NEUROIMAGING BIOMARKERS AND COGNITION IN ALZHEIMER'S DISEASE SPECTRUM, 2nd Edition

EDITED BY: Jiu Chen, Rong Chen and Yong Liu
PUBLISHED IN: Frontiers in Aging Neuroscience and Frontiers in Neuroscience

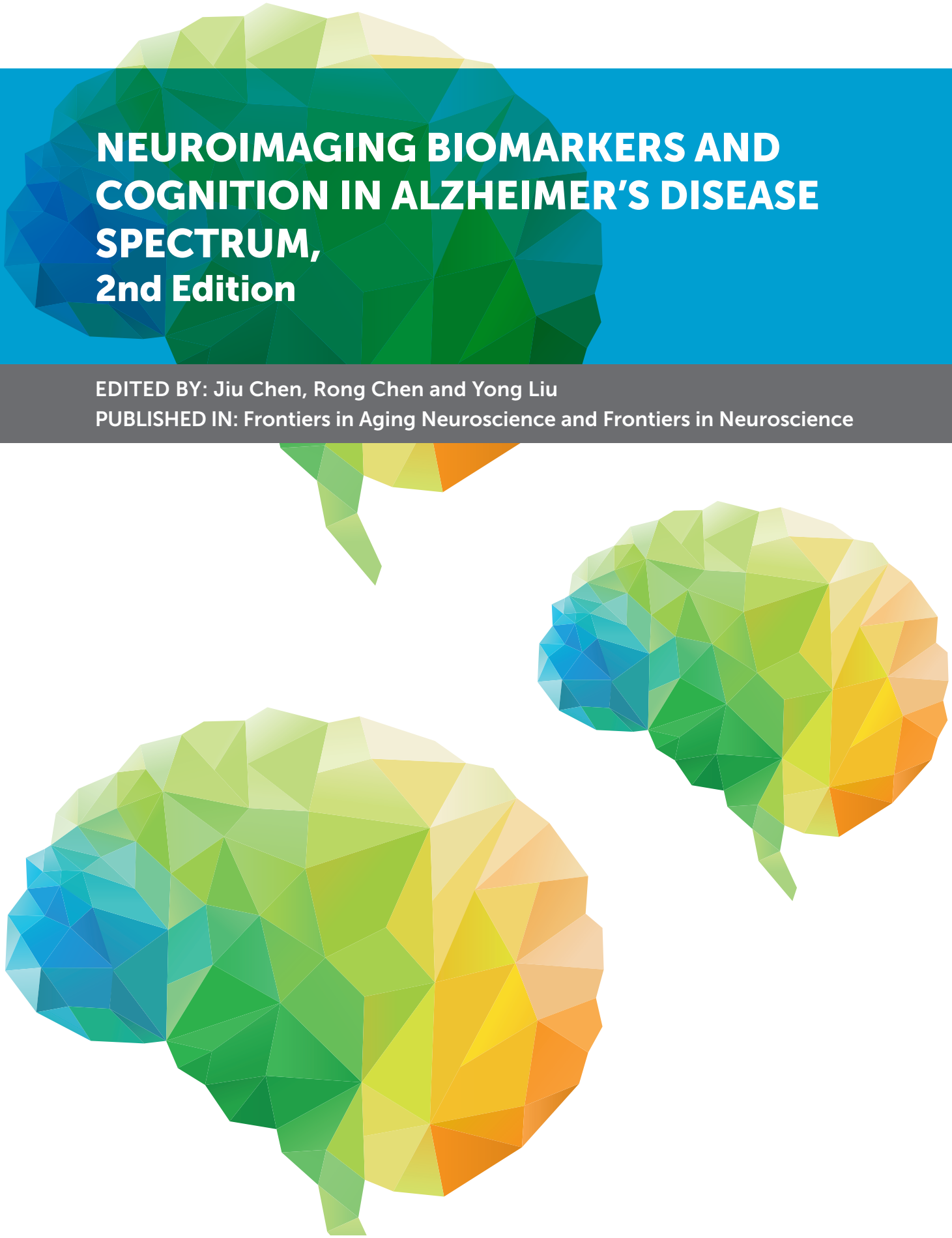

frontiers Research Topics

ISSN 1664-8714
ISBN 978-2-8325-4266-8
DOI 10.3389/978-2-8325-4266-8

About Frontiers

Frontiers is more than just an open-access publisher of scholarly articles: it is a pioneering approach to the world of academia, radically improving the way scholarly research is managed. The grand vision of Frontiers is a world where all people have an equal opportunity to seek, share and generate knowledge. Frontiers provides immediate and permanent online open access to all its publications, but this alone is not enough to realize our grand goals.

Frontiers Journal Series

The Frontiers Journal Series is a multi-tier and interdisciplinary set of open-access, online journals, promising a paradigm shift from the current review, selection and dissemination processes in academic publishing. All Frontiers journals are driven by researchers for researchers; therefore, they constitute a service to the scholarly community. At the same time, the Frontiers Journal Series operates on a revolutionary invention, the tiered publishing system, initially addressing specific communities of scholars, and gradually climbing up to broader public understanding, thus serving the interests of the lay society, too.

Dedication to Quality

Each Frontiers article is a landmark of the highest quality, thanks to genuinely collaborative interactions between authors and review editors, who include some of the world's best academicians. Research must be certified by peers before entering a stream of knowledge that may eventually reach the public - and shape society; therefore, Frontiers only applies the most rigorous and unbiased reviews.
Frontiers revolutionizes research publishing by freely delivering the most outstanding research, evaluated with no bias from both the academic and social point of view. By applying the most advanced information technologies, Frontiers is catapulting scholarly publishing into a new generation.

What are Frontiers Research Topics?

Frontiers Research Topics are very popular trademarks of the Frontiers Journals Series: they are collections of at least ten articles, all centered on a particular subject. With their unique mix of varied contributions from Original Research to Review Articles, Frontiers Research Topics unify the most influential researchers, the latest key findings and historical advances in a hot research area! Find out more on how to host your own Frontiers Research Topic or contribute to one as an author by contacting the Frontiers Editorial Office: frontiersin.org/about/contact

NEUROIMAGING BIOMARKERS AND COGNITION IN ALZHEIMER'S DISEASE SPECTRUM, 2nd Edition

Topic Editors:
Jiu Chen, Nanjing Medical University, China
Rong Chen, University of Maryland, Baltimore, United States
Yong Liu, Beijing University of Posts and Telecommunications (BUPT), China

Publisher's note: This is a 2nd edition due to an article retraction.

Citation: Chen, J., Chen, R., Liu, Y., eds. (2024). Neuroimaging Biomarkers and Cognition in Alzheimer's disease Spectrum, 2nd Edition. Lausanne: Frontiers Media SA. doi: 10.3389/978-2-8325-4266-8

Table of Contents

frontiers in Aging Neuroscience

EDITORIAL
published: 25 February 2022
doi: 10.3389/fnagi.2022.848719

Editorial: Neuroimaging Biomarkers and Cognition in Alzheimer's Disease Spectrum

Jiu Chen[1,2]*, *Siyu Wang*[1,2], *Rong Chen*[3] and *Yong Liu*[4]

[1] Institute of Neuropsychiatry, The Affiliated Brain Hospital, Fourth Clinical College, Nanjing Medical University, Nanjing, China, [2] Fourth Clinical College, Nanjing Medical University, Nanjing, China, [3] Department of Diagnostic Radiology and Nuclear Medicine, University of Maryland School of Medicine, Baltimore, MD, United States, [4] School of Artificial Intelligence, Beijing University of Posts and Telecommunications, Beijing, China

Keywords: Alzheimer's disease spectrum, subjective cognitive decline, mild cognitive impairment, neuroimaging, cognition

Editorial on the Research Topic

Neuroimaging Biomarkers and Cognition in Alzheimer's Disease Spectrum

Subjective cognitive decline (SCD) and mild cognitive impairment (MCI) are well recognized to be at high risk of converting to Alzheimer's disease (AD) and act as a clinical continuum of the AD spectrum. Neuroimaging is applied as a tool to figure out both anatomical and functional alterations in the AD spectrum and may further reveal the pathophysiologic mechanism of AD. This topic aimed to recruit worldwide articles focusing on neuroimaging biomarkers and cognition in the AD spectrum. A total of 30 contributions from 168 different authors have been included as of January 2022.

OPEN ACCESS

Edited and reviewed by:
Kristy A. Nielson, Marquette University, United States

***Correspondence:**
Jiu Chen
ericcst@aliyun.com

Specialty section:
This article was submitted to Neurocognitive Aging and Behavior, a section of the journal Frontiers in Aging Neuroscience

Received: *05 January 2022*
Accepted: *24 January 2022*
Published: *25 February 2022*

Citation:
Chen J, Wang S, Chen R and Liu Y (2022) Editorial: Neuroimaging Biomarkers and Cognition in Alzheimer's Disease Spectrum. Front. Aging Neurosci. 14:848719. doi: 10.3389/fnagi.2022.848719

STRUCTURAL AND METABOLIC ALTERATIONS CORRELATED WITH COGNITION IN THE AD SPECTRUM

Voxel-based morphometry (VBM) is a useful tool for detecting structural alterations in the preclinical AD spectrum. Zhang J. et al. assessed 31 VBM studies in amnestic MCI (aMCI) patients, discovering the highly robust deterioration in the left amygdala and right hippocampus. This indicates that specific gray matter (GM) atrophy may serve as a potential biomarker for early AD diagnoses. GM atrophy in the hippocampus and its subfield (HippSub) has long been recognized as typical lesions of AD. Several articles in our Research Topic focus on alterations in hippocampal volume. For example, Hansen et al. discovered alterations in HippSub volume in AD, but not in bipolar disorder (BD), or in major depressive disorder (MDD). This study reinforced the notion of different neural mechanisms in hippocampal degeneration. Except for HippSub volumes, atrophy in other brain regions has been observed to be correlated with cognitive dysfunction. Chen Q. et al. discovered reduced basal forebrain (BF) volume, especially in the Ch4p subfield in SCD patients compared with healthy controls, which was further associated with spatial disorientation. This indicates a structural basis for allocentric disorientation independent of hippocampal atrophy in SCD patients. To note, there is an increasing number of studies focusing on subdivided brain regions. We may expect that precisely subdividing regions could assist in improving the accuracy of locating preclinical AD lesions and further exploring the essence of disease changes.

White matter (WM) fiber bundles communicate with various brain regions and serve as important structural components of the brain. AD progression leads to potential damage to WM. One typical pathological change is white matter hyperintensities (WMHs). WMH reflects demyelination, which is a deterioration of neural pathways caused by decreasing blood flow and/or disease. WMHs have been widely observed in dementia such as AD. At the same time, diffusion tensor imaging (DTI) is used for detecting water molecule diffusion and is sensitive in white matter atrophy detection. Fractional anisotropy (FA), mean diffusivity (MD), and relative anisotropy (RA) are recognized as common DTI metrics. Diaz-Galvan et al. assessed cerebrovascular disease by applying WM signal abnormalities (WMSA) and MD. They further combined correlation, multiple regression, and mediation analyses to investigate the association between depressive symptomatology, cerebrovascular disease, and SCD. Likewise, several contributions of WM pay special attention to lesions in specific brain regions. Srisaikaew et al. focused on disruption of fornix integrity and fiber length in non-amnestic MCI (naMCI) compared to healthy controls, and its association with cognition. Based on their study results, the authors suggested that fornix fiber tract length played a crucial role in sustaining executive function in naMCI patients. To summarize, various studies focus on WM and GM separately. Still, since GM and WM together constitute the major part of the cerebrum, the internal relationship of atrophy between GM and WM is worth pondering, which may reveal the in-depth deteriorative and compensatory mechanism of the AD spectrum.

As for micro-alterations, fluorodeoxyglucose-B-positron emission tomography (FDG-PET) is utilized to reveal glucose metabolism in patients of the early AD spectrum. By GM volume analyses and glucose metabolism analyses, Lee S.-Y. et al. announced that tinnitus may lead to abnormal metabolism and altered cerebral architecture in MCI patients, providing insights into the combination of micro (metabolism) and macro (cerebellar structure) alterations to reveal AD pathology. Aβ and tau pathology are well established as AD typical biomarkers. By conducting partial correlation analyses under different amyloid statuses, Ge et al. calculated the relationship between tauopathy/volume of the hippocampal subfields and assessment scores. A significant decrease in hippocampal volume and increase in tau deposition of hippocampal subfields were observed in the Aβ-positive group compared to the negative one, indicating the feasibility of applying neuroimaging methods to explore traditional biomarkers.

FUNCTIONAL ALTERATIONS, NETWORK CONNECTIVITY, AND ENTROPY MAPPING CORRELATED WITH COGNITION IN THE AD SPECTRUM

Resting-state functional magnetic resonance imaging (rs-fMRI) is widely applied for AD early detection by means of functional connectivity (FC). Wang S. et al. applied data from the Nanjing Brain Hospital-Alzheimer's Disease Spectrum Neuroimaging Project (NBH-ADsnp) database (Dr. Jiu Chen serves as the principal investigator of NBH-ADsnp) to conduct FC in insular subnetworks for SCD and aMCI classification. Amplitude of low-frequency fluctuations (ALFF) can be utilized for measuring low-frequency oscillations of the blood-oxygen-level-dependent (BOLD) signal and localize altered spontaneous brain activities. Zhang X. et al. looked into previous studies on ALFF and fractional ALFF (fALFF) in amnestic and vascular MCI patients, suggesting the possibility of applying ALFF/fALFF for distinguishment. Except for FC and ALFF, other assessments such as regional homogeneity (ReHo), etc. can reflect neuronal activities.

Minor alterations pile up and eventually lead to the dysfunction of network connectivity. Many contributions in our Research Topic focus on brain networks. Sheng et al. conducted graph theory analysis to explore altered GM network metrics among healthy controls, MCI patients, and AD patients. Their study provided insight into the association between cognitive impairment and brain structural network compensation. To reveal executive function (EF) alterations, Liu et al. calculated fALFF and FC in an executive control network (ECN) and examined the relationship between altered fALFF or FC and EF composite score, uncovering the convergence and divergence in the MCI-high EF group and MCI-low EF group. Moreover, Lee P.-L. et al. suggested that the posterior cingulate cortex (PCC)-synchronized degeneration network (SDN) is spatially correlated with patterns of the GM atrophy rate, which is in better association with the AD spectrum than hippocampus-SDN. These contributions uncovered the deterioration and compensation of preclinical AD correlated to cognitions under diverse brain networks, which may also assist in revealing disease mechanism and progression.

Progressive brain deterioration leads to increasing brain entropy (BEN). In order to characterize BEN in AD and test the inverse-U-shape BEN model, Wang Z. et al. compared BEN between AD and normal aging, and further correlated BEN with age, education, etc. Abnormal decreasing BEN was discovered in association with severe cognitive impairment and daily function disability in an AD group, indicating an inverse-U trajectory of BEN evolution when normal aging progresses into AD dementia.

POTENTIAL CLASSIFICATION TOOLS FOR THE AD SPECTRUM

Optimizing classification tools for the early AD spectrum has always been a pursuit for researchers in this field. Research is conducted mainly by applying machine learning, pattern recognition, logistic regression, and deep learning strategy. For example, by integrating altered rCBF, ALFF, and ReHo, Zhang Q. et al. established a support-vector classifier model of machine learning to classify patients of the AD spectrum from HC. Except for applying various biomarkers, Wang S.-H. et al. proposed an Alzheimer's Disease VGG-Inspired Attention Network (ADVIAN) to better identify AD. Some researchers also chose to optimize the existing models. Du et al. suggested that anisotropy of anomalous diffusion improved the accuracy of classifying AD in a novel fractional motion model. These

studies cast light on the improved strategy of AD diagnoses. Still, more effort is needed for establishing AD diagnostic models based on the proper combination of stable biomarkers, which are accurate, convenient, and economical enough for clinical use.

POTENTIAL PREVENTION STRATEGY FOR THE AD SPECTRUM

Two other contributions focusing on intervention are included in our Research Topic. To measure the effect of aerobic exercises, Yu et al. examined hippocampal volume, temporal meta-regions of interest (ROI) cortical thickness, WMH volume, and network failure quotient (NFQ). They further performed correlation analyses between 6- and 12-month changes of MRI biomarkers and the AD Assessment Scale-Cognition (ADAS-Cog). The results revealed that hippocampal volume and temporal meta-ROI cortical thickness are slightly reduced only during the intervention period. By applying probabilistic tractography and voxel-based morphometry, Kim G.-W. et al. discovered that no significant changes in thalamo-cortical WM connectivity, cortical thickness, or GM volume exist between MCI patients with/without donepezil treatment. A reliable intervention strategy is urgently needed for slowing down the procession of AD. Thus, carrying out relevant longitudinal research is a necessity. Through structural and functional alterations and correspondent clinical symptoms, these two studies assessed the treatment effect of aerobic exercises and donepezil for preclinical stages of AD. This suggests that potential neuroimaging biomarkers can be further applied to evaluate the impact of diet, lifestyle intervention, and medication on AD progression. At the same time, the combination of multimodal interventions may have superimposed therapeutic effects, which is also worthy of researchers' attention.

AUTHOR CONTRIBUTIONS

JC, RC, and YL designed the topic. JC and SW prepared the manuscript. All authors contributed to the article and approved the submitted version.

FUNDING

This study was supported by the National Natural Science Foundation of China (No. 81701675), the Key Project supported by Medical Science and Technology Development Foundation, Nanjing Department of Health (No. JQX18005), and the Key Research and Development Plan (Social Development) Project of Jiangsu Province (No. BE2018608).

Conflict of Interest: The authors declare that the research was conducted in the absence of any commercial or financial relationships that could be construed as a potential conflict of interest.

frontiers in Aging Neuroscience

ORIGINAL RESEARCH
published: 10 November 2020
doi: 10.3389/fnagi.2020.596122

Brain Entropy Mapping in Healthy Aging and Alzheimer's Disease

Ze Wang and for the Alzheimer's Disease Neuroimaging Initiative†*

Department of Diagnostic Radiology and Nuclear Medicine, University of Maryland School of Medicine, Baltimore, United States

Alzheimer's disease (AD) is a progressive neurodegenerative disease, for which aging remains the major risk factor. Aging is under a consistent pressure of increasing brain entropy (BEN) due to the progressive brain deteriorations. Noticeably, the brain constantly consumes a large amount of energy to maintain its functional integrity, likely creating or maintaining a big "reserve" to counteract the high entropy. Malfunctions of this latent reserve may indicate a critical point of disease progression. The purpose of this study was to characterize BEN in aging and AD and to test an inverse-U-shape BEN model: BEN increases with age and AD pathology in normal aging but decreases in the AD continuum. BEN was measured with resting state fMRI and compared across aging and the AD continuum. Associations of BEN with age, education, clinical symptoms, and pathology were examined by multiple regression. The analysis results highlighted resting BEN in the default mode network, medial temporal lobe, and prefrontal cortex and showed that: (1) BEN increased with age and pathological deposition in normal aging but decreased with age and pathological deposition in the AD continuum; (2) AD showed catastrophic BEN reduction, which was related to more severe cognitive impairment and daily function disability; and (3) BEN decreased with education years in normal aging, but not in the AD continuum. BEN evolution follows an inverse-U trajectory when AD progresses from normal aging to AD dementia. Education is beneficial for suppressing the entropy increase potency in normal aging.

Keywords: resting state fMRI, entropy, pathology, reserve, AD, MCI

OPEN ACCESS

Edited by:
Yong Liu,
Chinese Academy of Sciences, China

Reviewed by:
Subapriya Suppiah,
Universiti Putra Malaysia, Malaysia
Mitsuru Shinohara,
Mayo Clinic, United States
Vesa J. Kiviniemi,
University of Oulu, Finland

****Correspondence:***
Ze Wang
ze.wang@som.umaryland.edu

†Data used in preparation of this article were obtained from the Alzheimer's Disease Neuroimaging Initiative (ADNI) database (adni.loni.usc.edu). As such, the investigators within the ADNI contributed to the design and implementation of ADNI and/or provided data but did not participate in analysis or writing of this report. A complete listing of ADNI investigators can be found at: http://adni.loni.usc.edu/wp-content/uploads/how_to_apply/ADNI_Acknowledgement_List.pdf.

Received: *18 August 2020*
Accepted: *06 October 2020*
Published: *10 November 2020*

Citation:
Wang Z (2020) Brain Entropy Mapping In Healthy Aging and Alzheimer's Disease. Front. Aging Neurosci. 12:596122. doi: 10.3389/fnagi.2020.596122

INTRODUCTION

Alzheimer's disease (AD) is a neurodegenerative disease that has impacted millions of elderly people but still remains incurable (Ferri et al., 2005; Reitz and Mayeux, 2014). Although AD has been well characterized by AD pathology and clinical symptoms, a major barrier to research progress is the unclear mechanism for how and when normal aging progresses into AD dementia (Kumar and Singh, 2015; Mehta and Yeo, 2017) and why AD symptoms often emerge many years later than AD pathology. This pathology vs. symptom discrepancy (Jack et al., 2010; Jack and Holtzman, 2013) suggests that there may exist a reserve of brain function according to the seminal "cognitive reserve" (CR; Stern, 2006; Stern et al., 2018) model. This reserve may compensate brain damage–induced functional abnormalities in normal aging but fails to do that after disease conversion. To characterize the brain function reserve, we need a more tangible proxy. One candidate is the resting-state brain activity which matches the latent function reserve in two perspectives: first, it is an ongoing process

non-specific to any overt brain function; second, it has been postulated to play a role in brain function facilitation (Raichle et al., 2001; Raichle and Gusnard, 2002; Raichle, 2011). Resting-state fMRI (rsfMRI) represents the most widely used tool for studying resting brain activity and has been used to assess neural correlates of brain reserve through the inter-regional functional connectivity (FC) analysis (Arenaza-Urquijo et al., 2013; Bozzali et al., 2015; Marques et al., 2016; Franzmeier et al., 2017; Li et al., 2020). An overall picture revealed by these studies is that higher CR measures are related to stronger FC in distributed brain regions including the default mode network (DMN) area and weaker FC in other restricted focal regions. Because FC is defined by the inter-regional signal correlation in the seed-based FC (Biswal et al., 1995) or the associations to a common temporal fluctuation pattern in the spatial independent component decomposition (Calhoun et al., 2001; Hyvärinen et al., 2001; Beckmann and Smith, 2004), it does not tell anything specific to regional brain activity.

In this study, we proposed entropy of each local voxel as a regional proxy of brain reserve. Entropy is a physical measure for a dynamic system with high entropy indicating less order and more irregularity. It may be informative for delineating the aforementioned AD pathology vs. symptom discrepancy because aging is known to have progressive brain deteriorations (Hayflick, 2004; Drachman, 2006) which inevitably increase the brain entropy. High entropy corresponds to low temporal coherence, which is detrimental to brain functional organization and has to be counteracted to keep the normal brain functionality. Because brain reserve is defined by brain function facilitation and compensation, assessing entropy of functional brain activity may provide a direct outcome measure of the latent brain reserve. In a pilot study (Wang, 2020a,b; full article under separate review) based on data from 862 healthy adults from the human connectome project (Van Essen et al., 2013), we found that brain entropy (BEN) in the DMN (including precuneus, bilateral parietal cortex, and part of temporal cortex) and the executive control network (ECN; including the dorsolateral prefrontal cortex and lateral parietal cortex) increases with age but decreases with education years (an indicator of cognitive reserve for compensating brain dysfunctions) and that lower BEN in DMN and ECN is associated with better performance of cognitive functions. These data suggest the feasibility of BEN for characterizing the latent brain reserve compensation outcome. Although the compensation may be sufficient in normal aging, they may become insufficient when disease progresses, which can reciprocally trigger reserve overactions, leading to a catastrophic reduction of BEN as found in previous biophysiological recording–based AD entropy studies (Stam et al., 2003; Jeong, 2004; Abásolo et al., 2006; Gómez and Hornero, 2010; Mizuno et al., 2010; Yang et al., 2013). To explain this apparent opposed entropy change pattern in normal aging and AD, we proposed a heuristic BEN model as shown in **Figure 1**. This model considers low BEN in DMN and ECN as beneficial for normal aging because low brain entropy corresponds to high temporal coherence which is evidenced to be important for brain function (Buzsáki and Draguhn, 2004; Buzsaki, 2006; Schroeder and Lakatos, 2009; Saleh et al., 2010; Buzsáki and Watson, 2012; Henry and Obleser, 2012; Lega et al., 2012; Thut et al., 2012; Calderone et al., 2014; Reinhart and Nguyen, 2019). However, in AD, our model predicts a detrimental large BEN reduction in DMN/ECN, indicating a failure of the functional compensation role of brain reserve in AD (Stern, 2006, 2012; Stern et al., 2018). The accumulating brain errors or deteriorations will increase BEN and the risk of brain dysfunction if no compensations occur. This potency, however, can be substantially counteracted by brain reserve or other compensatory mechanisms, resulting in a slowly increasing and then flat topping BEN evolution curve in normal aging (the dashed blue line in **Figure 1**). When the BEN increase latency reaches a critical point where brain dysfunction cannot be fully compensated anymore, reserve overaction may be triggered, leading to an apparent BEN reduction (the red solid curve in **Figure 1**). When disease progresses, BEN reduction may be accelerated further by other detrimental factors such as the accumulation of Aβ deposition and perfusion deficits. Both Aβ decomposition and hypoperfusion may cause or be associated with BEN reductions through the CBF vs. brain coherence associations: lower CBF correlates with higher brain activity coherence (Sharbrough et al., 1973; Foreman and Claassen, 2012; higher coherence corresponds to lower BEN).

The main purpose of this study was to assess the feasibility of BEN as an outcome measure of the latent brain function reserve and to evaluate the hypothetical BEN model by leveraging the relatively large data from the AD Neuroimaging Initiative (ADNI)[1] and our recently developed rsfMRI-based BEN mapping tool (Wang et al., 2014). The model was assessed using the cross-sectional ADNI rsfMRI data. We hypothesized that AD patients have lower BEN than cognitively healthy elderlies; BEN increases with age in normal aging but not in AD. The association of BEN to function reserve was examined through the correlation between BEN and education, cognitive function measures, and AD pathology measures. Education is a main contributing factor of cognitive reserve (Stern et al., 2018). Longer education years have been demonstrated to be beneficial for combating cognitive impairments. In accordance with the BEN model, we hypothesized that longer education years are associated with reduced BEN in normal aging but not in AD. The entire study reported in this paper is a full expansion of a small sample-based preliminary study (Li and Wang, 2016).

MATERIALS AND METHODS

Human Subjects

All human subjects' data included in this study were downloaded from the ADNI database[1]. Reanalysis of ADNI data was approved by institutional review boards of all participating institutions and written informed consent was obtained from all participants or authorized representatives. Subjects were limited to those with rsfMRI data acquired with the traditional gradient-echo-weighted echo-planar imaging sequence by May 2018. Full inclusion and exclusion criteria for ADNI are described at www.adni-info.org. In brief, patients with mild

[1] http://www.adni-info.org

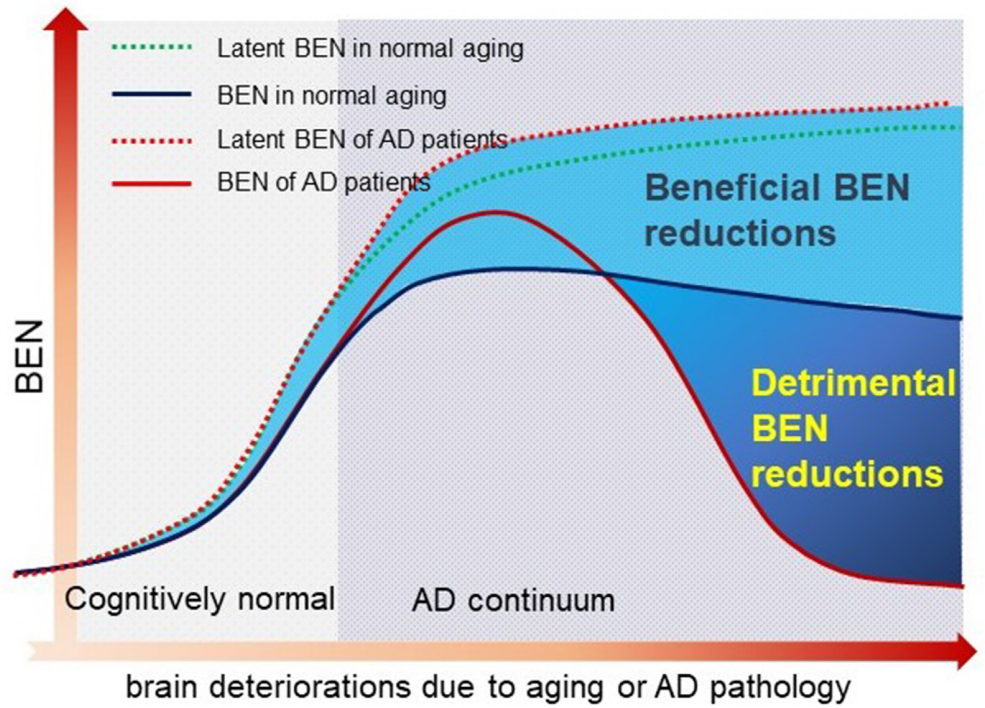

FIGURE 1 | A hypothetical brain entropy (BEN) model for normal aging and Alzheimer's disease (AD). The dotted line shows the latent BEN evolution trend as a result of the aging-related accumulated brain deteriorations. The dashed line represents the actual BEN evolution curve after brain reserve compensation which imposes negative entropy brings down the total BEN. Catastrophic BEN reduction may start at the disease conversion time due to a potential overaction of the brain reserve.

cognitive impairment (MCI) were classified essentially in the manner described by Petersen (2004), but were then further divided into "early" and "late" groups (i.e., EMCI and LMCI, respectively) based on performance on the Wechsler Memory Scale–Revised Logical Memory II (WMS-LM). The EMCI group was defined based on scores between the cutoff of normal and that of the LMCI group. A total of 211 subjects whose rsfMRI data met all QC criteria were analyzed. Detailed characteristic information and the number of subjects in each sub-group are listed in **Table 1**.

MRI Data Acquisition

Both high-resolution structural MRI data and rsfMRI data were downloaded from the ADNI website[1]. The structural images were acquired using a 3D magnetization-prepared rapid acquisition with gradient echo T1-weighted sequence with the following parameters: repetition time/echo time/inversion time = 2,300/2.98/900 ms, 176 sagittal slices, within plane field of view = 256 × 240 mm^2, voxel size = 1.1 × 1.1 × 1.2 mm^3, flip angle = 9°, bandwidth = 240 Hz/px. rsfMRI was acquired using a gradient echo-weighted echo-planar imaging sequence with the following acquisition parameters: repetition time/echo time = 3,000/30 ms, number of axial slices = 48, slice thickness = 3.3, flip angle = 80°, within plane field of view = 212 × 212 mm^2, and number of timepoints = 140.

MRI Data Preprocessing

MR image preprocessing was conducted using the pipeline included in BENtbx (Wang et al., 2014) with the following steps: slice timing correction, motion correction, temporal nuisance correction, spatial smoothing, inter-modality coregistration (structural image and rsfMRI images), and spatial normalization. These procedures were implemented in Matlab m-script. Coregistration and spatial normalization were based on functions provided by SPM (version 12[2]); other steps were based on custom code written by the author. The first two rsfMRI images were excluded to allow rsfMRI signal reach the steady state. Subjects included in the following analyses had no more than 2 mm translational motions and no more than 2° of angular motions. Subjects with mean framewise displacement (Power et al., 2012) greater than 0.5 mm were excluded too. Residual motions were regressed out from the rsfMRI time series in the temporal nuisance correction step. The Diffeomorphic Anatomical Registration Through Exponential Lie Algebra algorithm (Ashburner, 2007) implemented in SPM12 was used to generate a local brain template based on all subjects' gray matter and white matter probability maps. The template was registered into the Montreal Neurological Institute (MNI) standard space using a linear affine transformation. With these two transforms, each individual subject's rsfMRI

[2]https://www.fil.ion.ucl.ac.uk/spm/

TABLE 1 | Human subject characteristics.

Diagnosis group	HC	SMC	EMCI	LMCI	Alzheimer's disease	*P*-value
Number	54	27	58	38	34	–
Gender (M/F)	24/28	12/15	22/35	24/14	16/18	0.253
Age (mean ± SD, range)	75.3 ± 6.96, 65–95	72.44 ± 5.49, 65–83	71.53 ± 6.93, 56–89	71.89 ± 8.26, 57–88	72.47 ± 7.06, 56–87	0.082
APOE ε4 allele	30.00%	29.63%	45.61%	35.89%	70.59%	**1.9E−03**
MMSE (mean ± SD)	27.56 ± 5.71	28.78 ± 1.48	25.93 ± 7.94	26.59 ± 6.12	22.21 ± 4.47	**1.59E−4**

P-values were assessed due to significant differences among diagnosis groups and were computed using one-way ANOVA (except for gender using χ^2 test). HC, healthy control; SMC, significant memory concern; EMCI, early mild cognitive impairment; LMCI, late mild cognitive impairment; MMSE, Mini-Mental State Examination; values in bold signify $p < 0.05$.

was mapped into the MNI space for group-level analysis. BEN calculation was performed for each voxel of the preprocessed rsfMRI data using two iterative processes. Given the rsfMRI time series of any voxel, a sliding window with a length of m consecutive timepoints was used to extract all possible data segments as illustrated by the colored rectangles overlaid on the time series and the associated arrows. For the i-th data segment, its Chebyshev distance to another segment was calculated. If the distance was smaller than the cutoff threshold r, it was considered as a "match". r and m were selected to be $r = 0.6$ and $m = 3$ as evaluated in Wang et al. (2014). The same procedure was iterated until the seed segment was compared with all other segments and the total number of matches was recorded as $B_i^m(r)$ and the sum of B_i^m over all segments was recorded by $B_i^m(r)$. Next, the sliding window length was increased by 1 to be m + 1. The aforementioned matching process was repeated to get the total number of matches $A^{(m+1)}(r)$ for all segments with a length of m + 1. Following the Sample Entropy formula, entropy was finally calculated as the logarithm of the ratio of $B^m(r)/A^{(m+1)}(r)$. This process is theoretically equivalent to calculating the negative natural logarithm of the conditional probability that two temporal segments of the entire data time series similar for m points remain similar for m + 1.

Cerebrospinal Fluid (CSF) Biomarker

The amyloid-β 1–42 peptide ($A\beta_{1-42}$) and total tau (t-tau) measured in the baseline CSF samples were obtained from the ADNI database[1]. Sample acquisition and quality control of CSF were performed as described previously (Shaw et al., 2009). Mean and SD of t-tau/$A\beta_{1-42}$ ratio were calculated, while subjects with greater or smaller than 6 SD from the mean value were regarded as outliers. Only one subject was out of this range and was subsequently excluded from the following analysis.

Statistical Analysis

An ANOVA model was used to examine BEN difference between controls and patients at different disease stages. Disease diagnosis vs. pathology interactions were modeled. Age, sex, race, and education were included as variables. Cross-sectional BEN difference and age, sex, and education effects were assessed using *ad hoc* contrast analysis as mentioned previously. Disease vs. age, sex, and education interactions on BEN were examined. Voxelwise multiple regressions were used to assess age, sex, and education effects and the associations of BEN to delayed recall (for memory), memory test results in the Rey Auditory Verbal Learning Test (RAVLT; Schmidt, 1996), the total score of Functional Activity Questionnaire (FAQ; Pfeffer et al., 1982; Marshall et al., 2015), and the Mini-Mental State Examination (MMSE). The rationales for choosing these neuropsychological measures are memory dysfunction is a hallmark of clinical AD symptoms and is widely assessed by delayed recall and RAVLT; AD patients present characteristic daily function impairment which can be measured by FAQ; MMSE is the most often used short screening tool for measuring the overall cognitive impairment. Sex, age, and education level were included as nuisance covariates in these regression models. Additional multiple-regression models were used to assess associations of BEN vs. CSF Aβ ($A\beta_{1-42}$) concentration.

Data Availability

BENtbx used in this study is available from https://www.cfn.upenn.edu/∼zewang/BENtbx.php. ADNI data are available from loni.usc.edu/adni. Analysis results are available from the author by request.

RESULTS

Age difference was significant only between controls and EMCI (p = 0.02). **Figure 2** shows the one-way ANOVA results. BEN was significantly (F-test, $p < 0.05$, family-wise error corrected) different within the whole brain among the five populations (elderly controls, significant memory concern (SMC), EMCI, LMCI, and AD). The hot spots overlaid on the three axial image slices in **Figure 2** are the *post hoc* voxelwise BEN difference between AD and controls. At $p < 0.005$, cluster size > 300 [AlphaSim (the updated version) corrected], AD showed reduced BEN in MTL including hippocampus (HIPP), inferior temporal cortex, precuneus, and parietal cortex (part of the DMN). No BEN increase was observed across the brain in AD as compared with controls. BEN was extracted from a voxel in left parietal cortex as marked by the yellow dotted cross. Both the scatter plot and the fitted curve demonstrate an inverse-U shaped transition pattern of BEN from cognitively normal elderly controls to AD: BEN slightly increased from controls to SMC, then to EMCI, but quickly dropped to be below BEN of controls in LMCI, and fell further in AD at an accelerated pace. This curve was very similar at different voxels in DMN, PFC, and other brain regions.

Figure 3 shows the age and education effects of BEN. Controls showed age-related BEN increase [**Figure 3A**; $p < 0.005$, cluster size > 200 (corrected using AlphaSim)] in precuneus, MTL, and PFC. Education years were negatively correlated to BEN in controls (**Figure 3C**). By contrast, the age effects were mostly

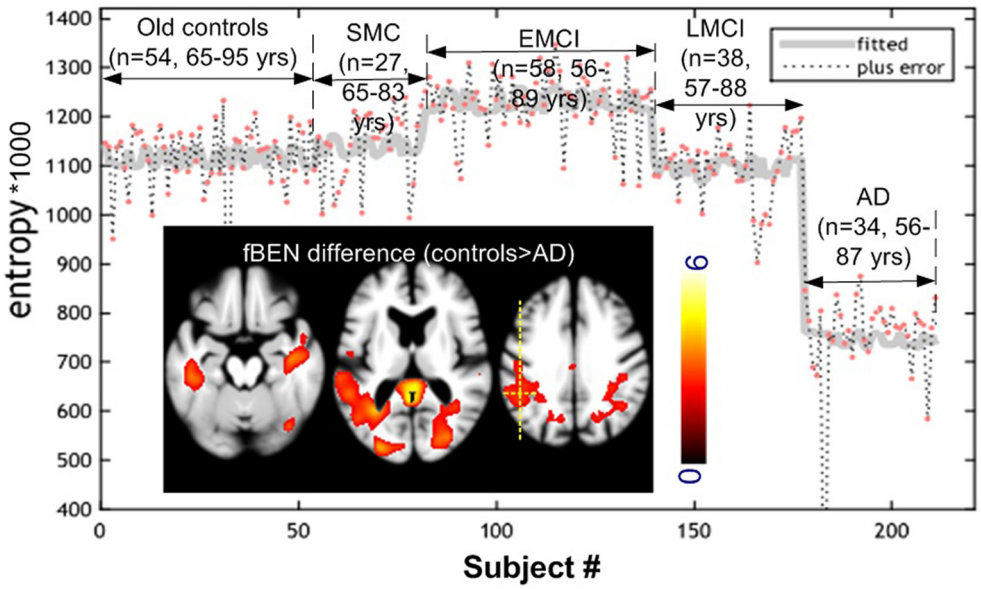

FIGURE 2 | Cross-sectional brain entropy (BEN) profile identified from ADNI rsfMRI. BEN slightly increased from old controls to significant memory concern (SMC) and then early mild cognitive impairment (EMCI), but reduced from EMCI to late mild cognitive impairment (LMCI), and then AD at an accelerated pace. The inset figure shows the post hoc control > AD (red spots in the three image slices) BEN difference ($P < 0.005$, cluster size > 300 corrected). The gray curve was the fitted line of BEN from different populations from the same position marked by the yellow cross. Color bar indicates the display window for the t-map shown in the three image slices.

flipped to the opposite direction (a negative correlation) in the combined patient group (SMC + EMCI + LMCI + AD; **Figure 3B**) and no education effects were found in the composite patient group at all (**Figure 3D**).

Figure 4 shows the results of BEN vs. AD pathology association analyses. AD pathology was measured by CSF $A\beta_{1-42}$ peptide concentration with lower CSF Aβ meaning higher brain Aβ depositions. Controls and patients showed opposite BEN vs. CSF Aβ associations in nearly the same brain regions. As CSF $A\beta_{1-42}$ is inversely related to beta amyloid depositions in the brain (Grimmer et al., 2009), the negative CSF Aβ-BEN correlation found in controls (**Figure 4A**) means BEN in DMN, MTL, lateral PFC, and visual cortex may increase with brain beta amyloid depositions. In patients (**Figure 4B**), BEN decreases with brain beta amyloid depositions. **Figure 4C** shows the scatter plots for all subgroups. Controls and SMC showed opposite BEN vs. CSF Aβ relationship though the correlation was statistically significant only in controls (r^2 = 0.282, p = 4.3e−4) and LMCI (r^2 = 0.14, p = 0.04). Similar BEN vs. AD pathology associations were found when we used tau/Aβ ratio or p-tau/Aβ ratio as the pathology indicator.

Figure 5 shows the associations of BEN to cognitive and daily functional impairment for the composite patient group. Age, sex, and education years were regressed out. Both **Figure 5A** (delayed-recall) and **5C** (RAVLT) show a positive correlation of BEN to memory function, meaning that a lower BEN in the elucidated regions (DMN, MTL) corresponds to a more severe memory deficit. BEN in DMN and hippocampus was positively related to MMSE (**Figure 5B**), suggesting patients with more cognitive impairments have lower BEN. Lower BEN in DMN, temporal cortex, and PFC was further related to more severe daily functional disability as measured by FAQ.

DISCUSSION

We assessed resting state BEN as a proxy for assessing the latent brain reserve and proposed a heuristic inverse-U shape BEN model to explain the aging-related functional brain alterations and the pathology vs. AD symptom discrepancy. The validity of BEN as a reserve proxy was examined by the BEN vs. age, education, and cognitive performance association studies. The inverse-U shape model was evaluated by comparing BEN across normal aging and patients with different stages of disease in the AD continuum as well as by the neurobehavioral and pathological association analyses. The major findings are as follows: (1) the cross-sectional analysis demonstrated that BEN first slightly increased from normal aging to SMC and to EMCI, but quickly fell below the BEN level of normal controls in LMCI, and reduced further in AD with an accelerated pace; (2) BEN presented different age and education effects in normal aging and AD continuum. It increases with age in normal aging but decreases with age in the AD continuum. It decreases with education years in normal aging, but is not correlated with education any more in the AD continuum; (3) BEN showed totally opposite associations with CSF Aβ depositions. The BEN vs. CSF Aβ correlation was negative in normal aging but became positive in the AD continuum; and (4) low BEN was correlated with more severe cognitive impairment and daily function disability in the AD continuum. These findings

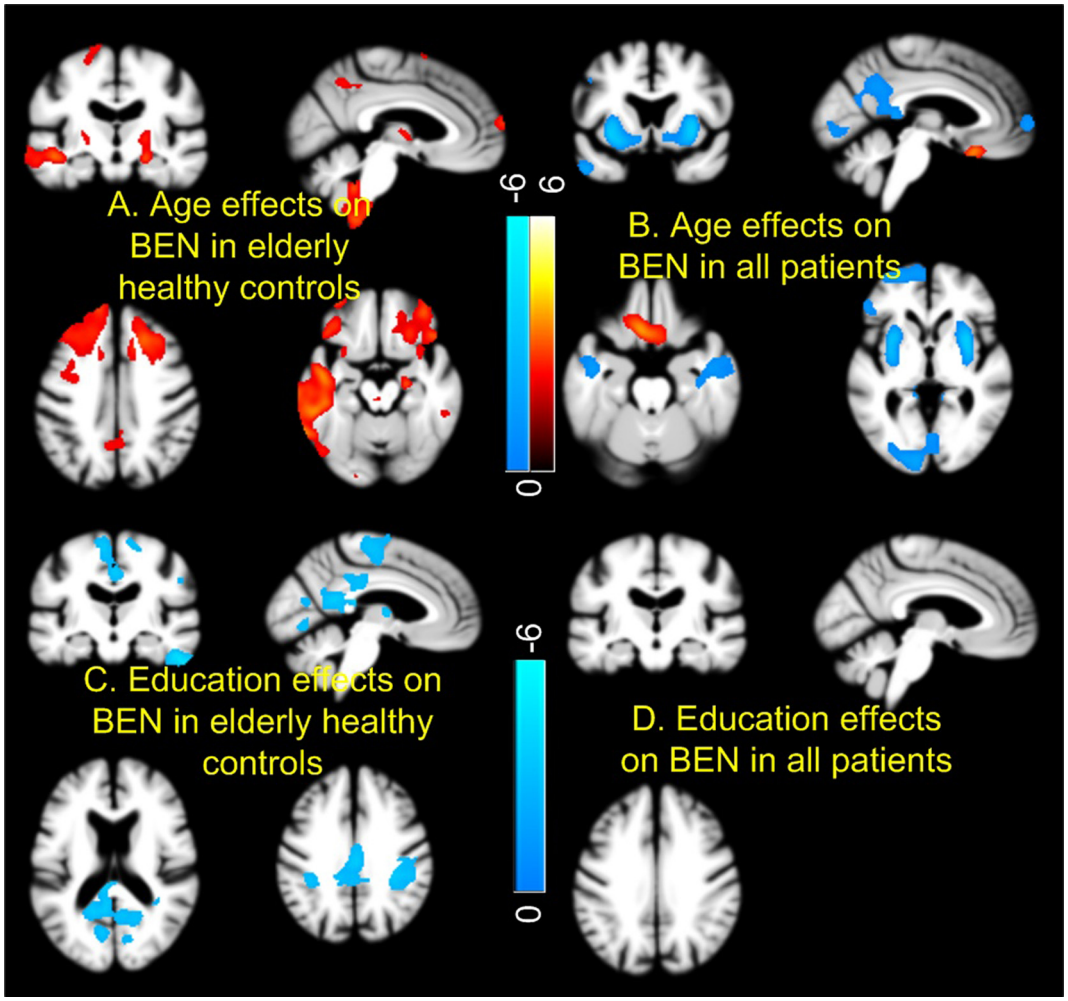

FIGURE 3 | Age and education effects of brain entropy (BEN). Controls and patients [mild cognitive impairment (MCI) and AD] showed opposite BEN vs. age relationship in most part of the brain **(A,B)**. Education years correlated with reduced BEN in default mode network in controls **(C)**, but not in patients **(D)**. Red and cool colors mean positive and negative correlations, respectively. Color bars indicate the display windows of the *t*-maps of the regression analysis.

highlighted resting BEN in DMN, MTL, and PFC, which have been implicated in different neuroimaging-based aging and AD studies (Ries et al., 2008; Ouchi and Kikuchi, 2012; Weiner et al., 2013; Wang, 2016; Badhwar et al., 2017; Anthony and Lin, 2018).

These findings proved the hypothetical inverse-U shape BEN model as depicted in **Figure 1**: resting BEN changed from cognitively normal controls to AD following an apparent inverse-U shape; BEN increases with age and pathological depositions but decreases with longer education years in normal aging; in the AD continuum, BEN decreases with age and is not correlated with education anymore as the reserve-based function compensations fail. Age had deleterious effects on BEN (BEN increases with age), but the effects were surpassed by a potential overaction of brain reserve after clinical observable memory or cognitive problems emerged. Controls and patients showed opposite age effects on BEN, which can be explained by the substantially reduced BEN in LMCI and AD. The lack of education effects in patients may suggest a failure of the compensation role of BEN especially in later stages of dementia. Education years showed effects of reducing BEN in the cognitively normal elderly, but the effects diminished in the AD continuum, indicating a weakening or failure of the reserve compensation as suggested by the brain reserve literature (Stern, 2006, 2012; Stern et al., 2018). This compensation weakening or failure was further supported by the BEN vs. behavior correlations showing that lower BEN in DMN/MTL/PFC is correlated to more severe cognitive impairment and daily functional disability. The opposite BEN evolution processes in normal controls and the disease continuum were supported by the AD pathology association findings: higher AD pathology deposition (reflected by lower CSF Abeta level) is associated with increased BEN in the cognitively normal elderly, suggesting an AD pathology–related functional deterioration in normal aging. In contrast, the pathology–BEN association was switched to the opposite in the AD continuum showing more brain pathology corresponding to lower DMN/MTL/PFC BEN. This

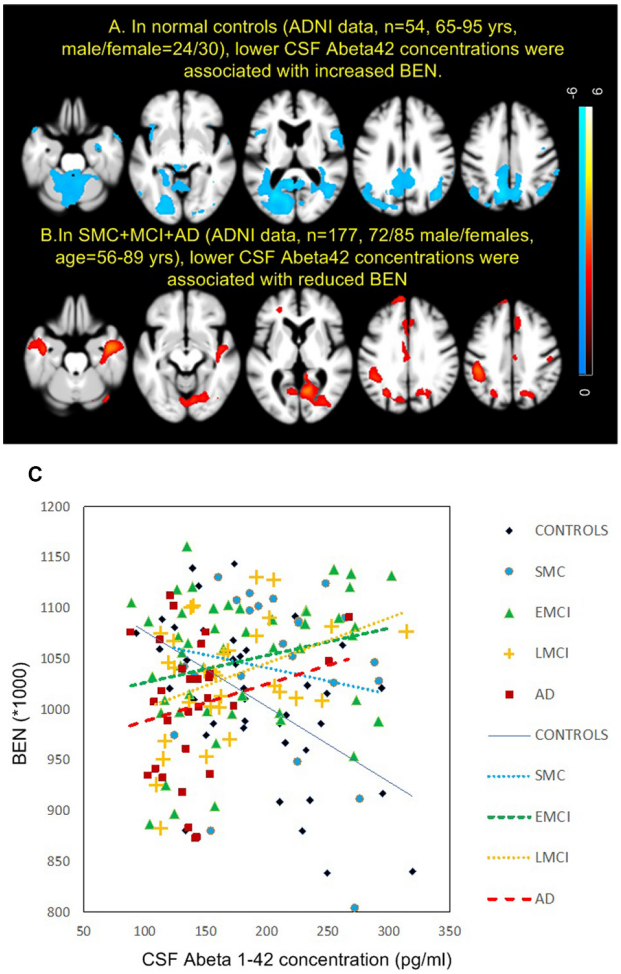

FIGURE 4 | Brain entropy (BEN) vs. cerebrospinal fluid (CSF) Aβ associations in panel **(A)** controls and **(B)** MCI and AD. **(C)** The associations for each sub-group in precuneus. The red cross in the 4th image in panel **(A)** indicates the location of the precuneus region of interest. The lines in panel **(C)** depict the linearly fitted associations. EMCI, early mild cognitive impairment; LMCI, late mild cognitive impairment.

pathology-related BEN reduction (rather than increase) indicates an escalated demand of compensation triggering a reserve overaction, which unfortunately cannot be achieved anymore. The dramatically reduced BEN eventually leads to accelerated functional impairments as the brain activity still needs a certain level of entropy to keep its functional flexibility (Tagliazucchi et al., 2012; Haimovici et al., 2013). Low entropy may also indicate a low energy state, which is supported by the well-known hypo-perfusion/hypo-metabolism state found in AD (Johnson et al., 2005; Ruitenberg et al., 2005; Chao et al., 2009; Hu et al., 2010; Chen et al., 2011; Musiek et al., 2012; Wang et al., 2013; Liu et al., 2014; Wang, 2014; Verclytte et al., 2016; Daulatzai, 2017).

The BEN variation patterns from normal aging to the AD continuum are consistent with our initial finding reported in 2016 (Li and Wang, 2016) and the AD hypo-entropy literature (Stam et al., 2003; Jeong, 2004; Abásolo et al., 2006; Gómez and Hornero, 2010; Mizuno et al., 2010; Yang et al., 2013; Wang et al., 2017). Different from these previous studies, the current study provided more comprehensive data regarding the change patterns of BEN across different disease stages, the associations of BEN to AD pathology, the associations with age and education, and the link to clinical consequences. The link of BEN to brain reserve was examined through its correlation to education years, which is a widely used index of cognitive reserve. The BEN–brain reserve association was also evidenced by the correlation to neurobehaviors in the patients. Although we did not find a significant correlation between BEN and neurobehavior measures in the healthy elderly controls, we observed significant negative correlation between BEN and cognitive function and education years but significant positive correlation between BEN and age in 866 young healthy adults in a article under peer review. Those data suggest that BEN vs. neurobehavior correlation in elderly controls may still exist but require a larger sample size to be identified.

Brain reserve was proposed to explain the individual difference of tolerating the pathology-induced functional alterations (Stern, 2006, 2012; Stern et al., 2018). Because

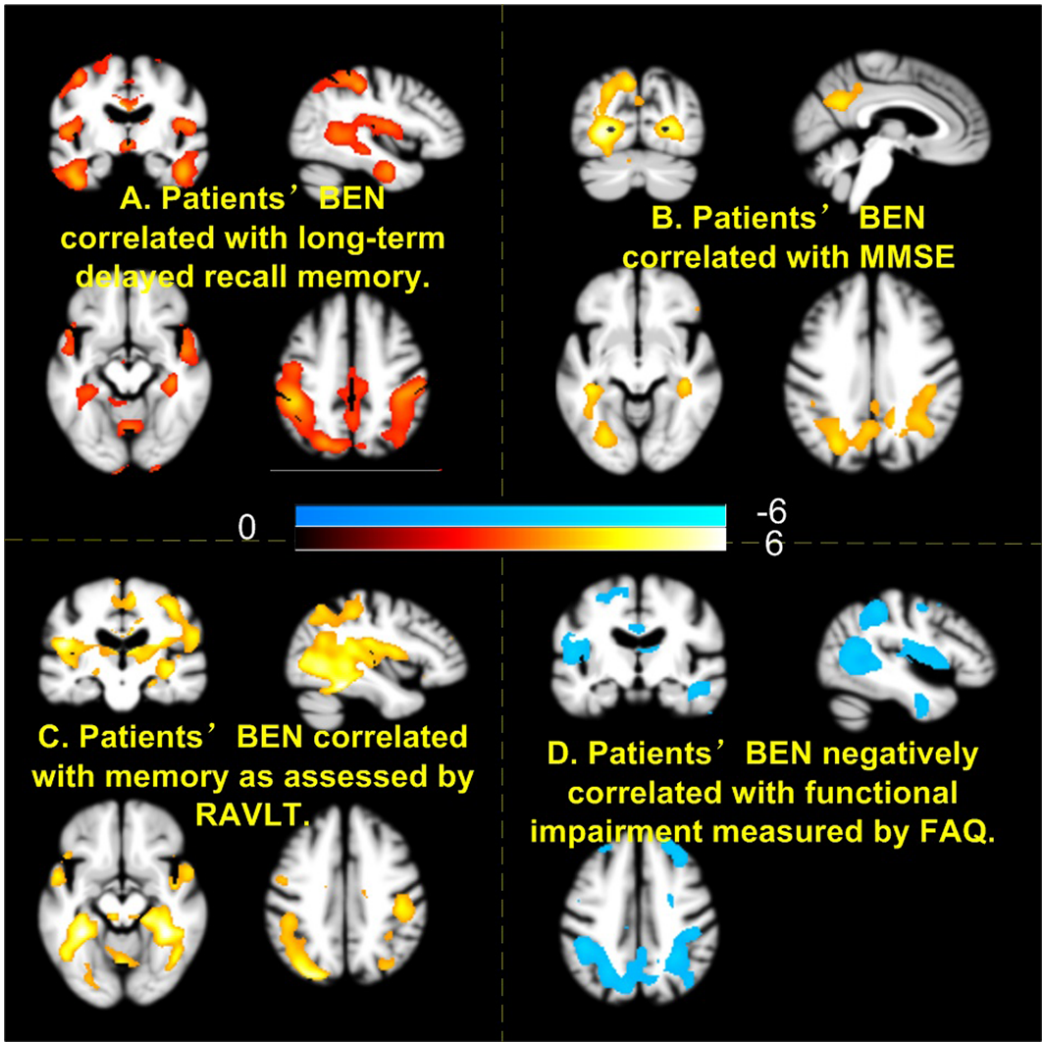

FIGURE 5 | Higher brain entropy (BEN) in parietal cortex, temporal cortex associated with more severe impairment of memory **(A,C)**, cognitive **(B)**, and daily functions **(D)**. Red and cool colors mean positive and negative correlations, respectively. MMSE, Mini-Mental State Examination; RAVLT, Rey Auditory Verbal Learning Test; FAQ, Functional Activity Questionnaire.

brain reserve is non-specific to any overt brain function, the null-hypothesis resting state activity which play a role in function facilitation (Raichle et al., 2001; Raichle and Gusnard, 2002; Raichle, 2006; Pizoli et al., 2011) has been postulated to be related to brain reserve in several studies (Arenaza-Urquijo et al., 2013; Bozzali et al., 2015; Marques et al., 2016; Franzmeier et al., 2017; Li et al., 2020). Different from these previous studies, the current study focused on regional resting brain activity, which may either be the action or the outcome of brain reserve facilitation or compensation. We chose entropy as the proxy to characterize the neural substrates of brain reserve because any system including human brain is prone to errors and deteriorations which inevitably leads to entropy increase (Finch et al., 2000; Hayflick, 2004, 2007a,b; Drachman, 2006). Without compensation, brain activity will be disrupted and provide no function. No matter how functional compensation by brain reserve works (which is unknown), the compensation outcome should be a reduction of entropy. Another rationale for choosing BEN is that BEN is inversely related to coherence (low BEN means high coherence) and brain activity coherence has been shown to be fundamental to high-order brain functions such as memory, attention, perception, and coordination (Pesaran et al., 2002, 2008; Buzsáki and Draguhn, 2004; Buzsaki, 2006; Womelsdorf et al., 2006; Buschman and Miller, 2007; Gregoriou et al., 2009; Schroeder and Lakatos, 2009; Siegel et al., 2009; Saleh et al., 2010; Hagan et al., 2011; Buzsáki and Watson, 2012; Dean et al., 2012; Henry and Obleser, 2012; Lega et al., 2012; Salazar et al., 2012; Thut et al., 2012; Rigotti et al., 2013; Calderone et al., 2014; Hawellek et al., 2016; Wong et al., 2016). Loss of temporal coherence interrupts inter-neuronal then inter-regional communications. Restoring brain coherence can therefore fix the related brain dysfunctions. For example, a recent study showed that enhancing coherence improved memory for older

people (Reinhart and Nguyen, 2019). However, too much coherence (very low BEN), such as in the sedation or coma state (Viertiö-Oja et al., 2004; Perez et al., 2019), will make the brain too rigid, unable to form variable brain activity patterns. This situation can happen in the AD continuum because of the escalated compensation demand from the progressive brain function deterioration caused by both aging and AD pathology.

Limitations exist in this study. First, these findings were based on cross-sectional data and must be further confirmed with longitudinal data. Second, the negative BEN vs. education correlations seem to be contradictory to a previous large size study showing positive correlations between BEN and intelligence (Saxe et al., 2018). We have to note that the suprathreshold regions between this study and Saxe et al. (2018) did not overlap with ours mainly in the parietal cortex and theirs in inferior frontal and temporal regions and cerebellum. In an independent study based on 862 young healthy adults' high-resolution, high signal-to-noise-ratio long rsfMRI data from the Human Connectome Project, we observed the same negative education vs. BEN correlations in parietal cortex as well as prefrontal cortex (Wang, 2020a,b). The consistent findings across two different cohorts with different age ranges and different imaging acquisition parameters prove the rigor of the negative BEN vs. education findings. Third, although the heuristic BEN model predicts a reserve compensation-related BEN reduction, the rsfMRI-derived BEN represents the sum of the aging-related BEN and the compensation-induced BEN reduction and we cannot separate them. In other words, we cannot assess the compensation-related BEN reduction independently. A fifth concern is the physiological noise such as motion, cardiac, and respiratory pulsations. Although we followed the standard processing steps for motion correction, residual motion effects removal, and physiological noise filtering, residual effects may still exist. As those confounds are unlikely correlated with all the assessed variables such as age, education, pathology, and cognitive measures, the major BEN effects identified in this article should be still related to neuronal events. Finally, BOLD signal is also contributed by vascular effects. Because vascular abnormality is a known risk factor of AD, vascular contributions to BOLD fMRI signal may be even larger than in healthy controls. Therefore, the observed resting BOLD fMRI-derived BEN effects likely contained both neuronal and vascular effects too.

In summary, rsfMRI-derived BEN provides a potential proxy to assess the brain circuits underlying brain reserve; BEN follows an inverse-U curve when normal aging progresses into AD. The heuristic BEN progression model may provide a potential tool for early detection of AD and disease modification development given the recent evidence of that resting BEN can be modulated using non-invasive transcranial magnetic resonance stimulation (Chang et al., 2018; Song et al., 2018).

DATA AVAILABILITY STATEMENT

The datasets presented in this study can be found in online repositories. The names of the repository/repositories and accession number(s) can be found below: http://adni.loni.usc.edu/.

ETHICS STATEMENT

The studies involving human participants were reviewed and approved by IRB of University of Maryland, Baltimore, MA, USA. The patients/participants provided their written informed consent to participate in this study.

AUTHOR CONTRIBUTIONS

The author confirms being the sole contributor of this work and has approved it for publication.

FUNDING

This work was supported by National Institute of Health/National Institute on Aging (NIH/NIA) Grant R01AG060054 and by the ATIP grant from Institute for Clinical and Translational Research (ICTR), University of Maryland, Baltimore, MD, USA.

ACKNOWLEDGMENTS

Data collection and sharing for this project was funded by the Alzheimer's Disease Neuroimaging Initiative (ADNI; National Institutes of Health Grant U01 AG024904) and DOD ADNI (Department of Defense award number W81XWH-12-2-0012). ADNI is funded by the National Institute on Aging, the National Institute of Biomedical Imaging and Bioengineering, and through generous contributions from the following: AbbVie; Alzheimer's Association; Alzheimer's Drug Discovery Foundation; Araclon Biotech; BioClinica, Inc.; Biogen; Bristol-Myers Squibb Company; CereSpir, Inc.; Cogstate; Eisai Inc.; Elan Pharmaceuticals, Inc.; Eli Lilly and Company; EuroImmun; F. Hoffmann-La Roche Limited and its affiliated company Genentech, Inc.; Fujirebio; GE Healthcare; IXICO Limited; Janssen Alzheimer Immunotherapy Research and Development, LLC; Johnson and Johnson Pharmaceutical Research and Development LLC; Lumosity; Lundbeck; Merck and Company, Inc.; Meso Scale Diagnostics, LLC; NeuroRx Research; Neurotrack Technologies; Novartis Pharmaceuticals Corporation; Pfizer Inc.; Piramal Imaging; Servier; Takeda Pharmaceutical Company; and Transition Therapeutics. The Canadian Institutes of Health Research is providing funds to support ADNI clinical sites in Canada. Private sector contributions are facilitated by the Foundation for the National Institutes of Health (www.fnih.org). The grantee organization is the Northern California Institute for Research and Education, and the study is coordinated by the Alzheimer's Therapeutic Research Institute at the University of Southern California. ADNI data are disseminated by the Laboratory for NeuroImaging at the University of Southern California, CA, USA.

REFERENCES

Abásolo, D., Hornero, R., Espino, P., Alvarez, D., and Poza, J. (2006). Entropy analysis of the EEG background activity in Alzheimer's disease patients. *Physiol. Meas.* 27, 241–253. doi: 10.1088/0967-3334/27/3/003

Anthony, M., and Lin, F. (2018). A systematic review for functional neuroimaging studies of cognitive reserve across the cognitive aging spectrum. *Arch. Clin. Neuropsychol.* 33, 937–948. doi: 10.1093/arclin/acx125

Arenaza-Urquijo, E. M., Landeau, B., La Joie, R., Mevel, K., Mézenge, F., Perrotin, A., et al. (2013). Relationships between years of education and gray matter volume, metabolism and functional connectivity in healthy elders. *NeuroImage* 83, 450–457. doi: 10.1016/j.neuroimage.2013.06.053

Ashburner, J. (2007). A fast diffeomorphic image registration algorithm. *NeuroImage* 38, 95–113. doi: 10.1016/j.neuroimage.2007.07.007

Badhwar, A., Tam, A., Dansereau, C., Orban, P., Hoffstaedter, F., and Bellec, P. (2017). Resting-state network dysfunction in Alzheimer's disease: a systematic review and meta-analysis. *Alzheimers Dement.* 8, 73–85. doi: 10.1016/j.dadm.2017.03.007

Beckmann, C. F., and Smith, S. M. (2004). Probabilistic independent component analysis for functional magnetic resonance imaging. *IEEE Trans. Med. Imaging* 23, 137–152. doi: 10.1109/TMI.2003.822821

Biswal, B., Yetkin, F. Z., Haughton, V. M., and Hyde, J. S. (1995). Functional connectivity in the motor cortex of resting human brain using echo-planar Mri. *Magn. Reson. Med.* 34, 537–541. doi: 10.1002/mrm.1910340409

Bozzali, M., Dowling, C., Serra, L., Spanò, B., Torso, M., Marra, C., et al. (2015). The impact of cognitive reserve on brain functional connectivity in Alzheimer's disease. *J. Alzheimers Dis.* 44, 243–250. doi: 10.3233/JAD-141824

Buschman, T. J., and Miller, E. K. (2007). Top-down versus bottom-up control of attention in the prefrontal and posterior parietal cortices. *Science* 315, 1860–1862. doi: 10.1126/science.1138071

Buzsaki, G. (2006). *Rhythms of the Brain.* New York, NY: Oxford University Press.

Buzsáki, G., and Draguhn, A. (2004). Neuronal oscillations in cortical networks. *Science* 304, 1926–1929. doi: 10.1126/science.1099745

Buzsáki, G., and Watson, B. O. (2012). Brain rhythms and neural syntax: implications for efficient coding of cognitive content and neuropsychiatric disease. *Dialogues Clin. Neurosci.* 14, 345–367.

Calderone, D. J., Lakatos, P., Butler, P. D., and Castellanos, F. X. (2014). Entrainment of neural oscillations as a modifiable substrate of attention. *Trends Cogn. Sci.* 18, 300–309. doi: 10.1016/j.tics.2014.02.005

Calhoun, V. D., Adali, T., Pearlson, G. D., and Pekar, J. J. (2001). Spatial and temporal independent component analysis of functional MRI data containing a pair of task-related waveforms. *Hum. Brain Mapp.* 13, 43–53. doi: 10.1002/hbm.1024

Chang, D., Zhang, J., Peng, W., Shen, Z., Gao, X., Du, Y., et al. (2018). Smoking cessation with 20 Hz repetitive transcranial magnetic stimulation (rTMS) applied to two brain regions: a pilot study. *Front. Hum. Neurosci.* 12:344. doi: 10.3389/fnhum.2018.00344

Chao, L. L., Pa, J., Duarte, A., Schuff, N., Weiner, M. W., Kramer, J. H., et al. (2009). Patterns of cerebral hypoperfusion in amnestic and dysexecutive MCI. *Alzheimer Dis. Assoc. Disord.* 23, 245–252. doi: 10.1097/WAD.0b013e318199ff46

Chen, Y., Wolk, D. A., Reddin, J. S., Korczykowski, M., Martinez, P. M., Musiek, E. S., et al. (2011). Voxel-level comparison of arterial spin-labeled perfusion MRI and FDG-PET in Alzheimer disease. *Neurology* 77, 1977–1985. doi: 10.1212/WNL.0b013e31823a0ef7

Daulatzai, M. A. (2017). Cerebral hypoperfusion and glucose hypometabolism: Key pathophysiological modulators promote neurodegeneration, cognitive impairment and Alzheimer's disease. *J. Neurosci. Res.* 95, 943–972. doi: 10.1002/jnr.23777

Dean, H. L., Hagan, M. A., and Pesaran, B. (2012). Only coherent spiking in posterior parietal cortex coordinates looking and reaching. *Neuron* 73, 829–841. doi: 10.1016/j.neuron.2011.12.035

Drachman, D. A. (2006). Aging of the brain, entropy and Alzheimer's disease. *Neurology* 67, 1340–1352. doi: 10.1212/01.wnl.0000240127.89601.83

Ferri, C. P., Prince, M., Brayne, C., Brodaty, H., Fratiglioni, L., Ganguli, M., et al. (2005). Global prevalence of dementia: a Delphi consensus study. *Lancet* 366, 2112–2117. doi: 10.1016/S0140-6736(05)67889-0

Finch, C. E., Kirkwood, T. B., and Kirkwood, T. (2000). *Chance, Development and Aging.* New York, NY: Oxford University Press.

Foreman, B., and Claassen, J. (2012). Quantitative EEG for the detection of brain ischemia. *Crit. Care* 16:216. doi: 10.1186/cc11230

Franzmeier, N., Buerger, K., Teipel, S., Stern, Y., Dichgans, M., Ewers, M., et al. (2017). Cognitive reserve moderates the association between functional network anti-correlations and memory in MCI. *Neurobiol. Aging* 50, 152–162. doi: 10.1016/j.neurobiolaging.2016.11.013

Gómez, C., and Hornero, R. (2010). Entropy and complexity analyses in Alzheimer's disease: an MEG study. *Open Biomed. Eng. J.* 4, 223–235. doi: 10.2174/1874120701004010223

Gregoriou, G. G., Gotts, S. J., Zhou, H., and Desimone, R. (2009). High-frequency, long-range coupling between prefrontal and visual cortex during attention. *Science* 324, 1207–1210. doi: 10.1126/science.1171402

Grimmer, T., Riemenschneider, M., Förstl, H., Henriksen, G., Klunk, W. E., Mathis, C. A., et al. (2009). Beta amyloid in Alzheimer's disease: increased deposition in brain is reflected in reduced concentration in cerebrospinal fluid. *Biol. Psychiatry* 65, 927–934. doi: 10.1016/j.biopsych.2009.01.027

Hagan, M. A., Dean, H. L., and Pesaran, B. (2011). Spike-field activity in parietal area LIP during coordinated reach and saccade movements. *J. Neurophysiol.* 107, 1275–1290. doi: 10.1152/jn.00867.2011

Haimovici, A., Tagliazucchi, E., Balenzuela, P., and Chialvo, D. R. (2013). Brain organization into resting state networks emerges at criticality on a model of the human connectome. *Phys. Rev. Lett.* 110, 178101–178104. doi: 10.1103/PhysRevLett.110.178101

Hawellek, D. J., Wong, Y. T., and Pesaran, B. (2016). Temporal coding of reward-guided choice in the posterior parietal cortex. *Proc. Natl. Acad. Sci. U S A* 113, 13492–13497. doi: 10.1073/pnas.1606479113

Hayflick, L. (2004). Aging: the reality: "Anti-Aging" is an Oxymoron. *J. Gerontol.* 59, B573–B578. doi: 10.1093/gerona/59.6.b573

Hayflick, L. (2007a). Biological aging is no longer an unsolved problem. *Ann. N Y Acad. Sci.* 1100, 1–13. doi: 10.1196/annals.1395.001

Hayflick, L. (2007b). Entropy explains aging, genetic determinism explains longevity and undefined terminology explains misunderstanding both. *PLoS Genet.* 3:e220. doi: 10.1371/journal.pgen.0030220

Henry, M. J., and Obleser, J. (2012). Frequency modulation entrains slow neural oscillations and optimizes human listening behavior. *Proc. Natl. Acad. Sci. U S A* 109, 20095–20100. doi: 10.1073/pnas.1213390109

Hu, W. T., Wang, Z., Lee, V. M., Trojanowski, J. Q., Detre, J. A., and Grossman, M. (2010). Distinct cerebral perfusion patterns in FTLD and AD. *Neurology* 75, 881–888. doi: 10.1212/WNL.0b013e3181f11e35

Hyvärinen, A., Karhunen, J., and Oja, E. (2001). *Independent Component Analysis.* New York, NY: John Wiley & Sons, Inc.

Jack, C. R., Jr., and Holtzman, D. M. (2013). Biomarker modeling of Alzheimer's disease. *Neuron* 80, 1347–1358. doi: 10.1016/j.neuron.2013.12.003

Jack, C. R., Jr., Knopman, D. S., Jagust, W. J., Shaw, L. M., Aisen, P. S., Weiner, M. W., et al. (2010). Hypothetical model of dynamic biomarkers of the Alzheimer's pathological cascade. *Lancet Neurol.* 9, 119–128. doi: 10.1016/S1474-4422(09)70299-6

Jeong, J. (2004). EEG dynamics in patients with Alzheimer's disease. *Clin. Neurophysiol.* 115, 1490–1505. doi: 10.1016/j.clinph.2004.01.001

Johnson, N. A., Jahng, G. H., Weiner, M. W., Miller, B. L., Chui, H. C., Jagust, W. J., et al. (2005). Pattern of cerebral hypoperfusion in Alzheimer disease and mild cognitive impairment measured with arterial spin-labeling MR imaging: initial experience. *Radiology* 234, 851–859. doi: 10.1148/radiol.2343040197

Kumar, A., and Singh, A. (2015). A review on Alzheimer's disease pathophysiology and its management: an update. *Pharmacol. Rep.* 67, 195–203. doi: 10.1016/j.pharep.2014.09.004

Lega, B. C., Jacobs, J., and Kahana, M. (2012). Human hippocampal theta oscillations and the formation of episodic memories. *Hippocampus* 22, 748–761. doi: 10.1002/hipo.20937

Li, T., Wang, B., Gao, Y., Wang, X., Yan, T., Xiang, J., et al. (2020). APOE ϵ4 and cognitive reserve effects on the functional network in the Alzheimer's disease spectrum. *Brain Imaging Behav.* doi: 10.1007/s11682-020-00283-w [Epub ahead of print].

Li, Z., and Wang, Z. (2016). "Alzheimer's Disease Is Associated with Hypo-Brain Entropy," in *Proceedings of the 2016 Annual Meeting of International Society of Magnetic Resonance in Medicine (ISMRM)*, (Singapore: ISMRM), 3825.

Liu, J., Zhu, Y. S., Khan, M. A., Brunk, E., Martin-Cook, K., Weiner, M. F., et al. (2014). Global brain hypoperfusion and oxygenation in amnestic mild cognitive impairment. *Alzheimers Dement.* 10, 162–170. doi: 10.1016/j.jalz.2013.04.507

Marques, P., Moreira, P., Magalhães, R., Costa, P., Santos, N., Zihl, J., et al. (2016). The functional connectome of cognitive reserve. *Hum. Brain Mapp.* 37, 3310–3322. doi: 10.1002/hbm.23242

Marshall, G. A., Zoller, A. S., Lorius, N., Amariglio, R. E., Locascio, J. J., Johnson, K. A., et al. (2015). Functional activities questionnaire items that best discriminate and predict progression from clinically normal to mild cognitive impairment. *Curr. Alzheimer Res.* 12, 493–502. doi: 10.2174/1567205012051505261150 03

Mehta, K. M., and Yeo, G. W. (2017). Systematic review of dementia prevalence and incidence in United States race/ethnic populations. *Alzheimers Dement.* 13, 72–83. doi: 10.1016/j.jalz.2016.06.2360

Mizuno, T., Takahashi, T., Cho, R. Y., Kikuchi, M., Murata, T., Takahashi, K., et al. (2010). Assessment of EEG dynamical complexity in Alzheimer's disease using multiscale entropy. *Clin. Neurophysiol.* 121, 1438–1446. doi: 10.1016/j.clinph.2010.03.025

Musiek, E. S., Chen, Y., Korczykowski, M., Saboury, B., Martinez, P. M., Reddin, J. S., et al. (2012). Direct comparison of fluorodeoxyglucose positron emission tomography and arterial spin labeling magnetic resonance imaging in Alzheimer's disease. *Alzheimers Dement.* 8, 51–59. doi: 10.1016/j.jalz.2011.06.003

Ouchi, Y., and Kikuchi, M. (2012). A review of the default mode network in aging and dementia based on molecular imaging. *Rev. Neurosci.* 23, 263–268. doi: 10.1515/revneuro-2012-0029

Perez, J. V., Mateos, D. M., and Guevara, R. E. (2019). On a simple general principle of brain organization. *Front. Neurosci.* 13:1106. doi: 10.3389/fnins.2019.01106

Pesaran, B., Nelson, M. J., and Andersen, R. A. (2008). Free choice activates a decision circuit between frontal and parietal cortex. *Nature* 453, 406–409. doi: 10.1038/nature06849

Pesaran, B., Pezaris, J. S., Sahani, M., Mitra, P. P., and Andersen, R. A. (2002). Temporal structure in neuronal activity during working memory in macaque parietal cortex. *Nat .Neurosci.* 5, 805–811. doi: 10.1038/nn890

Petersen, R. C. (2004). Mild cognitive impairment as a diagnostic entity. *J. Intern. Med.* 256, 183–194. doi: 10.1111/j.1365-2796.2004.01388.x

Pfeffer, R. I., Kurosaki, T. T., Harrah, C. H., Jr., Chance, J. M., and Filos, S. (1982). Measurement of functional activities in older adults in the community. *J. Gerontol.* 37, 323–329. doi: 10.1093/geronj/37.3.323

Pizoli, C. E., Shah, M. N., Snyder, A. Z., Shimony, J. S., Limbrick, D. D., Raichle, M. E., et al. (2011). Resting-state activity in development and maintenance of normal brain function. *Proc. Natl. Acad. Sci. U S A* 108, 11638–11643. doi: 10.1073/pnas.1109144108

Power, J. D., Barnes, K. A., Snyder, A. Z., Schlaggar, B. L., and Petersen, S. E. (2012). Spurious but systematic correlations in functional connectivity MRI networks arise from subject motion. *NeuroImage* 59, 2142–2154. doi: 10.1016/j.neuroimage.2011.10.018

Raichle, M. E. (2006). Neuroscience. The brain's dark energy. *Science* 314, 1249–1250. doi: 10.1126/science.1134405

Raichle, M. E. (2011). The restless brain. *Brain Connect.* 1, 3–12. doi: 10.1089/brain.2011.0019

Raichle, M. E., and Gusnard, D. A. (2002). Appraising the brain's energy budget. *Proc. Natl. Acad. Sci. U S A* 99, 10237–10239. doi: 10.1073/pnas.172399499

Raichle, M. E., MacLeod, A. M., Snyder, A. Z., Powers, W. J., Gusnard, D. A., and Shulman, G. L. (2001). A default mode of brain function. *Proc. Natl. Acad. Sci. U S A* 98, 676–682. doi: 10.1073/pnas.98.2.676

Reinhart, R. M. G., and Nguyen, J. A. (2019). Working memory revived in older adults by synchronizing rhythmic brain circuits. *Nat. Neurosci.* 22, 820–827. doi: 10.1038/s41593-019-0371-x

Reitz, C., and Mayeux, R. (2014). Alzheimer disease: epidemiology, diagnostic criteria, risk factors and biomarkers. *Biochem. Pharmacol.* 88, 640–651. doi: 10.1016/j.bcp.2013.12.024

Ries, M. L., Carlsson, C. M., Rowley, H. A., Sager, M. A., Gleason, C. E., Asthana, S., et al. (2008). Magnetic resonance imaging characterization of brain structure and function in mild cognitive impairment: a review. *J. Am. Geriatr. Soc.* 56, 920–934. doi: 10.1111/j.1532-5415.2008.01684.x

Rigotti, M., Barak, O., Warden, M. R., Wang, X. J., Daw, N. D., Miller, E. K., et al. (2013). The importance of mixed selectivity in complex cognitive tasks. *Nature* 497, 585–590. doi: 10.1038/nature12160

Ruitenberg, A., den Heijer, T., Bakker, S. L., van Swieten, J. C., Koudstaal, P. J., Hofman, A., et al. (2005). Cerebral hypoperfusion and clinical onset of dementia: the Rotterdam study. *Ann. Neurol.* 57, 789–794. doi: 10.1002/ana.20493

Salazar, R., Dotson, N., Bressler, S., and Gray, C. (2012). Content specific fronto parietal synchronization during visual working memory. *Science* 338, 1097–1100. doi: 10.1126/science.1224000

Saleh, M., Reimer, J., Penn, R., Ojakangas, C. L., and Hatsopoulos, N. G. (2010). Fast and slow oscillations in human primary motor cortex predict oncoming behaviorally relevant cues. *Neuron* 65, 461–471. doi: 10.1016/j.neuron.2010.02.001

Saxe, G. N., Calderone, D., and Morales, L. J. (2018). Brain entropy and human intelligence: A resting-state fMRI study. *PLoS One* 13:e0191582. doi: 10.1371/journal.pone.0191582

Schmidt, M. (1996). *Rey Auditory Verbal Learning Test: A Handbook*. Los Angeles, CA: Western Psychological Services.

Schroeder, C. E., and Lakatos, P. (2009). Low-frequency neuronal oscillations as instruments of sensory selection. *Trends Neurosci.* 32, 9–18. doi: 10.1016/j.tins.2008.09.012

Sharbrough, F. W., Messick, J. M., Jr., and Sundt, T. M., Jr. (1973). Correlation of continuous electroencephalograms with cerebral blood flow measurements during carotid endarterectomy. *Stroke* 4, 674–683. doi: 10.1161/01.str.4.4.674

Shaw, L. M., Vanderstichele, H., Knapik-Czajka, M., Clark, C. M., Aisen, P. S., Petersen, R. C., et al. (2009). Cerebrospinal fluid biomarker signature in Alzheimer's disease neuroimaging initiative subjects. *Ann. Neurol.* 65, 403–413. doi: 10.1002/ana.21610

Siegel, M., Warden, M. R., and Miller, E. K. (2009). Phase-dependent neuronal coding of objects in short-term memory. *Proc. Natl. Acad. Sci. U S A* 106, 21341–21346. doi: 10.1073/pnas.0908193106

Song, D., Chang, D., Zhang, J., Peng, W., Shang, Y., Gao, X., et al. (2018). Reduced brain entropy by repetitive transcranial magnetic stimulation on the left dorsolateral prefrontal cortex in healthy young adults. *Brain Imaging Behav.* 13, 421–429. doi: 10.1007/s11682-018-9866-4

Stam, C., Van Der Made, Y., Pijnenburg, Y., and Scheltens, P. (2003). EEG synchronization in mild cognitive impairment and Alzheimer's disease. *Acta Neurol. Scand.* 108, 90–96. doi: 10.1034/j.1600-0404.2003.02067.x

Stern, Y. (2006). Cognitive reserve and Alzheimer disease. *Alzheimer Dis. Assoc. Disord.* 20, 112–117. doi: 10.1097/01.wad.0000213815.20177.19

Stern, Y. (2012). Cognitive reserve in ageing and Alzheimer's disease. *Lancet Neurol.* 11, 1006–1012. doi: 10.1016/S1474-4422(12)70191-6

Stern, Y., Arenaza-Urquijo, E. M., Bartrés-Faz, D., Belleville, S., Cantilon, M., Chetelat, G., et al. (2018). Whitepaper: defining and investigating cognitive reserve, brain reserve and brain maintenance. *Alzheimers Dement.* 16, 1305–1311. doi: 10.1016/j.jalz.2018.07.219

Tagliazucchi, E., Balenzuela, P., Fraiman, D., and Chialvo, D. R. (2012). Criticality in large-scale brain fMRI dynamics unveiled by a novel point process analysis. *Front. Physiol.* 3:15. doi: 10.3389/fphys.2012.00015

Thut, G., Miniussi, C., and Gross, J. (2012). The functional importance of rhythmic activity in the brain. *Curr. Biol.* 22, R658–R663. doi: 10.1016/j.cub.2012.06.061

Van Essen, D. C., Smith, S. M., Barch, D. M., Behrens, T. E., Yacoub, E., Ugurbil, K., et al. (2013). The WU-Minn Human connectome project: an overview. *NeuroImage* 80, 62–79. doi: 10.1016/j.neuroimage.2013.05.041

Verclytte, S., Lopes, R., Lenfant, P., Rollin, A., Semah, F., Leclerc, X., et al. (2016). Cerebral hypoperfusion and hypometabolism detected by arterial spin labeling MRI and FDG-PET in early-onset Alzheimer's disease. *J. Neuroimaging* 26, 207–212. doi: 10.1111/jon.12264

Viertiö-Oja, H., Maja, V., Särkelä, M., Talja, P., Tenkanen, N., Tolvanen-Laakso, H., et al. (2004). Description of the entropy algorithm as applied in the Datex-Ohmeda S/5 Entropy Module. *Acta. Anaesth. Scand.* 48, 154–161. doi: 10.1111/j.0001-5172.2004.00322.x

Wang, Z. (2014). Characterizing early Alzheimer's disease and disease progression using hippocampal volume and arterial spin labeling perfusion MRI. *J. Alzheimers Dis.* 42, S495–S502. doi: 10.3233/JAD-141419

Wang, Z. (2016). "Longitudinal CBF changes predict disease conversion/revision in AD and MCI," in *Annual Meeting of Organization for Human Brain Mapping*, Geneva, 1009.

Wang, Z. (2020a). Assessing the neurocognitive correlates of resting brain entropy. *arXiv* [Preprint]. Available online at: https://arxiv.org/abs/2004.13256#.

Wang, Z. (2020b). "Resting brain entropy in the default mode network and the executive network may serve as a functional brain reserve," in *Annual Meeting of International Society of Magnetic Resonance in Medicine*, Paris, France, 1794.

Wang, Z., Das, S. R., Xie, S. X., Arnold, S. E., Detre, J. A., Wolk, D. A., et al (2013). Arterial spin labeled MRI in prodromal Alzheimer's disease: a multi-site study. *Neuroimage Clin.* 2, 630–636. doi: 10.1016/j.nicl.2013.04.014

Wang, Z., Li, Y., Childress, A. R., and Detre, J. A. (2014). Brain entropy mapping using fMRI. *PLoS One* 9:e89948. doi: 10.1371/journal.pone.0089948

Wang, B., Niu, Y., Miao, L., Cao, R., Yan, P., Guo, H., et al. (2017). Decreased complexity in Alzheimer's disease: resting-state fMRI evidence of brain entropy mapping. *Front. Aging Neurosci.* 9:378. doi: 10.3389/fnagi.2017.00378

Weiner, M. W., Veitch, D. P., Aisen, P. S., Beckett, L. A., Cairns, N. J., Green, R. C., et al. (2013). The Alzheimer's disease neuroimaging initiative: a review of papers published since its inception. *Alzheimers Dement.* 8, S1–S68. doi: 10.1016/j.jalz.2011.09.172

Womelsdorf, T., Fries, P., Mitra, P. P., and Desimone, R. (2006). Gamma-band synchronization in visual cortex predicts speed of change detection. *Nature* 439, 733–736. doi: 10.1038/nature04258

Wong, Y. T., Fabiszak, M. M., Novikov, Y., Daw, N. D., and Pesaran, B. (2016). Coherent neuronal ensembles are rapidly recruited when making a look-reach decision. *Nat. Neurosci.* 19, 327–334. doi: 10.1038/nn.4210

Yang, A. C., Wang, S. J., Lai, K. L., Tsai, C. F., Yang, C. H., Hwang, J. P., et al. (2013). Cognitive and neuropsychiatric correlates of EEG dynamic complexity in patients with Alzheimer's disease. *Prog. Neuropsychopharmacol. Biol. Psychiatry* 47, 52–61. doi: 10.1016/j.pnpbp.2013.07.022

Conflict of Interest: The author declares that the research was conducted in the absence of any commercial or financial relationships that could be construed as a potential conflict of interest.

frontiers in Aging Neuroscience

ORIGINAL RESEARCH
published: 19 November 2020
doi: 10.3389/fnagi.2020.594282

Effects of Chronic Tinnitus on Metabolic and Structural Changes in Subjects With Mild Cognitive Impairment

Sang-Yeon Lee[1†], Heejung Kim[2,3†], Jun Young Lee[4,5], Ju Hye Kim[4], Dong Young Lee[6,7], Inhee Mook-Jung[5,8], Young Ho Kim[9] and Yu Kyeong Kim[2]**

[1]Department of Otorhinolaryngology, Seoul National University Bundang Hospital, Seoul National University College of Medicine, Seoul, South Korea, [2]Department of Nuclear Medicine, Seoul National University Boramae Medical Center, Seoul National University College of Medicine, Seoul, South Korea, [3]Institute of Radiation Medicine, Medical Research Center, Seoul National University College of Medicine, Seoul, South Korea, [4]Department of Psychiatry, Seoul National University Boramae Medical Center, Seoul National University College of Medicine, Seoul, South Korea, [5]Neuroscience Research Institute, Seoul National University College of Medicine, Seoul, South Korea, [6]Departmentof Psychiatry, Seoul National University College of Medicine, Seoul, South Korea, [7]Institute of Human Behavioral Medicine, Medical Research Center, Seoul National University, Seoul, South Korea, [8]Department of Biochemistry and Biomedical Science, Seoul National University College of Medicine, Seoul, South Korea, [9]Department of Otorhinolaryngology, Seoul National University Boramae Medical Center, Seoul National University College of Medicine, Seoul, South Korea

OPEN ACCESS

Edited by:
Jiu Chen,
Nanjing Medical University, China

Reviewed by:
Amber Leaver,
Northwestern Medicine,
United States
Ricki Colman,
University of Wisconsin-Madison,
United States

***Correspondence:**
Young Ho Kim
yhkiment@snu.ac.kr
Yu Kyeong Kim
yk3181@snu.ac.kr

†These authors have contributed equally to this work

Received: *13 August 2020*
Accepted: *02 November 2020*
Published: *19 November 2020*

Citation:
Lee S-Y, Kim H, Lee JY, Kim JH, Lee DY, Mook-Jung I, Kim YH and Kim YK (2020) Effects of Chronic Tinnitus on Metabolic and Structural Changes in Subjects With Mild Cognitive Impairment. Front. Aging Neurosci. 12:594282. doi: 10.3389/fnagi.2020.594282

Tinnitus is a conscious auditory perception in the absence of an external stimulus. Despite previous reports of a recognized association between tinnitus and cognitive deficits, the effects of tinnitus on functional and structural brain changes associated with cognitive deficits remain unknown. We aimed to investigate the changes in glucose metabolism and gray matter (GM) volume in subjects diagnosed with mild cognitive impairment (MCI) depending on tinnitus. Twenty-three subjects were subclassified into MCI with the chronic tinnitus (MCI_T) and MCI without tinnitus (MCI_NT) groups. Encouraged by the identification of neural substrates associated with tinnitus and cognitive deficits, we correlated the extent of tinnitus severity with the changes in glucose metabolism and GM volume and conducted a glucose metabolic connectivity study. Compared to the MCI_NT group, the MCI_T group showed significantly lower metabolism in the right superior temporal pole and left fusiform gyrus. Additionally, the GM volume in the right insula was markedly lower in the MCI_T group compared to the MCI_NT group. Moreover, correlation analyses in metabolism or GM volumes revealed specific brain regions associated with the cognitive decline with increasing tinnitus severity. Metabolic connectivity analysis revealed that MCI_NT had markedly strengthened intra-hemispheric connectivity in the frontal, parietal, and occipital regions than did MCI_T. Furthermore, MCI_NT showed a strong negative association between the parietal and temporal and parietal and limbic regions, but the association was not observed in MCI_T. These findings indicate that tinnitus may cause metabolic and

structural changes in the brain and alters complex inter- or intra-hemispheric networks in MCI. Considering the impact of MCI on accelerating dementia, these results provide a valuable basis on which yet-to-be-identified neurodegenerative markers of tinnitus can be refined.

Keywords: tinnitus, mild cognitive impairment, voxel-based morphometry, positron emission tomography, Alzheimer's dementia

INTRODUCTION

Tinnitus, a "phantom sound," is a conscious auditory perception in the absence of an external stimulus (Lee et al., 2017). Recently, tinnitus is considered to be a consequence of the complex interplay between auditory and non-auditory cortical regions after auditory deafferentation, likely recapitulating maladaptive cortical plasticity (Langguth et al., 2013). A meta-analysis of PET studies, coupled with other neuroimaging-based researches, has shown an association between tinnitus and multiple brain regions concerning attention, emotion, memory, and cognition (Song et al., 2012).

With a growing body of evidence on the association between chronic tinnitus and cognitive deficits, several studies have suggested that a decrease in attention and working memory is associated with the mechanism between chronic tinnitus and cognitive deficits (Rossiter et al., 2006; Trevis et al., 2016; Zarenoe et al., 2017). Furthermore, by correlating resting-state cortical oscillatory changes with tinnitus severity, a recent study has proposed that specific brain regions related to memory, such as the parahippocampus, may serve as a bridge between chronic tinnitus and cognitive decline. This, in turn, led us to hypothesize that neurophysiological changes may explain the association between tinnitus and cognitive impairment.

Specifically, mild cognitive impairment (MCI) is a predementia condition with a substantial risk of advancing to dementia (Snowden, 2004), particularly Alzheimer's disease (Levey et al., 2006; Langa and Levine, 2014). Therefore, evaluating the risk factors associated with MCI is important for prognosis and protection. It was recently observed that chronic tinnitus accompanies a relatively high rate of MCI in approximately 17% of elderly subjects (i.e., >65 years; Lee et al., 2020). Further, a significant correlation between tinnitus severity and cognitive performance suggests that chronic tinnitus might be a potential determinant for accelerating MCI (Wang et al., 2018; Lee et al., 2020). The rationale behind this association would rely on a couple of previous studies, demonstrating that tinnitus may closely link to a reduced cognitive function on selective and divided attention, memory, and learning (Das et al., 2012; Vanneste et al., 2016). Despite the existence of recognized evidence regarding the association between tinnitus and cognitive deficits, the effects of chronic tinnitus on functional and structural brain changes in subjects with MCI have never been investigated, and no neurodegenerative markers of chronic tinnitus have thus far been identified.

Herein, we thus aimed to investigate the changes in glucose metabolism and gray matter (GM) volume in subjects diagnosed with MCI depending on tinnitus using [^{18}F]fluoro-2-deoxyglucose-positron emission tomography (FDG-PET) and voxel-based morphometry (VBM). A recent neuroimaging study demonstrated that the combination of FDG-PET and VBM makes it possible to predict the conversion from MCI to Alzheimer's dementia (Ottoy et al., 2019). Encouraged by the identification of neural substrates associated with tinnitus and cognitive deficits, we correlated the extent of tinnitus severity with the changes in glucose metabolism and GM volume. Furthermore, we conducted a glucose metabolic connectivity study based on the correlation of FDG uptakes between predefined regions of interest by templates to reveal the specific tinnitus-related metabolic pattern in the MCI group, similar to functional reorganization. Certainly, the functional connectivity analyses based on FDG-PET have been developed (Yakushev et al., 2017), allowing to evaluate cerebral metabolic connectivity using inter-regional correlation analysis (Lee et al., 2008). Overall, the present study not only provides insights regarding the effects of chronic tinnitus on metabolic and structural changes in patients with MCI but also sets the stage for potential neural substrates that may link tinnitus and cognitive decline.

MATERIALS AND METHODS

Subjects

This study retrospectively reviewed subjects diagnosed with MCI who were nested in the prospective, longitudinal cohort registry of the Korean Brain Aging Study for the Early Diagnosis and Prediction of Alzheimer's disease. Only subjects whose baseline neuroimaging was performed and audiograms met the criteria of having a mean hearing threshold <40 dB hearing loss (HL) in both ears were initially included. Subsequently, subjects with otologic disorders such as otosclerosis and Meniere's disease, psychiatric or neurological disorders, and chronic headache, subjects receiving psychotropic/central nervous system-active medications, and subjects with a history of drug/alcohol abuse and/or history of a head injury (with loss of consciousness) or seizures were excluded from this study. Ultimately, 23 eligible subjects were enrolled in this study. To test the hypothesis, 23 subjects were subclassified into two groups: MCI with chronic subjective tinnitus (the MCI_T group, $N = 12$) and MCI without chronic subjective tinnitus (the MCI_NT group, $N = 11$). All subjects in the MCI_T group experienced perception of tinnitus with a duration of more than 6 months. Specifically, two subjects who reported no subjective tinnitus but had positive Tinnitus Handicap Inventory (THI) scores of 5 or less were assigned to the MCI_NT group. This study was approved by the Seoul National University Hospital Institutional Review Board (IRB-B-20-2019-44) and was conducted following the Declaration of Helsinki.

Mild Cognitive Impairment Criteria and Neurocognition Battery

All subjects were diagnosed with MCI based on Peterson criteria, as documented in a previous study (Byun et al., 2017). The subjects had a global Clinical Dementia Rating score of 0.5 and were assessed at baseline and follow-up according to the Korean version of Consortium to Establish a Registry for Alzheimer's Disease (CERAD-K) neuropsychological battery (Lee et al., 2004). The CERAD-K neuropsychological battery comprised the Verbal Fluency Test, Boston Naming Test, Mini-Mental State Exam in the Korean version of the CERAD assessment packet, Word List Memory, Constructional Praxis, Word List Recall, Word List Recognition, and Constructional Recall Test. General exclusion criteria for all patients were a history of major neurological or untreated major medical conditions.

Positron Emission Tomography (PET)/Magnetic Resonance Image Acquisition

Subjects underwent FDG-PET and magnetic resonance (MR) imaging using a PET/MR scanner (Biograph mMR, Siemens Healthcare, Knoxville, TN, USA). Subjects received an intravenous injection of 370 MBq or less of [^{18}F] FDG, the subjects remained in a dimly lit waiting room, and the brain emission scans were acquired after 40 min on bolus injection and continued for 20 min. For attenuation correction of PET, MR images were acquired simultaneously with PET using a dual-echo ultrashort echo time (UTE) sequence (echo time = 0.07 and 2.46 ms, repetition time = 11.9 ms, flip angle = 10°). The UTE images were reconstructed into a 192 × 192 × 192 matrix with an isotropic voxel size of 1.33 mm. The PET images were reconstructed using the ordered subset expectation maximization algorithm (subset = 21, iteration = 6) into 344 × 344 × 127 matrices with voxel size 1.04 × 1.04 × 2.03 mm. A 6-mm Gaussian post-filter was applied to the reconstructed PET images. A T1-weighted three-dimensional ultrafast gradient echo sequence was also acquired on an integrated PET/MR scanner in a 208 × 256 × 256 matrix with voxel sizes of 1.0 × 0.98 × 0.98 mm.

Audiological and Psychoacoustic Evaluations

At the baseline evaluation, a structured history of the characteristics of tinnitus on the affected ear and the psychoacoustic properties (pure-tone or narrow-band noise) of the tinnitus was obtained. As described in previous studies (Lee et al., 2017, 2020), all subjects underwent pure-tone audiometry (PTA) testing that included psychoacoustic tests of tinnitus such as tinnitus pitch matching, tinnitus loudness matching, and the minimum masking level test. The hearing thresholds for seven different octave frequencies (0.25, 0.5, 1, 2, 3, 4, and 8 kHz) were evaluated using PTA in a sound-proof booth. The mean hearing threshold was calculated by the average of the hearing thresholds at 0.5, 1, and 2 kHz. The severity of perceived tinnitus was based on the THI scores.

PET Analysis

Pre-processing and statistical analyses were performed using Statistical Parametric Mapping (SPM12, Wellcome Department of Imaging Neuroscience, London, UK[1]) implemented in MATLAB 9.1 (The MathWorks Inc., Natick, MA, USA). Co-registration was performed to align functional and structural images from the same subject to map functional information into anatomical space, and the co-registered FDG images were subsequently spatially transformed into the Montreal Neurological Institute standard PET template. The spatially normalized image was smoothed with an isotropic Gaussian kernel of 12 mm full width at half maximum (FWHM). Brain glucose metabolism at each voxel was proportionally scaled to the global mean value to reduce individual variation; hence, the relative regional glucose metabolic rate was calculated.

Voxel-Based Morphometry Image Analyses

VBM was performed using the CAT12 toolbox[2]; Structural Brain Mapping Group, Jena University Hospital, Jena, Germany) implemented in SPM12 to identify structural changes. Each anatomical image was segmented into GM, white matter, and cerebrospinal fluid and non-linearly normalized to a standard stereotactic space using DARTEL (diffeomorphic anatomical registration through an exponentiated Lie algebra) algorithm. The spatially normalized images were subsequently rescaled to preserve relative tissue volumes and smoothed using an 8-mm FWHM Gaussian kernel to reduce residual interindividual variability. For the exclusion of artifacts on the GM, we applied an absolute GM threshold of 0.1.

FDG-PET Metabolic Connectivity

For whole-brain FDG-PET metabolic connectivity, we used a region of interest (ROI)-based metabolic connectivity. First, the pre-processed and normalized FDG-PET image for subjects was parcellated based on the Automated Anatomical Labeling (AAL) template, which divides the brain into 90 anatomical ROIs, except the cerebellum (**Supplementary Table 1**, Tzourio-Mazoyer et al., 2002). To evaluate FDG-PET metabolic connectivity, we extracted the count normalized mean glucose uptake values divided by global mean from each ROI of the AAL template for all subjects, calculated the Pearson's correlation between each pair of ROIs across subjects within each group, and created a pairwise FDG-PET metabolic connectivity matrix (90 × 90 ROIs) for the whole brain in each group. Age was included as a nuisance variable. A connectivity matrix was constructed by converting the correlation coefficient values into Fisher's Z values to obtain an approximately normal distribution. Moreover, individual FDG-PET metabolic connectivity maps were constructed for each group separately at a threshold of $p < 0.01$, and the difference in each real FDG-PET metabolic connectivity matrix between the two groups (e.g., MCI_T vs. MCI_NT) was also constructed with significance at a $p < 0.01$ (two-tailed). For validation, we performed nonparametric permutation testing to test the probability that the

[1]http://www.fil.ion.ucl.ac.uk/spm
[2]http://www.neuro.uni-jena.de/cat

observed difference of metabolic connectivity between the two groups occurred by chance (the null hypothesis) and to validate significant differences. To determine the null distribution of the difference in the correlation between the determined ROIs, we went back to the data matrix. The subject number was randomly into two pseudo-group data matrices (e.g., pseudo-MCI_T and pseudo-MCI_NT). On each pseudo-data matrix, correlation matrices were generated, and differences between two pseudo-groups were computed. Subsequently, null distributions of the FDG-PET metabolic connectivity matrix were generated, and this procedure was repeated 10,000 times. The difference in each real FDG-PET metabolic connectivity matrix between the two groups was compared with the null distribution. Significance was set at a $p < 0.01$ (two-tailed).

Statistical Analysis

To evaluate differences between the MCI_T and MCI_NT groups in glucose metabolism and gray matter volume, statistical tests were performed using a two-sample *t*-test. The age variable was included as a nuisance covariate for glucose metabolism differences and age and total intracranial volume (TIV) were included as covariates of no interest for differences of gray matter volume. Because of the small sample size, the statistical voxel-wise threshold was set at uncorrected $p < 0.005$ with a cluster extent threshold of 100 in group comparison. For correlation analysis, after a log conversion of the THI scores due to the wide range (from 0 to 88), an evaluation of the correlation between the severity of tinnitus based on THI scores and gray matter volume and between the severity of tinnitus based on THI scores and glucose metabolism were also evaluated using regression analysis for whole-brain volume and glucose metabolism. The age variable was included as a nuisance covariate in regression analysis in glucose metabolism and the TIV variable was added in regression analysis in gray matter volume. For regression analysis, an exploratory uncorrected statistical threshold was set at $p < 0.005$ and a minimum cluster extent of 100 voxels in regression analysis in gray matter volume and a minimum cluster extent of 50 voxels in regression analysis in glucose metabolism. For validation of metabolic connectivity analysis, we performed non-parametric permutation testing by 10,000 times. The difference in metabolic connectivity matrix between two groups was set at a $p < 0.01$ (two-tailed).

RESULTS

Demographic and Clinical Characteristics of the Subjects

The clinical characteristics of 23 subjects diagnosed with MCI are summarised in **Table 1**. The mean age of the 23 subjects was 74.0 ± 6.1 years (range, 63–83 years), and 13 were male. The demographics and clinical characteristics in terms of age, sex, educational level, and mean hearing thresholds of subjects in the MCI_T and MCI_NT groups did not have a statistically significant difference. In particular, each hearing threshold across all frequencies did not differ between the MCI_T and MCI_NT groups (**Figure 1**). Regarding the neuropsychological test, no significant differences were observed for any domain involved in CERAD-K between the two groups. As expected, THI scores and the duration of tinnitus were significantly higher in the MCI_T group than those in the MCI_NT group. In the MCI_T group (N = 12), the most frequent characteristic of tinnitus was pure tone (N = 7, 58.3%), followed by narrow-band noise (N = 5, 41.7%).

Group Comparison of Gray Matter Volume and Glucose Metabolism

Compared with the MCI_NT group, the MCI_T group exhibited significantly lower GM volume in the right insula (**Figure 2A**; **Table 2**). Compared with the MCI_NT group, the MCI_T group showed a lower metabolism in the right superior temporal pole and the left fusiform gyrus and higher metabolism in the right postcentral gyrus (**Figure 2B**; **Table 2**).

Association Between Tinnitus Severity and Gray Matter Volume and Metabolism

The THI score was inversely correlated with the GM volume in multiple brain regions, including the bilateral superior frontal gyrus, left frontal gyrus, right supplementary motor area (SMA), right insula, bilateral fusiform gyrus, and right rectal gyrus (**Figure 3A**; **Table 3**). Additionally, a putative rank in terms of the T-score was observed. Specifically, the left superior frontal gyrus showed the highest correlation, whereas the SMA and insula belonged to the second-tier group. However, the THI score was positively associated with glucose metabolism in the SMA/middle cingulate gyrus but was inversely associated with that in the olfactory/rectal gyrus (**Figure 3B**; **Table 3**).

Metabolic Connectivity of Glucose Metabolism

In MCI_NT, negative metabolic connectivity was mainly detected between the parietal and temporal regions, such as Heschl's gyrus, and between the parietal and limbic regions, including the amygdala, hippocampus, and parahippocampus. Moreover, MCI_NT showed strong metabolic connectivity within the intra-hemispheric regions, such as the frontal, parietal, and occipital regions, and between the frontoparietal regions (**Figure 4**). In contrast, in MCI_T, different from MCI_NT, inter-parietal connectivity was weakened or absent with the other regions, but there was strong connectivity between the motor regions and both temporal and limbic regions (**Figure 4**). Compared with the MCI_NT group, the MCI_T group had significantly lower metabolic connectivity between the rectal gyrus and inferior frontal gyrus; between the SMA and parietal region, including the angular gyrus and precuneus; between the orbitofrontal and inferior temporal region; between the precuneus and inferior occipital gyrus; and between the fusiform gyrus and insula but had higher metabolic connectivity between the parietal and temporal and parietal and limbic regions (**Figure 4**).

DISCUSSION

This is the first study that investigated the effects of chronic tinnitus on metabolic and structural brain changes concerning

TABLE 1 | Demographic and clinical characteristics of the study population.

	MCI_T group (MCI patients with from mild, to severe tinnitus handicap)	MCI_NT group (MCI patients without tinnitus handicap)	*P*-value
No. of patients	12	11	
Gender (M:F)	6:6	7:4	
Age (years)	73.27 ± 5.83	74.83 ± 6.56	n.s
Education (years)	8.00 ± 4.43	11.82 ± 4.51	$p = 0.053$
Duration of tinnitus (years)	3.50 ± 3.19	0.09 ± 0.20	$p < 0.01$
THI	38.50 ± 20.06	0.55 ± 1.29	$p < 0.01$
Hearing loss (right)	32.71 ± 7.21	33.50 ± 8.42	n.s
Hearing loss (left)	29.69 ± 6.93	32.84 ± 6.94	n.s
Hearing loss (average)	31.20 ± 5.86	33.17 ± 7.22	n.s
Neuropsychological test			
MMSE	23.42 ± 2.75	24.73 ± 3.10	n.s
Semantic fluency	13.50 ± 3.66	11.64 ± 4.90	n.s
Boston naming	11.75 ± 1.60	11.64 ± 2.34	n.s
Word list immediate memory	15.33 ± 2.74	15.45 ± 3.67	n.s
Constructional praxis	9.50 ± 1.78	9.64 ± 1.21	n.s
Word list delayed recall	4.83 ± 1.19	4.00 ± 2.24	n.s
Word list recognition recall	8.75 ± 1.29	7.73 ± 2.53	n.s
Memory delayed call	6.08 ± 2.64	6.09 ± 3.33	n.s

Data shows mean ± SD (SD, standard deviation). M, male; F, female; MMSE, mini mental state exam; THI, tinnitus handicap inventory; n.s, no statistical significance.

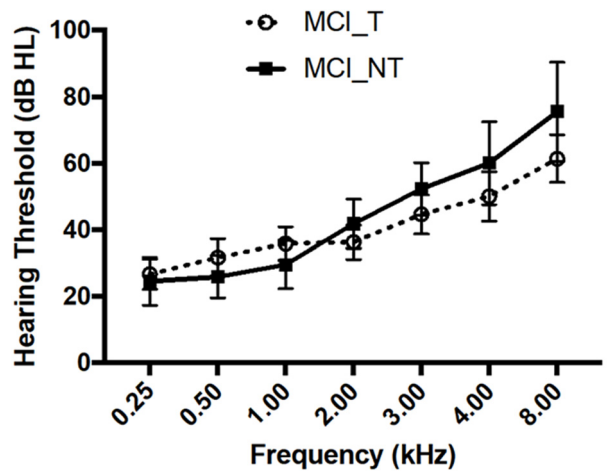

FIGURE 1 | No significant differences in hearing thresholds across all frequencies were observed between mild cognitive impairment (MCI) with tinnitus handicap (MCI_T) and MCI without tinnitus handicap (MCI_NT). Data show the mean ± SEM (SEM, standard error of the mean).

MCI. It clearly showed that at least chronic tinnitus contributes to hypometabolic changes in the fusiform gyrus and the superior temporal gyrus and volumetric atrophy in the insula. These results, coupled with correlation and connectivity analyses, merit attention because the specific brain regions tied to tinnitus and cognitive deficits may serve as neurodegenerative markers indicating the progression of cognitive deficits over time. However, the biomarkers that reveal the linkage between tinnitus and cognitive decline may be only relevant to the particular situation of MCI with tinnitus. Our findings cannot necessarily represent all cases of MCI transitioning dementia, requiring careful interpretation.

Importantly, the MCI_T group demonstrated more distinctive hypometabolic changes in the superior temporal pole and the fusiform gyrus compared to the MCI_NT group. Anatomically, the superior temporal region comprises the auditory cortex, which is known to play a critical role in tinnitus perception (Maudoux et al., 2012). As is known, the superior temporal region interacts with the parietal and limbic regions in the social cognitive process (Zilbovicius et al., 2006). A recent meta-analysis on PET studies reported higher regional cerebral blood flow in primary and secondary auditory cortices in tinnitus subjects compared with normal controls (Song et al., 2012). According to these results, the group with tinnitus should have high intrinsic activity or metabolism, but our result shows that metabolism in the tinnitus group is lower than that with the no tinnitus group. Possibly, the neurodegeneration might be still more advanced, despite an increase in intrinsic activity by tinnitus. This suggests that the hypometabolic changes in the superior temporal pole, as evidenced here, might be more associated with cognitive deficits and underlying tinnitus, rather than perceived tinnitus itself. Additionally, a recent study on changes in resting-state brain function networks in subjects with amnestic MCI showed that regional abnormalities in functional brain areas, including the superior temporal gyrus, could be associated with cognitive deficits (Wang et al., 2011). Several lines of evidence indicate that the superior temporal region plays a critical role in cognition. In particular, the superior temporal gyrus is an essential structure for auditory processing, which has been implicated as a hub for social perception and cognition (Ramot et al., 2019). For example, impaired social interaction and visual object discrimination deficiency, both early signs of MCI or Alzheimer's dementia, are closely associated with the functional and structural abnormality of the superior temporal gyrus (Pietschnig et al., 2016; Ramot et al., 2019).

Additionally, compared with the MCI_NT group, a significant hypometabolism in the fusiform gyrus in the

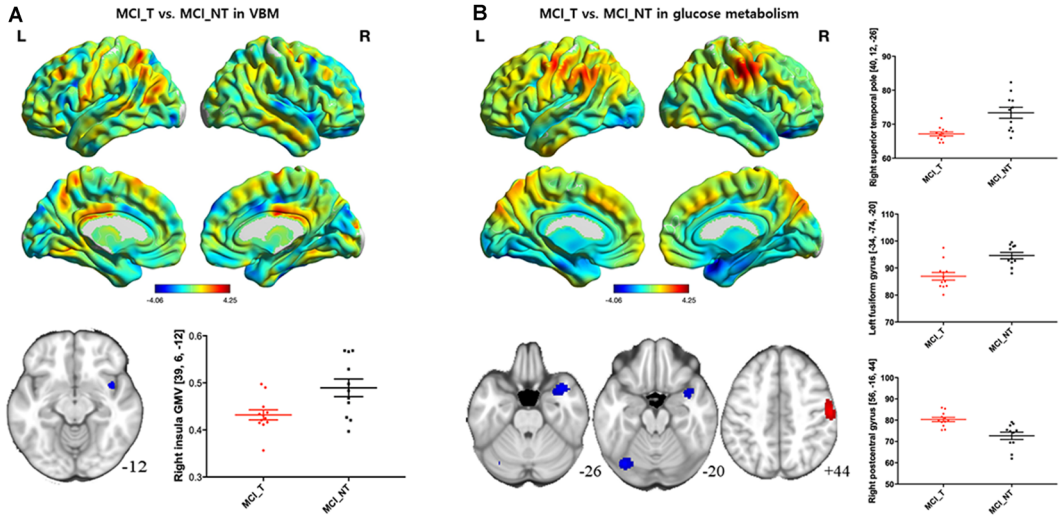

FIGURE 2 | Brain regions showing structural and metabolic differences in MCI_T, compared with MCI_NT. **(A)** Three-dimensional visualization of comparison of MCI_T with MCI_NT in gray matter (GM) volumes by voxel-based morphometry (VBM). The red-spectrum color indicates the MCI_T-increase in GM volumes, and blue-spectrum color indicates the MCI_T-decrease in GM volumes compared with MCI_NT. MCI_T showed a significant decrease in GM volume, compared with MCI_NT (middle). The bottom figure shows a scatter plot of individual GM volume in the region showing significant volume reduction. The horizontal lines represent the mean and standard error of the mean (±SEM). **(B)** Three-dimensional visualization of comparison of MCI_T with MCI_NT in mean metabolic uptake of [^{18}F]fluoro-2-deoxyglucose-positron emission tomography (FDG-PET). The red-spectrum color indicates the MCI_T-increase in metabolism, and blue-spectrum color indicates the MCI_T-decrease in metabolism compared with MCI_NT. Middle figures indicate brain regions showing significant glucose metabolic differences, in which red color indicates higher metabolism and blue color indicates lower metabolism in the MCI_T compared with the MCI_NT. The bottom figure shows a scatter plot of individual glucose metabolism in the regions showing significantly increased or decreased metabolic uptakes. The horizontal lines represent the mean and standard error of the mean (±SEM; $p < 0.005$ uncorrected, $k > 100$).

MCI_T group was observed. Furthermore, it shows that an increase in tinnitus severity is associated with the reduced GM volume of the fusiform gyrus. The fusiform gyrus is a part of the temporal lobe in Brodmann area 37, which has been associated with various neural pathways related to recognition (Mummery et al., 2000). A previous FDG-PET study revealed that the fusiform gyrus, but not the temporal pole, exerted a significant effect on semantic disruptions in semantic dementia (Cai et al., 2015). Moreover, the GM volume of the left fusiform gyrus was significantly correlated with the semantic scores in subjects with semantic dementia, after adjusting for the GM volumes of the other related regions (Ding et al., 2016). Collectively, these results suggest that perceived tinnitus in MCI subjects is closely associated with reduced activation of the superior temporal pole and fusiform gyrus. The specific brain regions tied to tinnitus and cognitive deficits, such as the superior temporal pole and fusiform gyrus, may act as potential neurodegenerative markers that may accelerate cognitive decline, which deserves further study.

Metabolic connectivity analysis revealed that, in MCI_NT, strong negative correlations were observed between the parietal regions and both temporal and limbic regions, which was less pronounced or absent in MCI_T. Negative correlations between a region and other brain areas indicate that when the region has a high FDG uptake, the negatively connected areas have a low FDG uptake and vice versa. In functional MRI (fMRI) network analyses, negative correlations between brain areas were frequently observed, but those had been considered artifacts caused by methodological peculiarities of fMRI analysis because their biological relevance was unclear (Parente et al., 2018). However, our results using FDG-PET were not influenced by short-term hemodynamics or time series artifacts. In recent studies, negative correlations tend to be considered in the biological state. Furthermore, negative correlations might reflect regulatory interactions between brain regions, such as modulations, inhibition, suppression, and neurofeedback (Gopinath et al., 2015). In the MCI_NT group, the inter-hemispheric parietal connectivity was negatively strengthened in temporal including Heschl's gyrus and limbic regions, including the hippocampus, amygdala, and parahippocampal gyrus, although that was not observed in the MCI group with tinnitus. In particular, the MCI_T group showed hypermetabolism in the parietal regions. Our results suggested that hypermetabolism in the parietal regions was affected by chronic tinnitus in the MCI_T group, which was abnormally altered metabolic connectivity with several regions that impairs salience network and hearing, cognitive, and emotional processing.

It is worth noting that chronic tinnitus only leads to a decrease in the insula volume in subjects with MCI. As depicted in **Figure 3**, an inverse correlation between tinnitus severity and insula volume supports the putative association. The insula is responsible for emotion and sympathetic activation and, according to an integrative model of tinnitus (De Ridder et al., 2014), has been considered a critical node of the salience network in the context of tinnitus (Vanneste and De Ridder, 2012). The

TABLE 2 | Brain regions showing significant gray matter (GM) volume or glucose metabolic differences between MCI_T and MCI_NT groups.

	Regions	L/R	BA	Clusters (voxels)	T-score	MNI Coordinates		
						x	*y*	*z*
Gray matter volumes differences								
MCI_T < MCI_NT	Insula	R	13	142	3.59	39	6	−12
Glucose metabolic differences								
MCI_T > MCI_NT	Postcentral gyrus	R	4	305	4.25	56	−16	44
MCI_T < MCI_NT	Superior temporal pole	R	38	246	4.06	40	12	−26
	Fusiform gyrus/cerebellum	L	19	184	4.05	−34	−74	−20

The statistical threshold was $p < 0.005$ (uncorrected) with cluster threshold of 100 voxels.

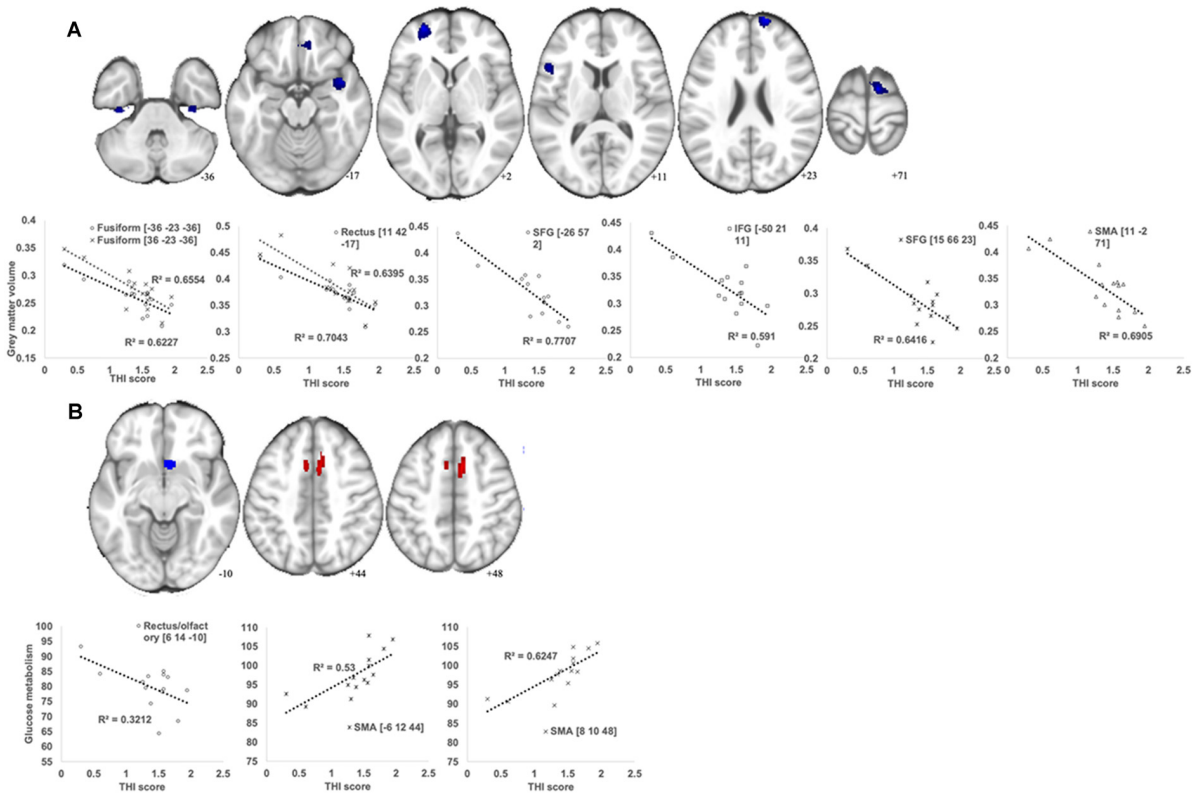

FIGURE 3 | Brain regions showing significant correlations between the Tinnitus Handicap Inventory (THI) score and GM volume **(A)** and glucose metabolism **(B)** in the MCI_T group. **(A)** A voxel-wise multiple regression analysis was performed to detect specific areas in which the GM volume changes are associated with the THI score in MCI_T. The plot figure shows the linear regression line in each region. All analysis was controlled by age and total intracranial volume (TIV; $p < 0.005$ uncorrected, $k > 100$). **(B)** A voxel-wise multiple regression analysis was performed to detect specific areas in which the glucose metabolic changes are associated with the THI score in MCI_T. The plot figure shows the linear regression line in each region. All analysis was controlled by age ($p < 0.005$ uncorrected, $k > 50$).

salience network is a distributed functional-anatomical network that supports emotion and cognition (Uddin, 2015). Importantly, the insula intensively connects with the medial temporal lobe and the posteromedial part of the parietal cortex, which are known biomarkers showing the accelerating conversion from MCI to Alzheimer dementia (Lee et al., 2002; Ferreira et al., 2017; Xu et al., 2019). The results were consistent with those of a previous meta-analysis, indicating that the precuneus and posterior cingulate cortex play a significant role in the transition from MCI to Alzheimer's dementia (Ma et al., 2018). Indeed, Carpenter-Thompson et al. (2015a) also proposed that the posterior cingulate and insula may be associated with an early emotional reaction to develop tinnitus in both task and resting states. Further, the recruitment of more frontal regions makes it possible to better control their emotional response and exhibit altered connectivity in the default mode network (Carpenter-Thompson et al., 2015a). The precuneus and posterior cingulate cortex resided in the posteromedial part of the parietal cortex are core components of the default mode network (Huijbers et al., 2012), a distributed functional-anatomic network exhibiting a high rate of metabolism in subjects not focused on the outside world, and decreases in

TABLE 3 | Correlation analysis between glucose metabolism or gray matter volume and tinnitus severity in MCI_T group.

Regions		L/R	BA	Clusters (voxels)	T-score	MNI Coordinates x	y	z
Gray matter volume correlation with tinnitus severity								
Negative correlation	Superior frontal gyrus	L	10	417	7.90	−26	57	2
	Superior frontal gyrus	R	10	228	7.15	15	66	23
	Inferior frontal gyrus	L	45	158	5.13	−50	21	11
	SMA	R	6	290	7.18	11	−2	71
	Insula	R	13	425	6.08	42	6	−17
	Fusiform gyrus	L	36	167	5.02	−36	−23	−36
	Fusiform gyrus	R	36	161	4.65	36	−23	−36
	Gyrus rectus	R	11	330	4.32	11	42	−17
Glucose metabolism correlation with tinnitus severity								
Positive correlation	SMA/middle cingulate gyrus	R	6	201	4.81	8	10	48
	SMA/middle cingulate gyrus	L	6	61	3.73	−6	12	44
Negative correlation	Olfactory/ Gyrus rectus	R	32	95	3.59	6	14	−10

The statistical threshold was $p < 0.005$ (uncorrected) with cluster threshold of 100 voxels (gray matter volume) and cluster threshold of 50 voxels (glucose metabolism).

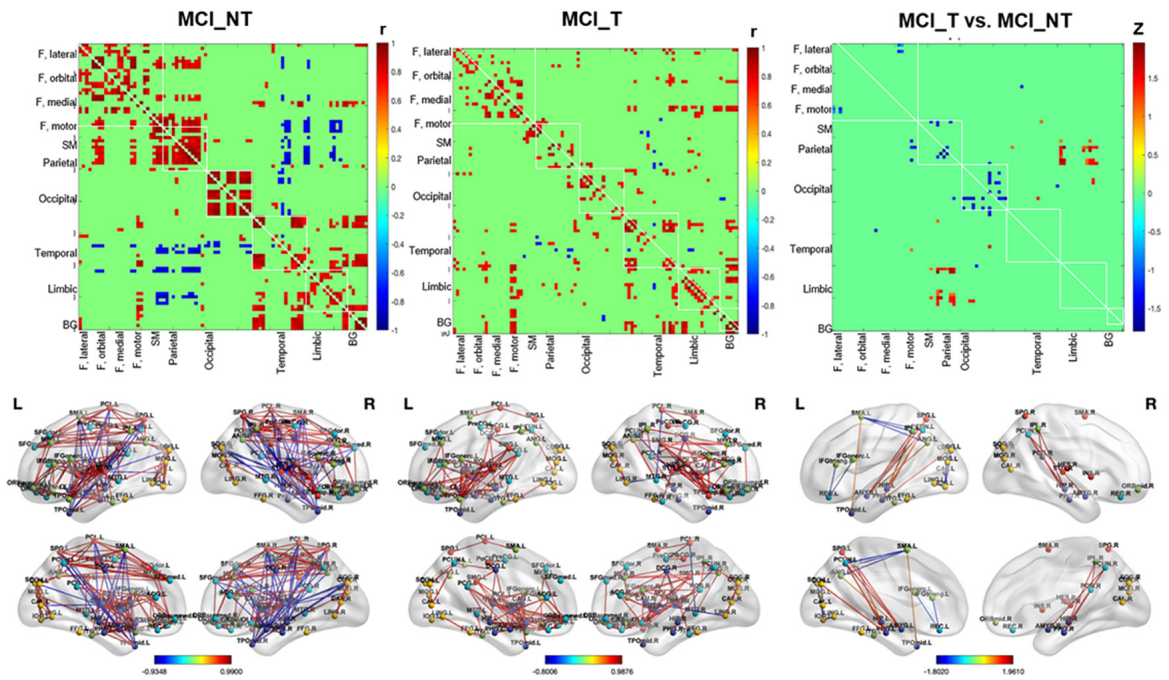

FIGURE 4 | Whole-brain glucose metabolic connectivity. (First left and middle column) Figures show the whole-brain metabolic connectivity matrix among 90 by 90 regions of MCI_NT and MCI_T based on correlation, respectively, with color gradient representing the strength of correlation between two nodes, at p-value < 0.01. (Right column) The figure shows differences in metabolic connectivity in MCI_T compared to MCI_NT, at p-value < 0.01. Values were based on the z-transformed correlations within (diagonal) and between (off-diagonal) ROIs. The color bar represents Fisher's Z. The difference in real connectivity matrix was compared with the null distribution, generated by permutation testing. The second row shows connections between two nodes projected on a 3D template.

activity across a range of cognitive loads (Shulman et al., 1997; Raichle et al., 2001; Kim, 2010). Overall, the volumetric atrophy in the insula is an important morphological marker that selectively develops along with tinnitus in MCI patients and may contribute to the progressive cognitive decline by impairing the connectivity between the brain regions involved in the salience network.

Additionally, a significant inverse correlation between GM volume in the frontal gyrus and THI score was also distinct in MCI subjects. In line with this, Carpenter-Thompson et al. (2015b) demonstrated that individuals with lower tinnitus distress engaged frontal regions to a greater extent to better control their emotional response to affective sounds. Indeed, the frontal regions, such as the prefrontal cortex and orbitofrontal cortex, are considered key areas for the integration of sensory and emotional aspects of tinnitus and the modulation of autonomic physiological responses (Vanneste et al., 2010). Interestingly, the structural abnormalities of the frontal lobe have been reported to weaken the role of auditory memory storage, resulting in the inhibitory

modulation of input to the auditory cortex (Voisin et al., 2006). Given this, severely attenuated GM volume in the frontal gyrus observed herein may represent the deficiency of auditory attention relevant to cognitive decline. As proposed in recent literature (Carpenter-Thompson et al., 2015b), changes in the function or structure of frontal gyrus might serve as a guide when evaluating the efficacy of tinnitus treatment for MCI subjects. Furthermore, it was observed that functional and structural changes in the SMA correlate with THI scores in subjects with MCI. Similarly, a recent study suggested that the conscious perception of tinnitus may be part of the synchronised theta activity in the SMA (Vanneste and De Ridder, 2012). Considering a potential link between the SMA and cognition (Nachev et al., 2008), hypermetabolic or diminished changes in the SMA, such as increasing tinnitus severity, may accelerate cognitive decline. Overall, these specific brain regions, yet-to-be-determined, may influence the progression of cognitive deficits over time, depending on the severity of tinnitus.

This milestone study merits special attention considering the significant impact of *chronic tinnitus* on developing dementia. These results enhance the understanding of the effects of chronic tinnitus on functional and structural brain changes in MCI subjects and offer some potential neurodegenerative markers indicative of cognitive decline. Nevertheless, several limitations require future follow-up investigations. First, our results are limited by the relatively small number of subjects in both groups, mainly due to the difficulty of recruiting MCI subjects with and without tinnitus presenting normal or mild hearing loss. Additionally, the current study was designed as a cross-sectional evaluation, which, along with the retrospective study design, may weaken the clinical implications of our results. Therefore, a prospective and longitudinal follow-up study in large-scale cases is required to support the hypotheses. Second, confounding variables concerning cognition were minimized, but not eliminated. Although only tinnitus subjects with normal hearing or mild hearing loss were enrolled, previous studies have noted that mild hearing loss still acts as a confounder that affects cognitive impairment, eventually leading to dementia (van Boxtel et al., 2000; Thomson et al., 2017). Moreover, combined tinnitus and hyperacusis were not taken into account. Tinnitus subjects may have different cortical activity patterns according to the degree of hearing loss or combined hyperacusis (Vanneste and De Ridder, 2016). Thus, more efforts to minimize the confounders that have cognition-related functional and structural brain changes are required to draw a firm conclusion. Third, lack of correction for multiple comparisons is also a major limitation of the study; future studies employing correction for multiple comparisons in large-scale cases would be the best fit for proving the effects of chronic tinnitus on functional and structural brain changes relevant to MCI. Fourth, since the average age is 74 and younger adults were not included, all results could be simply related to tinnitus, and not relevant to MCI or aging. All subjects in the present study were diagnosed with MCI based on Peterson criteria, which is consistent with the previous study in Korea (Byun et al., 2017). Also, the CERAD-K neuropsychological battery was employed to assess the psychometric properties of the various cognitive domains in both studies, including this study (Byun et al., 2017). As shown in **Supplementary Table 2**, compared with the "CN-old group by Byun et al. (2017)," MCI group in this study markedly showed impairments of cognitive metrics in most cognitive metrics, except for Boston naming test and Memory delayed call. Nevertheless, the differences in neuropsychological status between the two groups were not completely adjusted by other confounding factors, such as age, gender, and education. Also, cognitive metrics were not rigorously included in the PET/MRI analyses. Thus, our results may still be inconclusive whether the effects of chronic tinnitus on functional and structural brain changes are relevant to MCI or the aging process or not, when considering additional potential confounders. Fifth, this study only included subjects with normal or mild hearing loss, raising a question that the relationships discovered herein might be different with higher levels of hearing loss. If not perfectly, previous studies could tell to some extent whether the relationships discovered herein will be different with higher levels of hearing loss or not. Hearing loss *per se* has been identified as the potentially largest modifiable risk factor for cognitive decline (Lin et al., 2011). Recent neuroimaging studies have shown that aberrant activity in the brain may interact with dementia pathology in people with hearing loss (Griffiths et al., 2020; Ha et al., 2020). Specifically, a longitudinal population study demonstrated that the risk of dementia increased with hearing loss severity for individuals older than 60 years (Lin et al., 2011). In collaboration with this, the worsening hearing was positively correlated with a higher β-amyloid burden, a pathologic biomarker of AD, measured *in vivo* with PET scans (Golub et al., 2020). Given this, the effects of chronic tinnitus on functional and structural brain changes in subjects with MCI would be different according to levels of hearing loss, but this awaits further confirmation. Nevertheless, we believe that our protocol that recruits only normal or mild hearing loss subjects exerts major strength because it can minimize bias related to hearing loss-induced metabolic and structural changes. Finally, subjects enrolled in this study show relatively heterogeneous tinnitus severity. To replicate current results, future studies comprising a large number of cases and subsequent normal distribution of tinnitus severity should be considered.

CONCLUSIONS

Taken together, these results show, for the first time, that chronic tinnitus elicits differential metabolic and structural brain changes in subjects diagnosed with MCI. Given the significant impact of MCI on developing dementia, specifically Alzheimer's disease, this study merits strong attention because the results provide a valuable basis on which neurodegenerative markers of tinnitus, yet-to-be-identified, can be polished accordingly.

DATA AVAILABILITY STATEMENT

The raw data supporting the conclusions of this article will be made available by the authors, without undue reservation.

ETHICS STATEMENT

The studies involving human participants were reviewed and approved by the Seoul National University Hospital Institutional Review Board (IRB-B-20-2019-44) and was conducted in accordance with the Declaration of Helsinki. The patients/participants provided their written informed consent to participate in this study.

AUTHOR CONTRIBUTIONS

S-YL, YHK, and YKK: conceptualization. S-YL, HK, and YKK: methodology. JL and JK: software. YHK and YKK: validation and supervision. S-YL and HK: formal analysis, investigation and writing—original draft preparation. YKK: resources and funding acquisition. S-YL, HK, DL, JK, and JL: data curation. DL and I-MJ: writing—review and editing. HK: visualization. S-YL: project administration. All authors contributed to the article and approved the submitted version.

FUNDING

This work was supported by a clinical research grant-in-aid from the Seoul Metropolitan Government Seoul National University Boramae Medical Center (03-2019-14) and by a grant from the National Research Foundation of Korea (NRF) grant funded by the Korea government (MEST; Grant Nos. NRF-2018R1A5A2025964 and NRF- 2014M3C7A1046042).

SUPPLEMENTARY MATERIAL

The Supplementary Material for this article can be found online at: https://www.frontiersin.org/articles/10.3389/fnagi.2020.594282/full#supplementary-material.

REFERENCES

Byun, M. S., Yi, D., Lee, J. H., Choe, Y. M., Sohn, B. K., Lee, J. Y., et al. (2017). Korean brain aging study for the early diagnosis and prediction of Alzheimer's disease: methodology and baseline sample characteristics. *Psychiatry Investig.* 14, 851–863. doi: 10.4306/pi.2017.14.6.851

Cai, S., Chong, T., Zhang, Y., Li, J., Von Deneen, K. M., Ren, J., et al. (2015). Altered functional connectivity of fusiform gyrus in subjects with amnestic mild cognitive impairment: a resting-state fMRI study. *Front. Hum. Neurosci.* 9:471. doi: 10.3389/fnhum.2015.00471

Carpenter-Thompson, J. R., Schmidt, S. A., and Husain, F. T. (2015a). Neural plasticity of mild tinnitus: an fMRI investigation comparing those recently diagnosed with tinnitus to those that had tinnitus for a long period of time. *Neural Plast.* 2015:161478. doi: 10.1155/2015/161478

Carpenter-Thompson, J. R., Schmidt, S., Mcauley, E., and Husain, F. T. (2015b). Increased frontal response may underlie decreased tinnitus severity. *PLoS One* 10:e0144419. doi: 10.1371/journal.pone.0144419

Das, S. K., Wineland, A., Kallogjeri, D., and Piccirillo, J. F. (2012). Cognitive speed as an objective measure of tinnitus. *Laryngoscope* 122, 2533–2538. doi: 10.1002/lary.23555

De Ridder, D., Vanneste, S., Weisz, N., Londero, A., Schlee, W., Elgoyhen, A. B., et al. (2014). An integrative model of auditory phantom perception: tinnitus as a unified percept of interacting separable subnetworks. *Neurosci. Biobehav. Rev.* 44, 16–32. doi: 10.1016/j.neubiorev.2013.03.021

Ding, J., Chen, K., Chen, Y., Fang, Y., Yang, Q., Lv, Y., et al. (2016). The left fusiform gyrus is a critical region contributing to the core behavioral profile of semantic dementia. *Front. Hum. Neurosci.* 10:215. doi: 10.3389/fnhum.2016.00215

Ferreira, D., Machado, A., Molina, Y., Nieto, A., Correia, R., Westman, E., et al. (2017). Cognitive variability during middle-age: possible association with neurodegeneration and cognitive reserve. *Front. Aging Neurosci.* 9:188. doi: 10.3389/fnagi.2017.00188

Golub, J. S., Sharma, R. K., Rippon, B. Q., Brickman, A. M., and Luchsinger, J. A. (2020). The association between early age-related hearing loss and brain β-amyloid. *Laryngoscope* doi: 10.1002/lary.28859 [Epub ahead of print].

Gopinath, K., Krishnamurthy, V., Cabanban, R., and Crosson, B. A. (2015). Hubs of anticorrelation in high-resolution resting-state functional connectivity network architecture. *Brain Connect.* 5, 267–275. doi: 10.1089/brain.2014.0323

Griffiths, T. D., Lad, M., Kumar, S., Holmes, E., McMurray, B., Maguire, E. A., et al. (2020). How can hearing loss cause dementia? *Neuron* doi: 10.1016/j.neuron.2020.08.003 [Epub ahead of print].

Ha, J., Cho, Y. S., Kim, S. J., Cho, S. H., Kim, J. P., Jung, Y. H., et al. (2020). Hearing loss is associated with cortical thinning in cognitively normal older adults. *Eur. J. Neurol.* 27, 1003–1009. doi: 10.1111/ene.14195

Huijbers, W., Vannini, P., Sperling, R., Pennartz, C., Cabeza, R., and Daselaar, S. (2012). Explaining the encoding/retrieval flip: memory-related deactivations and activations in the posteromedial cortex. *Neuropsychologia* 50, 3764–3774. doi: 10.1016/j.neuropsychologia.2012.08.021

Kim, H. (2010). Dissociating the roles of the default-mode, dorsal and ventral networks in episodic memory retrieval. *NeuroImage* 50, 1648–1657. doi: 10.1016/j.neuroimage.2010.01.051

Langa, K. M., and Levine, D. A. (2014). The diagnosis and management of mild cognitive impairment: a clinical review. *JAMA* 312, 2551–2561. doi: 10.1001/jama.2014.13806

Langguth, B., Kreuzer, P. M., Kleinjung, T., and De Ridder, D. (2013). Tinnitus: causes and clinical management. *Lancet Neurol.* 12, 920–930. doi: 10.1016/S1474-4422(13)70160-1

Lee, D. S., Kang, H., Kim, H., Park, H., Oh, J. S., Lee, J. S., et al. (2008). Metabolic connectivity by interregional correlation analysis using statistical parametric mapping (SPM) and FDG brain PET; methodological development and patterns of metabolic connectivity in adults. *Eur. J. Nucl. Med. Mol. Imaging* 35, 1681–1691. doi: 10.1007/s00259-008-0808-z

Lee, S.-Y., Lee, J. Y., Han, S.-Y., Seo, Y., Shim, Y. J., and Kim, Y. H. (2020). Neurocognition of aged patients with chronic tinnitus: focus on mild cognitive impairment. *Clin. Exp. Otorhinolaryngol.* 13, 8–14. doi: 10.21053/ceo.2018.01914

Lee, D. Y., Lee, K. U., Lee, J. H., Kim, K. W., Jhoo, J. H., Kim, S. Y., et al. (2004). A normative study of the CERAD neuropsychological assessment battery in the Korean elderly. *J. Int. Neuropsychol. Soc.* 10, 72–81. doi: 10.1017/S1355617704101094

Lee, S.-Y., Nam, D. W., Koo, J.-W., De Ridder, D., Vanneste, S., and Song, J.-J. (2017). No auditory experience, no tinnitus: lessons from subjects with congenital-and acquired single-sided deafness. *Hear. Res.* 354, 9–15. doi: 10.1016/j.heares.2017.08.002

Lee, T. M., Yip, J. T., and Jones-Gotman, M. (2002). Memory deficits after resection from left or right anterior temporal lobe in humans: a meta-analytic review. *Epilepsia* 43, 283–291. doi: 10.1046/j.1528-1157.2002.09901.x

Levey, A., Lah, J., Goldstein, F., Steenland, K., and Bliwise, D. (2006). Mild cognitive impairment: an opportunity to identify patients at high risk for progression to Alzheimer's disease. *Clin. Ther.* 28, 991–1001. doi: 10.1016/j.clinthera.2006.07.006

Lin, F. R., Metter, E. J., O'brien, R. J., Resnick, S. M., Zonderman, A. B., and Ferrucci, L. (2011). Hearing loss and incident dementia. *Arch. Neurol.* 68, 214–220. doi: 10.1001/archneurol.2010.362

Ma, H. R., Sheng, L. Q., Pan, P. L., Di Wang, G., Luo, R., Shi, H. C., et al. (2018). Cerebral glucose metabolic prediction from amnestic mild cognitive impairment to Alzheimer's dementia: a meta-analysis. *Transl. Neurodegener.* 7:9. doi: 10.1186/s40035-018-0114-z

Maudoux, A., Lefebvre, P., Cabay, J.-E., Demertzi, A., Vanhaudenhuyse, A., Laureys, S., et al. (2012). Auditory resting-state network connectivity in tinnitus: a functional MRI study. *PLoS One* 7:e36222. doi: 10.1371/journal.pone.0036222

Mummery, C. J., Patterson, K., Price, C. J., Ashburner, J., Frackowiak, R. S., and Hodges, J. R. (2000). A voxel-based morphometry study of semantic dementia: relationship between temporal lobe atrophy and semantic memory. *Ann. Neurol.* 47, 36–45. doi: 10.1002/1531-8249(200001)47:1<36::aid-ana8>3.0.co;2-l

Nachev, P., Kennard, C., and Husain, M. (2008). Functional role of the supplementary and pre-supplementary motor areas. *Nat. Rev. Neurosci.* 9, 856–869. doi: 10.1038/nrn2478

Ottoy, J., Niemantsverdriet, E., Verhaeghe, J., De Roeck, E., Struyfs, H., Somers, C., et al. (2019). Association of short-term cognitive decline and MCI-to-AD dementia conversion with CSF, MRI, amyloid-and ^{18}F-FDG-PET imaging. *NeuroImage Clin.* 22:101771. doi: 10.1016/j.nicl.2019.101771

Parente, F., Frascarelli, M., Mirigliani, A., Di Fabio, F., Biondi, M., and Colosimo, A. (2018). Negative functional brain networks. *Brain Imaging Behav.* 12, 467–476. doi: 10.1007/s11682-017-9715-x

Pietschnig, J., Aigner-Wöber, R., Reischenböck, N., Kryspin-Exner, I., Moser, D., Klug, S., et al. (2016). Facial emotion recognition in patients with subjective cognitive decline and mild cognitive impairment. *Int. Psychogeriatr.* 28, 477–485. doi: 10.1017/S1041610215001520

Raichle, M. E., Macleod, A. M., Snyder, A. Z., Powers, W. J., Gusnard, D. A., and Shulman, G. L. (2001). A default mode of brain function. *Proc. Natl. Acad. Sci. U S A* 98, 676–682. doi: 10.1073/pnas.98.2.676

Ramot, M., Walsh, C., and Martin, A. (2019). Multifaceted integration—memory for faces is subserved by widespread connections between visual, memory, auditory, and social networks. *J. Neurosci.* 39, 4976–4985. doi: 10.1523/JNEUROSCI.0217-19.2019

Rossiter, S., Stevens, C., and Walker, G. (2006). Tinnitus and its effect on working memory and attention. *J. Speech Lang. Hear. Res.* 49, 150–160. doi: 10.1044/1092-4388(2006/012)

Shulman, G. L., Fiez, J. A., Corbetta, M., Buckner, R. L., Miezin, F. M., Raichle, M. E., et al. (1997). Common blood flow changes across visual tasks: II. Decreases in cerebral cortex. *J. Cogn. Neurosci.* 9, 648–663. doi: 10.1162/jocn.1997.9.5.648

Snowden, J. (2004). *Mild Cognitive Impairment: Aging To Alzheimer's Disease.* New York: NY: Oxford University Press.

Song, J.-J., De Ridder, D., Van de Heyning, P., and Vanneste, S. (2012). Mapping tinnitus-related brain activation: an activation-likelihood estimation metaanalysis of PET studies. *J. Nucl. Med.* 53, 1550–1557. doi: 10.2967/jnumed.112.102939

Thomson, R. S., Auduong, P., Miller, A. T., and Gurgel, R. K. (2017). Hearing loss as a risk factor for dementia: a systematic review. *Laryngoscope Investig. Otolaryngol.* 2, 69–79. doi: 10.1002/lio2.65

Trevis, K. J., McLachlan, N. M., and Wilson, S. J. (2016). Cognitive mechanisms in chronic tinnitus: psychological markers of a failure to switch attention. *Front. Psychol.* 7:1262. doi: 10.3389/fpsyg.2016.01262

Tzourio-Mazoyer, N., Landeau, B., Papathanassiou, D., Crivello, F., Etard, O., Delcroix, N., et al. (2002). Automated anatomical labeling of activations in SPM using a macroscopic anatomical parcellation of the MNI MRI single-subject brain. *NeuroImage* 15, 273–289. doi: 10.1006/nimg.2001.0978

Uddin, L. Q. (2015). Salience processing and insular cortical function and dysfunction. *Nat. Rev. Neurosci.* 16, 55–61. doi: 10.1038/nrn3857

van Boxtel, M. P., van Beijsterveldt, E. C., Houx, P. J., Anteunis, L. J., Metsemakers, J. F., and Jolles, J. (2000). Mild hearing impairment can reduce verbal memory performance in a healthy adult population. *J. Clin. Exp. Neuropsychol.* 22, 147–154. doi: 10.1076/1380-3395(200002)22:1;1-8;FT147

Vanneste, S., and De Ridder, D. (2012). The auditory and non-auditory brain areas involved in tinnitus. An emergent property of multiple parallel overlapping subnetworks. *Front. Syst. Neurosci.* 6:31. doi: 10.3389/fnsys.2012.00031

Vanneste, S., and De Ridder, D. (2016). Deafferentation-based pathophysiological differences in phantom sound: tinnitus with and without hearing loss. *NeuroImage* 129, 80–94. doi: 10.1016/j.neuroimage.2015.12.002

Vanneste, S., Faber, M., Langguth, B., and De Ridder, D. (2016). The neural correlates of cognitive dysfunction in phantom sounds. *Brain Res.* 1642, 170–179. doi: 10.1016/j.brainres.2016.03.016

Vanneste, S., Plazier, M., van der Loo, E., van de Heyning, P., Congedo, M., and De Ridder, D. (2010). The neural correlates of tinnitus-related distress. *NeuroImage* 52, 470–480. doi: 10.1016/j.neuroimage.2010.04.029

Voisin, J., Bidet-Caulet, A., Bertrand, O., and Fonlupt, P. (2006). Listening in silence activates auditory areas: a functional magnetic resonance imaging study. *J. Neurosci.* 26, 273–278. doi: 10.1523/JNEUROSCI.2967-05.2006

Wang, Z., Yan, C., Zhao, C., Qi, Z., Zhou, W., Lu, J., et al. (2011). Spatial patterns of intrinsic brain activity in mild cognitive impairment and Alzheimer's disease: a resting-state functional MRI study. *Hum. Brain Mapp.* 32, 1720–1740. doi: 10.1002/hbm.21140

Wang, Y., Zhang, J.-N., Hu, W., Li, J.-J., Zhou, J.-X., Zhang, J.-P., et al. (2018). The characteristics of cognitive impairment in subjective chronic tinnitus. *Brain Behav.* 8:e00918. doi: 10.1002/brb3.918

Xu, X.-M., Jiao, Y., Tang, T.-Y., Lu, C.-Q., Zhang, J., Salvi, R., et al. (2019). Altered spatial and temporal brain connectivity in the salience network of sensorineural hearing loss and tinnitus. *Front. Neurosci.* 13:246. doi: 10.3389/fnins.2019.00246

Yakushev, I., Drzezga, A., and Habeck, C. (2017). Metabolic connectivity: methods and applications. *Curr. Opin. Neurol.* 30, 677–685. doi: 10.1097/WCO.0000000000000494

Zarenoe, R., Hällgren, M., Andersson, G., and Ledin, T. (2017). Working memory, sleep and hearing problems in patients with tinnitus and hearing loss fitted with hearing aids. *J. Am. Acad. Audiol.* 28, 141–151. doi: 10.3766/jaaa.16023

Zilbovicius, M., Meresse, I., Chabane, N., Brunelle, F., Samson, Y., and Boddaert, N. (2006). Autism, the superior temporal sulcus and social perception. *Trends Neurosci.* 29, 359–366. doi: 10.1016/j.tins.2006.06.004

Conflict of Interest: The authors declare that the research was conducted in the absence of any commercial or financial relationships that could be construed as a potential conflict of interest.

frontiers in Aging Neuroscience

ORIGINAL RESEARCH
published: 19 November 2020
doi: 10.3389/fnagi.2020.602510

Anisotropy of Anomalous Diffusion Improves the Accuracy of Differentiating and Grading Alzheimer's Disease Using Novel Fractional Motion Model

Lei Du[1,2†], Zifang Zhao[3†], Boyan Xu[4†], Wenwen Gao[1], Xiuxiu Liu[1], Yue Chen[1], Yige Wang[1], Jian Liu[5], Bing Liu[1], Shilong Sun[1], Guolin Ma[1,2] and Jiahong Gao[6,7,8]*

[1] Department of Radiology, China-Japan Friendship Hospital, Beijing, China, [2] Graduate School of Peking Union Medical College, Chinese Academy of Medical Sciences and Peking Union Medical College, Beijing, China, [3] Department of Anesthesiology, Peking University First Hospital, Peking University, Beijing, China, [4] Beijing Intelligent Brain Cloud Inc., Beijing, China, [5] Department of Ultrasound Diagnosis, China-Japan Friendship Hospital, Beijing, China, [6] Beijing City Key Lab for Medical Physics and Engineering, Institute of Heavy Ion Physics, School of Physics, Peking University, Beijing, China, [7] Center for MRI Research, Academy for Advanced Interdisciplinary Studies, Peking University, Beijing, China, [8] McGovern Institute for Brain Research, Peking University, Beijing, China

OPEN ACCESS

Edited by:
Jiu Chen,
Nanjing Medical University, China

Reviewed by:
Xi-jian Dai,
The Chinese University of Hong Kong, China
Xiaochun Wang,
First Hospital of Shanxi Medical University, China

***Correspondence:**
Guolin Ma
maguolin1007@qq.com

† These authors have contributed equally to this work

Received: *03 September 2020*
Accepted: *19 October 2020*
Published: *19 November 2020*

Citation:
Du L, Zhao Z, Xu B, Gao W, Liu X, Chen Y, Wang Y, Liu J, Liu B, Sun S, Ma G and Gao J (2020) Anisotropy of Anomalous Diffusion Improves the Accuracy of Differentiating and Grading Alzheimer's Disease Using Novel Fractional Motion Model. Front. Aging Neurosci. 12:602510. doi: 10.3389/fnagi.2020.602510

Background and Purpose: Recent evidence shows that the fractional motion (FM) model may be a more appropriate model for describing the complex diffusion process of water in brain tissue and has shown to be beneficial in clinical applications of Alzheimer's disease (AD). However, the FM model averaged the anomalous diffusion parameter values, which omitted the impacts of anisotropy. This study aimed to investigate the potential feasibility of anisotropy of anomalous diffusion using the FM model for distinguishing and grading AD patients.

Methods: Twenty-four patients with AD and 11 matched healthy controls were recruited, diffusion MRI was obtained from all participants and analyzed using the FM model. Generalized fractional anisotropy (gFA), an anisotropy metric, was introduced and the gFA values of FM-related parameters, Noah exponent (α) and the Hurst exponent (H), were calculated and compared between the healthy group and AD group and between the mild AD group and moderate AD group. The receiver-operating characteristic (ROC) analysis and the multivariate logistic regression analysis were used to assess the diagnostic performances of the anisotropy values and the directionally averaged values.

Results: The gFA(α) and gFA(H) values of the moderate AD group were higher than those of the mild AD group in left hippocampus. The gFA(α) value of the moderate AD group was significantly higher than that of the healthy control group in both the left and right hippocampus. The gFA(ADC) values of the moderate AD group were significantly lower than those of the mild AD group and healthy control group in the right hippocampus. Compared with the gFA(α), gFA(H), α, and H, the ROC analysis showed larger areas under the curves for combination of α + gFA(α) and the combination of H + gFA(H) in differentiating the mild AD and moderate AD groups, and larger area under the curves for combination of α + gFA(α) in differentiating the healthy controls and AD groups.

Conclusion: The anisotropy of anomalous diffusion could significantly differentiate and grade patients with AD, and the diagnostic performance was improved when the anisotropy metric was combined with commonly used directionally averaged values. The utility of anisotropic anomalous diffusion may provide novel insights to profoundly understand the neuropathology of AD.

Keywords: diffusion magnetic resonance imaging, fractional motion model, anisotropy, Alzheimer's disease, hippocampus

INTRODUCTION

Alzheimer's disease (AD), manifested as progressive cognitive decline and memory loss, is the most common neurodegenerative disease (Reddy and Oliver, 2019). Approximately accounting for 60–70% of dementia patients, AD has been the most prevalent type of dementia (Wortmann, 2012; Alzheimer's, 2016; Khan et al., 2017). The underlying neuropathological mechanisms of AD include the hyperphosphorylation of tau protein and the deposition of β-amyloid (Aβ), which lead to the formation of intracellular neurofibrillary tangles (NFTs) and Aβ plaques separately (Kidd, 1963; Hyman et al., 1984; Braak and Braak, 1991; Wegmann et al., 2010; Mattsson et al., 2019) and ultimately result in the apoptosis of neurons. Neuropathological changes can occur and persist for decades before the appearance of cognitive degeneration. Recently, a variety of magnetic resonance imaging (MRI) techniques have been widely investigated for the diagnosis of AD; however, these methods are insufficient to make a specific diagnosis of AD (Cummings, 2017; Mattsson et al., 2019).

Diffusion MRI (dMRI) can non-invasively describe the random motion of water molecules in and around brain structures such as cell bodies or brain white matter fibers, which provides rich information of microscopic properties than other traditional MRI sequences (Le Bihan, 1995; Le Bihan and Johansen-Berg, 2012; Harrison et al., 2020) and has become a widely used imaging practice in clinical practice and relevant researches (La Rocca et al., 2018; Anckaerts et al., 2019; Bergamino et al., 2020; Finsterwalder et al., 2020). Directional dependence (i.e., anisotropy) is one of the most important microscopic properties obtained from the nervous system by dMRI. Anisotropy results from the dense accumulation of axons and inherent axonal membranes, which prevent the diffusion of water perpendicular to the long axis of fibers (Beaulieu, 2002). One of the most commonly used diffusion MRI technologies, the apparent diffusion coefficient (ADC), was found useful in differentiating AD patients (Takahashi et al., 2017; Xue et al., 2019) and AD transgenic mice (Thiessen et al., 2010). Moreover, the ADC value of white matter in the frontal lobe was correlated with mini-mental state examination (MMSE) scale (Xue et al., 2019). Diffusion tensor imaging (DTI) is another commonly used diffusion MRI technology to measure the anisotropy in the research (Basser et al., 1994a,b). DTI has been increasingly applied to the diagnosis of AD in both basic and clinical studies. The degree of diffusion anisotropy is mostly quantified by two DTI-derived metrics, the fractional anisotropy (FA) and mean diffusivity (MD), in patients with AD (Mayo et al., 2017; Brueggen et al., 2019; Marcos Dolado et al., 2019). Several studies found that the FA values reduced and MD values increased in the hippocampus of AD patients and amnestic mild cognitive impairment (aMCI) patients when compared with healthy control. And the FA and MD might be used to differentiate healthy controls, aMCI patients, and AD patients (Hong et al., 2013; Tang et al., 2016; Schouten et al., 2017). Moreover, the FA value or MD value of hippocampus could be used to predict the progression of AD or aMCI, which is evaluated by MMSE scale (Hong et al., 2013; Lee et al., 2017), indicating the possibility of diffusivity as a biomarker for disease progression. In addition to DTI combined with functional MRI, structural MRI can improve the diagnostic accuracy of AD (Dyrba et al., 2015; Tang et al., 2016; Bouts et al., 2018).

DTI presumes a normal diffusion process in brain tissues and is consequently quantified using a mono-exponential model, $S/S_0 = \exp(-b \cdot \mathrm{ADC})$. The b-value represents the applied magnetic field gradient sequence. However, it has been recognized that the observed dMRI signal decay curve deviates from the mono-exponential form in brain tissues, especially at high b-values (De Santis et al., 2011). To solve this problem, several models have been developed based on different theories of anomalous diffusion processes to find the optimal consistency between the observed signal decay curve and the fitted curves. Representative models include the stretched exponential model (Bennett et al., 2003), the bi-exponential model (Mulkern et al., 1999), the kurtosis model (Jensen et al., 2005), and the statistical model (Yablonskiy et al., 2003). Additionally, several physics-motivated dMRI models have also been proposed (Magin et al., 2008; Ingo et al., 2014).

The fractional motion (FM) model has been proposed as a more appropriate approach to describe the complex diffusion process of biological systems (Magdziarz et al., 2009; Burnecki and Weron, 2010; Weiss, 2013). Theoretically, the FM model presumes that the diffusion process of water molecules is α-stable and H-self-similar and has stationary increments. The symbol α represents the Noah exponent, which describes the fluctuations of the random process. The symbol H represents the Hurst exponent, which depicts the self-similarity property of molecular trajectories. The FM model possesses a relevantly more excellent consistency between experimental data and fitting curves. Many studies have demonstrated the clinical feasibility of anomalous diffusion using the FM model (Kwee et al., 2010a,b; Sui et al., 2015; Karaman et al., 2016; Xu et al., 2017b, 2018; Du et al., 2020). In the aforementioned studies, researchers averaged

the anomalous diffusion parameter values that were acquired in different gradient directions, which ignored the impacts of anisotropy. However, existing literature elucidated that the anisotropy of anomalous diffusion should not be neglected as it revealed a different image contrast and provided unique information (Hall and Barrick, 2012; Xu et al., 2017a). At present, the availability regarding the clinical application of the anisotropy of anomalous diffusion in AD patients remains unclear. The purpose of this study was to investigate the potential feasibility of anisotropy of anomalous diffusion for distinguishing AD patients from healthy controls and grading AD patients.

MATERIALS AND METHODS

Subjects

This research was approved by the ethics committee of the China-Japan Friendship Hospital, and the informed consent was obtained from all subjects. The cognitive function of all participants was assessed by the MMSE scale and Montreal cognitive assessment (MoCA) scale. Initially, MRI examinations were performed on 13 healthy controls and 50 patients with AD. The patients with AD visited the Department of Neurology of the China-Japan Friendship Hospital from November 2015 to March 2019. The clinical diagnosis of AD met the criteria of the National Institute of Neurological and Communicative Disorders and Stroke and the Alzheimer's Disease and Related Disorders Association (NINCDS-ADRDA) (1984) (McKhann et al., 1984; Mattsson et al., 2019). Only the mild-to-moderate AD patients ($11 \leq$ MMSE score ≤ 25) (Folstein et al., 1975; Perneczky et al., 2006; Tchalla et al., 2018) who met the following criteria were considered for inclusion: (a) the participants' acquired MR image had no artifacts; (b) the participants had no other brain diseases, such as cerebral ischemia or infarction; and (c) the participants had no visual and hearing impairment disorders, aphasia, and limb activity disorder. Finally, 24 patients with AD were eligible and enrolled in this study (9 males and 15 females, mean age, 69.0 years, age range, 50–79 years). Healthy controls were recruited from the local community. Inclusion criteria were as follows: (a) ages range from 50 to 79 years (including 50 and 79 years); (b) a degree of primary education or above; and (c) neurological examination showed no obvious anomalies, and the MMSE scores were between 26 and 30. Healthy controls who suffered from cardiovascular, neurologic, metabolic, and psychiatric disorders or brain abnormalities were excluded. Eventually, 11 healthy controls (2 males and 9 females, mean age 65.3 years, range 54–78 years) were enrolled in the present study. Detailed demographic and clinical characteristics of all participants are summarized in **Table 1**.

TABLE 1 | Demographic and clinical information of all participants.

	Healthy controls	AD patients		*P*–value
		Mild AD	Moderate AD	
Number	11	12	12	-
Male/female	2/9	6/6	3/9	>0.05
Age	65.3 ± 6.6	65.8 ± 10.1	72.1 ± 3.8	> 0.05
Education	10.6 ± 3.3	13.4 ± 3.1	10.5 ± 3.9	> 0.05
MMSE score	28.8 ± 1.1	23.2 ± 1.3	19.1 ± 1.4	< 0.05
MoCA score	-	19.5 ± 2.4	16.5 ± 2.2	< 0.05

The MoCA score was only compared between mild AD group and moderate AD group using a two-sample t-test.

AD, Alzheimer's disease; MMSE, mini-mental state examination; MoCA, Montreal cognitive assessment.

Image Acquisition

All participants received conventional MRI, 3D T1-weighted imaging, and dMRI. The MRI scans were performed on a 3.0-T MRI scanner (GE Healthcare, Discovery MR750, USA) equipped with an eight-channel head coil. dMR images of all participants were obtained using a special Stejskal–Tanner single-shot spin-echo echo-planar-imaging sequence.

To fit the FM model, we did not fix the diffusion gradient separation time (Δ) during the scanning process as the conventional dMRI sequence. Specifically, Δ was arrayed at 27.060, 39.560, and 52.060 ms. For each Δ value, the diffusion gradient amplitude (G_0) was 15.67, 19.68, 24.73, 31.06, 39.01, and 49.00 mT/m in sequence, which were selected to be approximately evenly spaced on the log axis. The gradient duration constant (δ) was set to 20.676 ms. Thereafter, 18 non-zero b-values (151, 239, 377, 595, 939, and 1,481 s/mm^2 for Δ at 27.060 ms; 245, 387, 611, 964, 1,521, and 2,399 s/mm^2 for Δ at 39.560 ms; and 339, 535, 845, 1,333, 2,103, and 3,317 s/mm^2 for Δ at 52.060 ms) were obtained in each gradient direction. In order to decrease the effect of diffusion anisotropy, we successively applied the diffusion gradients in three orthogonal directions (the x-axis, y-axis, and z-axis) in turn. Moreover, a total of 12 images without diffusion sensitization ($b = 0$) were acquired.

The dMRI scanning parameters included the following: repetition time (TR)/echo time (TE) = 3,800 ms/110 ms; accelerating factor = 2; flip angle = 90°; number of excitations = 2; field of view (FOV) = 240 mm × 240 mm; matrix size = 128 × 128; slice thickness = 5.0 mm; number of slices = 27; voxel size = 1.875 × 1.875 × 5 mm^3. Since high in-plane resolution was preferable, a large slice thickness had to be chosen to achieve a decent signal-to-noise ratio (SNR). The total scan time was 8 min 33 s, which facilitated the clinical use. T1 structure image parameters were as follows: TR = 6.7 ms; TE = min full; flip angle = 12°; FOV = 256 mm × 256 mm; matrix size = 256 × 256; slice thickness = 1.0 mm; number of slices = 192; scan time = 4 min 10 s.

Image Segmentation

In the present study, the hippocampus was chosen as the region of interest (ROI) (**Figure 1**). At first, the hippocampus was manually drawn slice by slice using MRICRON by a radiologist (LD, 5 years' working experience) on the T1 structure images, and then the drawn ROIs were registered onto lower-resolution dMRI, to more easily define the boundary of hippocampus. The ROIs' boundary was accurately segmented, and ambiguous voxels would be eliminated in all participants. Then the average values

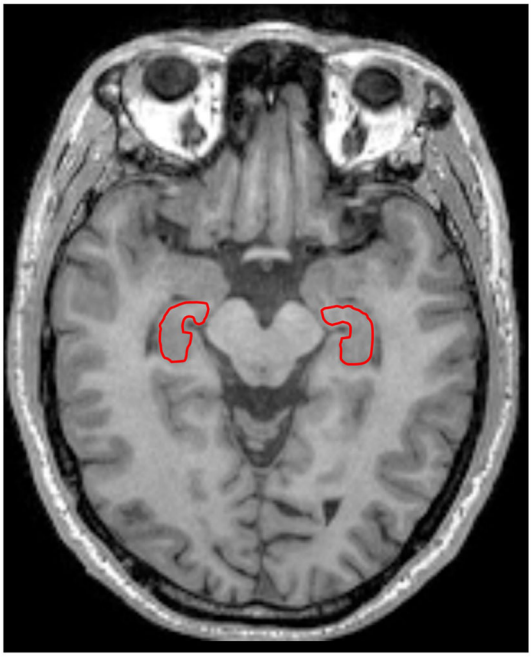

FIGURE 1 | A 67-year-old male healthy control. The left and right hippocampus are outlined in red line in T1-weighted imaging.

of α, H, ADC, generalized FA (gFA)(α), gFA(H), and gFA(ADC) in the left and right hippocampus were acquired.

Image Analysis

First, the obtained images were corrected for head motion and eddy current distortions by FSL tools (Cha, 2006). In the dMRI acquisition, ADC maps were calculated using the images obtained at b-values of 0 and 954 s/mm^2 (closest to conventional 1,000 s/mm^2 b-value). We used the FM model to analyze the images. According to the FM-based dMRI theory (Sui et al., 2015), the following formula can be used to calculate diffusion-induced signal decay:

$$S/S_0 = \exp(-\eta D_{\alpha,H}\gamma^{\alpha}G_0^{\alpha}\Delta^{\alpha+\alpha H}) \quad (1)$$

where $D_{\alpha,H}$ represents the diffusion coeffcient of anomalous diffusion and γ represents the gyromagnetic ratio. G_0 represents the diffusion gradient amplitude, and Δ represents the gradient separation time. η is a dimensionless number, which can be calculated using α, H, δ, and Δ in the following formula (Xu et al., 2017b, 2018):

$$\eta = \frac{1}{(1+\mu)^{\alpha}}\left[\int_0^{\delta/\Delta}\left|\left(\frac{\delta}{\Delta}+1-u\right)^{1+\mu} - (1-u)^{1+\mu} - \left(\frac{\delta}{\Delta}-u\right)^{1+\mu}\right|^{\alpha}du + \int_{\delta/\Delta}^{1}\left|\left(\frac{\delta}{\Delta}+1-u\right)^{1+\mu} - (1-u)^{1+\mu}\right|^{\alpha}du + \int_1^{1+\delta/\Delta}\left(\frac{\delta}{\Delta}+1-u\right)^{\alpha+\alpha\mu}du\right] \quad (2)$$

where $\mu = H - 1/\alpha$, and μ is the memory parameter. Along each direction, the signal attenuation at each voxel is fitted to **Equation 1** separately. We used the trust-region-reflective non-linear fitting algorithm in MATLAB (MathWorks, Natick, MA) to perform the fitting procedures.

A metric similar to FA, called gFA, is introduced to quantify anisotropy, where the sample standard deviation is divided by the root mean square [35]:

$$gFA(V) = \sqrt{\frac{N}{N-1}\frac{\sum_{i=1}^{N}(V_i-\overline{V})^2}{\sum_{i=1}^{N}V_i^2}} \quad (3)$$

where N represents the number of sampling directions, including three directions in this research, and V refers to the parameter values to be measured. $\overline{V}$ is the directionally averaged value, and V_i is the value in the i-th direction. The gFA maps of α, H, and ADC were calculated.

Statistical Analysis

Among the mild AD group, moderate AD group, and healthy control group, gender was analyzed using the chi-square (χ^2) test, and the age, education, and MMSE score were compared using one-way ANOVA. The MoCA score was compared using a two-sample t-test between the mild AD group and moderate AD group, since the MoCA score was not assessed in healthy control. Except for gender, the data were shown in the form of mean ± SD.

The gFA values of α, H, and ADC were compared using a one-way ANOVA test and *post-hoc* Tukey test among the healthy group, mild AD group, and moderate AD group. Moreover, receiver-operating characteristic (ROC) curves were performed to evaluate the diagnostic capability of each gFA value in differentiating AD patients from healthy controls and distinguishing mild AD patients from moderate AD patients by the area under the curve (AUC). Additionally, multivariate logistic regression analysis was utilized to assess the diagnostic performances of the combination of the anisotropy value and the directionally averaged value. For example, the probability of the combination of H and gFA(H) can be expressed as

$$P(\text{high}-\text{grade}|\{\text{gFA}(\alpha),\ \text{gFA}(H)\}) = \frac{\exp(a_0 + a_1\text{gFA}(\alpha) + a_2\text{gFA}(H))}{1+\exp(a_0 + a_1\text{gFA}(\alpha) + a_2\text{gFA}(H))} \quad (4)$$

where a_1 and a_2 are the regression coeffcients for H and gFA(H), respectively, and a_0 is a constant. The probabilities of other combinations can be expressed in a similar method. These probability values were used as the test variables in the ROC analysis.

In AD patients, the correlations between gFA(α), gFA(H), and gFA(ADC) values and the cognitive functions evaluated by MMSE and MoCA scales were investigated using Pearson correlation analysis. P-values < 0.05 were considered statistically significant.

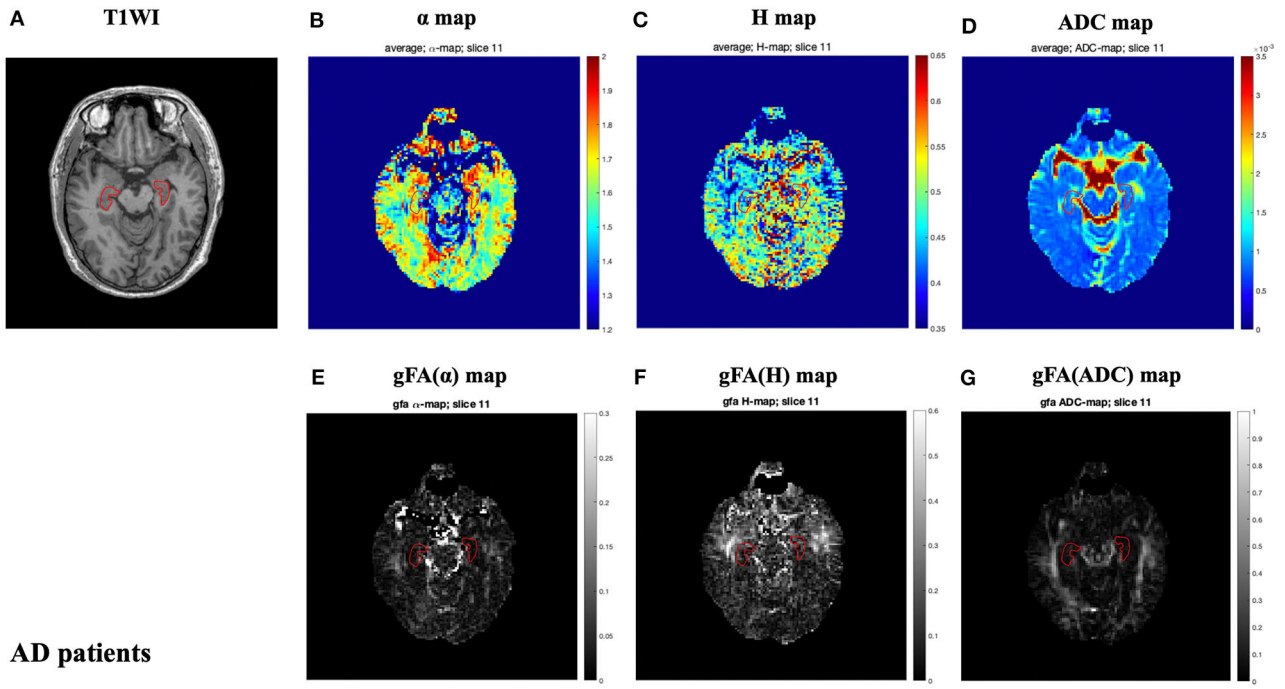

FIGURE 2 | A 58-year-old male patient with AD. Top row: T1-weighed image **(A)** and directionally averaged maps of α, H, and ADC [**(B–D)**, respectively]. Bottom row: generalized fractional anisotropy (gFA) maps of α, H, and ADC [**(E–G)**, respectively]. The bilateral hippocampus is shown with red outlines in all maps. AD, Alzheimer's disease; ADC, apparent diffusion coefficient; gFA, generalized fractional anisotropy.

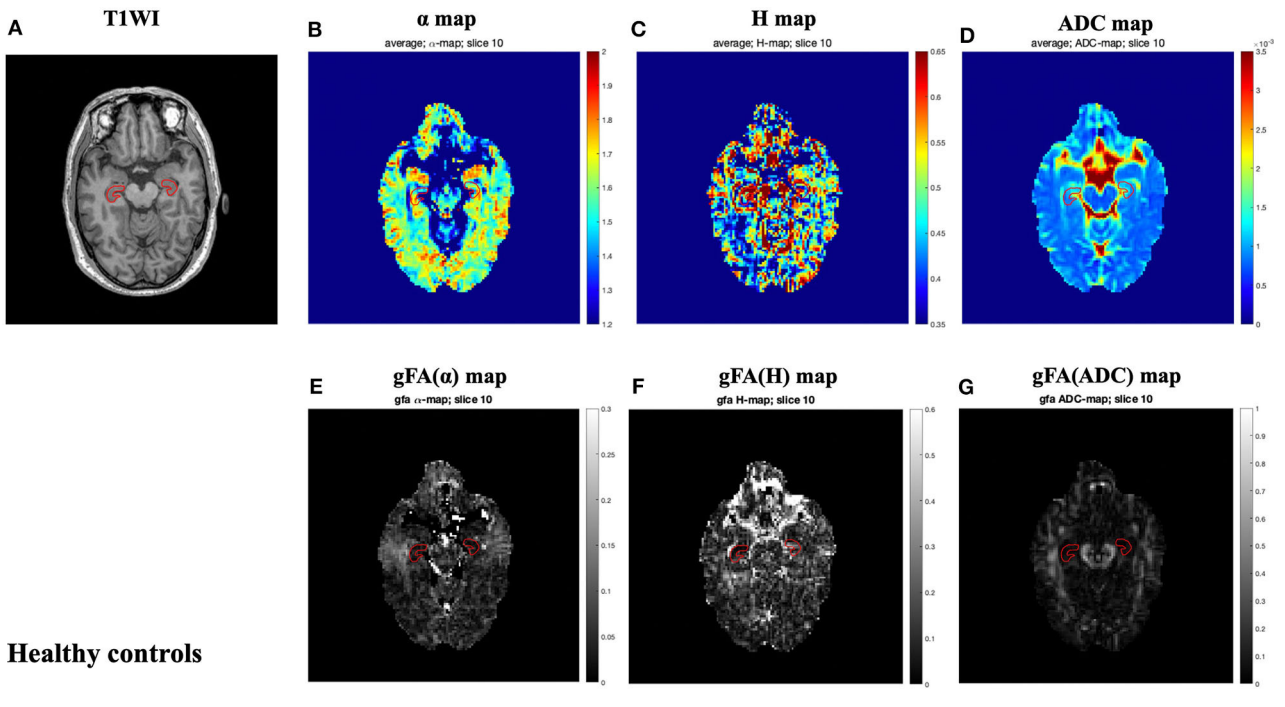

FIGURE 3 | A 60-year-old male healthy control. Top row: axial T1-weighed image **(A)** and directionally averaged maps of α, H, and ADC [**(B–D)**, respectively]. Bottom row: gFA maps of α, H, and ADC [**(E–G)**, respectively]. The bilateral hippocampus is shown with red outlines in all maps. ADC, apparent diffusion coefficient; gFA, generalized fractional anisotropy.

RESULTS

Characteristics of All Subjects

The demographic information and clinical cognition scores in all subjects are summarized in **Table 1**. Ultimately, 24 AD patients (69.0 ± 8.1 years) and 11 healthy controls (65.3 ± 6.6 years) were enrolled in this study. Then patients with AD were divided into two groups [the mild AD group (six males and six females, mean age 65.8 ± 10.1 years) and the moderate AD group (three males and nine females, mean age 72.1 ± 3.8 years)] according to their MMSE score and education level. The general division criteria are as follows: 21 ≤ MMSE score ≤ 25 was considered as mild AD, and 11 ≤ MMSE score ≤ 20 was considered as moderate AD (Perneczky et al., 2006). As demonstrated in **Table 1**, the age, gender, and education level of the three groups were matched ($P > 0.05$), while there was a significant difference in the MMSE score among the three groups ($P < 0.05$). MoCA score was significantly different between the mild AD group and moderate AD group, and a significant difference was found between the two groups ($P < 0.05$).

The locations of the bilateral hippocampus in the T1-weighted image are shown in **Figure 1**. **Figures 2**, **3** show the representative maps of a 58-year-old male patient with AD and a 60-year-old male healthy patient, including the 3D T1-weighted images; directionally averaged maps of α, H, and ADC; and the gFA maps of α, H, and ADC. From **Figures 2**, **3**, we found that there no outstanding contrasts between the hippocampus and other brain regions were observed by the naked eye.

Comparisons of gFA(α), gFA(H), and gFA(ADC) Values Among Three Groups

The gFA values of α, H, and ADC of the left and right hippocampus in all participants are summarized in **Table 2**. Data are presented in the form of mean ± SD. The comparisons among three groups in gFA(α), gFA(H), and gFA(ADC) are shown in **Figure 4**. From **Figure 4**, we found that the gFA(α) and gFA(H) values of the moderate AD group were higher than those of the mild AD group ($P = 0.003$, $P = 0.008$, separately) in the left ROI (**Figures 4A,C**). We also found that the gFA(α) values of the moderate AD group were higher than those of the healthy control group ($P < 0.001$, $P = 0.003$, separately, **Figures 4A,B**) in the bilateral ROI, and the gFA(ADC) values of the moderate AD group were lower than those of the healthy control group and mild AD group in the right ROI ($P = 0.038$, $P = 0.035$, separately, **Figure 4F**). No significant differences were found between the healthy control group and mild AD group ($P > 0.05$ for all, **Figures 4A–F**).

The performances in differentiating mild AD and moderate AD were illustrated by ROC analysis. **Figure 5** depicts the ROC curves calculated from individual gFA values and directionally averaged maps of α, H, and ADC. **Figure 5** shows that gFA(α) (AUC = 0.833) and gFA(H) (AUC = 0.826) of the left ROI and gFA(ADC) (AUC = 0.764) of the right ROI exhibited good capacity to differentiate the two groups. The other anisotropy measures of gFA parameters did not perform well. **Figure 6** demonstrates the ROC curves calculated by combinations of different parameters, and some positive results were elucidated. More specifically, {α, gFA(α)} and {α, gFA(α), H, gFA(H)} of the bilateral ROI and {H, gFA(H)} and {gF(α) + gFA(H)} of the left ROI showed inspiring potencies in differentiating mild AD and moderate AD. It was noteworthy that, by combining the anisotropy information, the α combination {α, gFA(α)} (AUC = 0.806, left ROI; AUC = 0.819, right ROI) and the H combination {H, gFA(H)} (AUC = 0.861, left ROI; AUC = 0.549, right ROI) were significantly superior to the separate performances of the individual directionally averaged α (AUC = 0.674, left ROI; AUC = 813, right ROI) or H (AUC = 0.524, left ROI; AUC = 0.569, right ROI).

Similarly, ROC analysis in differentiating AD patients and healthy controls was also made. **Figure 7** presents the ROC curves calculated from the individual gFA values and directionally averaged maps of α, H, and ADC for differentiating AD patients and healthy controls. As depicted in **Figure 7**, gFA(α) (AUC = 0.801, left ROI; AUC = 0.758, right ROI) values of the bilateral ROI exhibited a good capacity to differentiate the two groups. The anisotropy measures of gFA(H) and gFA(ADC) did not perform well. **Figure 8** shows the ROC curves calculated from the combinations of different parameters, and the results validated some significant findings. Specifically, {α, gFA(α)}, {gF(α) + gFA(H)}, and {α, gFA(α), H, gFA(H)} of the bilateral ROI can perfectly separate AD patients and healthy controls. By combining the anisotropy information, the α combination {α, gFA(α)} (AUC = 0.852, left ROI; AUC = 0.826, right ROI) outperformed the individual directionally averaged α (AUC = 0.780, left ROI; AUC = 0.811, right ROI).

Correlations Between Fractional Motion-Related Parameters and Mini-Mental State Examination Scores and Montreal Cognitive Assessment Scores

Figure 9 shows that the gFA(α) and gFA(H) values of the left hippocampus were negatively correlated to corresponding MMSE score ($P = 0.017$, $P = 0.037$, respectively) in patients with AD. However, the correlations were not so strong, and there was no significant correlation after false discovery rate (FDR) correction and family-wise error rate (FWER) correction. Moreover, no significant correlations were found in other gFA parameters.

DISCUSSION

In the current study, we investigated the feasibility and effectiveness of the anisotropy of anomalous diffusion assessed by the FM model to differentiate and grade AD patients. We introduced a new anisotropy metric called gFA, and we explored its potencies in identifying AD patients and healthy controls and distinguishing mild AD and moderate AD patients. Our results demonstrated that the anisotropy of α and H of the left ROI exhibited good performances to grade AD patients, and the anisotropy of α of the bilateral ROI

TABLE 2 | Mean and SD of the gFA(α), gFA(H), and gFA(ADC) values of left and right hippocampus in all participants.

Subjects	No.	ROIs	gFA(α)	gFA(H)	gFA(ADC)
Controls	11	Left-hippocampus	0.0403 ± 0.0088	0.1588 ± 0.0431	0.0859 ± 0.0340
		Right-hippocampus	0.0390 ± 0.0066	0.1497 ± 0.0364	0.0770 ± 0.0075
Mild AD	12	Left-hippocampus	0.0451 ± 0.0069	0.1443 ± 0.0244	0.0705 ± 0.0102
		Right-hippocampus	0.0461 ± 0.0143	0.1542 ± 0.0351	0.0787 ± 0.0126
Moderate AD	12	Left-hippocampus	0.0573 ± 0.0105	0.1829 ± 0.0393	0.0695 ± 0.0144
		Right-hippocampus	0.0555 ± 0.0150	0.1667 ± 0.0539	0.0663 ± 0.0144

SD, standard deviation; gFA, generalized fractional anisotropy; ADC, apparent diffusion coefficient; AD, Alzheimer's disease; ROI, region of interest.

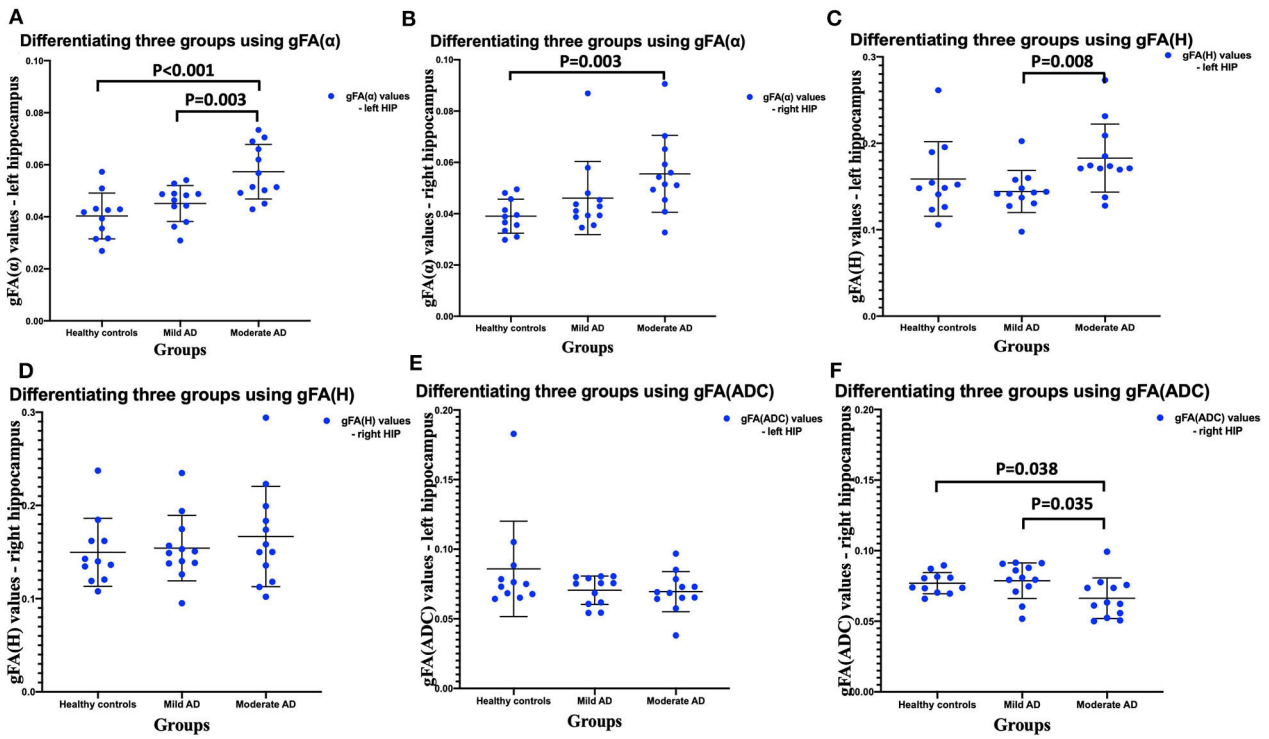

FIGURE 4 | Comparisons among three groups: healthy control group, mild AD patient group, and moderate AD patient group **(A–F)**. Scatter plots show that gFA(α) and gFA(H) of the left hippocampus **(A,C)**, and gFA(ADC) values of the right hippocampus **(F)** can readily separate the mild AD patients and moderate AD patients, and gFA(α) of the bilateral hippocampus **(A,B)**, gFA(ADC) values of right hippocampus **(F)** can easily distinguish the moderate AD patients and healthy controls. n = 12 for mild AD patients, n = 12 for moderate AD patients, and n = 11 for healthy controls. $P < 0.05$ was considered as significant. AD, Alzheimer's disease; gFA, generalized fractional anisotropy; ADC, apparent diffusion coefficient.

possessed good potencies to differentiate AD patients and healthy controls. It was worth noting that the diagnostic accuracy was increased when combined with the anisotropy metric with the commonly used directionally averaged value, indicating that the anisotropy metric could improve the diagnostic performances of directionally averaged values in identifying and grading AD patients.

An important finding in the present study was that the anisotropy of α and H showed significant superiority to distinguish mild AD and moderate AD patients and identify AD patients from healthy controls, in particular the α. In combination with the results of our previous study (Du et al., 2020), we reached a conclusion that both directionally averaged value and the anisotropy value of α exhibited excellent capacity to identify and grade AD patients, which indicated that α-related values may possess a specific advantage in the diagnosis and grading of AD. In line with the currently available data, α-related diffusion values probably already provide sufficient information regarding the differentiation and classification of AD, which is beneficial to shorten the scan time, simplify the test procedure, and improve medical efficiency. However, it should be validated by future studies with larger sample size.

Possible explanations for the diagnostic performance of gFA(α) are as follows. The symbol α describes the fluctuations

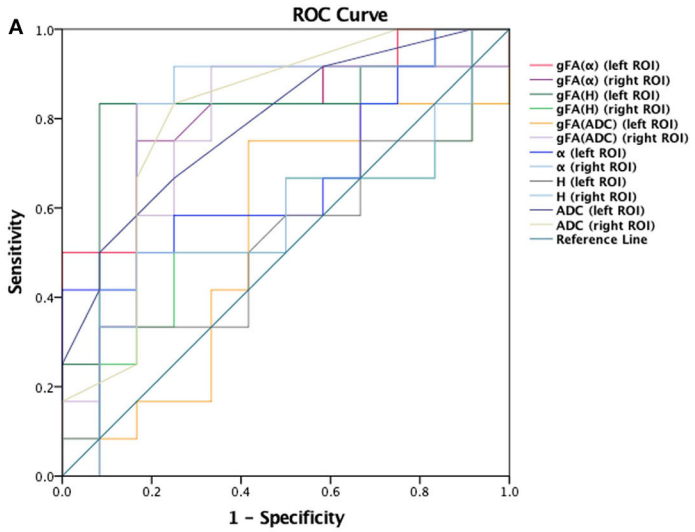

B

ROIs	AUC
L-hippocampus (gFA (α))	0.833
R-hippocampus (gFA (α))	0.753
L-hippocampus (gFA (H))	0.826
R-hippocampus (gFA (H))	0.549
L-hippocampus (gFA (ADC))	0.542
R-hippocampus (gFA (ADC))	0.764
L-hippocampus (α)	0.674
R-hippocampus (α)	0.813
L-hippocampus (H)	0.524
R-hippocampus (H)	0.569
L-hippocampus (ADC)	0.792
R-hippocampus (ADC)	0.806

FIGURE 5 | Receiver-operating characteristic (ROC) curve was generated using the individual gFA values and directionally averaged values of α, *H*, and ADC for differentiating mild and moderate AD patients ($n = 12$ in each group). **(A,B)** The area under the curve (AUC) of gFA(α) and gFA(*H*) values of the left hippocampus (AUC = 0.833, AUC = 0.826, separately) were larger than those of others. ROC, receiver operating characteristic; ROI, region of interest; gFA, generalized fractional anisotropy; ADC, apparent diffusion coefficient; AD, Alzheimer's disease; AUC, area under the curve.

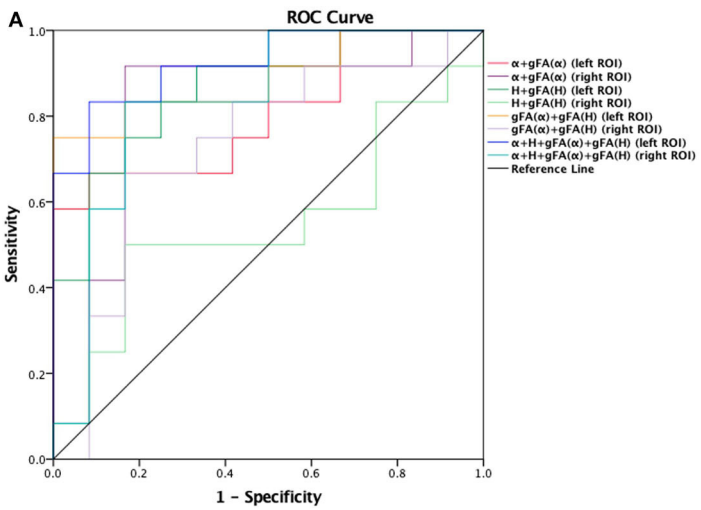

B

ROIs	AUC
L-hippocampus (α+gFA (α))	0.806
R-hippocampus (α+gFA (α))	0.819
L-hippocampus (H+gFA (H))	0.861
R-hippocampus (H+gFA (H))	0.549
L-hippocampus (gFA (α)+gFA (H))	0.889
R-hippocampus (gFA (α)+gFA (H))	0.729
L-hippocampus (α+H+gFA (α)+gFA (H))	0.924
R-hippocampus (α+H+gFA (α)+gFA (H))	0.833

FIGURE 6 | Receiver-operating characteristic (ROC) curve was generated using the combination of gFA values and averaged values of α, *H*, and ADC for differentiating mild and moderate AD patients ($n = 12$ in each group). **(A,B)** The combinations {α, gFA(α)} and {α, gFA(α), *H*, gFA(*H*)} of the bilateral ROI and {*H*, gFA(*H*)} and {gF(α) + gFA(*H*)} of the left ROI perfectly differentiate mild AD and moderate AD patients. The α combination {α, gFA(α)} and the *H* combination {*H*, gFA(*H*)} outperformed the directionally averaged α and *H*, respectively. ROC, receiver operating characteristic; ROI, region of interest; AUC, area under the curve; gFA, generalized fractional anisotropy; ADC, apparent diffusion coefficient; AD, Alzheimer's disease.

of the random process. Excessive deposition of Aβ protein and neurofibrillary tangles in brain tissue are two main pathological changes in AD patients and can lead to neuronal apoptosis (Wang et al., 2015). These pathological alterations that emerged along with AD progression can result in subsequent neuronal apoptosis and encephalatrophy, which eventually reduce the volume of affected brain regions (especially the hippocampus). Moreover, it is well acknowledged that the α values depend on the structural complexity of the brain regions. The non-Gaussian water molecule diffusion is more active in a more complex brain region, and accordingly, the measured α values would be higher and gFA(α) values would be lower. Consistently, the degenerative pathological alterations (neuronal apoptosis and encephalatrophy) that occurred in AD progression can markedly decrease the structural complexity of the hippocampus (Jensen et al., 2005; Grinberg et al., 2011; Yoshida et al., 2013) and

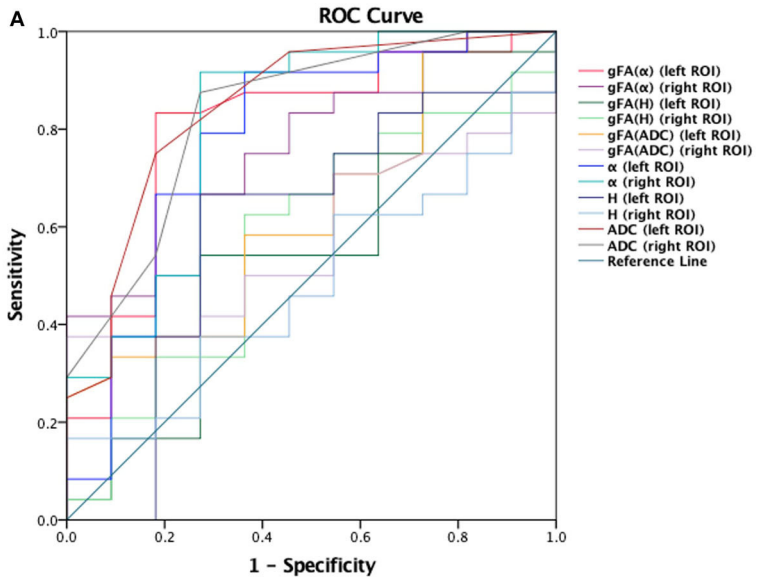

B

ROIs	AUC
L-hippocampus (gFA (α))	0.801
R-hippocampus (gFA (α))	0.758
L-hippocampus (gFA (H))	0.561
R-hippocampus (gFA (H))	0.576
L-hippocampus (gFA (ADC))	0.629
R-hippocampus (gFA (ADC))	0.578
L-hippocampus (α)	0.780
R-hippocampus (α)	0.811
L-hippocampus (H)	0.598
R-hippocampus (H)	0.519
L-hippocampus (ADC)	0.847
R-hippocampus (ADC)	0.833

FIGURE 7 | Receiver-operating characteristic (ROC) curve was generated using the individual gFA values and directionally averaged values of α, H, and ADC for differentiating healthy controls and AD patients. **(A,B)** The area under the curve (AUC) of gFA(α) values of the bilateral hippocampus (AUC = 0.801, AUC = 0.758, separately) was larger. ROC, receiver operating characteristic; ROI, region of interest; gFA, generalized fractional anisotropy; ADC, apparent diffusion coefficient; AD, Alzheimer's disease; AUC, area under the curve.

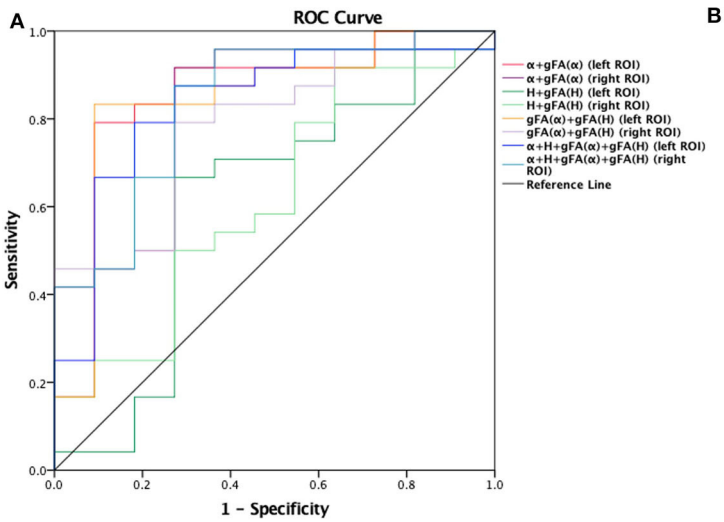

B

ROIs	AUC
L-hippocampus (α+gFA (α))	0.852
R-hippocampus (α+gFA (α))	0.826
L-hippocampus (H+gFA (H))	0.606
R-hippocampus (H+gFA (H))	0.617
L-hippocampus (gFA (α)+gFA (H))	0.845
R-hippocampus (gFA (α)+gFA (H))	0.788
L-hippocampus (α+H+gFA (α)+gFA (H))	0.833
R-hippocampus (α+H+gFA (α)+gFA (H))	0.837

FIGURE 8 | Receiver-operating characteristic (ROC) curve was generated using the combination of gFA values and averaged values of α, H, and ADC for differentiating AD patients and healthy controls ($n = 24$, $n = 11$, respectively). **(A,B)** The combinations {α, gFA(α)}, {gF(α) + gFA(H)}, and {α, gFA(α), H, gFA(H)} of the bilateral ROI perfectly separated AD patients and healthy controls. The α combination {α, gFA(α)} outperformed the directionally averaged α. ROC, receiver operating characteristic; ROI, region of interest; AUC, area under the curve; gFA, generalized fractional anisotropy; ADC, apparent diffusion coefficient; AD, Alzheimer's disease.

can manifest as different α values and gFA(α) values among healthy controls, mild AD, and moderate AD patients, which were observed in the current study.

Compared with other commonly used traditional techniques, such as DTI, using the FM model to calculate anisotropy of anomalous diffusion possesses several potential advantages. On the one hand, DTI quantifies the diffusion process of water molecule using a mono-exponential form. However, the observed dMRI signal decay curve in the brain deviates from the mono-exponential form. In this regard, the FM model was introduced and showed a better agreement between the measured signal decay curve and the fitted curves (Magin et al., 2008). On the other hand, the detected diffusion-time dependence of the MR signal shows a non-Gaussian nature of diffusion, while the DTI

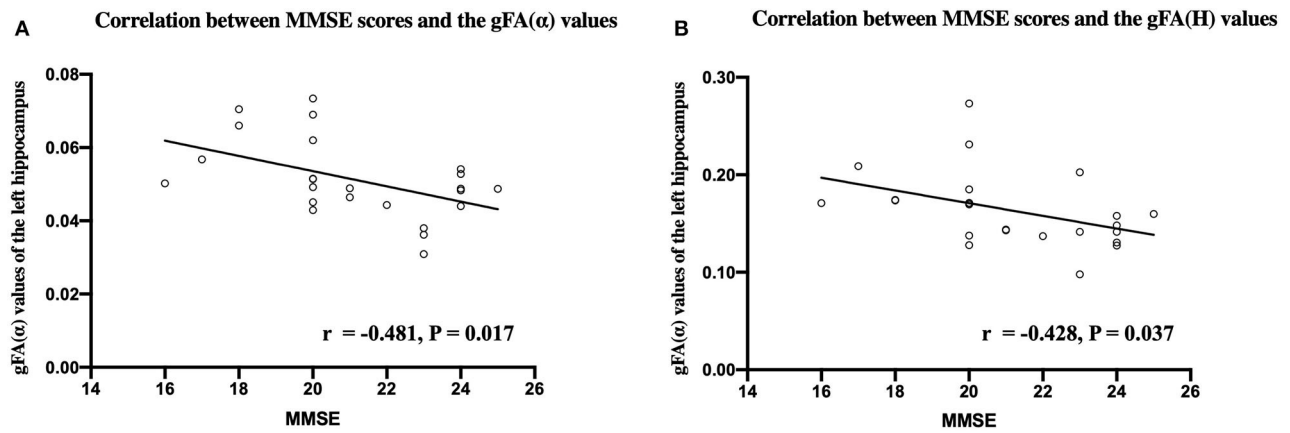

FIGURE 9 | Correlations between MMSE scores and the gFA(α) **(A)** and gFA(H) **(B)** values of the left hippocampus in patients with AD. Pearson correlation was conducted. $n = 24$. MMSE, mini-mental state examination; gFA, generalized fractional anisotropy; AD, Alzheimer's disease.

model assumes the molecular displacement in brain tissues with a 3D Gaussian ellipsoid (Fieremans et al., 2016). This defect was circumvented by the FM model.

The feasibility and effectiveness of anisotropy calculated by the FM model have been verified in this research. But potential clinical applications are not limited to the FM model. As shown in **Equation 1**, the α is an exponent of the diffusion gradient, which is proportional to the parameters of other dMRI models, like the stretching parameter γ in the stretched-exponential model (Bennett et al., 2003; Hall and Barrick, 2008; Zhou et al., 2010). Therefore, the clinical feasibility of anisotropy may be generalized to the α-like parameters of other models because of the intrinsic consistency of their anisotropic properties (Xu et al., 2017a).

The current results indicated that the gFA(α) and gFA(H) values of the left hippocampus were negatively correlated with MMSE score in patients with AD. This finding was partially consistent with the results of our previous study using directionally averaged values (Du et al., 2020), which further provided evidence for the reliability and repeatability of our findings. However, the correlations were not so strong and even not significant after FDR and FWER correction. This may be explained by the following reasons. In addition to the hippocampus, pathological alterations of AD affected other brain regions such as the prefrontal cortex and basal ganglion region, which synergistically contributed to cognitive impairments in AD patients. So there might be no linear relationship between cognitive scores and anisotropic values in the hippocampus. Moreover, the small sample size of this study may also affect the results, and further researches with larger sample size are needed to confirm these findings.

The limitations of the present study must be acknowledged. First, this is a single-institution study with a limited number of healthy controls and AD patients, and the results should be validated by further study with larger samples. We hope the independent validation of our results can be done at separated institutions. Second, the voxel of imaging is large, and a single voxel displays an average measurement of neuronal environment, which may decrease the sensitivity for brain tissue components occupying a small part of a voxel. Third, the x-, y-, and z-axes are the only three directions being applied by the diffusion gradients, and the accuracy of this study may be affected, as increased sampling directions are conducive to measuring the anisotropy of anomalous diffusion.

CONCLUSIONS

In summary, the anisotropy of anomalous diffusion was successfully applied in differentiating and grading patients with AD. It was worth noting that the diagnostic performance was improved when the anisotropy metric was combined with commonly used directionally averaged value in identifying and grading AD patients. The anisotropy of anomalous diffusion calculated by the FM model may provide novel insights to profoundly elucidate the neuropathology process of AD.

DATA AVAILABILITY STATEMENT

The original contributions presented in the study are included in the article/Supplementary Materials, further inquiries can be directed to the corresponding author.

ETHICS STATEMENT

The studies involving human participants were reviewed and approved by China-Japan Friendship Hospital. The participants provided their written informed consent to participate in this study. Written informed consent was obtained from the individuals for the publication of any potentially identifiable images or data included in this article.

AUTHOR CONTRIBUTIONS

LD, ZZ, and BX designed this research, analyzed the MRI data, and drafted this manuscript. SS, WG, XL, YC, YW,

JL, and BL did the MRI scanning. BX and JG wrote and revised the content of the FM model theory, separately. GM revised the whole manuscript. All authors approved the final manuscript.

FUNDING

This research was supported by the National Key Research and Development Program of China (Nos. 2020YFC2003903, 2019YFC0120903, and 2016YFC1307001) and grants from the National Natural Science Foundation of China (NSFC) (Nos. 81971585, 81571641, and 91959123).

ACKNOWLEDGMENTS

We thank all the patients with AD and healthy controls who participated in our study. The authors thank Dr. Lizhi Xie from GE Healthcare for help in solving MR technical problems.

REFERENCES

Alzheimer's, Association (2016). 2016 Alzheimer's disease facts and figures. *Alzheimers Dement* 12, 459–509. doi: 10.1016/j.jalz.2016.03.001

Anckaerts, C., Blockx, I., Summer, P., Michael, J., Hamaide, J., Kreutzer, C., et al. (2019). Early functional connectivity deficits and progressive microstructural alterations in the TgF344-AD rat model of Alzheimer's Disease: a longitudinal MRI study. *Neurobiol. Dis.* 124, 93–107. doi: 10.1016/j.nbd.2018.11.010

Basser, P. J., Mattiello, J., and LeBihan, D. (1994a). Estimation of the effective self-diffusion tensor from the NMR spin echo. *J. Magn. Reson. B* 103, 247–254. doi: 10.1006/jmrb.1994.1037

Basser, P. J., Mattiello, J., and LeBihan, D. (1994b). MR diffusion tensor spectroscopy and imaging. *Biophys. J.* 66, 259–267. doi: 10.1016/S0006-3495(94)80775-1

Beaulieu, C. (2002). The basis of anisotropic water diffusion in the nervous system - a technical review. *NMR Biomed.* 15, 435–455. doi: 10.1002/nbm.782

Bennett, K. M., Schmainda, K. M., Bennett, R. T., Rowe, D. B., Lu, H., and Hyde, J. S. (2003). Characterization of continuously distributed cortical water diffusion rates with a stretched-exponential model. *Magn. Reson. Med.* 50, 727–734. doi: 10.1002/mrm.10581

Bergamino, M., Nespodzany, A., Baxter, L. C., Burke, A., Caselli, R. J., Sabbagh, M. N., et al. (2020). Preliminary assessment of intravoxel incoherent motion diffusion-weighted MRI (IVIM-DWI) metrics in Alzheimer's disease. *J. Magn. Reson. Imaging* 4:e27272. doi: 10.1002/jmri.27272

Bouts, M., Moller, C., Hafkemeijer, A., van Swieten, J. C., Dopper, E., van der Flier, W. M., et al. (2018). Single subject classification of alzheimer's disease and behavioral variant frontotemporal dementia using anatomical, diffusion tensor, and resting-state functional magnetic resonance imaging. *J. Alzheimers Dis.* 62, 1827–1839. doi: 10.3233/JAD-170893

Braak, H., and Braak, E. (1991). Neuropathological stageing of Alzheimer-related changes. *Acta Neuropathol.* 82, 239–259. doi: 10.1007/bf00308809

Brueggen, K., Dyrba, M., Cardenas-Blanco, A., Schneider, A., Fliessbach, K., Buerger, K., et al. (2019). Structural integrity in subjective cognitive decline, mild cognitive impairment and Alzheimer's disease based on multicenter diffusion tensor imaging. *J. Neurol.* 266, 2465–2474. doi: 10.1007/s00415-019-09429-3

Burnecki, K., and Weron, A. (2010). Fractional Levy stable motion can model subdiffusive dynamics. *Phys. Rev. E Stat. Nonlin. Soft Matter Phys.* 82:021130. doi: 10.1103/PhysRevE.82.021130

Cha, S. (2006). Update on brain tumor imaging: from anatomy to physiology. *AJNR Am. J. Neuroradiol.* 27, 475–487.

Cummings, J. (2017). Disease modification and neuroprotection in neurodegenerative disorders. *Transl. Neurodegener.* 6:25. doi: 10.1186/s40035-017-0096-2

De Santis, S., Gabrielli, A., Bozzali, M., Maraviglia, B., Macaluso, E., and Capuani, S. (2011). Anisotropic anomalous diffusion assessed in the human brain by scalar invariant indices. *Magn. Reson. Med.* 65, 1043–1052. doi: 10.1002/mrm.22689

Du, L., Xu, B., Zhao, Z., Han, X., Gao, W., Shi, S., et al. (2020). Identification and classification of Alzheimer's disease patients using novel fractional motion model. *Front. Neurosci.* 14:767. doi: 10.3389/fnins.2020.00767

Dyrba, M., Barkhof, F., Fellgiebel, A., Filippi, M., Hausner, L., Hauenstein, K., et al. (2015). Predicting prodromal Alzheimer's disease in subjects with mild cognitive impairment using machine learning classification of multimodal multicenter diffusion-tensor and magnetic resonance imaging data. *J. Neuroimaging* 25, 738–747. doi: 10.1111/jon.12214

Fieremans, E., Burcaw, L. M., Lee, H. H., Lemberskiy, G., Veraart, J., and Novikov, D. S. (2016). *In vivo* observation and biophysical interpretation of time-dependent diffusion in human white matter. *Neuroimage* 129, 414–427. doi: 10.1016/j.neuroimage.2016.01.018

Finsterwalder, S., Vlegels, N., Gesierich, B., Araque Caballero, M. A., Weaver, N. A., Franzmeier, N., et al. (2020). Small vessel disease more than Alzheimer's disease determines diffusion MRI alterations in memory clinic patients. *Alzheimers Dement*. 18. doi: 10.1002/alz.12150

Folstein, M. F., Folstein, S. E., and McHugh, P. R. (1975). "Mini-mental state". A practical method for grading the cognitive state of patients for the clinician. *J. Psychiatr. Res.* 12, 189–198. doi: 10.1016/0022-3956(75)90026-6

Grinberg, F., Farrher, E., Kaffanke, J., Oros-Peusquens, A. M., and Shah, N. J. (2011). Non-Gaussian diffusion in human brain tissue at high b-factors as examined by a combined diffusion kurtosis and biexponential diffusion tensor analysis. *Neuroimage* 57, 1087–1102. doi: 10.1016/j.neuroimage.2011.04.050

Hall, M. G., and Barrick, T. R. (2008). From diffusion-weighted MRI to anomalous diffusion imaging. *Magn. Reson. Med.* 59, 447–455. doi: 10.1002/mrm.21453

Hall, M. G., and Barrick, T. R. (2012). Two-step anomalous diffusion tensor imaging. *NMR Biomed.* 25, 286–294. doi: 10.1002/nbm.1747

Harrison, J. R., Bhatia, S., Tan, Z. X., Mirza-Davies, A., Benkert, H., Tax, C. M. W., et al. (2020). Imaging Alzheimer's genetic risk using diffusion MRI: a systematic review. *Neuroimage Clin.* 27:102359. doi: 10.1016/j.nicl.2020.102359

Hong, Y. J., Yoon, B., Lim, S. C., Shim, Y. S., Kim, J. Y., Ahn, K. J., et al. (2013). Microstructural changes in the hippocampus and posterior cingulate in mild cognitive impairment and Alzheimer's disease: a diffusion tensor imaging study. *Neurol. Sci.* 34, 1215–1221. doi: 10.1007/s10072-012-1225-4

Hyman, B. T., Van Hoesen, G. W., Damasio, A. R., and Barnes, C. L. (1984). Alzheimer's disease: cell-specific pathology isolates the hippocampal formation. *Science* 225, 1168–1170. doi: 10.1126/science.6474172

Ingo, C., Magin, R. L., Colon-Perez, L., Triplett, W., and Mareci, T. H. (2014). On random walks and entropy in diffusion-weighted magnetic resonance imaging studies of neural tissue. *Magn. Reson. Med.* 71, 617–627. doi: 10.1002/mrm.24706

Jensen, J. H., Helpern, J. A., Ramani, A., Lu, H., and Kaczynski, K. (2005). Diffusional kurtosis imaging: the quantification of non-gaussian water diffusion by means of magnetic resonance imaging. *Magn. Reson. Med.* 53, 1432–1440. doi: 10.1002/mrm.20508

Karaman, M. M., Sui, Y., Wang, H., Magin, R. L., Li, Y., and Zhou, X. J. (2016). Differentiating low- and high-grade pediatric brain tumors using a continuous-time random-walk diffusion model at high b-values. *Magn. Reson. Med.* 76, 1149–1157. doi: 10.1002/mrm.26012

Khan, A., Corbett, A., and Ballard, C. (2017). Emerging treatments for Alzheimer's disease for non-amyloid and non-tau targets. *Expert Rev. Neurother.* 17, 683–695. doi: 10.1080/14737175.2017.1326818

Kidd, M. (1963). Paired helical filaments in electron microscopy of Alzheimer's disease. *Nature* 197, 192–193. doi: 10.1038/197192b0

Kwee, T. C., Galban, C. J., Tsien, C., Junck, L., Sundgren, P. C., Ivancevic, M. K., et al. (2010a). Comparison of apparent diffusion coefficients and distributed

diffusion coefficients in high-grade gliomas. *J. Magn. Reson. Imaging* 31, 531–537. doi: 10.1002/jmri.22070

Kwee, T. C., Galban, C. J., Tsien, C., Junck, L., Sundgren, P. C., Ivancevic, M. K., et al. (2010b). Intravoxel water diffusion heterogeneity imaging of human high-grade gliomas. *NMR Biomed*. 23, 179–187. doi: 10.1002/nbm.1441

La Rocca, M., Amoroso, N., Monaco, A., Bellotti, R., and Tangaro, S. (2018). A novel approach to brain connectivity reveals early structural changes in Alzheimer's disease. *Physiol. Meas*. 39:074005. doi: 10.1088/1361-6579/aacf1f

Le Bihan, D. (1995). Molecular diffusion, tissue microdynamics and microstructure. *NMR Biomed*. 8, 375–386. doi: 10.1002/nbm.1940080711

Le Bihan, D., and Johansen-Berg, H. (2012). Diffusion MRI at 25: exploring brain tissue structure and function. *Neuroimage* 61, 324–341. doi: 10.1016/j.neuroimage.2011.11.006

Lee, P., Ryoo, H., Park, J., Jeong, Y., and Alzheimer's Disease Neuroimaging Initiative. (2017). Morphological and microstructural changes of the hippocampus in early MCI: a study utilizing the alzheimer's disease neuroimaging initiative database. *J. Clin. Neurol.* 13, 144–154. doi: 10.3988/jcn.2017.13.2.144

Magdziarz, M., Weron, A., Burnecki, K., and Klafter, J. (2009). Fractional brownian motion versus the continuous-time random walk: a simple test for subdiffusive dynamics. *Phys. Rev. Lett*. 103:180602. doi: 10.1103/PhysRevLett.103.180602

Magin, R. L., Abdullah, O., Baleanu, D., and Zhou, X. J. (2008). Anomalous diffusion expressed through fractional order differential operators in the Bloch-Torrey equation. *J. Magn. Reson*. 190, 255–270. doi: 10.1016/j.jmr.2007.11.007

Marcos Dolado, A., Gomez-Fernandez, C., Yus Fuertes, M., Barabash Bustelo, A., Marcos-Arribas, L., Lopez-Mico, C., et al. (2019). Diffusion tensor imaging measures of brain connectivity for the early diagnosis of Alzheimer's disease. *Brain Connect* 9, 594–603. doi: 10.1089/brain.2018.0635

Mattsson, N., Insel, P. S., Donohue, M., Jogi, J., Ossenkoppele, R., Olsson, T., et al. (2019). Predicting diagnosis and cognition with (18)F-AV-1451 tau PET and structural MRI in Alzheimer's disease. *Alzheimers Dement* 15, 570–580. doi: 10.1016/j.jalz.2018.12.001

Mayo, C. D., Mazerolle, E. L., Ritchie, L., Fisk, J. D., Gawryluk, J. R., and Alzheimer's Disease Neuroimaging Initiative. (2017). Longitudinal changes in microstructural white matter metrics in Alzheimer's disease. *Neuroimage Clin*. 13, 330–338. doi: 10.1016/j.nicl.2016.12.012

McKhann, G., Drachman, D., Folstein, M., Katzman, R., Price, D., and Stadlan, E. M. (1984). Clinical diagnosis of Alzheimer's disease: report of the NINCDS-ADRDA work group under the auspices of department of health and human services task force on Alzheimer's disease. *Neurology* 34, 939–944. doi: 10.1212/wnl.34.7.939

Mulkern, R. V., Gudbjartsson, H., Westin, C. F., Zengingonul, H. P., Gartner, W., Guttmann, C. R., et al. (1999). Multi-component apparent diffusion coefficients in human brain. *NMR Biomed*. 12, 51–62. doi: 10.1002/(sici)1099-1492(199902)12:1<51::aid-nbm546>3.0.co;2-e

Perneczky, R., Wagenpfeil, S., Komossa, K., Grimmer, T., Diehl, J., and Kurz, A. (2006). Mapping scores onto stages: mini-mental state examination and clinical dementia rating. *Am. J. Geriatr. Psychiatry* 14, 139–144. doi: 10.1097/01.JGP.0000192478.82189.a8

Reddy, P. H., and Oliver, D. M. (2019). Amyloid beta and phosphorylated tau-induced defective autophagy and mitophagy in Alzheimer's disease. *Cells* 8:488. doi: 10.3390/cells8050488

Schouten, T. M., Koini, M., Vos, F., Seiler, S., Rooij, M., Lechner, A., et al. (2017). Individual classification of Alzheimer's disease with diffusion magnetic resonance imaging. *Neuroimage* 152, 476–481. doi: 10.1016/j.neuroimage.2017.03.025

Sui, Y., Wang, H., Liu, G., Damen, F. W., Wanamaker, C., Li, Y., et al. (2015). Differentiation of low- and high-grade pediatric brain tumors with high b-value diffusion-weighted MR imaging and a fractional order calculus model. *Radiology* 277, 489–496. doi: 10.1148/radiol.2015142156

Takahashi, H., Ishii, K., Kashiwagi, N., Watanabe, Y., Tanaka, H., Murakami, T., et al. (2017). Clinical application of apparent diffusion coefficient mapping in voxel-based morphometry in the diagnosis of Alzheimer's disease. *Clin. Radiol.* 72, 108–115. doi: 10.1016/j.crad.2016.11.002

Tang, X., Qin, Y., Wu, J., Zhang, M., Zhu, W., and Miller, M. I. (2016). Shape and diffusion tensor imaging based integrative analysis of the hippocampus and the amygdala in Alzheimer's disease. *Magn. Reson. Imaging* 34, 1087–1099. doi: 10.1016/j.mri.2016.05.001

Tchalla, A. E., Clement, J. P., Saulnier, I., Beaumatin, B., Lachal, F., Gayot, C., et al. (2018). Predictors of rapid cognitive decline in patients with mild-to-moderate alzheimer disease: a prospective cohort study with 12-month follow-up performed in memory clinics. *Dement Geriatr. Cogn. Disord.* 45, 56–65. doi: 10.1159/000487938

Thiessen, J. D., Glazner, K. A., Nafez, S., Schellenberg, A. E., Buist, R., Martin, M., et al. (2010). Histochemical visualization and diffusion MRI at 7 Tesla in the TgCRND8 transgenic model of Alzheimer's disease. *Brain Struct. Funct.* 215, 29–36. doi: 10.1007/s00429-010-0271-z

Wang, D., Guo, Z. H., Liu, X. H., Li, Y. H., and Wang, H. (2015). Examination of hippocampal differences between Alzheimer disease, amnestic mild cognitive impairment and normal aging: diffusion kurtosis. *Curr. Alzheimer Res.* 12, 80–87. doi: 10.2174/1567205012666141218142422

Wegmann, S., Jung, Y. J., Chinnathambi, S., Mandelkow, E. M., Mandelkow, E., and Muller, D. J. (2010). Human Tau isoforms assemble into ribbon-like fibrils that display polymorphic structure and stability. *J. Biol. Chem*. 285, 27302–27313. doi: 10.1074/jbc.M110.145318

Weiss, M. (2013). Single-particle tracking data reveal anticorrelated fractional Brownian motion in crowded fluids. *Phys. Rev. E Stat. Nonlin. Soft Matter Phys*. 88:010101. doi: 10.1103/PhysRevE.88.010101

Wortmann, M. (2012). Dementia: a global health priority - highlights from an ADI and World Health Organization report. *Alzheimers Res. Ther*. 4:40. doi: 10.1186/alzrt143

Xu, B., Gong, G., Fan, Y., Wu, B., and Gao, J. H. (2017a). Directional sensitivity of anomalous diffusion in human brain assessed by tensorial fractional motion model. *Magn. Reson. Imaging* 42, 74–81. doi: 10.1016/j.mri.2017.05.006

Xu, B., Su, L., Wang, Z., Fan, Y., Gong, G., Zhu, W., et al. (2017b). Anomalous diffusion in cerebral glioma assessed using a fractional motion model. *Magn. Reson. Med*. 78, 1944–1949. doi: 10.1002/mrm.26581

Xu, B., Su, L., Wang, Z., Fan, Y., Gong, G., Zhu, W., et al. (2018). Anisotropy of anomalous diffusion improves the accuracy of differentiating low- and high-grade cerebral gliomas. *Magn. Reson. Imaging* 51, 14–19. doi: 10.1016/j.mri.2018.04.005

Xue, Y., Zhang, Z., Wen, C., Liu, H., Wang, S., Li, J., et al. (2019). Characterization of alzheimer's disease using ultra-high b-values apparent diffusion coefficient and diffusion kurtosis imaging. *Aging Dis*. 10, 1026–1036. doi: 10.14336/AD.2018.1129

Yablonskiy, D. A., Bretthorst, G. L., and Ackerman, J. J. (2003). Statistical model for diffusion attenuated MR signal. *Magn. Reson. Med*. 50, 664–669. doi: 10.1002/mrm.10578

Yoshida, S., Oishi, K., Faria, A. V., and Mori, S. (2013). Diffusion tensor imaging of normal brain development. *Pediatr. Radiol.* 43, 15–27. doi: 10.1007/s00247-012-2496-x

Zhou, X. J., Gao, Q., Abdullah, O., and Magin, R. L. (2010). Studies of anomalous diffusion in the human brain using fractional order calculus. *Magn. Reson. Med*. 63, 562–569. doi: 10.1002/mrm.22285

Conflict of Interest: BX was employed by Beijing Intelligent Brain Cloud Inc company.

The remaining authors declare that the research was conducted in the absence of any commercial or financial relationships that could be construed as a potential conflict of interest.

frontiers in Aging Neuroscience

ORIGINAL RESEARCH
published: 02 December 2020
doi: 10.3389/fnagi.2020.594002

Fornix Integrity Is Differently Associated With Cognition in Healthy Aging and Non-amnestic Mild Cognitive Impairment: A Pilot Diffusion Tensor Imaging Study in Thai Older Adults

Patcharaporn Srisaikaew[1,2], *Nahathai Wongpakaran*[3], *Nicole D. Anderson*[4,5], *J. Jean Chen*[4,6], *Suchart Kothan*[7], *Pairada Varnado*[3], *Kittisak Unsrisong*[8] *and Pasuk Mahakkanukrauh*[2,9]*

[1] Ph.D. Program in Anatomy, Faculty of Medicine, Chiang Mai University, Chiang Mai, Thailand, [2] Department of Anatomy, Faculty of Medicine, Chiang Mai University, Chiang Mai, Thailand, [3] Geriatric Psychiatry Unit, Department of Psychiatry, Faculty of Medicine, Chiang Mai University, Chiang Mai, Thailand, [4] Rotman Research Institute, Baycrest Health Science, Toronto, ON, Canada, [5] Department of Psychology and Psychiatry, University of Toronto, Toronto, ON, Canada, [6] Department of Medical Biophysics, University of Toronto, Toronto, ON, Canada, [7] Department of Radiologic Technology, Faculty of Associated Medical Sciences, Chiang Mai University, Chiang Mai, Thailand, [8] Department of Radiology, Faculty of Medicine, Chiang Mai University, Chiang Mai, Thailand, [9] Excellence in Osteology Research and Training Center (ORTC), Chiang Mai University, Chiang Mai, Thailand

OPEN ACCESS

Edited by:
Jiu Chen,
Nanjing Medical University, China

Reviewed by:
Andrew Budson,
VA Boston Healthcare System, United States
Arun Bokde,
Trinity College Dublin, Ireland

***Correspondence:**
Pasuk Mahakkanukrauh
pasuk034@gmail.com

Received: *12 August 2020*
Accepted: *02 November 2020*
Published: *02 December 2020*

Citation:
Srisaikaew P, Wongpakaran N, Anderson ND, Chen JJ, Kothan S, Varnado P, Unsrisong K and Mahakkanukrauh P (2020) Fornix Integrity Is Differently Associated With Cognition in Healthy Aging and Non-amnestic Mild Cognitive Impairment: A Pilot Diffusion Tensor Imaging Study in Thai Older Adults. Front. Aging Neurosci. 12:594002. doi: 10.3389/fnagi.2020.594002

Damage to the fornix leads to significant memory impairment and executive dysfunction and is associated with dementia risk. We sought to identify if fornix integrity and fiber length are disrupted in mild cognitive impairment (MCI) and how they associate with cognition. Data from 14 healthy older adult controls (HCs) and 17 subjects with non-amnestic MCI (n-aMCI) were analyzed. Diffusion tensor imaging (DTI) at 1.5 Tesla MRI was performed to enable manual tracing of the fornix and calculation of DTI parameters. Higher fractional anisotropy of body and column of the fornix was associated with better executive functioning and memory, more strongly in the HC than in the n-aMCI group. Fornix fiber tract length (FTL) was associated with better executive function, more strongly in the n-aMCI than in the HC group, and with better memory, more strongly in the HC than in the n-aMCI group. These results highlight a decline in the contributions of the fornix to cognition in n-aMCI and suggest that maintenance of fornix FTL is essential for sustaining executive functioning in people with n-aMCI.

Keywords: non-amnestic mild cognitive impairment (n-aMCI), fornix, diffusion tensor imaging (DTI), fractional anisotropy (FA), fiber tract length (FTL), cognitive performance, executive function, vascular dementia (VaD)

INTRODUCTION

Approximately 60% of the world's population lives in the Asia-Pacific region, where the prevalence of dementia is expected to rise from 23 million in 2015 to 71 million in 2050 (Venketasubramanian et al., 2010; Alzheimer's Disease International, 2014, 2018, 2019), among which vascular dementia (VaD) is more prevalent than in western populations. Mild cognitive impairment (MCI) is generally

considered the transitional state between healthy aging and dementia (Petersen et al., 2001; American Psychiatric Association, 2013; Anderson, 2019). The criteria for MCI (termed minor cognitive disorder by the American Psychiatric Association) include concerns about changes in cognition, impairment in one or more cognitive domains, preservation of independence in functional abilities, and no dementia (American Psychiatric Association, 2013). People with MCI can be categorized as amnestic (aMCI) or non-amnestic (n-aMCI). aMCI is likely to progress to Alzheimer's disease (AD), whereas n-aMCI most typically develops into other types of dementia, prominently into VaD but also into frontotemporal dementia (FTD) or Lewy body dementia (LBD), but can also progress to AD (Petersen et al., 1995; Farlow et al., 2004; Petersen, 2004). VaD is the second most common cause of dementia after AD, causing 20–30% of global dementia cases (Alzheimer's Disease International, 2014), 15–20% in North America and Europe (Plassman et al., 2007; Rizzi et al., 2014), and ∼30% in Asia (Jhoo et al., 2008; Chan et al., 2013).

VaD is usually caused by decreased blood flow to the brain, with the risk of incident dementia within 5 years being 6.5 times higher after a stroke and 1.5 times higher after a transient ischemic attack (TIA) (Pendlebury et al., 2019). In VaD, white matter (WM) inflammation is associated with oxidative stress, cerebral hypoperfusion, and thromboembolism (Venkat et al., 2015). Clinical signs and symptoms of VaD depend on the cause of VaD, affected areas, and size of infarction. A decrease in cerebral blood flow (CBF) and hypoxia in the prefrontal cortex (PFC), basal ganglia, and hippocampus is typically associated with cognitive decline and behavioral changes in VaD (Iadecola, 2013; Venkat et al., 2015). In a recent study, patients with small- and large-vessel VaD showed dysfunction in memory, executive function, and attention domains (Sengupta et al., 2019).

A WM tract that plays a major role in supporting these functional domains is the fornix, a discrete bidirectional tract bundle that connects the hippocampus to other limbic structures that is crucial for normal cognitive function and is a subcortical component of the limbic system (Teipel et al., 2008; Christiansen et al., 2016; Rabin et al., 2019). As a part of the fornix extends from the hippocampal–diencephalic system, the fornix plays an important role in the Papez circuit (Papez, 1937). It is the major efferent pathway in the human memory circuit and is thought to be especially key for maintaining episodic memory (EM) (Thomas et al., 2011; Douet and Chang, 2015) and executive function (EF) (Sasson et al., 2013).

Damage to the fornix has been shown to lead to significant memory and cognitive impairment (Oishi et al., 2009; Thomas et al., 2011; Mielke et al., 2012; Fletcher et al., 2013; Wang et al., 2018; Metzler-Baddeley et al., 2019). Likewise, infarction of the fornix can lead to neurodegeneration of the fornix, cognitive function decline, and VaD or subcortical VaD (SVD) (Cummings, 1994; Kalaria and Erkinjuntti, 2006; Zhuang et al., 2013; Mugikura and Takahashi, 2015; Takano et al., 2018; Zhu et al., 2018). Neuropsychological evaluation demonstrated the existence of an amnesia syndrome with deficit of executive functions in patients with bilateral infarction of the fornix, especially in the anterior column of the fornix (Nestor et al., 2007; Rizek et al., 2013; Salvalaggio et al., 2018). Given these findings, we expected reduced fornix integrity in n-aMCI compared to healthy older adults and for fornix integrity to be related to memory and executive functioning performance.

Diffusion tensor imaging (DTI) has been used fruitfully to study *in vivo* WM microstructure in the human brain *via* voxelwise analysis, region-of-interest (ROI) analysis, or fiber tractography (FT) (Liu et al., 2009). The majority of DTI studies have revealed a reduction of fractional anisotropy (FA) and an increase in mean diffusivity (MD), also known as the apparent diffusion coefficient (ADC), with advancing age (Beaulieu, 2002; Peters, 2002; DeBoy et al., 2007; Lebel et al., 2008; Mamere et al., 2009; Klawiter et al., 2011; Aung et al., 2013). These findings have been attributed to the breakdown of the myelin sheath and axonal membrane degradation such as axonal disintegration, oligodendrocytosis, astrocytosis, and Wallerian degeneration (WD) (Werring et al., 2000; Pierpaoli et al., 2001; Kiuchi et al., 2009; Kantarci et al., 2011; Dimitra et al., 2013). Indeed, abnormal fornix tissue cytoarchitecture has been associated with neuropathological abnormalities in those who are cognitively normal and later progress to MCI (Chao et al., 2013). Patients with MCI and/or AD show significant reductions of FA of the fornix, which highlights the importance of this key structure as an imaging marker to predict early disease progression (Liu et al., 2011; Thomas et al., 2011; Mielke et al., 2012; Pelletier et al., 2013; Yu et al., 2014; Metzler-Baddeley et al., 2019; da Rocha et al., 2020). Moreover, pathology of the fornix affects several brain networks with which it is interconnected (Nowrangi and Rosenberg, 2015).

In this study, we used DTI to assess the WM microstructure of the fornix in a cohort of Thai older adults. While the current literature has focused more on DTI markers of aMCI and AD and on whole-brain analyses, our aim was to specifically target the fornix, as its unique connectivity can shed light on the pathophysiology of n-aMCI, which is particularly prevalent in the Asia-Pacific region. Importantly, we approached this aim through both volumetric analysis and tractography. Our hypothesis was that WM integrity and fiber tract length (FTL) of the fornix would be sensitive to n-aMCI and would associate with cognitive functioning.

MATERIALS AND METHODS

Participants and Study Design

Participants aged 60 years and older with no history of dementia, no active depression disorders, and normal levels of daily function were recruited through the Maharaj Nakorn Chiang Mai Hospital and the local community. This study received institutional ethical approval. All participants in this study had voluntarily offered to undergo blood collection, cognitive screening tests, neuropsychological battery testing by a geriatric psychologist, and MRI scan by a well-trained radiologic technologist. Participants provided written informed consent before beginning the study. Participants were excluded from enrollment if they had (1) a history of infection, infarction, or other focal lesions in a brain structure critically associated with memory; (2) alcohol or substance abuse or dependence within

the past 2 years; (3) significant neurologic diseases within the past 1 year; active claustrophobia, hypothyroidism, hyperthyroidism, vitamin B12 deficiency, neurosyphilis [rapid plasma reagin (RPR) or Treponema pallidum hemagglutination (THPA) positive], or the human immunodeficiency virus (HIV); (4) current use of psychoactive medications; significant head trauma with post-traumatic loss of consciousness for at least 30 min at any point in their life; (5) loss of senses (blindness, deafness) or photosensitive epilepsy; presence of any metallic implants; and (6) any significant systemic illness or unstable medical condition that could lead to difficulty complying with the protocol.

Eighty participants were recruited, of which 39 were excluded after screening due to (1) 10 cases of mild anemia, (2) three cases of incomplete screening, (3) three cases of claustrophobia, (4) two cases of depression, (5) two cases of abnormal thyroid function, (6) two cases of obstructive sleep apnea, (7) two cases where participants were taking medications that affect cognition (i.e., prostatitis treatment), (8) one case of contracted syphilis, (9) one case of color blindness, (10) one case of generalized anxiety disorder, and (11) one case of low white blood cell count. Eleven other participants were excluded due to an unclear diagnosis after neuropsychological testing. Forty-one participants met the initial inclusion criteria, consisting of 20 healthy controls (HCs) and 21 with MCI. All of the participants with MCI met the criteria for non-amnestic MCI (n-aMCI), all presenting with executive dysfunction. Ten participants were excluded from the imaging analysis due to incomplete MRI acquisitions and/or atypical projection of the fornix. Therefore, data from 31 participants are presented. The resulting cohort consists of 14 HCs and 17 n-aMCI.

Clinical Evaluation

Each participant received multidisciplinary clinical evaluations at the Geriatric Psychiatry Clinic, Maharaj Nakorn Chiang Mai Hospital. Evaluations included (1) a detailed medical history; (2) physical and neurological examinations; (3) medical blood tests including fasting blood sugar (FBS), lipid profile (cholesterol and triglyceride), complete blood count (CBC), blood–urea–nitrogen (BUN) and creatinine (Cr), blood electrolytes (sodium, potassium, chloride, bicarbonate, calcium, magnesium, and phosphorus), triiodothyronine (T3), thyroxine (T4), thyroid-stimulating hormone (TSH) levels, and vitamin B12 (cobalamin), the RPR test, TPHA test, and HIV testing by a well-trained HIV counselor; and (4) cognitive screening tests including Montreal Cognitive Assessment (MoCA) (Nasreddine et al., 2005; Hemrungrojn, 2011), Mini-Cog Test (Borson et al., 2000; Trongsakul et al., 2015), Thai Geriatric Depression Scale-15 (TGDS-15) (Sheik, 1986; Wongpakaran and Wongpakaran, 2012), and The Barthel Index for Activities of Daily Living (ADL). In order to proceed in the study, participants needed to pass the Mini-Cog Test (score $\geq$3) and TGDS-15 (score $<$ 6) and to have no abnormal blood work results indicating conditions that could affect cognition.

Neuropsychological Testing

Subtests of the Wechsler Memory Scale-Third Edition (WMS-III) and the Wechsler Adult Intelligence Scale-Fourth Edition (WAIS-IV) were used to measure three cognitive domains: attention, executive function, and memory.

To correct for multiple comparisons, composite scores were calculated. A z-score was calculated for each participant's performance on each cognitive test relative to the mean and standard deviation across all participants. The z-scores were multiplied by −1 in cases where higher scores indicated worse performance and then averaged within the domain:

- Attention: Digit Span Test, Digit Symbol-Coding Test, and Trail Making Test (TMT) Part.
- Executive function: TMT Part B, Block Design test, Verbal Fluency test (Phonemic and Animal), and the Stroop Color and Word Test (SCWT).
- Memory: Letter-Number Sequencing Test and Word List Memory I and II.

Diagnosis of cognitively normal or MCI (minor neurocognitive disorder) was made according to the American Psychiatric Association's (APA) Diagnostic and Statistical Manual of Mental Disorders-Fifth Edition (DSM-5®) criteria (American Psychiatric Association, 2013) by a consensus conference of a geriatric psychiatrist and neuropsychologist.

MRI Acquisition

All participants were scanned on a 1.5 Tesla MR Philips Ingenia system equipped with a 15-channel head/spine array coil at the Associated Medical Science (AMS) Clinical Service Center, Department of Radiologic Technology, Faculty of Associated Medical Sciences, Chiang Mai University. The examination protocol included: axial DTI, T2 weighted (T2W) imaging, fluid-attenuated inversion recovery (FLAIR), and T1 weighted (T1W) imaging. The DTI protocol used the following parameters: repetition time (TR) = 5.0 s, echo time (TE) = 90 ms, FOV = 224 mm, matrix = 128 × 128, 49 directions, slice/gap 5.0/1 mm, b-value = 0 (1 volume per acquisition) and 1,000 s/mm^2 applied in 12 diffusion gradient orientations, and 75 slices. The total scan time was 25 min.

Preprocessing

The DTI data were analyzed using the FMRIB (University of Oxford's Center for Functional Magnetic Resonance Imaging of the Brain) Software Library (FSL) Diffusion Toolbox FSL release 5.0.10 (https://fsl.fmrib.ox.ac.uk/fsl/fslwiki). All DICOM files were converted into NIFTI files using the MRICron utility dcm2nii (http://www.nitrc.org/projects/mricron), and the first volume (the b = 0 image) was used to generate a binary brain mask with a threshold of 0.2 by using Brain Extraction Tool (BET). Then, the DTI parameters FA, axial diffusivity (AxD), mean diffusivity (MD), and radial diffusivity (RD) were derived from each participant's preprocessed DTI data.

Non-linear registration to the FMRIB58_FA space was applied to align the individual FA maps into a Montreal Neurological Institute (MNI) 152 standard space (http://imaging.mrc-cbu.cam.ac.uk/imaging/MniTalairach). The mean FA image was created from across all participants to generate a mean FA skeleton, which represents the center of WM tracts shared by all participants. To exclude voxels containing peripheral tracts,

partial volume effects with gray matter (GM), and cerebrospinal fluid (CSF), the mean FA skeleton voxel was thresholded at FA ≥ 0.2.

Given the small size and high intersubject variability of fornix anatomy, in our group analyses, we used standard-space binary masks to isolate specific anatomical substrates of the fornix based on the JHU ICBM-DTI-81 WM Labels Atlas (Mori et al., 2005, 2008) (**Figure 1**). Subsequently, FSL's fslmeants (https://fsl.fmrib.ox.ac.uk/fsl/fslwiki/Fslutils) was used to extract the average time course of FA and ADC values over 2 JHU-atlas masks for each participant: the whole tract of the fornix (denoted by subscript "whole") and the body and column (BC) of the fornix.

Fiber Tract Length Measurement

We performed fornix tractography using the Phillips proprietary software, FiberTrak, which is based on the Fiber Assignment with Continuous Tracking (FACT) algorithm (Mukherjee et al., 2008; Christidi et al., 2016). This deterministic DTI fiber tracking technique was performed with an FA threshold of 0.2. The fornix was manually drawn on the axial plane based on anatomical knowledge on the color-coded first eigenvector FA (FEFA) map by an experienced radiologic technologist and by three raters: (1) a professional rater with experience with DTI of the brain and manual tracing, (2) an intermediate rater who knew about DTI but had no experience with the protocol or manual tracing, and (3) a novice rater who was unfamiliar with DTI, the protocol, and manual tracing. Then, the fornix FTL was computed using the FACT algorithm length distributions across the fornix following the main direction of its principal eigenvector in each individual using Euler's method (Yeh et al., 2013). Each completed the tracings three times within 1-month interval to determine intra- and inter-rater reliability of the manual tracings. The FEFA maps were calculated based on a combination of direction and anisotropic diffusion, represented in red, green, and blue. **Figure 2** shows the manually traced tract (red line) drawn on the 2D FEFA map on the axial plane of the fornix (green color diffusion direction).

Statistical Analysis

Statistical analyses were performed using IBM-SPSS version 26 (IBM Corp. Released 2019 from the manual tracing IBM SPSS Statistics for Windows, Version 26.0; IBM Corp., Armonk, NY). Independent *t*-tests were used to compare age and education level between the HC and n-aMCI groups. ANOVAs were used to compare groups on MoCA, attention, executive functioning, memory, and the DTI parameters; FTL from the manual tracing (FiberTrak) and (FA_{whole}, ADC_{whole}, FA_{BC}, FA_{ST}, ADC_{BC}, and ADC_{ST}) extracted from the JHU-atlas masks, all controlling for age and education level. Pearson correlation coefficients were calculated to determine the strength of the linear association among DTI parameters and cognitive composites (**Supplementary Table 4**). Separate hierarchical linear regressions for each DTI parameter were performed to predict the cognitive composites, controlling for age and education. To achieve this, the HC group was coded as 1 and the n-aMCI group as 2, and age and education were entered first. Because age and education correlated with FTL (**Supplementary Table 4**), the interactions of FTL with age and education were included as a second step to account for these relationships. Next entered was a DTI parameter (e.g., FA of the entire fornix) and then the group × DTI parameter interactions. The group × DTI interaction term allowed us to determine if the relationship between DTI parameters and cognition differed between groups over and above any effects of age or education. The alpha level was set at 0.05 throughout.

RESULTS

Demographic Data

Table 1 shows the descriptive statistics of the demographic data. The HC group was significantly younger (64.36 ± 3.93 years) than the n-aMCI group (71.24 ± 8.15 years), $p = 0.005$, and significantly more educated (HC = 15.79 ± 2.61, n-aMCI = 12.18 ± 5.71), $p = 0.029$. Furthermore, age and education were correlated with cognition and with FTL from the manual tracing; **Supplementary Table 4**). Therefore, age and education were controlled in all remaining group comparisons.

Qualitative Analysis

Although the anatomy of the fornix is well-established, substantial intersubject anatomical variability is observed. The 3D reconstruction of the manually labeled fornix tracts was classified into seven classes of projection based on a skilled neuroanatomist's knowledge of the typical complete projection of the fornix consisting of fimbriae, crura, body, and column. The seven classes identified included three types of typical projection, two types of typical projection with missing features, and two types of atypical projection (**Figure 3**). Six cases (14.6% of all cases) of Type 6 and Type 7 were excluded due to the atypical projection of the fornix tract.

Intra- and Inter-rater Reliability

Intra-rater consistency of the manual tracing in fornix FTL ranged from acceptable to excellent, with Cronbach's alpha of 0.733 to 0.972, as shown in **Table 2**. Inter-rater consistency was excellent, with Cronbach's alpha ranging from 0.950 to 0.990. The inter-rater reliability of FTL in the HC group showed the highest reproducibility among both groups. In addition, the intra/inter-rater consistency averaged across all iterations and raters was excellent, with the highest Cronbach's alpha of 0.993. It was these latter averages that were brought forward for analysis.

Group Differences in Diffusion Tensor Imaging Parameters and Cognition

Descriptive statistics for cognitive screening scores, DTI parameters, and the z-scores of attention, executive function, and memory domains for each group are shown in **Table 3**. The HC group outperformed the n-aMCI group in the executive function and memory domains, but not in the attention domain,

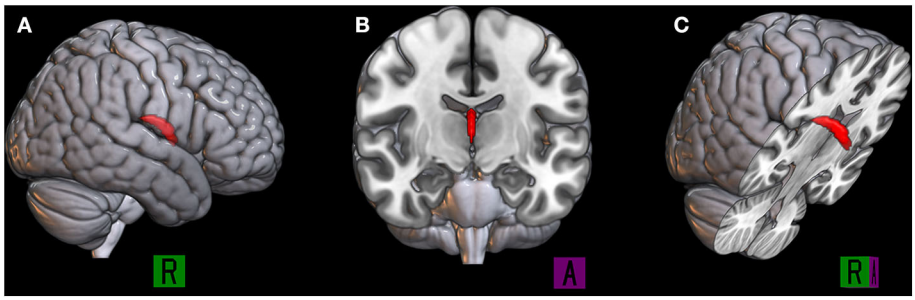

FIGURE 1 | The binary mask of the body and column of the fornix is represented in red, the 3D rendered by using MRIcroGL (https://www.mccauslandcenter.sc.edu/mricrogl/) in the sagittal plane **(A)**, coronal plane **(B)**, and right oblique plane **(C)**.

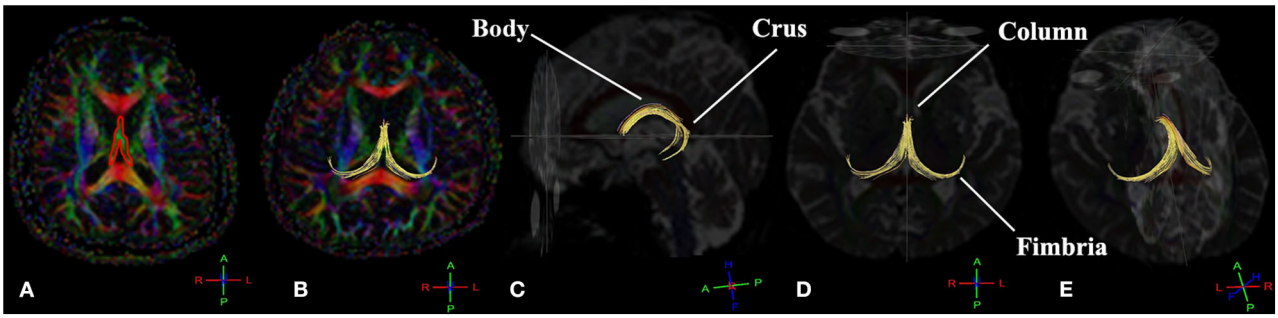

FIGURE 2 | The deterministic tractography of the complete projection of the fornix tract (yellow tract) consists of fimbriae, crura, body, and column. The manual tracing region of interest (ROI) draws on the 2D first eigenvector fractional anisotropy (FEFA) map on the axial plane of the fornix **(A)**. The fornix fiber tract in the axial plane **(B)**, sagittal plane **(C)**, axial plane **(D)**, and left oblique view **(E)**. The conventional red-green-blue color-coding was used for display purposes (red for right–left, blue for dorsal–ventral, and green for anterior–posterior) (Müller and Kassubek, 2007).

TABLE 1 | Descriptive statistics of participants' demographics.

Variables	Mean ± SD		Group comparison	
	HC	n-aMCI	*F*	*p*
Subjects (*n*)	14	17	–	–
Age (years)	64.36 ± 3.93	71.24 ± 8.15	4.868	**0.005**
Education level (years)	15.79 ± 2.61	12.18 ± 5.71	1.713	**0.029**
Gender (M:F)	0:14	3:14	4.278	0.098

Age and education level were compared using an independent t-test and a chi-square test, respectively. HCs, healthy older adult controls, n-aMCI, non-amnestic mild cognitive impairment (MCI) group. Significant values are bolded.

after controlling for age and education. No significant difference between groups was found in the age- and education-adjusted DTI parameters.

Group Differences in the Relationship Between Diffusion Tensor Imaging Parameters and Cognition

Hierarchical linear regressions revealed no significant relationship of the whole-fornix FA or ADC with cognition. The same was true for the ADC of the BC of the fornix. However, significant relationships with cognition were identified in FA_{BC} and FTL, and these relationships furthermore differed between groups after accounting for the influence of age and education. FA_{BC} was positively associated with both executive function ($p = 0.003$) and memory ($p = 0.035$) overall, but more strongly in the HC than in the n-aMCI group ($p < 0.001$ and $p = 0.028$, respectively) (**Table 4**). While the association of FTL with executive function and memory was not significant overall, these relationships also differed between groups ($p < 0.001$ and $p = 0.011$, respectively) (**Table 5**). The association of FTL with memory was stronger in the HC group than that in the n-aMCI group, but contrary to the case of FA_{BC}, the association of FTL with executive functioning was stronger in the n-aMCI group than that in the HC group. Importantly, these differences in the relationship between FA_{BC} and FTL with cognition were independent of any influence of age or education.

DISCUSSION

Demographics

All participants with MCI in our study were classified as n-aMCI with deficits in executive functioning. This is consistent with the high prevalence of cerebrovascular and cardiovascular conditions in the Asia-Pacific region compared to other regions (Jhoo et al.,

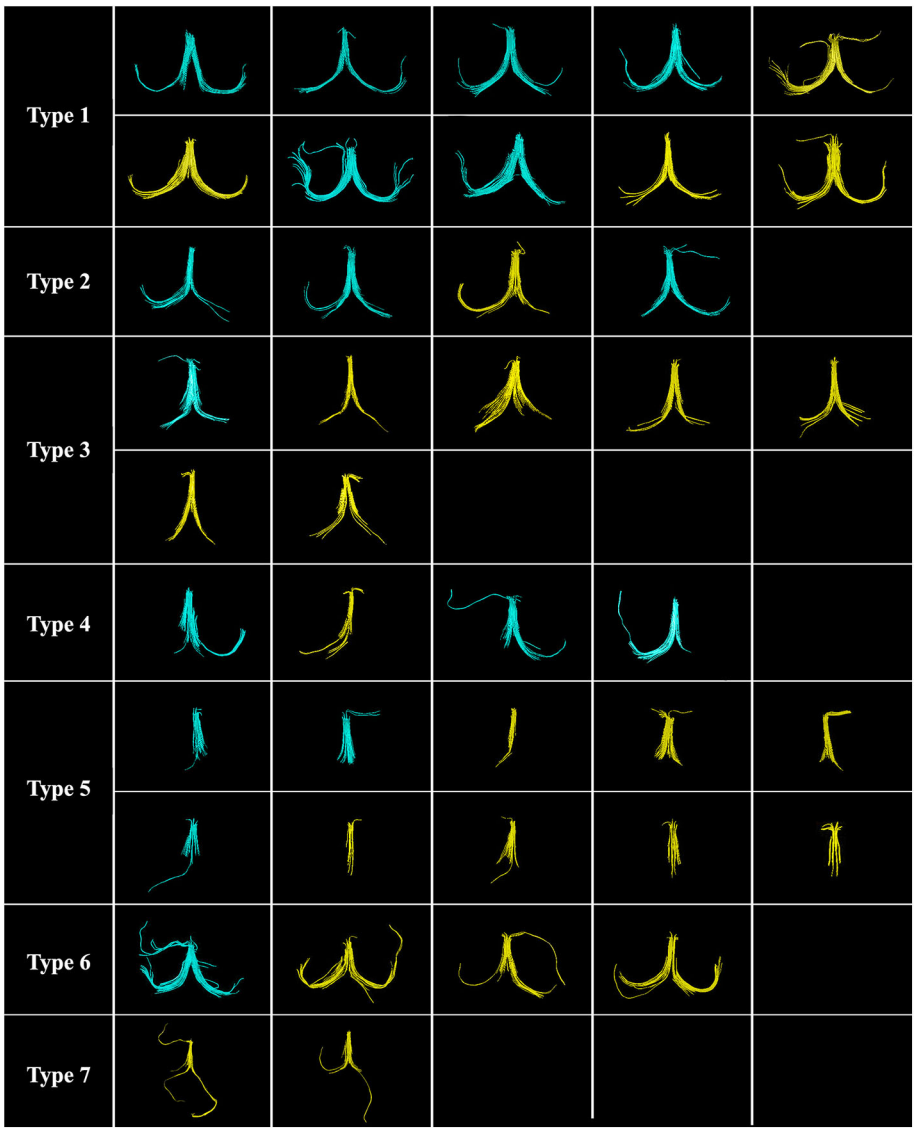

FIGURE 3 | Seven classes of the fornix projection are classified by using a single region of interest (ROI) ($n = 41$). Ten cases (24.4%) of Type 1, the complete typical projection; four cases (9.8%) of Type 2, complete typical projection with short fimbria (one side, Lt/Rt); seven cases (17.1%) of Type 3, complete typical projection with short fimbriae (both sides, Lt. and Rt.); four cases (9.7%) of Type 4, atypical projection with missing crus and/or fimbria (one side, Lt/Rt); 10 cases (24.4%) of Type 5, atypical projection with missing both crura and fimbriae (both sides, Lt. and Rt.); four cases (9.8%) of Type 6, complete typical projection with addition atypical projection; and two cases (4.9%) of Type 7, the atypical projection of fimbriae (both sides, Lt. and Rt.). Six cases (14.6%) of Type 6 and Type 7 were excluded due to the atypical projection of the fornix tract. Note: Healthy control (HC) group is shown in blue, and non-amnestic mild cognitive impairment (MCI) group (n-aMCI) group is shown in yellow.

2008; Chan et al., 2013), although it should be noted that n-aMCI can progress to AD, and individuals with AD often have mixed neuropathology that includes neurovascular events such as WM hyperintensities (Alber et al., 2019). Earlier studies have reported a higher prevalence of VaD than AD with an overall ratio of 2:1 in the Asia-Pacific population due to lifestyle and food preference (Narasimhalu et al., 2008). The HC group was significantly younger and had higher education levels than the n-aMCI group; therefore, all other group comparisons in this study accounted for these differences. Our findings in this regard are consistent with several studies that have demonstrated a link between educational attainment and cognitive functioning (Ardila et al., 2000; Le Carret et al., 2003; Narasimhalu et al., 2008; Falch and Sandgren Massih, 2011; Guerra-Carrillo et al., 2017).

Fornix Projections and Integrity

DTI tractography was performed using the novel deterministic FACT algorithm. In the FACT algorithm, the fornix fiber tract is reconstructed voxel by voxel following the main direction of its principal eigenvector. Hence, this algorithm provided

TABLE 2 | The internal consistency (Cronbach's alpha) of the manual tracing of the fornix, both intra-observer and among three levels of inter-observer including professional, intermediate, and novice levels.

DTI parameters	Intra-rater consistency (α)		Inter-rater consistency (α)		Average of intra/inter-rater consistency (α)	
	HC ($n = 14$)	n-aMCI ($n = 17$)	HC ($n = 14$)	n-aMCI ($n = 17$)	HC ($n = 14$)	n-aMCI ($n = 17$)
FTL (mm)	0.972	0.733	0.990	0.950	0.993	0.966

HCs, healthy older adult controls; n-aMCI, non-amnestic mild cognitive impairment (MCI) group; FA, fractional anisotropy; ADC, apparent diffusion coefficient; FTL, fiber tract length.

TABLE 3 | Descriptive statistics of participants' MoCA score, cognitive composites, and diffusion tensor imaging (DTI) parameters.

Variables	Mean ± SD		Group comparison	
	HC	n-aMCI	*F*	*p*
MoCA	26.07 ± 3.10	19.88 ± 4.06	7.804	**0.009**
Attention (z)	0.05 ± 0.46	−0.10 ± 0.44	0.000	0.988
Executive Function (z)	0.46 ± 0.39	−0.46 ± 0.44	19.703	**<0.001**
Memory (z)	0.24 ± 0.37	−0.19 ± 0.46	5.680	**0.024**
JHU-atlas				
FA_{whole}	0.43 ± 0.03	0.42 ± 0.03	0.167	0.686
ADC_{whole}	1.11 ± 0.09	1.15 ± 0.12	0.683	0.416
FA_{BC}	0.33 ± 0.07	0.29 ± 0.08	2.366	0.136
ADC_{BC}	1.71 ± 0.24	1.84 ± 0.30	1.722	0.200
Manual tracing: FiberTrak				
FTL (mm)	44.25 ± 9.66	37.59 ± 10.89	0.326	0.573

The group comparisons were made using univariate ANOVA, controlling for age and education. HCs, healthy older adult controls; n-aMCI, non-amnestic mild cognitive impairment (MCI) group; MoCA, Montreal Cognitive Assessment; FA, fractional anisotropy; ADC, apparent diffusion coefficient; FTL, fornix fiber tract length; FA_{BC}, FA value of the body and column of the fornix; FA_{whole}, FA value of the whole fornix tract; ADC_{BC}, ADC value of the body and column of the fornix; ADC_{whole}, the ADC value of the whole fornix tract. Significant values are bolded.

a reliable estimate of fornix FTL (Mori and Van Zijl, 2002; Hagler et al., 2009). Based on neuroanatomy knowledge, we found 35 of the 41 participants (85.37%) to have successfully represented the projection of fornix entirely and only six (9.76%) to have unsuccessful tracking results (presenting with the unlikely scenario of fiber projecting within subcortical WM) (Bürgel et al., 2009). For this reason, it was necessary to exclude these six aberrant fiber cases. Fornix WM integrity begins to decrease after its maturation peak during late adolescence because it is one of the earliest WM tracts to mature in the human brain (Douet and Chang, 2015). With advancing age, total WM fiber length in older adults has been reported to be decreased by 27 to 45% compared to younger adults (Tang et al., 1997; Marner et al., 2003). In our study, 14 cases had shortened or missing crura and/or fimbriae of the fornix including six cases (42.85%) of HC and eight cases (57.15%) of the n-aMCI group (as you can see in **Figure 3**; Type 4 and Type 5). Aging, together with the WM lesions (WMLs), in particular, specific frontal or medial temporal lobe (MTL) areas, could lead to a higher prevalence of atypical or incomplete fornix projection in n-aMCI than in the control group.

The Relationship Between Fornix Integrity and Executive Function

Executive function (EF) encompasses higher-order cognitive processes that generally refer to the coordinated operation of organization, regulation, planning, working memory, problem-solving, cognitive flexibility, and cognitive fluency (Denckla, 1994; Alvarez and Emory, 2006; Chan et al., 2008). It has long been known that the PFC is a pivotal area for sustaining executive functioning (Welsh et al., 1991; Moriguchi and Hiraki, 2013; Yuan and Raz, 2014). As the fornix connects the limbic system with both prefrontal and subcortical regions, it is a critical component of the Papez circuit and serves a major efferent pathway from the hippocampus to the medial PFC. Indeed, executive dysfunction was found to be related to cerebral hypoperfusion in regions connected to the fornix, specifically the middle frontal cortex and posterior cingulate gyrus in people with n-aMCI and executive dysfunction (Chao et al., 2009). Moreover, infarction of the fornix also leads to amnesia with executive dysfunction (Rizek et al., 2013; Salvalaggio et al., 2018).

We found a significant relationship between executive function and integrity in the BC (FA_{BC}) of the fornix as well as with fornix FTL, independent of the influence of age and education. Our results suggest that FA_{BC} does not support executive function as efficiently in n-aMCI compared to HC, as FA is less strongly associated with EF in the former group (**Table 4**). Interestingly, FTL was more strongly associated with EF in n-aMCI than the control group, and FTL was significantly positively related to EF over all participants ($r = 0.60$, $p < 0.01$; **Supplementary Table 4**). In n-aMCI, we found that most cases (57% of all n-aMCI cases) had missing crura and fimbriae, which are extended from the hippocampus. On the other hand, the BC of the fornix was intact in all cases. The column of the fornix projects to septal nuclei and the PFC *via* the precommissural fornix. As mentioned above, the PFC plays a critical role in executive functioning. Those with longer fornix FTL had better executive functioning, and this was particularly the case in the n-aMCI group. Given that the precommissural fornix projects to the PFC *via* the septal nuclei (Yeo et al., 2013; Cho et al., 2015; Coad et al., 2020), this finding suggests that, particularly among those with n-aMCI, executive functioning was sustained among those with fornix FTL long enough to make these connections.

The Relationship Between Fornix Integrity and Memory

Episodic memory involves the ability to learn, store, and retrieve information (Dickerson and Eichenbaum, 2010). In our study, FA_{BC} and FTL both showed a significant positive relationship with memory performance, over and above the influences of age and education. Moreover, this relationship was stronger in the HC than in the n-aMCI group. These results replicate previous findings showing that fornix integrity is supportive of memory performance in healthy young and older adults (e.g., Rudebeck et al., 2009; Metzler-Baddeley et al., 2011) but also highlight the breakdown of the contribution of the fornix to episodic memory in individuals with n-aMCI. As is well known,

TABLE 4 | Hierarchical linear regression analysis of fractional anisotropy (FA) of the body and column of the fornix and cognition among HC and non-amnestic mild cognitive impairment (MCI) group (n-aMCI) groups, with attention, executive function, and memory domains as dependent variables, adjusted for age and education.

Model	Unstandardized coefficient		Standardized coefficient	*t*	*p*	*F*	*R*	R^2	ΔR^2
	B	SE	Beta						
1. Attention domain									
Age	−0.005	0.013	−0.086	−0.413	0.683				
Edu	0.031	0.019	0.343	1.685	0.104				
FA_{BC}	0.615	1.214	0.107	0.507	0.617				
FA_{BC}*Group	0.057	0.598	0.023	0.095	0.925	1.244	0.401	0.161	<0.001
2. Executive function domain									
Age	−0.013	0.010	−0.159	−1.299	0.205				
Edu	0.042	0.015	0.330	2.770	**0.010**				
FA_{BC}	3.199	0.990	0.401	3.230	**0.003**				
FA_{BC}*Group	−2.097	0.488	−0.596	−4.298	**0.000**	16.169	0.845	0.713	0.204
3. Memory domain									
Age	0.013	0.012	0.210	1.136	0.266				
Edu	0.029	0.017	0.299	1.663	0.108				
FA_{BC}	2.513	1.131	0.416	2.221	**0.035**				
FA_{BC}*Group	−1.295	0.558	−0.487	−2.323	**0.028**	3.419	0.587	0.345	0.136

*Edu, education level; FA_{BC}, the FA value in the body and column of the fornix; FA_{BC}*Group, group difference in FA_{BC}. Significant values are bolded.*

TABLE 5 | Hierarchical linear regression analysis of fornix fiber length and cognition among HC and non-amnestic mild cognitive impairment (MCI) group (n-aMCI) groups, with attention, executive function, and memory domains as dependent variables, adjusted for age and education.

Model	Unstandardized coefficient		Standardized coefficient	*t*	*p*	*F*	*R*	R^2	ΔR^2
	B	SE	Beta						
1. Attention domain									
Age	−0.007	0.048	−0.108	−0.135	0.894				
Edu	−0.136	0.072	−1.495	−1.892	0.071				
Age * FTL	0.000	0.001	−0.509	−0.335	0.741				
Edu * FTL	0.005	0.002	3.052	2.443	**0.022**				
FTL	−0.53	0.100	−1.275	−0.530	0.601				
FTL * Group	0.002	0.004	0.116	0.571	0.573	2.323	0.606	0.367	0.209
2. Executive function domain									
Age	−0.022	0.042	−2.55	−0.515	0.612				
Edu	0.065	0.063	0.508	1.035	0.311				
Age * FTL	0.001	0.001	0.703	0.744	0.464				
Edu * FTL	−0.001	0.002	−0.353	−0.455	0.653				
FTL	0.005	0.086	0.086	0.057	0.955				
FTL * Group	−0.015	0.003	−0.569	−4.491	**<0.001**	12.374	0.869	0.756	0.695
3. Memory domain									
Age	0.012	0.049	0.194	0.252	0.803				
Edu	0.082	0.073	0.855	1.123	0.273				
Age * FTL	0.001	0.001	0.704	0.480	0.636				
Edu * FTL	−0.02	0.002	−0.999	−0.830	0.415				
FTL	0.020	0.101	0.465	0.200	0.843				
FTL * Group	−0.011	0.004	−0.540	−2.750	**0.011**	2.799	0.642	0.412	0.265

*Edu, education level; FTL, fornix fiber tract length; Age * FTL, age by FTL interaction; Edu * FTL, education by FTL interaction; FTL * Group, group difference in FTL. Significant values are bolded.*

the hippocampus–fornix–mammillary body system plays a role in episodic memory (Gaffan, 1992). Similar to hippocampus lesions, neurodegeneration of the fornix microstructure leads to the inability to create and/or store new memories (Thomas et al., 2011). This joint biological mechanism can potentially include Wallerian-like degeneration (WD) of the fornix axons, which is secondary to early injury of the neuronal degeneration in the hippocampus (Fletcher et al., 2013; Chen et al., 2017). The earliest study to our knowledge identifying WD in the fornix was after transection of the fimbria–fornix during temporal lobe epilepsy surgery for intractable epilepsy (Liu et al., 2013). More recently, Wang et al. (2020) reported that poorer fornix WM integrity was significantly correlated with reduced functional connectivity of the hippocampus due to the WD of the fornix axons in patients with MCI and AD (Wang et al., 2020). WD can be secondary to some cerebrovascular diseases (Uchino et al., 2004; Thomalla et al., 2005; Xie et al., 2012; Zhang et al., 2018), especially in the first week after ischemic stroke. It has been reported that the FA values of the affected tract begin to decrease 3 days after onset of the stroke (Thomalla et al., 2005; Xie et al., 2012; Zhang et al., 2018). Moreover, the fornix microstructure has been shown to predict episodic memory performance in several MRI studies (Vann et al., 2009; Sexton et al., 2010; Metzler-Baddeley et al., 2011; Zhuang et al., 2012).

Infarction of the fornix can lead to VaD or SVD, which also leads to a decline in memory performance (Cummings, 1994; Kalaria and Erkinjuntti, 2006). Likewise, the MTL is commonly affected by traumatic brain injury (TBI), which typically results in a variety of cognitive deficits. The pathophysiology of TBI is characterized by impaired regulation of cerebral blood flow (Werner and Engelhard, 2007; Prins et al., 2013), tissue damage involving the damage of limbic WM, and other factors such as edema, excitotoxicity, and hemorrhage (Gale et al., 1993). WM disruption in the fornix has been found to be associated with memory performance in both TBI patients and control groups (Kinnunen et al., 2011) and the reduction of FA of the fornix is correlated with poorer memory performance (Tomaiuolo et al., 2004), working memory (Palacios et al., 2011), and learning (Kinnunen et al., 2011) in patients with TBI.

In addition, anterograde amnesia, the inability to create new memories, is one of the earliest symptoms in patients with fornix infarction or after TBI that damages limbic-related structures including the fornix (Baweja et al., 2015; Gupta et al., 2015; Turine et al., 2016; Kauppila et al., 2018; Takano et al., 2018; Wang et al., 2018; Zhu et al., 2018). These results suggest that one contributor to episodic memory deficits in n-aMCI is the subtle degradation of fornix integrity.

The Relationship Between Fornix Integrity and Attention

Attention refers to the ability to selectively attend or concentrate on specific relevant information while ignoring irrelevant information (McGuinness et al., 2010). The dorsolateral PFC and anterior cingulate gyrus are two areas involved in attention (Perry and Hodges, 1999). Because the fornix is one of the WM tracts carrying signals from the MTL to the PFC, damage to the fornix could lead to a decline in attention ability. Although our participants with n-aMCI had intact attention and there was no significant relationship between the DTI parameters and attention in the present study, several studies have found that patients with VaD have attentional deficits and more so than patients with AD (Mendez and Ashla-Mendez, 1991; Barr et al., 1992; Almkvist et al., 1993). Therefore, we might expect a significant decline in attention ability and its relationship with fornix integrity in the later stages of VaD in our sample. It is also the case that our measures of attention did not assess higher-order attention skills such as divided attention. Perhaps we would have seen group differences had we administered more complex attention tasks.

Fornix and Its Association With Vascular Dementia

Changes in fornix diffusivity are common among patients with VaD (Douaud et al., 2011; Mayo et al., 2017; Salvadores et al., 2017), especially the reduction of FA and an increase of ADC, which reflect its integrity. The higher the frequency of ischemic heart disease, TIA, or stroke in a sample, the more WMLs are found in n-aMCI compared to aMCI patients (Mariani et al., 2007). Likewise, those with n-aMCI typically have increased vascular burden and are more likely to have cardiovascular risk factors as well as basal forebrain atrophy than those with aMCI (He et al., 2009; Jak et al., 2009). These vascular burdens, such as small ischemic and vascular lesions that involve subcortical areas (where the fornix is situated) are commonly associated with cognitive decline (Cummings, 1994). As is well known, n-aMCI is more likely to develop into non-AD dementia, notably VaD (Petersen et al., 2001).

Limitations and Future Directions

One limitation of this pilot study is the small sample size, which may have limited the power of investigation. We initially recruited 80 participants but were very conservative in excluding conditions that might affect cognition, other than preclinical neurodegeneration. Thus, although our sample is small, we are highly confident in the clinical diagnosis of our sample. Another limitation of our data is that age and education are strongly associated with cognition; age and education differed between the patient and control groups. However, we have shown that the significance relationship between cognition and DTI parameters in our study is independent of any influence of age or education. Another limitation is the deterministic tractography, which can only detect local diffusion that passes through the chosen ROI and is unable to distinguish between afferent and efferent fibers within the WM tract; hence, it cannot be assumed that the detected projection reflects the true anatomical structure (Mori et al., 1999; Bürgel et al., 2009).

Because the fornix is small and located between the lateral ventricles beneath the corpus callosum along with septum pellucidum, it is susceptible to partial volume effects by the surrounding CSF, which can potentially affect the measurement of the thinner parts of it (i.e., crura and fimbriae). By contrast, the BC of the fornix is the most prominent structure, making it least

susceptible to partial volume effects and thus a good candidate for representing the WM integrity of the entire fornix.

CONCLUSION

The FA of the BC of the fornix and fornix FTL were positively associated with executive function and memory among both groups. These relationships were stronger in the healthy older adults than those in the n-aMCI, with the exception of the FTL–executive functioning association. This pilot study provides the first evidence for a decline in the contributions of fornix integrity to memory and executive functioning in n-aMCI and suggests that maintenance of fornix FTL is critical for sustaining executive functioning in people with presumptive preclinical VaD.

DATA AVAILABILITY STATEMENT

The raw data supporting the conclusions of this article will be made available by the authors, without undue reservation.

ETHICS STATEMENT

This study was reviewed and approved by Research Ethics Committee of the Faculty of Medicine, Chiang Mai University. The patients/participants provided their written informed consent to participate in this study.

AUTHOR CONTRIBUTIONS

JC and SK contributed to the provision of software and computational resources. JC, NW, NA, PV, PM, PS, and SK contributed to the study design. JC, KU, NW, NA, PV, PM, and SK contributed to the review and editing of the manuscript. JC contributed to the supervision of imaging analysis. NW contributed to the supervision of investigation-clinical aspects of the work, field mentorship, and ethics. NA contributed to the supervision of statistical analysis and clinical aspects of the work. PM contributed to the supervision and project administration. SK contributed to the supervision of DTI and MRI. NW, PV, and PS contributed to the data collection. PM and PS obtained funding for the study. PS contributed to the conceptualization and writing the original draft. All authors contributed to the article and approved the submitted version.

FUNDING

This research was funded by the Thailand Research Fund (TRF) through the Royal Golden Jubilee Ph.D. Programme (Grant No. PHD/0069/2559) to PS and PM, Faculty of Medicine Research Fund (Grant No. 087/2562), and the Excellence in Osteology Research and Training Center (ORTC) with partially support by Chiang Mai University is acknowledged.

ACKNOWLEDGMENTS

We gratefully thank the Rotman Research Institute at Baycrest, Toronto, Canada, for hosting PS as a visiting graduate student. We would like to especially thank Jordan A. Chad and Jacob L. Matthew for their advice, knowledge, and kind support throughout the imaging analysis step in this study.

SUPPLEMENTARY MATERIAL

The Supplementary Material for this article can be found online at: https://www.frontiersin.org/articles/10.3389/fnagi.2020.594002/full#supplementary-material

REFERENCES

Alber, J., Alladi, S., Bae, H.-J., Barton, D. A., Beckett, L. A., Bell, J. M., et al. (2019). White matter hyperintensities in vascular contributions to cognitive impairment and dementia (VCID): knowledge gaps and opportunities. *Alzheimers Dement*. 5, 107–117. doi: 10.1016/j.trci.2019.02.001

Almkvist, O., Bäckman, L., Basun, H., and Wahlund, L.-O. (1993). Patterns of neuropsychological performance in Alzheimer's disease and vascular dementia. *Cortex* 29, 661–673. doi: 10.1016/S0010-9452(13)80289-4

Alvarez, J. A., and Emory, E. (2006). Executive function and the frontal lobes: a meta-analytic review. *Neuropsychol. Rev*. 16, 17–42. doi: 10.1007/s11065-historyof 006-9002-x

Alzheimer's Disease International (2014). *Dementia in the Asia Pacific Region*. London. Available online at: www.alz.co.uk. (accessed March 25, 2020).

Alzheimer's Disease International (2018). *World Alzheimer Report: The State of the Art of Dementia Research: New Frontiers.* London: Alzheimer's Disease International (ADI). Available online at: www.alz.co.uk. (accessed February 19, 2020).

Alzheimer's Disease International (2019). *World Alzheimer Report: Attitudes to Dementia*. London: Alzheimer's Disease International (ADI). Available online at: www.alz.co.uk. (accessed March 25, 2020).

American Psychiatric Association (2013). *Diagnostic and Statistical Manual of Mental Disorders: Diagnostic and Statistical Manual of Mental Disorders, Fifth Edition*. Arlington, VA. doi: 10.1176/appi.books.9780890425596

Anderson, N. D. (2019). State of the science on mild cognitive impairment (MCI). *CNS Spectr*. 24, 78–87. doi: 10.1017/S1092852918001347

Ardila, A., Ostrosky-Solis, F., Rosselli, M., and Gómez, C. (2000). Age-related cognitive decline during normal aging: the complex effect of education. *Arch. Clin. Neuropsychol*. 15, 495–513. doi: 10.1093/arclin/15.6.495

Aung, W. Y., Mar, S., and Benzinger, T. L. (2013). Diffusion tensor MRI as a biomarker in axonal and myelin damage. *Imaging Med*. 5:427. doi: 10.2217/iim.13.49

Barr, A., Benedict, R., Tune, L., and Brandt, J. (1992). Neuropsychological differentiation of Alzheimer's disease from vascular dementia. *Int. J. Geriatr. Psychiatry* 7, 621–627. doi: 10.1159/000477344

Baweja, R., Mensinkai, A., Reddy, K., and Sahlas, D. J. (2015). Fornix infarction after clipping of anterior communicating artery aneurysm. *Can. J. Neurol. Sci*. 42, 205–207. doi: 10.1017/cjn.2015.27

Beaulieu, C. (2002). The basis of anisotropic water diffusion in the nervous system–a technical review. *NMR Biomed*. 15, 435–455. doi: 10.1002/nbm.782

Borson, S., Scanlan, J., Brush, M., Vitaliano, P., and Dokmak, A. (2000). The mini-cog: a cognitive 'vital signs' measure for dementia screening in multi-lingual elderly. *Int. J. Geriatr. Psychiatry* 15, 1021–1027. doi: 10.1002/1099-1166(200011)15:11<1021::AID-GPS234>3.0.CO;2-6

Bürgel, U., Mädler, B., Honey, C., Thron, A., Gilsbach, J., and Coenen, V. (2009). Fiber tracking with distinct software tools results in a clear diversity in anatomical fiber tract portrayal. *Cent. Eur. Neurosurg.* 70, 27–35. doi: 10.1055/s-0028-1087212

Chan, K. Y., Wang, W., Wu, J. J., Liu, L., Theodoratou, E., Car, J., et al. (2013). Epidemiology of Alzheimer's disease and other forms of dementia in China, 1990–2010: a systematic review and analysis. *Lancet* 381, 2016–2023. doi: 10.1016/S0140-6736(13)60221-4

Chan, R. C., Shum, D., Toulopoulou, T., and Chen, E. Y. (2008). Assessment of executive functions: review of instruments and identification of critical issues. *Arch. Clin. Neuropsychol.* 23, 201–216. doi: 10.1016/j.acn.2007.08.010

Chao, L. L., DeCarli, C., Kriger, S., Truran, D., Zhang, Y., Laxamana, J., et al. (2013). Associations between white matter hyperintensities and β amyloid on integrity of projection, association, and limbic fiber tracts measured with diffusion tensor MRI. *PLoS ONE* 8:e65175. doi: 10.1371/journal.pone.0065175

Chao, L. L., Pa, J., Duarte, A., Schuff, N., Weiner, M. W., Kramer, J. H., et al. (2009). Patterns of cerebral hypoperfusion in amnestic and dysexecutive MCI. *Alzheimers Dis. Assoc. Dis.* 23:245. doi: 10.1097/WAD.0b013e318199ff46

Chen, Y. J., Nabavizadeh, S. A., Vossough, A., Kumar, S., Loevner, L. A., and Mohan, S. (2017). Wallerian degeneration beyond the corticospinal tracts: conventional and advanced MRI findings. *J. Neuroimaging* 27, 272–280. doi: 10.1111/jon.12404

Cho, Z.-H., Chi, J.-G., Choi, S.-H., Oh, S.-H., Park, S.-Y., Paek, S. H., et al. (2015). A newly identified frontal path from fornix in septum pellucidum with 7.0 T MRI track density imaging (TDI)–the septum pellucidum tract (SPT). *Front. Neuroanat.* 9:151. doi: 10.3389/fnana.2015.00151

Christiansen, K., Aggleton, J. P., Parker, G. D., O'Sullivan, M. J., Vann, S. D., and Metzler-Baddeley, C. (2016). The status of the precommissural and postcommissural fornix in normal ageing and mild cognitive impairment: an MRI tractography study. *Neuroimage* 130, 35–47. doi: 10.1016/j.neuroimage.2015.12.055

Christidi, F., Karavasilis, E., Samiotis, K., Bisdas, S., and Papanikolaou, N. (2016). Fiber tracking: a qualitative and quantitative comparison between four different software tools on the reconstruction of major white matter tracts. *Eur. J. Radiol. Open* 3, 153–161. doi: 10.1016/j.ejro.2016.06.002

Coad, B. M., Craig, E., Louch, R., Aggleton, J. P., Vann, S. D., and Metzler-Baddeley, C. (2020). Precommissural and postcommissural fornix microstructure in healthy aging and cognition. *Brain Neurosci. Adv.* 4:2398212819899316. doi: 10.1177/2398212819899316

Cummings, J. L. (1994). Vascular subcortical dementias: clinical aspects. *Dement. Geriatr. Cogn. Disord.* 5, 177–180. doi: 10.1159/000106718

da Rocha, J. L. D., Bramati, I., Coutinho, G., Moll, F. T., and Sitaram, R. (2020). Fractional Anisotropy changes in parahippocampal cingulum due to Alzheimer's Disease. *Sci. Rep.* 10, 1–8. doi: 10.1038/s41598-020-59327-2

DeBoy, C. A., Zhang, J., Dike, S., Shats, I., Jones, M., Reich, D. S., et al. (2007). High resolution diffusion tensor imaging of axonal damage in focal inflammatory and demyelinating lesions in rat spinal cord. *Brain* 130, 2199–2210. doi: 10.1093/brain/awm122

Denckla, M. B. (1994). "Measurement of executive function," in *Frames of Reference for the Assessment of Learning Disabilities: New Views on Measurement Issues,* ed G. R. Lyon (Baltimore, MD: Paul H Brookes Publishing Co.), 117–142.

Dickerson, B. C., and Eichenbaum, H. (2010). The episodic memory system: neurocircuitry and disorders. *Neuropsychopharmacology* 35, 86–104. doi: 10.1038/npp.2009.126

Dimitra, S., Verganelakis, D., Gotsis, E., Toulas, P., Papatriantafillou, J., Karageorgiou, C., et al. (2013). Diffusion tensor imaging (DTI) in the detection of white matter lesions in patients with mild cognitive impairment (MCI). *Acta Neurol. Belg.* 113, 441–451. doi: 10.1007/s13760-013-0224-4

Douaud, G., Jbabdi, S., Behrens, T. E., Menke, R. A., Gass, A., Monsch, A. U., et al. (2011). DTI measures in crossing-fibre areas: increased diffusion anisotropy reveals early white matter alteration in MCI and mild Alzheimer's disease. *Neuroimage* 55, 880–890. doi: 10.1016/j.neuroimage.2010.12.008

Douet, V., and Chang, L. (2015). Fornix as an imaging marker for episodic memory deficits in healthy aging and in various neurological disorders. *Front. Aging. Neurosci.* 6:343. doi: 10.3389/fnagi.2014.00343

Falch, T., and Sandgren Massih, S. (2011). The effect of education on cognitive ability. *Econ. Inq.* 49, 838–856. doi: 10.1111/j.1465-7295.2010.00312.x

Farlow, M., He, Y., Tekin, S., Xu, J., Lane, R., and Charles, H. (2004). Impact of APOE in mild cognitive impairment. *Neurology* 63, 1898–1901. doi: 10.1212/01.WNL.0000144279.21502.B7

Fletcher, E., Raman, M., Huebner, P., Liu, A., Mungas, D., Carmichael, O., et al. (2013). Loss of fornix white matter volume as a predictor of cognitive impairment in cognitively normal elderly individuals. *JAMA Neurol.* 70, 1389–1395. doi: 10.1001/jamaneurol.2013.3263

Gaffan, D. (1992). "The role of the hippocampus-fornix-mammillary system in episodic memory," in *Neuropsychology of Memory, 2nd Edn*, eds L. R. Squire and N. Butter (New York, NY: Guilford Press), 336–346.

Gale, S., Burr, R., Bigler, E. D., and Blatter, D. (1993). Fornix degeneration and memory in traumatic brain injury. *Brain Res. Bull.* 32, 345–349. doi: 10.1016/0361-9230(93)90198-K

Guerra-Carrillo, B., Katovich, K., and Bunge, S. A. (2017). Does higher education hone cognitive functioning and learning efficacy? Findings from a large and diverse sample. *PLoS ONE* 12:e0182276. doi: 10.1371/journal.pone.0182276

Gupta, M., Kantor, M. A., Tung, C. E., Zhang, N., and Albers, G. W. (2015). Transient global amnesia associated with a unilateral infarction of the fornix: case report and review of the literature. *Front. Neurol.* 5:291. doi: 10.3389/fneur.2014.00291

Hagler D. J. Jr., Ahmadi, M. E., Kuperman, J., Holland, D., McDonald, C. R., Halgren, E., et al. (2009). Automated white-matter tractography using a probabilistic diffusion tensor atlas: Application to temporal lobe epilepsy. *Hum. Brain Mapp.* 30, 1535–1547. doi: 10.1002/hbm.20619

He, J., Farias, S., Martinez, O., Reed, B., Mungas, D., and DeCarli, C. (2009). Differences in brain volume, hippocampal volume, cerebrovascular risk factors, and apolipoprotein E4 among mild cognitive impairment subtypes. *Arch. Neurol.* 66, 1393–1399. doi: 10.1001/archneurol.2009.252

Hemrungrojn, S. (2011). *Thai Version of Montreal Cognitive Assessment (MOCA)*. Available online at: www.mocatest.org.

Iadecola, C. (2013). The pathobiology of vascular dementia. *Neuron* 80, 844–866. doi: 10.1016/j.neuron.2013.10.008

Jak, A. J., Bangen, K. J., Wierenga, C. E., Delano-Wood, L., Corey-Bloom, J., and Bondi, M. W. (2009). Contributions of neuropsychology and neuroimaging to understanding clinical subtypes of mild cognitive impairment. *Int. Rev. Neurobiol.* 84, 81–103. doi: 10.1016/S0074-7742(09)00405-X

Jhoo, J. H., Kim, K. W., Huh, Y., Lee, S. B., Park, J. H., Lee, J. J., et al. (2008). Prevalence of dementia and its subtypes in an elderly urban Korean population: results from the Korean Longitudinal Study on Health and Aging (KLoSHA). *Dement. Geriatr. Cogn. Disord.* 26, 270–276. doi: 10.1159/000160960

Kalaria, R. N., and Erkinjuntti, T. (2006). Small vessel disease and subcortical vascular dementia. *J. Clin. Neurol.* 2, 1–11. doi: 10.3988/jcn.2006.2.1.1

Kantarci, K., Senjem, M., Avula, R., Zhang, B., Samikoglu, A., Weigand, S., et al. (2011). Diffusion tensor imaging and cognitive function in older adults with no dementia. *Neurology* 77, 26–34. doi: 10.1212/WNL.0b013e31822313dc

Kauppila, L. A., Alves, P. N., Reimão, S., Fonseca, A. C., e Melo, T. P., and Martins, I. P. (2018). Memory impairment due to bilateral fornix infarction: characterisation and follow-up. *J. Neurol. Sci.* 390, 10–13. doi: 10.1016/j.jns.2018.03.034

Kinnunen, K. M., Greenwood, R., Powell, J. H., Leech, R., Hawkins, P. C., Bonnelle, V., et al. (2011). White matter damage and cognitive impairment after traumatic brain injury. *Brain* 134, 449–463. doi: 10.1093/brain/awq347

Kiuchi, K., Morikawa, M., Taoka, T., Nagashima, T., Yamauchi, T., Makinodan, M., et al. (2009). Abnormalities of the uncinate fasciculus and posterior cingulate fasciculus in mild cognitive impairment and early Alzheimer's disease: a diffusion tensor tractography study. *Brain Res. J.* 1287, 184–191. doi: 10.1016/j.brainres.2009.06.052

Klawiter, E. C., Schmidt, R. E., Trinkaus, K., Liang, H.-F., Budde, M. D., Naismith, R. T., et al. (2011). Radial diffusivity predicts demyelination in *ex vivo* multiple sclerosis spinal cords. *Neuroimage* 55, 1454–1460. doi: 10.1016/j.neuroimage.2011.01.007

Le Carret, N., Lafont, S., Letenneur, L., Dartigues, J.-F., Mayo, W., and Fabrigoule, C. (2003). The effect of education on cognitive performances and its implication for the constitution of the cognitive reserve. *Dev. Neuropsychol.* 23, 317–337. doi: 10.1207/S15326942DN2303_1

Lebel, C., Walker, L., Leemans, A., Phillips, L., and Beaulieu, C. (2008). Microstructural maturation of the human brain from childhood to

adulthood. *Neuroimage* 40, 1044–1055. doi: 10.1016/j.neuroimage.2007.12.053

Liu, M., Gross, D. W., Wheatley, B. M., Concha, L., and Beaulieu, C. (2013). The acute phase of Wallerian degeneration: longitudinal diffusion tensor imaging of the fornix following temporal lobe surgery. *Neuroimage* 74, 128–139. doi: 10.1016/j.neuroimage.2013.01.069

Liu, Y., Spulber, G., Lehtimäki, K. K., Könönen, M., Hallikainen, I., Gröhn, H., et al. (2011). Diffusion tensor imaging and tract-based spatial statistics in Alzheimer's disease and mild cognitive impairment. *Neurobiol. Aging* 32, 1558–1571. doi: 10.1016/j.neurobiolaging.2009.10.006

Liu, Z., Zhu, H., Marks, B. L., Katz, L. M., Goodlett, C. B., Gerig, G., et al. (2009). "Voxel-wise group analysis of DTI," *Paper Presented at the IEEE International Symposium on Biomedical Imaging: From Nano to Macro* (Boston, MA), 807–810. doi: 10.1109/ISBI.2009.5193172

Mamere, A., Saraiva, L., Matos, A., Carneiro, A., and Santos, A. (2009). Evaluation of delayed neuronal and axonal damage secondary to moderate and severe traumatic brain injury using quantitative MR imaging techniques. *AJNR Am. J. Neuroradiol.* 30, 947–952. doi: 10.3174/ajnr.A1477

Mariani, E., Monastero, R., Ercolani, S., Mangialasche, F., Caputo, M., Feliziani, F., et al. (2007). Vascular risk factors in mild cognitive impairment subtypes. *Dement. Geriatr. Cogn. Disord.* 24, 448–456. doi: 10.1159/000110653

Marner, L., Nyengaard, J. R., Tang, Y., and Pakkenberg, B. (2003). Marked loss of myelinated nerve fibers in the human brain with age. *J. Comp. Neurol.* 462, 144–152. doi: 10.1002/cne.10714

Mayo, C. D., Mazerolle, E. L., Ritchie, L., Fisk, J. D., and Gawryluk, J. R. (2017). Longitudinal changes in microstructural white matter metrics in Alzheimer's disease. *Neuroimage Clin.* 13, 330–338. doi: 10.1016/j.nicl.2016.12.012

McGuinness, B., Barrett, S. L., Craig, D., Lawson, J., and Passmore, A. P. (2010). Attention deficits in Alzheimer's disease and vascular dementia. *J. Neurol. Neurosurg. Psychiatry* 81, 157–159. doi: 10.1136/jnnp.2008.164483

Mendez, M. F., and Ashla-Mendez, M. (1991). Differences between multi-infarct dementia and Alzheimer's disease on unstructured neuropsychological tasks. *J. Clin. Exp. Neuropsychol.* 13, 923–932. doi: 10.1080/01688639108405108

Metzler-Baddeley, C., Jones, D. K., Belaroussi, B., Aggleton, J. P., and O'Sullivan, M. J. (2011). Frontotemporal connections in episodic memory and aging: a diffusion MRI tractography study. *J. Neurosci.* 31, 13236–13245. doi: 10.1523/JNEUROSCI.2317-11.2011

Metzler-Baddeley, C., Mole, J. P., Sims, R., Fasano, F., Evans, J., Jones, D. K., et al. (2019). Fornix white matter glia damage causes hippocampal gray matter damage during age-dependent limbic decline. *Sci. Rep.* 9, 1–14. doi: 10.1038/s41598-019-51737-1

Mielke, M. M., Okonkwo, O. C., Oishi, K., Mori, S., Tighe, S., Miller, M. I., et al. (2012). Fornix integrity and hippocampal volume predict memory decline and progression to Alzheimer's disease. *Alzheimers Dement.* 8, 105–113. doi: 10.1016/j.jalz.2011.05.2416

Mori, S., Crain, B. J., Chacko, V. P., and Van Zijl, P. C. (1999). Three-dimensional tracking of axonal projections in the brain by magnetic resonance imaging. *Ann. Neurol.* 45, 265–269. doi: 10.1002/1531-8249(199902)45:2<265::AID-ANA21>3.0.CO;2-3

Mori, S., Oishi, K., Jiang, H., Jiang, L., Li, X., Akhter, K., et al. (2008). Stereotaxic white matter atlas based on diffusion tensor imaging in an ICBM template. *Neuroimage* 40, 570–582. doi: 10.1016/j.neuroimage.2007.12.035

Mori, S., and Van Zijl, P. C. (2002). Fiber tracking: principles and strategies–a technical review. *NMR Biomed.* 15, 468–480. doi: 10.1002/nbm.781

Mori, S., Wakana, S., Van Zijl, P. C., and Nagae-Poetscher, L. M. (2005). *MRI Atlas of Human White Matter*. Amsterdam: Elsevier B.V.

Moriguchi, Y., and Hiraki, K. (2013). Prefrontal cortex and executive function in young children: a review of NIRS studies. *Front. Hum. Neurosci.* 7:867. doi: 10.3389/fnhum.2013.00867

Mugikura, S., and Takahashi, S. (2015). Infarction in the pars libera of the column of fornix including pre (cholinergic)-and post (circuit of Papez fiber tracts)-commissural fibers causes "basal forebrain" amnesia. *Neuroradiology* 57, 757–759. doi: 10.1007/s00234-015-1504-x

Mukherjee, P., Berman, J., Chung, S., Hess, C., and Henry, R. (2008). Diffusion tensor MR imaging and fiber tractography: theoretic underpinnings. *AJNR Am. J. Neuroradiol.* 29, 632–641. doi: 10.3174/ajnr.A1051

Müller, H.-P., and Kassubek, J. (2007). Multimodal imaging in neurology: special focus on MRI applications and MEG. *Synth. Lect. Biomed. Eng.* 2, 1–75. doi: 10.2200/S00099ED1V01Y200710BME016

Narasimhalu, K., Lee, J., Auchus, A. P., and Chen, C. P. (2008). Improving detection of dementia in Asian patients with low education: combining the Mini-Mental State Examination and the Informant Questionnaire on Cognitive Decline in the Elderly. *Dement. Geriatr. Cogn. Disord.* 25, 17–22. doi: 10.1159/000111128

Nasreddine, Z. S., Phillips, N. A., Bédirian, V., Charbonneau, S., Whitehead, V., Collin, I., et al. (2005). The Montreal Cognitive Assessment, MoCA: a brief screening tool for mild cognitive impairment. *J. Am. Geriatr. Soc.* 53, 695–699. doi: 10.1111/j.1532-5415.2005.53221.x

Nestor, P. G., Kubicki, M., Kuroki, N., Gurrera, R. J., Niznikiewicz, M., Shenton, M. E., et al. (2007). Episodic memory and neuroimaging of hippocampus and fornix in chronic schizophrenia. *Psychiatry Res. Neuroimaging* 155, 21–28. doi: 10.1016/j.pscychresns.2006.12.020

Nowrangi, M. A., and Rosenberg, P. B. (2015). The fornix in mild cognitive impairment and Alzheimer's disease. *Front. Aging Neurosci.* 7:1. doi: 10.3389/fnagi.2015.00001

Oishi, K., Faria, A., Jiang, H., Li, X., Akhter, K., Zhang, J., et al. (2009). Atlas-based whole brain white matter analysis using large deformation diffeomorphic metric mapping: application to normal elderly and Alzheimer's disease participants. *Neuroimage* 46, 486–499. doi: 10.1016/j.neuroimage.2009.01.002

Palacios, E. M., Fernandez-Espejo, D., Junque, C., Sanchez-Carrion, R., Roig, T., Tormos, J., et al. (2011). Diffusion tensor imaging differences relate to memory deficits in diffuse traumatic brain injury. *BMC Neurol.* 11:24. doi: 10.1186/1471-2377-11-24

Papez, J. W. (1937). A proposed mechanism of emotion. *Arch. Neurol. Psychiatry* 38, 725–743. doi: 10.1001/archneurpsyc.1937.02260220069003

Pelletier, A., Periot, O., Dilharreguy, B., Hiba, B., Bordessoules, M., Pérès, K., et al. (2013). Structural hippocampal network alterations during healthy aging: a multi-modal MRI study. *Front. Aging Neurosci.* 5:84. doi: 10.3389/fnagi.2013.00084

Pendlebury, S. T., Rothwell, P. M., and Study, O. V. (2019). Incidence and prevalence of dementia associated with transient ischaemic attack and stroke: analysis of the population-based Oxford Vascular Study. *Lancet Neurol.* 18, 248–258. doi: 10.1016/S1474-4422(18)30442-3

Perry, R. J., and Hodges, J. R. (1999). Attention and executive deficits in Alzheimer's disease: a critical review. *Brain* 122, 383–404. doi: 10.1093/brain/122.3.383

Peters, A. (2002). The effects of normal aging on myelin and nerve fibers: a review. *J. Neurocytol.* 31, 581–593. doi: 10.1023/A:1025731309829

Petersen, R. C. (2004). Mild cognitive impairment as a diagnostic entity. *J. Intern. Med.* 256, 183–194. doi: 10.1111/j.1365-2796.2004.01388.x

Petersen, R. C., Doody, R., Kurz, A., Mohs, R. C., Morris, J. C., Rabins, P. V., et al. (2001). Current concepts in mild cognitive impairment. *Arch. Neurol.* 58, 1985–1992. doi: 10.1001/archneur.58.12.1985

Petersen, R. C., Smith, G. E., Ivnik, R. J., Tangalos, E. G., Schaid, D. J., Thibodeau, S. N., et al. (1995). Apolipoprotein E status as a predictor of the development of Alzheimer's disease in memory-impaired individuals. *JAMA* 273, 1274–1278. doi: 10.1001/jama.1995.03520400044042

Pierpaoli, C., Barnett, A., Pajevic, S., Chen, R., Penix, L., Virta, A., et al. (2001). Water diffusion changes in Wallerian degeneration and their dependence on white matter architecture. *Neuroimage* 13, 1174–1185. doi: 10.1006/nimg.2001.0765

Plassman, B. L., Langa, K. M., Fisher, G. G., Heeringa, S. G., Weir, D. R., Ofstedal, M. B., et al. (2007). Prevalence of dementia in the United States: the aging, demographics, and memory study. *Neuroepidemiology* 29, 125–132. doi: 10.1159/000109998

Prins, M., Greco, T., Alexander, D., and Giza, C. C. (2013). The pathophysiology of traumatic brain injury at a glance. *Dis. Model. Mech.* 6, 1307–1315. doi: 10.1242/dmm.011585

Rabin, J. S., Perea, R. D., Buckley, R. F., Johnson, K. A., Sperling, R. A., and Hedden, T. (2019). Synergism between fornix microstructure and beta amyloid accelerates memory decline in clinically normal older adults. *Neurobiol. Aging* 81, 38–46. doi: 10.1016/j.neurobiolaging.2019.05.005

Rizek, P., Pasternak, S., Leung, A., and Jenkins, M. E. (2013). Acute-onset anterograde amnesia caused by isolated bilateral fornix infarction. *Can. J. Neurol. Sci.* 40, 738–739. doi: 10.1017/S0317167100015031

Rizzi, L., Rosset, I., and Roriz-Cruz, M. (2014). Global epidemiology of dementia: Alzheimer's and vascular types. *Biomed. Res. Int.* 2014:908915. doi: 10.1155/2014/908915

Rudebeck, S. R., Scholz, J., Millington, R., Rohenkohl, G., Johansen-Berg, H., and Lee, A. C. (2009). Fornix microstructure correlates with recollection but not familiarity memory. *J. Neurosci.* 29, 14987–14992. doi: 10.1523/JNEUROSCI.4707-09.2009

Salvadores, N., Sanhueza, M., and Manque, P. (2017). Axonal degeneration during aging and its functional role in neurodegenerative disorders. *Front. Neurosci.* 11:451. doi: 10.3389/fnins.2017.00451

Salvalaggio, A., Cagnin, A., Nardetto, L., Manara, R., and Briani, C. (2018). Acute amnestic syndrome in isolated bilateral fornix stroke. *Eur. J. Neurol.* 25, 787–789. doi: 10.1111/ene.13592

Sasson, E., Doniger, G. M., Pasternak, O., Tarrasch, R., and Assaf, Y. (2013). White matter correlates of cognitive domains in normal aging with diffusion tensor imaging. *Front. Neurosci.* 7:32. doi: 10.3389/fnins.2013.00032

Sengupta, P., Ganguly, J., Pal, S., and Ghosal, M. (2019). Pattern of cognitive deficits in vascular dementia. *Indian J. Med. Res.* 149:503. doi: 10.4103/ijmr.IJMR_1336_17

Sexton, C. E., Mackay, C. E., Lonie, J. A., Bastin, M. E., Terrière, E., O'Carroll, R. E., et al. (2010). MRI correlates of episodic memory in Alzheimer's disease, mild cognitive impairment, and healthy aging. *Psychiatry Res. Neuroimaging* 184, 57–62. doi: 10.1016/j.pscychresns.2010.07.005

Sheik, J. (1986). Geriatric Depression Scale (GDS): recent findings and development of a shorter version. *Clin. Gerontol.* 5, 165–173. doi: 10.1300/J018v05n01_09

Takano, Y., Tatewaki, Y., Mutoh, T., Ohara, Y., Yamamoto, S., and Taki, Y. (2018). Isolated fornix infarction with damage to the limbic system as a cause of persistent amnesia: a case report. *Am. J. Med. Case Rep.* 19:1382. doi: 10.12659/AJCR.912508

Tang, Y., Nyengaard, J., Pakkenberg, B., and Gundersen, H. (1997). Age-induced white matter changes in the human brain: a stereological investigation. *Neurobiol. Aging* 18, 609–615. doi: 10.1016/S0197-4580(97)00155-3

Teipel, S. J., Meindl, T., Grinberg, L., Heinsen, H., and Hampel, H. (2008). Novel MRI techniques in the assessment of dementia. *Eur. J. Nucl. Med. Mol. Imaging* 35, 58–69. doi: 10.1007/s00259-007-0703-z

Thomalla, G., Glauche, V., Weiller, C., and Röther, J. (2005). Time course of wallerian degeneration after ischaemic stroke revealed by diffusion tensor imaging. *J. Neurol. Neurosurg. Psychiatry* 76, 266–268. doi: 10.1136/jnnp.2004.046375

Thomas, A. G., Koumellis, P., and Dineen, R. A. (2011). The fornix in health and disease: an imaging review. *Radiographics* 31, 1107–1121. doi: 10.1148/rg.314105729

Tomaiuolo, F., Carlesimo, G., Di Paola, M., Petrides, M., Fera, F., Bonanni, R., et al. (2004). Gross morphology and morphometric sequelae in the hippocampus, fornix, and corpus callosum of patients with severe non-missile traumatic brain injury without macroscopically detectable lesions: a T1 weighted MRI study. *J. Neurol. Neurosurg. Psychiatry* 75, 1314–1322. doi: 10.1136/jnnp.2003.017046

Trongsakul, S., Lambert, R., Clark, A., Wongpakaran, N., and Cross, J. (2015). Development of the Thai version of Mini-Cog, a brief cognitive screening test. *Geriatr. Gerontol. Int.* 15, 594–600. doi: 10.1111/ggi.12318

Turine, G., Gille, M., Druart, C., Rommel, D., and Rutgers, M. P. (2016). Bilateral anterior fornix infarction: the "amnestic syndrome of the subcallosal artery". *Acta Neurol. Belg.* 116, 371–373. doi: 10.1007/s13760-015-0553-6

Uchino, A., Sawada, A., Takase, Y., Egashira, R., and Kudo, S. (2004). Transient detection of early wallerian degeneration on diffusion-weighted MRI after an acute cerebrovascular accident. *Neuroradiology* 46, 183–188. doi: 10.1007/s00234-003-1159-x

Vann, S. D., Tsivilis, D., Denby, C. E., Quamme, J. R., Yonelinas, A. P., Aggleton, J. P., et al. (2009). Impaired recollection but spared familiarity in patients with extended hippocampal system damage revealed by 3 convergent methods. *Proc. Natl. Acad. Sci. U.S.A.* 106, 5442–5447. doi: 10.1073/pnas.0812097106

Venkat, P., Chopp, M., and Chen, J. (2015). Models and mechanisms of vascular dementia. *Exp. Neurol.* 272, 97–108. doi: 10.1016/j.expneurol.2015.05.006

Venketasubramanian, N., Sahadevan, S., Kua, E., Chen, C., and Ng, T.-P. (2010). Interethnic differences in dementia epidemiology: global and Asia-Pacific perspectives. *Dement. Geriatr. Cogn. Disord.* 30, 492–498. doi: 10.1159/000321675

Wang, J., Ke, J., Zhou, C., and Yin, C. (2018). Amnesia due to the injury of papez circuit following isolated fornix column infarction. *J. Stroke Cerebrovasc. Dis.* 27, 1431–1433. doi: 10.1016/j.jstrokecerebrovasdis.2017.12.040

Wang, P., Zhou, B., Yao, H., Xie, S., Feng, F., Zhang, Z., et al. (2020). Aberrant hippocampal functional connectivity is associated with fornix white matter integrity in Alzheimer's disease and mild cognitive impairment. *J Alzheimers Dis.* 75, 1153–1168. doi: 10.3233/JAD-200066

Welsh, M. C., Pennington, B. F., and Groisser, D. B. (1991). A normative-developmental study of executive function: a window on prefrontal function in children. *Dev. Neuropsychol.* 7, 131–149. doi: 10.1080/87565649109540483

Werner, C., and Engelhard, K. (2007). Pathophysiology of traumatic brain injury. *Br. J. Anaesth.* 99, 4–9. doi: 10.1093/bja/aem131

Werring, D. J., Toosy, A. T., Clark, C. A., Parker, G. J., Barker, G. J., Miller, D. H., et al. (2000). Diffusion tensor imaging can detect and quantify corticospinal tract degeneration after stroke. *J. Neurol. Neurosurg. Psychiatry* 69, 269–272. doi: 10.1136/jnnp.69.2.269

Wongpakaran, N., and Wongpakaran, T. (2012). Prevalence of major depressive disorders and suicide in long-term care facilities: a report from northern Thailand. *Psychogeriatrics* 12, 11–17. doi: 10.1111/j.1479-8301.2011.00383.x

Xie, R., Fang, M., Zhou, L., Fan, S., Liu, J., Quan, H., et al. (2012). Diffusion tensor imaging detects Wallerian degeneration of the corticospinal tract early after cerebral infarction. *Neural Regen. Res.* 7, 900–905. doi: 10.3969/j.issn.1673-5374.2012.12.004

Yeh, F.-C., Verstynen, T. D., Wang, Y., Fernández-Miranda, J. C., and Tseng, W. Y. I. (2013). Deterministic diffusion fiber tracking improved by quantitative anisotropy. *PLoS ONE* 8:e80713. doi: 10.1371/journal.pone.0080713

Yeo, S. S., Seo, J. P., Kwon, Y. H., and Jang, S. H. (2013). Precommissural fornix in the human brain: a diffusion tensor tractography study. *Yonsei Med. J.* 54, 315–320. doi: 10.3349/ymj.2013.54.2.315

Yu, Q., Peng, Y., Mishra, V., Ouyang, A., Li, H., Zhang, H., et al. (2014). Microstructure, length, and connection of limbic tracts in normal human brain development. *Front. Aging Neurosci.* 6:228. doi: 10.3389/fnagi.2014.00228

Yuan, P., and Raz, N. (2014). Prefrontal cortex and executive functions in healthy adults: a meta-analysis of structural neuroimaging studies. *Neurosci. Biobehav. Rev.* 42, 180–192. doi: 10.1016/j.neubiorev.2014.02.005

Zhang, Z.-Y., Liu, Z.-Q., Qin, W., Chen, Y.-W., and Liu, Z.-J. (2018). Clinical and radiological features of wallerian degeneration of the middle cerebellar peduncles secondary to pontine infarction. *Chin. Med. J.* 131, 665–671. doi: 10.4103/0366-6999.226890

Zhu, Q. Y., Zhu, H. C., and Song, C. R. (2018). Acute amnesia associated with damaged fiber tracts following anterior fornix infarction. *Neurology* 90, 706–707. doi: 10.1212/WNL.0000000000005306

Zhuang, L., Sachdev, P. S., Trollor, J. N., Reppermund, S., Kochan, N. A., Brodaty, H., et al. (2013). Microstructural white matter changes, not hippocampal atrophy, detect early amnestic mild cognitive impairment. *PLoS ONE* 8:e58887. doi: 10.1371/journal.pone.0058887

Zhuang, L., Wen, W., Trollor, J. N., Kochan, N. A., Reppermund, S., Brodaty, H., et al. (2012). Abnormalities of the fornix in mild cognitive impairment are related to episodic memory loss. *J. Alzheimers Dis.* 29, 629–639. doi: 10.3233/JAD-2012-111766

Conflict of Interest: The authors declare that the research was conducted in the absence of any commercial or financial relationships that could be construed as a potential conflict of interest.

frontiers in Aging Neuroscience

ORIGINAL RESEARCH
published: 15 December 2020
doi: 10.3389/fnagi.2020.608667

Posterior Cingulate Cortex Network Predicts Alzheimer's Disease Progression

Pei-Lin Lee[1], *Kun-Hsien Chou*[1,2], *Chih-Ping Chung*[3,4], *Tzu-Hsien Lai*[3,5], *Juan Helen Zhou*[6,7], *Pei-Ning Wang*[2,3,4]* and *Ching-Po Lin*[1,2]*

[1] Institute of Neuroscience, National Yang-Ming University, Taipei, Taiwan, [2] Brain Research Center, National Yang-Ming University, Taipei, Taiwan, [3] Department of Neurology, School of Medicine, National Yang-Ming University, Taipei, Taiwan, [4] Department of Neurology, The Neurological Institute, Taipei Veterans General Hospital, Taipei, Taiwan, [5] Department of Neurology, Far Eastern Memorial Hospital, New Taipei, Taiwan, [6] Department of Medicine, Yong Loo Lin School of Medicine, National University of Singapore, Singapore, Singapore, [7] Center for Cognitive Neuroscience, Neuroscience & Behavioral Disorders Program, Duke-National University of Singapore Medical School, Singapore, Singapore

Alzheimer's disease (AD) is a progressive neurodegenerative disorder characterized by the accumulation of toxic misfolded proteins, which are believed to have propagated from disease-specific epicenters through their corresponding large-scale structural networks in the brain. Although previous cross-sectional studies have identified potential AD-associated epicenters and corresponding brain networks, it is unclear whether these networks are associated with disease progression. Hence, this study aims to identify the most vulnerable epicenters and corresponding large-scale structural networks involved in the early stages of AD and to evaluate its associations with multiple cognitive domains using longitudinal study design. Annual neuropsychological and MRI assessments were obtained from 23 patients with AD, 37 patients with amnestic mild cognitive impairment (MCI), and 33 healthy controls (HC) for 3 years. Candidate epicenters were identified as regions with faster decline rate in the gray matter volume (GMV) in patients with MCI who progressed to AD as compared to those regions in patients without progression. These epicenters were then further used as pre-defined regions of interest to map the synchronized degeneration network (SDN) in HCs. Spatial similarity, network preference and clinical association analyses were used to evaluate the specific roles of the identified SDNs. Our results demonstrated that the hippocampus and posterior cingulate cortex (PCC) were the most vulnerable AD-associated epicenters. The corresponding PCC-SDN showed significant spatial association with the patterns of GMV atrophy rate in each patient group and the overlap of these patterns was more evident in the advanced stages of the disease. Furthermore, individuals with a higher GMV atrophy rate of the PCC-SDN also showed faster decline in multiple cognitive domains. In conclusion, our findings suggest the PCC and hippocampus are two vulnerable regions involved early in AD pathophysiology. However, the PCC-SDN, but not hippocampus-SDN, was more closely associated with AD progression. These results may provide insight into the pathophysiology of AD from large-scale network perspective.

Keywords: Alzheimer's disease, mild cognitive impairment, structural covariance network, synchronized degeneration network, hippocampus, posterior cingulate cortex

OPEN ACCESS

Edited by:
Yong Liu,
Chinese Academy of Sciences, China

Reviewed by:
Natalia Salvadores,
Universidad Mayor, Chile
Ni Shu,
Beijing Normal University, China

***Correspondence:**
Pei-Ning Wang
pnwang@vghtpe.gov.tw
Ching-Po Lin
cplin@ym.edu.tw

Received: *21 September 2020*
Accepted: *24 November 2020*
Published: *15 December 2020*

Citation:
Lee P-L, Chou K-H, Chung C-P, Lai T-H, Zhou JH, Wang P-N and Lin C-P (2020) Posterior Cingulate Cortex Network Predicts Alzheimer's Disease Progression. Front. Aging Neurosci. 12:608667. doi: 10.3389/fnagi.2020.608667

INTRODUCTION

The human brain is traditionally considered to be a patchwork composed of neurons with specific functions and has been thoroughly dissected into histologically distinct regions based on functional organization or cellular cytoarchitecture. Advances in neuroimaging techniques have generated a novel view of the brain as a complex interconnected system that exerts its functions via both local and long-range connections (Biswal et al., 1995). Although the exact roles of these large-scale brain networks are not fully understood, disruptions of these networks have been demonstrated in various neurological diseases (Ahmed et al., 2016).

A pathological hallmark of neurodegenerative diseases is misfolded protein deposition in specific brain areas. In patients with Alzheimer's disease (AD), β-amyloid and tau proteins are widespread in many cortical regions and are correlated with clinical symptoms and cognitive functions (Braak and Braak, 1991). Recent studies further suggested that these misfolded proteins may be deposited in certain vulnerable anatomical regions early on, and spread along their corresponding large-scale networks in the brain as the disease progresses (Pievani et al., 2014; Franzmeier et al., 2020). According to this brain network degeneration hypothesis, the process may begin in epicenters of disease-specific networks, which are specific brain regions that are structurally and/or functionally vulnerable to the disease (Seeley et al., 2009). Misfolded proteins then spread along corresponding brain networks rather than by geographical proximity (Iba et al., 2013). Based on this hypothesis, several cross-sectional studies have identified AD epicenters as brain areas with maximal atrophy in patients with AD compared to healthy controls (HCs). These epicenters were then used as seeds to determine their corresponding structural and functional brain networks in HCs (Seeley et al., 2009; Dickerson et al., 2017). However, the epicenters identified using this approach may not be the earliest disease-involved regions, as AD pathology accumulates in the brain prior to the onset of clinical symptoms (Jack et al., 2010). In addition, it is also unclear whether these identified brain networks are associated with disease progression.

To identify AD-associated structural brain networks based on characteristics of disease progression, a 3-year-prospective study was conducted and the epicenters were posited as regions with greater annual atrophy rates in gray matter volume (GMV) in patients with mild cognitive impairment (MCI) who progressed to AD during the follow-up period as well as AD patients who were at an earlier stage. These regions were used as candidate epicenters to establish synchronized degeneration networks (SDNs) based on covariance patterns of annual GMV atrophy rates in HCs. This approach has been proposed as a surrogate marker for investigating longitudinal changes in large-scale structural networks (Alexander-Bloch et al., 2013). In contrast with the widely-used structural covariance network approach, which models the cross-sectional co-variance pattern of morphometric features across the study participants, the SDN approach uses longitudinal GMV atrophy rates as a coupling factor to construct the related structural network. Consequently, brain networks established using the SDN approach would more likely capture the progressive characteristic of neurodegenerative disease. We hypothesized that large-scale SDNs established with our identified epicenters could predict disease progression and provide further evidence supporting the network degeneration hypothesis for AD pathophysiology from a longitudinal perspective.

MATERIALS AND METHODS

Participants

Patients with amnestic MCI, patients with AD dementia, and HCs were recruited for the study. During the 3-year follow up, patients with MCI who progressed to AD were classified as MCIp; those that remained stable were classified as MCIs. All patients were recruited from the memory clinic at Taipei Veterans General Hospital (TVGH), Taiwan. Before the study began, written informed consent was obtained from all participants and guardians for AD patients. This study was approved by the Local Ethics Committee of Human Research in TVGH (N0.97-04-1OA). Every subject was interviewed by the neurologist for history-taking and neuropsychological evaluation. Laboratory and MR examinations were used to exclude other major neurological diseases such as tumors, strokes, and severe white matter disease. None of the participants had a history of major head injury, brain tumor, stroke, epilepsy, alcoholism, major psychiatric illness, or other systemic diseases affecting cognitive function. HCs were volunteers with no neurological disease and no cognitive complaints.

Clinical Assessments

The Mini-Mental State Examination (MMSE) was administered to assess global cognitive function (Folstein et al., 1975). To evaluate performance in different cognitive domains, the following cognitive tests were used:

- Verbal memory: the Chinese version of the Verbal Learning Test (CVVLT; nine items, four trials, and 10-min delayed recall) (Chang et al., 2010)
- Language: the categorical (animals) Verbal Fluency Test (VFT) and 30-item Boston Naming Test (BNT) (Cheung et al., 2004)
- Visuospatial function: the modified Rey-Osterrieth Complex Figure Test (CFT) (Boxer et al., 2003)
- Executive function: the modified Trail-Making Test, Part B (TMT-B) (Kramer et al., 2003)

The diagnosis of AD was based on the criteria from the National Institute of Neurological and Communicative Disorders and Stroke-Alzheimer's Disease and Related Disorders Association (NINCDS/ADRDA) (McKhann et al., 1984). All patients with AD had mild dementia with a baseline CDR score of 1 at the time of enrollment. All patients with amnestic MCI fulfilled the Petersen criteria (Petersen et al., 1999): (1) memory complaints, preferably corroborated by an informant; (2) objective memory impairment (verbal memory test, CVVLT $\leq$5, below 1.5 standard deviations of normal data) (Chang et al., 2010); (3) normal general cognitive function (MMSE $\geq$24); (4) intact daily living activities; and (5) dementia criteria not

met. As defined for amnestic MCI, only patients with isolated memory impairments and without neuropsychological evidence of dysfunction in other cognitive domains were recruited. All participants were scheduled to receive clinical and imaging tests annually for 3 years. Only subjects that received at least two MRI examinations (17 participants with 2 consecutive scans and 76 participants with 3 consecutive scans) were included in subsequent analyses.

Image Acquisition

The MRI scans were acquired using an eight-channel phased-array head coil on the identical 1.5 T Excite-II MRI scanner (General Electric Healthcare, Milwaukee, Wisconsin, USA) at TVGH. Foam pads were used to minimize head movement during image acquisition. T1 weighted anatomical images were acquired using a 3-dimensional fluid-attenuated inversion-recovery fast spoiled gradient recalled echo sequence with the following imaging parameters: repetition time/echo time/inversion time = 8.548/1.836/400 ms; flip angle = 15 degrees; number of excitations = 1; matrix size = 256 × 256 × 124 without inter-slice gap and interpolation; and voxel size = 1.02 × 1.02 × 1.50 mm^3. Each individual brain scan was manually inspected for image artifacts and gross anatomical abnormalities by an experienced radiologist before the morphometry analysis. No participant was excluded for brain abnormalities. Before subsequent image processing, we reoriented all images to have an approximate point of origin at the anterior commissure.

Image Analysis

A general overview of the analytical framework is illustrated in **Figure 1**. Details of the analytic pipeline are summarized below.

Estimating Individual Voxel-Wise Anatomical Changing Rate Map

To estimate voxel-wise anatomical brain changes over time and enable subsequent statistical analyses independent of the number of time points, a two-stage tensor-based morphometry approach was applied using Statistical Parametric Mapping software (SPM12 version 7487, Wellcome Institute of Neurology, University College London, UK, http://www.fil.ion.ucl.ac.uk/spm/) with default settings and in-house MATLAB codes (R2018a, Mathworks, Natick, MA). In the first stage, all available native space T1w scans for each individual were warped longitudinally to their corresponding midpoint average image using an inverse-consistent non-linear registration approach available in the "Serial Longitudinal Registration" module of SPM12 (Ashburner and Ridgway, 2012). Experiment times for each scan were entered into the registration algorithm, generating Jacobian determinant maps of each time point and the corresponding midpoint average images for each individual. All midpoint average anatomical images were subsequently segmented into three distinct tissue types (gray matter, white matter, and cerebrospinal fluid) using a unified segmentation approach (Ashburner and Friston, 2005). The resulting gray and white matter tissue segments were used to construct group-specific tissue templates and estimate deformation fields using a fast diffeomorphic image registration algorithm (Ashburner, 2007). This procedure enabled the transformation of individual Jacobian determinant maps into the standard Montreal Neurological Institute (MNI) space. Subsequently, to estimate voxel-wise changing rate maps, a linear regression model was applied to the MNI-space Jacobian determinant maps of each time point for each individual participant. The estimated slope of the regression model presented the changing rate of the brain across multiple time points. The resulting changing rate maps were then further smoothed using an isotropic 8 mm full-width at half-maximum Gaussian kernel. These preprocessed data encoded the relative speed of brain expansion or contraction per individual, and were used for subsequent voxel- and network-level analyses. To exclude partial volume effects of borders between different tissue types, individual unmodulated gray matter segments of corresponding midpoint average images were averaged and set at a threshold (0.2 intensity) to create explicit masks. Individual native space baseline T1w scans were used to estimate total intracranial volume.

Voxel-Wise Statistical Analyses of Changing Rate Maps

The GLM Flex toolbox (http://mrtools.mgh.harvard.edu/index.php?title=GLM_Flex) with appropriate statistical models was used for the following voxel-wise statistical analyses. A single-factor-four-level (HC, MCIp, MCIs, and AD) analysis of covariance with age, sex, educational years, and total intracranial volume as nuisance covariates was used to identify between-group differences in GMV changing rates of local brain areas. A separate one-sample *t*-test was performed for each study group to map group-specific degenerative patterns (different from zero) over time. Voxel-wise statistical results were set at a voxel-level uncorrected $p < 0.005$ and extent threshold of family wise error (FWE) corrected $p < 0.05$ (cluster extent = 513 voxels) using the updated "3dFWHMx" and "3dClustSim" programs implemented in the Analysis of Functional Neuroimages software (AFNI, version 19.3.17). For transparency and reusability of statistical results, all unthresholded statistical maps of direct group comparisons and group-specific degenerative patterns can be downloaded from the NeuroVault website (https://neurovault.org/collections/3273/).

Disease-Specific Epicenter Identification and Synchronized Structural Degeneration Network Analysis

Disease-specific epicenters for synchronized SDN analysis were identified by placing 6-mm-radius spheres at the most-significant voxel from the above direct-group voxel-wise changing rate analysis (MCIp vs. MCIs). Brain regions with significantly higher GMV changing rates in MCIp were defined as early AD-associated epicenters and further selected as seed regions-of-interest (ROIs) for mapping large-scale SDNs in HCs. In accordance with previous longitudinal studies (Alexander-Bloch et al., 2013), we extracted mean changing rate values of seed ROIs (hippocampus and the posterior cingulate cortex [PCC]) and

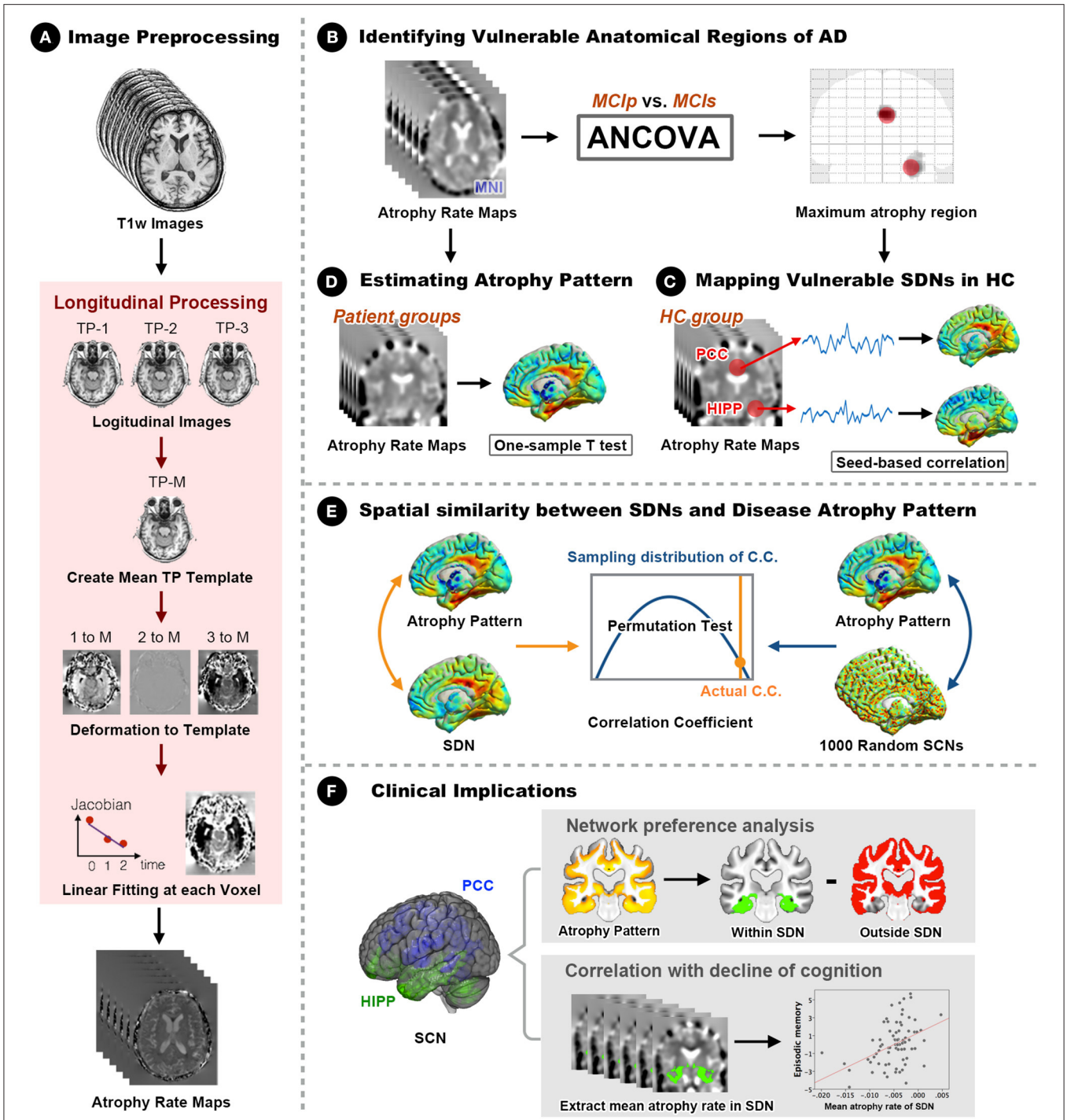

FIGURE 1 | Framework of the study design and analyses. **(A)** The optimized longitudinal anatomical image preprocessing pipeline was used to generate individual annual changing rate maps in Montreal Neurological Institute (MNI) standard space. **(B)** Vulnerable regions (hippocampus and PCC) were identified by comparing MNI space annual changing rate maps between MCIp and MCIs groups. **(C)** Seed-based correlation analyses were conducted to identify corresponding large-scale synchronized degeneration networks (SDNs) in the HC group. **(D)** A one-sample *t*-test was performed for each patient group to map group-specific degenerative patterns (different than zero) over time. **(E)** Permutation test was conducted to assess the spatial similarity between SDNs and group-specific degenerative patterns by comparing the strength of actual correlations with the distribution from randomly generated SDNs. **(F)** Network preference analysis and Spearman correlation analysis were conducted to investigate clinical implications. AD, Alzheimer's disease; ANCOVA, analysis of covariance; C.C., correlation coefficient; HC, healthy control; HIPP, hippocampus; MCIp, mild cognitive impairment with progression to AD; MCIs, mild cognitive impairment stable without progression to AD; PCC, posterior cingulate cortex; TP, time point; SDN, synchronized degeneration network.

then entered these values into respective general linear models to identify possible coupling patterns between seed ROIs and voxels across the rest of the brain in HCs. The same nuisance covariate settings and statistical criteria were used for SDN analyses. Unthresholded statistical maps of these SDNs are also available at the NeuroVault website (https://neurovault.org/collections/3273/).

Spatial Similarity and Network Preference Analyses

To investigate whether AD-specific SDNs predicted the longitudinal GMV atrophy rate in each disease group, a voxel-wise spatial cross-correlation approach was used to assess similarities between spatial distributions of unthresholded group-specific degenerative maps and SDN maps (Douaud et al., 2014). Using non-parametric permutation tests to assess the statistical significance of observed spatial relationships, 1,000 random Gaussian noise maps were generated and smoothed with corresponding estimated smoothness from SDN maps. We then calculated 1,000 spatial cross-correlations between simulated SDNs and group-specific degenerative maps, and compared the strength of observed correlations with the empirically generated null distribution. To test whether AD-specific SDNs exhibited different vulnerability levels in each disease group, network preference analysis was conducted (Seeley et al., 2009). First, binarized network-level ROIs were generated from previous SDN analysis with statistical thresholding (cluster-level FWE corrected $p < 0.05$). We then calculated the goodness-of-fit (GOF) score between binarized network ROIs and group-specific degenerative patterns (from previous one-sample *t*-tests of voxel-wise changing rate map analysis). The GOF score reflected how well SDNs fit each group-specific degenerative pattern, and was defined by the difference between the mean *z*-value within and outside the binarized network ROIs. Furthermore, to confirm the stability and reliability of the results of the network preference analysis, we performed an additional GOF analysis using binarized network-level ROIs with fixed network size. More specifically, we first ranked the whole brain voxels from highest to lowest according to the corresponding voxel-wise *z*-value of PCC- and hippocampus-epicentered network analyses. After voxel ranking procedure, 10 binarized network ROIs with different network sizes from the top 1 to 10 percent of all brain voxels with 1 percent intervals were generated for the PCC- and hippocampus-epicentered SDNs, respectively. This procedure provides a more identical network size for both AD-specific SDNs to be used in the GOF-based network preference analysis. The GOFs scores were then calculated using the same approach which was mentioned above.

Relationship Between Cognitive Decline and the Mean Changing Rate of AD-Specific Synchronized Structural Degeneration Networks

To investigate the relationships between AD-specific SDNs and cognitive decline, mean GMV changing rates of AD-specific SDNs were extracted, averaged, and entered into MATLAB software to perform partial Spearman's rank order correlation analysis with the changing rate of neuropsychological test scores. Participants' age, sex, education years, and total intracranial volume were included as nuisance variables. A Bonferroni correction was applied to correct for multiple comparisons for correlation analyses, excluding the MMSE which was considered a separate test representing global cognition. The threshold for statistical significance was set at corrected $p < 0.05$.

Statistical Analyses of Demographic, Clinical Characteristics, and Global Tissue Volume at Baseline

The statistical analyses of non-voxel-wise data were performed with IBM SPSS Statistics Version 25 (Armonk, NY). We used the Shapiro-Wilk normality test to check that each variable was normally distributed. The Chi-square test was used to examine categorical data. The Analysis of Variance and Kruskal-Wallis rank sum tests were used to identify differences in continuous variables after considering distributional assumptions. Two-tailed $p < 0.05$ were considered statistically significant.

RESULTS

Patients' Characteristics and Clinical Data

In total, 23 patients with AD, 37 patients with MCI, and 33 HCs were included at baseline. During the 3-year follow-up, 12 of the patients with MCI progressed to AD (MCIp); the remaining 25 patients remained stable (MCIs). Patient demographics and baseline cognitive function test results are listed in **Table 1**. Age and sex were similar among study groups. Differences in education years were noted. *Post-hoc* analysis revealed greater education years in HCs than in MCIp ($p = 0.011$) and AD patients ($p = 0.036$). Significant differences were observed in the baseline cognitive function test results between study groups with the exception of the complex figure test copy section (CFT copy). In the majority of tests, HCs performed better than MCIs, followed by MCIp and AD.

Epicenter Identification and Group Differences in Annual GMV Atrophy Rate

Using the direct group comparison of voxel-wise annual GMV atrophy rate maps between patients with MCIp and MCIs, the hippocampus and PCC were identified as the early AD-associated disease epicenters (**Figure 2A**). Additionally, all possible group differences in the regional GMV atrophy rate are illustrated in **Supplementary Figure 1**; detailed anatomical locations are listed in **Supplementary Table 1**. Overall, the AD group had the fastest atrophy rate, followed by MCIp, MCIs, and HC groups. More specifically, compared to HCs, patients with AD had faster atrophy rates in the hippocampus, temporal pole, frontal lobe, cingulate gyrus, and cuneus/precuneus. No brain areas exhibited a decreased annual GMV atrophy rate when comparing disease groups and HCs.

Spatial Distribution of Vulnerable SDNs

The spatial distribution of large-scale hippocampus- and PCC-epicenter SDNs are illustrated in **Figure 2B** and the detailed anatomical locations of the corresponding SDNs are listed in **Supplementary Table 2**. The hippocampus-epicentered SDN involved brain areas surrounding the hippocampus

TABLE 1 | Demographics and baseline clinical characteristics.

	HC	MCIs	MCIp	AD	*p*-value	*Post-hoc* comparisons
Number	33	25	12	23		
Female [*n*, (%)]	18 (54.5%)	16 (64.0%)	6 (50.0%)	12 (52.2%)	0.804[a]	
Age (years)	74.9 (5.46)	77.1 (6.08)	77.1 (6.24)	78.3 (5.79)	0.066[b]	
Education (years)	13.1 (3.21)	12.4 (3.53)	9.58 (4.48)	10.3 (4.87)	0.035[b]	HC>MCIp/AD
MMSE	28.5 (1.42)	27.2 (1.87)	24.7 (2.50)	20.7 (2.86)	<0.001[b]	HC>MCIs>MCIp>AD
CVVLT	7.79 (1.29)	5.04 (1.43)	3.50 (2.81)	1.04 (1.40)	<0.001[c]	HC>MCIs/MCIp>AD
CFT copy	15.7 (1.57)	15.4 (1.71)	14.8 (2.01)	15.0 (1.72)	0.352[b]	
CFT recall	11.5 (3.28)	6.96 (3.43)	4.58 (4.19)	0.83 (1.85)	<0.001[b]	HC>MCIs/MCIp>AD
VFT	16.8 (3.88)	12.7 (3.08)	13.6 (3.85)	12.3 (4.08)	<0.001[b]	HC>MCIs/MCIp/AD
BNT	28.2 (2.32)	26.6 (2.23)	24.5 (3.50)	23.5 (3.36)	<0.001[b]	HC>MCIs/MCIp/AD; MCIs>AD
TMT-B lines	13.3 (2.28)	11.4 (3.76)	11.2 (3.97)	8.59 (5.03)	<0.001[b]	HC>MCIs/MCIp/AD; MCIs>AD
GMV (cm^3)	592 (57.1)	578 (56.9)	569 (51.5)	544 (47.0)	0.015[c]	HC/MCIs>AD
WMV (cm^3)	398 (50.8)	399 (47.5)	385 (46.0)	375 (33.9)	0.230[c]	
CSFV (cm^3)	471 (92.7)	504 (80.4)	506 (88.9)	499 (87.5)	0.073[c]	
TIV (cm^3)	1,460 (146)	1,481 (118)	1,461 (152)	1,451 (131)	0.895[c]	

[a] *Chi-square test was used for group comparison in categorical variables.*

[b] *Kruskal-Wallis rank sum test was used for comparing of group differences in continuous variables with non-normal distributions.*

[c] *Analysis of variance test was used for comparing group differences in continuous variables with a normal distribution.*

AD, Alzheimer's disease; BNT, Boston Naming Test; CFT, Complex Figure Test; CSFV, Cerebrospinal fluid volume; CVVLT, Chinese version of the Verbal Learning Test; GMV, gray matter volume; HC, healthy controls; MCIp, mild cognitive impairment-progression; MCIs, mild cognitive impairment-stable; MMSE, Mini-Mental Screening Examination; TIV, total intracranial volume; TMT-B lines, Trail-making Test Part B lines completed in 120 s; VFT, Verbal Fluency Test; WMV, white matter volume.

(parahippocampus, entorhinal cortex, temporal pole, and temporal fusiform cortex), frontal poles, and the cerebellum. On the other hand, the PCC-epicentered SDN included more widespread brain areas, including the cingulate, frontal lobe, temporal lobe, insula, and cerebellum.

Spatial Similarity Between Vulnerable SDNs and GMV Atrophy Rate Patterns in Disease Groups

The voxel-wise spatial patterns of GMV atrophy rates for each disease group are illustrated in **Figure 2C**. Significant spatial correlation between atrophy patterns and SDNs were noted for PCC-epicentered SDN (MCIs: $r = 0.571$, $p < 0.001$; MCIp: $r = 0.639$, $p < 0.001$; AD: $r = 0.570$, $p < 0.001$) and hippocampus-epicentered SDN (MCIs: $r = 0.285$, $p < 0.001$; MCIp: $r = 0.415$, $p < 0.001$), with the exception of the hippocampus-epicentered SDN in the AD group ($r = 0.1$, $p > 0.99$).

Network Preference Analysis Revealed the Specific Role of Each SDN

To examine network preferences across different disease stages, we investigated the fitness between hippocampus/PCC-epicentered SDNs and whole-brain atrophy rate patterns of all disease groups (**Figure 3**). We first generated binarized masks of hippocampus- and PCC-epicentered SDNs (FWE-corrected $p < 0.05$, **Figure 3A**), and calculated the GOF according to the different disease stages (**Figure 3B**). A higher GOF represented more similarity between the SDN and disease atrophy pattern. For the PCC-epicentered SDN, overlaps were more evident with more advanced disease stages (GOF scores in MCIs = 0.610; MCIp = 0.827; AD = 0.874). This trend was not observed for the hippocampus-epicentered SDN (GOF scores in MCIs = 0.380; MCIp = 0.213; AD = 0.230). Furthermore, the additional GOF-based network preference analysis, which uses a different degree of fixed size approach to determine the network ROIs, also demonstrated the same relationship between SDN and disease atrophy pattern across different disease stages (**Supplementary Figure 2**).

Correlations Between the GMV Atrophy Rate of SDNs and Cognitive Decline

To test whether large-scale SDNs were associated with progressive cognitive decline, we performed exploratory correlation analyses between mean annual GMV atrophy rates of each SDN and deterioration slopes of neuropsychological test scores (**Table 2**). Significant correlations between PCC-epicentered SDN, but not hippocampus-epicentered SDN, and cognitive decline were observed in most domains (including MMSE, CVVLT, CFT recall, VFT, and BNT).

DISCUSSION

The results from this 3-year longitudinal study support the network degeneration hypothesis of AD. Our results indicated that the PCC and hippocampus were the two most vulnerable regions involved in the early-stage of AD. Spatial correlation analysis further demonstrated PCC- and hippocampus-epicentered SDNs in HCs strongly associated with the GMV atrophy patterns of disease groups. However, only the PCC-epicentered SDN was associated with disease severity, and its GMV atrophy rate predicted cognitive decline in multiple domains. These findings collectively indicate the

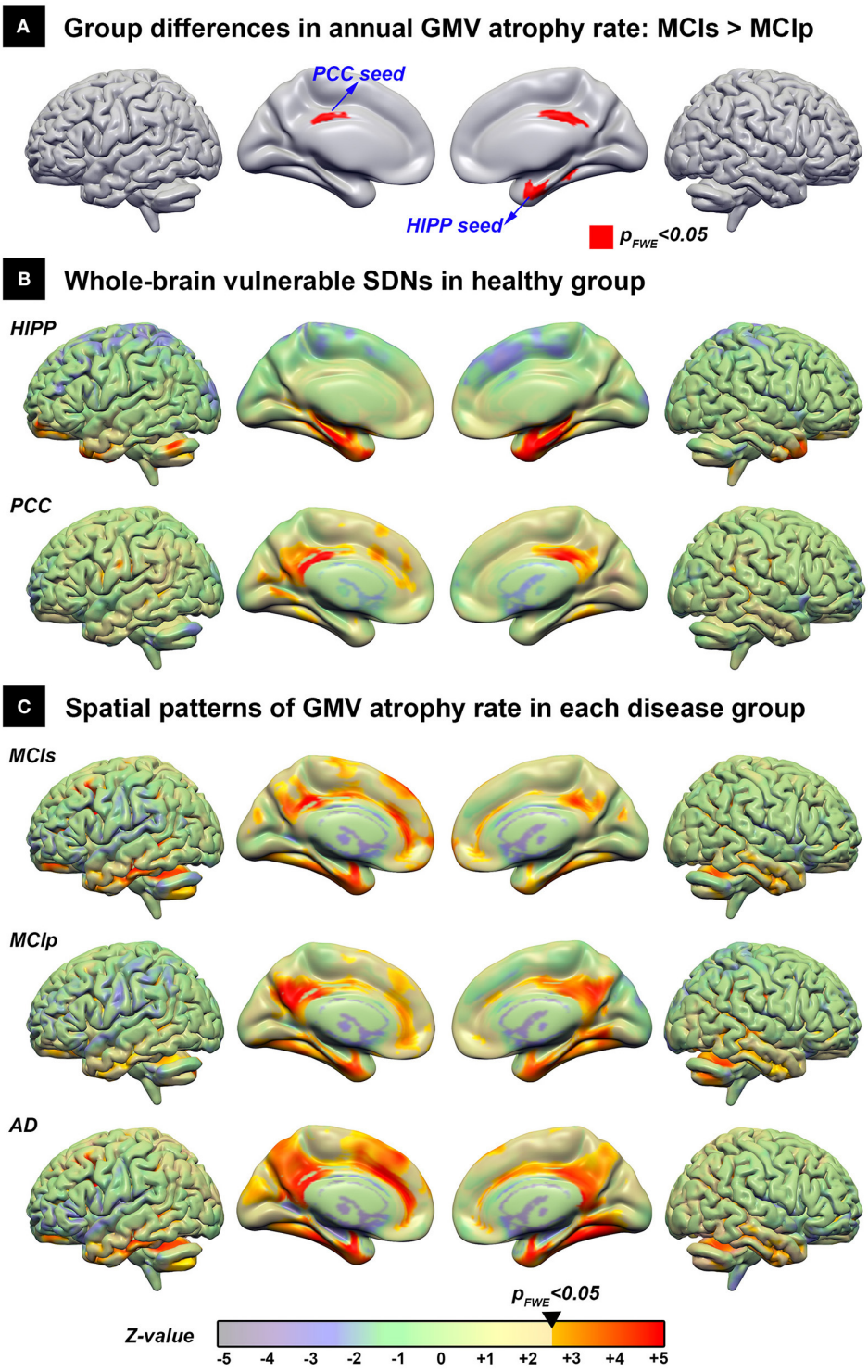

FIGURE 2 | The spatial distribution of the vulnerable SDNs and GMV atrophy rate patterns in disease groups. **(A)** Direct group comparison of the annual gray matter atrophy rate between MCIs and MCIp groups to identify early AD-associated epicenters. **(B)** Whole brain vulnerable SDNs illustrated in the HC group by seed-based correlation analyses in the epicenters on **(A)**. **(C)** Group-specific spatial patterns in each patient group based on one-sample *t*-tests. The transparent colors indicate the *z*-value of statistical results without a significant threshold; the solid colors show the significant regions. AD, Alzheimer's disease; HC, healthy control; HIPP, hippocampus; GMV, gray matter volume; MCIp, mild cognitive impairment with progression to AD; MCIs, mild cognitive impairment stable without progression to AD; PCC, posterior cingulate cortex; SDN, synchronized degeneration network.

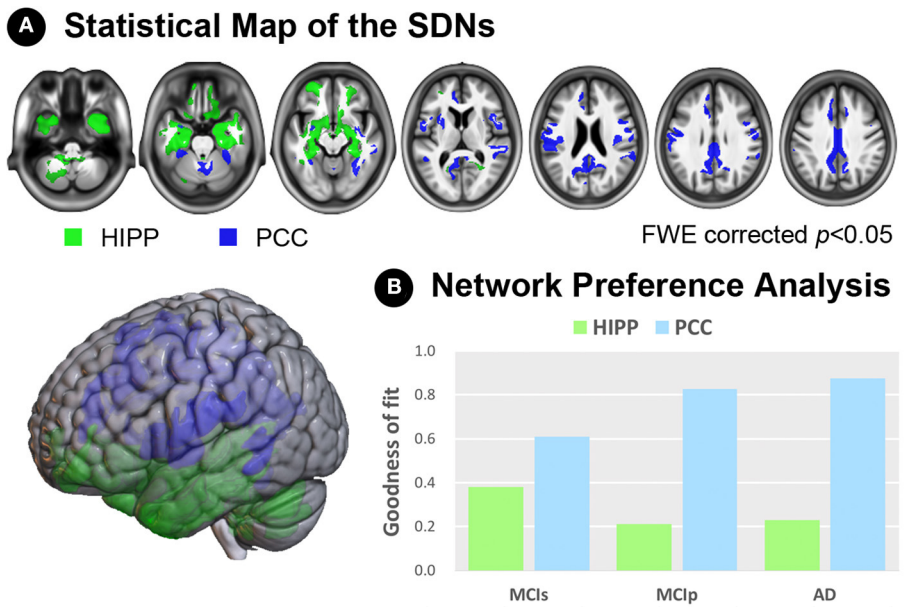

FIGURE 3 | Network preference analysis. **(A)** Statistical maps of the hippocampus- and PCC-SDNs. **(B)** Preference determined by goodness-of-fit showed a stronger association of the PCC-SDN than that of the hippocampus-SDN, especially in the MCIp and AD groups. AD, Alzheimer's disease; FWE, family-wise error; HIPP, hippocampus; MCIp, mild cognitive impairment with progression to AD; MCIs, mild cognitive impairment stable without progression to AD; PCC, posterior cingulate cortex; SDN, synchronized degeneration network.

TABLE 2 | Correlations between the mean annual gray matter volume atrophy rate and slopes of neuropsychological test scores.

	Spearman rank order test correlation coefficients			
	Hippocampus-SDN		PCC-SDN	
	rho	*p*-value	rho	*p*-value
MMSE	0.001	0.994	**0.245**	**0.035***
CVVLT	0.093	0.432	**0.400**	**<0.001†**
CFT copy	−0.030	0.799	0.052	0.659
CFT recall	0.089	0.455	**0.336**	**0.004†**
VFT	0.150	0.202	**0.429**	**<0.001†**
BNT	0.298	0.010	**0.304**	**0.008†**
Trail B line	0.052	0.668	0.215	0.076

*$p < 0.05$.
†$p < 0.008$ (statistically significant correlation after Bonferroni correction).
BNT, Boston Naming Test; CFT, Complex Figure Test; CVVLT, Chinese version of the Verbal Learning Test; MMSE, Mini-Mental Screening Examination; PCC, posterior cingulate cortex; SDN, synchronized degeneration network; TMT-B lines, Trail-making Test Part B lines completed in 120 s; VFT, Verbal Fluency Test.
Significant values are bolded.

distinct roles of PCC- and hippocampus-epicentered SDNs in the pathophysiology of AD.

The hippocampus, which plays an important role in declarative memory, is the anatomical signature of AD (Schröder and Pantel, 2016). Hippocampal atrophy, and more specifically, its atrophy rate, may be potential biomarkers to predict the conversion from MCI to AD (Henneman et al., 2009). Our voxel-wise atrophy rate analyses supported the regional role of the hippocampus in AD progression. In addition to its regional significance, the hippocampus has also been shown to be an important node in several large-scale brain networks and has been implicated as part of the subsystem of the default mode network (DMN) (Andrews-Hanna et al., 2010). Decreased integrity of hippocampus-associated functional and structural networks has also been reported (Zhou et al., 2008; O'Callaghan et al., 2019). In this study, we used the coupling atrophy rate as a surrogate image marker for longitudinal mapping of potential large-scale brain SDNs. We identified the parahippocampus, temporal pole, temporal fusiform cortex, frontal poles, and cerebellum within a single hippocampus-epicentered SDN. Although network mapping approaches vary among studies, the spatial distribution of identified hippocampus-epicentered SDNs is highly accordant with previous studies (Bai et al., 2009; Zhu et al., 2018). Close connections between the hippocampus and nearby regions, collectively referred to as the medial temporal lobe, have been reported in various histopathological and neuroimaging findings of AD (Braak and Braak, 1985, 1991). Beyond the limbic system, considerable evidence indicates that the hippocampus and prefrontal cortex become coupled via oscillatory synchrony reflecting bidirectional information flow (Battaglia et al., 2011) and may play an important role in memory and learning (Eichenbaum, 2017). Taken together, these regional and network-level findings underscore the importance of the hippocampus and its corresponding functionally/structurally connected areas in AD pathophysiology.

The PCC is an area in the brain with higher metabolic activity and dense anatomical and functional connections to many

other brain regions. PCC hypometabolism, volume atrophy, and connectivity corruption have been reported in patients with AD (Leech and Sharp, 2014). Longitudinal follow-up in patients with MCI revealed that changes in PCC connectivity over time were correlated with declines in MMSE and other cognitive test scores (Wang et al., 2012). From a global network perspective, the PCC is considered to be a central hub of the DMN and is interconnected with several large-scale brain networks (Raichle et al., 2001). Based on its regional and global characteristics, previous studies have indicated that the PCC may be involved in multiple cognitive functions including autobiographical/episodic memory retrieval, attention, salience, attention, and emotion (Leech and Sharp, 2014). These domains of cognitive function also changed during AD progression (Mortamais et al., 2017). Among these multiple PCC-connected large-scale brain networks, DMN is the first and most consistently reported network to be involved in AD (Badhwar et al., 2017). DMN failure begins early in the course of AD, even prior to measurable amyloid accumulation (Jones et al., 2016). Furthermore, using various network mapping approaches, including intrinsic functional connectivity and the cross-sectional structural covariance method, previous studies have reported that the integrity of the PCC-epicentered DMN may be associated with the clinical severity and progression of AD (Zhang et al., 2010), suggesting that the PCC and its corresponding brain networks have important roles in AD progression.

In our study, the PCC-epicentered SDN involved widespread frontal, temporal, insular, and cerebellar areas. Most of these areas overlap with the classical DMN that includes the precuneus, medial and lateral parietal, medial prefrontal, and medial and lateral temporal cortices (Raichle, 2015). The insular cortex is a notable exception, as it is typically not included in the DMN. The insular cortex is a core limbic area, historically and phylogenetically associated with emotion, and may underpin the behavioral and emotional symptoms in AD (Spalletta et al., 2010). The insular and anterior cingulate cortices are key hubs of the salience network that is also involved in AD and MCI. The insula may play a role in connecting the salience network and DMN, switching from externally-oriented to internally-oriented mental status (Sridharan et al., 2008). Functional and structural disruptions to the switching mechanism occur with disease progression in patients with AD (Xie et al., 2012; Liu et al., 2018). On the other hand, the cerebellum was shown to be involved in the PCC-epicentered SDN. Although traditionally considered to be involved in motor coordination, recent studies have further suggested that the cerebellum may be involved in multiple domains of cognitive function based on its complex spatial connectivity profile with large-scale cortical brain networks (King et al., 2019). Beyond its spatial characteristics, recent intrinsic functional connectivity studies have further suggested that the cerebellum may engage in a domain-general function in the adaptive control of the cortical process which may impaired in the progression of AD (Bai et al., 2011; Zheng et al., 2017; Marek et al., 2018). Taken together, these findings suggest the potential importance of the cerebellum in the pathogenesis of AD.

The findings of our study demonstrated that compared to the hippocampus-epicentered SDN, the PCC-epicentered SDN atrophy rate was more strongly correlated with deterioration slopes of cognitive tests in multiple domains. Moreover, the PCC-epicentered SDN predicted AD progression better than did the hippocampus SDN. One possible explanation is that the hippocampus and the surrounding entorhinal cortex are involved earliest in the course of AD (Braak and Braak, 1991), which might suggest that further atrophy rate in the hippocampus SDN is not as relevant. In addition, compared to the hippocampus, the PCC may be an integrative hub which mediates information flow across whole-brain networks (Leech and Sharp, 2014). Although the PCC and hippocampus are both components of the DMN, and considering the different functional roles in the DMN (central vs. peripheral), we propose that deficits in the PCC-epicentered network may better represent overall AD progression in terms of structural changes and cognitive decline in multiple domains. In addition, the fact that we did not observe any correlation between hippocampus-epicentered network and cognitive decline might be due to the small sample size in the current study. Future studies with a larger sample size will be needed to confirm the potential role of core PCC region and related connected brain areas and to determine the exact mechanism of the involvement of this region in the pathophysiology of AD.

To the best of our knowledge, this study is the first to investigate the associations between structural network changes, brain volume atrophy, and cognitive decline using an SDN approach from a longitudinal perspective. One strength of our study was its longitudinal follow-up design, which enabled us to identify AD-related epicenters involved early in the course of AD. Additionally, we demonstrated a relationship between large-scale structural brain networks and AD progression. However, our results should be interpreted with caution; first, due to the longitudinal design, the dropout rate was high, limiting the generalizability of our results to large disease populations. However, our exploratory findings may guide future studies with larger samples. Second, AD and MCI diagnoses were made according to characteristic clinical presentation and neuropsychological performance. Although these criteria are widely accepted for both clinical and research purposes, potential bias may exist due to a lack of amyloid and tau biomarkers. Third, we defined the structural networks based on brain regions with maximal changes during the conversion from MCI to AD; earlier changes occurring during the progression from HC to MCI might have been overlooked.

In conclusion, the PCC and hippocampus are two vulnerable regions involved early in AD pathophysiology. Notably, the PCC-epicentered, but not hippocampus-epicentered, network predicts AD progression, including brain atrophy and cognitive decline. Our results support the network degeneration hypothesis of AD and suggest that PCC large-scale SDNs may be used as potential markers for disease progression. Further, the results provide insight regarding the mechanisms of network pathology in AD.

DATA AVAILABILITY STATEMENT

Unthresholded statistical maps of all voxel-wise analyses are available to download from the NeuroVault repository (https://neurovault.org/collections/3273/). Requests to access the datasets should be directed to Ching-Po Lin, cplin@ym.edu.tw.

ETHICS STATEMENT

The studies involving human participants were reviewed and approved by Local Ethics Committee of Human Research in Taipei Veterans General Hospital (N0.97-04-1OA). The patients/participants provided their written informed consent to participate in this study.

AUTHOR CONTRIBUTIONS

C-PL and P-NW were responsible for study concept and design. P-LL and K-HC were responsible for data acquisition and analyses. P-LL, K-HC, C-PC, T-HL, and JZ were responsible for drafting the manuscript, tables, and figures. All authors contributed to the article and approved the submitted version.

FUNDING

This work was supported in part by funds from Taiwan Ministry of Science and Technology (MOST 103-2321-B-010-014, MOST 109-2634-F-010-001, MOST 108-2420-H-010-001, MOST 108-2321-B-010-010-MY2 to C-PL; MOST 107-2221-E-010-010-MY3 to K-HC; MOST 108-2321-B-010-013-MY2 to C-PL, K-HC, and P-NW), the Brain Research Center, National Yang-Ming University from The Featured Areas Research Center Program within the framework of the Higher Education Sprout Project by the Ministry of Education (MOE) in Taiwan, and the Taipei Veterans General Hospital (V106C-075, V107C-090 to P-NW; VGHUST109-V1-3-3, VGHUST109-V1-2-2 to C-PL).

ACKNOWLEDGMENTS

We would like to thank the study participants and the research assistants for actively participating.

SUPPLEMENTARY MATERIAL

The Supplementary Material for this article can be found online at: https://www.frontiersin.org/articles/10.3389/fnagi.2020.608667/full#supplementary-material

REFERENCES

Ahmed, R. M., Devenney, E. M., Irish, M., Ittner, A., Naismith, S., Ittner, L. M., et al. (2016). Neuronal network disintegration: common pathways linking neurodegenerative diseases. *J. Neurol. Neurosurg. Psychiatr.* 87, 1234–1241. doi: 10.1136/jnnp-2014-308350

Alexander-Bloch, A., Raznahan, A., Bullmore, E., and Giedd, J. (2013). The convergence of maturational change and structural covariance in human cortical networks. *J. Neurosci.* 33, 2889–2899. doi: 10.1523/JNEUROSCI.3554-12.2013

Andrews-Hanna, J. R., Reidler, J. S., Sepulcre, J., Poulin, R., and Buckner, R. L. (2010). Functional-anatomic fractionation of the Brain's default network. *Neuron* 65, 550–562. doi: 10.1016/j.neuron.2010.02.005

Ashburner, J. (2007). A fast diffeomorphic image registration algorithm. *Neuroimage* 38, 95–113. doi: 10.1016/j.neuroimage.2007.07.007

Ashburner, J., and Friston, K. J. (2005). Unified segmentation. *Neuroimage* 26, 839–851. doi: 10.1016/j.neuroimage.2005.02.018

Ashburner, J., and Ridgway, G. R. (2012). Symmetric diffeomorphic modeling of longitudinal structural MRI. *Front. Neurosci.* 6:197. doi: 10.3389/fnins.2012.00197

Badhwar, A., Tam, A., Dansereau, C., Orban, P., Hoffstaedter, F., and Bellec, P. (2017). Resting-state network dysfunction in Alzheimer's disease: A systematic review and meta-analysis. *Alzheimers Dement.* 8, 73–85. doi: 10.1016/j.dadm.2017.03.007

Bai, F., Liao, W., Watson, D. R., Shi, Y., Yuan, Y., Cohen, A. D., et al. (2011). Mapping the altered patterns of cerebellar resting-state function in longitudinal amnestic mild cognitive impairment patients. *J. Alzheimers. Dis.* 23, 87–99. doi: 10.3233/JAD-2010-101533

Bai, F., Zhang, Z., Watson, D. R., Yu, H., Shi, Y., Yuan, Y., et al. (2009). Abnormal functional connectivity of hippocampus during episodic memory retrieval processing network in amnestic mild cognitive impairment. *Biol. Psychiatry.* 65, 951–958. doi: 10.1016/j.biopsych.2008.10.017

Battaglia, F. P., Benchenane, K., Sirota, A., Pennartz, C. M., and Wiener, S. I. (2011). The hippocampus: hub of brain network communication for memory. *Trends Cogn. Sci.* 15, 310–318. doi: 10.1016/j.tics.2011.05.008

Biswal, B., Y. F., Haughton, V. M., and Hyde, J. S. (1995). Functional connectivity in the motor cortex of resting human brain using echo-planar MRI. *Magn. Reson. Med.* 34, 537–541. doi: 10.1002/mrm.1910340409

Boxer, A. L., Kramer, J. H., Du, A. T., Schuff, N., Weiner, M. W., Miller, B. L., et al. (2003). Focal right inferotemporal atrophy in AD with disproportionate visual constructive impairment. *Neurology* 61, 1485–1491. doi: 10.1212/01.WNL.0000090568.34810.47

Braak, H., and Braak, E. (1985). On areas of transition between entorhinal allocortex and temporal isocortex in the human brain. normal morphology and lamina-specific pathology in Alzheimer's disease. *Acta Neuropathol.* 68, 325–332. doi: 10.1007/BF00690836

Braak, H., and Braak, E. (1991). Neuropathological stageing of Alzheimer-related changes. *Acta Neuropathol.* 82, 239–259. doi: 10.1007/BF00308809

Chang, C. C., Kramer, J. H., Lin, K. N., Chang, W. N., Wang, Y. L., Huang, C. W., et al. (2010). Validating the Chinese version of the verbal learning test for screening Alzheimer's disease. *J. Int. Neuropsychol. Soc.* 16, 244–251. doi: 10.1017/S1355617709991184

Cheung, R. W., Cheung, M. C., and Chan, A. S. (2004). Confrontation naming in Chinese patients with left, right or bilateral brain damage. *J. Int. Neuropsychol. Soc.* 10, 46–53. doi: 10.1017/S1355617704101069

Dickerson, B. C., Brickhouse, M., McGinnis, S., and Wolk, D. A. (2017). Alzheimer's disease: The influence of age on clinical heterogeneity through the human brain connectome. *Alzheimers Dement.* 6, 122–135. doi: 10.1016/j.dadm.2016.12.007

Douaud, G., Groves, A. R., Tamnes, C. K., Westlye, L. T., Duff, E. P., Engvig, A., et al. (2014). A common brain network links development, aging, and vulnerability to disease. *Proc. Natl. Acad. Sci. U.S.A.* 111, 17648–17653. doi: 10.1073/pnas.1410378111

Eichenbaum, H. (2017). Prefrontal-hippocampal interactions in episodic memory. *Nat. Rev. Neurosci.* 18, 547–558. doi: 10.1038/nrn.2017.74

Folstein, M. F., Folstein, S. E., and McHugh, P. R. (1975). "Mini-mental state." A practical method for grading the cognitive state of patients for the clinician. *J. Psychiatr. Res.* 12, 189–198. doi: 10.1016/0022-3956(75)90026-6

Franzmeier, N., Neitzel, J., Rubinski, A., Smith, R., Strandberg, O., Ossenkoppele, R., et al. (2020). Functional brain architecture is associated with the

rate of tau accumulation in Alzheimer's disease. *Nat. Commun.* 11:347. doi: 10.1038/s41467-019-14159-1

Henneman, W. J., Sluimer, J. D., Barnes, J., van der Flier, W. M., Sluimer, I. C., Fox, N. C., et al. (2009). Hippocampal atrophy rates in Alzheimer disease: added value over whole brain volume measures. *Neurology* 72, 999–1007. doi: 10.1212/01.wnl.0000344568.09360.31

Iba, M., Guo, J. L., McBride, J. D., Zhang, B., Trojanowski, J. Q., and Lee, V. M. (2013). Synthetic tau fibrils mediate transmission of neurofibrillary tangles in a transgenic mouse model of Alzheimer's-like tauopathy. *J. Neurosci.* 33, 1024–1037. doi: 10.1523/JNEUROSCI.2642-12.2013

Jack, C. R. Jr, Knopman, D. S., Jagust, W. J., Shaw, L. M., Aisen, P. S., Weiner, M. W., et al. (2010). Hypothetical model of dynamic biomarkers of the Alzheimer's pathological cascade. *Lancet Neurol.* 9, 119–128. doi: 10.1016/S1474-4422(09)70299-6

Jones, D. T., Knopman, D. S., Gunter, J. L., Graff-Radford, J., Vemuri, P., Boeve, B. F., et al. (2016). Cascading network failure across the Alzheimer's disease spectrum. *Brain* 139, 547–562. doi: 10.1093/brain/awv338

King, M., Hernandez-Castillo, C. R., Poldrack, R. A., Ivry, R. B., and Diedrichsen, J. (2019). Functional boundaries in the human cerebellum revealed by a multi-domain task battery. *Nat. Neurosci.* 22, 1371–1378. doi: 10.1038/s41593-019-0436-x

Kramer, J. H., Jurik, J., Sha, S. J., Rankin, K. P., Rosen, H. J., Johnson, J. K., et al. (2003). Distinctive neuropsychological patterns in frontotemporal dementia, semantic dementia, and Alzheimer disease. *Cogn. Behav. Neurol.* 16, 211–218. doi: 10.1097/00146965-200312000-00002

Leech, R., and Sharp, D. J. (2014). The role of the posterior cingulate cortex in cognition and disease. *Brain 137(Pt* 1), 12–32. doi: 10.1093/brain/awt162

Liu, X., Chen, X., Zheng, W., Xia, M., Han, Y., Song, H., et al. (2018). Altered functional connectivity of insular subregions in Alzheimer's disease. *Front. Aging Neurosci.* 10:107. doi: 10.3389/fnagi.2018.00107

Marek, S., Siegel, J. S., Gordon, E. M., Raut, R. V., Gratton, C., Newbold, D. J., et al. (2018). Spatial and temporal organization of the individual human cerebellum. *Neuron* 100, 977–993.e977. doi: 10.1016/j.neuron.2018.10.010

McKhann, G., Drachman, D., Folstein, M., Katzman, R., Price, D., and Stadlan, E. M. (1984). Clinical diagnosis of Alzheimer's disease: report of the NINCDS-ADRDA work group under the auspices of department of health and human services task force on Alzheimer's disease. *Neurology* 34, 939–944. doi: 10.1212/WNL.34.7.939

Mortamais, M., Ash, J. A., Harrison, J., Kaye, J., Kramer, J., Randolph, C., et al. (2017). Detecting cognitive changes in preclinical Alzheimer's disease: a review of its feasibility. *Alzheimers. Dement.* 13, 468–492. doi: 10.1016/j.jalz.2016.06.2365

O'Callaghan, C., Shine, J. M., Hodges, J. R., Andrews-Hanna, J. R., and Irish, M. (2019). Hippocampal atrophy and intrinsic brain network dysfunction relate to alterations in mind wandering in neurodegeneration. *Proc. Natl. Acad. Sci. U.S.A.* 116, 3316–3321. doi: 10.1073/pnas.1818523116

Petersen, R. C., Smith, G. E., Waring, S. C., Ivnik, R. J., Tangalos, E. G., et al. (1999). Mild cognitive impairment: clinical characterization and outcome. *Arch. Neurol.* 56, 303–308. doi: 10.1001/archneur.56.3.303

Pievani, M., Filippini, N., van den Heuvel, M. P., Cappa, S. F., and Frisoni, G. B. (2014). Brain connectivity in neurodegenerative diseases–from phenotype to proteinopathy. *Nat. Rev. Neurol.* 10, 620–633. doi: 10.1038/nrneurol.2014.178

Raichle, M. E. (2015). The brain's default mode network. *Annu. Rev. Neurosci.* 38, 433–447. doi: 10.1146/annurev-neuro-071013-014030

Raichle, M. E., MacLeod, A. M., Snyder, A. Z., Powers, W. J., Gusnard, D. A., and Shulman, G. L. (2001). A default mode of brain function. *Proc. Natl. Acad. Sci. U.S.A.* 98, 676–682. doi: 10.1073/pnas.98.2.676

Schröder, J., and Pantel, J. (2016). Neuroimaging of hippocampal atrophy in early recognition of Alzheimer's disease–a critical appraisal after two decades of research. *Psychiatry Res. Neuroimaging* 247, 71–78. doi: 10.1016/j.pscychresns.2015.08.014

Seeley, W. W., Crawford, R. K., Zhou, J., Miller, B. L., and Greicius, M. D. (2009). Neurodegenerative diseases target large-scale human brain networks. *Neuron* 62, 42–52. doi: 10.1016/j.neuron.2009.03.024

Spalletta, G., Musicco, M., Padovani, A., Rozzini, L., Perri, R., Fadda, L., et al. (2010). Neuropsychiatric symptoms and syndromes in a large cohort of newly diagnosed, untreated patients with Alzheimer disease. *Am. J. Geriatr. Psychiatry* 18, 1026–1035. doi: 10.1097/JGP.0b013e3181d6b68d

Sridharan, D., Levitin, D. J., and Menon, V. (2008). A critical role for the right fronto-insular cortex in switching between central-executive and default-mode networks. *Proc. Natl. Acad. Sci. U.S.A.* 105, 12569–12574. doi: 10.1073/pnas.0800005105

Wang, Z., Liang, P., Jia, X., Jin, G., Song, H., Han, Y., et al. (2012). The baseline and longitudinal changes of PCC connectivity in mild cognitive impairment: a combined structure and resting-state fMRI study. *PLoS ONE* 7:e36838. doi: 10.1371/journal.pone.0036838

Xie, C., Bai, F., Yu, H., Shi, Y., Yuan, Y., Chen, G., et al. (2012). Abnormal insula functional network is associated with episodic memory decline in amnestic mild cognitive impairment. *Neuroimage* 63, 320–327. doi: 10.1016/j.neuroimage.2012.06.062

Zhang, H. Y., Wang, S. J., Liu, B., Ma, Z. L., Yang, M., Zhang, Z. J., et al. (2010). Resting brain connectivity: changes during the progress of Alzheimer disease. *Radiology* 256, 598–606. doi: 10.1148/radiol.10091701

Zheng, W., Liu, X., Song, H., Li, K., and Wang, Z. (2017). Altered functional connectivity of cognitive-related cerebellar subregions in Alzheimer's disease. *Front. Aging Neurosci.* 9:143. doi: 10.3389/fnagi.2017.00143

Zhou, Y., Dougherty, J. H. Jr, Hubner, K. F., Bai, B., Cannon, R. L., and Hutson, R. K. (2008). Abnormal connectivity in the posterior cingulate and hippocampus in early Alzheimer's disease and mild cognitive impairment. *Alzheimers Dement.* 4, 265–270. doi: 10.1016/j.jalz.2008.04.006

Zhu, L., Shu, H., Liu, D., Guo, Q., Wang, Z., and Zhang, Z. (2018). Apolipoprotein E epsilon4 specifically modulates the hippocampus functional connectivity network in patients with amnestic mild cognitive impairment. *Front. Aging Neurosci.* 10:289. doi: 10.3389/fnagi.2018.00289

Conflict of Interest: The authors declare that the research was conducted in the absence of any commercial or financial relationships that could be construed as a potential conflict of interest.

frontiers in Aging Neuroscience

ORIGINAL RESEARCH
published: 05 January 2021
doi: 10.3389/fnagi.2020.599112

Altered Weibull Degree Distribution in Resting-State Functional Brain Networks Is Associated With Cognitive Decline in Mild Cognitive Impairment

Yifei Zhang[1], *Xiaodan Chen*[2,3], *Xinyuan Liang*[2,3], *Zhijiang Wang*[4,5,6], *Teng Xie*[4,5,6], *Xiao Wang*[4,5,6], *Yuhu Shi*[1], *Weiming Zeng*[1] *and Huali Wang*[4,5,6]*

[1] College of Information Engineering, Shanghai Maritime University, Shanghai, China, [2] State Key Laboratory of Cognitive Neuroscience and Learning and IDG/McGovern Institute for Brain Research, Beijing Normal University, Beijing, China, [3] Beijing Key Laboratory of Brain Imaging and Connectomics, Beijing Normal University, Beijing, China, [4] Dementia Care and Research Center, Peking University Institute of Mental Health (Sixth Hospital), Beijing, China, [5] Beijing Key Laboratory for Translational Research on Diagnosis and Treatment of Dementia, Beijing, China, [6] National Clinical Research Center for Mental Disorders (Peking University Sixth Hospital), Beijing, China

The topological organization of human brain networks can be mathematically characterized by the connectivity degree distribution of network nodes. However, there is no clear consensus on whether the topological structure of brain networks follows a power law or other probability distributions, and whether it is altered in Alzheimer's disease (AD). Here we employed resting-state functional MRI and graph theory approaches to investigate the fitting of degree distributions of the whole-brain functional networks and seven subnetworks in healthy subjects and individuals with amnestic mild cognitive impairment (aMCI), i.e., the prodromal stage of AD, and whether they are altered and correlated with cognitive performance in patients. Forty-one elderly cognitively healthy controls and 30 aMCI subjects were included. We constructed functional connectivity matrices among brain voxels and examined nodal degree distributions that were fitted by maximum likelihood estimation. In the whole-brain networks and all functional subnetworks, the connectivity degree distributions were fitted better by the Weibull distribution [$f(x) \sim x^{(\beta-1)}e^{(-\lambda x^{\beta})}$] than power law or power law with exponential cutoff. Compared with the healthy control group, the aMCI group showed lower Weibull β parameters (shape factor) in both the whole-brain networks and all seven subnetworks (false-discovery rate-corrected, $p < 0.05$). These decreases of the Weibull β parameters in the whole-brain networks and all subnetworks except for ventral attention were associated with reduced cognitive performance in individuals with aMCI. Thus, we provided a short-tailed model to capture intrinsic connectivity structure of the human brain functional networks in health and disease.

Keywords: Alzheimer's disease, mild cognitive impairment, resting-state functional MRI, degree distribution, Weibull, network

OPEN ACCESS

Edited by:
Yong Liu,
Chinese Academy of Sciences, China

Reviewed by:
Riccardo Zucca,
Hospital del Mar Medical Research Institute (IMIM), Spain
Tuo Zhang,
Northwestern Polytechnical University, China

***Correspondence:**
Huali Wang
huali_wang@bjmu.edu.cn

Received: *26 August 2020*
Accepted: *24 November 2020*
Published: *05 January 2021*

Citation:
Zhang Y, Chen X, Liang X, Wang Z, Xie T, Wang X, Shi Y, Zeng W and Wang H (2021) Altered Weibull Degree Distribution in Resting-State Functional Brain Networks Is Associated With Cognitive Decline in Mild Cognitive Impairment. Front. Aging Neurosci. 12:599112. doi: 10.3389/fnagi.2020.599112

INTRODUCTION

Resting-state functional magnetic resonance imaging (rsfMRI) studies have suggested that the human brain can be considered an efficiently integrated network that is divided into several functionally linked subnetworks. Examining the topology of brain networks can provide valuable information about the organization of the networks such as hub regions, robustness levels, and ability to communicate information (Bullmore and Sporns, 2012; Dai et al., 2015; Liao et al., 2017). One of the most important properties describing the network topology is the degree distribution of network nodes, a graph theory property that characterizes the probability distribution of the number of connections between pairs of nodes in a network. In resting-state brain networks, there is no agreement on which model can better describe the degree distribution. One view is that the degree distribution follows the heavy-tailed power law (Van Den Heuvel et al., 2008; Hanson et al., 2016; Forlim et al., 2019) based on the simple growth mechanisms, such as preferential attachment (Barabási and Albert, 1999). Another view is that the degree distribution can be better fitted by a short-tailed distribution such as power law with exponential cutoff (Bassett et al., 2006; Hayasaka and Laurienti, 2010; Cao et al., 2016) and Weibull distribution (Nakamura et al., 2009; Gupta and Rajapakse, 2018), considering the wiring-cost constrains (Bullmore and Sporns, 2012) in the human brain. These suggest that power law, power law with exponential cutoff (also called truncated power law), and Weibull distribution (also called stretched exponential) are the three most frequently reported models for fitting the degree distribution of human brain networks, but the findings are not conclusive.

Amnestic mild cognitive impairment (aMCI) is an intermediate stage between healthy aging and (most likely to develop into) Alzheimer's disease (AD) (Petersen et al., 2001). For elderly subjects with cognitive impairment, rsfMRI is acquired without engaging the subjects in a particular cognitive task (i.e., during rest) and therefore has the advantages of clinical practice. It has been argued that neuropsychiatric disorders including AD can be considered as "dysconnectivity syndrome" and that a combination of graph theory method enables a quantitative study of the topology of the network (Bullmore and Sporns, 2009; Xie and He, 2012). In resting-state networks, functional connectivity (FC), the synchronization of spontaneous low-frequency fluctuations in brain activity between different brain regions, is the most commonly used measure of the number of connections in a degree distribution. Alterations of FC in resting-state networks have been identified in the early stages of AD, including elderly cognitively normal subjects with increased amyloid-beta (Aβ) level and aMCI patients (Hedden et al., 2009; Wang et al., 2013a; Zhang et al., 2016). Such aberrant FCs were observed even when controlling for gray matter atrophy (Sorg et al., 2007; Agosta et al., 2012; Wang et al., 2013b). Together, these results suggest that alterations of degree distribution in resting-state networks could be occurred in AD.

In the prodromal stage of AD, changes in network structures are usually accompanied by a variety of alterations in cognitive functions, such as memory, attention, and executive functions. Previous rsfMRI studies suggest that brain regions involving the medial and lateral prefrontal and parietal cortices, insula, and thalamus are preferentially affected in AD (Buckner et al., 2009; Dai et al., 2015, 2019). Two recent meta-analyses have explored resting-state brain changes in the progression of AD and overlaid the coordinates of these changes onto functional subnetworks. In the meta-analysis of Li et al. (2015a), they included 25 resting-state and 75 task-based fMRI studies, and the results revealed that compared to healthy controls, MCI patients showed altered brain activities in default, frontoparietal, and limbic networks during rest; when fulfilling cognitive tasks, there were also abnormalities in ventral attention and somatomotor networks in addition to these three networks. Including 40 resting-state fMRI studies, Badhwar et al. (2017) found that MCI and AD patients showed connectivity alterations in default, salience, and limbic networks. However, very few studies have examined AD-related changes in the topology architecture of functional subnetworks as described by the degree distribution.

Areas commonly activated during complex cognitive tasks are distributed across several of the classic resting-state networks (Li et al., 2015b). For example, a meta-analysis showed widespread memory-related activities across temporal, frontal parietal, and other regions of the brain (Spaniol et al., 2009). Also, these areas can also be observed to have functional synchronization during rest (Zhang et al., 2016). Therefore, to understand changes in degree distributions and whether they are related to cognitive performance, not only the connections within a specific functional subnetwork need to be considered, but also the connections of that network to other regions in the whole brain. Many studies have also found that resting-state FC changes, both within and in between the classic networks, are significantly associated with the patients' cognitive performance (Dai et al., 2015; Pasquini et al., 2015; Zhang et al., 2016). However, most of these studies have focused on some specific functional connections. The changes in the degree distributions of global connections in different functional subnetworks remain to be elucidated.

To address these issues, we used rsfMRI to investigate connectivity degree distributions of nodes in the whole-brain functional networks and within functional subnetworks in aMCI and healthy controls. The seven referenced functional subnetworks were defined according to Thomas Yeo et al. (2011). Using the three most likely candidate models (power law, power law with exponential cutoff, and Weibull distribution), we sought to determine whether degree distributions of these networks (1) can be better fitted by one of the candidate models, (2) are altered in aMCI, and (3) are associated with cognitive performance as assessed by standard neuropsychological tests.

MATERIALS AND METHODS

Participants

Seventy-one subjects (30 aMCI patients and 41 healthy controls, HC) were included in this study. The aMCI patients were recruited from the Dementia Care and Research Center (memory clinic) at Peking University Sixth Hospital. Elderly cognitively HC were screened from local communities. All

participants' demographic information was collected through detailed clinical consultations, including age, sex, education level (years of education), history of depression, treatment information, and current medication use. All participants were right-handed, drug-naive, and aged between 55 and 85 years. All participants received a neuropsychiatric and neuropsychological examination, and a geriatric psychiatrist provided a definitive diagnosis and Clinical Dementia Rating (CDR) (Chan and Siu, 2005) score after a clinical interview. Participants with aMCI met Petersen's MCI criteria (Petersen, 2004), which are as follows: (1) complaints of memory problems that are confirmed by an informant, (2) preserved general cognitive function (Mini-Mental State Examination (MMSE) (Folstein et al., 1975) scores $\geq$ 24), (3) intact or mildly impaired daily living ability (an ADL score $\leq$ 26) (Lawton and Brody, 1969), and (4) do not meet the diagnosis of dementia (World Health Organization, 2010). All HC had no cognitive complaints and did not meet clinical criteria for cognitive impairment or depression. MMSE cutoff scores were $\geq$24 for the HC group. The requirement for global CDR was $\leq$0.5 in the aMCI group and 0 in the HC group. For all participants, exclusion criteria were as follows: (1) history of stroke, tumor, subdural hematoma, other cerebrovascular disease or intracranial space-occupying disease, and obvious risk factors for cerebrovascular disease, (2) currently taking anti-dementia or antidepressant medications, (3) history of drug or substance abuse, (4) history of neurological or psychiatric disorders, and (5) presence of a physical illness that may affect cognition or emotion. Written informed consent was obtained from each participant, and this study was approved by the Medical Research Ethics Committee of Peking University Sixth Hospital, Beijing, China. The data of eight subjects were discarded during scanning, preprocessing, diagnosis, or analysis (for details, see **Supplementary Figure 1**). Neuropsychological and demographic summary statistics for each diagnostic group are provided in **Table 1**. No significant between-group differences were found in gender and education level (gender: $p = 0.45$; education level: $p = 0.81$). The age of the HC group was significantly lower than that of the aMCI group ($p < 0.01$). The MMSE and the Montreal Cognitive Assessment (MoCA) (Nasreddine et al., 2005) scores in the HC group were significantly higher than those in the aMCI group (ps < 0.001).

TABLE 1 | Characteristics of each diagnostic group.

Variable	HC	aMCI	*p*-value
N	41	30	-
Gender (F/M)	28/13	17/13	0.45[b]
Age (y)	70.3 [7.0]	74.8 [5.7]	<0.01[a]
Education	4.3 [0.9]	4.2 [1.1]	0.81[a]
MMSE	28.5 [1.3]	26.7[1.9]	<0.001[a]
MoCA	25.7 [2.8]	22.2 [3.5]	<0.001[a]

Values represent the mean [standard deviation] or number of subjects. HC, cognitively healthy; aMCI, amnestic mild cognitive impairment; N, number of subjects; F, female; M, male; MMSE, Mini-Mental State Examination; MoCA, Montreal Cognitive Assessment.
[a] The P-value was obtained by the two-sample two-tailed t-test.
[b] The P-value was obtained by the two-tailed Pearson χ^2 test.

Assessment of Cognitive Ability

Cognitive ability was quantified by a mean score of the MMSE and the MoCA. The MMSE and the MoCA are two widely used screening assessments for detecting cognitive impairment. Both tests have a 30-point questionnaire and cover a wide range of cognitive functions, with the MMSE testing dysfunctions of attention and calculation, recall, language, orientation, abilities to repeat named prompts and to follow simple commands, and the MoCA screening for dysfunctions of attention, executive function, language, visual, memory, abstracting thinking, structure calculation, and directional force.

MRI Acquisition

All MRI data were acquired on a 3T Siemens Magnetom Prisma scanner (Siemens, Erlangen, Germany). Foam pads and headphones were used to minimize head movement and scanner noise. For rsfMRI, the following acquisition parameters were used: T2*-weighted multi-band echo planer imaging (EPI) pulse sequence in transverse slice orientation, with multiband acceleration factor of 4, repetition time (TR)/echo time (TE) = 500/30 ms, flip angle (FA) = 47°, field of view (FOV) = 231 × 231 mm^2, matrix = 66 × 66, slices = 36, thickness = 3.5 mm, voxel size = 3.5 × 3.5 × 3.5 mm^3, echo spacing = 0.4 ms, and bandwidth = 3,444 Hz/pixel. The subjects were instructed to keep their eyes closed but not fall asleep, relax their minds, and minimize their movement during data acquisition. rsfMRI scan lasted for 480 s and included 960 functional volumes for each subject. T1-weighted magnetization-prepared rapid gradient echo (MPRAGE) sagittal images were also scanned with the following sequence: TR/TE = 2,530 ms/2.98 ms, FA = 7°, inversion time = 1,100 ms, FOV = 256 × 224 mm^2, slices = 192, thickness = 1 mm, voxel size = 0.5 × 0.5 × 1 mm^3.

Image Pre-processing

The first 10 rsfMRI volumes were discarded to ensure steady-state magnetization. The remaining volumes were then realigned to the first volume to correct for head motion. Subjects were excluded if the head motion is larger than 3 mm and 3°. The mean functional image after motion correction was coregistered to the individual T1-weighted images using a linear transformation (Collignon et al., 1995) and were then segmented into gray matter (GM), white matter (WM), and cerebrospinal fluid (CSF) with a priori tissue maps of SPM by using a unified segmentation algorithm (Ashburner and Friston, 2005). The resultant GM, WM, and CSF images were further non-linearly registered into the Montreal Neurological Institute (MNI) space with the information estimated in unified segmentation and then averaged across all subjects to create custom GM, WM, and CSF templates. Then, the custom templates were used as reference images to segment the coregistered T1 images for the second time. This two-step registration procedure based on custom template could minimize the inaccuracies of the spatial normalization of rsfMRI volumes caused by GM atrophy in elderly people. The transformation parameters estimated during unified segmentation were applied to motion-corrected

rsfMRI images and then the images resampled to 3-mm isotropic voxels, which reflect the neuronal pattern of the columnar grain (Kriegeskorte et al., 2010) and are the minimum spatial resolution to capture cortical folding (Kiselev et al., 2003). Subsequently, a linear trend was removed and 24 head motion parameters, mean global signal, and the WM and CSF time courses were regressed out from the spatially normalized rsfMRI scans. A bandpass filter was used to remove frequencies outside of the 0.01–0.1-Hz range. It should be noted that no spatial smoothing was applied to the rsfMRI time series, avoiding local artificial correlations between voxels. The MATLAB-based Statistical Parametric Mapping (SPM12, Wellcome Department of Cognitive Neurology, London, http://www.fil.ion.ucl.ac.uk/spm/) and graph theoretical network analysis toolbox (GRETNA, Beijing Normal University, http://www.nitrc.org/projects/gretna/) (Wang et al., 2015) were used to carry out all functional imaging data pre-processing.

Degree Distribution Analysis

Creating Brain Networks and Degree Calculation

The degree distribution analyses were based on binarized brain networks according to the original definition of nodal degree (i.e., the number of binary edges of a node). To establish the whole-brain networks, for each subject, FC matrices were computed by Pearson's correlation between the times series of any pairs of brain voxels. This procedure was constrained within a GM mask ($N_{voxels} = 47{,}294$) generated by thresholding (cutoff = 0.2) the mean GM probability map of all subjects. A threshold T between 0.4 and 0.6 (with steps of 0.1) defined links between any pairs of nodes (voxels) in the networks. The maximum T value was empirically set to 0.6 to maintain the network integrity, minimizing the number of disconnected voxels, and the minimum value was set to 0.4 to keep the small-world property of the networks and to ensure that the matrices were sufficiently sparse for voxel-based networks (Van Den Heuvel et al., 2008). For each given voxel, *i*, its degree was calculated by the following equation:

$$degree\,(i) = \sum_{j=1,\, j\neq i}^{N_{voxels}} a_{ij}, \quad \begin{cases} a_{ij} = 1 \; if \; r_{ij} \geq T \\ a_{ij} = 0 \; if \; r_{ij} < T \end{cases},$$

where r_{ij} was the correlation coefficient between voxel *i* and voxel *j*. The seven referenced functional subnetworks were obtained from previous studies based on the rsfMRI data from 1,000 participants and a data-driven clustering approach (Thomas Yeo et al., 2011) (see **Supplementary Figure 2**), including visual (V), sensorimotor (SM), dorsal attention (DA), ventral attention (VA), limbic (Lim), frontoparietal (FP), and default mode (DM). For each subnetwork, nodal degrees were still computed by summing the connections of a voxel to any other voxels in the whole brain (not only the connections within the subnetwork), which we refer to here as the global degree of nodes in a particular subnetwork.

For validity reasons, to identify the whole strength pattern of degree distribution in both the HC and aMCI groups, we performed a functional connectivity strength (FCS) analysis, also called degree centrality of a weighted network (Buckner et al., 2009; Zuo et al., 2012; Dai et al., 2015). For each subject, we built whole-brain FC matrices by computing Pearson's correlations between the time series of any pairs of brain voxels. This process was constrained within the same GM mask. For each voxel, *i*, the FCS was computed by the following equation:

$$FCS\,(i) = \frac{1}{N_{voxels}} \sum_{j=1,\, j\neq i}^{N_{voxels}} z_{ij}, \quad r_{ij} > r_0\,,$$

where z_{ij} is the Fisher's z-transformation of r_{ij}, r_0 is a threshold that eliminates weak correlations possibly arising from noise [here $r_0 = 0.2$, based on a previous study that evaluated different thresholds (Dai et al., 2015)].

Notably, only positive correlations between voxels were considered in the calculation of the nodal degree and FCS; connectivity terminating within 20 mm of each source voxel center was set to zero to avoid potential shared signals between nearby voxels. These voxel-wise brain network analyses were performed using an in-house toolbox (developed by Dr. Mingrui Xia, Beijing Normal University).

Degree Distribution Fit

Based on published literatures, we chose three most likely models, including power law, power law with exponential cutoff, and Weibull, as candidate models for the fittings of the degree distributions (see **Table 2** for their probability density function). The fittings of the alternative models and the estimations of the model parameters followed the statistical methods from previous study (Clauset et al., 2009) and used the *powerlaw* Python package (Alstott and Bullmore, 2014) (https://github.com/jeffalstott/powerlaw). In general, the visual form of the Complementary Cumulative Distribution Function (CCDF) is more frequently preferred than that of the Probability Distribution Function (PDF) against fluctuations due to finite sample sizes (Clauset et al., 2009). In the fitting procedure, for each network, a vector containing voxels' degrees was sorted in ascending order for each correlation threshold. For every generated network, the maximum likelihood estimation method was used to estimate model parameters. The obtained degrees could only take values in integers. For the power law distribution, there is no exact closed-form expression for the maximum likelihood estimator of the parameter α in the discrete case. The *powerlaw* Python package uses an analytic estimation of α with the method mentioned by Clauset et al. (2009) that provides a faster way to obtain a more precise estimation. The approximate expression of α is

$$\hat{\alpha} \simeq 1 + n\left[\sum_{i=1}^{n} ln\frac{x_i}{x_{min} - \frac{1}{2}}\right]^{-1},$$

where x_i, $i = 1 \cdots n$ are the observed voxels' degree values in the vector. In practice, the power law tends to apply only when the values of empirical phenomena are greater than some minimum value $x_{\min}$. Thus, when initially fitting with the power law, the optimal value of $x_{\min}$ was obtained by selecting the one that

TABLE 2 | The three candidate models for the fit of the degree distribution.

Distribution name	Probability density function
Power law	$x^{-\alpha}$
Power law with exponential cutoff	$x^{-\alpha}e^{-\lambda x}$
Weibull	$x^{\beta-1}e^{-\lambda x^{\beta}}$

resulted in the minimal Kolmogorov–Smirnov distance between the data and the fit. The initial fit showed that the CCDF of degree distributions of functional brain networks was curved on the double logarithmic axis, and the selection of different optimal $x_{\min}$ values resulted in a large shift of the fitted lines on the sample curves for different subjects. Thus, the power-law model might not be appropriate. The $x_{\min}$ was then fixed to 1 in the fittings and comparisons of the other alternative models. Discrete forms of the other alternative models are not defined analytically. Discrete forms of probability distributions are often more difficult to calculate. The *powerlaw* package performs discretization by rounding, summing the continuous distribution to the nearest integer, to calculate approximations to the discrete form of the alternative distribution. For comparison between models, a normalized loglikelihood ratio R and an associated significance value p were used to evaluate the goodness of fit between two competing distributions to identify a better fit. The positive or negative sign of the R indicates which model is better, or a ratio close to zero indicates the two models have similar effects, if the *p*-value is small enough ($<$ 0.05). Therefore, we used the mean of *R*-values to determine which model and to what extent is more appropriate at the group level.

Statistical Analyses

To investigate whether the degree distribution parameter(s) of the best-fit model changed in the aMCI group compared to the HC group, we applied analyses of the following general linear model including diagnosis (HC vs. aMCI), age, gender, and education as independent variables and model parameter as dependent variable:

$$Model\ parameter\ \sim\ \beta_0 + \beta_1 \times Diagnostic\ group + \beta_2 \times Age + \beta_3 \times Gender + \beta_4 \times Education.$$

Then, to detect the relationship between a parameter of a degree model and cognition ability, the parameters of degree distribution that were found significantly altered in the aMCI group were tested as predictors of cognition scores in the aMCI group. We used the following linear regression model, including cognitive ability as dependent variable and model parameter, age, gender and education as independent variables:

$$Cognitive\ ability\ \sim\ \beta_0 + \beta_1 \times Model\ parameter + \beta_2 \times Age + \beta_3 \times Gender + \beta_4 \times Education.$$

For validity reasons, we generated mean FCS maps for the HC and the aMCI groups. The group difference of the FCS maps was evaluated via two-sample *t*-tests controlling for age, gender, and education. A false discovery rate (FDR) procedure was used to correct for multiple comparisons within the GM.

Without other statements, the analyses were corrected for multiple comparisons, FDR-corrected at p = 0.05. All group-level statistical analyses were done with the stats package of statistical software R implemented in R Studio v. 0.98.953 (Boston, MA, https://www.rstudio.com/).

RESULTS

Weibull Distribution Fits Brain Networks Better

In order to estimate connectivity degree distributions of the whole-brain networks and different functional subnetworks, we tested the three candidate models for each subject by using normalized loglikelihood ratios *R* and *p*-values (calculated by R and its standard deviation σ, indicating whether the observed sign of R is statistically significant). A positive R suggests a better fit of the data to the first model, while a negative R suggests a better fit to the second, if the *p*-value is small ($<$ 0.05 here). The results of the group-averaged normalized loglikelihood ratios (only counted if ps $<$ 0.05) for the fittings of degree distributions between two of the three models in the whole-brain networks and subnetworks are listed in **Table 3**. In the whole-brain networks and all subnetworks, the connectivity degree distributions were fitted better by a Weibull distribution than power law or power law with exponential cutoff. Examples of the CCDF plots and their fittings of the three candidate models in the whole-brain network and the seven subnetworks (correlation threshold T = 0.4) for an aMCI subject are shown (fittings were similar for other subjects and thresholds); see **Figure 1**. For the fittings compared between Weibull and power law, in all networks, both the HC and the aMCI groups, all of the averaged R ratios were positive and sufficiently larger than zero, indicating that the Weibull is better than the power law in human brain rsfMRI networks. For the 48 times fitting compared between Weibull and power law with exponential cutoff, in all generated networks, 85.4% of the R-values were positive, suggesting that the Weibull is better than the power law with exponential cutoff. While the other 14.6% comparisons have negative R-values, these values were very close to zero, suggesting that the two models fit similarly for these 14.6% comparisons (**Table 3**). It should be noted that, in general, all R-values tended to decrease as the correlation threshold increases. Consequently, out of the three correlation thresholds, T = 0.4 and 0.5 were more compatible with the Weibull distribution. The reason could be that lower threshold preserves more weak connections. No significant between-group difference in R-values was found in any of the networks.

Degree Distribution Changes in aMCI

Focusing on the Weibull distribution, we tested whether its two parameters, β and γ, were altered in the aMCI group. The Weibull distribution can be used to describe a distribution between the power law and the exponential function, where the

parameter $\beta \in (0, 1)$ denoting the extent it falls between the two distributions. When $\beta = 0$, it reduces to a power law distribution and when $\beta = 1$, it becomes an exponential distribution. Compared with the HC group, the aMCI group showed lower Weibull β parameters (shape factor) in both the whole-brain network and all the seven subnetworks. When T = 0.4, decreased Weibull β parameters were found in aMCI for connectivity degree distributions in the whole-brain networks ($p = 0.05$) and within functional subnetworks: in FP & DM (ps < 0.01), in V & SM (ps $= 0.05$), and a tendency in VA ($p = 0.06$, uncorrected $p = 0.04$). When T = 0.5, the β parameters of the Weibull distribution in the whole-brain network and within all seven subnetworks decreased significantly: in V (p = 0.001), in SM, DA, VA, FP, DM, and whole brain (ps ≤ 0.01), and in Lim ($p = 0.05$). When $T = 0.6$, the β parameters were also decreased in V, DA, and the whole brain (ps < 0.05), and a tendency to decrease in SM and DM (ps < 0.1, uncorrected ps < 0.05). All p-values reported were FDR-corrected, unless otherwise noted. As shown in **Figure 2**, the value of β parameters in aMCI were lower than that for HC in the whole-brain network and within all seven subnetworks (correlation threshold T = 0.5). No changes of λ parameter in aMCI were observed compared to HC. For validity reasons, we also examined the group difference of the FCS map between the HC and the aMCI groups (see **Supplementary Figure 3**). Visual inspection indicated that the spatial distributions of FCS in the aMCI group were similar but weaker than those of the HC group; the FCS of some voxels distributed in regions including the angular and precuneus were increased in the aMCI group. No significant between-group difference was found after an FDR multiple comparisons at p < 0.05 (for the number of connections between voxels in GM).

TABLE 3 | Group-averaged loglikelihood ratios between candidate models for the fittings of connectivity degree distributions.

	WB vs. PL in HC	WB vs. PL in aMCI	WB vs. PLEC in HC	WB vs. PLEC in aMCI
V	66.9/37.9/25.9	63.8/32.5/21.2	33.8/12.5/7.4	29.8/7.2/2.7
SM	57.6/28.7/18.4	54.8/ 25.0/16.4	27.0/4.2/2.5	23.3/−1.3/0.8
DA	52.6/29.1/18.8	51.1/ 25.9/16.2	25.4/7.5/4.4	23.3/3.8/1.7
VA	48.8/24.9/15.8	46.6/ 22.7/14.8	22.1/4.6/1.6	19.5/0.5/0.5
Lim	43.6/19.0/11.6	40.2/ 16.3/9.8	19.2/−0.1/−1.8	16.5/2.9/2.0
FP	64.8/36.7/22.0	60.7/ 32.2/19.8	34.3/12.3/4.9	29.6/6.8/2.7
DM	80.6/44.5/27.3	75.5/ 39.3/24.6	42.3/13.7/4.8	36.4/7.8/2.2
Whole brain	164.9/87.1/57.2	157.5/ 78.0/51.3	67.3/9.7/4.3	59.0/−2.1/−1.4

Values represent the mean normalized loglikelihood ratios (ps < 0.05) between candidate models for the fittings of networks generated at threshold of 0.4/0.5/0.6 in the HC and the aMCI groups. V, visual; SM, somatomotor; DA, dorsal attention; VA, ventral attention; Lim, limbic; FP, frontoparietal; DM, default model; WB, Weibull; PL, power law, PLEC, power law with exponential cutoff; HC, cognitively healthy; aMCI, amnestic mild cognitive impairment.

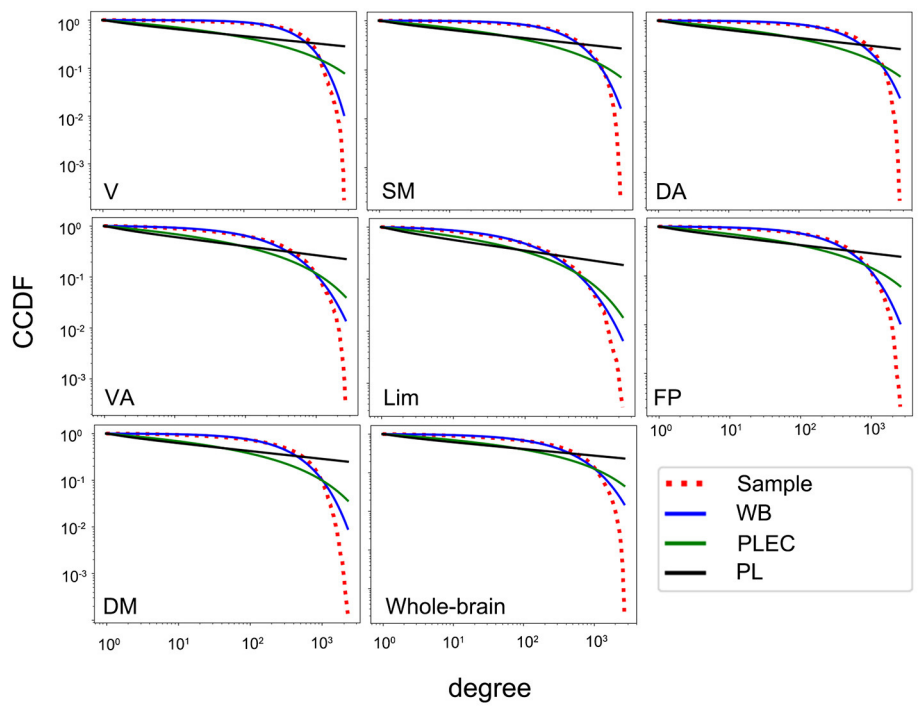

FIGURE 1 | The CCDF plots of the degree distributions for an aMCI subject in the whole-brain network and seven subnetworks and their fit with the three candidate models (correlation threshold $T = 0.4$). V, visual; SM, somatomotor; DA, dorsal attention; VA, ventral attention; Lim, limbic; FP, frontoparietal; DM, default model; WB, Weibull; PL, power law, PLEC, power law with exponential cutoff; CCDF, complementary cumulative distribution function.

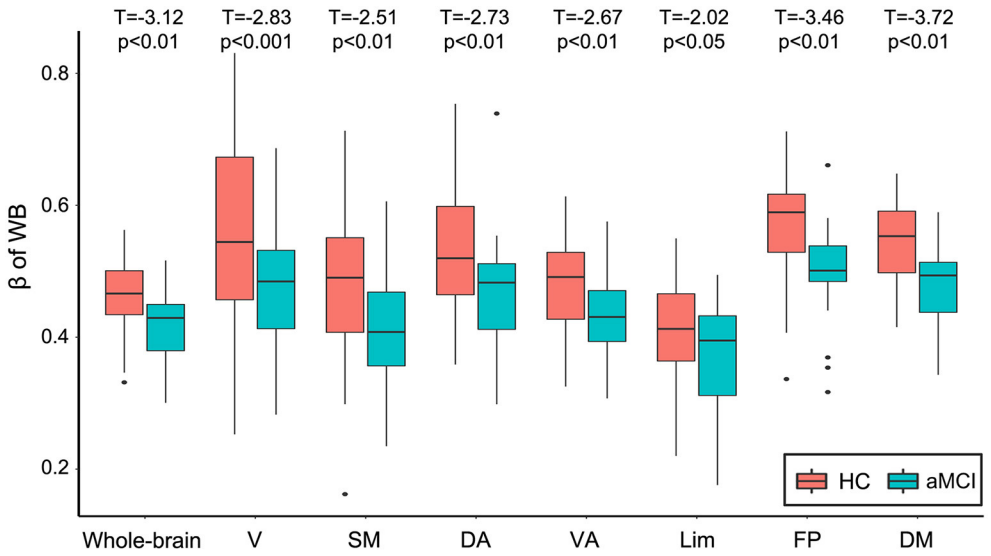

FIGURE 2 | Boxplot of the Weibull β parameters as a function of diagnosis on the degree distributions of the whole-brain network and seven subnetworks (correlation threshold $T = 0.5$). *P*-values of between-group differences were FDR adjusted. V, visual; SM, somatomotor; DA, dorsal attention; VA, ventral attention; Lim, limbic; FP, frontoparietal; DM, default model; HC, cognitively healthy; aMCI, amnestic mild cognitive impairment; FDR, false-discovery rate.

Association Between Weibull β Parameter and Cognitive Decline in aMCI

Focusing on the Weibull β parameter for which the value was found to be decreased in aMCI, we found lower values of the Weibull β parameter to be associated with reduced cognitive ability in aMCI (mainly in the networks with T = 0.4). Specifically, for connectivity degree distributions in rsfMRI, we found the above associations for the whole-brain network and all subnetworks excluding VA (for the *t*-values and FDR-corrected *p*-values, see **Figure 3**). We also found the association in Lim with T = 0.5 (t = 2.99, FDR-corrected $p = 0.04$). We computed the diagnosis (HC, aMCI) × Weibull β parameter interactions, controlled for age, gender, and education to correlate cognitive ability in the networks showed the above relationship. The results showed that the slopes of the Weibull β parameter in HC differed significantly from those in aMCI (**Supplementary Figure 4**).

DISCUSSION

The first major finding of the present study was that the Weibull distribution fits brain networks better in resting-state fMRI. The second major finding was the decreased Weibull β parameters in the whole-brain network and all seven subnetworks in aMCI subjects compared to HC. The third major finding was that the abnormal decrease in the values of Weibull β parameter in the whole-brain network and the functional subnetworks were associated with reduced cognitive performance in aMCI.

The current finding of Weibull distribution fits brain networks better is in line with previous reports of the nodal degree of human brain functional networks that follow short-tailed distribution such as the Weibull distribution and the power law with exponential cutoff (Nakamura et al., 2009; Hayasaka and Laurienti, 2010; Gupta and Rajapakse, 2018; Zucca et al., 2019). In contrast, the heavy-tailed power law distribution (also called scale-free network) has been extensively discussed (Eguíluz et al., 2005; Van Den Heuvel et al., 2008; Ciuciu et al., 2014; Hanson et al., 2016; Forlim et al., 2019). Most of these studies on the power law had a strong hypothesis that brain networks are structured with simple growth mechanisms, such as preferential attachment (Barabási and Albert, 1999). Under this assumption, the network has scale-free property that allows for efficient communication of information through a few hub nodes. To characterize this property, more complicated network construction methods were adopted in these studies. For example, Hanson et al. (2016) reported brain networks that fit for power law distribution by using a conditional probability-based Bayes network search model that "allows for the node structure to express more subtle hub and modular configurations." Another rsfMRI study also found that a machine learning-based k-nearest neighbor graph construction of brain networks presents scale-free properties (Forlim et al., 2019). However, a recent study analyzing over a thousand power law distributions from various disciplines concluded that scale-free networks are rare in real-world data, and alternative models such as log-normal often fit degree distributions better than the power law (Broido and Clauset, 2019).

For the present study, we found that the Weibull distribution outperforms the other two commonly reported brain network models in the whole-brain networks and all the seven subnetworks, in both the HC and the aMCI subjects. We agree with the assumption of wiring-cost constrains in human brain (Bullmore and Sporns, 2012). In addition to the fact that the human brain has mechanisms to reduce information processing cost and maximize efficiency, the organization of functional networks is also limited by the spatial structure of the brain. The

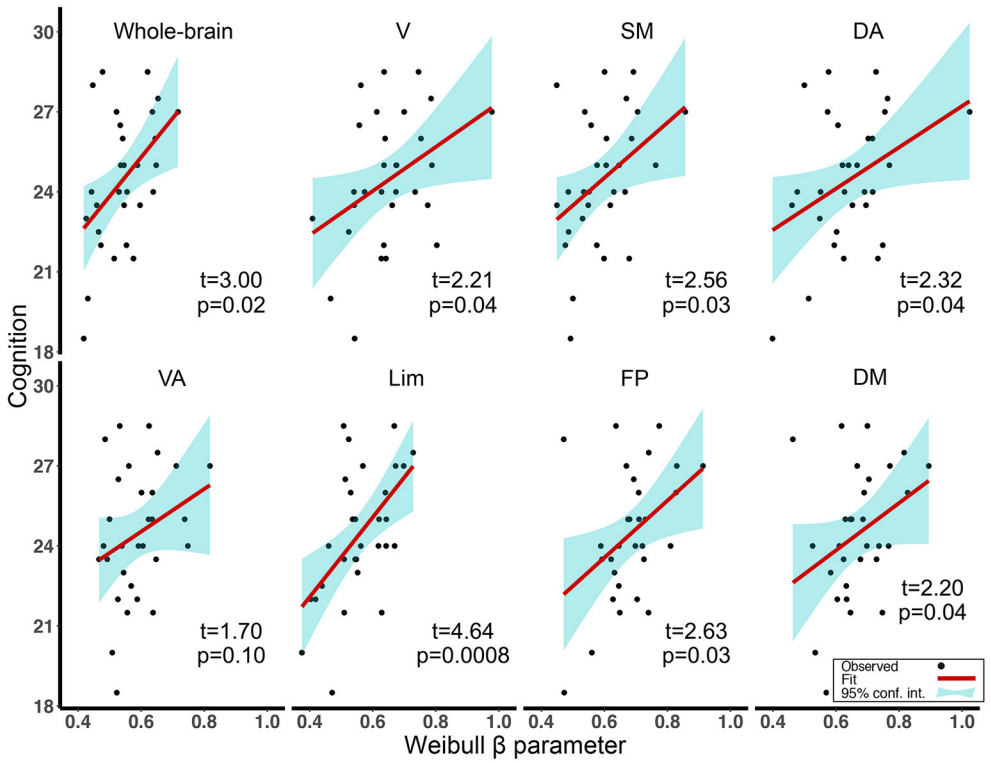

FIGURE 3 | Regression plots of the association between Weibull β parameters and cognitive ability scores for aMCI in the whole-brain network and seven subnetworks (correlation threshold $T = 0.4$). All *p*-values were FDR adjusted. V, visual; SM, somatomotor; DA, dorsal attention; VA, ventral attention; Lim, limbic; FP, frontoparietal; DM, default model; aMCI, amnestic mild cognitive impairment; FDR, false-discovery rate.

dynamic properties of functional networks such as their topology and synchronization ability are strongly influenced by small world and other structural connectivity constraints (Bullmore and Sporns, 2009). The architectural constraints prevent the occurrence of long-distance hubs, as the corresponding remote anatomical connections consume more energy. Therefore, on a CCDF plot of the nodal degree with logarithmic axes, the tail of the Weibull distribution may show a downward bend compared to the power law distribution. Notably, it has been suggested that the estimation of the degree distribution is still dependent on several factors such as the pre-processing process, region-based or voxel-based node scale, edge calculation, and fitting method (Clauset et al., 2009; Hayasaka and Laurienti, 2010; Zucca et al., 2019). For example, the earliest studies usually used the least-square fitting method on log–log plots to test whether a degree distribution is power law. This fitting method is systematically biased and does not take into account the goodness of fit and selection of prospective degree distributions (Clauset et al., 2009). Another study comparing functional brain networks at multiple resolutions found that although the degree distributions of all networks followed the power law with exponential cutoff, the higher the resolution (up to the voxel level), the more the distribution tended to be a power law (Hayasaka and Laurienti, 2010). In summary, in this study, we aimed to use a generally applicable, easily understood approach to discuss degree distribution of functional brain networks in rsfMRI. We used the Pearson association of FC to construct binary networks at the finest voxel level. To avoid the flaws of the least-squares, the maximum likelihood estimation and loglikelihood ratio methods were used to estimate and compare proposed models. Our results suggest that the short-tailed Weibull distribution is superior to the other two models in all generated networks.

The second major finding showed decreased Weibull β parameters of the global degree distribution in the whole-brain network and all seven functional subnetworks in aMCI. These nodal degrees were computed from themselves to all the other nodes in the whole brain. The calculation of the degree distribution was based on the strength of functional connectivity between paired voxels. Therefore, these findings are at least partially in agreement with previous reports that found alterations in resting-state connectivity in aMCI. Specifically, two meta-analyses reported increased connectivity in default mode, salience, and limbic networks, while decreased connectivity in default mode, frontoparietal, visual, and limbic networks (Li et al., 2015a; Badhwar et al., 2017). Another study that explored topological pattern changes of brain networks in aMCI reported decreased nodal centrality in the medial temporal lobe and

increased nodal centrality in the occipital regions (Liu et al., 2012). Here we extended these findings to the network level, showing that the overall topology features of these functional subnetworks have changed in aMCI.

The underlying nature of the decrease in Weibull β parameter in aMCI is unclear. The Weibull distribution used here that describes the degree distribution of functional brain networks is a two-parameter model. Although no statistically significant between-group differences were found for the second γ parameter, it is difficult to determine the specific variation of the curve on the CCDF plot based on just one β parameter. The β parameter is the shape factor of the Weibull distribution. Its slight decrease may be thought of as a small shifting of the degree distribution from exponential to power law distribution, reflecting an increase in the number of hub nodes in the network. One possible explanation is that the decrease in Weibull β parameter reflects less efficient neural network activity. According to the dedifferentiation hypothesis, inefficient neural processing results in age-related brain functional changes that lead to more diffuse brain activity (Dennis and Cabeza, 2011). In line with the dedifferentiation hypothesis, a study found that age-related decreased modularity of resting-state FC within networks and increased inter-network connectivity in elderly cognitively healthy subjects (Geerligs et al., 2015). Another study showed increased number of FC connections in aMCI and AD compared to HC. The number of connections peaked in aMCI and is significantly higher compared to AD. Furthermore, increased strength of FC was found for connections that spanned different functional clusters were identified, including the FP network, the posterior DM network, the medial temporal lobe subsystem, and a subcortical cluster (Zhang et al., 2016). The human brain has the capacity to buffer or reserve itself against some extent of the changes brought on by aging and disease (Staff, 2012). It is possible that this more diffuse, less efficient neural processing may require an increase in the strength or the number of FC, with compensatory recruitment of additional neural resources to try to maintain task performance in early stage of AD (Grady et al., 2003; Dickerson et al., 2004). An alternative explanation is that the increase in FC results from increased deposition of Aβ (Elman et al., 2014; Huijbers et al., 2015). However, this hypothesis is still in doubt. The present study did not collect Aβ from the subjects, and therefore, no Aβ-related experimental manipulation was involved.

The third major findings found that the abnormal decrease in the value of Weibull β parameter was associated with reduced cognitive performance in aMCI. These findings are consistent with previous reports of increased DM network connectivity contributes to semantic memory deficits in MCI patients (Gardini et al., 2014). The abnormal increase in the strength of FC, not confined to the DM network but connected between the FP network and medial temporal lobe subsystem, was found to be associated with reduced episodic memory performance in MCI and AD (Zhang et al., 2016). Task-related studies have also shown that MCI patients had enhanced activation in the hippocampus (Dickerson et al., 2004) and its association with faster subsequent cognitive decline in MCI (Miller et al., 2008). Although most of the previous findings were related to the DM network, complex cognitive functions, such as memory, are distributed across several resting-state networks (Li et al., 2015b). Here we addressed the associations between changes in nodal degree distributions and cognitive ability at the functional network level. Negative correlations were found between the cognitive ability and the Weibull β parameters of several subnetworks' global degree distributions in aMCI. Notably, we focus on the number of FC-based connections for each node in the network, with each connection potentially linking to other functional networks. In other words, increase in the number of hub nodes in these networks is associated with cognitive decline in aMCI. Thus, the inverse association may reflect a failed compensatory attempt to recruit additional neural resources to maintain task performance. These results suggest that decrease in the Weibull β parameter characterizing the functional brain network is detrimental to cognitive performance in aMCI.

It is important to acknowledge the potential limitations of our study. Firstly, the number of subjects used in this study was relatively small, which may lead to potential statistical instability. Secondly, the determination of the connections during network construction will have an influence on the results. We used absolute thresholds so that connections that surpass the fixed connectivity strength were kept and set to 1. However, there is no consistent standard for the selection of threshold. In this study, the selection was based on the small-world characteristic and the integrity of the network. The networks generated with multiple thresholds were all well-fitted by the Weibull distribution. For validity reasons, we performed a FCS analysis, using the weighted degree centrality to avoid the selection of thresholds. The results also revealed enhanced degree centrality of several hub regions in aMCI (**Supplementary Figure 3**), which is consistent with the results of reduced Weibull β parameters using the absolute thresholds. Additionally, in rsfMRI, the spontaneous brain activation is sampled without reference to external tasks, so its interpretation is inherently less well-understood. Therefore, we attempted to frame the study in a hypothesis-driven manner, focusing on functional subnetworks derived from a data-driven approach based on 1,000 participants. However, the combination of resting-state and specific task-related fMRI studies would be important for future researches.

Overall, the current results on the altered degree distributions of functional brain subnetworks support that the degree distribution gives a window to evaluate the neural network topology underlying cognitive performance. This study offers a method for designing resting-state analysis to assess variations in degree distribution for providing insight into cognitive decline in aMCI. Degree distribution is currently not established as a biomarker for neuroimaging. Longitudinal studies are needed to examine the value of degree distribution to predict subsequent cognitive decline.

DATA AVAILABILITY STATEMENT

The raw data supporting the conclusions of this article will be made available by the authors, without undue reservation.

ETHICS STATEMENT

The studies involving human participants were reviewed and approved by the Medical Research Ethics Committee of Peking University Sixth Hospital, Beijing, China. The patients/participants provided their written informed consent to participate in this study.

AUTHOR CONTRIBUTIONS

YZ designed the study, performed the statistical analysis, interpreted the results, and wrote the manuscript. XC, ZW, TX, and XW carried out the data collection. XL pre-processed the rsfMRI data. YS and WZ revised the manuscript. HW carried out the data collection, provided advices, and revised the manuscript. All authors contributed to the article and approved the submitted version.

FUNDING

This research was funded by the National Natural Science Foundation of China (61701298, 61906117, 31870979, and 81500918), National Key Research & Development Project of Ministry of Science and Technology (2017YFC1311100), and Shanghai Sailing Program (19YF1419000).

ACKNOWLEDGMENTS

The author (YZ) thanks Prof. Yong He, Dr. Xuhong Liao, and Dr. Mingrui Xia for their useful comments.

SUPPLEMENTARY MATERIAL

The Supplementary Material for this article can be found online at: https://www.frontiersin.org/articles/10.3389/fnagi.2020.599112/full#supplementary-material

REFERENCES

Agosta, F., Pievani, M., Geroldi, C., Copetti, M., Frisoni, G. B., and Filippi, M. (2012). Resting state fMRI in Alzheimer's disease: beyond the default mode network. *Neurobiol. Aging* 33, 1564–1578. doi: 10.1016/j.neurobiolaging.2011.06.007

Alstott, J., and Bullmore, D. P. (2014). powerlaw: a python package for analysis of heavy-tailed distributions. *PLoS ONE* 9:e85777. doi: 10.1371/journal.pone.0085777

Ashburner, J., and Friston, K. J. (2005). Unified segmentation. *Neuroimage* 26, 839–851. doi: 10.1016/j.neuroimage.2005.02.018

Badhwar, A., Tam, A., Dansereau, C., Orban, P., Hoffstaedter, F., and Bellec, P. (2017). Resting-state network dysfunction in Alzheimer's disease: a systematic review and meta-analysis. *Alzheimers Dement.* 8, 73–85. doi: 10.1016/j.dadm.2017.03.007

Barabási, A.-L., and Albert, R. (1999). Emergence of scaling in random networks. *Science* 286, 509–512. doi: 10.1126/science.286.5439.509

Bassett, D. S., Meyer-Lindenberg, A., Achard, S., Duke, T., and Bullmore, E. (2006). Adaptive reconfiguration of fractal small-world human brain functional networks. *Proc. Natl. Acad. Sci. U.S.A.* 103:19518. doi: 10.1073/pnas.0606005103

Broido, A. D., and Clauset, A. (2019). Scale-free networks are rare. *Nat. Commun.* 10:1017. doi: 10.1038/s41467-019-08746-5

Buckner, R. L., Sepulcre, J., Talukdar, T., Krienen, F. M., Liu, H., Hedden, T., et al. (2009). Cortical hubs revealed by intrinsic functional connectivity: mapping, assessment of stability, and relation to Alzheimer's disease. *J. Neurosci.* 29, 1860–1873. doi: 10.1523/JNEUROSCI.5062-08.2009

Bullmore, E., and Sporns, O. (2009). Complex brain networks: graph theoretical analysis of structural and functional systems. *Nat. Rev. Neurosci.* 10, 186–198. doi: 10.1038/nrn2575

Bullmore, E., and Sporns, O. (2012). The economy of brain network organization. *Nat. Rev. Neurosci.* 13, 336–349. doi: 10.1038/nrn3214

Cao, M., He, Y., Dai, Z., Liao, X., Jeon, T., Ouyang, M., et al. (2016). Early development of functional network segregation revealed by connectomic analysis of the preterm human brain. *Cereb. Cortex* 27, 1949–1963. doi: 10.1093/cercor/bhw038

Chan, I. H., and Siu, A. M. (2005). A study of the reliability and validity of the Chinese version of the dementia rating scale. *Int. Psychogeriatr.* 17, 69–79. doi: 10.1017/S1041610204000791

Ciuciu, P., Abry, P., and He, B. J. (2014). Interplay between functional connectivity and scale-free dynamics in intrinsic fMRI networks. *NeuroImage* 95, 248–263. doi: 10.1016/j.neuroimage.2014.03.047

Clauset, A., Shalizi, C. R., and Newman, M. E. (2009). Power-law distributions in empirical data. *SIAM Rev.* 51, 661–703. doi: 10.1137/070710111

Collignon, A., Maes, F., Delaere, D., Vandermeulen, D., Suetens, P., and Marchal, G. (1995). Automated multi-modality image registration based on information theory. *Inf. Process. Med. Imag. Citeseer* 3, 263–274.

Dai, Z., Lin, Q., Li, T., Wang, X., Yuan, H., Yu, X., et al. (2019). Disrupted structural and functional brain networks in Alzheimer's disease. *Neurobiol. Aging* 75, 71–82. doi: 10.1016/j.neurobiolaging.2018.11.005

Dai, Z., Yan, C., Li, K., Wang, Z., Wang, J., Cao, M., et al. (2015). Identifying and mapping connectivity patterns of brain network hubs in Alzheimer's disease. *Cereb. Cortex* 25, 3723–3742. doi: 10.1093/cercor/bhu246

Dennis, N. A., and Cabeza, R. (2011). Age-related dedifferentiation of learning systems: an fMRI study of implicit and explicit learning. *Neurobiol. Aging 32*, 2318.e2317–2330. doi: 10.1016/j.neurobiolaging.2010.04.004

Dickerson, B. C., Salat, D. H., Bates, J. F., Atiya, M., Killiany, R. J., Greve, D. N., et al. (2004). Medial temporal lobe function and structure in mild cognitive impairment. *Ann. Neurol.* 56, 27–35. doi: 10.1002/ana.20163

Eguíluz, V. M., Chialvo, D. R., Cecchi, G. A., Baliki, M., and Apkarian, A. V. (2005). Scale-free brain functional networks. *Phys. Rev. Lett.* 94:018102. doi: 10.1103/PhysRevLett.94.018102

Elman, J. A., Oh, H., Madison, C. M., Baker, S. L., Vogel, J. W., Marks, S. M., et al. (2014). Neural compensation in older people with brain amyloid-beta deposition. *Nat. Neurosci.* 17, 1316–1318. doi: 10.1038/nn.3806

Folstein, M. F., Folstein, S. E., and Mchugh, P. R. (1975). Mini-mental state. A practical method for grading the cognitive state of patients for the clinician. *J. Psychiatr. Res.* 12, 189–198. doi: 10.1016/0022-3956(75)90026-6

Forlim, C. G., Haghiri, S., Düzel, S., and Kühn, S. (2019). Efficient small-world and scale-free functional brain networks at rest using k-nearest neighbors thresholding. *bioRxiv [Preprint]* 628453. doi: 10.1101/628453

Gardini, S., Venneri, A., Sambataro, F., Cuetos, F., Fasano, F., Marchi, M., et al. (2014). Increased functional connectivity in the default mode network in mild cognitive impairment: a maladaptive compensatory mechanism associated with poor semantic memory performance. *J. Alzheimers Dis. JAD* 45, 457–470. doi: 10.3233/JAD-142547

Geerligs, L., Renken, R. J., Saliasi, E., Maurits, N. M., and Lorist, M. M. (2015). A brain-wide study of age-related changes in functional connectivity. *Cereb. Cortex* 25, 1987–1999. doi: 10.1093/cercor/bhu012

Grady, C. L., Mcintosh, A. R., Beig, S., Keightley, M. L., Burian, H., and Black, S. E. (2003). Evidence from functional neuroimaging of a compensatory prefrontal network in Alzheimer's disease. *J. Neurosci.* 23, 986–993. doi: 10.1523/JNEUROSCI.23-03-00986.2003

Gupta, S., and Rajapakse, J. C. (2018). "Nodal degree distributions of resting-state functional brain modules," in *2018 IEEE 15th International*

Symposium on Biomedical Imaging (ISBI 2018) (Washington, DC), 1256–1259. doi: 10.1109/ISBI.2018.8363799

Hanson, S. J. E., Mastrovito, D., Hanson, C., Ramsey, J., and Glymour, C. (2016). Scale-free exponents of resting state provide a biomarker for typical and atypical brain activity. *bioRxiv* 068841. doi: 10.1101/068841

Hayasaka, S., and Laurienti, P. J. (2010). Comparison of characteristics between region-and voxel-based network analyses in resting-state fMRI data. *Neuroimage* 50, 499–508. doi: 10.1016/j.neuroimage.2009.12.051

Hedden, T., Van Dijk, K. R. A., Becker, J. A., Mehta, A., Sperling, R. A., Johnson, K. A., et al. (2009). Disruption of Functional Connectivity in Clinically Normal Older Adults Harboring Amyloid Burden. *J. Neurosci.* 29, 12686–12694. doi: 10.1523/JNEUROSCI.3189-09.2009

Huijbers, W., Mormino, E. C., Schultz, A. P., Wigman, S., Ward, A. M., Larvie, M., et al. (2015). Amyloid-beta deposition in mild cognitive impairment is associated with increased hippocampal activity, atrophy and clinical progression. *Brain* 138, 1023–1035. doi: 10.1093/brain/awv007

Kiselev, V. G., Hahn, K. R., and Auer, D. P. (2003). Is the brain cortex a fractal? *Neuroimage* 20, 1765–1774. doi: 10.1016/S1053-8119(03)00380-X

Kriegeskorte, N., Cusack, R., and Bandettini, P. (2010). How does an fMRI voxel sample the neuronal activity pattern: compact-kernel or complex spatiotemporal filter? *Neuroimage* 49, 1965–1976. doi: 10.1016/j.neuroimage.2009.09.059

Lawton, M. P., and Brody, E. M. (1969). Assessment of older people: self-maintaining and instrumental activities of daily living1. *Gerontologist* 9, 179–186. doi: 10.1093/geront/9.3_Part_1.179

Li, H.-J., Hou, X.-H., Liu, H.-H., Yue, C.-L., He, Y., and Zuo, X.-N. (2015a). Toward systems neuroscience in mild cognitive impairment and Alzheimer's disease: a meta-analysis of 75 fMRI studies. *Hum. Brain Mapp.* 36, 1217–1232. doi: 10.1002/hbm.22689

Li, H.-J., Hou, X.-H., Liu, H.-H., Yue, C.-L., Lu, G.-M., and Zuo, X.-N. (2015b). Putting age-related task activation into large-scale brain networks: a meta-analysis of 114 fMRI studies on healthy aging. *Neurosci. Biobehav. Rev.* 57, 156–174. doi: 10.1016/j.neubiorev.2015.08.013

Liao, X., Vasilakos, A. V., and He, Y. (2017). Small-world human brain networks: perspectives and challenges. *Neurosci. Biobehav. Rev.* 77, 286–300. doi: 10.1016/j.neubiorev.2017.03.018

Liu, Z., Zhang, Y., Yan, H., Bai, L., Dai, R., Wei, W., et al. (2012). Altered topological patterns of brain networks in mild cognitive impairment and Alzheimer's disease: a resting-state fMRI study. *Psychiatr. Res. Neuroimag.* 202, 118–125. doi: 10.1016/j.pscychresns.2012.03.002

Miller, S. L., Fenstermacher, E., Bates, J., Blacker, D., Sperling, R. A., and Dickerson, B. C. (2008). Hippocampal activation in adults with mild cognitive impairment predicts subsequent cognitive decline. *J. Neurol. Neurosurg. Psychiatr.* 79:630. doi: 10.1136/jnnp.2007.124149

Nakamura, T., Hillary, F. G., and Biswal, B. B. (2009). Resting network plasticity following brain injury. *PLoS ONE* 4:e8220. doi: 10.1371/journal.pone.0008220

Nasreddine, Z. S., Phillips, N. A., Bedirian, V., Charbonneau, S., Whitehead, V., Collin, I., et al. (2005). The montreal cognitive assessment, MoCA: a brief screening tool for mild cognitive impairment. *J. Am. Geriatr. Soc.* 53, 695–699. doi: 10.1111/j.1532-5415.2005.53221.x

Pasquini, L., Scherr, M., Tahmasian, M., Meng, C., Myers, N. E., Ortner, M., et al. (2015). Link between hippocampus' raised local and eased global intrinsic connectivity in AD. *Alzheimer's Dement.* 11, 475–484. doi: 10.1016/j.jalz.2014.02.007

Petersen, R. C. (2004). Mild cognitive impairment as a diagnostic entity. *J. Intern. Med.* 256, 183–194. doi: 10.1111/j.1365-2796.2004.01388.x

Petersen, R. C., Doody, R., Kurz, A., Mohs, R. C., Morris, J. C., Rabins, P. V., et al. (2001). Current concepts in mild cognitive impairment. *Arch. Neurol.* 58, 1985–1992. doi: 10.1001/archneur.58.12.1985

Sorg, C., Riedl, V., Muhlau, M., Calhoun, V. D., Eichele, T., Laer, L., et al. (2007). Selective changes of resting-state networks in individuals at risk for Alzheimer's disease. *Proc. Natl. Acad. Sci. U.S.A.* 104, 18760–18765. doi: 10.1073/pnas.0708803104

Spaniol, J., Davidson, P. S., Kim, A. S., Han, H., Moscovitch, M., and Grady, C. L. (2009). Event-related fMRI studies of episodic encoding and retrieval: meta-analyses using activation likelihood estimation. *Neuropsychologia* 47, 1765–1779. doi: 10.1016/j.neuropsychologia.2009.02.028

Staff, R. T. (2012). Reserve, brain changes, and decline. *Neuroimag. Clin.* 22, 99–105. doi: 10.1016/j.nic.2011.11.006

Thomas Yeo, B., Krienen, F. M., Sepulcre, J., Sabuncu, M. R., Lashkari, D., Hollinshead, M., et al. (2011). The organization of the human cerebral cortex estimated by intrinsic functional connectivity. *J. Neurophysiol.* 106, 1125–1165. doi: 10.1152/jn.00338.2011

Van Den Heuvel, M. P., Stam, C. J., Boersma, M., and Hulshoff Pol, H. E. (2008). Small-world and scale-free organization of voxel-based resting-state functional connectivity in the human brain. *Neuroimage* 43, 528–539. doi: 10.1016/j.neuroimage.2008.08.010

Wang, J., Wang, X., Xia, M., Liao, X., Evans, A., and He, Y. (2015). GRETNA: a graph theoretical network analysis toolbox for imaging connectomics. *Front. Hum. Neurosci.* 9:386. doi: 10.3389/fnhum.2015.00386

Wang, J., Zuo, X., Dai, Z., Xia, M., Zhao, Z., Zhao, X., et al. (2013a). Disrupted functional brain connectome in individuals at risk for Alzheimer's disease. *Biol. Psychiatry* 73, 472–481. doi: 10.1016/j.biopsych.2012.03.026

Wang, Y., Risacher, S. L., West, J. D., Mcdonald, B. C., Magee, T. R., Farlow, M. R., et al. (2013b). Altered default mode network connectivity in older adults with cognitive complaints and amnestic mild cognitive impairment. *J. Alzheimers. Dis.* 35, 751–760. doi: 10.3233/JAD-130080

World Health Organization (2010). *International Statistical Classification of Diseases and Related Health Problems 10th Revision Instruction Manual*. Geneva: World health Organization.

Xie, T., and He, Y. (2012). Mapping the Alzheimer's brain with connectomics. *Front. Psychiatry* 2:77. doi: 10.3389/fpsyt.2011.00077

Zhang, Y., Simon-Vermot, L., Araque Caballero, M. A., Gesierich, B., Taylor, A. N. W., Duering, M., et al. (2016). Enhanced resting-state functional connectivity between core memory-task activation peaks is associated with memory impairment in MCI. *Neurobiol. Aging* 45, 43–49. doi: 10.1016/j.neurobiolaging.2016.04.018

Zucca, R., Arsiwalla, X. D., Le, H., Rubinov, M., Gurguí, A., and Verschure, P. (2019). The degree distribution of human brain functional connectivity is generalized pareto: a multi-scale analysis. *bioRxiv [Preprint]* 840066. doi: 10.1101/840066

Zuo, X.-N., Ehmke, R., Mennes, M., Imperati, D., Castellanos, F. X., Sporns, O., et al. (2012). Network centrality in the human functional connectome. *Cereb. Cortex* 22, 1862–1875. doi: 10.1093/cercor/bhr269

Conflict of Interest: The authors declare that the research was conducted in the absence of any commercial or financial relationships that could be construed as a potential conflict of interest.

frontiers in Aging Neuroscience

ORIGINAL RESEARCH
published: 15 January 2021
doi: 10.3389/fnagi.2020.625642

Retinal Thickness Changes Over Time in a Murine AD Model APP$^{NL-F/NL-F}$

Elena Salobrar-García[1,2†], Inés López-Cuenca[1†], Lídia Sánchez-Puebla[1], Rosa de Hoz[1,2], José A. Fernández-Albarral[1], Ana I. Ramírez[1,2], Isabel Bravo-Ferrer[3,4], Violeta Medina[5], María A. Moro[5], Takaomi C. Saido[6], Takashi Saito[7], Juan J. Salazar[1,2] and José M. Ramírez[1,8*]*

[1] Ramon Castroviejo Ophthalmological Research Institute, Complutense University of Madrid, Madrid, Spain, [2] Department of Immunology, Ophthalmology and Ear, Nose, and Throat, Faculty of Optics and Optometry, Complutense University of Madrid, Madrid, Spain, [3] Department of Pharmacology and Toxicology, Faculty of Medicine, Complutense University of Madrid, Madrid, Spain, [4] Edinburgh Medical School, UK Dementia Research Institute, University of Edinburgh, Edinburgh, United Kingdom, [5] Centro Nacional de Investigaciones Cardiovasculares (CNIC), Madrid, Spain, [6] Laboratory for Proteolytic Neuroscience, Brain Science Institute, RIKEN, Wako, Japan, [7] Department of Neurocognitive Science, Institute of Brain Science, Nagoya City University Graduate School of Medical Sciences, Nagoya, Japan, [8] Department of Immunology, Ophthalmology and ENT, School of Medicine, Complutense University of Madrid, Madrid, Spain

OPEN ACCESS

Edited by:
Rong Chen,
University of Maryland, Baltimore, United States

Reviewed by:
Sachchida Nand Rai,
University of Allahabad, India
Henri Leinonen,
University of California, Irvine, United States

****Correspondence:***
José M. Ramírez
ramirezs@med.ucm.es
Juan J. Salazar
jjsalaza@ucm.es

† These authors have contributed equally to this work

Received: *03 November 2020*
Accepted: *15 December 2020*
Published: *15 January 2021*

Citation:
Salobrar-García E, López-Cuenca I, Sánchez-Puebla L, de Hoz R, Fernández-Albarral JA, Ramírez AI, Bravo-Ferrer I, Medina V, Moro MA, Saido TC, Saito T, Salazar JJ and Ramírez JM (2021) Retinal Thickness Changes Over Time in a Murine AD Model APP$^{NL-F/NL-F}$. Front. Aging Neurosci. 12:625642. doi: 10.3389/fnagi.2020.625642

Background: Alzheimer's disease (AD) may present retinal changes before brain pathology, suggesting the retina as an accessible biomarker of AD. The present work is a diachronic study using spectral domain optical coherence tomography (SD-OCT) to determine the total retinal thickness and retinal nerve fiber layer (RNFL) thickness in an APP$^{NL-F/NL-F}$ mouse model of AD at 6, 9, 12, 15, 17, and 20 months old compared to wild type (WT) animals.

Methods: Total retinal thickness and RNFL thickness were determined. The mean total retinal thickness was analyzed following the Early Treatment Diabetic Retinopathy Study sectors. RNFL was measured in six sectors of axonal ring scans around the optic nerve.

Results: In the APP$^{NL-F/NL-F}$ group compared to WT animals, the total retinal thickness changes observed were the following: (i) At 6-months-old, a significant thinning in the outer temporal sector was observed; (ii) at 15-months-old a significant thinning in the inner temporal and in the inner and outer inferior retinal sectors was noticed; (iii) at 17-months-old, a significant thickening in the inferior and nasal sectors was found in both inner and outer rings; and (iv) at 20-months-old, a significant thinning in the inner ring of nasal, temporal, and inferior retina and in the outer ring of superior and temporal retina was seen. In RNFL thickness, there was significant thinning in the global analysis and in nasal and inner-temporal sectors at 6 months old. Thinning was also found in the supero-temporal and nasal sectors and global value at 20 months old.

Conclusions: In the APP$^{NL-F/NL-F}$ AD model, the retinal thickness showed thinning, possibly produced by neurodegeneration alternating with thickening caused by deposits and neuroinflammation in some areas of the retina. These changes over time are similar to those observed in the human retina and could be a biomarker for AD. The APP$^{NL-F/NL-F}$ AD model may help us better understand the different retinal changes during the progression of AD.

Keywords: Alzheimer, retina, OCT, mouse model of AD, APPNL-F/NL-F

INTRODUCTION

Alzheimer's disease (AD) is a neurodegenerative brain pathology characterized by a loss of neurons and their synapses, after which an atrophy of the cerebral cortex develops (Sharma and Singh, 2016). The main features of AD are extracellular deposits of the protein amyloid-β (Aβ), the formation of plaques, and intraneuronal hyper-phosphorylated tau (pTau) in the form of neurofibrillary tangles (Ghiso et al., 2013) leading to a neuroinflammatory process (Pan et al., 2011).

One important tissue to focus on in search of neurodegenerative disease biomarkers is the eye. It is widely known that patients with AD have visual problems, such as decreased visual acuity, contrast sensitivity, color perception, and visual integration (Salobrar-García et al., 2015a, 2016, 2019a,b). Retinal changes have also been documented *in vivo* using optical coherence tomography (OCT) both in humans (Iseri et al., 2006; Garcia-Martin et al., 2014; Salobrar-García et al., 2015b, 2016, 2019a,b; Polo et al., 2017; Ko et al., 2018; Lad et al., 2018) and in different AD animal models (Chiquita et al., 2019; Georgevsky et al., 2019; Harper et al., 2020). The retinal changes observed in the OCT results of AD patients showed macular thinning when the disease is in an early stage, followed by thinning of the peripapillary area when AD progresses (Garcia-Martin et al., 2014; Salobrar-García et al., 2015b, 2019a,b; Jáñez-Escalada et al., 2019). Retinal areas with an increased thickness were found in AD patients, specifically in the macular area (Jáñez-Escalada et al., 2019; Salobrar-García et al., 2019a), revealing areas of possible gliosis prior to neurodegeneration. These changes could be correlated with those found in the retinas of AD transgenic models, where marked neurodegeneration and a loss of optic nerve axons were observed (Gupta et al., 2016; Chiquita et al., 2019; Georgevsky et al., 2019), alongside retinal thickening and increased microglial activation in the early stages of the disease (Perez et al., 2009; Yang et al., 2013; Gao et al., 2015; Salobrar-García et al., 2020). In addition to the retinal structural changes, several functional changes have been observed by means of electroretinogram (ERG) in the $APP_{swe/PS1}$ transgenic mouse model of AD finding a significant reduction of the a and b wave amplitudes between 12 and 16 months of age (Perez et al., 2009). Other authors observed in this model, already at 3 months a significant reduction of the b-wave coinciding with the Aβ deposits in the hippocampus (Georgevsky et al., 2019). In addition, findings, such as a slightly shortened ERG latency in dark adapted conditions and the increased frequency of oscillatory potentials in the old $APP_{swe/PS1}$, could be related to inadequate cholinergic innervation (Leinonen et al., 2016). However, in this model, late-stage photopic ERG measurements revealed that the cone mediated retinal response was preserved in the $APP_{swe/PS1}$ mice (Joly et al., 2017). Therefore, the retina has been postulated as an accessible biomarker of AD.

Most cases of AD in humans are sporadic, and only <3% are caused by genetic mutations (Selkoe, 2001). There is currently no mouse model for sporadic AD (Foidl and Humpel, 2020). In recent decades, different transgenic AD models have been generated for mice to mimic the main neuropathological hallmarks of the disease (Foidl and Humpel, 2020), but there is no transgenic mouse model that presents all AD features. Most transgenic mice were made to overexpress mutant forms of APP and/or PS1 and show the onset of Aβ age-dependent brain deposition, gliosis, synaptic dysfunction, and memory deficits (Duyckaerts et al., 2008). Transgenic mice that overexpress APP have artificial phenotypes because, in addition to the Aβ, they overproduce other APP fragments that can interfere with intrinsic biological functions. In addition, these models use artificial promoters that produce transgenic expression in cells that are not always identical to those that express endogenous APP. Another feature of APP overexpression models is the sudden death that reflects a physiological alteration (Nilsson et al., 2014; Saito et al., 2014). A second generation of AD mouse models was developed to have both less artificial phenotypes and less altered physiology (Sakakibara et al., 2018). This alternative AD mouse models have been generated via knock-in (KI) of a humanized Aβ sequences harboring familial AD mutations [Swedish (NL), Beyreuther/Iberian (F), and Arctic (G)] (Sakakibara et al., 2019). One of these second generation AD mouse models is the $APP^{NL-F/NL-F}$ that harbors the Swedish mutation (NL) and the Iberian mutation (F). This model, unlike the models that overexpress APP, has normal levels of full-length APP, and its cleavage products produce a significantly higher level of $A\beta_{42}$ compared to wild type (WT) mice and APP overexpression models, as well as exhibits a significantly higher $A\beta_{42}/A\beta_{40}$ ratio (Saito et al., 2014). Increased $A\beta_{42}$ levels in this model cause pathological deposits of Aβ in the cerebral cortex and hippocampus, leading to infiltration of the microglia and astrocytes surrounding the Aβ plaques starting at 6 months old (Sasaguri et al., 2017). The $APP^{NL-F/NL-F}$ model reproduces several key pathologies found in AD patients. It has been suggested that this model may be useful as a preclinical AD mouse model to research the pathological role of amyloidosis and amyloids related to neuroinflammation (Saito and Saido, 2018). In addition, this model presents a number of neurological disturbances in an age-dependent manner, such as synaptic disorders and memory impairment, in a Y-maze test (Saito et al., 2014).

For retinal tissue, Aβ deposits have been found in several AD models that overexpress APP (Ning et al., 2008; Shimazawa et al., 2008; Dutescu et al., 2009; Perez et al., 2009; Koronyo-Hamaoui et al., 2011; Gupta et al., 2016). These Aβ deposits were located in the retinal nerve fiber layer (RNFL), ganglion cell layer (GCL), inner plexiform layer (IPL), outer plexiform layer (OPL), and inner nuclear layer (INL) (Ning et al., 2008; Dutescu et al., 2009; Perez et al., 2009; Koronyo-Hamaoui et al., 2011).

Recently, the retina has been studied by OCT in transgenic mouse models that overexpress APP, but these studies are scarce and controversial. In an APP/PS1 model analyzing the retina from 3 to 12 months of age, a significant decrease in retinal thickness in the inner layers was found at 9 months of age and in the outer layers at 12 months (Georgevsky et al., 2019). In the 3xTg-AD animal model, neurodegeneration was found to start at 4 months-old in the innermost retinal layers. As the disease progressed, significant changes were found in every analyzed layer, with the exception of the ONL, where a thickening was observed at 12 months of age (Chiquita et al., 2019), as well as a

significant thinning of the RNFL in AD mouse retinas compared to the WT controls (Song et al., 2020).

Despite the loss of neurons that occurs at ∼17 months-age, for most transgenic models of AD (APP/PS1 model) (Harper et al., 2020), diachronic studies that analyze the retinal changes observed by OCT in AD transgenic models from early stages to late stages of the disease could help us better understand the retinal observations. To the best of our knowledge, there is no study that analyzes the retina using SD-OCT in the $APP^{NL-F/NL-F}$ model. Given the aforementioned advantages of this model, the aim of this study was to analyze the changes in retinal thickness (total retinal thickness and RNFL thickness) over time (at 6, 9, 12, 15, 17, and 20 months of age) in a well-validated mouse model of AD ($APP^{NL-F/NL-F}$).

MATERIALS AND METHODS

Animals and Ethics

The experiments were performed on male $APP^{NL-F/NL-F}$ mice produced by manipulating the mouse APP gene using a knock-in strategy with Swedish (KM670/671NL) and Beyreuther/Iberian (I716F) mutations, as described previously (Saito et al., 2014). The experiments were also performed on age-matched WT animals (C57BL/6J). The animals were obtained from the research group led by Dr. Takaomi C. Saito at the laboratory for Proteolytic Neuroscience, RIKEN Brain Science Institute, Saitama, Japan.

The Aβ sequence within the mouse APP gene was humanized and, while the Swedish mutation (NL) elevates the total amount of $A\beta_{40}$ and $A\beta_{42}$, the Beyreuther/Iberian(F) mutation increases the ratio of $A\beta_{42}/A_{\beta 40}$ (Saito et al., 2014). The great advantage of this model is that the mouse Aβ sequence is humanized and the Swedish and Beyreuther/Iberian mutations are introduced by knock-in technology (Saito et al., 2014). In order to accelerate pathology and to remove murine endogenous Aβ, mutant mice are bred in homozygosity (Sasaguri et al., 2017) explaining why control mice are not littermates. However, this should not be a major problem considering that mutant mice have been backcrossed with genuine wild-type B6J mice for more than 10 generations.

The retinas of male $APP^{NL-F/NL-F}$ and WT animals were evaluated *in vivo* using SD-OCT at 6, 9, 12, 15, 17, and 20 months of age.

The animals were housed in light- and temperature-controlled rooms with a 12-h light/dark cycle and *ad libitum* access to food and water in the Medical School at the University Complutense of Madrid. Light intensity within the cages ranged from 9 to 24 lux. The SD-OCT analysis was performed under general anesthesia induced with an intraperitoneal (ip) injection of a mixture of ketamine (75 mg/kg; Anesketin®, Dechra Veterinary Products SLU, Barcelona, Spain) and medetomidine (0.26 mg/kg; Medetor®, Virbac España S.A., Barcelona, Spain), which can be reversed by the antagonist atipamezole (Antisedan, 5 mg/mL; Pfizer). During the recovery from anesthesia, the mice were placed in their cages with a heat source to maintain their core body temperature.

All procedures were performed in accordance with the European Parliament, the Council Directive 2010/63/EU, and Spanish legislation (Real Decreto 53/ 2013). The procedures were approved by the Ethics Committee on Animal Welfare of the University Complutense (PROEX No. 047/16) and reported according to the Association for Research in Vision and Ophthalmology (ARVO) statement of animal use. All procedures minimized the number of animals used and their suffering.

Experimental Groups

Two groups of mice were used for this study: an $APP^{NL-F/NL-F}$ group ($n = 55$) and an age-matched control (WT, $n = 41$) group, as indicated in **Table 1**. Only the left eyes of the animals were used in our study. This control-case study was performed at 6, 9, 12, 15, 17, and 20 months of age.

OCT Analysis

The retinal structures were evaluated using SD-OCT Spectralis with the Heidelberg Eye Explorer software v6.13 (Heidelberg Engineering, Heidelberg, Germany) after pupil dilation (tropicamide 10 mg/ml; colircusi tropicamide, Alcon Healthcare, Barcelona, Spain).

The cornea was kept moisturized using artificial tear eye drops. To prevent a reduction in body temperature, heating pads were placed underneath the mice.

An addition, a 25 diopter mouse lens (Heidelberg, Germany) was added in front of the OCT camera, and the murine eye was covered with a polymethyl methacrylate contact lens (3.2 mm diameter, base curve 1.7; Cantor&Nissel, UK), which served to create a uniform refractive surface.

Each mouse eye was aligned with respect to the measurement beam to ensure that the optic nerve head (ONH) was at the center of the OCT analysis. To compensate for small eye movements, such as those that occur as a result of respiration, motion artifacts were minimized through real-time eye tracking in the device software.

As in the Early Treatment Diabetic Retinopathy Study (ETDRS), retinal thickness data were displayed as three concentric rings 3 mm in total diameter centered in the optic nerve. These rings were distributed as follows: a central area with a diameter of 1 mm that was not considered for the measurements, an inner ring with a diameter of 2 mm, and an outer ring with a diameter of 3 mm. Both measured rings were divided into four quadrants (superior, inferior, nasal, and temporal) (**Figures 1A,B**). Due to the size of the mouse eye,

TABLE 1 | Number of mice used at different time points.

Age group	$APP^{NL-F/NL-F}$ group (*n*)	WT group (*n*)
6 months	5	7
9 months	14	6
12 months	10	7
15 months	6	7
17 months	8	7
20 months	12	7

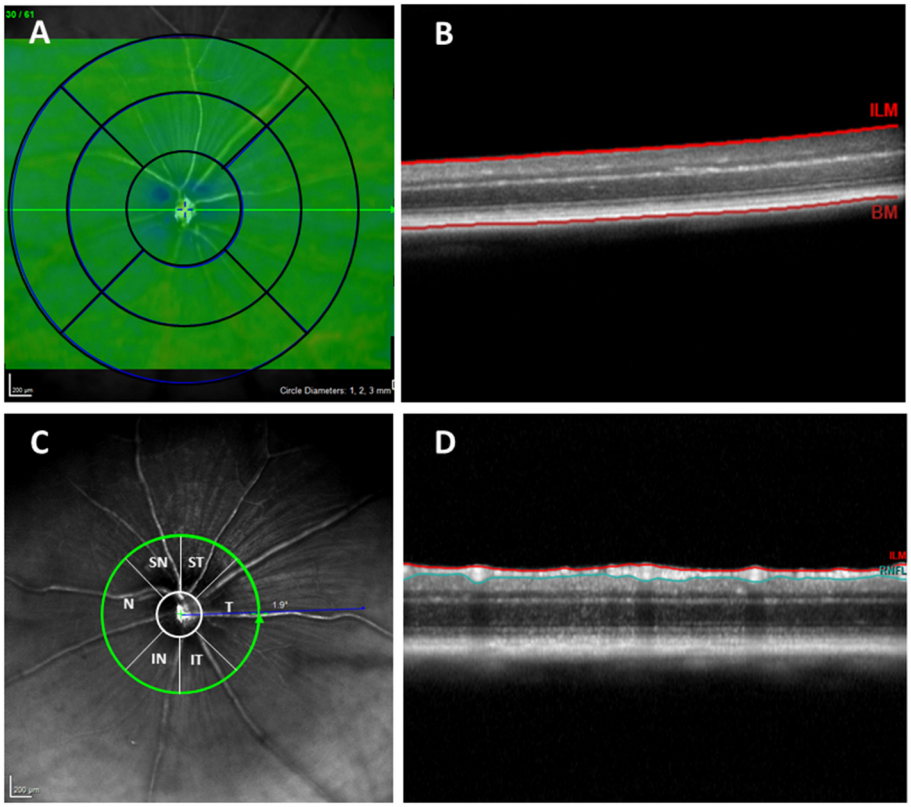

FIGURE 1 | (A) Concentric rings with 1, 2, and 3 mm diameters. **(B)** OCT section. Retinal thickness measured between the inner limiting membrane and the retinal pigment epithelium. **(C)** RNFL sectors (RNFL, Retinal Nerve Fiber Layer; ST, Supero–Temporal; SN, Supero–Nasal; N, Nasal; IN, Infero–Nasal; IT, Infero-Temporal; T, Temporal; G, Global). **(D)** OCT section. Result of segmentation of the OCT scan. RNFL delimited between the ILM and GCL + IPL. OCT, optical coherence tomography; RNFL, Retinal nerve fiber layer; ILM, inner limiting membrane; GCL + IPL, ganglion cell layer and inner plexiform layer.

which differs significantly from that of the human eye, a +25 diopter optical lens was used in addition to a contact lens, so the lateral distances were not entirely accurate. However, it was shown that axial measurements with OCT are accurate for the study of rodents (Dysli et al., 2015).

To analyze the RNFL, an axonal ring scan around the optic nerve head was carried out. The RNFL was measured in six sectors provided by the Heidelberg Software (Supero–Temporal, Superior, Supero–Nasal, Nasal, Infero–Nasal, Temporal, Inferior, and Temporal). The mean of all sectors is shown in the center as the global value (G) (**Figures 1C,D**).

The Spectralis OCT animal software allows automatic segmentation of the retinal layers and measurement of each layer's thickness through the same segmentation of the concentric circular sectors mentioned above. After collecting the images, if it was necessary to correct the automatic division of the layers, manual corrections were made by the same experienced examiner. The RNFL and total retinal thickness were then measured. The distance between the inner limiting membrane and the posterior surface of the RPE was defined as the total retinal thickness.

Statistical Analysis

For the statistical analysis, we used the SPSS software 25.0 (SPSS Inc., Inc., Chicago, IL, USA). The differences between study groups ($APP^{NL-F/NL-F}$ and WT) were analyzed using a non-parametric Mann–Whitney U Test. Data are reported as the mean values ± standard deviation (SD). A *P*-value <0.05 was considered statistically significant.

RESULTS

In this study, we evaluated the total retinal thickness and RNFL thickness in different age groups (at 6, 9, 12, 15, 17, and 20 months) using the $APP^{NL-F/NL-F}$ mouse model of AD ($APP^{NL-F/NL-F}$ group) and age-matched wild-type mice (WT group). Ninety-four mice were analyzed in total—55 $APP^{NL-F/NL-F}$ mice and 41 WT mice.

Total Retinal Thickness

At 6 months of age, for the $APP^{NL-F/NL-F}$ mice, we found that the total retinal thickness was significantly decreased in the temporal sector in the outer ring (244.40 ± 2.41) compared to the WT mice (253.00 ± 6.11; $p < 0.05$). In this same age group, compared to the WT mice, the remaining sectors showed slight thinning, except for the superior sector in the inner ring, which showed a slight thickening (without statistical significance in both cases) (**Table 2**, **Figure 2**).

When we analyzed the 9-months-age groups, the total retinal thickness of the $APP^{NL-F/NL-F}$ mice showed slight thinning

TABLE 2 | Total retinal thickness between groups.

			Total retinal thickness							
			Inner ring				Outer ring			
			S	I	N	T	S	I	N	T
6 months	$APP^{NL-F/NL-F}$	Mean	250.60	244.20	241.40	243.00	254.20	243.80	246.20	244.40
		SD	5.73	4.82	4.28	4.53	6.38	4.44	5.63	2.41
	WT	Mean	249.43	249.43	246.00	247.43	256.57	253.57	248.86	253.00
		SD	6.02	7.30	4.28	7.25	8.28	9.11	6.18	6.11
	P-value		0.935	0.255	0.101	0.221	0.684	0.061	0.624	**0.028***
9 months	$APP^{NL-F/NL-F}$	Mean	252.36	247.29	247.43	247.57	257.71	245.36	251.21	246.14
		SD	8.42	7.24	5.26	5.56	6.78	9.43	4.51	6.68
	WT	Mean	257.17	250.33	250.50	251.83	261.67	249.00	248.17	252.33
		SD	7.31	6.12	6.92	7.68	11.38	5.37	7.36	7.12
	P-value		0.246	0.342	0.230	0.185	0.282	0.535	0.320	0.063
12 months	$APP^{NL-F/NL-F}$	Mean	253.00	246.56	245.56	246.33	257.22	246.11	247.67	246.22
		SD	8.38	3.17	5.96	5.70	11.29	4.86	4.85	7.07
	WT	Mean	255.86	252.86	249.71	250.71	258.14	252.57	250.14	250.57
		SD	6.94	7.84	7.04	6.92	6.31	7.61	6.87	5.53
	P-value		0.366	0.089	0.202	0.123	0.560	0.100	0.243	0.110
15 months	$APP^{NL-F/NL-F}$	Mean	253.83	248.00	244.83	249.17	257.50	247.00	248.17	247.67
		SD	4.96	7.90	2.48	8.64	9.12	7.75	4.36	9.58
	WT	Mean	252.71	254.86	251.00	250.57	257.29	255.29	250.71	251.57
		SD	7.11	5.90	6.68	8.48	9.23	6.34	6.05	6.11
	P-value		0.429	**0.044***	**0.031***	0.473	0.617	**0.038***	0.418	0.195
17 months	$APP^{NL-F/NL-F}$	Mean	255.38	250.25	251.63	248.25	257.75	252.88	255.00	248.13
		SD	7.48	4.37	5.73	3.37	9.10	5.30	7.48	4.52
	WT	Mean	252.29	244.71	243.00	246.71	255.00	245.00	243.71	249.71
		SD	4.68	4.57	4.73	3.20	8.50	5.45	3.30	4.68
	P-value		0.450	**0.036***	**0.024***	0.415	0.602	**0.023***	**0.004****	0.523
20 months	$APP^{NL-F/NL-F}$	Mean	240.83	241.83	239.08	240.25	245.25	244.91	242.58	241.67
		SD	6.86	4.53	5.74	4.75	8.67	7.49	7.14	6.96
	WT	Mean	250.67	253.17	251.50	251.50	255.33	252.33	249.50	252.00
		SD	9.87	8.38	8.89	8.80	9.54	8.14	6.75	9.61
	P-value		0.054	**0.007****	**0.009****	**0.007****	**0.039**	0.076	0.100	**0.031**

** in bold: p-value <0.05; **in bold: p-value <0.01; Mann-Whitney U Test; WT, wild type; SD, standard deviation; S, superior; I, inferior; N, nasal; T, temporal.*

without statistical significance in all sectors, except for the nasal sector in the outer ring, which was slightly thickened compared to the WT group (**Table 2**, **Figure 2**).

At 12 months of age, total retinal thickness in the $APP^{NL-F/NL-F}$ group showed no statistically significant changes in comparison to the WT group. However, at 12 months old, all sectors showed slight thinning, with the inferior sectors in both the inner and outer rings being the thinnest (**Table 2**, **Figure 2**).

At 15 months of age, the total retinal thickness of the $APP^{NL-F/NL-F}$ mice group showed a significant decrease in the inferior sector in both the inner (248.00 ± 7.90) and outer ring (247 ± 7.75) and in the inner ring of the nasal sector (244.83 ± 2.48) compared to the WT group (254.86 ± 5.90, 255.29 ± 6.34, and 251 ± 4.73, respectively $p < 0.05$ in all cases). In this age group, the remaining sectors showed slight thinning, except for the superior sector in the inner ring, which showed a slight thickening (without statistical significance in both cases), in comparison to the WT mice group (**Table 2**, **Figure 2**).

At 17 months of age, in the $APP^{NL-F/NL-F}$ group compared to the WT group, we found a significant increase in thickness in the nasal and inferior sectors in the inner and outer rings. The nasal sectors in both the inner ring (251.63 ± 5.73 vs. 243 ± 4.73, for $APP^{NL-F/NL-F}$ and WT groups, respectively) and the outer ring (255.00 ± 7.48 vs. 243.71 ± 3.30, for $APP^{NL-F/NL-F}$ and WT groups, respectively) were significantly thicker ($p < 0.05$ for inner ring and $p < 0.01$ for outer ring) in the $APP^{NL-F/NL-F}$ group compared to the WT group. Similarly, in the $APP^{NL-F/NL-F}$ group, the inferior sectors in both the inner ring (250.25 ± 4.37 vs. 244.71 ± 4.57, for $APP^{NL-F/NL-F}$ and WT groups, respectively) and the outer ring (252.88 ± 5.30 vs. 245.00 ± 5.45, for $APP^{NL-F/NL-F}$ and WT groups, respectively) showed statistically significant thickening compared to the WT group ($p < 0.05$ in all cases; **Table 2**, **Figure 2**).

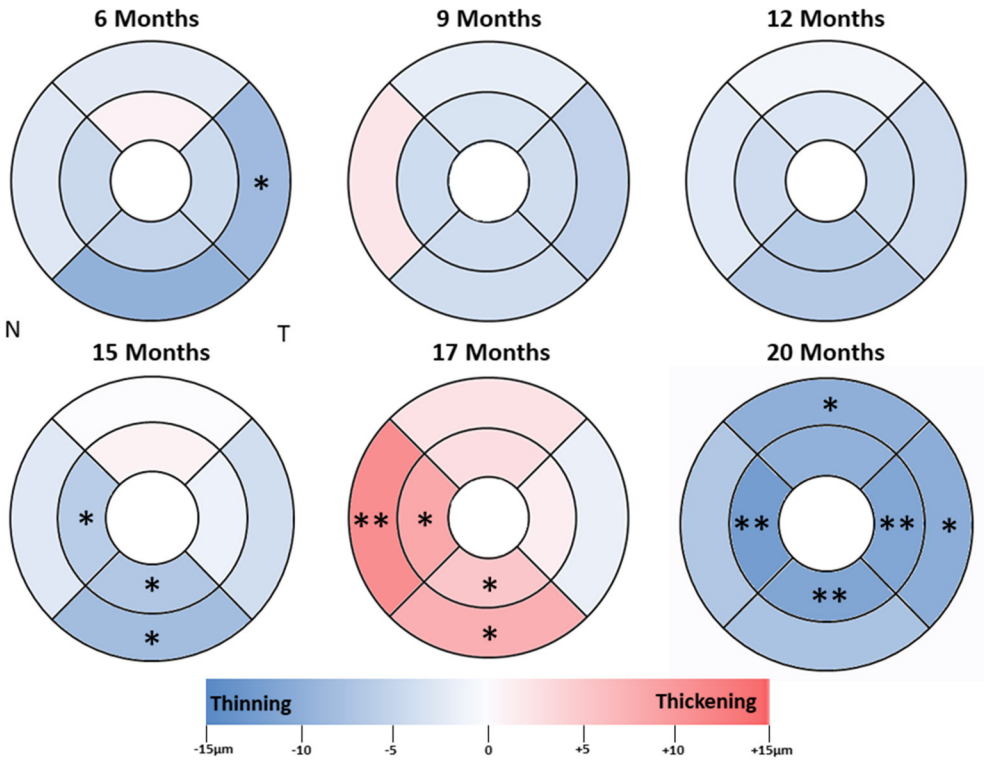

FIGURE 2 | Colorimetric differences of retinal thickness in each age group between the APP$^{NL-F/NL-F}$ and WT animal groups. OCT rings with 1, 2, and 3 mm diameters. Red: thickening; blue: thinning. APP$^{NL-F/NL-F}$, Single App Knock-in mouse model of Alzheimer's disease; WT, Wild type; OCT, optical coherence tomography; N, nasal; T, temporal.

When we compared the APP$^{NL-F/NL-F}$ group with the WT control group in the oldest animals (20 months), we found a significant thickness decrease in the inner and outer ring in the temporal sector ($p < 0.01$ and $p < 0.05$, respectively), in the inner ring of both inferior and nasal sectors ($p < 0.01$ in both cases) and in the outer ring of the superior sector ($p < 0.05$). In the APP$^{NL-F/NL-F}$ mice in comparison with the WT group: the temporal sectors showed a statistically significant decrease in both the inner ring (240.25 ± 4.75 vs. 251.50 ± 8.80, in APP$^{NL-F/NL-F}$ and WT, respectively) and in the outer ring (241.67 ± 6.96 vs. 252.00 ± 9.61, in APP$^{NL-F/NL-F}$ and WT, respectively); both the nasal sectors and inferior sectors showed statistically significant thinning in the inner ring (239.08 ± 5.74 vs. 251.50 ± 8.89 for nasal sector and 241.83 ± 4.53 vs. 253.17 ± 8.38 for inferior sector, in APP$^{NL-F/NL-}$F and WT, respectively) and the superior sectors showed statistically significant thinning, in the outer ring (245.25 ± 8.67 vs. 255.00 ± 9.54, in APP$^{NL-F/NL-F}$ and WT, respectively) (**Table 2**, **Figure 2**).

RNFL Thickness

Overall, in RNFL, there were no statistically significant changes over time observed in our study, except at 6 and 12 months of age. At early time point in the APP$^{NL-F/NL-F}$ group, we found a significant thickness decrease compared to the WT group in the nasal sector (21.80 ± 1.48 vs. 24.29 ± 1.80, in APP$^{NL-F/NL-F}$ and WT, respectively), in the infero–temporal sector (21.20 ± 1.30 *vs*. 25.57 ± 4.58, in APP$^{NL-F/NL-F}$ and WT, respectively), and in the global value (23.00 ± 1.00 vs. 26.71 ± 4.46, in APP$^{NL-F/NL-F}$ and WT, respectively; $p < 0.05$ in all cases) (**Table 3**, **Figure 3**).

At 9 months-old, the thickness of all sectors in the APP$^{NL-F/NL-F}$ group slightly decreased compared to the WT group without statistical significance (**Table 3**, **Figure 3**).

By contrast, at 12 and 15 months of age, in the APP$^{NL-F/NL-F}$ group, only four sectors showed a slight non-significant thickness decrease (in the supero–temporal, temporal, nasal, and infero–nasal sectors), and the remaining two sectors were slightly thickened without statistical significance (supero–nasal, and infero–temporal) compared to the WT group (**Table 3**, **Figure 3**).

When comparing APP$^{NL-F/NL-F}$ and WT mice at 17 months old, it was found that the RNFL thickness of all sectors increased slightly without statistical significance, except in the supero–temporal sector, where we found a slight non-significant thickness decrease (**Table 3**, **Figure 3**).

By contrast, at 20 months of age, the highest age in the APP$^{NL-F/NL-F}$ group, we found a significant thickness decrease in comparison to WT group in the nasal sector (24.83 ± 2.33

TABLE 3 | Retinal nerve fiber layer thickness between groups.

			Retinal nerve fiber layer thickness						
			N	**T**	**SN**	**ST**	**IN**	**IT**	**G**
6 months	$APP^{NL-F/NL-F}$	Mean	21.80	23.60	25.60	25.00	24.80	21.20	23.00
		SD	1.48	0.89	4.16	2.12	1.30	1.30	1.00
	WT	Mean	24.29	25.86	24.00	28.86	25.71	25.57	26.71
		SD	1.80	2.19	3.00	4.06	4.46	4.58	4.46
	P-value		**0.030***	0.062	0.741	0.087	0.868	**0.014***	**0.039***
9 months	$APP^{NL-F/NL-F}$	Mean	24.29	26.36	24.64	27.00	25.57	23.86	25.29
		SD	2.73	3.46	4.09	4.71	6.28	3.63	2.61
	WT	Mean	26.17	28.00	24.50	27.83	29.00	24.50	26.67
		SD	2.14	2.37	2.95	2.64	2.37	2.43	1.75
	P-value		0.133	0.213	0.708	0.868	0.299	0.617	0.170
12 months	$APP^{NL-F/NL-F}$	Mean	25.40	25.90	25.70	27.60	25.00	25.90	26.00
		SD	2.07	2.28	3.37	2.59	5.42	3.14	1.70
	WT	Mean	26.33	25.50	23.83	27.83	28.50	23.67	26.17
		SD	1.63	2.17	3.25	2.99	2.95	2.58	1.47
	P-value		0.352	0.659	0.414	0.869	0.190	0.272	0.868
15 months	$APP^{NL-F/NL-F}$	Mean	24.50	25.67	25.33	26.17	28.17	25.17	25.50
		SD	3.62	1.97	3.39	4.07	4.36	2.14	2.43
	WT	Mean	27.29	26.86	26.14	29.00	29.71	25.29	27.14
		SD	3.99	3.72	3.02	5.03	2.87	5.59	2.91
	P-value		0.311	0.718	0.829	0.194	0.251	0.665	0.348
17 months	$APP^{NL-F/NL-F}$	Mean	26.75	27.25	28.00	26.38	30.00	26.38	27.25
		SD	4.30	5.39	3.25	3.85	5.55	3.29	3.06
	WT	Mean	26.29	26.29	25.71	28.43	26.71	23.43	26.29
		SD	1.98	3.99	3.25	7.55	4.46	2.70	2.29
	P-value		0.861	0.861	0.244	0.636	0.270	0.077	0.481
20 months	$APP^{NL-F/NL-F}$	Mean	24.83	24.58	25.25	26.33	24.83	24.17	24.67
		SD	2.33	3.73	3.47	4.08	5.56	4.84	2.06
	WT	Mean	30.33	27.00	28.00	31.50	29.17	28.33	29.00
		SD	1.86	4.52	4.86	2.35	5.42	3.44	1.79
	P-value		**0.001***	0.257	0.343	**0.011***	0.158	0.081	**0.002***

** in bold: p-value <0.05, Mann-Whitney U Test; WT, wild type; SD, standard deviation; N, nasal; T, temporal; SN, supero-nasal; ST, supero-temporal; IN, ínfero-nasal; IT, ínfero-temporal; G, mean global thickness.*

vs. 30.33 ± 1.86, in $APP^{NL-F/NL-F}$ and WT, respectively), in the supero-temporal sector (26.33 ± 4.08 vs. 31.50 ± 2.35, in $APP^{NL-F/NL-F}$ and WT, respectively), and in the global value (24.67 ± 2.06 vs. 29.00 ± 1.79, in $APP^{NL-F/NL-F}$ and WT, respectively) (**Table 3**, **Figure 3**).

DISCUSSION

The present work is the first diachronic SD-OCT study of the RNFL thickness and total retinal thickness in $APP^{NL-F/NL-F}$ mice at 6, 9, 12, 15, 17, and 20 months of age compared with WT animals. In this way, the development of the retinas could be tracked as the disease progressed. This diachronic study covers a wider timeframe than any other study performed so far. Histological studies provide a wide spectrum of information, but the processing of retinal tissue for analysis causes thicknesses to vary, which makes it difficult to correlate directly with the data provided by current techniques like OCT, which allows us to analyze *in vivo* the changes experienced by the retina as the disease develops (Salobrar-García et al., 2016). In this study we demonstrated for the first time retinal changes from the early to late stages of AD using OCT in the $APP^{NL-F/NL-F}$ model.

The $APP^{NL-F/NL-F}$ model presents an age-related Aβ pathology, memory deterioration, behavioral problems, and neuroinflammation (Cash et al., 2013; Rochat et al., 2013; Saito et al., 2014; Masuda et al., 2016; Sasaguri et al., 2017; Shah et al., 2018) and allows us to estimate early changes in the retina.

It is now known that there are relationships between certain areas of the brain and the retina. Specifically, the thickness of peripapillary RNFL (pRNFL) in the temporal sector is related to the volume of the medial temporal lobes, especially with the volume of the hippocampus (Shi et al., 2020). In

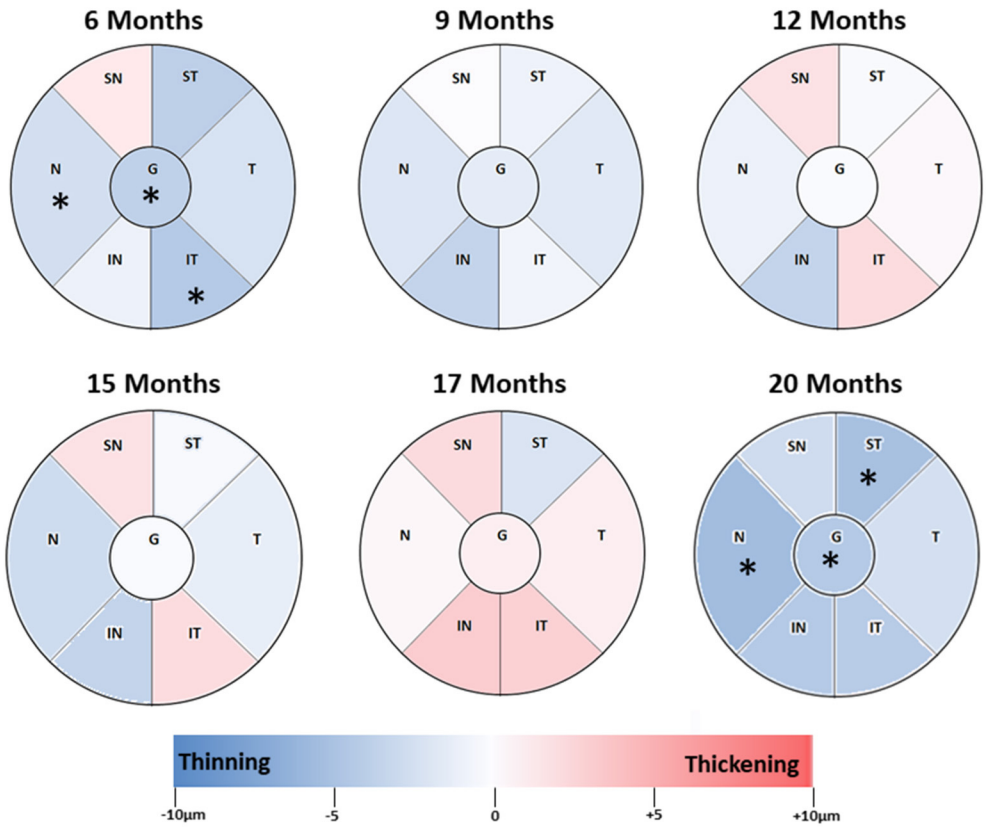

FIGURE 3 | Colorimetric differences of RNFL thickness at each time point between the APP$^{NL-F/NL-F}$ and WT groups. OCT sectors. Red: thickening; blue: thinning. APP$^{NL-F/NL-F}$, Single App Knock-in mouse model of Alzheimer's disease; WT, Wild type; RNFL, Retinal nerve fiber layer; N, nasal; SN, Supero–Nasal; ST, Supero–Temporal; T, temporal; IT, Infero-Temporal; IN, Infero–Nasal; G, global.

the lower sector the pRNFL thickness is associated with the volume of the occipital lobes and selectively with the volume of the lingual gyrus. Therefore, the cerebral changes observed in AD may be related to retinal changes and the retina may be useful as a biomarker of neurodegenerative diseases (Shi et al., 2020).

In APP$^{NL-F/NL-F}$ model, at 3 months old, there was no presence of Aβ pathology, although there was already an alteration of the proteome in both the hippocampus and the cortex compared to WT mice. The early increase in Tris-soluble Aβ$_{42}$ levels suggests that the pre-symptomatic stages of AD begin before amyloidosis Aβ (Schedin-Weiss et al., 2020). In addition, the accumulation of Aβ is age-dependent from 1 to 18 months (Petrache et al., 2019). Aβ brain deposits have been reported at 6 months of age in this AD model (Saito et al., 2014), developing first in the hippocampus and then becoming more significant in the cerebral cortex (Schedin-Weiss et al., 2020). At 9 months old, there was a significant amount of Aβ plaques in the parenchymal brain, with the Aβ plaque load reaching its maximum at 18 months (Schedin-Weiss et al., 2020). While the brain changes in this model have been studied, there are not works analyzing the retina. However, in other transgenic models retinal changes have been previously reported.

In the retina, the formation of Aβ plaques was described to occur at 6 months in the APP/PS1 model (Georgevsky et al., 2019), although other authors observed these plaques earlier in the retina at 2.5 months old (Koronyo-Hamaoui et al., 2011). Using the 3xTg-AD model, it was demonstrated that there is a positive correlation between retinal thickness and the volume of the visual cortex (Chiquita et al., 2019), as well as the behavior of the microglia in the retina, showing activation and migration between the different layers of the retina in whole-mount retinas (Salobrar-García et al., 2020). Histological alterations has been described in the retina, such as a decrease in the density of retinal ganglion cells and the nerve fiber layer, thinning of the inner plexiform layer, and the presence of Aβ plaques in the inner nuclear layer in a APP/PS1 model (Gupta et al., 2016).

Scarce studies have analyzed retinal changes using OCT in transgenic models (APP/PS1 and 3xTg-AD), however, to our knowledge, there is no study that analyses the retina in the APP$^{NL-F/NL-F}$ model. By analyzing two horizontal lines above and below the optic nerve, Georgevsky et al. (2019) showed, in

both APP/PS1 mice and WT controls, a significant age-related reduction in the inner retinal thickness from 3 to 12 months, with a significant difference between the APP/PS1 and WT mice in both the inner and outer retinal thickness starting at 9 months. In contrast, Harper et al. (2020) using multicontrast OCT, more recently found no significant changes in retinal thickness between APP/PS1 mice and control mice in any of the retinal regions analyzed by scanning an annulus around the ONH divided into two sectors. Finally, Song et al. (2020) using a multimodal imaging system with co-registered OCT and angle-resolved low-coherence interferometry, found a significant thinning of RNFL in 3xTg-AD mouse retinas compared to the WT controls.

Although the use of OCT gives us *in vivo* images at a very high resolution that allow us to analyze the retinal layers in animal model studies, most OCTs designed for animal studies have no tracker system. To date, no published studies have been conducted using this technique (Georgevsky et al., 2019; Harper et al., 2020). However, our diachronic study in $APP^{NL-F/NL-F}$ model was conducted using SD-OCT with a tracking system that allowed us to re-examine the exact same area, thereby avoiding measurement errors or unintentional movements and giving us the ability to analyse areas of the retina that cover almost the entire posterior pole instead of a single scan line.

In $APP^{NL-F/NL-F}$ mice the early retinal thinning observed with SD-OCT at 6 months of age (which was significant in total retinal thickness only in the outer temporal sector, as well as in the nasal, infero–temporal sectors and mean global value of the RNFL) appeared to develop toward more significant thinning by the final time point. It is possible that these initial changes are the consequence of the progressive accumulation of soluble oligomers of Aβ (in our model Tris-soluble $Aβ_{42}$), inducing early neuronal dysfunction due to their toxicity. These changes are in line with the observation that the APOE ε4 genotype of AD is associated with a decrease in GABAergic interneurons and glutamatergic signaling in the hippocampus, which is a risk factor for AD (Andrews-Zwilling et al., 2010; Busche and Konnerth, 2016; Shah et al., 2018). In the APP/PS1 model, primary visual cortex degeneration has also been observed in parallel with an increase in Aβ plaque with age. This is specific to the hyperactive neurons located near plaques, which are also found in the frontal cortex in AD (Busche et al., 2008). The hyperactive astrocytes located in the vicinity of the Aβ plaques that are formed may also contribute to neuronal protection, which can directly improve neuronal activity initially. This astrogliosis becomes noticeable very early and correlates with the slow development of AD in the $APP^{NL-F/NL-F}$ mice at 6 months (Saito et al., 2014; Petrache et al., 2019). The findings at this early time may also be secondary to the astrocyte reduction of glutamate synaptic recapture (Li et al., 2009) and to the excessive amount of Aβ dimers, as well as the $Aβ_{1-40}$ monomers and dimers, which increase the presynaptic release of glutamate (Fogel et al., 2014). Therefore, a combination of both causes could increase residual glutamate levels, thereby promoting neuronal hyperactivity, which is a precursor to plaque formation (Busche and Konnerth, 2016; Schedin-Weiss et al., 2020).

In the $APP^{NL-F/NL-F}$ mice, the time between 9 and 15 months of age was characterized by a slow and progressive tendency toward thickening of the retina with alternation of thinned retinal sectors, which vary over time and present only statistical significance at 15 months in some sectors of the total retinal thickness (outer and inner rings of inferior sector and inner ring of the temporal sector). These changes could correlate to the brain changes seen in this model at 9 months, when neuronal death was detected by necrosis in the cerebral cortex (Schedin-Weiss et al., 2020). At the same time, the effect of microgliosis and astrogliosis are significant in the $APP^{NL-F/NL-F}$ model in the cortex, hippocampus, and subcortical region compared to the WT mice (Masuda et al., 2016). These mechanisms could explain why, at 9 months, although there were changes in the OCT analysis in the $APP^{NL-F/NL-F}$ group compared to WT mice, these changes were not statistically significant since neuroinflammation could appears at the same time as neurodegeneration, masking the changes seen at 6 months of age (Saito et al., 2014; Masuda et al., 2016). These slow and minor changes in retinal thickness, which evolve steadily until 15 months of age, could be produced by the progressive deposit of Aβ plaques (Radde et al., 2006; Ferguson et al., 2013; Nilsson et al., 2014; Masuda et al., 2016; Stevanovic et al., 2017; Shah et al., 2018; Petrache et al., 2019; Schedin-Weiss et al., 2020) and by the mechanisms of inflammation, phagocytosis, and microglial migration between different retinal layers (Lee et al., 2020; Salobrar-García et al., 2020).

While in the APP/PS1 model, at 16 months of age, there was a heavy plaque burden throughout all cortical regions (Ferguson et al., 2013), as well as increased microglial activity (Perez et al., 2009), in the murine model used in our study, this heavy plaque load peaked at 18 months. At the same time, the mice showed alterations in different proteins of the hippocampus and the cortex, which are involved in various neuronal maintenance activities (Schedin-Weiss et al., 2020).

These findings may be linked to the overall increase in total retinal thickness at 17 months of age in the $APP^{NL-F/NL-F}$ group, with significance in the nasal and inferior sectors, the inner and outer sectors, and the RNFL (albeit without statistical significance); these changes were more noticeable in the nasal–superior, nasal–inferior, and temporal–inferior sectors. At this point in our study, where the greatest thickening was observed, we precisely observed that Aβ brain plaques accumulate at an accelerated rate (Koronyo-Hamaoui et al., 2011), which coincides with the findings of our model (Saito et al., 2014; Schedin-Weiss et al., 2020).

In addition, astrocytes are hyperreactive, surrounding the Aβ plaques and releasing proinflammatory factors that induce higher microglial activation (Saito et al., 2014; Busche and Konnerth, 2016; Masuda et al., 2016; Shah et al., 2018). In the APP/PS1model there was an increase in the microglial marker F4/80, inflammatory cytokine MCP-1, and TUNNEL-positive cells in the RGC layer (Ning et al., 2008). In addition, the activated microglia may trigger a neuroinflammatory response (Perez et al., 2009) that could contribute to retinal disorganization, as demonstrated by the functional alterations present in the electroretinogram of the APP/PS1 mouse model (Krasodomska et al., 2010; Ramirez et al., 2017). In $APP^{NL-F/NL-F}$ mice, high levels of $Aβ_{42}$ cause pathological Aβ

deposits in the cerebral cortex and hippocampus, which are accompanied by increased neuroinflammation, with activation of the astrocytes and microglia surrounding the plaques from 6 months of age (Saito et al., 2014; Sasaguri et al., 2017; Schedin-Weiss et al., 2020). In our study, Iba-1+ cells located in the OPL and IPL were larger, with thicker and larger somas and processes than in the WT group (**Supplementary Figures 1D,F**). In addition, in the GCL-NFL the Iba-1+ cells had a more amoeboid appearance with thicker somas and retracted processes (**Supplementary Figures 1D,F**). In the $APP^{NL-F/NL-F}$ group there was an increase in GFAP+ immunostaining with astrocytes accumulating in areas where Iba-1+ cells also clustered (**Supplementary Figures 1E,F**). When the microglia is activated, it undergoes morphological changes and it is transformed into cells with an amoeboid appearance and phagocytic properties, capable of releasing substances that induce an inflammatory response (Rowland and Shneider, 2001). These morphological changes are gradual, ranging from the branched resting state to an intermediate, early activated or "primed" state, and finally reaching the amoeboid phagocytic state (Perry, 2004). In the "primed" state, the microglia increases its vigilance state and shows a thickening of the cell body and its processes. This change in the microglia can occur in response to primary factors derived from neurons or astrocytes. Astrogliosis has also been observed in patients with AD in the GCL (Grimaldi et al., 2018, 2019). All microglial and astroglial cell changes, which may be associated with the neuroinflammatory process, could result in the increased retinal thickness observed in $APP^{NL-F/NL-F}$ group.

Finally, at 20 months of age, which is the latest time point we analyzed, the findings of SD-OCT show significant thinning of the total retina thickness in the inner ring of nasal, inferior and temporal sectors and in the outer rings of superior and temporal sectors, contrary to where the thickening occurred at 17 months, which could be the result of the generalized thinning of the retina. It should be noted that the outer temporal sector, the first sector with a significant change at 6 months, again showed significant thinning being more pronounced than that at earlier time points. The RNFL showed generalized thinning reaching statistical significance in nasal, supero-temporal sectors and mean global value. This situation could be a consequence of the neurodegeneration caused by high levels of Aβ and oligomers, which could be promoting neurotoxicity at this time point (Schedin-Weiss et al., 2020). At the same time, a decrease in retinal ganglion cell density due to apoptosis (Ning et al., 2008; Gupta et al., 2016), a decrease in the axon density of the optic nerve, and a significant thinning of the inner plexiform layer were found in the APP/PS1 model (Gupta et al., 2016).

Notably, in the SD-OCT analysis from 6 to 20 months of age, in the RNFL, the only sector that did not increase in thickness was the superior temporal sector, while that with the most fluctuations was the superio–nasal sector, which correlates with the temporal sectors in total retinal thickness because, again, the sector that exhibited the least thickness variation was the outer temporal sector. These structural changes are consistent with the functional findings of the electroretinogram (ERG), which show dysfunction of the RGCs and cones, as well as a response from bipolar and other interneuronal cells in the inner retina in the APP/PS1 mice (Gupta et al., 2016), which could support the diminished thickness of the retina detected in our $APP^{NL-F/NL-F}$ mice.

It must be considered that this data should be corroborate in future works with molecular biological investigations that confirm the findings in this model.

In summary, the first changes observed at 6 months of age included a significant thinning of the total retinal thickness in the outer temporal sector, and significant thinning of the RNFL in the nasal and inferior–temporal sectors, and mean global value. At the later time points, which correspond to 9 and 12 months of age, there was a slow and progressive evolution toward thickening, with alternation of the thinned sectors, albeit without statistical significance. At 15 months of age, there was a significant thinning of the total retinal thickness in the inner rings of temporal and inferior sectors and in the outer ring of inferior sector. At 17 months of age there were a widespread thickening of the total retina, which was significant in the inferior and nasal sectors of both the inner and outer ring. This thickening could be due to a neuroinflammatory process produced by astrocytes and microglia changes. Finally, at 20 months of age, the SD-OCT showed generalized non-significant thinning of the RNFL and a considerable thinning of the total retinal thickness, with greatest significance in the superior and temporal sectors of both the inner and outer ring.

CONCLUSIONS

In conclusion, this diachronic study of the murine model of $APP^{NL-F/NL-F}$ of AD from 6 to 20 months of age provides significant information on the variations in total retinal thickness and RNFL measured by SD-OCT. In this model, the retinal thickness showed thinning, possibly produced by neurodegeneration alternating with thickening that could be caused by deposits and neuroinflammation in some areas of the retina.

Retinal changes over time, similar to those observed in the human retina could be a biomarker for AD. The $APP^{NL-F/NL-F}$ AD model may help us better understand the different retinal changes during the progression of AD.

DATA AVAILABILITY STATEMENT

The datasets generated for this study can be found in online repositories. The names of the repository/repositories and accession number(s) can be found at: https://figshare.com/s/b3303423bc9cac47ac09.

ETHICS STATEMENT

The animal study was reviewed and approved by Ethics Committee on Animal Welfare of the University Complutense (PROEX No. 047/16).

AUTHOR CONTRIBUTIONS

ES-G, IL-C, RdH, and JR: conceptualization. ES-G, IL-C, LS-P, JF-A, IB-F, VM, TCS, and TS: methodology. ES-G, IL-C, LS-P, and JF-A: investigation. ES-G, IL-C, and LS-P: formal analysis. AR and JS: project administration. AR, JS, MM, TCS, TS, RdH, and JR: funding acquisition. ES-G, IL-C, RdH, and JR: writing—original draft. ES-G, IL-C, AR, TS, JS, MM, RdH, and JR: writing—review and editing. All authors read and approved the final manuscript.

FUNDING

This research was funded by the Ophthalmological Network OFTARED (RD16/0008/0005) of the Institute of Health of Carlos III of the Spanish Ministry of Science and Innovation; and the Research Network RETIBRAIN (RED2018-102499-T) and Grant PID2019-106581RB-I00 of the Spanish Ministry of Science and Innovation; and Leducq Foundation for Cardiovascular Research TNE-19CVD01. IL-C was currently supported by a Predoctoral Fellowship (CT42/18-CT43/18) from the Complutense University of Madrid. JF-A was currently supported by a Predoctoral Fellowship (FPU17/01023) from the Spanish Ministry of Science, Innovation, and Universities.

ACKNOWLEDGMENTS

The authors would like to thank Desireé Contreras for technical assistance and Lucía García del Arco for the English style editing.

SUPPLEMENTARY MATERIAL

The Supplementary Material for this article can be found online at: https://www.frontiersin.org/articles/10.3389/fnagi.2020.625642/full#supplementary-material

REFERENCES

Andrews-Zwilling, Y., Bien-Ly, N., Xu, Q., Li, G., Bernardo, A., Yoon, S. Y., et al. (2010). Apolipoprotein E4 causes age- and Tau-dependent impairment of GABAergic interneurons, leading to learning and memory deficits in mice. *J. Neurosci.* 30, 13707–13717. doi: 10.1523/JNEUROSCI.4040-10.2010

Busche, M. A., Eichhoff, G., Adelsberger, H., Abramowski, D., Wiederhold, K. H., Haass, C., et al. (2008). Clusters of hyperactive neurons near amyloid plaques in a mouse model of Alzheimer's disease. *Science* 321, 1686–1689. doi: 10.1126/science.1162844

Busche, M. A., and Konnerth, A. (2016). Impairments of neural circuit function in Alzheimer's disease. *Philos. Trans. R. Soc. B Biol. Sci.* 371:1700. doi: 10.1098/rstb.2015.0429

Cash, D. M., Ridgway, G. R., Liang, Y., Ryan, N. S., Kinnunen, K. M., Yeatman, T., et al. (2013). The pattern of atrophy in familial alzheimer disease: volumetric MRI results from the DIAN study. *Neurology* 81, 1425–1433. doi: 10.1212/WNL.0b013e3182a841c6

Chiquita, S., Campos, E. J., Castelhano, J., Ribeiro, M., Sereno, J., Moreira, P. I., et al. (2019). Retinal thinning of inner sub-layers is associated with cortical atrophy in a mouse model of Alzheimer's disease: a longitudinal multimodal *in vivo* study. *Alzheimers Res. Ther.* 11:90. doi: 10.1186/s13195-019-0542-8

Dutescu, R. M., Li, Q. X., Crowston, J., Masters, C. L., Baird, P. N., and Culvenor, J. G. (2009). Amyloid precursor protein processing and retinal pathology in mouse models of Alzheimer's disease. *Graefes Arch. Clin. Exp. Ophthalmol.* 247, 1213–1221. doi: 10.1007/s00417-009-1060-3

Duyckaerts, C., Potier, M. C., and Delatour, B. (2008). Alzheimer disease models and human neuropathology: similarities and differences. *Acta Neuropathol.* 115, 5–38. doi: 10.1007/s00401-007-0312-8

Dysli, C., Enzmann, V., Sznitman, R., and Zinkernagel, M. S. (2015). Quantitative analysis of mouse retinal layers using automated segmentation of spectral domain optical coherence tomography images. *Transl. Vis. Sci. Technol.* 4:9. doi: 10.1167/tvst.4.4.9

Ferguson, S. A., Sarkar, S., and Schmued, L. C. (2013). Longitudinal behavioral changes in the APP/PS1 transgenic Alzheimer's disease model. *Behav. Brain Res.* 242, 125–134. doi: 10.1016/j.bbr.2012.12.055

Fogel, H., Frere, S., Segev, O., Bharill, S., Shapira, I., Gazit, N., et al. (2014). APP homodimers transduce an amyloid-β-mediated increase in release probability at excitatory synapses. *Cell Rep.* 7, 1560–1576. doi: 10.1016/j.celrep.2014.04.024

Foidl, B., and Humpel, C. (2020). Can mouse models mimic sporadic Alzheimer's disease? *Neural Regen. Res.* 15, 401–406. doi: 10.4103/1673-5374.266046

Gao, L., Chen, X., Tang, Y., Zhao, J., Li, Q., Fan, X., et al. (2015). Neuroprotective effect of memantine on the retinal ganglion cells of APPswe/PS1δE9 mice and its immunomodulatory mechanisms. *Exp. Eye Res.* 135, 47–58. doi: 10.1016/j.exer.2015.04.013

Garcia-Martin, E. S., Rojas, B., Ramirez, A. I., de Hoz, R., Salazar, J. J., Yubero, R., et al. (2014). Macular thickness as a potential biomarker of mild Alzheimer's disease. *Ophthalmology* 121, 1149–1151. doi: 10.1016/j.ophtha.2013.12.023

Georgevsky, D., Retsas, S., Raoufi, N., Shimoni, O., and Golzan, S. M. (2019). A longitudinal assessment of retinal function and structure in the APP/PS1 transgenic mouse model of Alzheimer's disease. *Transl. Neurodegener.* 8:30. doi: 10.1186/s40035-019-0170-z

Ghiso, J. A., Doudevski, I., Ritch, R., and Rostagno, A. A. (2013). Alzheimer's disease and glaucoma: mechanistic similarities and differences. *J. Glaucoma* 22, S36–S38. doi: 10.1097/IJG.0b013e3182934af6

Grimaldi, A., Brighi, C., Peruzzi, G., Ragozzino, D., Bonanni, V., Limatola, C., et al. (2018). Inflammation, neurodegeneration and protein aggregation in the retina as ocular biomarkers for Alzheimer's disease in the 3xTg-AD mouse model. *Cell Death Dis.* 9:685. doi: 10.1038/s41419-018-0740-5

Grimaldi, A., Pediconi, N., Oieni, F., Pizzarelli, R., Rosito, M., Giubettini, M., et al. (2019). Neuroinflammatory processes, A1 astrocyte activation and protein aggregation in the retina of Alzheimer's disease patients, possible biomarkers for early diagnosis. *Front. Neurosci.* 13:925. doi: 10.3389/fnins.2019.00925

Gupta, V. K., Chitranshi, N., Gupta, V. B., Golzan, M., Dheer, Y., Wall, R. Vander, et al. (2016). Amyloid β accumulation and inner retinal degenerative changes in Alzheimer's disease transgenic mouse. *Neurosci. Lett.* 623, 52–56. doi: 10.1016/j.neulet.2016.04.059

Harper, D. J., Augustin, M., Lichtenegger, A., Gesperger, J., Himmel, T., Muck, M., et al. (2020). Retinal analysis of a mouse model of Alzheimer's disease with multicontrast optical coherence tomography. *Neurophotonics* 7:015006. doi: 10.1117/1.nph.7.1.015006

Iseri, P. K., Altinas, Ö., Tokay, T., and Yüksel, N. (2006). Relationship between cognitive impairment and retinal morphological and visual functional abnormalities in Alzheimer disease. *J. Neuroophthalmol.* 26, 18–24. doi: 10.1097/01.wno.0000204645.56873.26

Jáñez-Escalada, L., Jáñez-García, L., Salobrar-García, E., Santos-Mayo, A., de Hoz, R., Yubero, R., et al. (2019). Spatial analysis of thickness changes in ten retinal layers of Alzheimer's disease patients based on optical coherence tomography. *Sci. Rep.* 9:13000. doi: 10.1038/s41598-019-49353-0

Joly, S., Lamoureux, S., and Pernet, V. (2017). Nonamyloidogenic processing of amyloid beta precursor protein is associated with retinal function improvement in aging male APPswe/PS1ΔE9 mice. *Neurobiol. Aging* 53, 181–191. doi: 10.1016/j.neurobiolaging.2017.02.004

Ko, F., Muthy, Z. A., Gallacher, J., Sudlow, C., Rees, G., Yang, Q., et al. (2018). Association of retinal nerve fiber layer thinning with current and future cognitive decline: a study using optical coherence tomography. *JAMA Neurol.* 75, 1198–1205. doi: 10.1001/jamaneurol.2018.1578

Koronyo-Hamaoui, M., Koronyo, Y., Ljubimov, A. V., Miller, C. A., Ko, M. K. H. K., Black, K. L., et al. (2011). Identification of amyloid plaques in retinas from Alzheimer's patients and noninvasive *in vivo* optical imaging of retinal plaques in a mouse model. *Neuroimage* 54, S204–S217. doi: 10.1016/j.neuroimage.2010.06.020

Krasodomska, K., Lubiński, W., Potemkowski, A., and Honczarenko, K. (2010). Pattern electroretinogram (PERG) and pattern visual evoked potential (PVEP) in the early stages of Alzheimer's disease. *Doc. Ophthalmol.* 121, 111–121. doi: 10.1007/s10633-010-9238-x

Lad, E. M., Mukherjee, D., Stinnett, S. S., Cousins, S. W., Potter, G. G., Burke, J. R., et al. (2018). Evaluation of inner retinal layers as biomarkers in mild cognitive impairment to moderate Alzheimer's disease. *PLoS ONE* 13:e0192646. doi: 10.1371/journal.pone.0192646

Lee, J., Kim, D. E., Griffin, P., Sheehan, P. W., Kim, D. H., Musiek, E. S., et al. (2020). Inhibition of REV-ERBs stimulates microglial amyloid-beta clearance and reduces amyloid plaque deposition in the 5XFAD mouse model of Alzheimer's disease. *Aging Cell* 19:13078. doi: 10.1111/acel.13078

Leinonen, H., Lipponen, A., Gurevicius, K., and Tanila, H. (2016). Normal amplitude of electroretinography and visual evoked potential responses in AβPP/PS1 mice. *J. Alzheimers Dis.* 51, 21–26. doi: 10.3233/JAD-150798

Li, S., Hong, S., Shepardson, N. E., Walsh, D. M., Shankar, G. M., and Selkoe, D. (2009). Soluble oligomers of amyloid β protein facilitate hippocampal long-term depression by disrupting neuronal glutamate uptake. *Neuron* 62, 788–801. doi: 10.1016/j.neuron.2009.05.012

Masuda, A., Kobayashi, Y., Kogo, N., Saito, T., Saido, T. C., and Itohara, S. (2016). Cognitive deficits in single app knock-in mouse models. *Neurobiol. Learn. Mem.* 135, 73–82. doi: 10.1016/j.nlm.2016.07.001

Nilsson, P., Saito, T., and Saido, T. C. (2014). New mouse model of Alzheimer's. *ACS Chem. Neurosci.* 5, 499–502. doi: 10.1021/cn500105p

Ning, A., Cui, J., To, E., Ashe, K. H., and Matsubara, J. (2008). Amyloid-β deposits lead to retinal degeneration in a mouse model of Alzheimer disease. *Investig. Opthalmology Vis. Sci.* 49:5136. doi: 10.1167/iovs.08-1849

Pan, X. D., Zhu, Y. G., Lin, N., Zhang, J., Ye, Q. Y., Huang, H. P., et al. (2011). Microglial phagocytosis induced by fibrillar β-amyloid is attenuated by oligomeric β-amyloid: implications for Alzheimer's disease. *Mol. Neurodegener.* 6:45. doi: 10.1186/1750-1326-6-45

Perez, S. E., Lumayag, S., Kovacs, B., Mufson, E. J., and Xu, S. (2009). β-amyloid deposition and functional impairment in the retina of the APPswe/PS1ΔE9 transgenic mouse model of Alzheimer's disease. *Investig. Opthalmology Vis. Sci.* 50, 793–800. doi: 10.1167/iovs.08-2384

Perry, V. H. (2004). The influence of systemic inflammation on inflammation in the brain: implications for chronic neurodegenerative disease. *Brain. Behav. Immun.* 18, 407–413. doi: 10.1016/j.bbi.2004.01.004

Petrache, A. L., Rajulawalla, A., Shi, A., Wetzel, A., Saito, T., Saido, T. C., et al. (2019). Aberrant excitatory-inhibitory synaptic mechanisms in entorhinal cortex microcircuits during the pathogenesis of Alzheimer's disease. *Cereb. Cortex* 29, 1–17. doi: 10.1093/cercor/bhz016

Polo, V., Rodrigo, M. J., Garcia-Martin, E., Otin, S., Larrosa, J. M., Fuertes, M. I., et al. (2017). Visual dysfunction and its correlation with retinal changes in patients with Alzheimer's disease. *Eye (Lond).* 31, 1034–1041. doi: 10.1038/eye.2017.23

Radde, R., Bolmont, T., Kaeser, S. A., Coomaraswamy, J., Lindau, D., Stoltze, L., et al. (2006). Aβ42-driven cerebral amyloidosis in transgenic mice reveals early and robust pathology. *EMBO Rep.* 7, 940–946. doi: 10.1038/sj.embor.7400784

Ramirez, A. I., de Hoz, R., Salobrar-Garcia, E., Salazar, J. J., Rojas, B., Ajoy, D., et al. (2017). The role of microglia in retinal neurodegeneration: Alzheimer's disease, Parkinson, and glaucoma. *Front. Aging Neurosci.* 9:214. doi: 10.3389/fnagi.2017.00214

Rochat, L., Billieux, J., Juillerat Van der Linden, A. C., Annoni, J. M., Zekry, D., Gold, G., et al. (2013). A multidimensional approach to impulsivity changes in mild Alzheimer's disease and control participants: cognitive correlates. *Cortex* 49, 90–100. doi: 10.1016/j.cortex.2011.08.004

Rowland, L. P., and Shneider, N. A. (2001). Amyotrophic lateral sclerosis. *N. Engl. J. Med.* 344, 1688–1700. doi: 10.1056/NEJM200105313442207

Saito, T., Matsuba, Y., Mihira, N., Takano, J., Nilsson, P., Itohara, S., et al. (2014). Single app knock-in mouse models of Alzheimer's disease. *Nat. Neurosci.* 17, 661–663. doi: 10.1038/nn.3697

Saito, T., and Saido, T. C. (2018). Neuroinflammation in mouse models of Alzheimer's disease. *Clin. Exp. Neuroimmunol.* 9, 211–218. doi: 10.1111/cen3.12475

Sakakibara, Y., Sekiya, M., Saito, T., Saido, T. C., and Iijima, K. M. (2018). Cognitive and emotional alterations in app knock-in mouse models of Aβ amyloidosis. *BMC Neurosci.* 19:46. doi: 10.1186/s12868-018-0446-8

Sakakibara, Y., Sekiya, M., Saito, T., Saido, T. C., and Iijima, K. M. (2019). Amyloid-β plaque formation and reactive gliosis are required for induction of cognitive deficits in app knock-in mouse models of Alzheimer's disease. *BMC Neurosci.* 20:13. doi: 10.1186/s12868-019-0496-6

Salobrar-García, E., de Hoz, R., Ramírez, A. I., López-Cuenca, I., Rojas, P., Vazirani, R., et al. (2019a). Changes in visual function and retinal structure in the progression of Alzheimer's disease. *PLoS ONE* 14:e0220535. doi: 10.1371/journal.pone.0220535

Salobrar-García, E., de Hoz, R., Ramírez, A. I., Salazar, J. J., Rojas, P., López- Cuenca, I., et al. (2019b). "Ocular exploration in the diagnosis and followup of the Alzheimer's dementia," in *Alzheimer's Disease*, ed T. Wisniewski (Brisbane, QLD: Codon Publications), 159–177. doi: 10.15586/alzheimersdisease.2019.ch10

Salobrar-García, E., de Hoz, R., Rojas, B., Ramirez, A. I., Salazar, J. J., Yubero, R., et al. (2015a). Ophthalmologic psychophysical tests support OCT findings in mild Alzheimer's disease. *J. Ophthalmol.* 2015:736949. doi: 10.1155/2015/736949

Salobrar-García, E., Hoyas, I., Leal, M., de Hoz, R., Rojas, B., Ramirez, A. I., et al. (2015b). Analysis of retinal peripapillary segmentation in early Alzheimer's disease patients. *Biomed Res. Int.* 2015, 1–8. doi: 10.1155/2015/636548

Salobrar-García, E., Ramírez, A. I., de Hoz, R., Rojas, P., Salazar, J. J., Rojas, B., et al. (2016). "Chapter 15: The impact of the eye in dementia: the eye and its role in diagnosis and follow-up," in *Update on Dementia*, ed D. Moretti (London: IntechOpen). doi: 10.5772/64490

Salobrar-García, E., Rodrigues-Neves, A. C., Ramírez, A. I., de Hoz, R., Fernández-Albarral, J. A., López-Cuenca, I., et al. (2020). Microglial activation in the retina of a triple-transgenic Alzheimer's disease mouse model (3xTg-AD). *Int. J. Mol. Sci.* 21:816. doi: 10.3390/ijms21030816

Sasaguri, H., Nilsson, P., Hashimoto, S., Nagata, K., Saito, T., De Strooper, B., et al. (2017). APP mouse models for Alzheimer's disease preclinical studies . *EMBO J.* 36, 2473–2487. doi: 10.15252/embj.201797397

Schedin-Weiss, S., Nilsson, P., Sandebring-Matton, A., Axenhus, M., Sekiguchi, M., Saito, T., et al. (2020). Proteomics time-course study of app knock-in mice reveals novel presymptomatic Aβ42-induced pathways to Alzheimer's disease pathology. *J. Alzheimers Dis.* 75, 1–15. doi: 10.3233/jad-200028

Selkoe, D. J. (2001). Alzheimer's disease: genes, proteins, and therapy. *Physiol. Rev.* 81, 741–766. doi: 10.1152/physrev.2001.81.2.741

Shah, D., Latif-Hernandez, A., De Strooper, B., Saito, T., Saido, T., Verhoye, M., et al. (2018). Spatial reversal learning defect coincides with hypersynchronous telencephalic BOLD functional connectivity in APPNL-F/NL-F knock-in mice. *Sci. Rep.* 8:6264. doi: 10.1038/s41598-018-24657-9

Sharma, N., and Singh, A. N. (2016). Exploring biomarkers for Alzheimer's disease. *J. Clin. Diagn. Res.* 10, KE01–KE06. doi: 10.7860/JCDR/2016/18828166

Shi, Z., Cao, X., Hu, J., Jiang, L., Mei, X., Zheng, H., et al. (2020). Retinal nerve fiber layer thickness is associated with hippocampus and lingual gyrus volumes in nondemented older adults. *Prog. Neuropsychopharmacol. Biol. Psychiatry* 99:109824. doi: 10.1016/j.pnpbp.2019.109824

Shimazawa, M., Inokuchi, Y., Okuno, T., Nakajima, Y., Sakaguchi, G., Kato, A., et al. (2008). Reduced retinal function in amyloid precursor protein-over-expressing transgenic mice via attenuating glutamate-N-methyl-d-aspartate receptor signaling. *J. Neurochem.* 107, 279–290. doi: 10.1111/j.1471-4159.2008.05606.x

Song, G., Steelman, Z. A., Finkelstein, S., Yang, Z., Martin, L., Chu, K. K., et al. (2020). Multimodal coherent imaging of retinal biomarkers of Alzheimer's disease in a mouse model. *Sci. Rep.* 10:7912. doi: 10.1038/s41598-020-64827-2

Stevanovic, K., Yunus, A., Joly-Amado, A., Gordon, M., Morgan, D., Gulick, D., et al. (2017). Disruption of normal circadian clock function in a mouse model of tauopathy. *Exp. Neurol.* 294, 58–67. doi: 10.1016/j.expneurol.2017.04.015

Yang, Y., Shiao, C., Hemingway, J. F., Jorstad, N. L., Shalloway, B. R., Chang, R., et al. (2013). Suppressed retinal degeneration in aged wild type and APPswe/PS1ΔE9 mice by bone marrow transplantation. *PLoS ONE* 8:e64246. doi: 10.1371/journal.pone.0064246

Conflict of Interest: The authors declare that the research was conducted in the absence of any commercial or financial relationships that could be construed as a potential conflict of interest.

frontiers in Aging Neuroscience

ORIGINAL RESEARCH
published: 22 January 2021
doi: 10.3389/fnagi.2020.597491

Visual Abnormalities Associate With Hippocampus in Mild Cognitive Impairment and Early Alzheimer's Disease

Aonan Zhao[1†], Fang Fang[2†], Binyin Li[1], Yan Chen[3], Yinghui Qiu[1], Yanli Wu[3], Wei Xu[1] and Yulei Deng[1,4*]*

[1] Department of Neurology, Institute of Neurology, Ruijin Hospital, Shanghai Jiao Tong University School of Medicine, Shanghai, China, [2] Department of Geriatrics, Ruijin Hospital, Shanghai Jiao Tong University School of Medicine, Shanghai, China, [3] Department of Ophthalmology, Ruijin Hospital, Shanghai Jiao Tong University School of Medicine, Shanghai, China, [4] Department of Neurology, Ruijin Hospital, Luwan Branch, Shanghai Jiao Tong University School of Medicine, Shanghai, China

Background and Objective: Alzheimer's disease (AD) has been shown to affect vision in human patients and animal models. This study was conducted to explore ocular abnormalities in the primary visual pathway and their relationship with hippocampal atrophy in patients with AD and mild cognitive impairment (MCI). The aim of this study was to investigate the potential value of ocular examinations as a biomarker during the AD progression.

Methods: Patients with MCI ($n = 23$) or AD ($n = 17$) and age-matched cognitively normal controls (NC; $n = 19$) were enrolled. Pattern visual-evoked potentials (PVEP), flash electroretinogram (FERG) recordings and optical coherence tomography (OCT) were performed for all participants. Hippocampal volumes were measured by 3T magnetic resonance imaging. Cognitive function was assessed by Mini Mental State Examination (MMSE), Montreal Cognitive Assessment (MoCA) and Alzheimer's Disease Assessment Scale-cognitive subscale (ADAS-cog). Pearson correlation was employed to analyze the potential associations between ocular abnormalities and hippocampal volumes. Hierarchical regression models were conducted to determine associations between cognitive performances and ocular abnormalities as well as hippocampal volumes after adjusting for confounding factors including age, sex, cognitive reserve, and APOE4 status.

Results: PVEP amplitude of P100 waveform was significantly decreased in AD patients compared to MCI and normal individuals. In FERG test, delayed latencies of rod response, rod cone response and 3.0 flicker time were found in cognitively impaired groups, indicating dysfunctions of both the rod and cone systems in the disease progression. OCT test revealed reduced macular retinal nerve fiber layer (m-RNFL) thickness in MCI and AD patients, which significantly correlated with brain structure of hippocampus particularly vulnerable during the progression of AD. Interestingly, P100 amplitude showed a significant association with hippocampal volumes even after adjusting confounding factors including age, sex, and cognitive reserve. Hierarchical

OPEN ACCESS

Edited by:
Jiu Chen,
Nanjing Medical University, China

Reviewed by:
Nicole J. Gervais,
University of Toronto, Canada
María Jesús Rodrigo,
Hospital Universitario Miguel Servet, Spain

***Correspondence:**
Wei Xu
xw11246@rjh.com.cn
Yulei Deng
dyl10786@rjh.com.cn

[†]These authors have contributed equally to this work and share first authorship

Received: *21 August 2020*
Accepted: *28 December 2020*
Published: *22 January 2021*

Citation:
Zhao A, Fang F, Li B, Chen Y, Qiu Y, Wu Y, Xu W and Deng Y (2021) Visual Abnormalities Associate With Hippocampus in Mild Cognitive Impairment and Early Alzheimer's Disease. Front. Aging Neurosci. 12:597491. doi: 10.3389/fnagi.2020.597491

regression analysis further demonstrated that m-RNFL thickness, as well as hippocampal volumes, significantly associated with ADAS-cog scores.

Conclusion: P100 amplitude and m-RNFL thickness showed significant correlations with brain structure involved in AD-related neurodegeneration, and therefore proved to be potential indicators of brain imaging pathologies.

Keywords: Alzheimer's disease, mild cognitive impairment, hippocampus, visual abnormalities, P100 amplitude, m-RNFL thickness

INTRODUCTION

Alzheimer's disease (AD) is the most common cause of degenerative dementia in older people (Livingston et al., 2020). The early symptoms begin with short-term memory loss and gradually progress to severe impairment in memory, thinking and behavior (Chan et al., 2013). Mild cognitive impairment (MCI) is defined as an early stage of dementia and more than 50% of MCI patients progress to AD in a period of 4–5 years (Petersen, 2006). Therefore, screening, diagnosis and targeted treatment in this stage to prevent conversion to AD is of great importance. Various studies have attempted to identify and evaluate biomarkers for AD and MCI, including state-of-the-art neuroimaging techniques and biochemical analysis of the cerebrospinal fluid. However, time-consuming, radiation, high cost, and invasiveness have hampered their widespread availability.

In recent years, ocular tests have received substantial attention from the scientific community for ocular structural and functional changes in AD through non-invasive and inexpensive evaluation (Heaton et al., 2015). Lots of evidence indicates that visual disturbance is common for AD patients (Cormack et al., 2000). In some AD patients, visual disturbances present as the initial complaint, such as impairment in visual acuity, spatial contrast sensitivity, color sensitivity, and blurred vision (Croningolomb, 1995; Armstrong, 1996). Quantitative data supports the assessment that in the primary visual pathway including retina and lens amyloid-beta accumulation, retinal nerve fiber layer loss, and visual cortex changes can be valuable for the diagnosis of AD (Goldstein et al., 2003; Ohno-Matsui, 2011; Ikram et al., 2012). Optical coherence tomography (OCT) is a non-invasive imaging technique that captures high-resolution and three-dimensional images of the retina. Previous studies in AD patients demonstrated that the retinal nerve fiber layer (RNFL) thickness was attenuated in comparison to healthy controls (Iseri et al., 2006). In addition, the decrease in parapapillary and macular RNFL thickness, and macular volume were related to the cognitive ability of AD patients (Ikram et al., 2012). Other than structural measures, flash electroretinogram (FERG), and pattern visual evoked potential (PVEP) are classic tests to assess full retinal function and retinal ganglion cells, respectively. Abnormal changes are reported in FERG and PVEP in early AD patients as well (Krasodomska et al., 2010).

In this study, we aim to perform ophthalmological examinations including PVEP, FERG and OCT tests to explore ocular functional and structural changes in patients with AD or MCI and age-matched cognitively normal individuals. Since the hippocampus is well-known to be involved in neurodegenerative processes and atrophy of hippocampus predicts the conversion from MCI to AD (Erten-Lyons et al., 2006), we investigated hippocampal volumes by MRI and attempt to identify the relationship between hippocampal volumes and visual system impairment. Our research's goal was to evaluate the potential availability of the application of non-invasive, cost-effective ophthalmic screening tests for AD.

Abbreviations: AD, Alzheimer's disease; MCI, Mild cognitive impairment; PVEP, Pattern visual-evoked potentials; FERG, Flash electroretinogram; OCT, Optical coherence tomography; MMSE, Mini Mental State Examination; MoCA, Montreal Cognitive Assessment; ADAS-cog, Alzheimer's Disease Assessment Scale-cognitive subscale; m-RNFL, Macular retinal nerve fiber layer; SDS, Self-rating depression scale; SAS, Self-rating anxiety scale; MRI, Magnetic resonance imaging.

MATERIALS AND METHODS

Patients Enrolment

Participants ($N = 59$) in this study were enrolled at the neurology clinic of Ruijin Hospital affiliated to the Shanghai Jiao Tong University School of Medicine, Shanghai, China, from September 2016 to December 2020. All volunteers gave their informed, written consent prior to study participation. This study was approved by the Research Ethics Committee of Ruijin Hospital. All patients with AD dementia were diagnosed as probable AD dementia following the National Institute on Aging and Alzheimer's Association (NIA-AA) diagnostic guidelines for probable AD dementia with support of structural MRI images (McKhann et al., 2011). To ensure volunteers understood the task, only patients with mild to moderate AD dementia [24 $\geq$ Mini Mental State Examination (MMSE) $\geq$ 10] participated on the tests. MCI with deficits in memory function were diagnosed according to the Mayo Clinic criteria (Petersen, 2004). The criteria include subjective memory complaint corroborated by an informant together with preserved everyday activities, a memory impairment based on a standard neuropsychological test, preserved global cognitive functions and finally the exclusion of dementia. Age- and education-adjusted scores falling 1.5 standard deviations below that expected for age and education level may indicate MCI but these are considered as guidelines rather than diagnostic cut-offs. The cognitively normal participants were age-, sex-, and education-matched and were recruited from the local community in Shanghai. Inclusion criteria for normal controls required a MMSE score $\geq$ 28 without any memory-related complaint. Participants with the presence

of dementia or other neurological diseases such as Parkinson's disease were excluded. Besides, individuals were excluded if they have any of the following medical problems: acute diabetic complications, history of acute cerebrovascular accident, history of acute cardiovascular accident, systemic disorders such as malignancy and lupus which were not cured, severe infection, drug abuse or dependency condition and severe psychiatric disorders which were not cured. Individuals with any ocular disease, high refractive error, systemic disease affecting vision or history of ophthalmic surgery were excluded.

Neuropsychological Assessment

Each participant received a detailed neuropsychological assessment by a memory-related specialist. Additionally, patients with vascular dementia, mental disorders, other neurological diseases, and history of alcohol or drug abuse were also excluded. Specialists assessed cognitive ability in all participants utilizing Mini-Mental State Examination (MMSE, developed by Zhang et al., 1990), Montreal Cognitive Assessment (MoCA) Beijing version, Self-rating depression scale (SDS), Self-rating anxiety scale (SAS), and the 12-item Chinese version of Alzheimer's Disease Assessment Scale-cognitive subscale (ADAS-cog). The cut point established for the MMSE that defines "Alzheimer's disease" was set at 24 (Lopez et al., 2005). We used MoCA cut-off scores of $\leq$24 points for MCI and $\leq$22 points for dementia and for individual within 6 years or fewer of formal education, one point was added to the score as a correction (Goldstein et al., 2014). The clinical cut-off raw scores for SAS and SDS were set at 36 and 40, respectively (Dunstan and Scott, 2018). The optimal cut-off score for ADAS-Cog 12-item scale to discriminate between MCI and mild AD was $\geq$21 (Zainal et al., 2016).

Optical Coherence Tomography

All participants underwent the OCT examination using the STRATUS OCT Model 3000 (Carl Zeiss Meditec, Inc., Dublin, California, USA). The retinal mapping software was used to calculate the average retinal thickness of the central ring. All eyes were scanned in a radial-spoked pattern centered on the foveola with the scan length of 6 mm. The mean and standard deviations of the macular RNFL (m-RNFL) were calculated in superior, inferior hemiretina. These measurements were performed out to one disc diameter inferiorly and superiorly to the fovea. Optic disc head scans were recorded with optimized z-offset and polarization. The Fast Optic Disc Scan Protocol (OCT-DISC) was used. The software determined automatically the disc margin setting a point at the edge of the retinal pigment epithelium (RPE)/choriocapillaris layer on each side of the disc along a cross-section. The operator was permanently monitoring for steady eye fixation, correct scan position, and good signal-to-noise ratio. Scans were repeated until an image of satisfying quality was obtained.

Pattern Visual Evoked Potential

All the PVEP examinations (UTAS-E3000, LKC Technologies Inc., Gaithersburg, USA) were performed in an electrically shielded room. Cup-shaped electrodes of Ag/AgCl were placed according to the International 10/20 system (Odom et al., 2004) at the following positions: active electrode in Oz, reference electrode in Fz, ground electrode on earlobes. The recordings were performed in a quiet and dimmed room. The electrical potentials of the occipital cortex were recorded while the participant was looking at the fixation point in the middle of the moving checkboard patterns on the screen one meter in front. The luminance of the white areas was 80 cd m^{-2}, and the contrast between the checks was 100%. The checkerboard pattern reversed at the rate of 2 Hz and the viewing distance was 100 cm, the check edges subtended at 15′of visual angle. The signals were fed into an amplifier with the low frequency cut-off filter set at 1.0 Hz and the high frequency cut-off filter set at 100 Hz. The amplified responses were fed to a signal-averaging computer, and 100 responses were averaged with an analysis time of 500 ms. The impedance was kept below 5 kOhm. An alternant checkboard pattern was used as a stimulating pattern and the check size was 23 min. There are three separate phases in the VEP waveform: an initial negative deflection (N75), a prominent positive deflection (P100), and a later negative deflection (N135). The peak latency and peak to peak amplitudes of these waves are measured (Mishra and Kalita, 2004). N75 reflects the activity of fovea and primary visual cortex. P100 originates from dorsal and ventral extrastriate cortex and represents the processing of stimulus characteristics and visuospatial selection (Di Russo et al., 2005; Hamilton et al., 2020). The latency and amplitude of N75 and P100 were calculated in this study.

Flash Electroretinogram

All participants underwent the FERG examinations using LKC UTAS-E 3000 system (LKC Technologies, Inc., Gaithersburg, USA). The white flash illumination was provided by Ganzfeld 2503D stimulator (LKC Technologies, Inc., Gaithersburg, MD, USA). The software LKC EM for Windows (EMwin v3.0; LKC Technologies, Inc., Gaithersburg, MD, USA) was used to control the recording setting and analyze the data. Signal amplification, luminance calibration, and bandpass filtering were integrated into the LKC system. Standard Ganzfeld scotopic (dark-adapted) and photopic (light- adapted) ERGs were obtained by specialists after pupillary dilation. Subjects took 10 min of light adaptation before recording light-adapted ERGs and were dark adapted for at least 30 min before dark-adapted ERGs were obtained. Topical anesthesia was used for contact lens electrodes. Electroretinographic waveforms were simultaneously obtained from each eye by positioning the active electrodes (ERG-jet monopolar contact lens electrodes; UniversoPlastique SA, Le Cret-Du-Locle, Switzerland) on each cornea. The reference and ground electrodes (Grass subdermal needle electrode; Astro-Med, Inc., West Warwick, RI) were placed subcutaneously in the pinna.

Three ERG recordings were obtained per stimulus intensity. The scotopic and photopic white flash stimuli were performed with an intrastimulus interval of 1 min. The intrastimulus background recovery interval allowed the retina to recover from the previous flash. Photopic tests included: a 100 Td-s ($\sim$4 cd-s/m2 [assuming a 6 mm pupil diameter]) flash stimulus presented at a 1 Hz repetition rate with no background luminance (P1); a 58 Td-s ($\sim$2 cd-s/m2 [assuming a 6 mm pupil diameter]) red

stimulus presented at 3.4 Hz, with a 380 Td blue background (P2); a 100 Td-s (∼4 cd-s/m2 [assuming a 6 mm pupil diameter]) flash stimulus presented at a 2 Hz repetition rate with a 340 Td background (P3); and an 85 Td-s (∼3 cd-s/m2 [assuming a 6 mm pupil diameter]) flickering (at 28.3 Hz) stimulus (PF). For scotopic tests, stimulus intensity increased by a factor of 10 for each trial, beginning with a 2.8 Td-s (∼0.10 cd-s/m2 [assuming a 6 mm pupil diameter]) flash stimulus presented at 0.25 Hz (S1), then a 28 Td-s (∼1 cd-s/m2 [assuming a 6 mm pupil diameter]) flash stimulus presented at 0.1 Hz (S2), and finally, a 280 Td-s (∼10 cd-s/m2 [assuming a 6 mm pupil diameter]) flash stimulus presented at 0.05 Hz (S3). Flicker ERG was obtained under the same conditions of light adaptation as the light-adapted ERG. And flashes were presented at a rate of ∼30 stimuli per second.

Magnetic Resonance Imaging

MRI Scans were performed on a 3.0T EXCITE HD MR imaging system (Echo-speed plus, General Electric, Milwaukee, WI, USA) with an 8NVHEAD-A coil using a three- dimensional, spoiled gradient recalled echo 3D-SPGR-T1 weighted sequence using the following parameters: repetition time (TR) = 7.7 ms; echo time = 1.6 ms; flip angle = 15′; number of excitations = 1; section thickness = 0.5 mm; field of view = 240 × 240 mm; and matrix size = 256 × 256 mm. The voxel size was 1 × 1 × 1 mm. The voxel-based morphometry was used to analyze the hippocampal volume, with the Biological Parametric Mapping (WFU PickAtlas Tool, http://fmri.wfubmc.edu/) and the MATLAB platform (version 7.0, Mathworks Inc. Sherbom, MA, USA) was used to calculate the hippocampal structure volume.

Statistical Analysis

Both eyes for each subject were examined and the average of these measurements was taken for the both eyes. Hippocampal volumes of both sides were obtained and the mean value of both sides was included in the analysis. Statistical analysis was performed using SPSS Version 26.0 (SPSS Inc., Chicago, IL, USA) and $P < 0.05$ was considered significant. One-way ANOVAs were used to compare group differences in demographic and clinical variables between the three groups (AD, MCI, and cognitively normal control). We used chi-squared and split chi-squared tests to identify differences in sex and APOE 4 carrier status between the three groups. The Pearson correlation was used to determine the associations between hippocampal volume and ocular indexes, while the partial correlation coefficient (r) and associated probability (P) were calculated using partial correlation analysis after adjusting for confounding factors, such as age, sex, and years of education. We performed a Bonferroni correction by dividing the critical P-value by the number of comparisons being made. For multiple comparisons of demographic characteristics, ocular measurements and hippocampus volumes among AD, MCI, and cognitively normal group, the adjusted P-value required for significance is $0.05/3 = 0.017$. For correlation analysis, P-value is adjusted at $0.05/5 = 0.01$. We conducted hierarchical multiple stepwise linear regression analysis to evaluate the possible factors affecting the scores of ADAS-cog, MMSE and MoCA, including age, sex, years of education, APOE 4 carrier status, ophthalmologic measurements and hippocampal volumes. For each model, the regression coefficients (β), R-squared (R^2), change of R^2 (ΔR^2), and change of F (ΔF) were calculated, respectively.

TABLE 1 | Demographic characteristics of all participants.

Demographics	NC	MCI	AD	*P*-value
N	19	23	17	–
Age, y, (SD)	66.63 (6.17)	68.43 (5.70)	70.24 (7.53)	0.251
Sex M/F	8/11	12/11	9/8	0.756
Education, y, (SD)	10.74 (3.00)	12.78 (3.48)	10.47 (3.47)	0.057
ApoE4 carrier (%)	15.8%	30.4%	41.2%	0.238
MMSE (SD)	28.79 (1.03)	26.91 (1.47)[#]	21.18 (3.09)[*§]	<0.001
MoCA (SD)	24.89 (2.13)	20.57 (2.21)[#]	15.65 (2.81)[*§]	<0.001
ADAS-cog (SD)	14.21 (4.57)	18.00 (3.22)[#]	31.88 (4.31)[*§]	<0.001
SAS (SD)	28.26 (5.11)	27.26 (4.87)	27.64 (4.78)	0.789
SDS (SD)	27.47 (6.44)	29.96 (6.15)	29.76 (6.10)	0.389

AD, Alzheimer's disease; MCI, mild cognitive impairment; NC, normal control; M, male; F, female; y, years; SD, standard deviation; MMSE, Mini-Mental State Examination; MoCA, Montreal Cognitive Assessment; ADAS-cog, Alzheimer's Disease Assessment Scale-cognitive subscale; SAS, Self-rating anxiety scale; SDS, Self-rating depression scale.
[#]*MCI vs. NC, P < 0.017.*
[*]*AD vs. MCI, P < 0.017.*
[§]*AD vs. NC, P < 0.017.*

RESULTS

In this research, 19 cognitively normal controls, 23 MCI patients and 17 AD patients were included. There was no significant difference in age, sex, years of education and *APOE* 4 carrier status among three groups. MMSE, MoCA and ADAS-cog were performed to assess cognitive function for all participants, and the scores of which revealed significantly typical trends among groups as expected ($P < 0.001$). Detailed demographic characteristics of each group are shown in **Table 1**.

Results of ocular measurements are listed in **Table 2**. Of the PVEP waveform components recognized, AD patients showed a decrease in the P100 amplitudes when compared to MCI group ($P = 0.016$), while comparison of the N75 wave revealed no statistically significant differences for the amplitudes or the latencies. In the FERG tests, eyes of AD patients had significantly prolonged rod response latency time when observed in the dark-adapted environment in comparison with age-matched cognitively normal controls ($P = 0.013$). As light stimulus in darkness was intensified to activate the cone system and mixed responses from both rod and cone systems were recorded, delayed rod cone response latency time was found in both MCI ($P = 0.003$) and AD ($P = 0.003$) patients compared to normal controls. In the light environment, where responses from the cone system were recorded, AD patients showed longer reaction time reflected as increased 3.0 flicker latencies when compared to MCI patients ($P = 0.013$) and healthy participants ($P = 0.008$). However, no statistically significant group difference was found in amplitudes of all responses. In addition, structural changes were examined by OCT tests. Remarkably reduced thickness of m-RNFL was observed in AD eyes than that in MCI eyes

TABLE 2 | PVEP, FERG, OCT results, and Hippocampal volumes for all participants.

Variable	NC	MCI	AD	*P*-value	*F*-value	Total *df*	Effect size (η_p^2)
N75 latency(ms), (SD)	63.84 (13.49)	63.76 (17.70)	62.15 (16.30)	0.938	0.064	58	0.003
N75 amplitude(μV), (SD)	2.41 (0.62)	2.32 (0.85)	2.48 (0.87)	0.808	0.214	58	0.027
P100 latency(ms), (SD)	99.89 (8.31)	104.33 (10.69)	104.65 (14.54)	0.354	1.058	58	0.054
P100 amplitude(μV), (SD)	6.23 (2.71)	6.92 (3.48)	4.61 (2.17)*	0.050	3.159	58	0.099
Rod response latency(ms), (SD)	49.93 (6.63)	51.55 (11.45)	59.47 (9.76)§	0.010	5.028	58	0.149
Rod response amplitude(μV), (SD)	90.69 (9.47)	88.95 (11.17)	92.68 (10.33)	0.537	0.629	58	0.025
Rod cone response latency(ms), (SD)	41.36 (7.21)	50.50 (10.52)#	50.82 (10.65)§	0.002	6.859	58	0.237
Rod cone response amplitude(μV), (SD)	110.63 (36.95)	130.14 (42.17)	108.97 (26.95)	0.125	2.157	58	0.048
Cone response latency(ms), (SD)	16.85 (2.12)	15.70 (2.58)	16.43 (2.97)	0.345	1.084	58	0.029
Cone response amplitude(μV), (SD)	93.47 (16.24)	90.50 (20.53)	91.84 (16.91)	0.871	0.138	58	0.008
3.0 flicker latency(ms), (SD)	25.85 (4.11)	26.31 (5.90)	30.63 (5.72)*§	0.015	4.554	58	0.121
3.0 flicker amplitude(μV), (SD)	75.09 (13.58)	68.96 (20.96)	73.73 (15.00)	0.482	0.740	58	0.018
m-RNFL thickness(μm), (SD)	96.76 (7.30)	88.65 (9.81)#	80.46 (8.37)*§	<0.001	15.94	58	0.393
Rim area(mm^2), (SD)	1.36 (0.14)	1.44 (0.32)	1.50 (0.24)	0.255	1.40	58	0.044
Disc area(mm^2), (SD)	2.08 (0.25)	1.98 (0.33)	2.09 (0.32)	0.441	0.831	58	0.055
Cup volume(mm^3), (SD)	0.30 (0.04)	0.28 (0.08)	0.30 (0.07)	0.476	0.752	58	0.020
Hippo volume(cm^3), (SD)	2.53 (0.45)	1.84 (0.30)#	1.33 (0.37)*§	<0.001	46.91	58	0.636

PVEP, pattern visual evoked potential; FERG, flash electroretinogram; OCT, optical coherence tomography; AD, Alzheimer's disease; MCI, mild cognitive impairment; NC, normal control; SD, standard deviation; m-RNFL, macular retinal nerve fiber layer; Hippo, hippocampus.

#*MCI vs. NC, P < 0.017.*

**AD vs. MCI, P < 0.017.*

§*AD vs. NC, P < 0.017.*

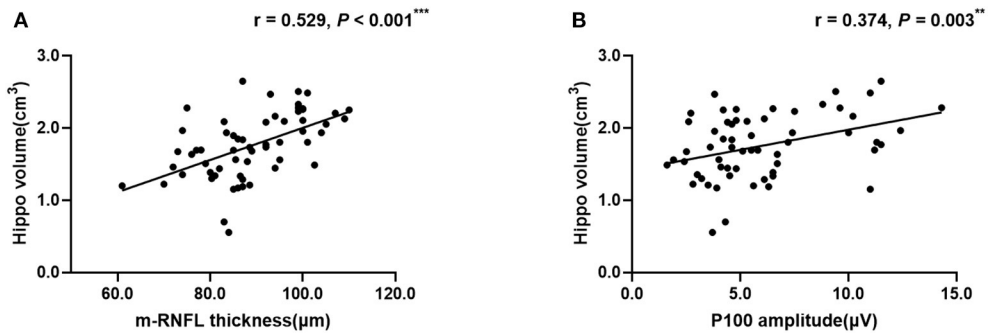

FIGURE 1 | Correlation analysis between hippocampal volume and m-RNFL thickness **(A)** or P100 amplitude **(B)**. The parameter was estimated using Pearson's correlation coefficients. Hippo, hippocampus; m-RNFL, macular retinal nerve fiber layer. ***$P < 0.001$, **$P < 0.01$.

($P = 0.014$) and NC eyes ($P < 0.001$). MCI patients showed significantly thinner m-RNFL compared to normal individuals ($P = 0.011$) as well. However, no significant morphological changes in the optic disc head were found for the rim area, disc area, and cup volume.

Regarding hippocampal volumes investigated by MRI, as shown in **Table 2**, significantly decreased size of hippocampus was found in patients with AD when compared to MCI group ($P < 0.001$) and healthy individuals ($P < 0.001$). A comparison of the MCI group with the NC group showed obviously shrunken structure of hippocampus as well ($P < 0.001$). Then we performed Pearson correlation analysis to explore associations between hippocampal volumes and ocular abnormalities as described in PVEP, FERG, and OCT examinations, respectively. As shown in **Figure 1**, m-RNFL thickness ($r = 0.529$, $P < 0.001$, **Figure 1A**) and P100 amplitude ($r = 0.374$, $P = 0.003$, **Figure 1B**) significantly correlated with hippocampal volumes. With adjustments made for the confounding factors of age, sex, years of education and *APOE* 4 carrier status, as shown in **Table 3**, associations remained significant between the volumes of hippocampus and m-RNFL thickness ($r = 0.521$, $P < 0.001$) as well as P100 amplitude ($r = 0.389$, $P = 0.003$). We did not find any significant associations between rod response latency, rod cone response latency, 3.0 flicker latency and the brain structure of hippocampus.

A hierarchical regression analysis was further conducted to determine the associations between ocular indexes, hippocampal volumes and cognitive function. After controlling for age, sex,

TABLE 3 | Partial correlation analysis between visual indexes and hippocampal volume.

Variable	*r*-value	*P*-value
m-RNFL thickness	0.521	<0.001*
P100 amplitude	0.389	0.003*
Rod response latency	−0.183	0.178
Rod cone response latency	0.078	0.570
3.0 flicker latency	−0.065	0.634

m-RNFL, macular retinal nerve fiber layer.
The partial correlation coefficient of the correlation analysis was corrected with confounding factors including age, gender, and years of education.
**P < 0.01.*

TABLE 4 | Hierarchical regression analysis for ADAS-cog score in all participants.

Variable	Regression 1	Regression 2	Regression 3
Age	0.141	0.032	−0.061
Gender	−0.068	−0.147	−0.111
Years of education	−0.205	−0.219	−0.167
ApoE4 status	0.146	0.090	0.083
Hippo volume		−0.667***	−0.490***
m-RNFL thickness			−0.242*
P100 amplitude			−0.028
Rod response latency			0.204
Rod cone response latency			0.044
3.0 flicker latency			0.173
R^2	0.107	0.528	0.635
ΔR^2	0.107	0.421	0.106
ΔF	1.625	47.262***	2.794*

ADAS-cog, Alzheimer's Disease Assessment Scale-cognitive subscale; Hippo, hippocampus; m-RNFL, macular retinal nerve fiber layer.
****P < 0.001, *P < 0.05.*

TABLE 5 | Hierarchical regression analysis for MMSE score in all participants.

Variable	Regression 1	Regression 2	Regression 3
Age	−0.006	0.095	0.219
Gender	−0.113	−0.040	−0.054
Years of education	0.218	0.230	0.159
ApoE4 status	−0.188	−0.136	−0.139
Hippo volume		0.617***	0.527***
m-RNFL thickness			0.134
P100 amplitude			−0.004
Rod response latency			−0.177
Rod cone response latency			−0.128
3.0 flicker latency			−0.022
R^2	0.076	0.437	0.491
ΔR^2	0.076	0.361	0.054
ΔF	1.115	33.942***	1.024

MMSE, Mini-Mental State Examination; Hippo, hippocampus; m-RNFL, macular retinal nerve fiber layer.
****P < 0.001.*

TABLE 6 | Hierarchical regression analysis for MoCA score in all participants.

Variable	Regression 1	Regression 2	Regression 3
Age	−0.041	0.068	0.068
Gender	−0.078	0.001	−0.075
Years of education	0.007	0.021	0.046
ApoE4 status	−0.191	−0.135	−0.108
Hippo volume		0.664***	0.664***
m-RNFL thickness			0.085
P100 amplitude			−0.170
Rod response latency			−0.050
Rod cone response latency			0.025
3.0 flicker latency			−0.123
R^2	0.042	0.460	0.506
ΔR^2	0.042	0.417	0.047
ΔF	0.597	40.957***	0.905

MoCA, Montreal Cognitive Assessment; Hippo, hippocampus; m-RNFL, macular retinal nerve fiber layer.
****P < 0.001.*

years of education and *APOE* 4 carrier status, hippocampal volumes ($\beta = -0.490$, $P < 0.001$) and m-RNFL thickness ($\beta = -0.242$, $P = 0.031$) were significantly associated with ADAS-cog scores (**Table 4**). Regarding scores of MMSE (**Table 5**) and MoCA (**Table 6**), however, just the parameter of hippocampal volumes demonstrated strongly positive associations ($\beta = 0.527$, $P < 0.001$; $\beta = 0.664$, $P < 0.001$; respectively), while parameters of ocular indexes revealed no significant association ($P > 0.05$).

DISCUSSION

This study performed ophthalmic measurements including PVEP, FERG and OCT tests to investigate functional and structural changes of retina and/or visual pathway in MCI and AD patients compared to cognitively normal aging. Our results demonstrated that PVEP amplitude of P100 waveform was significantly decreased in AD patients compared to MCI and normal individuals. In FERG test, delayed latencies of rod response, rod cone response and 3.0 flicker time were found in cognitively impaired groups, indicating dysfunctions of both the rod, and cone systems in the disease progression. OCT test revealed reduced m-RNFL thickness in MCI and AD patients, which significantly correlated with brain structure of hippocampus particularly vulnerable during the progression of AD. Strikingly, P100 amplitude showed significant association with hippocampal volumes even after adjusting confounding factors including age, sex, and years of education. Hierarchical regression analysis further demonstrated that m-RNFL thickness, as well as hippocampal volumes, had significant predictive value in assessing cognitive performance in terms of neuropsychological test of ADAS-cog.

PVEPs are used to evaluate the functional integrity of the visual pathway. P100, typically peaking at about 100 ms, is the major component of the PVEPs. It is considered to generate from dorsal and ventral extrastriate cortex and represent the

processing of stimulus characteristics and visuospatial selection (Di Russo et al., 2005). Extrastriate cortex belongs to part of visual association areas and shows significant microscopic pathology with beta-amyloid (Aβ) aggregates and neurofibrillary tangles in the post-mortem investigation of AD patients (Arnold et al., 1991). High synaptic complexity of the association cortices may enable and amplify the propagation of disease pathology (Mckee et al., 2006). In line with previous reports (Krasodomska et al., 2010; Stothart et al., 2015), we propose that reduced P100 amplitude in AD patients may reflect this pathology in visual association areas and prove a sensitive marker in examining cortical pathology in AD progression beyond currently available behavioral, imaging and biochemical tools. Interestingly, partial correlation analysis revealed that decreased P100 amplitude significantly positively correlated with atrophied volume of hippocampus. Recent findings suggest that hippocampus participates in visuospatial memory formation. Dysfunction of synaptic plasticity in the visual cortex may influence visuospatial information process and thus in turn hippocampal formation (Tsanov and Manahan-Vaughan, 2008). Close relationship between P100 amplitude and hippocampal volumes may strengthen the potential value of PVEP waveform of P100 in early screening and monitoring the disease progression.

FERG provides an objective measure of cellular function in retina. The cellular responses recorded can be specific to rod photoreceptors under dark-adapted conditions or cone photoreceptors in light-adapted environment. In our study, prolonged latencies of rod response and 3.0 flicker time were found in AD patients when compared to MCI group and/or normal aging, while delayed rod cone response latency was observed in both MCI and AD patients compared to healthy controls, indicative of being a potential marker in early stage of cognitive decline. In an animal study of mice carrying *APOE4*, the most prevalent genetic risk factor for AD, ERG recordings revealed significant attenuation of mixed rod cone responses in dark-adapted eyes, which is considered to be related to observed decrease in synaptic density of the retinal synaptic layers (Ran et al., 2013). However, our following correlation analysis demonstrated no significant association between FERG components and hippocampal volumes. In view of recent reports of FERG alterations in other neurodegenerative diseases (Devos et al., 2005; Pearl et al., 2017), more comprehensive longitudinal studies are needed to improve its specificity in clinical practice.

Retina has been viewed as an extension of central nervous system due to their developmental and structural similarities. Histopathological studies reported typical Aβ deposits, loss of retinal ganglion cells and optic nerve degeneration in AD patients, hence initiating in the retrograde damaged ganglion cell fibers and leading to the morphological changes, such as RNFL thinning (Blanks et al., 1996a,b). Consistent with recent evidence (den Haan et al., 2017b; Chan et al., 2018), we have found significantly reduced overall thickness of m-RNFL in AD and MCI patients compared to age-matched control counterparts in the current research. In addition, our results demonstrated a significant correlation between total m-RNFL thickness and hippocampal volumes, corroborating the link between retina and brain in the progression of cognitive impairment. Several studies have investigated the connections between retinal changes and MRI volumetric measurements of brain structures. In early-onset AD patients, den Haan et al. (2017a) found total macular thickness correlated with parietal cortical atrophy, suggestive of reflection of cerebral cortical changes in the retina, independent of AD pathological markers, such as amyloid. In non-demented older adults, thinner overall RNFL and peripapillary RNFL showed good associations with smaller volumes of medial temporal lobes and hippocampus, while no significant associations were found in the control regions, which were located outside the visual pathway and the regions involved in AD (Méndez-Gómez et al., 2018; Shi et al., 2020). In a recent study involving AD and MCI patients, better correlation was observed between inner perifovea retinal thickness and the hippocampal and entorhinal cortical volumes, which are specifically affected in the early stage of AD, although no correlation was found between m-RNFL thickness and cognitive performance, and no significant difference of m-RNFL thinning was shown in patients with MCI compared to those with AD (Tao et al., 2019). In our study, m-RNFL thickness exhibited a significant reduction in MCI patients in comparison to AD patients and presented as an independent predictor of ADAS-cog score, along with average hippocampal volumes, in the hierarchical regression model. The discrepancies may result from high degree of variability in the study inclusion/exclusion criteria, assessment of neuropsychological performance and the rigor of adjustment of confounding factors. However, our results have added more evidence for the availability of application of m-RNFL thickness as a promising biomarker for future AD diagnosis, monitoring, and prognosis.

In the current cross-sectional study we have enrolled relatively small sample size, partially due to strict exclusion criteria of patient enrollment and adaptability to full screen of ocular structural and functional measurements. A longitudinal study with expanded sample size is required to validate the retina-brain association in the neurodegenerative process of cognitive decline. Owing to the lack of Aβ or Tau-related markers, we were unable to analyze the relationship between those pathological markers and ocular measurements, and hence the present findings cannot directly confirm whether the alterations in the ophthalmological examinations are specific to AD. Additionally, quandrant-specific changes of peripapillary RNFL thickness have been reported in recent studies, although results remained controversial (Alber et al., 2020). Evidence from numerous neuropsychological and functional neuroimaging studies suggested that right posterior hippocampus is implicated in visual information and visuospatial memory formation. Changes in the volume of the anterior and posterior hippocampus can be compensated and therefore underestimate the alteration of the hippocampus most involved in vision (Hüfner et al., 2011). Braak's staging of AD showed that neurodegeneration began in entorhinal and perirhinal cortex suggesting the area most and earliest affected by neurofibrillary tangles in Alzheimer's disease, even before the hippocampus (Braak and Braak, 1995). Further detailed studies with investigations of

changes of different segmentation of RNFL thickness and more brain regions including entorhinal cortex, perirhinal cortex and subareas of hippocampus are needed to assist in clarification of possible mechanisms underlying retina-brain association in the disease progression of cognitive decline and AD.

In conclusion, our results presented significant alterations in ophthalmological examinations including PVEP, FERG responses and m-RNFL thickness in patients with MCI and AD. P100 amplitude and m-RNFL thickness showed significant correlations with brain structure involved in AD-related neurodegeneration, and therefore proved to be potential indicators of brain imaging pathologies. Future prospective researches are required to determine the reliability of ocular investigations, especially measurement of RNFL thickness during AD progression and recognize whether retina has broad implications in AD pathology to serve as a promising non-invasive and cost-effective biomarker.

DATA AVAILABILITY STATEMENT

The raw data supporting the conclusions of this article will be made available by the authors, without undue reservation.

ETHICS STATEMENT

The studies involving human participants were reviewed and approved by Ruijin Hospital Ethics Committee, Shanghai Jiao Tong University School of Medicine. The patients/participants provided their written informed consent to participate in this study.

AUTHOR CONTRIBUTIONS

YD and WX designed the study, edited the manuscript, and validated the statistics. AZ and FF collected the data, wrote and edited the manuscript, and performed the statistics. YC and YW collected the data and help revised the manuscript. BL and YQ collected the data. All authors contributed to the article and approved the submitted version.

FUNDING

This study was supported by grants from the National Natural Science Foundation of China (No. 81571029) and the Natural Science Foundation of Shanghai (No. 19ZR1432500) to YD; the Shanghai Municipal Commission of Health and Family Planning (No. 201640042) to WX; the National Natural Science Foundation of China (No. 81801261) to FF.

REFERENCES

Alber, J., Goldfarb, D., Thompson, L. I., Arthur, E., Hernandez, K., Cheng, D., et al. (2020). Developing retinal biomarkers for the earliest stages of Alzheimer's disease: what we know, what we don't, and how to move forward. *Alzheimers Dement.* 16, 229–243. doi: 10.1002/alz.12006

Armstrong, R. A. (1996). Visual field defects in alzheimer's disease patients may reflect differential pathology in the primary visual cortex. *Optom Vis Sci.* 73:677–682. doi: 10.1097/00006324-199611000-00001

Arnold, S. E., Hyman, B. T., Flory, J., Damasio, A. R., and Hoesen, G. W. V. (1991). The topographical and neuroanatomical distribution of neurofibrillary tangles and neuritic plaques in the cerebral cortex of patients with Alzheimer's disease. *Cereb. Cortex* 1, 103–116. doi: 10.1093/cercor/1.1.103

Blanks, J. C., Schmidt, S. Y., Torigoe, Y., Porrello, K. V., Hinton, D. R., and Blanks, R. H. (1996a). Retinal pathology in Alzheimer's disease. II. Regional neuron loss and glial changes in GCL. *Neurobiol. Aging* 17, 385–395. doi: 10.1016/0197-4580(96)00009-7

Blanks, J. C., Torigoe, Y., Hinton, D. R., and Blanks, R. H. (1996b). Retinal pathology in Alzheimer's disease. I. Ganglion cell loss in foveal/parafoveal retina. *Neurobiol. Aging* 17, 377–384. doi: 10.1016/0197-4580(96)00010-3

Braak, H., and Braak, E. (1995). Staging of Alzheimer's disease-related neurofibrillary changes. *Neurobiol. Aging* 16, 271–278; discussion 278–84. doi: 10.1016/0197-4580(95)00021-6

Chan, K. Y., Campbell, H., Wang, W., Rudan, I., Wang, W., Wu, J. J., et al. (2013). Epidemiology of Alzheimer's disease and other forms of dementia in China, 1990-2010:a systematic review and analysis. *Lancet* 381, 2016–2023. doi: 10.1016/S0140-6736(13)60221-4

Chan, V. T. T., Sun, Z., Tang, S., Chen, L. J., Wong, A., Tham, C. C., et al. (2018). Spectraldomain OCT measurements in Alzheimer's disease: a systematic review and meta analysis. *Ophthalmology* 126, 497–510. doi: 10.1016/j.ophtha.2018.08.009

Cormack, F. K., Tovee, M., and Ballard, C. (2000). Contrast sensitivity and visual acuity in patients with Alzheimer's disease. *Int. J. Geriatr. Psychiatry* 15, 614–620. doi: 10.1002/1099-1166(200007)15:7<614::AID-GPS153>3.0.CO;2-0

Croningolomb, A. (1995). Vision in Alzheimer's disease. *Gerontologist* 35, 370–376. doi: 10.1093/geront/35.3.370

den Haan, J., Janssen, S. F., van de Kreeke, J. A., Scheltens, P., Verbraak, F. D., and Bouwman, F. H. (2017a). Retinal thickness correlates with parietal cortical atrophy in early-onset Alzheimer's disease and controls. *Alzheimers Dement.* 10, 49–55. doi: 10.1016/j.dadm.2017.10.005

den Haan, J., Verbraak, F. D., Visser, P. J., and Bouwman, F. H. (2017b). Retinal thickness in Alzheimer's disease: a systematic review and meta-analysis. *Alzheimers Dement.* 25, 162–170. doi: 10.1016/j.dadm.2016.12.014

Devos, D., Tir, M., Maurage, C. A., Waucquier, N., Defebvre, L., Defoort-Dhellemmes, S., et al. (2005). ERG and anatomical abnormalities suggesting retinopathy in dementia with Lewy bodies. *Neurology* 65, 1107–1110. doi: 10.1212/01.wnl.0000178896.44905.33

Di Russo, F., Pitzalis, S., Spitoni, G., Aprile, T., Patria, F., Spinelli, D., et al. (2005). Identification of the neural sources of the pattern-reversal VEP. *Neuroimage* 24, 874–886. doi: 10.1016/j.neuroimage.2004.09.029

Dunstan, D. A., and Scott, N. (2018). Assigning clinical significance and symptom severity using the zung scales: levels of misclassification arising from confusion between index and raw scores. *Depress. Res. Treat.* 2018:9250972. doi: 10.1155/2018/9250972

Erten-Lyons, D., Howieson, D., Moore, M. M., Quinn, J., Sexton, G., Silbert, L., et al. (2006). Brain volume loss in MCI predicts dementia. *Neurology* 66, 233–235. doi: 10.1212/01.wnl.0000194213.50222.1a

Goldstein, F. C., Ashley, A. V., Miller, E., Alexeeva, O., Zanders, L., and King, V. (2014). Validity of the montreal cognitive assessment as a screen for mild cognitive impairment and dementia in African Americans. *J. Geriatr. Psychiatry Neurol.* 27, 199–203. doi: 10.1177/0891988714524630

Goldstein, L. E., Muffat, J. A., Cherny, R. A., Moir, R. D., Ericsson, M. H., Huang, X., et al. (2003). Cytosolic beta-amyloid deposition and supranuclear cataracts in lenses from people with Alzheimer's disease. *Lancet* 361, 1258–1265. doi: 10.1016/S0140-6736(03)12981-9

Hamilton, R., Bach, M., Heinrich, S. P., Hoffmann, M. B., Odom, J. V., McCulloch, D. L., et al. (2020). ISCEV extended protocol for VEP methods of estimation of visual acuity. *Doc Ophthalmol.* doi: 10.1007/s10633-020-09780-1

Heaton, G. R., Davis, B. M., Turner, L. A., and Cordeiro, M. F. (2015). Ocular biomarkers of Alzheimer's disease. *Cent. Nerv. Syst. Agents Med. Chem*. 15, 117–125. doi: 10.2174/1871524915666150319123015

Hüfner, K., Strupp, M., Smith, P., Brandt, T., and Jahn, K. (2011). Spatial separation of visual and vestibular processing in the human hippocampal formation. *Ann. N. Y. Acad. Sci.* 1233, 177–186. doi: 10.1111/j.1749-6632.2011.06115.x

Ikram, M. K., Cheung, C. Y., Wong, T. Y., and Chen, C. P. (2012). Retinal pathology as biomarker for cognitive impairment and Alzheimer's disease. *J. Neurol. Neurosurg. Psychiatr*. 83, 917–922. doi: 10.1136/jnnp-2011-301628

Iseri, P. K., Altina,ş, O., Tokay, T., and Yüksel, N. (2006). Relationship between cognitive impairment and retinal morphological and visual functional abnormalities in Alzheimer disease. *J. Neuroophthalmol*. 26, 18–24. doi: 10.1097/01.wno.0000204645.56873.26

Krasodomska, K., Lubiński, W., Potemkowski, A., and Honczarenko, K. (2010). Pattern electroretinogram (PERG) and pattern visual evoked potential (PVEP) in the early stages of Alzheimer's disease. *Doc. Ophthalmol*. 121, 111–121. doi: 10.1007/s10633-010-9238-x

Livingston, G., Huntley, J., Sommerlad, A., Ames, D., Ballard, C., Banerjee, S., et al. (2020). Dementia prevention, intervention, and care: 2020 report of the lancet commission. *Lancet* 396, 413–446. doi: 10.1016/S0140-6736(20)30367-6

Lopez, M. N., Charter, R. A., Mostafavi, B., Nibut, L. P., and Smith, W. E. (2005). Psychometric properties of the folstein mini-mental state examination. *Assessment* 12, 137–144. doi: 10.1177/1073191105275412

Mckee, A. C., Au, R., Cabral, H. J., Kowall, N. W., Seshadri, S., Kubilus, C. A., et al. (2006). Visual association pathology in preclinical Alzheimer disease. *J. Neuropathol. Exp. Neurol*. 65, 621–630. doi: 10.1097/00005072-200606000-00010

McKhann, G. M., Knopman, D. S., Chertkow, H., Hyman, B. T., Jack, C. R., Kawas, C. H., et al. (2011). The diagnosis of dementia due to Alzheimer's disease: recommendations from the national institute on aging-Alzheimer's association workgroups on diagnostic guidelines for Alzheimer's disease. *Alzheimers Dement*. 7, 263–269. doi: 10.1016/j.jalz.2011.03.005

Méndez-Gómez, J. L., Pelletier, A., Rougier, M. B., Korobelnik, J. F., Schweitzer, C., Delyfer, M. N., et al. (2018). Association of retinal nerve fiber layer thickness with brain alterations in the visual and limbic networks in elderly adults without dementia. *JAMA Netw. Open*. 1:e184406. doi: 10.1001/jamanetworkopen.2018.4406

Mishra, U. K., and Kalita, J. (2004). "Clinical neurophysiology,"in *Visual Evoked Potential,* 1st Edn, eds U. K. Mishra and J. Kalita (New Delhi: Elsevier), 249–266.

Odom, J. V., Bach, M., Barber, C., Brigell, M., Marmor, M. F., Tormene, A. P., et al. (2004). Visual evoked potentials standard. *Doc. Ophthalmol.* 108, 115–123. doi: 10.1023/B:DOOP.0000036790.67234.22

Ohno-Matsui, K. (2011). Parallel findings in age-related macular degeneration and Alzheimer's disease. *Prog. Retin. Eye Res.* 30, 217–238. doi: 10.1016/j.preteyeres.2011.02.004

Pearl, J. R., Heath, L. M., Bergey, D. E., Kelly, J. P., Smith, C., Laurino, M. Y., et al. (2017). Enhanced retinal responses in Huntington's disease patients. *J. Huntingtons. Dis.* 6, 237–247. doi: 10.3233/JHD-170255

Petersen, R. C. (2004). Mild cognitive impairment as a diagnostic entity. *J. Intern. Med*. 256, 183–194. doi: 10.1111/j.1365-2796.2004.01388.x

Petersen, R. C. (2006). Mild cognitive impairment. *Lancet* 367:1979. doi: 10.1016/S0140-6736(06)68881-8

Ran, A., Ezraelia, R., Weinberger, D., Solomon, A., Ofri, R., and Michaelson, D. M. (2013). ApoE4 induces synaptic and ERG impairments in the retina of young targeted replacement ApoE4 mice. *PLoS ONE* 8:e64949. doi: 10.1371/journal.pone.0064949

Shi, Z., Cao, X., Hu, J., Jiang, L., Mei, X., Zheng, H., et al. (2020). Retinal nerve fiber layer thickness is associated with hippocampus and lingual gyrus volumes in nondemented older adults. *Prog. Neuropsychopharmacol. Biol. Psychiatry*. 99:109824. doi: 10.1016/j.pnpbp.2019.109824

Stothart, G., Kazanina, N., Näätänen, R., Haworth, J., and Tales, A. (2015). Early visual evoked potentials and mismatch negativity in Alzheimer's disease and mild cognitive impairment. *J. Alzheimers Dis*. 44, 397–408. doi: 10.3233/JAD-140930

Tao, R., Lu, Z., Ding, D., Fu, S., Hong, Z., Liang, X., et al.(2019). Perifovea retinal thickness as an ophthalmic biomarker for mild cognitive impairment and early Alzheimer's disease. *Alzheimers Dement.* 11, 405–414. doi: 10.1016/j.dadm.2019.04.003

Tsanov, M., and Manahan-Vaughan, D. (2008). Synaptic plasticity from visual cortex to hippocampus: systems integration in spatial information processing. *Neuroscientist* 14, 584–597. doi: 10.1177/1073858408315655

Zainal, N. H., Silva, E., Lim, L. L., and Kandiah, N. (2016). Psychometric properties of Alzheimer's disease assessment scale-cognitive subscale for mild cognitive impairment and mild Alzheimer's disease patients in an Asian context. *Ann. Acad. Med. Singap*. 45, 273–283.

Zhang, M. Y., Katzman, R., Salmon, D., Jin, H., Cai, G. J., Wang, Z. Y., et al. (1990). The prevalence of dementia and Alzheimer's disease in Shanghai, China: impact of age, gender, and education. *Ann. Neurol.* 27, 428–437. doi: 10.1002/ana.410270412

Conflict of Interest: The authors declare that the research was conducted in the absence of any commercial or financial relationships that could be construed as a potential conflict of interest.

frontiers in Aging Neuroscience

ORIGINAL RESEARCH
published: 10 February 2021
doi: 10.3389/fnagi.2021.597455

Altered Insular Subregional Connectivity Associated With Cognitions for Distinguishing the Spectrum of Pre-clinical Alzheimer's Disease

Siyu Wang[1,2], *Haiting Sun*[3], *Guanjie Hu*[1,4], *Chen Xue*[5], *Wenzhang Qi*[5], *Jiang Rao*[6], *Fuquan Zhang*[7], *Xiangrong Zhang*[3,8]* *and Jiu Chen*[1,2]*

[1] *Institute of Neuropsychiatry, The Affiliated Brain Hospital of Nanjing Medical University, Fourth Clinical College of Nanjing Medical University, Nanjing, China,* [2] *Fourth Clinical College of Nanjing Medical University, Nanjing, China,* [3] *Department of Pediatrics, Xijing Hospital, The Fourth Military Medical University, Xi'an, China,* [4] *Institute of Brain Functional Imaging, Nanjing Medical University, Nanjing, China,* [5] *Department of Radiology, The Affiliated Brain Hospital of Nanjing Medical University, Nanjing, China,* [6] *Department of Rehabilitation, The Affiliated Brain Hospital of Nanjing Medical University, Nanjing, China,* [7] *Department of Psychiatry, The Affiliated Brain Hospital of Nanjing Medical University, Nanjing, China,* [8] *Department of Geriatric Psychiatry, The Affiliated Brain Hospital of Nanjing Medical University, Nanjing, China*

Background: Subjective cognitive decline (SCD) and amnestic mild cognitive impairment (aMCI) are regarded as part of the pre-clinical Alzheimer's disease (AD) spectrum. The insular subregional networks are thought to have diverse intrinsic connectivity patterns that are involved in cognitive and emotional processing. We set out to investigate convergent and divergent altered connectivity patterns of the insular subregions across the spectrum of pre-clinical AD and evaluated how well these patterns can differentiate the pre-clinical AD spectrum.

Method: Functional connectivity (FC) analyses in insular subnetworks were carried out among 38 patients with SCD, 56 patients with aMCI, and 55 normal controls (CNs). Logistic regression analyses were used to construct models for aMCI and CN, as well as SCD and CN classification. Finally, we conducted correlation analyses to measure the relationship between FCs of altered insular subnetworks and cognition.

Results: Patients with SCD presented with reduced FC in the bilateral cerebellum posterior lobe and increased FC in the medial frontal gyrus and the middle temporal gyrus. On the other hand, patients with aMCI largely presented with decreased FC in the bilateral inferior parietal lobule, the cerebellum posterior lobe, and the anterior cingulate cortex, as well as increased FC in the medial and inferior frontal gyrus, and the middle and superior temporal gyrus. Logistic regression analyses indicated that a model composed of FCs among altered insular subnetworks in patients with SCD was able to appropriately classify 83.9% of patients with SCD and CN, with an area under the receiver operating characteristic (ROC) curve (AUC) of 0.876, 81.6% sensitivity, and 81.8% specificity. A model consisting of altered insular subnetwork FCs in patients with aMCI was able to appropriately classify 86.5% of the patients with aMCI and CNs, with an AUC of 0.887, 80.4% sensitivity, and 83.6% specificity. Furthermore, some of the FCs

OPEN ACCESS

Edited by:
Oury Monchi,
University of Calgary, Canada

Reviewed by:
Takahito Yoshizaki,
Keio University, Japan
Claudia Jacova,
Pacific University, United States

***Correspondence:**
Jiu Chen
ericcst@aliyun.com
Xiangrong Zhang
drxrz@hotmail.com

Received: *21 August 2020*
Accepted: *15 January 2021*
Published: *10 February 2021*

Citation:
Wang S, Sun H, Hu G, Xue C, Qi W, Rao J, Zhang F, Zhang X and Chen J (2021) Altered Insular Subregional Connectivity Associated With Cognitions for Distinguishing the Spectrum of Pre-clinical Alzheimer's Disease. Front. Aging Neurosci. 13:597455. doi: 10.3389/fnagi.2021.597455

among altered insular subnetworks were significantly correlated with episodic memory and executive function.

Conclusions: Patients with SCD and aMCI are likely to share similar convergent and divergent altered intrinsic FC patterns of insular subnetworks as the pre-clinical AD spectrum, and presented with abnormalities among subnetworks. Based on these abnormalities, individuals can be correctly differentiated in the pre-clinical AD spectrum. These results suggest that alterations in insular subnetworks can be utilized as a potential biomarker to aid in conducting a clinical diagnosis of the spectrum of pre-clinical AD.

Keywords: amnestic mild cognitive impairment, subjective cognitive decline, fMRI, insular subnetwork, functional connectivity, episodic memory, executive function

INTRODUCTION

Subjective cognitive decline (SCD) and amnestic mild cognitive impairment (aMCI), which are part of the clinical continuum of dementia progression and the spectrum of pre-clinical Alzheimer's disease (AD), are well-established risk factors for the development of AD (van der Flier et al., 2004; Stewart et al., 2008; Striepens et al., 2010; Scheef et al., 2012; Jessen et al., 2014b, 2020; Buckley et al., 2016; Xue et al., 2019). Many studies have suggested that individuals with SCD go on to develop aMCI, and then AD (Jessen et al., 2014b; Berger-Sieczkowski et al., 2019). Therefore, our in-depth understanding of neuroimaging-based continual pathology across the spectrum of pre-clinical AD can help assist in the development of a new method in pre-clinical AD diagnosis and treatment.

Neuroimaging can help reveal the pathological mechanisms behind AD progression. The insula and its network connectivity are anatomically connected to the limbic and frontal-parietal-temporal lobes and are functionally involved in a higher-order cognitive and emotional processing (Allen et al., 2008; Naqvi and Bechara, 2010), which has a significant role in AD progression (Fan et al., 2008; Guo et al., 2012). Numerous studies have reported the presence of insular gray matter atrophy in AD (Guo et al., 2012), as well as altered insular activities and networks in aMCI (Xie et al., 2012; Lin et al., 2017). In particular, studies have demonstrated that insula atrophy can help correctly distinguish patients with AD from normal controls (CNs; Fan et al., 2008; Guo et al., 2012). Therefore, it is reasonable to hypothesize that the insula is an extremely vulnerable area, as well as a critical hub, in delaying the progression of the pre-clinical spectrum of AD, including SCD and aMCI.

Recently, several studies have consistently suggested that the insula demonstrates heterogeneity and may be divided into the ventral anterior insula (vAI), the dorsal anterior insula (dAI), and the posterior insula (PI) (Deen et al., 2011; Peng et al., 2018; Lu et al., 2020). These insula subregional networks have different roles in information processing (Taylor et al., 2009) and therefore, have distinct intrinsic connectivity patterns (Deen et al., 2011; Peng et al., 2018; Lu et al., 2020). Studies have demonstrated that patients with aMCI and AD present with distinct disruption in the connectivity of insular subregions (Xie et al., 2012; Liu et al., 2018; Lu et al., 2020), which is associated with episodic memory deficits (Xie et al., 2012). Increasing evidence indicates that insular subregional networks can reveal neuroimaging-based continuum pathology across the spectrum of pre-clinical AD in a sensitive and specific manner. However, there is still a lack of knowledge with regards to altered network connectivity patterns of the insular subregions across the spectrum of pre-clinical AD (SCD and aMCI), as well as its relationship with cognition. In particular, it is unclear whether altered connectivity patterns of the insula subregions can help distinguish the spectrum of pre-clinical AD.

We conducted this study to identify altered intrinsic connectivity patterns of the insular subregions across the spectrum of pre-clinical AD. After identification of intrinsic connectivity pathology, we further evaluated how well this can be used to distinguish the spectrum of pre-clinical AD. Finally, we hypothesized that patients with SCD and aMCI present with different altered intrinsic connectivity patterns of the insular subregions. Additionally, we further hypothesized that integration of altered intrinsic functional connectivity (FC) can accurately distinguish individuals in the spectrum of pre-clinical AD.

MATERIALS AND METHODS

Participants

The data used in this study were acquired from our in-home database, the Nanjing Brain Hospital-Alzheimer's Disease Spectrum Neuroimaging Project (NBH-ADsnp) (Nanjing, China), which is continuously updated. The relevant information obtained from the NBH-ADsnp is summarized in **Supplementary Methods S.1**. This study was granted approval by the responsible Human Participants Ethics Committee of the Affiliated Brain Hospital of Nanjing Medical University (Nos. 2018-KY010-01 and 2020-KY010-02), located in Nanjing, China. Signed informed consent was obtained from each participant.

Initially, 460 individuals, who were of Han Chinese origin and right-handed, were enrolled in the NBH-ADsnp database from the memory clinic of hospitals and local communities through the use of advertising and broadcasting. All patients with SCD ($n = 116$) and CNs ($n = 190$) were recruited from local communities, while aMCI subjects ($n = 154$) were enrolled from both memory clinics and local communities. According

to our criteria, a total of 169 elderly individuals participated in this study. Among them, two CNs, two patients with SCD, and 16 patients with aMCI were excluded due to excessive head movement during MRI scan (defined as cumulative translation or rotation of >3.0 mm or 3.0° and individual time points with mean frame-wise displacement (FD) of >0.5 mm and scans with >50% volumes removed; Brady et al., 2019), and incomplete or missing MRI data. The remaining 55 CNs, 38 patients with SCD, and 56 patients with aMCI were enrolled in the final study. The inclusion and exclusion criteria were outlined in accordance with previously published studies (Jessen et al., 2014a, 2020; Chen et al., 2015a, 2016a, 2019a; Dubois et al., 2016; Xue et al., 2019). The diagnosis was performed independently by three neuropsychiatric physicians (Dr. Jiang Rao, Fuquan Zhang, and Xiangrong Zhang) who had 12–15 years of experience. Any disagreement between the three neuropsychiatric physicians was solved by reaching a consensus through group discussions.

The inclusion criteria of SCD subjects included the published SCD research criteria proposed by the Subjective Cognitive Decline Initiative (SCD-I; Jessen et al., 2014a). The detailed inclusion criteria were described in our previously published study (Xue et al., 2019), and is as follows: (a) self-reported persistent memory decline, confirmed by the caretaker or a family member; (b) a Subjective Cognitive Decline Questionnaire (SCD-Q) score > 5 (Hao et al., 2017; Yan et al., 2018; Cedres et al., 2019); (c) performance within a normal range on the Mini-Mental State Examination (MMSE) and the Montreal Cognitive Assessment (MoCA) (adjusted for age and education); (d) Clinical Dementia Rating (CDR) = 0; (e) subjects must be between the ages of 50 and 80; and (f) subjects must have Hamilton Depression Scale (HAMD) scores of < 7.

The inclusion criteria of aMCI subjects included the diagnostic criteria that were previously defined by Petersen et al. (1999) and the revised consensus standards reported by Winblad et al. (2004). The detailed inclusion criteria have been previously described in our published studies (Chen et al., 2016b, 2019a; Xue et al., 2019) and includes: (a) complaint of loss of memory, preferably corroborated by an informant or the subject for more than 3 months; (b) objective memory impairment (adjusted for age and educational level); (c) normal general cognitive function with MMSE score ≥ 24; (d) no or minimal impairment in daily life activities; (e) CDR = 0.5; (f) subjects must be between the ages of 50 and 80; (g) absence of dementia symptoms not sufficient to meet the criteria of the National Institute of Neurological and Communicative Disorders and Stroke or the AD and Related Disorders Association criteria for AD; and (h) subjects must have HAMD scores of < 7.

The inclusion criteria of CN were as follows: (a) no complaints of loss of memory; (b) normal cognitive performance (matched for age and education); (c) CDR = 0; (d) MMSE ≥ 26; (e) subjects must be between the ages of 50 and 80 (Chen et al., 2019b; Xue et al., 2019); and (f) subjects must have a HAMD score of < 7.

Detailed exclusion criteria for all subjects were described in our previously published studies (Chen et al., 2016b, 2019a; Xue et al., 2019), and included (a) past history of stroke (modified Hachinski Ischemic Scale score > 4), alcoholism, head injury, brain tumors, Parkinson's disease, epilepsy, encephalitis, major depression (excluded by HAMD), or other neurological or psychiatric diseases (excluded by clinical assessment and case history); (b) diagnosis of a major medical illness (i.e., cancer, anemia, thyroid dysfunction, syphilis, or HIV); (c) severe loss of vision or hearing; (d) inability to complete neuropsychological tests or a contraindication for MRI, and (e) T2-weighted MRI displaying major changes in white matter (WM), infarction, or additional lesions, as determined by the scan analysis done by two experienced radiologists. None of the subjects used any medications.

All participants underwent a standardized clinical evaluation protocol, including sequencing, demographic inventory, medical history, neurological and mental status examination, and MRI scan. The neuropsychologic tests were conducted by two different neurologists (Dr. Jiang Rao and Dr. Chen Xue) who had 3–5 years of experience. Specific demographics and neuropsychological characteristics of each group are provided in **Table 1**.

Neuropsychological Assessment

Neuropsychological assessments were similar to those used in our previous studies (Chen et al., 2015a, 2016a, 2019a,b; Xue et al., 2019). These assessments were utilized for evaluating the general cognitive function, episodic memory, speed of information processing, executive function, and visuospatial function. Details regarding each of the assessments are listed in **Supplementary Methods**.

MRI Data Acquisition

The detailed parameters of MRI acquisition of the NBH-ADsnp are summarized in **Supplementary Methods**. Imaging analysts were blinded to the status of diagnosis.

Functional MRI Data Pre-processing

We utilized MATLAB2015b and DPABI software (Yan et al., 2016) to preprocess all functional MRI (fMRI) data. The image processing procedure was conducted as previously described (Yan et al., 2013) and is summarized in **Supplementary Methods**. In brief, the first 10 time-points were removed, and the data were adjusted for time and motion effects with several nuisance variables [Friston 24-parameter model, with WM, cerebrospinal fluid (CSF), global signals and the linear trend removed; Ashburner and Friston, 2009]. Then, the functional images were spatially normalized, smoothed, and temporal band-pass filtered. The voxels within a group gray matter (GM) mask created by DARTEL were used for further analyses.

Structural MRI Data Pre-processing

Structural MRI analysis was carried out during fMRI data preprocessing using the DPABI image processing software. First, we manually reoriented and shifted the structural images to define the anterior commissure as the origin. Next, we used the DARTEL technique for normalization and segmentation, which divided the structural images into GM, WM, and CSF (Almairac et al., 2018), and created a group-specific GM (functional connection analysis was restricted to voxels within the GM mask) and WM template. Then, the native and DARTEL versions were

TABLE 1 | Demographics, clinical measures, and head rotation parameters of aMCI, SCD, and CN subjects.

Characteristics	CN	SCD	aMCI	*F*-values (χ^2)	*p*-values
	n = 55	*n* = 38	*n* = 56		
Age (years)	62.91 (5.94)	65.84 (7.73)	64.30 (7.70)	1.927	0.149
Gender (male/female)	23/32	8/30	15/41	5.243	0.074
Education level (years)	12.51 (2.51)	12.22 (2.72)	11.15 (2.87)[b]	3.813	0.024*
MMSE	28.58 (1.43)	28.32 (2.63)	27.29 (1.59)[b,c]	11.426	0.000*
MoCA	25.05 (2.42)	24.92 (1.79)	22.73 (2.88)[b,c]	14.787	0.000*
MDRS	141.46 (2.33)	140.37 (3.05)	136.45 (6.67)[b,c]	17.874	0.000*
SCD-Q	3.55 (1.50)	6.51 (0.90)[a]	5.06 (1.79)[b,c]	44.589	0.000*
HAMD	1.82 (2.26)	3.92 (3.17)[a]	3.80 (3.64)[b]	7.614	0.001*
Composite Z scores of each cognitive domain					
Episodic memory	0.27 (0.53)	0.34 (0.59)	−0.49 (0.61)[b,c]	33.177	0.000*
Information processing speed	0.27 (0.67)	0.18 (0.71)	−0.38 (0.74)[b,c]	13.325	0.000*
Executive function	0.27 (0.48)	0.30 (0.57)	−0.46 (0.62)[b,c]	31.026	0.000*
Visuospatial function	0.17 (0.66)	0.26 (0.50)	−0.34 (0.96)[b,c]	9.400	0.000*
Head rotation parameters					
FD_VanDijk	0.05 (0.03)	0.04 (0.03)	0.04 (0.03)	0.880	0.417
FD_Power	0.18 (0.08)	0.16 (0.09)	0.16 (0.09)	1.046	0.354
FD_Jenkinson	0.09 (0.04)	0.09 (0.05)	0.08 (0.05)	0.667	0.515

*Data are presented as mean (standard deviation, SD). CN, normal control; SCD, subjective cognitive decline; aMCI, amnestic mild cognitive impairment; MMSE, Mini-Mental State Examination; MoCA, Montreal Cognitive Assessment; MDRS, Mattis Dementia Rating Scale; HAMD, Hamilton Depression Scale; CDR, Clinical Dementia Rating; SCD-Q, Subjective Cognitive Decline-Questionnaire; FD, frame-wise displacement. *Significant differences were found among CN, SCD, and aMCI subjects. Most p-values were obtained using ANOVA, except for gender (chi-square test). Comparisons of each paired group were conducted to further reveal the source of ANOVA difference (a: SCD vs. CN; b: aMCI vs. CN; c: aMCI vs. SCD). Bonferroni correction was applied for multiple group comparisons. MMSE, MoCA, and MDRS were displayed as raw scores. This study utilized the composite Z scores to determine the level of each cognitive domain.* ***Supplementary Table 2*** *displays detailed raw scores and the corresponding Z scores of neuropsychological assessments.*

provided for GM, WM, and CSF tissues, and native versions were utilized to compute the global intracranial volumes (ITV).

Quality Assurance

The Effect of Brain Atrophy

Given that significant GM atrophies that are present within patients with SCD (Scheef et al., 2012) and aMCI (Trzepacz et al., 2013; Chen et al., 2015a,b, 2020), the anatomical differences between each group may affect the FCs of insular subregions. In order to investigate this issue, we computed ITV based on native GM, WM, and CSF in CN, SCD, and aMCI groups through the use of in-home MATLAB codes. We explored the differences among each group on the FC of insular subnetworks using ITV as an additional covariate in the general linear model (GLM) analysis.

Head Motion Effect

We used three different approaches to control for head motion effect, both at an individual and group level. First, we excluded CNs and patients with SCD and aMCI that had excessive head motion (defined as cumulative translation or rotation > 3.0 mm or 3.0°). Next, a Friston 24-parameter model was applied for regressing out the effects of head motion from the realigned data (Friston et al., 1996). Then, a "scrubbing" procedure was performed to scrub frames (volumes) that had an excessively high whole-brain root mean square (RMS) signal change over time in the preprocessed fMRI data for each participant (Sheline et al., 2010; Power et al., 2012; Van Dijk et al., 2012). Furthermore, any volume with an FD that was > 0.2 mm as nuisance covariates was regressed out, and scans with 50% of volumes were removed and discarded, as previously described in a study (Brady et al., 2019). Overall, two CNs, two patients with SCD, and 16 patients with aMCI were excluded on the account of excessive head movement. There were no significant changes with regards to between-group differences found in quality assurance parameters of head motion in qualified subjects (**Table 1**).

Strict Multiple Comparison Correction Strategy

In order to ensure reproducibility, test-retest reliability, and replicability using the fMRI metrics, we conducted a strict multiple comparison correction (Chen et al., 2018). That is, statistical maps were set with a threshold applying the permutation test with Threshold-Free Cluster Enhancement (TFCE; Smith and Nichols, 2009) and the family-wise error (FWE), as was implemented in DPABI (Yan et al., 2016).

Definition of Insular Subregions

For this study, we created six 6-mm radius spherical seeds. Our definition of insular subregions was in accordance with recent studies (Deen et al., 2011; Peng et al., 2018; Lu et al., 2020). Essentially, the insula was separated into six subregions, which included the left and right bilateral ventral anterior insula (L-vAI and R-vAI), the left and right bilateral dorsal anterior insula (L-dAI and R-dAI), and the left and right bilateral posterior insula (L-PI and R-PI) (Peng et al., 2018; Lu et al.,

2020). **Supplementary Table 1** details the Montreal Neurological Institute (MNI) seed coordinates.

Functional Connectivity Analyses

For each participant, we extracted the average time courses for all voxels within each insula subregional seed and used that as the reference time course. Next, we conducted voxel-wise cross-correlation analysis between the averaged time courses of all voxels within the insular subregional seed, as well as each voxel in the remainder of the entire brain within the group-specific GM mask. Finally, we increased the normality of correlation coefficients, and a Fisher's z-transformation analysis was performed.

Statistical Analyses

Demographics and Neuropsychological Data

ANOVA and chi-square tests were conducted for a comparison of differences of the demographic data, clinical measures, and head rotation parameters among the SCD, aMCI, and CN subjects. Notably, in order to improve the statistical power of the study, we applied a re-sampling method of stationary bootstrap (10,000 bootstrap samplings) to obtain significance.

We also set out to improve statistical power by diminishing random variability, as was done in a previous study (Chen et al., 2016b). This was done by compositing neuropsychological assessments into four cognitive domains (episodic memory, information processing speed, executive function, and visuospatial function), and the raw scores were then transformed into four composite Z scores. The details of raw and composite scores for the neuropsychological tests are outlined in **Supplementary Table 2**.

Identification of Altered Connectivity Patterns of the Insula Subregions

Using GLM analysis, we evaluated the differences of the FCs of insula subregions among subjects with aMCI, SCD, and CN (1,000 permutations, TFCE-corrected; $p < 0.001$ and cluster size > 227 mm^3). Then, we constructed a mask based on the different brain regions. Comparisons between any two groups (i.e., CN vs. SCD, CN vs. aMCI) were performed under this mask after adjusting for age, sex, education, ITV, and mean FD (1,000 permutations, TFCE-FWE-corrected $p < 0.05$, and cluster size > 227 mm^3).

Classification Based on Altered Connectivity Patterns of Insular Subregions

In order to further identify the FC patterns of insular subregions, closely related to patients with SCD and aMCI, we applied an approach based on binary logistic regression analysis using alterations in the identified ROIs as biomarkers to evaluate how well these can help distinguish patients with SCD or aMCI from CN subjects. The receiver operating characteristic (ROC) curve was applied to determine the classification power of this model, as well as to assess its accuracy, sensitivity, and specificity.

Relationship Between Altered Connectivity Patterns of the Insula Subregions and Cognition

In order to empirically verify the behavioral significance of altered FC within insular subnetworks in patients with SCD and aMCI, a Pearson's correlation analysis was performed to calculate the relationship between abnormal FC patterns of insula subregions, cognition, and clinical measure (HAMD scores) after adjusting for age, sex, and education. Furthermore, we assessed the significance of these correlation analyses through the use of a leave-one-out cross-validation procedure in 10,000 Monte-Carlo simulation tests to measure how often these results would be expected by chance in a study of multiple comparisons and a re-sampling method of stationary bootstrap (10,000 bootstrap samplings) in order to obtain significance.

RESULTS

Demographic and Neuropsychological Characteristics

We found no significant differences with regard to age and gender across each of the three groups ($p > 0.05$; **Table 1**). In comparison with CNs, patients with aMCI had significantly decreased education level ($p < 0.05$), while patients with SCD were not significantly different. In comparison to CNs, patients with SCD only showed significantly increased SCD-Q and HAMD scores, while patients with aMCI exhibited significantly reduced MMSE, MoCA, and MDRS scores, higher SCD-Q and HAMD scores, and a significant decline in executive function, episodic memory, information processing speed, and visuospatial cognition ($p < 0.05$).

Functional Connectivity of Insular Subnetworks in Patients With SCD and aMCI

In the left vAI subnetwork, in comparison to CNs, patients with SCD displayed reduced FC in the left cerebellum posterior lobe and increased FC in the bilateral medial frontal gyrus (MFG), the right middle temporal gyrus (MTG), and the right inferior frontal gyrus (orbital part) (IFGorb) ($P_{\mathrm{TFCE-FWE}} < 0.05$, cluster size > 227 mm^3) (**Figure 1A**, **Table 2**). Additionally, in the left dAI subnetwork, compared to CNs, patients with SCD showed decreased FC in the bilateral cerebellum posterior lobe and the left cerebellum anterior lobe, with increased FC in the left MTG ($P_{\mathrm{TFCE-FWE}} < 0.05$, cluster size > 227 mm^3) (**Figure 1B**, **Table 2**). Furthermore, in the right PI subnetwork, patients with SCD exhibited increased FC in right MTG in comparison with CNs ($P_{\mathrm{TFCE-FWE}} < 0.05$, cluster size > 227 mm^3) (**Figure 1C**, **Table 2**).

In the left vAI subnetwork, compared to CNs, patients with aMCI exhibited decreased FC in bilateral inferior parietal lobule (IPL) and increased FC in bilateral MFG, and right, middle, and superior temporal gyrus (STG; $P_{\mathrm{TFCE-FWE}} < 0.05$, cluster size > 227 mm^3) (**Figure 2A**, **Table 2**). In addition, in the left dAI subnetwork, compared with CNs, patients with aMCI showed decreased FC in the bilateral cerebellum posterior lobe, the left cerebellum anterior lobe, and the bilateral

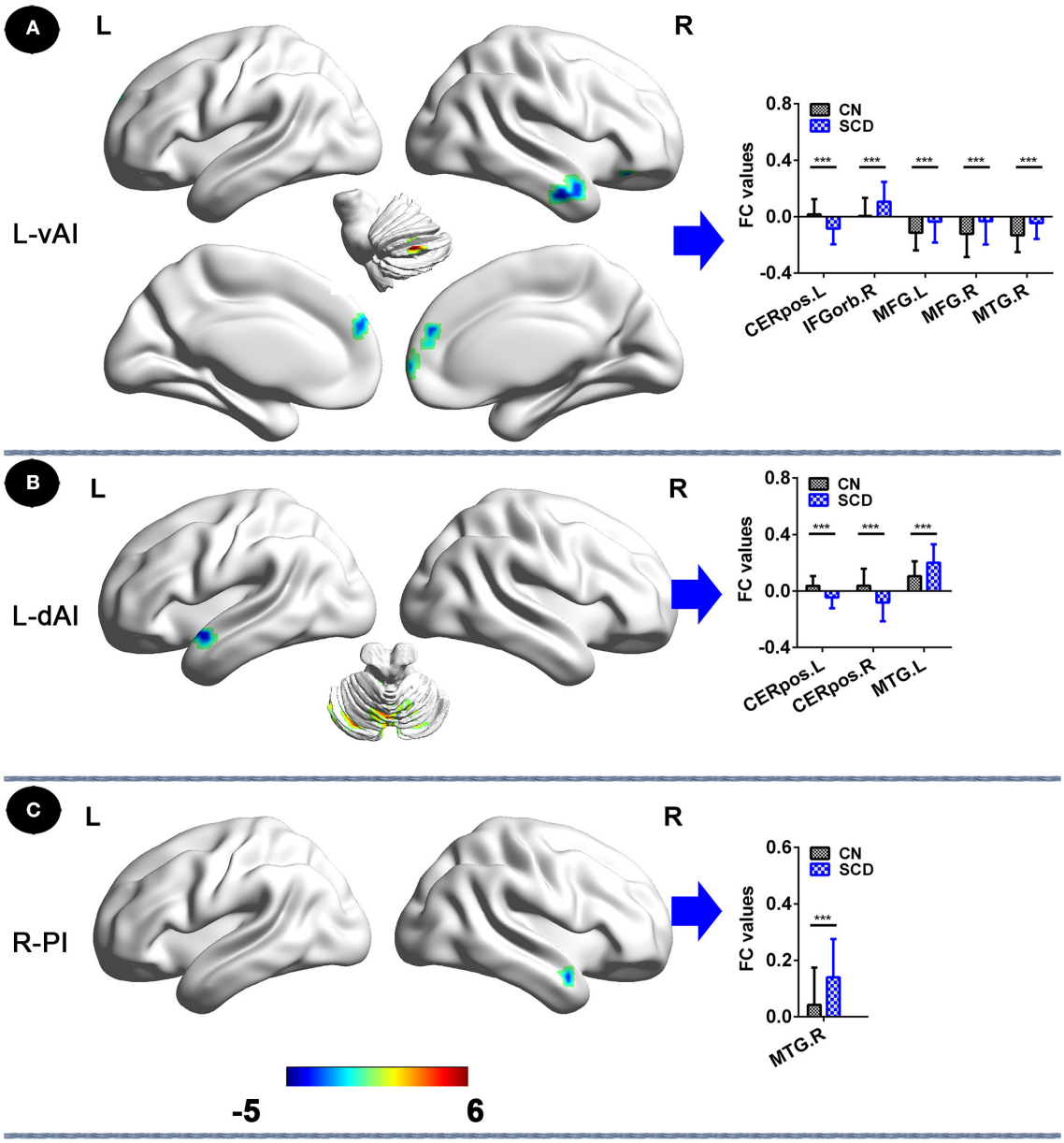

FIGURE 1 | Insular subnetwork functional connectivity in patients with SCD compared to CNs. **(A)** The different brain regions of the FC of the left vAI subregion between CN and SCD. A bar chart indicating the quantitative comparison of functional connectivity between these regions. **(B)** FC of left dAI subregion between CN and SCD. A bar chart indicating the quantitative comparison of FC between these regions. **(C)** FC of the right PI subregion between CN and SCD. A bar chart indicating the quantitative comparison of FC between these regions. *$P_{TFCE-FWE} < 0.05$. Note: only subnetworks that show significant differences in between-group comparisons are shown here. All results are displayed after adjusting for age, sex, education, ITV, and FD. A threshold of $p < 0.05$ was applied, and TFCE-FWE correction with cluster size >270 mm^3. FC, functional connectivity; CN, normal control; SCD, subjective cognitive decline; L-vAI, left ventral anterior insula; L-dAI, left dorsal anterior insula; R-PI, right posterior insula; TFCE, threshold-free cluster enhancement; FEW, family-wise error; ITV, intracranial volume; FD, frame-wise displacement; CERpos.L, left cerebellum posterior lobe; CERpos.R, right cerebellum posterior lobe; MTG.R, right middle temporal gyrus; IFGorb.R, right inferior frontal gyrus, orbital part; MFG.R, right medial frontal gyrus; MFG.L, left medial frontal gyrus; MTG.L, left middle temporal gyrus.

anterior cingulate cortex (ACC) ($P_{TFCE-FWE} < 0.05$, cluster size $>$ 227 mm^3) (**Figure 2B**, **Table 2**). Finally, in the right PI subnetwork, in comparison with CNs, patients with aMCI displayed increased FC in right IFGrob and IFGtri (triangular part) ($P_{TFCE-FWE} < 0.05$, cluster size $>$ 227 mm^3) (**Figure 2C**, **Table 2**). All results were adjusted for age, sex, education, ITV, and FD.

However, it is important to note that other insular subnetworks did not show significant differences among CN, SCD, and aMCI subjects.

TABLE 2 | Comparisons of functional connectivity of insular subregions among aMCI, SCD, and CN subjects.

Brain regions	L/R	BA	MNI			*F*/*T*-values	Cluster size (mm^3)
			x	y	z		
L-vAI FUNCTIONAL CONNECTIVITY							
CN vs. SCD							
Cerebellum posterior lobe	L		−51	−63	−33	5.7672	864
Middle temporal gyrus	R	21	60	−9	−27	−3.8771	2,241
Inferior frontal gyrus, orbital part	R	11	39	33	−15	−4.0899	324
Medial frontal gyrus	R	10	6	63	3	−3.3068	432
Medial frontal gyrus	L	9	6	51	24	−3.3713	1,026
CN vs. aMCI							
Medial frontal gyrus	L/R	11	−9	54	−15	−4.0347	14,121
Middle temporal gyrus	R	11	63	−63	3	−3.6545	297
Superior temporal gyrus	R	39	51	−57	21	−3.7118	297
Inferior parietal lobule	R	40	33	−54	42	4.7854	864
Inferior parietal lobule	L	40	−42	−51	51	3.8108	1,728
SCD vs. aMCI							
None							
L-dAI FUNCTIONAL CONNECTIVITY							
CN vs. SCD							
Cerebellum posterior lobe	R		36	−60	−57	4.1111	486
Cerebellum posterior lobe/Cerebellum anterior lobe	L		3	−60	−18	4.5395	15,147
Middle temporal gyrus	L	38	−51	3	−12	−4.5773	405
CN vs. aMCI							
Cerebellum posterior lobe	L		−33	−87	−27	3.4273	2,025
Cerebellum posterior lobe/Cerebellum anterior lobe	L		−6	−69	−21	3.5586	2,052
Anterior cingulate cortex	L/R	24	0	15	24	4.1218	567
SCD vs. aMCI							
None							
R-PI FUNCTIONAL CONNECTIVITY							
CN vs. SCD							
Middle temporal gyrus	R	21	48	0	−24	−4.0283	297
CN vs. aMCI							
Inferior frontal gyrus, orbital part	R	47	42	21	−3	−3.7377	2,160
Inferior frontal gyrus, triangular part	R	46	51	33	15	−3.2717	540
SCD vs. aMCI							
None							

CN, normal control; SCD, subjective cognitive decline; aMCI, amnestic mild cognitive impairment; TFCE, threshold-free cluster enhancement; FEW, family-wise error; ITV, intracranial volume; FD, frame-wise displacement; L-vAI, left ventral anterior insula; L-dAI, left dorsal anterior insula; R-PI, right posterior insula; MNI, Montreal neurological institute; L, left hemisphere; R, right hemisphere. To note, only the subnetworks that have significant between-group differences are shown here. All results are displayed after adjusting for age, sex, education, ITV, and FD at a threshold of $p < 0.05$, after applying TFCE-FWE correction with cluster size > 270 mm^3.

Classification of SCD, aMCI, and CN Using the Binary Logistic Regression

Binary logistic regression analyses revealed that the best-fitting model that combined altered insular subnetwork connectivity in patients with SCD was able to correctly classify 83.9% of SCD and CN subjects ($\chi^2 = 66.239$, $p < 0.001$; Nagelkerke $R^2 = 0.777$). The ROC curve of each altered insular subnetwork connectivity is presented in **Figure 3A**. The best-fitting model for this analysis had an area under the ROC curve (AUC) of 0.876, with 81.6% sensitivity and 81.8% specificity.

Next, using binary logistic regression analyses, we found that the best-fitting model combining altered insular subnetwork connectivity in patients with aMCI was able to correctly classify 86.5% of aMCI and CN subjects ($\chi^2 = 71.785$, $p < 0.001$; Nagelkerke $R^2 = 0.635$). The ROC curve of each altered insular subnetwork connectivity is displayed in **Figure 3B**. The best-fitting model had an AUC of 0.887, with 80.4% sensitivity and 83.6% specificity.

Behavioral Significance of Altered FC Within Insular Subnetworks in Patients With SCD and aMCI

Functional connectivity between the left vAI and left cerebellum posterior lobe in patients with SCD was negatively correlated with episodic memory score ($r = -0.357$, $p = 0.028$) (**Figure 4A**).

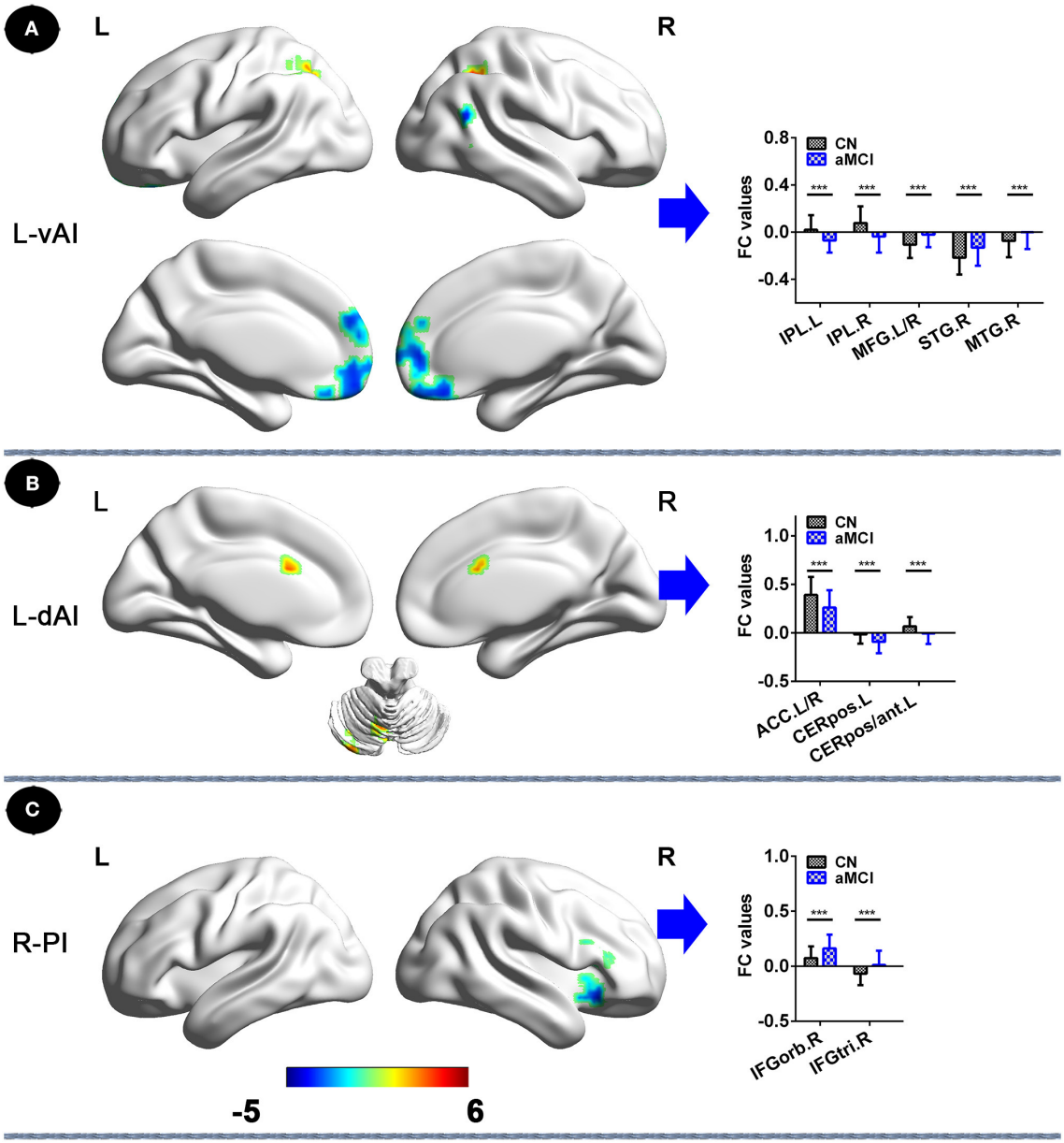

FIGURE 2 | Insular subnetwork functional connectivity in patients with aMCI compared to CNs. **(A)** FC of left vAI subregion between CN and aMCI patients. A bar chart indicating the quantitative comparison of FC between these regions. **(B)** Functional connectivity of the left dAI subregion between CN and aMCI patients. A bar chart indicating the quantitative comparison of FC between these regions. **(C)** FC of right PI subregion between CN and aMCI patients. A bar chart indicating the quantitative comparison of FC between these regions. $^{*}P_{TFCE-few} < 0.05$. Note: only the subnetworks that show between-group differences are shown here. All results are displayed after adjusting for age, sex, education, ITV, and FD. A threshold of $p < 0.05$ was applied, with a TFCE-FWE correction with cluster size > 270 mm^3. FC, functional connectivity; CN, normal controls; aMCI, amnestic mild cognitive impairment; L-vAI, left ventral anterior insula; L-dAI, left dorsal anterior insula; R-PI, right posterior insula; TFCE, threshold-free cluster enhancement; FEW, family-wise error; ITV, intracranial volume; FD, frame-wise displacement; IPL.L, left inferior parietal lobule; IPL.R, right inferior parietal lobule; STG.R, right superior temporal gyrus; MTG.R, right middle temporal gyrus; MFG. L/R, left/right medial frontal gyrus; ACC.L/R, anterior cingulate cortex; CERpos.L, left cerebellum posterior lobe; CERpos/ant.L, left cerebellum posterior lobe/cerebellum anterior lobe; IFGorb.R, right inferior frontal gyrus, orbital part; IFGtri.R, right inferior frontal gyrus, triangular part.

Furthermore, FC between the left vAI and left IPL within patients with aMCI was positively correlated with episodic memory score ($r = 0.292$; $p = 0.034$), while FC between left vAI and right STG ($r = -0.348$; $p = 0.011$), and FC between right PI and right IFGtri was negatively correlated with executive function scores ($r = -0.388$, $p = 0.004$) (**Figures 4B–D**). Furthermore, we did not find any correlation between depression (HAMD scores) and changes in FC in patients with SCD and aMCI ($p > 0.05$).

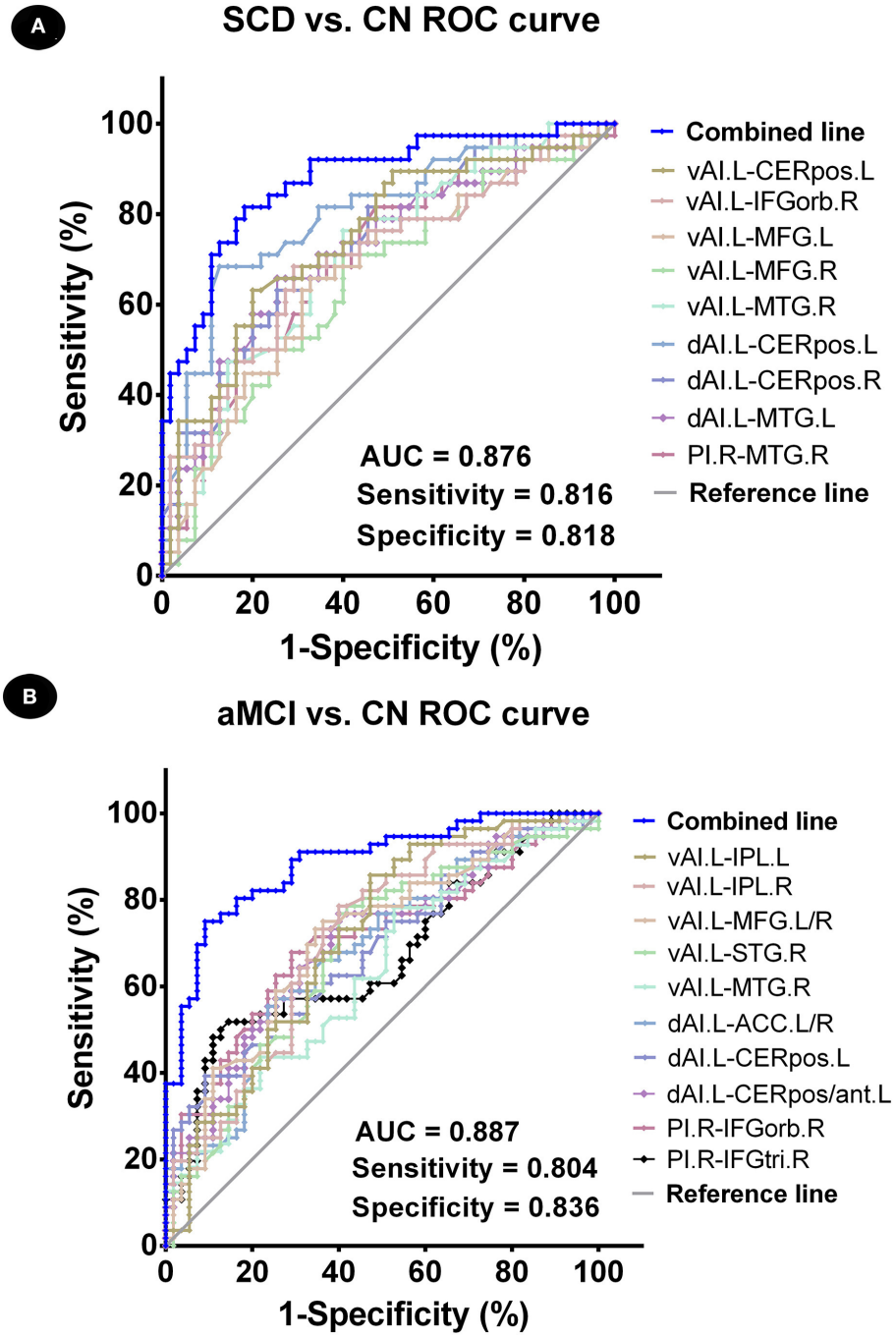

FIGURE 3 | Classification of individuals as SCD vs. CN and aMCI vs. CN using an MRI-based classifier. **(A)** ROC curve showcasing the classification power using an MRI-based "classifier" of SCD from CN. **(B)** ROC curve presetting the classification power using MRI-based "classifier" of aMCI from CN. Note: the values of AUC, sensitivity, and specificity are displayed in the lower right region of the figure. The combined line reflects the combination of indices of abnormal insular subnetwork functional connectivity. CN, normal control; SCD, subjective cognitive decline; aMCI, amnestic mild cognitive impairment; AUC, area under the ROC curve; ROC, receiver operating characteristic; vAI.L, left ventral anterior insula; dAI.L, left dorsal anterior insula; PI.R, right posterior insula; CERpos.L, left cerebellum posterior lobe; CERpos.R, right cerebellum posterior lobe; MTG.R, right middle temporal gyrus; IFGorb.R, right inferior frontal gyrus, orbital part; MFG.R, right medial frontal gyrus; MFG.L, left medial frontal gyrus; MTG.L, left middle temporal gyrus; IPL.L, left inferior parietal lobule; IPL.R, right inferior parietal lobule; STG.R, right superior temporal gyrus; ACC.L/R, anterior cingulate cortex; CERpos/ant.L, left cerebellum posterior lobe/cerebellum anterior lobe; IFGtri.R, right inferior frontal gyrus, triangular part.

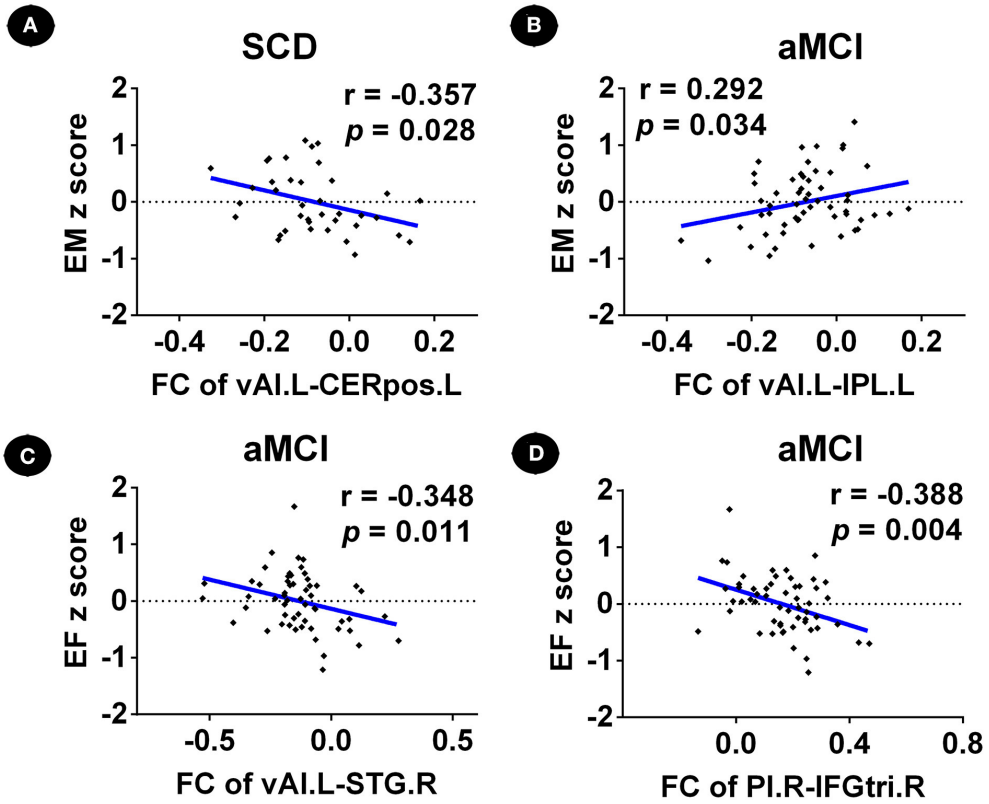

FIGURE 4 | Relationship between abnormal insular subnetwork functional connectivity and cognition in patients with SCD and aMCI. **(A)** Relationship between the insular subnetwork FC and cognition in patients with SCD. **(B–D)** Relationship between the insular subnetwork FC and cognition in patients with aMCI. FC, functional connectivity; CN, normal control; SCD, subjective cognitive decline; aMCI, amnestic mild cognitive impairment; vAI.L, left ventral anterior insula; PI.R, right posterior insula; CERpos.L, left cerebellum posterior lobe; IPL.L, left inferior parietal lobule; STG.R, right superior temporal gyrus; IFGtri.R, right inferior frontal gyrus, triangular part; EM, episodic memory; EF, executive function.

DISCUSSION

To the best of our knowledge, this is the first study to evaluate altered FC patterns of insular subnetworks in the pre-clinical spectrum of AD, and investigate the relationship between altered FC and behavioral significance. Binary logistic regression analyses were further applied for the classification of pre-clinical AD stages. According to our study results, we discovered that altered FC, if found, were mainly in overlapping areas among insular subnetworks (vAI, dAI, and PI) (Nomi et al., 2018), part of which is correlated with the abnormal cognition. Nonetheless, similarities and differences do exist between the two pre-clinical AD stages, and this utilization of abnormalities is able to precisely distinguish the spectrum of pre-clinical AD. Taken together, our results could imply that altered FCs within insular subnetworks may act as a biomarker for prompt detection, intervention, and treatment for pre-clinical AD.

Altered FC Patterns of Insular Subnetworks in Patients With SCD

We detected reduced FC within the L-vAI and L-dAI of cerebellum posterior lobe in patients with SCD compared to CN subjects. Furthermore, early studies discovered that the cerebellum posterior lobe contributes to episodic memory coding (Fliessbach et al., 2007). Additionally, altered FC within this area is closely related to abnormal episodic memory in patients with aMCI (Bai et al., 2011). In accordance with earlier observations, we identified a negative relationship between altered FCs of vAI in the cerebellum posterior lobe and episodic memory. With a gradual deterioration of FC, the episodic memory scores of patients with SCD turn out to increase. One possible explanation for this phenomenon is that while the connection between the cerebellum and insula gradually collapses, the compensatory brain regions (i.e., IFG, MFG, and MTG) become abnormally activated. These excessive intrinsic FCs contribute to transiently improved clinical performance. Notably, a dysfunction in episodic memory is thought to be a typical syndrome of aMCI (Seo and Choo, 2016). Furthermore, apart from aMCI, altered FC in the cerebellum was found to be highly correlated with deteriorated episodic memory performance of patients with SCD. This result implies that SCD may share some similarities in neuronal deterioration with aMCI, and may actually represent as a prodromal aMCI stage.

Altered FC Patterns of Insular Subnetworks in Patients With aMCI

In comparison to subjects with CN, patients with aMCI presented with reduced FCs of the L-vAI in IPL and in the cerebellum posterior lobe and ACC of L-dAI. IPL is known to be a region of heterogeneity that is associated with diverse brain networks, including DMN, salience network (SAN), and executive control network (ECN) (Wang et al., 2015). IPL has a role in multiple functions, such as the executive and salience effect (Uddin et al., 2011). Moreover, Kwok and Macaluso have demonstrated that IPL may be modulated under the episodic memory retrieval process, which indicates a tight relationship with episodic memory (Kwok and Macaluso, 2015). In addition, Xie et al. (2012) have reported that aberrant insular networks may play a key role in the processes of episodic memory. Consistently, we detected a positive correlation between FCs of L-vAI in IPL and episodic memory. With a reduction in FC, the severity of damage exceeds the degree of compensation, which leads to irreversible disrupted episodic memory performance. This implies decreased neuroactivity between IPL and L-vAI, which eventually causes worsened clinical performance. ACC is engaged in various processes, which includes attention, memory, and emotion (Fillinger et al., 2018). To date, numerous studies have demonstrated strong functional or structural connections between the dorsal ACC and dAI (Chang et al., 2013; Wiech et al., 2014; Ghaziri et al., 2017). Consistently, our result reveals a functional relationship between ACC and dAI, which indicates a potential deterioration mechanism of aMCI.

Convergent altered intrinsic FC remains in MFG, STG, and MTG under L-vAI, and in IFG under R-PI. MFG and MTG both belong to DMN and are relevant in cognitive processes. The abnormally increased FCs of patients with aMCI between these two regions and L-vAI implies possible recruitment of activated DMN for an early functional complement. Additionally, STG is in charge of primary and secondary auditory and lingual processes (Luo et al., 2018). Furthermore, Mwansisya et al. (2017) have reported convergent neuronal abnormalities within activated STG, which is closely related to executive dysfunction in schizophrenia. Consistently, we discovered a negative relationship between executive function and altered FC of L-vAI in STG, which validates an intimate relationship between STG and executive dysfunction of patients with aMCI. These results indicate that aMCI (or AD) may share similarities with regard to psychopathology and compensatory mechanisms.

Convergent and Divergent Altered FC of Insular Subnetworks in Patients With SCD and aMCI

Subjective cognitive decline and aMCI share both similarities and differences in altered FC of insular subnetworks. To summarize, we found that there were compensatory brain regions in patients with SCD, including MFG, MTG, and IFG. In addition, we also discovered that the compensatory phenomenon exists in STG in patients with aMCI. Furthermore, altered FC in MTG was detected across all three insular subnetworks, suggesting that STG may represent the main compensatory region in patients with SCD. However, compensation in patients with aMCI is more prominent, which further reflects the adaptation of deepened atrophy. With regards to the distribution of affected regions, IFG and MFG belong to the frontal regions while MTG and STG belong to the temporal regions. With the ever-expanding influence of neurotoxicity, researchers have discovered the presence of excessive strengthened intrinsic neuroactivities among the frontal and temporal regions (Qi et al., 2010; Gour et al., 2011; Yang et al., 2018). Combined with our results, we infer that the frontal and temporal regions may serve as the major and the earliest regions that regulate compensatory activities in pre-clinical AD stages. These results suggest a tendency to recruit advanced brain regions to compensate for early functional loss.

In addition, our study showed no insular differences in FC in the SCD group compared to the aMCI group. This is a surprising finding given the clear-cut cognitive differences that are present between the SCD and aMCI groups, as well as the different stages that are attributed to these groups in the clinical and pathological progression of AD. Our results suggest that even though these groups are clinically different, their underlying insular pathology may not be. Previous studies have highlighted the similarities and the overlap of the cerebral amyloid burden between patients with SCD and MCI (Wolfsgruber et al., 2017; Jessen et al., 2018). The explanation may be that SCD, in the presence of AD pathology, may represent the stage at which there is the first subtle cognitive dysfunction in pre-clinical AD (Sperling et al., 2011). At this stage, SCD reflects an individual's experience of this subtle cognitive decline, which is still in a significant compensatory phase (Erk et al., 2011). Furthermore, our previous study discovered that the compensatory phenomenon of neural networks in SCD individuals is associated with clinical cognition measures (Xue et al., 2019). This further indicates that AD pathology occurs in a temporally ordered manner, along with disease progression (Jack et al., 2013; Chen et al., 2019a). Therefore, SCD is considered a highly attractive stage for future early interventions in pre-clinical AD, as the brain function remains largely preserved with intact compensatory processes.

Our results also indicated that SCD and aMCI subjects have significantly higher HAMD scores in comparison to controls, despite the fact none of the subjects were depressed (HAMD score < 7). This suggests that depression may be a confounding factor of insular connectivity changes in SCD and aMCI. Recently, Liew (2019) investigated the independent risk factors for neurocognitive disorders associated with depression in a large sample study. Their results suggested that SCD and depression were both independent risks of MCI/dementia, but the combination of depression and SCD was a higher risk compared to SCD alone. However, in order to avoid this confounding factor, all subjects had depression scores of <7. Furthermore, there were no correlations found between depression scores and insular connectivity. Therefore, it is reasonable to speculate that the connectivity changes seen are indicative of SCD and aMCI, and are not representative of a state of depression.

Distinctly Altered Connectivity Patterns of Insular Subnetworks Within the Separate Spectrum of Pre-clinical AD

Even within the same group, there are differences among vAI, dAI, and PI. Based on our study results, we can infer that vAI is more sensitive with regard to the manifestation of compensation. Furthermore, vAI delivers more evident clinical manifestations of deterioration and compensation compared to dAI and PI and is associated with strong clinical significance. Liu et al. (2018) have reported that vAI, dAI, and PI are closely associated with SAN, ECN, and somatomotor network, respectively, indicating separate engagement in cognitive, affective, and interoceptive processes. The insula is highly associated with neuronal nodes that are related to episodic memory (Sugar and Moser, 2019) and possesses the function of executive control (Menon and Uddin, 2010). Our data have revealed that vAI is recruited in the functioning of episodic memory and executive function. Additionally, our results reveal a strong relationship between executive function and PI. Since there are distinct brain regions located within the hub of insular subnetworks, we infer that FC among these interactive subregions possesses multimodal functions. Under certain circumstances in which a specific function of a subregion is impaired, FC is increased within that region. However, further experimentation is required to verify specific mechanisms. Our preliminary results suggest that altered FC detection in pre-clinical AD patients may reversely play an essential role in revealing the internal relationships within insular subnetworks.

Precise Classification of the Spectrum of Pre-clinical AD by Model Combining Altered Insular Subnetwork Connectivity

To date, this is the first time that aberrant FC of insular subnetworks has been applied to identify the stages of the spectrum of pre-clinical AD. Utilizing binary logistic regression, we were able to obtain two separate optimal models for each pre-clinical stage, SCD, and aMCI. The accuracy of classification for the SCD model was 83% (81% sensitivity and 81.8% specificity), while the accuracy of the aMCI model was 86.5% (80% sensitivity and 83.6% specificity). Through this comparison, we are able to conclude that the aMCI classification model has higher overall accuracy. While the SCD classification model has increased competence in the identification of real patients, the aMCI classification model possesses a greater capability of excluding healthy individuals. Based on these results, as well as a combination of abnormal FCs in several altered brain regions, which belong to the overlapping areas of vAI, dAI, and PI, we are able to precisely distinguish the spectrum of pre-clinical AD. Therefore, abnormal connectivity among these regions can be utilized as a tool for early clinical diagnosis, and these altered regions can also be used as therapeutic targets for early intervention and treatment.

LIMITATION

There are several limitations to our study. Firstly, we have a small sample size, and only 55 CNs, 38 patients with SCD, and 56 patients with aMCI were included in this study. This may have led to a bias of the results. To enhance the statistical power of our results, we applied a non-parametric permutation test, which allows control of the false positive rate in cluster-level inference. Meanwhile, our NBH-ADsnp database is constantly being updated and recruits new volunteers, and therefore, we will further verify our conclusions shortly. Secondly, we studied the behavioral significance of FC abnormalities in its resting state, which has some limitations. The task-based fMRI may be utilized to verify these results and further evaluate the behavioral significance of FC alterations. Finally, we found no differences in FC between SCD and aMCI, which may limit the validity of insular FC measures in staging individuals that are on the spectrum of pre-clinical AD. This may suggest that insular FC features may simply serve as biological markers of disease, rather than markers of disease progression. The reason for these findings may be that aMCI subjects were recruited from the memory clinic and local communities. In the future, we hope to further expand the sample size in order to assess the characteristics of insular FC differences in patients with aMCI from the local community vs. patients enrolled from the memory clinic.

CONCLUSION

Subjective cognitive decline and aMCI, part of the spectrum of pre-clinical AD, share some convergent and divergent altered intrinsic connectivity of insular subnetworks, with differences in abnormalities existing among subnetworks. These abnormalities can be applied to accurately identify patients that are within the spectrum of pre-clinical AD, which suggests that aberrant functional connectivity within insular networks may serve as a strong potential biomarker in the diagnosis of pre-clinical AD stages.

DATA AVAILABILITY STATEMENT

The raw data supporting the conclusions of this article will be made available by the authors, without undue reservation.

ETHICS STATEMENT

The studies involving human participants were reviewed and approved by the responsible Human Participants Ethics Committee of the Affiliated Brain Hospital of Nanjing Medical University. The patients/participants provided their written informed consent to participate in this study.

AUTHOR CONTRIBUTIONS

JC, XZ, SW, and HS: study design. SW, HS, GH, CX, WQ, JR, and FZ: data acquisition. SW and HS: data analyses. SW and HS:

manuscript preparation. All authors contributed to the article and approved the submitted version.

FUNDING

This study was supported by the National Natural Science Foundation of China (Nos. 81701675; 2018YFC1314300; 81971255; and 81700666); the Key Project was supported by the Medical Science and technology development Foundation, Nanjing Department of Health (No. JQX18005); the Cooperative Research Project of Southeast University-Nanjing Medical University (No. 2018DN0031); the Key Research and Development Plan (Social Development) Project of Jiangsu Province (Nos. BE2018608 and BE2019610); the Innovation and Entrepreneurship Training Program for College Students in Jiangsu Province (Nos. 201810312061X and 201910312035Z); and the Key Scientific Research Projects of Colleges and Universities in Henan Province (No. 18A190003).

SUPPLEMENTARY MATERIAL

The Supplementary Material for this article can be found online at: https://www.frontiersin.org/articles/10.3389/fnagi.2021.597455/full#supplementary-material

REFERENCES

Allen, J. S., Emmorey, K., Bruss, J., and Damasio, H. (2008). Morphology of the insula in relation to hearing status and sign language experience. *J. Neurosci.* 28, 11900–11905. doi: 10.1523/JNEUROSCI.3141-08.2008

Almairac, F., Duffau, H., and Herbet, G. (2018). Contralesional macrostructural plasticity of the insular cortex in patients with glioma: a VBM study. *Neurology* 91, e1902–e1908. doi: 10.1212/WNL.0000000000006517

Ashburner, J., and Friston, K. J. (2009). Computing average shaped tissue probability templates. *Neuroimage* 45, 333–341. doi: 10.1016/j.neuroimage.2008.12.008

Bai, F., Liao, W., Watson, D. R., Shi, Y., Yuan, Y., Cohen, A. D., et al. (2011). Mapping the altered patterns of cerebellar resting-state function in longitudinal amnestic mild cognitive impairment patients. *J. Alzheimers. Dis.* 23, 87–99. doi: 10.3233/JAD-2010-101533

Berger-Sieczkowski, E., Gruber, B., Stogmann, E., and Lehrner, J. (2019). Differences regarding the five-factor personality model in patients with subjective cognitive decline and mild cognitive impairment. *Neuropsychiatrie* 33, 35–45. doi: 10.1007/s40211-018-0292-z

Brady, R. O. Jr., Gonsalvez, I., Lee, I., Ongur, D., Seidman, L. J., Schmahmann, J. D., et al. (2019). Cerebellar-prefrontal network connectivity and negative symptoms in schizophrenia. *Am. J. Psychiatry* 176, 512–520. doi: 10.1176/appi.ajp.2018.18040429

Buckley, R. F., Maruff, P., Ames, D., Bourgeat, P., Martins, R. N., Masters, C. L., et al. (2016). Subjective memory decline predicts greater rates of clinical progression in preclinical Alzheimer's disease. *Alzheimers. Dement* 12, 796–804. doi: 10.1016/j.jalz.2015.12.013

Cedres, N., Machado, A., Molina, Y., Diaz-Galvan, P., Hernandez-Cabrera, J. A., Barroso, J., et al. (2019). Subjective cognitive decline below and above the age of 60: a multivariate study on neuroimaging, cognitive, clinical, and demographic measures. *J. Alzheimers. Dis.* 68, 295–309. doi: 10.3233/JAD-180720

Chang, L. J., Yarkoni, T., Khaw, M. W., and Sanfey, A. G. (2013). Decoding the role of the insula in human cognition: functional parcellation and large-scale reverse inference. *Cerebral Cortex* 23, 739–749. doi: 10.1093/cercor/bhs065

Chen, J., Chen, G., Shu, H., Chen, G., Ward, B. D., Wang, Z., et al. (2019a). Predicting progression from mild cognitive impairment to Alzheimer's disease on an individual subject basis by applying the CARE index across different independent cohorts. *Aging* 11, 2185–2201. doi: 10.18632/aging.101883

Chen, J., Duan, X., Shu, H., Wang, Z., Long, Z., Liu, D., et al. (2016a). Differential contributions of subregions of medial temporal lobe to memory system in amnestic mild cognitive impairment: insights from fMRI study. *Sci. Rep.* 6:26148. doi: 10.1038/srep26148

Chen, J., Shu, H., Wang, Z., Liu, D., Shi, Y., Zhang, X., et al. (2015a). The interaction of APOE genotype by age in amnestic mild cognitive impairment: a voxel-based morphometric study. *J. Alzheimers. Dis.* 43, 657–668. doi: 10.3233/JAD-141677

Chen, J., Shu, H., Wang, Z., Zhan, Y., Liu, D., Liao, W., et al. (2016b). Convergent and divergent intranetwork and internetwork connectivity patterns in patients with remitted late-life depression and amnestic mild cognitive impairment. *Cortex* 83, 194–211. doi: 10.1016/j.cortex.2016.08.001

Chen, J., Shu, H., Wang, Z., Zhan, Y., Liu, D., Liu, Y., et al. (2019b). Intrinsic connectivity identifies the sensory-motor network as a main cross-network between remitted late-life depression- and amnestic mild cognitive impairment-targeted networks. *Brain Imaging Behav.* 14, 1130–1142. doi: 10.1007/s11682-019-00098-4

Chen, J., Zhang, Z., and Li, S. (2015b). Can multi-modal neuroimaging evidence from hippocampus provide biomarkers for the progression of amnestic mild cognitive impairment? *Neurosci. Bull* 31, 128–140. doi: 10.1007/s12264-014-1490-8

Chen, S., Xu, W., Xue, C., Hu, G., Ma, W., Qi, W., et al. (2020). Voxelwise meta-analysis of gray matter abnormalities in mild cognitive impairment and subjective cognitive decline using activation likelihood estimation. *J. Alzheimers Dis.* 77, 1495–1512. doi: 10.3233/JAD-200659

Chen, X., Lu, B., and Yan, C. G. (2018). Reproducibility of R-fMRI metrics on the impact of different strategies for multiple comparison correction and sample sizes. *Hum. Brain Mapp.* 39, 300–318. doi: 10.1002/hbm.23843

Deen, B., Pitskel, N. B., and Pelphrey, K. A. (2011). Three systems of insular functional connectivity identified with cluster analysis. *Cereb. Cortex* 21, 1498–1506. doi: 10.1093/cercor/bhq186

Dubois, B., Hampel, H., Feldman, H. H., Scheltens, P., Aisen, P., Andrieu, S., et al. (2016). Preclinical Alzheimer's disease: definition, natural history, and diagnostic criteria. *Alzheimers. Dement.* 12, 292–323. doi: 10.1016/j.jalz.2016.02.002

Erk, S., Spottke, A., Meisen, A., Wagner, M., Walter, H., and Jessen, F. (2011). Evidence of neuronal compensation during episodic memory in subjective memory impairment. *Arch. Gen. Psychiatry* 68, 845–852. doi: 10.1001/archgenpsychiatry.2011.80

Fan, Y., Resnick, S. M., Wu, X., and Davatzikos, C. (2008). Structural and functional biomarkers of prodromal Alzheimer's disease: a high-dimensional pattern classification study. *Neuroimage* 41, 277–285. doi: 10.1016/j.neuroimage.2008.02.043

Fillinger, C., Yalcin, I., Barrot, M., and Veinante, P. (2018). Efferents of anterior cingulate areas 24a and 24b and midcingulate areas 24a' and 24b' in the mouse. *Brain Struct. Funct.* 223, 1747–1778. doi: 10.1007/s00429-017-1585-x

Fliessbach, K., Trautner, P., Quesada, C. M., Elger, C. E., and Weber, B. (2007). Cerebellar contributions to episodic memory encoding as revealed by fMRI. *Neuroimage* 35, 1330–1337. doi: 10.1016/j.neuroimage.2007.02.004

Friston, K. J., Williams, S., Howard, R., Frackowiak, R. S., and Turner, R. (1996). Movement-related effects in fMRI time-series. *Magn. Reson. Med.* 35, 346–355. doi: 10.1002/mrm.1910350312

Ghaziri, J., Tucholka, A., Girard, G., Houde, J.-C., Boucher, O., Gilbert, G., et al. (2017). The corticocortical structural connectivity of the human insula. *Cerebral Cortex* 27, 1216–1228. doi: 10.1093/cercor/bhv308

Gour, N., Ranjeva, J.-P., Ceccaldi, M., Confort-Gouny, S., Barbeau, E., Soulier, E., et al. (2011). Basal functional connectivity within the anterior temporal network is associated with performance on declarative memory tasks. *Neuroimage* 58, 687–697. doi: 10.1016/j.neuroimage.2011.05.090

Guo, X., Han, Y., Chen, K., Wang, Y., and Yao, L. (2012). Mapping joint grey and white matter reductions in Alzheimer's disease using

joint independent component analysis. *Neurosci. Lett.* 531, 136–141. doi: 10.1016/j.neulet.2012.10.038

Hao, L., Wang, X., Zhang, L., Xing, Y., Guo, Q., Hu, X., et al. (2017). Prevalence, risk factors, and complaints screening tool exploration of subjective cognitive decline in a large cohort of the Chinese population. *J. Alzheimers. Dis.* 60, 371–388. doi: 10.3233/JAD-170347

Jack, C. R. Jr., Knopman, D. S., Jagust, W. J., Petersen, R. C., Weiner, M. W., Aisen, P. S., et al. (2013). Tracking pathophysiological processes in Alzheimer's disease: an updated hypothetical model of dynamic biomarkers. *Lancet Neurol.* 12, 207–216. doi: 10.1016/S1474-4422(12)70291-0

Jessen, F., Amariglio, R. E., Buckley, R. F., van der Flier, W. M., Han, Y., Molinuevo, J. L., et al. (2020). The characterisation of subjective cognitive decline. *Lancet Neurol.* 19, 271–278. doi: 10.1016/S1474-4422(19)30368-0

Jessen, F., Amariglio, R. E., van Boxtel, M., Breteler, M., Ceccaldi, M., Chetelat, G., et al. (2014a). A conceptual framework for research on subjective cognitive decline in preclinical Alzheimer's disease. *Alzheimers. Dement* 10, 844–852. doi: 10.1016/j.jalz.2014.01.001

Jessen, F., Spottke, A., Boecker, H., Brosseron, F., Buerger, K., Catak, C., et al. (2018). Design and first baseline data of the DZNE multicenter observational study on predementia Alzheimer's disease (DELCODE). *Alzheimers. Res. Ther.* 10:15. doi: 10.1186/s13195-017-0314-2

Jessen, F., Wolfsgruber, S., Wiese, B., Bickel, H., Mosch, E., Kaduszkiewicz, H., et al. (2014b). AD dementia risk in late MCI, in early MCI, and in subjective memory impairment. *Alzheimers. Dement* 10, 76–83. doi: 10.1016/j.jalz.2012.09.017

Kwok, S. C., and Macaluso, E. (2015). Exogenous features versus prior experiences modulate different subregions of the right IPL during episodic memory retrieval. *Sci. Rep.* 5:11248. doi: 10.1038/srep11248

Liew, T. M. (2019). Depression, subjective cognitive decline, and the risk of neurocognitive disorders. *Alzheimers. Res. Ther.* 11:70. doi: 10.1186/s13195-019-0527-7

Lin, F., Ren, P., Lo, R. Y., Chapman, B. P., Jacobs, A., Baran, T. M., et al. (2017). Insula and inferior frontal gyrus' activities protect memory performance against alzheimer's disease pathology in old age. *J. Alzheimers Dis.* 55, 669–678. doi: 10.3233/JAD-160715

Liu, X., Chen, X., Zheng, W., Xia, M., Han, Y., Song, H., et al. (2018). Altered functional connectivity of insular subregions in Alzheimer's disease. *Front. Aging Neurosci.* 10:107. doi: 10.3389/fnagi.2018.00107

Lu, L., Li, F., Chen, H., Wang, P., Zhang, H., Chen, Y. C., et al. (2020). Functional connectivity dysfunction of insular subdivisions in cognitive impairment after acute mild traumatic brain injury. *Brain Imaging Behav.* 14, 941–948. doi: 10.1007/s11682-020-00288-5

Luo, X., Jiaerken, Y., Huang, P., Xu, X. J., Qiu, T., Jia, Y., et al. (2018). Alteration of regional homogeneity and white matter hyperintensities in amnestic mild cognitive impairment subtypes are related to cognition and CSF biomarkers. *Brain Imaging Behav.* 12, 188–200. doi: 10.1007/s11682-017-9680-4

Menon, V., and Uddin, L. Q. (2010). Saliency, switching, attention and control: a network model of insula function. *Brain Struct. Funct.* 214, 655–667. doi: 10.1007/s00429-010-0262-0

Mwansisya, T. E., Hu, A., Li, Y., Chen, X., Wu, G., Huang, X., et al. (2017). Task and resting-state fMRI studies in first-episode schizophrenia: a systematic review. *Schizophr. Res.* 189, 9–18. doi: 10.1016/j.schres.2017.02.026

Naqvi, N. H., and Bechara, A. (2010). The insula and drug addiction: an interoceptive view of pleasure, urges, and decision-making. *Brain Struct. Funct.* 214, 435–450. doi: 10.1007/s00429-010-0268-7

Nomi, J. S., Schettini, E., Broce, I., Dick, A. S., and Uddin, L. Q. (2018). Structural connections of functionally defined human insular subdivisions. *Cerebral Cortex* 28, 3445–3456. doi: 10.1093/cercor/bhx211

Peng, X., Lin, P., Wu, X., Gong, R., Yang, R., and Wang, J. (2018). Insular subdivisions functional connectivity dysfunction within major depressive disorder. *J. Affect. Disord.* 227, 280–288. doi: 10.1016/j.jad.2017.11.018

Petersen, R. C., Smith, G. E., Waring, S. C., Ivnik, R. J., Tangalos, E. G., and Kokmen, E. (1999). Mild cognitive impairment: clinical characterization and outcome. *Arch. Neurol.* 56, 303–308. doi: 10.1001/archneur.56.3.303

Power, J. D., Barnes, K. A., Snyder, A. Z., Schlaggar, B. L., and Petersen, S. E. (2012). Spurious but systematic correlations in functional connectivity MRI networks arise from subject motion. *Neuroimage* 59, 2142–2154. doi: 10.1016/j.neuroimage.2011.10.018

Qi, Z., Wu, X., Wang, Z., Zhang, N., Dong, H., Yao, L., et al. (2010). Impairment and compensation coexist in amnestic MCI default mode network. *Neuroimage* 50, 48–55. doi: 10.1016/j.neuroimage.2009.12.025

Scheef, L., Spottke, A., Daerr, M., Joe, A., Striepens, N., Kolsch, H., et al. (2012). Glucose metabolism, gray matter structure, and memory decline in subjective memory impairment. *Neurology* 79, 1332–1339. doi: 10.1212/WNL.0b013e31826c1a8d

Seo, E. H., and Choo, I. L. H. (2016). Amyloid-independent functional neural correlates of episodic memory in amnestic mild cognitive impairment. *Eur. J. Nucl. Med. Mol. Imaging* 43, 1088–1095. doi: 10.1007/s00259-015-3261-9

Sheline, Y. I., Raichle, M. E., Snyder, A. Z., Morris, J. C., Head, D., Wang, S., et al. (2010). Amyloid plaques disrupt resting state default mode network connectivity in cognitively normal elderly. *Biol. Psychiatry* 67, 584–587. doi: 10.1016/j.biopsych.2009.08.024

Smith, S. M., and Nichols, T. E. (2009). Threshold-free cluster enhancement: addressing problems of smoothing, threshold dependence and localisation in cluster inference. *Neuroimage* 44, 83–98. doi: 10.1016/j.neuroimage.2008.03.061

Sperling, R. A., Aisen, P. S., Beckett, L. A., Bennett, D. A., Craft, S., Fagan, A. M., et al. (2011). Toward defining the preclinical stages of Alzheimer's disease: recommendations from the National Institute on Aging-Alzheimer's Association workgroups on diagnostic guidelines for Alzheimer's disease. *Alzheimers. Dement* 7, 280–292. doi: 10.1016/j.jalz.2011.03.003

Stewart, R., Dufouil, C., Godin, O., Ritchie, K., Maillard, P., Delcroix, N., et al. (2008). Neuroimaging correlates of subjective memory deficits in a community population. *Neurology* 70, 1601–1607. doi: 10.1212/01.wnl.0000310982.99438.54

Striepens, N., Scheef, L., Wind, A., Popp, J., Spottke, A., Cooper-Mahkorn, D., et al. (2010). Volume loss of the medial temporal lobe structures in subjective memory impairment. *Dement. Geriatr. Cogn. Disord.* 29, 75–81. doi: 10.1159/000264630

Sugar, J., and Moser, M.-B. (2019). Episodic memory: neuronal codes for what, where, and when. *Hippocampus* 29, 1190–1205. doi: 10.1002/hipo.23132

Taylor, K. S., Seminowicz, D. A., and Davis, K. D. (2009). Two systems of resting state connectivity between the insula and cingulate cortex. *Hum. Brain Mapp.* 30, 2731–2745. doi: 10.1002/hbm.20705

Trzepacz, P. T., Yu, P., Bhamidipati, P. K., Willis, B., Forrester, T., Tabas, L., et al. (2013). Frontolimbic atrophy is associated with agitation and aggression in mild cognitive impairment and Alzheimer's disease. *Alzheimers. Dement* 9, S95–S104 e101. doi: 10.1016/j.jalz.2012.10.005

Uddin, L. Q., Supekar, K. S., Ryali, S., and Menon, V. (2011). Dynamic reconfiguration of structural and functional connectivity across core neurocognitive brain networks with development. *J. Neurosci.* 31, 18578–18589. doi: 10.1523/JNEUROSCI.4465-11.2011

van der Flier, W. M., van Buchem, M. A., Weverling-Rijnsburger, A. W., Mutsaers, E. R., Bollen, E. L., Admiraal-Behloul, F., et al. (2004). Memory complaints in patients with normal cognition are associated with smaller hippocampal volumes. *J. Neurol.* 251, 671–675. doi: 10.1007/s00415-004-0390-7

Van Dijk, K. R., Sabuncu, M. R., and Buckner, R. L. (2012). The influence of head motion on intrinsic functional connectivity MRI. *Neuroimage* 59, 431–438. doi: 10.1016/j.neuroimage.2011.07.044

Wang, Z., Xia, M., Dai, Z., Liang, X., Song, H., He, Y., et al. (2015). Differentially disrupted functional connectivity of the subregions of the inferior parietal lobule in Alzheimer's disease. *Brain Struct. Funct.* 220, 745–762. doi: 10.1007/s00429-013-0681-9

Wiech, K., Jbabdi, S., Lin, C. S., Andersson, J., and Tracey, I. (2014). Differential structural and resting state connectivity between insular subdivisions and other pain-related brain regions. *Pain* 155, 2047–2055. doi: 10.1016/j.pain.2014.07.009

Winblad, B., Palmer, K., Kivipelto, M., Jelic, V., Fratiglioni, L., Wahlund, L. O., et al. (2004). Mild cognitive impairment–beyond controversies, towards a consensus: report of the International Working Group on Mild Cognitive Impairment. *J. Intern. Med.* 256, 240–246. doi: 10.1111/j.1365-2796.2004.01380.x

Wolfsgruber, S., Polcher, A., Koppara, A., Kleineidam, L., Frolich, L., Peters, O., et al. (2017). Cerebrospinal fluid biomarkers and clinical progression in patients with subjective cognitive decline and mild cognitive impairment. *J. Alzheimers. Dis.* 58, 939–950. doi: 10.3233/JAD-161252

Xie, C., Bai, F., Yu, H., Shi, Y., Yuan, Y., Chen, G., et al. (2012). Abnormal insula functional network is associated with episodic memory decline in amnestic mild cognitive impairment. *Neuroimage* 63, 320–327. doi: 10.1016/j.neuroimage.2012.06.062

Xue, C., Yuan, B., Yue, Y., Xu, J., Wang, S., Wu, M., et al. (2019). Distinct disruptive patterns of default mode subnetwork connectivity across the spectrum of preclinical Alzheimer's disease. *Front. Aging Neurosci.* 11:307. doi: 10.3389/fnagi.2019.00307

Yan, C. G., Craddock, R. C., Zuo, X. N., Zang, Y. F., and Milham, M. P. (2013). Standardizing the intrinsic brain: towards robust measurement of inter-individual variation in 1000 functional connectomes. *Neuroimage* 80, 246–262. doi: 10.1016/j.neuroimage.2013.04.081

Yan, C. G., Wang, X. D., Zuo, X. N., and Zang, Y. F. (2016). DPABI: data processing & analysis for (resting-state) brain imaging. *Neuroinformatics* 14, 339–351. doi: 10.1007/s12021-016-9299-4

Yan, T., Wang, W., Yang, L., Chen, K., Chen, R., and Han, Y. (2018). Rich club disturbances of the human connectome from subjective cognitive decline to Alzheimer's disease. *Theranostics* 8, 3237–3255. doi: 10.7150/thno.23772

Yang, L., Yan, Y., Wang, Y., Hu, X., Lu, J., Chan, P., et al. (2018). Gradual disturbances of the Amplitude of Low-Frequency Fluctuations (ALFF) and Fractional ALFF in Alzheimer spectrum. *Front. Neurosci.* 12:975. doi: 10.3389/fnins.2018.00975

Conflict of Interest: The authors declare that the research was conducted in the absence of any commercial or financial relationships that could be construed as a potential conflict of interest.

frontiers in Aging Neuroscience

ORIGINAL RESEARCH
published: 15 February 2021
doi: 10.3389/fnagi.2021.596025

Basal Forebrain Atrophy Is Associated With Allocentric Navigation Deficits in Subjective Cognitive Decline

Qian Chen[1†], Sichu Wu[2†], Xin Li[1†], Yi Sun[2], Wenqian Chen[2], Jiaming Lu[2], Wen Zhang[2], Jiani Liu[2], Zhao Qing[2,3], Zuzana Nedelska[4,5], Jakub Hort[4,5], Xin Zhang[1,2] and Bing Zhang[1,2,3]*

[1] Department of Radiology, Drum Tower Hospital, Clinical College of Nanjing Medical University, Nanjing, China, [2] Department of Radiology, Drum Tower Hospital, Medical School of Nanjing University, Nanjing, China, [3] Institute of Brain Science, Nanjing University, Nanjing, China, [4] Memory Clinic, Department of Neurology, 2nd Faculty of Medicine, Charles University, University Hospital Motol, Prague, Czechia, [5] International Clinical Research Center, St. Anne's University Hospital Brno, Brno, Czechia

OPEN ACCESS

Edited by:
Rong Chen,
University of Maryland, Baltimore, United States

Reviewed by:
Kamil Vlcek,
Academy of Sciences of the Czech Republic (ASCR), Czechia
Natalia Ladyka-Wojcik,
University of Toronto, Canada
Lok-Kin Yeung,
Columbia University, United States

***Correspondence:**
Bing Zhang
zhangbing_nanjing@nju.edu.cn

[†] These authors share first authorship

Received: *18 August 2020*
Accepted: *27 January 2021*
Published: *15 February 2021*

Citation:
Chen Q, Wu S, Li X, Sun Y, Chen W, Lu J, Zhang W, Liu J, Qing Z, Nedelska Z, Hort J, Zhang X and Zhang B (2021) Basal Forebrain Atrophy Is Associated With Allocentric Navigation Deficits in Subjective Cognitive Decline. Front. Aging Neurosci. 13:596025. doi: 10.3389/fnagi.2021.596025

Individuals with subjective cognitive decline (SCD) are at higher risk of incipient Alzheimer's disease (AD). Spatial navigation (SN) impairments in AD dementia and mild cognitive impairment patients have been well-documented; however, studies investigating SN deficits in SCD subjects are still lacking. This study aimed to explore whether basal forebrain (BF) and entorhinal cortex (EC) atrophy contribute to spatial disorientation in the SCD stage. In total, 31 SCD subjects and 24 normal controls were enrolled and administered cognitive scales, a 2-dimensional computerized SN test, and structural magnetic resonance imaging (MRI) scanning. We computed the differences in navigation distance errors and volumes of BF subfields, EC, and hippocampus between the SCD and control groups. The correlations between MRI volumetry and navigation distance errors were also calculated. Compared with the controls, the SCD subjects performed worse in both egocentric and allocentric navigation. The SCD group showed volume reductions in the whole BF ($p < 0.05$, uncorrected) and the Ch4p subfield ($p < 0.05$, Bonferroni corrected), but comparable EC and hippocampal volumes with the controls. In the SCD cohort, the allocentric errors were negatively correlated with total BF ($r = -0.625, p < 0.001$), Ch4p ($r = -0.625, p < 0.001$), total EC ($r = -0.423, p = 0.031$), and left EC volumes ($r = -0.442$, $p = 0.024$), adjusting for age, gender, years of education, total intracranial volume, and hippocampal volume. This study demonstrates that SN deficits and BF atrophy may be promising indicators for the early detection of incipient AD patients. The reduced BF volume, especially in the Ch4p subfield, may serve as a structural basis for allocentric disorientation in SCD subjects independent of hippocampal atrophy. Our findings may have further implications for the preclinical diagnosis and intervention for potential AD patients.

Keywords: subjective cognitive decline, basal forebrain, entorhinal cortex, spatial navigation, allocentric

INTRODUCTION

Alzheimer's disease (AD), a global concern, is a progressive neurodegenerative disorder that contains three stages: the preclinical stage, mild cognitive impairment (MCI), and dementia (Sperling et al., 2011). Subjective cognitive decline (SCD), a self-perceived worsening of cognitive function without objective deficits in neuropsychological evaluations, is considered to be a clinically-based approach for the detection of subjects at a potentially higher risk of developing AD (Jessen et al., 2014, 2020). SCD corresponds to the preclinical stage of the AD spectrum; thus, it is of critical importance to fully investigate features and biomarkers of this stage to pave the way for early diagnosis and intervention in AD (Howard, 2020; Jessen et al., 2020).

It has been well-established by histopathological studies that AD is associated with the loss of cholinergic neurons (Davies and Maloney, 1976; Mcgeer et al., 1984). Treatment with cholinesterase inhibitors has proven effective in improving global cognitive function, the activities of daily living, and behavioral symptoms in patients with mild to moderate AD (Raskind et al., 2000; Tariot et al., 2000; Rockwood et al., 2006). The basal forebrain (BF), consisting of different subfields such as Ch1-4, is a key structure for cholinergic input to the hippocampus, amygdala, and cerebral cortex (Mesulam et al., 1983). Studies based on magnetic resonance imaging (MRI) volumetry have shown significant volume reductions of the BF in MCI and AD dementia patients (Teipel et al., 2011; Grothe et al., 2012, 2013). The reduced volumes in specific subfields correlated with impairments in different cognitive domains (Grothe et al., 2010). However, to our knowledge, only one recent study has reported Ch4p volume reductions in the BF in a cohort of 24 SCD subjects (Scheef et al., 2019).

The entorhinal cortex (EC) is recognized as one of the earliest affected regions by AD pathology, and previous studies have shown cortical thinning and volume reductions in the EC in SCD subjects (Jessen et al., 2006; Meiberth et al., 2015; Ryu et al., 2017). Furthermore, a longitudinal study using the Alzheimer's Disease Neuroimaging Initiative (ADNI) cohort revealed that BF atrophy preceded entorhinal volume reduction and could predict the cortical spread of AD pathology and memory impairments in MCI patients (Schmitz et al., 2016).

Patients with MCI and AD dementia experience difficulties with spatial navigation (SN), which is the ability to determine and maintain a route from one place to another (Hort et al., 2007; Nedelska et al., 2012; Lithfous et al., 2013). Two SN strategies have been well-established: egocentric navigation and allocentric navigation (O'Keefe and Nadel, 1978). Egocentric navigation relies on subject-to-object relations and leads to the constitution of self-centered representations, while allocentric navigation depends on object-to-object relations and contributes to the construction of world-centered representations (Colombo et al., 2017). Lesion studies in mice have provided direct evidence that BF lesions result in both egocentric and allocentric disorientation (Berger-Sweeney et al., 2001; Hamlin et al., 2013). Previous studies have shown that BF atrophy was associated with allocentric impairments in AD patients (Kerbler et al., 2015b). Furthermore, treatment with donepezil, a cholinesterase inhibitor, has suggested improved performance in allocentric but not egocentric navigation in AD patients (Hort et al., 2014). The EC contains grid cells, which show a six-fold modulated firing pattern and play a critical role in allocentric representations (Hafting et al., 2005; Doeller et al., 2010). However, whether BF and EC atrophy contribute to SN deficits in SCD subjects remains unresolved.

In the present study, we aimed to determine the alterations in volumes of BF subfields and the bilateral EC in SCD subjects and to further elucidate the associations between MRI volumetry and navigation performance assessed by a 2-dimensional computerized SN test. We hypothesized that SCD individuals would show reduced volumes in the BF, most pronounced in the Ch4p subregion, and reduced volumes in the EC compared to the control subjects. Consistent with previous studies, we also expected significant associations between structural measures and allocentric navigation performance, which may indicate the structural neural basis of allocentric navigation deficits in SCD subjects.

MATERIALS AND METHODS

Subjects

Fifty-six individuals with Chinese Han nationality were recruited from the Drum Tower District of Nanjing by advertisement, and one subject showing bad homogeneity of imaging data was excluded. In total, 55 subjects were enrolled in the present study. The inclusion criteria were 55–75 years old, right-handedness, and equal to or more than 9 years of education experience. Participants with a history of stroke, other neurological disorders that could lead to cognitive decline (Parkinson's disease, encephalitis, epilepsy, brain tumors, etc.), severe anxiety or depression, and contraindications for MRI scanning were excluded from the study. Subjects who met the diagnostic for MCI in the standardized neuropsychological evaluation were also excluded from the current study. Specifically, three cognitive domains each containing two subtests were assessed: Auditory Verbal Learning Test (AVLT) long-delayed memory and AVLT recognition (Zhao et al., 2012) for episodic memory; Trail Making Test Part A (TMT-A) and Part B (TMT-B) (Zhao et al., 2013) for executive function; and Boston Naming Test (BNT) (Mack et al., 1992) and Animal Fluency Test (AFT) (Henry et al., 2004) for language ability. Participants were considered MCI patients with scores >1 standard deviation (SD) below the normative means in both subtests within one cognitive domain or >1 SD below the normative means in three single tests in three different domains (Jak et al., 2009; Li et al., 2019). The participants were assigned to the SCD group if they complained of memory decline within the last 5 years and expressed worries associated with memory decline. In total, 31 subjects were assigned to the SCD group. Twenty-four age-, sex-, and education-matched old people without memory complaints and cognitive impairments were recruited as normal controls (NCs). All participants signed an informed consent statement after gaining a sufficient understanding of the study procedures.

The experiment was approved by the Medical Research Ethics Committee of Nanjing Drum Tower Hospital.

Neuropsychological Evaluation

Each participant completed a set of standardized neuropsychological tests. The cognitive evaluation was performed by a psychologist with 10 years of working experience. The Mini-Mental State Examination (MMSE) (Tombaugh and Mcintyre, 1992) was implemented to measure global cognition, and the SCD questionnaire (SCD-Q) was employed for a quantitative assessment of the severity of SCD (**Supplementary Box 1**) and was not the inclusion criteria for SCD (Gifford et al., 2015; Li et al., 2019). Except for AVLT, TMT-A, TMT-B, BNT, and AFT mentioned above, we also used the Rey-Osterrieth Complex Figure (ROCF) (Shin et al., 2006) recall test to measure visuospatial memory, ROCF copy test and the Clock Drawing Test (CDT) (Shulman, 2000) to assess visuospatial abilities, and the Symbol Digit Modalities Test (SDMT) (Sheridan et al., 2006) to evaluate processing speed. The measures from the TMT-A and TMT-B tests are reported as the time (in seconds) spent on the test, with longer times representing worse executive function. Higher scores in the SCD-Q suggest worse self-assessment of cognition. For the other cognitive tests, measures are reported as the numbers of correct responses, with higher scores reflecting better function in the corresponding cognitive domains.

Spatial Navigation Assessment

The navigation behavior was measured by the Amunet test battery (NeuroScios, Austria, Gmbh), a computer-based version of the Morris water maze (hMWM), which used a similar paradigm as the hidden goal task (Kalová et al., 2005; Hort et al., 2007; Nedelska et al., 2012). Participants were presented with a computer screen (640 × 480 pixels) that showed a large white circle with 280 pixels in diameter representing the overhead view of the arena. Briefly, a red dot was the starting point, and yellow and green lines on the edge of a large white circle were the orienting cues. A purple hollow circle with 16 pixels in diameter was the goal, which was shown at the beginning and then disappeared in each trial. The examinee was asked to draw a path from the start to the goal as accurately as possible using a mouse. After the subject indicated the supposed goal position, the correct position was shown and the subject again was encouraged to notice its relative position to the starting point or cues. The task contained four phases from simple to complex: (a) Mixed alloegocentric navigation (**Figure 1A**): The least demanding subtask, which was considered a training task designed to get familiarized with the SN test. The examinee could find the goal by its spatial relationship with both the starting point and the orienting cues. (b) Egocentric navigation (**Figure 1B**): The examinee could locate the hidden goal only by its mutual relationship with the starting point, as the orienting cues were not displayed on the screen. (c) Allocentric navigation (**Figure 1C**): The examinee could locate the hidden goal using only its relationship with the orienting cues, as the position of the starting point was unrelated to the goal. (d) Delayed allocentric navigation (**Figure 1D**): This subtest was performed 30 min later using the same strategy as allocentric navigation to measure the delayed recall ability, during which the correct goal position was not shown so as

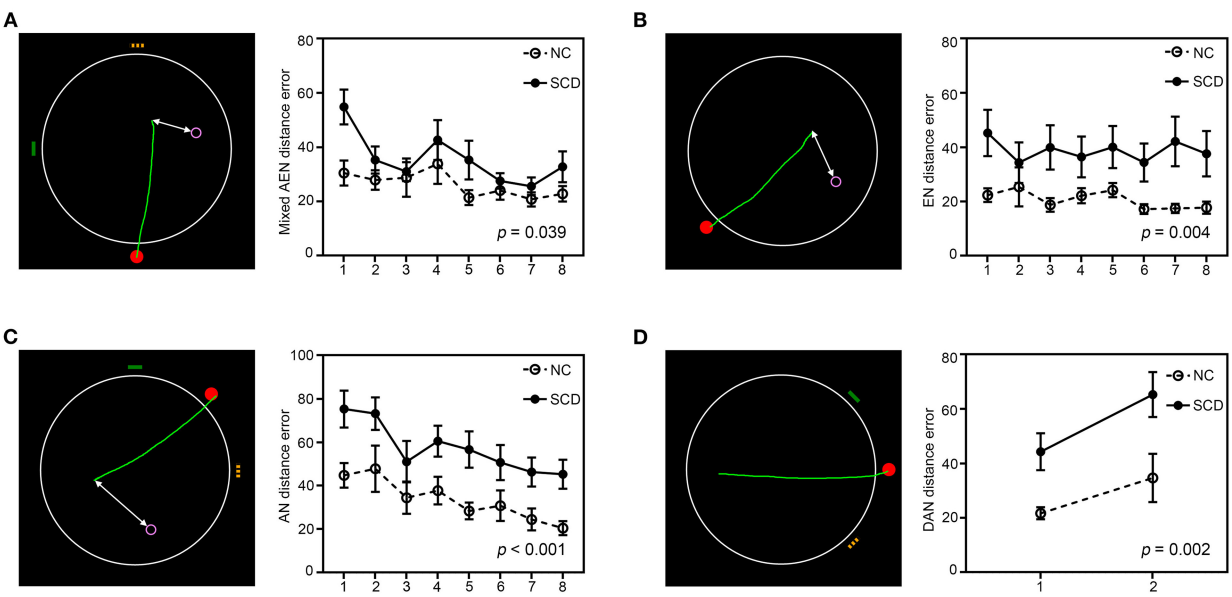

FIGURE 1 | The 2-dimensional computerized hidden goal task and corresponding navigation distance errors in each subtest. The images show an aerial view of the arena (large white circle), the starting point (red filled circle), orientation cues (yellow and green lines), and the goal (purple hollow circle). The green lines represent tracking by a subject from the start point to the supposed goal position, and the white lines represent the distance errors. Navigation distance errors in the normal control (NC) and subjective cognitive decline (SCD) groups in each trial of the **(A)** mixed alloegocentric navigation subtest (AEN), **(B)** egocentric navigation subtest (EN), **(C)** allocentric navigation subtest (AN), and **(D)** delayed allocentric navigation subtest (DAN) are shown. Values are the mean ± SEM (For interpretation of the references to colors in this figure, the reader is referred to the web version of this article).

to prevent the subjects from learning (Laczó et al., 2011). It is analogous to the probe trial in the original MWM task, where the hidden platform is removed and only distal orientation cues are used for navigation (Laczó et al., 2015). There were eight trials each of the mixed alloegocentric, egocentric, and allocentric subtests, while there were two trials of the delayed allocentric subtest. SN performance was recorded automatically as the average distance errors (from the position drawn by the examinee to the correct position of the goal on the computer screen in pixels) across all trials of each subtest. The SN task was not time-restricted to reduce bias by differences in cognitive, sensory, and physical functioning (Laczo et al., 2014). The examiner was blind to the diagnosis. Two SCD participants did not complete the delayed subtest; thus, they were excluded from the following analyses related to delayed allocentric navigation.

Imaging Data Acquisition

All participants were scanned on a 3T MRI scanner with an 8-channel phased-array head coil (Philips, Achieva TX) at the Department of Radiology, Nanjing Drum Tower Hospital. The T_1-weighted images (T_1WI) were acquired with the following parameters: 192 sagittal slices, repetition time (TR) = 9.74 ms, echo time (TE) = 4.60 ms, slice thickness = 1 mm, field of view (FOV) = 256 × 256 mm^2, and voxel size = 1 × 1 × 1 mm^3.

Basal Forebrain Subfield and Entorhinal Cortex Volumetry

MRI data were processed by the Computational Anatomy Toolbox (CAT12) for Statistics Parametric Mapping version 12 (SPM12). Briefly, MRI data were automatically segmented into gray matter (GM), white matter (WM), and cerebrospinal fluid (CSF) partitions. Then, the GM partitions were non-linearly normalized to the CAT12 default template (IXI555-MNI152) using the Diffeomorphic Anatomical Registration Through Exponentiated Lie Algebra (DARTEL) (Ashburner, 2007). Subject with a correlation between volumes that was two SDs below the mean suggested bad homogeneity of the data was excluded from the following analysis (Dahnke et al., 2013). The images were smoothed with a 4-mm full-width at half-maximum (FWHM) (Kilimann et al., 2014; Wolf et al., 2014). The GM, WM, and CSF partitions were summarized as the total intracranial volume (TIV), which was calculated to adjust for head size differences.

Calculation of the individual BF volumes was obtained by summing up the modulated GM voxel values within a cytoarchitectonic BF mask in the MNI space, which was derived from histological sections of a postmortem brain (Wolf et al., 2014). Regions of interest (ROIs) corresponding to the following BF subfields were derived (**Figure 2**): Ch1/2 (the nucleus of the vertical limb of the diagonal band), Ch3 (the nucleus of the horizontal limb of the diagonal band), Ch4a_i (anterior and

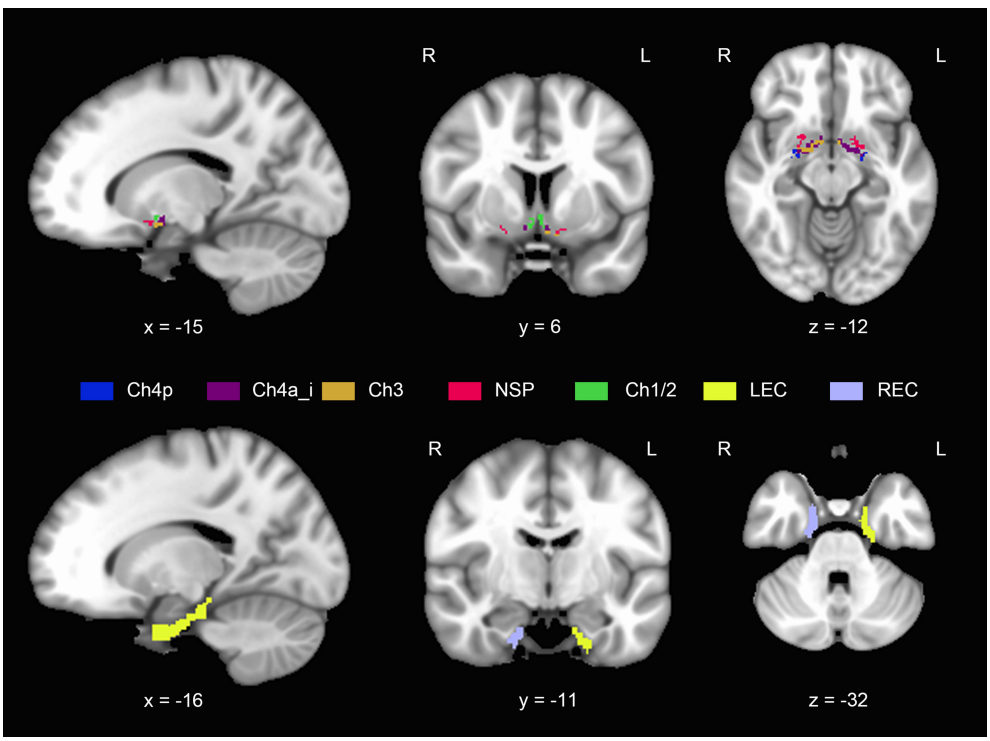

FIGURE 2 | Anatomical position and extent of the basal forebrain and entorhinal cortex. Different colors refer to different subregions. NSP, nucleus subputaminalis; LEC, left entorhinal cortex; REC, right entorhinal cortex (For interpretation of the references to colors in this figure, the reader is referred to the web version of this article).

intermediate parts of the nucleus basalis of Meynert), Ch4p (posterior part of the nucleus basalis of Meynert), and the nucleus subputaminalis (NSP). The entire volumes of the BF were defined as the sum of the volume of all subfields.

We extracted the subregions labeled 115 and 116 from the Brainnetome Atlas as the left EC and right EC mask, respectively (Fan et al., 2016) (**Figure 2**), using the Data Processing Assistant for Resting-State fMRI, advanced edition (DPARSF) (Chao-Gan and Yu-Feng, 2010). Individual EC volumes were calculated by summing up the modulated GM voxel values within the left or right EC mask.

We also calculated the hippocampal volume of each subject using FreeSurfer version 6.0.0 image analysis suites (http://freesurfer.net/), which was extracted as a covariate in subsequent correlation analyses.

Apolipoprotein E Genotyping

DNA extraction from 300 μL of whole blood per subject was performed using an SK2884 DNA extraction kit (Sangon Biotech, Shanghai, China). Apolipoprotein E (APOE) single nucleotide polymorphism (SNP) genotyping was performed for rs429358 and rs7412 using PCR technology with the support of the BGI Tech Solutions Beijing Liuhe Company. We determined APOE ε4 status for 42 of the 55 participants (15/24 in the NC group and 27/31 in the SCD group).

Statistical Analysis

Age, years of education, cognitive measures, and navigation distance errors were compared by two-sample *t*-tests. Gender distribution and APOE ε4 status were calculated by chi-square tests. We also applied paired t-tests to assess the differences in distance errors between egocentric and allocentric strategies within the whole cohort and in the NC and SCD cohorts. We also evaluated between-group differences in the total BF, BF subfields, EC, and hippocampal volumes, controlling for age, gender, years of education, and TIV.

The associations of SN errors with cognitive variables were assessed, adjusting for age, gender, and years of education. The correlations between the total BF, significant BF subfield volumes, total EC, and hippocampal volumes were calculated within the whole cohort and in the NC and SCD cohorts, adjusting for age, gender, years of education, and TIV. The associations between BF and EC volumetry and navigation distance errors on each subtest were also evaluated, adjusting for age, gender, years of education, TIV, and hippocampal volume. We further evaluated the differences in volumetry-navigation correlations between the two groups. Statistical analyses were performed with SPSS version 21.0 and the SurfStat package (http://www.math.mcgill.ca/keith/surfstat/). The significance level was set at $p < 0.05$ with two-tailed tests. Bonferroni corrections were applied for multiple comparisons.

RESULTS

Demographic and Neuropsychological Data

As shown in **Table 1**, the SCD and NC groups did not significantly differ in age, gender distribution, or educational level. Following Bonferroni correction with an adjusted α of 0.003, the SCD group showed higher scores on the SCD-Q [$t_{(53)} = -5.140$, $p < 0.001$]. Under uncorrected criteria, the SCD group also performed worse on the ROCF recall test [$t_{(53)} = 2.858$, $p = 0.006$] and the SDMT [$t_{(53)} = 2.034$, $p = 0.047$]. No significant differences in MMSE scores, episodic memory, executive, language or visuospatial abilities were observed between the NC and SCD groups. The two groups did not significantly differ in APOE ε4 status [$\chi^2_{(1)} = 0.380, p = 0.567$].

TABLE 1 | Demographic, neuropsychological, and APOE genotyping data.

	NC ($n = 24$)	SCD ($n = 31$)	Statistics (degree of freedom)	*P*
Age	63.50 ± 5.35	64.68 ± 5.21	$t_{(53)} = -0.822$	0.415
Gender	8/16	5/26	$\chi^2_{(1)} = 2.218$	0.136[a]
Education	13.25 ± 3.35	11.97 ± 2.60	$t_{(53)} = 1.598$	0.116
MMSE	29.04 ± 1.33	28.35 ± 1.43	$t_{(53)} = 1.820$	0.074
SCD-Q	3.19 ± 2.43	6.02 ± 1.65	$t_{(53)} = -5.140$	<0.001**
Episodic memory				
AVLT immediate	18.79 ± 4.75	16.55 ± 5.07	$t_{(53)} = 1.673$	0.100
AVLT short-term	5.83 ± 2.60	4.45 ± 2.57	$t_{(53)} = 1.969$	0.054
AVLT long-term	5.46 ± 2.50	4.39 ± 2.79	$t_{(53)} = 1.477$	0.146
AVLT cued recall	5.46 ± 2.17	4.19 ± 2.54	$t_{(53)} = 1.953$	0.056
AVLT recognition	21.67 ± 1.46	21.87 ± 1.15	$t_{(53)} = -0.580$	0.564
Visuospatial memory				
ROCF recall	18.13 ± 4.88	13.94 ± 5.76	$t_{(53)} = 2.858$	0.006*
Executive function				
TMT-A	58.04 ± 15.48	55.55 ± 17.34	$t_{(53)} = 0.554$	0.582
TMT-B	135.33 ± 46.04	153.32 ± 54.64	$t_{(53)} = -1.295$	0.201
Language ability				
AFT	19.17 ± 4.23	17.97 ± 4.57	$t_{(53)} = 0.996$	0.324
BNT	27.25 ± 2.71	27.16 ± 2.58	$t_{(53)} = 0.124$	0.902
Visuospatial ability				
ROCF copy	35.33 ± 1.24	34.23 ± 2.68	$t_{(53)} = 1.873$	0.067
CDT	27.67 ± 2.44	26.94 ± 2.71	$t_{(53)} = 1.036$	0.305
Processing speed				
SDMT	43.04 ± 9.68	37.45 ± 10.42	$t_{(53)} = 2.034$	0.047*
Genotyping				
APOE ε4 (carriers/non-carriers)	4/11	5/22	$\chi^2_{(1)} = 0.380$	0.537[a,b]

Values are the mean ± SD.

NC, normal control; SCD, subjective cognitive decline; MMSE, Mini-Mental State Examination; SCD-Q, SCD questionnaire; AVLT, Auditory Verbal Learning Test; ROCF, Rey-Osterrieth Complex Figure; TMT-A, Trail Making Test part A; TMT-B, Trail Making Test part B; AFT, Animal Fluency Test; BNT, Boston Naming Test; CDT, Clock Drawing Test; SDMT, Symbol Digit Modalities Test; APOE, apolipoprotein E.

**$p < 0.05$, uncorrected; **$p < 0.003$ (Bonferroni-adjusted α, 0.05/15 cognitive scales measured).*

[a]chi-square test; [b]APOE ε4 status not determined for the whole cohort.

Comparisons of Navigation Behavior Performance and Associations With Cognitive Variables

As **Table 2** and **Figure 1** show, the SCD subjects demonstrated larger distance errors in all the navigation subtests than the controls [mixed alloegocentric navigation: $t_{(53)} = -2.115$, $p = 0.039$, Cohen's $d = 0.60$; egocentric navigation: $t_{(53)} = -3.048$, $p = 0.004$, Cohen's $d = 0.88$; allocentric navigation: $t_{(53)} = -3.664$, $p < 0.001$, Cohen's $d = 1.03$; delayed allocentric navigation: $t_{(51)} = -3.328$, $p = 0.002$, Cohen's $d = 0.93$], but the differences in mixed alloegocentric navigation errors did not survive Bonferroni correction with an adjusted α of 0.0125. In addition, the two groups did not significantly differ in average duration in each subtest.

Regarding the within-group differences in two navigation strategies, we observed significantly larger distance errors in the allocentric strategy compared to the egocentric strategy in the whole [$t_{(54)} = -5.519$, $p = <0.001$, Cohen's $d = 0.74$], NC [$t_{(23)} = -4.458$, $p < 0.001$, Cohen's $d = 0.91$], and SCD cohorts [$t_{(30)} = -3.982$, $p < 0.001$, Cohen's $d = 0.72$] (**Supplementary Table 1**).

Supplementary Figure 1 shows the correlations between SN errors and cognitive measures in the whole cohort adjusting for age, gender, and years of education. The ROCF recall scores showed significant negative associations with distance errors in all the SN subtests.

TABLE 2 | Spatial navigation distance errors.

	NC ($n = 24$)	SCD ($n = 31$)	Statistics (degree of freedom)	*P*	Cohen's *d*
Mixed AEN	26.23 ± 9.86	35.60 ± 19.86	$t_{(53)} = -2.115$	0.039*	0.60
EN	20.63 ± 6.69	38.74 ± 28.44	$t_{(53)} = -3.048$	0.004**	0.88
AN	33.59 ± 15.74	57.35 ± 28.54	$t_{(53)} = -3.664$	<0.001**	1.03
DAN	28.16 ± 22.69	54.78 ± 33.27	$t_{(51)} = -3.328$	0.002**,a	0.93

Average distance errors (in pixels) in mixed alloegocentric (AEN), egocentric (EN), allocentric (AN), and delayed allocentric navigation (DAN) subtests in the normal control (NC) and subjective cognitive decline (SCD) groups. Values are the mean ± SD.

**p < 0.05, uncorrected; **p < 0.0125 (Bonferroni-adjusted α, 0.05/4 navigation tests measured).*

[a] Two SCD participants did not complete the DAN subtest; thus, they were excluded from the comparison.

Comparisons of BF, EC, and Hippocampal Volumes

After adjusting for age, gender, education level, and TIV, the SCD group showed reduced total BF volumes compared to the NC group [$F_{(1)} = 4.258$, $p = 0.044$, partial $\eta^2 = 0.08$] under uncorrected criteria. Considering the BF subfields, volume reduction in Ch4p in the SCD group [$F_{(1)} = 8.187$, $p = 0.006$, partial $\eta^2 = 0.14$] survived the Bonferroni adjusted α of 0.01. No significant differences in total and bilateral EC volumes, and in total and bilateral hippocampal volumes were observed (**Figure 3**).

Correlations Between BF Volumes and EC and Hippocampal Volumes

After adjusting for age, gender, education level, and TIV, we observed significant positive correlations between the Ch4p volumes and the total EC volumes ($r = 0.332$, $p = 0.017$) (**Supplementary Figure 2A**), and between total BF and hippocampal volumes ($r = 0.369$, $p = 0.008$) (**Supplementary Figure 3A**) in the whole cohort. In the SCD group, the total BF volumes showed positive correlations with total EC volumes ($r = 0.394$, $p = 0.042$) (**Supplementary Figure 2B**) and hippocampal volumes ($r = 0.572$, $p = 0.002$) (**Supplementary Figure 3B**). The Ch4p volumes also showed positive correlations with total EC volumes ($r = 0.609$, $p < 0.001$) (**Supplementary Figure 2C**) and hippocampal volumes ($r = 0.558$, $p = 0.002$) (**Supplementary Figure 3C**) in the SCD group. No significant associations between BF and EC volumes and between BF

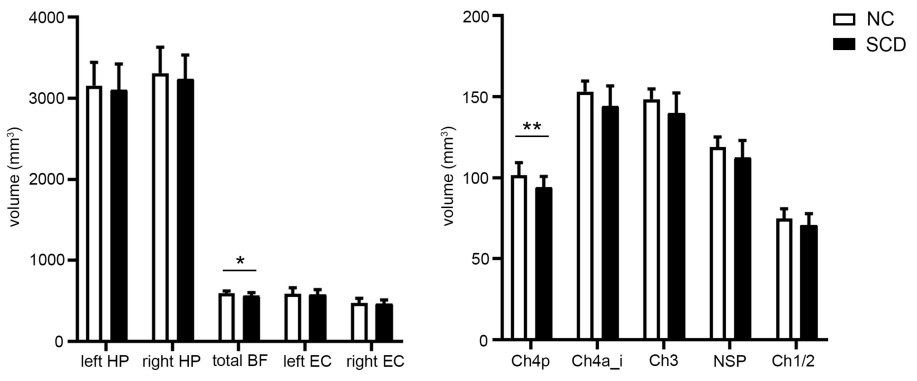

FIGURE 3 | Group comparisons of the basal forebrain (BF), entorhinal cortex (EC), and hippocampal (HP) volumes between the normal control (NC) and subjective cognitive decline (SCD) groups. Values are the mean ± *SD*. *$p < 0.05$; **$p < 0.01$ (Bonferroni-adjusted α, 0.05/5 BF subfields measured). *P*-values were adjusted for age, gender, years of education, and total intracranial volume.

and hippocampal volumes were observed in the NC group (**Supplementary Table 2**).

Correlations Between BF and EC Volumes and Navigation Performance

In the whole cohort (**Supplementary Table 3**), the total BF volumes were negatively correlated with allocentric errors ($r = -0.587$, $p < 0.001$) (**Figure 4A**) and delayed allocentric errors ($r = -0.294$, $p = 0.043$) (**Figure 4B**). The Ch4p volumes were negatively correlated with both allocentric errors ($r = -0.468$, $p < 0.001$) (**Figure 4C**) and delayed allocentric errors ($r = -0.355$, $p = 0.013$) (**Figure 4D**), controlling for age, gender, years of education, TIV, and hippocampal volume.

In the SCD group (**Supplementary Table 4**), the reduced total BF volumes were associated with larger allocentric errors ($r = -0.625$, $p < 0.001$) (**Figure 5A**), and the reduced Ch4p volumes were associated with larger allocentric errors ($r = -0.625$, $p < 0.001$) (**Figure 5B**). We also observed a negative correlation between the total EC volumes and allocentric errors ($r = -0.423$, $p = 0.031$) (**Figure 5C**) and between the left EC volumes and allocentric errors ($r = -0.442$, $p = 0.024$) (**Figure 5D**) in the SCD group, controlling for age, gender, years of education, TIV, and hippocampal volume.

In the NC group (**Supplementary Table 5**), no significant associations between BF, EC volumes, and navigation errors were observed.

Comparisons of Correlations Between BF and EC Volumes and Navigation Performance

Regarding the brain-behavior correlation comparison, we observed significant differences in the Ch4p volume-allocentric error correlation [$F_{(1,46)} = 10.07$, $p = 0.003$], total EC volume-allocentric error correlation [$F_{(1,46)} = 4.75$, $p = 0.034$], and left EC volume-allocentric error correlation [$F_{(1,46)} = 5.22$, $p = 0.027$] between the NC and SCD groups, controlling for age, gender, years of education, TIV, and hippocampal volume (**Supplementary Figure 4**).

DISCUSSION

In the present study, we observed worse egocentric and allocentric navigation performance in the SCD subjects.

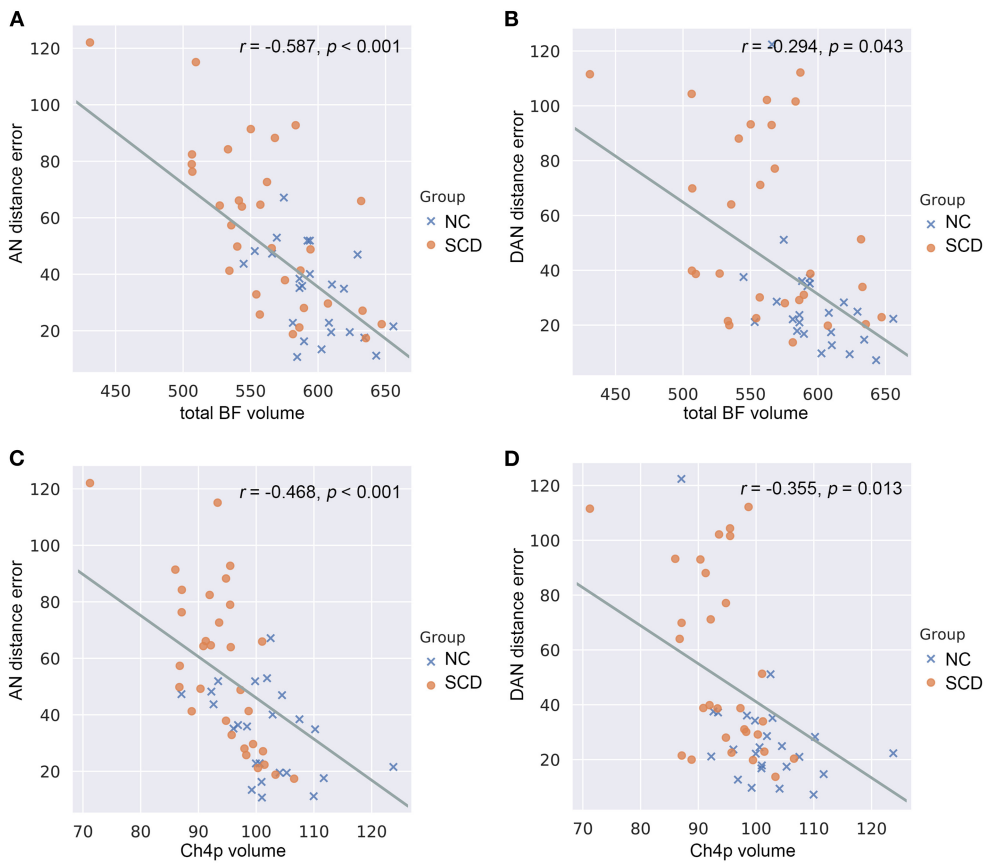

FIGURE 4 | Correlations between basal forebrain (BF) volumetry and navigation distance errors in the whole cohort. **(A)** Correlations between allocentric navigation (AN) distance errors and total BF volumes. **(B)** Correlations between delayed allocentric navigation (DAN) distance errors and total BF volumes. **(C)** Correlations between AN distance errors and Ch4p volumes. **(D)** Correlations between DAN distance errors and Ch4p volumes. NC, normal control; SCD, subjective cognitive decline. *P*-values were adjusted for age, gender, years of education, total intracranial volume, and hippocampal volume.

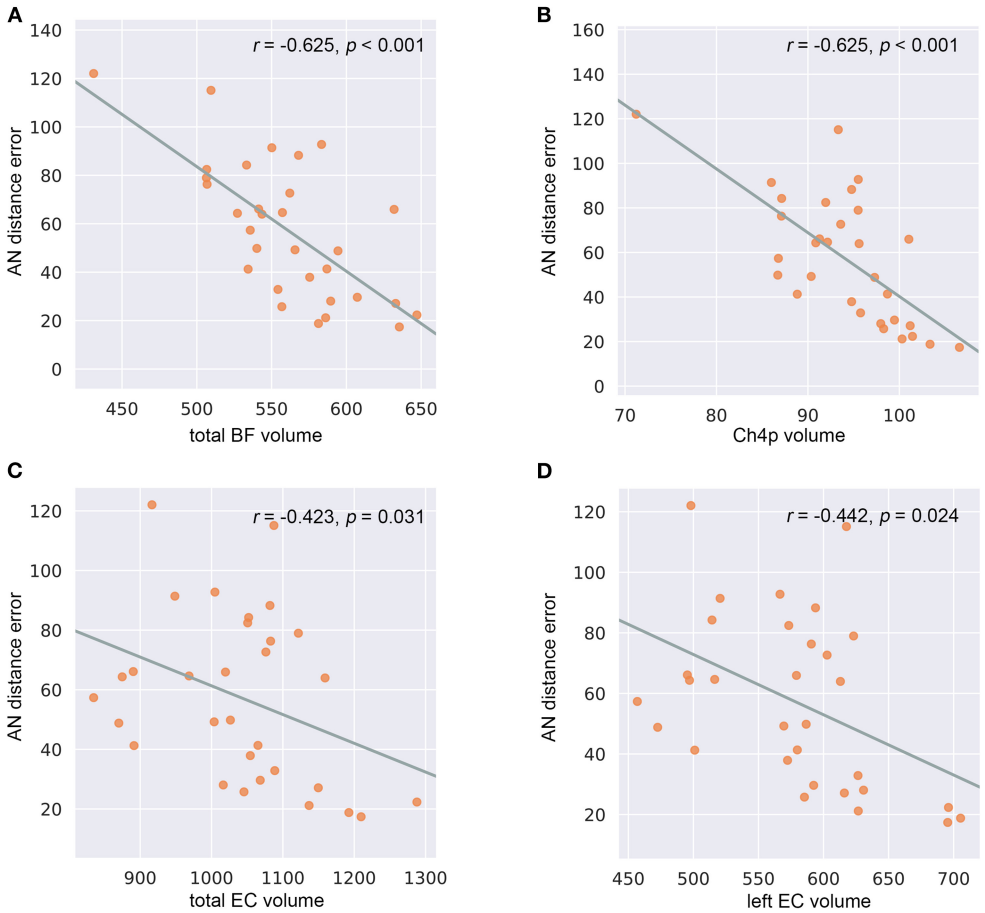

FIGURE 5 | Correlations between basal forebrain (BF) and entorhinal cortex (EC) volumetry and navigation distance errors in the subjective cognitive decline (SCD) cohort. **(A)** Correlations between allocentric navigation (AN) distance errors and total BF volumes. **(B)** Correlations between AN distance errors and Ch4p volumes. **(C)** Correlations between AN distance errors and total EC volumes. **(D)** Correlations between AN distance errors and left EC volumes. *P*-values were adjusted for age, gender, years of education, total intracranial volume, and hippocampal volume.

Additionally, we found that SCD subjects showed reduced volumes in the Ch4p subfield of BF, which were negatively correlated with allocentric distance errors. Our findings support the hypothesis that BF atrophy and spatial disorientation are objective and sensitive biomarkers for the preclinical detection of subjects with potential AD and point to the critical role of the BF, especially the Ch4p subfield, in allocentric disorientation in the SCD stage.

SCD Subjects Showed Egocentric and Allocentric Disorientation

With the exception of SCD-Q, the SCD subjects revealed comparable function to the controls in all the cognitive domains based on the neuropsychological evaluation after Bonferroni correction. Regarding the navigation test, the SCD subjects showed disorientation with both egocentric and allocentric representations, consistent with that observed in MCI and AD dementia patients in previous studies using the same paradigm (Hort et al., 2007; Laczo et al., 2010). Notably, the study by Hort et al. (2007) did not reveal significant differences in navigation performance between NCs and participants with subjective memory complaints (SMC). We speculated that differences in diagnostic criteria for SMC and SCD, sample size, and demographic characteristics may be possible factors contributing to the discrepancies. Our study extended previous findings by showing that spatial deficits exist in preclinical subjects at a higher risk of AD.

Egocentric is self-centered and depends on the parietal cortex and caudate nucleus, while allocentric is world-centered and hippocampus-driven (Laczó et al., 2018). Navigation likely represents a distinguishable cognitive domain that could provide promising methods for detecting individuals with incipient AD. In the present study, navigation performance revealed significant correlations with a broad range of cognitive domains, especially visuospatial memory, visuospatial ability, and processing speed. These relationships support the notion that SN is a complex process that associates with various navigational skills including spatial memory and visuospatial ability (Botly and De Rosa, 2009; Lithfous et al., 2013; Li and King, 2019). A recent study has also suggested a relation between SN impairments and processing

speed (Glikmann-Johnston et al., 2019). Of note, compared to the traditional cognitive scales, navigation tests could overcome limits based on ethnic origins and cultural restrictions, which may benefit longitudinal studies with large cohorts in the future (Coughlan et al., 2018).

Regarding the within-group analysis, we found that participants showed larger distance errors in allocentric compared to egocentric navigation. According to previous studies, older people prefer to use the egocentric strategy for navigation (Harris et al., 2012; Wiener et al., 2013; Lester et al., 2017). Our findings suggest that more accurate navigation using the egocentric rather than allocentric strategy may be an explanation for this bias. Still, this might also imply the absence of significant associations between mixed alloegocentric distance errors and BF volumes while the presence of strong correlations between allocentric performance and BF volumes discussed below in the present study, considering old subjects might tend to choose egocentric strategy when both egocentric and allocentric references were provided.

SCD Subjects Showed Reduced Ch4p Subfield Volumes of BF

We observed reduced Ch4p subfield volumes of BF in the SCD group compared to the NC group. Postmortem studies have documented cholinergic neuron loss in the BF in AD patients (Vogels et al., 1990), which was most pronounced in the Ch4p region (Liu et al., 2015). Previous studies have demonstrated significant volume reductions in all BF subfields except for Ch2 in MCI patients in a multicentre cohort, and the subsequent receiver operating characteristics (ROC) analysis for the separation between subjects with MCI and NCs revealed a higher diagnostic value of the Ch4p region than the hippocampus (Kilimann et al., 2014). A recent study investigating BF volumes in SCD subjects showed a significant total volume reduction in the BF, with the largest effect sizes in the Ch1/2 and Ch4p subregions, and the latter was associated with reduced glucose metabolism in the right precuneus, which had been reported to predict subsequent memory decline (Scheef et al., 2019). In addition, studies have reported negative correlations between BF volume and cortical amyloid deposition in presymptomatic subjects, suggesting intrinsic associations between cholinergic degeneration and amyloid pathology in the preclinical stages of AD (Grothe et al., 2014). Our findings provide evidence that SCD represents a higher risk of preclinical AD from the perspective of BF volumetry, which also suggests that Ch4p atrophy may serve as a sensitive imaging marker for the identification of incipient AD patients.

By contrast, we did not find significant differences in EC and hippocampal volumes between the two groups, which has been considered the earliest regions demonstrating neurofibrillary tangles and amyloid deposition in the initial stages of AD (Braak and Del Tredici, 2015). Previous studies have shown cortical thinning or reduced volumes of EC and hippocampus in SCD subjects, which reflected early alterations related to AD pathology in the SCD stage (Jessen et al., 2006; Saykin et al., 2006; Meiberth et al., 2015; Ryu et al., 2017; Zhao et al., 2019). Similar to our findings, these studies also did not find significant EC or hippocampal volumetry differences between controls and SCD subjects (Selnes et al., 2012; Hong et al., 2016; Ryu et al., 2017). Factors such as SCD definition, recruitment site, and calculation methods may contribute to the discrepant results. Notably, the SCD participants in the present study may be in a relatively earlier phase of SCD, while the SCD cohorts in previous studies showing remarkable EC or hippocampal atrophy may be representative of a later phase of SCD that is closer to MCI.

Since the SCD cohort in the present study showed volume reductions in the Ch4p subfield of BF while comparable EC and hippocampal volumes with the controls, we speculated that reduced BF volumes might have an advantage over EC or hippocampal atrophy as sensitive imaging markers for the detection of potential AD patients. However, since no pathology biomarkers and no follow-up data were available, the conclusion that cholinergic degeneration of the BF precedes neurofibrillary tangles or amyloid deposits in the EC and hippocampus in the initial stage of AD should be made with caution. In line with previous studies (Kerbler et al., 2015a,b)(Kerbler et al., 2015a,b), the positive relationships between BF and EC and hippocampal volumetry observed in the whole cohort and the SCD group may suggest covariation of these pathological processes, which remains to be further validated by studies with AD pathology biomarkers and more accurate volumetric methods.

BF Atrophy, Especially in the Ch4p Subfield, Contributed to Allocentric Disorientation in SCD Subjects

In the whole cohort, greater BF and Ch4p volumes were associated with better allocentric navigation performance. Studies in rats have revealed the role of cholinergic neurons in the posterior BF in visuospatial attention during feature binding (Botly and De Rosa, 2012). Furthermore, cholinesterase inhibitors have been reported to increase the selectivity of neural responses during visual working memory encoding in humans, which are crucial for allocentric navigation (Furey et al., 2000). Our findings were consistent with previous studies in that greater BF volumes predicted better allocentric navigation ability.

In the SCD group, the significant correlations between total BF and Ch4p volumes and allocentric errors suggested that BF degeneration, especially in the Ch4p subfield, contributes to allocentric disorientation in SCD subjects. Previous studies have demonstrated marked correlations between allocentric performance and anterior BF volumes, which covered Ch1-3 and the anterior region of Ch4, while no significant correlations between egocentric performance and BF volumes were found in AD dementia patients (Kerbler et al., 2015b). However, we did not observe significant Ch1-2 and Ch3 volume reductions in the SCD group, indicating that the allocentric disorientation may not be due to Ch1-3 atrophy in the preclinical stage. Previous studies also suggested that AD-related neurodegenerative changes in the BF may lead to less effective allocentric processing and increased reliance on egocentric representations in the early clinical stages of AD (Parizkova et al., 2018). Furthermore, mild

AD patients treated with cholinesterase inhibitors demonstrated improved delayed allocentric performance after 3 months (Hort et al., 2014). Our findings provide additional evidence that Ch4p atrophy contributes to allocentric navigation deficits in the SCD stage independent of hippocampal atrophy and have implications for the potential use of the SN test for prognostic evaluation of drugs targeting the cholinergic system in preclinical AD patients.

The Ch4 region mainly projects to the medial frontal, cingulate, retrosplenial, and visual cortices (Solari and Hangya, 2018). The medial frontal cortex has been implicated in the upstream processing of spatial memory (Ito, 2018). The retrosplenial cortex has been identified as crucial for allocentric navigation and the flexible transition between egocentric representations and allocentric representations (Vann et al., 2009). Ch4p atrophy may lead to disrupted projections from the BF to the medial frontal cortex and retrosplenial cortex and thus subsequent allocentric deficits. Although Ch4 also projects to the posterior parietal cortex (PPC), which mainly contributes to egocentric route planning, we did not observe significant correlations between Ch4p volumes and egocentric performance. We speculated that the Ch4-PPC cholinergic neurons were insusceptible to the earliest AD-related alterations and thus did not predict egocentric deficits in the SCD stage. Longitudinal studies with direct detection of functional assessment of cholinergic activity rather than mere BF volumetry are needed to further elucidate these speculations.

Neurons in Ch4p also project to the adjacent EC (Mesulam et al., 1983; Parizkova et al., 2018). We observed marked associations between total and left EC volumes and allocentric performance in the SCD group. The EC, particularly the medial part, processes self-motion generated and environmental landmark orienting signals to create an allocentric representation (Wang et al., 2020). In addition, the medial EC contains grid cells, which encode spatial information to form a cognitive map critical for allocentric strategies. Critically, young adults at genetic risk of AD (APOE ε4 carriers) exhibited reduced grid-cell-like representations and altered SN behavior in a virtual arena (Kunz et al., 2015). No significant associations between EC volumetry and navigation performance were detected either in the whole cohort or in the NC group. Therefore, we speculated that the negative relationships between EC volumes and allocentric errors did not represent a normal aging process but an SCD-related covariation.

The SCD vs. NC group difference may also modulate the relationship between BF and EC volumes and navigation behavior, with greater volume predicting better performance being more evident in the SCD group. These findings highlighted that stage specificity should be taken into consideration while investigating the associations between brain measures and behavior in AD-related studies (Qing et al., 2017).

LIMITATIONS

This study has some limitations. First, we conducted this cross-sectional study in a small cohort, which was mainly composed of female subjects; thus, enlarging the sample size, increasing the number of male participants, and collecting follow-up data is necessary for our future studies. Second, the SN test was performed on the computer, which might be difficult for participants with no computer experience, although the skill demands were relatively basic. Notably, although the computerized SN test has been suggested highly associated with the real-space SN test (Hort et al., 2007), we need to examine SN ability in virtual reality or real space in our future study to make the present findings more convincing (Coughlan et al., 2018). Third, since preclinical AD is a designation for individuals who exhibit pathological amyloid-β and tau deposits, it is critical to collect data on these biomarkers and direct evidence of cholinergic neurodegeneration in our future research, which may benefit a better understanding of the directionality between reports of SCD and BF atrophy. Further, a recent study has reported the effects of APOE ε4 on navigation (Coughlan et al., 2020), thus in our future study with a larger sample size, we need to regress out the potential effects of APOE genotype. Last, a more sophisticated EC mask containing subregions is needed, since the posteromedial part of the EC was believed to be more relevant to SN than the anterolateral part (Howett et al., 2019). Longitudinal studies with large cohorts, novel navigation paradigms, and sophisticated segmentation methods are needed for the systemic clarification of the neural basis underlying spatial deficits in SCD individuals in the future.

CONCLUSION

In the present study, we observed spatial disorientation in the SCD subjects, which may serve as a promising biomarker for the early detection of potential AD patients and indicate future cognitive deterioration. Furthermore, the volume reductions in the Ch4p subfield of BF suggested the structural neural basis for allocentric navigation deficits in the SCD stage. Our findings may provide novel insights into the early diagnosis and prognostic evaluation of subjects at higher risk of incipient AD.

DATA AVAILABILITY STATEMENT

The raw data supporting the conclusions of this article will be made available by the authors, without undue reservation.

ETHICS STATEMENT

The studies involving human participants were reviewed and approved by Human Participants Ethics Committee of Nanjing Drum Tower Hospital. The patients/participants provided their written informed consent to participate in this study.

AUTHOR CONTRIBUTIONS

QC was responsible for the conception and design of the present study, execution of the experimental work, and wrote the first draft of the manuscript. SW and XL undertook the conception of the study and the review and critique of the

manuscript. YS and WC executed the experimental work. JLu, WZ, JLi, and ZQ organized the research project and reviewed and critiqued the statistical analysis. ZN and JH provided the computerized spatial navigation test paradigm. XZ and BZ guided the design of the study protocol and reviewed and critiqued the manuscript. All authors contributed to the article and approved the submitted version.

FUNDING

This work was supported by the National Natural Science Foundation of China (81720108022, BZ, 81971596, XZ, 81701672, ZQ); the Fundamental Research Funds for the Central Universities, Nanjing University (2020-021414380462); the key project of Jiangsu Commission of Health (K2019025); the social development project of science and technology project in Jiangsu Province (BE2017707); key medical talents of the Jiangsu province, the 13th Five-Year health promotion project of the Jiangsu province (ZDRCA2016064); Jiangsu Provincial Key Medical Discipline (Laboratory) (ZDXKA2016020); the project of the sixth peak of talented people (WSN−138). The funders had no role in the study design, data collection, analysis, and decision to publish, or preparation of the manuscript.

SUPPLEMENTARY MATERIAL

The Supplementary Material for this article can be found online at: https://www.frontiersin.org/articles/10.3389/fnagi.2021.596025/full#supplementary-material

Supplementary Figure 1 | Correlations between spatial navigation distance errors and cognitive variables in the whole cohort. AEN, mixed alloegocentric navigation; EN, egocentric navigation; AN, allocentric navigation; DAN, delayed allocentric navigation; MMSE, Mini-mental state examination; SCD-Q, subjective cognitive decline questionnaire; AVLT, auditory verbal learning test; ROCF, Rey-Osterrieth complex figure; TMT-A, trail making test part A; TMT-B, trail making test part B; AFT, animal fluency test; BNT, Boston naming test; CDT, clock drawing test; SDMT, symbol digit modalities test. $^{*}p < 0.05$; $^{**}p < 0.01$; $^{***}p < 0.001$. Findings were adjusted for age, gender, and years of education.

Supplementary Figure 2 | Correlations between basal forebrain (BF) and entorhinal cortex (EC) volumes. NC, normal control; SCD, subjective cognitive decline. *P*-values were adjusted for age, gender, years of education, and total intracranial volume.

Supplementary Figure 3 | Correlations between basal forebrain (BF) and hippocampal (HP) volumes. NC, normal control; SCD, subjective cognitive decline. *P*-values were adjusted for age, gender, years of education, and total intracranial volume.

Supplementary Figure 4 | Comparisons of the correlations between basal forebrain (BF) and entorhinal cortex (EC) volumetry and spatial navigation distance errors between the subjective cognitive decline (SCD) and normal control (NC) groups. AN, allocentric navigation. *P*-values were adjusted for age, gender, years of education, total intracranial volume, and hippocampal volume.

Supplementary Table 1 | Comparisons of navigation distance errors between egocentric and allocentric strategies.Average distance errors (in pixels) in egocentric navigation (EN) and allocentric navigation (AN) subtests within the whole cohort, normal control (NC), and subjective cognitive decline (SCD) groups. Values are the mean ± SD. $^{*}p < 0.05$.

Supplementary Table 2 | Correlations between total EC and HP volumes and BF volumes.BF, basal forebrain; EC, entorhinal cortex; HP, hippocampus; NC, normal control; SCD, subjective cognitive decline. $^{*}p < 0.05$. P values were adjusted for age, gender, years of education, and total intracranial volume.

Supplementary Table 3 | Correlations between BF and EC volumetry and navigation distance errors in the whole cohort.AEN, alloegocentric navigation; EN, egocentric navigation; AN, allocentric navigation; DAN, delayed allocentric navigation; BF, basal forebrain; EC, entorhinal cortex. $^{*}p < 0.05$. P values were adjusted for age, gender, years of education, total intracranial volume, and hippocampal volume.

Supplementary Table 4 | Correlations between BF and EC volumetry and navigation distance errors in the SCD group.SCD, subjective cognitive decline; AEN, alloegocentric navigation; EN, egocentric navigation; AN, allocentric navigation; DAN, delayed allocentric navigation; BF, basal forebrain; EC, entorhinal cortex. $^{*}p < 0.05$. P values were adjusted for age, gender, years of education, total intracranial volume, and hippocampal volume.

Supplementary Table 5 | Correlations between BF and EC volumetry and navigation distance errors in the NC group. NC, normal control; AEN, alloegocentric navigation; EN, egocentric navigation; AN, allocentric navigation; DAN, delayed allocentric navigation; BF, basal forebrain; EC, entorhinal cortex. P values were adjusted for age, gender, years of education, total intracranial volume, and hippocampal volume.

Supplementary Box 1 | Subjective cognitive decline questionnaire.

REFERENCES

Ashburner, J. (2007). A fast diffeomorphic image registration algorithm. *Neuroimage* 38, 95–113. doi: 10.1016/j.neuroimage.2007.07.007

Berger-Sweeney, J., Stearns, N. A., Murg, S. L., Floerke-Nashner, L. R., Lappi, D. A., and Baxter, M. G. (2001). Selective immunolesions of cholinergic neurons in mice: effects on neuroanatomy, neurochemistry, and behavior. *J. Neurosci.* 21, 8164–8173. doi: 10.1523/JNEUROSCI.21-20-08164.2001

Botly, L. C., and De Rosa, E. (2009). Cholinergic deafferentation of the neocortex using 192 IgG-saporin impairs feature binding in rats. *J. Neurosci.* 29, 4120–4130. doi: 10.1523/JNEUROSCI.0654-09.2009

Botly, L. C., and De Rosa, E. (2012). Impaired visual search in rats reveals cholinergic contributions to feature binding in visuospatial attention. *Cereb. Cortex* 22, 2441–2453. doi: 10.1093/cercor/bhr331

Braak, H., and Del Tredici, K. (2015). The preclinical phase of the pathological process underlying sporadic Alzheimer's disease. *Brain* 138, 2814–2833. doi: 10.1093/brain/awv236

Chao-Gan, Y., and Yu-Feng, Z. (2010). DPARSF: a MATLAB toolbox for "pipeline" data analysis of resting-state fMRI. *Front. Syst. Neurosci.* 4:13. doi: 10.3389/fnsys.2010.00013

Colombo, D., Serino, S., Tuena, C., Pedroli, E., Dakanalis, A., Cipresso, P., et al. (2017). Egocentric and allocentric spatial reference frames in aging: a systematic review. *Neurosci. Biobehav. Rev.* 80, 605–621. doi: 10.1016/j.neubiorev.2017.07.012

Coughlan, G., Laczo, J., Hort, J., Minihane, A. M., and Hornberger, M. (2018). Spatial navigation deficits - overlooked cognitive marker for preclinical Alzheimer disease? *Nat. Rev. Neurol.* 14, 496–506. doi: 10.1038/s41582-018-0031-x

Coughlan, G., Zhukovsky, P., Puthusseryppady, V., Gillings, R., Minihane, A. M., Cameron, D., et al. (2020). Functional connectivity between the entorhinal and posterior cingulate cortices underpins navigation discrepancies in at-risk Alzheimer's disease. *Neurobiol. Aging* 90, 110–118. doi: 10.1016/j.neurobiolaging.2020.02.007

Dahnke, R., Yotter, R. A., and Gaser, C. (2013). Cortical thickness and central surface estimation. *Neuroimage* 65, 336–348. doi: 10.1016/j.neuroimage.2012.09.050

Davies, P., and Maloney, A. J. (1976). Selective loss of central cholinergic neurons in Alzheimer's disease. *Lancet* 2:1403. doi: 10.1016/S0140-6736(76)91936-X

Doeller, C. F., Barry, C., and Burgess, N. (2010). Evidence for grid cells in a human memory network. *Nature* 463, 657–661. doi: 10.1038/nature08704

Fan, L., Li, H., Zhuo, J., Zhang, Y., Wang, J., Chen, L., et al. (2016). The human brainnetome atlas: a new brain atlas based on connectional architecture. *Cereb. Cortex* 26, 3508–3526. doi: 10.1093/cercor/bhw157

Furey, M. L., Pietrini, P., and Haxby, J. V. (2000). Cholinergic enhancement and increased selectivity of perceptual processing during working memory. *Science* 290, 2315–2319. doi: 10.1126/science.290.5500.2315

Gifford, K. A., Liu, D., Romano, R. 3rd, Jones, R. N., and Jefferson, A. L. (2015). Development of a subjective cognitive decline questionnaire using item response theory: a pilot study. *Alzheimers Dement.* 1, 429–439. doi: 10.1016/j.dadm.2015.09.004

Glikmann-Johnston, Y., Carmichael, A. M., Mercieca, E. C., and Stout, J. C. (2019). "Real-life" hippocampal-dependent spatial memory impairments in Huntington's disease. *Cortex* 119, 46–60. doi: 10.1016/j.cortex.2019.04.006

Grothe, M., Heinsen, H., and Teipel, S. (2013). Longitudinal measures of cholinergic forebrain atrophy in the transition from healthy aging to Alzheimer's disease. *Neurobiol. Aging* 34, 1210–1220. doi: 10.1016/j.neurobiolaging.2012.10.018

Grothe, M., Heinsen, H., and Teipel, S. J. (2012). Atrophy of the cholinergic Basal forebrain over the adult age range and in early stages of Alzheimer's disease. *Biol. Psychiatry* 71, 805–813. doi: 10.1016/j.biopsych.2011.06.019

Grothe, M., Zaborszky, L., Atienza, M., Gil-Neciga, E., Rodriguez-Romero, R., Teipel, S. J., et al. (2010). Reduction of basal forebrain cholinergic system parallels cognitive impairment in patients at high risk of developing Alzheimer's disease. *Cereb. Cortex* 20, 1685–1695. doi: 10.1093/cercor/bhp232

Grothe, M. J., Ewers, M., Krause, B., Heinsen, H., and Teipel, S. J. (2014). Basal forebrain atrophy and cortical amyloid deposition in nondemented elderly subjects. *Alzheimers Dement.* 10, S344–S353. doi: 10.1016/j.jalz.2013.09.011

Hafting, T., Fyhn, M., Molden, S., Moser, M. B., and Moser, E. I. (2005). Microstructure of a spatial map in the entorhinal cortex. *Nature* 436, 801–806. doi: 10.1038/nature03721

Hamlin, A. S., Windels, F., Boskovic, Z., Sah, P., and Coulson, E. J. (2013). Lesions of the basal forebrain cholinergic system in mice disrupt idiothetic navigation. *PLoS ONE* 8:e53472. doi: 10.1371/journal.pone.0053472

Harris, M. A., Wiener, J. M., and Wolbers, T. (2012). Aging specifically impairs switching to an allocentric navigational strategy. *Front. Aging Neurosci.* 4:29. doi: 10.3389/fnagi.2012.00029

Henry, J. D., Crawford, J. R., and Phillips, L. H. (2004). Verbal fluency performance in dementia of the Alzheimer's type: a meta-analysis. *Neuropsychologia* 42, 1212–1222. doi: 10.1016/j.neuropsychologia.2004.02.001

Hong, Y. J., Kim, C. M., Jang, E. H., Hwang, J., Roh, J. H., and Lee, J. H. (2016). White matter changes may precede gray matter loss in elderly with subjective memory impairment. *Dement. Geriatr. Cogn. Disord.* 42, 227–235. doi: 10.1159/000450749

Hort, J., Andel, R., Mokrisova, I., Gazova, I., Amlerova, J., Valis, M., et al. (2014). Effect of donepezil in Alzheimer disease can be measured by a computerized human analog of the Morris water maze. *Neurodegener. Dis.* 13, 192–196. doi: 10.1159/000355517

Hort, J., Laczo, J., Vyhnalek, M., Bojar, M., Bures, J., and Vlcek, K. (2007). Spatial navigation deficit in amnestic mild cognitive impairment. *Proc. Natl. Acad. Sci. U. S. A.* 104, 4042–4047. doi: 10.1073/pnas.0611314104

Howard, R. (2020). Subjective cognitive decline: what is it good for? *Lancet Neurol.* 19, 203–204. doi: 10.1016/S1474-4422(20)30002-8

Howett, D., Castegnaro, A., Krzywicka, K., Hagman, J., Marchment, D., Henson, R., et al. (2019). Differentiation of mild cognitive impairment using an entorhinal cortex-based test of virtual reality navigation. *Brain* 142, 1751–1766. doi: 10.1093/brain/awz116

Ito, H. T. (2018). Prefrontal-hippocampal interactions for spatial navigation. *Neurosci. Res.* 129, 2–7. doi: 10.1016/j.neures.2017.04.016

Jak, A. J., Bondi, M. W., Delano-Wood, L., Wierenga, C., Corey-Bloom, J., Salmon, D. P., et al. (2009). Quantification of five neuropsychological approaches to defining mild cognitive impairment. *Am. J. Geriatr. Psychiatry* 17, 368–375. doi: 10.1097/JGP.0b013e31819431d5

Jessen, F., Amariglio, R. E., Buckley, R. F., Van Der Flier, W. M., Han, Y., Molinuevo, J. L., et al. (2020). The characterisation of subjective cognitive decline. *Lancet Neurol.* 19, 271–278. doi: 10.1016/S1474-4422(19)30368-0

Jessen, F., Amariglio, R. E., Van Boxtel, M., Breteler, M., Ceccaldi, M., Chételat, G., et al. (2014). A conceptual framework for research on subjective cognitive decline in preclinical Alzheimer's disease. *Alzheimers Dement.* 10, 844–852. doi: 10.1016/j.jalz.2014.01.001

Jessen, F., Feyen, L., Freymann, K., Tepest, R., Maier, W., Heun, R., et al. (2006). Volume reduction of the entorhinal cortex in subjective memory impairment. *Neurobiol. Aging* 27, 1751–1756. doi: 10.1016/j.neurobiolaging.2005.10.010

Kalová, E., Vlcek, K., Jarolímová, E., and Bures, J. (2005). Allothetic orientation and sequential ordering of places is impaired in early stages of Alzheimer's disease: corresponding results in real space tests and computer tests. *Behav. Brain Res.* 159, 175–186. doi: 10.1016/j.bbr.2004.10.016

Kerbler, G. M., Fripp, J., Rowe, C. C., Villemagne, V. L., Salvado, O., Rose, S., et al. (2015a). Basal forebrain atrophy correlates with amyloid β burden in Alzheimer's disease. *Neuroimage Clin.* 7, 105–113. doi: 10.1016/j.nicl.2014.11.015

Kerbler, G. M., Nedelska, Z., Fripp, J., Lacz,ó, J., Vyhnalek, M., Lis,ý, J., et al. (2015b). Basal forebrain atrophy contributes to allocentric navigation impairment in Alzheimer's disease patients. *Front. Aging Neurosci.* 7:185. doi: 10.3389/fnagi.2015.00185

Kilimann, I., Grothe, M., Heinsen, H., Alho, E. J., Grinberg, L., Amaro, E. Jr., et al. (2014). Subregional basal forebrain atrophy in Alzheimer's disease: a multicenter study. *J. Alzheimers Dis.* 40, 687–700. doi: 10.3233/JAD-132345

Kunz, L., Schröder, T. N., Lee, H., Montag, C., Lachmann, B., Sariyska, R., et al. (2015). Reduced grid-cell-like representations in adults at genetic risk for Alzheimer's disease. *Science* 350, 430–433. doi: 10.1126/science.aac8128

Laczó, J., Andel, R., Vlček, K., Macoška, V., Vyhnálek, M., Tolar, M., et al. (2011). Spatial navigation and APOE in amnestic mild cognitive impairment. *Neurodegener Dis.* 8, 169–177. doi: 10.1159/000321581

Laczó, J., Andel, R., Vyhnalek, M., Matoska, V., Kaplan, V., Nedelska, Z., et al. (2015). The effect of TOMM40 on spatial navigation in amnestic mild cognitive impairment. *Neurobiol. Aging* 36, 2024–2033. doi: 10.1016/j.neurobiolaging.2015.03.004

Laczo, J., Andel, R., Vyhnalek, M., Vlcek, K., Magerova, H., Varjassyova, A., et al. (2010). Human analogue of the morris water maze for testing subjects at risk of Alzheimer's disease. *Neurodegener. Dis.* 7, 148–152. doi: 10.1159/000289226

Laczo, J., Andel, R., Vyhnalek, M., Vlcek, K., Nedelska, Z., Matoska, V., et al. (2014). APOE and spatial navigation in amnestic MCI: results from a computer-based test. *Neuropsychology* 28, 676–684. doi: 10.1037/neu0000072

Laczó, J., Parizkova, M., and Moffat, S. D. (2018). Spatial navigation, aging and Alzheimer's disease. *Aging* 10, 3050–3051. doi: 10.18632/aging.101634

Lester, A. W., Moffat, S. D., Wiener, J. M., Barnes, C. A., and Wolbers, T. (2017). The aging navigational system. *Neuron* 95, 1019–1035. doi: 10.1016/j.neuron.2017.06.037

Li, A. W. Y., and King, J. (2019). Spatial memory and navigation in ageing: a systematic review of MRI and fMRI studies in healthy participants. *Neurosci. Biobehav. Rev.* 103, 33–49. doi: 10.1016/j.neubiorev.2019.05.005

Li, X., Wang, X., Su, L., Hu, X., and Han, Y. (2019). Sino Longitudinal Study on Cognitive Decline (SILCODE): protocol for a Chinese longitudinal observational study to develop risk prediction models of conversion to mild cognitive impairment in individuals with subjective cognitive decline. *BMJ Open* 9:28188. doi: 10.1136/bmjopen-2018-028188

Lithfous, S., Dufour, A., and Després, O. (2013). Spatial navigation in normal aging and the prodromal stage of Alzheimer's disease: insights from imaging and behavioral studies. *Ageing Res. Rev.* 12, 201–213. doi: 10.1016/j.arr.2012.04.007

Liu, A. K., Chang, R. C., Pearce, R. K., and Gentleman, S. M. (2015). Nucleus basalis of Meynert revisited: anatomy, history and differential involvement in Alzheimer's and Parkinson's disease. *Acta Neuropathol.* 129, 527–540. doi: 10.1007/s00401-015-1392-5

Mack, W. J., Freed, D. M., Williams, B. W., and Henderson, V. W. (1992). Boston Naming Test: shortened versions for use in Alzheimer's disease. *J. Gerontol.* 47, P154–158. doi: 10.1093/geronj/47.3.P154

Mcgeer, P. L., Mcgeer, E. G., Suzuki, J., Dolman, C. E., and Nagai, T. (1984). Aging, Alzheimer's disease, and the cholinergic system of the basal forebrain. *Neurology* 34, 741–745. doi: 10.1212/WNL.34.6.741

Meiberth, D., Scheef, L., Wolfsgruber, S., Boecker, H., Block, W., Träber, F., et al. (2015). Cortical thinning in individuals with subjective memory impairment. *J. Alzheimers Dis.* 45, 139–146. doi: 10.3233/JAD-142322

Mesulam, M. M., Mufson, E. J., Levey, A. I., and Wainer, B. H. (1983). Cholinergic innervation of cortex by the basal forebrain: cytochemistry and cortical connections of the septal area, diagonal band nuclei, nucleus basalis (substantia innominata), and hypothalamus in the rhesus monkey. *J. Comp. Neurol.* 214, 170–197. doi: 10.1002/cne.902140206

Nedelska, Z., Andel, R., Lacz,ó, J., Vlcek, K., Horinek, D., Lisy, J., et al. (2012). Spatial navigation impairment is proportional to right hippocampal volume. *Proc. Natl. Acad. Sci. U. S. A.* 109, 2590–2594. doi: 10.1073/pnas.1121588109

O'Keefe, J., and Nadel, L. (1978). *The Hippocampus as a Cognitive Map.*

Parizkova, M., Lerch, O., Moffat, S. D., Andel, R., Mazancova, A. F., Nedelska, Z., et al. (2018). The effect of Alzheimer's disease on spatial navigation strategies. *Neurobiol. Aging* 64, 107–115. doi: 10.1016/j.neurobiolaging.2017.12.019

Qing, Z., Li, W., Nedelska, Z., Wu, W., Wang, F., Liu, R., et al. (2017). Spatial navigation impairment is associated with alterations in subcortical intrinsic activity in mild cognitive impairment: a resting-state fMRI Study. *Behav. Neurol.* 2017:6364314. doi: 10.1155/2017/6364314

Raskind, M. A., Peskind, E. R., Wessel, T., and Yuan, W. (2000). Galantamine in AD: a 6-month randomized, placebo-controlled trial with a 6-month extension. the Galantamine USA-1 Study Group. *Neurology* 54, 2261–2268. doi: 10.1212/WNL.54.12.2261

Rockwood, K., Fay, S., Song, X., Macknight, C., and Gorman, M. (2006). Attainment of treatment goals by people with Alzheimer's disease receiving galantamine: a randomized controlled trial. *Cmaj* 174, 1099–1105. doi: 10.1503/cmaj.051432

Ryu, S. Y., Lim, E. Y., Na, S., Shim, Y. S., Cho, J. H., Yoon, B., et al. (2017). Hippocampal and entorhinal structures in subjective memory impairment: a combined MRI volumetric and DTI study. *Int. Psychogeriatr.* 29, 785–792. doi: 10.1017/S1041610216002349

Saykin, A. J., Wishart, H. A., Rabin, L. A., Santulli, R. B., Flashman, L. A., West, J. D., et al. (2006). Older adults with cognitive complaints show brain atrophy similar to that of amnestic MCI. *Neurology* 67, 834–842. doi: 10.1212/01.wnl.0000234032.77541.a2

Scheef, L., Grothe, M. J., Koppara, A., Daamen, M., Boecker, H., Biersack, H., et al. (2019). Subregional volume reduction of the cholinergic forebrain in subjective cognitive decline (SCD). *Neuroimage Clin.* 21:101612. doi: 10.1016/j.nicl.2018.101612

Schmitz, T. W., Spreng, R. N., and Alzheimer's Dis Neuroimaging, I. (2016). Basal forebrain degeneration precedes and predicts the cortical spread of Alzheimer's pathology. *Nat. Commun.* 7:13249. doi: 10.1038/ncomms13249

Selnes, P., Fjell, A. M., Gjerstad, L., Bjørnerud, A., Wallin, A., Due-Tønnessen, P., et al. (2012). White matter imaging changes in subjective and mild cognitive impairment. *Alzheimers Dement.* 8, S112–S121. doi: 10.1016/j.jalz.2011.07.001

Sheridan, L. K., Fitzgerald, H. E., Adams, K. M., Nigg, J. T., Martel, M. M., Puttler, L. I., et al. (2006). Normative symbol digit modalities test performance in a community-based sample. *Arch. Clin. Neuropsychol.* 21, 23–28. doi: 10.1016/j.acn.2005.07.003

Shin, M. S., Park, S. Y., Park, S. R., Seol, S. H., and Kwon, J. S. (2006). Clinical and empirical applications of the Rey-Osterrieth Complex Figure Test. *Nat. Protoc.* 1, 892–899. doi: 10.1038/nprot.2006.115

Shulman, K. I. (2000). Clock-drawing: Is it the ideal cognitive screening test? *Int. J. Geriatr. Psychiatry* 15, 548–561. doi: 10.1002/1099-1166(200006)15:6<548::AID-GPS242>3.0.CO;2-U

Solari, N., and Hangya, B. (2018). Cholinergic modulation of spatial learning, memory and navigation. *Eur. J. Neurosci.* 48, 2199–2230. doi: 10.1111/ejn.14089

Sperling, R. A., Aisen, P. S., Beckett, L. A., Bennett, D. A., Craft, S., Fagan, A. M., et al. (2011). Toward defining the preclinical stages of Alzheimer's disease: recommendations from the National Institute on Aging-Alzheimer's Association workgroups on diagnostic guidelines for Alzheimer's disease. *Alzheimers Dement.* 7, 280–292. doi: 10.1016/j.jalz.2011.03.003

Tariot, P. N., Solomon, P. R., Morris, J. C., Kershaw, P., Lilienfeld, S., and Ding, C. (2000). A 5-month, randomized, placebo-controlled trial of galantamine in AD. the galantamine USA-10 study group. *Neurology* 54, 2269–2276. doi: 10.1212/WNL.54.12.2269

Teipel, S. J., Meindl, T., Grinberg, L., Grothe, M., Cantero, J. L., Reiser, M. F., et al. (2011). The cholinergic system in mild cognitive impairment and Alzheimer's disease: an *in vivo* MRI and DTI study. *Hum. Brain Mapp.* 32, 1349–1362. doi: 10.1002/hbm.21111

Tombaugh, T. N., and Mcintyre, N. J. (1992). The mini-mental state examination: a comprehensive review. *J. Am. Geriatr. Soc.* 40, 922–935. doi: 10.1111/j.1532-5415.1992.tb01992.x

Vann, S. D., Aggleton, J. P., and Maguire, E. A. (2009). What does the retrosplenial cortex do? *Nat. Rev. Neurosci.* 10, 792–802. doi: 10.1038/nrn2733

Vogels, O. J., Broere, C. A., Ter Laak, H. J., Ten Donkelaar, H. J., Nieuwenhuys, R., and Schulte, B. P. (1990). Cell loss and shrinkage in the nucleus basalis Meynert complex in Alzheimer's disease. *Neurobiol. Aging* 11, 3–13. doi: 10.1016/0197-4580(90)90056-6

Wang, C., Chen, X., and Knierim, J. J. (2020). Egocentric and allocentric representations of space in the rodent brain. *Curr. Opin. Neurobiol.* 60, 12–20. doi: 10.1016/j.conb.2019.11.005

Wiener, J. M., De Condappa, O., Harris, M. A., and Wolbers, T. (2013). Maladaptive bias for extrahippocampal navigation strategies in aging humans. *J. Neurosci.* 33, 6012–6017. doi: 10.1523/JNEUROSCI.0717-12.2013

Wolf, D., Grothe, M., Fischer, F. U., Heinsen, H., Kilimann, I., Teipel, S., et al. (2014). Association of basal forebrain volumes and cognition in normal aging. *Neuropsychologia* 53, 54–63. doi: 10.1016/j.neuropsychologia.2013.11.002

Zhao, Q., Guo, Q., Li, F., Zhou, Y., Wang, B., and Hong, Z. (2013). The Shape Trail Test: application of a new variant of the Trail making test. *PLoS ONE* 8:e57333. doi: 10.1371/journal.pone.0057333

Zhao, Q., Lv, Y., Zhou, Y., Hong, Z., and Guo, Q. (2012). Short-term delayed recall of auditory verbal learning test is equivalent to long-term delayed recall for identifying amnestic mild cognitive impairment. *PLoS ONE* 7:e51157. doi: 10.1371/journal.pone.0051157

Zhao, W., Wang, X., Yin, C., He, M., Li, S., and Han, Y. (2019). Trajectories of the hippocampal subfields atrophy in the Alzheimer's disease: a structural imaging study. *Front. Neuroinform.* 13:13. doi: 10.3389/fninf.2019.00013

Conflict of Interest: The authors declare that the research was conducted in the absence of any commercial or financial relationships that could be construed as a potential conflict of interest.

frontiers in Aging Neuroscience

ORIGINAL RESEARCH
published: 22 February 2021
doi: 10.3389/fnagi.2021.630382

Altered Regional Cerebral Blood Flow and Brain Function Across the Alzheimer's Disease Spectrum: A Potential Biomarker

Qianqian Zhang[1], Qing Wang[1], Cancan He[1], Dandan Fan[1], Yao Zhu[1], Feifei Zang[1], Chang Tan[1], Shaoke Zhang[1], Hao Shu[1], Zhijun Zhang[1,2,3], Haixia Feng[4], Zan Wang[1] and Chunming Xie[1,2,3]**

[1] Department of Neurology, Affiliated ZhongDa Hospital, School of Medicine, Southeast University, Nanjing, China, [2] Neuropsychiatric Institute, Affiliated ZhongDa Hospital, School of Medicine, Southeast University, Nanjing, China, [3] The Key Laboratory of Developmental Genes and Human Disease, Southeast University, Nanjing, China, [4] Department of Nursing, Affiliated ZhongDa Hospital, School of Medicine, Southeast University, Nanjing, China

Objective: To investigate variation in the characteristics of regional cerebral blood flow (rCBF), brain activity, and intrinsic functional connectivity (FC) across the Alzheimer's disease spectrum (ADS).

Methods: The study recruited 20 individuals in each of the following categories: Alzheimer's disease (AD), mild cognitive impairment (MCI), subjective cognitive decline (SCD), and healthy control (HC). All participants completed the 3.0T resting-state functional MRI (rs-fMRI) and arterial spin labeling scans in addition to neuropsychological tests. Additionally, the normalized CBF, regional homogeneity (ReHo), and amplitude of low-frequency fluctuation (ALFF) of individual subjects were compared in the ADS. Moreover, the changes in intrinsic FC were investigated across the ADS using the abnormal rCBF regions as seeds and behavioral correlations. Finally, a support-vector classifier model of machine learning was used to distinguish individuals with ADS from HC.

Results: Compared to the HC subjects, patients with AD showed the poorest level of rCBF in the left precuneus (LPCUN) and right middle frontal gyrus (RMFG) among all participants. In addition, there was a significant decrease in the ALFF in the bilateral posterior cingulate cortex (PCC) and ReHo in the right PCC. Moreover, RMFG- and LPCUN-based FC analysis revealed that the altered FCs were primarily located in the posterior brain regions. Finally, a combination of altered rCBF, ALFF, and ReHo in posterior cingulate cortex/precuneus (PCC/PCUN) showed a better ability to differentiate ADS from HC, AD from SCD and MCI, but not MCI from SCD.

Conclusions: The study demonstrated the significance of an altered rCBF and brain activity in the early stages of ADS. These findings, therefore, present a potential diagnostic neuroimaging-based biomarker in ADS. Additionally, the study provides a better understanding of the pathophysiology of AD.

Keywords: Alzheimer's disease, arterial spin labeling, resting-state functional MRI, regional homogeneity, cerebral blood flow, amplitude of low frequency fluctuation

OPEN ACCESS

Edited by:
Rong Chen,
University of Maryland, Baltimore, United States

Reviewed by:
Xun-Heng Wang,
Hangzhou Dianzi University, China
Carlos Ayala Grosso,
Instituto Venezolano de Investigaciones Científicas (IVIC), Venezuela
Feng Bai,
Nanjing Drum Tower Hospital, China

***Correspondence:**
Chunming Xie
chmxie@163.com
Zan Wang
ujs_yingxiang0401@126.com

Received: *17 November 2020*
Accepted: *20 January 2021*
Published: *22 February 2021*

Citation:
Zhang Q, Wang Q, He C, Fan D, Zhu Y, Zang F, Tan C, Zhang S, Shu H, Zhang Z, Feng H, Wang Z and Xie C (2021) Altered Regional Cerebral Blood Flow and Brain Function Across the Alzheimer's Disease Spectrum: A Potential Biomarker. Front. Aging Neurosci. 13:630382. doi: 10.3389/fnagi.2021.630382

INTRODUCTION

Alzheimer's disease (AD) is one of the most important public health burdens worldwide. Notably, constant frustrations in drug development against the disease revealed the complexity of the pathogenic mechanism of AD. This, therefore, suggested that a more comprehensive study of specific neurobiological changes should be performed across the Alzheimer's disease spectrum (ADS), at both the preclinical and clinical stages. Moreover, the search for effective biomarkers is essential for the implementation of effective interventions before the development of significant neuronal damage.

Multimodal MRI has extensively been applied to investigate the abnormalities in brain structure and function in the ADS. In addition, the estimation of medial temporal lobe atrophy (MTA) by structural MRI (sMRI) is used as a neuroimaging biomarker in the diagnosis of AD (Ten et al., 2017). However, the obvious brain structure atrophy might imply the appearance of irreversible neuronal damage in the process of AD pathophysiology. In contrast, the resting-state functional MRI (rs-fMRI) can detect early functional changes in the brain reflected by the intrinsic blood-oxygen-level-dependent (BOLD) signals before the appearance of cognitive decline and brain structural atrophy (Galvin et al., 2011; Habib et al., 2017; Kawagoe et al., 2019). Moreover, several brain regions, including the hippocampus (HIP), posterior cingulate cortex (PCC), precuneus (PCUN), prefrontal cortex (PFC), temporal lobe, and angular gyrus (ANG) (Kawagoe et al., 2019; Xue et al., 2019; Zheng et al., 2019), have been reported as the core hub of brain networks involved in the pathophysiology of AD. Importantly, functional changes in the brain are independent of and even more sensitive than brain structure atrophy during the early stages of AD (Galvin et al., 2011; Xie et al., 2015; Kawagoe et al., 2019).

In addition, arterial spin labeling (ASL), utilizing intravascular water as an endogenous contrast agent, can measure regional cerebral blood flow (rCBF) (Ma et al., 2017). Notably, several studies consistently reported that rCBF displayed a decreasing trend with the progression of cognitive impairment in ADS (Binnewijzend et al., 2013; Ding et al., 2014; Trebeschi et al., 2016; Ma et al., 2017; Li et al., 2020). Moreover, compared to the age-matched subjects of health control (HC) and subjects of subjective cognitive decline (SCD), subjects of the mild cognitive impairment (MCI) and patients with AD presented decreased perfusion in the parietal lobe, PCC/PCUN, and occipital lobe (Binnewijzend et al., 2013; Ding et al., 2014; Trebeschi et al., 2016; Ma et al., 2017; Duan et al., 2020). Furthermore, the perfusion patterns identified by ASL were highly congruent with that provided by PET (Schroeter et al., 2009; Riederer et al., 2018; Dolui et al., 2020). PCC/PCUN, as one of the core regions in the default mode network (DMN), has been widely reported to be associated with a decreased rCBF, disrupted activity, and a destructive brain network in subjects with MCI and subjects with AD (Yoshiura et al., 2009; Sierra-Marcos, 2017; Xue et al., 2019). Notably, functional abnormalities of PCC/PCUN were also associated with the increased amyloid burden and decreased hippocampal volume (Khan et al., 2020). Additionally, a recent study, which explored the correlation between an altered rCBF and brain function in AD, revealed that the combination of ASL and the amplitude of low-frequency fluctuations (ALFF) in the PCC/PCUN could be used as a potential biomarker for the diagnosis of AD (Zheng et al., 2019). However, whether the integration of an altered rCBF and functional parameters in PCC/PCUN is capable of predicting various stages of AD is still unclear.

Therefore, the present study aimed to investigate the altered brain perfusion and function in all phases of ADS. First, the study measured whole-brain rCBF, regional homogeneity (ReHo), and the ALFF in each subject through the ASL and rs-fMRI approaches. Second, a partial correlation analysis was performed between the altered regions of each modality image and neuropsychological tests in ADS to obtain the behavioral significance of these altered brain functions. Third, the study investigated the changes in whole-brain functional connectivity of the identified rCBF regions as a seed in the ADS. Finally, the altered rCBF, ALFF, and ReHo in PCC/PCUN were integrated to get an imaging biomarker for the prediction of the ADS using a linear support vector machine (SVM) based on the machine learning approach.

MATERIALS AND METHODS

Participants

Participants were recruited from media advertisements and neurology outpatient clinics of the Affiliated Zhongda Hospital, Southeast University (Nanjing, China). All the subjects and their relatives were then provided with all relevant details before signing a written informed consent to participate in the study. A total of 80 Han Chinese individuals from eastern China were included in the study. Additionally, the participants underwent a full neuropsychological test battery, physical examination, blood tests, and a multi-modal MRI brain scan. This study was approved by the Research Ethics Committee of the Affiliated Zhongda Hospital, Southeast University (Nanjing, China).

Neuropsychological Assessments

Comprehensive cognitive function assessment and neurological examination were conducted on all the participants by two experienced neuropsychiatrists. The items specifically included activities of daily living (ADL), the Hamilton Depression Scale (HAMD), the Hachinski Ischemic Scale (HIS), the Mini-Mental State Examination (MMSE), and additional tests that covered the four previously characterized cognitive domains, namely: memory (episodic memory), information processing speed, visuospatial function, and executive function. In addition, memory tests included the Auditory Verbal Learning Test-20-min-Delayed Recall (AVLT-20-min-DR), Logical Memory Test-20-min-Delayed Recall (LMT-20-min-DR), and the Rey–Osterrieth Complex Figure Test-20-min-Delayed Recall (ROCFT-20-min-DR). On the other hand, the information processing speed was measured using the Symbol Digit Modalities Test (DSST), Trail Making Tests-A (TMT-A), and the Stroop Color and Word Test A and B. Moreover, the visuospatial function domain included the Clock Drawing Test (CDT) and the ROCFT. Additionally, the executive function domain was

measured using the Stroop Color and Word Test C, the Digit Span Test (DST), the Verbal Fluency Test (VFT), the Trail Making Tests-B (TMT-B), and the Semantic Similarity Test (Shi et al., 2019). Finally, the raw scores of each test were transformed into *z*-scores using the mean and SD in order to calculate the composite score of each cognitive domain (Xie et al., 2012).

Inclusion and Exclusion Criteria

All subjects were independently evaluated and diagnosed by two experienced neuropsychiatrists. Participants were required to meet the following criteria: (1) 55–85 years old, (2) educational years ≥8, (3) right-handed, and (4) should have been from the Han Chinese population. In addition, the inclusion criteria for HC contained: (1) no memory complaints and normal in ADL, (2) all neuropsychological tests were within the normal range, and (3) no abnormal findings in routine brain MRI (Dubois et al., 2014; Yan et al., 2018). On the other hand, the eligibility criteria for SCD contained: (1) frequent complaints of memory problems; (2) normal neuropsychological performance of age- and education-matched norms; and (3) lack of impairments in the ADL (Dubois et al., 2014; Yan et al., 2018). Moreover, the inclusion criteria for MCI contained: (1) complaints of memory impairment for more than 3 months; (2) MMSE score ≥24 and HAMD ≤7; (3) objective impairment in at least one cognitive domain, AVLT-20-min-DR score within ≤1.5 SD of the same age- and education-adjusted norms (cut-off of ≤4 correct responses on 12 items for subjects); and (4) no dementia (Dunn et al., 2014; Shi et al., 2019). The clinical diagnosis of AD was based on the criteria by the National Institute of Neurological and Communicative Disorders and Stroke and the Alzheimer's Disease and Related Disorders Association (NINCDS-ADRDA). They included (1) a clear-cut history of worsening cognition over 6 months; (2) MMSE score <24; (3) impairments in the ADL; and (4) dementia (McKhann et al., 2011; Arevalo-Rodriguez et al., 2015).

On the other hand, the exclusion criteria were as follows: (1) history of serious neurological and psychiatric diseases including major depressive disorders, schizophrenia, hydrocephalus, significant cerebrovascular disorders, and brain trauma; (2) systemic illnesses, such as uncontrolled hypertension, diabetes, abnormalities in the thyroid hormone, folic acid levels, vitamin B12, or significant liver and kidney diseases; and (3) the inability to undergo an MRI scan (Xie et al., 2012; Shi et al., 2019).

Acquisition of MRI Data

All MRI data was obtained using the Siemens Verio 3Tesla MRI Scanner with an 8-channel head-coil. In addition, the rs-fMRI images were obtained using the following parameters: 240 time points, repetition time (TR) = 2,000 ms, echo time (TE) = 25 ms, flip angle = 90°, number of slices = 36, slice thickness = 4 mm, spatial resolution = 3.75 × 3.75 × 4 mm^3, acquisition matrix = 64 × 64, and field of view (FOV) = 240 × 240 mm^2. Additionally, the 3D magnetization-prepared rapid gradient echo (MP-RAGE) were acquired to get the T1-weighted images with the following data parameters: TR = 1,900 ms, TE = 2.48 ms, slice thickness = 1 mm, FA = 90°, FOV = 256 × 256 mm, gap = 0 mm, and number of slices = 176. Moreover, the ASL data was obtained using the following parameters: TI1 = 600 ms, TI2 = 1.6 s, flip angle = 90°, number of slices = 27, slice thickness = 4.0 mm, TR = 4 s, TE = 12 ms, FOV = 220 × 220 mm^2, and matrix size = 64 × 64.

Data Pre-processing

SPM8 software (http://www.fil.ion.ucl.ac.uk/spm) was used to analyze the T1-weighted and ASL images. First, the T1-weighted images were segmented into three parts [cerebrospinal fluid (CSF), gray matter (GM), and white matter] using the VBM8 toolbox (http://dbm.neuro.uni-jena.de/wordpress/vbm/). Out of these, the segmented GM volume was normalized and regressed out as a covariate to control the effects of GM volume on the analysis of rCBF, ALFF, ReHo, and FC. Thereafter, deformation matrices were used to co-register the ASL images to the corresponding native GM images, which were spatially normalized to the Montreal Neurological Institute (MNI) space. During spatial normalization, the ASL images were resampled into 2 × 2 × 2 mm^3 voxel size. Finally, the resulting ASL images were smoothened using an isotropic 6 mm Gaussian filter for subsequent multiple comparison analysis.

Additionally, Data Processing & Analysis for Brain Imaging (DPABI, http://www.rfmri.org) was used to perform ALFF, ReHo, and seed-based FC analysis on the rs-fMRI images (Yan et al., 2016). Briefly, the first 10 volumes for each subject were removed in case of possible instability in the rs-fMRI signal. The remaining 230 points in time were then corrected for timing differences before adopting the Friston 24-parameter model to regress out the effects of head motion from realignment (Qi et al., 2020). All subjects with cumulative translation and rotation of head motion were <2 mm or 2°. Thereafter, the original space was registered to the MNI space with a resampled voxel size of 3 mm isotropic by using the DARTEL templates created during the preprocessing of T1-weighted images (Ashburner, 2007), which could alleviate the interference from different brain structures between subjects. Following this, the normalized images were smoothed with a 6 × 6 × 6 mm Gaussian kernel to reduce variation. The effects of confounding factors were then removed and they included the global mean signal, CSF signal, and white matter signal (Zheng et al., 2019). Finally, the previously generated images were filtered between 0.01 and 0.08 Hz so as to control noise interferences.

Moreover, a seed-based connectivity analysis was adopted to investigate FC changes in the ADS. Regions showing significant differences in rCBF among the groups were selected as regions of interest (ROIs). The mean time series of the seed regions was extracted for each participant and correlated with each voxel of the whole brain to obtain the seed-based FC maps, which were then transformed to *z*-maps based on the Fisher *z*-transformation (Waltz et al., 2013; Wang et al., 2019).

Statistical Analyses

The analysis of variance (ANOVA) and chi-square tests were used for demographic characteristics. Additionally, the mixed analysis of covariance (ANCOVA) was used to calculate differences in clinical scores and images among subjects ($p < 0.05$, SPSS 20.0) after controlling for age, gender, and education. For image data analysis (voxel-wised ANCOVA), GM volume, age, and education were controlled as covariates of no interest, and the

Gaussian random field (GRF) theory was used for multiple comparison correction (cluster level $p < 0.05$, voxel-level $p < 0.001$). *Post hoc* analysis was also performed with the Bonferroni correction to evaluate differences between the four groups ($p < 0.05$).

Thereafter, a partial correlation analysis was used to investigate relationships between the behavioral scores and the altered rCBF, functional activity, and connectivity in all the subjects, after controlling for age, gender, and education as nuisance covariates ($p < 0.05/5 = 0.01$).

Finally, an SVM model based on the machine learning approach was adopted to obtain an imaging biomarker for the classification of the ADS by integrating the altered rCBF, ALFF, and ReHo in specific regions. Briefly, we used an SVM package, which was built in MATLAB, the LIBSVM toolbox to get optimal classifiers and test the power of classification (Pirooznia and Deng, 2006). The mean values of PCC/PCUN that showed significant group differences in rCBF, ALFF, and ReHo were employed as input features, which were all based on voxel-wise measures. Due to our limited sample size, the leave-one-out cross-validation (LOOCV) was used to quantify the power of classification (Wee et al., 2011). At last, receiver operating characteristic (ROC) curves were utilized to assess the performance of the classifier using the results from the LOOCV data. The classification performance was manifested at the area under the ROC curve (AUC), and the larger the AUC, the better the performance. Detailed information can be found in the **Supplementary Material**.

RESULTS

Demographic and Neuropsychological Tests

Table 1, **Supplementary Table 1**, and **Supplementary Figure 1** show the main demographic and clinical scores of all the subjects. There were no significant differences in age, gender, and education, as well as HAMD and HIS scores ($p > 0.05$), among the subjects. However, there were obvious differences in the MMSE, ADL, and composite *z*-scores of each cognitive domain between AD and the other three groups. *Post hoc* analysis revealed that the AD groups showed the worst behavioral performance when compared with the other three groups. In addition, more importantly, the four groups showed significant differences with each other in the episodic memory scores which decreased with disease severity (i.e., HC > SCD > MCI > AD).

Differences in Brain rCBF in the Four Groups

The voxel-wise ASL analysis showed that the altered rCBF was primarily located in the left PCUN (LPCUN) and the right middle frontal gyrus (MFG) in the four groups (**Figure 1A**). In addition, *post hoc* analysis indicated that patients with AD suffered the most severe CBF loss in both altered brain regions compared to the other three groups (**Figure 1B**). **Figure 1C** shows the correlations between the different brain rCBF regions and clinical tests in the SCD, MCI, and AD groups. The rCBF in the LPCUN showed a clear positive association with MMSE ($R^2 = 0.298$, $p < 0.001$), episodic memory ($R^2 = 0.125$, $p = 0.006$), information processing speed ($R^2 = 0.150$, $p = 0.002$), and executive function ($R^2 = 0.266$, $p < 0.001$). However, it was only related to MMSE ($R^2 = 0.160$, $p = 0.002$) and episodic memory ($R^2 = 0.122$, $p = 0.006$) (adjusted *p*-values were < 0.01) in the right MFG. Notably, the higher the neuropsychological scores, the higher the rCBF value was in these regions of the brain.

Altered Brain Activities Among Groups

Thereafter, the study measured intrinsic brain activity in each region using ALFF and ReHo (**Figures 2**, **3**). Significant changes in ALFF were shown in the bilateral PCC, LPCUN, and left paracentral lobule (PCL) as shown in **Figure 2A**. Additionally,

TABLE 1 | Comparison of demographic, clinical characteristics, and cognitive function in all subjects.

	HC ($n = 20$)	SCD ($n = 20$)	MCI ($n = 20$)	AD ($n = 20$)	*p*-Value
Age (years)	70.75 ± 5.37	68.60 ± 7.30	71.95 ± 5.93	73.00 ± 6.03	0.144
Gender (F/M)	8/12	16/4	12/8	10/10	0.067†
Education (years)	13.38 ± 2.89	12.35 ± 3.63	11.40 ± 3.73	10.75 ± 3.52	0.096
HAMD scores	0.50 ± 0.89	2.40 ± 3.96	2.85 ± 2.96	2.55 ± 3.46	0.176
HIS scores	1.75 ± 0.85	1.05 ± 1.32	1.60 ± 1.35	1.70 ± 1.26	0.459
ADL scores	20.00 ± 0.00	20.10 ± 0.45	20.15 ± 0.37	26.45 ± 7.20[cef]	<0.001
MMSE scores	28.60 ± 1.19	28.80 ± 1.28	26.95 ± 2.09	19.60 ± 3.27[cef]	<0.001
Composite *z*-scores of each cognitive domain					
Episodic memory	2.75 ± 1.27	1.37 ± 1.86[a]	−1.51 ± 1.16[bd]	−2.85 ± 0.94[cef]	<0.001
Visuospatial function	0.64 ± 0.66	0.50 ± 1.16	0.13 ± 1.20	−1.19 ± 2.57[ef]	0.002
Information processing speed	2.46 ± 2.31	1.16 ± 2.23	0.32 ± 2.83	−4.10 ± 2.71[cef]	<0.001
Executive function	2.49 ± 1.79	0.84 ± 1.98	0.62 ± 1.92[b]	−4.35 ± 2.61[cef]	<0.001

The values of p were obtained from the one-way ANOVA (age and education) and the ANCOVA (controlled for age, gender, and education) analysis, while the † p-value was obtained from the χ^2 test. Data are presented as mean ± SD. Significant differences were found in MMSE, ADL, and four cognitive domains among all the groups. Post hoc analysis (Bonferroni correction) further revealed the source of ANCOVA differences: (a) HC vs. SCD; (b) HC vs. MCI; (c) HC vs. AD; (d) SCD vs. MCI; (e) SCD vs. AD; (f) MCI vs. AD. HC, Healthy Control; SCD, Subjective Cognitive Decline; MCI, Mild Cognitive Impairment; AD, Alzheimer's Disease; F/M, Female/Male; MMSE, Mini-Mental State Examination; ADL, Activities of Daily Living; HAMD, Hamilton Depression Scale; HIS, Hachinski Ischemic Scale.

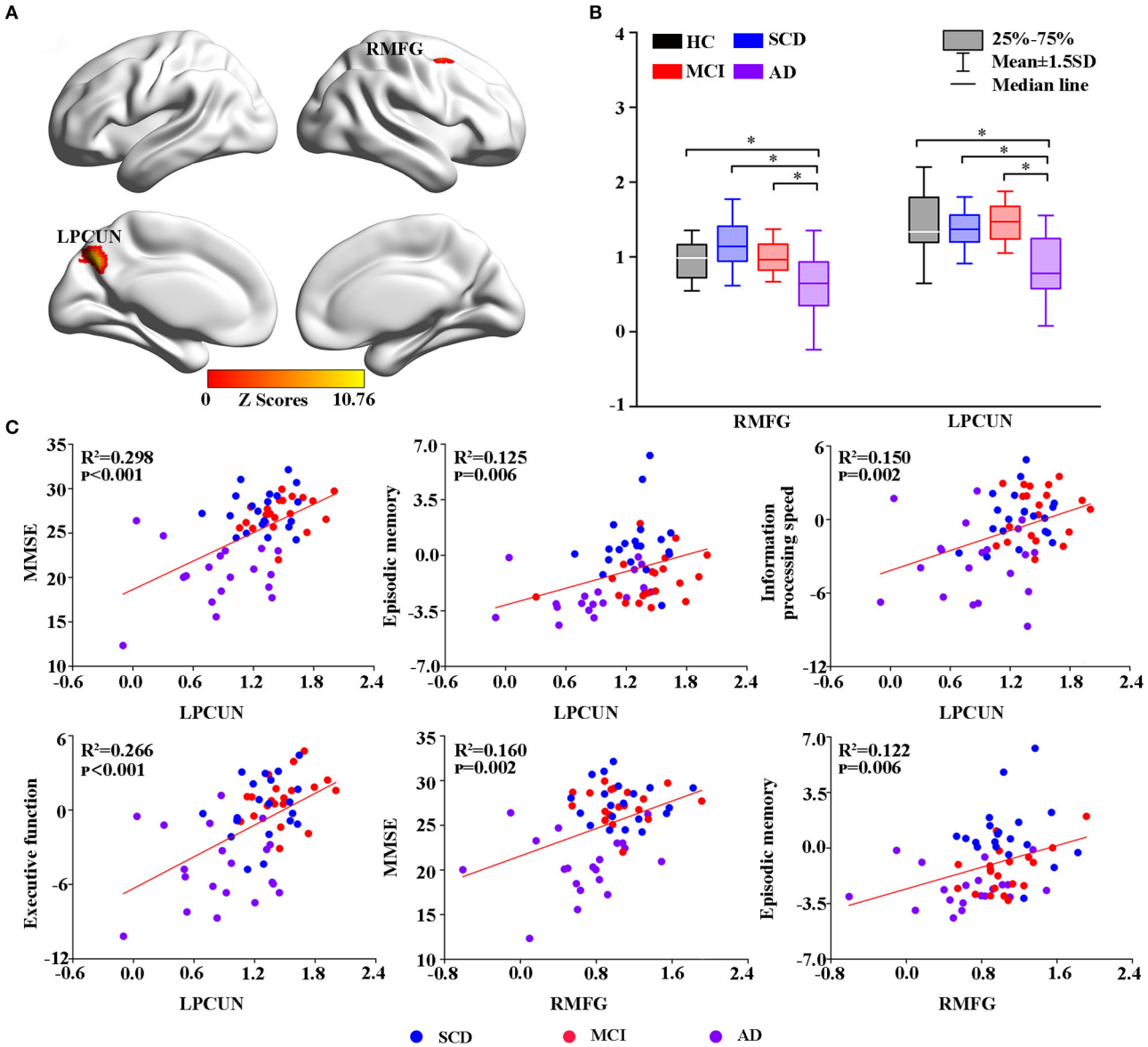

FIGURE 1 | Group-level differences in rCBF among all subjects and behavioral significance. **(A)** The result revealed altered rCBF regions among the groups including LPCUN and RMFG (GRF-corrected, cluster level $p < 0.05$, voxel-level $p < 0.001$). The color bar represents the *z*-scores. **(B)** *Post hoc* analysis of the altered rCBF in the LPCUN and RMFG regions in all the groups (Bonferroni correction, $p < 0.05$). Box plots show the 25 percentile, the median, and the 75 percentile, and whisker plots are in mean ± SD. *Represents statistical difference ($p < 0.05$). **(C)** Significant correlations between the altered rCBF and cognitive performance in the SCD, MCI, and AD groups after controlling the effects of age, gender, education, and GM volumes as covariates of no interest ($p < 0.01$). AD, Alzheimer's Disease; MCI, Mild Cognitive Impairment; SCD, Subjective Cognitive Decline; HC, Healthy Control; MMSE, Mini-Mental State Examination; rCBF, Regional Cerebral Blood Flow; LPCUN, Left Precuneus; RMFG, Right Middle Frontal Gyrus; GM, Gray Matter; GRF, Gaussian Random Field.

ReHo was significantly altered in the bilateral PCUN, left inferior parietal (IPL), left middle temporal gyrus (MTG), and right superior occipital gyrus (SOG) among the groups (**Figure 3A**). Moreover, the groups with the disease showed decreased ALFF and ReHo compared to the HC group (**Figures 2B**, **3B**). It is also worth noting that ReHo significantly increased in the MCI group in most of the altered brain regions except for the right PCUN (**Figure 3B**). Furthermore, partial correlation analysis revealed the relationship between brain activity and the neuropsychological scores (adjusted *p*-values were < 0.01) as shown in **Figures 2C**, **3C**. The results revealed a negative correlation between the ALFF in the LPCL and MMSE ($R^2 = 0.121$, $p = 0.006$), as indicated in **Figure 2C**. In contrast, ReHo was positively associated with MMSE (LPCUN: $R^2 = 0.229$, $p < 0.001$; LMTG: $R^2 = 0.191$, $p = 0.001$), information processing speed (LPCUN: $R^2 = 0.254$, $p < 0.001$; LMTG: $R^2 = 0.147$, $p =$

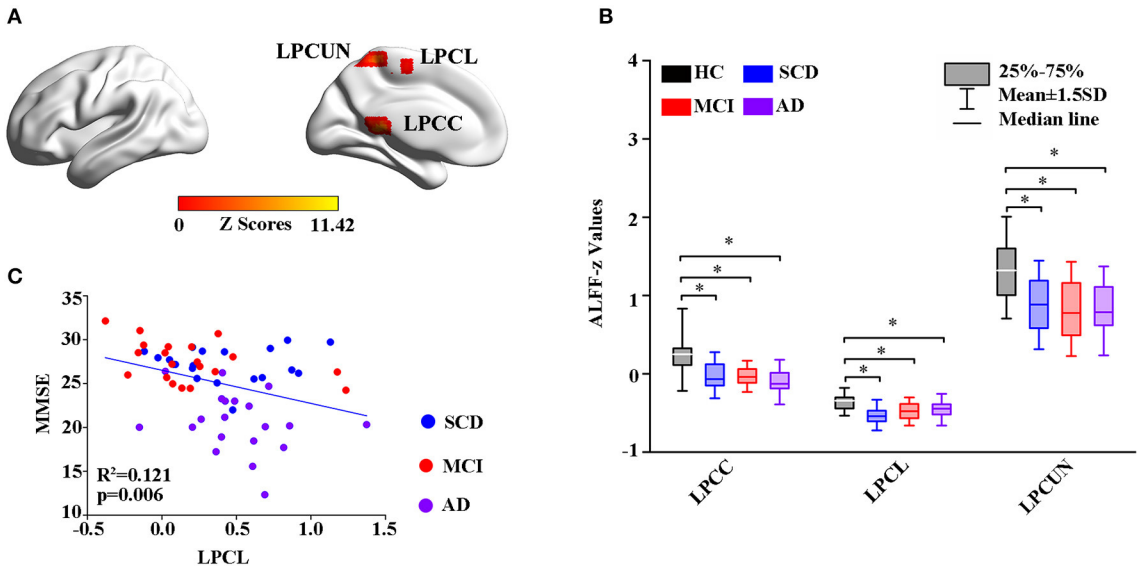

FIGURE 2 | Group-level differences in ALFF among the subjects and behavioral significance. **(A)** The results showed the altered ALFF regions among the groups including LPCUN, LPCL, and LPCG (GRF-corrected, cluster level $p < 0.05$, voxel-level $p < 0.001$). Color bars represent the *z*-scores. **(B)** *Post hoc* analysis for the altered ALFF regions in all the groups (Bonferroni correction, $p < 0.05$). Box plots show the 25 percentile, the median, and the 75 percentile, and whisker plots are in mean ± SD. *Represents statistical difference ($p < 0.05$). **(C)** Significant correlations between the altered ALFF and neuropsychological tests in the SCD, MCI, and AD groups after controlling the effects of age, gender, education, and GM volumes as covariates of no interest ($p < 0.01$). AD, Alzheimer's Disease; MCI, Mild Cognitive Impairment; SCD, Subjective Cognitive Decline; HC, Healthy Control; MMSE, Mini-Mental State Examination; ALFF, Amplitude of Low-Frequency Fluctuation; LPCUN, Left Precuneus; LPCL, Left Paracentral Lobule; BPCG, Bilateral Posterior Cingulate Gyrus; GM, Gray Matter; GRF, Gaussian Random Field.

0.002), and executive function (LPCUN: $R^2 = 0.266$, $p < 0.001$; LMTG: $R^2 = 0.185$, $p = 0.001$) in the LPCUN and left MTG as shown in **Figure 3C**. Moreover, there was a significant positive correlation between the ReHo of the LPCUN and the episodic memory ($R^2 = 0.118$, $p = 0.007$), as highlighted in **Figure 3C**.

Functional Connectivity Changes in the Resting State

Using the altered rCBF regions as ROIs, the study then performed a seed-based FC analysis (**Figures 4**, **5**). The results showed significant differences in the FC of RMFG with bilateral SOG, right supramarginal gyrus (SMG), and right fusiform gyrus (RFFG) among the groups (**Figure 4A**). Notably, the bilateral SOG and right SMG showed decreased FC strength in MCI compared to SCD, while the maximum reduction was only observed in the AD group across all regions (**Figure 4B**). After adjusting the values of *p*, the partial correlation analysis also revealed that the FC strength of RMFG-RSOG significantly affected the visuospatial function in the disease groups ($R^2 = 0.109$, $p = 0.009$) (adjusted *p*-values are < 0.01) as shown in **Figure 4C**.

Moreover, group changes were widely observed between LPCUN and the left median cingulate, between paracingulate gyrus (DCG) and olfactory cortex (OLF), right cuneus (RCUN), superior temporal gyrus (STG), lingual gyrus (LING), and FFG (**Figure 5A**). Interestingly, although FC was significantly decreased in ADS compared to the HC group, patients with AD displayed an obvious increase in all the different regions compared to the SCD and MCI groups (**Figure 5B**). Furthermore, the partial correlation analysis revealed significant negative correlations between the FC strength of LPCUN-RCUN and MMSE ($R^2 = 0.177$, $p = 0.001$), episodic memory ($R^2 = 0.121$, $p = 0.007$), and executive function ($R^2 = 0.131$, $p = 0.005$) (adjusted *p*-values are < 0.01) as shown in **Figure 5C**.

Analysis of the Altered rCBF, ALFF, and ReHo as Biomarkers in PCC/PCUN

Finally, the altered rCBF, ALFF, and ReHo in PCC/PCUN were used to conduct a ROC analysis. The results in **Supplementary Figure 2** show that the study was able to differentiate all the disease groups from HC through the classification of altered ReHo (**Supplementary Figure 2B**) or ALFF (**Supplementary Figure 2C**) but not altered rCBF, which could only differentiate AD from HC (**Supplementary Figure 2A**). Within the disease groups, the altered rCBF (**Supplementary Figure 2D**) and ReHo (**Supplementary Figure 2E**) were satisfactory in their ability to classify AD and MCI, AD, and SCD but not MCI and SCD. However, the altered ALFF showed the worst performance with regard to classification (**Supplementary Figure 2F**). Nonetheless, a combination of altered rCBF, ALFF, and ReHo in PCC/PCUN showed a better differentiating ability across the AD spectrum (**Figure 6**). Therefore, using this classification, the AUC was 0.978 (95% confidence intervals from 0.942 to 1.000, $p < 0.001$), 0.958 (95% confidence intervals from 0.897 to 1, $p < 0.001$), and 0.915 (95% confidence intervals from 0.82 to 1,

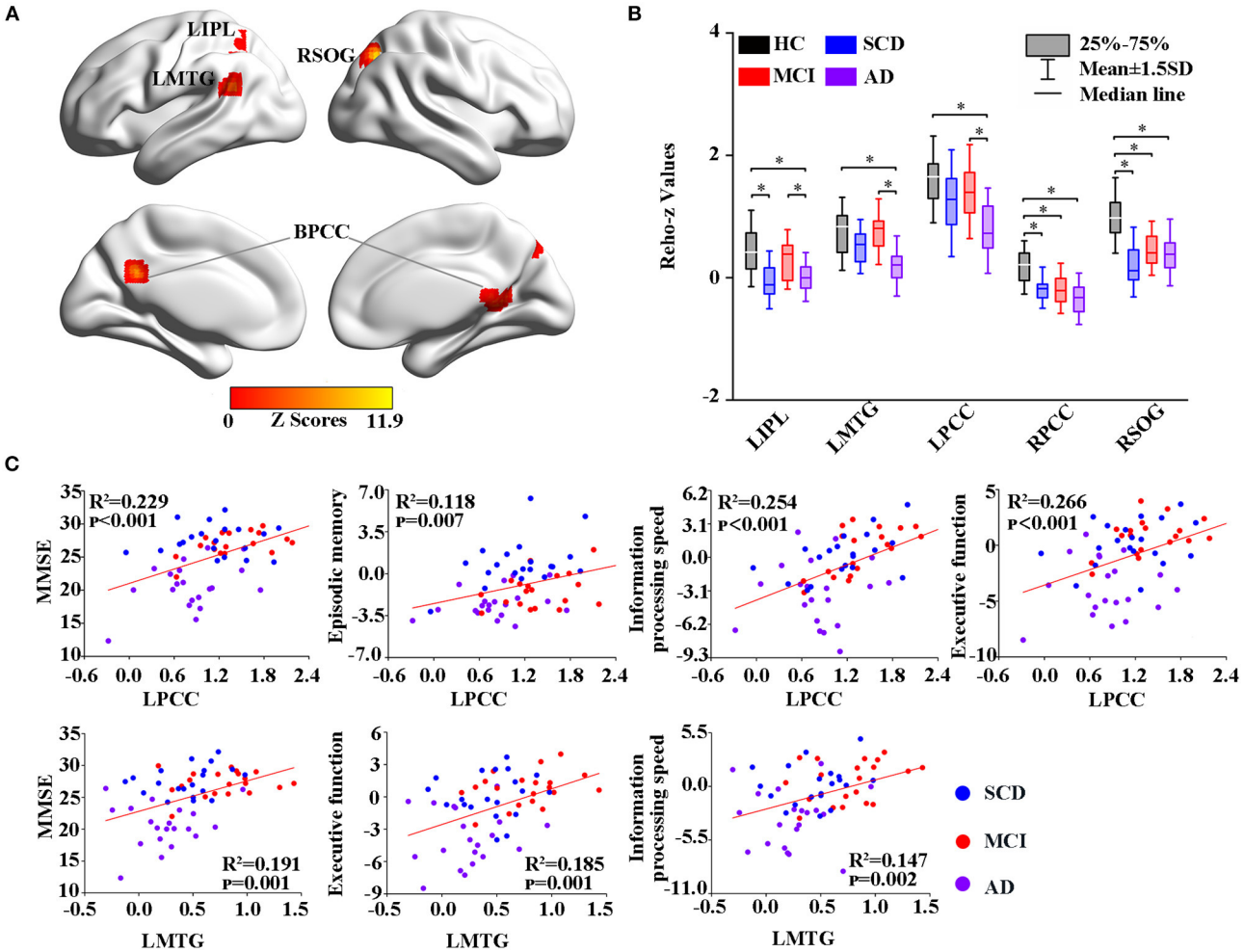

FIGURE 3 | Group-level differences in ReHo among all the subjects and behavioral significance. **(A)** The results showed the altered ReHo regions among the groups, including BPCG, LIPL, LMTG, and RSOG (GRF-corrected, cluster level $p < 0.05$, voxel-level $p < 0.001$). **(B)** *Post hoc* analysis of the altered ReHo regions in all the groups (Bonferroni correction, $p < 0.05$). Box plots show the 25 percentile, the median, and the 75 percentile, and whisker plots are in mean ± SD. *Represents statistical difference ($p < 0.05$). **(C)** Significant correlations between the altered ReHo and neuropsychological tests in the SCD, MCI, and AD groups after controlling the effects of age, gender, education, and GM volumes as covariates of no interest ($p < 0.01$). AD, Alzheimer's Disease; MCI, Mild Cognitive Impairment; SCD, Subjective Cognitive Decline; HC, Healthy Control; MMSE, Mini-Mental State Examination; ReHo, Regional Homogeneity; BPCG, Bilateral Posterior Cingulate Gyrus; LIPL, Left Inferior Parietal; LMTG, Left middle Temporal gyrus; RSOG, Right Superior Occipital Gyrus; GM, Gray Matter; GRF, Gaussian Random Field.

$p < 0.001$) in the distinction of AD, MCI, and SCD from HC, respectively (**Figure 6A**). Moreover, the AUC of the difference between MCI and AD was 0.933 (95% confidence intervals from 0.855 to 1, $p < 0.001$) while that of SCD and AD was 0.86 (95% confidence intervals from 0.744 to 0.977, $p < 0.001$). However, the combination displayed a poor ability to differentiate MCI from SCD (AUC value = 0.623, 95% confidence intervals from 0.445 to 0.8, $p = 0.224$) as shown in **Figure 6B**.

DISCUSSION

This study aimed to explore the changing patterns in rCBF, brain function, and the behavioral significance across the ADS. First, the results showed that the rCBF in LPCUN and RMFG of the AD group decreased significantly compared to the other three groups. It also had a significant positive association with most cognitive tests except for visuospatial function. Second, the results revealed that the aberrant activity and function were mainly in the posterior brain regions. Compared to the HC group, the ALFF in LPCC/PCUN and the LPCL as well as ReHo in RPCC and RSOG showed an obvious decrease across the disease groups. In addition, ReHo in LMTG, LPCC, and LIPL of the MCI group was higher than that of the AD group. Furthermore, the partial correlation analysis revealed that there was a negative association between ALFF in the LPCL and the MMSE scores, while ReHo in LPCC and LMTG had a positive association with most of the behavioral tests. Additionally, it was shown that the identified regions of the brain had a significant dysfunction in FC and were closely related to cognitive performance. Finally, a combination of altered rCBF, ALFF,

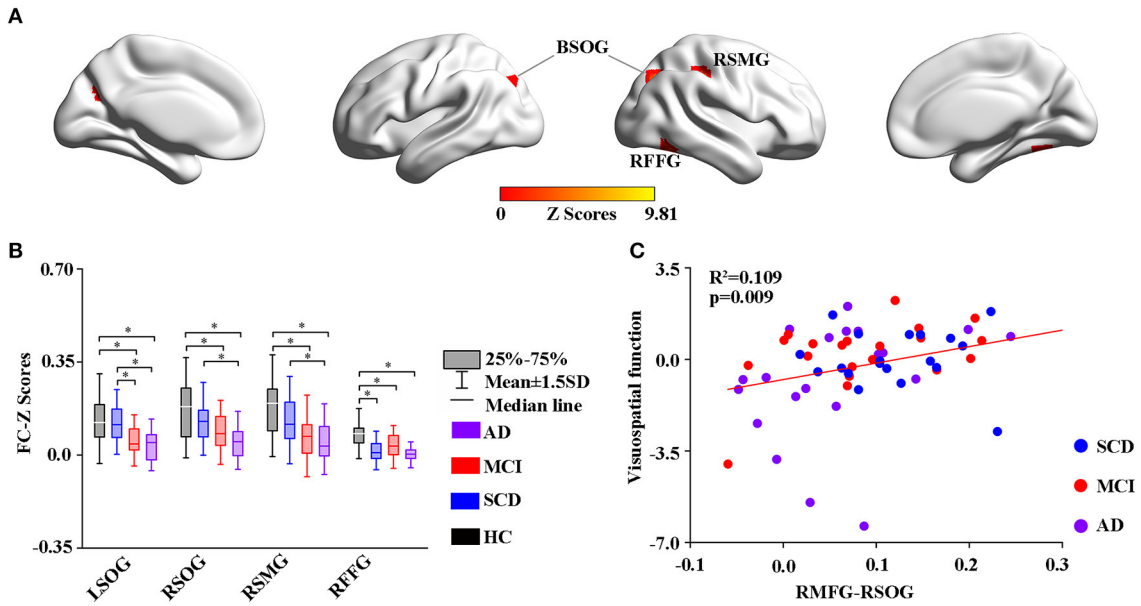

FIGURE 4 | Group-level differences in RMFG-based functional connectivity among the subjects and behavioral significance. **(A)** The results showed the altered FC brain regions among the groups including BSOG, RITG, and RSMG (GRF-corrected, cluster level $p < 0.05$, voxel-level $p < 0.001$). **(B)** *Post hoc* analysis of the altered FC regions in all the groups (Bonferroni correction, $p < 0.05$). Box plots show the 25 percentile, the median, and the 75 percentile, whisker plots are in mean ± SD. *Indicates statistical difference ($p < 0.05$). **(C)** Significant correlations between the altered FC and cognitive performance in the SCD, MCI, and AD groups ($p < 0.01$) after controlling the effects of age, gender, education, and GM volumes as covariates of no interest ($p < 0.01$). AD, Alzheimer's Disease; MCI, Mild Cognitive Impairment; SCD, Subjective Cognitive Decline; HC, Healthy Control; FC, Function Connectivity; BSOG, Bilateral Superior Occipital Gyrus; RFFG, Right Fusiform Gyrus; RSMG, Right Supramarginal Gyrus; GM, Gray Matter; GRF, Gaussian Random Field.

and ReHo in PCC/PCUN showed a better differentiating ability across the ADS.

Differences in rCBF in the ADS

In this study, there was a significant decrease in rCBF in the LPCUN and the RMFC of the AD group. In addition, rCBF was positively associated with cognitive function, consistent with the previous studies (Johnson et al., 2005; Alexopoulos et al., 2012; Hays et al., 2016; Kawagoe et al., 2019; Thomas et al., 2019; Duan et al., 2020). Additionally, a community-based cohort study showed that higher levels of rCBF were associated with better attention, executive function, and memory (Leeuwis et al., 2018). A previous study also showed that the lower the level of rCBF, the worse the cognitive performance was in patients with AD (Leeuwis et al., 2017). Notably, the DMN has two core regions, namely the MFG and the PCUN. The MFG is mainly related to attention, working memory, and regulation of emotions (Seminowicz and Moayedi, 2017), while PCUN is primarily involved in the retrieval of episodic memory, self-consciousness, and processing of the self-relevant effect (Zhang and Li, 2012). Moreover, necropsy revealed that MFG and PCUN were susceptible to Aβ deposition and hypoperfusion in the early stages of AD (Thomas et al., 2015; Miners et al., 2016). According to a previous report, a decrease in CBF starts from the PCUN and propagates along the PCC to other regions of the brain. More importantly, hypoperfusion in these regions showed no significant association with the distribution of brain atrophy in the early onset of familial AD (Benzinger et al., 2013). However, similar hypoperfusion was identified in the late-onset sporadic AD and showed the most pronounced decrease of CBF in PCUN and PCC, as well as in the prefrontal, parietal, and occipital cortices (Binnewijzend et al., 2013). Moreover, CBF in the prefrontal cortex was shown to be highly sensitive in the prediction of future cognitive performance (De Vis et al., 2018), while decreased CBF in the PCUN was considered to be a marker of severity in cognitive impairment (Binnewijzend et al., 2013). Intriguingly, aberrant local perfusion in the brain revealed that neurovascular dysfunction is commonly present in ADS. This also implied that the reduction in rCBF may be closely related to the progression of pathological processes in AD (Leeuwis et al., 2017), forming a vicious circle. Notably, decreased brain perfusion reduces the clearance of Aβ, leading to the accumulation of amyloid plaques and neurofibrillary tangles, which further impair vascular function and exacerbate the reduction of CBF (Popa-Wagner et al., 2015). As such, the altered rCBF may interfere with brain function and aggravate cognitive decline in the ADS.

Changes in Brain Activity and FC Among the Subjects

The study identified multiple areas of the brain with decreased activity and disrupted FC (Liu et al., 2008; Han et al., 2012; Zhang et al., 2012; Pan et al., 2017; Min et al., 2019). Additionally, two recent meta-analyses demonstrated that the decreased ALFF

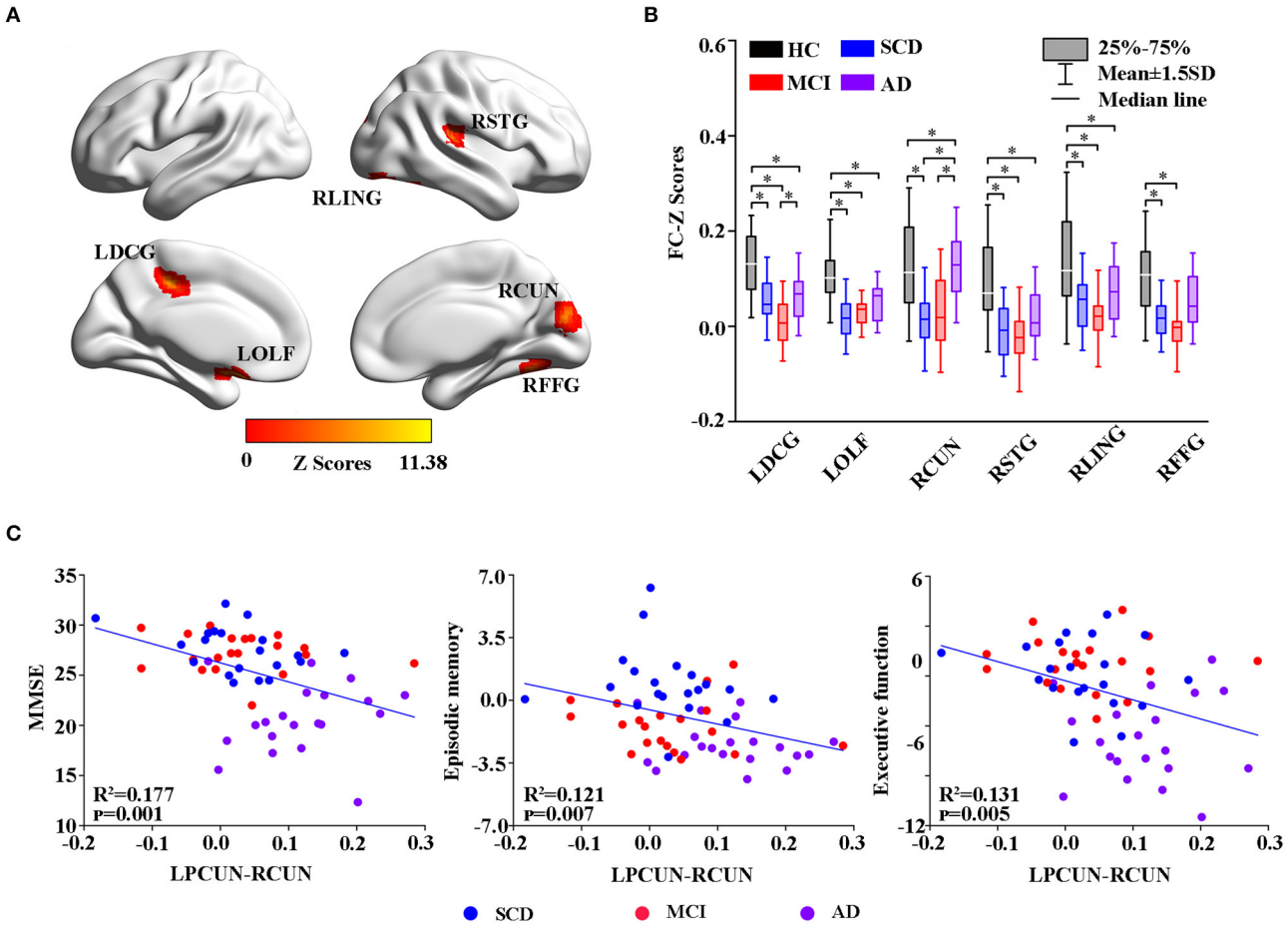

FIGURE 5 | Group-level differences in the LPCUN-based functional connectivity across the subjects and behavioral significance. **(A)** The results showed the altered FC brain regions among the groups including LDCG, LOLF, RCUN, RSTG, RLING, and RFFG (GRF-corrected, cluster level $p < 0.05$, voxel-level $p < 0.001$). **(B)** *Post hoc* analysis of the altered FC regions in all the groups (Bonferroni correction, $p < 0.05$). Box plots show the 25 percentile, the median, and the 75 percentile, whisker plots are in mean ± SD. *Indicates statistical difference ($p < 0.05$). **(C)** Significant correlations between the altered FC and neuropsychological tests in the SCD, MCI, and AD groups after controlling the effects of age, gender, education, and GM volumes as covariates of no interest ($p < 0.01$). AD, Alzheimer's Disease; MCI, Mild Cognitive Impairment; SCD, Subjective Cognitive Decline; HC, Healthy Control; FC, Function Connectivity; LDCG, Left Median Cingulate and Paracingulate Gyri; LOLF, Left Olfactory Cortex; RCUN, Right Cuneus; RSTG, Right Superior Temporal Gyrus; RLING, Right Lingual Gyrus; RFFG, Right Fusiform Gyrus; GM, Gray Matter; GRF, Gaussian Random Field.

and ReHo in patients with MCI were primarily located in the BPCC/PCUN, bilateral frontal, left occipitotemporal cortex, and parietal lobule compared to HC (Pan et al., 2017; Zhen et al., 2018). In the present study, the findings showed that the altered regions were mainly located in the posterior areas of the brain, including the PCC/PCUN, LMTG, IPL, SOG, FFG, and LING. These constitute parts of the DMN, the executive control network (ECN), and the visual network (VN) (Pan et al., 2017; Zhen et al., 2018). Moreover, numerous studies reported on the interruption of the connectivity of DMN, ECN, and VN in MCI/AD (Bokde et al., 2006; Sorg et al., 2007; Brier et al., 2012; Wang et al., 2015; Joo et al., 2016; Eyler et al., 2019). It is also well-known that visual impairment is one of the most important clinical signs of AD and accounts for about 30% in MCI (Mapstone et al., 2003) and up to 50% in AD (Mendola et al., 1995). Additionally, a marked decrease in glucose metabolism was reported in the parietal and occipital cortices of patients with AD (Pietrini et al., 1996). Existing evidence suggests that visual impairment might arise from the abnormal connectivity of the VN and other regions of the brain (Bokde et al., 2006; Vannini et al., 2008; Zheng et al., 2019). However, it is important to note that both brain activity and FC significantly decreased as early as in SCD. This suggests that dysregulation of brain neuronal excitability appears before objective impairment upon formal testing and that might be a potential biomarker (Mattson and Arumugam, 2018; Si et al., 2020). Interestingly, the FC strength between LPCUN and the altered regions of the brain in the AD group showed an increasing trend compared to the SCD and MCI groups. Moreover, there was a significant negative correlation between the FC of LPCUN-RCUN and MMSE, episodic memory, and executive functioning. This may have been due to the slight global cognitive impairment in the preclinical stage of AD,

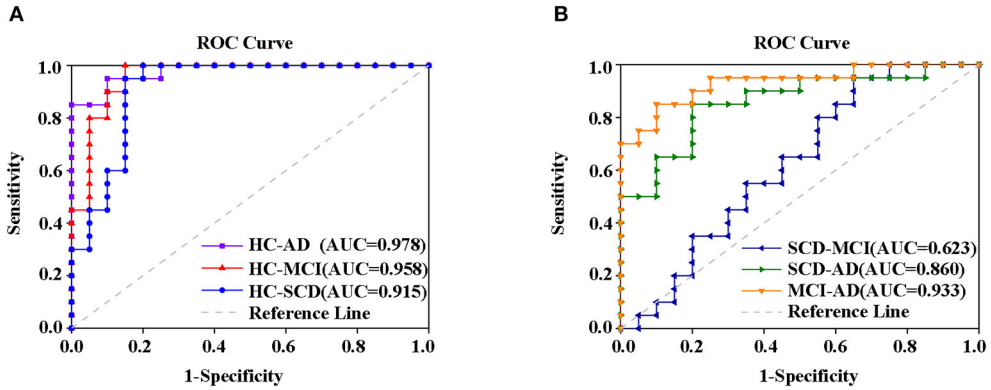

FIGURE 6 | ROC curve from the support vector machine classifier and the general ROC model for classification of the AD spectrum. The results revealed that the combination of altered rCBF, ALFF, and ReHo in PCC/PCUN had more power in differentiating subjects with ADS from HC **(A)** MCI and SCD from patients with AD but not **(B)** SCD from MCI. The classification was able to differentiate disease groups from HC. Specifically, the AUC for the AD patients was 0.978 (95% confidence intervals from 0.942 to 1.000, $p < 0.001$), the MCI had 0.958 (95% confidence intervals from 0.897 to 1, $p < 0.001$), and SCD had 0.915 (95% confidence intervals from 0.82 to 1, $p < 0.001$) **(A)**. Within disease groups, the combination showed a good ability to distinguish AD from MCI (AUC value = 0.933, 95% confidence intervals from 0.855 to 1, $p < 0.001$) as well as AD from SCD (AUC value = 0.86, 95% confidence intervals from 0.744 to 0.977, $p < 0.001$), but not MCI from SCD (AUC value = 0.623, 95% confidence intervals from 0.445 to 0.8, $p = 0.224$) **(B)**. The blue line represents the HC and AD group, the red line represents the HC and MCI group, the purple line represents the HC and AD group, the orange line represents the AD and MCI group, the green line represents the AD and SCD group, the dark blue line represents the MCI and SCD group, and the gray line represents the reference. AD, Alzheimer's Disease; MCI, Mild Cognitive Impairment; SCD, Subjective Cognitive Decline; HC, Healthy Normal; ROC, Receiver Operating Characteristic, AUC, Area Under the Curve; ALFF, Amplitude of Low-Frequency Fluctuation; ReHo, Regional Homogeneity.

which only manifested as decreased FC. However, the FC in the core hub of DMN led to a compensatory rise in order to maintain cognitive function during the progression of the disease (Qi et al., 2010). It is noteworthy that with continued amyloid deposition and substantial loss of neurons in the late stages of AD, DMN gradually falls out of the compensatory mode, leading to a severe decrease in FC (Tuovinen et al., 2016; Scherr et al., 2019). Furthermore, the results showed that the ALFF in LPCL had a negative association with the MMSE score. The PCL is located in the posterior ventral region of the inferior frontal gyrus (IFG), which is a crucial cortical node for the cognitive control in the circuits. Additionally, with the aggravation of cognitive impairment, the cortical motor regions in the circuits compensate for the damaged brain function by part activation (Zhang et al., 2020). In summary, the results suggested that there is a significant difference in brain activity and FC across the ADS, and the difference appears as early as in SCD. Moreover, the difference is closely correlated with cognitive performance and can be used as a potential imaging biomarker for monitoring disease progression in AD.

Altered rCBF, ALFF, and ReHo as Biomarkers in PCC/PCUN

Numerous studies have reported on the altered rCBF, the deposition of AD pathology biomarkers, and decreased brain function in the PCC/PCUN of AD (Benzinger et al., 2013; Aghakhanyan et al., 2018; Zhu et al., 2019). In addition, the rCBF was validated in a previous study as a diagnostic marker for AD but not for preclinical AD (Zheng et al., 2019). It is well-known that the machine learning method is widely employed for classification in clinical research and has been used for the prediction of AD and preclinical AD (Liu et al., 2013; Xu et al., 2018). Therefore, using SVM, the study performed an integrated analysis of altered rCBF, ALFF, and ReHo in PCC/PCUN as biomarkers to uncover the differentiating power across the AD spectrum. The results revealed that a combination of the three measured brain functional changes in PCC/PCUN has a better differentiating power across the ADS compared to each parameter. Notably, the combination was able to differentiate the disease groups from HC. Moreover, the combination displayed a good ability to distinguish between AD and MCI, AD and SCD, but not MCI and SCD in the disease groups. Therefore, the study demonstrated that a combination of multimodal neuroimaging in PCC/PCUN might be an effective biomarker for differentiating the ADS.

LIMITATIONS

Although the study supplemented and refined similar reports from the past, it had a number of limitations. First, there was no evidence of a biomarker for amyloid pathology and genetic data. Secondly, the study was a single-center cross-sectional study and might therefore have presented insufficient data. Thirdly, the sample size was relatively small and some analyses may have had insufficient power. Moving forward, more volunteers will be recruited to participate in the study. In addition, the study will refine the detection of pathological markers of AD and obtain genetic data. Finally, regular follow-up will be conducted in the future in order to further confirm the results.

CONCLUSION

This study demonstrated obvious changes in CBF, brain activity, and FC in the ADS, and these could appear in the early stages of the disease. In addition, a disrupted FC, decreased CBF, and brain

activity were associated with more serious cognitive impairment, reflecting brain neurovascular dysfunction in ADS. Finally, the combination of altered rCBF, ALFF, and ReHo in PCC/PCUN proved to be a powerful tool in differentiating the ADS and is therefore a potential neuroimaging biomarker.

DATA AVAILABILITY STATEMENT

The raw and processed data in this study cannot be shared at this time due to the ethics and the protection of privacy issues of the participants. And these data also forms part of an ongoing study.

ETHICS STATEMENT

The studies involving human participants were reviewed and approved by Research Ethics Committee of the Affiliated ZhongDa Hospital, Southeast University (Nanjing, China). The patients/participants provided their written informed consent to participate in this study.

AUTHOR CONTRIBUTIONS

ZZ, ZW, and CX were responsible for coordinating the entire data collection process and checking the quality of data during the collection period. YZ, FZ, CT, SZ, and HS were responsible for data collection. QW, CH, and DF were responsible for cognitive function assessment and neurological examination. QZ made a draft of the manuscript. HF polished the manuscript and language revision. All authors read and approved the final manuscript.

FUNDING

This research was supported by the National Key Projects for Research and Development Program of China (2016YFC1305800, 2016YFC1305802, CX); the National Natural Science Foundation of China (81671256, 81871069, 81271204, CX); the Key Project for Research and Development Program of Jiangsu Province (BE2018741); the social science fund of Jiangsu Province (19GLB025); and the Nanjing International Joint Research and Development Project (201715013).

SUPPLEMENTARY MATERIAL

The Supplementary Material for this article can be found online at: https://www.frontiersin.org/articles/10.3389/fnagi.2021.630382/full#supplementary-material

REFERENCES

Aghakhanyan, G., Vergallo, A., Gennaro, M., Mazzarri, S., Guidoccio, F., Radicchi, C., et al. (2018). The precuneus–a witness for excessive abeta gathering in Alzheimer's disease pathology. *Neurodegener. Dis.* 18, 302–309. doi: 10.1159/000492945

Alexopoulos, P., Sorg, C., Forschler, A., Grimmer, T., Skokou, M., Wohlschlager, A., et al. (2012). Perfusion abnormalities in mild cognitive impairment and mild dementia in Alzheimer's disease measured by pulsed arterial spin labeling MRI. *Eur. Arch. Psychiatry Clin. Neurosci.* 262, 69–77. doi: 10.1007/s00406-011-0226-2

Arevalo-Rodriguez, I., Smailagic, N., Roque, I. F. M., Ciapponi, A., Sanchez-Perez, E., Giannakou, A., et al. (2015). Mini-Mental State Examination (MMSE) for the detection of Alzheimer's disease and other dementias in people with mild cognitive impairment (MCI). *Cochrane Database Syst. Rev.* 2015:D10783. doi: 10.1002/14651858.CD010783.pub2

Ashburner, J. (2007). A fast diffeomorphic image registration algorithm. *Neuroimage* 38, 95–113. doi: 10.1016/j.neuroimage.2007.07.007

Benzinger, T. L., Blazey, T., Jack, C. J., Koeppe, R. A., Su, Y., Xiong, C., et al. (2013). Regional variability of imaging biomarkers in autosomal dominant Alzheimer's disease. *Proc. Natl. Acad. Sci. U.S.A.* 110, E4502–E4509. doi: 10.1073/pnas.1317918110

Binnewijzend, M. A., Kuijer, J. P., Benedictus, M. R., van der Flier, W. M., Wink, A. M., Wattjes, M. P., et al. (2013). Cerebral blood flow measured with 3D pseudocontinuous arterial spin-labeling MR imaging in Alzheimer disease and mild cognitive impairment: a marker for disease severity. *Radiology* 267, 221–230. doi: 10.1148/radiol.12120928

Bokde, A. L., Lopez-Bayo, P., Meindl, T., Pechler, S., Born, C., Faltraco, F., et al. (2006). Functional connectivity of the fusiform gyrus during a face-matching task in subjects with mild cognitive impairment. *Brain* 129, 1113–1124. doi: 10.1093/brain/awl051

Brier, M. R., Thomas, J. B., Snyder, A. Z., Benzinger, T. L., Zhang, D., Raichle, M. E., et al. (2012). Loss of intranetwork and internetwork resting state functional connections with Alzheimer's disease progression. *J. Neurosci.* 32, 8890–8899. doi: 10.1523/JNEUROSCI.5698-11.2012

De Vis, J. B., Peng, S. L., Chen, X., Li, Y., Liu, P., Sur, S., et al. (2018). Arterial-spin-labeling (ASL) perfusion MRI predicts cognitive function in elderly individuals: a 4-year longitudinal study. *J. Magn. Reson. Imaging* 48, 449–458. doi: 10.1002/jmri.25938

Ding, B., Ling, H. W., Huang, J., Zhang, H., Wang, T., Yan, F. H., et al. (2014). Pattern of cerebral hyperperfusion in Alzheimer's disease and amnestic mild cognitive impairment using voxel-based analysis of 3D arterial spin-labeling imaging: initial experience. *Clin. Interv. Aging* 9, 493–500. doi: 10.2147/CIA.S58879

Dolui, S., Li, Z., Nasrallah, I. M., Detre, J. A., and Wolk, D. A. (2020). Arterial spin labeling versus 18F-FDG-PET to identify mild cognitive impairment. *Neuroimage Clin.* 25:102146. doi: 10.1016/j.nicl.2019.102146

Duan, W., Sehrawat, P., Balachandrasekaran, A., Bhumkar, A. B., Boraste, P. B., Becker, J. T., et al. (2020). Cerebral blood flow is associated with diagnostic class and cognitive decline in Alzheimer's disease. *J. Alzheimers Dis.* 76, 1103–1120. doi: 10.3233/JAD-200034

Dubois, B., Feldman, H. H., Jacova, C., Hampel, H., Molinuevo, J. L., Blennow, K., et al. (2014). Advancing research diagnostic criteria for Alzheimer's disease: the IWG-2 criteria. *Lancet Neurol.* 13, 614–629. doi: 10.1016/S1474-4422(14)70090-0

Dunn, C. J., Duffy, S. L., Hickie, I. B., Lagopoulos, J., Lewis, S. J. G., Naismith, S. L., et al. (2014). Deficits in episodic memory retrieval reveal impaired default mode network connectivity in amnestic mild cognitive impairment. *Neuroimage Clin.* 4, 473–480. doi: 10.1016/j.nicl.2014.02.010

Eyler, L. T., Elman, J. A., Hatton, S. N., Gough, S., Mischel, A. K., Hagler, D. J., et al. (2019). Resting state abnormalities of the default mode network in mild cognitive impairment: a systematic review and meta-analysis. *J. Alzheimers Dis.* 70, 107–120. doi: 10.3233/JAD-180847

Galvin, J. E., Price, J. L., Yan, Z., Morris, J. C., and Sheline, Y. I. (2011). Resting bold fMRI differentiates dementia with Lewy bodies vs Alzheimer disease. *Neurology* 76, 1797–1803. doi: 10.1212/WNL.0b013e31821ccc83

Habib, M., Mak, E., Gabel, S., Su, L., Williams, G., Waldman, A., et al. (2017). Functional neuroimaging findings in healthy middle-aged adults at risk of Alzheimer's disease. *Ageing Res. Rev.* 36, 88–104. doi: 10.1016/j.arr.2017.03.004

Han, Y., Lui, S., Kuang, W., Lang, Q., Zou, L., and Jia, J. (2012). Anatomical and functional deficits in patients with amnestic mild cognitive impairment. *PLoS ONE* 7:e28664. doi: 10.1371/journal.pone.0028664

Hays, C. C., Zlatar, Z. Z., and Wierenga, C. E. (2016). The utility of cerebral blood flow as a biomarker of preclinical Alzheimer's disease. *Cell. Mol. Neurobiol.* 36, 167–179. doi: 10.1007/s10571-015-0261-z

Johnson, N. A., Jahng, G. H., Weiner, M. W., Miller, B. L., Chui, H. C., Jagust, W. J., et al. (2005). Pattern of cerebral hypoperfusion in Alzheimer disease and mild cognitive impairment measured with arterial spin-labeling MR imaging: initial experience. *Radiology* 234, 851–859. doi: 10.1148/radiol.2343040197

Joo, S. H., Lim, H. K., and Lee, C. U. (2016). Three large-scale functional brain networks from resting-state functional MRI in subjects with different levels of cognitive impairment. *Psychiatry Investig.* 13, 1–7. doi: 10.4306/pi.2016.13.1.1

Kawagoe, T., Onoda, K., and Yamaguchi, S. (2019). Subjective memory complaints are associated with altered resting-state functional connectivity but not structural atrophy. *Neuroimage Clin.* 21:101675. doi: 10.1016/j.nicl.2019.101675

Khan, W., Amad, A., Giampietro, V., Werden, E., De Simoni, S., O'Muircheartaigh, J., et al. (2020). The heterogeneous functional architecture of the posteromedial cortex is associated with selective functional connectivity differences in Alzheimer's disease. *Hum. Brain Mapp.* 41, 1557–1572. doi: 10.1002/hbm.24894

Leeuwis, A. E., Benedictus, M. R., Kuijer, J., Binnewijzend, M., Hooghiemstra, A. M., Verfaillie, S., et al. (2017). Lower cerebral blood flow is associated with impairment in multiple cognitive domains in Alzheimer's disease. *Alzheimers Dement.* 13, 531–540. doi: 10.1016/j.jalz.2016.08.013

Leeuwis, A. E., Smith, L. A., Melbourne, A., Hughes, A. D., Richards, M., Prins, N. D., et al. (2018). Cerebral blood flow and cognitive functioning in a community-based, multi-ethnic cohort: the SABRE study. *Front. Aging Neurosci.* 10:279. doi: 10.3389/fnagi.2018.00279

Li, D., Liu, Y., Zeng, X., Xiong, Z., Yao, Y., Liang, D., et al. (2020). Quantitative study of the changes in cerebral blood flow and iron deposition during progression of Alzheimer's disease. *J. Alzheimers Dis.* 78, 439–452. doi: 10.3233/JAD-200843

Liu, X., Tosun, D., Weiner, M. W., and Schuff, N. (2013). Locally linear embedding (LLE) for MRI based Alzheimer's disease classification. *Neuroimage* 83, 148–157. doi: 10.1016/j.neuroimage.2013.06.033

Liu, Y., Wang, K., Yu, C., He, Y., Zhou, Y., Liang, M., et al. (2008). Regional homogeneity, functional connectivity and imaging markers of Alzheimer's disease: a review of resting-state fMRI studies. *Neuropsychologia* 46, 1648–1656. doi: 10.1016/j.neuropsychologia.2008.01.027

Ma, H. R., Pan, P. L., Sheng, L. Q., Dai, Z. Y., Wang, G. D., Luo, R., et al. (2017). Aberrant pattern of regional cerebral blood flow in Alzheimer's disease: a voxel-wise meta-analysis of arterial spin labeling MR imaging studies. *Oncotarget* 8, 93196–93208. doi: 10.18632/oncotarget.21475

Mapstone, M., Steffenella, T. M., and Duffy, C. J. (2003). A visuospatial variant of mild cognitive impairment: getting lost between aging and AD. *Neurology* 60, 802–808. doi: 10.1212/01.WNL.0000049471.76799.DE

Mattson, M. P., and Arumugam, T. V. (2018). Hallmarks of brain aging: adaptive and pathological modification by metabolic states. *Cell Metab.* 27, 1176–1199. doi: 10.1016/j.cmet.2018.05.011

McKhann, G. M., Knopman, D. S., Chertkow, H., Hyman, B. T., Jack, C. R. J., Kawas, C. H., et al. (2011). The diagnosis of dementia due to Alzheimer's disease: recommendations from the National Institute on Aging-Alzheimer's Association workgroups on diagnostic guidelines for Alzheimer's disease. *Alzheimers Dement.* 7, 263–269. doi: 10.1016/j.jalz.2011.03.005

Mendola, J. D., Cronin-Golomb, A., Corkin, S., and Growdon, J. H. (1995). Prevalence of visual deficits in Alzheimer's disease. *Optom Vis. Sci.* 72, 155–167. doi: 10.1097/00006324-199503000-00003

Min, J., Zhou, X. X., Zhou, F., Tan, Y., and Wang, W. D. (2019). A study on changes of the resting-state brain function network in patients with amnestic mild cognitive impairment. *Braz. J. Med. Biol. Res.* 52:e8244. doi: 10.1590/1414-431x20198244

Miners, J. S., Palmer, J. C., and Love, S. (2016). Pathophysiology of hypoperfusion of the precuneus in early Alzheimer's disease. *Brain Pathol.* 26, 533–541. doi: 10.1111/bpa.12331

Pan, P., Zhu, L., Yu, T., Shi, H., Zhang, B., Qin, R., et al. (2017). Aberrant spontaneous low-frequency brain activity in amnestic mild cognitive impairment: a meta-analysis of resting-state fMRI studies. *Ageing Res. Rev.* 35, 12–21. doi: 10.1016/j.arr.2016.12.001

Pietrini, P., Furey, M. L., Graff-Radford, N., Freo, U., Alexander, G. E., Grady, C. L., et al. (1996). Preferential metabolic involvement of visual cortical areas in a subtype of Alzheimer's disease: clinical implications. *Am. J. Psychiatry* 153, 1261–1268. doi: 10.1176/ajp.153.10.1261

Pirooznia, M., and Deng, Y. (2006). SVM classifier–a comprehensive java interface for support vector machine classification of microarray data. *BMC Bioinformatics* 7:S25. doi: 10.1186/1471-2105-7-S4-S25

Popa-Wagner, A., Buga, A. M., Popescu, B., and Muresanu, D. (2015). Vascular cognitive impairment, dementia, aging and energy demand. A vicious cycle. *J. Neural Transm. (Vienna)* 122, S47–S54. doi: 10.1007/s00702-013-1129-3

Qi, R., Luo, Y., Zhang, L., Weng, Y., Surento, W., Li, L., et al. (2020). Effects of COMT rs4680 and BDNF rs6265 polymorphisms on brain degree centrality in Han Chinese adults who lost their only child. *Transl. Psychiatry* 10:46. doi: 10.1038/s41398-020-0728-7

Qi, Z., Wu, X., Wang, Z., Zhang, N., Dong, H., Yao, L., et al. (2010). Impairment and compensation coexist in amnestic MCI default mode network. *Neuroimage* 50, 48–55. doi: 10.1016/j.neuroimage.2009.12.025

Riederer, I., Bohn, K. P., Preibisch, C., Wiedemann, E., Zimmer, C., Alexopoulos, P., et al. (2018). Alzheimer disease and mild cognitive impairment: integrated pulsed arterial spin-labeling MRI and (18)F-FDG PET. *Radiology* 288, 198–206. doi: 10.1148/radiol.2018170575

Scherr, M., Utz, L., Tahmasian, M., Pasquini, L., Grothe, M. J., Rauschecker, J. P., et al. (2019). Effective connectivity in the default mode network is distinctively disrupted in Alzheimer's disease-A simultaneous resting-state FDG-PET/fMRI study. *Hum Brain Mapp*. doi: 10.1002/hbm.24517. [Epub ahead of print].

Schroeter, M. L., Stein, T., Maslowski, N., and Neumann, J. (2009). Neural correlates of Alzheimer's disease and mild cognitive impairment: a systematic and quantitative meta-analysis involving 1351 patients. *Neuroimage* 47, 1196–1206. doi: 10.1016/j.neuroimage.2009.05.037

Seminowicz, D. A., and Moayedi, M. (2017). The dorsolateral prefrontal cortex in acute and chronic pain. *J. Pain* 18, 1027–1035. doi: 10.1016/j.jpain.2017.03.008

Shi, Y., Gu, L., Wang, Q., Gao, L., Zhu, J., Lu, X., et al. (2019). Platelet amyloid-β protein precursor (AβPP) ratio and phosphorylated tau as promising indicators for early Alzheimer's disease. *J. Gerontol. A* 75, 664–670. doi: 10.1093/gerona/glz005

Si, T., Xing, G., and Han, Y. (2020). Subjective cognitive decline and related cognitive deficits. *Front. Neurol.* 11:247. doi: 10.3389/fneur.2020.00247

Sierra-Marcos, A. (2017). Regional cerebral blood flow in mild cognitive impairment and Alzheimer's disease measured with arterial spin labeling magnetic resonance imaging. *Int. J. Alzheimers Dis.* 2017:5479597. doi: 10.1155/2017/5479597

Sorg, C., Riedl, V., Muhlau, M., Calhoun, V. D., Eichele, T., Laer, L., et al. (2007). Selective changes of resting-state networks in individuals at risk for Alzheimer's disease. *Proc. Natl. Acad. Sci. U.S.A.* 104, 18760–18765. doi: 10.1073/pnas.0708803104

Ten, K. M., Barkhof, F., Boccardi, M., Visser, P. J., Jack, C. J., Lovblad, K. O., et al. (2017). Clinical validity of medial temporal atrophy as a biomarker for Alzheimer's disease in the context of a structured 5-phase development framework. *Neurobiol. Aging* 52, 167–182. doi: 10.1016/j.neurobiolaging.2016.05.024

Thomas, B., Sheelakumari, R., Kannath, S., Sarma, S., and Menon, R. N. (2019). Regional cerebral blood flow in the posterior cingulate and precuneus and the entorhinal cortical atrophy score differentiate mild cognitive impairment and dementia due to Alzheimer disease. *Am. J. Neuroradiol.* 40, 1658–1664. doi: 10.3174/ajnr.P0057

Thomas, T., Miners, S., and Love, S. (2015). Post-mortem assessment of hypoperfusion of cerebral cortex in Alzheimer's disease and vascular dementia. *Brain* 138, 1059–1069. doi: 10.1093/brain/awv025

Trebeschi, S., Riederer, I., Preibisch, C., Bohn, K. P., Forster, S., Alexopoulos, P., et al. (2016). Diagnostic potential of pulsed arterial spin labeling in Alzheimer's disease. *Front. Neurosci.* 10:154. doi: 10.3389/fnins.2016.00154

Tuovinen, T., Rytty, R., Moilanen, V., Abou, E. A., Veijola, J., Remes, A. M., et al. (2016). The effect of gray matter ICA and coefficient of variation mapping of BOLD data on the detection of functional connectivity changes in Alzheimer's disease and bvFTD. *Front. Hum. Neurosci.* 10:680. doi: 10.3389/fnhum.2016.00680

Vannini, P., Lehmann, C., Dierks, T., Jann, K., Viitanen, M., Wahlund, L. O., et al. (2008). Failure to modulate neural response to increased task demand in mild Alzheimer's disease: fMRI study of visuospatial processing. *Neurobiol. Dis.* 31, 287–297. doi: 10.1016/j.nbd.2008.04.013

Waltz, J. A., Kasanova, Z., Ross, T. J., Salmeron, B. J., McMahon, R. P., Gold, J. M., et al. (2013). The roles of reward, default, and executive control networks in set-shifting impairments in schizophrenia. *PLoS ONE* 8:e57257. doi: 10.1371/journal.pone.0057257

Wang, Z., Wang, Y., Sweeney, J. A., Gong, Q., Lui, S., and Mosconi, M. W. (2019). Resting-state brain network dysfunctions associated with visuomotor impairments in autism spectrum disorder. *Front. Integr. Neurosci.* 13:17. doi: 10.3389/fnint.2019.00017

Wang, Z., Xia, M., Dai, Z., Liang, X., Song, H., He, Y., et al. (2015). Differentially disrupted functional connectivity of the subregions of the inferior parietal lobule in Alzheimer's disease. *Brain Struct. Funct.* 220, 745–762. doi: 10.1007/s00429-013-0681-9

Wee, C. Y., Yap, P. T., Li, W., Denny, K., Browndyke, J. N., Potter, G. G., et al. (2011). Enriched white matter connectivity networks for accurate identification of MCI patients. *Neuroimage* 54, 1812–1822. doi: 10.1016/j.neuroimage.2010.10.026

Xie, C., Bai, F., Yu, H., Shi, Y., Yuan, Y., Chen, G., et al. (2012). Abnormal insula functional network is associated with episodic memory decline in amnestic mild cognitive impairment. *Neuroimage* 63, 320–327. doi: 10.1016/j.neuroimage.2012.06.062

Xie, C., Bai, F., Yuan, B., Yu, H., Shi, Y., Yuan, Y., et al. (2015). Joint effects of gray matter atrophy and altered functional connectivity on cognitive deficits in amnestic mild cognitive impairment patients. *Psychol. Med.* 45, 1799–1810. doi: 10.1017/S0033291714002876

Xu, L., Liang, G., Liao, C., Chen, G. D., and Chang, C. C. (2018). An efficient classifier for Alzheimer's disease genes identification. *Molecules* 23:3140. doi: 10.3390/molecules23123140

Xue, C., Yuan, B., Yue, Y., Xu, J., Wang, S., Wu, M., et al. (2019). Distinct disruptive patterns of default mode subnetwork connectivity across the spectrum of preclinical Alzheimer's disease. *Front. Aging Neurosci.* 11:307. doi: 10.3389/fnagi.2019.00307

Yan, C., Wang, X., Zuo, X., and Zang, Y. (2016). DPABI: Data processing & analysis for (resting-state) brain imaging. *Neuroinformatics* 14, 339–351. doi: 10.1007/s12021-016-9299-4

Yan, T., Wang, W., Yang, L., Chen, K., Chen, R., and Han, Y. (2018). Rich club disturbances of the human connectome from subjective cognitive decline to Alzheimer's disease. *Theranostics* 8, 3237–3255. doi: 10.7150/thno.23772

Yoshiura, T., Hiwatashi, A., Noguchi, T., Yamashita, K., Ohyagi, Y., Monji, A., et al. (2009). Arterial spin labelling at 3-T MR imaging for detection of individuals with Alzheimer's disease. *Eur Radiol* 19, 2819–2825. doi: 10.1007/s00330-009-1511-6

Zhang, L., Li, W., Wang, L., Bai, T., Ji, G. J., Wang, K., et al. (2020). Altered functional connectivity of right inferior frontal gyrus subregions in bipolar disorder: a resting state fMRI study. *J. Affect. Disord.* 272, 58–65. doi: 10.1016/j.jad.2020.03.122

Zhang, S., and Li, C. S. (2012). Functional connectivity mapping of the human precuneus by resting state fMRI. *Neuroimage* 59, 3548–3562. doi: 10.1016/j.neuroimage.2011.11.023

Zhang, Z., Liu, Y., Jiang, T., Zhou, B., An, N., Dai, H., et al. (2012). Altered spontaneous activity in Alzheimer's disease and mild cognitive impairment revealed by regional homogeneity. *Neuroimage* 59, 1429–1440. doi: 10.1016/j.neuroimage.2011.08.049

Zhen, D., Xia, W., Yi, Z. Q., Zhao, P. W., Zhong, J. G., Shi, H. C., et al. (2018). Alterations of brain local functional connectivity in amnestic mild cognitive impairment. *Transl. Neurodegener.* 7:26. doi: 10.1186/s40035-018-0140-x

Zheng, W., Cui, B., Han, Y., Song, H., Li, K., He, Y., et al. (2019). Disrupted regional cerebral blood flow, functional activity and connectivity in Alzheimer's disease: a combined ASL perfusion and resting state fMRI study. *Front. Neurosci.* 13:738. doi: 10.3389/fnins.2019.00738

Zhu, Y., Gong, L., He, C., Wang, Q., Ren, Q., and Xie, C. (2019). Default mode network connectivity moderates the relationship between the APOE genotype and cognition and individualizes identification across the Alzheimer's disease spectrum. *J. Alzheimers Dis.* 70, 843–860. doi: 10.3233/JAD-190254

Conflict of Interest: The authors declare that the research was conducted in the absence of any commercial or financial relationships that could be construed as a potential conflict of interest.

frontiers in Aging Neuroscience

ORIGINAL RESEARCH
published: 24 February 2021
doi: 10.3389/fnagi.2021.625511

Blood Hemoglobin, *in-vivo* Alzheimer Pathologies, and Cognitive Impairment: A Cross-Sectional Study

Jee Wook Kim[1,2] Min Soo Byun[3], Dahyun Yi[4], Jun Ho Lee[5], So Yeon Jeon[6], Kang Ko[5], Haejung Joung[7], Gijung Jung[7], Jun-Young Lee[8], Chul-Ho Sohn[9], Yun-Sang Lee[10], Yu Kyeong Kim[11] and Dong Young Lee[3,7,12] for the KBASE Research Group[†]*

[1] Department of Neuropsychiatry, Hallym University Dongtan Sacred Heart Hospital, Hwaseong, South Korea, [2] Department of Psychiatry, Hallym University College of Medicine, Chuncheon, South Korea, [3] Department of Neuropsychiatry, Seoul National University Bundang Hospital, Seongnam, South Korea, [4] Institute of Human Behavioral Medicine, Medical Research Center Seoul National University, Seoul, South Korea, [5] Department of Geriatric Psychiatry, National Center for Mental Health, Seoul, South Korea, [6] Department of Psychiatry, Chungnam National University Hospital, Daejeon, South Korea, [7] Department of Neuropsychiatry, Seoul National University Hospital, Seoul, South Korea, [8] Department of Neuropsychiatry, Seoul Metropolitan Government - Seoul National University Boramae Medical Center, Seoul, South Korea, [9] Department of Radiology, Seoul National University Hospital, Seoul, South Korea, [10] Department of Nuclear Medicine, Seoul National University College of Medicine, Seoul, South Korea, [11] Department of Nuclear Medicine, Seoul Metropolitan Government - Seoul National University Boramae Medical Center, Seoul, South Korea, [12] Department of Psychiatry, Seoul National University College of Medicine, Seoul, South Korea

OPEN ACCESS

Edited by:
Rong Chen, University of Maryland, Baltimore, United States

Reviewed by:
Owen T. Carmichael, Pennington Biomedical Research Center, United States
Michael Malek-Ahmadi, Banner Alzheimer's Institute, United States

***Correspondence:**
Dong Young Lee
selfpsy@snu.ac.kr

[†] *The coinvestigators of the KBASE Research Group are listed in elsewhere (http://kbase.kr)*

Received: *03 November 2020*
Accepted: *02 February 2021*
Published: *24 February 2021*

Citation:
Kim JW, Byun MS, Yi D, Lee JH, Jeon SY, Ko K, Joung H, Jung G, Lee J-Y, Sohn C-H, Lee Y-S, Kim YK and Lee DY (2021) Blood Hemoglobin, in-vivo Alzheimer Pathologies, and Cognitive Impairment: A Cross-Sectional Study. Front. Aging Neurosci. 13:625511. doi: 10.3389/fnagi.2021.625511

Background: Despite known associations between low blood hemoglobin level and Alzheimer's disease (AD) or cognitive impairment, the underlying neuropathological links are poorly understood. We aimed to examine the relationships of blood hemoglobin levels with *in vivo* AD pathologies (i.e., cerebral beta-amyloid [Aβ] deposition, tau deposition, and AD-signature degeneration) and white matter hyperintensities (WMHs), which are a measure of cerebrovascular injury. We also investigated the association between hemoglobin level and cognitive performance, and then assessed whether such an association is mediated by brain pathologies.

Methods: A total of 428 non-demented older adults underwent comprehensive clinical assessments, hemoglobin level measurement, and multimodal brain imaging, including Pittsburgh compound B-positron emission tomography (PET), AV-1451 PET, fluorodeoxyglucose (FDG)-PET, and magnetic resonance imaging. Episodic memory score and global cognition scores were also measured.

Results: A lower hemoglobin level was significantly associated with reduced AD-signature cerebral glucose metabolism (AD-CM), but not Aβ deposition, tau deposition, or WMH volume. A lower hemoglobin level was also significantly associated with poorer episodic memory and global cognition scores, but such associations disappeared when AD-CM was controlled as a covariate, indicating that AD-CM has a moderating effect.

Conclusion: The present findings suggest that low blood hemoglobin in older adults is associated with cognitive decline via reduced brain metabolism, which seems to be independent of those aspects of AD-specific protein pathologies and cerebrovascular injury that are reflected in PET and MRI measures.

Keywords: hemoglobin, anemia, Alzheimer's disease, cerebral hypometabolism, cognitive impairment

INTRODUCTION

Hemoglobin, a protein molecule present in red blood cells, contributes to the oxygen-carrying capacity of blood and related energy metabolism (Feig et al., 1971, 1972; Zauner et al., 2002; Schechter, 2008). Anemia, characterized by a decrease in the level of blood hemoglobin, is one of the most common blood disorders and has been reported to increase the risk of acute stroke (Tanne et al., 2010) and coronary heart disease (Astor et al., 2006; Mahmoodi et al., 2007). Many human studies have also found associations of low blood hemoglobin or anemia with increased risk of Alzheimer's disease (AD) (Shah et al., 2011; Faux et al., 2014; Wolters et al., 2019) or overall dementia (Atti et al., 2006; Hong et al., 2013; Wolters et al., 2019) and poorer cognitive performance (Shah et al., 2011).

Despite such associations of a lower blood hemoglobin level with AD and related cognitive impairment, the pathological mechanisms that underlie the associations are still poorly understood. A couple of preclinical and postmortem brain studies indicated that hemoglobin binds beta-amyloid protein (Aβ) and co-localizes with amyloid plaques (Oyama et al., 2000; Wu et al., 2004). Hemoglobin was also reported to alter the Aβ aggregation state (Chuang et al., 2012) and suppress Aβ-mediated inflammatory reactions (Sankar et al., 2018). A recent magnetic resonance imaging (MRI) study in a non-demented population showed an association of low blood hemoglobin level with altered white matter integrity and cerebral perfusion (Wolters et al., 2019). However, as of yet, no studies have investigated the relationship between blood hemoglobin and AD-specific pathologies in a living human brain.

Therefore, the present study was performed to investigate the associations between low blood hemoglobin and *in vivo* AD pathologies in non-demented older adults. We first examined the relationships of blood hemoglobin level with three AD pathologies (i.e., cerebral Aβ deposition, tau deposition, and AD-signature neurodegeneration) and white matter hyperintensities (WMHs), which are a measure of cerebrovascular injury. We then tried to examine whether the association of blood hemoglobin with cognitive impairment is affected by brain pathology which shows a significant relationship with lower hemoglobin level.

MATERIALS AND METHODS

Participants

This study was part of the Korean Brain Aging Study for Early Diagnosis and Prediction of Alzheimer's Disease (KBASE), which is an ongoing prospective cohort study (Byun et al., 2017). As of February 2017, a total of 428 non-demented [289 cognitive normal (CN) and 139 mild cognitive impairment (MCI)] older adults between 55 and 90 years of age were enrolled in the study. The CN group consisted of participants with a Clinical Dementia Rating (CDR) (Morris, 1993) score of 0 and no diagnosis of MCI or dementia. All individuals with MCI met the current consensus criteria for amnestic MCI, which are as follows: (1) memory complaints confirmed by an informant; (2) objective memory impairments, (3) preserved global cognitive function; (4) independence in functional activities; and (5) no dementia. With regard to criterion 2, the age-, education-, and gender-adjusted z-scores for at least one of four episodic memory tests were < -1.0. The four memory tests were the Word List Memory, Word List Recall, Word List Recognition, and Constructional Recall tests, which are included in the Korean version of the Consortium to Establish a Registry for Alzheimer's Disease (CERAD-K) neuropsychological battery (Lee et al., 2004). All MCI individuals had a CDR score of 0.5. The exclusion criteria were as follows: (1) presence of a major psychiatric illness; (2) significant neurological (e.g., cerebrovascular disease) or medical conditions that could affect mental function; (3) contraindications for MRI (e.g., pacemaker or claustrophobia); (4) illiteracy; (5) the presence of significant visual/hearing difficulties and/or severe communication or behavioral problems that would make clinical examinations or brain scans difficult; (6) taking an investigational drug; and (7) pregnant or breastfeeding. The presence of any of the exclusion criteria was determined by research clinicians that referred to laboratory examination, MRI results, as well as clinical data collected by trained nurses during systematic interviews of participants and their reliable informants during the screening period. More detailed information on the recruitment of the KBASE cohort is presented in a previous report from our research group (Byun et al., 2017).

Clinical Assessments

All participants underwent comprehensive clinical and neuropsychological assessments administered by trained psychiatrists and neuropsychologists based on the KBASE assessment protocol (Byun et al., 2017), which incorporates the Korean version of the CERAD neuropsychological battery (Morris et al., 1989; Lee et al., 2002, 2004). The episodic memory score (EMS) was calculated by summing the scores of the four episodic memory tests (i.e., Word List Memory, Word List Recall, Word List Recognition, and Constructional Recall) included in the CERAD neuropsychological battery. A CERAD total score (TS) was generated by summing the scores of seven tests in the CERAD neuropsychological battery including the Verbal Fluency, modified Boston Naming Test, Word List Memory, Constructional Praxis, Word List Recall, Word List Recognition, and Constructional recall tests (Seo et al., 2010). EMS and TS were selected as measures of episodic memory function and global cognitive function, respectively. Importantly, episodic memory decline is the earliest cognitive change observed in AD (Howieson et al., 1997; Grober et al., 2000). The comorbidity rates of vascular risk factors (e.g., hypertension, diabetes mellitus, dyslipidemia, coronary heart disease, transient ischemic attack, and stroke) were assessed based on data collected by trained nurses during systematic interviews of participants and their informants. A vascular risk score (VRS) was calculated based on the number of vascular risk factors present and reported as a percentage (Decarli et al., 2004). Body mass index (BMI) was calculated by dividing the weight in kilograms by the square of the height in meters. Annual income was evaluated and categorized into three groups [below the minimum cost of living (MCL), more than MCL but below twice the MCL, twice the MCL or more] (http://www.law.go.kr). Regarding occupational

complexity, we considered only the longest-held occupation and then classified into four levels based on the skill levels described in International Standard Classification of Occupations (http://www.ilo.org/public/english/bureau/stat/isco/). The details of annual income and occupational complexity were described in **Supplementary Material**. Medication use within 4 weeks (no/yes), declined food intake over the past 3 months due to loss of appetite or swallowing difficulties (no/moderate/severe) (Vellas et al., 1999) smoking status (never/ex-smoker/smoker), and alcohol intake status (never/former/drinker) were also evaluated through nurse interviews and medical record review. To acquire accurate information, reliable informants were interviewed.

Laboratory Tests of Blood Samples

After an overnight fast, blood samples were obtained via venipuncture in the morning (8–9 a.m.). Hemoglobin levels were measured using a flow cytometry method (ADVIA 2120i, Siemens, USA). The normal ranges for hemoglobin level are 12–15.5 g/dL in women and 13–17.5 g/dL in men (Shah et al., 2011). Serum creatinine levels were measured using a colorimetry method (ADVIA 1800 Auto Analyzer, Siemens, USA). Serum folate and vitamin B_{12} were measured using a radioimmunoassay method (Gamma-counter) with a vitamin B_{12} [^{57}Co] / folate [^{125}I] radioassay kit. Additionally, genomic DNA was extracted from whole blood and apolipoprotein E (*APOE*) genotyping was performed as previously described (Wenham et al., 1991). APOE ε4 (*APOE4*) positivity was defined as the presence of at least one ε4 allele.

Measurement of Cerebral Aβ Deposition

All participants underwent simultaneous three-dimensional (3D) [^{11}C] Pittsburgh compound B (PiB)-positron emission tomography (PET) and 3D T1-weighted MRI scanning using a 3.0T Biograph mMR (PET-MR) scanner (Siemens; Washington DC, WC, USA), in accordance with the manufacturer's guidelines. The details of the PiB-PET imaging acquisition and preprocessing were described previously (Park et al., 2019). An automatic anatomical labeling algorithm and a region-combining method(Reiman et al., 2009) were applied to determine regions of interest (ROIs) for characterization of PiB retention levels in the frontal, lateral parietal, posterior cingulate-precuneus, and lateral temporal regions. Standardized uptake value ratio (SUVR) values for each ROI were calculated by dividing the mean value for all voxels within each ROI by the mean cerebellar uptake value in the same image. A global cortical ROI consisting of the four ROIs was defined and a global Aβ retention value was generated by dividing the mean value for all voxels of the global cortical ROI by the mean cerebellar uptake value in the same image (Reiman et al., 2009; Choe et al., 2014). Participants were classified as Aβ-positive (Aβ+) if the SUVR value was > 1.4 in at least one of the four ROIs or as Aβ-negative (Aβ-) if the SUVR value was ≤ 1.4 for all four ROIs (Reiman et al., 2009; Jack et al., 2014).

Measurement of Cerebral Tau Deposition

A subset of subjects ($n = 107$) underwent [^{18}F] AV-1451 PET scans using a Biograph True point 40 PET/CT scanner (Siemens; Washington DC, WC, USA), in accordance with the manufacturer's guidelines. While all the other neuroimaging scans were performed during the baseline visit, AV-1451 PET imaging was performed at an average of 2.6 (standard deviation 0.3) years after the baseline visit. The details of AV-1451 PET imaging acquisition and preprocessing were described previously (Park et al., 2019). To estimate cerebral tau deposition, we quantified the AV-1541 SUVR of an a priori ROI of "AD-signature regions" of tau accumulation, which was composed of a size-weighted average of partial volume-corrected uptake in entorhinal, amygdala, parahippocampal, fusiform, inferior temporal, and middle temporal ROIs, in accordance with the method used in a previous report (Jack et al., 2017). The AV-1451 SUVR of the abovementioned ROI was used as an outcome variable for cerebral tau deposition.

Measurement of AD-Signature Neurodegeneration

All participants underwent [^{18}F] fluorodeoxyglucose (FDG)-PET imaging using the above-described PET-MR machine; the details of FDG-PET image acquisition and preprocessing were described previously (Park et al., 2019). AD-signature FDG ROIs that are sensitive to the changes associated with AD, such as the angular gyri, posterior cingulate cortex, and inferior temporal gyri (Jack et al., 2014), were determined. AD-signature cerebral glucose metabolism (AD-CM) was defined as the voxel-weighted mean SUVR extracted from the AD-signature FDG ROIs.

Measurement of WMH

All participants underwent MRI scans including T1 weighted images and fluid-attenuated inversion recovery (FLAIR) images using the abovementioned 3.0T PET-MR machine. WMH volume was measured though a validated automatic procedure previously reported (Tsai et al., 2014). Briefly, the procedure consists of 11 steps: spatial co-registration of T1 and FLAIR images, fusion of T1 and FLAIR images, segmentation of T1 images, acquisition of transformation parameters, deformation and acquisition of the white matter mask, acquisition of FLAIR within the white matter mask, intensity normalization of the masked FLAIR, nomination of candidate WMH with a designated threshold, creation of a junction map, and elimination of the junction. There were two modifications in the current processing procedure relative to that used in the original study: (a) an optimal threshold of 70 was applied, as it was more suitable for our data than the threshold of 65 that was used in the original study; and, (b) given that individuals with acute cerebral infarcts were not enrolled in our sample, we did not use diffusion-weighted imaging in the current automated procedure. Using the final WMH candidate image, WMH volume was extracted in the native space in each subject.

Statistical Analysis

To examine the relationships between hemoglobin level and neuroimaging biomarkers, multiple logistic, and linear regression analyses were performed as appropriate. Hemoglobin level, an independent variable for each analysis, was first entered as a continuous variable, and then as a stratified categorical

TABLE 1 | Participant characteristics.

Characteristic	Overall, $N = 428$
Age, y	70.61 (8.01)
Female, *n* (%)	240 (56.07)
Education, y	11.18 (4.78)
APOE4 positivity, *n* (%)	99 (23.13)
Clinical diagnosis, CN, %	289 (67.52)
MMSE	25.45 (3.47)
Hemoglobin level	
Overall hemoglobin, g/dL	13.87 (1.30)
Categorized hemoglobin	
High, *n* (%)	2 (0.05)
High-normal, *n* (%)	181 (42.89)
Low-normal, *n* (%)	203 (47.43)
Anemia, *n* (%)	42 (9.81)
Red cell distribution width	12.89 (0.83)
Hematocrit	42.36 (3.87)
Iron ($n = 376$)	118.65 (39.14)
Transferrin ($n = 376$)	271.77 (40.65)
Ferritin ($n = 376$)	121.84 (92.87)
Body mass index, kg/m^2	24.37 (3.03)
Vascular risk score, %	17.76 (16.33)
Annual income status	
<MCL, *n* (%)	35 (8.18)
≥MCL, <2×MCL, *n* (%)	190 (44.39)
≥2×MCL, *n* (%)	203 (47.43)
Occupational complexity ($N = 427$)	
None, *n* (%)	78 (18.27)
Skill level 1, *n* (%)	29 (6.79)
Skill level 2, *n* (%)	141 (33.02)
Skill level 3, *n* (%)	56 (13.11)
Skill level 4, *n* (%)	123 (28.81)
Smoking status, *n* (%)	
Never/Former/ Smoker	287 (67.21)/119 (27.87)/21 (4.92)
Alcohol intake status, *n* (%) ($n = 427$)	
Never/former/ drinker	231 (54.10)/57 (13.35)/139 (32.55)
Vitamin B_{12}	580.93 (336.05)
Folic acid	10.01 (5.56)
Platelet, 10^9/L	239.28 (57.49)
Serum creatinine, mg/dL	1.01 (0.20)
Medication use within 4 weeks ($n = 427$)	
No, *n* (%)/Yes, *n* (%)	85 (19.91)/ 342 (80.09)
Declined food intake over past 3 months (n = 426)	
No, *n* (%)/Moderate, *n* (%)/Severe, *n* (%)	354 (83.10)/54 (12.68)/18 (4.23)
CERAD neuropsychological test, *z*-score	
Episodic memory score	−0.19 (1.21)
Memory total score	−0.19 (1.10)
Cognitive test score	−0.10 (0.86)
AD neuroimage biomarkers	
Cerebral Aβ deposition ($n = 420$)	
Aβ positivity, *n* (%)	101 (24.05)
Aβ retention, SUVR	11.28 (0.35)
Cerebral tau deposition ($n = 106$)	
AV-1451, SUVR	1.60 (0.79)
AD-CM, SUVR ($n = 420$)	1.40 (0.13)
WMH volume, cm^3 ($n = 376$)	5.99 (5.41)

MMSE, mini-mental state examination; APOE4, apolipoprotein ε4; CN, cognitively normal; MCL, minimum cost of living; Aβ, beta-amyloid; AD, Alzheimer's disease; AD-CM, Alzheimer's disease signature cerebral glucose metabolism; SUVR, standardized uptake value ratio.

Unless otherwise indicated, data are expressed as mean (standard deviation).

variable. Subjects were divided into three strata [<12 g/dL in female and <13 g/dL in male (anemia), ≤14 g/dL (low-normal level), and 14< g/dL (high-normal level)]. Within the normal range of hemoglobin level, the median value (i.e., 14 g/dL) was used as a cutoff to divide the low-normal and high-normal levels. To analyze the associations between hemoglobin and neuroimaging biomarkers, three models were tested for stepwise control of potential confounders. The first model did not include any covariates, the second model included age and sex as covariates, and the third model included all potential covariates (i.e., age, sex, education, *APOE4* positivity, VRS, clinical diagnosis, BMI, annual income status, occupational complexity, smoking, alcohol intake, vitamin B_{12}, folate, platelet level, serum creatinine, medication use within 4 weeks, and declined food intake over past 3 months) that might confound the relationship between hemoglobin level and brain changes (Ballard, 1997; Vellas et al., 1999; Borroni et al., 2002; Chan and Mike, 2014; Shi et al., 2018). In multiple linear regression analyses, the normality was checked using the Kolmogorov-Smirnov test for dependent variable(s). While AD-CM was found to be normally distributed (statistic = 0.032, $df = 420$, p = 0.20), the other neuroimaging markers were not (statistic = 0.294, $df = 420$, $p < 0.05$ in global Aβ retention; statistic = 0.266, $df = 106$, $p < 0.05$ in AV-1451; and statistic = 0.139, $df = 376$, $p < 0.05$ in WMH). Therefore, the markers except AD-CM were used after natural log-transformation to achieve normal distribution. For the sensitivity analyses, the same analyses were performed for the subjects without cognitive impairment (i.e., CN subjects) or those without decreased food intake over the past 3 months due to loss of appetite or swallowing difficulties that could affect the hemoglobin level. For neuroimaging biomarkers that showed significant associations with hemoglobin level in the above analyses, further multiple linear regression analyses were performed that included hemoglobin×age (or sex or education or *APOE4* positivity or VRS or clinical diagnosis or BMI or annual income or occupational complexity) interaction term, as well as hemoglobin and age (or sex or education or *APOE4* positivity or VRS or clinical diagnosis or BMI or annual income or occupational complexity) as independent variables. In these analyses, the neuroimaging biomarker was used as a dependent variable, and the analyses were controlled for all potential covariates. To investigate the association between hemoglobin level and cognitive performance, a multiple

linear regression model with hemoglobin as an independent variable and each of EMS and TS as a dependent variable was tested. Then, the same regression model was tested again while controlling for the neuroimaging biomarker that showed significant association with hemoglobin level as an additional covariate, to examine whether the relationship between blood hemoglobin and cognitive impairment is affected by the brain pathological marker. All statistical analyses were performed using IBM SPSS Statistics software (version 24, IBM Corp., Armonk, NY, USA).

RESULTS

Participants

Demographic and clinical characteristics of the participants are presented in **Table 1**. Among the total of 428 participants, 183 had high or high-normal hemoglobin levels, 203 had low-normal hemoglobin levels, and 42 had low hemoglobin levels (anemia).

Association Between Hemoglobin Level and Neuroimaging Biomarkers

As shown in **Tables 2** and **3**, neither Aβ biomarkers (i.e., Aβ positivity and Aβ deposition) nor tau deposition showed association with hemoglobin level (or strata) even after controlling for potential confounders. Hemoglobin level (or strata) was also not associated with WMH volume. In contrast, hemoglobin level (or strata) showed a significant positive association with AD-CM (**Tables 2**, **3** and **Figures 1A**, **2A**). Both anemia and the low-normal stratum of hemoglobin showed significantly decreased AD-CM compared to the high-normal stratum. Sensitivity analyses that included only CN individuals produced very similar results for the relationships between hemoglobin and AD-CM (**Supplementary Tables 1**, **2**; **Figures 1B**, **2B**). Even when individuals without reduced food intake over the past 3 months were excluded, the results were not changed (**Supplementary Tables 3**, **4**). Additional analyses to determine the moderation effects of age, sex, education, *APOE4* positivity, VRS, clinical diagnosis, BMI, annual income status, and occupational complexity on the association between hemoglobin and AD-CM did not reveal any significant results (**Supplementary Table 5**).

Association Between Hemoglobin and Cognition

Both EMS and TS were significantly different among the three hemoglobin strata (**Table 4**). The high-normal stratum had a significantly higher EMS and TS than the other two strata with lower hemoglobin levels (**Figure 3**). When AD-CM was controlled as an additional covariate, the relationship between hemoglobin strata and EMS or TS was no longer significant (**Table 4**).

TABLE 2 | Results of multiple logistic and linear regression analyses for assessing the relationship between hemoglobin level and Aβ, AV-1451, AD-CM, or WMH in non-demented older adults.

	OR	95% CI	*P*
Aβ positivity			
Model 1	0.816	0.684–0.974	0.024
Model 2	0.866	0.699–1.073	0.187
Model 3	0.894	0.682 to 1.171	0.416
	B	**95% CI**	***P***
Aβ retention, SUVR			
Model 1	−0.021	−0.038 to −0.004	0.014
Model 2	−0.012	−0.033 to 0.009	0.254
Model 3	−0.005	−0.025 to 0.014	0.590
AV-1451, SUVR			
Model 1	−0.020	−0.079 to 0.039	0.511
Model 2	−0.027	−0.097 to 0.042	0.439
Model 3	−0.038	−0.113 to 0.036	0.305
AD-CM, SUVR			
Model 1	0.019	0.010 to 0.029	< 0.001
Model 2	0.020	0.008 to 0.032	0.001
Model 3	0.018	0.006 to 0.030	0.004
WMH, cm^3			
Model 1	−0.031	−0.105 to 0.042	0.404
Model 2	−0.015	−0.101 to 0.071	0.732
Model 3	−0.017	−0.110 to 0.077	0.722

Aβ beta-amyloid; AD–CM Alzheimer's disease signature cerebral glucose metabolism; OR odds ratio; CI confidence interval.

The results of multivariate logistic or linear regression analyses are presented with OR or B coefficient values, 95% CI and P value.

Global Aβ retention, AV-1451, and WMH were used after natural log-transformation to achieve normal distribution.

Model 1 did not include any covariates, model 2 included age and sex as covariates, and model 3 included all potential covariates, including age, sex, education, apolipoprotein ε4, vascular risk score, clinical diagnosis, body mass index, annual income status, occupational complexity, smoking, alcohol intake, vitamin B_{12}, folate, platelet level, serum creatinine, medication use, and declined food intake.

DISCUSSION

In the present study, a lower blood hemoglobin was associated with reduced AD-CM, but not Aβ deposition, tau deposition or WMH volume, in non-demented older adults. There was also a significant association between lower hemoglobin and decreased cognitive performance. To the best of our knowledge, this is the first study to investigate the relationship between hemoglobin and AD-specific pathologies in the living human brain.

We found a strong association between anemia or a low-normal level of hemoglobin and decreased AD-CM. The present findings are in line with previous reports that found a strong relationship between a low level of hemoglobin and AD dementia (Shah et al., 2011; Wolters et al., 2019). Regarding the association between lower hemoglobin and deceased AD-CM, there are a couple of possible explanations. First, lower hemoglobin or anemia itself can decrease the delivery of oxygen to brain tissues (Kosenko et al., 2017), and cause oxidative damage to key enzymes involved in glycolysis, the tricarboxylic acid cycle and adenosine triphosphate (ATP) biosynthesis (Butterfield and Halliwell, 2019). This damage to energy-related processes negatively affects the metabolism of glucose, a key source of energy for the brain, and subsequently results in the characteristic

TABLE 3 | Results of multiple logistic and linear regression analyses for assessing the relationship between hemoglobin strata and Aβ, AV-1451, AD-CM, or WMH in non-demented older adults.

	Stratified hemoglobin level				
	Anemia		Low-normal (≤14 g/dL)		High-normal (>14 g/dL)
	OR (95% CI)	*P*	OR (95% CI)	*P*	
Aβ positivity					
Model 1	2.410 (1.153 to 5.037)	0.019	1.421 (0.868 to 2.326)	0.163	Reference
Model 2	1.649 (0.748 to 3.637)	0.215	1.216 (0.674 to 2.196)	0.515	Reference
Model 3	1.466 (0.541 to 3.977)	0.452	1.091 (0.554 to 2.151)	0.801	Reference
	B (95% CI)	***P***	**B (95% CI)**	***P***	
Aβ retention, SUVR					
Model 1	0.100 (0.022 to 0.179)	0.013	0.051 (0.005 to 0.098)	0.032	Reference
Model 2	0.062 (−0.019 to 0.143)	0.134	0.032 (−0.023 to 0.087)	0.249	Reference
Model 3	0.030 (−0.046 to 0.106)	0.442	0.020 (−0.028 to 0.068)	0.410	Reference
AV-1451, SUVR					
Model 1	0.095 (−0.174 to 0.364)	0.485	0.101 (−0.042 to 0.244)	0.165	Reference
Model 2	0.109 (−0.166 to 0.383)	0.433	0.165 (−0.019 to 0.348)	0.078	Reference
Model 3	0.112 (−0.179 to 0.403)	0.446	0.129 (−0.038 to 0.296)	0.129	Reference
AD-CM, SUVR					
Model 1	−0.092 (−0.136 to −0.048)	<0.001	−0.045 (−0.071 to −0.019)	0.001	Reference
Model 2	−0.081 (−0.127 to −0.036)	0.001	−0.047 (−0.078 to −0.016)	0.003	Reference
Model 3	−0.063 (−0.111 to −0.015)	0.010	−0.045 (−0.076 to −0.015)	0.003	Reference
WMH, cm^3					
Model 1	0.141 (−0.189 to 0.471)	0.402	0.165 (−0.039 to 0.369)	0.112	Reference
Model 2	−0.006 (−0.339 to 0.327)	0.971	0.187 (−0.046 to 0.420)	0.116	Reference
Model 3	−0.028 (−0.392 to 0.337)	0.882	0.191 (−0.047 to 0.430)	0.116	Reference

Aβ, beta-amyloid; AD-CM, Alzheimer's disease signature cerebral glucose metabolism; OR, odds ratio; CI, confidence interval.
Global Aβ retention, AV-1451, and WMH were used after natural log-transformation to achieve normal distribution.
Model 1 did not include any covariates, model 2 included age and sex as covariates, and model 3 included all potential covariates, including age, sex, education, apolipoprotein ε4, vascular risk score, clinical diagnosis, body mass index, annual income status, occupational complexity, smoking, alcohol intake, vitamin B_{12}, folate, platelet level, serum creatinine, medication use, and declined food intake.

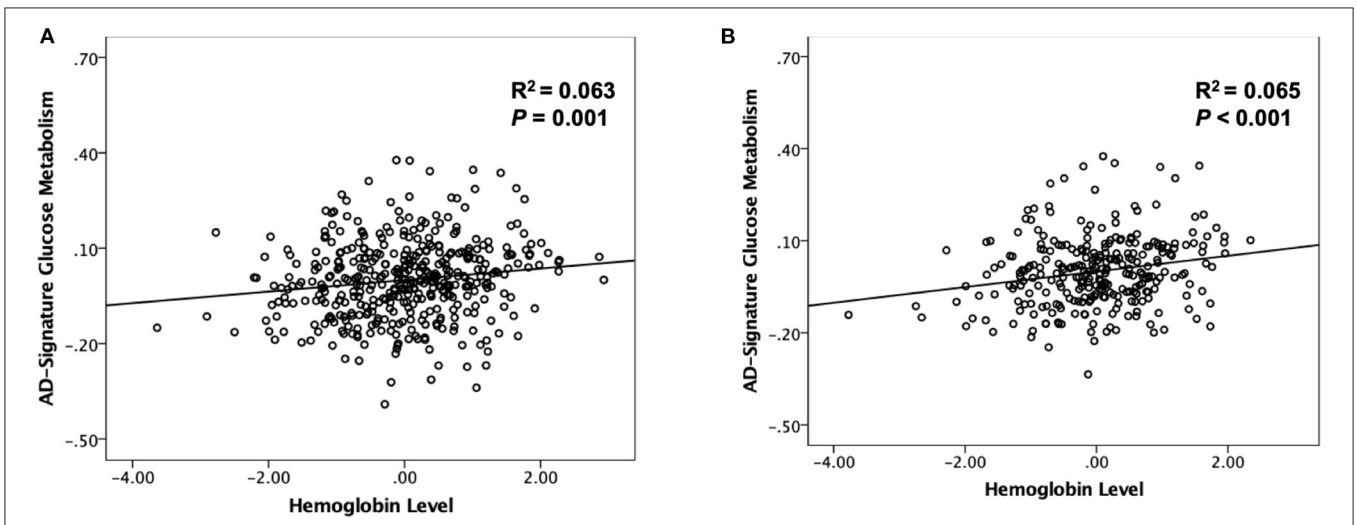

FIGURE 1 | Partial regression plot showing the relationship between hemoglobin level and AD-signature cerebral glucose metabolism (AD-CM) in **(A)** non-demented and **(B)** cognitive normal older participants. Multiple linear regression analyses were performed after adjusting for age and sex.

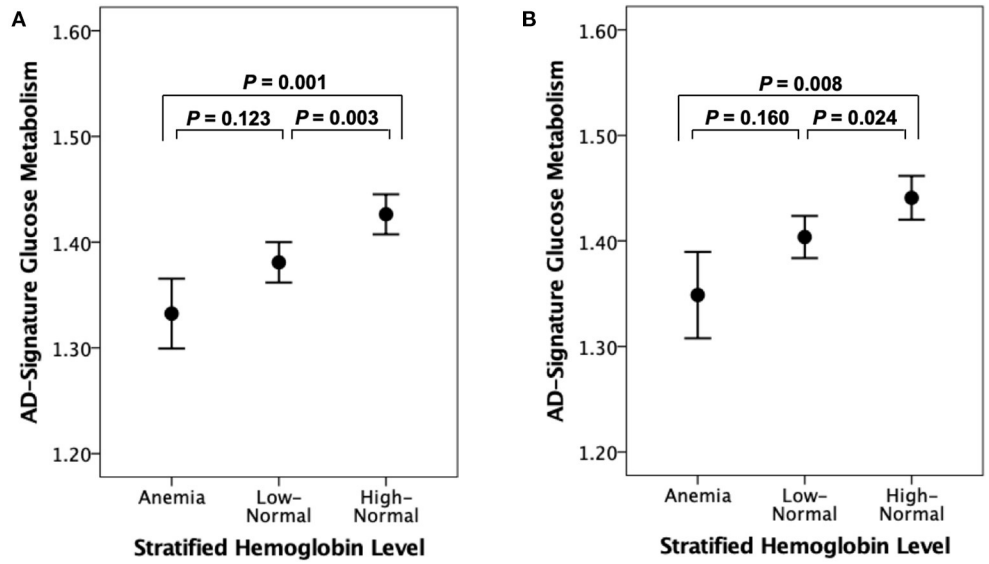

FIGURE 2 | Error bar charts displaying AD-signature cerebral glucose metabolism and stratified hemoglobin level in **(A)** non-demented and **(B)** cognitive normal older participants. Error bars indicate standard error. Multiple linear regression analyses were performed after adjusting for age and sex.

TABLE 4 | Results of multiple linear regression analyses for assessing the relationship between hemoglobin strata and cognitive performance in non-demented older adults.

	Stratified hemoglobin level				
	Anemia		Low-normal (≤14 g/dL)		High-normal (>14 g/dL)
	B (95% CI)	*P*	B (95% CI)	*P*	
EMS, *z*-score	−0.432 (−0.834 to −0.030)	0.035	−0.282 (−0.524 to −0.040)	0.023	Reference
EMS, *z*-score[†]	−0.266 (−0.670 to 0.138)	0.196	−0.202 (−0.443 to 0.040)	0.101	Reference
TS, *z*-score	−0.376 (−0.659 to −0.093)	0.009	−0.205 (−0.375 to −0.035)	0.018	Reference
TS, *z*-score[†]	−0.238 (−0.520 to 0.044)	0.098	−0.138 (−0.306 to 0.030)	0.108	Reference

AD-CM, Alzheimer's disease signature cerebral glucose metabolism; CI, confidence interval; EMS, episodic memory score; TS, total score.

[†] To examine whether the association between hemoglobin and cognitive impairment is mediated by the brain pathological marker, we included AD-CM which showed a significant relationship with hemoglobin as an additional covariate in the multiple linear regression model with hemoglobin as an independent variable and each of EMS and TS as a dependent variable.

reduction of cerebral glucose metabolism that is found in AD dementia (Aliev et al., 2003; Perry et al., 2003; Butterfield and Halliwell, 2019). Second, hemoglobin may also be lowered by decreased oral intake and poor nutrition in individuals with cognitive impairment. However, this possibility seems very low since the sensitivity analysis for CN subjects or those without declined food intake over the past 3 months revealed similar findings. Additionally, lower socio-economic status (SES) may just mediate the association between lower hemoglobin and deceased AD-CM because it could be related with not only low hemoglobin level via chronic poor nutritional intake and limited access to medical care, but also reduced brain metabolism and poor cognition (Farah, 2017). Given that the result did not change even after controlling annual income and occupational complexity as indicators for SES as covariates (in Model 3), however, this possibility appears very low.

Although several preclinical and postmortem studies showed a possible association between hemoglobin and Aβ pathology itself or its downstream pathological changes (Oyama et al., 2000; Wu et al., 2004), we could not find any association of hemoglobin with Aβ or tau pathologies. This indicates that AD-specific protein pathologies are not associated with lower hemoglobin and dementia or cognitive decline. Additionally, WMH volume, a measure of cerebrovascular injury, was not associated with hemoglobin in the present study. This finding is not in line with the result from a recent human study, which reported that a lower level of hemoglobin was associated with increased WMH volume in non-demented individuals (Wolters et al., 2019). This discrepancy may be explained by differences in the characteristics of study participants regarding the presence of severe cerebrovascular disease. While the aforementioned study included individuals with severe cerebrovascular lesions, the present study did

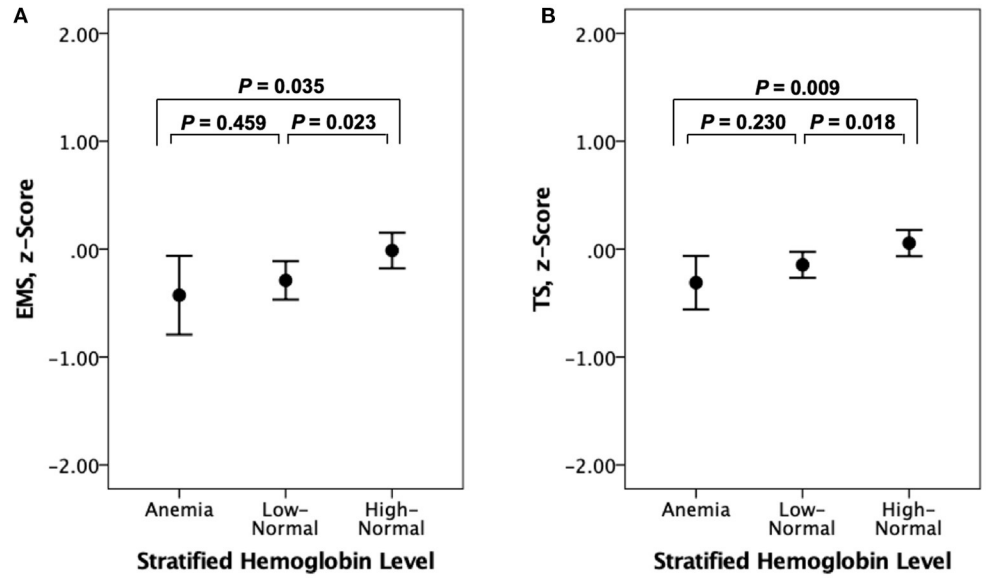

FIGURE 3 | Error bar charts displaying **(A)** episodic memory score (EMS) and **(B)** CERAD total score (TS) according to stratified hemoglobin levels in non-demented older participants. Error bars indicate standard error.

not. The null finding in the current study may be related to the low variability or relatively low burden of WMH or cerebrovascular injury.

We also found a relationship between low hemoglobin and poorer episodic memory or overall cognition, consistent with previous similar observations (Deal et al., 2009; Shah et al., 2011; Qin et al., 2019). When AD-CM, which showed significant association with hemoglobin, was adjusted as an additional covariate, the positive relationship between hemoglobin level and cognitive function was no longer significant. These findings further support the possibility that low hemoglobin or anemia may contribute to the development of AD dementia and related cognitive decline via cerebral hypometabolism.

There were a few limitations in the present study. First, because this was a cross-sectional study, causal relationships cannot be easily inferred from the findings. Long term prospective studies are still needed to confirm the etiological contribution of low hemoglobin. Second, we did not assess the relationships between an abnormally high level of hemoglobin (<15.5 g/dL in female and <17.5 g/dL in male) and neuroimaging markers or cognition, although such high levels of hemoglobin, as well as anemia, have been reported to increase the risk of poor cognitive performance (Shah et al., 2011). This was because only two subjects had a high level of hemoglobin in the present study. Further studies that include individuals within the entire range of possible hemoglobin levels will be helpful to obtain a more comprehensive understanding of the association between hemoglobin and brain pathologies or related cognitive impairment. Third, tau PET was applied after an average of 2.6 years from the baseline visit, whereas other neuroimaging scans were performed at baseline. This temporal gap may have influenced the association between hemoglobin and tau. When we controlled for the temporal gap as an additional covariate, however, the results did not change. In addition, only a subset of participants ($n = 107$) underwent tau PET, while all participants underwent the other imaging modalities. This relatively reduced sample size for tau PET may have decreased the statistical power and contributed to the null result for the relationship between hemoglobin and tau deposition. A study with a larger sample size is still needed to confirm this finding. Lastly, history of vascular risk factors, included as one of the covariates in the Model 3, was assessed only based on the data collected through systematic interviews of participants and their informants. Detailed review of medical record or use of direct physiological or biochemical measurements may help to obtain more accurate information.

CONCLUSION

The present findings suggest that low blood hemoglobin in older adults is associated with cognitive decline via reduced brain metabolism, which seems to be independent of those aspects of AD-specific protein pathologies and cerebrovascular injury that are reflected in PET and MRI measures.

DATA AVAILABILITY STATEMENT

The data of the current study can be available from the independent data sharing committee of the KBASE research group on reasonable request. Requests for data access can be submitted to the administrative coordinator of the KBASE group by e-mail (kbasecohort@gmail.com).

ETHICS STATEMENT

This study was approved by the Institutional Review Boards of Seoul National University Hospital (IRB No: C-1401-027547) and SNU-SMG Boramae Center (IRB No: 26-2015-60), Seoul, South Korea, and was conducted in accordance with the recommendations of the current version of the Declaration of Helsinki. All subjects or their legal representatives gave written and informed consent.

AUTHOR CONTRIBUTIONS

JK and DL conceived and designed the study. MB, DY, JL, SJ, KK, HJ, GJ, J-YL, C-HS, Y-SL, YK, and DL were involved in acquisition, or analysis and interpretation of the data and helped to draft the manuscript. JK, MB, DY, JL, and DL were major contributors in writing the manuscript and critically revising the manuscript for intellectual content. DL served as principal investigator and supervised the study. All authors read and approved the final manuscript.

FUNDING

This study was supported by a grant from the Ministry of Science, ICT, and Future Planning, Republic of Korea (Grant No: NRF-2014M3C7A1046042) and a grant of the Korea Health Technology R&D Project through the Korea Health Industry Development Institute (KHIDI), funded by the Ministry of Health & Welfare, Republic of Korea (Grant Nos: HI18C0630 and HI19C0149). The funding source had no role in the study design, data collection, data analysis, data interpretation, writing of the manuscript, or decision to submit it for publication.

ACKNOWLEDGMENTS

We thank all the members of the KBASE Research Group for their contribution. Members of the KBASE Research Group are listed in elsewhere (http://kbase.kr). We sincerely thank the subjects for their participation in this study. The precursor of [18F] AV-1451 was provided by AVID Radiopharmaceuticals. We also thank AVID Radiopharmaceuticals for providing the precursor.

SUPPLEMENTARY MATERIAL

The Supplementary Material for this article can be found online at: https://www.frontiersin.org/articles/10.3389/fnagi.2021.625511/full#supplementary-material

REFERENCES

Aliev, G., Obrenovich, M. E., Smith, M. A., and Perry, G. (2003). Hypoperfusion, mitochondria failure, oxidative stress, and alzheimer disease. *J. Biomed. Biotechnol.* 2003, 162–163. doi: 10.1155/S1110724303305029

Astor, B. C., Coresh, J., Heiss, G., Pettitt, D., and Sarnak, M. J. (2006). Kidney function and anemia as risk factors for coronary heart disease and mortality: the atherosclerosis risk in communities (ARIC) study. *Am. Heart J.* 151, 492–500. doi: 10.1016/j.ahj.2005.03.055

Atti, A. R., Palmer, K., Volpato, S., Zuliani, G., Winblad, B., and Fratiglioni, L. (2006). Anaemia increases the risk of dementia in cognitively intact elderly. *Neurobiol. Aging* 27, 278–284. doi: 10.1016/j.neurobiolaging.2005.02.007

Ballard, H. S. (1997). The hematological complications of alcoholism. *Alcohol Health Res World* 21, 42–52.

Borroni, B., Akkawi, N., Martini, G., Colciaghi, F., Prometti, P., Rozzini, L., et al. (2002). Microvascular damage and platelet abnormalities in early Alzheimer's disease. *J. Neurol. Sci.* 203–204, 189–193. doi: 10.1016/S0022-510X(02)00289-7

Butterfield, D. A., and Halliwell, B. (2019). Oxidative stress, dysfunctional glucose metabolism and Alzheimer disease. *Nat. Rev. Neurosci.* 20, 148–160. doi: 10.1038/s41583-019-0132-6

Byun, M. S., Yi, D., Lee, J. H., Choe, Y. M., Sohn, B. K., Lee, J. Y., et al. (2017). Korean brain aging study for the early diagnosis and prediction of alzheimer's disease: methodology and baseline sample characteristics. *Psychiatry Investig.* 14, 851–863. doi: 10.4306/pi.2017.14.6.851

Chan, L. N., and Mike, L. A. (2014). The science and practice of micronutrient supplementations in nutritional anemia: an evidence-based review. *JPEN J. Parenter Enteral. Nutr.* 38, 656–672. doi: 10.1177/0148607114533726

Choe, Y. M., Sohn, B. K., Choi, H. J., Byun, M. S., Seo, E. H., Han, J. Y., et al. (2014). Association of homocysteine with hippocampal volume independent of cerebral amyloid and vascular burden. *Neurobiol. Aging* 35, 1519–1525. doi: 10.1016/j.neurobiolaging.2014.01.013

Chuang, J. Y., Lee, C. W., Shih, Y. H., Yang, T., Yu, L., and Kuo, Y. M. (2012). Interactions between amyloid-beta and hemoglobin: implications for amyloid plaque formation in Alzheimer's disease. *PLoS ONE* 7:e33120. doi: 10.1371/journal.pone.0033120

Deal, J. A., Carlson, M. C., Xue, Q. L., Fried, L. P., and Chaves, P. H. (2009). Anemia and 9-year domain-specific cognitive decline in community-dwelling older women: the Women's health and aging study II. *J. Am. Geriatr. Soc.* 57, 1604–1611. doi: 10.1111/j.1532-5415.2009.02400.x

Decarli, C., Mungas, D., Harvey, D., Reed, B., Weiner, M., Chui, H., et al. (2004). Memory impairment, but not cerebrovascular disease, predicts progression of MCI to dementia. *Neurology* 63, 220–227. doi: 10.1212/01.WNL.0000130531.90205.EF

Farah, M. J. (2017). The neuroscience of socioeconomic status: correlates, causes, and consequences. *Neuron* 96, 56–71. doi: 10.1016/j.neuron.2017.08.034

Faux, N. G., Rembach, A., Wiley, J., Ellis, K. A., Ames, D., Fowler, C. J., et al. (2014). An anemia of Alzheimer's disease. *Mol. Psychiatr.* 19, 1227–1234. doi: 10.1038/mp.2013.178

Feig, S. A., Segel, G. B., Shohet, S. B., and Nathan, D. G. (1972). Energy metabolism in human erythrocytes. II. Effects of glucose depletion. *J. Clin. Invest.* 51, 1547–1554. doi: 10.1172/JCI106951

Feig, S. A., Shohet, S. B., and Nathan, D. G. (1971). Energy metabolism in human erythrocytes. I. Effects of sodium fluoride. *J. Clin. Invest.* 50, 1731–1737. doi: 10.1172/JCI106662

Grober, E., Lipton, R. B., Hall, C., and Crystal, H. (2000). Memory impairment on free and cued selective reminding predicts dementia. *Neurology* 54, 827–832. doi: 10.1212/WNL.54.4.827

Hong, C. H., Falvey, C., Harris, T. B., Simonsick, E. M., Satterfield, S., Ferrucci, L., et al. (2013). Anemia and risk of dementia in older adults: findings from the Health ABC study. *Neurology* 81, 528–533. doi: 10.1212/WNL.0b013e31829e701d

Howieson, D. B., Dame, A., Camicioli, R., Sexton, G., Payami, H., and Kaye, J. A. (1997). Cognitive markers preceding Alzheimer's dementia in the healthy oldest old. *J. Am. Geriatr. Soc.* 45, 584–589. doi: 10.1111/j.1532-5415.1997.tb03091.x

Jack, C. R. Jr., Wiste, H. J., Weigand, S. D., Rocca, W. A., Knopman, D. S., Mielke, M. M., et al. (2014). Age-specific population frequencies of cerebral beta-amyloidosis and neurodegeneration among people with normal cognitive function aged 50-89 years: a cross-sectional study. *Lancet Neurol.* 13, 997–1005. doi: 10.1016/S1474-4422(14)70194-2

Jack, C. R. Jr., Wiste, H. J., Weigand, S. D., Therneau, T. M., Lowe, V. J., Knopman, D. S., et al. (2017). Defining imaging biomarker cut points for brain aging and Alzheimer's disease. *Alzheimers Dement* 13, 205–216. doi: 10.1016/j.jalz.2016.08.005

Kosenko, E. A., Tikhonova, L. A., Montoliu, C., Barreto, G. E., Aliev, G., and Kaminsky, Y. G. (2017). Metabolic abnormalities of erythrocytes as a risk factor for alzheimer's disease. *Front. Neurosci*. 11:728. doi: 10.3389/fnins.2017.00728

Lee, D. Y., Lee, K. U., Lee, J. H., Kim, K. W., Jhoo, J. H., Kim, S. Y., et al. (2004). A normative study of the CERAD neuropsychological assessment battery in the Korean elderly. *J. Int. Neuropsychol. Soc.* 10, 72–81. doi: 10.1017/S1355617704101094

Lee, J. H., Lee, K. U., Lee, D. Y., Kim, K. W., Jhoo, J. H., Kim, J. H., et al. (2002). Development of the Korean version of the Consortium to establish a registry for alzheimer's disease assessment packet (CERAD-K): clinical and neuropsychological assessment batteries. *J. Gerontol. Psychol. Sci. Soc. Sci*. 57, P47–53. doi: 10.1093/geronb/57.1.P47

Mahmoodi, M. R., Kimiagar, S. M., and Abadi, A. R. (2007). Is anemia an independent predictor of occurrence of acute coronary syndrome? Results from the modares heart study. *Am. Heart Hosp. J.* 5, 73–79. doi: 10.1111/j.1541-9215.2007.06110.x

Morris, J. C. (1993). The Clinical Dementia Rating (CDR): current version and scoring rules. *Neurology* 43, 2412–2414. doi: 10.1212/WNL.43.11.2412-a

Morris, J. C., Heyman, A., Mohs, R. C., Hughes, J. P., Van Belle, G., Fillenbaum, G., et al. (1989). The Consortium to Establish a Registry for Alzheimer's Disease (CERAD). Part I. Clinical and neuropsychological assessment of Alzheimer's disease. *Neurology* 39, 1159–1165. doi: 10.1212/WNL.39.9.1159

Oyama, R., Yamamoto, H., and Titani, K. (2000). Glutamine synthetase, hemoglobin alpha-chain, and macrophage migration inhibitory factor binding to amyloid beta-protein: their identification in rat brain by a novel affinity chromatography and in Alzheimer's disease brain by immunoprecipitation. *Biochim. Biophys. Acta* 1479, 91–102. doi: 10.1016/S0167-4838(00)00057-1

Park, J. C., Han, S. H., Yi, D., Byun, M. S., Lee, J. H., Jang, S., et al. (2019). Plasma tau/amyloid-beta1-42 ratio predicts brain tau deposition and neurodegeneration in Alzheimer's disease. *Brain* 142, 771–786. doi: 10.1093/brain/awy347

Perry, G., Nunomura, A., Raina, A. K., Aliev, G., Siedlak, S. L., Harris, P. L., et al. (2003). A metabolic basis for Alzheimer disease. *Neurochem. Res*. 28, 1549–1552. doi: 10.1023/A:1025678510480

Qin, T., Yan, M., Fu, Z., Song, Y., Lu, W., Fu, A., et al. (2019). Association between anemia and cognitive decline among Chinese middle-aged and elderly: evidence from the China health and retirement longitudinal study. *BMC Geriatr*. 19:305. doi: 10.1186/s12877-019-1308-7

Reiman, E. M., Chen, K., Liu, X., Bandy, D., Yu, M., Lee, W., et al. (2009). Fibrillar amyloid-beta burden in cognitively normal people at 3 levels of genetic risk for Alzheimer's disease. *Proc. Natl. Acad. Sci. U.S.A*. 106, 6820–6825. doi: 10.1073/pnas.0900345106

Sankar, S. B., Donegan, R. K., Shah, K. J., Reddi, A. R., and Wood, L. B. (2018). Heme and hemoglobin suppress amyloid beta-mediated inflammatory activation of mouse astrocytes. *J. Biol. Chem*. 293, 11358–11373. doi: 10.1074/jbc.RA117.001050

Schechter, A. N. (2008). Hemoglobin research and the origins of molecular medicine. *Blood* 112, 3927–3938. doi: 10.1182/blood-2008-04-078188

Seo, E. H., Lee, D. Y., Lee, J. H., Choo, I. H., Kim, J. W., Kim, S. G., et al. (2010). Total scores of the CERAD neuropsychological assessment battery: validation for mild cognitive impairment and dementia patients with diverse etiologies. *Am. J. Geriatr. Psychiatr.* 18, 801–809. doi: 10.1097/JGP.0b013e3181cab764

Shah, R. C., Buchman, A. S., Wilson, R. S., Leurgans, S. E., and Bennett, D. A. (2011). Hemoglobin level in older persons and incident Alzheimer disease: prospective cohort analysis. *Neurology* 77, 219–226. doi: 10.1212/WNL.0b013e318225aaa9

Shi, Y., Liu, Z., Shen, Y., and Zhu, H. (2018). A novel perspective linkage between kidney function and alzheimer's disease. *Front Cell Neurosci*. 12:384. doi: 10.3389/fncel.2018.00384

Tanne, D., Molshatzki, N., Merzeliak, O., Tsabari, R., Toashi, M., and Schwammenthal, Y. (2010). Anemia status, hemoglobin concentration and outcome after acute stroke: a cohort study. *BMC Neurol*. 10:22. doi: 10.1186/1471-2377-10-22

Tsai, J. Z., Peng, S. J., Chen, Y. W., Wang, K. W., Li, C. H., Wang, J. Y., et al. (2014). Automated segmentation and quantification of white matter hyperintensities in acute ischemic stroke patients with cerebral infarction. *PLoS ONE* 9:e104011. doi: 10.1371/journal.pone.0104011

Vellas, B., Guigoz, Y., Garry, P. J., Nourhashemi, F., Bennahum, D., Lauque, S., et al. (1999). The mini nutritional assessment (MNA) and its use in grading the nutritional state of elderly patients. *Nutrition* 15, 116–122. doi: 10.1016/S0899-9007(98)00171-3

Wenham, P. R., Price, W. H., and Blandell, G. (1991). Apolipoprotein E genotyping by one-stage PCR. *Lancet* 337, 1158–1159. doi: 10.1016/0140-6736(91)92823-K

Wolters, F. J., Zonneveld, H. I., Licher, S., Cremers, L. G. M., Heart Brain Connection Collaborative Research, G., Ikram, M. K., et al. (2019). Hemoglobin and anemia in relation to dementia risk and accompanying changes on brain MRI. *Neurology* 93, e917–e926. doi: 10.1212/WNL.0000000000008003

Wu, C. W., Liao, P. C., Yu, L., Wang, S. T., Chen, S. T., Wu, C. M., et al. (2004). Hemoglobin promotes Abeta oligomer formation and localizes in neurons and amyloid deposits. *Neurobiol. Dis*. 17, 367–377. doi: 10.1016/j.nbd.2004.08.014

Zauner, A., Daugherty, W. P., Bullock, M. R., and Warner, D. S. (2002). Brain oxygenation and energy metabolism: part I-biological function and pathophysiology. *Neurosurgery 51*, 289–301; discussion 302. doi: 10.1097/00006123-200208000-00003

Conflict of Interest: The authors declare that the research was conducted in the absence of any commercial or financial relationships that could be construed as a potential conflict of interest.

frontiers in Neuroscience

ORIGINAL RESEARCH
published: 25 February 2021
doi: 10.3389/fnins.2021.630278

Brain Structural Network Compensation Is Associated With Cognitive Impairment and Alzheimer's Disease Pathology

Xiaoning Sheng[1], Haifeng Chen[1,2,3], Pengfei Shao[1], Ruomeng Qin[1,2,3], Hui Zhao[1,2,3], Yun Xu[1,2,3], Feng Bai[1,2,3] and Alzheimer's Disease Neuroimaging Initiative[†]*

[1] Department of Neurology, Affiliated Drum Tower Hospital of Medical School and The State Key Laboratory of Pharmaceutical Biotechnology, Institute of Brain Science, Nanjing University, Nanjing, China, [2] Jiangsu Province Stroke Center for Diagnosis and Therapy, Nanjing, China, [3] Nanjing Neuropsychiatry Clinic Medical Center, Nanjing, China

Background: Structural network alterations in Alzheimer's disease (AD) are related to worse cognitive impairment. The aim of this study was to quantify the alterations in gray matter associated with impaired cognition and their pathological biomarkers in AD-spectrum patients.

Methods: We extracted gray matter networks from 3D-T1 magnetic resonance imaging scans, and a graph theory analysis was used to explore alterations in the network metrics in 34 healthy controls, 70 mild cognitive impairment (MCI) patients, and 40 AD patients. Spearman correlation analysis was computed to investigate the relationships among network properties, neuropsychological performance, and cerebrospinal fluid pathological biomarkers (i.e., Aβ, t-tau, and p-tau) in these subjects.

Results: AD-spectrum individuals demonstrated higher nodal properties and edge properties associated with impaired memory function, and lower amyloid-β or higher tau levels than the controls. Furthermore, these compensations at the brain regional level in AD-spectrum patients were mainly in the medial temporal lobe; however, the compensation at the whole-brain network level gradually extended from the frontal lobe to become widely distributed throughout the cortex with the progression of AD.

Conclusion: The findings provide insight into the alterations in the gray matter network related to impaired cognition and pathological biomarkers in the progression of AD. The possibility of compensation was detected in the structural networks in AD-spectrum patients; the compensatory patterns at regional and whole-brain levels were different and the clinical significance was highlighted.

Keywords: cognitive impairment, pathological biomarkers, Alzheimer's disease, structural compensation ability, gray matter (GM) atrophy

OPEN ACCESS

Edited by:
Yong Liu,
Beijing University of Posts and Telecommunications (BUPT), China

Reviewed by:
Jiu Chen,
Nanjing Medical University, China
Swati Rane,
University of Washington, United States

****Correspondence:***
Feng Bai
baifeng515@126.com

[†]Data used in preparation of this article were obtained from the Alzheimer's Disease Neuroimaging Initiative (ADNI) database (adni.loni.usc.edu). As such, the investigators within the ADNI contributed to the design and implementation of ADNI and/or provided data but did not participate in the analysis or writing of this report. A complete listing of ADNI investigators can be found at http://adni.loni.usc.edu/wp-content/uploads/how_to_apply/ADNI_Acknowledgement_List.pdf.

Specialty section:
This article was submitted to Brain Imaging Methods, a section of the journal Frontiers in Neuroscience

Received: *17 November 2020*
Accepted: *26 January 2021*
Published: *25 February 2021*

Citation:
Sheng X, Chen H, Shao P, Qin R, Zhao H, Xu Y, Bai F and Alzheimer's Disease Neuroimaging Initiative (2021) Brain Structural Network Compensation Is Associated With Cognitive Impairment and Alzheimer's Disease Pathology. Front. Neurosci. 15:630278. doi: 10.3389/fnins.2021.630278

INTRODUCTION

Alzheimer's disease (AD), the most prevalent cause of dementia, is characterized by progressive loss in the activities of daily living and cognitive impairment, which causes a very large socioeconomic burden (van der Lee et al., 2018). The number of individuals with AD is increasing significantly every year, and 10–20% of people aged 65 or older suffer from mild cognitive impairment (MCI)

which is known as a prodromal clinical stage of AD (Kim et al., 2020). However, the effective period of symptomatic treatment is limited (Patnode et al., 2020). Therefore, the early diagnosis and prognosis of clinical AD-spectrum patients is of great importance as it increases the time window to implement interventions that attenuate or reverse deterioration (Luo et al., 2019).

Structural magnetic resonance imaging (MRI) is a promising approach used to identify the progression of disease (Lane et al., 2019). Evidence has been accumulating that changes leading to cognitive impairment and dementia are not limited to specific regions but rather exhibit widespread changes in connectivity and topological properties that have emerged as potential intermediate biomarkers for AD (Verfaillie et al., 2018). The pattern of gray matter morphology can be defined as a network that consists of multiple regions (i.e., nodes) that are interconnected when structural similarity is exhibited within the cortex across subjects (Beheshti et al., 2017). The advantage of examining the morphology of gray matter networks is that it provides the possibility to accurately quantify individual brains using tools from graph theory (Batalle et al., 2013; Beheshti et al., 2017). For example, the small world coefficient provides an indication of whether the organization of connections in the network is different from a randomly organized network (Zhao et al., 2017). Although the biological significance of structural similarities is not fully understood, the similarity within gray matter has been shown to be related to synchronized maturation between brain regions, which may reflect a higher degree of clustering (Wang et al., 2018). Previous studies have shown that changes in structural properties in gray matter are related to the degree of cognitive impairment and disease severity in individuals with AD (Vipin et al., 2018). In the early and preclinical stages of dementia, the gray matter network might commence reorganization and show high resilience to network integrity damages (Lin et al., 2020). Previous studies have further demonstrated that lower cerebrospinal fluid (CSF) Aβ42 levels in individuals with cognitive impairment were closely associated with the perceived decline in memory performance (Zhang et al., 2018). In a series of structural neuroimaging studies, it was reported that individuals with cognitive impairment exhibited, from the perspective of topological properties, higher nodal degree centrality and lower nodal betweenness in the bilateral hippocampus, compared to the healthy controls (Chen et al., 2020). Recently, structural similarity within the gray matter network in individuals with cognitive impairment was mainly related to the thalamus, insula, and occipital cortex and was associated with poor memory performance (Ahmed et al., 2019). However, there has been no research exploring the altered structural network measures related to pathological biomarkers in combination with the structural similarity and topological properties in patients with cognitive impairment. If individuals with cognitive impairment at the early stage of AD could be identified, they may benefit from early targeted intervention. With developments in neuroimaging, an increasing number of studies have focused on identifying brain functional and structural alterations related to the AD continuum, which may potentially be considered a biomarker of AD pathology.

To this end, we compared the structural networks and the structural similarity within gray matter in AD-spectrum patients using a graph theoretical approach (Rubinov and Sporns, 2010). In the present study, the aim was to explore whether gray matter network parameters were linked to declines in cognitive impairment and abnormal CSF pathology in AD-spectrum patients.

MATERIALS AND METHODS

Data used in the preparation of our study were obtained from the Alzheimer's Disease Neuroimaging Initiative (ADNI) database[1]. The protocol was authorized by the ADNI and informed consent was obtained according to the Declaration of Helsinki. The ADNI was launched in 2003 as a non-profit organization, led by Principal Investigator Michael W. Weiner, MD. The aim of the ADNI is to test whether neuroimaging, neuropsychological assessment, and biological markers could track the progression of AD and conduct early diagnosis. For up-to-date information, see adni-info.org.

Study Population

This study included 34 healthy controls (HC), 70 early or late MCI patients, and 40 AD patients, and used a subset of T1-weighted MRI images for these 144 subjects. Subjects were originally recruited for ADNI-GO or ADNI-2. Group inclusion criteria were as follows. HC subjects had no memory complaints, a CDR score of 0 and Mini-Mental State Examination (MMSE) scores between 26 and 30. MCI subjects had a CDR score of 0.5, MMSE scores between 21 and 30, as well as memory complaints and abnormal memory function according to the Logical Memory II subscale (Delayed Paragraph Recall) from the Weschler Memory Scaled—Revised (=8 for 16 years and more of education; =4 for 8–15 years of education; and =2 for 0–7 years of education), but an absence of dementia. To be included in the AD group, participants had memory complaints, CDR scores between 0.5 and 2.0, MMSE scores less than 26, and presented the criteria for probable AD diagnosis according to National Institute of Neurological and Communicative Disorders and Stroke/Alzheimer's Disease and Related Disorders Association (NINCDS/ADRDA) (Lu et al., 2019). In addition, we also excluded participants with a history of significant psychiatric and neurological illness (e.g., depression, stroke, traumatic brain injury, and others). All participants were required to provide informed consent compatible with the local sites (Institutional Review Board regulations). **Table 1** shows the detailed clinical and demographic information for these subjects.

Clinical and Neuropsychological Measurement

All participants received a series of cognitive evaluations in the primary analyses, including the MMSE, Montreal Cognitive Assessment (MoCA); Functional Activities Questionnaire (FAQ); Clinical Dementia Rating Sum of Boxes (CDRSB); Alzheimer's

[1] adni.loni.usc.edu

TABLE 1 | Demographic and neuropsychological data.

Items	HC (n = 34)	MCI (n = 70)	AD (n = 40)	F/χ 2	P
Demographics					
Age (years)	72.38 ± 0.87	73.78 ± 0.84	74.85 ± 1.37	1.082	0.342[b]
Education (years)	16.21 ± 0.48	15.73 ± 0.34	15.15 ± 0.45	1.273	0.283[b]
Gender (male/female)	13/21	42/28	23/17	4.614	0.100[a]
General cognition					
MMSE	28.76 ± 0.26	27.61 ± 0.21	23.25 ± 0.30	9.653	<0.001[b]*
MoCA	25.85 ± 0.40	22.44 ± 0.34	17.28 ± 0.68	61.959	<0.001[b]*
FAQ	0.41 ± 0.24	2.77 ± 0.37	15.1 ± 1.06	143.618	<0.001[b]*
CDRSB	0.15 ± 0.07	1.66 ± 0.10	5.03 ± 0.22	268.077	<0.001[b]*
ADAS13	8.09 ± 0.68	17.3 ± 0.83	30.68 ± 1.35	102.456	<0.001[b]*
EcogSPMem	1.47 ± 0.11	2.21 ± 0.09	3.25 ± 0.10	63.732	<0.001[b]*
EcogSPLang	1.33 ± 0.09	1.56 ± 0.07	2.47 ± 0.13	36.699	<0.001[b]*
EcogSPVisspat	1.14 ± 0.05	1.42 ± 0.06	2.60 ± 0.15	61.820	<0.001[b]*
EcogSPPlan	1.30 ± 0.09	1.49 ± 0.07	2.76 ± 0.13	63.467	<0.001[b]*
EcogSPOrgan	1.38 ± 0.11	1.64 ± 0.08	3.03 ± 0.12	71.906	<0.001[b]*
EcogSPDivatt	1.44 ± 0.11	1.85 ± 0.09	3.09 ± 0.13	54.816	<0.001[b]*
EcogSPTotal	1.35 ± 0.08	1.70 ± 0.06	2.83 ± 0.10	78.533	<0.001[b]*
Cerebrospinal fluid					
Aβ (pg/mL)	1293.73 ± 84.83	901.05 ± 57.21	647.98 ± 41.89	23.100	<0.001[b]*
t-tau (pg/mL)	210.03 ± 13.12	290.83 ± 22.36	358.16 ± 26.69	7.873	0.001[b]*
p-tau (pg/mL)	19.32 ± 1.24	28.25 ± 2.45	35.43 ± 2.81	7.913	0.001[b]*

Values are presented as the mean ± standard error (SE).
[a]The p-value was obtained by χ^2 test, [b]the p-value was obtained by one-way ANOVA.
**Indicates a statistical difference between groups, $p < 0.05$.*
MMSE, mini mental state examination; MoCA, Montreal Cognitive Assessment; FAQ, Functional Activities Questionnaire; CDRSB, Clinical Dementia Rating Sum of Boxes; ADAS13, Alzheimer's Disease Assessment Scale; EcogSP, Everyday Cognition by the patient's study; Mem, Memory; Lang, Language; Visspat, Visuospatial; Plan, Planning; Organ, Organization; Divatt, Divided Attention; Aβ, amyloid-β; t-tau, total tau; p-tau, phosphorylated tau.

Disease Assessment Scale (ADAS13), and Everyday Cognition by the patient's study partner (EcogSP), that provided memory, language, visuospatial abilities, planning, organization, divided attention, and total scores (**Table 1**).

Cerebrospinal Fluid Biomarkers

Lumbar puncture and the preparation of the CSF sample were described in the ADNI manual[2]. CSF Aβ, t-tau, and p-tau were measured based on the reagents (Innotest, Fujirebio, Ghent, Belgium) from INNOBIA AlzBio3 immunoassay kit. Not all subjects had CSF sample data because lumbar puncture is an invasive procedure. In this study, 23 out of 34 HC subjects, 46 out of 70 MCI subjects, and 34 out of 40 AD subjects had a CSF sample available (**Table 1**).

MRI Acquisition

The standardized T1-weighted image protocol used volumetric 3-dimensional sagittal MPRAGE[3]. Briefly, the ADNI protocol includes T1-weighted acquisition based on a sagittal volumetric magnetization-prepared rapid gradient-echo sequence collected from a variety of 3.0 Tesla MRI systems with protocols optimized for each type of scanner. Representative of each scan, parameters were as follows: repetition time = 2300 ms; flip angle = 8°; inversion time = 1000 ms; field of view = 240 mm × 240 mm; and a 256 × 256 matrix yielding, a voxel size of 0.94 mm × 0.94 mm × 1.2 mm. The workflow graphic about the processing of the gray matter structural network is presented in **Figure 1**.

Image Pre-processing

We used the Computational Anatomy Toolbox (CAT12[4]) as implemented in the Statistical Parametric Mapping analysis package (SPM12[5]) to pre-process the structural images. First, the raw MRI data were checked manually to ensure no obvious artifacts. Second, individual 3D-T1 images were segmented into white matter (WM), gray matter (GM), and cerebrospinal fluid (CSF) using an adaptive Maximum A Posterior technique (Wang et al., 2016). The intracranial volume was obtained by summing the volumes of the GM, WM, and CSF. Last, the resultant GM images were normalized to the Montreal Neurological Institute (MNI) space and the GM volume maps were smoothed spatially (Gaussian kernel of 8 mm full width at half maximum). To define the network nodes, an automated anatomical labeling (AAL) atlas was used to divide the brain into 90 regions of interest (ROIs) (abbreviations provided in **Supplementary Table 1**). We calculated the gray matter network density considered as the total number of edges in the network, divided by the possible

[2]http://adni.loni.usc.edu/research/protocols/bios-pecimens-protocols/
[3]http://adni.loni.usc.edu/
[4]http://www.neuro.uni-jena.de/cat/
[5]http://www.fil.ion.ucl.ac.uk/spm/soft-ware/spm12/

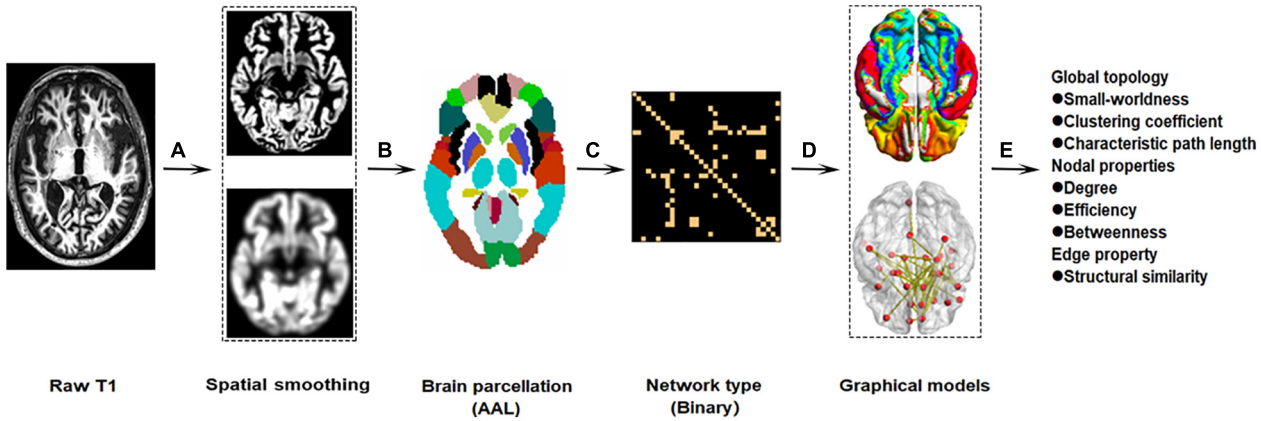

FIGURE 1 | Workflow graphic of gray matter structural networks. The processing of gray matter structural network roughly includes preprocessing (**A:** spatial smoothing), brain parcelation **(B)**, network type **(C)**, graphical models **(D)**, and network reconstruction **(E)**.

number of edges, and average network strength considered as the sum of all weighted edges for every node, using the Graph Theoretical Network Analysis Toolbox (GRETNA[6]) based on Brain Connectivity Toolbox (Wang et al., 2015).

Network Parameters and Network Reconstruction

Every subject's gray matter network from gray matter segmentations was extracted, using a fully automated method to implement in MATLAB[7]. Briefly, we defined nodes as $3 \times 3 \times 3$ voxel regions in gray matter through an atlas free approach (Rimkus et al., 2019). We then defined connectivity using statistical similarity in gray matter structures by Spearman's correlations across intensity values of corresponding voxels between one node and neighbor nodes in the gray matter (Tijms et al., 2016). All similarity values were collected in a matrix. Nodes connected were ensured that all subjects had a threshold that they had a similar chance including at most 5% spurious connections through a random permutation method (Toppi et al., 2012). To reduce the number of local tests, the nodal network characteristics for nodes were averaged in 90 regions of interest as defined by the automatic anatomical labeling (AAL) brain atlas (Tzourio-Mazoyer et al., 2002; Jin et al., 2020). The network metrics were classified as "basic" or "higher-order" parameters (Liu et al., 2020). The basic parameters included the local and global degree and the small-worldness. Higher-order network parameters consisted of the clustering coefficient, characteristic path length, degree centrality, and betweenness centrality (Rubinov and Sporns, 2010). To further explore the topological structure of the network, we calculated the small-worldness, global efficiency, and local efficiency. To obtain the network edge, we calculated the connectivity referred to the statistical similarity between each pair of 90 ROIs, which is computed by the Spearman's correlation of the grey matter intensity values of the corresponding voxels in the ROIs. All similarity values are arranged in a similarity matrix. ROIs are connected when the similarity value of ROIs exceeds the statistical threshold ($P < 0.05$, False Discovery Rate, FDR corrected) determined by the random arrangement method (Toppi et al., 2012). A brief description of specific definitions, calculating formula, and topological property descriptions for the network G with N nodes and V edges follows below (Xu et al., 2016; Yang et al., 2020).

[6]http://www.nitrc.org/projects/gretna/

[7]https://github.com/bettytijms/Single_Subject_Grey_Matter_Networks

Global Topological Properties

The inverse of the harmonic mean of the shortest path length between every two nodes in the network is considered as Global efficiency. It efficiently measures the information communication capacity of the whole network. It is calculated as:

$$Eglobal\,(G) = \frac{1}{N\,(N-1)} \sum_{i \neq j \in G} \frac{1}{dij}$$

d_{ij} is the shortest path length between node i and j of the network.

Local efficiency of the network measures how efficiently the communication information is among the neighbors of a specific node when that node is removed, which shows how fault tolerant the network is and is calculated as:

$$Elocal(G) = \frac{1}{N} \sum_{i \in G} Eglobal(Gi)$$

G_i is the subgraph consisting of the nearest neighbors of node *i*.

Nodal Topological Properties

Nodal global efficiency quantifies how efficiently the parallel information transfers from one node in the network and is calculated as:

$$Enodal\_global\,(i) = \frac{1}{N-1} \sum_{i \neq j \in G} \frac{1}{dij}$$

d_{ij} indicates the shortest path length between node i and j of the network.

Nodal local efficiency indicates the efficiency of the communication among the first neighbors of one node when it is

removed. It is calculated as:

$$E_{nodal\_local}(i) = \frac{1}{N_i(N_i-1)} \sum_{m \neq n \in G_i} \frac{1}{d_{mn}}$$

G_i is the sub-graph which consists of node i and its local neighbors.

Nodal strength is defined as the sum of the edge weights in a subnetwork G_i, which is the graph that includes the nodes that are direct neighbors of node i. It can be defined as:

$$S_{nodai}(i) = \sum_{j \in G_i} w_{ij}$$

where w_{ij} is the edge weight linking node i and j in the subnetwork G_i.

Statistical Analysis

Statistical analyses were performed with the Statistical Package for the Social Sciences (SPSS, IBM v22). A one-way analysis of variance (ANOVA) was performed in the analyses of age, education, and data volume, with significance at $P < 0.05$ among the control group, the MCI group, and the AD group. The Chi-squared (χ^2) test was applied in the analysis of gender, among the three groups. Because the neuropsychological data was of non-normal distribution, the Kruskal–Wallis test was applied in the analyses of the neuropsychological data with significance at $P < 0.05$ among the three groups (Zhu et al., 2016).

At the level of the edge properties of the brain network, we used the two-sample t test to investigate group differences between any two groups, adjusting for age, sex, and education years with a false discovery rate (FDR) correction for multiple comparisons.

One-way analysis of covariance (ANCOVA) was used to explore the group differences in the structural networks (degree centrality, betweenness centrality, global efficiency, and local efficiency) while adjusting based on age, sex, and education years. Correction of multiple testing used the FDR. Subsequently, we conducted a *post hoc* analysis to investigate the group differences between any pair of all groups.

Additionally, a multiple linear regression analysis was conducted to investigate the relationships among CSF pathology indicators, gray matter network graph theoretical properties, and cognitive function adjusting for age, gender, and education years at $P < 0.05$, uncorrected (Lu et al., 2017; Wang et al., 2020).

RESULTS

Demographic, Neuropsychological, and CSF Data

The characteristic demographic, neuropsychological and CSF data of the participants are presented in **Table 1**. No significant differences among the three groups were observed in age, gender, or education years ($P > 0.05$). Multiple cognitive functions were more impaired in MCI and AD patients than in the controls, and the largest differences were between AD patients and the controls (all $P < 0.05$), including scores on the MMSE, MoCA, FAQ, CDRSB, ADAS13, and EcogSP.

We observed a significant reduction in CSF Aβ levels ($P < 0.001$) and increased CSF t-tau ($P = 0.001$) and p-tau ($P = 0.001$) levels with the progression of AD.

Global Topology of Gray Matter Structural Networks

The properties of the global network analysis are shown in **Figure 2**. No significant differences were calculated among the three groups in global efficiency or the small-worldness ($P > 0.05$, FDR corrected).

Node-Based Analysis of Gray Matter Structural Networks

The nodal analysis is shown in **Figure 3**. Abnormal nodal levels (betweenness centrality, degree centrality, and nodal efficiency) were observed in AD-spectrum patients ($P < 0.05$, FDR corrected). In general, gradually increasing nodal properties in the medial temporal lobe (right parahippocampal gyrus and right amygdala) were associated with the progression of AD across the three groups (from HC to MCI to AD), with the exception of decreased betweenness centrality of the right parahippocampal gyrus in the MCI group.

In the present study, significant relationships between altered nodal (i.e., right parahippocampal gyrus and right amygdala) properties and multidomain cognitive impairments were observed in AD-spectrum patients (**Table 2**; for more details, see **Supplementary Table 2**). In addition, no significant correlation was calculated between altered nodal properties and CSF biomarkers in HC and MCI patients, and the betweenness centrality in the right parahippocampal gyrus was negatively correlated with CSF t-tau (r =-0.373, P = 0.03) (**Figure 4A**) and p-tau (r = -0.386, P = 0.024) (**Figure 4B**) concentration in AD patients.

Connectivity-Based Analysis

By using correcting for multiple comparisons with FDR correction, the AD-spectrum patients had significant differences in the structural similarity within the gray matter network when compared to the controls. In addition to a few edges showing decreased structural similarity, most of the others showed increases with the development of AD. In detail, the abnormal connections were mainly related to the frontal lobe in the MCI group (**Figure 5A**), but were more widely distributed in the frontal lobe, thalamus, and subcortical structures in the AD group (**Figures 5B,C**) ($P < 0.05$, FDR corrected).

Significant associations between altered edge properties and cognitive impairments were detected in AD-spectrum patients. Interestingly, most of these connections between edges were associated with the frontal lobe in both the MCI and AD groups (**Table 3**, for more details, see **Supplementary Tables 3, 4**). In addition, the connection between the right medial superior frontal gyrus and left precentral gyrus (t-tau: r = -0.293, P = 0.049) (**Figure 6A**) was negatively correlated with the CSF tau concentrations in MCI patients. In the AD group, the connection

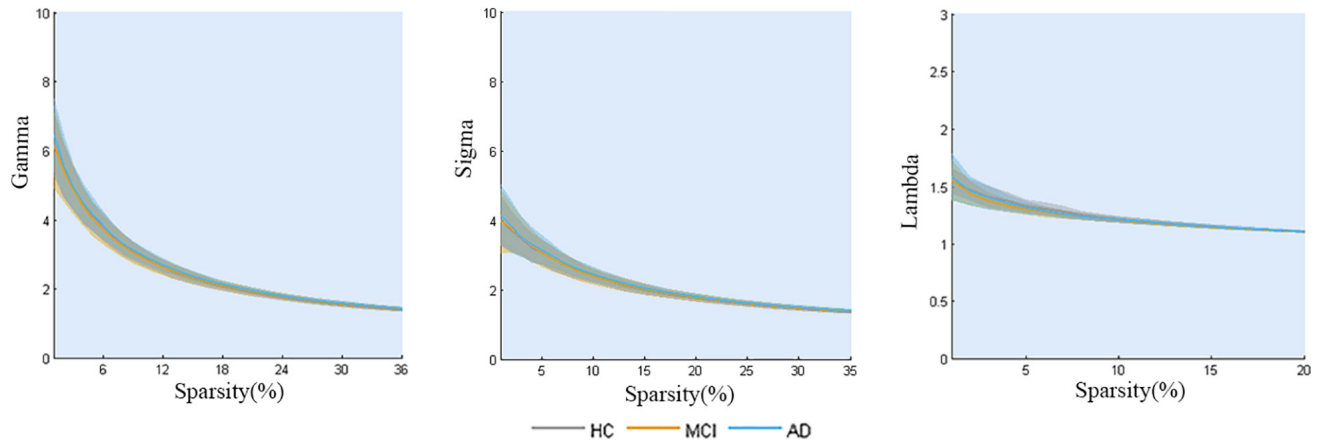

FIGURE 2 | Global topology of gray matter structural networks in AD-spectrum patients. No significant differences were calculated among the three groups (all $P > 0.05$, FDR corrected).

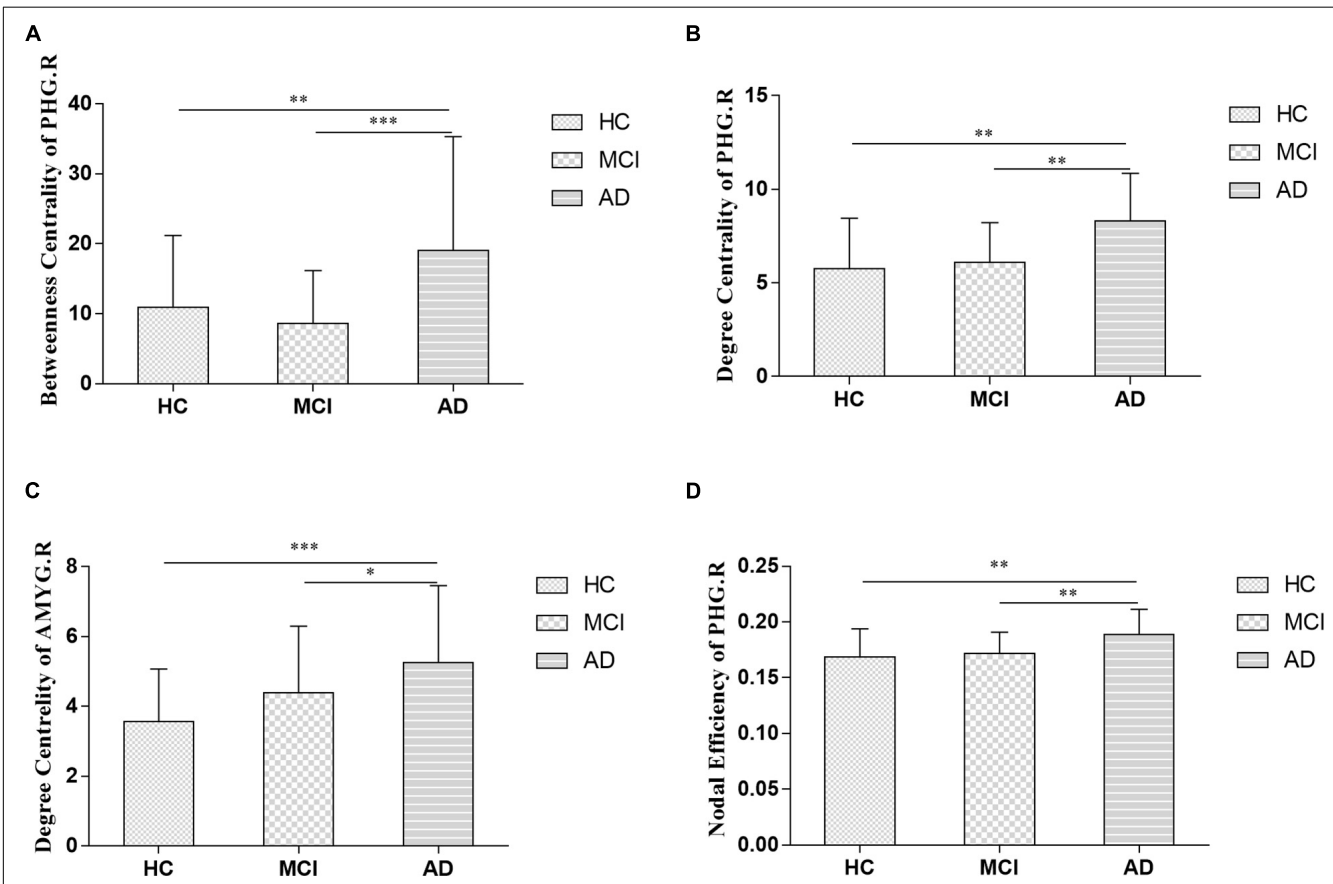

FIGURE 3 | Between-groups comparisons showed the altered betweenness centrality (**A:** right parahippocampal gyrus), degree centrality (**B:** right parahippocampal gyrus; **C:** right amygdala) and nodal efficiency (**D:** right parahippocampal gyrus) in AD-spectrum patients. PHG.R, right parahippocampal gyrus; AMYG.R, right amygdala; $^{*}P < 0.05$, $^{**}P < 0.01$, $^{***}P < 0.001$ indicates a statistical difference between groups by FDR corrected.

TABLE 2 | Significant correlations between altered graph theoretical properties and neuropsychological performance in AD-spectrum patients.

Neuropsychological scale	Group	Network properties	Spearman's correlation coefficient	*P*-values
FAQ	HC	DC of PHG.R	0.352	0.041*
		DC of AMYG.R	0.36	0.037*
		NE of PHG.R	0.362	0.035*
	MCI	BC of PHG.R	0.301	0.011*
	AD	DC of PHG.R	0.334	0.035*
		DC of AMYG.R	0.335	0.034*
		NE of PHG.R	0.342	0.031*
CDRSB	HC	BC of PHG.R	0.37	0.031*
		DC of PHG.R	0.424	0.012*
		DC of AMYG.R	0.388	0.023*
		NE of PHG.R	0.433	0.011*
	MCI	BC of PHG.R	0.295	0.013*
		DC of PHG.R	0.343	0.004**
		NE of PHG.R	0.286	0.016*
	AD	DC of PHG.R	0.339	0.032*
		NE of PHG.R	0.362	0.022*
ADAS13	AD	DC of PHG.R	0.395	0.012*
		NE of PHG.R	0.364	0.021*
EcogSP Mem	MCI	DC of AMYG.R	− 0.236	0.049*
EcogSP Lang	HC	BC of PHG.R	0.392	0.022*
	MCI	NE of PHG.R	0.248	0.038*
EcogSP Visspat	HC	BC of PHG.R	0.355	0.039*
		DC of PHG.R	0.492	0.003**
		NE of PHG.R	0.477	0.004**
	MCI	DC of AMYG.R	− 0.244	0.041*
	AD	BC of PHG.R	0.334	0.035*
		DC of PHG.R	0.462	0.003**
		DC of AMYG.R	0.384	0.014*
		NE of PHG.R	0.511	0.001**
EcogSP Plan	HC	BC of PHG.R	0.386	0.024*
		DC of PHG.R	0.436	0.01**
		NE of PHG.R	0.454	0.007**
	MCI	BC of PHG.R	0.326	0.006**
	AD	DC of AMYG.R	0.395	0.012*
		NE of PHG.R	0.336	0.034*
EcogSP Organ	HC	BC of PHG.R	0.464	0.006**
		DC of PHG.R	0.484	0.004**
		NE of PHG.R	0.494	0.003**
EcogSP Divatt	HC	BC of PHG.R	0.348	0.044*
		DC of PHG.R	0.491	0.003**
		NE of PHG.R	0.498	0.003**
	AD	NE of PHG.R	0.328	0.039*
EcogSP Total	HC	BC of PHG.R	0.394	0.021*
		DC of PHG.R	0.4	0.019*
		NE of PHG.R	0.413	0.015*
	AD	DC of PHG.R	0.407	0.009**
		DC of AMYG.R	0.389	0.013*
		NE of PHG.R	0.446	0.004**

**P < 0.05, **P < 0.01 indicates an uncorrected relevant analysis.*

HC, healthy controls; MCI, mild cognitive impairment; AD, Alzheimer's disease; BC, Betweenness Centrality; DC, Degree Centrality; NE, Nodal Efficiency; PHG.R, right parahippocampal gyrus; AMYG.R, right amygdala; MMSE, mini mental state examination; MoCA, Montreal Cognitive Assessment; FAQ, Functional Activities Questionnaire; CDRSB, Clinical Dementia Rating Sum of Boxes; ADAS13, Alzheimer's Disease Assessment Scale; EcogSP, Everyday Cognition by the patient's study; Mem, Memory; Lang, Language; Visspat, Visuospatial; Plan, Planning; Organ, Organization; Divatt, Divided Attention.

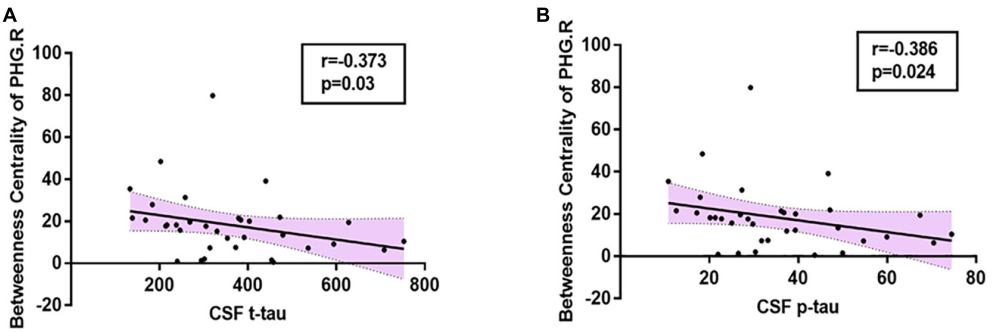

FIGURE 4 | Relationships between altered nodal properties and CSF biomarkers in AD group. The betweenness centrality in the right parahippocampal gyrus was negatively correlated with CSF t-tau (**A:** r = -0.373, P = 0.03) and CSF p-tau (**B:** r = -0.386, P = 0.024) in AD patients. PHG.R, right parahippocampal gyrus.

between the right medial superior frontal gyrus and left cuneus was positively correlated with CSF t-tau (r = 0.399, P = 0.019) (**Figure 6B**) and CSF p-tau (r = 0.420, P = 0.013) (**Figure 6C**).

DISCUSSION

In the present study, we investigated topological alterations in the structural network within gray matter, the relationships to pathological biomarkers, and their behavioral significance in AD-spectrum patients. The three main findings are as follows: (i) The local regional rearrangements in AD-spectrum patients are mainly in the medial temporal lobe. (ii) The rearrangements in the whole-brain networks gradually extended from the frontal lobe to become widely distributed in the cortex with the progression of AD. (iii) These rearrangements in gray matter might be associated with compensation, which was influenced following multidomain cognitive impairments and AD-related CSF.

Research interest is transforming to increasingly earlier diagnoses, since the origin of AD and the key to treatment probably lie in preventing progression to a fully-fledged disease (Hem et al., 2016; Slot et al., 2018). It should be noted that compensation in the structural network has been shown to be manifested earlier in AD-spectrum patients (Liu et al., 2020), and there is increasing interest in the study of structural network alterations to assess the progression in subjects who have a higher risk of AD (Sanchez-Benavides et al., 2018). Therefore, it is essential to evaluate alterations in structural networks related to cognition and pathology (Dicks et al., 2020). In the present study, we deduced that there was the possibility of compensation in the structural networks in AD-spectrum patients, as expected from previous AD-spectrum studies which also provided additional evidence for our research results (Wook Yoo et al., 2015; Caso et al., 2016). Our findings demonstrate that brain regional compensation may start from the medial temporal lobe, and the level of compensation within the whole gray matter network moved from the frontal lobe to the more extensive cortex as the disease progressed. We confirmed that the gray matter network might commence reorganization and show high resilience to network integrity damages in the early and preclinical stages of dementia, which is similar to previous studies (De Vogelaere et al., 2012). Thus, structural network properties can be a sensitive and reliable index to detect changes in the evolution of AD.

These findings are in line with previous studies reporting altered graph theoretical properties in these regions in AD-spectrum patients (Shah et al., 2018; Liu et al., 2020). Most of the network graph theoretical properties referring to the frontal lobe, medial temporal lobe, and subcortical structures–areas that play a role in perception, executive control, episodic memory, and understanding–have consistently been found to be affected across the development of AD (Geib et al., 2017; Danti et al., 2018; Luo et al., 2018). Furthermore, our study may reflect reorganization and high resilience to network integrity damage. Previous studies evaluating graph theoretical properties have described compensation at the level of hippocampal/parahippocampal regions and the frontal and occipital lobes (van Duinkerken et al., 2016; Li et al., 2018). In line with prior studies, in our analysis, network integrity was widely increased due to the compensation in specific nodes related to cognition. Despite differences in methodologies, compensation has been described in other neurological and psychiatric disorders, such as schizophrenia (Sapara et al., 2014) and early stages of Parkinson's disease (Nonnekes et al., 2019). Increased global connectivity in the frontal lobe, hippocampus, and occipital areas has been previously reported for mild AD patients (Bai et al., 2011; De Vogelaere et al., 2012). Similarly, our study shows that the compensation appears in the medial temporal lobe at the brain regional level, while it gradually spread from the frontal lobe to the widely distributed throughout the cortex at the whole-brain network level with AD degenerative processes. However, there is no specific report about the potential mechanism revealing the patterns of this compensation within structural networks of AD-spectrum patients. In that sense, our findings present novel evidence of pathophysiological mechanisms in alterations within the gray matter network of AD-spectrum patients.

In addition, little is known about the pathological basis of structural network compensation (Jackson et al., 2019). The findings of impaired graph theoretical properties with reference to the frontal lobe, medial temporal lobe, and

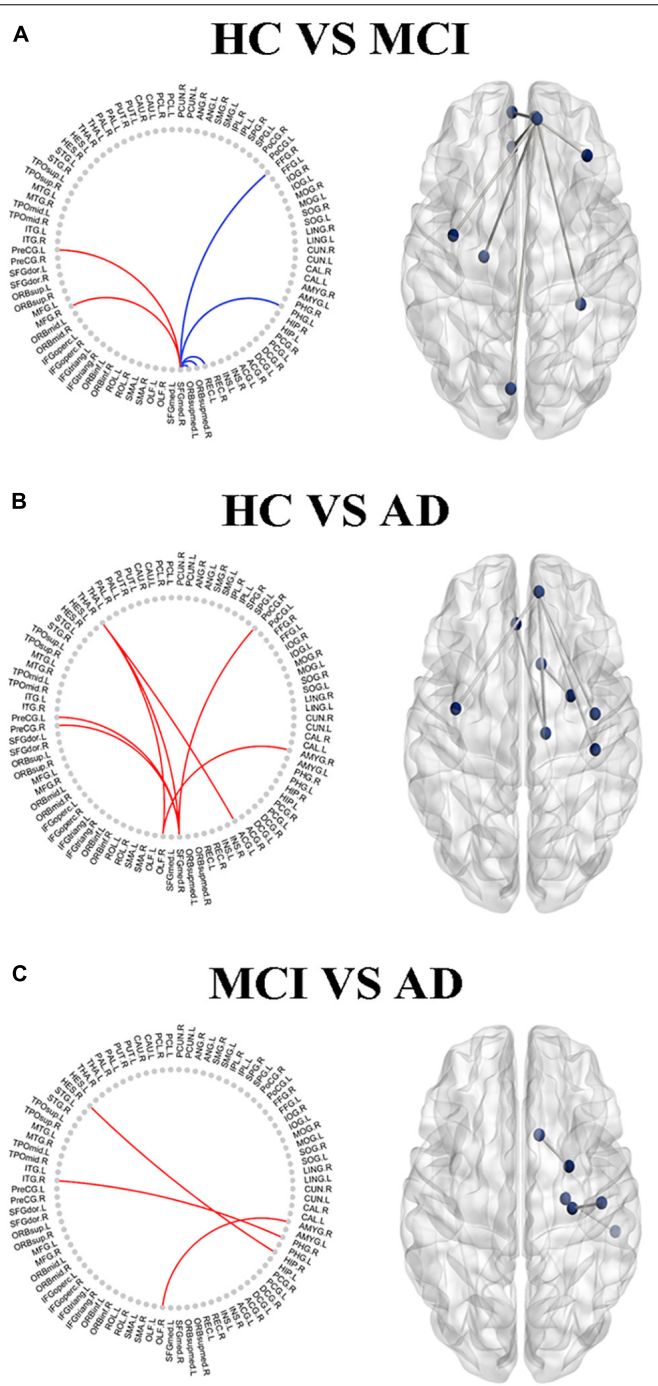

FIGURE 5 | The altered edge based on the node analysis in AD-spectrum patients. Edges with significant ($P < 0.05$, FDR correction) increase (in red) or decrease (in blue) in MCI **(A)** and AD **(B)** in patients compared with HC, and MCI group compared with AD **(C)**. Results are shown in anatomical view (left panels) and in connectograms (right panels).

subcortical structures involved alterations affecting gray matter structures in the present AD spectrum patients, which is in line with previous studies reporting increased Aβ deposition and pathological tau accumulation in these regions in AD (Buckley et al., 2017). This study demonstrates the compensation related to cognitive impairments, which exists with a potential AD pathological basis behind them. Taken together, our findings and those from structural network studies suggest structural brain compensation in response to brain damage (Wook Yoo et al., 2015; Liu et al., 2020). However, the relationship between structural changes and disease progression remains controversial. Modifications in

TABLE 3 | Significant correlations between the altered edge properties and neuropsychological performance in MCI and AD patients.

Neuropsychological scale	Group	Edge	Spearman's correlation coefficient	*P*-values
MMSE	MCI	SFGmed.R – MFG.R	0.356	0.002**
		SFGmed.R – ORBsupmed.L	– 0.277	0.02*
	AD	SFGmed.R – PreCG.R	– 0.396	0.011*
MoCA	AD	SFGmed.R – PreCG.R	– 0.35	0.027*
		SFGmed.R – PoCG.R	– 0.395	0.012*
		ACG.L – THA.R	– 0.349	0.027*
FAQ	AD	SFGmed.R – PreCG.R	0.385	0.014*
CDRSB	AD	SFGmed.R – PoCG.R	0.315	0.048*
ADAS13	AD	ACG.L – THA.R	0.354	0.025*
EcogSP Lang	AD	SFGmed.R – ORBsupmed.R	0.319	0.045*
EcogSP Plan	MCI	SFGmed.R – FFG.R	0.308	0.009**

**P<0.05, **P<0.01 indicates an uncorrected relevant analysis.*
MCI, mild cognitive impairment; AD, Alzheimer's disease; MMSE, mini mental state examination; MoCA, Montreal Cognitive Assessment; FAQ, Functional Activities Questionnaire; CDRSB, Clinical Dementia Rating Sum of Boxes; ADAS13, Alzheimer's Disease Assessment Scale; EcogSP, Everyday Cognition by the patient's study; Lang, Language; Plan, Planning; PreCG.R, right precentral gyrus; MFG.R, right middle frontal gyrus; SFGmed.R, right superior frontal gyrus-medial part; ORBsupmed.L, left superior frontal gyrus-medial orbital part; ORBsupmed.R, right superior frontal gyrus-medial orbital part; THA.R, right thalamus; PoCG.R, right postcentral gyrus; ACG.L, left anterior cingulate and paracingulate gyri; FFG.R, right fusiform gyrus.

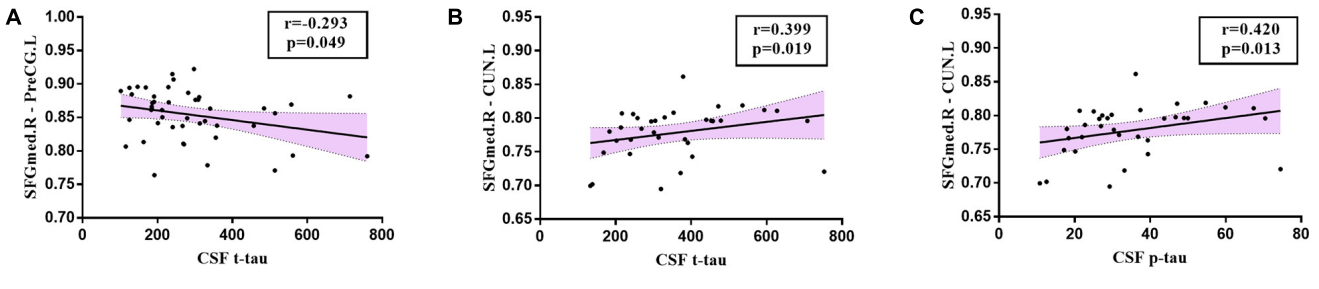

FIGURE 6 | Relationships between altered edges and CSF biomarkers in MCI and AD group. In MCI group, **(A)** the connection between right medial superior frontal gyrus and left precentral gyrus (t-tau: r = -0.293, P = 0.049) was correlated with CSF tau concentration in MCI patients. In the AD group, the connection between right medial superior frontal gyrus and left cuneus was positively correlated with CSF t-tau (**B:** r = 0.399, P = 0.019) and CSF p-tau (**C:** r = 0.420, P = 0.013). SFGmed.R, right medial superior frontal gyrus; PreCG.L, left precentral gyrus; CUN.L, left cuneus.

the cerebral structure could be integral mechanisms that reflect maladaptive changes promoting clinical dysfunction or maintaining optimal network functioning (Llufriu et al., 2017). Therefore, longitudinal studies are required to understand the positive or negative consequences of these compensatory brain changes.

Although our study attempted to provide a new perspective for understanding the aberrant structural network architecture and early identification in AD-spectrum patients, a few limitations still require future study. First, to explore the relationships among CSF pathology indicators, gray matter network graph theoretical properties, and cognitive function, we did not perform a correction for multiple comparisons. The present study was a preliminary exploration and this study, at least in part, revealed these interactions. Second, this study was cross-sectional, and no directionality or causal inferences were made. We still require large sample and longitudinal studies to further confirm these findings and to formulate a personalized evaluation system for disease progression in patients with cognitive impairment in the future. Third, the structural network parameters were calculated according to the binary adjacency matrix rather than the weighted network analysis. The latter analysis may provide additional findings in future studies. Fourth, the whole brain was divided coarsely into 90 regions based on the AAL template for structural network construction. The parcelation of the brain regions might influence the network properties and may result in various outcomes in the graph theoretical metrics. Different parcelation strategies are required to validate our findings.

CONCLUSION

In summary, this study explored the differences in gray matter network properties by graph theory and revealed a reorganization mechanism of structural networks related to cognitive impairments and CSF pathological biomarkers in AD-spectrum patients. Our findings present novel evidence of compensatory mechanisms in gray matter networks of AD

spectrum patients and highlight the potential for applying structural network metrics to monitor disease progression.

DATA AVAILABILITY STATEMENT

The raw data supporting the conclusions of this article will be made available by the authors, without undue reservation.

ETHICS STATEMENT

The studies involving human participants were reviewed, approved by the ADNI database (http://adni.loni.usc.edu) as well as the written informed consents from the patients/participant.

AUTHOR CONTRIBUTIONS

FB, HZ, and YX designed the study and edited the manuscript. XS and HC analyzed the data and wrote the manuscript. HC, RQ, and PS validated the statistics. ADNI collected the data. All the authors contributed to the article and approved the submitted version.

FUNDING

This work was supported partly by grants from the National Natural Science Foundation of China (Nos. 81822013 and 82071186), Jiangsu Provincial Key Medical Talents (No. ZDRCA2016085), the Key Research and Development Program of Jiangsu Province of China (BE2016610), the National Key Research and Development Program of China (2016YFC1300500–504), and Jiangsu Province Key Medical Discipline (ZDXKA2016020). Data collection and sharing for this project was in part funded by the Alzheimer's Disease Neuroimaging Initiative (ADNI) (National Institutes of Health Grant U01 AG024904) and DOD ADNI (Department of Defense award number W81XWH-12-2-0012). ADNI is funded by the National Institute on Aging, the National Institute of Biomedical Imaging and Bioengineering, and through generous contributions from the following: AbbVie, Alzheimer's Association; Alzheimer's Drug Discovery Foundation; Araclon Biotech; BioClinica, Inc.; Biogen; BristolMyers Squibb Company; CereSpir, Inc.; Cogstate; Eisai Inc.; Elan Pharmaceuticals, Inc.; Eli Lilly and Company; EuroImmun; F. Hoffmann-La Roche Ltd and its affiliated company Genentech, Inc.; Fujirebio; GE Healthcare; IXICO Ltd.; Janssen Alzheimer Immunotherapy Research & Development, LLC; Johnson & Johnson Pharmaceutical Research & Development LLC; Lumosity; Lundbeck; Merck & Co., Inc.; Meso Scale Diagnostics, LLC; NeuroRx Research; Neurotrack Technologies; Novartis Pharmaceuticals Corporation; Pfizer Inc.; Piramal Imaging; Servier; Takeda Pharmaceutical Company; and Transition Therapeutics. The Canadian Institutes of Health Research is providing funds to support ADNI clinical sites in Canada. Private sector contributions are facilitated by the Foundation for the National Institutes of Health (www.fnih.org). The grantee organization is the Northern California Institute for Research and Education, and the study is coordinated by the Alzheimer's Therapeutic Research Institute at the University of Southern California. ADNI data are disseminated by the Laboratory for Neuro Imaging at the University of Southern California.

SUPPLEMENTARY MATERIAL

The Supplementary Material for this article can be found online at: https://www.frontiersin.org/articles/10.3389/fnins.2021.630278/full#supplementary-material

REFERENCES

Ahmed, R. M., Landin-Romero, R., Liang, C. T., Keogh, J. M., Henning, E., Strikwerda-Brown, C., et al. (2019). Neural networks associated with body composition in frontotemporal dementia. *Ann. Clin. Transl. Neurol.* 6, 1707–1717. doi: 10.1002/acn3.50869

Bai, F., Liao, W., Watson, D. R., Shi, Y., Wang, Y., Yue, C., et al. (2011). Abnormal whole-brain functional connection in amnestic mild cognitive impairment patients. *Behav. Brain Res.* 216, 666–672. doi: 10.1016/j.bbr.2010.09.010

Batalle, D., Muñoz-Moreno, E., Figueras, F., Bargallo, N., Eixarch, E., and Gratacos, E. (2013). Normalization of similarity-based individual brain networks from gray matter MRI and its association with neurodevelopment in infants with intrauterine growth restriction. *Neuroimage* 83, 901–911. doi: 10.1016/j.neuroimage.2013.07.045

Beheshti, I., Maikusa, N., Matsuda, H., Demirel, H., and Anbarjafari, G. (2017). Histogram-based feature extraction from individual gray matter similarity-matrix for Alzheimer's Disease classification. *J. Alzheimers Dis.* 55, 1571–1582. doi: 10.3233/jad-160850

Buckley, R. F., Hanseeuw, B., Schultz, A. P., Vannini, P., Aghjayan, S. L., Properzi, M. J., et al. (2017). Region-specific association of subjective cognitive decline with tauopathy independent of global beta-amyloid burden. *JAMA Neurol.* 74, 1455–1463. doi: 10.1001/jamaneurol.2017.2216

Caso, F., Agosta, F., and Filippi, M. (2016). Insights into white matter damage in Alzheimer's Disease: from postmortem to in vivo diffusion tensor MRI studies. *Neurodegener. Dis.* 16, 26–33. doi: 10.1159/000441422

Chen, H., Sheng, X., Luo, C., Qin, R., Ye, Q., Zhao, H., et al. (2020). The compensatory phenomenon of the functional connectome related to pathological biomarkers in individuals with subjective cognitive decline. *Transl. Neurodegener.* 9:21.

Danti, S., Handjaras, G., Cecchetti, L., Beuzeron-Mangina, H., Pietrini, P., and Ricciardi, E. (2018). Different levels of visual perceptual skills are associated with specific modifications in functional connectivity and global efficiency. *Int. J. Psychophysiol.* 123, 127–135. doi: 10.1016/j.ijpsycho.2017.10.002

De Vogelaere, F., Santens, P., Achten, E., Boon, P., and Vingerhoets, G. (2012). Altered default-mode network activation in mild cognitive impairment compared with healthy aging. *Neuroradiology* 54, 1195–1206. doi: 10.1007/s00234-012-1036-6

Dicks, E., van der Flier, W. M., Scheltens, P., Barkhof, F., Tijms, B. M., and Alzheimer's Disease Neuroimaging Initiative (2020). Single-subject gray matter networks predict future cortical atrophy in preclinical Alzheimer's disease. *Neurobiol. Aging* 94, 71–80. doi: 10.1016/j.neurobiolaging.2020.05.008

Geib, B. R., Stanley, M. L., Wing, E. A., Laurienti, P. J., and Cabeza, R. (2017). Hippocampal contributions to the large-scale episodic memory network predict vivid visual memories. *Cereb. Cortex* 27, 680–693. doi: 10.1093/cercor/bhv272

Hem, S., Albite, R., Loresi, M., Rasmussen, J., Ajler, P., Yampolsky, C., et al. (2016). Pathological changes of the hippocampus and cognitive dysfunction following frontal lobe surgery in a rat model. *Acta Neurochir.* 158, 2163–2171. doi: 10.1007/s00701-016-2938-6

Jackson, J., Jambrina, E., Li, J., Marston, H., Menzies, F., Phillips, K., et al. (2019). Targeting the synapse in Alzheimer's Disease. *Front. Neurosci.* 13:735. doi: 10.3389/fnins.2019.00735

Jin, M., Wang, L., Wang, H., Han, X., Diao, Z., Guo, W., et al. (2020). Altered resting-state functional networks in patients with hemodialysis: a graph-theoretical based study. *Brain Imaging Behav.* [Epub ahead of print]. doi: 10.1007/11682-020-00293-8

Kim, G. W., Kim, B. C., Park, K. S., and Jeong, G. W. (2020). A pilot study of brain morphometry following donepezil treatment in mild cognitive impairment: volume changes of cortical/subcortical regions and hippocampal subfields. *Sci. Rep.* 10:10912.

Lane, C. A., Barnes, J., Nicholas, J. M., Sudre, C. H., Cash, D. M., Parker, T. D., et al. (2019). Associations between blood pressure across adulthood and late-life brain structure and pathology in the neuroscience substudy of the 1946 British birth cohort (Insight 46): an epidemiological study. *Lancet Neurol.* 18, 942–952. doi: 10.1016/s1474-4422(19)30228-5

Li, W., Yang, C., Wu, S., Nie, Y., Zhang, X., Lu, M., et al. (2018). Alterations of graphic properties and related cognitive functioning changes in mild Alzheimer's Disease revealed by individual morphological brain network. *Front. Neurosci.* 12:927. doi: 10.3389/fnins.2018.00927

Lin, X., Chen, Y., Wang, M., Song, C., Lin, B., Yuan, X., et al. (2020). Altered topological patterns of gray matter networks in tinnitus: a graph-theoretical-based study. *Front. Neurosci.* 14:541. doi: 10.3389/fnins.2020.00541

Liu, H., Hu, H., Wang, H., Han, J., Li, Y., Qi, H., et al. (2020). A brain network constructed on an L1-norm regression model is more sensitive in detecting small world network changes in early AD. *Neural Plast.* 2020:9436406.

Llufriu, S., Martinez-Heras, E., Solana, E., Sola-Valls, N., Sepulveda, M., Blanco, Y., et al. (2017). Structural networks involved in attention and executive functions in multiple sclerosis. *Neuroimage Clin.* 13, 288–296. doi: 10.1016/j.nicl.2016.11.026

Lu, F. M., Liu, C. H., Lu, S. L., Tang, L. R., Tie, C. L., Zhang, J., et al. (2017). Disrupted topology of frontostriatal circuits is linked to the severity of insomnia. *Front. Neurosci.* 11:214. doi: 10.3389/fnins.2017.00214

Lu, J., Testa, N., Jordan, R., Elyan, R., Kanekar, S., Wang, J., et al. (2019). Functional connectivity between the resting-state olfactory network and the hippocampus in Alzheimer's Disease. *Brain Sci.* 9:338. doi: 10.3390/brainsci9120338

Luo, C., Li, M., Qin, R., Chen, H., Yang, D., Huang, L., et al. (2019). White matter microstructural damage as an early sign of subjective cognitive decline. *Front. Aging Neurosci.* 11:378. doi: 10.3389/fnagi.2019.00378

Luo, Y., Schulz, K. P., Alvarez, T. L., Halperin, J. M., and Li, X. (2018). Distinct topological properties of cue-evoked attention processing network in persisters and remitters of childhood ADHD. *Cortex* 109, 234–244. doi: 10.1016/j.cortex.2018.09.013

Nonnekes, J., Ruzicka, E., Nieuwboer, A., Hallett, M., Fasano, A., and Bloem, B. R. (2019). Compensation strategies for gait impairments in parkinson disease: a review. *JAMA Neurol.* 76, 718–725. doi: 10.1001/jamaneurol.2019.0033

Patnode, C. D., Perdue, L. A., Rossom, R. C., Rushkin, M. C., Redmond, N., Thomas, R. G., et al. (2020). Screening for cognitive impairment in older adults: updated evidence report and systematic review for the US preventive services task force. *JAMA* 323, 764–785. doi: 10.1001/jama.2019.22258

Rimkus, C. M., Schoonheim, M. M., Steenwijk, M. D., Vrenken, H., Eijlers, A. J., Killestein, J., et al. (2019). Gray matter networks and cognitive impairment in multiple sclerosis. *Mult. Scler.* 25, 382–391. doi: 10.1177/1352458517751650

Rubinov, M., and Sporns, O. (2010). Complex network measures of brain connectivity: uses and interpretations. *Neuroimage* 52, 1059–1069. doi: 10.1016/j.neuroimage.2009.10.003

Sanchez-Benavides, G., Grau-Rivera, O., Suarez-Calvet, M., Minguillon, C., Cacciaglia, R., Gramunt, N., et al. (2018). Brain and cognitive correlates of subjective cognitive decline-plus features in a population-based cohort. *Alzheimers Res. Ther,* 10:123.

Sapara, A., Ffytche, D. H., Birchwood, M., Cooke, M. A., Fannon, D., Williams, S. C., et al. (2014). Preservation and compensation: the functional neuroanatomy of insight and working memory in schizophrenia. *Schizophr. Res.* 152, 201–209. doi: 10.1016/j.schres.2013.11.026

Shah, P., Bassett, D. S., Wisse, L. E. M., Detre, J. A., Stein, J. M., Yushkevich, P. A., et al. (2018). Mapping the structural and functional network architecture of the medial temporal lobe using 7T MRI. *Hum. Brain Mapp.* 39, 851–865. doi: 10.1002/hbm.23887

Slot, R. E. R., Verfaillie, S. C. J., Overbeek, J. M., Timmers, T., Wesselman, L. M. P., Teunissen, C. E., et al. (2018). Subjective cognitive impairment cohort (SCIENCe): study design and first results. *Alzheimers Res. Ther.* 10:76.

Tijms, B. M., Kate, M. T., Wink, A. M., Visser, P. J., Ecay, M., Clerigue, M., et al. (2016). Gray matter network disruptions and amyloid beta in cognitively normal adults. *Neurobiol. Aging* 37, 154–160. doi: 10.1016/j.neurobiolaging.2015.10.015

Toppi, J., De Vico Fallani, F., Vecchiato, G., Maglione, A. G., Cincotti, F., Mattia, D., et al. (2012). How the statistical validation of functional connectivity patterns can prevent erroneous definition of small-world properties of a brain connectivity network. *Comput. Math Methods Med.* 2012:130985.

Tzourio-Mazoyer, N., Landeau, B., Papathanassiou, D., Crivello, F., Etard, O., Delcroix, N., et al. (2002). Automated anatomical labeling of activations in SPM using a macroscopic anatomical parcellation of the MNI MRI single-subject brain. *Neuroimage* 15, 273–289. doi: 10.1006/nimg.2001.0978

van der Lee, S. J., Wolters, F. J., Ikram, M. K., Hofman, A., Ikram, M. A., Amin, N., et al. (2018). The effect of APOE and other common genetic variants on the onset of Alzheimer's disease and dementia: a community-based cohort study. *Lancet Neurolo.* 17, 434–444. doi: 10.1016/s1474-4422(18)30053-x

van Duinkerken, E., Ijzerman, R. G., Klein, M., Moll, A. C., Snoek, F. J., Scheltens, P., et al. (2016). Disrupted subject-specific gray matter network properties and cognitive dysfunction in type 1 diabetes patients with and without proliferative retinopathy. *Hum. Brain Mapp.* 37, 1194–1208. doi: 10.1002/hbm.23096

Verfaillie, S. C. J., Slot, R. E. R., Dicks, E., Prins, N. D., Overbeek, J. M., Teunissen, C. E., et al. (2018). A more randomly organized grey matter network is associated with deteriorating language and global cognition in individuals with subjective cognitive decline. *Hum. Brain Mapp.* 39, 3143–3151. doi: 10.1002/hbm.24065

Vipin, A., Foo, H. J. L., Lim, J. K. W., Chander, R. J., Yong, T. T., Ng, A. S. L., et al. (2018). Regional white matter hyperintensity influences grey matter atrophy in mild cognitive impairment. *J. Alzheimers Dis.* 66, 533–549. doi: 10.3233/jad-180280

Wang, H., Jin, X., Zhang, Y., and Wang, J. (2016). Single-subject morphological brain networks: connectivity mapping, topological characterization and test-retest reliability. *Brain Behav.* 6:e00448.

Wang, J., Khosrowabadi, R., Ng, K. K., Hong, Z., Chong, J. S. X., Wang, Y., et al. (2018). Alterations in brain network topology and structural-functional connectome coupling relate to cognitive impairment. *Front. Aging Neurosci.* 10:404. doi: 10.3389/fnagi.2018.00404

Wang, J., Wang, X., Xia, M., Liao, X., Evans, A., and He, Y. (2015). GRETNA: a graph theoretical network analysis toolbox for imaging connectomics. *Front. Hum. Neurosci.* 9:386. doi: 10.3389/fnhum.2015.00386

Wang, J., Zhang, Y., Zhu, D., Yang, Z., Liu, F., Qin, W., et al. (2020). A common variant in OXTR rs53576 impacts topological patterns of brain functional networks. *Eur. Child Adolesc. Psychiatry* 29, 993–1002. doi: 10.1007/s00787-019-01414-5

Wook Yoo, S., Han, C. E., Shin, J. S., Won Seo, S., Na, D. L., Kaiser, M., et al. (2015). A network flow-based analysis of cognitive reserve in normal ageing and Alzheimer's Disease. *Sci. Rep.* 5:10057.

Xu, T., Cullen, K. R., Mueller, B., Schreiner, M. W., Lim, K. O., Schulz, S. C., et al. (2016). Network analysis of functional brain connectivity in borderline personality disorder using resting-state fMRI. *Neuroimage Clin.* 11, 302–315. doi: 10.1016/j.nicl.2016.02.006

Yang, D., Huang, L., Luo, C., Li, M., Qin, R., Ma, J., et al. (2020). Impaired structural network properties caused by white matter hyperintensity related to cognitive decline. *Front. Neurol.* 11:250. doi: 10.3389/fneur.2020.00250

Zhang, H., Therriault, J., Kang, M. S., Ng, K. P., Pascoal, T. A., Rosa-Neto, P., et al. (2018). Cerebrospinal fluid synaptosomal-associated protein 25 is a key player in synaptic degeneration in mild cognitive impairment and Alzheimer's disease. *Alzheimer's Res. Ther.* 10:80.

Zhao, C., Jiang, J., Xu, Z., and Guan, Y. (2017). A study of EMR-based medical knowledge network and its applications. *Comput. Methods Programs Biomed.* 143, 13–23. doi: 10.1016/j.cmpb.2017.02.016

Zhu, J., Zhuo, C., Liu, F., Qin, W., Xu, L., and Yu, C. (2016). Distinct disruptions of resting-state functional brain networks in familial and sporadic schizophrenia. *Sci. Rep.* 6:23577.

Conflict of Interest: The authors declare that the research was conducted in the absence of any commercial or financial relationships that could be construed as a potential conflict of interest.

frontiers in Aging Neuroscience

ORIGINAL RESEARCH
published: 16 March 2021
doi: 10.3389/fnagi.2020.604940

White Matter Connectivity and Gray Matter Volume Changes Following Donepezil Treatment in Patients With Mild Cognitive Impairment: A Preliminary Study Using Probabilistic Tractography

Gwang-Won Kim[1,2], *Shin-Eui Park*[1], *Kwangsung Park*[1,3] *and Gwang-Woo Jeong*[4]*

[1] *Advanced Institute of Aging Science, Chonnam National University, Gwangju, South Korea,* [2] *Department of Psychiatry, Massachusetts General Hospital and Harvard Medical School, Boston, MA, United States,* [3] *Department of Urology, Chonnam National University Hospital, Chonnam National University Medical School, Gwangju, South Korea,* [4] *Department of Radiology, Chonnam National University Hospital, Chonnam National University Medical School, Gwangju, South Korea*

OPEN ACCESS

Edited by:
Jiu Chen,
Nanjing Medical University, China

Reviewed by:
Giulia Donzuso,
University of Catania, Italy
Ye Wu,
University of North Carolina at Chapel Hill, United States

***Correspondence:**
Gwang-Woo Jeong
gwjeong100@hanmail.net

Received: *10 September 2020*
Accepted: *21 December 2020*
Published: *16 March 2021*

Citation:
Kim G-W, Park S-E, Park K and Jeong G-W (2021) White Matter Connectivity and Gray Matter Volume Changes Following Donepezil Treatment in Patients With Mild Cognitive Impairment: A Preliminary Study Using Probabilistic Tractography. Front. Aging Neurosci. 12:604940. doi: 10.3389/fnagi.2020.604940

The donepezil treatment is associated with improved cognitive performance in patients with mild cognitive impairment (MCI), and its clinical effectiveness is well-known. However, the impact of the donepezil treatment on the enhanced white matter connectivity in MCI is still unclear. The purpose of this study was to evaluate the thalamo-cortical white matter (WM) connectivity and cortical thickness and gray matter (GM) volume changes in the cortical regions following donepezil treatment in patients with MCI using probabilistic tractography and voxel-based morphometry. Patients with MCI underwent magnetic resonance examinations before and after 6-month donepezil treatment. Compared with healthy controls, patients with MCI showed decreased WM connectivity of the thalamo-lateral prefrontal cortex, as well as reduced thickness in the medial/lateral orbitofrontal cortices ($p < 0.05$). The thalamo-lateral temporal cortex connectivity in patients with MCI was negatively correlated with Alzheimer's disease assessment scale-cognitive subscale (ADAS-cog) ($r = -0.76$, $p = 0.01$). The average score of the Korean version of the mini-mental state examination (K-MMSE) in patients with MCI was improved by 7.9% after 6-months of donepezil treatment. However, the patterns of WM connectivity and brain volume change in untreated and treated patients were not significantly different from each other, resulting from multiple comparison corrections. These findings will be valuable in understanding the neurophysiopathological mechanism on MCI as a prodromal phase of Alzheimer's disease in connection with brain functional connectivity and morphometric change.

Keywords: white matter connectivity, probabilistic tractography algorithm, mild cognitive impairment, gray matter volume, donepezil treatment, cortical thickness

INTRODUCTION

Alzheimer's disease (AD) is a chronic brain disorder that is associated with neurodegeneration and the progressive development of dementia (Fumagalli et al., 2006). AD generally progresses slowly in three stages, including preclinical AD, mild cognitive impairment (MCI) due to AD pathology, and AD-dementia. MCI is a prodromal stage of AD, which is a relatively broad clinical condition that involves a slight memory deficit, and in many cases, the condition may represent a transitional state between normal cognition and AD (Morris, 2005). Among the neuropathological alterations in AD, relevant neuronal loss, and synaptic pathology have been studied to be most strongly related to dementia severity and cognitive deficits (Hoy et al., 2017). White matter (WM) degeneration occurs early in the development of AD and is useful in evaluating pathologic AD progression before AD becomes clinically evident (Caso et al., 2015). Several postmortem studies have reported that the early neuropathology in AD manifests in the medial temporal lobe (Hyman et al., 1984; Krasuski et al., 1998).

The key clinical symptom of AD is the progressive deterioration of learning and memory, which further leads to reduced acetylcholine (ACh) levels in the brain (Hashimoto et al., 2005). Treatment with acetylcholinesterase inhibitors (AChEIs) prevents the breakdown of ACh and impacts an increase in cholinergic transmission. Acetylcholinesterase inhibitors are among the approved drugs currently used to treat AD, wherein, and the most frequently prescribed drug is donepezil (Cavedo et al., 2017). Donepezil has been demonstrated to inhibit acetylcholinesterase activity in the cerebral cortex, hippocampus, and striatum of the rat brain, by impacting the increased production of ACh activity in the brain areas associated with cognitive function (Kasa et al., 2000; Scali et al., 2002). Kim et al. (2020) reported that donepezil treatment in patients with MCI is associated with improved cognitive performance. However, it is as yet unknown how donepezil treatment influences the brain cortical thickness and WM connectivity in MCI.

Diffusion weighted imaging (DWI) facilitates measuring the effects of tissue microstructure on the random translational motion of water molecules in biologic tissues and has been reported to be highly sensitive to WM microstructural damage (Caso et al., 2015). Several DWI studies (Wang et al., 2012; Mito et al., 2018) focusing on MCI and AD have analyzed the DWI data based on the diffusion tensor model. For the detection of WM integrity of an entire bundle, probabilistic tractography in DTI has recently emerged as an increasing medium, allowing us to evaluate structural connectivity through estimating the likelihood that two areas of the brain are interconnected (Jaimes et al., 2017). This tool may advantageously provide more valuable information and insight regarding the early signs of microstructural change in MCI and brain structural connectivity following the donepezil treatment. Most brain structural connectivity studies focusing on MCI and AD have exclusively explored the specific brain region-of-interest (ROI), hippocampus, or medial temporal lobe. AD has largely been considered a disease of the cerebral cortex, and thus it is important to screen cortical dysfunction at an early stage before the development of AD. The thalamus is an evolutionarily conserved structure with extensive reciprocal connections to cortical regions, and it plays an important role in learning and memory (Nakajima and Halassa, 2017). Alderson et al. (2017) have reported that patients with MCI showed significantly decreased fractional anisotropy between the thalamus and inferior parietal lobe compared with healthy controls. To date, however, no neuroimaging studies on the interaction between the thalamus and cortical regions using probabilistic tractography in patients with MCI following donepezil treatment have been attempted. We have previously reported on a study that evaluated the thalamo-cortical WM connectivity in patients with MCI using probabilistic tractography. Voxel-based morphometry (VBM) has grown in popularity since its introduction because of its ability to perform statistical tests across all voxels in the image, identifying volume differences between groups (Whitwell, 2009; Kim et al., 2018b). Therefore, a combined study of probabilistic tractography and VBM could further understanding of gray matter (GM) atrophy and the WM networks that can cause disconnection among neural cells in MCI.

The purpose of this study was to evaluate the thalamo-cortical WM connectivity before and after donepezil treatment in patients with MCI using probabilistic tractography, as well as to assess the cortical thickness and GM volume changes in the cortical regions.

SUBJECTS AND METHOD

Ethics

This is study a retrospective that has been approved by the Institutional Review Board of Chonnam National University Hospital (IRB-CNUH). Before MR scanning, the experimental procedure was explained to all volunteers, and written informed consent was obtained. All the experimental procedures and methods were performed in accordance with the relevant guidelines and regulations approved by IRB-CNUH.

Subjects

Ten patients with MCI (male:female = 4:6, mean age = 72.4 ± 7.9 years) and 9 age-matched healthy controls (male:female = 3:6, mean age = 70.7 ± 3.5 years) participated in this study (**Table 1**). The patients with MCI were inpatients or outpatients of the CNUH. We included the patients with MCI based on the following criteria: first, the MCI of Alzheimer-type by the criteria of both the DSM-IV and the National Institute of Neurological and Communicative Diseases and Stroke-Alzheimer Disease and Related Disorders Association (NINCDS-ADRDA); second, no history of MCI treatment and other neurological or psychiatric illnesses; third, a score of 0.5 or 1 on the Clinical Dementia Rating (CDR); fourth, a score <26 on the Korean version of the Mini-Mental State Examination (K-MMSE); fifth, reconfirmation through the typical symptom severity including change in cognition recognized by the affected individual or observers, objective impairment in one or more

TABLE 1 | Demographic and clinical characteristics of patients with MCI (baseline), donepezil-treated patients (follow-up), and healthy controls (HC).

	MCI patients		Healthy controls (n = 9)	Statistical analysis (*p*-value)		
	Baseline ($n = 10$)	Follow-up ($n = 10$)		Baseline vs. follow-up	HC vs. baseline	HC vs. follow-up
Age (years)	73.1 ± 7.9	-	70.7 ± 3 .5	-	$p = 0.092$	$p = 0.092$
Gender	7 F, 3 M	-	6 F, 3 M	-	$p = 0.876$	$p = 0.876$
K-MMSE	16.5 ± 4.9	17.5 ± 2.9	28.6 ± 1.1	$p = 0.031$[a]	$p < 0.001$[b]	$p < 0.001$[b]
ADAS-Cog	25.6 ± 6.2	24.4 ± 5.9	-	$p = 0.506$	-	-
CDR	0.6 ± 0.2	0.6 ± 0.2	-	$p = 0.317$	-	-
GDS	13.2 ± 5.2	12.7 ± 4.9	-	$p = 0.372$	-	-

[a] *Significant difference (Wilcoxon's signed-ranks; $p < 0.05$) between MCI patients (baseline) and treated patients (follow-up).*

[b] *Significant differences (Mann-Whitney U; $p < 0.001$) in both "healthy controls (HC) vs. MCI patients" and "HC vs. treated patients".*

K-MMSE, the Korean version of the mini-mental state examination; ADAS-Cog, AD assessment scale-cognitive subscale; CDR, clinical dementia rating; GDS, geriatric depression scale.

cognitive domains, independence in functional activities, and absence of dementia (Morris, 2012).

Ten patients underwent MR examinations before (baseline) and after (follow-up) donepezil treatment. After performing the first MR examination, 10 patients received 5 mg/day of Aricept (donepezil hydrochloride; Pfizer Inc., New York, NY) for the initial 28 days, and 10 mg/day thereafter. The mean time gap between before and after donepezil treatment was 194.0 ± 29.5 days.

Neuropsychological Tests

The MCI symptom severity was evaluated in the two separated groups, receiving and not receiving donepezil treatment, using the questionnaires of the K-MMSE, AD assessment scale-cognitive subscale (ADAS-Cog), CDR scale, and geriatric depression scale (GDS). Patients with MCI completed questionnaires before and after the 6-months of donepezil treatment. The contrasts of "healthy controls vs. patients with MCI" and "healthy controls vs. using donepezil-treated patients" were analyzed by using a Mann-Whitney *U*-test. A Wilcoxon's signed-ranks test was used to compare the scores on the K-MMSE, ADAS-Cog, CDR, and GDS between untreated and treated patients.

Image Acquisition

T1- and T2-weighted images and DWI were performed on a 3.0-T Magnetom Tim Trio MR Scanner (Siemens Medical Solutions, Erlangen, Germany) with a head coil of birdcage type. The axial DW images were acquired using echo-planar imaging pulse sequence with the following parameters: TR/TE = 5,200/105 ms, matrix = 128 × 128, field of view (FOV) = 220 mm^2, and resolution = 1.7 mm × 1.7 mm. Diffusion sensitizing gradient-echo encoding was applied in 24 directions using a diffusion-weighting b factor of 1,000 s/mm^2 and 5 images without diffusion weighting (b factor = 0 s/mm^2). Phase-encoding was in the anterior → posterior direction and a factor of 2 in-plane acceleration (GRAPPA) was used. T1-weighted sagittal images (TR/TE = 1,700/2.2 ms) and T2-weighted axial images (TR/TE = 5,000/90 ms) were acquired with the following parameters: FOV = 256 × 256 mm^2, matrix = 512 × 512, slice thickness = 5 mm, and slice gap = 2 mm.

Data Processing and Analysis

DWI data were analyzed using Functional Magnetic Resonance Imaging of the Brain (FMRIB) Software Library (FSL) v6.0 software (Behrens et al., 2003, 2007; Jenkinson et al., 2012). Based on the findings of previous studies (Marenco et al., 2012; Cho et al., 2016) that used probabilistic tractography, we identified 9 brain regions of interest (ROIs) in all, individual T1 images using the FreeSurfer v6.0 software (MGH, Boston, MA, USA) with Desikan-Killiany cortical parcellation as following: seed region; thalamus, target regions; orbitofrontal cortex (OFC), medial prefrontal cortex (MPFC), lateral prefrontal cortex (LPFC), sensorimotor cortex (SMC), parietal cortex (PC), medial temporal cortex (MTC), lateral temporal cortex (LTC), and occipital cortex (OC) (**Figure 1**) (Dale et al., 1999; Fischl et al., 2002, 2004). The DWI data were preprocessed using skull removal and eddy current as well as motion correction. The first non-diffusion weighted image was set as the target image, into which the remaining images (24 diffusion weighted image and 4 non-diffusion weighted images) were registered using an affine transformation to adjust for distortions caused by eddy currents and head motion (Tsai, 2018). The individual T1 images were rigidly registered to their corresponding non-diffusion weighted (B0) images using FMRIB's Linear Image Registration Tool (FLIRT) in combination with mutual information cost function and trilinear interpolation. Diffusion parameters were modeled using Bayesian Estimation of Diffusion Parameters Obtained using Sampling Techniques (BEDPOSTX) with crossing-fibers modeling. One patient had motion artifact in the T1 images obtained after treatment, thus nine ROIs in the patient were extracted in the T1 image obtained before treatment to register their T1 images to diffusion space. BEDPOSTX models of diffusion signal as a ball (isotropic) and stick (anisotropic) components were used to generate a distribution of likely fiber orientations within each voxel as well as an estimate of the uncertainty on these orientations (Theisen et al., 2017). To determine WM connectivity between seed region and target regions, we used FSL probabilistic tractography (connectivity

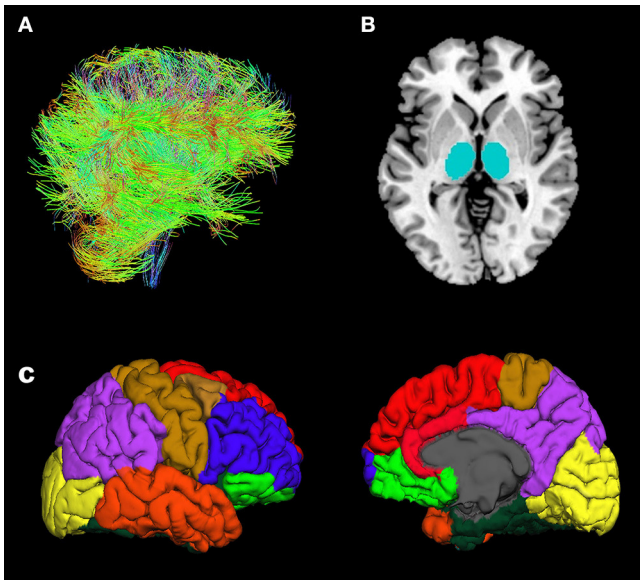

FIGURE 1 | Illustration of fiber tracts **(A)**, thalamus ROIs (seed regions) **(B)**, and cortical ROIs (target regions) **(C)**: orbitofrontal cortex (yellow-green), medial prefrontal cortex (red), lateral prefrontal cortex (blue), sensorimotor cortex (brown), parietal cortex (purple), lateral temporal cortex (orange), medial temporal cortex (dark-green), and occipital cortex (yellow).

modeling) as following: 5,000 streamlines per each voxel in the thalamus, 0.2 curvature threshold, 0.5 mm step length, and loop check. The connectivity values were routinely thresholded at 10% to remove the aberrant connections arising from noise and errors (Cho et al., 2016). To take into account the individual variances in total connectivity between the thalamus and eight cortical ROIs, each thalamo-cortical WM connectivity value was divided by the sum of connectivity values from all cortical ROIs, named "relative connectivity" (Cho et al., 2016).

For the group analysis, a Wilcoxon's signed-ranks test was conducted using the SPSS (version 24.0, IBM, Armonk, NY, USA) to compare the thalamo-cortical WM connectivity between patients receiving and not receiving donepezil treatment. A Mann-Whitney U-test was used to compare the connectivity between patients and healthy controls. The significance level was set to 0.05 after Bonferroni correction for 8 brain cortices to adjust multiple comparisons (level of significance after Bonferroni correction: $p < 0.0063$).

The cortical thickness of the entire brain was calculated using the FreeSurfer v6.0 software (MGH, Boston, MA, USA). T1 data of 1 subject was excluded from the cortical thickness and VBM analyses due to a motion artifact detected in the anatomical scan. Post-processing of images comprised the following steps: correction for head motion and non-uniformity of intensity, Talairach transformation of each subject's brain, removal of non-brain tissue, segmentation of cortical gray, subcortical white and deep GM volumetric structures, triangular tessellation of the GM/WM matter interface and GM/CSF boundary, and topology correction. The images were then smoothed with a 10-mm FWHM Gaussian kernel. Cortical thickness was calculated as the shortest distance between the GM/WM boundary and pial surface at each vertex across the cortical mantle, measured in millimeters (Gerrits et al., 2016). The cortical maps were generated by computing mean cortical thickness for each subject at each vertex, right and left hemispheres separately, and mapping these data to the surface of an average brain template enabling visualization of data across the entire cortical surface (Han et al., 2014). Cortical thickness was compared between patients receiving and not receiving donepezil treatment using Wilcoxon's signed-ranks test, and between patients and healthy controls using the Mann-Whitney U-test.

Brain GM volume was analyzed using SPM8 software (Statistical Parametric Mapping, Wellcome Department of Cognitive Neurology, University College, London, U.K.) with diffeomorphic anatomical registration through exponentiated Lie algebra (DARTEL) analysis (Kim et al., 2018a, 2019). Prior to processing data, all individual T1 images were aligned with the anterior and posterior commissure line on the transverse plane. After correcting the non-uniformity field bias on images, the images were segmented to GM, WM, and cerebrospinal fluid (CSF) using the tissue probability maps based on the International Consortium of Brain Mapping (ICBM) space template type of East Asian Brains. In addition, the mean templates of GM and WM were created using individual GM and WM images. Subsequently, all the images were normalized to the Montreal Neurological Institute template and smoothed with an 8 mm full width at a half maximum (FWHM) isotropic Gaussian kernel.

To compare the GM volumes between healthy controls and patients with MCI before or after donepezil treatment, a two sample *t*-test, with whole brain volume as covariate, was used in the Statistical non-Parametric Mapping (SnPM13). A paired *t*-test was used to compare the GM volumes between patients with MCI and treated patients with MCI. The results were thresholded at a cluster level corrected threshold of $p < 0.05$ [$n = 5{,}000$ permutations, family-wise error (FWE)-corrected] with a cluster-determining threshold at the voxel level $p < 0.0001$.

RESULTS

Changes in Symptom Severity

The average scores of K-MMSE in healthy control, patients with MCI, and donepezil-treated patients with MCI were 28.6 ± 1.1, 16.5 ± 4.9, and 17.5 ± 2.9, respectively (**Table 1**). The average score of K-MMSE in untreated patients with MCI was improved by 7.9% after donepezil treatment ($p = 0.031$). The average scores of ADAS-Cog and GDS in untreated patients were decreased by 5.0% (25.6 ± 6.2 → 24.4 ± 5.9; $p = 0.506$) and 4.0% (13.2 ± 5.2 → 12.7 ± 4.9; $p = 0.372$) after donepezil treatment, respectively (**Table 1**). In addition, the average score of CDR in untreated patients and donepezil-treated patients were 0.6 ± 0.2, and 0.6 ± 0.2, respectively ($p = 0.317$) (**Table 1**).

White Matter Connectivity Changes

Compared with healthy controls, the untreated and treated patients showed significantly decreased thalamo-LPFC relative connectivity ($p < 0.05$, Bonferroni corrected) (**Figure 2**,

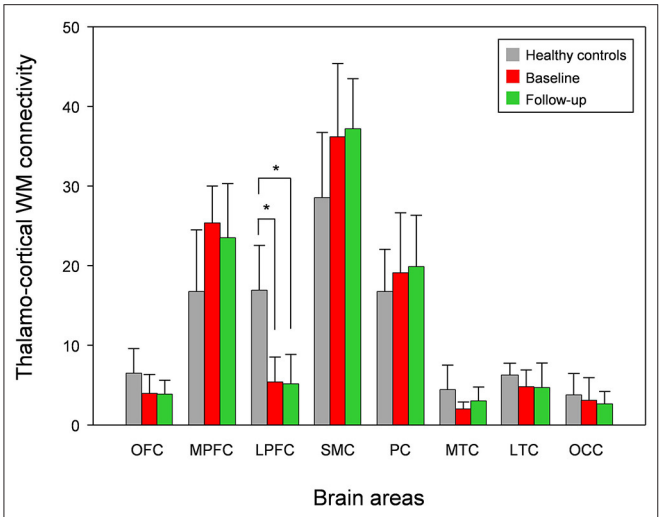

FIGURE 2 | Mean white matter (WM) connectivity between the thalamus and each cortex in patients with MCI (baseline), donepezil-treated patients (Follow-up), and healthy controls. OFC, orbitofrontal cortex; MPFC, medial prefrontal cortex; LPFC, lateral prefrontal cortex; SMC, sensorimotor cortex; PC, parietal cortex; MTC, medial temporal cortex; LTC, lateral temporal cortex; OC, occipital cortex. *significant difference (Bonferroni corrected, $p < 0.05$).

Table 2). Treated patients showed increased thalamo-MTC relative connectivity after donepezil treatment ($p < 0.05$). Interestingly, thalamo-LPFC relative connectivity in patients with MCI was positively correlated with the K-MMSE ($r = 0.80$, $p = 0.005$) and thalamo-LTC relative connectivity was negatively correlated with the ADAS-Cog ($r = -0.76$, $p = 0.010$) (**Figure 3**).

Cortical Thickness

Compared with the healthy controls, patients with MCI showed significantly reduced thickness in the medial orbitofrontal cortex ([x, y, z = −9, 37, −21], t-value = 3.6) and lateral orbitofrontal cortex ([x, y, z = −13, 34, −19], t-value = 3.0) (Monte-Carlo corrected, $p < 0.01$) (**Figure 4**). However, no significant differences were found between untreated and treated patients.

Global Gray Matter Volume Changes

The overall GM volumes in healthy control, patients with MCI, and donepezil-treated patients were 589.9 ± 54.7 mL, 574.0 ± 36.8 mL, and 578.9 ± 32.8 mL, respectively. In comparison with the healthy controls, patients with MCI showed significantly reduced GM volumes in the hippocampus ([x, y, z = 32, −16, −14], t-value = 5.8) (FWE corrected, $p < 0.05$) (**Figure 5**). Furthermore, when comparing the untreated and treated patients, the treated patients showed significantly higher GM volumes in the putamen ([x, y, z = −30, −10, 6], t-value = 5.5), globus pailldus ([x, y, z = 16, 6, 0], t-value = 6.0), and inferior frontal cortex ([x, y, z = 46, 24, −4], t-value = 5.2) (uncorrected; $p < 0.001$) (**Figure 5**).

DISCUSSION

To our knowledge, this is the first study evaluating the thalamo-cortical WM connectivity after donepezil treatment in patients with MCI using probabilistic tractography. Patients with MCI showed decreased thalamo-LPFC WM connectivity, as well as reduced thickness in the medial/lateral orbitofrontal cortices compared with the healthy controls. In addition, the thalamo-SMC WM connectivity in patients with MCI was positively correlated with K-MMSE scores, and the thalamo-LTC connectivity was negatively correlated with ADAS-cog scores. This suggests that decreased thalamo-LPFC WM connectivity and reduced thickness of medial/lateral orbitofrontal cortices are closely related to MCI and/or early stages of AD.

It is widely recognized that WM abnormalities are detectable in the early stages of AD and MCI, suggesting that abnormalities in the cortico-cortical and cortico-subcortical WM interconnections are associated with an increased risk of progression from MCI to AD (Radanovic et al., 2013). A previous study (Wang et al., 2012) using VBM has reported that the MCI group showed lower fractional anisotropy (FA) and higher radial diffusivity (RD) in the parahippocampal WM compared with the control group. Another similar study (Palesi et al., 2012) demonstrated that patients with MCI showed decreased volume in the hippocampus and increased MD in the hippocampus-precuneus/posterior cingulate cortex tracts when compared with the healthy controls. The current study revealed that in comparison with the control group, the MCI group showed a significant decrease in the thalamo-LPFC WM connectivity. In addition, the thalamo-SMC WM connectivity in the MCI group was positively correlated with K-MMSE scores. The LPFC was shown to play an important role in cognitive function. There is evidence that cognitive deficits in patients with MCI are related to dysfunction of the LPFC (Duarte et al., 2006; Zhou et al., 2013). According to the study by Duarte et al. (Duarte et al., 2006), patients with MCI showed GM volume loss in the LPFC compared with the healthy controls. Zhou et al. (2013) evaluated the functional connectivity in the thalmo-cortical network in patients with AD. They reported a decrease in the functional connectivity between the left thalamus and left inferior frontal cortex. A cerebral perfusion study (Chao et al., 2009) demonstrated that MCI patients with executive dysfunctions showed hypoperfusion in the prefrontal cortex relative to controls. This indicates that thalamo-LPFC WM connectivity in the MCI patients may be associated with characteristics of the pathobiology of MCI.

We also found evidence that the decreased thickness of the medial/lateral orbitofrontal cortices in patients with MCI compared with healthy controls. The orbitofrontal cortex occupies the anterior part of the prefrontal cortex, which plays in complex human behaviors such as evaluation, affect regulation, and reward-based decision-making (Fettes et al., 2017). The orbitofrontal cortex atrophy was associated with cognitive deficits (Hornberger et al., 2010; Zhao et al., 2015). Both MCI and AD subjects had a thinner cortex in the lateral orbitofrontal cortex compared with healthy controls (Zhao et al., 2015). A positron emission tomography study

TABLE 2 | Mean white matter connectivity between the thalamus and each cortex in patients with MCI (baseline), donepezil-treated patients (follow-up), and healthy controls (HC).

Brain cortex	MCI patients (baseline)	Treated patients (follow-up)	Healthy controls (HC)	Statistical analysis		
				Baseline vs. follow-up	HC vs. baseline	HC vs. follow-up
OFC	0.04 ± 0.02	0.04 ± 0.02	0.06 ± 0.03	$p = 0.959$	$p = 0.027$	$p = 0.034$
MPFC	0.25 ± 0.05	0.24 ± 0.07	0.17 ± 0.08	$p = 0.575$	$p = 0.014$	$p = 0.086$
LPFC	0.05 ± 0.03	0.05 ± 0.04	0.17 ± 0.06	$p = 0.959$	$^*p < 0.001$	$^*p = 0.001$
SMC	0.36 ± 0.09	0.37 ± 0.06	0.29 ± 0.08	$p = 0.575$	$p = 0.060$	$p = 0.022$
PC	0.19 ± 0.08	0.20 ± 0.06	0.17 ± 0.05	$p = 0.959$	$p = 0.514$	$p = 0.221$
MTC	0.02 ± 0.01	0.03 ± 0.02	0.04 ± 0.03	$p = 0.037$	$p = 0.022$	$p = 0.221$
LTC	0.05 ± 0.02	0.05 ± 0.03	0.06 ± 0.01	$p = 0.444$	$p = 0.165$	$p = 0.050$
OCC	0.03 ± 0.03	0.03 ± 0.02	0.04 ± 0.03	$p = 0.445$	$p = 0.327$	$p = 0.253$

OFC, orbitofrontal cortex; MPFC, medial prefrontal cortex; LPFC, lateral prefrontal cortex; SMC, sensorimotor cortex; PC, parietal cortex; MTC, medial temporal cortex; LTC, lateral temporal cortex; OC, occipital cortex.
**significant difference (Bonferroni corrected, $p < 0.05$).*

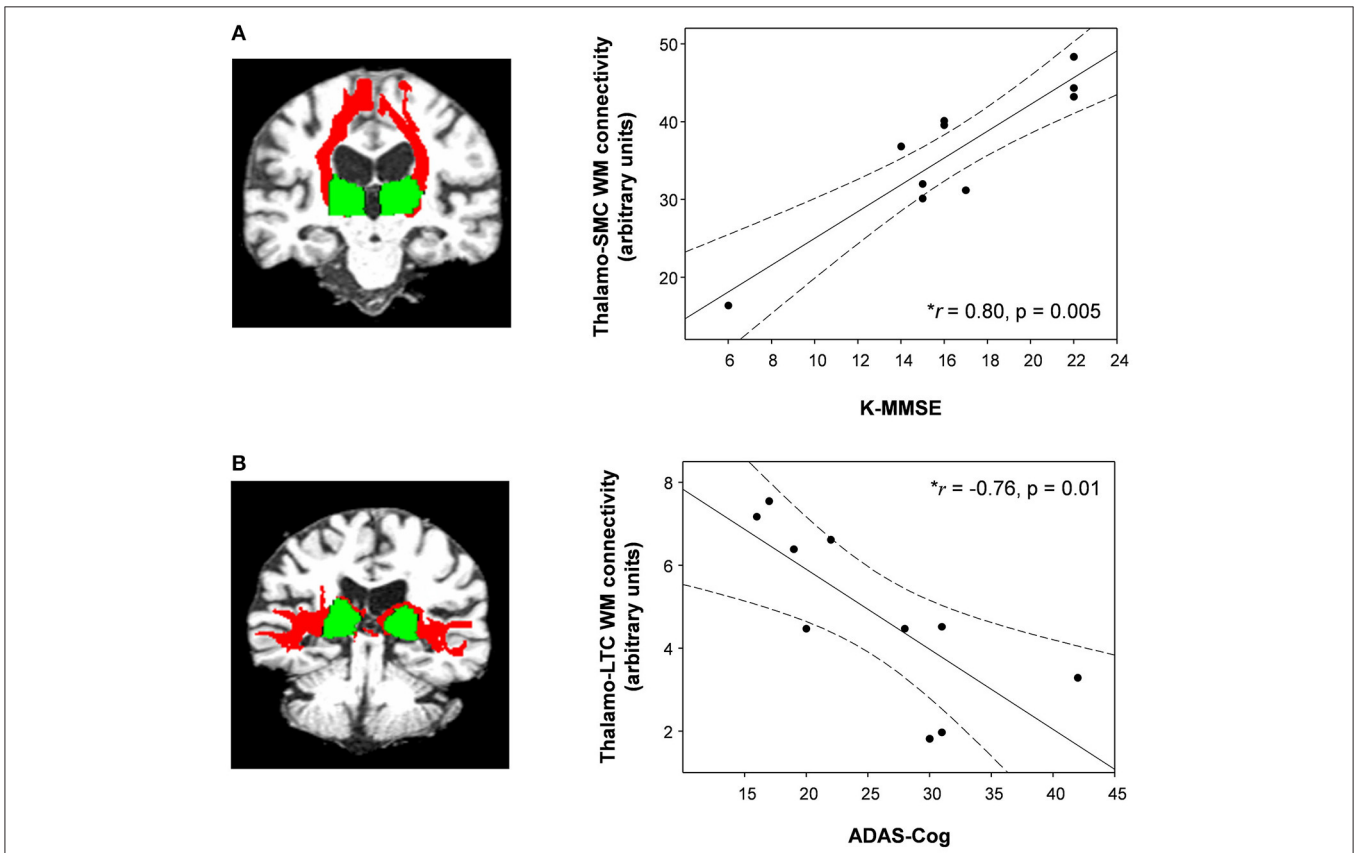

FIGURE 3 | (A) The thalamo-sensorimotor cortex (SMC) white matter connectivity in patients with MCI was positively correlated with K-MMSE scores (Spearman's rho = 0.80, $p = 0.005$) and **(B)** the thalamo-lateral temporal cortex (LTC) was negatively correlated with ADAS-cog scores (Spearman's rho = −0.76, $p = 0.01$). Dotted lines show 95% confidence intervals. Red, white matter connectivity; green, thalamus ROIs (seed regions). • Shows WM connectivity and K-MMSE or ADAS-Cog in patients with MCI.

(Mentis et al., 1995) demonstrated hypometabolism in the orbitofrontal cortex in patients with AD. Notably, observations with simultaneously decreased thalamo-LPFC WM connectivity, thickness in the orbitofrontal cortex, and reduced K-MMSE scores can be attributed to the cognitive dysfunction in the MCI patients.

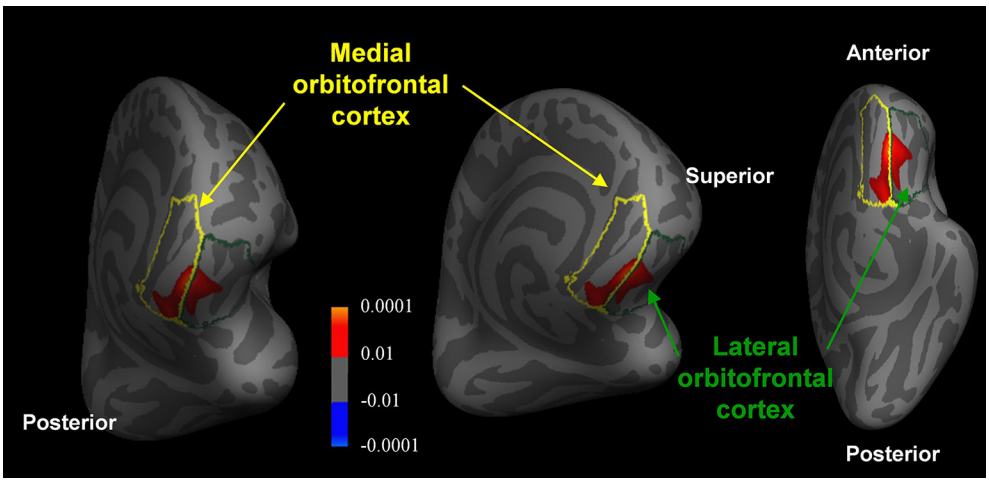

FIGURE 4 | Reduced orbitofrontal cortex thickness in patients with MCI compared with healthy controls (Monte-Carlo corrected, $p < 0.01$). The p-values of the clusters are represented by warm (healthy controls > MCI patients) and cool (MCI patients > healthy controls) colors.

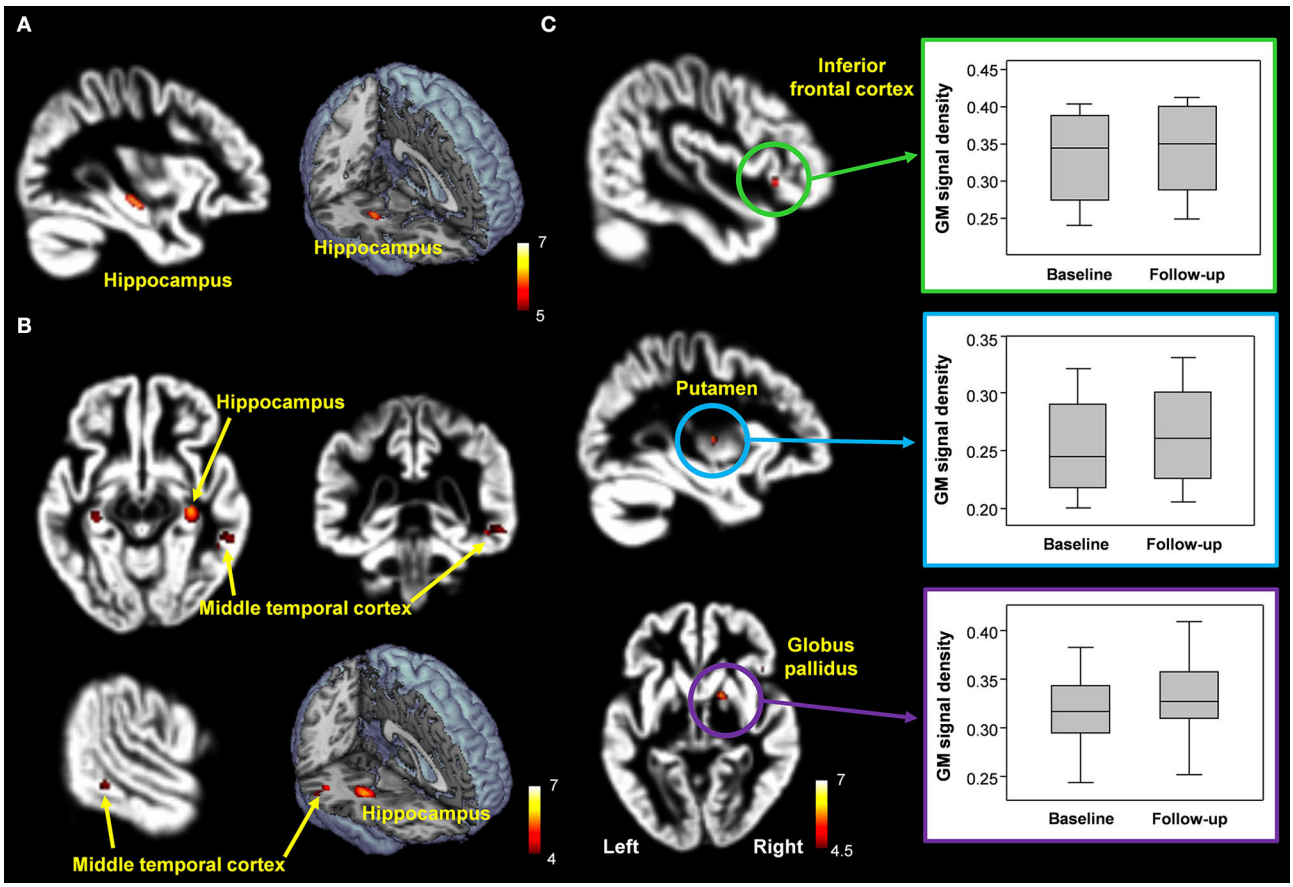

FIGURE 5 | (A,B) Decreased hippocampal volume in patients with MCI compared with healthy controls [FWE corrected, $p < 0.05$ **(A)**; uncorrected $p < 0.0005$ **(B)**]. **(C)** Brain regions with significantly increased GM volumes in donepezil-treated patients compared with patients with MCI (uncorrected, $p < 0.001$).

Furthermore, atrophy in the temporal lobe and hippocampus has proven to be an important biomarker in the diagnosis of MCI and AD. Especially, hippocampal atrophy has also been an important predictor of progression from MCI to AD and may be a marker for early AD in patients with MCI (Jack et al., 1999, 2005; Apostolova et al., 2006; He et al., 2009).

According to He et al. (2009), patients with amnestic multiple-domain MCI had significant hippocampal atrophy compared with the patients with amnestic single-domain MCI. The work of Apostolova et al. (2006) suggested that smaller hippocampal volume is associated with increased risk for conversion from MCI to AD. The current study found that patients with MCI showed significantly decreased volume in the hippocampus and middle temporal cortex compared with the healthy controls. This result is in concurrence with the finding that the most prominent structural changes at the initial stage in AD occur in the temporal lobe and hippocampus (Jack et al., 1999, 2005; Apostolova et al., 2006; He et al., 2009). Although the patients with MCI showed decreased GM volume in the middle temporal cortex, the significance level by multiple comparison correction is not high enough to validate this finding. In addition, the thalamo-LTC WM connectivity in the patients with MCI was negatively correlated with the ADAS-cog scores. The ADAS-Cog is a validated and robust scale for measuring the change in AD and continues to remain the regulatory standard outcome for AD trials (Schrag et al., 2012). Based on these findings, decreased thalamo-LPFC WM connectivity, reduced orbitofrontal cortical thickness, and hippocampal atrophy can be useful for diagnosing and tracking MCI.

In the current study, the MMSE scores in patients with MCI improved after donepezil treatment by 7.9%. Additionally, after 6 months of treatment, patients with MCI showed increased thalamo-MTC WM connectivity and higher GM volume in the inferior frontal cortex. However, the patterns of WM connectivity and brain volume change in untreated and treated patients were not significantly different from each other, resulting from multiple comparison corrections. However, these findings might not be clear due to the short follow-up period for donepezil treatment. Therefore, future studies comprising a larger population with a long period of follow-up are needed to generate more accurate and reliable data.

This study has some limitations. The small sample size means it does not have high statistical power. To compensate for this limitation, we considered a statistical threshold of P-value <0.05 using FWE or Bonferroni correction. Another limitation relates to the quality inspection of DWI data, which is based on a visual inspection and individual processing in FSL software, without correction for the geometric distortion induced by B0 inhomogeneity. Thus, further correction through unwarping is needed to rectify susceptibility-induced geometric distortions. Another limitation involves the short follow-up period of about 6 months for donepezil treatment, hindering optimal evaluation of the time course of donepezil treatment efficacy. Therefore, large population studies with long-term follow-up are needed to obtain more accurate and reliable findings. Furthermore, a placebo-controlled study of MCI patients is recommended to validate and establish the efficacy of drug treatments.

CONCLUSION

This study has demonstrated altered thalamo-cortical WM connectivity, cortical thickness, and GM volume following donepezil treatment in patients with MCI. More specifically, patients with MCI showed decreased thalamo-LPC WM connectivity and reduced thickness in the medial/lateral orbitofrontal cortices. Taken altogether, these findings could be valuable in the early detection of MCI as a prodromal phase of AD, as well as furthering understanding of the neurophysiopathological mechanism of MCI in connection with structural and functional abnormalities.

DATA AVAILABILITY STATEMENT

The data that support the findings of this study are available from the corresponding author upon reasonable request.

ETHICS STATEMENT

The studies involving human participants were reviewed and approved by the Institutional Review Board of Chonnam National University Hospital. The patients/participants provided their written informed consent to participate in this study.

AUTHOR CONTRIBUTIONS

G-WK, S-EP, KP, and G-WJ designed the study, contributed to the analysis and interpretation of results, wrote the first draft of the manuscript. G-WK and G-WJ performed the majority of experiments. G-WJ has approved the final manuscript and completed manuscript. All authors agree with the content of the manuscript.

FUNDING

This research was supported by the grants from the National Research Foundation funded by the Korea government (MSIT; 2021R1C1C2011748, Ministry of Education; 2014R1A1A2006730, MSICT; 2018R1A2B2006260 and 2018R1C1B6005456) and the Chonnam National University (CNU) Research Fund for the CNU distinguished research professor (2017–2022).

REFERENCES

Alderson, T., Kehoe, E., Maguire, L., Farrell, D., Lawlor, B., Kenny, R. A., et al. (2017). Disrupted thalamus white matter anatomy and posterior default mode network effective connectivity in amnestic mild cognitive impairment. *Front. Aging Neurosci.* 9:370. doi: 10.3389/fnagi.2017.00370

Apostolova, L. G., Dutton, R. A., Dinov, I. D., Hayashi, K. M., Toga, A. W., Cummings, J. L., et al. (2006). Conversion of mild cognitive impairment to Alzheimer disease predicted by hippocampal atrophy maps. *Arch. Neurol.* 63, 693–699. doi: 10.1001/archneur.63.5.693

Behrens, T. E., Berg, H. J., Jbabdi, S., Rushworth, M. F., and Woolrich, M. W. (2007). Probabilistic diffusion tractography with multiple

fibre orientations: what can we gain? *Neuroimage* 34, 144–155. doi: 10.1016/j.neuroimage.2006.09.018

Behrens, T. E., Woolrich, M. W., Jenkinson, M., Johansen-Berg, H., Nunes, R. G., Clare, S., et al. (2003). Characterization and propagation of uncertainty in diffusion-weighted MR imaging. *Magn. Reson. Med.* 50, 1077–1088. doi: 10.1002/mrm.10609

Caso, F., Agosta, F., Mattavelli, D., Migliaccio, R., Canu, E., Magnani, G., et al. (2015). White matter degeneration in atypical Alzheimer disease. *Radiology* 277, 162–172. doi: 10.1148/radiol.2015142766

Cavedo, E., Grothe, M. J., Colliot, O., Lista, S., Chupin, M., Dormont, D., et al. (2017). Reduced basal forebrain atrophy progression in a randomized Donepezil trial in prodromal Alzheimer's disease. *Sci. Rep.* 7:11706. doi: 10.1038/s41598-017-09780-3

Chao, L. L., Pa, J., Duarte, A., Schuff, N., Weiner, M. W., Kramer, J. H., et al. (2009). Patterns of cerebral hypoperfusion in amnestic and dysexecutive MCI. *Alzheimer Dis. Assoc. Disord.* 23, 245–252. doi: 10.1097/WAD.0b013e318199ff46

Cho, K. I., Shenton, M. E., Kubicki, M., Jung, W. H., Lee, T. Y., et al. (2016). Altered thalamo-cortical white matter connectivity: probabilistic tractography study in clinical-high risk for psychosis and first-episode psychosis. *Schizophr. Bull.* 42, 723–731. doi: 10.1093/schbul/sbv169

Dale, A. M., Fischl, B., and Sereno, M. I. (1999). Cortical surface-based analysis. I. Segmentation and surface reconstruction. *Neuroimage* 9, 179–194. doi: 10.1006/nimg.1998.0395

Duarte, A., Hayasaka, S., Du, A., Schuff, N., Jahng, G. H., Kramer, J., et al. (2006). Volumetric correlates of memory and executive function in normal elderly, mild cognitive impairment and Alzheimer's disease. *Neurosci. Lett.* 406, 60–65. doi: 10.1016/j.neulet.2006.07.029

Fettes, P., Schulze, L., and Downar, J. (2017). Cortico-striatal-thalamic loop circuits of the orbitofrontal cortex: promising therapeutic targets in psychiatric illness. *Front. Syst. Neurosci.* 11:25. doi: 10.3389/fnsys.2017.00025

Fischl, B., Salat, D. H., Busa, E., Albert, M., Dieterich, M., Haselgrove, C., et al. (2002). Whole brain segmentation: automated labeling of neuroanatomical structures in the human brain. *Neuron* 33, 341–355. doi: 10.1016/S0896-6273(02)00569-X

Fischl, B., Van Der Kouwe, A., Destrieux, C., Halgren, E., Segonne, F., Salat, D. H., et al. (2004). Automatically parcellating the human cerebral cortex. *Cereb. Cortex* 14, 11–22. doi: 10.1093/cercor/bhg087

Fumagalli, F., Racagni, G., and Riva, M. A. (2006). The expanding role of BDNF: a therapeutic target for Alzheimer's disease? *Pharmacogenomics J.* 6, 8–15. doi: 10.1038/sj.tpj.6500337

Gerrits, N. J., Van Loenhoud, A. C., Van Den Berg, S. F., Berendse, H. W., Foncke, E. M., Klein, M., et al. (2016). Cortical thickness, surface area and subcortical volume differentially contribute to cognitive heterogeneity in Parkinson's disease. *PLoS ONE* 11:e0148852. doi: 10.1371/journal.pone.0148852

Han, K. M., Choi, S., Jung, J., Na, K. S., Yoon, H. K., Lee, M. S., et al. (2014). Cortical thickness, cortical and subcortical volume, and white matter integrity in patients with their first episode of major depression. *J. Affect Disord.* 155, 42–48. doi: 10.1016/j.jad.2013.10.021

Hashimoto, M., Kazui, H., Matsumoto, K., Nakano, Y., Yasuda, M., and Mori, E. (2005). Does donepezil treatment slow the progression of hippocampal atrophy in patients with Alzheimer's disease? *Am. J. Psychiatry* 162, 676–682. doi: 10.1176/appi.ajp.162.4.676

He, J., Farias, S., Martinez, O., Reed, B., Mungas, D., and Decarli, C. (2009). Differences in brain volume, hippocampal volume, cerebrovascular risk factors, and apolipoprotein E4 among mild cognitive impairment subtypes. *Arch. Neurol.* 66, 1393–1399. doi: 10.1001/archneurol.2009.252

Hornberger, M., Savage, S., Hsieh, S., Mioshi, E., Piguet, O., and Hodges, J. R. (2010). Orbitofrontal dysfunction discriminates behavioral variant frontotemporal dementia from Alzheimer's disease. *Dement Geriatr. Cogn. Disord.* 30, 547–552. doi: 10.1159/000321670

Hoy, A. R., Ly, M., Carlsson, C. M., Okonkwo, O. C., Zetterberg, H., Blennow, K., et al. (2017). Microstructural white matter alterations in preclinical Alzheimer's disease detected using free water elimination diffusion tensor imaging. *PLoS ONE* 12:e0173982. doi: 10.1371/journal.pone.0173982

Hyman, B. T., Van Hoesen, G. W., Damasio, A. R., and Barnes, C. L. (1984). Alzheimer's disease: cell-specific pathology isolates the hippocampal formation. *Science* 225, 1168–1170. doi: 10.1126/science.6474172

Jack, C. R. Jr., Petersen, R. C., Xu, Y. C., O'brien, P. C., Smith, G. E., Ivnik, R. J., et al. (1999). Prediction of AD with MRI-based hippocampal volume in mild cognitive impairment. *Neurology* 52, 1397–1403. doi: 10.1212/WNL.52.7.1397

Jack, C. R. Jr., Shiung, M. M., Weigand, S. D., O'brien, P. C., Gunter, J. L., Boeve, B. F., et al. (2005). Brain atrophy rates predict subsequent clinical conversion in normal elderly and amnestic MCI. *Neurology* 65, 1227–1231. doi: 10.1212/01.wnl.0000180958.22678.91

Jaimes, C., Cheng, H. H., Soul, J., Ferradal, S., Rathi, Y., Gagoski, B., et al. (2017). Probabilistic tractography-based thalamic parcellation in healthy newborns and newborns with congenital heart disease. *J. Magn. Reson. Imaging* 47, 1626–1637. doi: 10.1002/jmri.25875

Jenkinson, M., Beckmann, C. F., Behrens, T. E., Woolrich, M. W., and Smith, S. M. (2012). FSL. *Neuroimage* 62, 782–790. doi: 10.1016/j.neuroimage.2011.09.015

Kasa, P., Papp, H., Kasa, P. Jr., and Torok, I. (2000). Donepezil dose-dependently inhibits acetylcholinesterase activity in various areas and in the presynaptic cholinergic and the postsynaptic cholinoceptive enzyme-positive structures in the human and rat brain. *Neuroscience* 101, 89–100. doi: 10.1016/S0306-4522(00)00335-3

Kim, G. W., Kim, B. C., Park, K. S., and Jeong, G. W. (2020). A pilot study of brain morphometry following donepezil treatment in mild cognitive impairment: volume changes of cortical/subcortical regions and hippocampal subfields. *Sci. Rep.* 10:10912. doi: 10.1038/s41598-020-67873-y

Kim, G. W., Kim, Y. H., Park, K., and Jeong, G. W. (2019). A comparative study of white matter volume between postoperative female-to-male transsexuals and healthy female. *Int. J. Impot. Res.* 31, 432–438. doi: 10.1038/s41443-019-0111-5

Kim, G. W., Park, K., and Jeong, G. W. (2018a). Effects of sex hormones and age on brain volume in post-menopausal women. *J. Sex Med.* 15, 662–670. doi: 10.1016/j.jsxm.2018.03.006

Kim, G. W., Yoon, W., and Jeong, G. W. (2018b). Whole-brain volume alteration and its correlation with anxiety severity in patients with obsessive-compulsive disorder and generalized anxiety disorder. *Clin. Imaging* 50, 164–170. doi: 10.1016/j.clinimag.2018.03.008

Krasuski, J. S., Alexander, G. E., Horwitz, B., Daly, E. M., Murphy, D. G., Rapoport, S. I., et al. (1998). Volumes of medial temporal lobe structures in patients with Alzheimer's disease and mild cognitive impairment (and in healthy controls). *Biol. Psychiatry* 43, 60–68. doi: 10.1016/S0006-3223(97)00013-9

Marenco, S., Stein, J. L., Savostyanova, A. A., Sambataro, F., Tan, H. Y., Goldman, A. L., et al. (2012). Investigation of anatomical thalamo-cortical connectivity and FMRI activation in schizophrenia. *Neuropsychopharmacology* 37, 499–507. doi: 10.1038/npp.2011.215

Mentis, M. J., Weinstein, E. A., Horwitz, B., Mcintosh, A. R., Pietrini, P., Alexander, G. E., et al. (1995). Abnormal brain glucose metabolism in the delusional misidentification syndromes: a positron emission tomography study in Alzheimer disease. *Biol. Psychiatry* 38, 438–449. doi: 10.1016/0006-3223(94)00326-X

Mito, R., Raffelt, D., Dhollander, T., Vaughan, D. N., Tournier, J. D., Salvado, O., et al. (2018). Fibre-specific white matter reductions in Alzheimer's disease and mild cognitive impairment. *Brain* 141, 888–902. doi: 10.1093/brain/awx355

Morris, J. C. (2005). Mild cognitive impairment and preclinical Alzheimer's disease. *Geriatrics* 9–14.

Morris, J. C. (2012). Revised criteria for mild cognitive impairment may compromise the diagnosis of Alzheimer disease dementia. *Arch. Neurol.* 69, 700–708. doi: 10.1001/archneurol.2011.3152

Nakajima, M., and Halassa, M. M. (2017). Thalamic control of functional cortical connectivity. *Curr. Opin. Neurobiol.* 44, 127–131. doi: 10.1016/j.conb.2017.04.001

Palesi, F., Vitali, P., Chiarati, P., Castellazzi, G., Caverzasi, E., Pichiecchio, A., et al. (2012). DTI and MR Volumetry of Hippocampus-PC/PCC circuit: in search of early micro- and macrostructural signs of Alzheimers's disease. *Neurol. Res. Int.* 2012:517876. doi: 10.1155/2012/517876

Radanovic, M., Pereira, F. R., Stella, F., Aprahamian, I., Ferreira, L. K., Forlenza, O. V., et al. (2013). White matter abnormalities associated with Alzheimer's disease and mild cognitive impairment: a critical review of MRI studies. *Expert Rev. Neurother.* 13, 483–493. doi: 10.1586/ern.13.45

Scali, C., Casamenti, F., Bellucci, A., Costagli, C., Schmidt, B., and Pepeu, G. (2002). Effect of subchronic administration of metrifonate, rivastigmine and donepezil on brain acetylcholine in aged F344 rats. *J. Neural. Transm.* 109, 1067–1080. doi: 10.1007/s007020200090

Schrag, A., Schott, J. M., and Initia, A. D. N. (2012). What is the clinically relevant change on the ADAS-Cog? *J. Neurol. Neurosurg. Psychiatry* 83, 171–173. doi: 10.1136/jnnp-2011-300881

Theisen, F., Leda, R., Pozorski, V., Oh, J. M., Adluru, N., Wong, R., et al. (2017). Evaluation of striatonigral connectivity using probabilistic tractography in Parkinson's disease. *Neuroimage Clin.* 16, 557–563. doi: 10.1016/j.nicl.2017.09.009

Tsai, S. Y. (2018). Reproducibility of structural brain connectivity and network metrics using probabilistic diffusion tractography. *Sci. Rep.* 8:11562. doi: 10.1038/s41598-018-29943-0

Wang, Y., West, J. D., Flashman, L. A., Wishart, H. A., Santulli, R. B., Rabin, L. A., et al. (2012). Selective changes in white matter integrity in MCI and older adults with cognitive complaints. *Biochim. Biophys. Acta* 1822, 423–430. doi: 10.1016/j.bbadis.2011.08.002

Whitwell, J. L. (2009). Voxel-based morphometry: an automated technique for assessing structural changes in the brain. *J. Neurosci.* 29, 9661–9664. doi: 10.1523/JNEUROSCI.2160-09.2009

Zhao, H., Li, X., Wu, W., Li, Z., Qian, L., Li, S., et al. (2015). Atrophic patterns of the frontal-subcortical circuits in patients with mild cognitive impairment and Alzheimer's disease. *PLoS ONE* 10:e0130017. doi: 10.1371/journal.pone.0130017

Zhou, B., Liu, Y., Zhang, Z., An, N., Yao, H., Wang, P., et al. (2013). Impaired functional connectivity of the thalamus in Alzheimer's disease and mild cognitive impairment: a resting-state fMRI study. *Curr. Alzheimer Res.* 10, 754–766. doi: 10.2174/15672050113109990146

Conflict of Interest: The authors declare that the research was conducted in the absence of any commercial or financial relationships that could be construed as a potential conflict of interest.

frontiers in Aging Neuroscience

SYSTEMATIC REVIEW
published: 31 March 2021
doi: 10.3389/fnagi.2021.627919

Gray Matter Atrophy in Amnestic Mild Cognitive Impairment: A Voxel-Based Meta-Analysis

Jinhuan Zhang[1,2], Yongfeng Liu[3], Kai Lan[1], Xingxian Huang[3], Yuhai He[1], Fuxia Yang[3], Jiaying Li[2], Qingmao Hu[2], Jinping Xu[2] and Haibo Yu[1,3]**

[1] The Fourth Clinical Medical College of Guangzhou University of Chinese Medicine, Shenzhen, China, [2] Institute of Biomedical and Health Engineering, Shenzhen Institutes of Advanced Technology, Chinese Academy of Sciences, Shenzhen, China, [3] Department of Acupuncture and Moxibustion, Shenzhen Traditional Chinese Medicine Hospital, Shenzhen, China

Background: Voxel-based morphometry (VBM) has been widely used to investigate structural alterations in amnesia mild cognitive impairment (aMCI). However, inconsistent results have hindered our understanding of the exact neuropathology related to aMCI.

Objectives: Our aim was to systematically review the literature reporting VBM on aMCI to elucidate consistent gray matter alterations, their functional characterization, and corresponding co-activation patterns.

Methods: The PubMed, Web of Science, and EMBASE databases were searched for VBM studies on aMCI published from inception up to June 2020. Peak coordinates were extracted from clusters that showed significant gray matter differences between aMCI patients and healthy controls (HC). Meta-analysis was performed using seed-based *d* mapping with the permutation of subject images (SDM-PSI), a newly improved meta-analytic method. Functional characterization and task-based co-activation patterns using the BrainMap database were performed on significant clusters to explore their functional roles. Finally, VBM was performed based on the Alzheimer's Disease Neuroimaging Initiative (ADNI) dataset to further support the findings.

Results: A total of 31 studies with 681 aMCI patients and 837 HC were included in this systematic review. The aMCI group showed significant gray matter atrophy in the left amygdala and right hippocampus, which was consistent with results from the ADNI dataset. Functional characterization revealed that these regions were mainly associated with emotion, cognition, and perception. Further, meta-regression analysis demonstrated that gray matter atrophy in the left inferior frontal gyrus and the left angular gyrus was significantly associated with cognitive impairment in the aMCI group.

Conclusions: The findings of gray matter atrophy in the left amygdala and right hippocampus are highly consistent and robust, and not only offer a better understanding of the underlying neuropathology but also provide accurate potential biomarkers for aMCI.

Keywords: amnestic mild cognitive impairment, voxel-based morphometry, gray matter volume, meta-analysis, seed-based *d* mapping

OPEN ACCESS

Edited by:
Jiu Chen,
Nanjing Medical University, China

Reviewed by:
Cecilia Beatriz Conde,
Medical Research Institute Mercedes and Martín Ferreyra (INIMEC), Argentina
Carmen Jiménez-Mesa,
University of Granada, Spain

***Correspondence:**
Haibo Yu
13603066098@163.com
Jinping Xu
jp.xu@siat.ac.cn

Received: *10 November 2020*
Accepted: *02 March 2021*
Published: *31 March 2021*

Citation:
Zhang J, Liu Y, Lan K, Huang X, He Y, Yang F, Li J, Hu Q, Xu J and Yu H (2021) Gray Matter Atrophy in Amnestic Mild Cognitive Impairment: A Voxel-Based Meta-Analysis. Front. Aging Neurosci. 13:627919. doi: 10.3389/fnagi.2021.627919

INTRODUCTION

Mild cognitive impairment (MCI) is a transitional stage between normal cognitive function and dementia, mainly characterized by mild impaired cognitive function but without significant impairment of function (Bennett et al., 2002; Petersen, 2004). Amnestic MCI (aMCI), is a subtype of MCI characterized by objective memory impairment without dementia, preserved general cognitive function, and highly intact functional activities (Petersen, 2004). aMCI conveys a high risk for developing Alzheimer's disease (AD), with an annual rate of ∼25% of patients (Petersen et al., 2001b; Zhao et al., 2014). Although numerous studies have reported gray matter atrophy in many brain regions and have suggested it to be associated with the pathophysiology of aMCI, the results are inconsistent (Threlkeld et al., 2011; Baglio et al., 2012; Migo et al., 2015), and need to be verified.

In recent years, numerous systematic reviews have been performed to analyze the difference in gray matter between MCI and HC (Schroeter et al., 2009; Shi et al., 2009; Yang et al., 2012; Tabatabaei-Jafari et al., 2015; Minkova et al., 2017; Gu and Zhang, 2019). However, the studies showed that MCI, including both aMCI and non-aMCI, is a heterogeneous clinical identity displaying the loss of different neurodegenerative entities (Costafreda et al., 2009; Serra et al., 2013), thus, should be studied at the subtype level. The most recent meta-analysis (Nickl-Jockschat et al., 2012) on the gray matter differences between aMCI and HC was conducted in 2012, and revealed significant atrophy in the bilateral amygdala, hippocampus, left superior temporal gyrus, and the left thalamus. An increasing number of voxel-based morphometry (VBM) studies have investigated gray matter differences between aMCI and HC. However, due to the small and heterogeneous samples of participants as well as substantial methodological differences between studies, results from VBM studies remain inconsistent and controversial (Costafreda et al., 2009). For example, some studies report that regional gray matter atrophy is mainly restricted to the bilateral hippocampus (Pa et al., 2009; Gili et al., 2011), whereas other studies only report gray matter volume (GMV) loss in the unilateral hippocampus (left or right) (Bonekamp et al., 2010; Xie et al., 2015). Moreover, a statistical method of the meta-analysis has been optimized (Albajes-Eizagirre et al., 2019a,b). A new-generation algorithm for coordinate-based meta-analysis (CBMA), seed-based *d* mapping with the permutation of subject images (SDM-PSI), has been successfully used in previous VBM meta-analysis studies (Albajes-Eizagirre et al., 2019b; Wang et al., 2020). This method has led to significant improvements, such as using threshold-free cluster enhancement (TFCE) statistics, small bias estimates of the overall size estimates, and multiple imputations of the study image, to avoid bias associated with single imputation (Albajes-Eizagirre et al., 2019a).

Therefore, in this systematic review of VBM studies, SDM-PSI was used to determine the most prominent and replicable areas that can distinguish aMCI from healthy controls. Further, meta-analytic connectivity modeling (MACM) analysis was performed to understand the role of significance clusters at the functional network level. Behavioral domains (BD) and paradigm classes (PC) were used to determine functional characterization of significance clusters. A dataset (144 aMCI and 87 HC) from the Alzheimer's Disease Neuroimaging Initiative (ADNI) database was used to compare gray matter atrophy of aMCI and HC to further validate the results of our meta-analysis.

MATERIALS AND METHODS

The meta-analysis was conducted in accordance with the Preferred Reporting Items for Systematic Reviews and Meta-analyses (PRISMA) statement (Moher et al., 2009; Muller et al., 2018) (**Supplementary Table 1**). The present meta-analysis was undertaken following the recent guidelines and recommendations for CBMA (Winblad et al., 2004; Tahmasian et al., 2019). The protocol of this meta-analysis was registered at PROSPERO (http://www.crd.york.ac.uk/PROSPERO) (registration number: CRD42020204050).

Literature Search and Study Selection

A systematic search strategy was conducted in PubMed, EMBASE, and Web of Science (https://www.webofknowledge.com/) from inception to June 2020. The search keywords used were ("cognitive impairment" OR "mild cognitive impairment" OR "cognitive decline" [Title/Abstract]) OR "neurocognitive disorder" OR "MCI") AND ("voxel-based morphometry" OR "VBM" OR "morphometry") OR "volumetry" OR "gray matter" OR "structural MRI"). Besides, the references of the included studies were manually screened to avoid omission of relevant studies, and all the identified studies were imported into EndNote. After a review of the title and abstracts, studies that did not meet the inclusion criteria were excluded. A final exclusion of studies was performed after a full-text review.

Studies were included if they met the following criteria: (1) the patients met the clear diagnostic criteria for aMCI (McKhann et al., 1984; Petersen et al., 2001a,b; Petersen, 2004; Du et al., 2014); (2) the study utilized the VBM method to estimate GMV or differences in gray matter density at the whole-brain level between aMCI and HC; (3) the study used stereotactic coordinates (i.e., Talairach space or Montreal Neurological Institute (MNI) space); and (4) the study was an original article, peer-reviewed, and published in English. The appropriate results of the meta-analysis were based on the overall effect in the subgroups. Studies reporting aMCI patients with other neurological, psychiatric, or systemic diseases or postoperative complications were also excluded (i.e.; stroke, Parkinson's disease, or diabetes). For longitudinal design studies, only baseline preprocessing data were included. Authors of published studies were contacted for additional information by email. Following this approach, 31 studies were selected (**Figure 1**).

Data Extraction and Quality Assessment

The extracted data included study characteristics (author and year of publication), subject characteristics [sample size, age, gender, education, and mini-mental state examination (MMSE)], peak coordinates, and the significance level. Moreover, coordinates in different stereotactic spaces were converted to MNI space, while Z- or *P*-values for significant

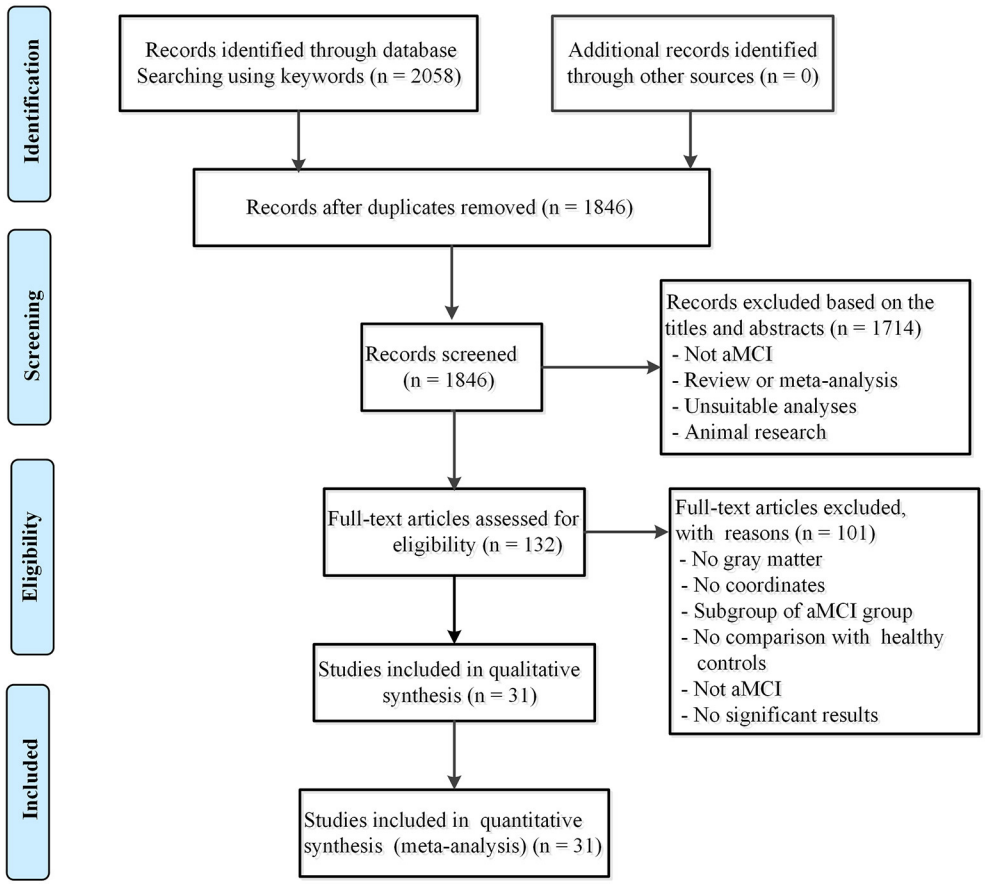

FIGURE 1 | Flow diagram of inclusion and exclusion process of selected articles of VBM studies in patients with aMCI. aMCI, amnestic mild cognitive impairment.

clusters were converted to *T*-values using SDM utilities (https://www.sdmproject.com/utilities/?show=Statistics).

A 12-point checklist (**Supplementary Table 2**) containing the inclusion criteria, demographic characteristics, sample size, technical details of the imaging procedure, analysis method, and the quality of the reported results was assessed to determine the quality of each selected article (Radua et al., 2015). All the steps were independently performed by two authors, and all inconsistencies were resolved by a third author.

Coordinate-Based Meta-Analysis

CBMA was carried out using SDM-PSI version 6.21 (https://www.sdmproject.com/), with the following procedure: (1) collection of information regarding the peak coordinates of significant GM differences between aMCI and HC; (2) calculation of the maps of the lower and upper bounds of possible effect sizes within a GM mask, full anisotropy = 1, isotropic full width half maximum (FWHM) = 20 mm, and voxel = 2 mm; (3) the mean analysis: estimation of the map of most likely effect size and its standard error based on the MetaNSUE algorithms (Radua et al., 2012; Albajes-Eizagirre et al., 2019b); (4) conducting multiple imputations of the maps of the effect size of individual studies; (5) meta-analysis of these maps using a standard random-effects model, and Rubin rules to pool the different meta-analyses resulting from the multiple imputations (Albajes-Eizagirre et al., 2019b); (6) family-wise error (FWE) correction for multiple comparisons; and (7) using threshold-free cluster enhancement (TFCE) in the statistical thresholding ($p < 0.05$, voxel extent ≥ 10). The details of these procedures have been extensively described in prior publications (Albajes-Eizagirre et al., 2019a,b) and the SDM-PSI reference manual (https://www.sdmproject.com/manual/).

Reliability Analysis, Subgroup Meta-Analysis, and Meta-Regressions

To test the replicability of the results, a systematic whole-brain voxel-based jackknife sensitivity analysis was performed using the leave-one-out method (Radua and Mataix-Cols, 2009; Albajes-Eizagirre et al., 2019a).

Subgroup meta-analyses were performed to investigate the potential confounding effects. Imaging methodology variables including datasets using a 3.0 T MRI scanner, statistical parametric mapping (SPM) software versions 8 or 12, a smoothing kernel of 8 mm, and the corrected thresholds for multiple comparisons, respectively, were performed. Statistical significance was determined using the TFCE-based FWE

corrected threshold ($p < 0.05$, voxel extent ≥ 10) (Radua et al., 2014; Albajes-Eizagirre et al., 2019b).

Finally, meta-regression analyses were conducted to examine the potential effects of demographic characteristics and clinical confounders (age, gender, education, and MMSE) on GMV by linear regression. Confounders were weighted based on the square root of the sample size and restricted to only predict possible SDM values (Radua et al., 2014). Statistical significance was determined using a stringent threshold of $p < 0.05$ and cluster extent ≥ 10 voxels in the meta-regression analyses (Higgins et al., 2003; Radua and Mataix-Cols, 2009).

Analyses of Heterogeneity and Publication Bias

The values from peak coordinates reported in the CBMA were extracted for information to guide heterogeneity statistics and publication bias analyses. Heterogeneity between studies was assessed using the I^2 statistic using a random-effects model, where $I^2 < 50\%$ indicates low heterogeneity (Egger et al., 1997). Publication bias was examined using funnel plots and Egger tests (Eickhoff et al., 2011). An asymmetric plot and $p < 0.05$ were considered statistically significant.

Analysis of Co-activation Patterns and Functional Characterization

To determine the role of these clusters at the functional network level, we performed MACM to obtain the task-dependent co-activated patterns of each brain region in the BrainMap database (http://brainmap.org/) by performing an activation likelihood estimation (ALE) (Eickhoff et al., 2009; Tench et al., 2014). The ALE scores were compared to a null-distribution of random spatial association between experiments with a fixed within-experiment distribution of foci (Eickhoff et al., 2012) yielding a p-value based on the proportion of equal or higher random values (Eickhoff et al., 2011). These non-parametric p-values were converted to z-scores and corrected at a cluster-level FWE-corrected threshold of $p < 0.05$ (a voxel-level $p < 0.001$).

Functional characterization determines the functional role of the brain region in terms of behavioral domains (BD) and paradigm classes (PC) using forward inference in the BrainMap database (Laird et al., 2009; Turner and Laird, 2012) (http://www.brainmap.org). Behavioral domains include the main categories of cognition, action, perception, emotion, and interception, as well as their related sub-categories. Paradigm classes classify the specific task employed (Muller et al., 2013) (http://brainmap.org/scribe/) for complete BrainMap taxonomy. Significance was assessed using a binomial test ($p < 0.05$, corrected for multiple comparisons using FDR) (Weiner et al., 2013).

Alzheimer's Disease Neuroimaging Initiative Database

The gray matter differences between aMCI and HC were further studied using the ADNI database, to support the meta-analysis results. Inclusive and exclusive criteria are described in detail at http://www.adni-info.org.

Data were downloaded from the ADNI database up to July 2020 (Chetelat et al., 2002) (http://adni.loni.ucla.edu/). The search included insertion of MCI and HC in the research group and selecting MRI modalities from the ADNI.

The T1 images were preprocessed using DPABI (http://rfmri.org/dpabi). First, each image was segmented into gray matter, white matter, and cerebrospinal fluid, and the images were transformed to MNI space. The gray matter images were modulated to preserve regional volume information. Finally, the modulated images were smoothed with a 6 mm FWHM. Two-sample t-tests were performed to identify GMV differences between aMCI and HC. Age and sex were entered into the models as covariates. Results were corrected for Gaussian Random Field (GRF) with a voxel level of $p < 0.001$ and a cluster level of $p < 0.05$.

RESULTS

Included Studies and Sample Characteristics

Thirty-one studies (Bell-McGinty et al., 2005; Hirata et al., 2005; Saykin et al., 2006; Shiino et al., 2006; Trivedi et al., 2006; Hämäläinen et al., 2007; Bai et al., 2008; Barbeau et al., 2008; Barnes et al., 2009; Guedj et al., 2009; Pa et al., 2009; Rami et al., 2009; Bonekamp et al., 2010; Agosta et al., 2011; Derflinger et al., 2011; Threlkeld et al., 2011; Venneri et al., 2011; Baglio et al., 2012; Han et al., 2012; Wang et al., 2012; Xie et al., 2012, 2015; Bastin et al., 2013; Hoppstädter et al., 2013; Serra et al., 2013; Zhao et al., 2014, 2015; Hong et al., 2015; Migo et al., 2015; Sheelakumari et al., 2018; Chen et al., 2020) were included comprising 681 aMCI patients (211 male and 207 female) and 837 HC (257 male and 301 female). An unbalanced age distribution was observed between aMCI and HC (standardized mean difference [SMD] $= -0.20$, 95% confidence interval [CI] $= [-0.31, -0.10]$, z $= 3.74$, $p < 0.01$), and one dataset (Pa et al., 2009) did not report the mean age and standard deviation of HC. Significant differences were observed between aMCI and HC regarding gender ($\chi^2 = 4.7$, $p = 0.03$), however, the sex ratios of the two datasets (Saykin et al., 2006; Chen et al., 2020) were not provided. In terms of educational level, the aMCI group had fewer years of education compared with the HC group (SMD $= -1.32$, 95%CI $= [-1.45, -1.18]$, z $= 19.23$, $p < 0.01$), the education levels in six datasets (Bell-McGinty et al., 2005; Saykin et al., 2006; Trivedi et al., 2006; Guedj et al., 2009; Pa et al., 2009; Agosta et al., 2011) were not provided. Besides, the aMCI groups had significantly lower MMSE scores than the HC group (SMD $= -0.19$, 95% CI $= [-0.31, -0.07]$, z $= 3.19$, $p < 0.01$). The MMSE scores in seven datasets were not provided.

The quality of each included study (**Supplementary Table 2**) was acceptable, with a quality score not <10 (a maximum score =11.5). The demographic, clinical, and quality score of each eligible study are summarized in **Table 1**. Technical characteristics are shown in **Supplementary Table 3**.

Gray Matter Atrophy

In the pooled meta-analysis, aMCI patients showed significant gray matter atrophy in two brain regions relative to HC; one in

TABLE 1 | Demographic and clinical characteristics of the included VBM studies.

Study	Gender (F/M)		Age (SD)		Education (SD)		MMSE (SD)		Quality scores (out of 12)
	HC	MCI	HC	MCI	HC	MCI	HC	aMCI	
Chetelat et al. (2002), Chetelat et al. (2002), Bell-McGinty et al. (2005)	22 (12/10)	22 (12/10)	66.6 (7.2)	71.0 (8.0)	NA	NA	NA	NA	11
Bell-McGinty et al. (2005), Hirata et al. (2005)	47 (20/27)	9 (5/4)	66.9 (7.3)	71.9 (7.6)	15.7 (2.7)	13.7 (2.1)	29.4 (0.4)	23.1 (3.8)	10.5
Hirata et al. (2005), Saykin et al. (2006)	30	41	70.6 (8.4)	71.1 (7.7)	NA	NA	28.7 (1.5.)	26.0 (1.5)	10.5
Saykin et al. (2006), Shiino et al. (2006)	40 (28/12)	40 (17/23)	63.4 (8.9)	70.9 (9.0)	16.6 (2.7)	16.3 (3.3)	29.1 (1.0)	27.2 (2.2)	11.5
Shiino et al. (2006), Trivedi et al. (2006)	88 (48/40)	20 (10/10)	68.7 (8.7)	67.7 (9.0)	NA	NA	29.09 (1.47)	26.80 (1.88)	11
Trivedi et al. (2006), Hämäläinen et al. (2007)	15 (6/9)	15 (6/9)	73.6 (7.1)	73.3 (6.7)	16.7 (2.5)	16.3 (2.8)	29.7 (0.5)	27.8 (1.8)	11.5
Hämäläinen et al. (2007), Bai et al. (2008)	21 (17/4)	14 (10/4)	71.2 (4.9)	72.4 (7.3)	7.9 (2.9)	8.1 (2.6)	27.7 (2.0)	5.6 (3.1)	11
Bai et al. (2008), Barbeau et al. (2008)	20 (11/9)	20 (10/10)	69.4 (3.8)	71.3 (3.8)	13.8 (4)	14.0 (3.1)	28.3 (1.4)	27.2 (1.6)	11
Barbeau et al. (2008), Guedj et al. (2009)	28 (13/15)	28 (16/12)	63.3 (7.2)	69.3 (8.6)	NA	NA	28.9 (1.0)	27.4 (1.4)	11
Guedj et al. (2009), Pa et al. (2009)	28	19 (10/9)	NA	69.9 (9.5)	NA	NA	28.8 (1.0)	27.1 (1.1)	10
Pa et al. (2009), Rami et al. (2009)	36 (23/13)	26 (13/13)	64.8 (8.2)	68.0 (6.6)	17.0 (2.0)	17.5 (1.7)	NA	NA	11
Rami et al. (2009), Bonekamp et al. (2010)	27 (17/10)	14 (10/4)	74.3 (5.3)	72.9 (4.8)	9.4 (5.2)	7.4 (4.2)	27.4 (1.0)	26.0 (2.0)	11
Bonekamp et al. (2010), Agosta et al. (2011)	20 (10/10)	10 (5/5)	75.5 (4.6)	73.5 (5.5)	NA	NA	28.9 (1.2)	26.3 (2.9)	11.5
Agosta et al. (2011), Derflinger et al. (2011)	15 (9/6)	15 (7/8)	69.8 (6.0)	70.4 (7.2)	12.3 (3.6)	9.0 (4.6)	28.8 (1.5)	25.8 (0.9)	11.5
Derflinger et al. (2011), Threlkeld et al. (2011)	30 (20/10)	24 (13/11)	67.0 (8.7)	69.0 (9.0)	10.6 (1.7)	10.4 (2.0)	NA	26.8 (1.7)	11.5
Threlkeld et al. (2011)	24 (11/13)	18 (8/10)	77.9 (7.1)	77.1 (5.8)	16.2 (2.4)	15.8 (2.6)	28.4 (1.1)	27.1 (1.3)	11
Venneri et al. (2011), Venneri et al. (2011)	25 (15/10)	25 (12/13)	70.3 (6.5)	70.5 (6.4)	9.32 (4.46)	8.96 (4.41)	28.68 (1.52)	28.24 (1.23)	10.5
Baglio et al. (2012), Baglio et al. (2012)	15 (9/6)	16 (7/9)	71.0 (5.8)	66.9 (6.4)	10.8 (3.5)	9.9 (4.8)	29.0 (1.3)	27.0 (1.8)	10.5

(Continued)

TABLE 1 | Continued

Study	Gender (F/M)		Age (SD)		Education (SD)		MMSE (SD)		Quality scores (out of 12)
	HC	MCI	HC	MCI	HC	MCI	HC	aMCI	
Han et al. (2012), Han et al. (2012), Wang et al. (2012)	18 (11/7)	17 (10/7)	66.5 (6.2)	69.7 (7.6)	8.4 (5.6)	8.8 (4.0)	29.2 (0.7)	25.2 (3.5)	11
Wang et al. (2012), Xie et al. (2012)	30 (11/19)	40 (16/24)	76.1 (7.2)	68.07 (7.46)	13.5 (2.6)	11.4 (4.3)	NA	NA	11.5
Xie et al. (2012), Bastin et al. (2013)	25 (12/13)	17 (11/6)	74.3 (8.3)	75.1 (6.6)	15.3 (2.9)	13.5 (2.1)	28.9 (1.2)	27.3 (1.8)	11
Bastin et al. (2013), Hoppstädter et al. (2013)	24 (18/6)	35 (12/23)	73.2 (7.2)	73.9 (6.6)	12.5 (2.8)	13.0 (3.5)	NA	NA	11.5
Hoppstädter et al. (2013), Serra et al. (2013)	10 (6/4)	14 (4/10)	67.8 (4.7)	68.0 (4.0)	12.90 (3.80)	11.30 (2.50)	28.88 (1.05)	27.85 (1.29)	11.5
Serra et al. (2013), Zhao et al. (2014)	28 (10/18)	15 (4/11)	63.4 (8.9)	70.9 (9.0)	13.1 (3.5)	11.3 (4.4)	28.4 (1.7)	25.4 (1.7)	11
Zhao et al. (2014), Hong et al. (2015)	18 (10/8)	20 (12/8)	66.8 (7.4)	65.1 (9.9)	12.0 (2.9)	11.8 (3.3)	29.3 (1.2)	25.2 (2.2)	11.5
Hong et al. (2015), Migo et al. (2015)	28 (19/9)	29 (19/10)	70.6 (6.5)	70.5 (5.2)	8.8 (6.16)	8.6 (4.36)	28.7 (1.36)	25.5 (2.81)	11.5
Migo et al. (2015)	11 (4/7)	10 (5/5)	70.3 (6.2)	71.4 (6.4)	15.64 (4.13)	16.00 (4.30)	NA	NA	10.5
Xie et al. (2015), Xie et al. (2015), Zhao et al. (2015)	26 (12/14)	30 (11/19)	64.8 (7.59)	67.14 (9.3)	14.3 (3.2)	14.3 (3.2)	28.2 (1.3)	27.1 (1.6)	11.5
Zhao et al. (2015), Sheelakumari et al. (2018)	34 (16/18)	34 (20/14)	66.9 (6.7)	68.0 (7.6)	11.5 (3.9)	10.8 (3.3)	29.2 (0.9)	25.5 (1.6)	11.5
Sheelakumari et al. (2018), Chen et al. (2020)	25	24	63.24 (6.94)	69.8 3(5.76)	12.80 (3.68)	11.29 (3.25)	NA	NA	11.5
Chen et al. (2020)	29 (17/12)	20 (7/13)	70.69 (5.4)	71.35 (5.9)	12.17 (3.2)	10.88 (2.9)	28.55 (1.4)	27.45 (2.1)	11.5

aMCI, amnestic mild cognitive impairment; SD, standard deviation; MMSE, mini-mental state examination; NA, not available; F, female; and M, male.

the left amygdala ($p = 0.000999987 < 0.001$) extending to the left hippocampus, left temporal pole, superior temporal gyrus, left amygdala, cingulum, and left parahippocampal gyrus. The other in the right hippocampus ($p = 0.000999987 < 0.001$), extending to the right amygdala and right parahippocampal gyrus (**Figure 2**; **Table 2**).

Jackknife Sensitivity Analysis and Subgroup Analysis

Whole-brain jackknife sensitivity analysis showed that gray matter atrophy in the left amygdala and right hippocampus were highly replicable (**Table 2**). The results of the right amygdala and left thalamus remained significant in all but one combination (Trivedi et al., 2006).

The results remained largely unchanged when the meta-analysis was restricted to the datasets corrected for multiple comparisons ($n = 14$). However, when the meta-analysis was restricted to the datasets acquiring images with a 3.0 T MRI scanner ($n = 16$), datasets using statistical parametric mapping (SPM) software, versions 8 or 12 ($n = 19$), only the left amygdala was found (**Table 3**).

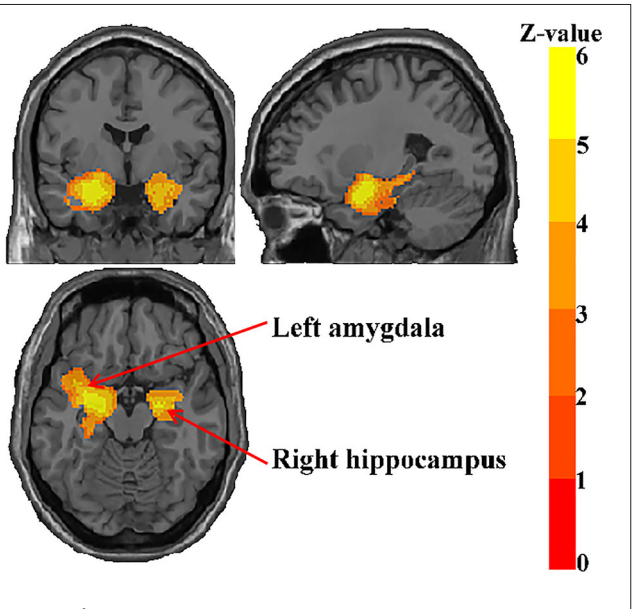

FIGURE 2 | Regions showing reduced gray matter in aMCI patients.

Analyses of Heterogeneity and Publication Bias

The low I^2 statistic (0.0%) (**Supplementary Figures 1, 2**) indicated low heterogeneity between-study variability in gray matter atrophy in the right hippocampus and left amygdala.

Although the funnel plot showed no obvious asymmetry for the right hippocampus and the left amygdala (**Figure 3**), Egger tests revealed possible publication bias in the left amygdala ($p < 0.05$) (**Supplementary Table 4**).

Meta-Regression Analysis

GMV atrophy in the left orbital part of the inferior frontal gyrus (IFG.L) (BA 47, MNI coordinate: $x = -36$, $y = 26$, $z = -16$, SDM-Z value = 2.469, $r = 0.19$, $p = 0.006$, and 112 voxels), the left triangular part of the inferior frontal gyrus (BA 48, MNI coordinate: $x = -52$, $y = 16$, $z = 8$; SDM-Z value = 1.965, $r = 0.16$, $p = 0.024$, 47 voxels), and the left angular gyrus (AG.L) (BA 39, MNI coordinate: $x = -48$, $y = -62$, $z = 48$, SDM-Z value = 2.037, $r = 0.17$, $p = 0.020$, 19 voxels) was found to be positively correlated with the MMSE scores in the aMCI patients after removing the covariates of age and education (**Figure 4**).

Results From ADNI

A total of 144 patients with aMCI (82 male/62 female, mean age = 74.97, mean MMSE = 29.64) and 83 HC (38 male/45 female, mean age = 75.90, mean MMSE = 26.85) were included in the current study. No significant difference was reported for age and gender between both groups ($p > 0.05$). The aMCI group showed significantly higher MMSE compared with the HC group ($p < 0.01$).

VBM analysis revealed that there were two clusters with a statistical significant difference: the left hippocampus (MNI coordinate: $x = -25.5$, $y = -9$, $z = -16.5$, $t = 4.450$, 2,609 voxels) and right amygdala (peak MNI coordinate: $x = 21$, $y = -4.5$, $z = -18$, $t = 4.453$). These results showed high overlap with the meta-analysis results (**Supplementary Figure 3**).

TABLE 2 | Regional differences in GM volume between patients with aMCI and healthy controls in the meta-analysis.

Brain regions	MNI coordinate	SDM-Z value	*P*-value	Number of voxels	Cluster breakdown (number of voxels)	Jackknife sensitivity
Left amygdala	−26, −2, −16	−6.635	<0.001	2,633	Left hippocampus, BA 20 (177); left temporal pole, superior temporal gyrus, BA 38 (165); left median network, cingulum (128); left parahippocampal gyrus, BA 28 (125); left inferior network, inferior longitudinal fasciculus (112); left inferior network, uncinate fasciculus (94); left insula, BA 48 (91);	31/31
Right hippocampus	20, −6, −14	−5.973	<0.001	836	Right amygdala, BA 34 (86); right parahippocampal gyrus, BA 28 (66)	30/31

BA, Brodmann area.

TABLE 3 | Results of analyses of subgroups.

	Decreased gray matter	
	Left amygdala	**Right hippocampus**
Studies Hämäläinen et al., 2007; Barnes et al., 2009; Threlkeld et al., 2011; Venneri et al., 2011; Baglio et al., 2012; Han et al., 2012; Wang et al., 2012; Bastin et al., 2013; Hoppstädter et al., 2013; Serra et al., 2013; Zhao et al., 2014; Hong et al., 2015; Migo et al., 2015; Sheelakumari et al., 2018 with acquiring images with a 3.0T MRI scanner (n = 14)	Yes	No
Studies Barnes et al., 2009; Venneri et al., 2011; Wang et al., 2012; Bastin et al., 2013; Hoppstädter et al., 2013; Serra et al., 2013; Zhao et al., 2014, 2015; Migo et al., 2015; Sheelakumari et al., 2018; Chen et al., 2020 employing statistical parametric mapping (SPM) software, versions 8 or 12 (n =11)	Yes	No
Studies Bell-McGinty et al., 2005; Saykin et al., 2006; Trivedi et al., 2006; Bai et al., 2008; Barbeau et al., 2008; Guedj et al., 2009; Pa et al., 2009; Rami et al., 2009; Agosta et al., 2011; Derflinger et al., 2011; Threlkeld et al., 2011; Han et al., 2012; Wang et al., 2012; Xie et al., 2012; Bastin et al., 2013; Zhao et al., 2014, 2015 with correction for multiple comparisons (n = 16)	Yes	Yes

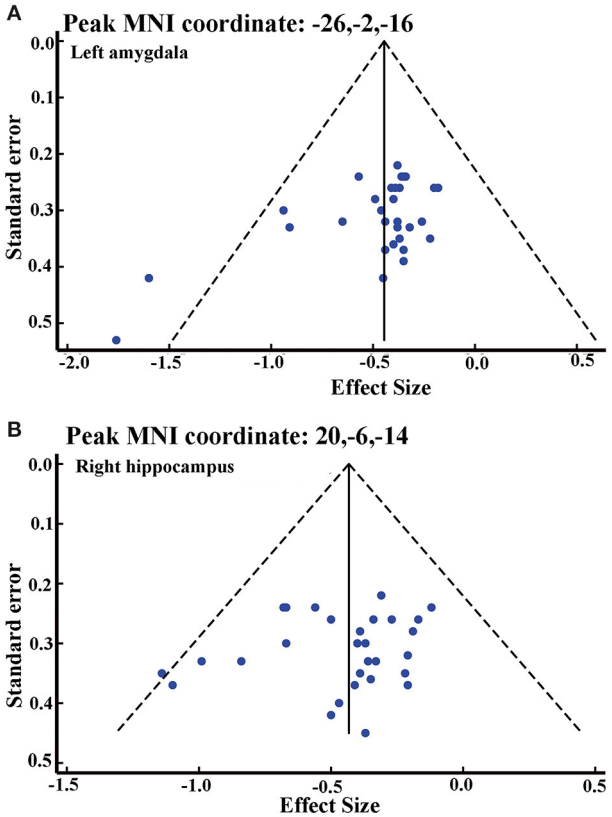

FIGURE 3 | Funnel plot of effect size of left amygdala **(A)** and right hippocampus **(B)**.

Co-activation Patterns and Functional Characterization

To further investigate the role of significance clusters (the left amygdala and right hippocampus) at the functional network level, MACM analysis was performed; at the same time, functional characterizations was performed to explore the detailed functions and behavioral profiles of the left amygdala and the right hippocampus.

The bilateral cerebrum, limbic lobe, parahippocampal gyrus, amygdala, inferior frontal gyrus, sub-lobar, frontal lobe, inferior frontal gyrus, temporal lobe, extra-nuclear, superior frontal gyrus, and fusiform gyrus were co-activated with the left amygdala (**Figures 5A,B**). Functional characterization showed that the left amygdala was mainly associated with emotion, perception, and cognition, and the PCs showed similar results (**Figure 5C**).

The bilateral cerebrum, limbic lobe, parahippocampal gyrus, amygdala, temporal lobe, inferior frontal gyrus, sub-lobar, extra-nuclear, fusiform gyrus, and cingulate gyrus were co-activated with the right hippocampus (**Figures 5D,E**). Functional characterization demonstrated that the right hippocampus was associated with emotion, perception, and cognition, and the PCs also showed similar results (**Figure 5F**).

DISCUSSION

In the current study, a newly improved SDM-PSI method was used to perform a meta-analysis on VBM studies on GMV alterations in aMCI compared to HC. This quantitative meta-analysis comprised 31 whole-brain VBM studies with 681 aMCI patients and 837 HC. aMCI patients were found to exhibit significant gray matter atrophy in the left amygdala and the right hippocampus compared to HC. Jackknife sensitivity analysis and subgroup analysis revealed that the results were highly consistent and robust. Moreover, VBM analyses based on the ADNI dataset showed similar results with high overlap. Further meta-regression analysis demonstrated that GMV atrophy in the left inferior frontal gyrus and left angular gyrus is associated with the severity of cognitive impairment in aMCI. Functional characterization revealed that these regions were mainly associated with emotion, cognition, and memory.

Our findings of robust GMV atrophy in the left amygdala and right hippocampus were consistent with a previous meta-analysis based on ALE studies which reported evidence of volume reduction in the bilateral amygdala and hippocampus in aMCI (Albajes-Eizagirre et al., 2019b). Our results were also consistent with various longitudinal studies which showed that subjects with AD have higher rates of hippocampal and amygdala volumetric

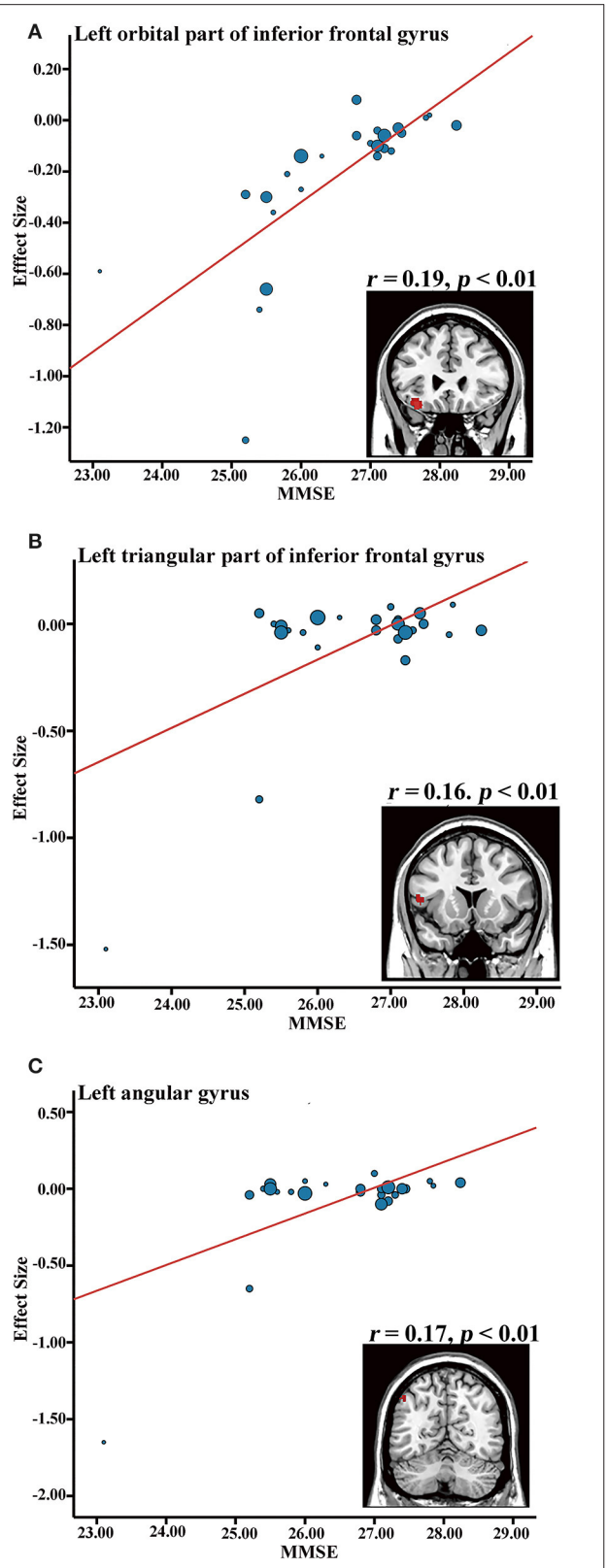

FIGURE 4 | Meta-regression results showing an association between MMSE and gray matter volume in the aMCI group, in the left inferior frontal gyrus **(A)**, left inferior frontal gyrus **(B)**, and left angular gyrus **(C)**. MMSE, mini-mental state examination.

atrophy compared with HC (Jack et al., 1998; van de Pol et al., 2007; Wolz et al., 2010; Zhang et al., 2012; Miller et al., 2013). Moreover, the results were also supported by the previous meta-analysis between MCI and HC (Yang et al., 2012; Minkova et al., 2017; Gu and Zhang, 2019), however, there were some statistically significant clusters not reported in this study, which may be related to a heterogeneous subgroup of MCI patients (that is, aMCI and non-aMCI) (Hirata et al., 2005). These differences may be related to risk factors or physiology that is unique to each MCI subtype. Previous studies demonstrate that gray matter atrophy in MCI subtypes differs from HC (Whitwell et al., 2007; Bai et al., 2009a), aMCI showed more atrophy in the hippocampus, parahippocampus, and temporal lobes, whereas non-aMCI showed atrophy in the inferior and medial frontal gyrus, anterior cingulate gyrus, superior temporal gyrus, and insula (Whitwell et al., 2007). Most importantly, functional MRI studies report that aMCI patients show decreased medial temporal lobe activation (Chen et al., 2016) and decreased sub-regional functional connectivity (Remondes and Schuman, 2004; Bai et al., 2009b) compared with HC. It is important to note that the amygdala and hippocampus are two important medial temporal lobes (MTL) structures. MTL, involved in encoding and retrieval of episodic and spatial memory (Braak and Braak, 1991; Schwindt and Black, 2009; Ranganath and Ritchey, 2012), is considered to be initially targeted in AD-related pathology (Braak and Braak, 1991; Ranganath and Ritchey, 2012) and aMCI patients (Scheltens et al., 1992; Karas et al., 2004; Korf et al., 2004; Bai et al., 2009a). The results indicate that GMV atrophy in the left amygdala and right hippocampus might provide accurate potential biomarkers for aMCI.

This meta-analysis revealed GMV atrophy of the amygdala in aMCI, which has been reported in numerous other studies (Maren and Fanselow, 1995; Trivedi et al., 2006; Bastin et al., 2013; Migo et al., 2015). The important role of the amygdala in emotional processing and emotional memory has been emphasized by functional imaging experiments and lesion studies in animal models (Roozendaal et al., 2009; Pape and Pare, 2010; Mendez-Bertolo et al., 2016). Human studies further demonstrate the central roles of the amygdala in emotion processing (Adolphs et al., 1999; Sotres-Bayon et al., 2012), memory, and storage. Growing evidence suggests that aMCI patients have impaired recognition of facial emotional expression (McCade et al., 2011; Richard-Mornas et al., 2012; Varjassyova et al., 2013), which is mainly related to the amygdala. Results of our behavioral analysis for the amygdala also support this opinion. More importantly, impairments of emotional recognition and emotional facial expressions have been reported in aMCI patients (Lavenu et al., 1999), and are related to the transition of aMCI into AD (Bediou et al., 2009; Chen et al., 2015). Based on these findings, amygdala atrophy may help explain the clinical manifestations of aMCI.

Consistent with previous studies in aMCI patients (Maren and Fanselow, 1995; Apostolova et al., 2006; Shi et al., 2009; Bartsch and Wulff, 2015), this meta-analysis also showed GMV atrophy in the hippocampus, which is the most validated, easily accessible, and widely used biomarker for AD. The hippocampus, located in the MTL, plays a pivotal role in the learning, formation,

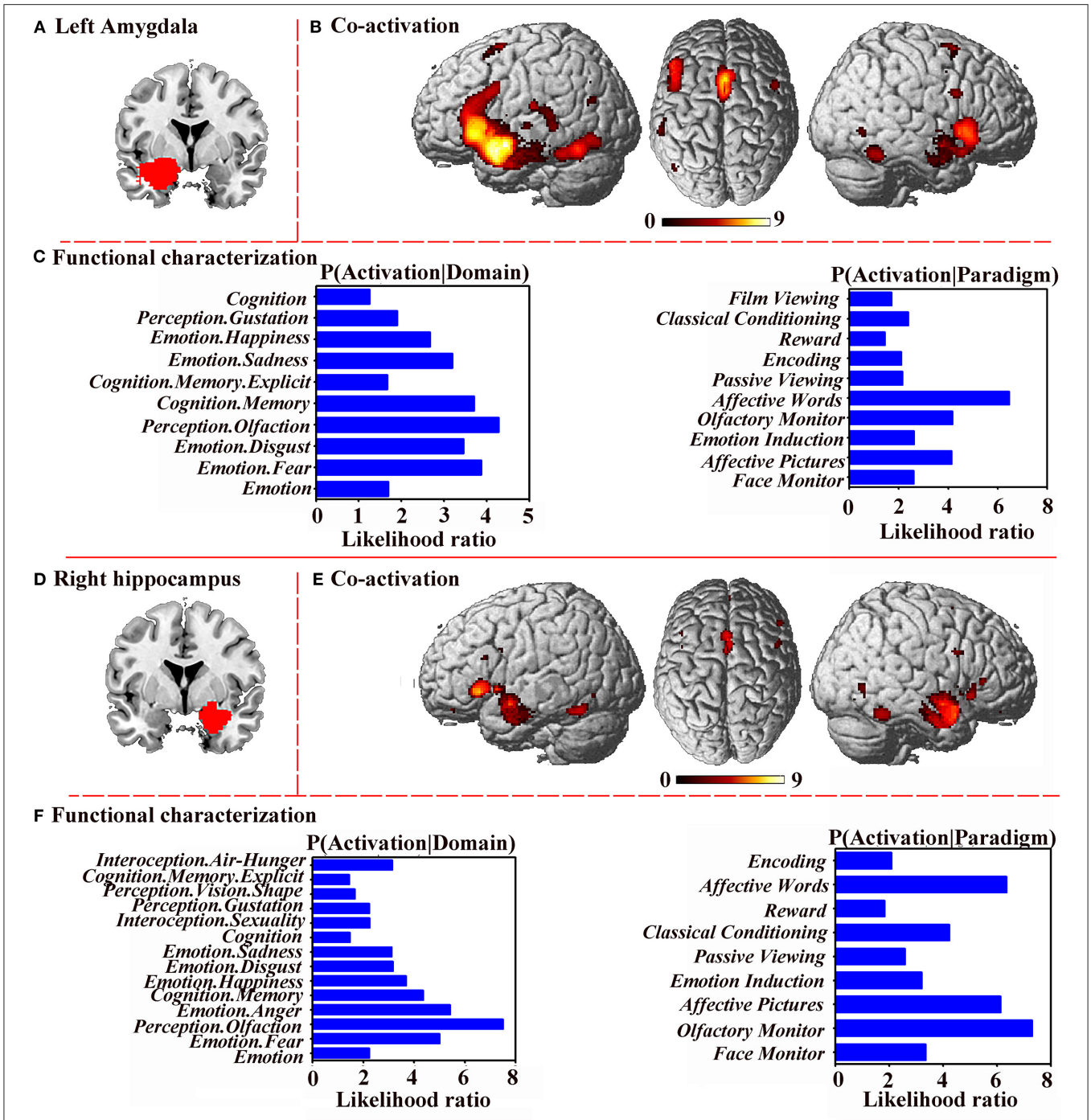

FIGURE 5 | Functional connectivity and characterization. **(A)** Left amygdala. **(B)** Co-activation connectivity analysis for left amygdala. **(C)** Functional characterization of left amygdala. **(D)** Right hippocampus. **(E)** Co-activation connectivity analysis for right hippocampus. **(F)** Functional characterization of right hippocampus. Functional characterization of significance levels was thresholded at $p < 0.05$, cluster-level FWE-corrected, cluster-forming threshold at voxel-level $p < 0.001$. Co-activation connectivity of significance levels was thresholded at $p < 0.05$, corrected for multiple comparisons using FDR.

and consolidation of memory (Knierim, 2015). Lesion studies on humans and animals demonstrate that the hippocampus performs a critical function in the brain's ability to store and retrieve memories (particularly episodic memories in humans) (Kontaxopoulou et al., 2018). Recent findings indicate that aMCI patients have difficulties with episodic memory, incidental memory, and long-term memory with greater hippocampal atrophy (Lee et al., 2014; Zhao et al., 2014; de Mendonca

et al., 2018). Lee's study also showed that recognition memory can be used to identify aMCI patients at greater risk for progressing to dementia (Leung et al., 2013). These findings are consistent with our functional characteristics findings. An important study by Leung et al. found that hippocampal atrophy in MCI patients was estimated to accelerate by an average of 0.22%/year^2 (Defrancesco et al., 2014). Therefore, our findings on hippocampal atrophy in patients with aMCI further emphasize the important role of the hippocampus in the pathobiology of aMCI.

MMSE, a general cognitive screening test commonly used to assess MCI in previous studies, has been correlated with GMV atrophy. In this study, lower MMSE was positively correlated with decreased GMV in the IFG.L, which was consistent with previous studies (Prince et al., 2005; Wang et al., 2012). The IFG.L has been implicated as an important part in the pathology of MCI, and is thought to be associated with attention and memory processes, including encoding and retrieval and long- and short-term memory (Wagner et al., 2001; Chambers et al., 2004; Prince et al., 2007). Similarly, lower MMSE was positively correlated with decreased GMV in the AG.L, which plays a major role in spatial attention and orienting (Dehaene et al., 2004), mathematical cognition (Thakral et al., 2017), and especially, episodic simulation and episodic memory (Bokde et al., 2010). Previous studies have shown that lower resting-state activity in the angular gyrus in aMCI may be related to poorer verbal working memory performance that involves short-term storage and retrieval of phonological representations (Jonides et al., 1998; Lin et al., 2020). These findings indicated that the IFG.L and AG.L may be used as potential markers to monitor aMCI progression and cognitive decline. Subgroup meta-analyses revealed that the main results were affected by the MR field-strength and SPM software to some extent, whereas GMV atrophy in the left amygdala and right hippocampus were independent of correction methods. These results provide insights to future VBM investigations, indicating the need to control for the potentially confounding factors of MR field-strength and SPM software.

The current study has several strengths. The most important one is the use of SDM-PSI, an updated CBMA, which has been presented and recommended in several previous studies (Yu et al., 2017; Albajes-Eizagirre et al., 2019b; Sheng et al., 2020a,b; Wang et al., 2020). This technique has made significant methodological improvements to overcome the drawbacks of alternative procedures and produce accurate results (Albajes-Eizagirre et al., 2019a). Besides, functional characterization and task-based co-activation using the BrainMap database was performed to explore the functional roles of the abnormal regions between aMCI and HC. Finally, the ADNI database was used to investigate the reliability of our findings.

Despite these strengths, this study has several potential limitations. First, the study shows that there may be publication bias in the gray matter atrophy of the amygdala. This may be related to the fact that we include only studies published in English that have been peer-reviewed. However, one study performed by Yu et al. also showed that publication bias did not have a major influence on the results in general (Salimi-Khorshidi et al., 2009). Our VBM results from the ADNI database showed similar patterns with those of the meta-analysis, which further supports the findings. Future comprehensively pooled big neuroimaging data from worldwide populations is still warranted. Second, voxel-based meta-analyses are based on summarized coordinates from published studies rather than raw data, which may result in less accurate results (Li and Zhang, 2015). However, obtaining and analyzing the raw images from these studies is logistically and technically difficult. Third, we did not perform subgroup analyses on the aMCI-single domain (aMCI-sd) and aMCI-multiple domain (aMCI-md), yet, distinct clinical features of aMCI subtypes may indicate different conversion rates to AD (Li and Zhang, 2015). Finally, since MMSE scores are a rather unspecific measure for aMCI (Nickl-Jockschat et al., 2012), the relationship between MMSE and brain structure should be used with caution. More specific memory tests are needed in future studies to better explore the relationship between gray matter atrophy and cognitive impairment in aMCI.

CONCLUSIONS

The current meta-analysis supports that GMV atrophy in the left amygdala and right hippocampus is highly consistent in aMCI patients. Additionally, functional characterization demonstrates that the consistent regions of brain atrophy are functionally linked to "emotion," "perception," and "cognition." This not only offers a better understanding of the underlying neuropathology but also provides accurate potential biomarkers for aMCI.

DATA AVAILABILITY STATEMENT

The original contributions presented in the study are included in the article/**Supplementary Material**, further inquiries can be directed to the corresponding authors.

AUTHOR CONTRIBUTIONS

JZ and JX designed the whole study, analyzed the data, and wrote the manuscript. XH and JL searched for and selected the studies. YL and FY participated in the interpretation of data. KL and YH participated in the revision of the article. HY and QH offered good suggestions. All authors read and approved the final manuscript.

FUNDING

This work was supported by the National Key R&D Program of China (No. 2017YFC1703600), the Key Technology Research on Effect Mechanism of Acupuncture-Moxibustion on Dominant Diseases (No. 2017YFC1703606), and the Natural Science Foundation of Guangdong Province (No. 2018A030313975).

SUPPLEMENTARY MATERIAL

The Supplementary Material for this article can be found online at: https://www.frontiersin.org/articles/10.3389/fnagi.2021.627919/full#supplementary-material

REFERENCES

Adolphs, R., Tranel, D., Hamann, S., Young, A. W., Calder, A. J., Phelps, E. A., et al. (1999). Recognition of facial emotion in nine individuals with bilateral amygdala damage. *Neuropsychologia* 37, 1111–1117. doi: 10.1016/S0028-3932(99)00039-1

Agosta, F., Pievani, M., Sala, S., Geroldi, C., Galluzzi, S., Frisoni, G. B., et al. (2011). White matter damage in Alzheimer disease and its relationship to gray matter atrophy. *Radiology* 258, 853–863. doi: 10.1148/radiol.10101284

Albajes-Eizagirre, A., Solanes, A., Fullana, M. A., Ioannidis, J., Fusar-Poli, P., Torrent, C., et al. (2019b). Meta-analysis of voxel-based neuroimaging studies using Seed-based d Mapping with Permutation of Subject Images (SDM-PSI). *J. Vis. Exp.* 153:59841. doi: 10.3791/59841

Albajes-Eizagirre, A., Solanes, A., Vieta, E., and Radua, J. (2019a). Voxel-based meta-analysis via permutation of subject images (PSI): theory and implementation for SDM. *Neuroimage* 186, 174–184. doi: 10.1016/j.neuroimage.2018.10.077

Apostolova, L. G., Dinov, I. D., Dutton, R. A., Hayashi, K. M., Toga, A. W., Cummings, J. L., et al. (2006). 3D comparison of hippocampal atrophy in amnestic mild cognitive impairment and Alzheimer's disease. *Brain* 129, 2867–2873. doi: 10.1093/brain/awl274

Baglio, F., Castelli, I., Alberoni, M., Blasi, V., Griffanti, L., Falini, A., et al. (2012). Theory of mind in amnestic mild cognitive impairment: an fMRI study. *J. Alzheimers Dis.* 29, 25–37. doi: 10.3233/JAD-2011-111256

Bai, F., Zhang, Z., Watson, D. R., Yu, H., Shi, Y., Yuan, Y., et al. (2009b). Abnormal functional connectivity of hippocampus during episodic memory retrieval processing network in amnestic mild cognitive impairment. *Biol. Psychiatry* 65, 951–958. doi: 10.1016/j.biopsych.2008.10.017

Bai, F., Zhang, Z., Watson, D. R., Yu, H., Shi, Y., Zhu, W., et al. (2009a). Absent gender differences of hippocampal atrophy in amnestic type mild cognitive impairment. *Neurosci. Lett.* 450, 85–89. doi: 10.1016/j.neulet.2008.11.055

Bai, F., Zhang, Z., Yu, H., Shi, Y., Yuan, Y., Zhu, W., et al. (2008). Default-mode network activity distinguishes amnestic type mild cognitive impairment from healthy aging: a combined structural and resting-state functional MRI study. *Neurosci. Lett.* 438, 111–115. doi: 10.1016/j.neulet.2008.04.021

Barbeau, E. J., Ranjeva, J. P., Didic, M., Confort-Gouny, S., Felician, O., Soulier, E., et al. (2008). Profile of memory impairment and gray matter loss in amnestic mild cognitive impairment. *Neuropsychologia* 46, 1009–1019. doi: 10.1016/j.neuropsychologia.2007.11.019

Barnes, J., Bartlett, J. W., van de Pol, L. A., Loy, C. T., Scahill, R. I., Frost, C., et al. (2009). A meta-analysis of hippocampal atrophy rates in Alzheimer's disease. *Neurobiol. Aging* 30, 1711–1723. doi: 10.1016/j.neurobiolaging.2008.01.010

Bartsch, T., and Wulff, P. (2015). The hippocampus in aging and disease: from plasticity to vulnerability. *Neuroscience* 309, 1–16. doi: 10.1016/j.neuroscience.2015.07.084

Bastin, C., Feyers, D., Jedidi, H., Bahri, M. A., Degueldre, C., Lemaire, C., et al. (2013). Episodic autobiographical memory in amnestic mild cognitive impairment: what are the neural correlates? *Hum. Brain Mapp.* 34, 1811–1825. doi: 10.1002/hbm.22032

Bediou, B., Ryff, I., Mercier, B., Milliery, M., Henaff, M. A., D'Amato, T., et al. (2009). Impaired social cognition in mild Alzheimer disease. *J. Geriatr. Psychiatry Neurol.* 22, 130–140. doi: 10.1177/0891988709332939

Bell-McGinty, S., Lopez, O. L., Meltzer, C. C., Scanlon, J. M., Whyte, E. M., Dekosky, S. T., et al. (2005). Differential cortical atrophy in subgroups of mild cognitive impairment. *Arch. Neurol.* 62, 1393–1397. doi: 10.1001/archneur.62.9.1393

Bennett, D. A., Wilson, R. S., Schneider, J. A., Evans, D. A., Beckett, L. A., Aggarwal, N. T., et al. (2002). Natural history of mild cognitive impairment in older persons. *Neurology* 59, 198–205.. doi: 10.1212/WNL.59.2.198

Bokde, A. L., Karmann, M., Born, C., Teipel, S. J., Omerovic, M., Ewers, M., et al. (2010). Altered brain activation during a verbal working memory task in subjects with amnestic mild cognitive impairment. *J. Alzheimers Dis.* 21, 103–118. doi: 10.3233/JAD-2010-091054

Bonekamp, D., Yassa, M. A., Munro, C. A., Geckle, R. J., Yousem, D. M., Barker, P. B., et al. (2010). Gray matter in amnestic mild cognitive impairment: voxel-based morphometry. *Neuroreport* 21, 259–263. doi: 10.1097/WNR.0b013e328335642a

Braak, H., and Braak, E. (1991). Neuropathological stageing of Alzheimer-related changes. *Acta Neuropathol.* 82, 239–259. doi: 10.1007/BF00308809

Chambers, C. D., Payne, J. M., Stokes, M. G., and Mattingley, J. B. (2004). Fast and slow parietal pathways mediate spatial attention. *Nat. Neurosci.* 7, 217–218. doi: 10.1038/nn1203

Chen, J., Duan, X., Shu, H., Wang, Z., Long, Z., Liu, D., et al. (2016). Differential contributions of subregions of medial temporal lobe to memory system in amnestic mild cognitive impairment: insights from fMRI study. *Sci. Rep.* 6:26148. doi: 10.1038/srep26148

Chen, J., Shu, H., Wang, Z., Liu, D., Shi, Y., Zhang, X., et al. (2015). The interaction of APOE genotype by age in amnestic mild cognitive impairment: a voxel-based morphometric study. *J. Alzheimers Dis.* 43, 657–668. doi: 10.3233/JAD-141677

Chen, J., Yan, Y., Gu, L., Gao, L., and Zhang, Z. (2020). Electrophysiological processes on motor imagery mediate the association between increased gray matter volume and cognition in amnestic mild cognitive impairment. *Brain Topogr.* 33, 255–266. doi: 10.1007/s10548-019-00742-8

Chetelat, G., Desgranges, B., De La Sayette, V., Viader, F., Eustache, F., and Baron, J. C. (2002). Mapping gray matter loss with voxel-based morphometry in mild cognitive impairment. *Neuroreport* 13, 1939–1943. doi: 10.1097/00001756-200210280-00022

Costafreda, S. G., David, A. S., and Brammer, M. J. (2009). A parametric approach to voxel-based meta-analysis. *Neuroimage* 46, 115–122. doi: 10.1016/j.neuroimage.2009.01.031

de Mendonca, A., Felgueiras, H., Verdelho, A., Camara, S., Grilo, C., Maroco, J., et al. (2018). Memory complaints in amnestic mild cognitive impairment: more prospective or retrospective? *Int. J. Geriatr. Psychiatry* 33, 1011–1018. doi: 10.1002/gps.4886

Defrancesco, M., Egger, K., Marksteiner, J., Esterhammer, R., Hinterhuber, H., Deisenhammer, E. A., et al. (2014). Changes in white matter integrity before conversion from mild cognitive impairment to Alzheimer's disease. *PLoS ONE* 9:e106062. doi: 10.1371/journal.pone.0106062

Dehaene, S., Molko, N., Cohen, L., and Wilson, A. J. (2004). Arithmetic and the brain. *Curr. Opin. Neurobiol.* 14, 218–224. doi: 10.1016/j.conb.2004.03.008

Derflinger, S., Sorg, C., Gaser, C., Myers, N., Arsic, M., Kurz, A., et al. (2011). Grey-matter atrophy in Alzheimer's disease is asymmetric but not lateralized. *J. Alzheimers Dis.* 25, 347–357. doi: 10.3233/JAD-2011-110041

Du, M., Liu, J., Chen, Z., Huang, X., Li, J., Kuang, W., et al. (2014). Brain grey matter volume alterations in late-life depression. *J. Psychiatry Neurosci.* 39, 397–406. doi: 10.1503/jpn.130275

Egger, M., Davey, S. G., Schneider, M., and Minder, C. (1997). Bias in meta-analysis detected by a simple, graphical test. *BMJ* 315, 629–634. doi: 10.1136/bmj.315.7109.629

Eickhoff, S. B., Bzdok, D., Laird, A. R., Kurth, F., and Fox, P. T. (2012). Activation likelihood estimation meta-analysis revisited. *Neuroimage* 59, 2349–2361. doi: 10.1016/j.neuroimage.2011.09.017

Eickhoff, S. B., Bzdok, D., Laird, A. R., Roski, C., Caspers, S., Zilles, K., et al. (2011). Co-activation patterns distinguish cortical modules, their connectivity and functional differentiation. *Neuroimage* 57, 938–949. doi: 10.1016/j.neuroimage.2011.05.021

Eickhoff, S. B., Laird, A. R., Grefkes, C., Wang, L. E., Zilles, K., and Fox, P. T. (2009). Coordinate-based activation likelihood estimation meta-analysis of neuroimaging data: a random-effects approach based on empirical estimates of spatial uncertainty. *Hum Brain Mapp* 30, 2907–2926. doi: 10.1002/hbm.20718

Gili, T., Cercignani, M., Serra, L., Perri, R., Giove, F., Maraviglia, B., et al. (2011). Regional brain atrophy and functional disconnection across Alzheimer's disease evolution. *J. Neurol. Neurosurg. Psychiatry* 82, 58–66. doi: 10.1136/jnnp.2009.199935

Gu, L., and Zhang, Z. (2019). Exploring structural and functional brain changes in mild cognitive impairment: a whole brain ALE meta-analysis for multimodal MRI. *ACS Chem. Neurosci.* 10, 2823–2829. doi: 10.1021/acschemneuro.9b00045

Guedj, E., Barbeau, E. J., Didic, M., Felician, O., de Laforte, C., Ranjeva, J., et al. (2009). Effects of medial temporal lobe degeneration on brain perfusion in amnestic MCI of AD type: deafferentation and functional compensation? *Eur. J. Nucl. Med. Mol. Imaging* 36, 1101–1112. doi: 10.1007/s00259-009-1060-x

Hämäläinen, A., Pihlajamäki, M., Tanila, H., Hänninen, T., Niskanen, E., Tervo, S., et al. (2007). Increased fMRI responses during encoding in mild cognitive impairment. *Neurobiol. Aging.* 28, 1889–1903. doi: 10.1016/j.neurobiolaging.2006.08.008

Han, Y., Lui, S., Kuang, W., Lang, Q., Zou, L., and Jia, J. (2012). Anatomical and functional deficits in patients with amnestic mild cognitive impairment. *PLoS ONE* 7:e28664. doi: 10.1371/journal.pone.0028664

Higgins, J. P., Thompson, S. G., Deeks, J. J., and Altman, D. G. (2003). Measuring inconsistency in meta-analyses. *BMJ* 327, 557–560. doi: 10.1136/bmj.327.7414.557

Hirata, Y., Matsuda, H., Nemoto, K., Ohnishi, T., Hirao, K., Yamashita, F., et al. (2005). Voxel-based morphometry to discriminate early Alzheimer's disease from controls. *Neurosci. Lett.* 382, 269–274. doi: 10.1016/j.neulet.2005.03.038

Hong, Y. J., Yoon, B., Shim, Y. S., Ahn, K. J., Yang, D. W., and Lee, J. (2015). Gray and white matter degenerations in subjective memory impairment: comparisons with normal controls and mild cognitive impairment. *J. Korean Med. Sci.* 30:1652. doi: 10.3346/jkms.2015.30.11.1652

Hoppstädter, M., King, A. V., Frölich, L., Wessa, M., Flor, H., and Meyer, P. (2013). A combined electrophysiological and morphological examination of episodic memory decline in amnestic mild cognitive impairment. *Front. Aging Neurosci.* 5:51. doi: 10.3389/fnagi.2013.00051

Jack, C. J., Petersen, R. C., Xu, Y., O'Brien, P. C., Smith, G. E., Ivnik, R. J., et al. (1998). Rate of medial temporal lobe atrophy in typical aging and Alzheimer's disease. *Neurology* 51, 993–999. doi: 10.1212/WNL.51.4.993

Jonides, J., Schumacher, E. H., Smith, E. E., Koeppe, R. A., Awh, E., Reuter-Lorenz, P. A., et al. (1998). The role of parietal cortex in verbal working memory. *J. Neurosci.* 18, 5026–5034. doi: 10.1523/JNEUROSCI.18-13-05026.1998

Karas, G. B., Scheltens, P., Rombouts, S. A., Visser, P. J., van Schijndel, R. A., Fox, N. C., et al. (2004). Global and local gray matter loss in mild cognitive impairment and Alzheimer's disease. *Neuroimage* 23, 708–716. doi: 10.1016/j.neuroimage.2004.07.006

Knierim, J. J. (2015). The hippocampus. *Curr. Biol.* 25, R1116–R1121. doi: 10.1016/j.cub.2015.10.049

Kontaxopoulou, D., Beratis, I. N., Fragkiadaki, S., Pavlou, D., Andronas, N., Yannis, G., et al. (2018). Exploring the profile of incidental memory in patients with amnestic mild cognitive impairment and mild Alzheimer's disease. *J. Alzheimers Dis.* 65, 617–627. doi: 10.3233/JAD-180328

Korf, E. S., Wahlund, L. O., Visser, P. J., and Scheltens, P. (2004). Medial temporal lobe atrophy on MRI predicts dementia in patients with mild cognitive impairment. *Neurology* 63, 94–100. doi: 10.1212/01.WNL.0000133114.92694.93

Laird, A. R., Eickhoff, S. B., Kurth, F., Fox, P. M., Uecker, A. M., Turner, J. A., et al. (2009). ALE meta-analysis workflows via the brainmap database: progress towards a probabilistic functional brain atlas. *Front. Neuroinform.* 3:23. doi: 10.3389/neuro.11.023.2009

Lavenu, I., Pasquier, F., Lebert, F., Petit, H., and Van der Linden, M. (1999). Perception of emotion in frontotemporal dementia and Alzheimer disease. *Alzheimer Dis. Assoc. Disord.* 13, 96–101. doi: 10.1097/00002093-199904000-00007

Lee, M., Lim, T. S., Lee, H. Y., and Moon, S. Y. (2014). Profile of memory impairment as a prognostic marker in amnestic mild cognitive impairment. *J. Neurol. Sci.* 347, 124–128. doi: 10.1016/j.jns.2014.09.031

Leung, K. K., Bartlett, J. W., Barnes, J., Manning, E. N., Ourselin, S., and Fox, N. C. (2013). Cerebral atrophy in mild cognitive impairment and Alzheimer disease: rates and acceleration. *Neurology* 80, 648–654. doi: 10.1212/WNL.0b013e318281ccd3

Li, X., and Zhang, Z. J. (2015). Neuropsychological and neuroimaging characteristics of amnestic mild cognitive impairment subtypes: a selective overview. *CNS Neurosci. Ther.* 21, 776–783. doi: 10.1111/cns.12391

Lin, X., Zhen, D., Li, H., Zhong, J., Dai, Z., Yuan, C., et al. (2020). Altered local connectivity in chronic pain: A voxel-wise meta-analysis of resting-state functional magnetic resonance imaging studies. *Medicine (Baltimore)* 99:e21378. doi: 10.1097/MD.0000000000021378

Maren, S., and Fanselow, M. S. (1995). Synaptic plasticity in the basolateral amygdala induced by hippocampal formation stimulation *in vivo*. *J. Neurosci.* 15, 7548–7564. doi: 10.1523/JNEUROSCI.15-11-07548.1995

McCade, D., Savage, G., and Naismith, S. L. (2011). Review of emotion recognition in mild cognitive impairment. *Dement. Geriatr. Cogn. Disord.* 32, 257–266. doi: 10.1159/000335009

McKhann, G., Drachman, D., Folstein, M., Katzman, R., Price, D., and Stadlan, E. M. (1984). Clinical diagnosis of Alzheimer's disease: report of the NINCDS-ADRDA Work Group under the auspices of Department of Health and Human Services Task Force on Alzheimer's Disease. *Neurology* 34, 939–944. doi: 10.1212/WNL.34.7.939

Mendez-Bertolo, C., Moratti, S., Toledano, R., Lopez-Sosa, F., Martinez-Alvarez, R., Mah, Y. H., et al. (2016). A fast pathway for fear in human amygdala. *Nat. Neurosci.* 19, 1041–1049. doi: 10.1038/nn.4324

Migo, E. M., Mitterschiffthaler, M., O., Daly, O., Dawson, G. R., Dourish, C. T., et al. (2015). Alterations in working memory networks in amnestic mild cognitive impairment. *Aging Neuropsychol. Cogn.* 22, 106–127. doi: 10.1080/13825585.2014.894958

Miller, M. I., Younes, L., Ratnanather, J. T., Brown, T., Trinh, H., Postell, E., et al. (2013). The diffeomorphometry of temporal lobe structures in preclinical Alzheimer's disease. *Neuroimage Clin.* 3, 352–360. doi: 10.1016/j.nicl.2013.09.001

Minkova, L., Habich, A., Peter, J., Kaller, C. P., Eickhoff, S. B., and Kloppel, S. (2017). Gray matter asymmetries in aging and neurodegeneration: a review and meta-analysis. *Hum. Brain Mapp.* 38, 5890–5904. doi: 10.1002/hbm.23772

Moher, D., Liberati, A., Tetzlaff, J., and Altman, D. G. (2009). Preferred reporting items for systematic reviews and meta-analyses: the PRISMA statement. *Ann. Intern. Med.* 151, 264–269. doi: 10.7326/0003-4819-151-4-200908180-00135

Muller, V. I., Cieslik, E. C., Laird, A. R., Fox, P. T., and Eickhoff, S. B. (2013). Dysregulated left inferior parietal activity in schizophrenia and depression: functional connectivity and characterization. *Front. Hum. Neurosci.* 7:268. doi: 10.3389/fnhum.2013.00268

Muller, V. I., Cieslik, E. C., Laird, A. R., Fox, P. T., Radua, J., Mataix-Cols, D., et al. (2018). Ten simple rules for neuroimaging meta-analysis. *Neurosci. Biobehav. Rev.* 84, 151–161. doi: 10.1016/j.neubiorev.2017.11.012

Nickl-Jockschat, T., Kleiman, A., Schulz, J. B., Schneider, F., Laird, A. R., Fox, P. T., et al. (2012). Neuroanatomic changes and their association with cognitive decline in mild cognitive impairment: a meta-analysis. *Brain Struct. Funct.* 217, 115–125. doi: 10.1007/s00429-011-0333-x

Pa, J., Boxer, A., Chao, L. L., Gazzaley, A., Freeman, K., Kramer, J., et al. (2009). Clinical-neuroimaging characteristics of dysexecutive mild cognitive impairment. *Ann. Neurol.* 65, 414–423. doi: 10.1002/ana.21591

Pape, H. C., and Pare, D. (2010). Plastic synaptic networks of the amygdala for the acquisition, expression, and extinction of conditioned fear. *Physiol. Rev.* 90, 419–463. doi: 10.1152/physrev.00037.2009

Petersen, R. C. (2004). Mild cognitive impairment as a diagnostic entity. *J. Intern. Med.* 256, 183–194. doi: 10.1111/j.1365-2796.2004.01388.x

Petersen, R. C., Doody, R., Kurz, A., Mohs, R. C., Morris, J. C., Rabins, P. V., et al. (2001b). Current concepts in mild cognitive impairment. *Arch. Neurol.* 58, 1985–1992. doi: 10.1001/archneur.58.12.1985

Petersen, R. C., Stevens, J. C., Ganguli, M., Tangalos, E. G., Cummings, J. L., and DeKosky, S. T. (2001a). Practice parameter: early detection of dementia: mild cognitive impairment (an evidence-based review). Report of the Quality Standards Subcommittee of the American Academy of Neurology. *Neurology* 56, 1133–1142. doi: 10.1212/WNL.56.9.1133

Prince, S. E., Daselaar, S. M., and Cabeza, R. (2005). Neural correlates of relational memory: successful encoding and retrieval of semantic and perceptual associations. *J. Neurosci.* 25, 1203–1210. doi: 10.1523/JNEUROSCI.2540-04.2005

Prince, S. E., Tsukiura, T., and Cabeza, R. (2007). Distinguishing the neural correlates of episodic memory encoding and semantic memory retrieval. *Psychol. Sci.* 18, 144–151. doi: 10.1111/j.1467-9280.2007.01864.x

Radua, J., and Mataix-Cols, D. (2009). Voxel-wise meta-analysis of grey matter changes in obsessive-compulsive disorder. *Br. J. Psychiatry* 195, 393–402. doi: 10.1192/bjp.bp.108.055046

Radua, J., Mataix-Cols, D., Phillips, M. L., El-Hage, W., Kronhaus, D. M., Cardoner, N., et al. (2012). A new meta-analytic method for neuroimaging studies that combines reported peak coordinates and statistical parametric maps. *Eur. Psychiatry.* 27, 605–611. doi: 10.1016/j.eurpsy.2011.04.001

Radua, J., Rubia, K., Canales-Rodriguez, E. J., Pomarol-Clotet, E., Fusar-Poli, P., and Mataix-Cols, D. (2014). Anisotropic kernels for coordinate-based meta-analyses of neuroimaging studies. *Front. Psychiatry* 5:13. doi: 10.3389/fpsyt.2014.00013

Radua, J., Schmidt, A., Borgwardt, S., Heinz, A., Schlagenhauf, F., McGuire, P., et al. (2015). Ventral striatal activation during reward processing in psychosis: a neurofunctional meta-analysis. *JAMA Psychiat.* 72, 1243–1251. doi: 10.1001/jamapsychiatry.2015.2196

Rami, L., Gómez-Anson, B., Monte, G. C., Bosch, B., Sánchez-Valle, R., and Molinuevo, J. L. (2009). Voxel based morphometry features and follow-up of amnestic patients at high risk for Alzheimer's disease conversion. *Int. J. Geriatr. Psych.* 24, 875–884. doi: 10.1002/gps.2216

Ranganath, C., and Ritchey, M. (2012). Two cortical systems for memory-guided behaviour. *Nat. Rev. Neurosci.* 13, 713–726. doi: 10.1038/nrn3338

Remondes, M., and Schuman, E. M. (2004). Role for a cortical input to hippocampal area CA1 in the consolidation of a long-term memory. *Nature* 431, 699–703. doi: 10.1038/nature02965

Richard-Mornas, A., Borg, C., Klein-Koerkamp, Y., Paignon, A., Hot, P., and Thomas-Anterion, C. (2012). Perceived eye region and the processing of fearful expressions in mild cognitive impairment patients. *Dement. Geriatr. Cogn. Disord.* 33, 43–49. doi: 10.1159/000336599

Roozendaal, B., McEwen, B. S., and Chattarji, S. (2009). Stress, memory, and the amygdala. *Nat. Rev. Neurosci.* 10, 423–433. doi: 10.1038/nrn2651

Salimi-Khorshidi, G., Smith, S. M., Keltner, J. R., Wager, T. D., and Nichols, T. E. (2009). Meta-analysis of neuroimaging data: a comparison of image-based and coordinate-based pooling of studies. *Neuroimage* 45, 810–823. doi: 10.1016/j.neuroimage.2008.12.039

Saykin, A. J., Wishart, H. A., Rabin, L. A., Santulli, R. B., Flashman, L. A., West, J. D., et al. (2006). Older adults with cognitive complaints show brain atrophy similar to that of amnestic MCI. *Neurology* 67, 834–842. doi: 10.1212/01.wnl.0000234032.77541.a2

Scheltens, P., Leys, D., Barkhof, F., Huglo, D., Weinstein, H. C., Vermersch, P., et al. (1992). Atrophy of medial temporal lobes on MRI in "probable" Alzheimer's disease and normal ageing: diagnostic value and neuropsychological correlates. *J. Neurol. Neurosurg. Psychiatry* 55, 967–972. doi: 10.1136/jnnp.55.10.967

Schroeter, M. L., Stein, T., Maslowski, N., and Neumann, J. (2009). Neural correlates of Alzheimer's disease and mild cognitive impairment: a systematic and quantitative meta-analysis involving 1351 patients. *Neuroimage* 47, 1196–1206. doi: 10.1016/j.neuroimage.2009.05.037

Schwindt, G. C., and Black, S. E. (2009). Functional imaging studies of episodic memory in Alzheimer's disease: a quantitative meta-analysis. *Neuroimage* 45, 181–190. doi: 10.1016/j.neuroimage.2008.11.024

Serra, L., Giulietti, G., Cercignani, M., Spano, B., Torso, M., Castelli, D., et al. (2013). Mild cognitive impairment: same identity for different entities. *J. Alzheimers Dis.* 33, 1157–1165. doi: 10.3233/JAD-2012-121663

Sheelakumari, R., Kesavadas, C., Lekha, V. S., Justus, S., Sarma, P. S., and Menon, R. (2018). Structural correlates of mild cognitive impairment: a clinicovolumetric study. *Neurol. India* 66, 370–376. doi: 10.4103/0028-3886.227298

Sheng, L., Zhao, P., Ma, H., Qi, L., Yi, Z., Shi, Y., et al. (2020b). Gray matter alterations in restless legs syndrome: a coordinate-based meta-analysis. *Medicine (Baltimore)* 99:e21374. doi: 10.1097/MD.0000000000021374

Sheng, L., Zhao, P., Ma, H., Radua, J., Yi, Z., Shi, Y., et al. (2020a). Cortical thickness in Parkinson disease: a coordinate-based meta-analysis. *Medicine (Baltimore)* 99:e21403. doi: 10.1097/MD.0000000000021403

Shi, F., Liu, B., Zhou, Y., Yu, C., and Jiang, T. (2009). Hippocampal volume and asymmetry in mild cognitive impairment and Alzheimer's disease: meta-analyses of MRI studies. *Hippocampus* 19, 1055–1064. doi: 10.1002/hipo.20573

Shiino, A., Watanabe, T., Maeda, K., Kotani, E., Akiguchi, I., and Matsuda, M. (2006). Four subgroups of Alzheimer's disease based on patterns of atrophy using VBM and a unique pattern for early onset disease. *Neuroimage* 33, 17–26. doi: 10.1016/j.neuroimage.2006.06.010

Sotres-Bayon, F., Sierra-Mercado, D., Pardilla-Delgado, E., and Quirk, G. J. (2012). Gating of fear in prelimbic cortex by hippocampal and amygdala inputs. *Neuron* 76, 804–812. doi: 10.1016/j.neuron.2012.09.028

Tabatabaei-Jafari, H., Shaw, M. E., and Cherbuin, N. (2015). Cerebral atrophy in mild cognitive impairment: a systematic review with meta-analysis. *Alzheimers Dement.* 1, 487–504. doi: 10.1016/j.dadm.2015.11.002

Tahmasian, M., Sepehry, A. A., Samea, F., Khodadadifar, T., Soltaninejad, Z., Javaheripour, N., et al. (2019). Practical recommendations to conduct a neuroimaging meta-analysis for neuropsychiatric disorders. *Hum. Brain Mapp.* 40, 5142–5154. doi: 10.1002/hbm.24746

Tench, C. R., Tanasescu, R., Auer, D. P., Cottam, W. J., and Constantinescu, C. S. (2014). Coordinate based meta-analysis of functional neuroimaging data using activation likelihood estimation; full width half max and group comparisons. *PLoS ONE* 9:e106735. doi: 10.1371/journal.pone.0106735

Thakral, P. P., Madore, K. P., and Schacter, D. L. (2017). A role for the left angular gyrus in episodic simulation and memory. *J. Neurosci.* 37, 8142–8149. doi: 10.1523/JNEUROSCI.1319-17.2017

Threlkeld, Z. D., Jicha, G. A., Smith, C. D., and Gold, B. T. (2011). Task deactivation reductions and atrophy within parietal default mode regions are overlapping but only weakly correlated in mild cognitive impairment. *J. Alzheimers Dis.* 27, 415–427. doi: 10.3233/JAD-2011-110206

Trivedi, M. A., Wichmann, A. K., Torgerson, B. M., Ward, M. A., Schmitz, T. W., Ries, M. L., et al. (2006). Structural MRI discriminates individuals with Mild Cognitive Impairment from age-matched controls: a combined neuropsychological and voxel based morphometry study. *Alzheimers Dement.* 2:Z200606001. doi: 10.1016/j.jalz.2006.06.001

Turner, J. A., and Laird, A. R. (2012). The cognitive paradigm ontology: design and application. *Neuroinformatics* 10, 57–66. doi: 10.1007/s12021-011-9126-x

van de Pol, L. A., Barnes, J., Scahill, R. I., Frost, C., Lewis, E. B., Boyes, R. G., et al. (2007). Improved reliability of hippocampal atrophy rate measurement in mild cognitive impairment using fluid registration. *Neuroimage* 34, 1036–1041. doi: 10.1016/j.neuroimage.2006.10.033

Varjassyova, A., Horinek, D., Andel, R., Amlerova, J., Laczo, J., Sheardova, K., et al. (2013). Recognition of facial emotional expression in amnestic mild cognitive impairment. *J. Alzheimers Dis.* 33, 273–280. doi: 10.3233/JAD-2012-120148

Venneri, A., Gorgoglione, G., Toraci, C., Nocetti, L., Panzetti, P., and Nichelli, P. (2011). Combining neuropsychological and structural neuroimaging indicators of conversion to Alzheimer's disease in amnestic mild cognitive impairment. *Curr. Alzheimer Res.* 8, 789–797. doi: 10.2174/15672051179763160

Wagner, A. D., Pare-Blagoev, E. J., Clark, J., and Poldrack, R. A. (2001). Recovering meaning: left prefrontal cortex guides controlled semantic retrieval. *Neuron* 31, 329–338. doi: 10.1016/S0896-6273(01)00359-2

Wang, H. Z., Wang, W. H., Shi, H. C., and Yuan, C. H. (2020). Is there a reliable brain morphological signature for migraine? *J. Headache Pain* 21:89. doi: 10.1186/s10194-020-01158-7

Wang, P., Chou, K., Lirng, J., Lin, K., Chen, W., and Lin, C. (2012). Multiple diffusivities define white matter degeneration in amnestic mild cognitive impairment and Alzheimer's disease. *J. Alzheimers Dis.* 30, 423–437. doi: 10.3233/JAD-2012-111304

Weiner, M. W., Veitch, D. P., Aisen, P. S., Beckett, L. A., Cairns, N. J., Green, R. C., et al. (2013). The Alzheimer's disease neuroimaging initiative: a review of papers published since its inception. *Alzheimers Dement.* 9, e111–e194. doi: 10.1016/j.jalz.2013.05.1769

Whitwell, J. L., Przybelski, S. A., Weigand, S. D., Knopman, D. S., Boeve, B. F., Petersen, R. C., et al. (2007). 3D maps from multiple MRI illustrate changing atrophy patterns as subjects progress from mild cognitive impairment to Alzheimer's disease. *Brain* 130, 1777–1786. doi: 10.1093/brain/awm112

Winblad, B., Palmer, K., Kivipelto, M., Jelic, V., Fratiglioni, L., Wahlund, L. O., et al. (2004). Mild cognitive impairment—beyond controversies, towards a consensus: report of the International Working Group on Mild Cognitive Impairment. *J. Intern. Med.* 256, 240–246. doi: 10.1111/j.1365-2796.2004.01380.x

Wolz, R., Heckemann, R. A., Aljabar, P., Hajnal, J. V., Hammers, A., Lotjonen, J., et al. (2010). Measurement of hippocampal atrophy using 4D graph-cut segmentation: application to ADNI. *Neuroimage* 52, 109–118. doi: 10.1016/j.neuroimage.2010.04.006

Xie, C., Bai, F., Yuan, B., Yu, H., Shi, Y., Yuan, Y., et al. (2015). Joint effects of gray matter atrophy and altered functional connectivity on cognitive deficits in amnestic mild cognitive impairment patients. *Psychol. Med.* 45, 1799–1810. doi: 10.1017/S0033291714002876

Xie, C., Li, W., Chen, G., Douglas Ward, B., Franczak, M. B., Jones, J. L., et al. (2012). The co-existence of geriatric depression and amnestic mild cognitive impairment detrimentally affect gray matter volumes: Voxel-based morphometry study. *Behav. Brain Res.* 235, 244–250. doi: 10.1016/j.bbr.2012.08.007

Yang, J., Pan, P., Song, W., Huang, R., Li, J., Chen, K., et al. (2012). Voxelwise meta-analysis of gray matter anomalies in Alzheimer's disease and mild cognitive impairment using anatomic likelihood estimation. *J. Neurol. Sci.* 316, 21–29. doi: 10.1016/j.jns.2012.02.010

Yu, J., Lam, C., and Lee, T. (2017). White matter microstructural abnormalities in amnestic mild cognitive impairment: a meta-analysis of whole-brain and ROI-based studies. *Neurosci. Biobehav. Rev.* 83, 405–416. doi: 10.1016/j.neubiorev.2017.10.026

Zhang, H., Sachdev, P. S., Wen, W., Kochan, N. A., Crawford, J. D., Brodaty, H., et al. (2012). Gray matter atrophy patterns of mild cognitive impairment subtypes. *J. Neurol. Sci.* 315, 26–32. doi: 10.1016/j.jns.2011.12.011

Zhao, Z., Fan, F., Lu, J., Li, H., Jia, L., Han, Y., et al. (2015). Changes of gray matter volume and amplitude of low-frequency oscillations in amnestic MCI: an integrative multi-modal MRI study. *Acta Radiol.* 56, 614–621. doi: 10.1177/0284185114533329

Zhao, Z., Lu, J., Jia, X., Chao, W., Han, Y., Jia, J., et al. (2014). Selective changes of resting-state brain oscillations in aMCI: an fMRI study using ALFF. *Biomed. Res. Int.* 2014:920902. doi: 10.1155/2014/920902

Conflict of Interest: The authors declare that the research was conducted in the absence of any commercial or financial relationships that could be construed as a potential conflict of interest.

frontiers in Aging Neuroscience

BRIEF RESEARCH REPORT
published: 01 April 2021
doi: 10.3389/fnagi.2021.659618

Event-Related Potential Measures of the Passive Processing of Rapidly and Slowly Presented Auditory Stimuli in MCI

Farooq Kamal[1,2], *Cassandra Morrison*[1,2], *Kenneth Campbell*[1] *and Vanessa Taler*[1,2]*

[1]School of Psychology, University of Ottawa, Ontario, ON, Canada, [2]Bruyère Research Institute, Ottawa, ON, Canada

Much research effort is currently devoted to the development of a simple, low-cost method to determine early signs of Alzheimer's disease (AD) pathology. The present study employs a simple paradigm in which event-related potentials (ERPs) were recorded to a single auditory stimulus that was presented rapidly or very slowly while the participant was engaged in a visual task. A multi-channel EEG was recorded in 20 healthy older adults and 20 people with mild cognitive impairment (MCI). In two different conditions, a single 80 dB sound pressure level (SPL) auditory stimulus was presented every 1.5 s (fast condition) or every 12.0 s (slow condition). Participants were instructed to watch a silent video and ignore the auditory stimuli. Auditory processing thus occurred passively. When the auditory stimuli were presented rapidly (every 1.5 s), N1 and P2 amplitudes did not differ between the two groups. When the stimuli were presented very slowly, the amplitude of N1 and P2 increased in both groups and their latencies were prolonged. The amplitude of N1 did not significantly differ between the two groups. However, the subsequent positivity was reduced in people with MCI compared to healthy older adults. This late positivity in the slow condition may reflect a delayed P2 or a summation of a composite P2 + P3a. In people with MCI, the priority of processing may not be switched from the visual task to the potentially much more relevant auditory input. ERPs offer promise as a means to identify the pathology underlying cognitive impairment associated with MCI.

Keywords: mild cognitive impairment, MCI, event-related potentials, ERPs, biomarker

OPEN ACCESS

Edited by:
Rong Chen,
University of Maryland, Baltimore, United States

Reviewed by:
Hanjun Liu,
Sun Yat-Sen University, China
Alexandra Key,
Vanderbilt University Medical Center, United States

***Correspondence:**
Vanessa Taler
vtaler@uottawa.ca

Received: *27 January 2021*
Accepted: *12 March 2021*
Published: *01 April 2021*

Citation:
Kamal F, Morrison C, Campbell K and Taler V (2021) Event-Related Potential Measures of the Passive Processing of Rapidly and Slowly Presented Auditory Stimuli in MCI. Front. Aging Neurosci. 13:659618. doi: 10.3389/fnagi.2021.659618

INTRODUCTION

Mild cognitive impairment (MCI) is a condition in which individuals demonstrate cognitive impairment with no impairments in social or occupational function. MCI may represent a transitional stage between healthy aging and Alzheimer's disease (AD) with 20–40% of people with MCI progressing to dementia (Roberts and Knopman, 2013). The early identification of MCI and prediction of decline associated with progression to AD has been the subject of intense research (Sperling et al., 2011). Much of this research is devoted to the development of a simple, low-cost, and readily available biomarker to determine the early signs of neuropathology underlying AD.

Neuropsychological tests are often used to diagnose AD. Performance on almost all neuropsychological and cognitive tasks will inevitably be affected by the participant's ability and willingness to maintain attention (Sturm et al., 1999; Buschman and Miller, 2010; Oberauer, 2019). Attentional control and the maintenance of attention may be a challenge for older adults, and particularly for people with MCI (Saunders and Summers, 2010). A good deal of early processing of sensory input is said to be automatic; that is, it is completed whether or not the participant attends to the sensory channel. Determining the extent of processing of unattended input is methodologically difficult. The processing of unattended input can be measured by event-related potentials (ERPs), the changes in the electrical activity of the brain elicited by an external stimulus or internal psychological event. ERPs consist of a series of negative- and positive-going components, thought to reflect different aspects of information processing. Some of these ERP components are elicited independently of attention.

All auditory stimuli elicit an obligatory negative component, the N1, occurring around 100 ms post-stimulus, followed by a later positivity, the P2, occurring around 180 ms. In the classic Näätänen (1990) model of auditory processing, a transient detector system detects abrupt onsets and offsets of auditory stimuli. The output of this system, reflected by the amplitude of N1, varies directly with the rate of stimulus presentation and the energy (intensity) of the stimulus, thus defining its salience. N1 and the P2 will therefore be larger for higher intensity auditory stimuli and stimuli presented slowly. Critically, it has long been known that attention to the auditory channel has relatively little effect on N1 and P2 (Picton and Hillyard, 1974), especially when stimuli are presented slower than every 1 s (Schwent et al., 1976; Hansen and Hillyard, 1988; Woldorff, 1995).

In the Näätänen (1990) model, sufficiently high activation of the transient detector system will result in an interrupt signal being sent to the frontoparietal network controlling processing priorities (Goulden et al., 2014). Attention may then be switched from the ongoing cognitive activities to the processing of the highly salient stimulus event. A later positivity, the P3a, peaking between 200 and 300 ms, is thought to reflect processes associated with the switching of attention (Escera et al., 1998; Masson and Bidet-Caulet, 2019).

The P3a is often elicited in oddball paradigms by a deviant representing a large change from the frequently occurring standard stimulus. There is evidence that a P3a can also be elicited by a single, rarely presented stimulus. When the rate of stimulus presentation is very slow (> than every 10 s), N1 and P2 become very large and their peak latencies are delayed by about 20–30 ms (Alcaini et al., 1994; Budd et al., 1998; Muller-Gass et al., 2008; Pereira et al., 2014). Berti (2013) questioned whether this P2 might be better described as a P3a. The Berti study required subjects to decide on a visual stimulus. On 13% of trials, the visual stimulus was preceded by an irrelevant auditory stimulus. Performance on the visual task subsequently deteriorated, compared to trials in which no auditory stimulus preceded the visual stimulus. This suggested that attention had been switched from the processing of the visual task to the processing of the auditory stimulus. Such processing is associated with the P3a rather than the P2. In the present study, we describe the positivity following the very slow presentation of the stimulus as a composite P2/P3a. Rinne et al. (2006) and Muller-Gass et al. (2007) employed oddball paradigms in which the rare deviant was created by either decreasing or increasing the intensity of the standard. Only the intensity increase elicited a large P3a, presumably because it resulted in large output from the transient detector system. In this regard, Cecchi et al. (2015) employed an oddball paradigm with a white noise burst deviant. The intensity of white noise at times increases and as such will be detected by the transient detector system. A P3a was elicited by the noise burst in healthy older adults but was reduced in amplitude in people with MCI.

There is disagreement about how the N1 and P2 change with aging. In most studies, stimuli are presented relatively rapidly, every 1–3 s. Many of these studies have failed to find N1 or P2 differences between younger and older adults, while some have reported larger responses for younger adults and others have reported larger responses for older adults (Pfefferbaum et al., 1980; Cranford and Martin, 1991; Bertoli et al., 2005; Harkrider et al., 2005; Čeponiene et al., 2008; McCullagh and Shinn, 2013; Stothart and Kazanina, 2016; Kamal et al., 2021). Stimulus features and experimental parameters differ widely across studies, making comparison difficult. In general, even when differences between younger and older participants are observed, they tend to be small. More consistent results have been observed when stimuli are presented very slowly. Berti et al. (2017) and Kamal et al. (2021) varied the rate of stimulus presentation of the to-be-ignored auditory stimuli. When the auditory stimuli were presented very slowly (every 10 and 12 s respectively), the amplitude of both N1 and P2/P3a was much reduced in the older compared to younger adults.

A limited number of studies have examined the N1 and P2 in people with MCI (for a review see Morrison et al., 2018). When the stimuli are presented relatively rapidly, most studies have not found N1 and P2 differences between healthy older adults and people with MCI (Golob et al., 2002; Lai et al., 2010; Lister et al., 2016; Bidelman et al., 2017; Buján et al., 2019). Some studies have reported a somewhat larger N1 or a reduced P2 in people with MCI, at least in certain conditions (Irimajiri et al., 2005; Golob et al., 2007; Lister et al., 2016; Buján et al., 2019). While some of these differences have been attributed to the severity of MCI, experimental parameters again tend to vary widely across studies.

The effects of very slowly presented stimuli have yet to be examined in people with MCI. The large age-related changes in N1 and P2/P3a elicited by auditory stimuli presented very slowly offer much promise for early identification of MCI. The paradigm used by Kamal et al. (2021) has many advantages. Testing can be completed within 15 minutes. Moreover, the participant does not need to attend to the auditory stimuli; the ERPs are elicited passively, independent of attention. In the present study, participants were asked to ignore the auditory stimuli while engaged in a visual task. We compared the passive processing of the auditory stimuli in people with MCI and cognitively healthy older adults. The auditory

stimuli were presented rapidly and very slowly in separate conditions. Berti et al. (2017) and Kamal et al. (2021) observed large N1 and P2/P3a differences between younger and older adults only when stimuli were presented very slowly. It was therefore expected that with the additional decline observed in people with MCI compared to healthy older adults, ERP amplitude differences would also only be observed in the slow condition.

MATERIALS AND METHODS

Participants

Forty-one participants took part in this study. One participant was excluded from the analysis because of noisy EEG data (see "EEG Data Recording" section). A total of 40 participants' data were therefore analyzed: 20 cognitively healthy older adults (12 females; age range = 67–81 years; M = 72.4 years) and 20 people with MCI (10 females; age range = 68–84 years; M = 74.2 years). Older adults were recruited through word-of-mouth and announcements displayed at community centers. Participants with MCI were recruited from the Bruyère Memory Program. They were diagnosed with MCI based on the clinical history and a neurological exam by a physician with expertise in neurodegenerative conditions. They underwent a CT scan and blood work to rule out reversible causes of cognitive impairment. Participants were not included if their cognitive decline was thought to be related to other comorbidities.

The Montreal Cognitive Assessment (MoCA) was used to screen for cognitive decline (Nasreddine et al., 2005). The cutoff for the MoCA in cognitively healthy older adults was 24. Healthy older adults scored significantly higher ($p < 0.001$) on the MoCA (M = 27.05, SD = 1.46) than people with MCI (M = 22.79, SD = 3.24). Participants also completed a one-hour neuropsychological battery to assess general cognitive functioning (see **Supplementary Table 1**). The healthy older adults also participated in the Kamal et al. (2021) study. All participants reported no history of neurological or psychiatric conditions. All participants reported normal hearing but also completed pure tone audiometric testing for 500, 1,000, and 2,000 Hz frequencies.

This study was approved by the University of Ottawa and Bruyère Research Institute ethics boards. Participants provided informed written consent before starting the study and an honorarium was given as compensation.

Stimuli and Procedure

Participants were seated in a sound-attenuated testing room. A single 80 dB SPL (sound pressure level) 1,000 Hz pure tone auditory stimulus, having a total duration of 55 ms (5 ms rise/fall time) was presented binaurally through Sony MDR-V6 headphones. The stimuli were presented every 1.5 s in a fast condition and every 12.0 s in a slow condition. A total of 400 and 50 stimuli were presented in the fast and slow conditions, respectively. Each condition lasted 10 min. The order of the two conditions was randomized across participants. The auditory conditions were presented a second time in reverse order. A total of 100 and 800 stimuli were therefore presented in the slow and fast conditions, respectively. The repetition of stimulus presentations served to reduce the amplitude of the random background noise in the EEG.

Participants were instructed to watch a silent, subtitled video and to ignore the presentation of the irrelevant auditory stimuli. Processing of the auditory stimuli thus occurred passively.

EEG Data Recording

Continuous EEG activity was recorded from 31 active silver-silver chloride electrodes, attached to an electrode cap placed according to the international 10-10 system. An EOG electrode was placed on the infraorbital ridge of the left eye to monitor vertical eye movements and blinks. An electrode placed on the tip of the nose served as a reference for all channels. An advantage of active electrodes is that impedance can be relatively high (Kappenman and Luck, 2010). Inter-electrode impedance was kept below 20 kΩ. The impedance at F3, Fz, F4, and C3, Cz, C4, which comprised regions of interest (ROIs), was below 10 kΩ. The EEG and EOG signals were sampled at a rate of 500 Hz.

The EEG was then visually examined to remove channels containing high levels of noise. These channels were substituted by interpolating the data of the surrounding electrode sites (Perrin et al., 1989). Interpolation was not applied to any of the ROI sites. The data of one participant were removed from further analysis because more than four channels with excessive noise were rejected. A 0.5 Hz high-pass and a 20 Hz low-pass digital filter (24 dB/octave roll-off) were then applied to the data.

Eye movement and blink artifacts occurring independently of EEG activity were identified and corrected using Independent Component Analysis (ICA; Makeig et al., 1996). To do so required computation of vertical and horizontal EOG activity. A vertical EOG was computed by subtracting FP1 from the inferior orbital activity. Horizontal eye movements were computed by subtracting the FT9 and FT10 activity. The EEG was subsequently reconstructed into single 700 ms epochs starting 100 ms before stimulus onset. The average of all activity in the pre-stimulus period served as a zero-voltage baseline. Drifts in post-stimulus voltage from this baseline were then corrected for each epoch. Epochs containing EEG activity exceeding ±100 μV were subsequently rejected from the averaging. In the fast condition, fewer than 1% of trials were rejected for healthy older adults, while fewer than 3% were rejected for people with MCI (p = 0.20). In the slow condition, fewer than 2% of trials were rejected for either group.

ERP Quantification

The amplitude of N1 and P2/P3a was quantified as the mean of all data points within ± 25 ms of their peak amplitude identified in the grand average of each group. In both groups, N1 peaked at 95 ms in the fast condition and 115 ms in the slow condition. The subsequent P2/P3a positivity peaked at 205 ms in the fast condition and 230 ms in the slow condition.

N1 and P2/P3a were quantified at frontal (F3, Fz, F4) and central (C3, Cz, C4) ROIs, where they are largest. Separate 2-way ANOVAs were initially run at these ROIs for both the N1 and

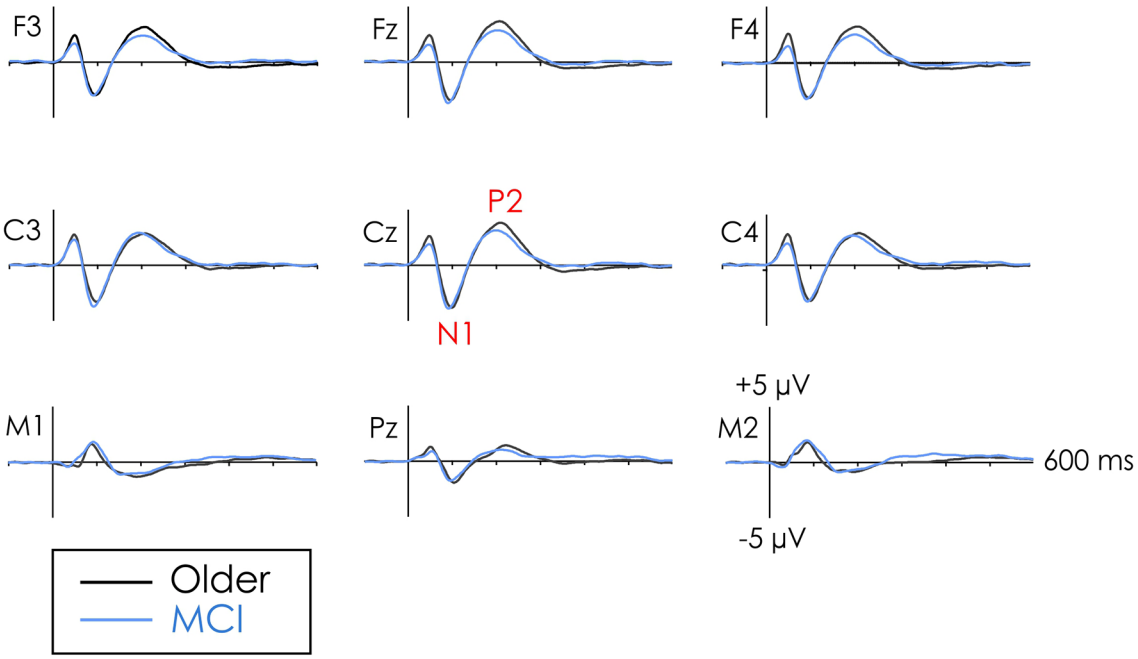

FIGURE 1 | Grand averaged event-related potentials (ERPs) from healthy older adults and people with mild cognitive impairment (MCI) in the fast rate of presentation condition. N1 and P2 amplitude did not differ between the two groups.

P2/P3a with a single between-subjects factor, Group (Older, MCI), and a single within-subjects factor, Rate of Presentation (Fast, Slow). The results were quite similar at both electrode sites. For this reason, the data were collapsed across ROIs. A 3-way ANOVA was then run with the between-subjects factor, Group (Older, MCI), and two within-subjects factors, Rate (Fast, Slow) and ROI (Frontal, Central). Previous research has shown large ERP differences between younger and older participants but only when stimuli were presented very slowly. We, therefore, expected to observe differences between MCI and healthy older adults only in this condition. For this reason, planned comparisons were run on interactions involving Group and Rate of Presentation.

RESULTS

Figures 1, **2** illustrate the multi-channel ERPs for both groups in the fast and slow conditions, respectively. As may be observed, a robust negative peak, N1, occurring at about 100 ms was elicited in both conditions followed by a later positivity, P2/P3a, occurring at about 200 in the fast condition and 230 ms in the slow condition.

N1

A main effect of Rate of Presentation was observed for the amplitude of N1, $F_{(1,38)} = 29.05$, $p < 0.001$, $\eta_p^2 = 0.43$. N1 was larger in the slow than in the fast condition. Overall Group differences were not significant ($F < 1$) and interactions involving Group were not significant ($F < 1$). Thus, regardless of the rate of presentation, the amplitude of N1 did not significantly differ between groups at either frontal or central ROIs.

Figure 3A presents the grand averaged ERPs at Cz including SDs around the average. A pirate plot illustrating both descriptive and inferential statistics (Phillips, 2017) of the N1 data is presented in **Figure 3B**. As may be observed, the confidence intervals (CIs) for N1 were very similar for both groups. There was considerable overlap between healthy older adults and people with MCI in both the fast and slow conditions.

P2/P3a

An overall significant main effect of the Rate of the presentation was also observed for P2/P3a. P2/P3a was larger in the slow than the fast condition, $F_{(1,38)} = 28.30$, $p < 0.001$, $\eta_p^2 = 0.43$. The Group × Rate interaction was not significant $F_{(1,38)} = 2.53$, $p = 0.12$, $\eta_p^2 = 0.06$. The trend of the interactions was, however, in keeping with *a priori* predictions. Follow-up Fisher's Least Square Significance procedures revealed the source of the interactions. Group differences were not significant in the fast condition ($p < 0.20$). However, in the slow condition, P2 was significantly larger for healthy older adults than for people with MCI ($p < 0.03$). The Group × Condition × ROI interaction was not significant, $F < 1$.

A pirate plot of the P2/P3a at the central ROI is presented in **Figure 3C**. The mean amplitude of the P2/P3a was larger for the older than the MCI group, but only in the slow condition. There

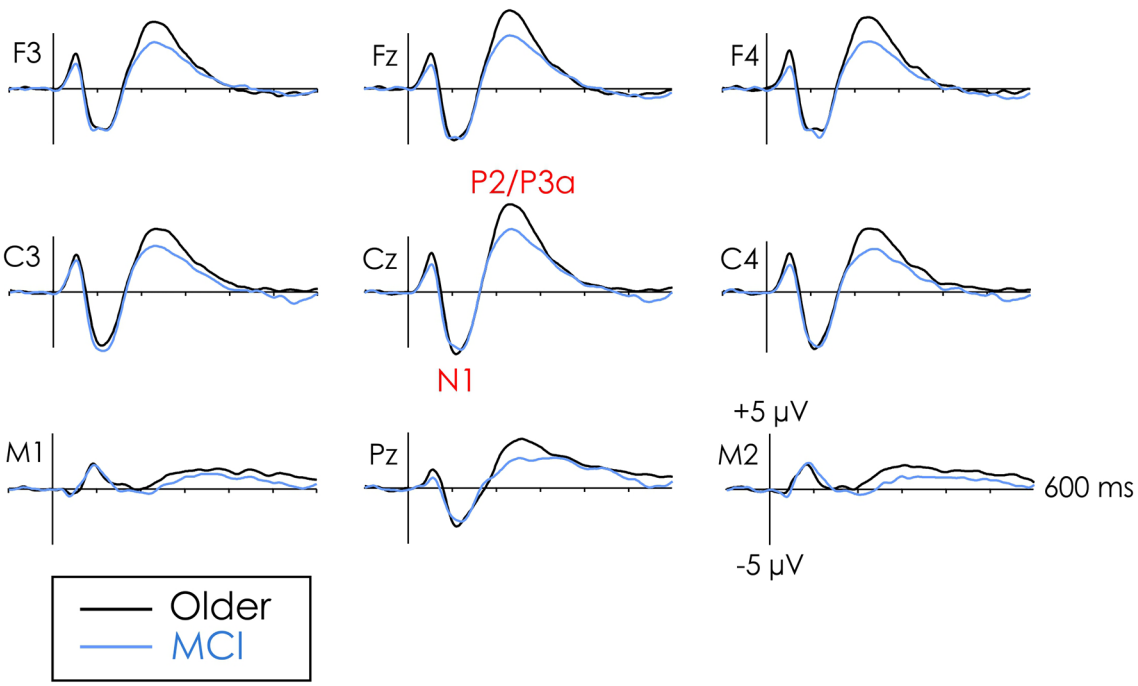

FIGURE 2 | Grand averaged ERPs from healthy older adults and people with MCI in the slow rate of presentation condition. The amplitude of N1 did not differ between the groups. The amplitude of P2 was larger for healthy older adults than people with MCI at both the frontal and central regions of interest (ROIs).

was, however, considerable overlap in individual participants' amplitudes within the two groups.

Changes Across Quarters

A reduced P2/P3a was observed in people with MCI in slow condition (see **Figure 4**). Possibly, their ERPs varied over time, while being more consistent for healthy older adults. The data were separated into four equal quarters to explore changes over time. The first trial was excluded from this analysis because it marked the initiation of a new condition. Thus, for the slow condition trials 2–13, 14–25, 26–37, and 38–49 were averaged separately. The main effect of the Quarter was not significant ($F < 1$). Importantly, the Group x Quarter interaction was also not significant ($F < 1$).

Correlations

Correlations were also computed between the P2/P3a amplitude and the MoCA scores within the MCI group. In the fast condition, no significant correlations were found $r = 0.24$, $p = 0.22$ at Fz, and $r = 0.32$, $p = 0.22$ at Cz. In the slow condition, the correlations were also not significant, $r = 0.32$, $p = 0.19$ at Fz, and $r = 0.40$, $p = 0.09$ at Cz.

Scalp Distribution

N1 and P2/P3a were both large over fronto-central areas of the scalp. Interactions involving Site and Group and Site and Rate were not significant for either N1 or P2/P3a ($F < 1$ in all comparisons). Spline-interpolated scalp distribution maps of N1 are illustrated in the **Supplementary Figure 1**.

DISCUSSION

The auditory stimulus in both the fast and slow conditions elicited a robust N1 and P2/P3a. In both healthy older adults and people with MCI, the amplitude of N1 and P2/P3a increased and their latencies were prolonged when the stimuli were presented very slowly. This finding replicates several other studies in younger adults (Alcaini et al., 1994; Budd et al., 1998; Muller-Gass et al., 2008; Pereira et al., 2014). There is evidence that the sources of the auditory N1 differ depending on the rate of stimulus presentation. When stimuli are presented relatively rapidly, the sources have been identified to be in and around the auditory cortex. When stimuli are presented very slowly, the large increase in the amplitude of the N1 and P2/P3a, and their prolonged latencies has been explained by activation of additional widespread sources, particularly in the frontal lobes (Sams et al., 1993; Alcaini et al., 1994; Giard et al., 1994; McEvoy et al., 1997). Many imaging studies have noted a deterioration and loss of function in the frontal regions with age and in early dementia (Driscoll et al., 2009; Machulda et al., 2009; Madden et al., 2012; Salami et al., 2012).

It was expected that differences between healthy older adults and people with MCI would be largest when stimuli were presented very slowly, and smallest when stimuli were presented

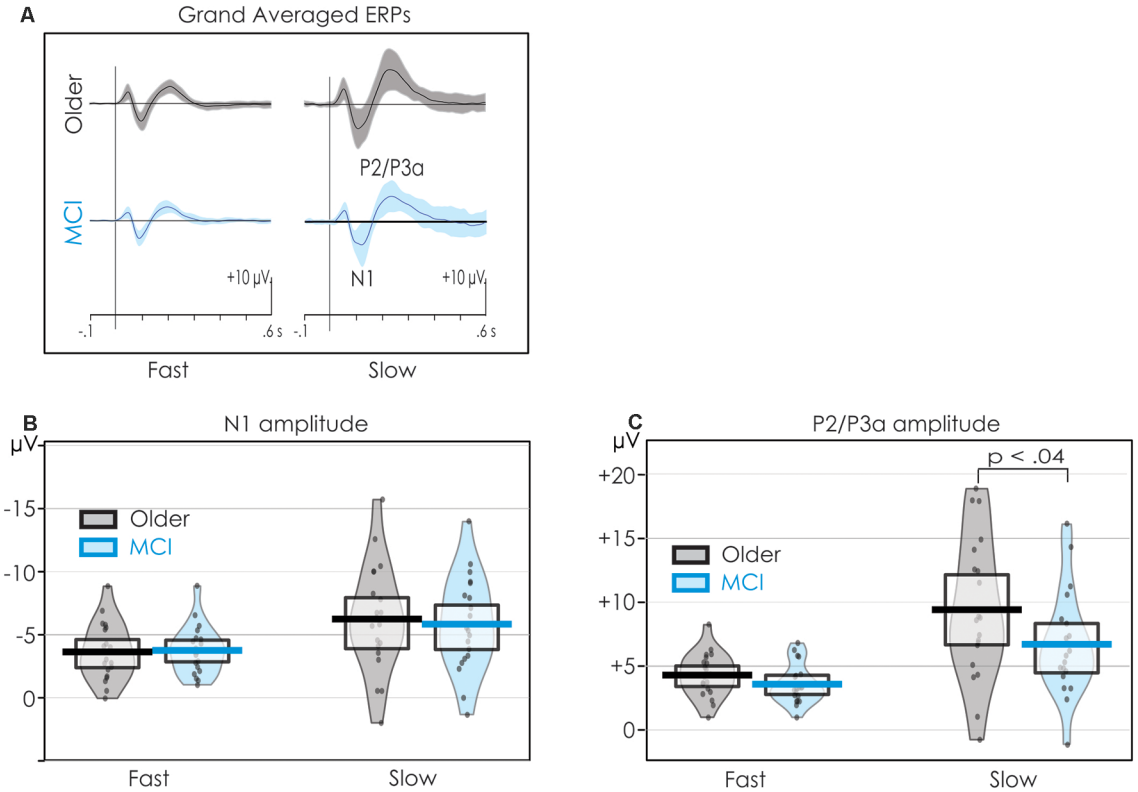

FIGURE 3 | Pirateplots of N1 and P2 data providing both descriptive and inferential statistics. Data are collapsed across all central electrode (C3, Cz, C4) sites. The grand averages and SDs (shaded) are illustrated in panel **(A)**. The mean amplitudes of N1 and P2 (thick, solid horizontal line), 95% confidence intervals (CIs; light horizontal box), smooth frequency distribution (shaded area), and individual data points (jittered) are presented in panels **(B,C)** respectively. The mean amplitude of N1 did not differ between the groups in the fast condition. On the other hand, P2 was larger for the healthy older adults when stimuli were presented slowly.

rapidly. The finding that the N1 and P2 amplitudes did not differ between the two groups in the fast condition is consistent with other studies (Golob et al., 2002; Lai et al., 2010; Lister et al., 2016; Bidelman et al., 2017; Buján et al., 2019). However, contrary to expectations, the amplitude of N1 was not significantly reduced in people with MCI when stimuli were presented slowly. The amplitude of N1 can be used to define the salience of stimulus input. N1 amplitude is larger when transient energy (intensity) is higher or when the time between the onset of stimuli is very long (i.e., when stimuli are presented slowly). In the present study, there is thus little evidence that at the early level of processing, people with MCI have a deficit in computing the salience of unattended auditory stimuli compared to healthy older adults.

In the present study, when stimuli were presented very slowly, planned comparisons indicated that the P2/P3a was significantly larger in older adults than in people with MCI. Its peak latency, around 230 ms, is more consistent with that of a P3a than a P2. Distinguishing between the P2 and P3a processes can be difficult because they may overlap and summate both temporally (occurring at about the same time) and spatially (sharing a similar scalp distribution).

When stimuli were presented slowly, it could be argued that the reduced P2/P3a in people with MCI is a result of a variable response within this condition. The reduction in this positivity in people with MCI in the slow condition might have been a result of rapid habituation, or a fatigue effect throughout the study. Ruusuvirta (2021) notes that the ERP response will be large in the initial trials but will decay upon repetition of the stimulus. Thus, in people with MCI, it is possible that the P2/P3a response was large in the initial trials but subsequently became much smaller. By contrast, in healthy older adults, the P2/P3a response may not have varied within the condition. However, there was

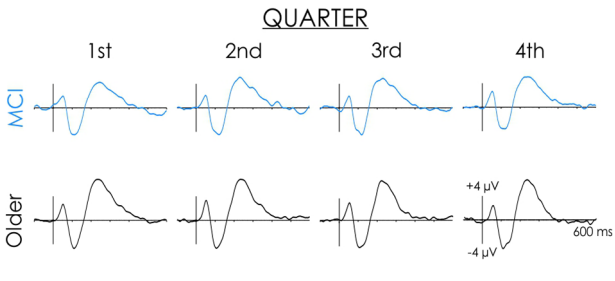

FIGURE 4 | Healthy older adult and MCI grand averaged ERP waveforms across the four quarters of the slow rate of presentation condition. Data presented are from the Cz electrode site. Note the N1 and P2 did not change across the four quarters for either healthy older adults or people with MCI.

little evidence to support this notion. When the averages were computed across each quarter of the study, ERP response showed little variance over time for either group.

The reduced P2/P3a in MCI, also observed by Cecchi et al. (2015), supports the view that the operations of the frontoparietal network may be dysfunctional in MCI. At first glance, the reduced P2/P3a does seem to contradict the theory that people with MCI are less able to inhibit the processing of irrelevant, unattended stimulus input (Belleville et al., 2008; Johns et al., 2012; Rabi et al., 2020; but see Rey-Mermet and Gade, 2018). In the present study, although the auditory stimuli were not attended to, their very rare occurrence should have been deemed to be a potentially highly *relevant* event. The amplitude of N1 did not significantly differ between people with MCI and healthy older adults. This finding suggests that people with MCI can establish the relevance/salience of the incoming stimulus event. To determine the actual relevance of such input would require a switch of processing priorities and the continuation, rather than the inhibition, of further processing. The dysfunction in people with MCI, therefore, appears to occur later as a result of a reduction in the ability to determine processing priorities.

In people with MCI, the correlational analyses indicated a small positive relationship between the amplitude of P2/P3a and MoCA scores. Nevertheless, the correlations did not attain statistical significance, perhaps because of the limited range of MoCA scores. It is also possible that the specific cognitive functions reflected by the P2/P3a are different from the more global cognitive functions measured by the MoCA.

CONCLUSION

Several studies have proposed the use of electrophysiological measures as a biomarker of MCI (Gu and Zhang, 2017; Morrison et al., 2018; Paitel et al., 2020). The very simple paradigm used in the present study has the advantage that it could be readily implemented on almost any low-cost commercial system. Testing can be completed in a short 15-min period. It has the marked advantage that the ERP responses elicited by the slowly-presented auditory stimuli occur relatively independent of attention, task demands, and what the participant is doing. From a clinical and applied perspective, whether the positivity occurring around 230 ms reflects P2 or P3a activity may be somewhat incidental. What is critical for its use as a biomarker is how accurately ERPs can classify people with MCI and cognitively healthy older adults. Despite overlap among individual participants, the P2/P3a group differences in the slow condition were significant. ERPs thus offers promise as a means to identify the pathology underlying cognitive impairment associated with MCI. Future research should examine the effects of even slower rates of stimulus presentation and different intensity levels. The use of an oddball paradigm which includes white noise and novel environmental sound deviants, known to elicit a large P3a, might also be employed. A longitudinal design should also be employed to examine differences between MCI participants who convert to dementia and those who remain stable. These studies could reveal the electrophysiological changes associated with conversion to dementia at an individual level.

DATA AVAILABILITY STATEMENT

The datasets presented in this article are not readily available because research ethics board restrictions preclude the sharing of data. Requests to access the datasets should be directed to vtaler@uottawa.ca.

ETHICS STATEMENT

The studies involving human participants were reviewed and approved by the University of Ottawa and Bruyère Research Institute Ethics Boards. The patients/participants provided their written informed consent to participate in this study.

AUTHOR CONTRIBUTIONS

FK, CM, KC, and VT contributed to the rationale and the design of the study and edited and approved the final manuscript. The manuscript was written by FK. FK and CM assisted with the collection and analysis of the EEG data. KC, CM, and VT provided feedback and revisions on written drafts of the manuscript. All authors contributed to the article and approved the submitted version.

FUNDING

This work was funded by a Natural Sciences and Engineering Research Council of Canada grant to KC (210405-190799) and VT (210924-190799).

SUPPLEMENTARY MATERIAL

The Supplementary Material for this article can be found online at: https://www.frontiersin.org/articles/10.3389/fnagi.2021.659618/full#supplementary-material.

REFERENCES

Alcaini, M., Giard, M. H., Thevenet, M., Thomas, A., and Pernier, J. (1994). Two separate frontal components in the N1 wave of the human auditory evoked response. *Psychophysiology* 31, 611–615. doi: 10.1111/j.1469-8986.1994.tb02354.x

Belleville, S., Bherer, L., Lepage, É., Chertkow, H., and Gauthier, S. (2008). Task switching capacities in persons with Alzheimer's disease and mild cognitive impairment. *Neuropsychologia* 46, 2225–2233. doi: 10.1016/j.neuropsychologia.2008.02.012

Berti, S. (2013). The role of auditory transient and deviance processing in distraction of task performance: a combined behavioral and event-related brain potential study. *Front. Hum. Neurosci.* 7:352. doi: 10.3389/fnhum.2013.00352

Berti, S., Vossel, G., and Gamer, M. (2017). The orienting response in healthy aging': novelty P3 indicates no general decline but reduced efficacy for fast stimulation rates. *Front. Psychol.* 8, 1–14. doi: 10.3389/fpsyg.2017.01780

Bertoli, S., Smurzynski, J., and Probst, R. (2005). Effects of age, age-related hearing loss and contralateral cafeteria noise on the discrimination of small frequency changes: psychoacoustic and electrophysiological measures. *J. Assoc. Res. Otolaryngol.* 6, 207–222. doi: 10.1007/s10162-005-5029-6

Bidelman, G. M., Lowther, J. E., Tak, S. H., and Alain, C. (2017). Mild cognitive impairment is characterized by deficient brainstem and cortical representations of speech. *J. Neurosci.* 37, 3610–3620. doi: 10.1523/JNEUROSCI.3700-16.2017

Budd, T. W., Barry, R. J., Gordon, E., Rennie, C., and Michie, P. T. (1998). Decrement of the N1 auditory event-related potential with stimulus repetition': habituation vs. refractoriness. *Int. J. Psychophysiol.* 31, 51–68. doi: 10.1016/s0167-8760(98)00040-3

Buján, A., Lister, J. J., O'Brien, J. L., and Edwards, J. D. (2019). Cortical auditory evoked potentials in mild cognitive impairment: evidence from a temporal-spatial principal component analysis. *Psychophysiology* 56, 1–22. doi: 10.1111/psyp.13466

Buschman, T. J., and Miller, E. K. (2010). Shifting the spotlight of attention: evidence for discrete computations in cognition. *Front. Hum. Neurosci.* 4, 1–9. doi: 10.3389/fnhum.2010.00194

Cecchi, M., Moore, D. K., Sadowsky, C. H., Solomon, P. R., Doraiswamy, P. M., Smith, C. D., et al. (2015). A clinical trial to validate event-related potential markers of Alzheimer's disease in outpatient settings. *Alzheimers Dement.* 1, 387–394. doi: 10.1016/j.dadm.2015.08.004

Čeponiene, R., Westerfield, M., Torki, M., and Townsend, J. (2008). Modality-specificity of sensory aging in vision and audition: evidence from event-related potentials. *Brain Res.* 1215, 53–68. doi: 10.1016/j.brainres.2008.02.010

Cranford, J. L., and Martin, D. R. (1991). Age-related changes in binaural processing: I. Evoked potential findings. *Am. J. Otol.* 12, 357–364.

Driscoll, I., Davatzikos, C., An, Y., Wu, X., Shen, D., Kraut, M., et al. (2009). Longitudinal pattern of regional brain volume change differentiates normal aging from MCI. *Neurology* 72, 1906–1913. doi: 10.1212/WNL.0b013e3181a82634

Escera, C., Alho, K., Winkler, I., and Näätänen, R. (1998). Neural mechanisms of involuntary attention to acoustic novelty and change. *J. Cogn. Neurosci.* 10, 590–604. doi: 10.1162/089892998562997

Giard, M. H., Perrin, F., Echallier, J. F., Thevenet, M., Froment, J. C., and Pernier, J. (1994). Dissociation of temporal and frontal components in the human auditory N1 wave: a scalp current density and dipole model analysis. *Electroencephalogr. Clin. Neurophysiol.* 92, 238–252. doi: 10.1016/0168-5597(94)90067-1

Golob, E. J., Irimajiri, R., and Starr, A. (2007). Auditory cortical activity in amnestic mild cognitive impairment: Relationship to subtype and conversion to dementia. *Brain* 130, 740–752. doi: 10.1093/brain/awl375

Golob, E. J., Johnson, J. K., and Starr, A. (2002). Auditory event-related potentials during target detection are abnormal in mild cognitive impairment. *Clin. Neurophysiol.* 113, 151–161. doi: 10.1016/s1388-2457(01)00713-1

Goulden, N., Khusnulina, A., Davis, N. J., Bracewell, R. M., Bokde, A. L., McNulty, J. P., et al. (2014). The salience network is responsible for switching between the default mode network and the central executive network: replication from DCM. *NeuroImage* 99, 180–190. doi: 10.1016/j.neuroimage.2014.05.052

Gu, L., and Zhang, Z. (2017). Exploring potential electrophysiological biomarkers in mild cognitive impairment: a systematic review and meta-analysis of event-related potential studies. *J. Alzheimers Dis.* 58, 1283–1292. doi: 10.3233/JAD-161286

Hansen, J. C., and Hillyard, S. A. (1988). Temporal dynamics of human auditory selective attention. *Psychophysiology* 25, 316–329. doi: 10.1111/j.1469-8986.1988.tb01249.x

Harkrider, A. W., Plyler, P. N., and Hedrick, M. S. (2005). Effects of age and spectral shaping on perception and neural representation of stop consonant stimuli. *Clin. Neurophysiol.* 116, 2153–2164. doi: 10.1016/j.clinph.2005.05.016

Irimajiri, R., Golob, E. J., and Starr, A. (2005). Auditory brain-stem, middle- and long-latency evoked potentials in mild cognitive impairment. *Clin. Neurophysiol.* 116, 1918–1929. doi: 10.1016/j.clinph.2005.04.010

Johns, E. K., Phillips, N. A., Belleville, S., Goupil, D., Babins, L., Kelner, N., et al. (2012). The profile of executive functioning in aMCI: disproportionate deficits in inhibitory control. *J. Int. Neuropsychol. Soc.* 18, 541–555. doi: 10.1017/S1355617712000069

Kamal, F., Morrison, C., Campbell, K., and Taler, V. (2021). Event-related potential evidence that very slowly presented auditory stimuli are passively processed differently in younger and older adults. *Neurobiol. Aging* doi: 10.1016/j.neurobiolaging.2021.02.014

Kappenman, E. S., and Luck, S. J. (2010). The effects of electrode impedance on data quality and statistical significance in ERP recordings. *Psychophysiology* 47, 888–904. doi: 10.1111/j.1469-8986.2010.01009.x

Lai, C. L., Lin, R. T., Liou, L. M., and Liu, C. K. (2010). The role of event-related potentials in cognitive decline in Alzheimer's disease. *Clin. Neurophysiol.* 121, 194–199. doi: 10.1016/j.clinph.2009.11.001

Lister, J. J., Harrison, A. L., Andel, R., Matthews, C., Morgan, D., and Edwards, J. D. (2016). Clinical Neurophysiology Cortical auditory evoked responses of older adults with and without probable mild cognitive impairment. *Clin. Neurophysiol.* 127, 1279–1287. doi: 10.1016/j.clinph.2015.11.007

Machulda, M. M., Senjem, M. L., Weigand, S. D., Smith, G. E., Ivnik, R. J., Boeve, B. F., et al. (2009). Functional magnetic resonance imaging changes in amnestic and nonamnestic mild cognitive impairment during encoding and recognition tasks. *J. Int. Neuropsychol. Soc.* 15, 372–382. doi: 10.1017/S1355617709090523

Madden, D. J., Bennett, I. J., Burzynska, A., Potter, G. G., Chen, N. K., Song, A. W., et al. (2012). Diffusion tensor imaging of cerebral white matter integrity in cognitive aging. *Biochim. Biophys. Acta* 1822, 386–400. doi: 10.1016/j.bbadis.2011.08.003

Makeig, S., Bell, A. J., Jung, T.-P., and Sejnowski, T. J. (1996). Independent component analysis of electroencephalographic data. *Adv. Neural. Inf. Process. Syst.* 145–151.

Masson, R., and Bidet-Caulet, A. (2019). Fronto-central P3a to distracting sounds: an index of their arousing properties. *NeuroImage* 185, 164–180. doi: 10.1016/j.neuroimage.2018.10.041

McCullagh, J., and Shinn, J. B. (2013). Auditory cortical processing in noise in younger and older adults. *Hear. Balance Commun.* 11, 182–190. doi: 10.3109/21695717.2013.855374

McEvoy, L., Levanen, S., and Loveless, N. (1997). Temporal characteristics of auditory sensory memory: neuromagnetic evidence. *Psychophysiology* 34, 308–316. doi: 10.1111/j.1469-8986.1997.tb02401.x

Morrison, C., Rabipour, S., Knoefel, F., Sheppard, C., and Taler, V. (2018). Auditory event-related potentials in mild cognitive impairment and Alzheimer's disease. *Curr. Alzheimer Res.* 15, 702–715. doi: 10.2174/1567205015666180123123209

Muller-Gass, A., Macdonald, M., Schröger, E., Sculthorpe, L., and Campbell, K. (2007). Evidence for the auditory P3a reflecting an automatic process: elicitation during highly-focused continuous visual attention. *Brain Res.* 1170, 71–78. doi: 10.1016/j.brainres.2007.07.023

Muller-Gass, A., Marcoux, A., Jamshidi, P., and Campbell, K. (2008). The effects of very slow rates of stimulus presentation on event-related potential estimates of hearing threshold The effects of very slow rates of stimulus presentation on event-related potential estimates of hearing threshold. *Int. J. Audiol.* 47, 34–43. doi: 10.1080/14992020701647934

Näätänen, R. (1990). The role of attention in auditory information processing as revealed by event-related potentials and other brain measures of cognitive function. *Behav. Brain Sci.* 13, 201–233. doi: 10.1017/S0140525X00078407

Nasreddine, Z. S., Phillips, N. A., Bédirian, V., Charbonneau, S., Whitehead, V., Collin, I., et al. (2005). The montreal cognitive assessment, MoCA: a brief screening tool for mild cognitive impairment. *J. Am. Geriatr. Soc.* 53, 695–699. doi: 10.1111/j.1532-5415.2005.53221.x

Oberauer, K. (2019). Working memory and attention-A conceptual analysis and review. *J. Cogn.* 2:36. doi: 10.5334/joc.58

Paitel, E. R., Samii, M. R., and Nielson, K. A. (2020). A systematic review of cognitive event-related potentials in mild cognitive impairment and Alzheimer's disease. *Behav. Brain Res.* 396:112904. doi: 10.1016/j.bbr.2020.112904

Pereira, D. R., Cardoso, S., Ferreira-Santos, F., Fernandes, C., Cunha-Reis, C., Paiva, T. O., et al. (2014). Effects of inter-stimulus interval (ISI) duration on the N1 and P2 components of the auditory event-related potential. *Int. J. Psychophysiol.* 94, 311–318. doi: 10.1016/j.ijpsycho.2014.09.012

Perrin, F., Pernier, J., Bertrand, O., Echallier, J. F., Inserm, U., Thomas, C. A., et al. (1989). Spherical splines for scalp potential and current density mapping. *Electroencephalogr. Clin. Neurophysiol.* 72, 184–187. doi: 10.1016/0013-4694(89)90180-6

Pfefferbaum, A., Ford, J. M., Roth, W. T., and Kopell, B. S. (1980). Age-related changes in auditory event-related potentials. *Electroencephalogr. Clin. Neurophysiol.* 49, 266–276. doi: 10.1016/0013-4694(80)90221-7

Phillips, N. D. (2017). Yarrr! The pirate's guide to R. *APS Observer*, 30.

Picton, T. W., and Hillyard, S. A. (1974). Human auditory evoked potentials. II: effects of attention. *Electroencephalogr. Clin. Neurophysiol.* 36, 191–200. doi: 10.1016/0013-4694(74)90156-4

Rabi, R., Vasquez, B. P., Alain, C., Hasher, L., Belleville, S., and Anderson, N. D. (2020). Inhibitory control deficits in individuals with amnestic mild cognitive impairment: A meta-analysis. *Neuropsychol. Rev.* 30, 97–125. doi: 10.1007/s11065-020-09428-6

Rey-Mermet, A., and Gade, M. (2018). Inhibition in aging: What is preserved? What declines? A meta-analysis. *Psychon. Bull. Rev.* 25, 1695–1716. doi: 10.3758/s13423-017-1384-7

Rinne, T., Särkkä, A., Degerman, A., Schröger, E., and Alho, K. (2006). Two separate mechanisms underlie auditory change detection and involuntary control of attention. *Brain Res.* 1077, 135–143. doi: 10.1016/j.brainres.2006.01.043

Roberts, R., and Knopman, D. S. (2013). Classification and epidemiology of MCI. *Clin. Geriatr. Med.* 29, 753–772. doi: 10.1016/j.cger.2013.07.003

Ruusuvirta, T. (2021). The release from refractoriness hypothesis of N1 of event-related potentials needs reassessment. *Hear. Res.* 399:107923. doi: 10.1016/j.heares.2020.107923

Salami, A., Eriksson, J., Nilsson, L. G., and Nyberg, L. (2012). Age-related white matter microstructural differences partly mediate age-related decline in processing speed but not cognition. *Biochim. Biophys. Acta* 1822, 408–415. doi: 10.1016/j.bbadis.2011.09.001

Sams, M., Hari, R., Rif, J., and Knuutila, J. (1993). The human auditory sensory memory trace persists about 10 sec: neuromagnetic evidence. *J. Cogn. Neurosci.* 5, 363–370. doi: 10.1162/jocn.1993.5.3.363

Saunders, N. L. J., and Summers, M. J. (2010). Attention and working memory deficits in mild cognitive impairment. *J. Clin. Exp. Neuropsychol.* 32, 350–357. doi: 10.1080/13803390903042379

Schwent, V. L., Hillyard, S. A., and Galambos, R. (1976). Selective attention and the auditory vertex potential. I. Effects of stimulus delivery rate. *Electroencephalogr. Clin. Neurophysiol.* 40, 604–614. doi: 10.1016/0013-4694(76)90135-8

Sperling, R. A., Aisen, P. S., Beckett, L. A., Bennett, D. A., Craft, S., Fagan, A. M., et al. (2011). Toward defining the preclinical stages of Alzheimer's disease: Recommendations from the National Institute on Aging-Alzheimer's Association workgroups on diagnostic guidelines for Alzheimer's disease. *Alzheimers Dement.* 7, 280–292. doi: 10.1016/j.jalz.2011.03.003

Stothart, G., and Kazanina, N. (2016). Auditory perception in the aging brain: the role of inhibition and facilitation in early processing. *Neurobiol. Aging* 47, 23–34. doi: 10.1016/j.neurobiolaging.2016.06.022

Sturm, W., De Simone, A., Krause, B. J., Specht, K., Hesselmann, V., Radermacher, I., et al. (1999). Functional anatomy of intrinsic alertness: evidence for a fronto-parietal-thalamic-brainstem network in the right hemisphere. *Neuropsychologia* 37, 797–805. doi: 10.1016/s0028-3932(98)00141-9

Woldorff, M. G. (1995). Selective listening at fast stimulus rates: so much to hear, so little time. *Electroencephalogr. Clin. Neurophysiol. Suppl.* 44, 32–54.

Conflict of Interest: The authors declare that the research was conducted in the absence of any commercial or financial relationships that could be construed as a potential conflict of interest.

frontiers in Aging Neuroscience

ORIGINAL RESEARCH
published: 21 April 2021
doi: 10.3389/fnagi.2021.626974

Hippocampal and Hippocampal-Subfield Volumes From Early-Onset Major Depression and Bipolar Disorder to Cognitive Decline

Niels Hansen[1,2], Aditya Singh[1,2], Claudia Bartels[1], Frederic Brosseron[3,4], Katharina Buerger[5,6], Arda C. Cetindag[7,8], Laura Dobisch[9], Peter Dechent[10], Birgit B. Ertl-Wagner[11], Klaus Fliessbach[3,4], John D. Haynes[12], Michael T. Heneka[3,4], Daniel Janowitz[6], Ingo Kilimann[13,14], Christoph Laske[15,16,17], Coraline D. Metzger[9,18,19], Matthias H. Munk[15,16,17], Oliver Peters[7,8], Josef Priller[8,20], Nina Roy[3], Klaus Scheffler[21], Anja Schneider[3,4], Annika Spottke[3,22], Eike J. Spruth[8,20], Stefan Teipel[13,14], Maike Tscheuschler[23], Ruth Vukovich[1], Jens Wiltfang[1,24,25], Emrah Duezel[9,18], Frank Jessen[23,26] and Roberto Goya-Maldonado[1,2]**

[1] Department of Psychiatry and Psychotherapy, Göttingen, Germany, [2] Laboratory of Systems Neuroscience and Imaging in Psychiatry, University Medical Center Göttingen, Göttingen, Germany, [3] German Center for Neurodegenerative Diseases (DZNE), Bonn, Germany, [4] Department for Neurodegenerative Diseases and Geriatric Psychiatry, University Hospital Bonn, Bonn, Germany, [5] German Center for Neurodegenerative Diseases (DZNE, Munich), Munich, Germany, [6] Institute for Stroke and Dementia Research (ISD), University Hospital, LMU Munich, Munich, Germany, [7] Berlin Institute of Health, Institute of Psychiatry and Psychotherapy, Charité—Universitätsmedizin Berlin, Corporate Member of Freie Universität Berlin, Humboldt-Universität zu Berlin, Berlin, Germany, [8] German Center for Neurodegenerative Diseases (DZNE), Berlin, Germany, [9] German Center for Neurodegenerative Diseases (DZNE), Magdeburg, Germany, [10] MR-Research in Neurology and Psychiatry, University Medical Center Göttingen, Göttingen, Germany, [11] Institute for Clinical Radiology, Ludwig-Maximilians-University, Munich, Germany, [12] Bernstein Center for Computational Neuroscience, Charité—Universitätsmedizin, Berlin, Germany, [13] German Center for Neurodegenerative Diseases (DZNE), Rostock, Germany, [14] Department of Psychosomatic Medicine, Rostock University Medical Center, Rostock, Germany, [15] German Center for Neurodegenerative Diseases (DZNE), Tübingen, Germany, [16] Section for Dementia Research, Hertie Institute for Clinical Brain Research, Tübingen, Germany, [17] Department of Psychiatry and Psychotherapy, University of Tübingen, Tübingen, Germany, [18] Institute of Cognitive Neurology and Dementia Research (IKND), Otto-von-Guericke University, Magdeburg, Germany, [19] Department of Psychiatry and Psychotherapy, Otto-von-Guericke University, Magdeburg, Germany, [20] Department of Psychiatry and Psychotherapy, Berlin, Germany, [21] Department for Biomedical Magnetic Resonance, University of Tübingen, Tübingen, Germany, [22] Department of Neurology, University of Bonn, Bonn, Germany, [23] Department of Psychiatry and Psychotherapy, University of Cologne, Medical Faculty, Cologne, Germany, [24] German Center for Neurodegenerative Diseases (DZNE), Göttingen, Germany, [25] Neurosciences and Signaling Group, Department of Medical Sciences, Institute of Biomedicine (iBiMED), University of Aveiro, Aveiro, Portugal, [26] Excellence Cluster on Cellular Stress Responses in Aging-Associated Diseases (CECAD), University of Cologne, Köln, Germany

Background: The hippocampus and its subfields (HippSub) are reported to be diminished in patients with Alzheimer's disease (AD), bipolar disorder (BD), and major depressive disorder (MDD). We examined these groups vs healthy controls (HC) to reveal HippSub alterations between diseases.

Methods: We segmented 3T-MRI T2-weighted hippocampal images of 67 HC, 58 BD, and MDD patients from the AFFDIS study and 137 patients from the DELCODE study assessing cognitive decline, including subjective cognitive decline (SCD), amnestic mild cognitive impairment (aMCI), and AD, via Free Surfer 6.0 to compare volumes across groups.

OPEN ACCESS

Edited by:
Yong Liu,
Beijing University of Posts and Telecommunications (BUPT), China

Reviewed by:
Sarah M. Szymkowicz,
Vanderbilt University Medical Center, United States
Baiying Lei,
Shenzhen University, China

***Correspondence:**
Niels Hansen
niels.hansen@med.uni-goettingen.de
Roberto Goya-Maldonado
roberto.goya@med.uni-goettingen.de

Received: 07 November 2020
Accepted: 10 March 2021
Published: 21 April 2021

Citation:
Hansen N, Singh A, Bartels C, Brosseron F, Buerger K, Cetindag AC, Dobisch L, Dechent P, Ertl-Wagner BB, Fliessbach K, Haynes JD, Heneka MT, Janowitz D, Kilimann I, Laske C, Metzger CD, Munk MH, Peters O, Priller J, Roy N, Scheffler K, Schneider A, Spottke A, Spruth EJ, Teipel S, Tscheuschler M, Vukovich R, Wiltfang J, Duezel E, Jessen F and Goya-Maldonado R (2021) Hippocampal and Hippocampal-Subfield Volumes From Early-Onset Major Depression and Bipolar Disorder to Cognitive Decline. Front. Aging Neurosci. 13:626974. doi: 10.3389/fnagi.2021.626974

Results: Groups differed significantly in several HippSub volumes, particularly between patients with AD and mood disorders. In comparison to HC, significant lower volumes appear in aMCI and AD groups in specific subfields. Smaller volumes in the left presubiculum are detected in aMCI and AD patients, differing from the BD group. A significant linear regression is seen between left hippocampus volume and duration since the first depressive episode.

Conclusions: HippSub volume alterations were observed in AD, but not in early-onset MDD and BD, reinforcing the notion of different neural mechanisms in hippocampal degeneration. Moreover, duration since the first depressive episode was a relevant factor explaining the lower left hippocampal volumes present in groups.

Keywords: Alzheimer's disease, cognitive impairment, early-onset depression, hippocampus, hippocampal subfields, MRI volumetry

INTRODUCTION

The human hippocampus is known as a brain structure pivotal for memory formation. It is the plasticity of the hippocampus to form memory that makes it particularly vulnerable to damage and volume reduction. In Alzheimer's disease (AD), hippocampal volume is reduced due to neurodegeneration as evidenced in brain MRIs of specific hippocampal subfields (HippSub). A variety of human studies have reported that specific HippSubs such as the cornu ammonis 1–3 (CA1–3), presubiculum or subiculum are more prone to neurodegenerative processes than others (Hanseeuw et al., 2011; La Joie et al., 2013; Carlesimo et al., 2015; de Flores et al., 2015). The degeneration pattern may depend on the AD stage, as indicated by cognitive performance, varying from subjective cognitive decline (SCD) to dementia. HippSub fields are suitable biological imaging markers of early stages of AD, as the presubiculum-subiculum complex (Carlesimo et al., 2015; Jacobs et al., 2020), CA2–3 (Hanseeuw et al., 2011), or CA1 region (de Flores et al., 2015) are often atrophied. Supporting this idea, recent work indicates that lower subicular volumes in patients with memory impairment are related to the grade of ß-amyloid depositions independent of the presence of neurodegeneration assessed by fluorescence desoxyglucose positron emission tomography (FDG PET) (Filho et al., 2021). More broadly, another study confirmed the association of ß-amyloid deposition in conjunction with higher iron content in the medial temporal lobe and subjects' age (even in cognitively unimpaired subjects) in terms of specific HippSub volume decreases, i.e., in the subiculum, CA1/2, CA3/dentate gyrus (DG) subregions (Foster et al., 2020). ß-amyloid accumulation is a key underlying mechanism in the loss of hippocampal volume across the spectrum of cognitive impairment in preclinical and clinical AD. Another study suggest that both reduced cerebrospinal fluid (CSF) ß-amyloid 1-42 and elevated CSF tau levels are seen in AD patients who exhibit smaller subiculum volumes (Tardif et al., 2018). This evidence suggests that both tau-based neurodegeneration and ß-amyloid pathology are crucial for HippSub volume loss in patients with AD. Other mechanisms underlying the loss of hippocampal volume might be polygenic, as a higher polygenic risk score for AD was observed in cognitively normal patients in a study by Foo (Foo et al., 2020), possibly depicting preclinical AD. Protective mechanisms might also play a role, such as carrying the TREML2 rs3747742-C polymorphism, which seem related to higher CA1 volumes in cognitively normal subjects (Wang et al., 2020). The interrelationship between depression and AD is a well-replicated finding (Heser et al., 2013; Donovan et al., 2018). It remains unclear whether depression is a relevant risk factor for AD (Enache et al., 2011), or if depression is an early manifestation thereof (Singh-Manoux et al., 2017). Furthermore, there is recent evidence that a decrease in hippocampal volume and functional connectivity is an important feature of major depressive disorder (MDD) associated with cognitive impairment (Genzel et al., 2015; Schmaal et al., 2016). Thus, it is of major interest to compare HippSub volumes which might give us hints about common underlying mechanisms in affective disorders and AD. In depressive disorders, diverse mechanisms such as the number of depressive episodes, stressful life events, oxidative stress, childhood physical, or sexual abuse or metabolic changes are potential underlying mechanisms of lower HippSub volumes such as CA1 or dentate gyrus (DG) or fimbria (Treadway et al., 2015; Elvsåshagen et al., 2016; Xu et al., 2018; Weissman et al., 2020; Yuan et al., 2020). These studies depict that in depression, the mechanisms of hippocampal volume loss seem to be even broader than in hippocampal degeneration due to AD's spectrum. HippSub loss does not just concern unipolar depression; it is also present in bipolar disorder (BD); the pattern of subfield loss was considerably more extensive than in controls in a recent multicentric study with 1,472 BD patients (Haukvik et al., 2020). Another recent study indicated one possible common pathogenic mechanism between BD and AD (Berridge, 2013), which is why we added a BD group in our study. BD could could result in a HippSub-specific fingerprint like reduced volume in the CA1 (Cao et al., 2017; Haukvik et al., 2020), cornu ammonis 4 (CA4) (Cao et al., 2017; Haukvik et al., 2020), the granule cell layer (GCL) (Cao et al., 2017; Haukvik et al., 2020), molecular layer (ML) (Cao et al., 2017; Haukvik et al., 2020), subiculum (Sub) (Cao et al., 2017; Haukvik et al., 2020), hippocampal amygdala transition area (Haukvik et al., 2020) and tail (Cao et al., 2017; Haukvik et al., 2020) depending on the duration and type of BD

(Cao et al., 2017), but also on antipsychotic and antiepileptic drug history (Haukvik et al., 2020). On the other hand, it has been suggested that depressive symptoms might reduce age-related hippocampal atrophy and result in larger Sub and CA1 subfields (Szymkowicz et al., 2017). However, most studies showed smaller hippocampal volumes due to ongoing depressive symptoms, thus the controversy about how depression's duration relates to HippSub volumes. The aforementioned studies show that the mechanism of hippocampal volume loss might differ even in two distinct affective disorders and AD and that it is not fully understood. However, we wondered whether there might be a similar pattern of HippSub loss in some HippSubs implying similar mechanisms of degeneration.

In the current investigation, we thus aimed [a] to analyze HippSub volumes and hippocampal volumes between cohorts with cognitive impairment, early-onset major depression and BD, and [b] to identify potential disorder-specific alterations and any shared trajectories of hippocampal volume decrease in the hippocampus and HippSub in SCD, aMCI, AD, BD, and MDD groups. Our study covers the spectrum ranging from subjective complaints (SCD) to amnestic mild cognitive impairment (aMCI) and AD. SCD patients do not reveal objective cognitive impairment. Therefore, it is worth seeking novel biomarker tools such as hippocampus and HippSub imaging to diagnose early AD more accurately. In addition, we are looking for molecular markers in the CSF such as ß-amyloid and tau protein to detect any underlying pathomechanism for HippSub in AD; a recent study by Tardif (Tardif et al., 2018) proved a relevant relationship between HippSub decline and ß-amyloid and tau-based neuropathology in AD. Our study does not focus on specific HippSubs, as there is controversy about which HippSubs are reduced among different diseases. The intersection between lower HippSub volumes and various diseases associated with cognitive dysfunction is inconsistent in studies of AD's spectrum (Hanseeuw et al., 2011; La Joie et al., 2013; Carlesimo et al., 2015; de Flores et al., 2015; Cao et al., 2017; Szymkowicz et al., 2017; Jacobs et al., 2020), MDD (Treadway et al., 2015; Elvsåshagen et al., 2016; Xu et al., 2018; Weissman et al., 2020; Yuan et al., 2020), and BD (Cao et al., 2017; Haukvik et al., 2020). Therefore, we plan to take a more exploratory look at the volumes of various HippSubs. Furthermore, we aimed to discover whether specific factors show a relevant impact on our HippSub and hippocampal volumes in certain disease groups; i.e., sex, age, disease duration, age at condition onset, number of depressive episodes, duration since first depression, and intracranial volume. In addition, we expected to uncover potential relationships not yet investigated between hippocampal volume and HippSub volumes and duration since the first occurrence of a depressive episode between all groups that might be clinically relevant and thus support the relevance of very early, effective treatment to impede further hippocampal degeneration that might accompany disease progression. By analyzing early-onset depression and BD patients, we will demonstrate a wide spectrum of time duration in years between the first episode of depression and hippocampal and HippSub volumes to answer how a lifetime's duration of suffering intermittent depressive and no depressive episodes since the first one's occurrence relates to hippocampus volumetry. Analyzing hippocampal volumes in addition to the HippSubs is an important endeavor, as they involve functional aspects of memory such as pattern separation and recognition in AD (Rizzolo et al., 2021), stress sensitization (Weissman et al., 2020), as does the number of depressive episodes in prior life (Videbech and Ravnkilde, 2004).

METHODS

Participants

We compared data of two independent cohorts from 137 patients of the DELCODE study and 58 patients of the AFFDIS study in this retrospective investigation. The German DELCODE [**D**eutsches Zentrum für Neurodegenerative **E**rkrankungen (DZNE, German Center for Neurodegenerative Diseases) **L**ongitudinal **CO**gnitive impairment and **De**mentia] is assessing cognitive decline and dementia in an ongoing, memory clinic-based, observational, longitudinal, multicentric study (Jessen et al., 2018). The AFFDIS study investigated differential neural correlates in **AFF**ective **DIS**orders (AFFDIS) and medication-related changes from 2015 to 2017. For a detailed description of the DELCODE study design and study population, please see Jessen et al. (2018). In short, participants from the DELCODE cohort were grouped into SCD ($n = 32$; mean age: 72 ± 6.2 years, age range: 60–89 years), amnestic mild cognitive impairment (aMCI) ($n = 63$; mean age: 72.5 ± 5.9 years, age range: 62–88 years), and AD ($n = 42$; mean age: 72.9 ± 6.9 years, age range: 61–87 years). The AD patients were selected according to McKhann's criteria (McKhann et al., 2011). Probable AD is diagnosed according to McKhann's criteria (McKhann et al., 2011) when the following deficits and other alternative causes have been excluded: a gradual, not acute onset of symptoms, worsening cognition resulting in dementia with a prominent amnestic presentation of cognitive dysfunction, difficulty finding words and solving problems, defective spatial cognition, impaired reasoning, or judgement. We randomly selected the patients from the DELCODE cohort for comparable size between study cohorts (AFFDIS, DELCODE) and their subgroups. Participants were classified as having SCD in case of self-reported subjective cognitive decline and a neuropsychological test achievement superior than −1.5 standard deviation (SD) on each subtest of the Consortium to Establish a Registry for Alzheimer's Disease (CERAD) test battery (according to normative data adapted for age, education and sex) (Jessen et al., 2014, 2018, 2020). According to research criteria (Jessen et al., 2018), participants with aMCI were defined as those whose neuropsychological performance was below −1.5 SD in the delayed recall test of the CERAD word list, which is indicative of episodic memory. For the HC group ($n = 67$, age: 54.0 ± 16.7 years, age range: 19–78 years) from the DELCODE study, the same test criteria for SCD were applied, but subjective cognitive concerns were absent. In a subgroup of patients with cognitive impairment in the DELCODE study [21/32 (66%) SCD, 46/63 (73%) aMCI, and 19/42 (45%) AD patients] cerebrospinal fluid (CSF) biomarkers were assessed. As part of the DELCODE protocol, Tau-protein, phosphorylated 181 Tau-protein (pTau181), ß-Amyloid 42, ß-Amyloid 40, and

the ratio of ß-Amyloid 42/40 were analyzed in cerebrospinal fluid (CSF) with cut-off values for AD's molecular markers established at the University Hospital in Bonn as previously described (Jessen et al., 2018). AD's molecular signature (AD pathology+) was present if Aß42 or the Aß42/Aß40 ratio in CSF was reduced and Tau protein or pTau181 were elevated in CSF in line with Jack's criteria for biological AD (Jack et al., 2018).

Major exclusion criteria were significant sensory impairment, major or neurological psychiatric disorder, current major depressive episode, malignant disease, cerebral ischemia, Vitamin B12 deficiency, and any unstable medical condition. A medical history derived from the participant's and caregiver's self-reports was collected and covered depression history (e.g., age of depression onset, number of previous mood episodes, if applicable). In the AFFDIS cohort, participants with affective disorders were diagnosed with BD ($n = 28$, age: 54.0 $\pm$ 16.7 years, and age range: 26–63 years) and MDD ($n = 30$, age: 38.2 $\pm$ 15.9 years, and age range: 19–65 years), according to the DSM-5 criteria, and were assessed by the Beck Depression Inventory-II (BDI-II), while HC participants were evaluated by the Symptom Checklist-90-R (SCL-90-R) to ensure the absence of psychopathological symptoms. By pooling HC from the two cohorts (DELCODE $n = 32$, AFFDIS $n = 35$), the HC group consisted of 67 participants in total. Informed consent was received from all participants. Approval was obtained for DELCODE [ethics committee of the University Hospital Bonn and subsequent local ethics committee's of the participating centers of Berlin (Charité-Universitätsmedizin Berlin), Göttingen (University Medical Center of Göttingen), Cologne (University Hospital Cologne), Magdeburg (Otto-von-Guericke University Magdeburg), Munich (LMU Munich), Rostock (University Medical Center of Rostock), and Tübingen (University of Tübingen)] and AFFDIS (ethics committee of the University Medical Center of Göttingen) from our local ethics committee and for DELCODE from the executive board of the DZNE in Bonn, Germany. The study was in agreement with the guidelines of the Declaration of Helsinki.

Neuroimaging

We used whole-brain T1-weighted images (1 mm isotropic) and high-resolution T2-weighted images ($0.5 \times 0.5 \times 1.5\text{mm}^3$) spanning the hippocampus to segment it into its constituent substructures. These structural images were acquired using 3T MRI Siemens scanner systems [TIM Trio and Verio systems, Skyra, and Prisma system, both the DELCODE and AFFDIS cohorts. We used the already established and reliable method, corroborated by longitudinal studies (Brown et al., 2020; Garimella et al., 2020; Xu et al., 2020), of FreeSurfer (Version 6.0, software: http://surfer.nmr.mgh.harvard.edu/) to segment the whole brain T1-weighted structural images using the default standard recon-all processing stream (Dale et al., 1999; Fischl et al., 1999). This step usually takes about 7–10 h for each subject image, and outputs the segmentation results from both cortical and subcortical structures. Standard preprocessing comprises brain extraction, B1 bias field correction, segmentation of gray as well as white matter, reconstruction of gray matter–white matter boundary and pial surfaces, labeling of regions in both the cortex and subcortex, and non-linearly co-registering the individual T1's cortical surface to a spherical atlas to allow comparison across subjects. To obtain HippSub segmentation, we employed the higher-resolution T2-weighted scans using the revised module available in FreeSurfer 6.0 (Iglesias et al., 2015; Whelan et al., 2016). The step takes ∼45 min for each subject's hippocampal segmentation and provides a label for the following subregions: hippocampal tail, subiculum (Sub), CA1, fissure, presubiculum (PreSub), parasubiculum (ParaSub), molecular layer (ML), granule cell layer-molecular layer of the DG, CA3, cornu ammonis 4 (CA4), fimbria, and hippocampus-amygdala transition area (Hata) region in both hemispheres. After this, we used automated scripts (courtesy of P. Saemann of the ENIGMA consortium [https://enigma.ini.usc.edu]) to extract the HippSub volumes of each hemisphere for further statistical analysis. Finally, we created 2D and 3D (**Figure 1**) renderings to perform careful quality check (QC) to ensure correct segmentation of all cases before running statistical analysis. Cases of poorly segmented hippocampus or HippSub were absent.

Statistical Analysis

We performed ANOVA to detect differences between groups and controls in relevant variables such as sex, age, disease duration, age at condition onset, number of depressive episodes, duration since first depression, and intracranial volume (eTIV). We examined the potential contribution of covariates (age, age at condition onset, and eTIV) to the HippSub volumes as they showed significant group differences. Only those covariates exhibiting relevant group differences among all patients were regarded as significant covariates in our HippSub analysis. To investigate volume differences between all groups, we analyzed HippSub volumes from FreeSurfer using ANOVA with group as a factor (SCD, aMCI, AD, BD, and MDD) with and without HC and with covariates age and eTIV. An additional one-way ANOVA was performed only with the cognitive-decline-groups as factor with or without CSF pathology suggestive of Alzheimer's disease (SCD, aMCI, AD, SCD-CSF pathology+, aMCI-CSF pathology+, and AD-CSF pathology+). A further ANOVA was performed for AFFDIS patient groups and their AFFDIS control group with eTIV as covariate. To investigate the potential impact of time since first depressive episode on volume reduction, we ran a linear regression analysis in all patient groups that had history of depression. The length of time since the first depressive episode is defined as the cumulative amount of time someone had been depressed including transient time periods with no depression in their lifetime before hippocampal volume was assessed. Statistical analysis was performed via SPSS (Version 25, IBM Inc., Chicago, Illinois, USA). Graphs were constructed by Sigma Plot (Version 11, Sigma Plot, USA). Statistical analyses were two-sided with a p-level of significance ≤ 0.05, including, if applicable, LSD *post-hoc* tests including Bonferroni correction.

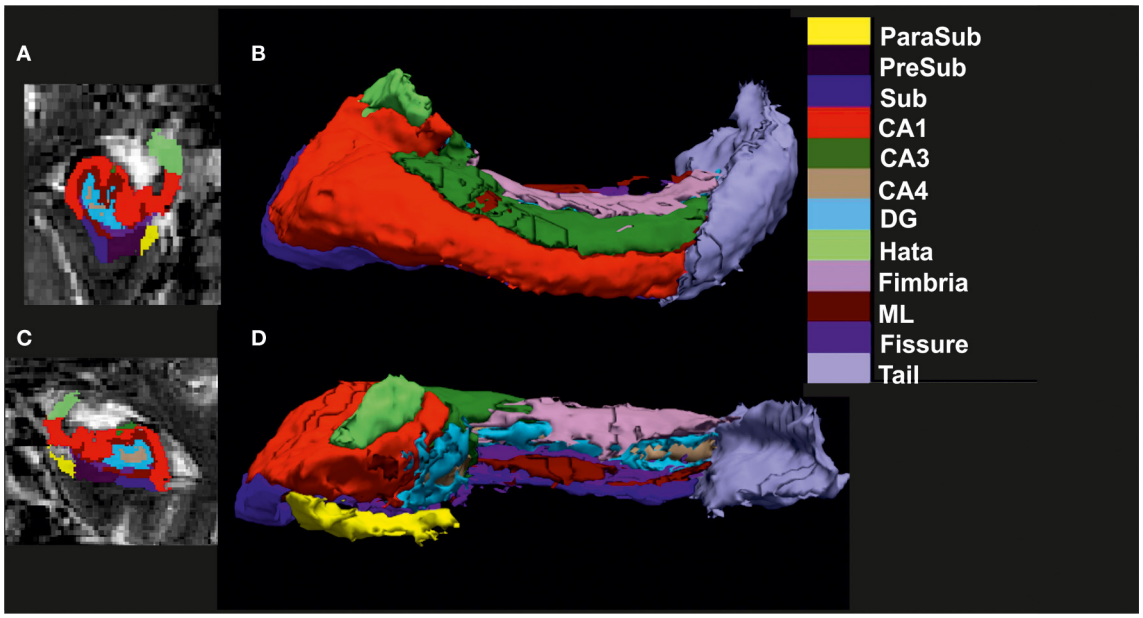

FIGURE 1 | Visualization of hippocampal subfield segmentation. **(A)** Left hippocampal subfields (HippSub) presented in a coronal MRI section, **(B)** Left HippSub illustrated in a 3D reconstruction, **(C)** Right HippSub presented in a coronal MRI section, and **(D)** Right HippSub illustrated in a 3D reconstruction. HippSub color code is on the right side of the figure. CA1/3/4, cornu ammonis 1/3/4; DG, granule cell layer-molecular layer of the dentate gyrus; Hata, hippocampus-amygdala transition area; ML, molecular layer; ParaSub, Parasubiculum; PreSub, Presubiculum; Sub, Subiculum.

TABLE 1 | Demographic and clinical information of patient and control groups.

		DELCODE cohort			AFFDIS cohort		Statistics
	SCD	MCI	AD	BD	MDD	HC (HCDELCODE, HCAFFDIS)	*F*, *p*
Number of subjects/patients	$n = 32$	$n = 63$	$n = 42$	$n = 28$	$n = 30$	$n = 67$ (32, 35)	
Sex (females/ males)	15/17	34/29	18/24	17/11	16/14	26/ 41 (22/ 10, 19/ 16)	68.9, 0.371 (0.342)
Age (y)	72 ± 6.2	72.5 ± 5.9	72.9 ± 6.9	44 ± 9.7	38.2 ± 15.9	54.0 ± 16.7 (67.4 ± 4.3, 41.4 ± 14.3)	1.082, <0.005 (<0.0005)
Age at disease onset (y)	56.7 ± 6.9	57.8 ± 5.0	59.5 ± 7.9	26.4 ± 9.8	28 ± 15.6	na	102.6, <0.0005
Onset of depressive episodes (y)	46.9 ± 17.7	36.4 ± 22.2	49.75 ± 15.9	25.7 ± 11.1	28.7 ± 15.9	na	4.81, <0.0005
Number of depressive episodes	2.7 ± 3.3	2.25 ± 1.2	2 ± 1.15	6.6 ± 5.5	4.8 ± 4.4	na	2.07, 0.095
Duration of depression (y)	21 ± 18.7	33.8 ± 26.4	17.5 ± 15.5	5 ± 12.75	9.4 ± 9.3	na	4.42, <0.005

AD, Alzheimer's disease dementia; BD, bipolar disorders; HC, healthy controls; HCDELCODE, healthy controls DELCODE; HCAFFDIS, healthy controls AFFDIS; MCI, mild cognitive impairment; MDD, major depressive disorder; na, not available; SCD, subjective cognitive decline; y, years; Mean ± standard deviation.

RESULTS

Baseline Characteristics of Groups

We pooled HC ($n = 67$) from the AFFDIS cohort ($n = 35$) and DELCODE cohort ($n = 32$) to serve as a reference for potential effects of age-related differences in hippocampus and HippSub volumes. Clinic and demographic data of study participants ($n = 195$) are presented in **Table 1**, showing sex, age, onset age of depressive episodes, number of depressive episodes, age at onset of condition, and duration since first depression compared across all groups (HC, SCD, aMCI, AD, BD, and MDD). Past depressive episodes were identified in 7/32 (22%) of SCD, in 5/63 (7.9%) of aMCI and in 4/42 (9.5%) of AD patients. The BP and MDD patients revealed a moderate degree of current depressive mood a s indexed by BDI-II (BDI-II scores: BD: 19 ± 12.8; MDD: 25 ± 11.3). Age ($F = 68.9$, $p < 0.005$), disease condition's onset age ($F = 90.7$, $p < 0.005$), and the onset age of depressive episodes ($F = 4.3$, $p < 0.005$) and the duration of depression ($F = 4.4$, $p < 0.005$) differed significantly between groups, whereas sex and number of depressive episodes did not. The eTIV differed significantly between groups ($F = 4.98$, $p < 0.0005$). In *post-hoc* analysis, only SCD and HC differed significantly from BD and MDD patients (*post-hoc* test: $p < 0.05$), while the other groups did not (LSD *post-hoc* test: $p > 0.05$). However, when comparing the HC in the AFFDIS cohort only with BD and MDD patients in eTIV volume, we detected no significant differences (LSD *post-hoc* test:

TABLE 2 | Neuroimaging data of patient and control groups.

	DELCODE cohort			AFFDIS cohort		
	SCD	**aMCI**	**AD**	**BD**	**MDD**	**HC**
eTIV	1,412,486 ± 223,372	1,490,137 ± 267,502	1,468,571 ± 141,138	1,575,000 ± 188,277	1,575,667 ± 134,976	141,908 ± 194,631
Right side						
Whole Hippocampus	2,921 ± 361	2,714 ± 436	2,205 ± 426	3,179 ± 339	3,229 ± 307	3,051 ± 351
CA1	590 ± 88	549 ± 99	445 ± 102	636 ± 82	649 ± 70	613 ± 86
CA3	171 ± 25	159 ± 32	128 ± 30	180 ± 29	189 ± 26	171 ± 26
CA4	239 ± 31	219 ± 41	179 ± 35	249 ± 29	260 ± 31	242 ± 30
DG	270 ± 35	248 ± 45	202 ± 39	287 ± 34	296 ± 34	277 ± 35
Fimbria	68 ± 19	65 ± 21	45 ± 20	93 ± 19	96 ± 18	80 ± 27
Fissure	180 ± 29	170 ± 32	148 ± 39	168 ± 29	171 ± 34	168 ± 31
Hata	54 ± 11	52 ± 14	43 ± 10	63 ± 10	63 ± 10	58 ± 9
Molecular Layer	270 ± 35	414 ± 79	324 ± 70	287 ± 34	465 ± 48	447 ± 57
ParaSub	51 ± 12	49 ± 11	42 ± 10	53 ± 8	54 ± 7	52 ± 9
PreSub	215 ± 46	201 ± 45	167 ± 38	240 ± 48	224 ± 36	226 ± 41
Sub	376 ± 52	337 ± 58	270 ± 62	416 ± 60	419 ± 45	400 ± 54
Tail	443 ± 66	422 ± 86	360 ± 77	488 ± 68	513 ± 79	485 ± 87
Left side						
Whole hippocampus	2,927 ± 307	2,652 ± 401	2,182 ± 426	3,233 ± 34	3,295 ± 320	3,058 ± 356
CA1	568 ± 73	519 ± 87	437 ± 94	596 ± 72	634 ± 74	586 ± 78
CA3	163 ± 28	149 ± 29	125 ± 28	174 ± 27	175 ± 26	161 ± 24
CA4	231 ± 27	206 ± 38	171 ± 34	251 ± 28	260 ± 32	238 ± 30
DG	261 ± 31	234 ± 41	194 ± 39	289 ± 33	299 ± 35	271 ± 35
Fimbria	60 ± 19	57 ± 20	39 ± 20	83 ± 15	93 ± 17	75 ± 18
Fissure	167 ± 29	162 ± 33	143 ± 36	155 ± 21	153 ± 32	161 ± 32
Hata	53 ± 12	49 ± 11	43 ± 10	58 ± 10	59 ± 11	54 ± 11
Molecular Layer	446 ± 60	411 ± 79	322 ± 76	289 ± 33	485 ± 59	452 ± 57
ParaSub	52 ± 11	48 ± 12	42 ± 10	52 ± 9	51 ± 8	50 ± 8
PreSub	246 ± 43	216 ± 43	175 ± 42	278 ± 47	257 ± 31	251 ± 43
Sub	381 ± 50	333 ± 59	271 ± 64	426 ± 54	432 ± 46	407 ± 48
Tail	443 ± 66	429 ± 82	361 ± 74	539 ± 75	550 ± 79	513 ± 97

AD, Alzheimer's disease dementia; BD, bipolar disorders; HC, healthy controls; HCDELCODE,healthy controls DELCODE; HCAFFDIS, healthy controls AFFDIS; MCI, mild cognitive impairment; MDD, major depressive disorder; na, not available; SCD, subjective cognitive decline; y, years; Mean ± standard deviation.

$p > 0.05$). Thus, the eTIV difference was driven by the SCD group compared with BD and MDD patients. Overall, age and eTIV showed relevant group differences among all patients and were considered as relevant covariates for our HippSub analysis as well as linear regression of hippocampus and HippSub volumes in patients with and without controls.

Comparison of Hippocampal Subfield Volumes Between Cognitive Decline and Affective Disease Groups Without Controls

ANOVA revealed a significant difference ($F = 2.24$, $p < 0.0005$, see **Table 2** for neuroimaging data of patients and controls) in hippocampus and HippSub volumes between all groups including cognitive decline (SCD, aMCI, and AD) and early-onset mood conditions (MDD and BD). The hippocampus in both hemispheres exhibited smaller volumes in AD patients, but not in MDD and BD patients (LSD *post-hoc* test: $p < 0.0005$; **Figure 2A**). Bilateral CA1, CA4, DG, ML, Sub, fimbria, and left tail revealed the same pattern of a diminished volume in AD, but not in MDD and BD groups (LSD *post-hoc* test: $p < 0.05$, **Figures 2B,C**). Significantly lower volumes in the left PreSub were observed in aMCI and AD patients when compared to BD (LSD *post-hoc* test: $p < 0.005$, **Figures 2B,C**). No differences between hippocampal volumes in AD vs. BD or MDD patients were identified in bilateral CA3, ParaSub, fissure, hata, and right PreSub regions (**Figures 2B,C**).

Hippocampal Subfield Volumes in Cognitive Decline Groups

Considering the hippocampus, aMCI and AD (but not SCD) groups presented significantly smaller volumes bilaterally in comparison to HC (*post-hoc* tests: $p < 0.05$, **Figure 2A**). Moreover, in aMCI and AD groups, but not in SCD group, we detected lower volumes in left CA1, left CA4, left DG, left tail, left PreSub, and bilateral Sub when compared to HC (LSD *post-hoc* test: $p < 0.05$, **Figures 2B,C**). In the right CA1, right CA4,

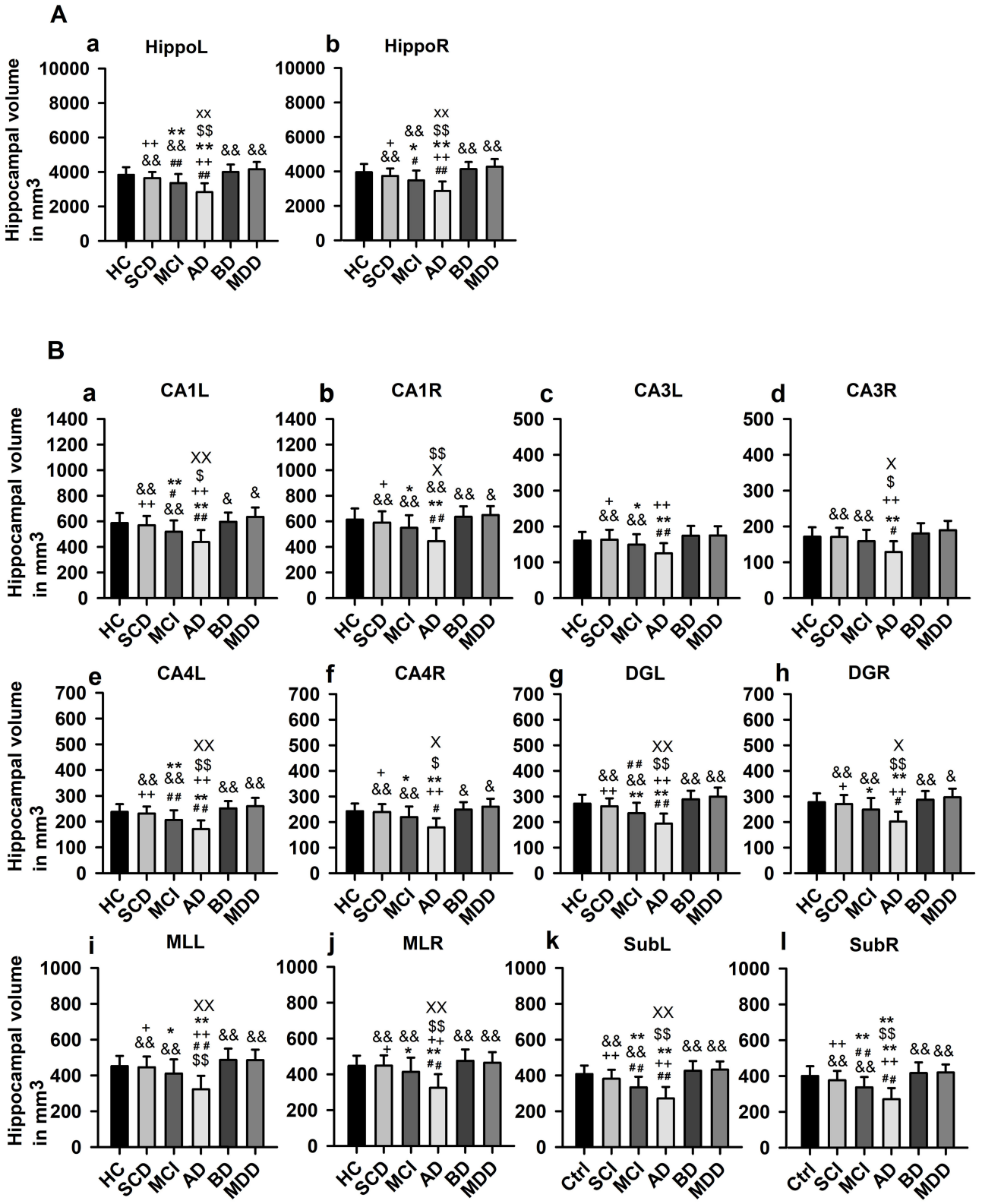

FIGURE 2 | Continued

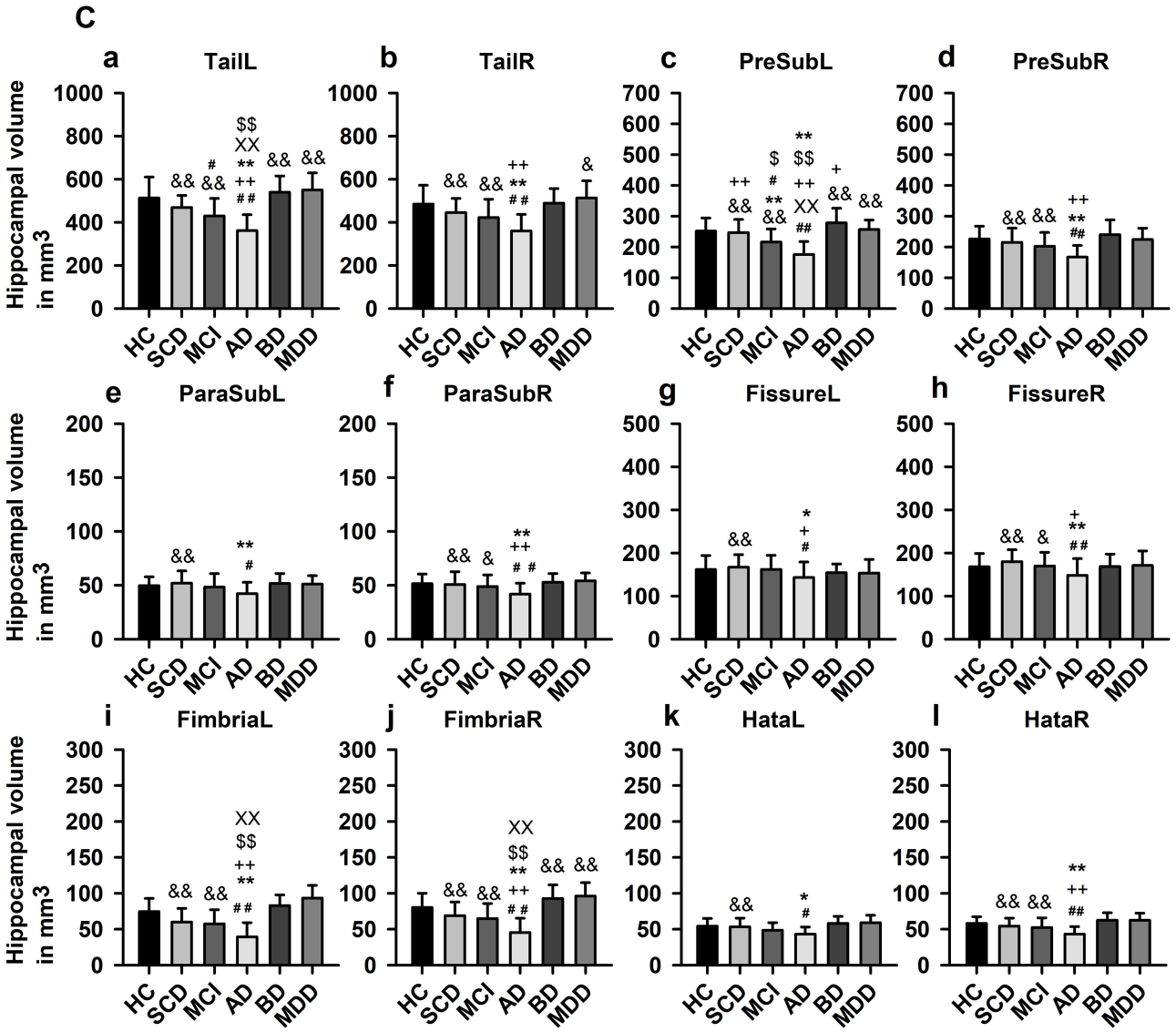

FIGURE 2 | Hippocampal subfield volumes across groups. **(A)** Whole hippocampus volumes compared in each hemisphere, **(B)** Hippocampal subfield (HippSub) volumes, including the CA1, CA3, CA4, DG, ML, and Sub as part of the hippocampus, compared in each hemisphere, and **(C)** Additional HippSub volumes including tail, PreSub, ParaSub, fissure, fimbria, Hata, compared in each hemisphere. Results refer to LSD *post-hoc t*-tests (two-sided) with Bonferroni correction between each condition. The significance level is indicated by different symbols: $^{\#\#}p < 0.005$ vs. HC, $^{**}p < 0.005$ vs. SCD, $^{++}p < 0.005$ vs. aMCI, $^{\&}p < 0.005$ vs. AD, $^{\$\$}p < 0.005$ vs. BD, $^{xx}p < 0.005$ vs. MDD, $^{*}p < 0.05$ vs. SCD, $^{+}p < 0.05$ vs. aMCI, $^{\&}p < 0.05$ vs. AD, $^{\$}p < 0.05$ vs. BD, $^{x}p < 0.05$ vs. MDD. AD, Alzheimer's disease; BD, bipolar disorder; CA1/3/4, cornu ammonis 1/3/4; HC, healthy controls; DG, granule cell layer-molecular layer of the dentate gyrus; Hata, hippocampus-amygdala transition area; L, left; aMCI, amnestic mild cognitive impairment; MDD, major depressive disorder; ML, molecular layer; ParaSub, Parasubiculum; PreSub, Presubiculum; R, right; SCD, subjective cognitive decline; Sub, Subiculum.

right DG, right tail, right PreSub, bilateral CA3, bilateral ParaSub, bilateral fimbria, and bilateral fissure regions (**Figures 2B,C**) we found no volume differences in HippSub in aMCI and SCD groups compared to HC.

In additional subgroup analyses, we investigated subjects presenting neuropathological abnormalities typical of AD. Concerning those DELCODE patients, for 6/32 (19%) patients with SCD, 20/63 (38%) with aMCI, and 16/42 (38%) patients with AD, their CSF pathology suggests AD. When we compared subgroups with a positive AD pathology to those without, we detected no significant between-group differences in HippSub (all $p > 0.05$, data not shown).

Hippocampal Subfield Volumes in Affective Disorder Groups

No significant differences were detected on hippocampal and HippSub volumes when we compared MDD and BD groups to HC ($p > 0.05$).

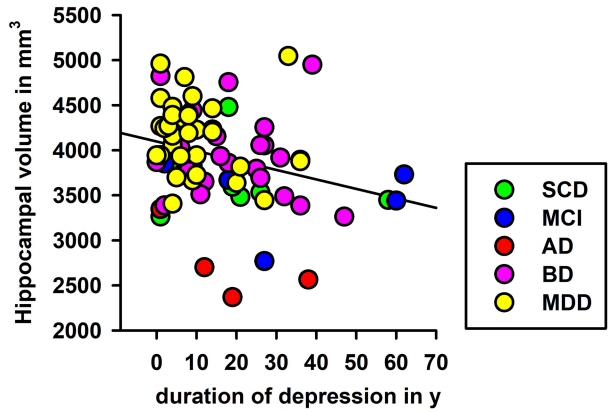

FIGURE 3 | Linear regression of depression duration and left hippocampal volumes. Significant regression analyses of depression duration and left hippocampal volume are shown. AD, Alzheimer's disease; BD, bipolar disorder; L, left; aMCI, amnestic mild cognitive impairment; MDD, major depressive disorder; SCD, subjective cognitive decline; y, years.

Hippocampal-Subfield Volumes and Duration of Depression

To explore the role duration plays in years since depression onset on hippocampus volume in each hemisphere, we conducted a linear regression analysis, and noted that left, but not right hippocampal volume was significantly associated with time since first depressive episode (left hippocampus: $F = 6.5$, $p < 0.05$; **Figure 3**). We explored this effect further in HippSub volumes, and observed no relevant association with the time since first depressive episode and the left Sub, left CA1, left PreSub, left DG, left CA4, left fimbria, right tail, and right fimbria.

DISCUSSION

The main findings of our investigation are that using MRI data, hippocampal and specific HippSub volumes differed between major cognitive decline due to possible AD and early-onset of unipolar and bipolar disorders. Smaller hippocampus and most HippSub volumes were detected almost exclusively in aMCI and AD groups, while SCD, BD, and MDD groups revealed no significant smaller volumes in relation to HC. Early markers of possible neurodegeneration can therefore be seen predominantly in the left CA1, CA4, DG, tail, PreSub, and bilateral Sub regions, since significant smaller volumes were found in aMCI and ADD groups, but not in early-onset mood disorders (MDD, BD). Of note, the duration in years since first depressive episode was significantly related to the volume of left hippocampus in all patient groups. Based on the present study, the HippSub right CA1, CA4, DG, tail, PreSub, and bilateral CA3, ParaSub, fimbria, and fissure regions seem more resilient against neurodegeneration in aMCI and SCD patients. These findings may partially reflect the existing variability at certain stages of cognitive decline, as other studies have already demonstrated a volume decrease in MCI patients (Zhao et al., 2019).

A unique finding in this investigation was the significant difference seen between aMCI and BD in the left PreSub region, which could function as a suitable imaging marker. If replicated, smaller volumes in the left PreSub might prove to be the earliest indications of hippocampal-volume differences due to cognitive impairment distinct from those with bipolar mood disorders. There is evidence that both ß-amyloid and tau pathology assessed via CSF are relevant factors in lower HippSub volumes due to AD's cognitive spectrum (Tardif et al., 2018; Filho et al., 2021). As we failed to detect significant volume differences in patients with cognitive impairment with and without AD-typical CSF pathology, there might be additional mechanisms contributing to HippSub decline in our patients. Nevertheless, we could not exclude the possibility of insufficient power to detect differences, considering the relatively few subgroup samples. Further studies are needed with larger patient cohorts to differentiate the proposed underlying mechanisms of AD in HippSub volume loss. The aforementioned literature suggests other mechanisms of HippSub volume degeneration in the AD spectrum such as genes, iron accumulation, or even neuroprotective factors (Foo et al., 2020; Foster et al., 2020; Wang et al., 2020). Some of these factors may be partly responsible for the PreSub volume loss in AD, aMCI vs BD patients that we detected.

Overall, we identified neither smaller hippocampal nor HippSub volumes in early-onset mood disorder groups. That may be attributable both groups' similar age and similar severity of depressive symptoms. Furthermore, another explanation for no relevant differences in HippSub in mood disorder groups might be that structural differences between MDD-BD patients are likely less evident in the hippocampus or HippSub than in other brain regions such as thalamus, dorsolateral, and medial prefrontal cortex as well as parietal regions (Schmaal et al., 2020). The lack of smaller HippSub volumes in MDD and BD might be due to the fact that the AFFDIS cohort recruited patients undergoing antidepressant therapy. As shown lately in a survey by Han et al. (2016), drug-naïve MDD patients revealed a pattern of smaller volumes in Sub, CA2-4, DG in comparison to healthy controls. On the other hand, other factors such as early-life stress, or rs1360780 polymorphism of the FKBP5 gene (referring to the hypothalamic-pituitary-adrenal axis) associated with some smaller HippSub volumes (Mikolas et al., 2019) might also have enabled variation in our sample (data not available). Genetic architecture with different genetic loci (Hibar et al., 2017) could have a major influence on disease-specific HippSub volumes, which might explain the absence of HippSub volume reduction observed in groups with mood disorders. In contrast to our findings, BD patients have also demonstrated reduced hippocampal CA1, GCL volumes (Han et al., 2019). Smaller volumes have been observed in the PreSub and Sub regions in a subgroup of BD patients (Janiri et al., 2019), an evidence to which our left PreSub findings, in contrast to aMCI, appear to be in line with. One factor that might explain why our BD patients revealed no major hippocampal volume reductions is that, differently from ours, their cohort was heterogeneous, and not characterized by a predominantly depressive subtype. Our results, however, support the findings from a recent investigation showing no smaller volumes in MDD patients via high-resolution 7-Tesla MRI (Tannous et al., 2020). As in this study only HippSub volumes and not shape alterations were assessed, therefore we cannot identify if HippSub deformations coinciding with

unaltered volumes were seen, as has been reported in MDD (Ballmaier et al., 2008; Cole et al., 2010).

Our findings suggest that depression's duration has a significant impact on left hippocampal volume, indicating that the time since first depressive episode plays an important role in hippocampal degeneration. This concurs with the knowledge that lower hippocampal volumes are associated with a poorer clinical outcome and more depressive episodes (Videbech and Ravnkilde, 2004; MacQueen and Frodl, 2011). However, when further exploring specific HippSub volumes, we observed no relationship between the duration since first depressive episode and HippSub volumes. Further studies with larger cohorts should be conducted to identify whether the duration since depressive manifestation affects HippSub volumes in a more relevant manner.

The limitations of our study concern the sample size of groups and subgroups, restricting additional conclusions in terms of clinical representation, applicability and neurobiological foundations. For instance, cognitive assessments comparable to DELCODE were not available in the AFFDIS cohort, with which we could have additionally investigated whether cognitive impairment across disorders relate to hippocampus or HippSub volume decline. A further potential limitation is the age difference between groups in both cohorts, with younger patients in the AFFDIS than the DELCODE cohort. Our analyses were controlled for age and eTIV (as covariates), but it would have been interesting to see if differences across patient groups would indeed hold when comparing older participants in mood disorder groups. Future studies addressing this aspect should also consider the potential risk of misclassifying participants with late-onset depression, since depressive episodes can be initial manifestations of neurodegeneration. However, as molecular markers have not yet been assessed in patients with affective disorders or in some patients with cognitive decline and possible AD, no general conclusions about the molecular mechanisms of neurodegeneration can be drawn for our patient groups. Cognitive decline in early-onset depression is usually not clinically associated with the neurodegenerative process, and it is often less severe (Jamieson et al., 2019) and affects specific cognitive subdomains such as language, memory, and cognitive flexibility, as recently reported (Ang et al., 2020). Thus, the manifestation age of depression is clinically relevant for the pattern and severity of cognitive decline, while also being a risk factor for later cognitive decline (Brzezińska et al., 2020). The increasing grade of severity in cognitive decline observed in late-onset compared to early-onset depression age might thus be accompanied by decreasing hippocampal and HippSub volumes.

In addition, our findings comprised cross-sectional structural imaging data and not longitudinal comparisons, through which more insight into intraindividual changes in HippSub volumes can be gained. Further studies combining functional data could better elucidate the significance of neuropathological processes in the HippSub for cognitive impairment. Lastly, potential influences of the treatment history on hippocampal and HippSub volumes could not be determined in the absence of comparable information across disorders.

Our study showed that hippocampus and HippSub volumes differ between cognitive decline due to possible AD and early-onset mood disorders. The left PreSub is a structure apparently affected in aMCI and AD subjects, but not in BD patients. This sheds new light into a possible marker differentiating correlates of neurodegeneration due to minor and major cognitive decline and BD. Conversely, we detected no relevant field and subfield volume decline in BD and MDD groups. Most strikingly, we found that the time since the first depressive episode was negatively associated with left hippocampal volume in all disorder groups. This time effect is a potentially important hallmark supporting hippocampal volume reduction as a continuum extending from mood disorders, and cognitive deterioration to AD. This finding may advance the comprehension of the relationship between depression and AD. The usage of sophisticated tools, such as machine learning, in identifying multivariate patterns in much larger groups should consider this feature.

DATA AVAILABILITY STATEMENT

The raw data supporting the conclusions of this article will be made available by the authors, without undue reservation.

ETHICS STATEMENT

The studies involving human participants were reviewed and approved by ethical committee's. The DELCODE study protocol was coordinated by the ethical committee of the medical faculty of the University of Bonn and approved by all participating sites ethical committees [Berlin (Charité, University Medicine), Bonn, Cologne, Göttingen, Magdeburg, Munich (Ludwig-Maximilians-University), Rostock, and Tübingen]. The AFFDIS study protocol was approved by the ethical committee of the medical faculty of the University of Goettingen. The patients/participants provided their written informed consent to participate in this study. Written informed consent was obtained from the individual(s) for the publication of any potentially identifiable images or data included in this article.

FINANCIAL DISCLOSURE STATEMENT

ASc got funding from Novartis, Diagnostik Netz BB (travel and speaker honoraria) and gained research support from German Federal Ministry of Research (BMBF), Actelion and Helmholtz Foundation Michael J Fox Foundation. CB received honoraria as a diagnostic consultant for Boehringer Ingelheim. DJ has obtained funding for travel from Pfizer GmbH. IK has obtained funding from the German ministry of economic cooperation and development. JP got research support for travel or speaker honoraria from Axon, CHDI, and UK DRI. He received research funding from DFG, BMBF, and UK DRI. JW has obtained research support from the Eli Lilly Advisory Board, Pfizer, MSD, and med Update GmbH (travel and speaker honoraria). He obtained research support from the BMBF. MH received funding for research support from the DFG. OP has obtained research support for travel or speaker honoraria from Schwabe. He has received funding from Eli Lilly,

Lundbeck, Genentech, Biogen, Roche, Pharmatrophix, Novartis, Janssen, and Probiodrug. ST has gained support (travel or speaker honoraria) from MSD Sharp and Dohme GmbH Quality circle for physicians in Kühlungsborn and research support from ROCHE, Roche Pharma AG, Lilly Deutschland GmbH, BMBF, and Ministry of Economics of the State Mecklenburg Western Pomerania.

AUTHOR CONTRIBUTIONS

RG-M designed the study. NH and RG-M wrote the manuscript. ASi, NH, and RG-M analyzed the data. AC, ASi, ASc, ASp, BE-W, CB, CM, DJ, ED, ES, FB, FJ, JH, JP, JW, KB, KF, KS, LD, MM, MT, MH, NR, OP, PD, RG-M, RV, and ST contributed to data collection. All authors critically revised the manuscript. All authors made significant intellectual contributions, reviewed, and accepted this work before submission.

ACKNOWLEDGMENTS

This work was promoted by the University Medical Center Göttingen (UMG) and the German Federal Ministry of Education and Research (Bundesministerium fuer Bildung und Forschung, BMBF: 01 ZX 1507, PreNeSt—e:Med). We thank Christine Werner, Sören Noack, Maria Keil, Tracy Erwin-Grabner, Vladimir Belov, and Esther Semmelhack for their contribution to data collection and organization.

REFERENCES

Ang, Y. S., Frontero, N., Belleau, E., and Pizzagalli, D. A. (2020). Disentangling vulnerability, state and trait features of neurocognitive impairments in depression. *Brain* 143, 3865–3877. doi: 10.1093/brain/awaa314

Ballmaier, M., Narr, K. L., Toga, A. W., Elderkin-Thompson, V., Thompson, P.M., Hamilton, L, et al. (2008). Hippocampal morphology and distinguishing late-onset from early-onset elderly depression. *Am. J. Psychiatry.* 165, 229–237. doi: 10.1176/appi.ajp.2007.07030506

Berridge, M. J. (2013). Dysregulation of neural calcium signaling in Alzheimer disease, bipolar disorder and schizophrenia. *Prion* 7, 2–13. doi: 10.4161/pri.21767

Brown, E. M., Pierce, M. E., Clark, D. C., Fischl, B. R., Iglesias, J. E., Milberg, W. P., et al. (2020). Test-retest reliability of FreeSurfer automated hippocampal subfield segmentation within and across scanners *Neuroimage* 210:116563. doi: 10.1016/j.neuroimage.2020.116563

Brzezińska, A., Bourke, J., Rivera-Hernández, R, Tsolaki, M., Wozniak, J., and Kazmierski, J. (2020). Depression in dementia or dementia in depression? systematic review of studies and hypotheses. *Curr. Alzheimer Res*. (2020) 17, 16–28. doi: 10.2174/1567205017666200217104114

Cao, B., Passos, I. C., Mwangi, B., Amaral-Silva, H., Tannous, J., and Wu, M. J. (2017). Hippocampal subfield volumes in mood disorders. *Mol. Psychiatry* 22, 1352–1358. doi: 10.1038/mp.2016.262

Carlesimo, G. A., Piras, F., Orfei, M. D., Iorio, M., Caltagirone, C., and Spalletta, G. (2015). Atrophy of presubiculum and subiculum is the earliest hippocampal anatomical marker of Alzheimer's disease. *Alzheimers Dement (Amst)*. 1, 24–32. doi: 10.1016/j.dadm.2014.12.001

Cole, J., Toga, A. W., Hojatkashani, C., Thompson, P., Costafreda, S. G., Cleare, A. J., et al. (2010). Subregional hippocampal deformations in major depressive disorder. *J. Affect. Disord*. 126, 272–277. doi: 10.1016/j.jad.2010.03.004

Dale, A. M., Fischl, B., and Sereno, M. I. (1999). Cortical surface-based analysis. I. Segmentation and surface reconstruction. *Neuroimage* 9, 179–194. doi: 10.1006/nimg.1998.0395

de Flores, R., La Joie, R., and Chételat, G. (2015). Structural imaging of hippocampal subfields in healthy aging and Alzheimer's disease. *Neuroscience* 309, 29–50. doi: 10.1016/j.neuroscience.2015.08.033

Donovan, N. J., Locascio, J. J., Marshall, G. A., Gatchel, J., Hanseeuw, B.J., Rentz, D. M., et al. (2018). Harvard aging brain study: longitudinal association of amyloid beta and anxious-depressive symptoms in cognitively normal older adults. *Am. J. Psychiatry* 175, 530–537. doi: 10.1176/appi.ajp.2017.17040442

Elvsåshagen, T., Zuzarte, P., Westlye, L. T., Bøen, E., Josefsen, D., Boye, B., et al. (2016). Dentate gyrus-cornu ammonis (CA) 4 volume is decreased and associated with depressive episodes and lipid peroxidation in bipolar II disorder: Longitudinal and cross-sectional analyses. *Bipolar Disord*. 18, 657–668. doi: 10.1111/bdi.12457

Enache, D., Winblad, B., and Aarsland, D. (2011). Depression in dementia: epidemiology, mechanisms, and treatmen. *Curr. Opin. Psychiatry* 24, 461–472. doi: 10.1097/YCO.0b013e32834bb9d4

Filho, G. B., de Souza Duran, F. L., Squarzoni, P., Coutinho, N. A. M., Rosa, P. G. P., Torralbo, L., et al. (2021). Hippocampal subregional volume changes in elders classified using positron emission tomography-based Alzheimer's biomarkers of β-amyloid deposition and neurodegeneration. *J. Neurosci. Res.* 99, 481–501. doi: 10.1002/jnr.24739

Fischl, B., Sereno, M.I., and Dale, A. M. (1999). Cortical surface-based analysis. II: Inflation, flattening, and a surface-based coordinate system. *Neuroimage* 9, 195–207. doi: 10.1006/nimg.1998.0396

Foo, H., Thalamuthu, A., Jiang, J, Koch, F, Mather, K. A., Wen, W., and Sachdev, P. S. (2020). Associations between Alzheimer's disease polygenic risk scores and hippocampal subfield volumes in 17,161 UK Biobank participants. *Neurobiol. Aging* 98, 108–115. doi: 10.1016/j.neurobiolaging.2020.11.002

Foster, C. M., Kennedy, K.M., Daugherty, A. M., and Rodrigue, K. M. (2020). Contribution of iron and Abeta to age differences in entorhinal and hippocampal subfield volume. *Neurology* 95, e2586–e2594. doi: 10.1212/WNL.0000000000010868

Garimella, A., Rajguru, S., Singla, U. K., and Alluri, V. (2020). Marijuana and the hippocampus: a longitudinal study on the effects of marijuana on hippocampal subfields. *Prog. Neuropsychopharmacol. Biol. Psychiatry* 101:109897. doi: 10.1016/j.pnpbp.2020.109897

Genzel, L., Dresler, M., Cornu, M., Jäger, E., Konrad, B., Adamczyk, M., et al. (2015). Medial prefrontal-hippocampal connectivity and motor memory consolidation in depression and schizophrenia. *Biol. Psychiatry* 77, 177–186. doi: 10.1016/j.biopsych.2014.06.004

Han, K. M., Kim, A., Kang, W., Kang, Y., Kang, J., Won, E., et al. (2019). Hippocampal subfield volumes in major depressive disorder and bipolar disorder. *Eur. Psychiatry* 57, 70–77. doi: 10.1016/j.eurpsy.2019.01.016

Han, K. M., Won, E., Sim, Y., and Tae, W. S. (2016). Hippocampal subfield analysis in medication-naïve female patients with major depressive disorder. *J. Affect. Disord*. 194, 21–29. doi: 10.1016/j.jad.2016.01.019

Hanseeuw, B. J., Van Leemput, K., Kavec, M., Grandin, C., Seron, X., and Ivanoiu, A. (2011). Mild cognitive impairment: differential atrophy in the hippocampal subfields. *AJNR Am. J. Neuroradiol.* 32, 1658–1661. doi: 10.3174/ajnr.A2589

Haukvik, U. K., Gurholt, T. P., Nerland, S., Elvsåshagen, T., Akudjedu, T. N., Alda, M., et al. (2020). *In vivo* hippocampal subfield volumes in bipolar disorder-A mega-analysis from the enhancing neuro imaging genetics through meta-analysis Bipolar Disorder Working Group. *Hum Brain Mapp*. (2020). doi: 10.1002/hbm.25249. [Epub ahead of print].

Heser, K., Tebarth, F., Wiese, B., Eisele, M., Bickel, H., Köhler, M., et al. (2013). Age of major depression onset, depressive symptoms, and risk for subsequent dementia: results of the German study on Ageing, Cognition, and Dementia in Primary Care Patients (AgeCoDe). *Psychol. Med.* 43, 1597–1610. doi: 10.1017/S0033291712002449

Hibar, D. P., Adams, H. H. H., Jahanshad, N., Chauhan, G., Stein, J. L., Hofer, E., et al. (2017). Novel genetic loci associated with hippocampal volume. *Nat. Commun.* 8:13624. doi: 10.1038/ncomms13624

Iglesias, J. E., Augustinack, J. C., Nguyen, K., Player, C. M., Player, A., Wright, M., et al. (2015). A computational atlas of the hippocampal formation using

ex vivo, ultra-high resolution MRI: Application to adaptive segmentation of *in vivo* MRI. *Neuroimage* 115, 117–137. doi: 10.1016/j.neuroimage.2015.04.042

Jack, C. R. Jr., Bennett, D. A., Blennow, K., Carrillo, M. C., Dunn, B., Haeberlein, S. B., et al. (2018). NIA-AA Research Framework: toward a biological definition of Alzheimer's disease. *Alzheimers Dement.* 14, 535–562. doi: 10.1016/j.jalz.2018.02.018

Jacobs, H. I. L., Augustinack, J. C., Schultz, A. P., Hanseeuw, B. J., Locascio, J., Amariglio, R. E., et al. (2020). The presubiculum links incipient amyloid and tau pathology to memory function in older persons. *Neurology* 94, e1916–e1928. doi: 10.1212/WNL.0000000000009362

Jamieson, A., Goodwill, A. M., Termine, M., Campbell, S., and Szoeke, C. (2019). Depression related cerebral pathology and its relationship with cognitive functioning: a systematic review. *J. Affect. Disord.* 250, 410–418. doi: 10.1016/j.jad.2019.03.042

Janiri, D., Sani, G., De Rossi, P., Piras, F., Banaj, N., Ciullo, V., et al. (2019). Hippocampal subfield volumes and childhood trauma in bipolar disorders. *J. Affect. Disord.* 253, 35–43. doi: 10.1016/j.jad.2019.04.071

Jessen, F., Amariglio, R. E., Buckley, R. F., van der Flier, W. M., Han, Y., Molinuevo, J. L., et al. (2020). The characterisation of subjective cognitive decline. *Lancet Neurol.* 19, 271–278. doi: 10.1016/S1474-4422(19)30368-0

Jessen, F., Amariglio, R. E., van Boxtel, M., Breteler, M., Ceccaldi, M., Chételat, G., et al. (2014). Subjective Cognitive Decline Initiative (SCD-I) Working Group: a conceptual framework for research on subjective cognitive decline in preclinical Alzheimer's disease. *Alzheimers Dement.* 10, 844–852. doi: 10.1016/j.jalz.2014.01.001

Jessen, F., Spottke, A., Boecker, H., Brosseron, F., Buerger, K., Catak, C., et al. (2018). Design and first baseline data of the DZNE multicenter observational study on predementia Alzheimer's disease (DELCODE). *Alzheimers Res. Ther.* 10:15. doi: 10.1186/s13195-017-0314-2

La Joie, R., Perrotin, A., de La Sayette, V., Egret, S., Doeuvre, L., Belliard, S., et al. (2013). Hippocampal subfield volumetry in mild cognitive impairment, Alzheimer's disease and semantic dementia. *Neuroimage Clin.* 14, 155–162. doi: 10.1016/j.nicl.2013.08.007

MacQueen, G., and Frodl, T. (2011). The hippocampus in major depression: evidence for the convergence of the bench and bedside in psychiatric research? *Mol. Psychiatry* (2011) 16, 252–264. doi: 10.1038/mp.2010.80

McKhann, G. M., Knopman, D. S., Chertkow, H., Hyman, B. T., Jack, C. R. Jr, Kawas, C. H., et al. (2011). The diagnosis of dementia due to Alzheimer's disease: recommendations from the National Institute on Aging-Alzheimer's Association workgroups on diagnostic guidelines for Alzheimer's disease. *Alzheimers Dement.* 7, 263–269. doi: 10.1016/j.jalz.2011.03.005

Mikolas, P., Tozzi, L., Doolin, K., Farrell, C., O'Keane, V., and Frodl, T. (2019). Effects of early life adversity and FKBP5 genotype on hippocampal subfields volume in major depression. *J. Affect. Disord.* 252, 152–159. doi: 10.1016/j.jad.2019.04.054

Rizzolo, L., Narbutas, J., Van Egroo, M., Chylinski, D., Besson, G., and Baillet, M. (2021). Relationship between brain AD biomarkers and episodic memory performance in healthy aging. *Brain Cogn.* 148:105680. doi: 10.1016/j.bandc.2020.105680

Schmaal, L., Pozzi, E., Ho, T. C., van Velzen, L.S., Veer, I. M., Opel, N., et al. (2020). ENIGMA MDD: seven years of global neuroimaging studies of major depression through worldwide data sharing. *Transl. Psych.* 10:172. doi: 10.1038/s41398-020-0842-6

Schmaal, L., Veltman, D. J., van Erp, T. G., Sämann, P. G., Frodl, T., Jahanshad, N., et al. (2016). Subcortical brain alterations in major depressive disorder: findings from the ENIGMA Major Depressive Disorder working group. *Mol. Psychiatry* 21, 806–812. doi: 10.1038/mp.2015.69

Singh-Manoux, A., Dugravot, A., Fournier, A., Abell, J., Ebmeier, K., Kivimäki, M., et al. (2017). Trajectories of depressive symptoms before diagnosis of dementia: a 28-year follow-up study. *JAMA Psychiatry* 74, 712–718. doi: 10.1001/jamapsychiatry.2017.0660

Szymkowicz, S. M., McLaren, M. E., O'Shea, A., Woods, A. J., Anton, S. D., and Dotson, V. M. (2017). Depressive symptoms modify age effects on hippocampal subfields in older adults. *Geriatr. Gerontol. Int.* 17, 1494–1500. doi: 10.1111/ggi.12901

Tannous, J., Godlewska, B. R., Tirumalaraju, V., Soares, J. C., Cowen, P. J., and Selvaraj, S. (2020). Stress, inflammation and hippocampal subfields in depression: a 7 Tesla MRI Study. *Transl. Psychiatry* 10:78. doi: 10.1038/s41398-020-0759-0

Tardif, C. L., Devenyi, G. A., Amaral, R. S. C., Pelleieux, S., Poirier, J., Rosa-Neto, P., et al. (2018). Regionally specific changes in hippocampal circuity accompany progression of cerebrospinal fluid biomarkers in preclinical Alzheimer's disease. *Hum. Brain Mapp.* 39, 971–984. doi: 10.1002/hbm.23897

Treadway, M. T., Waskom, M. L., Dillon, D. G., Holmes, A. J., Park, M. T. M., Chakravarty, M. M., et al. (2015). Illness progression, recent stress, and morphometry of hippocampal subfields and medial prefrontal cortex in major depression. *Biol. Psychiatry* 77, 285–294. doi: 10.1016/j.biopsych.2014.06.018

Videbech, P., and Ravnkilde, B. (2004). Hippocampal volume and depression: a meta-analysis of MRI studies. *Am. J. Psychiatry* 161, 1957–1966. doi: 10.1176/appi.ajp.161.11.1957

Wang, S. Y., Xue, X., Duan, R., Gong, P. Y., Jiang, T., Zhang, Y. D., et al. (2020). A TREML2 missense variant influences specific hippocampal subfield volumes in cognitively normal elderly subjects. *Brain Behav.* 10:e01573. doi: 10.1002/brb3.1573

Weissman, D. G., Lambert, H. K., Rodman, A.M., Peverill, M., Sheridan, M. A., and McLaughlin, K. A. (2020). Reduced hippocampal and amygdala volume as a mechanism underlying stress sensitization to depression following childhood trauma. *Depress Anxiety.* 37, 916–925. doi: 10.1002/da.23062

Whelan, C. D., Hibar, D. P., van Velzen, L. S., Zannas, A. S., Carrillo-Roa, T., McMahon, K., et al. (2016). Heritability and reliability of automatically segmented human hippocampal formation subregions. *Neuroimage* 128, 125–137. doi: 10.1016/j.neuroimage.2015.12.039

Xu, J., Tang, Y., Baro, C. C., Zhang, X., Meng, Z., and Li, Y. (2018). Left fimbria atrophy is associated with hippocampal metabolism in female major depressive disorder patients. *Annu. Int. Conf. IEEE Eng. Med. Biol. Soc.* 2018, 1136–1139. doi: 10.1109/EMBC.2018.8512472

Xu, R., Hu, X., Jiang, X., Zhang, Y., Wang, J., and Zeng, X. (2020). Longitudinal volume changes of hippocampal subfields and cognitive decline in Parkinson's disease. *Quant. Imaging Med. Surg.* 10, 220–232. doi: 10.21037/qims.2019.10.17

Yuan, M., Rubin-Falcone, H., Lin, X., Rizk, M. M., Miller, J. M., Sublette, M. E., et al. (2020). Smaller left hippocampal subfield CA1 volume is associated with reported childhood physical and/or sexual abuse in major depression: a pilot study. *J. Affect. Disord.* 272, 348–354. doi: 10.1016/j.jad.2020.03.169

Zhao, W., Wang, X., Yin, C., He, M., Li, S., and Han, Y. (2019). Trajectories of the hippocampal subfields atrophy in the Alzheimer's disease: a structural imaging study. *Front. Neuroinform.* 13:1. doi: 10.3389/fninf.2019.00013

Conflict of Interest: The authors declare that the research was conducted in the absence of any commercial or financial relationships that could be construed as a potential conflict of interest.

frontiers in Aging Neuroscience

ORIGINAL RESEARCH
published: 07 June 2021
doi: 10.3389/fnagi.2021.631587

The Significance of EEG Alpha Oscillation Spectral Power and Beta Oscillation Phase Synchronization for Diagnosing Probable Alzheimer Disease

Haifeng Zhang[1,2,3†], Xinling Geng[4†], Yuanyuan Wang[2], Yanjun Guo[5], Ya Gao[6], Shouzi Zhang[7], Wenjin Du[8], Lixin Liu[7], Mingyan Sun[9], Fubin Jiao[1,2,3], Fang Yi[2,10], Xiaoli Li[11*] and Luning Wang[1,2*]*

[1] Medical School of Chinese People's Liberation Army, Beijing, China, [2] Department of Neurology, The 2nd Medical Center, National Clinical Research Center for Geriatric Disease, Chinese People's Liberation Army General Hospital, Beijing, China, [3] Health Service Department of the Guard Bureau of the Joint Staff Department, Joint Staff of the Central Military Commission of Chinese PLA, Beijing, China, [4] School of Biomedical Engineering, Capital Medical University, Beijing, China, [5] Department of Neurology, Beijing Tongren Hospital, Capital Medical University, Beijing, China, [6] Department of Geriatrics, The Second Hospital of Hebei Medical University, Shijiazhuang, China, [7] The Psycho Department of Beijing Geriatric Hospital, Beijing, China, [8] Department of Neurology, Air Force Medical Center, Chinese People's Liberation Army, Beijing, China, [9] Ninth Health Care Department of the Second Medical Center of PLA General Hospital, Beijing, China, [10] Department of Neurology, Lishilu Outpatient, Jingzhong Medical District, Chinese People's Liberation Army General Hospital, Beijing, China, [11] State Key Laboratory of Cognitive Neuroscience and Learning, Beijing Normal University, Beijing, China

OPEN ACCESS

Edited by:
Rong Chen, University of Maryland, Baltimore, United States

Reviewed by:
Görsev Yener, Izmir Biomedicine and Genome Center, Dokuz Eylul University, Turkey
Yang Jiang, College of Medicine, University of Kentucky, United States

***Correspondence:**
Fang Yi
yifang211@163.com
Xiaoli Li
xiaoli@bnu.edu.cn
Luning Wang
luning_w@126.com

[†] *These authors have contributed equally to this work*

Received: 20 November 2020
Accepted: 11 May 2021
Published: 07 June 2021

Citation:
Zhang H, Geng X, Wang Y, Guo Y, Gao Y, Zhang S, Du W, Liu L, Sun M, Jiao F, Yi F, Li X and Wang L (2021) The Significance of EEG Alpha Oscillation Spectral Power and Beta Oscillation Phase Synchronization for Diagnosing Probable Alzheimer Disease. Front. Aging Neurosci. 13:631587. doi: 10.3389/fnagi.2021.631587

Alzheimer disease (AD) is the most common cause of dementia in geriatric population. At present, no effective treatments exist to reverse the progress of AD, however, early diagnosis and intervention might delay its progression. The search for biomarkers with good safety, repeatable detection, reliable sensitivity and community application is necessary for AD screening and early diagnosis and timely intervention. Electroencephalogram (EEG) examination is a non-invasive, quantitative, reproducible, and cost-effective technique which is suitable for screening large population for possible AD. The power spectrum, complexity and synchronization characteristics of EEG waveforms in AD patients have distinct deviation from normal elderly, indicating these EEG features can be a promising candidate biomarker of AD. However, current reported deviation results are inconsistent, possibly due to multiple factors such as diagnostic criteria, sample sizes and the use of different computational measures. In this study, we collected two neurological tests scores (MMSE and MoCA) and the resting-state EEG of 30 normal control elderly subjects (NC group) and 30 probable AD patients confirmed by Pittsburgh compound B positron emission tomography (PiB-PET) inspection (AD group). We calculated the power spectrum, spectral entropy and phase synchronization index features of these two groups' EEG at left/right frontal, temporal, central and occipital brain regions in 4 frequency bands: δ oscillation (1–4 Hz), θ oscillation (4–8 Hz), α

oscillation (8–13 Hz), and β oscillation (13–30 Hz). In most brain areas, we found that the AD group had significant differences compared to NC group: (1) decreased α oscillation power and increased θ oscillation power; (2) decreased spectral entropy in α oscillation and elevated spectral entropy in β oscillation; and (3) decrease phase synchronization index in δ, θ, and β oscillation. We also found that α oscillation spectral power and β oscillation phase synchronization index correlated well with the MMSE/MoCA test scores in AD groups. Our study suggests that these two EEG features might be useful metrics for population screening of probable AD patients.

Keywords: Alzheimer disease, electroencephalogram (EEG), power spectrum, spectral entropy (SE), phase synchronization index

INTRODUCTION

Alzheimer disease (AD) is the most common cause of dementia, accounting for an estimated 60–80% of cases (Garre-Olmo, 2018). It is characterized by progressive decline in memory, language function, orientation, and executive function, etc. AD is a continuous disease process, divided into preclinical, prodromal, and overt dementia (Babiloni et al., 2020a). Besides seriously affecting patients' own quality of life, AD also brings heavy economic and psychological burdens to family members and caregivers, and has become one of the serious public health problems. The exact pathogenesis of AD is unclear yet; its related pathological hypotheses may involve synapse damage and loss, amyloid plaques and neurofibrillary tangles (Colom-Cadena et al., 2020). The pathophysiological process of AD is thought to start up to 20 years before clinical symptoms can be detectable (Sperling et al., 2014). At present, no effective medication exist for curing this pathology and reversing the course of AD (Cassani et al., 2018). Current therapeutic treatments at the early stage might improve the symptoms and delay the evolution of the disease (Houmani et al., 2018). Therefore, early diagnosis and active intervention are of great significance for mitigating the epidemic.

Current diagnosis of AD usually depends on the biomarkers in cerebrospinal fluid (CSF), neuropsychological tests, and neuroimaging, neurophysiological examinations (Maestu et al., 2019). The CSF biomarker like amyloid-β (Aβ) or tau protein level has high sensitivity and specificity in diagnosing probable AD (Lim et al., 2016). But the CSF biomarker is obtained from invasive lumber puncture operation, which is not easy to be accepted by patients and their families. Neuroimaging biomarker like the Pittsburgh compound B positron emission tomography (PiB-PET) inspection is highly specific in detecting the accumulation of in vivo amyloid-β, making it almost comparable to the golden standard of autopsy (Cohen et al., 2019). However, the PET inspection is very expensive, and it requires complex hardware equipment, inspection environment, and repeat exposure to radiation. Therefore, the above-mentioned two well-established biomarkers are not suitable for large-scale population screening. On the other hand, the neuropsychological test like the Mini-Mental Status Exam (MMSE) and Montreal Cognitive Assessment (MoCA) is easy to perform and can quickly evaluate a patient's cognitive function. Therefore, these neurological tests are frequently used in clinical practice for screening large populations of possible AD. However, performing these tests is time-consuming, requires well-cooperated subjects and experienced clinicians (Cassani et al., 2018). Even though, the test scores are very subjective, and usually affected by the educational background of subjects.

As a non-invasive, cost-effective electrophysiological examination technique, electroencephalogram (EEG) can directly record the neural activity in different brain states. It can objectively and quantitatively reflect the neurological changes in pathological conditions with high time resolution, although its spatial resolution is lower than neuroimaging devices like magnetic resonance imaging (MRI). EEG has been widely used in the study of various neurological diseases including AD. Recently, Babiloni and many researchers have proposed an international initiative to include the use of EEG/MEG biomarkers in the regulatory requirements and guidelines for AD studies (Babiloni et al., 2020a). A variety of quantitative analysis techniques was used to characterize the EEG changes, looking for EEG biomarkers suitable for AD diagnosis. Compared to normal elderly, the resting state EEG activity in AD patients diffusely slows down, usually manifested by a decrease in the spectral power of the high frequency (α and/or β) oscillations and an increase of spectral power of low frequency (θ and/or δ) oscillations (Jeong, 2004; Cassani et al., 2018; Horvath et al., 2018; Babiloni et al., 2020a; Benwell et al., 2020; Wicki et al., 2021). Besides, AD is also characterized as a brain disconnection syndrome (Delbeuck et al., 2003). The synchronization of EEG activity is usually perturbed in AD patients, especially demonstrated by the decreased functional connectivity in different brain areas (Cassani et al., 2018; Musaeus et al., 2019a,b; Nunez et al., 2019; Song et al., 2019; Briels et al., 2020). Furthermore, the decline in the structure and functional connection of the brain may lead to a reduction in the complexity of EEG signals in AD patients, as reported in Azami et al. (2017), Deng et al. (2017), Kulkarni (2017), Simons and Abásolo (2017), Al-Nuaimi et al. (2018), Cassani et al. (2018), Horvath et al. (2018), Li et al. (2018), Simons et al. (2018). However, with respect to specific EEG frequency bands, current studies usually have inconsistent results, possibly due to multiple factors such as the severity level of disease, educational background of subjects, diagnostic criteria, sample sizes and the use of different computational measures (Briels et al., 2020). For example,

Babiloni et al. found that subjective memory complaint seniors with AD neuropathology (amyloid PET-positive) and high education attainment showed higher temporal α3 power density and lower posterior α2 power density, suggesting that preclinical Alzheimer's neuropathology may interact with education attainment (Babiloni et al., 2020b). Gaubert and colleagues found an increase in high frequency oscillations (higher β and γ power) and a decrease in low frequency oscillations (lower δ power), higher spectral entropy, higher complexity and increased functional connectivity in θ band in the frontocentral regions in preclinical AD patients (Gaubert et al., 2019). They found a nonlinear relationship between amyloid burden and EEG metrics in neurodegeneration positive subjects, suggesting the EEG patterns are modulated differently depending on the degree of amyloid burden. Briels and colleagues also found that the choice of functional connectivity measures and frequency bands can have a large impact on the outcome of EEG studies in AD. Their results showed that the corrected amplitude envelope correlation are reproducible in the α and β bands, and phase-based measures with correction for volume conduction showed reproducible effects in the θ band (Briels et al., 2020).

Considering the above inconsistent results, in this study we try to find significant and reliable EEG biomarkers for AD diagnosis. We collected 30 probable AD patients confirmed by PiB-PET inspection (AD group) with a wide neurological tests scores (MMSE and MoCA) range, resulting an AD population with great varieties of impaired cognitive functions. We calculated the power spectrum, spectral entropy and phase synchronization index metrics of their resting-state EEG in four frequency bands, and compared these metrics with that of 30 normal controlled elderly subjects (NC group). To investigate whether these EEG metrics could reflect the impaired cognitive functions in AD groups, we further calculated the correlation of these EEG metrics with the MMSE and MoCA test scores.

MATERIALS AND METHODS

Participants

In this study, patients who were diagnosed clinically as probable AD were screened for inclusion from the outpatients in the Department of Neurology, the Second Medical Center of Chinese People's Liberation Army General Hospital from 2016 to 2019. All patients in AD group meet the core criteria for probable AD diagnosis developed by the National Institute of Aging and the Alzheimer's Disease Society (NIA-AA) in 2011 (McKhann et al., 2011). Besides, they all underwent the PiB-PET neuroimaging test and their results are all positive. At the same time, their family members and volunteers who matched their gender, age and education level were selected as normal controls (NC).

Thirty AD patients and 30 NC subjects were evaluated by two or more senior neurological physicians and were included in this study. The studies involving human participants were reviewed and approved by the Medical Ethics Committee of Chinese People's Liberation Army General Hospital. The patients/participants provided their written informed consent to participate in this study.

EEG Acquisition and Processing

EEG Acquisition

The EEG data acquisition of all the participants was completed in the fixed clinic of the Department of Neurology, Chinese People's Liberation Army General Hospital. Before the test, the subjects were asked whether they took food or beverages containing stimulants such as nicotine, caffeine, and alcohol on the day, and the non-users were checked after washing their hair.

Participants sat in a comfortable chair, kept quiet and relaxed, and kept their bodies as motionless as possible to reduce artifacts. Because the EEG data collected when the eyes are open has more eye movement artifacts, the previous literature mostly uses the EEG data when the eyes are closed for research. Therefore, this study only records the resting state EEG data when the eyes are closed. The recording time is 5 min.

The EEG detection equipment used is a portable 8-channel high-performance EEG signal acquisition instrument (JL-EEG8w), developed by the State Key Laboratory of Cognition and Learning of Beijing Normal University, which is designed for quick EEG examination from outpatients who usually have very limited time at the clinic. The bandwidth of the EEG amplifier is 0.1–80 Hz with a sampling frequency of 1,000 Hz. According to the 10–20 international standard electrode system, 8 electrode position is used, i.e., F3, F4, T3, T4, C3, C4, O1, and O2. The reference electrode is in Cz, and the ground electrode is in Fpz (**Figure 1**). There is no parietal electrode used due to the recording device's limitation. The impedance of each active electrode is controlled below 100 kΩ before the start of recording EEG, and further checked after finishing recording. The data is saved in EDF format for subsequent offline analysis.

EEG Data Preprocessing

Several conventional preprocessing steps are taken following the recommendations from the OHBM COBIDAS MEEG committee (Pernet et al., 2020). Firstly, the recorded EEG data is bandpass filtered to 0.5–45 Hz, using the eegfiltfft function in EEGLab toolbox. Next, the continuous filtered data of each channel is divided into 4 s epoch. Then, for each epoch, the automatic artifact detection algorithm is applied to remove eye movement, breathing, EMG, 50 Hz power supply interference and outlier data segments, according to Durka et al. (2003). Finally, the remaining data epochs are manually checked to remove data segments that are not automatically eliminated with big artifacts or drowsy characteristics. The first 30 segments without artifacts (30×4 s = 120 s) of each channel of the participants were selected for analysis.

Relative Spectral Power of EEG

As mentioned in the above preprocessing section, the EEG signal has been divided into 30 epochs of 4 s data segment. We further reduce the sampling rate to 250 Hz, so that there are 1,000 points of EEG samples in each epoch. A Hamming window of 125 points (0.5 s) is used to slide over each piece of data in a step of 50 points (0.2 s). The Fourier transform of 1024 points is calculated to obtain the estimated power spectrum of each piece of data. The frequency resolution is about 0.25 Hz ($\Delta f = Fs/Nfft = 250/1,024$).

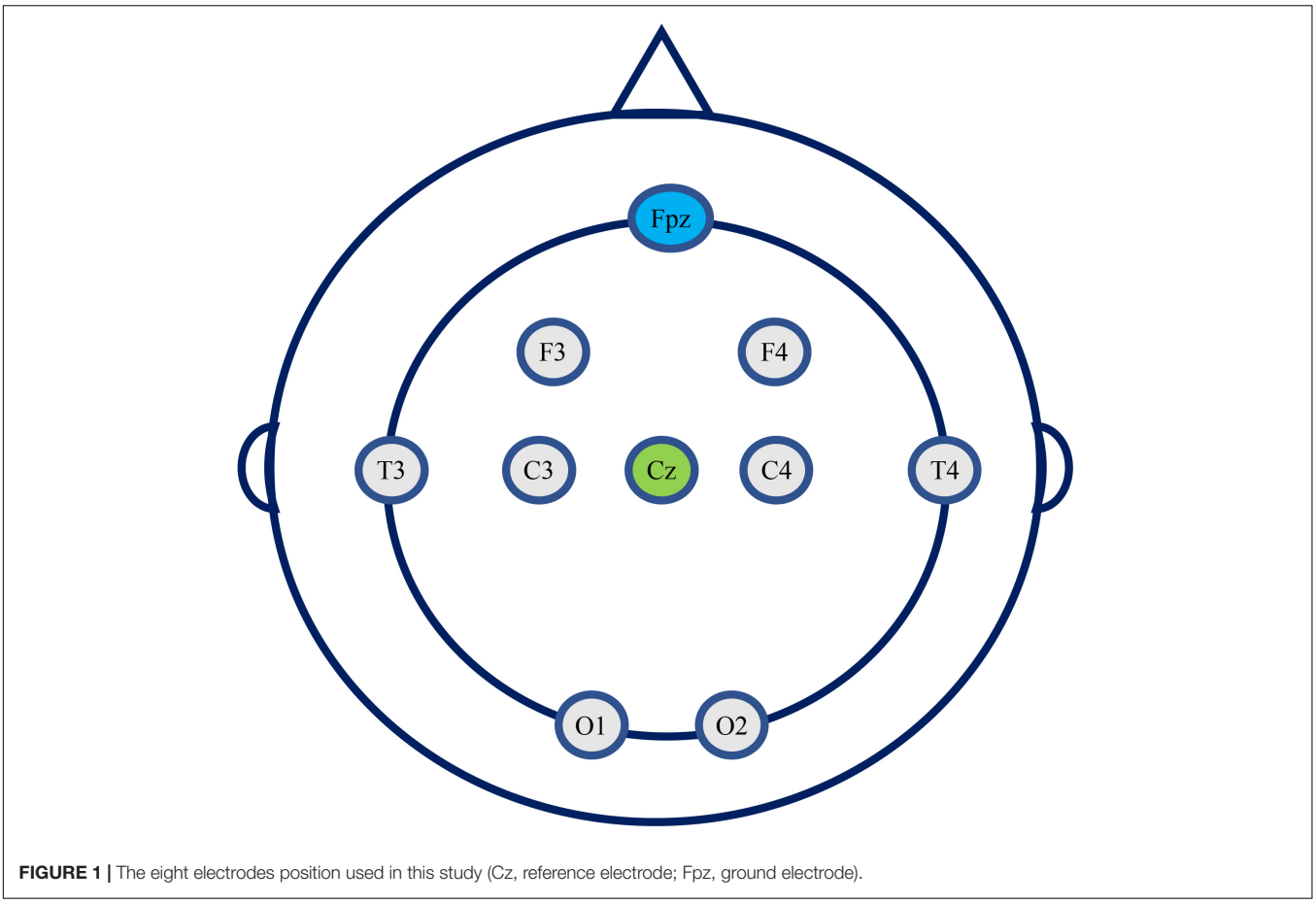

FIGURE 1 | The eight electrodes position used in this study (Cz, reference electrode; Fpz, ground electrode).

Then, the power spectrum estimates calculated for all 30 epochs are averaged, and the absolute powers are calculated in the following 4 canonical frequency bands: δ oscillation (1–4 Hz), θ oscillation (4–8 Hz), α oscillation (8–13 Hz), and β oscillation (13–30 Hz). In this study, we did not consider the γ oscillation as this frequency band EEG is easily contaminated by muscle artifacts.

Since the absolute power varies greatly among individual subjects, we further calculated the relative power of each oscillation for comparison between groups. Use the sum of the power in the frequency range of 1–45 Hz as the normalization factor, and define the ratio of each oscillation's absolute powers to the normalization factor as the relative power of that oscillation. The pwelch function in Matlab software is used to estimate the power spectral density.

Spectral Entropy of EEG

In addition to the power spectrum characteristics of EEG signals, the complexity of EEG signals is also an important parameter reflecting the characteristics of EEG. EEG signals are generally considered to be a chaotic signal between random and deterministic signals. Entropy values can be used to quantitatively describe the uncertainty of EEG signals.

Spectral entropy refers to the degree of uncertainty of the signal power spectrum distribution. It regards the normalized power distribution of a signal in the frequency domain as a probability distribution, and then calculates its information entropy. For a signal x(n), its power spectrum is represented by S(ω), and the probability distribution p(ω) of the spectrum is defined as (Wang et al., 2015):

$$p(\omega) = \frac{S(\omega)}{\sum_i S(i)} \tag{1}$$

Then the spectral entropy H is defined as:

$$H = -\sum_{\omega=1}^{N} p(\omega) \log_2 p(\omega) \tag{2}$$

Here N is the total frequency point. Normalized spectral entropy is usually used and is defined as:

$$H_n = -\frac{\sum_{m=1}^{N} P(m) log_2 P(m)}{log_2 N} \tag{3}$$

Here the denominator $\log_2 N$ represents the maximum spectral entropy of white noise evenly distributed in the frequency domain. The higher the spectral entropy of a signal, the more disordered (complex) the signal is. Conversely, the lower the spectral entropy, the more ordered (simple) the signal is.

In this study, the 8-s data sampled at 250 Hz is taken as one segment. There are a total of 15 segments. Calculate the spectral entropy in δ, θ, α, and β oscillation, and the frequency sampling points are 1,024 points. Then average the spectral entropy at each oscillation calculated from 15 data segments to obtain the spectral entropy value of each subject at each channel.

Phase Synchronization Index of EEG

Because brain information transmission needs to integrate the functions of various regions and the cooperation of neurons in multiple brain regions, the EEG in many diseases like AD are manifested as abnormal synchrony or connectivity between neurons in different brain regions. According to Dauwels et al. (2010), many of those synchronization measures are strongly correlated (or anti-correlated) with the correlation coefficient, providing little complementary information about EEG synchrony. While the phase synchrony indices are one of the metrics that are weakly correlated with the correlation coefficient, hence, it may capture a specific kind of interdependence of the EEG time series. The instantaneous phase φ_x of an EEG signal x is extracted as follows (Dauwels et al., 2010):

$$\varphi_x(k) = \arg[x(k) + i\tilde{x}(k)] \quad (4)$$

where $\tilde{x}$ is the Hilbert transform of x. The phase synchronization index is defined as:

$$\gamma = \left|\left\langle e^{i(n\varphi_x - m\varphi_y)}\right\rangle\right| \quad (5)$$

where n and m are integers, $\langle\cdot\rangle$ denotes time average. If γ tends to 1 in the above formula, the two signals are in phase synchronization, and if γ tends to 0, the phase difference of the two signals is randomly distributed.

In this study, phase synchronization index was used to investigate the connectivity difference in EEG signals between AD and NC groups. After pre-processing, the data is resampled to 250 Hz and divided into 4-s epochs. One-second Hamming window is used, with a 0.5-second sliding steps. The phase synchronization index of δ, θ, α, and β oscillation of each subject's EEG is calculated.

Neuropsychological Scale Evaluation

Two senior neurological physicians used MMSE and MoCA to evaluate the participants' cognitive functions. The test environment was quiet and the test scale versions were uniform. Among 60 participants, three AD patients and 7 NC subjects failed to complete MMSE/MoCA assessment because of noncooperation.

Statistical Analysis

Two-sample t-test was used to compare the age differences between AD and NC groups. Chi-square test was used to compare their gender differences. Using a two-sample t-test with false discovery rate (FDR) correction, the differences in the relative power, spectral entropy and phase synchronization index in δ, θ, α, and β oscillation of EEG signals between AD patients and NC subjects are compared. Further, in the AD patient group, Spearman correlation analysis with FDR correction was used to calculate the correlation between EEG metrics and the degree of cognitive impairment (2 neuropsychological evaluation scores). Subject's age was used as a control factor to eliminate its effect on the results. $P < 0.05$ was considered statistically significant.

RESULTS

Demographic Information and Neuropsychological Test Comparisons Between AD and NC Groups

As shown in **Table 1**, there was no statistical difference in age and gender between the AD and NC groups ($P > 0.05$), and there were statistically significant differences in the neuropsychological evaluation results ($P < 0.001$). The MMSE and MoCA scores in AD group were significantly lower than those in the NC group.

Sex Differences of EEG Metrics in AD or NC Groups

To evaluation the sex differences in each group, we further compared the relative spectral power, spectral entropy and phase synchronization indices between female (n = 18) and male (n = 12) participants in AD or NC groups. Two-sample t-test with FDR correction was used for the comparison. Results were shown in the **Supplementary Materials** (**Supplementary Figure 1**).

Differences of EEG Metrics Between AD and NC Groups

Relative Spectral Power

The comparison of the relative power of each oscillation at each electrode in the AD and NC groups is shown in **Figure 2**. The relative power of the slow wave oscillation (δ and θ oscillation) at each electrode in the AD group is higher than that in the NC group, and the relative power of fast-wave oscillation (α and β oscillation) at each electrode is lower than that in the NC group, suggesting that the relative power of EEG in AD patients is widely changed compared with NC subjects. Specifically, the relative spectral power of α oscillation at all electrodes and θ oscillation at seven electrodes (F3, T3, T4, C3, C4, O1, and O2) has significant difference, suggesting a diffuse slowing effect of the EEG spectrum in AD patients.

Spectral Entropy

In **Figure 3**, we show the comparison of the spectral entropy of each oscillation at each electrode of the EEG in AD and NC groups. For the α oscillation, the spectral entropy in the frontal, temporal and central regions of the AD

TABLE 1 | Participants demographic information.

	AD (n = 30)	NC (n = 30)	P value
Age(year)	68.83 ± 10.18	64.43 ± 10.55	0.106
Male : Female	12:18	12:18	0.879
MMSE[a]	12.89 ± 9.98	29.39 ± 0.89	0.000
MoCA[a]	10.48 ± 7.90	28.22 ± 1.98	0.000

[a]*Three AD patients and 7 NC subjects failed to complete MMSE/MoCA assessment.*

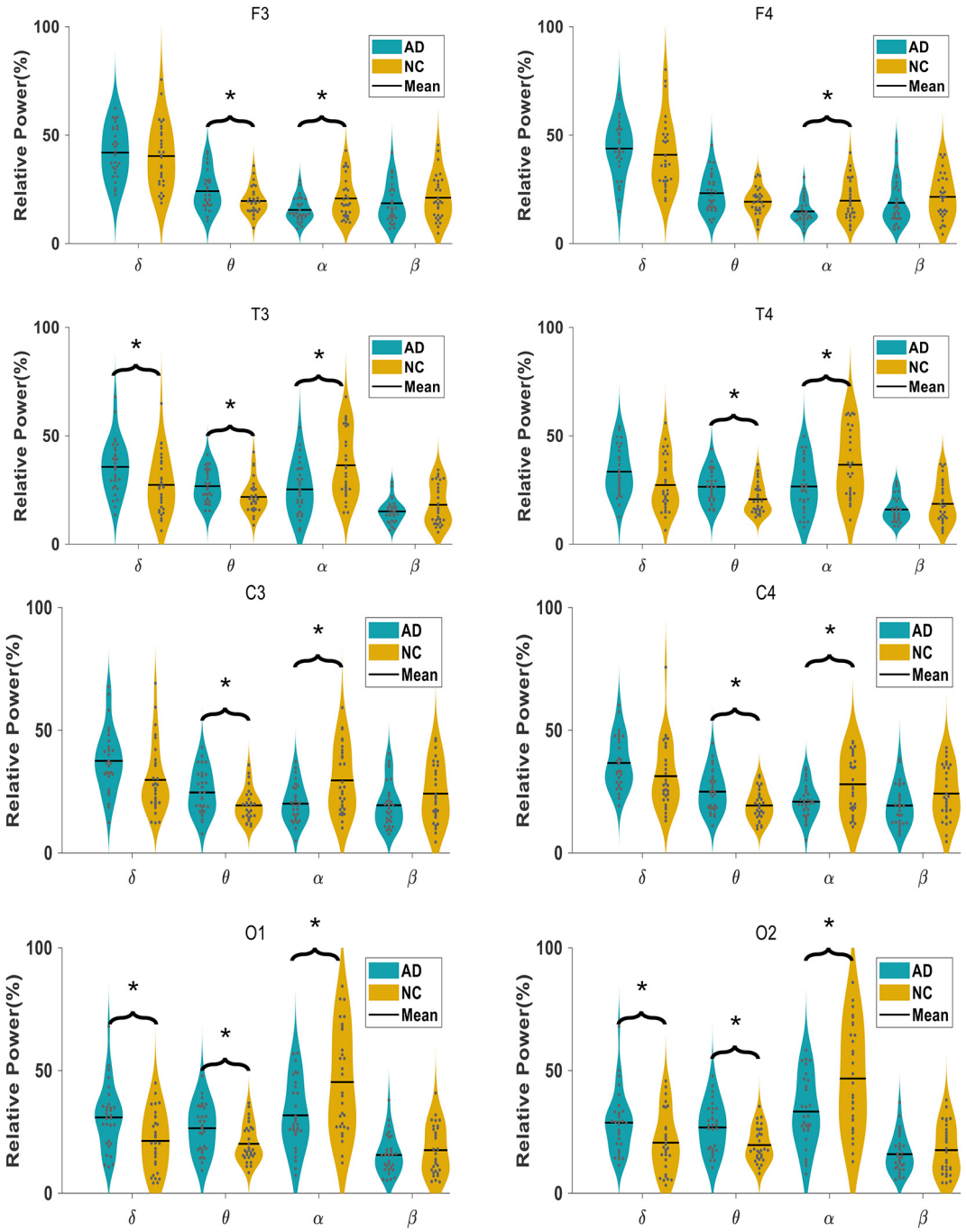

FIGURE 2 | Comparison of relative spectral power in AD and NC group at each electrode in four frequency bands.

group is significantly decreased compared to NC group, while in the occipital electrodes the spectral entropy has no significant difference between groups. For the β oscillation, the spectral entropy in the temporal, central and occipital regions of the AD group is significantly higher than that of the NC group, but in the frontal area the spectral entropy has no significant difference between groups. The spectral entropy of the θ oscillation in the occipital areas of AD group was higher than that of the NC group. However, the spectral entropy in the δ oscillation does not show statistical difference between groups.

Phase Synchronization Index

The phase synchronization comparison of each oscillation (δ, θ, α, and β) at each electrode pairs in the AD and NC groups is shown in **Figure 4**. The phase synchronization in AD group

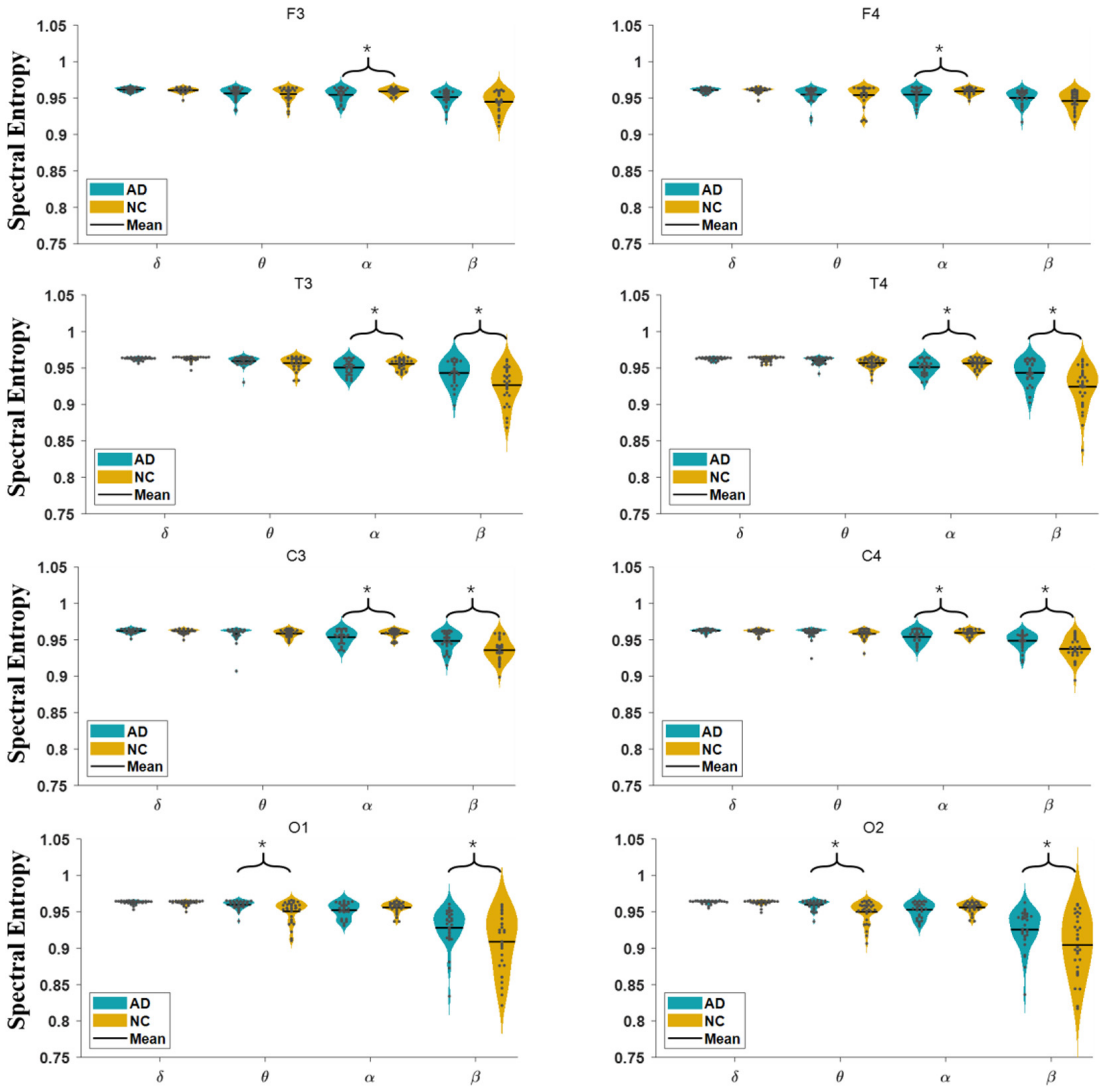

FIGURE 3 | Comparison of spectral entropy in AD and NC group at each electrode in four frequency bands.

is significantly lower than that of the NC group, specifically in frontal and temporal related areas in δ, θ, and β oscillations. While for α oscillation, the phase synchronization index of AD groups in most areas (apart from T3 and C4 electrode pairs) does not show statistical significance.

Association Between EEG Metrics and Neuropsychological Test Scores in AD Group

The Spearman correlation analysis with FDR correction was performed to investigate whether these EEG metrics could reflect the impaired cognitive functions in AD patients. Here we only demonstrate the association between EEG metrics and neuropsychological test scores in AD group. The neuropsychological tests and EEG correlation analysis in NC group and in both groups is listed in **Supplementary Materials** (**Supplementary Tables 1–6**).

Association Between Relative Spectral Power and MMSE/MoCA Scores

The correlation analysis between relative spectral power of each oscillation at each electrode of the EEG and the neuropsychological test scores in AD groups were calculated. As shown in **Table 2**, the relative power of δ and θ oscillations in AD patients is negatively correlated with the MMSE score, while the relative power of α and β oscillations is positively correlated with the MMSE score. Among them, the correlation of the relative power of α oscillation at bilateral frontal and central electrodes and the MMSE score is beyond statistical significance. The correlation between the power of each oscillation and the MoCA score has similar trend. The relative power of α oscillation

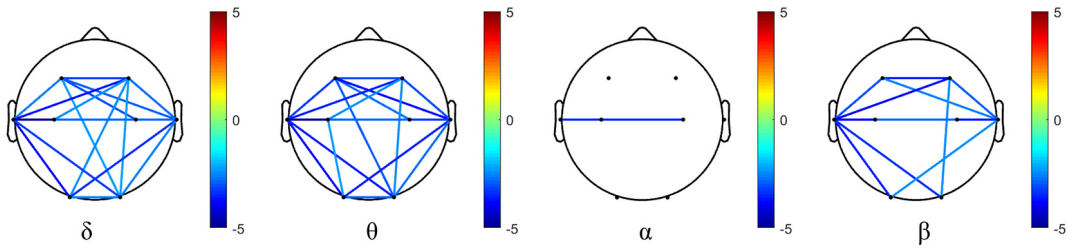

FIGURE 4 | Differences of phase synchronization indices between AD and NC group in four frequency bands. Values beyond statistical significance after FDR correction is demonstrated, and the color bar denotes the *t*-value.

TABLE 2 | Relationship between relative spectral power and MMSE/MoCA scores.

Electrode Position	MMSE				MoCA			
	ρ_{δ_power}	ρ_{θ_power}	ρ_{α_power}	ρ_{β_power}	ρ_{δ_power}	ρ_{θ_power}	ρ_{α_power}	ρ_{β_power}
F3	0.0376	–0.3085	0.3736	0.2806	0.0523	–0.2197	0.4711	0.2207
F4	–0.1044	–0.2596	0.3267	0.4013	–0.0886	–0.1642	0.4369	0.3361
T3	–0.2575	–0.1636	0.6540** 0.1698	–0.2813	–0.2107	0.7103** 0.2199		
T4	–0.2596	–0.4019	0.5671* 0.4610	–0.2704	–0.3270	0.5871* 0.3999		
C3	–0.1034	–0.4856	0.5972* 0.3485	–0.0667	–0.4643	0.6320** 0.2894		
C4	–0.2275	–0.3480	0.5753* 0.0229	–0.2838	–0.3685	0.6470** 0.0838		
O1	–0.3660	–0.3205	0.4334	0.3962	–0.3380	–0.3951	0.4722	0.4280
O2	–0.4541	–0.2908	0.4717	0.3719	–0.3953* –0.3696	0.5315* 0.3902		

*$P < 0.05$; **$P < 0.01$.

at bilateral frontal-central and right occipital electrodes is significantly positively correlated with the MoCA score.

Association Between Spectral Entropy and MMSE/MoCA Scores

We examined the correlation between δ, θ, α, and β oscillation spectrum entropy and the degree of cognitive impairment in the AD group. As shown in **Table 3**, the spectral entropy does not exhibit significant correlation to the MMSE and MoCA scores.

Association Between Phase Synchronization and MMSE/MoCA Scores

We further investigated the association between δ, θ, α, and β oscillation phase synchronization indices and the degree of cognitive impairment in the AD group. From **Table 4**, we can see the phase synchronization index of β oscillation is significantly correlated with MoCA scores, specifically at left frontal-central and temporal-central electrode pairs. Besides, the correlation of phase synchronization index of θ oscillation at left central to right frontal and right temporal electrode pairs to MoCA scores also beyond statistical significance after FDR correction.

DISCUSSION

In this study, we found that, almost in the whole brain regions, the AD group had higher θ oscillation spectral power and lower α oscillation spectral power than that in the NC group, which is consistent with many former studies as reviewed in Jeong (2004); Engels et al. (2017), Malek et al. (2017); Cassani et al. (2018), Horvath et al. (2018), and Babiloni et al. (2020a). We further found that in the AD group the α oscillation spectral power was positively correlated with the MMSE and MoCA scores. Basar and colleagues has suggested α oscillations have multifold functional correlates including sensory, motor and memory functions (Basar and Guntekin, 2012). As a universal code or universal operator, α oscillations serve as building blocks in several functions and can be used as clinical biomarkers of cognitive impairment in schizophrenia, Alzheimer's disease and bipolar disorders (Basar and Guntekin, 2012). Our results showed that α oscillation spectral power could be a significant EEG biomarker for differentiating probable AD patients from normal elderly, and could also indirectly reflect the severity and prognosis of disease.

Previous studies have shown that the EEG complexity of AD patients is lower than that of NC subjects, which is manifested by changes in entropy-related parameters such as spectral entropy, approximate entropy, and sample entropy (Abasolo et al., 2006; Simons et al., 2018; Tylová et al., 2018), etc. While on different time scales or frequency bands, the complexity of EEG signals associated with cognitive impairment may be inconsistent. When multi-scale entropy analysis is used, the entropy in the AD group was lower than that in the NC group on smaller scales, while the AD patients had higher complexity than NC subjects at larger scales on long scales (Mizuno et al., 2010; Maturana-Candelas et al., 2019). The smaller/larger scales can be considered to correspond to higher/lower frequencies of spectral power, respectively. Spectral entropy considers the complexity at specific frequency

TABLE 3 | Relationship between spectral entropy and MMSE/MoCA scores.

Electrode Position	MMSE				MoCA			
	$\rho_{\delta\_entropy}$	$\rho_{\theta\_entropy}$	$\rho_{\alpha\_entropy}$	$\rho_{\beta\_entropy}$	$\rho_{\delta\_entropy}$	$\rho_{\theta\_entropy}$	$\rho_{\alpha\_entropy}$	$\rho_{\beta\_entropy}$
F3	–0.3907	0.0542	0.3497	–0.2381	–0.2962	0.1014	0.3191	–0.1973
F4	–0.2999	0.0548	0.3027	0.0034	–0.2310	0.0440	0.2837	–0.0041
T3	–0.1264	0.2411	0.2387	–0.4739	–0.0734	0.1217	0.2947	–0.5415
T4	–0.2981	0.1387	0.3903	–0.3828	–0.2232	0.1133	0.3452	–0.4503
C3	–0.3528	0.0843	0.4075	–0.2785	–0.3027	0.0360	0.4055	–0.3572
C4	–0.4294	0.0854	0.2896	–0.5550	–0.3723	0.0434	0.3380	–0.5788
O1	–0.1919	0.1229	0.1812	–0.1962	–0.2445	0.0599	0.2598	–0.2075
O2	–0.1433	0.0294	0.1976	–0.1833	–0.2279	–0.0177	0.2609	–0.1996

TABLE 4 | Relationship between phase synchronization index and MMSE/MoCA scores.

Electrode pairs	MMSE				MoCA			
	$\rho_{\delta\_pha\_syn}$	$\rho_{\theta\_pha\_syn}$	$\rho_{\alpha\_pha\_syn}$	$\rho_{\beta\_pha\_syn}$	$\rho_{\delta\_pha\_syn}$	$\rho_{\theta\_pha\_syn}$	$\rho_{\alpha\_pha\_syn}$	$\rho_{\beta\_pha\_syn}$
F3-F4	0.0815	0.1249	–0.0084	0.3389	0.1377	0.1998	0.0650	0.4273
F3-T3	0.2913	0.2540	0.2156	0.4963	0.2882	0.3319	0.2902	0.5567*
F3-C3	0.0091	–0.0461	–0.0222	0.4796	–0.0025	–0.0057	0.0163	0.5542*
F3-C4	0.2166	0.2798	0.2513	0.4190	0.3530	0.3985	0.3314	0.5295
F3-T4	0.1624	0.4192	0.3108	0.4441	0.0978	0.4371	0.3564	0.5225
F3-O1	0.1683	0.3735	0.3115	0.4464	0.1610	0.4383	0.3258	0.5139
F3-O2	0.1017	0.2733	0.2059	0.4327	0.1030	0.3747	0.2548	0.5077
F4-T3	0.2546	0.2519	0.3283	0.3906	0.3551	0.3541	0.4125	0.4913
F4-C3	0.4255	0.5059	0.4528	0.4413	0.4387	0.5941*	0.4808	0.5127
F4-C4	–0.0245	0.0095	0.1032	0.0578	0.0641	0.0736	0.1711	0.1645
F4-T4	0.1470	0.2754	0.2773	0.2804	0.1856	0.2939	0.3197	0.3700
F4-O1	0.2665	0.2875	0.3547	0.4078	0.2822	0.3388	0.3568	0.4835
F4-O2	0.1943	0.1756	0.2995	0.3473	0.2252	0.2208	0.3278	0.4240
T3-C3	0.3450	0.3806	0.2854	0.4770	0.4309	0.4585	0.3698	0.6104*
T3-C4	0.3059	0.3649	0.4134	0.4915	0.3630	0.4391	0.4683	0.5555*
T3-T4	0.1137	0.3751	0.3269	0.3407	0.0761	0.3285	0.2606	0.3260
T3-O1	0.0124	0.2274	0.2194	0.2123	0.0076	0.1793	0.1252	0.2145
T3-O2	0.0426	0.1717	0.1869	0.2107	–0.0014	0.1135	0.0591	0.1840
C3-C4	0.4031	0.3382	0.3449	0.4251	0.4693	0.4209	0.3630	0.5261
C3-T4	0.3343	0.5681	0.4578	0.5410	0.3246	0.5836*	0.4782	0.6553*
C3-O1	0.3655	0.3330	0.2635	0.4735	0.3362	0.3667	0.2670	0.5600*
C3-O2	0.1847	0.2222	0.2591	0.3949	0.1630	0.2534	0.2691	0.5277
C4-T4	–0.0414	0.1907	0.2125	0.3301	0.0520	0.3367	0.3223	0.4557
C4-O1	0.2332	0.2900	0.3895	0.3570	0.2160	0.3039	0.3517	0.4109
C4-O2	0.2106	0.2772	0.2908	0.2874	0.1481	0.2765	0.2575	0.3198
T4-O1	0.0493	0.2618	0.1802	0.2722	0.0244	0.1878	0.0611	0.2347
T4-O2	–0.0439	0.2368	0.2054	0.2378	–0.0782	0.1744	0.1074	0.2288
O1-O2	–0.0826	–0.0150	-0.0980	0.1018	–0.1033	–0.0979	–0.2208	0.0197

*$P < 0.05$.

bands. Our study found that the spectral entropy of the α oscillations in the frontal, temporal and central regions of the AD group was lower than that in the NC group, which is consistent with former studies (Sun et al., 2020). On the other hand, we found the β oscillation spectral entropy in the temporal, central and occipital regions was higher than that in the NC group. Because the spectral entropy represents the degree of uncertainty in the power distribution of EEG signals, our results suggest that the power fluctuations of the α oscillations of AD patients become smaller, while the power fluctuations of the β oscillations become larger. In preclinical amyloid positive patients, Gaubert and colleagues also found increased spectral entropy, which is suggested to be related to a compensatory mechanism in AD patients during memory load and cognitive performance (Gaubert et al., 2019).

Many functional connectivity measures has been used in evaluating the synchronization characteristics in different brain areas in AD patients, and many of them are correlated (Dauwels et al., 2010). The phase-based measures are robust and reproducible, insensitive to volume conduction (Briels et al., 2020). Our study found the phase synchronization index of δ, θ, and β oscillations of AD patients was decreased than that of the NC subjects, especially in the frontal, temporal and central areas. Further, we found the phase synchronization index of β oscillations at these brain areas correlated well with the MoCA scores in AD patients. According to Pini et al. (2016), cortical atrophy in AD patients affects the medial temporal lobe very early, then extending to the other parts of the cortex along a temporal-parietal-frontal trajectory. Due to the recording device's limitation, we lack the neural activity in the parietal electrodes. Instead, our results suggests the neuronal functional connectivity at the temporal-central-frontal areas in AD patients is greatly impaired, and the phase synchronization index of β oscillations might be an indicator of the impairment of brain functions. However, the phase synchronization index of α oscillation seemed less damaged and less correlated with the neurological scores, suggesting the phase synchronization feature of α oscillations may not reflect the severity of disease.

In conclusion, our study suggest that quantitative EEG spectral power in α oscillations and phase synchronization characteristics in β oscillations could reflect the severity of AD disease and are beneficial to the diagnosis and screening of probable AD patients. As the PiB-PET examination is rather expensive, the number of AD patients included in this study is relatively small. In addition, the parietal neural activity is not recorded in current study, which hindered us evaluating the impaired cognitive functions in parietal areas of AD patients. Further, this study is a retrospective, cross-sectional group study. In the future we should consider a longitudinal and individualized study with a larger sample size and with more electrode sites.

DATA AVAILABILITY STATEMENT

The data that support the findings of this study are available from the corresponding authors, upon reasonable request.

ETHICS STATEMENT

The studies involving human participants were reviewed and approved by Medical Ethics Committee of Chinese People's Liberation Army General Hospital. The patients/participants provided their written informed consent to participate in this study.

AUTHOR CONTRIBUTIONS

YW, SZ, YG, WD, YG, LL, and MS recruited the participants and collected their information. HZ carried out the statistical analysis. XG collected and processed the EEG signals. FY interpreted the results. XL and LW designed the study. HZ, XG, and FY wrote the manuscript. All authors reviewed the manuscript.

FUNDING

This work was supported by the Scientific Research Common Program of Beijing Municipal Commission of Education (Grant No. KM201810025015) and Military Special Health Care Project (Grant No. 15BJZ38).

ACKNOWLEDGMENTS

We are very grateful to all the participants of the study. This work was supported by the Department of Nuclear Medicine in Chinese PLA General Hospital and we deeply appreciate all the work done by clinicians in the Department of Nuclear Medicine.

SUPPLEMENTARY MATERIAL

The Supplementary Material for this article can be found online at: https://www.frontiersin.org/articles/10.3389/fnagi.2021.631587/full#supplementary-material

REFERENCES

Abasolo, D., Hornero, R., Espino, P., Alvarez, D., and Poza, J. (2006). Entropy analysis of the EEG background activity in Alzheimer's disease patients. *Physiol. Meas.* 27, 241–253. doi: 10.1088/0967-3334/27/3/003

Al-Nuaimi, A. H. H., Jammeh, E., Sun, L., and Ifeachor, E. (2018). Complexity measures for quantifying changes in electroencephalogram in Alzheimer's disease. *Complexity* 2018, 1–12. doi: 10.1155/2018/8915079

Azami, H., Abásolo, D., Simons, S., and Escudero, J. (2017). Univariate and Multivariate Generalized Multiscale Entropy to Characterise EEG Signals in Alzheimer's disease. *Entropy* 19:31. doi: 10.3390/e19010031

Babiloni, C., Blinowska, K., Bonanni, L., Cichocki, A., De Haan, W., Del Percio, C., et al. (2020a). What electrophysiology tells us about Alzheimer's disease: a window into the synchronization and connectivity of brain neurons. *Neurobiol. Aging* 85, 58–73. doi: 10.1016/j.neurobiolaging.2019.09.008

Babiloni, C., Lopez, S., Del Percio, C., Noce, G., Pascarelli, M. T., Lizio, R., et al. (2020b). Resting-state posterior alpha rhythms are abnormal in subjective memory complaint seniors with preclinical Alzheimer's neuropathology and high education level: the INSIGHT-preAD study. *Neurobiol. Aging* 90, 43–59. doi: 10.1016/j.neurobiolaging.2020.01.012

Basar, E., and Guntekin, B. (2012). A short review of alpha activity in cognitive processes and in cognitive impairment. *Int. J. Psychophysiol.* 86, 25–38. doi: 10.1016/j.ijpsycho.2012.07.001

Benwell, C. S. Y., Davila-Perez, P., Fried, P. J., Jones, R. N., Travison, T. G., Santarnecchi, E., et al. (2020). EEG spectral power abnormalities and their relationship with cognitive dysfunction in patients with Alzheimer's disease and type 2 diabetes. *Neurobiol. Aging* 85, 83–95. doi: 10.1016/j.neurobiolaging.2019.10.004

Briels, C. T., Schoonhoven, D. N., Stam, C. J., de Waal, H., Scheltens, P., and Gouw, A. A. (2020). Reproducibility of EEG functional connectivity in Alzheimer's disease. *Alzheimers Res. Ther.* 12:68. doi: 10.1186/s13195-020-00632-3

Cassani, R., Estarellas, M., San-Martin, R., Fraga, F. J., and Falk, T. H. (2018). Systematic review on resting-state EEG for Alzheimer's disease diagnosis and progression assessment. *Dis. Mark.* 2018:5174815. doi: 10.1155/2018/5174815

Cohen, A. D., Landau, S. M., Snitz, B. E., Klunk, W. E., Blennow, K., and Zetterberg, H. (2019). Fluid and PET biomarkers for amyloid pathology in Alzheimer's disease. *Mol. Cell Neurosci.* 97, 3–17. doi: 10.1016/j.mcn.2018.12.004

Colom-Cadena, M., Spires-Jones, T., Zetterberg, H., Blennow, K., Caggiano, A., DeKosky, S. T., et al. (2020). The clinical promise of biomarkers of synapse damage or loss in Alzheimer's disease. *Alzheimers Res. Ther.* 12:21. doi: 10.1186/s13195-020-00588-4

Dauwels, J., Vialatte, F., Musha, T., and Cichocki, A. (2010). A comparative study of synchrony measures for the early diagnosis of Alzheimer's disease based on EEG. *Neuroimage* 49, 668–693. doi: 10.1016/j.neuroimage.2009.06.056

Delbeuck, X., Van der Linden, M., and Collette, F. (2003). Alzheimer's disease as a disconnection syndrome? *Neuropsychol. Rev.* 13, 79–92. doi: 10.1023/a:1023832305702

Deng, B., Cai, L., Li, S., Wang, R., Yu, H., Chen, Y., et al. (2017). Multivariate multi-scale weighted permutation entropy analysis of EEG complexity for Alzheimer's disease. *Cogn. Neurodyn.* 11, 217–231. doi: 10.1007/s11571-016-9418-9

Durka, P. J., Klekowicz, H., Blinowska, K. J., Szelenberger, W., and Niemcewicz, S. (2003). A simple system for detection of EEG artifacts in polysomnographic recordings. *IEEE Trans. Biomed. Eng.* 50, 526–528. doi: 10.1109/TBME.2003.809476

Engels, M. M. A., van der Flier, W. M., Stam, C. J., Hillebrand, A., Scheltens, P., and van Straaten, E. C. W. (2017). Alzheimer's disease: the state of the art in resting-state magnetoencephalography. *Clin. Neurophysiol.* 128, 1426–1437. doi: 10.1016/j.clinph.2017.05.012

Garre-Olmo, J. (2018). Epidemiology of Alzheimer's disease and other dementias. *Rev. Neurol.* 66, 377–386.

Gaubert, S., Raimondo, F., Houot, M., Corsi, M. C., Naccache, L., Diego Sitt, J., et al. (2019). EEG evidence of compensatory mechanisms in preclinical Alzheimer's disease. *Brain* 142, 2096–2112. doi: 10.1093/brain/awz150

Horvath, A., Szucs, A., Csukly, G., Sakovics, A., Stefanics, G., and Kamondi, A. (2018). EEG and ERP biomarkers of Alzheimer's disease: a critical review. *Front. Biosci. (Landmark Ed)* 23:183–220. doi: 10.2741/4587

Houmani, N., Vialatte, F., Gallego-Jutgla, E., Dreyfus, G., Nguyen-Michel, V. H., Mariani, J., et al. (2018). Diagnosis of Alzheimer's disease with Electroencephalography in a differential framework. *PLoS One* 13:e0193607. doi: 10.1371/journal.pone.0193607

Jeong, J. (2004). EEG dynamics in patients with Alzheimer's disease. *Clin. Neurophysiol.* 115, 1490–1505. doi: 10.1016/j.clinph.2004.01.001

Kulkarni, N. (2017). Use of complexity based features in diagnosis of mild Alzheimer disease using EEG signals. *Int. J. Inform. Technol.* 10, 59–64. doi: 10.1007/s41870-017-0057-0

Li, X., Zhu, Z., Zhao, W., Sun, Y., Wen, D., Xie, Y., et al. (2018). Decreased resting-state brain signal complexity in patients with mild cognitive impairment and Alzheimer's disease: a multiscale entropy analysis. *Biomed. Opt. Express* 9, 1916–1929. doi: 10.1364/BOE.9.001916

Lim, J. K., Li, Q. X., He, Z., Vingrys, A. J., Wong, V. H., Currier, N., et al. (2016). The eye as a biomarker for Alzheimer's disease. *Front. Neurosci.* 10:536. doi: 10.3389/fnins.2016.00536

Maestu, F., Cuesta, P., Hasan, O., Fernandez, A., Funke, M., and Schulz, P. E. (2019). The importance of the validation of M/EEG With current biomarkers in Alzheimer's disease. *Front. Hum. Neurosci.* 13:17. doi: 10.3389/fnhum.2019.00017

Malek, N., Baker, M. R., Mann, C., and Greene, J. (2017). Electroencephalographic markers in dementia. *Acta Neurol. Scand.* 135, 388–393. doi: 10.1111/ane.12638

Maturana-Candelas, A., Gómez, C., Poza, J., Pinto, N., and Hornero, R. (2019). EEG Characterization of the Alzheimer's disease continuum by means of multiscale entropies. *Entropy* 21:544. doi: 10.3390/e21060544

McKhann, G. M., Knopman, D. S., Chertkow, H., Hyman, B. T., Jack, C. R., Kawas, C. H., et al. (2011). The diagnosis of dementia due to Alzheimer's disease: recommendations from the national institute on aging-alzheimer's association workgroups on diagnostic guidelines for Alzheimer's disease. *Alzheimers Dement.* 7, 263–269. doi: 10.1016/j.jalz.2011.03.005

Mizuno, T., Takahashi, T., Cho, R. Y., Kikuchi, M., Murata, T., Takahashi, K., et al. (2010). Assessment of EEG dynamical complexity in Alzheimer's disease using multiscale entropy. *Clin. Neurophysiol.* 121, 1438–1446. doi: 10.1016/j.clinph.2010.03.025

Musaeus, C. S., Engedal, K., Hogh, P., Jelic, V., Morup, M., Naik, M., et al. (2019a). Oscillatory connectivity as a diagnostic marker of dementia due to Alzheimer's disease. *Clin. Neurophysiol.* 130, 1889–1899. doi: 10.1016/j.clinph.2019.07.016

Musaeus, C. S., Nielsen, M. S., and Hogh, P. (2019b). Altered low-frequency EEG connectivity in mild cognitive impairment as a sign of clinical progression. *J. Alzheimers Dis.* 68, 947–960. doi: 10.3233/JAD-181081

Nunez, P., Poza, J., Gomez, C., Rodriguez-Gonzalez, V., Hillebrand, A., Tola-Arribas, M. A., et al. (2019). Characterizing the fluctuations of dynamic resting-state electrophysiological functional connectivity: reduced neuronal coupling variability in mild cognitive impairment and dementia due to Alzheimer's disease. *J. Neural. Eng.* 16:056030. doi: 10.1088/1741-2552/ab234b

Pernet, C., Garrido, M. I., Gramfort, A., Maurits, N., Michel, C. M., Pang, E., et al. (2020). Issues and recommendations from the OHBM COBIDAS MEEG committee for reproducible EEG and MEG research. *Nat. Neurosci.* 23, 1473–1483. doi: 10.1038/s41593-020-00709-0

Pini, L., Pievani, M., Bocchetta, M., Altomare, D., Bosco, P., Cavedo, E., et al. (2016). Brain atrophy in Alzheimer's disease and aging. *Ageing Res. Rev.* 30, 25–48. doi: 10.1016/j.arr.2016.01.002

Simons, S., and Abásolo, D. (2017). Distance-based lempel–ziv complexity for the analysis of electroencephalograms in patients with Alzheimer's disease. *Entropy* 19:129. doi: 10.3390/e19030129

Simons, S., Espino, P., and Abásolo, D. (2018). Fuzzy entropy analysis of the electroencephalogram in patients with Alzheimer's disease: is the method superior to sample entropy? *Entropy* 20:21. doi: 10.3390/e20010021

Song, Z., Deng, B., Wang, J., and Wang, R. (2019). Biomarkers for Alzheimer's disease defined by a novel brain functional network measure. *IEEE Trans. Biomed. Eng.* 66, 41–49. doi: 10.1109/TBME.2018.2834546

Sperling, R., Mormino, E., and Johnson, K. (2014). The evolution of preclinical Alzheimer's disease: implications for prevention trials. *Neuron* 84, 608–622. doi: 10.1016/j.neuron.2014.10.038

Sun, J., Wang, B., Niu, Y., Tan, Y., Fan, C., Zhang, N., et al. (2020). Complexity analysis of EEG. MEG, and fMRI in mild cognitive impairment and Alzheimer's disease: a review. *Entropy* 22:239. doi: 10.3390/e22020239

Tylová, L., Kukal, J., Hubata-Vacek, V., and Vyšata, O. (2018). Unbiased estimation of permutation entropy in EEG analysis for Alzheimer's disease classification. *Biomed. Signal Process. Control* 39, 424–430. doi: 10.1016/j.bspc.2017.08.012

Wang, R., Wang, J., Li, S., Yu, H., Deng, B., and Wei, X. (2015). Multiple feature extraction and classification of electroencephalograph signal for Alzheimers' with spectrum and bispectrum. *Chaos* 25:013110. doi: 10.1063/1.4906038

Wicki, M., Marmet, S., Studer, J., Epaulard, O., and Gmel, G. (2021). Curvilinear associations between sexual orientation and problematic substance use, behavioural addictions and mental health among young Swiss men. *Addict. Behav.* 112:106609. doi: 10.1016/j.addbeh.2020.106609

Conflict of Interest: The authors declare that the research was conducted in the absence of any commercial or financial relationships that could be construed as a potential conflict of interest.

frontiers in Aging Neuroscience

ORIGINAL RESEARCH
published: 23 June 2021
doi: 10.3389/fnagi.2021.670463

The Cerebellum Is Related to Cognitive Dysfunction in White Matter Hyperintensities

Shanshan Cao[1,2,3†], Jiajia Nie[1,2,3†], Jun Zhang[4], Chen Chen[1,2,3], Xiaojing Wang[1,3], Yuanyuan Liu[1,3], Yuting Mo[1,2,3], Baogen Du[1,2,3], Yajuan Hu[1,2,3], Yanghua Tian[1,2,3,5], Qiang Wei[1,2,3] and Kai Wang[1,2,3,5*]*

[1] The School of Mental Health and Psychological Sciences, Department of Neurology, The First Affiliated Hospital of Anhui Medical University, Anhui Medical University, Hefei, China, [2] Collaborative Innovation Center of Neuropsychiatric Disorders and Mental Health, Hefei, China, [3] Anhui Province Key Laboratory of Cognition and Neuropsychiatric Disorders, Hefei, China, [4] Department of Neurology, The Second Affiliated Hospital of Anhui Medical University, Hefei, China, [5] Institute of Artificial Intelligence, Hefei Comprehensive National Science Center, Hefei, China

Objective: White matter hyperintensities (WMHs) on magnetic resonance imaging (MRI) is frequently presumed to be secondary to cerebral small vessel disease (CSVD) and associated with cognitive decline. The cerebellum plays a key role in cognition and has dense connections with other brain regions. Thus, the aim of this study was to investigate if cerebellar abnormalities could occur in CSVD patients with WMHs and the possible association with cognitive performances.

Methods: A total of 104 right-handed patients with WMHs were divided into the mild WMHs group (n = 39), moderate WMHs group (n = 37), and severe WMHs group (n = 28) according to the Fazekas scale, and 36 healthy controls were matched for sex ratio, age, education years, and acquired resting-state functional MRI. Analysis of voxel-based morphometry of gray matter volume (GMV) and seed-to-whole-brain functional connectivity (FC) was performed from the perspective of the cerebellum, and their correlations with neuropsychological variables were explored.

Results: The analysis revealed a lower GMV in the bilateral cerebellum lobule VI and decreased FC between the left- and right-sided cerebellar lobule VI with the left anterior cingulate gyri in CSVD patients with WMHs. Both changes in structure and function were correlated with cognitive impairment in patients with WMHs.

Conclusion: Our study revealed damaged GMV and FC in the cerebellum associated with cognitive impairment. This indicates that the cerebellum may play a key role in the modulation of cognitive function in CSVD patients with WMHs.

Keywords: cerebellum, white matter hyperintensities, resting-state functional connectivity, voxel-based morphometry, magnetic resonance imaging

OPEN ACCESS

Edited by:
Rong Chen,
University of Maryland, Baltimore, United States

Reviewed by:
Daniele Corbo,
University of Brescia, Italy
Laura Lorenzo-López,
University of A Coruña, Spain

***Correspondence:**
Kai Wang
wangkai1964@126.com
Qiang Wei
weiqiang19890914@126.com

† These authors have contributed equally to this work

Received: *21 February 2021*
Accepted: *03 May 2021*
Published: *23 June 2021*

Citation:
Cao S, Nie J, Zhang J, Chen C, Wang X, Liu Y, Mo Y, Du B, Hu Y, Tian Y, Wei Q and Wang K (2021) The Cerebellum Is Related to Cognitive Dysfunction in White Matter Hyperintensities. Front. Aging Neurosci. 13:670463. doi: 10.3389/fnagi.2021.670463

INTRODUCTION

White matter hyperintensities (WMHs) is a state of chronic hypoperfusion in the white matter, which reflects the loss of axons and myelin, myelin pallor, and gliosis. It is described as hyperintense in the subcortical white matter displayed on T2-weighted MRI images and fluid-attenuated inversion recovery (FLAIR) images (Gebeily et al., 2014). Cerebral small vessel disease (CSVD), associated with the altered blood supply

to the brain white matter, can lead to localized ischemic areas of necrosis and cavitation and cause WMHs (Petito et al., 1998). The prevalence of WMHs in the general population aged 60 to 90 years is nearly 70% in the Chinese population (Han et al., 2018). Moreover, there is growing evidence that the WMHs is imperative to cognitive dysfunction, particularly in executive function. Niels et al. reported that increasing severity of periventricular WMHs was specifically associated with impaired information processing speed and executive function (Prins et al., 2005; Smith et al., 2011; Yamanaka et al., 2019).

The cerebellum has long been regarded as critical for intact motor functioning (Koziol et al., 2014). Until recently, it has been accepted that it plays a significant role in cognitive processing supported by the posterior cerebellum, which is noteworthy (Smith et al., 2015a). Increasing numbers of studies have proven this. A meta-analysis revealed that patients with focal cerebellar lesions performed significantly worse on neuropsychological tests including phonological fluency, semantic fluency, Stroop test, block design test (WAIS-R), and visual memory (Ahmadian et al., 2019). Furthermore, lesions of the posterior lobe (lobules VI, VII, and possibly lobule IX) are reported to result in cerebellar cognitive affective syndrome characterized by impairments in executive function (Schmahmann, 2019).

Previous studies investigating the associations between WMHs on MRI and cognitive impairment have reported different results, with the most possible key role for prefrontal cortex connectivity with other (sub-)cortical regions (Chen et al., 2019). Moreover, structural and functional brain abnormalities in the cerebellum have also been recently identified in WMHs recently (Buckner, 2013). Studies have reported that both the number and volume of WMHs are correlated with changes in brain connectivity, especially in the cerebellum (Hoogendam et al., 2012; Smith et al., 2015b). Accumulating evidence has led to the growing recognition of the cerebellum's role in cognitive function and its involvement in WMHs. However, in the vast majority of neuroimaging studies of WMHs, the cerebellum's role in cognition has been dismissed or remains largely on the periphery in favor of cortico-centric models. Therefore, all these findings paved the way for our in-depth examination of the emerging role of the cerebellum in cognitive function in WMHs.

All these studies suggested that the cerebellum may play a vital role in cognition, and cerebellar involvement is described in several neurodegenerative diseases. For this reason, the aims of this study were to investigate if cerebellar abnormalities could occur in CSVD patients with WMHs and to investigate the possible association with cognitive performances. Therefore, we conducted voxel-based morphometry analysis (VBM) to explore cerebellar gray matter volume (GMV) and seed-to-whole-brain functional connectivity (FC) to investigate abnormalities of FC related to the cerebellum. Seed regions for resting-state analysis were selected based on GMV differences between the WMHs group and healthy controls (HC) group. Meanwhile, we also performed a correlation analysis between GMV as well as FC changes and cognitive performance in CSVD patients with WMHs.

MATERIALS AND METHODS

Participants

This study included 104 patients with WMHs from the Department of Neurology of the First Affiliated Hospital of Anhui Medical University, Hefei, China. The inclusion criteria were as follows: (1) aged between 40 and 80 years and (2) visible WMHs on T2 fluid-attenuated inversion recovery (T2 FLAIR). The exclusion criteria were as follows: (1) intracranial and extracranial stenosis of $>50\%$; (2) Trial of Org 10172 in Acute Stroke Treatment classification suggestive of cardiogenic stroke; (3) non-CSVD-related WMHs (e.g., multiple sclerosis); (4) mental disorders, alcohol addiction; (5) tumors; (6) intracranial hemorrhage; (7) significant hearing or visual impairment and physical movement disorders that prevented cooperation during cognitive testing; (8) language barrier; and (9) MRI contraindications or known claustrophobia. Periventricular hyperintensity (PVH) and deep white matter hyperintensity (DWMH) were scored separately using the four-point scale according to the Fazekas scale on FLAIR images (Fazekas et al., 1987). The PVH scores were categorized as follows: 0, absent; 1, caps or pencil-thin lining; 2, smooth "halo"; and 3, irregular PVH lesions extending into the deep white matter. DWMH scores were categorized as follows: 0, absence; 1, punctate foci; 2, beginning confluence of foci; and 3, large confluent areas. The Fazekas score is the sum of the PVH and DWMH scores. Patients with WMHs were divided into three groups based on their Fazekas scores. The mild WMHs group scored 1–2, the moderate WMHs group scored 3–4, and the severe WMHs group scored 5–6. Finally, we included 39 patients in the mild group, 37 patients in the moderate group, and 28 patients in the severe group.

Thirty-six controls (HC) were relatives of patients with WMHs and social recruits studied during the same period who matched the demographic data of the patients with WMHs, including age, gender, and years of education, and had no previous history of neurological diseases or mental illnesses. Imaging showed no white matter hyperintensities. The study was approved by the Ethics Committee of Anhui Medical University. All participants provided written informed consent before the study.

Statistical Analyses

One-way analysis of variance was used to assess differences in age, education, and CSVD neuroimaging manifestations and differences between the neuropsychological test scores of the four groups (significant for $P < 0.05$), and the least significant difference was used for *post-hoc* analysis (significant for $P < 0.05$). The chi-squared test was used to determine gender differences in the four groups ($P < 0.05$).

Magnetic Resonance Parameters

Structural and functional MRI were performed with a 3-T scanner (Discovery 750; GE Healthcare, Milwaukee, WI, United States) at the Information Science Center of the University of Science and Technology of China. During resting-state functional MRI (rs-fMRI) scanning, participants were instructed

to keep their eyes closed, but not to fall asleep, and try to think of nothing in particular. A tight but comfortable foam padding was used to minimize head motion, and earplugs were used to reduce scanner noise. The parameters of the different sequences were set as follows: T2FLAIR: repetition time (TR) = 8,000 ms, echo time (TE) = 165 ms, TI = 2,000 ms, flip angle = 111°, matrix size = 512 × 512, field of view (FOV) = 256 mm × 256 mm, slice thickness = 5 mm, gap = 1 mm, and total slices = 20. Enhanced gradient echo T2 star-weighted angiography (ESWAN): TR = 52.189 ms, TE = 2.856 ms, flip angle = 12°, matrix size = 256 × 256, FOV = 220 mm × 220 mm, and slice thickness = 2 mm with no gap. Rs-fMRI: TR = 2,400 ms, TE = 30 ms, flip angle = 90°, matrix size = 64 × 64, FOV = 192 mm × 192 mm, slice thickness = 3 mm with no gap, and 46 continuous slices (one voxel = 3 mm × 3 mm × 3 mm).

Sagittal three-dimensional (3D) T1-weighted images were acquired using a brain volume (BRAVO) sequence with 188 slices (TR = 8.16 ms; TE = 3.18 ms; flip angle = 12°; FOV = 256 mm × 256 mm; slice thickness = 1 mm, no gap; voxel size = 1 mm × 1 mm × 1 mm).

Neuropsychological Test

The neuropsychological scale of the Chinese Cerebral Small Vessel Disease Clinical Evaluation Study was used to evaluate the global cognitive function and individual cognitive functions of all participants (Cao et al., 2020). The Montreal Cognitive Assessment (MoCA) was used to measure global cognitive function (Nasreddine et al., 2005). Anxiety was assessed using the Generalized Anxiety Disorder-7 (GAD-7; Buckner, 2013). Depression symptoms were assessed using the Patient Health Questionnaire-9 (PHQ-9; Smarr and Keefer, 2011). The Chinese version of the Auditory Verbal Learning Test (AVLT) was used to evaluate memory function. The AVLT is composed of immediate memory, delay memory, and recognition memory function (Schoenberg et al., 2006). The Symbol Digit Modalities Test (SDMT) was used to evaluate information processing speed (Silva et al., 2018). The Digital Span test consists of two parts, forward and backward, and was used to evaluate the attention of the subjects (Yamamoto et al., 2011), and the Stroop Color-Word Test was used to evaluate executive function. The Trail Making Test (TMT) was also used to evaluate the executive and attention function (Selnes et al., 1991), and the Boston Naming Test was used to evaluate word-finding ability (Mack et al., 1992). The testers were all graduate or doctoral students in neurology who had passed the unified training.

WMHs Volume

The WMHs volume was calculated using the UBO detector (Jiang et al., 2018)[1], which is a cluster-based software. The calculation process was described in a previous study (Wen et al., 2009).

Rs-fMRI Data Processing

All rs-fMRI data were preprocessed using the Data Processing Assistant for Resting-State Functional MR Imaging toolkit (Chao-Gan and Yu-Feng, 2010) (DPARSF; http://rfmri.org/content/dparsf) and statistical parametric mapping (SPM12; https://www.fil.ion.ucl.ac.uk/spm/software/spm12/). Preprocessing mainly includes the following. (1) The first five time points were removed to reduce the impact of the scanner during the initial scanning and facilitate the adaptation of the participants to the scanning environment. (2) The slice timing was used to correct the differences in acquisition time between layers of the volume. (3) Head correction was performed by removing participants with large head movements to reduce the effect on the result. (4) Space standardization was used to reduce the impact of human BRAVO and shape diversity. 3D T1 was used to register functional images for the spatial standardization of the participants in our study. A matrix was generated after registration and segmentation. The matrix data were applied to the functional images, which were used to register the participants from the functional to the standard space. (5) Smoothing was applied to reduce the incomplete effects of registration to ensure that the residuals were more consistent with the Gaussian distribution and improve the image signal-to-noise ratio. An 8-mm Gaussian kernel was chosen. (6) A detrending was applied at the end to reduce the effects of scanner heating. (7) Regression 24 Friston motion parameters, white matter high signal, and CSF were analyzed.

VBM Analysis

Voxel-based morphometry analyses were performed to determine potential differences in the cerebellum between patients in the WMHs group and the HC group. T1-weighted anatomic images were preprocessed using the VBM8 toolbox in SPM8 (Statistical Parametric Mapping software). Each structural image was segmented into gray matter (GM), white matter, and cerebrospinal fluid using a fully automated algorithm within SPM8 and subsequently transformed into the Montreal Neurological Institute (MNI) space using diffeomorphic anatomical registration through exponentiated Lie algebra (DARTEL) normalization. Next, the normalized GM images were smoothed (FWHM = 8 mm) for statistical analyses. Finally, a one-way ANOVA was conducted with age, education, gender, and whole-brain GM volume as covariates on these normalized cerebellum images to determine structural differences. The Gaussian random field (GRF) correction (significant for voxel levels at $P < 0.001$ and cluster at $P < 0.05$) was used for correction. Statistical analysis for saving masks was performed using the Data Processing and Analysis of Brain Imaging toolbox (Wu et al., 2020).

Rs-FC Calculation

We extracted the right-sided cerebellum lobule VI and the left-sided cerebellum lobule VI as the seed areas for resting-state FC analyses. The rs-FC between the mean time series of the seed and the time series of each voxel in the remainder of the GM was calculated using Pearson's correlation coefficient of the time course of each seed. To facilitate the normality of the data distribution, the correlation coefficients were converted to z-values using Fisher's r-to-z transformation.

Based on a GM template, a one-way analysis of covariance was used to assess the differences between the functional

[1]https://cheba.unsw.edu.au/group/neuroimagingpipeline

connectivities of the four groups. Age, education, GM volume, and gender were considered as covariates. Statistical analysis was performed voxel-wise using DPARSF and SPM software. Multiple comparisons during the analyses were corrected using the GRF (significant for voxel levels at $P < 0.001$ and cluster at $P < 0.05$).

Correlation Analysis

We performed a Pearson correlation analysis between each participant's volume of the cerebellum and neuropsychological tests and between each participant's FC and neuropsychological tests in significant regions to further explore whether neuroimaging indices were related to cognitive functions (significant for $P < 0.05$).

RESULTS

Demographic and Clinical Characteristics

There were no significant differences between the ages, years of education, and gender distributions of the HC and WMHs groups. The proportion of patients with hypertension was higher than that of HC, but there were no significant differences in the four groups in terms of diabetes, hyperlipidemia, smoking history, and drinking history. Demographic information and CSVD marker information are displayed in **Table 1**. Regarding the severity of WMHs, the quantitative assessment method we used was in good agreement with the Fazekas score ($P < 0.001$, $r = 0.499$). The distribution of lacunes and microbleed lesions is shown in **Table 2**. However, several participants did not complete the ESWAN sequence scan for specific reasons (HC group: 5 participants; mild WMHs group: 13 patients; moderate WMHs group: 7 patients; and severe WMHs group: 7 patients). Besides, neuropsychological tests of the participants in the four groups are shown in **Table 3**.

Group Comparison of Cerebellar Atrophy

Atrophy in the cerebellar subregions was apparent in patients with WMHs relative to HCs. Specifically, two large contiguous clusters were identified shown in **Figure 1**. One cluster included cerebellar subregions right-sided lobule VI (voxel size: 1961; peak MNI coordinates: $x = 22.5$, $y = -63$, $z = -15$; GRF for voxel levels at $P < 0.001$ and cluster at $P < 0.05$) and another included left-sided lobule VI (voxel size: 622; peak MNI coordinates: $x = -12$, $y = -82.5$, $z = -13.5$; GRF for voxel levels at $P < 0.001$ and cluster at $P < 0.05$). The volumes of the two ROIs were significantly higher in the HC group than in the patients with WMHs and gradually decreased in patients with WMHs from the mild to severe group (shown in **Figure 2**). The severe group also showed reduced volume both in right-sided lobule VI and left-sided lobule VI compared to the mild and moderate groups.

We identified significantly decreased functional connection between the left-sided cerebellum lobule VI with the left anterior cingulate gyrus (voxel size: 39; peak MNI coordinates: $x = -3$, $y = 33$, $z = -6$; cluster-level GRF for voxel levels at $P < 0.001$ and cluster at $P < 0.05$) in mild, moderate, and severe WMHs groups compared with HCs (shown in **Figure 3**).

Correlation analyses revealed that the volume of the left-sided cerebellum lobule VI was negatively correlated with TMT-A test ($P = 0.026$, $r = -0.361$) and TMT-B test ($P = 0.027$, $r = -0.363$) in the mild group, and positively correlated with AVLT-study test ($P < 0.001$, $r = 0.670$), AVLT-immediate test ($P = 0.002$, $r = 0.601$), AVLT-delay test ($P = 0.001$, $r = 0.644$), AVLT-recognition test ($P = 0.033$, $r = 0.437$) results in the severe group. The volume of the right-sided cerebellum lobule VI was positively correlated with the AVLT-immediate test ($P = 0.022$, $r = 0.398$), AVLT-delay test ($P = 0.015$, $r = 0.428$) results in the moderate group, and positively correlated with the AVLT-study test ($P = 0.001$, $r = 0.607$), AVLT-immediate test ($P < 0.001$, $r = 0.757$), AVLT-delay test ($P < 0.001$, $r = 0.800$), AVLT-recognition test ($P < 0.001$, $r = 0.628$) in the severe group.

DISCUSSION

In this study, we investigated the alterations in the volume and FC in the cerebellum due to WMHs and evaluated their relevance to cognitive function. Regarding imaging data, for the group difference, we have shown a lower volume in cerebellum lobule VI and lower FC between the left and right cerebellar lobule VI with the left anterior cingulate gyri in patients with WMHs. Moreover, both were closely related to WMHs scores and cognitive functions.

Recently, studies have demonstrated an increasing interest in elucidating the pattern of cerebellar atrophy across diseases and revealed its critical role in many neurodegenerative diseases (Guo et al., 2016). Although WMHs is commonly observed in cerebral white matter, CSVD-associated lesions can also occur in GM. We found cerebellar atrophy in lobule VI in WMHs patients, which is in line with numerous studies of neurodegenerative diseases (Tan et al., 2014). As for Alzheimer's disease (AD), atrophy of the posterior cerebellar regions was identified (Guo et al., 2016), and in Parkinson's disease (O'Callaghan et al., 2016), direct pathological change in the cerebellum, including atrophy, has also been confirmed (Borghammer et al., 2010). However, the functional consequences of GM loss in the cerebellum are not uniform across these studies. Cerebellar lobule VI has been implemented in executive functions that dovetail with the predominant cognitive impairment characteristic of WMHs (Habas et al., 2009). This is supported by our study that found a correlation between cerebellar lobule VI atrophy and cognitive decline in WMHs.

Reduced connectivity of the cerebellum lobule VI to the left anterior cingulate gyri owing to white matter hyperintensities was also found in this study. Observed gray matter loss in cerebellum lobule VI may drive this change in FC, and the WMHs can also disrupt white matter tracts or U-fibers that mediate cortical–cortical or cortical–subcortical connections (Ward et al., 2015). Furthermore, connectivity studies have confirmed that the posterior cerebellum has strong connections with the prelimbic, orbitofrontal, and anterior cingulate cortex, which provide anatomical substrates for our results (Badura et al., 2018). Aligning with our results, Schaefer et al. reported connectivity changes in cerebellar regions that are connected

TABLE 1 | Demographic and cerebral small vessel disease neuroimaging manifestations of participants in the four groups [mean (SD)].

	HC (n = 36)	Mild WMHs (n = 39)	Moderate WMHs (n = 37)	Severe WMHs (n = 28)	F/χ^2	P
Age (years)	60.58 (5.98)	63.77 (8.23)	65.08 (10.03)	65.04 (6.90)	2.424	0.068
Female	18	16	14	16	3.011	0.390
Education (years)	9.31 (3.32)	8.41 (4.16)	8.00 (3.84)	7.75 (3.88)	1.083	0.359
Hypertension	8	21	22	21	19.568	<0.001***
Diabetes	2	8	7	4	3.905	0.272
Hyperlipidemia	8	10	9	8	0.356	0.949
Smoking history	9	18	15	11	3.808	0.283
Drinking history	12	9	16	12	4.346	0.226
Fazekas	0.00 (0.00)[a,b,c]	1.64 (0.49)[a,d,e]	3.59 (0.50)[b,d,f]	5.43 (0.50)[c,e,f]	958.855	<0.001***
WMHs volume	/	11,457.35 (12,493.05)[d,e]	18,067.56 (10,873.84)[d,f]	30,658.38 (12,033.91)[e,f]	21.696	<0.001***
Lacunes	0.00 (0.00)[a,b,c]	0.51 (0.91)[a,d]	0.89 (1.29)[b,d]	0.79 (1.23)[c]	5.626	0.001**
Microbleeds	0.31 (0.59)[c]	2.26 (3.61) [e]	1.50 (2.35)[f]	6.29 (14.96)[c,e,f]	3.389	0.021**

*Volume is in cubic millimeters. HC, healthy controls; WMHs, white matter hyperintensities; and SD, standard deviation. [a]Healthy control group vs. mild WMHs group significantly different ($P < 0.05$). [b]Healthy control group vs. moderate WMHs group significantly different ($P < 0.05$). [c]Healthy control group vs. severe WMHs group significantly different ($P < 0.05$). [d]Mild WMHs group vs. moderate WMHs group significantly different ($P < 0.05$). [e]Mild WMHs group vs. severe WMHs group significantly different ($P < 0.05$). [f]Moderate WMHs group vs. severe WMHs group significantly different ($P < 0.05$). ***Significant at 0.001 level, **significant at 0.01 level.*

TABLE 2 | Distribution of neuroimaging manifestations in HC and patients with WMHs [mean (SD)].

	Lacunes				CMBs			
	HC (n = 36)	Mild WMHs (n = 39)	Moderate WMHs (n = 37)	Severe WMHs (n = 28)	HC (n = 32)	Mild WMHs (n = 27)	Moderate WMHs (n = 30)	Severe WMHs (n = 21)
Subcortical								
Frontal	0.00 (0.00)	0.18 (0.51)	0.11 (0.39)	0.14 (0.45)	0.03 (0.18)	0.11 (0.32)	0.13 (0.57)	0.33 (0.80)
Parietal	0.00 (0.00)	0.03 (0.16)	0.11 (0.39)	0.00 (0.00)	0.09 (0.30)	0.19 (0.68)	0.13 (0.35)	0.33 (0.91)
Occipital	0.00 (0.00)	0.00 (0.00)	0.05 (0.23)	0.04 (0.19)	0.03 (0.18)	0.07 (0.27)	0.07 (0.25)	0.57 (1.36)
Temporal	0.00 (0.00)	0.08 (0.27)	0.05 (0.33)	0.21 (0.50)	0.03 (0.18)	0.41 (1.15)	0.23 (0.63)	1.48 (3.12)
Any subcortical	0.00 (0.00)	0.03 (0.16)	0.08 (0.28)	0.11 (0.31)	0.00 (0.00)	0.04 (0.19)	0.00 (0.00)	0.19 (0.87)
Deep								
Basal ganglia	0.00 (0.00)	0.18 (0.51)	0.38 (0.79)	0.18 (0.61)	0.03 (0.18)	0.22 (0.51)	0.17 (0.38)	0.71 (1.23)
Thalamus	0.00 (0.00)	0.00 (0.00)	0.03 (0.16)	0.00 (0.00)	0.00 (0.00)	0.07 (0.27)	0.17 (0.46)	0.43 (1.33)
Internal capsule	0.00 (0.00)	0.00 (0.00)	0.03 (0.16)	0.00 (0.00)	0.03 (0.18)	0.44 (0.84)	0.23 (0.77)	0.62 (1.72)
Any deep	0.00 (0.00)	0.00 (0.00)	0.03 (0.16)	0.11 (0.31)	0.03 (0.18)	0.11 (0.32)	0.20 (0.66)	0.24 (0.89)
Infratentorial								
Cerebellum	0.00 (0.00)	0.00 (0.00)	0.03 (0.16)	0.00 (0.00)	0.03 (0.18)	0.15 (0.36)	0.13 (0.35)	0.86 (3.50)
Pons	0.00 (0.00)	0.03 (0.16)	0.00 (0.00)	0.00 (0.00)	0.00 (0.00)	0.11 (0.42)	0.03 (0.18)	0.14 (0.48)
Mesencephalon	0.00 (0.00)	0.00 (0.00)	0.00 (0.00)	0.00 (0.00)	0.00 (0.00)	0.15 (0.46)	0.03 (0.18)	0.14 (0.65)
Any	0.00 (0.00)	0.00 (0.00)	0.00 (0.00)	0.00 (0.00)	0.00 (0.00)	0.04 (0.19)	0.00 (0.00)	0.29 (1.10)
Any	0.00 (0.00)	0.51 (0.91)	0.89 (1.29)	0.79 (1.23)	0.31 (0.59)	2.11 (3.53)	1.53 (2.36)	6.33 (14.96)

SD, standard deviation; CMBs, cerebral microbleeds.

TABLE 3 | Neuropsychological tests of participants in the four groups [mean (SD)].

	HC (n = 36)	Mild WMHs (n = 39)	Moderate WMHs (n = 37)	Severe WMHs (n = 28)	F/χ^2	P
MoCA	22.33 (3.09)^{c}	21.16 (4.32)^{d}	21.06 (3.79)^{e}	17.81 (4.91)^{c,d,e}	6.850	<0.001***
AVLT-study	8.15 (1.59)^{c}	7.63 (2.24)^{d}	7.31 (1.52)	6.55 (2.00)^{c,d}	3.776	0.012*
AVLT-immediate	9.40 (2.30)^{c}	8.17 (3.84)^{d}	7.88 (2.65)^{e}	6.17 (3.27)^{c,d,e}	5.320	0.002**
AVLT-delay	9.06 (2.41)^{b,c}	7.95 (3.76)	7.31 (2.67)^{b}	6.50 (3.13)^{c}	3.731	0.013*
AVLT-recognition	13.63 (1.33)^{c}	13.53 (3.68)^{d}	13.16 (1.87)^{e}	11.13 (3.62)^{c,d,e}	4.734	0.004**
TMT-A	63.34 (24.76)^{a,b,c}	80.72 (33.12)^{a,d}	79.12 (33.73)^{b,e}	105.82 (37.72)^{c,d,e}	8.233	<0.001***
TMT-B	129.65 (44.44)^{c}	155.35 (70.69)^{d}	158.16 (73.16)^{e}	207.55 (81.24)^{c,d,e}	6.301	0.001**
BNT	13.94 (0.98)^{a,b,c}	12.89 (1.54)^{a}	13.25 (1.68)^{b}	12.74 (1.40)^{c}	4.797	0.003**
PHQ-9	3.31 (4.78)^{c,d}	3.74 (4.56)^{d}	5.00 (4.62)	7.39 (5.81)^{c,d}	4.272	0.006**
GAD-7	2.40 (3.24)^{c,d}	2.61 (4.10)^{d}	2.81 (3.43)^{e}	5.29 (5.48)^{c,d,e}	3.282	0.023*

*HC, healthy controls; WMHs, white matter hyperintensities; SD, standard deviation; MoCA, Montreal Cognitive Assessment; PHQ, Patient Health Questionnaire; GAD, generalized anxiety disorder; AVLT, Chinese Auditory Learning Test; TMT, Trial Making Test; and BNT, Boston Naming Test. [a]Healthy control group vs. mild WMHs group significantly different ($P < 0.05$). [b]Healthy control group vs. moderate WMHs group significantly different ($P < 0.05$). [c]Healthy control group vs. severe WMHs group significantly different ($P < 0.05$). [d]Mild WMHs group vs. severe WMHs group significantly different ($P < 0.05$). [e]Moderate WMHs group vs. severe WMHs group significantly different ($P < 0.05$). ***Significant at 0.001 level, **significant at 0.01 level, and *significant at 0.05 level (two tailed).*

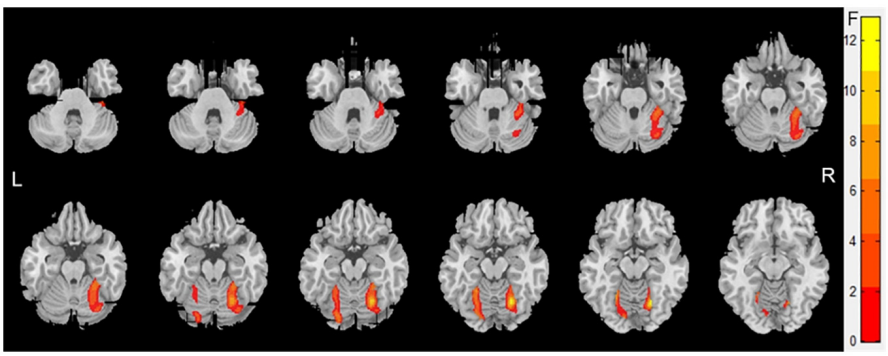

FIGURE 1 | Voxel-based morphometry showing gray matter loss in the cerebellar subregions for patients with White matter hyperintensities (WMHs) in comparison with controls. Areas of significant gray matter loss (red) included the cerebellar subregions right-sided lobule VI [voxel size: 2,106; peak MNI coordinates: x = 22.5, y = –63, and z = –15; Gaussian random field (GRF) for voxel levels at $P < 0.001$ and cluster at $P < 0.05$] and left-sided lobule VI (voxel size: 703; peak MNI coordinates: x = –22.5, y = –54, and z = –15; GRF for voxel levels at $P < 0.001$ and cluster at $P < 0.05$), for patients with WMHs vs. control subjects.

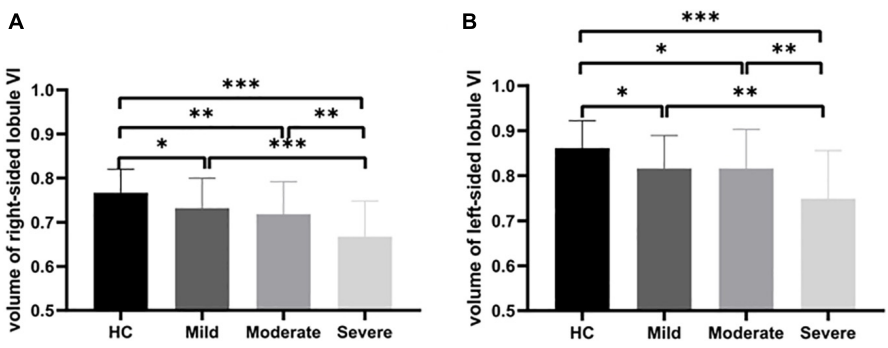

FIGURE 2 | Group comparison of cerebellar atrophy. Volume contrasts within two subregions of the cerebellum across four groups. *Post-hoc* analysis of the brain regions with significant differences among the four groups. **(A)** The gray matter volume (GMV) of the right-sided cerebellum lobule VI showing atrophy in WMHs groups. **(B)** The GMV of the left-sided cerebellum lobule VI showing atrophy in WMHs groups. ***$P < 0.001$, **$P < 0.01$, and *$P < 0.05$.

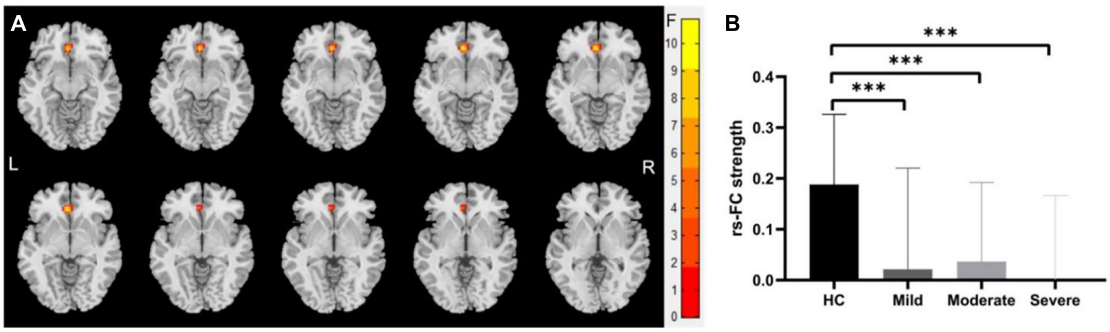

FIGURE 3 | Differences of functional connectivity (FC) between groups at the right-sided cerebellum lobule VI—whole brain level. **(A)** Significant differences were observed between patients with WMHs and healthy controls (HC) in the FC between the right-sided cerebellum lobule VI with the left anterior cingulate gyri (voxel size: 39; peak MNI coordinates: $x = -3$, $y = 33$, and $z = -6$; GRF for voxel levels at $P < 0.001$ and cluster at $P < 0.05$). **(B)** The functional connectivity of the right-sided cerebellum lobule VI with the left anterior cingulate gyri was significantly decreased in patients with WMHs. ***$P < 0.001$.

to frontoparietal cognitive networks (lobules crus II and VIIb) in patients with CSVD (Schaefer et al., 2014). Another study revealed that both the number and volume of WMHs were correlated with decreased FC of the cerebellum (Kerkovsky et al., 2019). Our findings provide further support for cerebellar involvement in WMHs. Despite the difficulties in interpreting WMHs pathology, the fact that atrophy and impaired FC correlated with WMHs severity observed in our study suggested that cerebellar changes should be at least partly related to the basic pathological process of WMHs.

The existing studies have shown that in patients with WMHs, memory, processing speed, and executive function impairments exist compared with HCs, and structural and functional brain abnormalities in the cerebellum have also been reported (Buckner, 2013; Kaskikallio et al., 2019). However, the association between cognitive decline and cerebellum in patients with WMHs is rarely discussed. The cerebellum has traditionally been thought to contribute mainly to motor coordination (Ito, 2000; Gao et al., 2012). However, increasing evidence has demonstrated that the cerebellum also plays an important role in cognitive processing, and memory and executive functions are mostly localized in the posterior cerebellum (E et al., 2014), which is supported by many researchers. Functional MRI evidence found cerebellar activation is a consistent finding with memory tasks predominantly in the posterior lobe of the cerebellum (Zacharia and Eslinger, 2019). Schmahmann found that lesions of the posterior lobe of the cerebellum were particularly important in impairments in executive function (Zhuang et al., 2017; Schmahmann, 2019). Researchers suspect that the most likely route for cerebellar contribution to cognition is *via* interactions with the neocortex (Wagner and Luo, 2020). This means that damage to the posterior lobe of the cerebellum and its connections may potentially degrade and disconnect cognition subserved by it. In line with previous studies, both atrophy and hypoconnectivity of cerebellum lobule VI were found to be related to cognitive decline in WMHs in our study, suggesting that the cerebellum with its influence on the cingulate cortex is responsible for cognitive decline in patients with WMHs. This is particularly relevant because the cerebellum's ability to work full time likely depends on its internal integrity and the integrity of its cortical connections, and local gray matter change in cerebellum lobule VI, or its functional connections (the cingulate), might influence cerebellar activity.

Several limitations of this study should be addressed. First, the sample size was relatively small, and therefore, our findings require validation in a larger cohort. Second, this cross-sectional study only provides correlational but no causal associations that need to be approached by longitudinal study designs. Third, it is impossible to eliminate the concomitant structural changes of WMHs, such as lacunes, although the lacunes were much less severe than WMHs in the current study. Further studies using a prospective design are needed to address these issues.

In conclusion, this study demonstrated that CSVD patients with WMHs display a lower bilateral GMV and a decreased FC in specific subregions of the cerebellum related to cognitive functions (VI). Moreover, correlations exist between these brain alterations and specific neurocognitive functions including memory and executive function. Together, it is quite a novelty to demonstrate that cerebellar abnormalities could occur in CSVD patients with WMHs and to introduce its unique contribution to cognitive functions, which led to the growing recognition of the cerebellum's role in CSVD patients with WMHs.

DATA AVAILABILITY STATEMENT

The raw data supporting the conclusions of this article will be made available by the authors, without undue reservation.

ETHICS STATEMENT

The studies involving human participants were reviewed and approved by Ethics Committee of the First Affiliated Hospital of Anhui Medical University. The patients/participants provided their written informed consent to participate in this study. Written informed consent was obtained from the individual(s)

for the publication of any potentially identifiable images or data included in this article.

AUTHOR CONTRIBUTIONS

SC and JN: performed the analysis and wrote the manuscript. KW: made substantial contribution to the conception of the work. KW, YT, and QW: designed the work. CC, XW, and YL: conducted acquisition and analysis. YM and BD: interpreted the data for the work. KW, YT, and QW: gave final approval of the version to be published and agreed to be accountable for all aspects of the work. All authors contributed to the article and approved the submitted version.

FUNDING

This study was supported by grants from the National Key Research and Development Program of China (2016YFC1300604) and National Science and Technology Fundamental Resources Investigation Program of China (2018FY100900).

ACKNOWLEDGMENTS

We would like to thank the Information Science Laboratory Center of the University of Science and Technology of China for their measurement services.

REFERENCES

Ahmadian, N., van Baarsen, K., van Zandvoort, M., and Robe, P. A. (2019). The cerebellar cognitive affective syndrome-a meta-analysis. *Cerebellum* 18, 941–950. doi: 10.1007/s12311-019-01060-2

Badura, A., Verpeut, J. L., Metzger, J. W., Pereira, T. D., Pisano, T. J., Deverett, B., et al. (2018). Normal cognitive and social development require posterior cerebellar activity. *Elife* 7:e36401.

Borghammer, P., Ostergaard, K., Cumming, P., Gjedde, A., Rodell, A., Hall, N., et al. (2010). A deformation-based morphometry study of patients with early-stage Parkinson's disease. *Eur. J. Neurol.* 17, 314–320. doi: 10.1111/j.1468-1331.2009.02807.x

Buckner, R. L. (2013). The cerebellum and cognitive function: 25 years of insight from anatomy and neuroimaging. *Neuron* 80, 807–815. doi: 10.1016/j.neuron.2013.10.044

Cao, S., Zhang, J., Wang, Z., Pan, W., Tian, Y., Hu, P., et al. (2020). Laterality of attentional networks in patients with cerebral small vessel disease. *Front. Aging Neurosci.* 12:21. doi: 10.3389/fnagi.2020.00021

Chao-Gan, Y., and Yu-Feng, Z. (2010). DPARSF: a MATLAB toolbox for "pipeline" data analysis of resting-state fMRI. *Front. Syst. Neurosci.* 4:13. doi: 10.3389/fnsys.2010.00013

Chen, X., Huang, L., Ye, Q., Yang, D., Qin, R., Luo, C., et al. (2019). Disrupted functional and structural connectivity within default mode network contribute to WMH-related cognitive impairment. *NeuroImage Clin.* 24:102088. doi: 10.1016/j.nicl.2019.102088

E, K. H., Chen, S. H., Ho, M. H., and Desmond, J. E. (2014). A meta-analysis of cerebellar contributions to higher cognition from PET and fMRI studies. *Hum. Brain Mapp.* 35, 593–615. doi: 10.1002/hbm.22194

Fazekas, F., Chawluk, J. B., Alavi, A., Hurtig, H. I., and Zimmerman, R. A. (1987). MR signal abnormalities at 1.5 T in Alzheimer's dementia and normal aging. *AJR Am. J. Roentgenol.* 149, 351–356.

Gao, Z., van Beugen, B. J., and De Zeeuw, C. I. (2012). Distributed synergistic plasticity and cerebellar learning. *Nat. Rev. Neurosci.* 13, 619–635. doi: 10.1038/nrn3312

Gebeily, S., Fares, Y., Kordahi, M., Khodeir, P., Labaki, G., and Fazekas, F. (2014). Cerebral white matter hyperintensities (WMH): an analysis of cerebrovascular risk factors in Lebanon. *Int. J. Neurosci.* 124, 799–805. doi: 10.3109/00207454.2014.884087

Guo, C. C., Tan, R., Hodges, J. R., Hu, X., Sami, S., and Hornberger, M. (2016). Network-selective vulnerability of the human cerebellum to Alzheimer's disease and frontotemporal dementia. *Brain* 139(Pt 5), 1527–1538. doi: 10.1093/brain/aww003

Habas, C., Kamdar, N., Nguyen, D., Prater, K., Beckmann, C. F., Menon, V., et al. (2009). Distinct cerebellar contributions to intrinsic connectivity networks. *J. Neurosci.* 29, 8586–8594. doi: 10.1523/jneurosci.1868-09.2009

Han, F., Zhai, F., Wang, Q., Zhou, L. X., Ni, J., Yao, M., et al. (2018). Prevalence and risk factors of cerebral small vessel disease in a Chinese population-based sample. *J. Stroke* 20, 239–246. doi: 10.5853/jos.2017.02110

Hoogendam, Y. Y., van der Geest, J. N., van der Lijn, F., van der Lugt, A., Niessen, W. J., Krestin, G. P., et al. (2012). Determinants of cerebellar and cerebral volume in the general elderly population. *Neurobiol. Aging.* 33, 2774–2781. doi: 10.1016/j.neurobiolaging.2012.02.012

Ito, M. (2000). Mechanisms of motor learning in the cerebellum. *Brain Res.* 886, 237–245.

Jiang, J., Liu, T., Zhu, W., Koncz, R., Liu, H., Lee, T., et al. (2018). UBO Detector - A cluster-based, fully automated pipeline for extracting white matter hyperintensities. *Neuroimage* 174, 539–549. doi: 10.1016/j.neuroimage.2018.03.050

Kaskikallio, A., Karrasch, M., Koikkalainen, J., Lötjönen, J., Rinne, J. O., Tuokkola, T., et al. (2019). White matter hyperintensities and cognitive impairment in healthy and pathological aging: a quantified brain MRI study. *Dement Geriatr. Cogn. Disord.* 48, 297–307. doi: 10.1159/000506124

Kerkovsky, M., Stulik, J., Dostal, M., Kuhn, M., Lošák, J., Praksová, P., et al. (2019). Structural and functional MRI correlates of T2 hyperintensities of brain white matter in young neurologically asymptomatic adults. *Eur. Radiol.* 29, 7027–7036. doi: 10.1007/s00330-019-06268-8

Koziol, L. F., Budding, D., Andreasen, N., D'Arrigo, S., Bulgheroni, S., Imamizu, H., et al. (2014). Consensus paper: the cerebellum's role in movement and cognition. *Cerebellum* 13, 151–177. doi: 10.1007/s12311-013-0511-x

Mack, W. J., Freed, D. M., Williams, B. W., and Henderson, V. W. (1992). Boston Naming Test: shortened versions for use in Alzheimer's disease. *J. Gerontol.* 47, 154–158.

Nasreddine, Z. S., Phillips, N. A., Bedirian, V., Charbonneau, S., Whitehead, V., Collin, I., et al. (2005). The montreal cognitive assessment, MoCA: a brief screening tool for mild cognitive impairment. *J. Am. Geriatr. Soc.* 53, 695–699. doi: 10.1111/j.1532-5415.2005.53221.x

O'Callaghan, C., Hornberger, M., Balsters, J. H., Halliday, G. M., Lewis, S. J., and Shine, J. M. (2016). Cerebellar atrophy in Parkinson's disease and its implication for network connectivity. *Brain* 139(Pt 3), 845–855. doi: 10.1093/brain/awv399

Petito, C. K., Olarte, J., Roberts, B., Nowak, T. S., and Pulsinelli, W. A. (1998). Selective glial vulnerability following transient global ischemia in rat brain. *J. Neuropath. Exp. Neur.* 57, 231–238. doi: 10.1097/00005072-199803000-00004

Prins, N. D., van Dijk, E. J., den Heijer, T., Vermeer, S. E., Jolles, J., Koudstaal, P. J., et al. (2005). Cerebral small-vessel disease and decline in information processing speed, executive function and memory. *Brain* 128(Pt 9), 2034–2041. doi: 10.1093/brain/awh553

Schaefer, A., Quinque, E. M., Kipping, J. A., Arélin, K., Roggenhofer, E., Frisch, S., et al. (2014). Early small vessel disease affects frontoparietal and cerebellar hubs in close correlation with clinical symptoms–a resting-state fMRI study. *J. Cereb. Blood Flow Metab.* 34, 1091–1095. doi: 10.1038/jcbfm.2014.70

Schmahmann, J. D. (2019). The cerebellum and cognition. *Neurosci. Lett.* 688, 62–75.

Schoenberg, M. R., Dawson, K. A., Duff, K., Patton, D., Scott, J. G., and Adams, R. L. (2006). Test performance and classification statistics for the Rey Auditory Verbal Learning Test in selected clinical samples. *Arch. Clin. Neuropsychol.* 21, 693–703. doi: 10.1016/j.acn.2006.06.010

Selnes, O. A., Jacobson, L., Machado, A. M., Becker, J. T., Wesch, J., Miller, E. N., et al. (1991). Normative data for a brief neuropsychological screening battery. Multicenter AIDS Cohort Study. *Percept. Mot. Skills* 73, 539–550. doi: 10.2466/pms.1991.73.2.539

Silva, P., Spedo, C. T., Barreira, A. A., and Leoni, R. F. (2018). Symbol digit modalities test adaptation for magnetic resonance imaging environment: a systematic review and meta-analysis. *Mult. Scler. Relat. Disord.* 20, 136–143. doi: 10.1016/j.msard.2018.01.014

Smarr, K. L., and Keefer, A. L. (2011). Measures of depression and depressive symptoms: beck depression inventory-II (BDI-II), Center for epidemiologic studies depression scale (CES-D), geriatric depression scale (GDS), hospital anxiety and depression scale (HADS), and Patient Health Questionnaire-9 (PHQ-9). *Arthritis Care Res. (Hoboken)* 63(Suppl. 11), S454–S466.

Smith, E. E., O'Donnell, M., Dagenais, G., Lear, S. A., Wielgosz, A., Sharma, M., et al. (2015b). Early cerebral small vessel disease and brain volume, cognition, and gait. *Ann. Neurol.* 77, 251–261.

Smith, E. E., O'Donnell, M., Dagenais, G., Lear, S. A., Wielgosz, A., Sharma, M., et al. (2015a). Early cerebral small vessel disease and brain volume, cognition, and gait. *Ann. Neurol.* 77, 251–261.

Smith, E. E., Salat, D. H., Jeng, J., McCreary, C. R., Schmahmann, J. D., Fischl, B., et al. (2011). Correlations between MRI white matter lesion location and executive function and episodic memory. *Neurology* 76, 1492–1499. doi: 10.1212/wnl.0b013e318217e7c8

Tan, R. H., Devenney, E., Dobson-Stone, C., Kwok, J. B., Hodges, J. R., Kiernan, M. C., et al. (2014). Cerebellar integrity in the amyotrophic lateral sclerosis-frontotemporal dementia continuum. *PLoS One* 9:e105632. doi: 10.1371/journal.pone.0105632

Wagner, M. J., and Luo, L. (2020). Neocortex–cerebellum circuits for cognitive processing. *Trends Neurosci.* 43, 42–54. doi: 10.1016/j.tins.2019.11.002

Ward, A. M., Mormino, E. C., Huijbers, W., Schultz, A. P., Hedden, T., and Sperling, R. A. (2015). Relationships between default-mode network connectivity, medial temporal lobe structure, and age-related memory deficits. *Neurobiol. Aging* 36, 265–272. doi: 10.1016/j.neurobiolaging.2014.06.028

Wen, W., Sachdev, P. S., Li, J. J., Chen, X., and Anstey, K. J. (2009). White matter hyperintensities in the forties: their prevalence and topography in an epidemiological sample aged 44-48. *Hum. Brain Mapp.* 30, 1155–1167. doi: 10.1002/hbm.20586

Wu, Y., Wu, X., Wei, Q., Wang, K., and Tian, Y. (2020). Differences in cerebral structure associated with depressive symptoms in the elderly with alzheimer's disease. *Front. Aging Neurosci.* 12:107. doi: 10.3389/fnagi.2020.00107

Yamamoto, D., Kazui, H., and Takeda, M. (2011). [Wechsler adult intelligence scale-III (WAIS-III)]. *Nihon Rinsho.* 69(Suppl. 8), 403–407.

Yamanaka, T., Uchida, Y., Sakurai, K., Kato, D., Mizuno, M., Sato, T., et al. (2019). Anatomical links between white matter hyperintensity and medial temporal atrophy reveal impairment of executive functions. *Aging Dis.* 10:711. doi: 10.14336/ad.2018.0929

Zacharia, T. T., and Eslinger, P. J. (2019). Functional MRI activation patterns of cerebellum in patients with epilepsy and brain tumors. *Clin. Anat.* 32, 1053–1060. doi: 10.1002/ca.23439

Zhuang, Y., Zeng, X., Wang, B., Huang, M., Gong, H., and Zhou, F. (2017). Cortical surface thickness in the middle-aged brain with white matter hyperintense lesions. *Front. Aging Neurosci.* 9:225. doi: 10.3389/fnagi.2017.00225

Conflict of Interest: The authors declare that the research was conducted in the absence of any commercial or financial relationships that could be construed as a potential conflict of interest.

frontiers in Aging Neuroscience

ORIGINAL RESEARCH
published: 14 July 2021
doi: 10.3389/fnagi.2021.672077

Association of Tau Pathology With Clinical Symptoms in the Subfields of Hippocampal Formation

Xinting Ge[1,2,3†], Dan Zhang[2†], Yuchuan Qiao[2], Jiong Zhang[2], Junhai Xu[4] and Yuanjie Zheng[1]* on behalf of Alzheimer's Disease Neuroimaging Initiative***

[1]School of Information Science and Engineering, Shandong Normal University, Jinan, China, [2]Laboratory of Neuro Imaging (LONI), USC Stevens Neuroimaging and Informatics Institute, Keck School of Medicine, University of Southern California, Los Angeles, CA, United States, [3]School of Medical Imaging, Xuzhou Medical University, Xuzhou, China, [4]College of Intelligence and Computing, Tianjin Key Lab of Cognitive Computing and Application, Tianjin University, Tianjin, China

Objective: To delineate the relationship between clinical symptoms and tauopathy of the hippocampal subfields under different amyloid statuses.

Methods: One hundred and forty-three subjects were obtained from the ADNI project, including 87 individuals with normal cognition, 46 with mild cognitive impairment, and 10 with Alzheimer's disease (AD). All subjects underwent the tau PET, amyloid PET, T1W, and high-resolution T2W scans. Clinical symptoms were assessed by the Neuropsychiatric Inventory (NPI) total score and Alzheimer's Disease Assessment Scale cognition 13 (ADAS-cog-13) total score, comprising memory and executive function scores. The hippocampal subfields including Cornu Ammonis (CA1–3), subiculum (Sub), and dentate gyrus (DG), as well as the adjacent para-hippocampus (PHC) and entorhinal cortex (ERC), were segmented automatically using the Automatic Segmentation of Hippocampal Subfields (ASHS) software. The relationship between tauopathy/volume of the hippocampal subfields and assessment scores was calculated using partial correlation analysis under different amyloid status, by controlling age, gender, education, apolipoprotein E (*APOE*) allele $\varepsilon 4$ carrier status, and, time interval between the acquisition time of tau PET and amyloid PET scans.

Results: Compared with amyloid negative (A−) group, individuals from amyloid positive (A+) group are more impaired based on the Mini-mental State Examination (MMSE; p = 3.82e-05), memory (p = 6.30e-04), executive function (p = 0.0016), and ADAS-cog-13 scores (p = 5.11e-04). Significant decrease of volume (CA1, DG, and Sub) and increase of tau deposition (CA1, Sub, ERC, and PHC) of the hippocampal subfields of both hemispheres were observed for the A+ group compared to the A- group. Tauopathy of ERC is significantly associated with memory score for the A- group, and the associated regions spread into Sub and PHC for the A+ group. The relationship between the impairment of behavior or executive function and tauopathy of the hippocampal subfield was discovered within the A+ group. Leftward asymmetry was observed with the association between assessment scores and tauopathy of the hippocampal subfield, which is more prominent for the NPI score for the A+ group.

OPEN ACCESS

Edited by:
Rong Chen, University of Maryland, Baltimore, United States

Reviewed by:
Muthuswamy Anusuyadevi, Bharathidasan University, India
Gabriel Gonzalez-Escamilla, Johannes Gutenberg University Mainz, Germany

***Correspondence:**
Junhai Xu
jhxu@tju.edu.cn
Yuanjie Zheng
yjzheng@sdnu.edu.cn

†These authors have contributed equally to this work

***Data used in preparation of this article were partly obtained from the Alzheimer's Disease Neuroimaging Initiative (ADNI) database (adni.loni.usc.edu). As such, the investigators within the ADNI contributed to the design and implementation of ADNI and/or provided data but did not participate in analysis or writing of this report. A complete listing of ADNI investigators can be found at: http://adni.loni.usc.edu/wp-content/uploads/how_to_apply/ADNI_Acknowledgement_List.pdf*

Received: *25 February 2021*
Accepted: *20 May 2021*
Published: *14 July 2021*

Citation:
Ge X, Zhang D, Qiao Y, Zhang J, Xu J and Zheng Y (2021) Association of Tau Pathology With Clinical Symptoms in the Subfields of Hippocampal Formation. Front. Aging Neurosci. 13:672077. doi: 10.3389/fnagi.2021.672077

Conclusion: The associations of tauopathy/volume of the hippocampal subfields with clinical symptoms provide additional insight into the understanding of local changes of the human HF during the AD continuum and can be used as a reference for future studies.

Keywords: Alzheimer's disease, hippocampal subfield, tau pathology, PET imaging, behavior symptoms

INTRODUCTION

Alzheimer's disease (AD) is characterized by the deposition of pathologic amyloid and tau proteins (Marks et al., 2017; Gordon et al., 2019; Scharre, 2019). Compared with β-amyloid (Aβ) plaques, tau deposition has been found to have a stronger association with cognitive decline during the AD continuum (Brier et al., 2016). Specimen research has revealed that the arise of tau deposition is firstly found in the trans-entorhinal cortex and then spreads into the temporal lobe regions such as the hippocampal formation (HF), and finally reaches the neocortex (Braak and Del Tredici, 2011; Braak et al., 2011). As the central node of the mnemonic circuitry, impairment of the HF has received much attention from other researchers (Yushkevich et al., 2015; Adler et al., 2018; Evans et al., 2018) to study the occurrence and progression of AD.

The HF has been associated with memory and cognitive functions and is conventionally used as one of the early biomarkers of several neuropsychiatric disorders including AD and Parkinson's disease (PD; Ikram et al., 2010; Adler et al., 2018; Das et al., 2019). AD subjects present a significant decrease in hippocampal volume and multifaceted impairment of adult hippocampal neurogenesis (AHN) compared to cognitively normal (CN) individuals (Adler et al., 2018; Moreno-Jiménez et al., 2019). However, morphometry changes of the whole HF may be insufficient to delineate the detailed neurodegenerative features during the progression of AD as the human HF is comprised of several substructures including the dentate gyrus (DG), the Cornu Ammonis (CA), the subiculum (Sub), and the associated white matter tracts (Naidich et al., 1987). Subfields of the HF may exhibit differential patterns in their association with cognitive performance in specific domains, as well as the subsequent risk of dementia. The atrophy of subiculum and pre-subiculum regions were found strongly associated with executive dysfunction (Evans et al., 2018). CA1 and fimbria also showed the trend toward significant volume reduction with the progression of AD (Parker et al., 2019; Zhao et al., 2019). In addition, the impairment of the HF can be regarded as the neurodegeneration assessment following the amyloid/tau/neurodegeneration (AT[N]) framework (Jack et al., 2016, 2019; Jack Jr et al., 2018). The spreading patterns of biomarker findings such as tau deposition of the hippocampal subfields, as well as its association with the clinical symptoms during the AD continuum, however, remain relatively underexplored.

In addition, behavioral changes are the accompanying characteristics with AD progression and severely impact the patients' quality of life and caregivers' burdens (Zhao et al., 2016; Deb et al., 2018). CN individuals with abnormal behavior symptoms were found to be at higher risk of developing mild cognitive impairment (MCI; Mok et al., 2004; Masters et al., 2015). Much research has demonstrated that the presence of mild behavioral impairment can be used as an "at-risk" state for cognitive decline and dementia (Ismail et al., 2016; Yoon et al., 2019). As one of the early markers of AD, impairment of the hippocampal subfield may also be associated with the rise of behavior symptoms. The characterization of these relationships will help us to determine if the presence of behavior symptoms provides additional information for the understanding of the AD continuum.

The specific aim of the current study was to observe the relationship between tau deposition of each hippocampal subfield and clinical symptoms (assessed by the memory, cognition, executive function, and behavior scores) under different amyloid status (amyloid negative and positive). The Alzheimer's Disease Assessment Scale-Cognitive (ADAS-cog) was used to measure the cognitive performance (Petersen et al., 2010; Kueper et al., 2018) and the Neuropsychiatric Inventory (NPI) was used to quantify the severity and frequency of behavior symptoms in the ADNI project (Cummings, 1997; Nunes et al., 2019). The volume of each hippocampal subfield was also assessed in the current research to calculate its association with the clinical scores. AD-related factors including age, gender, education, and apolipoprotein E (*APOE*) allele ε4 carrier status were considered in the statistical analysis based on previous studies (Tosun et al., 2017; McCartney et al., 2018). We hypothesize that the tauopathy/volume of different hippocampal subfields may have diverse association patterns with the clinical symptoms, even under the same amyloid status. They may exhibit an enhanced association between the tauopathy/volume of hippocampal subfield and the clinical symptoms with the presence of amyloid pathology. Our results may provide additional insight into the detailed analysis of the local changes of the human HF during the AD continuum and can be used as the reference for future AD studies.

MATERIALS AND METHODS

Participant

ADNI project was conducted to measure the progression of MCI and early AD based on serial MRI, PET, other biomarkers, and clinical and neuropsychological assessments (Weiner et al., 2015). The diagnostic criteria in ADNI was described beforehand and informed written consent was obtained from all participants

TABLE 1 | Data characteristics (A−: amyloid negative, A+ : amyloid positive, n.s.: no significant, $p < 0.05$).

Amyloid status	A−	A+	*P*-value
Number of subjects (*N*)	88	55	
CN/MCI/AD	59/28/1	28/18/9	
Age (years)	75.05 ± 6.77	77.99 ± 7.90	0.0192
Education (years)	16.40 ± 2.68	16.47 ± 2.73	n.s.
Gender (M/F)	40/48	24/31	n.s.
APOE ε4 (0/1/2)	71/15/1	25/22/7	1.96e-06
MMSE	28.75 ± 1.74	26.55 ± 4.35	3.82e-05
Memory	0.82 ± 0.69	0.31 ± 0.98	6.30e-04
Executive function	0.94 ± 0.95	0.33 ± 1.24	0.0016
ADAS-cog-13	14.23 ± 6.02	19.58 ± 10.10	1.33e-04
NPI	2.86 ± 6.40	5.07 ± 8.94	n.s.

at each site (Petersen et al., 2010). In our study, we firstly screened subjects who underwent both ^{18}F-AV-1451 PET and structural T1 scans in the latest visit. Subjects with amyloid florbetapir (AV-45) PET scans and T2 scans (High-resolution hippocampus sequence) within the time interval of 1 year before/after the acquisition time of tau PET scans were then selected. The Aβ status was determined by previous studies with a cutoff of 1.11 for AV-45 tracer (Landau et al., 2014). Participants with age >65 years and complete cognitive and behavioral assessments were included in our study as we focused on late-onset AD. By June 11th of 2019, 143 participants meeting the above requirements were selected from ADNI-2 and ADNI-3 (**Table 1**).

T1-Weighted and T2-Weighted MRI Acquisition and Processing

All subjects were scanned by 3.0 T MRI scanners using a 3D MP-RAGE or IR-SPGR T1-weighted sequences and high-resolution hippocampus T2-weighted sequence. The detailed protocol can be found online[1].

Tau PET Image Acquisition and Processing

Tau PET images were preprocessed according to the standardized protocols at each ADNI site. All images were verified with quality control and processed with realignment, averaging, and resampled to an isotropic voxel size of 8 mm. We obtained the brain ROIs based on the Desikan-Killiany Atlas (Desikan et al., 2006) and mapped the PET image to the structural T1-weighted MRI image. Standardized uptake value ratio (SUVR) images were calculated for each subject using the whole cerebellum gray matter as the reference region.

Segmentation of the Hippocampal Subfields

ASHS (Automatic Segmentation of Hippocampal Subfields) software was used for the automatic segmentation of the hippocampal subfields for each subject[2]. T1 weighted and high-resolution T2 weighted MRI data were imported into the ASHS to automatically parcellate the HF and adjacent brain regions into CA1, CA2, CA3, Sub, para-hippocampus (PHC), entorhinal cortex (ERC), and DG (**Figure 1**). The ERC and PHC were also considered in the current study as these two regions were adjacent to the HF and were closely related to the progression of AD. The CA2 and CA3 regions were considered together in the following analysis as the size of these regions were relatively small. Mean SUVRs of the six regions on each hemisphere were finally calculated from the SUVR images.

Clinical Symptoms

In the current research, we focus on the behavior score and the cognition score, as well as the comprised memory and executive function scores to delineate their relationship with tau pathology. The total score of NPI based on 12 domains was used to assess the behavioral symptoms. The total score of ADAS-cog based on 13 domains was used to measure cognitive symptoms. The composite score for memory was composed of scores of the Rey's Auditory Vocabulary List Test (RAVLT), Alzheimer's Disease Assessment Scale—cognitive subscale-11 (ADAS-Cog), Logical Memory (LM), and MMSE recall scores. The composite score for executive function included Category Fluency (animals and vegetables scores), Trail Making Test (TMT) A and B, Digit span backward, Wechsler Adult Intelligence Scale-Revised (WAIS-R) Digit Symbol Substitution, and five Clock drawing items (circle, symbol, numbers, hands, time). Clinical scores were acquired within the time interval of 3 months before/after the acquisition time of Tau PET scans.

Statistical Analysis

For paired group comparison based on amyloid status (A+ and A−), a two-tailed Student *t*-test was applied to the mean SUVR or volume of each hippocampal subfield between A− and A+ groups. For hemispheric comparison, a two-tailed Student *t*-test was applied to the mean SUVR or volume of each hippocampal subfield between the left and right hemisphere under different amyloid status.

To assess the association of clinical symptoms and mean SUVR (or volume) of each hippocampal subfield, partial correlation analysis was conducted on two groups (A+ and A−) for each hippocampal subfield. The NPI total score, ADAS-cog-13 total score, comprised memory score, and comprised executive function score were treated as the response variable and the mean SUVR or volume of each hippocampal subfield as the predictor. Age, gender, education, *APOE* allele ε4 carrier status, and the time interval between the acquisition time of amyloid PET and tau PET scans were used as the covariates of the partial correlation analysis. For all statistical tests, the false discovery rate (FDR) correction was applied for the correction of multiple comparisons. An adjusted *p*-value less than 0.05 was considered as statistically significant in all analyses.

Data Availability

All ADNI data used in our experiments are publicly available through LONI IDA[3].

[1]http://adni.loni.usc.edu/methods/documents/mri-protocols
[2]http://picsl.upenn.edu/software/ashs/
[3]https://ida.loni.usc.edu/

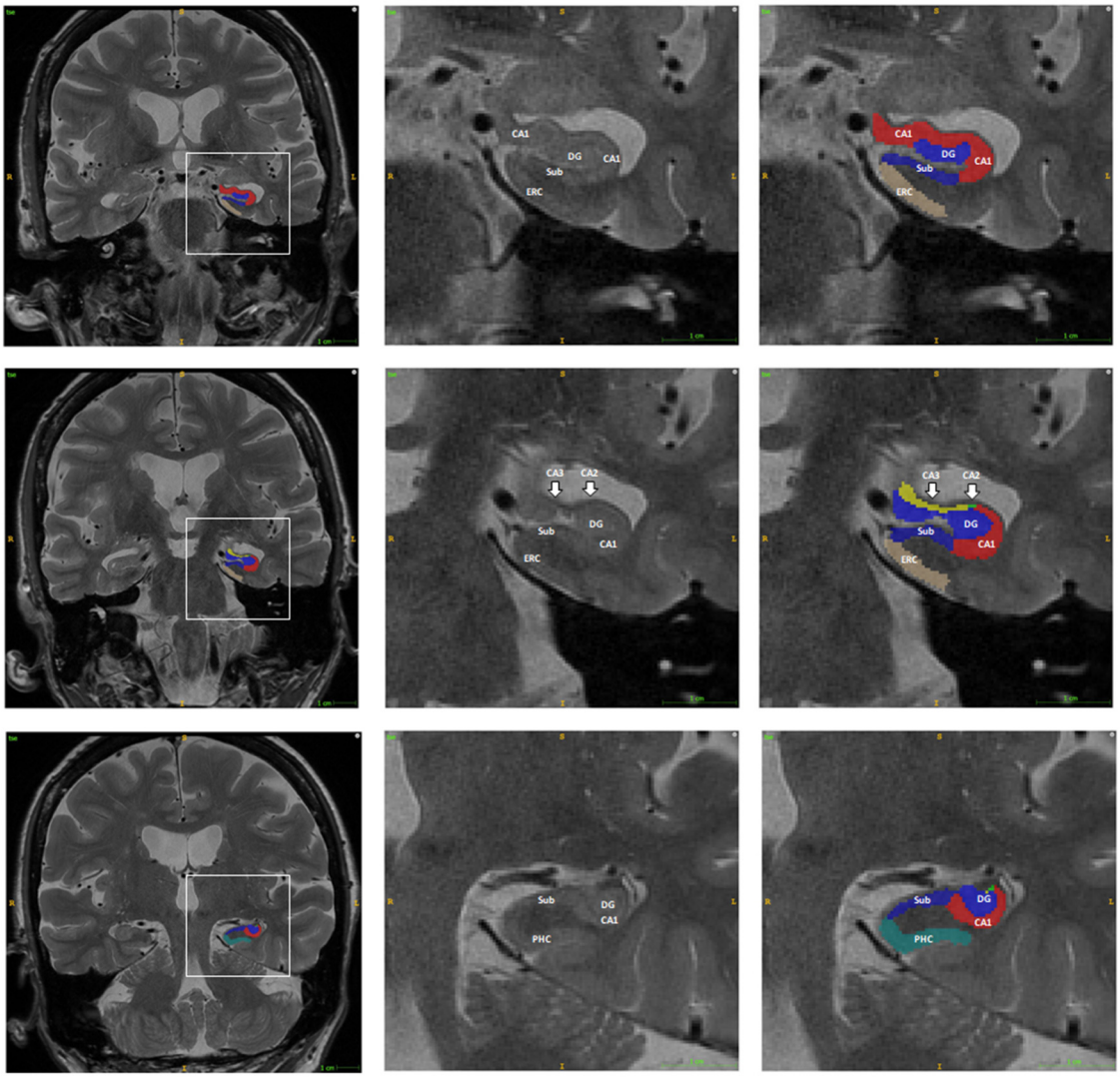

FIGURE 1 | Example of the automatic segmentation of the hippocampal subfield using ASHS software. The boundary of each hippocampal subfield of the hippocampal head (first row), body (second row), and tail (third row) are shown using ITK-SNAP software. The right two columns are the enlargement of the box in the left column. Abbreviations: DG, dentate gyrus; CA, Cornu Ammonis; Sub, subiculum; PHC, para-hippocampus; ERC, entorhinal cortex.

RESULTS

Data Characteristics

As we can see from **Table 1**, no significant difference in education level and gender distribution are found between the A− and A+ groups. Compared to the A− group, the A+ group has older subjects (p = 0.0192), more *APOE* allele ε4 carriers (p = 1.96e-06), and is more impaired based on the MMSE (p = 3.82e-05), memory (p = 6.30e-04), executive function (p = 0.0016), and ADAS-cog-13 scores (p = 5.11e-04).

The distribution of the mean tau SUVR and total volume of the whole region comprised of the six subfields in the current study were plotted in **Figure 2**. We should note that there may be several outliers in the current cohort. Outliers were then removed from each group based on the mean tau SUVR and total volume before the statistical analysis was conducted. If the outlier criterion was satisfied for any condition (mean SUVR or total volume for left or right hippocampi), this subject would be excluded as an outlier. These calculations were performed using the "isoutlier" function of MATLAB with the "mean" method. After outlier removal, three subjects in the amyloid negative group and one subject in the amyloid positive group were removed from the statistical analysis steps.

Comparison of Volume and Tau Deposition of the Hippocampal Subfields Between Amyloid Negative and Positive Groups

Significant volume decreases of the CA1, Sub, and DG for both hemispheres are observed from the A− group to the A+ group.

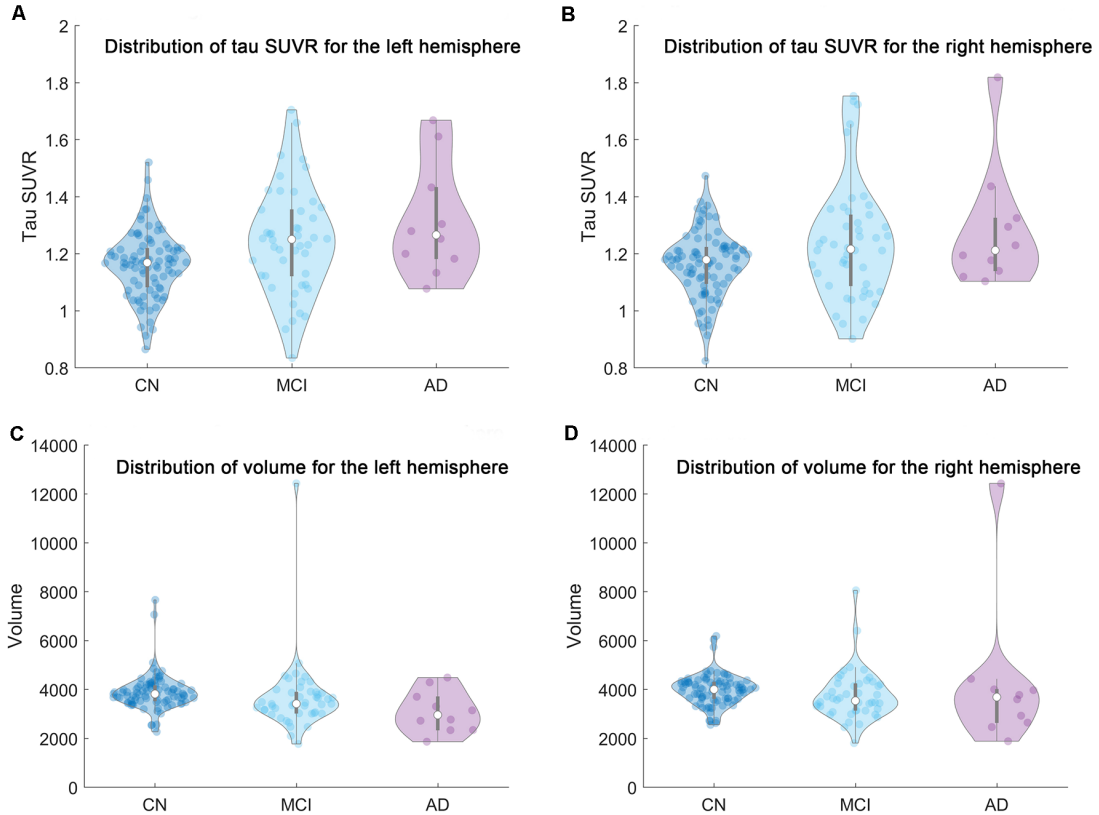

FIGURE 2 | The distribution of the mean tau SUVR and total volume of the whole region comprised of the six subfields in the current research for each group (CN/MCI/AD) were shown based on violin plot. From left to right and top to bottom are the distribution of **(A)** the mean tau SUVR for the left hemisphere, **(B)** the mean tau SUVR for the right hemisphere, **(C)** the total volume for the left hemisphere, and **(D)** the total volume for the right hemisphere, respectively.

Tau deposition of the CA1, Sub, ERC, and PHC for the A+ group increase significantly in both hemispheres compared to the A− group (**Table 2**).

Hemispheric Differences of the Hippocampal Subfields Within Specific Amyloid Status

For A− group, no significant difference is found between the left and right hippocampal subfield for tau SUVR. Hemispheric differences were prominent for hippocampal volume (leftward lower) mainly in the CA1 (p = 0.0069), DG (p = 0.0026), PHC (p = 0.0026), and CA2/CA3 (p = 1.92e-08) regions.

Similarly, no significant difference is found between the left and right hippocampal subfield for tau SUVR within the A+ group. The hemispheric difference is also prominent for hippocampal volume (leftward lower) mainly in the PHC (p = 0.0055) and CA2/CA3 (p = 2.57e-08) regions.

Partial Correlations Between Tau Deposition or Volume of the Hippocampal Subfields and Clinical Assessment Scores for A− Subjects

As can be seen from **Table 3**, the tau SUVR is found significantly correlated with memory score in the ERC for the left hemisphere, while no significant correlation was observed between the other clinical scores and tau SUVR of the hippocampal subfields for either hemisphere.

Differently, the volume of the left Sub and CA1 are significantly correlated with memory score, while no significant correlation is observed between the other assessment scores and hippocampal volumes (**Table 4**).

Partial Correlations Between Tau Deposition or Volume of the Hippocampal Subfields and Clinical Assessment Scores for A+ Subjects

As we can see from **Table 5**, significant correlations between the assessment scores and tau SUVR are found in the Sub, ERC, and PHC for the left hemisphere. Tau SUVR of CA1 region is also significantly associated with ADAS-cog-13 and NPI scores for the left hippocampi.

As to the right hemisphere, the correlations with tau SUVR are found in the ERC and the PHC with memory score, in the Sub, ERC, and PHC with ADAS-cog-13 score, and in the PHC with executive function score. No significant correlation is found between the NPI score and tau SUVR of the right hippocampal subfields.

TABLE 2 | Volume and tau deposition of the hippocampal subfields between different amyloid status ($p < 0.05$, FDR correction. n.s.: not significant).

	Hemisphere	CA1	DG	Sub	ERC	PHC	CA2/CA3
Volume	Left	0.0036	0.0414	0.0414	n.s.	n.s.	n.s.
	Right	0.0037	0.0037	0.017	n.s.	n.s.	n.s.
SUVR	Left	0.0110	n.s.	0.0027	0.0001	0.0014	n.s.
	Right	0.0417	n.s.	0.0006	0.0001	0.0006	n.s.

TABLE 3 | Associations between assessment scores and tau SUVR of the hippocampal subfields for A- group ($p < 0.05$, FDR correction).

Hemisphere	Assessment score	CA1	DG	Sub	ERC	PHC	CA2/CA3
Left	Memory	0.54	0.62	0.32	**0.04**	0.54	0.62
	ADAS-cog−13	0.49	0.49	0.18	0.18	0.35	0.49
	Executive function	0.47	0.47	0.47	0.47	0.47	0.47
	NPI	0.53	0.53	0.53	0.53	0.53	0.53
Right	Memory	0.67	0.81	0.52	0.051	0.67	0.81
	ADAS-cog-13	0.78	0.78	0.34	0.30	0.34	0.72
	Executive function	0.39	0.39	0.31	0.31	0.35	0.39
	NPI	0.30	0.30	0.30	0.30	0.30	0.30

Bold values mean the p's < 0.05 and statistically significant.

TABLE 4 | Associations between assessment scores and volume of the hippocampal subfields for A− group ($p < 0.05$, FDR correction).

Hemisphere	Assessment score	CA1	DG	Sub	ERC	PHC	CA2/CA3
Left	Memory	**0.01**	0.053	**0.004**	0.16	0.96	0.96
	ADAS-cog-13	0.07	0.43	0.07	0.61	0.96	0.48
	Executive function	0.50	0.86	0.09	0.86	0.86	0.48
	NPI	0.92	0.92	0.88	0.92	0.56	0.92
Right	Memory	0.27	0.21	0.21	0.21	0.31	0.78
	ADAS-cog-13	0.55	0.55	0.55	0.55	0.89	0.55
	Executive function	0.99	0.96	0.39	0.39	0.39	0.99
	NPI	0.51	0.51	0.51	0.67	0.51	0.67

Bold values mean the p's < 0.05 and statistically significant.

TABLE 5 | Associations between assessment scores and tau SUVR of the hippocampal subfields for A+ group ($p < 0.05$, FDR correction).

Hemisphere	Assessment score	CA1	DG	Sub	ERC	PHC	CA2/CA3
Left	Memory	0.08	0.64	**0.01**	**0.003**	**0.003**	0.20
	ADAS-cog-13	**0.02**	0.31	**0.001**	**0.0005**	**0.0005**	0.72
	Executive function	0.37	0.90	**0.048**	**0.008**	**0.008**	0.51
	NPI	**0.04**	0.25	**0.03**	**0.03**	**0.03**	0.83
Right	Memory	0.26	0.74	0.059	**0.03**	**0.02**	0.45
	ADAS-cog-13	0.06	0.51	**0.004**	**0.002**	**0.009**	0.84
	Executive function	0.43	0.74	0.11	0.054	**0.03**	0.74
	NPI	0.20	0.27	0.20	0.27	0.20	0.82

Bold values mean the p's < 0.05 and statistically significant.

TABLE 6 | Associations between assessment scores and volume of the hippocampal subfields for A+ group ($p < 0.05$, FDR correction).

Hemisphere	Assessment score	CA1	DG	Sub	ERC	PHC	CA2/CA3
Left	Memory	**0.008**	**0.008**	**0.03**	**0.008**	**0.02**	**0.04**
	ADAS_cog_13	0.14	0.23	0.11	0.11	0.74	0.68
	Executive function	0.16	0.12	0.19	0.35	0.12	0.83
	NPI	**0.008**	**0.008**	0.06	**0.005**	0.25	**0.008**
Right	Memory	**0.04**	0.053	0.053	**0.0004**	0.39	**0.04**
	ADAS_cog_13	0.09	0.17	0.09	**0.02**	0.91	0.15
	Executive function	0.10	**0.03**	0.12	**0.03**	0.12	0.12
	NPI	**0.07**	0.12	**0.01**	**0.003**	0.39	0.06

Bold values mean the p's < 0.05 and statistically significant.

Significant correlations between the volumes and memory score are found in all the subfields for the left hemisphere, while the association is only found with the CA1, ERC, and CA2/CA3 regions for the right hippocampi. The volume of the CA1, DG, ERC, and CA2/CA3 are found significantly correlated with the NPI score for the left hemisphere. However, there

is no significant correlation between the volume of the left subfields with either ADAS_cog_13 or executive function score. Differently, the ADAS_cog_13 score is found to be significantly correlated with the volume of the ERC and the executive function score is significantly correlated with the volume of the DG and ERC for the right hemisphere. The NPI total score is found associated with the volume of the CA1, Sub, and ERC for the right hippocampi (**Table 6**).

DISCUSSION

Atrophy of the HF is one of the early biomarkers for the diagnosis of neurodegenerative disorders including AD (Pizzi et al., 2016). However, neurodegeneration such as changes of the HF is not specific to AD and several neuropsychiatric disorders may have the same outcomes (Das et al., 2019). With the proposed AT[N] framework, the combination of the neurodegeneration assessed by the decrease of cortical thickness or the atrophy of HF and AD-related biomarkers such as pathology of amyloid and tau proteins were used to distinguish the stages of the AD continuum (Jack et al., 2016). In the current study, the memory score was found significantly associated with tau pathology in the ERC of the left hemisphere compared to the other hippocampal subfields, even for the amyloid negative individuals. On the contrary, impairment of cognition, behavior, and executive function were related to the changes of tauopathy/volume of hippocampal subfields when the amyloid status became positive. The impairment patterns of the hippocampal subfields observed in the current research are essential for the understanding of the AD spectrum and can be used as a reference for future AD studies.

Pathology of amyloid and tau proteins are the two defining hallmarks that can characterize the progression of AD. The presence of abnormal amyloid status was regarded as the 'disease state' to determine if the subject is during the Alzheimer's pathologic process (Brier et al., 2016). Individuals with positive amyloid biomarkers demonstrated a higher risk of the conversion from cognitive normal to mild cognitive impairment (Donohue et al., 2017). There is a strong association of elevated tau deposition in both medial temporal lobe structures and the neocortex with positive amyloid status across the normal aging to clinical dementia (Marks et al., 2017). In the current study, higher tau deposition is discovered in the CA1, Sub, ERC, and PHC of both hemispheres for the A+ group as compared to the A− group (**Table 2**). Significant volume decreases of the CA1, DG, and Sub of both hemispheres are also observed from the A- group to the A+ group. All confirm the increased disease severity with the presence of elevated amyloid pathology.

Previous studies showed that tau pathology in the medial temporal lobe (MTL) is a key driver of memory impairment in AD and is an important biomarker for neurodegeneration (Marks et al., 2017; Scott et al., 2020). Repeated tau PET scans have been an effective measurement to track the disease progression, while amyloid PET is more responsible for the detection of the early Alzheimer pathology (Hanseeuw et al., 2019). Tau deposition in the temporal lobe has been a better predictor of cognitive decline than the emergence of amyloid plaques in any region of the brain (Brier et al., 2016). The crucial role of tau deposition is recommended as a candidate target for AD therapy to deal with the limitations of the amyloid cascade hypothesis (Giacobini and Gold, 2013). We thus focused on the association of tau pathology with clinical symptoms in the hippocampal subfields under different amyloid statuses to delineate the detailed progression of AD. Tau SUVR of the ERC showed a significant correlation with the comprised memory score for the A− subjects in the current research (**Table 3**). ERC is one of the most vulnerable regions for the deposition of tau tangles and is closely associated with memory function (Braak et al., 2011). Impairment of the ERC has been regarded as an essential marker for the classical analysis of AD. Our results confirmed that the ERC should be paid more attention for the subsequent studies.

With the presence of amyloid pathology, the correlation between the tau SUVR with assessment scores spread into several subfields (**Table 5**). The tau SUVR of the Sub, ERC, and PHC are correlated with the comprised memory score, ADAS-cog-13 score, executive function score, and NPI total score for the left hippocampi. The tau SUVR of the CA1 region is also found significantly associated with the ADAS-cog-13 score and NPI total score for the left hemisphere. For the right hippocampi, the comprised memory score and ADAS-cog-13 score are found significantly correlated with the deposition of tau tangles in the ERC and PHC. It is known that the spatiotemporal spread of tau tangles follows a stereotypical trajectory starting from the locus coeruleus and the trans-entorhinal cortex, and then extending to the ERC, the HF, and finally the neocortex (Fuster-Matanzo et al., 2018). The associations between the tau deposition of the hippocampal subfields and assessment scores in the current research demonstrate that the development of AD may be affected in a progressive manner from the ERC and the PHC to the Sub, and eventually to the CA1 region on a smaller scale. On the other hand, the DG and the CA2/CA3 regions are less affected by the tau pathology. The DG is one of the few areas in the mammaliasn brain in which new excitatory neurons are continuously generated throughout life. The neural plasticity that results from the continuous integration of newly born excitatory granule cells may contribute to the DG network activity and withstand tau deposition. This could finally slow the disease progression (Tuncdemir et al., 2019; Christian et al., 2020). In addition, the NPI total score and executive function score were only found correlated with tau SUVR or volume of the hippocampal subfields with the presence of elevated amyloid pathology, which indicates that the decline of behavior and executive function is consistent with the neurodegenerative alterations of the HF when the subject was in the Alzheimer's pathologic process.

Volume changes of the hippocampal subfields are not as regular as the deposition of tau tangles. The CA1, DG, and Sub of both hemispheres have a volume decrease in the A+ group as compared to the A− group, while no significant difference is found in the ERC, PHC, and CA2/CA3 (**Table 2**). There is nearly no significant association between the volume

of the hippocampal subfields and assessment scores (except for the memory score) for the A- subjects (**Table 4**). With the presence of amyloid pathology, the relationship between the volume of the hippocampal subfields and assessment score is in conformity (**Table 6**). One possibility is that the volumetric changes of the hippocampal subfields are the sum of influences from normal aging and diverse neurodegenerative disorders such as AD, PD, and depression (Knopman et al., 2019). Individuals with diverse neuropsychiatric disorders may also be diagnosed as MCI or AD, which may affect the statistical results in the current study. Using volume changes of brain region without the help of AD-specific biomarkers is insufficient for the accurate diagnosis of AD (Edmonds et al., 2016; Sørensen et al., 2017).

Hemispheric difference is a classic topic in the neuroimaging area and still possesses a vital debate (Toga and Thompson, 2003; Pedraza et al., 2004; Woolard and Heckers, 2012). The left hippocampus was found more impaired than the right for individuals with subjective cognitive decline (Yue et al., 2018), as well as for the MCI and AD subjects (Shi et al., 2009). Similar results are discovered in the current research with the CA1 (p = 0.0069), DG (p = 0.0026), PHC (p = 0.0026), and CA2/CA3 (p = 1.92e-08) regions showing lower volume for the A− individuals. Lower volume of the left PHC (p = 0.0055) and CA2/CA3 (p = 2.57e-08) regions are also found for A+ group. In addition, the asymmetry of the association patterns between the tau SUVR of the hippocampal subfields and the assessment scores are obviously observed, and particularly more prominent for the NPI total score with the presence of elevated amyloid pathology (**Table 5**). Behavior symptoms including apathy, anxiety, and sleeping problems may be related to diverse brain functions and changes of specific hippocampal subfields (Chen et al., 2018; Campabadal et al., 2019; Dalton et al., 2019). The leftward asymmetry in the current research shows that the progression of AD may seriously affect the left hippocampi as compared to the right hemisphere.

LIMITATIONS

The diagnosis of the patients from ADNI is based on the clinical symptoms and clinical assessment scores other than the amyloid PET or tau PET scans. This is why one AD patient and some MCI individuals are included in the A- group, while many CN subjects are found in the A+ groups. Considering the integrity of the original data as well as the relatively small sample size, we put the CN, MCI, and AD subjects together for the statistical analysis in the current study. It is insufficient to observe the alterations of tau deposition or volume changes of the hippocampal subfields during a specific stage of AD (normal aging, mild cognitive impairment, or AD) based on the limited data. This is one of the reasons why the association between the volume of hippocampal subfields and assessment scores show no consistent patterns as compared to the tau deposition. In addition, there is a significant difference of age between the A− and A+ groups (**Table 1**). However, the influence of normal aging is not demonstrated thoroughly even if we considered age as a covariance in the partial correlation process. On the other hand, NPI has 12 domains to assess the behavior symptoms of each subject and is widely used for the assessment of treatment effect (Cummings, 1997). However, the sample size of the current study is insufficient for the analysis of one specific behavior domain. Further analysis focused on the cohort with the same clinical diagnosis, as well as with the matched distribution of age, gender, education, etc., should be conducted with the development of the ADNI project.

Another limitation is that the relatively low resolution of the PET images may influence the calculation of the tau deposition for each hippocampal subfield. No partial volume correction was performed in this study, which may introduce signal mixture to small brain regions (Brendel et al., 2015; Matsubara et al., 2016; Rullmann et al., 2016; Su et al., 2016; Baker et al., 2017; Gonzalez-Escamilla et al., 2017). This is one of the reasons why the CA2 and CA3 were considered together and relatively large regions such as the CA1, ERC, and PHC were considered in the statistical analysis.

Not enough longitudinal data of the high-resolution T2 weighted MR images and tau PET scans for the statistical analysis were acquired based on the current inclusion criteria. AD is a neurodegenerative disorder that may go through several decades before clinical diagnosis. Observation of the dynamic changes of the tau deposition of the hippocampal subfields and its association with assessment scores in the future is essential for the early diagnosis and prevention of AD dementia.

CONCLUSION

The current research has found that the development of AD may be affected in a progressive manner from the ERC to the PHC, the Sub, and eventually to the CA1 region on a smaller scale. The relationship between the clinical symptoms and tauopathy/volume of the hippocampal subfield showed diverse patterns under different amyloid statuses. Leftward asymmetry was observed with the association between assessment scores and tauopathy/volume of the hippocampal subfield, which is more prominent for the NPI total score in the current study. The associations of tauopathy/volume of the hippocampal subfields with the clinical symptoms are essential for the understanding of the AD spectrum and can be used as the reference for future AD studies.

DATA AVAILABILITY STATEMENT

The datasets presented in this study can be found in online repositories. The names of the repository/repositories and accession number(s) can be found in the article.

ETHICS STATEMENT

Written informed consent was obtained from the individual(s) for the publication of any potentially identifiable images or data included in this article.

AUTHOR CONTRIBUTIONS

XG wrote the first draft of the manuscript. YZ and JX contributed to conception and design of the study. YQ and JZ performed the statistical analysis. XG and DZ organized the database and designed the protocol. All authors contributed to the article and approved the submitted version.

FUNDING

This work was supported by the National Natural Science Foundation of China (No. 81801776), Natural Science Foundation of Jiangsu Province (No. BK20170256), and Science and Technology Development Program of Xuzhou (No. KC17164). The work of JX was supported by the Project funded by China: Postdoctoral Science Foundation (2020M680905).

ACKNOWLEDGMENTS

Data collection and sharing for this project was funded by the Alzheimer's Disease Neuroimaging Initiative (ADNI) (National Institutes of Health Grant U01 AG024904) and DOD ADNI (Department of Defense award number W81XWH-12-2-0012). ADNI is funded by the National Institute on Aging, the National Institute of Biomedical Imaging and Bioengineering, and through generous contributions from the following: AbbVie, Alzheimer's Association; Alzheimer's Drug Discovery Foundation; Araclon Biotech; BioClinica, Inc.; Biogen; Bristol-Myers Squibb Company; CereSpir, Inc.; Cogstate; Eisai Inc.; Elan Pharmaceuticals, Inc.; Eli Lilly and Company; EuroImmun; F. Hoffmann-La Roche Ltd. and its affiliated company Genentech, Inc.; Fujirebio; GE Healthcare; IXICO Ltd.; Janssen Alzheimer Immunotherapy Research & Development, LLC.; Johnson & Johnson Pharmaceutical Research & Development LLC.; Lumosity; Lundbeck; Merck & Co., Inc.; Meso Scale Diagnostics, LLC.; NeuroRx Research; Neurotrack Technologies; Novartis Pharmaceuticals Corporation; Pfizer Inc.; Piramal Imaging; Servier; Takeda Pharmaceutical Company; and Transition Therapeutics. The Canadian Institutes of Health Research is providing funds to support ADNI clinical sites in Canada. Private sector contributions are facilitated by the Foundation for the National Institutes of Health (www.fnih.org). The grantee organization is the Northern California Institute for Research and Education, and the study is coordinated by the Alzheimer's Therapeutic Research Institute at the University of Southern California. ADNI data are disseminated by the Laboratory for Neuro Imaging at the University of Southern California.

REFERENCES

Adler, D. H., Wisse, L. E., Ittyerah, R., Pluta, J. B., Ding, S.-L., Xie, L., et al. (2018). Characterizing the human hippocampus in aging and Alzheimer's disease using a computational atlas derived from *ex vivo* MRI and histology. *Proc. Natl. Acad. Sci. U S A* 115, 4252–4257. doi: 10.1073/pnas.1801093115

Baker, S. L., Maass, A., and Jagust, W. J. (2017). Considerations and code for partial volume correcting [18F]-AV-1451 tau PET data. *Data Brief* 15, 648–657. doi: 10.1016/j.dib.2017.10.024

Braak, H., and Del Tredici, K. (2011). Alzheimer's pathogenesis: is there neuron-to-neuron propagation. *Acta Neuropathol.* 121, 589–595. doi: 10.1007/s00401-011-0825-z

Braak, H., Thal, D. R., Ghebremedhin, E., and Del Tredici, K. (2011). Stages of the pathologic process in Alzheimer disease: age categories from 1 to 100 years. *J. Neuropathol. Exp. Neurol.* 70, 960–969. doi: 10.1097/NEN.0b013e318232a379

Brendel, M., Högenauer, M., Delker, A., Sauerbeck, J., Bartenstein, P., Seibyl, J., et al. (2015). Improved longitudinal [18F]-AV45 amyloid PET by white matter reference and VOI-based partial volume effect correction. *NeuroImage* 108, 450–459. doi: 10.1016/j.neuroimage.2014.11.055

Brier, M. R., Gordon, B., Friedrichsen, K., McCarthy, J., Stern, A., Christensen, J., et al. (2016). Tau and Aβ imaging, CSF measures and cognition in Alzheimer's disease. *Sci. Transl. Med.* 8:338ra366. doi: 10.1126/scitranslmed.aaf2362

Campabadal, A., Segura, B., Junque, C., Serradell, M., Abos, A., Uribe, C., et al. (2019). Cortical gray matter and hippocampal atrophy in idiopathic Rapid Eye Movement sleep behavior disorder. *Front. Neurol.* 10:312. doi: 10.3389/fneur.2019.00312

Chen, L. W., Sun, D., Davis, S. L., Haswell, C. C., Dennis, E. L., Swanson, C. A., et al. (2018). Smaller hippocampal CA1 subfield volume in posttraumatic stress disorder. *Depress. Anxiety* 35, 1018–1029. doi: 10.1002/da.22833

Christian, K. M., Ming, G.-L., and Song, H. (2020). Adult neurogenesis and the dentate gyrus: predicting function from form. *Behav. Brain Res.* 379:112346. doi: 10.1016/j.bbr.2019.112346

Cummings, J. L. (1997). The neuropsychiatric inventory: assessing psychopathology in dementia patients. *Neurology* 48, S10–S16. doi: 10.1212/wnl.48.5_suppl_6.10s

Dalton, M. A., McCormick, C., and Maguire, E. A. (2019). Differences in functional connectivity along the anterior-posterior axis of human hippocampal subfields. *NeuroImage* 192, 38–51. doi: 10.1016/j.neuroimage.2019.02.066

Das, T., Hwang, J. J., and Poston, K. L. (2019). Episodic recognition memory and the hippocampus in Parkinson's disease: a review. *Cortex* 113, 191–209. doi: 10.1016/j.cortex.2018.11.021

Deb, A., Sambamoorthi, U., Thornton, J. D., Schreurs, B., Innes, K. J. A., and health, M. (2018). Direct medical expenditures associated with Alzheimer's and related dementias (ADRD) in a nationally representative sample of older adults-an excess cost approach. *Aging Ment. Health* 22, 619–624. doi: 10.1080/13607863.2017.1286454

Desikan, R. S., Ségonne, F., Fischl, B., Quinn, B. T., Dickerson, B. C., Blacker, D., et al. (2006). An automated labeling system for subdividing the human cerebral cortex on MRI scans into gyral based regions of interest. *NeuroImage* 31, 968–980. doi: 10.1016/j.neuroimage.2006.01.021

Donohue, M. C., Sperling, R. A., Petersen, R., Sun, C.-K., Weiner, M. W., and Aisen, P. S. J. J. (2017). Association between elevated brain amyloid and subsequent cognitive decline among cognitively normal persons. *JAMA* 317, 2305–2316. doi: 10.1001/jama.2017.6669

Edmonds, E. C., Eppig, J., Bondi, M. W., Leyden, K. M., Goodwin, B., Delano-Wood, L., et al. (2016). Heterogeneous cortical atrophy patterns in MCI not captured by conventional diagnostic criteria. *Neurology* 87, 2108–2116. doi: 10.1212/WNL.0000000000003326

Evans, T. E., Adams, H. H., Licher, S., Wolters, F. J., van der Lugt, A., Ikram, M. K., et al. (2018). Subregional volumes of the hippocampus in relation to cognitive function and risk of dementia. *NeuroImage* 178, 129–135. doi: 10.1016/j.neuroimage.2018.05.041

Fuster-Matanzo, A., Hernández, F., and Ávila, J. (2018). Tau spreading mechanisms; implications for dysfunctional tauopathies. *Int. J. Mol. Sci.* 19:645. doi: 10.3390/ijms19030645

Giacobini, E., and Gold, G. (2013). Alzheimer disease therapy—moving from amyloid-β to tau. *Nat. Rev. Neurol.* 9, 677–686. doi: 10.1038/nrneurol.2013.223

Gonzalez-Escamilla, G., Lange, C., Teipel, S., Buchert, R., Grothe, M. J., and Initiative, A. S. D. N. (2017). PETPVE12: an SPM toolbox for partial volume effects correction in brain PET-application to amyloid imaging with AV45-PET. *NeuroImage* 147, 669–677. doi: 10.1016/j.neuroimage.2016.12.077

Gordon, B. A., Blazey, T. M., Christensen, J., Dincer, A., Flores, S., Keefe, S., et al. (2019). Tau PET in autosomal dominant Alzheimer's disease: relationship with cognition, dementia and other biomarkers. *Brain* 142, 1063–1076. doi: 10.1093/brain/awz019

Hanseeuw, B. J., Betensky, R. A., Jacobs, H. I., Schultz, A. P., Sepulcre, J., Becker, J. A., et al. (2019). Association of amyloid and tau with cognition in preclinical Alzheimer disease: a longitudinal study. *JAMA Neurol.* 76, 915–924. doi: 10.1001/jamaneurol.2019.1424

Ikram, M. A., Vrooman, H. A., Vernooij, M. W., den Heijer, T., Hofman, A., Niessen, W. J., et al. (2010). Brain tissue volumes in relation to cognitive function and risk of dementia. *Neurobiol. Aging* 31, 378–386. doi: 10.1016/j.neurobiolaging.2008.04.008

Ismail, Z., Smith, E. E., Geda, Y., Sultzer, D., Brodaty, H., Smith, G., et al. (2016). Neuropsychiatric symptoms as early manifestations of emergent dementia: provisional diagnostic criteria for mild behavioral impairment. *JAMA Neurol.* 12, 195–202. doi: 10.1016/j.jalz.2015.05.017

Jack Jr, C. R., Bennett, D. A., Blennow, K., Carrillo, M. C., Dunn, B., Haeberlein, S. B., et al. (2018). NIA-AA research framework: toward a biological definition of Alzheimer's disease. *Alzheimers Dement.* 14, 535–562. doi: 10.1016/j.jalz.2018.02.018

Jack, C. R., Bennett, D. A., Blennow, K., Carrillo, M. C., Feldman, H. H., Frisoni, G. B., et al. (2016). A/T/N: an unbiased descriptive classification scheme for Alzheimer disease biomarkers. *Neurology* 87, 539–547. doi: 10.1212/WNL.0000000000002923

Jack, C. R., Wiste, H. J., Therneau, T. M., Weigand, S. D., Knopman, D. S., Mielke, M. M., et al. (2019). Associations of amyloid, tau and neurodegeneration biomarker profiles with rates of memory decline among individuals without dementia. *JAMA* 321, 2316–2325. doi: 10.1001/jama.2019.7437

Knopman, D. S., Lundt, E. S., Therneau, T. M., Vemuri, P., Lowe, V. J., Kantarci, K., et al. (2019). Entorhinal cortex tau, amyloid-β, cortical thickness and memory performance in non-demented subjects. *Brain* 142, 1148–1160. doi: 10.1093/brain/awz025

Kueper, J. K., Speechley, M., and Montero-Odasso, M. (2018). The Alzheimer's disease assessment scale-cognitive subscale (ADAS-Cog): modifications and responsiveness in pre-dementia populations. a narrative review. *J. Alzheimer's Dis.* 63, 423–444. doi: 10.3233/JAD-170991

Landau, S., Thomas, B., Thurfjell, L., Schmidt, M., Margolin, R., Mintun, M., et al. (2014). Amyloid PET imaging in Alzheimer's disease: a comparison of three radiotracers. *Eur. J. Nucl. Med. Mol. Imaging* 41, 1398–1407. doi: 10.1007/s00259-014-2753-3

Marks, S. M., Lockhart, S. N., Baker, S. L., and Jagust, W. J. (2017). Tau and β-amyloid are associated with medial temporal lobe structure, function and memory encoding in normal aging. *J. Neurosci.* 37, 3192–3201. doi: 10.1523/JNEUROSCI.3769-16.2017

Masters, M. C., Morris, J. C., and Roe, C. M. J. N. (2015). "Noncognitive" symptoms of early Alzheimer disease: a longitudinal analysis. *Neurology* 84, 617–622. doi: 10.1212/WNL.0000000000001238

Matsubara, K., Ibaraki, M., Shimada, H., Ikoma, Y., Suhara, T., Kinoshita, T., et al. (2016). Impact of spillover from white matter by partial volume effect on quantification of amyloid deposition with [11C] PiB PET. *NeuroImage* 143, 316–324. doi: 10.1016/j.neuroimage.2016.09.028

McCartney, D. L., Stevenson, A. J., Walker, R. M., Gibson, J., Morris, S. W., Campbell, A., et al. (2018). Investigating the relationship between DNA methylation age acceleration and risk factors for Alzheimer's disease. *Alzheimers Dement. (Amst).* 10, 429–437. doi: 10.1016/j.dadm.2018.05.006

Mok, W. Y., Chu, L., Chung, C., Chan, N., and Hui, S. L. (2004). The relationship between non-cognitive symptoms and functional impairment in Alzheimer's disease. *Int. J. Geriatr. Psychiatry* 19, 1040–1046. doi: 10.1002/gps.1207

Moreno-Jiménez, E. P., Flor-García, M., Terreros-Roncal, J., Rábano, A., Cafini, F., Pallas-Bazarra, N., et al. (2019). Adult hippocampal neurogenesis is abundant in neurologically healthy subjects and drops sharply in patients with Alzheimer's disease. *Nat. Med.* 25, 554–560. doi: 10.1038/s41591-019-0375-9

Naidich, T., Daniels, D., Haughton, V., Williams, A., Pojunas, K., and Palacios, E. (1987). Hippocampal formation and related structures of the limbic lobe: anatomic-MR correlation. Part I. Surface features and coronal sections. *Radiology* 162, 747–754. doi: 10.1148/radiology.162.3.3809489

Nunes, P. V., Schwarzer, M. C., Leite, R. E. P., Ferretti-Rebustini, R. E. L., Pasqualucci, C. A., Nitrini, R., et al. (2019). Neuropsychiatric inventory in community-dwelling older adults with mild cognitive impairment and dementia. *J. Alzheimers Dis.* 68, 669–678. doi: 10.3233/JAD-180641

Parker, T. D., Slattery, C. F., Yong, K. X., Nicholas, J. M., Paterson, R. W., Foulkes, A. J., et al. (2019). Differences in hippocampal subfield volume are seen in phenotypic variants of early onset alzheimer's disease. *Neuroimage Clin.* 21:101632. doi: 10.1016/j.nicl.2018.101632

Pedraza, O., Bowers, D., and Gilmore, R. (2004). Asymmetry of the hippocampus and amygdala in MRI volumetric measurements of normal adults. *J. Int. Neuropsychol. Soc.* 10, 664–678. doi: 10.1017/S1355617704105080

Petersen, R. C., Aisen, P., Beckett, L. A., Donohue, M., Gamst, A., Harvey, D. J., et al. (2010). Alzheimer's disease neuroimaging initiative (ADNI): clinical characterization. *Neurology* 74, 201–209. doi: 10.1212/WNL.0b013e3181cb3e25

Pizzi, S. D., Franciotti, R., Bubbico, G., Thomas, A., Onofrj, M., and Bonanni, L. (2016). Atrophy of hippocampal subfields and adjacent extrahippocampal structures in dementia with Lewy bodies and Alzheimer's disease. *Neurobiol. Aging* 40, 103–109. doi: 10.1016/j.neurobiolaging.2016.01.010

Rullmann, M., Dukart, J., Hoffmann, K.-T., Luthardt, J., Tiepolt, S., Patt, M., et al. (2016). Partial-volume effect correction improves quantitative analysis of 18F-florbetaben β-amyloid PET scans. *J. Nucl. Med.* 57, 198–203. doi: 10.2967/jnumed.115.161893

Scharre, D. W. (2019). Preclinical, prodromal and dementia stages of Alzheimer's disease. *Pract. Neurol.* Available online at: https://practicalneurology.com/articles/2019-june/preclinical-prodromal-and-dementia-stages-ofalzheimers-disease/pdf.

Scott, M. R., Hampton, O. L., Buckley, R. F., Chhatwal, J. P., Hanseeuw, B. J., Jacobs, H. I., et al. (2020). Inferior temporal tau is associated with accelerated prospective cortical thinning in clinically normal older adults. *NeuroImage* 220:116991. doi: 10.1016/j.neuroimage.2020.116991

Shi, F., Liu, B., Zhou, Y., Yu, C., and Jiang, T. (2009). Hippocampal volume and asymmetry in mild cognitive impairment and Alzheimer's disease: meta-analyses of MRI studies. *Hippocampus* 19, 1055–1064. doi: 10.1002/hipo.20573

Sørensen, L., Igel, C., Pai, A., Balas, I., Anker, C., Lillholm, M., et al. (2017). Differential diagnosis of mild cognitive impairment and Alzheimer's disease using structural MRI cortical thickness, hippocampal shape, hippocampal texture and volumetry. *Neuroimage Clin.* 13, 470–482. doi: 10.1016/j.nicl.2016.11.025

Su, Y., Blazey, T. M., Owen, C. J., Christensen, J. J., Friedrichsen, K., Joseph-Mathurin, N., et al. (2016). Quantitative amyloid imaging in autosomal dominant Alzheimer's disease: results from the DIAN study group. *PLoS One* 11:e0152082. doi: 10.1371/journal.pone.0152082

Toga, A. W., and Thompson, P. M. (2003). Mapping brain asymmetry. *Nat. Rev. Neurosci.* 4, 37–48. doi: 10.1038/nrn1009

Tosun, D., Landau, S., Aisen, P. S., Petersen, R. C., Mintun, M., Jagust, W., et al. (2017). Association between tau deposition and antecedent amyloid-beta accumulation rates in normal and early symptomatic individuals. *Brain* 140, 1499–1512. doi: 10.1093/brain/awx046

Tuncdemir, S. N., Lacefield, C. O., and Hen, R. (2019). Contributions of adult neurogenesis to dentate gyrus network activity and computations. *Behav. Brain Res.* 374:112112. doi: 10.1016/j.bbr.2019.112112

Weiner, M. W., Veitch, D. P., Aisen, P. S., Beckett, L. A., Cairns, N. J., Cedarbaum, J., et al. (2015). 2014 Update of the Alzheimer's Disease Neuroimaging Initiative: a review of papers published since its inception. *Alzheimers Dement.* 11, e1–e120. doi: 10.1016/j.jalz.2014.11.001

Woolard, A. A., and Heckers, S. (2012). Anatomical and functional correlates of human hippocampal volume asymmetry. *Psychiatry Res.* 201, 48–53. doi: 10.1016/j.pscychresns.2011.07.016

Yoon, E. J., Ismail, Z., Hanganu, A., Kibreab, M., Hammer, T., Cheetham, J., et al. (2019). Mild behavioral impairment is linked to worse cognition and brain

atrophy in Parkinson disease. *Neurology* 93, e766–e777. doi: 10.1212/WNL.0000000000007968

Yue, L., Wang, T., Wang, J., Li, G., Wang, J., Li, X., et al. (2018). Asymmetry of hippocampus and amygdala defect in subjective cognitive decline among the community dwelling chinese. *Front. Psychiatry* 9:226. doi: 10.3389/fpsyt.2018.00226

Yushkevich, P. A., Pluta, J. B., Wang, H., Xie, L., Ding, S.-L., Gertje, E. C., et al. (2015). Automated volumetry and regional thickness analysis of hippocampal subfields and medial temporal cortical structures in mild cognitive impairment. *Hum. Brain Mapp.* 36, 258–287. doi: 10.1002/hbm.22627

Zhao, Q.-F., Tan, L., Wang, H.-F., Jiang, T., Tan, M.-S., Tan, L., et al. (2016). The prevalence of neuropsychiatric symptoms in Alzheimer's disease: systematic review and meta-analysis. *J. Affect. Disord.* 190, 264–271. doi: 10.1016/j.jad.2015.09.069

Zhao, W., Wang, X., Yin, C., He, M., Li, S., and Han, Y. (2019). Trajectories of the hippocampal subfields atrophy in the Alzheimer's disease: a structural imaging study. *Front. Neuroinform.* 13:13. doi: 10.3389/fninf.2019.00013

Conflict of Interest: The authors declare that the research was conducted in the absence of any commercial or financial relationships that could be construed as a potential conflict of interest.

frontiers in Aging Neuroscience

ORIGINAL RESEARCH
published: 27 July 2021
doi: 10.3389/fnagi.2021.656990

Cerebrovascular Disease and Depressive Symptomatology in Individuals With Subjective Cognitive Decline: A Community-Based Study

Patricia Diaz-Galvan[1,2†], *Nira Cedres*[1†], *Nerea Figueroa*[3], *Jose Barroso*[3], *Eric Westman*[1,4‡] *and Daniel Ferreira*[1,2,3*‡]

[1] *Department of Neurobiology, Care Sciences, and Society, Division of Clinical Geriatrics, Center for Alzheimer Research, Karolinska Institutet (KI), Stockholm, Sweden,* [2] *Department of Radiology, Mayo Clinic, Rochester, MN, United States,* [3] *Department of Clinical Psychology, Psychobiology, and Methodology, Faculty of Psychology, University of La Laguna, San Cristóbal de La Laguna, Tenerife, Spain,* [4] *Department of Neuroimaging, Center for Neuroimaging Sciences, Institute of Psychiatry, Psychology and Neuroscience, King's College London, London, United Kingdom*

Subjective cognitive decline (SCD) may be the first sign of Alzheimer's disease (AD), but it can also reflect other pathologies such as cerebrovascular disease or conditions like depressive symptomatology. The role of depressive symptomatology in SCD is controversial. We investigated the association between depressive symptomatology, cerebrovascular disease, and SCD. We recruited 225 cognitively unimpaired individuals from a prospective community-based study [mean age (SD) = 54.64 (10.18); age range 35–77 years; 55% women; 123 individuals with one or more subjective cognitive complaints, 102 individuals with zero complaints]. SCD was assessed with a scale of 9 memory and non-memory subjective complaints. Depressive symptomatology was assessed with established questionnaires. Cerebrovascular disease was assessed with magnetic resonance imaging markers of white matter signal abnormalities (WMSA) and mean diffusivity (MD). We combined correlation, multiple regression, and mediation analyses to investigate the association between depressive symptomatology, cerebrovascular disease, and SCD. We found that SCD was associated with more cerebrovascular disease, older age, and increased depressive symptomatology. In turn, depressive symptomatology was not associated with cerebrovascular disease. Variability in MD was mediated by WMSA burden, presumably reflecting cerebrovascular disease. We conclude that, in our community-based cohort, depressive symptomatology is associated with SCD but not with cerebrovascular disease. In addition, depressive symptomatology did not influence the association between cerebrovascular disease and SCD. We suggest that therapeutic interventions for depressive symptomatology could alleviate the psychological burden of negative emotions in people with SCD, and intervening on vascular risk factors to reduce cerebrovascular disease should be tested as an opportunity to minimize neurodegeneration in SCD individuals from the community.

Keywords: subjective cognitive decline, subjective cognitive complaints, DTI, mean diffusivity, cerebrovascular disease, depressive symptomatology, mediation

OPEN ACCESS

Edited by:
Jiu Chen,
Nanjing Medical University, China

Reviewed by:
Julie Suhr,
Ohio University, United States
Kiyoka Kinugawa,
Hôpital Charles-Foix, France

***Correspondence:**
Daniel Ferreira
daniel.ferreira.padilla@ki.se

†These authors share first authorship

‡These authors share last authorship

Received: *21 January 2021*
Accepted: *28 May 2021*
Published: *27 July 2021*

Citation:
Diaz-Galvan P, Cedres N, Figueroa N, Barroso J, Westman E and Ferreira D (2021) Cerebrovascular Disease and Depressive Symptomatology in Individuals With Subjective Cognitive Decline: A Community-Based Study. Front. Aging Neurosci. 13:656990. doi: 10.3389/fnagi.2021.656990

INTRODUCTION

It has been postulated that subjective cognitive decline (SCD) may be the first sign of Alzheimer's disease (AD) (Jessen et al., 2014). However, SCD has also been associated with other pathologies such as cerebrovascular disease (Diniz et al., 2013), especially in community-based studies (Slot et al., 2018). SCD has also been associated with other conditions like depressive symptomatology (Ginó et al., 2010; Zlatar et al., 2014; Cedres et al., 2019). Indeed, the role of depressive symptomatology in current diagnostic criteria of SCD is controversial (Jessen et al., 2014), and it is intensively discussed at the moment (Molinuevo et al., 2017; Rabin et al., 2017; Jessen et al., 2020).

Part of the discussion about the role of depressive symptomatology in SCD stems from the well-known association between depressive symptomatology and SCD (Clarnette et al., 2001; Reid and Maclullich, 2006; Ginó et al., 2010; Zlatar et al., 2014; Cedres et al., 2019). Due to this association, it was traditionally believed that SCD could merely reflect emotional factors (Apolinario et al., 2013; Yates et al., 2015; Burmester et al., 2016). However, there is convincing data showing that depressive symptomatology is a risk factor for future cognitive decline (Butters et al., 2008), or an early symptom of an underlying neurodegenerative disease (Alexopoulos et al., 2013). For example, late-life depression exacerbates the cognitive decline associated with both AD and cerebrovascular disease (Da Silva et al., 2013; Diniz et al., 2013). Also, cerebrovascular disease affects brain networks and causes early depressive symptoms (Murphy et al., 2007; Alexopoulos et al., 2013).

Cerebrovascular disease can be measured through markers assessed on magnetic resonance imaging (MRI) (Wardlaw et al., 2013). A common MRI marker of cerebrovascular disease is white matter signal abnormalities (WMSA), which can be assessed both on T1-weigthed images (white matter hypointensities) and T2-weigthed or fluid-attenuated inversion recovery (FLAIR) images (white matter hyperintensities). Another promising yet unspecific MRI marker is diffusion tensor imaging (DTI), which assesses microstructural alterations in the white matter that might be due to cerebrovascular disease (Zhou et al., 2008; Black et al., 2009; Kennedy and Raz, 2009; Salat et al., 2012). For example, DTI has been proposed as a marker to monitor the progression of cerebrovascular disease (Fu et al., 2012). Both WMSA and DTI alterations have been separately associated with depression (Murphy et al., 2007; Allan et al., 2016) and SCD (Wang et al., 2012; Selnes et al., 2013; Li et al., 2016; Cedres et al., 2019, 2020a; Ohlhauser et al., 2019). However, little is known about the association between cerebrovascular disease, depressive symptomatology, and SCD. This association is especially relevant in SCD individuals from the community, since the prevalence of cerebrovascular disease is significantly higher in community-based cohorts than in clinical cohorts of SCD individuals who seek medical help (Buckley et al., 2017; Slot et al., 2018).

In keeping with the recent contribution from the international working group on SCD (Jessen et al., 2020), the role of depressive symptomatology in SCD still needs to be elucidated (Molinuevo et al., 2017; Rabin et al., 2017). Therefore, the first aim of this study was to investigate the role of depressive symptomatology in SCD in a community-based cohort. We hypothesized three possible scenarios where depressive symptomatology would (A) co-exist with SCD, (B) influence SCD, or (C) reflect SCD (**Figure 1**). We addressed these hypotheses by combining correlation, multiple regression, and mediation analyses. We wanted to: (A) prove that depressive symptomatology and cerebrovascular disease are independently associated with SCD, but there is no association between depressive symptomatology and cerebrovascular disease (hypothesis: depressive symptomatology co-exists with SCD); (B) depressive symptomatology is associated with cerebrovascular disease and it mediates the association between cerebrovascular disease and SCD (hypothesis: depressive symptomatology influences SCD by mediating the association between cerebrovascular disease and SCD); and (C) SCD mediates the association between cerebrovascular disease and depressive symptomatology (hypothesis: depressive symptomatology reflects SCD). The second aim of this study was to test the hypothesis that variability in the unspecific DTI marker of neurodegeneration would be associated with cerebrovascular disease in our community-based SCD cohort. In addition to correlation analysis, we also used mediation analysis to demonstrate that T1 WMSA burden would mediate the association between DTI abnormalities and SCD. Further, older individuals in our cohort have an increased WMSA burden (Nemy et al., 2020), a higher frequency of SCD (Cedres et al., 2019), and higher levels of depressive symptomatology (Machado et al., 2018). Hence, our third aim was to investigate the effect of aging in our analyses. We hypothesized that DTI abnormalities in SCD are associated with increased WMSA burden and older age.

METHODS

Participants

A total of 225 cognitively unimpaired individuals from the GENIC-database (Machado et al., 2018) were included in the current study. The GENIC is a prospective community-based study from the Canary Islands (Spain). Recruitment was performed through primary care health centers, advertisements in local schools, and relatives, as well as acquaintances of the research staff. A more detailed description of the cohort is provided in previous publications (Ferreira et al., 2015; Machado et al., 2018; Gonzalez-Burgos et al., 2019).

All the individuals who received an MRI scan including both T1 and DTI sequences (see further down) were candidate cases for the current study. Inclusion criteria were in concordance

Abbreviations: ACME, average causal mediation effect; AD, Alzheimer's disease; ADE, average direct effect; BDI, Beck's Depression Inventory; BDRS, Blessed Dementia Rating Scale; CVD, cerebrovascular disease; DTI, diffusion tensor imaging; FAQ, Functional Activity Questionnaire; FSPGR, Fast Spoiled Gradient Echo; GDS, Geriatric Depression Scale; GENIC, *Grupo de Estudios Neuropsicológicos de las Islas Canarias;* ICV, Intracranial volume; MD, Mean diffusivity; MMSE, Mini Mental State Examination; MRI, Structural magnetic resonance imaging; SCC, Subjective Cognitive Complaints; SCD, Subjective Cognitive Decline; SCD-I, Subjective Cognitive Decline initiative; TBSS, tract-based spatial statistics; WMSA, White matter signal abnormalities.

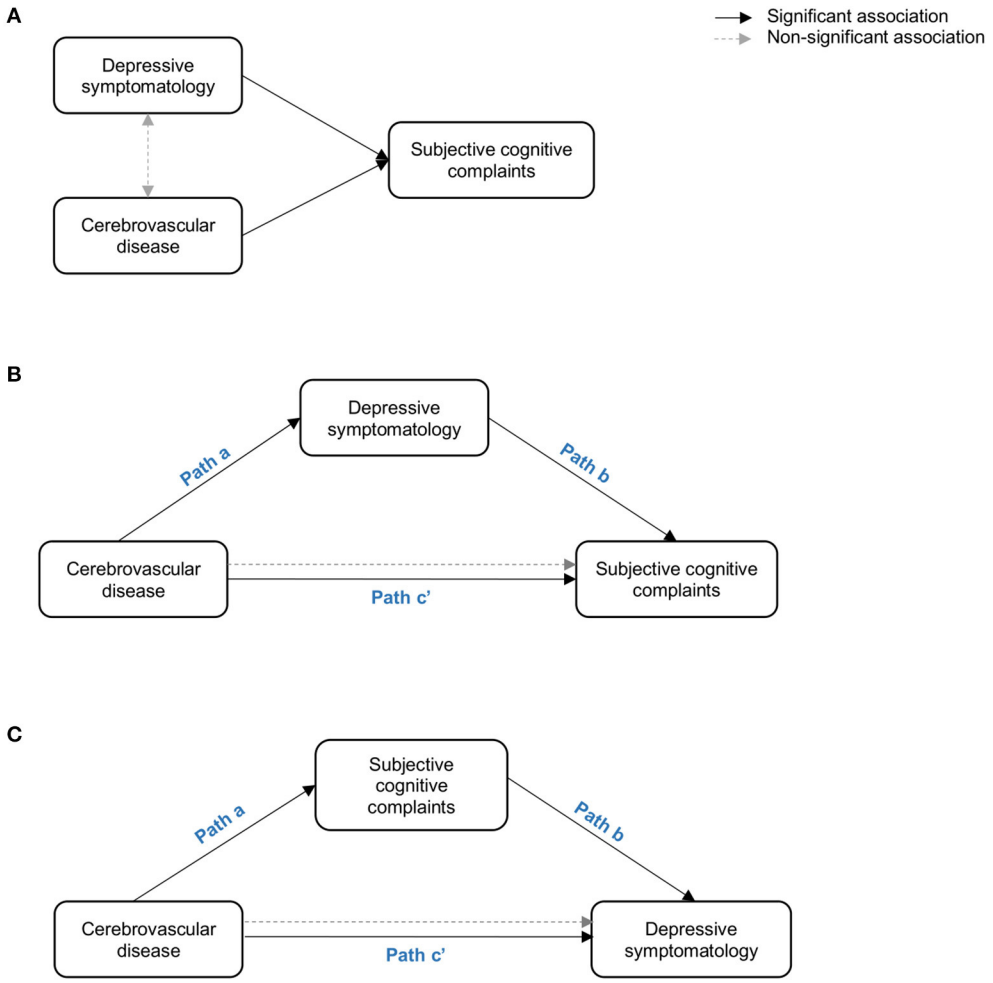

FIGURE 1 | Representation of the three hypothetical scenarios: **(A)** depressive symptomatology co-exist with SCD (i.e. depressive symptomatology and cerebrovascular disease are independently associated with SCD; **(B)** depressive symptomatology influeces SCD by mediating the association between cerebrovascular disease and SCD; **(C)** depressive symptomatology reflects SCD (i.e. SCD mediates the association between cerebrovascular disease and depressive symptomatology. Paths in the figure refer to the associations betwen the independent variable, the mediator, and the dependent variable as described in Baron and Kenny' mediation framework (Baron and Kenny, 1986).

with the SCD initiative (SCD-I) working group (Jessen et al., 2014): (1) Normal cognition, which was established in a two-step diagnostic procedure: Firstly, in a screening phase dementia was excluded based on altered activities of daily living and global cognition operationalized as a Blessed Rating Dementia Scale (BRDS) score >4 (Blessed et al., 1968), a Functional Activity Questionnaire (FAQ) score >5 (Pfeffer et al., 1982), and a Mini-Mental State Examination (MMSE) score <24 (Folstein et al., 1975); Secondly, mild cognitive impairment was excluded based on comprehensive neuropsychological assessment and age-, sex-, and education-adjusted normative data following current clinical criteria (Winblad et al., 2004). The neuropsychological protocol is summarized in the **Supplementary Table 1**. Briefly, the neuropsychological protocol was applied in two sessions and MRI scanning was conducted in a third session. In all participants, the time between neuropsychological assessment (first session) and MRI scanning was within 6 months (mean = 1.5 months, SD = 2.5); (2) No abnormal findings such as stroke, tumors, hippocampal sclerosis, etc., in MRI according to an experienced neuroradiologist; (3) no medical history of neurological and psychiatric disorders (including a diagnosis of major depression and/or individuals under treatment for depression), systemic diseases or head trauma; and (4) no history of substance abuse.

This study was approved by the ethics committee from the University of La Laguna (Spain). Participation was completely voluntarily, and all the individuals gave their written informed consent.

Subjective Cognitive Decline

SCD was assessed with a questionnaire that covers subjective cognitive complaints (SCC) in different cognitive domains,

including memory, orientation, executive functions, face recognition, language production, language comprehension, word-finding, reading and writing (Cedres et al., 2019). Participants answered nine yes/no questions referred to cognitive changes occurring during approximately the last 6 months. Answers were codified as 0 (absence of complaints) or 1 (presence of complaints). Answers were summed up and the total of complaints was obtained ranging from 0 to 9. In the current study, we use SCD when we refer to the clinical entity or concept of SCD, and we use SCC when we refer to the variable we used in our statistical analyses. The continuous variable of SCC was preferred to the dichotomous variable of SCD due to the nature of our statistical models and to avoid arbitrary clinical thresholds.

Depressive Symptomatology

Depressive symptomatology was assessed with two validated scales. The Beck Depression Inventory (BDI, 21-items version) (Beck et al., 1961) was used for participants younger than 63 years of age, and the Geriatric Depression Scale (GDS, 15-items version) (Yesavage et al., 1982) was used for participants 63 years old or older. Following previous publications, BDI and GDS scores were transformed into z-scores and combined into one single variable for statistical analysis (BDI-GDS composite) (Ferreira et al., 2017; Cedres et al., 2019).

MRI Data Acquisition and Image Processing

Participants were scanned using a 3.0T GE imaging system (General Electric, Milwaukee, WI, USA), located at the *Hospital Universitario de Canarias* in Tenerife, Spain. A three-dimensional T1-weighted Fast Spoiled Gradient Echo (FSPGR) sequence was acquired in sagittal plane: repetition time/echo time/inversion time = 8.73/1.74/650 ms., field of view = 250 × 250 mm, matrix = 250 × 250 mm, flip angle = 12°, slice thickness = 1 mm, voxel resolution = 1 × 1 × 1 mm. Also, a DTI sequence was acquired in axial plane: repetition time/echo time = 15.000/≈72 ms., field of view = 256 × 256 mm, matrix: 128 × 128 mm, directions = 31, *B*-value = 1,000, flip angle = 90°, slice thickness = 2.4 mm, voxel resolution = 2 × 2 × 2.4 mm. Full brain and skull coverage was required for the MRI datasets and detailed quality control was carried out on all MR images according to previously published criteria (Simmons et al., 2011).

T1-weighted images were processed and analyzed with the FreeSurfer 6.0.0 image analysis suite (http://surfer.nmr.mgh.harvard.edu/). The FreeSurfer measure of white matter hypointensities was used as a surrogate marker of cerebrovascular disease, and referred to as WMSA in the current study. Briefly, FreeSurfer uses a probabilistic procedure to detect hypointensities in the white matter and labels them as WMSA (Fischl et al., 2002). This procedure has previously demonstrated sensitivity in measuring white matter damage both in healthy individuals and in patients with Alzheimer's disease (Salat et al., 2010; Leritz et al., 2014). These T1-weighted WMSA correlate with hyperintensity volumes measured on T2/FLAIR, as well as with microstructural white matter changes as measured on diffusion tensor imaging data (Leritz et al., 2014; Riphagen et al., 2018; Cedres et al., 2020b; Nemy et al., 2020). The estimated total intracranial volume (TIV) was also obtained from FreeSurfer in order to adjust the WMSA volume by the TIV. This adjustment was performed by dividing the WMSA volume by the TIV of each individual (Voevodskaya, 2014). The TIV-adjusted WMSA measure was used for statistical analyses.

The DTI images were pre-processed and analyzed with the FSL software (http://www.fmrib.ox.ac.uk/fsl/index.html), using the FDT and tract-based spatial statistics (TBSS) tools. The mean diffusivity (MD) index was selected as our measure of interest in this study because MD has shown to be an earlier indicator of neurodegeneration compared to other diffusivity measures (Liu et al., 2013; Li et al., 2015).

All the data were processed through theHiveDB system (Muehlboeck et al., 2014). Careful visual quality control was performed on all output data obtained from both FreeSurfer and FSL, and manual edits were applied when needed.

Statistical Analysis

The DTI data was analyzed through a voxel-based approach on the white matter skeleton, using the FSL software (Smith et al., 2006). Separate general linear models were fitted at the voxel level with MD as the dependent variable and SCC, depressive symptomatology, WMSA, or age as independent variables. Permutation-based non-parametric testing with 5,000 iterations was used followed by threshold-free cluster enhancement (TFCE) and the family-wise error (FWE) correction for multiple testing ($p \leq 0.01$, two-sided). Average MD values of significant clusters in individual's native space were extracted as new measures for further analysis (e.g., SCC-related MD and WMSA-related MD, please see the results section below). In addition, the global MD was extracted as a measure of mean MD values in the whole white matter skeleton.

We designed an approach based on correlation, multiple regression, and mediation analyses to address our first aim: to investigate de role of the depressive symptomatology in SCD (**Figure 1**). Firstly, bivariate Pearson correlations were used to study relationships between SCC and depressive symptomatology, WMSA, and MD measures. Secondly, multiple linear regression models were used to further investigate partial associations of depressive symptomatology, WMSA, and MD measures (predictors) with SCC (outcome variable). Thirdly, these analyses were complemented with mediation models when the three basic conditions of mediation analysis were satisfied (Baron and Kenny, 1986): (1) there is a significant association between the mediator and the independent variable; (2) there is a significant association between the independent variable and the dependent variable; and (3) there is a significant association between the mediator and the dependent variable when the independent variable is also included in the model. For an illustration of the mediation models please see **Figure 1**.

Mediation analysis was also used to investigate our second aim: to investigate whether WMSA mediates the association between MD and SCC. Mediation was based on the average direct effect (ADE), the average causal mediation effect (ACME), and the total effect. Briefly, the ADE represents the direct effect of the independent variable on the dependent variable, while the ACME

TABLE 1 | Demographic and clinical characteristics.

	Whole sample ($n = 225$)	Individuals with one or more SCC ($n = 123$)	Individuals with zero SCC ($n = 102$)	*p*
Age	54.6 (10.2)	56.9 (11.0)	51.9 (8.3)	<0.001
Sex (% women)	55	64	43	0.002
Education level (% 0/1/2/3/4)[a]	0/3/35/25/37	4/42/26/29	2/28/25/45	0.07
Information (WAIS-III)	16.8 (6.0)	15.6 (6.0)	18.3 (5.7)	<0.001
MMSE	28.9 (1.2)	28.7 (1.3)	29.1 (1.0)	0.018
BDRS	0.6 (0.9)	0.7 (1.0)	0.4 (0.8)	0.017
FAQ	0.3 (0.7)	0.3 (0.6)	0.3 (0.8)	0.357
Subjective cognitive complaints[b]	0.9 (1.1)	1.7 (1.0)	0 (0)	–
Depressive symptomatology[c]	0 (1)	0.3 (1.0)	−0.3 (0.8)	<0.001
Cholesterol, n(%)	41 (18)	30 (73)	11 (27)	0.017
High blood pressure, n(%)	51 (23)	35 (69)	16 (31)	0.041
Diabetes, n(%)	5 (2)	4 (3)	1 (1)	0.507
Global MD[d]	7.4 (0.2)	7.5 (0.2)	7.4 (0.2)	0.018
WMSA volume	14.9 (13.1)	16.9 (15.6)	12.5 (8.7)	0.01

Values correspond to the mean (standard deviation), except for Sex and Education level, in which values correspond to percentage (%). P-values correspond to results of group comparisons between individuals with one or more subjective cognitive complaints (SCC) and individuals with zero SCC. [a]Education Level: illiterate (0); acquired reading and/or writing skills (1); primary level (2); secondary level (3); university level (4). [b]Subjective cognitive complaints were studied through nine yes/no questions as explained in the methods. [c]Depressive symptomatology was estimated by transforming BDI and GDS scores into z scores and then combined them into one single variable. [d]MD values were multiplied by 10,000. WAIS, Wechsler Adult Intelligence Scale; MMSE, Mini-Mental State Examination; BDRS, Blessed Dementia Rating Scale; FAQ, Functional Activity Questionnaire; BDI, Beck Depression Inventory; GDS, Geriatric Depression Scale; WMSA, White Matter Signal Abnormalities; MD, Mean Diffusivity.

represents the indirect effect of the independent variable on the dependent variable, through the mediator variable. The total effect represents the sum of the ACME and the ADE. When the ACME is statistically significant (in conjunction with a significant total effect) there is a mediation effect that can be of two types: full mediation, when the ACME is significant but the ADE is non-significant; and partial mediation, when both the ACME and the ADE are significant (Tingley et al., 2014). The ACME and the ADE were calculated by using confidence intervals based on non-parametric bootstrap sampling (1,s000 simulations).

To address our third aim—to investigate the effect of aging in our analyses—we repeated the above-mentioned regression models including age as a covariate, and we tested for bivariate Pearson's correlations for age with SCC, depressive symptomatology, WMSA, and MD.

Statistical analyses were conducted using the R statistical software (http://www.r-project.org). A $p < 0.05$ (two-tailed) was deemed significant in all these analyses.

RESULTS

The demographic and clinical characteristics of the cohort are described in **Table 1**. A total of 123 (55%) participants endorsed one or more SCC, while 102 (45%) participants reported zero SCC (number of complaints: mean = 0.92; SD = 1.1, range = 0–6). There were significantly more women in the subgroup of individuals with one or more SCC compared with those individuals with zero SCC (**Table 1**). Individuals with one or more SCC also showed significantly lower scores in the WAIS-III Information subtest after correcting for sex. Individuals with one or more SCC also had significantly lower scores in the MMSE; higher scores in the BDRS; and more depressive symptoms. These differences remained significant after controlling for the effect of sex and WAIS-III Information subtest. The proportion of individuals with high cholesterol and blood pressure was higher in the subgroup with one or more SCC than the group with zero SCC. Individuals with one or more SCC had a higher WMSA burden and worse white matter integrity (i.e., higher MD values) than individuals with zero SCC. Regarding depressive symptomatology irrespective of SCC, participants younger than 63 years scored between 0 and 23 in the BDI (mean = 5.6; SD = 4.6), and participants 63 years old or older scored between 0 and 9 in the GDS (mean = 2.3; SD = 2.1). The distributions of BDI, GDS, and the BDI-GDS composite variable are shown in **Figure 2**.

First Aim: The Role of Depressive Symptomatology

The first aim of this study was to investigate the role of depressive symptomatology in SCD, under the hypotheses that depressive symptomatology would (A) co-exist with SCD, (B) influence SCD, or (C) reflect SCD (**Figure 1**). Correlation analyses showed that higher scores in depressive symptomatology were associated with a higher number of SCC ($r = 0.340$, $p < 0.001$). In contrast, depressive symptomatology did not correlate with the global MD ($r = 0.076$, $p = 0.321$) or WMSA ($r = 0.003$, $p = 0.961$). Depressive symptomatology did not correlate with MD values at the voxel level either (**Figure 3A**). Based on these results, we could not satisfy some of the three basic conditions for mediation analysis proposed by Baron and Kenny's (1986) (i.e., the association between depressive symptomatology and MD or WMSA). Hence, we could not test for mediation models including depressive symptomatology together with WMSA or global MD (**Figures 1B,C**). We next conducted a multiple linear regression model to investigate the partial association of depressive symptomatology, WMSA, and MD with SCC. We

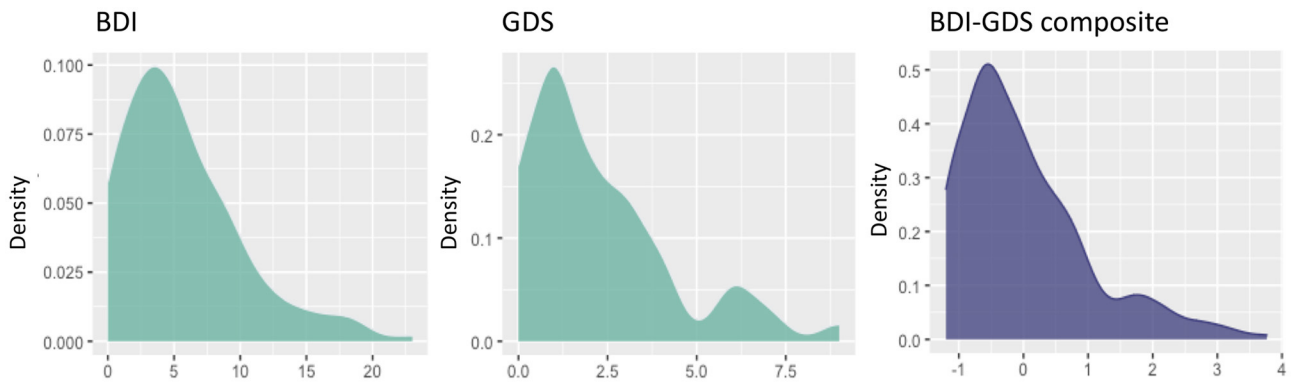

FIGURE 2 | Distribution of the variables of depressive symptomatology. Scores on the x-axis (original scores from the BDI and the GDS, or z-scores from the BDI-GDS composite measure), and densities on the y-axis. BDI, Beck Depression Inventory; GDS, Geriatric Depression Scale.

included SCC as the criterion variable, and WMSA, global MD, and depressive symptomatology as the predictors (**Table 2**; model 1). This model was significant [$F_{(3,221)} = 15.655$, $p < 0.001$, R^2 adj. $= 0.16$], indicating that depressive symptomatology and WMSA were independently associated with SCC. In contrast, global MD was not significant (**Table 2**). However, the lack of a significant effect for global MD may due to the fact that the measure of global MD may include areas that are not involved in SCC. Hence, in a second model, we restricted MD values to those voxels that were significantly related with SCC ("average SCC-related MD," see below). We observed that depressive symptomatology continued to be a significant predictor of SCC, but WMSA was no longer a significant predictor when the average SCC-related MD was also in the model [**Table 2**; model 2, full model: $F_{(3,221)} = 20.987$, $p < 0.001$, R^2 adj. $= 0.211$]. In correlation analysis, depressive symptomatology was not correlated with the average SCC-related MD either ($r = 0.117$, $p = 0.079$).

These results suggest that depressive symptomatology may co-exist with SCC (**Figure 1A**). To fully prove that hypothesis we had to demonstrate that cerebrovascular disease is also associated with SCC. Hence, we conducted complementary analyses to further characterize the association of WMSA and MD with SCC. A higher burden of WMSA and a higher global MD correlated with a higher number of SCC ($r = 0.216$, $p = 0.001$, and $r = 0.210$, $p = 0.002$, respectively). The voxel-based analysis showed that the association between higher MD values and a higher number of SCC involved most of the white matter skeleton, with a tendency to spare the occipital white matter and the anterior part of the cingulum bundle (**Figure 3B**). The average MD value of these SCC related areas was extracted in a new variable ("average SCC-related MD") for further analysis.

Second Aim: The Contribution of WMSA to Variability in MD

The second aim of this study was to test the hypothesis that variability in MD, an unspecific DTI biomarker of neurodegeneration, would mediate cerebrovascular disease as measured by WMSA. Correlation analyses showed that a higher global MD correlated with a higher burden of WMSA ($r = 0.370$, $p < 0.001$), and a higher MD in areas specifically associated with SCC ("average SCC-related MD") showed an even stronger correlation with a higher burden of WMSA ($r = 0.492$, $p < 0.001$). At the voxel level, the association between higher MD levels and higher WMSA burden involved most of the white matter skeleton, with a tendency to spare the internal capsule, the occipital white matter, and the cingulum bundle (**Figure 3C**). The average MD value of WMSA-related areas was extracted in a new variable ("average WMSA-related MD") for further analysis. Results showed that the correlation coefficient of the association between SCC and the average WMSA-related MD ($r = 0.267$) was larger than the correlation coefficient of the association between SCC and global MD ($r = 0.210$). We also assessed the conjunction between the association of MD with SCC and WMSA. When we overlapped these two maps, MD values in forceps minor, corpus callosum, superior longitudinal fasciculus, inferior fronto-occipital fasciculus, and thalamic radiation were associated with both SCC and WMSA burden (**Figure 3D**). The measure "average SCC&WMSA-related MD" was calculated as the conjunction between these two maps. A new multiple regression model was conducted to investigate the partial association of depressive symptomatology and the MD voxels that were associated with both SCC and WMSA burden ("average SCC&WMSA-related MD") with SCC. The model included depressive symptomatology and "average SCC&WMSA-related MD" as predictors, and SCC as the criterion (**Table 2**; model 3). This model was significant [$F_{(2,222)} = 28.534$, $p < 0.001$, R^2 adj. $= 0.197$], indicating that both the average SCC&WMSA-related MD ($\beta = 0.300$, $p < 0.001$) and depressive symptomatology ($\beta = 0.309$ $p < 0.001$) were independently associated with SCC.

Finally, we used mediation analysis to investigate whether WMSA mediates the association between global MD and SCC. We found that WMSA significantly mediated the association between global MD and SCC (ACME $= 2960.825$; $p = 0.026$). This mediation effect was partial because the direct effect of global MD on SCC was also significant (ADE $= 7590.678$, $p = 0.032$).

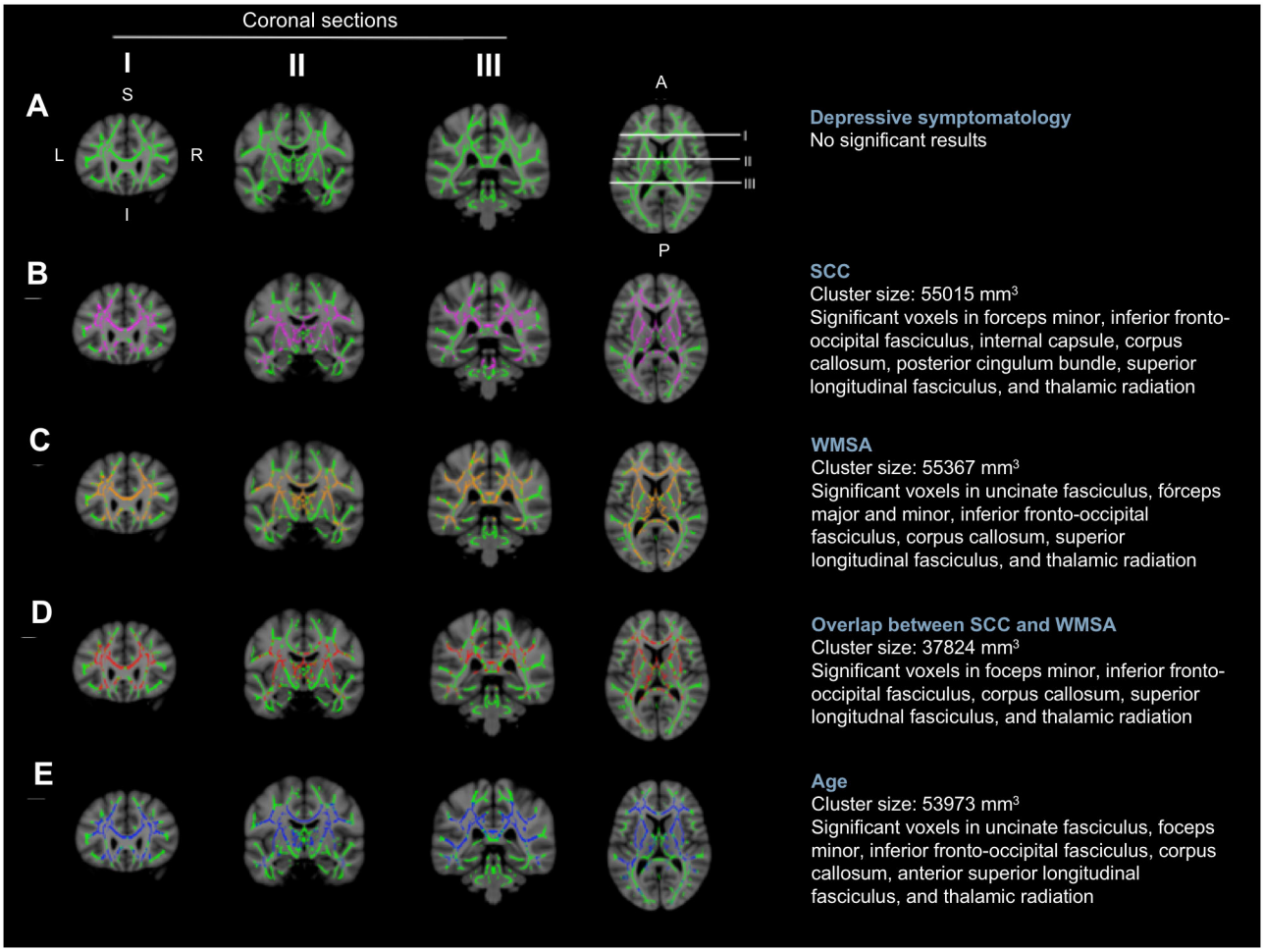

FIGURE 3 | Voxel-wise correlations of MD values with depressive symptomatology, SCC, WMSA, and age. The white matter skeleton is depicted in green. Significant voxels are colored in pink [**(B)** the association between MD values and SCC], orange [**(C)** the association between MD values and WMSA], red [**(D)** overlap of the association between MD values and SCC, and MD values and WMSA], and blue [**(E)** the association between MD values and age]. No significant voxels were obtained for the association between MD values and depressive symptomatology **(A)**. L, left; R, right; S, superior; I, inferior; A, anterior; P, posterior; MD, mean diffusivity; SCC, subjective cognitive complaints; WMSA, white matter signal abnormalities; mm, millimeters.

Third Aim: The Effect of Aging

The third aim of this study was to investigate the effect of aging in our data. Correlation analyses showed that an older age correlated with a higher volume of WMSA ($r = 0.521$, $p < 0.001$), a higher global MD ($r = 0.387$, $p < 0.001$), a higher number of SCC ($r = 0.373$, $p < 0.001$), and higher scores in depressive symptomatology ($r = 0.069$, $p = 0.030$). The voxel-based analysis showed that the association between an older age and higher MD values involved most of the white matter skeleton, with a tendency to spare the occipital and parietal white matter and tracts going through the internal capsule and the cingulum bundle (**Figure 3E**). Next, we added age as an extra predictor to the multiple regression models reported for the first and second aims. The model for global MD (model 4 in **Table 2**) was significant [$F_{(4, 222)} = 17.581$, $p < 0.001$, R^2 adj. $= 0.228$], showing that age was the main predictor of SCC, followed by depressive symptomatology. In contrast, WMSA and global MD were not significant as predictors. The model specific for MD areas involved in SCC ("average SCC-related MD," model 5 in **Table 2**) was significant [$F_{(4, 220)} = 19.466$, $p < 0.001$, R^2 adj. $= 0.248$], showing that age, depressive symptomatology, and the average SCC-related MD were significant predictors of SCC, while WMSA was not significant ($p = 0.900$). Finally, the model for the average SCC&WMSA-related MD (model 6 in **Table 2**) was significant [$F_{(3, 221)} = 24.676$, $p < 0.001$, R^2 adj. $= 0.241$], showing that both depressive symptomatology and age ($\beta = 0.268$, $p < 0.001$) were independently associated with SCC, with a trend to significance for the average SCC&WMSA-related MD to predict SCC ($\beta = 0.140$, $p = 0.055$).

DISCUSSION

In this study, we tested the role of depressive symptomatology in the context of SCD and cerebrovascular disease using cross-sectional data from a community-based cohort. We also investigated whether DTI abnormalities (increased MD values)

TABLE 2 | Partial association of depressive symptomatology, WMSA, MD, and age with SCC (multiple regression models).

	R^2	*B*	*SE B*	*β*	*p*
Model 1	**0.16**				**<0.001**
Depressive symptomatology		0.36	0.07	0.33	<0.001
WMSA		0.01	0.01	0.17	0.011
Global MD		0.63	0.33	0.13	0.059
Model 2	**0.21**				**<0.001**
Depressive symptomatology		0.34	0.07	0.31	<0.001
WMSA		0.01	0.01	0.08	0.271
Average SCC-related MD		0.12	0.03	0.28	<0.001
Model 3	**0.20**				**<0.001**
Depressive symptomatology		0.35	0.06	0.30	<0.001
Average SCC&WMSA-related MD		0.10	0.03	0.31	<0.001
Including age as predictor					
Model 4	**0.23**				**<0.001**
Depressive symptomatology		0.35	0.06	0.31	<0.001
WMSA		0.002	0.01	0.03	0.663
Global MD		0.28	0.33	0.06	0.391
Age		0.03	0.01	0.31	<0.001
Model 5	**0.25**				**<0.001**
Depressive symptomatology		0.33	0.06	0.30	<0.001
WMSA		−0.00	0.01	−0.01	0.90
Average SCC-related MD		0.08	0.03	0.19	0.012
Age		0.03	0.01	0.25	0.001
Model 6	**0.24**				**<0.001**
Depressive symptomatology		0.35	0.06	0.31	<0.001
Average SCC&WMSA-related MD		0.11	0.03	0.14	0.055
Age		0.03	0.01	0.27	<0.001

Values correspond to R^2 and its significance for each model. For each predictor in the models, values correspond to beta values (B) and their standard errors (SE B), as well as the standardized betas (β) and their significance values. BDI, Beck Depression Inventory; GDS, Geriatric Depression Scale; WMSA, White Matter Signal Abnormalities; MD, Mean Diffusivity; SCC, subjective cognitive complaints.

in SCD are associated with increased WMSA burden and older age. We operationalized SCD following the diagnostic criteria of the international working group on SCD (Jessen et al., 2014), and used the number of SCC (i.e., subjective cognitive complaints) in our statistical analyses. While our results showed that an increased depressive symptomatology is significantly associated with more SCC, we could not find a significant association of depressive symptomatology with WMSA or MD measures. We thus accepted the hypothesis of depressive symptomatology co-existing with SCC, independently of any MRI marker of cerebrovascular disease. In addition, we demonstrated that WMSA mediated the association between MD and SCC, and age had an important contribution to our findings.

The role of depressive symptomatology in SCD is controversial. While major depression is an exclusion criterion in current diagnostic criteria of SCD (Jessen et al., 2014), individual symptoms of depression that do not reach the threshold of a disorder are not considered a criterion for exclusion (Jessen et al., 2014). However, it is not clear what should be the exact threshold to exclude depression and how this type of symptomatology should be assessed in SCD (e.g., concurrent, past, subclinical, etc.). Currently, the most urgent need is to elucidate the role of subthreshold depressive symptomatology in SCD (Molinuevo et al., 2017; Jessen et al., 2020). In our relatively large community-based cohort, we approached this question by assessing subthreshold variability in depressive symptomatology in SCD individuals who did not have a diagnosis of major depression nor were under treatment for depression. Our analyses confirmed the well-known association between depressive symptomatology and SCD (Donovan et al., 2014, 2015; Buckley et al., 2016; Burmester et al., 2016; Lebedeva et al., 2018; Cedres et al., 2019), showing that a higher number of SCC was associated with increased depressive symptomatology in our cohort. In contrast, we could not demonstrate that an increased depressive symptomatology in our cohort is related with an older age, which would reflect the concept of late life depression (Diniz et al., 2013). In addition, we did not find an association of WMSA or MD measures with depressive symptomatology, as it would be predicted by the vascular depression hypothesis (Alexopoulos et al., 2013; Taylor et al., 2013). Altogether, our results suggest that the variability in depressive symptomatology in our cohort may be related to emotional factors rather than cerebrovascular disease or age-related factors. Moreover, despite its strong association with SCC, depressive symptomatology seems to

just co-exist with SCD in our cohort, without influencing associations of SCC with markers of cerebrovascular disease or, as demonstrated in previous studies using the same cohort, with markers of gray matter degeneration (Cedres et al., 2019, 2020a) or clinical-cognitive status (Diaz-Galvan et al., 2021). Hence, SCD in our cohort does not seem to merely reflect emotional factors, as traditionally postulated (Apolinario et al., 2013; Yates et al., 2015; Burmester et al., 2016), but may rather reflect neurodegeneration and subclinical cognitive decline.

We observed a strong association of SCC with both WMSA and MD. Since WMSA correlated with MD, and WMSA mediated the association between MD and SCC, we suggest that variability in our MD measure may be influenced by cerebrovascular disease. In other words, despite being an unspecific marker, our MD measure may be reflecting cerebrovascular disease in our study. Other studies also highlighted the contribution of non-AD pathologies such as cerebrovascular disease to SCD in community-based cohorts (Diniz et al., 2013). The novelty of our study is the use of DTI to investigate white matter neurodegeneration associated with cerebrovascular disease, and the analysis of its topographical distribution. The utility of DTI measures as markers of cerebrovascular disease has previously been noted (Zhou et al., 2008; Black et al., 2009; Fu et al., 2012; Salat et al., 2012). Interestingly, in our study, the association between WMSA and MD in areas related with SCC ("average SCC-related MD") was stronger than the association between WMSA and MD in the whole white matter skeleton ("global MD"). This suggests that the brain areas in which integrity of the white matter is associated with SCC seems to be more vulnerable to the effect of cerebrovascular disease than other white matter areas. Hence, cerebrovascular disease may be a contributor to SCC in our community-based cohort. This interpretation was further supported by our result showing that the association between SCC and MD in areas related with WMSA ("average WMSA-related MD") was stronger than the association between SCC and MD in the whole white matter skeleton ("global MD"). Another important observation is that our associations between SCC and markers of cerebrovascular disease were related with or accounted by the age, as discussed further down.

We demonstrated the strong association between an older age and increased SCC, a finding that is well-established in the SCD literature (Derouesné et al., 1993; Wang et al., 2004; Jessen et al., 2010; van Harten et al., 2018; Cedres et al., 2019). We also demonstrated the strong association between an older age and increased cerebrovascular disease, in line with previous reports (Raz et al., 2012; Habes et al., 2016; Nemy et al., 2020). Whether this cerebrovascular disease in cognitively unimpaired older individuals indicates preclinical stages of vascular cognitive impairment or is rather a feature of normal aging when not reaching the clinical threshold is currently not known. The hypothesis of a preclinical stage is attractive in the context of our study, highlighting the capacity of SCD to reflect underlying neurodegenerative processes of presumably vascular origin. In a recent study using the same cohort we demonstrated that the effect of WMSA on cholinergic white matter pathways goes beyond the effect of age (Nemy et al., 2020). In our current study, including the age in our models removed the predictive partial effect of global MD, but the effect of MD in white matter areas associated with SCC remained significant. This suggests that while the integrity of the white matter overall seems to be primarily driven by increasing age, variability in the integrity of areas specific to SCC goes beyond the effect of aging (and depressive symptomatology). This finding was attenuated when investigating the integrity of areas specific to both SCC and WMSA ($p = 0.055$), suggesting that the cerebrovascular component that is related to SCC in our cohort may primarily be explained by increasing age, and not to stroke or other major vascular disease. This interpretation is congruent with the current definition of SCD, where neurological diseases other than AD are a criterion for exclusion (Jessen et al., 2014).

This study has some limitations. Although we did not find a significant association between depressive symptomatology and MRI markers of cerebrovascular disease, we cannot exclude that depressive symptomatology in our cohort could be an early symptom of other brain pathologies previously reported in SCD, such as amyloid-beta or tau pathologies (Amariglio et al., 2012; Perrotin et al., 2012; Buckley et al., 2017). The lack of biomarkers for amyloid-beta and tau pathologies is thus a limitation of our study. Nonetheless, vascular risk factors are highly prevalent in community-based cohorts like the one used in our study (Buckley et al., 2017), while AD pathologies are more prevalent in clinical cohorts (Kern et al., 2018). In the same vein, variability in MD was strongly associated with WMSA, but other pathologies such as amyloid-beta and tau could also be contributing to MD. This interpretation is supported by our finding of SCC-related MD remaining in our model, while WMSA was automatically removed when including the age in the same model. We believe that SCC-related MD reflects neurodegeneration beyond that related with an older age or a higher WMSA burden. However, our measure of WMSA is global, and it would be interesting to investigate WMSA intersecting SCC-related white matter tracts in future studies. We partially circumvented this by investigating the conjunction between WMSA-related MD and SCC-related MD. We reported the frequency of some vascular risk factors but a more complete characterization of vascular risk factors, as well as their contribution to our current findings is warranted in the future. In any case, these limitations do not compromise our main interpretation of depressive symptomatology as an emotional factor co-existing but not related with neurodegenerative factors that underlie SCC, since MD and WMSA correlated with SCC but not with depressive symptomatology. We used correlation, regression, and mediation analyses to investigate associations on cross-sectional data. Longitudinal designs or clinical trials to demonstrate that treating emotional or vascular risk factors reduces SCD would help to support potential causality in our current associations. Finally, previous studies showed that individuals with SCD differed in the frequency of affective symptoms and underlying neurodegeneration depending on whether they are recruited in the community or in clinical settings (Perrotin et al., 2017; Slot et al., 2018). Therefore, our current findings could also be tested in clinical-based samples, including SCD individuals who seek medical help.

In conclusion, depressive symptomatology co-exists with SCD and reflects emotional factors but not cerebrovascular disease,

in our community-based cohort. In addition, we did not find any evidence for depressive symptomatology to influence the association between cerebrovascular disease and SCD. In our cohort, SCD reflected white matter neurodegeneration in spite of its association with depressive symptomatology. This highlights the clinical usefulness of SCD, especially in older individuals who often show subjective complaints, depressive symptomatology, and positive cerebrovascular disease biomarkers. A remark is that although SCD increased with age in our cohort, the association between white matter abnormalities and SCD was beyond the effect of aging. Therapeutic interventions for depressive symptomatology could alleviate the psychological burden of negative emotions in people SCD, and intervening on vascular risk factors to reduce cerebrovascular disease should be tested as an opportunity to minimize neurodegeneration in SCD individuals from the community. Another important contribution of the current study is the data reported to help understanding the association between cerebrovascular disease, depressive symptomatology, and SCD.

DATA AVAILABILITY STATEMENT

The raw data supporting the conclusions of this article will be available upon reasonable request from qualified researchers.

ETHICS STATEMENT

The studies involving human participants were reviewed and approved by the ethics committee from the University of La Laguna (Spain). The patients/participants provided their written informed consent to participate in this study.

AUTHOR CONTRIBUTIONS

PD-G: data acquisitions, interpretation of results, writing of portions of the manuscript, and preparing figures. NC: data acquisitions, analysis and interpretation of results, writing of portions of the manuscript, and preparing figures. NF: study concept and design, data acquisitions, analysis and interpretation of results, and writing of portions of the manuscript. JB: supervision of the project, revision of manuscript, and funding. EW: revision of manuscript and funding. DF: study concept and design, data acquisition, interpretation of results, writing of portions of the manuscript, supervision of the study, and funding. All authors contributed to the article and approved the submitted version.

FUNDING

This research was funded by the *Estrategia de Especialización Inteligente de Canarias RIS3 de la Consejería de Economía, Industria, Comercio y Conocimiento del Gobierno de Canarias*, co-funded by the *Programa Operativo FEDER Canarias* 2014–2020 (ProID2020010063); the *Fundación Canaria Dr. Manuel Morales* (calls in 2012, 2014, and 2017); *Fundación Cajacanarias*; Center for Innovative Medicine (CIMED), the Swedish Foundation for Strategic Research (SSF), the Strategic Research Programme in Neuroscience at Karolinska Institutet (StratNeuro), the Swedish Research Council (VR), the Åke Wiberg foundation, Hjärnfonden, Alzheimerfonden, Demensfonden Stiftelsen, Olle Engkvist Byggmästare, Birgitta och Sten Westerberg, Demensförbundet, Loo och Hans Ostermans Foundation, Gun och Bertil Stohnes Stiftelse, Foundation for Geriatric Diseases at Karolinska Institutet, Research Funding from Karolinska Institutet, and Stiftelsen För Gamla Tjänarinnor. The funders of the study had no role in the study design nor the collection, analysis, and interpretation of data, writing of the report, or decision to submit the manuscript for publication.

ACKNOWLEDGMENTS

The authors would like to thank Dr. Antonio Rodríguez for providing access to participants and helpful assistance; and the *Servicio de Resonancia Magnética para Investigaciones Biomédicas del SEGAI* (University of La Laguna, Spain). Data used in preparation of this article is part of the GENIC-database (Group of Neuropsychological Studies of the Canary Islands, University of La Laguna, Spain. Principal investigator: JB. Contact: DF, daniel.ferreira.padilla@ki.se). The following collaborators contributed to the GENIC-database but did not participate in analysis or writing of this report (in alphabetic order by family name): Rut Correia, Aida Figueroa, Eloy García, Lissett González, Teodoro González, Zaira González, Cathaysa Hernández, Edith Hernández, Nira Jiménez, Judith López, Cándida Lozano, Alejandra Machado, María Antonieta Nieto, María Sabucedo, Elena Sirumal, Marta Suárez, Manuel Urbano, and Pedro Velasco.

SUPPLEMENTARY MATERIAL

The Supplementary Material for this article can be found online at: https://www.frontiersin.org/articles/10.3389/fnagi.2021.656990/full#supplementary-material

REFERENCES

Alexopoulos, G. S., Young, R. C., Campbell, S., Silbersweig, D., and Charlson, M. (2013). Vascular depression' hypothesis. *J. Chem. Inf. Model.* 53, 1689–1699. doi: 10.1021/ci400128m

Allan, C. L., Sexton, C. E., Filippini, N., Topiwala, A., Mahmood, A., Zsoldos, E., et al. (2016). Sub-threshold depressive symptoms and brain structure: A magnetic resonance imaging study within the Whitehall II cohort. *J. Affect. Disord.* 204, 219–225. doi: 10.1016/j.jad.2016.06.049

Amariglio, R. E., Becker, J. A., Carmasin, J., Wadsworth, L. P., Lorius, N., Sullivan, C., et al. (2012). Subjective cognitive complaints and amyloid burden in cognitively normal older individuals. *Neuropsychologia* 50, 2880–2886. doi: 10.1016/j.neuropsychologia.2012.08.011

Apolinario, D., Miranda, R. B., Suemoto, C. K., Magaldi, R. M., Busse, A. L., Soares, A. T., et al. (2013). Characterizing spontaneously reported cognitive complaints: The development and reliability of a classification instrument. *Int. Psychogeriatr.* 25, 157–166. doi: 10.1017/S1041610212001494

Baron, R. M., and Kenny, D. A. (1986). The moderator-mediator variable distinction in social psychological research: Conceptual, strategic, and statistical considerations. *J. Pers. Soc. Psychol.* 51, 1173–1182. doi: 10.1037/0022-3514.51.6.1173

Beck, A. A. T., Ward, C. H. H., Mendelson, M., Mock, J., and Erbaugh, J. (1961). An inventory for measuring depression. *Arch. Gen. Psychiatry* 4, 561–571. doi: 10.1001/archpsyc.1961.01710120031004

Black, S., Gao, F., and Bilbao, J. (2009). Understanding white matter disease: Imaging-pathological correlations in vascular cognitive impairment. *Stroke* 40(Suppl. 3), S48–52. doi: 10.1161/STROKEAHA.108.537704

Blessed, G., Tomlinson, B. E., and Roth, M. (1968). The association between quantitative measures of dementia and of senile change in the cerebral grey matter of elderly subjects. *Br. J. Psychiatry* 114, 797–811. doi: 10.1192/bjp.114.512.797

Buckley, R. F., Hanseeuw, B., Schultz, A. P., Vannini, P., Aghjayan, S. L., Properzi, M. J., et al. (2017). Region-specific association of subjective cognitive decline with tauopathy independent of global β-amyloid burden. *JAMA Neurol.* 74, 1455–1463. doi: 10.1001/jamaneurol.2017.2216

Buckley, R. F., Maruff, P., Ames, D., Bourgeat, P., Martins, R. N., Masters, C. L., et al. (2016). Subjective memory decline predicts greater rates of clinical progression in preclinical Alzheimer's disease. *Alzheimer's Dement.* 12, 796–804. doi: 10.1016/j.jalz.2015.12.013

Burmester, B., Leathem, J., and Merrick, P. (2016). Subjective cognitive complaints and objective cognitive function in aging: a systematic review and meta-analysis of recent cross-sectional findings. *Neuropsychol. Rev.* 26, 376–393. doi: 10.1007/s11065-016-9332-2

Butters, M. A., Young, J. B., Lopez, O., Aizenstein, H. J., Mulsant, B. H., Reynolds, C. F., et al. (2008). Pathways linking late-life depression to persistent cognitive impairment and dementia. *Dialog. Clin. Neurosci.* 10, 345–357. doi: 10.31887/DCNS.2008.10.3/mabutters

Cedres, N., Ferreira, D., Machado, A., Shams, S., Sacuiu, S., Waern, M., et al. (2020b). Predicting Fazekas scores from automatic segmentations of white matter signal abnormalities. *Aging.* 12, 894–901. doi: 10.18632/aging.102662

Cedres, N., Institutet, K., Diaz-galvan, P., Institutet, K., Ferreira, D., and Institutet, K. (2020a). The interplay between gray matter and white matter neurodegeneration in subjective cognitive decline. *ResearchSquare.* doi: 10.21203/rs.3.rs-91497/v1

Cedres, N., Machado, A., Molina, Y., Diaz-Galvan, P., Hernández-Cabrera, J. A., Barroso, J., et al. (2019). Subjective cognitive decline below and above the age of 60: a multivariate study on neuroimaging, cognitive, clinical, and demographic measures. *J. Alzheimer's Dis.* 68, 295–309. doi: 10.3233/JAD-180720

Clarnette, R. M., Almeida, O. P., Forstl, H., Paton, A., and Martins, R. N. (2001). Clinical characteristics of individuals with subjective memory loss in Western Australia: results from a cross-sectional survey. *Int. J. Geriatr. Psychiatry* 16, 168–174. doi: 10.1002/1099-1166(200102)16:2<168::AID-GPS291>3.0.CO;2-D

Da Silva, J., Gonçalves-Pereira, M., Xavier, M., and Mukaetova-Ladinska, E. B. (2013). Affective disorders and risk of developing dementia: Systematic review. *Br. J. Psychiatry* 202, 177–186. doi: 10.1192/bjp.bp.111.101931

Derouesné, C., Dealberto, M., Boyer, P., Lubin, S., Sauron, B., Piette, F., et al. (1993). Empirical evaluation of the 'Cognitive Difficulties Scale' for assessment of memory complaints in general practice: a study of 1628 cognitively normal subjects aged 45–75 years. *Int. J. Geriatr. Psychiatry* 8, 599–607. doi: 10.1002/gps.930080712

Diaz-Galvan, P., Ferreira, D., Cedres, N., Falahati, F., Hernández-Cabrera, J. A., Ames, D., et al. (2021). Comparing different approaches for operationalizing subjective cognitive decline: impact on syndromic and biomarker profiles. *Sci. Rep.* 11, 1–15. doi: 10.1038/s41598-021-83428-1

Diniz, B. S., Butters, M. A., Albert, S. M., Dew, M. A., and Reynolds, C. F. (2013). Late-life depression and risk of vascular dementia and Alzheimer's disease: Systematic review and meta-analysis of community-based cohort studies. *Br. J. Psychiatry* 202, 329–335. doi: 10.1192/bjp.bp.112.118307

Donovan, N. J., Amariglio, R. E., Zoller, A. S., Rudel, R. K., Gomez-Isla, T., Blacker, D., et al. (2014). Subjective cognitive concerns and neuropsychiatric predictors of progression to the early clinical stages of Alzheimer's disease. *Am. J. Geriatr. Psychiatry* 22, 1642–1651. doi: 10.1016/j.jagp.2014.02.007

Donovan, N. J., Hsu, D. C., Dagley, A. S., Schultz, A. P., Amariglio, R. E., Mormino, E. C., et al. (2015). Depressive symptoms and biomarkers of Alzheimer's disease in cognitively normal older adults. *J. Alzheimers Dis.* 46, 63–73. doi: 10.3233/JAD-142940

Ferreira, D., Correia, R., Nieto, A., Machado, A., Molina, Y., and Barroso, J. (2015). Cognitive decline before the age of 50 can be detected with sensitive cognitive measures. *Psicothema* 27, 216–222. doi: 10.7334/psicothema2014.192

Ferreira, D., Machado, A., Molina, Y., Nieto, A., Correia, R., Westman, E., et al. (2017). Cognitive variability during middle-age: possible association with neurodegeneration and cognitive reserve. *Front. Aging Neurosci.* 9:188. doi: 10.3389/fnagi.2017.00188

Fischl, B., van Der Kouwe, A., Salat, D. H., Busa, E., Albert, M., Dieterich, M., et al. (2002). Whole brain segmentation: automated labeling of neuroanatomical structures in the human brain. *Neuron* 33, 341–355. doi: 10.1016/S0896-6273(02)00569-X

Folstein, M. F., Folstein, S. E., and McHugh, P. R. (1975). "Mini-mental state": A practical method for grading the cognitive state of patients for the clinician. *J. Psychiatr. Res.* 12, 189–198. doi: 10.1016/0022-3956(75)90026-6

Fu, J. L., Zhang, T., Chang, C., Zhang, Y. Z., and Li, W. B. (2012). The value of diffusion tensor imaging in the differential diagnosis of subcortical ischemic vascular dementia and Alzheimer's disease in patients with only mild white matter alterations on T2-weighted images. *Acta Radiol.* 53, 312–317. doi: 10.1258/ar.2011.110272

Ginó, S., Mendes, T., Maroco, J., Ribeiro, F., Schmand, B. A., De Mendonça, A., et al. (2010). Memory complaints are frequent but qualitatively different in young and elderly healthy people. *Gerontology* 56, 272–277. doi: 10.1159/000240048

Gonzalez-Burgos, L., Hernández-Cabrera, J. A., Westman, E., Barroso, J., and Ferreira, D. (2019). Cognitive compensatory mechanisms in normal aging: a study on verbal fluency and the contribution of other cognitive functions. *Aging* 11, 4090–4106. doi: 10.18632/aging.102040

Habes, M., Erus, G., Toledo, J. B., Zhang, T., Bryan, N., Launer, L. J., et al. (2016). White matter hyperintensities and imaging patterns of brain ageing in the general population. *Brain* 139, 1164–1179. doi: 10.1093/brain/aww008

Jessen, F., Amariglio, R. E., Buckley, R. F., van der Flier, W. M., Han, Y., Molinuevo, J. L., et al. (2020). The characterisation of subjective cognitive decline. *Lancet Neurol.* 4422, 1–8. doi: 10.1016/S1474-4422(19)30368-0

Jessen, F., Amariglio, R. E., van Boxtel, M., Breteler, M., Ceccaldi, M., Chételat, G., et al. (2014). A conceptual framework for research on subjective cognitive decline in preclinical Alzheimer's disease. *Alzheimers Dement.* 10, 844–852. doi: 10.1016/j.jalz.2014.01.001

Jessen, F., Wiese, B., Bachmann, C., Eifflaender-Gorfer, S., Haller, F., Kölsch, H., et al. (2010). Prediction of dementia by subjective memory impairment: effects of severity and temporal association with cognitive impairment. *Arch. Gen. Psychiatry* 67, 414–422. doi: 10.1001/archgenpsychiatry.2010.30

Kennedy, K. M., and Raz, N. (2009). Pattern of normal age-related regional differences in white matter microstructure is modified by vascular risk. *Brain Res.* 1297, 41–56. doi: 10.1016/j.brainres.2009.08.058

Kern, S., Zetterberg, H., Kern, J., Zettergren, A., Waern, M., Höglund, K., et al. (2018). Prevalence of preclinical Alzheimer disease: Comparison of current classification systems. *Neurology* 90, e1682–e1691. doi: 10.1212/WNL.0000000000005476

Lebedeva, A., Institutet, K., Ume, A. S., Westman, E., Institutet, K., and Ume, T. O. (2018). Longitudinal relationships among depressive symptoms, cortisol, and brain atrophy in the neocortex and the hippocampus. *Acta Psychiatr. Scand.* 137, 491–502. doi: 10.1111/acps.12860

Leritz, E. C., Shepel, J., Williams, V. J., Lipsitz, L. A., McGlinchey, R. E., Milberg, W. P., et al. (2014). Associations between T1 white matter lesion volume and regional white matter microstructure in aging. *Hum. Brain. Mapp.* 35, 1085–1100. doi: 10.1002/hbm.22236

Li, X., Westman, E., Stahlbom, A. K., Thordardottir, S., Almkvist, O., Blennow, K., et al. (2015). White matter changes in familial Alzheimer's disease. *J. Intern. Med.* 278, 211–218. doi: 10.1111/joim.12352

Li, X.-Y., Tang, Z.-C., Sun, Y., Tian, J., Liu, Z.-Y., and Han, Y. (2016). White matter degeneration in subjective cognitive decline: a diffusion tensor imaging study. *Oncotarget* 7, 54405–54414. doi: 10.18632/oncotarget.10091

Liu, J., Yin, C., Xia, S., Jia, L., Guo, Y., Zhao, Z., et al. (2013). White matter changes in patients with amnestic mild cognitive impairment detected by diffusion tensor imaging. *PLoS ONE* 8:59440. doi: 10.1371/journal.pone.0059440

Machado, A., Barroso, J., Molina, Y., Nieto, A., Díaz-Flores, L., Westman, E., et al. (2018). Proposal for a hierarchical, multidimensional, and multivariate approach to investigate cognitive aging. *Neurobiol. Aging*. 71, 179–188. doi: 10.1016/j.neurobiolaging.2018.07.017

Molinuevo, J. L., Rabin, L. A., Amariglio, R., Buckley, R., Dubois, B., Ellis, K. A., et al. (2017). Implementation of subjective cognitive decline criteria in research studies. *Alzheimers Dement*. 13, 296–311. doi: 10.1016/j.jalz.2016.09.012

Muehlboeck, J.-S., Westman, E., and Simmons, A. (2014). TheHivedb image data management and analysis framework. *Front. Neuroinform*. 6:49. doi: 10.3389/fninf.2013.00049

Murphy, C. F., Gunning-Dixon, F. M., Hoptman, M. J., Lim, K. O., Ardekani, B., Shields, J. K., et al. (2007). White-matter integrity predicts stroop performance in patients with geriatric depression. *Biol. Psychiatry* 61, 1007–1010. doi: 10.1016/j.biopsych.2006.07.028

Nemy, M., Cedres, N., Grothe, M. J., Muehlboeck, J. S., Lindberg, O., Nedelska, Z., et al. (2020). Cholinergic white matter pathways make a stronger contribution to attention and memory in normal aging than cerebrovascular health and nucleus basalis of Meynert. *Neuroimage* 211:116607. doi: 10.1016/j.neuroimage.2020.116607

Ohlhauser, L., Parker, A. F., Smart, C. M., and Gawryluk, J. R. (2019). White matter and its relationship with cognition in subjective cognitive decline. *Alzheimer's Dement. Diagn. Assess Dis. Monit*. 11, 28–35. doi: 10.1016/j.dadm.2018.10.008

Perrotin, A., La Joie, R., de La Sayette, V., Barré, L., Mézenge, F., Mutlu, J., et al. (2017). Subjective cognitive decline in cognitively normal elders from the community or from a memory clinic: differential affective and imaging correlates. *Alzheimers Dement*. 13, 550–560. doi: 10.1016/j.jalz.2016.08.011

Perrotin, A., Mormino, E. C., Madison, C. M., Hayenga, A. O., and Jagust, W. J. (2012). Subjective cognition and amyloid deposition imaging: a Pittsburgh Compound B positron emission tomography study in normal elderly individuals. *Arch. Neurol*. 69, 223–229. doi: 10.1001/archneurol.2011.666

Pfeffer, R. I., Kurosaki, T. T., Harrah, C. H., Chance, J. M., and Filos, S. (1982). Measurement of functional activities in older adults in the community. *J. Gerontol*. 37, 323–329. doi: 10.1093/geronj/37.3.323

Rabin, L. A., Smart, C. M., and Amariglio, R. E. (2017). Subjective cognitive decline in preclinical Alzheimer's disease. *Annu. Rev. Clin. Psychol*. 13, 369–396. doi: 10.1146/annurev-clinpsy-032816-045136

Raz, N., Yang, Y., and Dahle, C. L. (2012). Volume of white matter hyperintensities in healthy adults: Contribution of age, vascular risk factors, and inflammation-related genetic variants. *Biochim. Biophys. Acta*. 1822, 361–369. doi: 10.1016/j.bbadis.2011.08.007

Reid, L. M., and Maclullich, A. M. J. (2006). Subjective memory complaints and cognitive impairment in older people. *Dement. Geriatr. Cogn. Disord*. 22, 471–85. doi: 10.1159/000096295

Riphagen, J. M., Gronenschild, E. H. B. M., Salat, D. H., Freeze, W. M., Ivanov, D., Clerx, L., et al. (2018). Shades of white : diffusion properties of T1- and FLAIR-defined white matter signal abnormalities differ in stages from cognitively normal to dementia. *Neurobiol. Aging* 68, 48–58. doi: 10.1016/j.neurobiolaging.2018.03.029

Salat, D., Tusch, D., van der Kouwe, A., Greve, D., Pappu, V., Lee, S., et al. (2010). White matter pathology isolates the hippocampal formation in Alzheimer's disease. *Neurobiol. Aging* 31, 244–256. doi: 10.1016/j.neurobiolaging.2008.03.013

Salat, D. H., Williams, V. J., Leritz, E. C., Schnyer, D. M., Rudolph, J. L., Lipsitz, L. A., et al. (2012). Inter-individual variation in blood pressure is associated with regional white matter integrity in generally healthy older adults. *Neuroimage J*. 59, 181–192. doi: 10.1016/j.neuroimage.2011.07.033

Selnes, P., Aarsland, D., Bjørnerud, A., Gjerstad, L., Wallin, A., Hessen, E., et al. (2013). Diffusion tensor imaging surpasses cerebrospinal fluid as predictor of cognitive decline and medial temporal lobe atrophy in subjective cognitive impairment and mild cognitive impairment. *J. Alzheimers Dis*. 33, 723–736. doi: 10.3233/JAD-2012-121603

Simmons, A., Westman, E., Muehlboeck, S., Mecocci, P., Vellas, B., Tsolaki, M., et al. (2011). The AddNeuroMed framework for multi-centre MRI assessment of Alzheimer's disease: experience from the first 24 months. *Int. J. Geriatr. Psychiatry* 26, 75–82. doi: 10.1002/gps.2491

Slot, R. E. R., Sikkes, S. A. M., Berkhof, J., Brodaty, H., Buckley, R., Cavedo, E., et al. (2018). Subjective cognitive decline and rates of incident Alzheimer's disease and non-Alzheimer's disease dementia. *Alzheimer's Dement*. 15, 465–476. doi: 10.1016/j.jalz.2018.10.003

Smith, S. M., Jenkinson, M., Johansen-Berg, H., Rueckert, D., Nichols, T. E., Mackay, C. E., et al. (2006). Tract-based spatial statistics: Voxelwise analysis of multi-subject diffusion data. *Neuroimage* 31, 1487–1505. doi: 10.1016/j.neuroimage.2006.02.024

Taylor, W. D., Aizenstein, H. J., and Alexopoulos, G. S. (2013). The vascular depression hypothesis: mechanisms linking vascular disease with depression. *Mol. Psychiatry* 18, 963–974. doi: 10.1038/mp.2013.20

Tingley, D., Yamamoto, T., Hirose, K., Keele, L., and Imai, K. (2014). Mediation: R Package for Causal Mediation Analysis. *J. Stat. Soft*. 59:1–38. doi: 10.18637/jss.v059.i05

van Harten, A. C., Mielke, M. M., Swenson-Dravis, D. M., Hagen, C. E., Edwards, K. K., Roberts, R. O., et al. (2018). Subjective cognitive decline and risk of MCI: the mayo clinic study of aging. *Neurology* 91, e300–e312. doi: 10.1212/WNL.0000000000005863

Voevodskaya, O. (2014). The effects of intracranial volume adjustment approaches on multiple regional MRI volumes in healthy aging and Alzheimer's disease. *Front. Aging Neurosci*. 6:264. doi: 10.3389/fnagi.2014.00264

Wang, L., van Belle, G., Crane, P. K., Kukull, W. A., Bowen, J. D., McCormick, W. C., et al. (2004). Subjective memory deterioration and future dementia in people aged 65 and older. *J. Am. Geriatr. Soc*. 52, 2045–2051. doi: 10.1111/j.1532-5415.2004.52568.x

Wang, Y., West, J. D., Flashman, L. A., Wishart, H. A., Santulli, R. B., Rabin, L. A., et al. (2012). Selective changes in white matter integrity in MCI and older adults with cognitive complaints. *Biochim. Biophys. Acta* 1822, 423–430. doi: 10.1016/j.bbadis.2011.08.002

Wardlaw, J. M., Smith, E. E., Biessels, G. J., Cordonnier, C., Fazekas, F., Frayne, R., et al. (2013). Neuroimaging standards for research into small vessel disease and its contribution to ageing and neurodegeneration. *Lancet Neurol*. 12, 822–838. doi: 10.1016/S1474-4422(13)70124-8

Winblad, B., Palmer, K., Kivipelto, M., Jelic, V., Fratiglioni, L., Wahlund, L.-O., et al. (2004). Mild cognitive impairment–beyond controversies, towards a consensus: report of the International Working Group on Mild Cognitive Impairment. *J. Intern. Med*. 256, 240–246. doi: 10.1111/j.1365-2796.2004.01380.x

Yates, J. A., Clare, L., Woods, R. T., Matthews, F. E., Cognitive Function and Ageing Study Wales (2015). Subjective memory complaints are involved in the relationship between mood and mild cognitive impairment. *J. Alzheimers Dis*. 48(Suppl. 1), S115–S123. doi: 10.3233/JAD-150371

Yesavage, J. A., Brink, T. L., Rose, T. L., Lum, O., Huang, V., Adey, M., et al. (1982). Development and validation of a geriatric depression screening scale: a preliminary report. *J. Psychiatr. Res*. 17, 37–49. doi: 10.1016/0022-3956(82)90033-4

Zhou, Y., Lin, F., Zhu, J., Zhuang, Z., guo, Li, Y., sheng, Tao, J., et al. (2008). Whole brain diffusion tensor imaging histogram analysis in vascular cognitive impairment. *J. Neurol. Sci*. 268, 60–64. doi: 10.1016/j.jns.2007.11.005

Zlatar, Z. Z., Moore, R. C., Palmer, B. W., Thompson, W. K., and Jeste, D. V. (2014). Cognitive complaints correlate with depression rather than concurrent objective cognitive impairment in the successful aging evaluation baseline sample. *J. Geriatr. Psychiatry Neurol*. 27, 181–187. doi: 10.1177/0891988714524628

Conflict of Interest: The authors declare that the research was conducted in the absence of any commercial or financial relationships that could be construed as a potential conflict of interest.

Publisher's Note: All claims expressed in this article are solely those of the authors and do not necessarily represent those of their affiliated organizations, or those of the publisher, the editors and the reviewers. Any product that may be evaluated in this article, or claim that may be made by its manufacturer, is not guaranteed or endorsed by the publisher.

frontiers in Aging Neuroscience

ORIGINAL RESEARCH
published: 03 August 2021
doi: 10.3389/fnagi.2021.675016

Multi-Racial Normative Data for Lobar and Subcortical Brain Volumes in Old Age: Korean and Caucasian Norms May Be Incompatible With Each Other†

Yu Yong Choi[1,2], Jang Jae Lee[1], Kyu Yeong Choi[1], Uk-Su Choi[1], Eun Hyun Seo[1], IL Han Choo[3], Hoowon Kim[1,2,4], Min-Kyung Song[5], Seong-Min Choi[5], Soo Hyun Cho[5], Youngshik Choe[6], Byeong C. Kim[5] and Kun Ho Lee[1,6,7,8]**

[1] Gwangju Alzheimer's Disease and Related Dementia Cohort Research Center, Chosun University, Gwangju, South Korea, [2] Biomedical Technology Center, Chosun University Hospital, Gwangju, South Korea, [3] Department of Neuropsychiatry, Chosun University School of Medicine and Hospital, Gwangju, South Korea, [4] Department of Neurology, Chosun University School of Medicine and Hospital, Gwangju, South Korea, [5] Department of Neurology, Chonnam National University Medical School and Hospital, Gwangju, South Korea, [6] Korea Brain Research Institute, Daegu, South Korea, [7] Department of Biomedical Science, Chosun University, Gwangju, South Korea, [8] Neurozen Inc., Seoul, South Korea

Brain aging is becoming an increasingly important topic, and the norms of brain structures are essential for diagnosing neurodegenerative diseases. However, previous studies of the aging brain have mostly focused on Caucasians, not East Asians. The aim of this paper was to examine ethnic differences in the aging process of brain structures or to determine to what extent ethnicity affects the normative values of lobar and subcortical volumes in clinically normal elderly and the diagnosis in multi-racial patients with Alzheimer's disease (AD). Lobar and subcortical volumes were measured using FreeSurfer from MRI data of 1,686 normal Koreans (age range 59–89) and 851 Caucasian, non-Hispanic subjects in the ADNI and OASIS datasets. The regression models were designed to predict brain volumes, including ethnicity, age, sex, intracranial volume (ICV), magnetic field strength (MFS), and MRI scanner manufacturers as independent variables. Ethnicity had a significant effect for all lobar ($|\beta| > 0.20$, $p < 0.001$) and subcortical regions ($|\beta| > 0.08$, $p < 0.001$) except left pallidus and bilateral ventricles. To demonstrate the validity of the z-score for AD diagnosis, 420 patients and 420 normal controls were selected evenly from the Korean and Caucasian datasets. The four validation groups divided by race and diagnosis were matched on age and sex using a propensity score matching. We analyzed whether and to what extent the ethnicity adjustment improved the diagnostic power of the logistic regression model that was built using the only z-scores of six regions: bilateral temporal cortices, hippocampi, and amygdalae. The performance of the classifier after ethnicity adjustment was significantly improved compared with the classifier before ethnicity adjustment ($\Delta AUC = 0.10$, $D = 7.80$, $p < 0.001$; AUC comparison test using bootstrap). Korean AD

OPEN ACCESS

Edited by:
Jiu Chen,
Nanjing Medical University, China

Reviewed by:
Olivier Potvin,
Laval University, Canada
Hosung Kim,
University of Southern California, Los Angeles, United States

***Correspondence:**
Byeong C. Kim
byeong.kim7@gmail.com
Kun Ho Lee
leekho@chosun.ac.kr

†Some of Caucasian data were provided by the ADNI project launched in 2003 as a public–private partnership, led by Principal Investigator Michael W. Weiner (see http://www.adni-info.org/ for up-to-date information)

Received: 02 March 2021
Accepted: 15 June 2021
Published: 03 August 2021

Citation:
Choi YY, Lee JJ, Choi KY, Choi U-S, Seo EH, Choo IH, Kim H, Song M-K, Choi S-M, Cho SH, Choe Y, Kim BC and Lee KH (2021) Multi-Racial Normative Data for Lobar and Subcortical Brain Volumes in Old Age: Korean and Caucasian Norms May Be Incompatible With Each Other. Front. Aging Neurosci. 13:675016. doi: 10.3389/fnagi.2021.675016

dementia patients may not be classified by Caucasian norms of brain volumes because the brain regions vulnerable to AD dementia are bigger in normal Korean elderly peoples. Therefore, ethnicity is an essential factor in establishing normative data for regional volumes in brain aging and applying it to the diagnosis of neurodegenerative diseases.

Keywords: aging, norm, ethnic difference, Alzheimer's disease, brain magnetic resonance imaging

Findings

1. Brain structures of cognitively normal people mostly decayed with age from 59 to 89 years old.
2. Ethnicity had a significant effect on all lobar regions and subcortical regions except left pallidus and bilateral ventricles.
3. The z-scores for brain volumes based on the prediction model incorporating ethnicity as a predictor were effective for diagnosing multi-racial patients with AD.

INTRODUCTION

Neurodegenerative diseases, including Alzheimesr's disease (AD) dementia and other dementias, yield specific brain changes detectable by a group comparison of anatomical magnetic resonance imaging (MRI) between patients and normal controls. To measure the brain volume alternation of an individual, the normative value or reference standard is required for estimating the degree of abnormality or the deviation from the norm according to the characteristics of the person. Very few attempts had been made (Kruggel, 2006; Walhovd et al., 2011) because a large number of brain images of normal people are needed, and there are many factors to consider in producing the normative data for brain volumes using MRI: technical and physical characteristics of MRI as well as demographic and anatomical characteristics of individuals.

Recently, a series of remarkable studies for normative data (norms) of brain regions have emerged, considering almost all feasible factors (Potvin et al., 2016, 2017). However, their work missed an essential factor of racial characteristics, so they produced practically the norms for Caucasians only. Neuroanatomical differences in brain structures between Asians and Caucasians have been reported (Zilles et al., 2001; Tang et al., 2010; Chee et al., 2011). Thus, ethnicity or race should be a factor considered for producing norms of brain regions.

Particularly, the norms specific to the elderly encompassing Asians as well as Caucasians are becoming increasingly necessary. According to the United States Census Bureau (2020), people over 65 years old are 730 million people and under 10% of the world population in 2020. By 2050, the older population is expected to reach 1.6 billion. Older Asians are now 414 million, or more than half (56.8%) of the older population, and are projected to more than double to 967 million by 2050. Most researchers in the field of aging brain did not consider ethnic backgrounds and examined Western samples with a high percentage of white people. Existing findings are largely a reflection of the White or Caucasian (Resnick et al., 2003; Scahill et al., 2003; Sowell et al., 2003; Ledig et al., 2018). Moreover, the norms specific to a narrow age range have two advantages. Even with the same number of samples, the prediction model can provide more reliable and precise estimates. The predictive model could be kept simple and non-over-fitted since the relationship between age and volume can be assumed to be linear.

Moreover, racial or regional differences have long been known in the cranial cavity or intracranial space among Asia, America, Europe, Oceania, and Africa (Beals et al., 1984; Howells, 1990; Rushton, 2000). Head shape has long been documented to be different between Caucasian and East Asian populations (Ball et al., 2010). The racial comparison demonstrated that East Asians have a rounder head with a flatter back and forehead than Caucasians. The shape of the head or cranium considerably determines the morphometry of the brain. It means that the normative values of brain structures could vary across ethnic populations and that the norms that take into account ethnicity are needed.

The study aimed to present the normative data of lobar and subcortical brain volumes for both the Asians and Caucasian elderly and determine whether and to what extent ethnicity affects the volumes in normal brain aging. To this end, we selected brain MRIs of 1,686 cognitively normal (CN) elderly people from the Gwangju Alzheimer's and Related Dementia (GARD) cohort in the Republic of Korea. For a Caucasian sample, we collected 851 brain images from the AD Neuroimaging Initiative (ADNI) and Open Access Series of Imaging Studies (OASIS) datasets. Our methods differ in detail but followed the procedures outlined in Potvin et al. (2016). We estimated lobar and subcortical volumes using FreeSurfer, an automated segmentation software widely used in neuroimaging research and created prediction models for each brain region's volume according to ethnicity, age, sex, ICV, scanner manufacturer, MFS.

The z-score as the difference between expected and actual volumes allows testing each brain structure for volume abnormality and the effect size. Finally, our objective was to determine whether ethnicity as a predictive variable resulted in substantially improved diagnosis performance when the normative z-score was applied to patients with AD; for this purpose, we analyzed additionally 420 images from patients with AD and compared the z-scores and the classifiers before and after ethnicity adjustment in the area under the receiver operating characteristics curve (AUC).

METHODS

Normative Samples for Koreans and Caucasians

Koreans

The study protocol was approved by the institutional review board of Chosun University Hospital, Republic of Korea. All volunteers or the next of kin of patients gave written informed consent before participation. They were registered in the GARD cohort by GARD Cohort Research Center at Gwangju City, Republic of Korea, from April 2010 to March 2018.

A normative sample for Koreans aged 59–89 years was included from the Korean elderly cohort in this study. All participants were evaluated by comprehensive interviews, neurological examinations, and neuropsychological tests. Neuropsychological tests consist of the Korean version of mini-mental state examination (K-MMSE) (Folstein et al., 1975), Clinical Dementia Rating (CDR) (Morris, 1993), and Seoul Neuropsychological Screening Battery (SNSB) (Kang et al., 2012). The exclusion criteria for all subjects were the presence of a focal lesion on brain MRI, history of head trauma, or psychiatric disorders that could affect their mental function. Individuals with minor medical abnormalities were included.

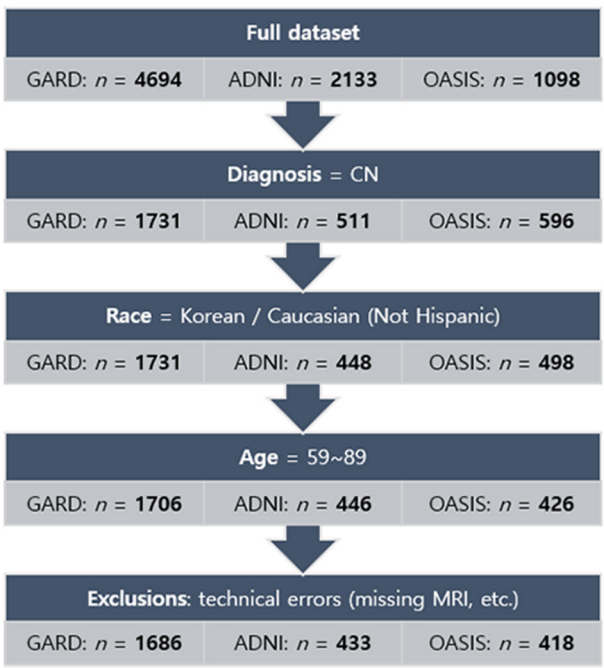

FIGURE 1 | Flowchart of the process of subject selection for the norms. The normative sample finally comprised 2,537 subjects: 1,686 for Koreans and 851 for Caucasians. GARD, Gwangju Alzheimer's and Related Dementia. ADNI, Alzheimer's Disease Neuroimaging Initiative. OASIS, Open Access Series of Imaging Studies.

Caucasians

To investigate ethnic differences, we collected Caucasians excluding Hispanic subjects (851 CN cases) from the ADNI database (http://adni.loni.usc.edu) and the OASIS project (https://www.oasis-brains.org). The age range was matched with our dataset (59–89 years). **Figure 1** showed the inclusion and exclusion criteria. In more technical detail, for ADNI, we applied one of the search conditions per step: VISCODE = "bl" (step 1) AND DX = "CN" (step 2) AND PTRACCAT = "White" AND PTETHCAT = "Not Hisp/Latino" (step 3) AND age > 59 AND age < 90 (step 4). Thirteen subjects were excluded in the final step. For OASIS, the search conditions were Visit ID = "d000" or the first date of MRI scans (step 1) AND DX1 = "Cognitively normal" (step 2) AND Race = "Caucasian" AND Ethnicity = "Non-Hispanic" (step 3) AND age > 59 AND age < 90 (step 4). Eight subjects were excluded in the final step.

Finally, the study sample for analysis comprised 2,537 subjects whose demographic information was described in **Table 1**.

Some of the Caucasian data used in the preparation of this article were obtained from the ADNI database (adni.loni.usc.edu). The ADNI was launched in 2003 as a public-private partnership led by Principal Investigator Michael W. Weiner, MD. The primary goal of ADNI has been to test whether serial magnetic resonance imaging (MRI), positron emission tomography (PET), other biological markers, and clinical and neuropsychological assessment can be combined to measure the progression of mild cognitive impairment (MCI) and early Alzheimer's disease (AD). For up-to-date information, see www.adni-info.org.

MRI Acquisition

The brain MRI images of Korean subjects were acquired using a 3.0 T scanner (Skyra, Siemens; 20-channel head coil; MPRAGE sagittal view; TR = 2,300 ms; TE = 2.143 ms; TI = 900 ms; FA = 9°; FoV = 256 mm × 256 mm; matrix = 320 × 320; slice thickness = 0.8 mm) and a 1.5 T scanner (Avanto, Siemens; 12-channel head coil; MPRAGE axial view; TR = 1,800 ms;

TABLE 1 | Cohort sizes and demographics for normal Koreans and Caucasians.

					Age (y)			MMSE		Education (y)	
Race	**Dataset**	***n***	**F**	**3T**	**Range**	**Mean**	**SD**	**Mean**	**SD**	**Mean**	**SD**
Korean	GARD	1686	62%	81%	59–89	73.1	5.5	27.0	2.1	9.6	4.6
Caucasian	ADNI, OASIS	851	55%	77%	59–89	73.2	6.3	29.1	1.1	16.3	2.6

GARD, Gwangju Alzheimer's Disease and Related Dementias; ADNI, Alzheimer's Disease Neuroimaging Initiative; OASIS, Open Access Series of Imaging Studies. F, female; 3T, MRI image using a 3 Tesla scanner; y, years; MMSE, mini mental state examination.

TABLE 2 | Standardized coefficients of the prediction model of lobar and subcortical gray matter volumes.

	Model				Coefficent															
	RMSE		R^2			Ethnicity	Sex	Intracrainial volume			MFS	Manufacturer		Intraction						
	M	*SD*	*M*	*SD*	Age	Caucasian/ Korean	M/F	ICV	ICV^2	ICV^3	1.5T/3.0T	GE/ Siemens	Philips/ Siemens	Ethnicity* Age.	Ethnicity* Sex	Sex* Age	MFS* GE	MFS * Philips	MFS* ICV	ICV* GE	ICV * Philips
Brain	44.42	1.88	0.78	0.02	***−0.29***	***−0.32***	***−0.08***	***0.94***	***0.03***	***−0.09***	***−0.26***	***0.08***	0.02	−0.01	***0.07***	**−0.03**	0.03	**0.04**	0.00	−0.01	**−0.03**
Lobar GM	22.14	1.10	0.71	0.03	***−0.23***	***−0.41***	***−0.06***	***0.83***	**0.03**	***−0.10***	***−0.45***	***0.09***	−0.02	−0.02	**0.05**	−0.02	0.03	***0.07***	0.00	**−0.03**	**−0.04**
Frontal L	4.45	0.19	0.61	0.04	***−0.18***	***−0.29***	**−0.06**	***0.83***	0.03	***−0.10***	***−0.36***	***0.09***	−0.03	**−0.03**	**0.04**	−0.02	−0.03	**0.05**	−0.01	**−0.03**	**−0.03**
Frontal R	4.51	0.19	0.62	0.03	***−0.19***	***−0.33***	**−0.05**	***0.83***	0.02	***−0.10***	***−0.37***	***0.10***	−0.02	−0.01	**0.04**	−0.03	−0.01	**0.05**	−0.01	**−0.03**	**−0.03**
Temporal L	3.31	0.13	0.63	0.03	***−0.33***	***−0.45***	**−0.05**	***0.73***	0.02	***−0.08***	***−0.38***	***0.12***	0.00	0.03	***0.08***	−0.02	0.03	***0.06***	0.01	**−0.03**	**−0.04**
Temporal R	3.22	0.15	0.63	0.03	***−0.30***	***−0.41***	**−0.05**	***0.76***	0.02	***−0.08***	***−0.39***	***0.11***	−0.01	0.01	***0.07***	−0.01	0.01	***0.06***	0.00	**−0.03**	−0.02
Parietal L	3.28	0.14	0.64	0.04	***−0.19***	***−0.44***	***−0.10***	***0.76***	**0.03**	***−0.11***	***−0.51***	**0.05**	**−0.04**	−0.03	**0.04**	−0.01	**0.07**	***0.09***	0.00	**−0.03**	**−0.04**
Parietal R	3.33	0.16	0.65	0.04	***−0.19***	***−0.44***	***−0.09***	***0.76***	**0.03**	***−0.10***	***−0.51***	**0.06**	**−0.05**	**−0.04**	**0.05**	−0.01	**0.05**	***0.08***	−0.01	**−0.03**	**−0.04**
Occipital L	1.98	0.08	0.50	0.04	***−0.25***	***−0.31***	−0.03	***0.59***	**0.03**	**−0.08**	***−0.50***	**0.07**	−0.03	−0.01	**0.06**	−0.01	**0.06**	***0.09***	0.01	**−0.03**	**−0.05**
Occipital R	2.01	0.08	0.51	0.04	***−0.24***	***−0.26***	0.00	***0.63***	0.02	***−0.09***	***−0.48***	0.04	**−0.04**	−0.02	**0.05**	−0.01	0.04	***0.09***	0.00	**−0.03**	**−0.04**
Cingulate L	1.02	0.04	0.46	0.03	***−0.17***	***−0.20***	−0.03	***0.74***	**0.04**	***−0.09***	***−0.30***	0.03	−0.02	−0.01	0.03	0.01	0.03	**0.05**	−0.03	−0.01	−0.03
Cingulate R	1.00	0.04	0.36	0.04	***−0.16***	***−0.31***	−0.03	***0.65***	0.01	***−0.11***	***−0.25***	***0.09***	**0.05**	0.00	0.02	0.01	−0.02	0.00	0.01	−0.02	**−0.04**
Insular L	0.45	0.02	0.41	0.04	**−0.05**	***−0.31***	0.00	***0.68***	0.01	**−0.07**	***−0.14***	***0.11***	0.02	−0.01	0.03	−0.01	−0.02	0.01	0.01	−0.01	−0.03
Insular R	0.47	0.02	0.44	0.04	**−0.07**	***−0.38***	**0.05**	***0.61***	0.01	−0.05	***−0.19***	**0.06**	0.01	0.01	0.03	−0.01	0.00	0.02	**0.04**	−0.01	−0.02
Subcortical GM	3.10	0.13	0.53	0.04	***−0.32***	***−0.25***	−0.03	***0.68***	0.01	**−0.05**	***−0.32***	0.01	0.01	0.03	**0.06**	−0.02	0.04	**0.05**	0.03	−0.01	−0.02
Thalamus L	0.80	0.04	0.38	0.04	***−0.13***	***−0.47***	**−0.08**	***0.53***	0.01	**−0.06**	***−0.32***	0.02	0.03	−0.01	**0.06**	−0.02	***0.10***	0.04	0.01	0.00	−0.01
Thalamus R	0.53	0.02	0.46	0.04	***−0.17***	***−0.44***	**−0.05**	***0.60***	0.03	−0.04	***−0.17***	***−0.12***	0.01	−0.03	0.04	−0.02	***0.15***	0.02	0.02	−0.03	−0.01
Putamen L	0.64	0.02	0.19	0.04	***−0.24***	***0.13***	0.01	***0.33***	−0.02	0.01	***−0.17***	−0.05	−0.04	**0.06**	0.01	−0.02	0.04	0.04	0.00	0.00	−0.02
Putamen R	0.54	0.02	0.20	0.05	***−0.28***	***0.08***	**0.06**	***0.30***	−0.01	0.01	***−0.14***	0.05	−0.03	***0.08***	0.01	−0.02	**−0.07**	0.02	0.03	0.01	**−0.05**
Hippocampus L	0.39	0.02	0.34	0.04	***−0.43***	***−0.28***	**−0.05**	***0.33***	0.00	−0.06	***−0.33***	**0.06**	**0.05**	0.02	0.05	0.00	0.03	0.00	**0.04**	0.00	−0.02
Hippocampus R	0.41	0.02	0.40	0.05	***−0.43***	***−0.34***	**−0.06**	***0.34***	−0.02	−0.03	***−0.40***	0.01	**0.06**	0.04	**0.07**	0.00	**0.08**	0.03	0.03	−0.02	−0.02
Caudate L	0.39	0.01	0.20	0.04	−0.04	**−0.08**	***−0.13***	***0.54***	0.00	−0.03	0.00	0.01	−0.04	0.04	0.00	0.00	−0.04	0.04	0.01	0.00	0.02
Caudate R	0.40	0.02	0.27	0.04	**−0.07**	***0.20***	**−0.07**	***0.48***	−0.01	0.00	***0.07***	0.05	**−0.06**	**0.07**	−0.01	−0.03	***−0.11***	0.02	0.04	−0.03	0.01
Amygdala L	0.19	0.01	0.40	0.04	***−0.31***	***−0.18***	**0.06**	***0.28***	−0.01	−0.03	***−0.54***	−0.04	0.02	**0.04**	0.04	−0.01	***0.10***	**0.05**	**0.04**	−0.02	−0.02
Amygdala R	0.20	0.01	0.38	0.05	***−0.28***	***−0.20***	***0.10***	***0.33***	−0.01	−0.04	***−0.50***	***0.10***	**0.06**	**0.04**	**0.06**	−0.01	0.03	0.04	0.02	−0.02	−0.03
Pallidus L	0.22	0.01	0.13	0.03	**0.07**	−0.04	0.05	***0.30***	0.02	0.03	0.00	**−0.09**	0.01	**−0.06**	−0.03	0.00	***0.11***	0.02	0.03	−0.03	−0.01
Pallidus R	0.18	0.01	0.22	0.04	0.01	***−0.22***	**−0.06**	***0.43***	−0.01	−0.02	***−0.35***	0.05	−0.02	**−0.07**	**0.06**	0.02	***0.12***	***0.10***	0.01	0.00	−0.02
Accumbens L	0.09	0.00	0.26	0.05	***−0.38***	***0.26***	−0.01	***0.14***	−0.02	−0.04	***−0.14***	***0.16***	**−0.05**	0.02	0.05	0.01	***−0.14***	0.02	**0.06**	**−0.04**	**−0.04**
Accumbens R	0.08	0.00	0.38	0.05	***−0.32***	***0.29***	**0.07**	***0.20***	−0.02	−0.04	***−0.41***	0.02	−0.02	0.01	0.02	0.00	−0.05	**0.06**	−0.02	0.00	**−0.04**
Ventral DC L	0.29	0.01	0.44	0.04	***−0.11***	***−0.22***	0.01	***0.66***	0.02	**−0.06**	***−0.28***	0.00	0.00	0.00	***0.08***	−0.03	**0.06**	***0.07***	−0.01	−0.01	−0.03
Ventral DC R	0.26	0.01	0.45	0.04	***−0.22***	***−0.14***	0.04	***0.65***	**0.05**	**−0.08**	***−0.25***	0.00	0.00	0.01	**0.06**	0.00	0.03	**0.04**	0.02	0.00	−0.02
Stem	1.61	0.07	0.42	0.04	***−0.16***	***−0.12***	**−0.06**	***0.70***	0.02	**−0.06**	***−0.06***	**−0.07**	0.03	0.01	***0.11***	−0.03	***0.11***	0.02	0.01	−0.02	−0.03
Corpuscallosum	0.36	0.01	0.20	0.04	***−0.28***	***−0.17***	***−0.15***	***0.36***	**−0.04**	−0.03	***−0.27***	−0.01	0.02	−0.02	**0.06**	0.00	0.06	0.04	0.02	0.00	−0.02
Ventricle	0.15	0.01	0.45	0.04	***0.49***	0.00	0.02	***0.47***	0.00	0.01	**−0.04**	0.03	0.00	**−0.05**	−0.01	**−0.04**	0.01	0.00	0.02	0.01	0.00
Lateral L	0.16	0.01	0.42	0.04	***0.48***	−0.01	0.00	***0.47***	0.00	0.01	**−0.04**	0.02	0.00	**−0.05**	−0.01	**−0.04**	0.01	0.01	0.01	0.01	0.00
Lateral R	0.17	0.01	0.42	0.05	***0.49***	**0.04**	0.00	***0.46***	−0.01	0.01	−0.03	0.03	0.00	**−0.06**	−0.01	**−0.04**	0.00	0.00	0.03	0.00	0.01
Inferior lateral L	0.23	0.01	0.39	0.04	***0.49***	**−0.04**	***0.17***	***0.21***	0.02	0.04	−0.02	0.02	−0.02	−0.02	−0.02	−0.02	**0.06**	0.04	0.03	**−0.04**	0.00
Inferior lateral R	0.26	0.01	0.36	0.04	***0.48***	0.02	***0.16***	***0.23***	0.00	0.00	0.02	**0.06**	**−0.06**	***−0.07***	−0.01	0.00	0.03	0.02	**0.05**	**−0.05**	0.00
3rd	0.12	0.00	0.44	0.05	***0.41***	***−0.18***	***0.19***	***0.39***	0.01	−0.01	***−0.06***	**0.07**	0.02	−0.01	−0.04	**−0.04**	0.04	0.00	0.02	−0.03	0.00
4th	0.12	0.00	0.14	0.04	***0.14***	***−0.12***	0.05	***0.25***	−0.01	0.07	**−0.05**	0.05	−0.01	−0.01	0.05	0.00	−0.06	−0.01	−0.02	0.03	0.02

The values with $p < 0.00125$ are presented in bold and italic. The values with $p < 0.05$ are presented in bold. L, left; R, right; MFS, magnetic field strength; GM, gray matter; DC, diencephalon.

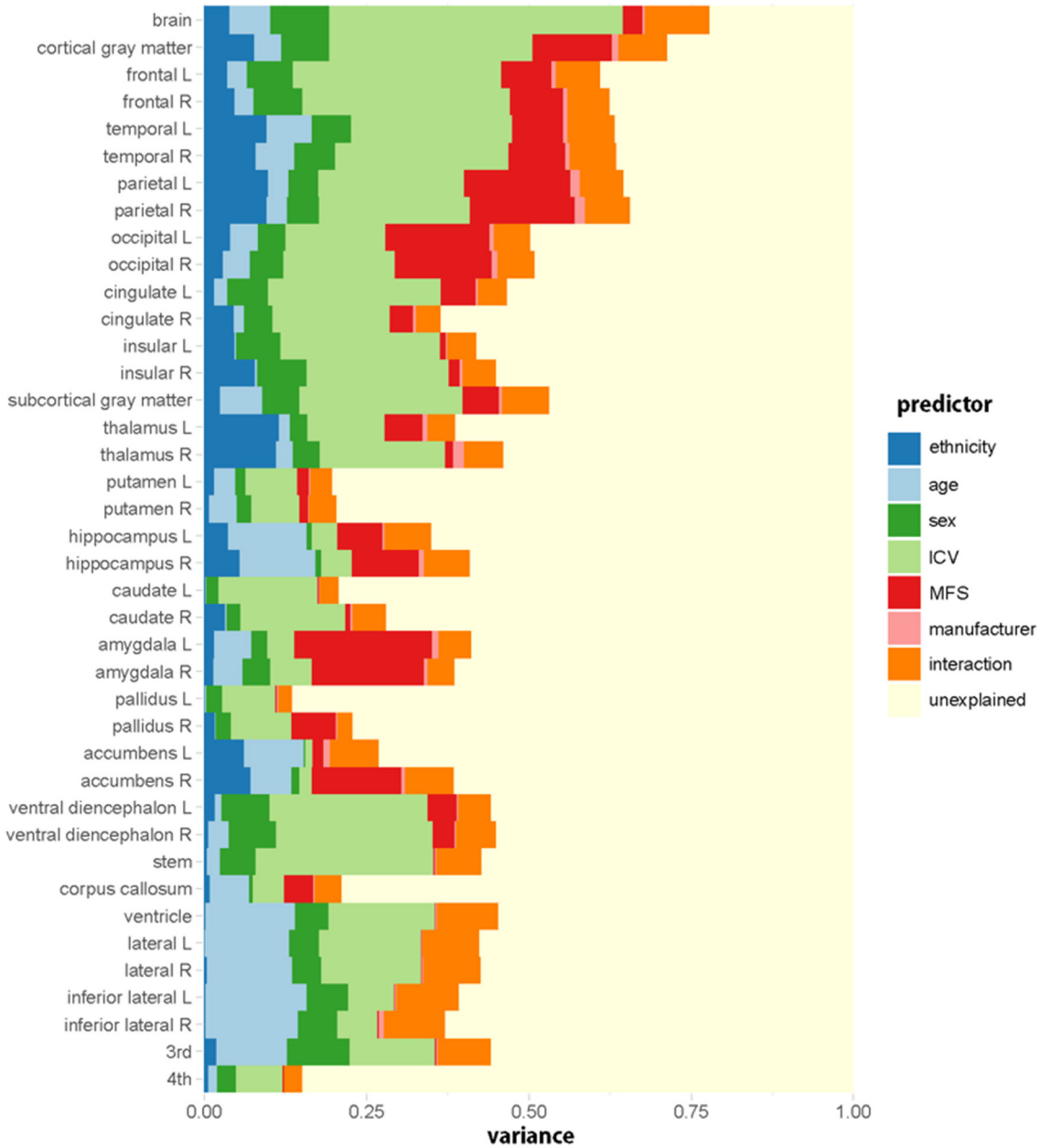

FIGURE 2 | Relative importance (R^2, proportion of the variance explained) of each predictive variable in the regression model for each regional volume. Ethnicity (dark blue) has a substantial effect on brain volumes. The relative importance is computed by averaging each predictor's explained proportion of the variance over all orderings of predictors. Interaction indicates the sum of the proportions of variance explained by all the interaction terms.

TE = 3.43 ms; TI = 1,100 ms; FA = 15°; FoV = 224 mm × 224 mm; matrix = 256 × 256; slice thickness = 0.9 mm) at Chosun University Hospital, Gwangju, Republic of Korea.

The brain images of Caucasians were selected with slice thickness ≤1.2 mm from ADNI and OASIS datasets. Since there are no sub-millimeter resolution images (voxel size < 1 mm^3) in the ADNI dataset, we selected 1- or near-millimeter resolution images (voxel size = 1−2 mm^3, 0.93–1.30 × 0.93–1.30 × 1.0–1.2 mm) of Caucasian brains, which were scanned at multiple centers. The MRI scanner protocols were described in detail according to each scanner model at the ADNI site (https://adni.loni.usc.edu/methods/documents/mri-protocols/) and the OASIS site (https://www.oasis-brains.org/files/OASIS-3_Imaging_Data_Dictionary_v1.5.pdf).

Measurement of Cortical and Subcortical Volumes

The volumes of cortical and subcortical structures were measured from each brain image using the standard recon-all processing

TABLE 3 | Percentage of the variance explained by each predictor in models predicting lobar and subcortical regional volumes.

	Ethnicity	Age	Sex	ICV	MFS	Manufacturer	Interaction	Unexplained
Brain	4.0	6.2	9.1	45.3	3.0	0.3	10.0	22.1
Cortical gray matter	7.7	4.2	7.4	31.3	12.3	1.0	7.5	28.7
Frontal L	3.6	3.0	7.2	32.0	7.8	0.7	6.8	39.0
Frontal R	4.7	2.9	7.5	32.0	8.2	0.7	6.5	37.5
Temporal L	9.6	7.0	6.0	24.9	7.8	0.7	7.3	36.7
Temporal R	8.0	6.0	6.3	26.7	8.7	0.7	7.1	36.5
Parietal L	9.9	3.1	4.7	22.4	16.3	1.5	6.8	35.3
Parietal R	9.6	3.1	5.0	23.2	16.2	1.5	7.0	34.4
Occipital L	4.0	4.3	4.2	15.4	16.1	0.7	5.5	49.8
Occipital R	2.9	4.1	5.2	17.2	15.0	0.8	5.7	49.1
Cingulate L	1.6	1.9	6.3	26.6	5.3	0.3	4.5	53.3
Cingulate R	4.6	1.6	4.3	18.0	3.6	0.4	3.8	63.5
Insular L	4.7	0.3	6.8	24.6	0.8	0.3	4.4	58.1
Insular R	7.8	0.4	7.7	21.8	1.7	0.5	5.1	55.1
Subcortical gray matter	2.5	6.5	5.7	25.2	5.6	0.5	7.3	46.8
Thalamus L	11.6	1.6	2.7	11.9	5.9	0.7	4.3	61.2
Thalamus R	11.1	2.5	4.2	19.3	1.3	1.7	6.0	53.9
Putamen L	1.6	3.3	1.6	8.0	1.8	0.2	3.4	80.2
Putamen R	0.8	4.3	2.2	7.4	1.4	0.1	4.2	79.6
Hippocampus L	3.7	12.2	0.7	4.0	6.9	0.4	7.1	65.0
Hippocampus R	5.5	11.7	0.9	4.7	10.4	0.8	7.0	59.1
Caudate L	0.3	0.1	1.9	15.3	0.2	0.2	2.9	79.2
Caudate R	3.2	0.3	2.1	16.1	0.8	0.3	5.2	72.0
Amygdala L	1.6	5.7	2.5	4.2	21.2	1.0	5.0	58.8
Amygdala R	1.5	4.4	4.4	6.3	17.3	0.5	4.2	61.4
Pallidus L	0.1	0.2	2.5	8.2	0.1	0.2	2.1	86.5
Pallidus R	1.7	0.0	2.4	9.3	6.9	0.2	2.3	77.2
Accumbens L	6.2	9.1	0.3	1.1	1.6	1.1	7.5	73.1
Accumbens R	7.2	6.3	1.2	2.0	13.8	0.5	7.6	61.5
Ventral diencephalon L	1.7	1.0	7.4	24.3	4.5	0.3	5.1	55.8
Ventral diencephalon R	0.7	3.1	7.3	24.0	3.4	0.2	6.2	55.0
Stem	0.4	2.1	5.4	27.4	0.2	0.3	6.9	57.3
Corpus callosum	1.0	6.0	0.5	4.9	4.5	0.3	4.2	78.7
Ventricle	0.2	13.8	5.2	16.4	0.1	0.1	9.5	54.7
Lateral L	0.1	13.1	4.5	15.7	0.1	0.1	8.8	57.6
Lateral R	0.5	13.1	4.4	15.4	0.1	0.2	8.8	57.4
Inferior lateral L	0.2	15.7	6.4	7.1	0.1	0.2	9.6	60.7
Inferior lateral R	0.2	14.3	6.0	6.2	0.3	0.8	9.4	62.9
3rd	1.9	10.9	9.6	13.2	0.2	0.2	8.2	55.8
4th	0.7	1.3	3.0	7.2	0.2	0.1	2.7	84.9

L, left; R, right; ICV, intracranial volume; MFS, magnetic field strength.

pipeline of FreeSurfer version 5.3.0, which is documented and available for download online (http://surfer.nmr.mgh.harvard.edu/). Briefly, the steps of the process include intensity normalization (Sled et al., 1998), segmentation of the gray matter (GM), white matter (WM), and cerebrospinal fluid (CSF), and surface modeling for the GM/WM and GM/CSF borders (Dale et al., 1999; Fischl et al., 2001). Once the cortical models are complete, a number of deformable procedures can be performed for in further data processing and analysis, including surface inflation (Fischl et al., 1999a), registration to a spherical atlas which utilized individual cortical folding patterns to match cortical geometry across subjects (Fischl et al., 1999b), parcellation of the cerebral cortex into units based on gyral and sulcal structure (Fischl et al., 2004; Desikan et al., 2006), and creation of a variety of surface-based data including maps of curvature and sulcal depth. This method uses both intensity and continuity information from the entire three-dimensional MR volume in segmentation and deformation procedures to produce

TABLE 4 | Sample sizes of normal people and AD patients of Koreans and Caucasians.

	Korean CN		Korean AD		Caucasian CN		Caucasian AD	
	Mean	**SD**	**Mean**	**SD**	**Mean**	**SD**	**Mean**	**SD**
n	210		210		210		210	
Age	75.1	5.5	74.6	6.1	75.6	5.8	74.8	6.5
Sex (M)	51.0%		50.0%		54.8%		50.0%	
Field strength (1.5T)	33.8%		37.1%		31.9%		37.6%	

M, male; CN, normal control; AD, Alzheimer's disease.

representations of cortical thickness, calculated as the closest distance from the GM/WM boundary to the GM/CSF boundary at each vertex on the tessellated surface (Fischl and Dale, 2000).

Subjects were excluded from all analyses if there were major errors in cortical and subcortical segmentation. To acquire consistent brain measures, we used the Desikan–Killiany–Tourville (DKT) atlas (Klein and Tourville, 2012), which has the advantages of having unambiguous regional definitions and boundaries well-suited to the FreeSurfer classifier algorithm.

Statistical Analysis

All statistical analyses, including regression models predicting cortical and subcortical volumes, were conducted in R version 3.6.3 (https://www.r-project.org/). In the previous study (Potvin et al., 2016), the regression model analyses were performed using age, sex, intracranial volume (ICV), magnetic field strength (MFS), and scanner manufacturers as predictors. Quadratic and cubic terms for ICV were tested, and the following interactions: age × sex, ICV × MFS, MFS × manufacturer. For age, unlike their model including quadratic and cubic terms, our prediction models adopted only a linear term because the age range was narrow for the subjects and the relations between age and GM volume are nearly linear from adulthood (Sowell et al., 2003; Fox and Schott, 2004; Fjell et al., 2009; Salthouse, 2011). The base model before including ethnicity as a predictor was as follows:

$$\hat{V} = \beta_1 \cdot age + \beta_2 \cdot sex + \beta_3 \cdot ICV + \beta_4 \cdot ICV^2 + \beta_5 \cdot ICV^3 + \beta_6 \cdot MFS + \beta_7 \cdot manufacturer + \beta_8 \cdot sex \times age + \beta_9 \cdot MFS \times manufacturer + \beta_{10} \cdot MFS \times ICV + \beta_{11} \cdot ICV \times manufacturer + \alpha$$

Our final model including ethnicity as well as the interaction terms: ethnicity × age, ethnicity × sex was as follows:

$$\hat{V} = \beta_1 \cdot \mathbf{ethnicity} + \beta_2 \cdot age + \beta_3 \cdot sex + \beta_4 \cdot ICV + \beta_5 \cdot ICV^2 + \beta_6 \cdot ICV^3 + \beta_7 \cdot MFS + \beta_8 \cdot manufacturer + \beta_9 \cdot \mathbf{ethnicity} \times \mathbf{age} + \beta_{10} \cdot \mathbf{ethnicity} \times \mathbf{sex} + \beta_{11} \cdot sex \times age + \beta_{12} \cdot MFS \times manufacturer + \beta_{13} \cdot MFS \times ICV + \beta_{14} \cdot ICV \times manufacturer + \alpha$$

To prevent overfitting and boost generalizability, 10-fold cross-validation was performed on all the predictive models using the caret package. Ventricular volumes were log-transformed to analyze because of the skewed distribution, and the estimated coefficients for the ventricular volumes were back-transformed to represent cm^3 or a % increase per year.

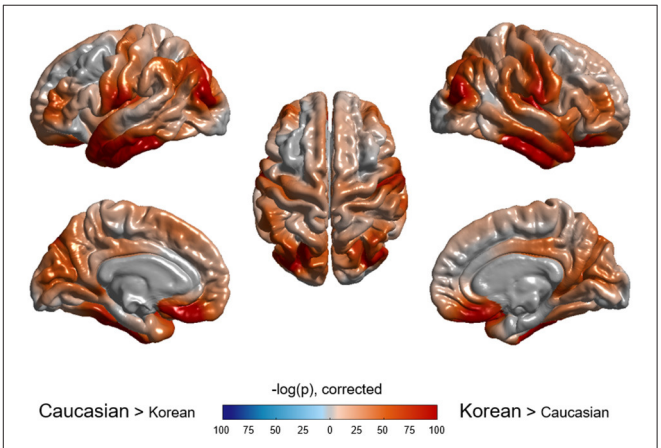

FIGURE 3 | Vertex-wise comparison of cortical volume between Caucasian and Korean normal controls. Korean elderly people were bigger in cortical volume than Caucasians. The *p*-value of ethnicity as a predictor was computed at each vertex based on the regression model described in the method section.

For the z-score distribution of normal controls and AD subjects of Koreans and Caucasians, the four groups were matched to each other based on age, sex, and MFS using a propensity score matching method of MatchIt package in R (see **Table 4** for the details of the four groups). The normal controls matched to patients with AD were selected again from the aforementioned normative samples.

Normative Statistics

We turn to the calculations required to draw inferences concerning the discrepancies between a given subject's obtained volume, V_0, and the volume predicted by the regression model, $\hat{V}$. The following methods are those developed by Crawford, Garthwaite (Crawford et al., 2012).

The first step is to calculate the standard error (SE) of a predicted volume for a new subject, denoted as s_{n+1}. This SE can

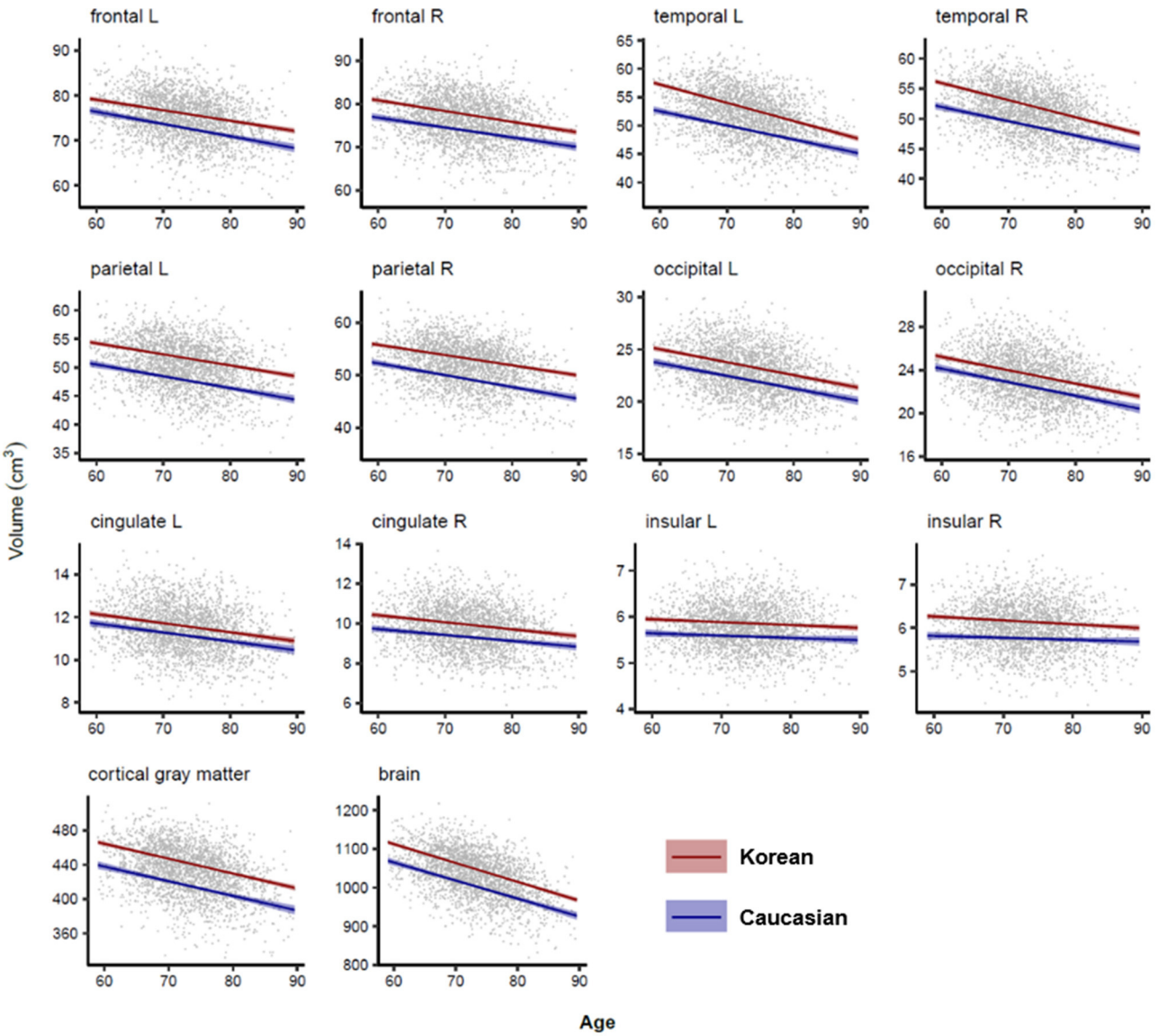

FIGURE 4 | Lobar volume changes with age in Caucasian and Korean elderly people. This figure illustrates ethnic contrast on age effect in each model predicting lobar volumes in a massive sample of cognitively normal people aged 59–89 years. Each line denotes mean volume with 95% confidence intervals in the colored shade.

be expressed in this form:

$$s_{n+1} = s_{V\cdot x}\sqrt{1 + \frac{1}{n} + \frac{1}{n-1}\sum r^{ii}z_{i0}^2 + \frac{2}{n-1}\sum r^{ij}z_{i0}z_{j0}}$$

where $s_{V\cdot x}$ represents the root mean square error (also called residual standard deviation or SE of estimate) of the model predicting normative values, r^{ii} identifies the main diagonal elements of the inverted correlation matrix (R^{-1}) for the k predictor variables, r^{ij} identifies off-diagonal elements, and $z_0 = (z_{10}, \ldots, z_{k0})'$ identifies the subject's values on the predictor variables in *z-score* form. We use the form $z_{i0} = (n-1)(x_{i0} - \bar{x}_i)/\Sigma(x_{ij} - \bar{x}_i)^2$. The first summation is over the k diagonal elements, and the second is over the $k(k\text{-}1)/2$ off-diagonal elements below (or above) the diagonal.

For effect size, a *z-score* (z) was computed by the formula below, using the discrepancy between a subject's actual (V_0) and predicted volumes ($\hat{V}$), divided by s_{n+1} the SE of the predicted volume:

$$z = \frac{V_0 - \hat{V}}{s_{n+1}.} \quad (1)$$

Vertex-Wise Analysis

Vertex-wise cortical volume comparisons were rendered on the cortical surface using the regression models implemented in the SurfStat toolbox (http://www.math.mcgill.ca/keith/surfstat/)

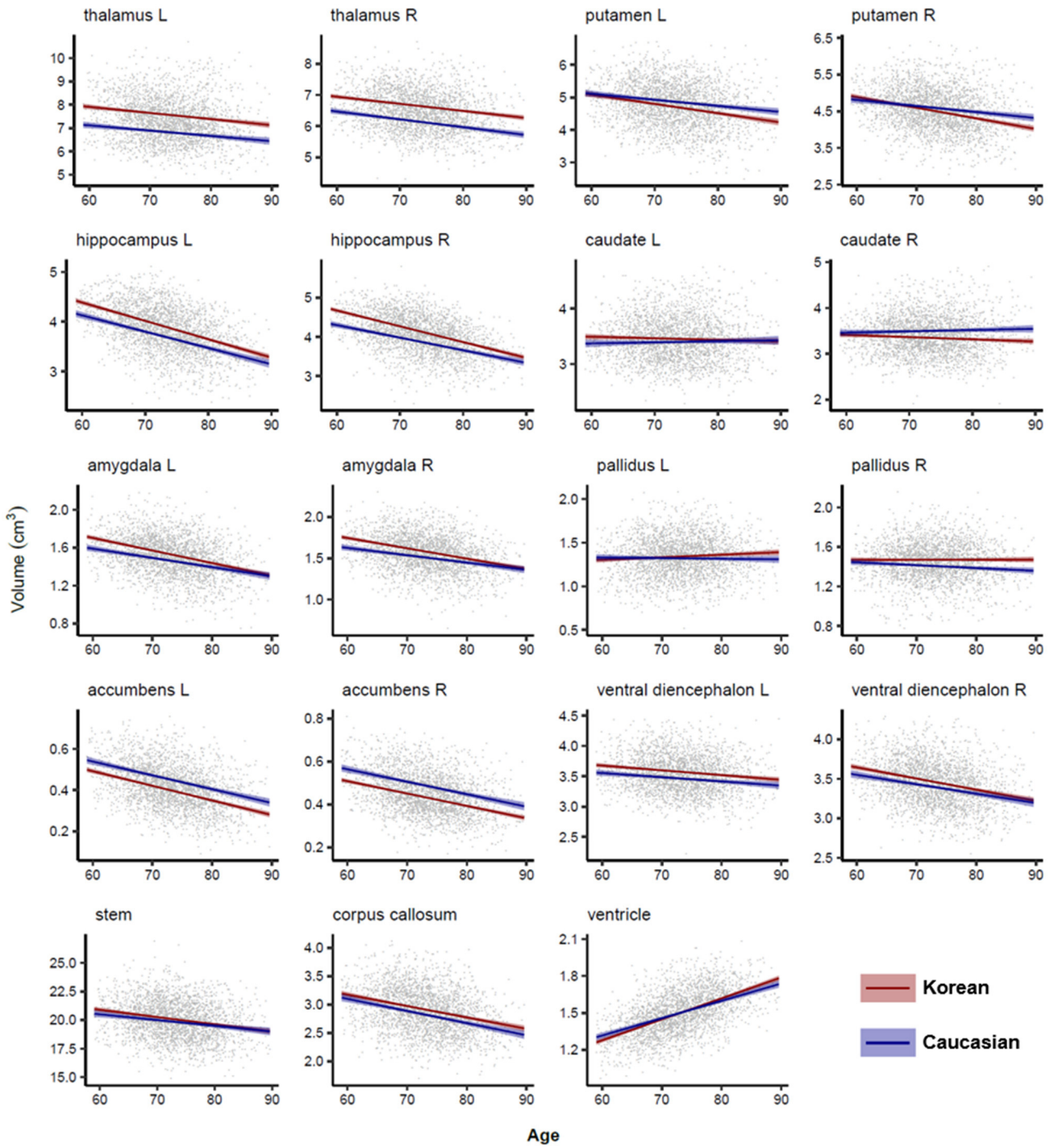

FIGURE 5 | Subcortical volume changes with age in Caucasian and Korean elderly peoples. This figure illustrates ethnic contrast in age effect in each model predicting subcortical volumes in a massive sample of cognitively normal people aged 59–89 years. Each line denotes mean volume with 95% confidence intervals in the colored shade. Ventricular volumes are $\log_{10}$ transformed.

in MATLAB R2016a (The Mathworks, Natick, MA, USA). A random field theory (RFT)-based correction for multiple comparisons was applied at the cluster level with $p = 0.05$ as the significance threshold.

Classification of Korean Patients With AD From Caucasian Normal People

The logistic regression model analyses were built using the only z-scores of six regions: bilateral temporal cortices, hippocampi, and

TABLE 5 | *Z*-scores and the differences between the observed volumes and the predicted volumes.

	Before ethnicity adjustment						After ethnicity adjustment					
	Kor.CN			Cau.CN			Kor.CN			Cau.CN		
	z	*t*	*p*	*z*	*t*	*p*	*z*	*t*	*p*	*z*	*t*	*p*
Brain	0.24	1.59	0.113	**−0.58**	−3.11	0.002	−0.02	−0.12	0.901	−0.02	0.35	0.728
Cortical gray matter	0.18	1.37	0.171	***−0.62***	−4.15	0.000	−0.14	−1.03	0.304	0.04	0.59	0.555
Frontal L	0.08	0.67	0.502	**−0.37**	−2.83	0.005	−0.13	−1.10	0.270	0.08	0.56	0.574
Frontal R	0.12	0.99	0.321	***−0.39***	−3.37	0.001	−0.11	−0.91	0.365	0.10	0.37	0.710
Temporal L	0.20	1.75	0.080	***−0.61***	−3.93	0.000	−0.08	−0.70	0.482	−0.01	1.27	0.204
Temporal R	0.19	1.57	0.117	***−0.56***	−3.76	0.000	−0.08	−0.75	0.453	0.01	1.04	0.297
Parietal L	0.17	1.45	0.149	***−0.71***	−5.43	0.000	−0.16	−1.30	0.196	−0.06	0.29	0.771
Parietal R	0.18	1.59	0.112	***−0.69***	−5.17	0.000	−0.15	−1.11	0.268	−0.04	0.32	0.745
Occipital L	0.12	0.97	0.333	**−0.34**	−3.20	0.001	−0.06	−0.81	0.419	0.06	0.54	0.588
Occipital R	0.11	1.05	0.294	**−0.34**	−2.62	0.009	−0.05	−0.47	0.636	0.00	0.44	0.662
Cingulate L	0.11	1.09	0.278	**−0.30**	−2.48	0.014	−0.01	−0.12	0.901	−0.03	−0.13	0.898
Cingulate R	0.07	0.70	0.482	***−0.33***	−3.99	0.000	−0.11	−1.25	0.212	0.06	0.14	0.885
Insular L	**0.18**	2.01	0.046	***−0.31***	−3.50	0.001	0.00	0.05	0.959	0.09	0.29	0.775
Insular R	**0.21**	2.44	0.015	***−0.40***	−4.88	0.000	0.00	0.07	0.945	0.08	−0.09	0.932
Subcortical gray matter	0.16	1.53	0.127	**−0.33**	−3.19	0.002	0.03	0.31	0.754	−0.03	−0.42	0.672
Thalamus L	**0.25**	2.90	0.004	***−0.58***	−8.17	0.000	0.00	−0.31	0.756	−0.04	−0.95	0.344
Thalamus R	**0.28**	2.97	0.003	***−0.56***	−7.53	0.000	0.02	−0.14	0.890	0.00	−1.02	0.307
Putamen L	−0.08	−0.53	0.598	**0.13**	2.45	0.015	0.01	0.58	0.563	−0.05	−0.13	0.897
Putamen R	0.00	0.19	0.848	0.20	1.64	0.103	0.07	1.06	0.288	0.06	−0.12	0.901
Hippocampus L	**0.19**	2.21	0.028	**−0.25**	−2.73	0.007	0.06	0.58	0.564	0.06	0.74	0.457
Hippocampus R	**0.21**	2.16	0.031	***−0.34***	−3.81	0.000	0.05	0.40	0.689	0.04	0.45	0.650
Caudate L	0.01	0.43	0.670	−0.19	−1.35	0.178	−0.03	0.04	0.970	−0.11	−0.34	0.737
Caudate R	−0.08	−0.65	0.517	**0.20**	2.96	0.003	0.05	0.76	0.450	−0.07	−0.12	0.902
Amygdala L	0.13	1.05	0.293	−0.20	−1.23	0.219	0.04	0.20	0.843	0.00	0.92	0.360
Amygdala R	0.08	0.45	0.657	−0.17	−1.45	0.148	0.00	−0.48	0.628	0.03	0.77	0.442
Pallidus L	0.03	0.55	0.580	**−0.06**	−2.20	0.029	−0.02	−0.10	0.923	0.02	−1.05	0.297
Pallidus R	0.15	1.94	0.053	**−0.22**	−3.21	0.001	0.04	0.48	0.628	0.02	0.29	0.769
Accumbens L	−0.15	−1.61	0.108	***0.40***	5.73	0.000	0.03	0.81	0.419	0.02	1.29	0.199
Accumbens R	**−0.21**	−2.00	0.047	***0.48***	4.45	0.000	−0.02	0.28	0.777	0.07	−0.05	0.964
Ventral diencephalon L	0.09	1.13	0.261	−0.23	−1.88	0.061	−0.01	0.09	0.930	0.00	0.32	0.751
Ventral diencephalon R	0.08	0.93	0.355	−0.10	−1.47	0.143	0.02	0.33	0.739	0.05	−0.11	0.912
Stem	0.08	0.95	0.344	−0.03	0.18	0.859	0.06	0.76	0.450	0.03	0.76	0.450
Corpus callosum	0.11	1.35	0.179	−0.06	−1.02	0.307	0.04	0.45	0.656	0.10	0.97	0.332
Ventricle	−0.05	−0.78	0.438	0.00	0.34	0.731	−0.07	−0.96	0.335	0.02	0.56	0.577
Lateral L	−0.03	−0.61	0.542	0.00	0.00	0.997	−0.06	−0.91	0.365	0.05	0.42	0.673
Lateral R	−0.07	−0.94	0.346	0.04	1.11	0.266	−0.07	−0.90	0.366	0.02	0.87	0.387
Inferior lateral L	−0.07	−0.82	0.414	−0.11	−0.85	0.398	−0.11	−1.26	0.210	−0.02	0.10	0.922
Inferior lateral R	−0.08	−0.99	0.325	−0.08	−0.43	0.665	−0.09	−1.07	0.284	−0.07	−0.45	0.654
3rd	0.08	0.71	0.480	***−0.33***	−3.44	0.001	−0.06	−0.60	0.546	−0.03	−0.45	0.652
4th	−0.06	−0.73	0.469	−0.20	−1.73	0.084	−0.10	−1.35	0.177	−0.09	−0.47	0.636

The z scores with $p < 0.00125$ are presented in bold and italic. The scores with $p < 0.05$ are presented in bold. L, left; R, right. Kor, Korean; Cau, Caucasian; CN, normal controls.

amygdalae. The best classification model was determined with 10-fold cross-validation using the caret package. The two receiver operating curves (ROCs) and the areas under the ROC (AUCs) were calculated using the pROC package. All the bootstrap operations for the significance of AUC comparison were performed with non-parametric stratified resampling (Carpenter and Bithell, 2000), and 10,000 bootstrap replicates to obtain a good estimate of the statistics.

TABLE 6 | Z-score differences between AD patients and controls before/after ethnicity adjustment.

	Before ethnicity adjustment												After ethnicity adjustment											
	Kor.AD vs. Kor.CN			Cau.AD vs. Kor.CN			Kor.AD vs. Cau.CN			Cau.AD vs. Cau.CN			Kor.AD vs. Kor.CN			Cau.AD vs. Kor.CN			Kor.AD vs. Cau.CN			Cau.AD vs. Cau.CN		
	Δz	t	p	Δz	t	p	Δz	t	p	Δz	t	p	Δz	t	p	Δz	t	p	Δz	t	p	Δz	t	p
Brain	***−0.92***	−10.43	0.000	***−1.75***	−18.53	0.000	−0.16	−1.59	0.113	***−0.99***	−9.42	0.000	***−1.03***	−10.26	0.000	***−1.20***	−11.49	0.000	***−1.12***	−10.35	0.000	***−1.28***	−11.52	0.000
Cortical GM	***−0.88***	−9.26	0.000	***−1.92***	−19.47	0.000	−0.12	−1.19	0.234	***−1.17***	−10.79	0.000	***−1.02***	−9.21	0.000	***−1.33***	−11.75	0.000	***−1.27***	−10.87	0.000	***−1.58***	−13.26	0.000
Frontal L	***−0.62***	−6.03	0.000	***−1.17***	−11.68	0.000	−0.17	−1.51	0.132	***−0.71***	−6.66	0.000	***−0.65***	−5.95	0.000	***−0.67***	−6.30	0.000	***−0.87***	−7.66	0.000	***−0.88***	−8.04	0.000
Frontal R	***−0.60***	−6.07	0.000	***−1.21***	−11.98	0.000	−0.03	−0.30	0.762	***−0.64***	−5.91	0.000	***−0.64***	−6.00	0.000	***−0.67***	−6.18	0.000	***−0.81***	−7.22	0.000	***−0.84***	−7.39	0.000
Temporal L	***−1.22***	−11.41	0.000	***−2.24***	−20.75	0.000	***−0.56***	−5.06	0.000	***−1.58***	−14.11	0.000	***−1.42***	−11.37	0.000	***−1.74***	-14.29	0.000	***−1.69***	−13.45	0.000	***−2.02***	−16.39	0.000
Temporal R	***−1.02***	−9.76	0.000	***−2.20***	−20.25	0.000	***−0.38***	−3.45	0.001	***−1.57***	−13.68	0.000	***−1.15***	−9.70	0.000	***−1.71***	−14.45	0.000	***−1.40***	−11.53	0.000	***−1.96***	−16.19	0.000
Parietal L	***−0.64***	−6.95	0.000	***−1.75***	−17.06	0.000	0.16	1.65	0.100	***−0.95***	−8.64	0.000	***−0.73***	−6.83	0.000	***−1.12***	−9.29	0.000	***−0.95***	−8.57	0.000	***−1.33***	−10.81	0.000
Parietal R	***−0.61***	−6.91	0.000	***−1.78***	−16.91	0.000	**0.20**	2.10	0.036	***−0.97***	−8.59	0.000	***−0.71***	−6.84	0.000	***−1.15***	−9.37	0.000	***−0.90***	−8.39	0.000	***−1.35***	−10.66	0.000
Occipital L	***−0.39***	−4.36	0.000	***−0.99***	−10.32	0.000	0.06	0.57	0.569	***−0.54***	−5.18	0.000	***−0.41***	−4.25	0.000	***−0.53***	−5.28	0.000	***−0.56***	−5.38	0.000	***−0.68***	−6.30	0.000
Occipital R	***−0.46***	−5.07	0.000	***−1.02***	−10.78	0.000	−0.05	−0.47	0.641	***−0.60***	−5.73	0.000	***−0.47***	−4.99	0.000	***−0.62***	−6.24	0.000	***−0.57***	−5.46	0.000	***−0.72***	−6.60	0.000
Cingulate L	***−0.58***	−5.97	0.000	***−1.01***	−10.45	0.000	−0.18	−1.86	0.064	***−0.61***	−6.29	0.000	***−0.59***	−5.90	0.000	***−0.70***	−7.09	0.000	***−0.59***	−5.94	0.000	***−0.69***	−7.14	0.000
Cingulate R	***−0.33***	−3.44	0.001	***−0.87***	−8.64	0.000	0.12	1.20	0.230	***−0.42***	−4.13	0.000	***−0.34***	−3.36	0.001	***−0.42***	−4.07	0.000	***−0.47***	−4.65	0.000	***−0.55***	−5.32	0.000
Insular L	***−0.65***	−6.71	0.000	***−1.10***	−10.75	0.000	−0.08	−0.82	0.415	***−0.54***	−4.90	0.000	***−0.67***	−6.62	0.000	***−0.65***	−6.11	0.000	***−0.70***	−6.55	0.000	***−0.68***	−6.08	0.000
Insular R	***−0.61***	−6.50	0.000	***−1.16***	−11.56	0.000	0.12	1.19	0.235	***−0.43***	−4.01	0.000	***−0.65***	−6.41	0.000	***−0.62***	−5.93	0.000	***−0.63***	−5.93	0.000	***−0.60***	−5.49	0.000
Subcortical GM	***−1.03***	−10.46	0.000	***−1.78***	−19.00	0.000	***−0.51***	−5.08	0.000	***−1.25***	−13.19	0.000	***−1.07***	−10.37	0.000	***−1.46***	−15.14	0.000	***−0.98***	−9.42	0.000	***−1.37***	-14.05	0.000
Thalamus L	***−0.37***	−4.47	0.000	***−0.88***	−10.44	0.000	***0.48***	5.71	0.000	−0.03	−0.39	0.699	***−0.40***	−4.33	0.000	***−0.25***	−2.71	0.007	***−0.34***	−3.74	0.000	***−0.19***	−2.11	0.035
Thalamus R	***−0.41***	−4.68	0.000	***−1.06***	−12.12	0.000	***0.50***	5.71	0.000	−0.15	−1.68	0.095	***−0.44***	−4.54	0.000	***−0.42***	−4.52	0.000	***−0.36***	−3.71	0.000	***−0.33***	−3.65	0.000
Putamen L	***−0.38***	−3.63	0.000	***−0.38***	−4.16	0.000	***−0.60***	−6.11	0.000	***−0.60***	−7.21	0.000	***−0.39***	−3.70	0.000	***−0.60***	−6.65	0.000	***−0.34***	−3.41	0.001	***−0.55***	−6.69	0.000
Putamen R	***−0.52***	−5.02	0.000	***−0.72***	−7.20	0.000	***−0.63***	−6.19	0.000	***−0.83***	−8.44	0.000	***−0.53***	−5.08	0.000	***−0.89***	−8.85	0.000	***−0.43***	−4.22	0.000	***−0.79***	−8.01	0.000
Hippocampus L	***−1.69***	−14.47	0.000	***−2.46***	−24.53	0.000	***−1.24***	−10.45	0.000	***−2.01***	−19.54	0.000	***−1.75***	−14.30	0.000	***−2.15***	−20.78	0.000	***−1.76***	−14.22	0.000	***−2.17***	−20.50	0.000
Hippocampus R	***−1.59***	−14.40	0.000	***−2.37***	−23.00	0.000	***−1.05***	−9.30	0.000	***−1.82***	−17.31	0.000	***−1.68***	−14.27	0.000	***−2.02***	−18.83	0.000	***−1.69***	−14.06	0.000	***−2.02***	−18.49	0.000
Caudate L	0.02	0.18	0.856	***−0.40***	−3.92	0.000	0.18	1.53	0.128	***−0.24***	−2.50	0.013	0.02	0.17	0.863	***−0.29***	−2.91	0.004	0.05	0.46	0.648	***−0.26***	−2.69	0.007
Caudate R	−0.13	−1.22	0.223	−0.13	−1.28	0.202	***−0.45***	−4.17	0.000	***−0.44***	−4.46	0.000	−0.15	−1.31	0.190	***−0.46***	−4.49	0.000	−0.07	−0.59	0.552	***−0.38***	−3.76	0.000
Amygdala L	***−1.16***	−9.90	0.000	***−1.97***	−19.47	0.000	***−0.93***	−7.75	0.000	***−1.74***	−16.65	0.000	***−1.18***	−9.81	0.000	***−1.75***	−16.65	0.000	***−1.25***	−10.14	0.000	***−1.82***	−17.24	0.000
Amygdala R	***−0.97***	−9.57	0.000	***−1.80***	−17.80	0.000	***−0.79***	−7.27	0.000	***−1.62***	−14.91	0.000	***−0.99***	−9.48	0.000	***−1.57***	−15.40	0.000	***−1.11***	−9.91	0.000	***−1.69***	−15.40	0.000
Pallidus L	0.14	1.52	0.129	−0.06	−0.61	0.540	***0.34***	3.67	0.000	0.15	1.60	0.111	0.15	1.57	0.116	0.04	0.49	0.626	**0.22**	2.32	0.021	0.11	1.26	0.208
Pallidus R	−0.13	−1.31	0.191	***−0.47***	−5.31	0.000	**0.25**	2.70	0.007	−0.10	−1.12	0.263	−0.12	−1.20	0.229	**−0.18**	−1.99	0.048	−0.10	−1.06	0.289	−0.16	−1.87	0.062
Accumbens L	***−0.77***	−8.31	0.000	***−0.45***	−4.50	0.000	***−1.38***	−13.47	0.000	***−1.05***	−9.74	0.000	***−0.81***	−8.47	0.000	***−0.93***	−9.06	0.000	***−0.87***	−8.26	0.000	***−0.98***	−8.85	0.000
Accumbens R	***−0.57***	−6.82	0.000	***−0.44***	−4.60	0.000	***−1.16***	−12.15	0.000	***−1.03***	−9.67	0.000	***−0.61***	−6.98	0.000	***−0.99***	−9.78	0.000	***−0.58***	−5.87	0.000	***−0.96***	−8.63	0.000
Ventral DC L	**−0.26**	−2.48	0.013	***−0.59***	−6.02	0.000	0.06	0.51	0.611	**−0.28**	−2.70	0.007	**−0.26**	−2.44	0.015	**−0.31**	−3.09	0.002	**−0.28**	−2.58	0.010	**−0.33**	−3.20	0.001
Ventral DC R	***−0.46***	−4.36	0.000	***−0.65***	−6.88	0.000	−0.20	−1.76	0.078	***−0.39***	−3.75	0.000	***−0.46***	−4.35	0.000	***−0.47***	−4.97	0.000	***−0.41***	−3.59	0.000	***−0.42***	−4.02	0.000
Stem	***−0.47***	−4.72	0.000	***−0.48***	−4.86	0.000	***−0.40***	−3.65	0.000	***−0.41***	−3.76	0.000	***−0.47***	−4.72	0.000	***−0.40***	−3.97	0.000	***−0.49***	−4.42	0.000	***−0.41***	−3.73	0.000
Corpus callosum	***−0.77***	−8.24	0.000	***−0.67***	−6.90	0.000	***−0.58***	−5.79	0.000	***−0.47***	−4.62	0.000	***−0.77***	−8.20	0.000	***−0.47***	−4.84	0.000	***−0.82***	−8.22	0.000	***−0.52***	−5.04	0.000
Ventricle	***1.02***	11.07	0.000	***0.97***	10.14	0.000	***0.90***	9.24	0.000	***0.86***	8.45	0.000	***1.02***	11.02	0.000	***1.00***	10.54	0.000	***0.86***	8.82	0.000	***0.84***	8.43	0.000
Lateral L	***0.93***	10.35	0.000	***0.87***	9.15	0.000	***0.87***	8.91	0.000	***0.81***	7.90	0.000	***0.93***	10.32	0.000	***0.92***	9.83	0.000	***0.80***	8.17	0.000	***0.79***	7.80	0.000
Lateral R	***0.90***	9.84	0.000	***0.91***	9.55	0.000	***0.69***	7.18	0.000	***0.70***	7.04	0.000	***0.90***	9.80	0.000	***0.88***	9.31	0.000	***0.72***	7.54	0.000	***0.70***	7.13	0.000
Inferior lateral L	***1.35***	12.97	0.000	***1.42***	14.78	0.000	***1.35***	13.33	0.000	***1.42***	15.27	0.000	***1.35***	12.99	0.000	***1.53***	16.00	0.000	***1.22***	12.00	0.000	***1.39***	15.06	0.000
Inferior lateral R	***1.30***	12.66	0.000	***1.43***	14.48	0.000	***1.25***	12.58	0.000	***1.38***	14.49	0.000	***1.31***	12.61	0.000	***1.43***	14.59	0.000	***1.24***	12.49	0.000	***1.37***	14.59	0.000
3rd	***0.75***	7.53	0.000	**0.28**	2.77	0.006	***1.17***	11.99	0.000	***0.70***	7.13	0.000	***0.78***	7.62	0.000	***0.65***	6.38	0.000	***0.76***	7.63	0.000	***0.63***	6.35	0.000
4th	***0.32***	3.34	0.001	−0.17	−1.64	0.101	***0.42***	4.11	0.000	−0.07	−0.66	0.513	***0.32***	3.38	0.001	−0.04	−0.35	0.724	**0.26**	2.57	0.010	−0.10	−0.86	0.389

L, left; R, right; ICV, intracranial volume; MFS, magnetic field strength; Kor, Korean; Cau, Caucasian; AD, AD patients; CN, normal controls; GM, gray matter; DC, diencephalon.

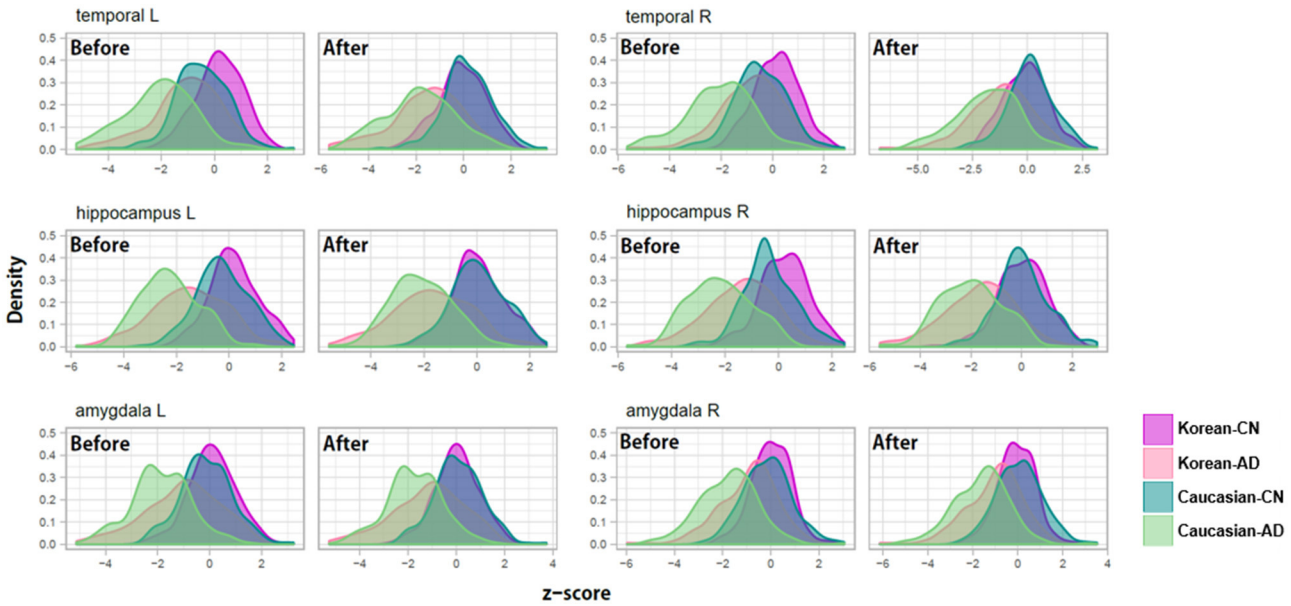

FIGURE 6 | Examples of z-score distributions of patients with Alzheimer's disease and normal controls before/after adjustment for ethnic differences. Before the adjustment, the z-score distributions of each diagnosis group were separated between Koreans and Caucasians and then overlapped after the adjustment.

RESULTS

Prediction Model Including Ethnicity as a Predictor

Table 2 describes fit measures and standardized coefficients of the models predicting lobar and subcortical volumes of the Korean and Caucasian subjects ($n = 2{,}537$). The models for subcortical GM volumes explained considerate portions of the variance (mean R^2: 31.8%, range: 12.7–45.5%). The models for lobar GM volumes explained more (mean R^2: 54.0%, range: 36.1–65.5%). As shown in **Table 2**, ethnicity had a substantial effect for all regions except left pallidus and bilateral ventricles, and age also had a substantial effect for all regions except bilateral pallidus.

Figure 2 shows the relative importance or explained variance predicted by each predictor (for detailed results, see **Table 3**). Focusing on ethnicity and age, the two main variables of interest, lobar volumes, were largely predicted by ethnicity (mean R^2: 5.9%, range: 1.6–9.9%) compared with age (mean R^2: 3.1%, range: 0.3–7%) whereas subcortical volumes were largely predicted by age (mean R^2: 4%, range: 0–12.2%) compared with ethnicity (mean R^2: 3.5%, range: 0.1–11.6%). The effects of ethnicity on the brain volumes were comparable to those of age. Even in some modified models, ethnic effects were substantial (**Supplementary Tables 2**, **3**).

As shown in **Table 2**, ethnicity had a substantial effect for all regions except left pallidus and bilateral ventricles, and age also had a substantial effect for all regions except bilateral pallidus. Cortical volumes of Koreans were larger than those of Caucasians at both lobar (**Table 2**) and vertex-wise levels (**Figure 3**). Subcortical volumes also were generally larger in Koreans, but the volumes of the putamen, accumbens, and right caudate were larger in Caucasians (**Table 2**).

Lobar and Subcortical Volume Changes in Normal Aging

Figures 4, **5** illustrated aging slopes of lobar and subcortical regions in Caucasians and Koreans aged 59 and 89 years, or the predicted volumes for lobar and subcortical regions according to age and ethnicity. As shown in **Table 2**, a marked age by race interaction was found in the right putamen and right inferior lateral ventricle. Additionally, a weak age by race interaction was found in the left frontal and right parietal lobes and the left putamen, right caudate, amygdalae, pallidi, and lateral ventricles.

Z-Scores of the Normal Controls Before/After Ethnicity Adjustment

For the validation of the z-scores based on our prediction model incorporating ethnicity, we selected Caucasian and Korean patients with AD and the matched normal controls. The four groups (two races × two diagnoses) were matched based on age, sex, and MFS (**Table 4**). To confirm whether the z-scores of the normal controls were close to zero, we calculated the z-scores of normal controls for Koreans and Caucasians, and the significances of the z-scores, or the differences between the observed and the predicted volumes. As shown in **Table 5**, the z-scores of the normal controls or the differences between the observed and the predicted volumes after ethnicity adjustment became not significant for both races. However, the differences before ethnicity adjustment were significant in most regions for either race. After ethnicity adjustment, the z-scores for lobar volumes became close to zero (mean z: −0.08, range: −0.16 to 0 for Korean; mean z: 0.03, range: −0.06 to 0.10 for Caucasian), and subcortical volumes also were close to zero (mean z: 0.02,

range: −0.03 to 0.07 for Korean; mean z: 0.01, −0.11 to 0.07 for Caucasian).

Crossover Classification of Korean Patients With AD From Caucasian Normal People

To verify the usefulness of our z-scoring system at diagnosis, we compared the z-scores of patients with AD and the normal controls (**Table 6**) and depicted the distributions of the three (bilaterally six) representative regions in **Figure 6**. The representative regions, the temporal cortices, hippocampi, and amygdalae were selected based on the criteria that all the four types of Δz values of each region were lesser than −1 after ethnicity adjustment (**Table 6**). The regions such as ventricles were not selected because they were not much affected by ethnicity.

As shown in **Figure 6**, before adjusting for racial differences, the z-score distributions of normal subjects were separated between Koreans and Caucasians and then overlapped after the adjustment. The distribution of patients with AD also shows a similar pattern, to a lesser extent than in normal people. An important point to look at is the distance change between the distributions of Korean patients with AD and Caucasian normal controls. Their distributions were overlapped before the adjustment and then separated after the adjustment. Their differences in z-value before ethnicity adjustment were close to zero and then became clear after ethnicity adjustment (see **Table 6**, particularly the columns named "Kor.AD vs. Cau.CN").

The result indicates that diagnostic errors could occur when doctors only diagnose Asian patients with AD with information from the Caucasian norms. They are likely to diagnose the patient as normal due to the highly overlapping distribution for Caucasian normal controls and Asian patients with AD before ethnicity adjustment.

Finally, we analyzed whether and to what extent the ethnicity adjustment improved the diagnostic power of the logistic regression models built using the only z-scores of six regions: bilateral temporal cortices, hippocampi, and amygdalae. The performances of the classifier models were visualized as the two ROCs (**Figure 7**). The performance of the classifier after ethnicity adjustment (AUC = 0.88) was significantly improved compared with the classifier before ethnicity adjustment (AUC =0.78) (ΔAUC = 0.10, $D = 7.80$, $p < 0.0001$; AUC comparison test using bootstrap).

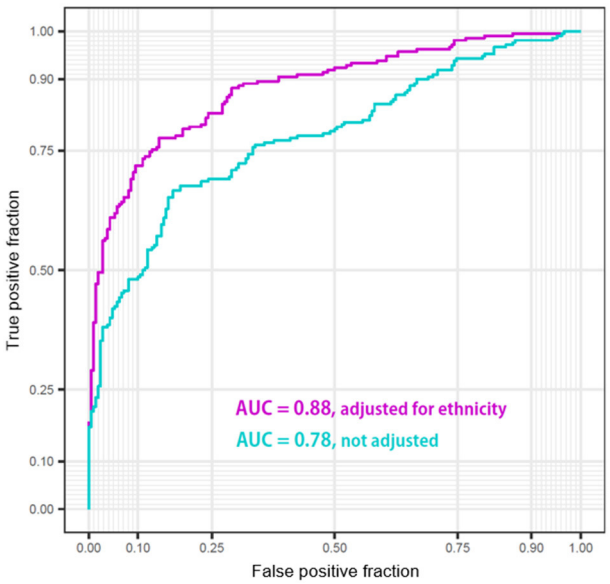

FIGURE 7 | Performance of the classifiers of Korean patients Alzheimer's disease from Caucasian normal people using z-scores of bilateral temporal cortices, hippocampi, and amygdalae before/after adjustment for ethnic differences.

DISCUSSION

General Summary

To our knowledge, the present study is the first to produce multi-racial normative volumes for lobar and subcortical structures in CN elderly individuals, considering ethnicity and age, sex, ICV, and characteristics of the MRI scanner using large samples restricted to old age. Even with the same number of samples, the sample dense in an age group can help the prediction model provide more reliable and precise estimates. The predictive model could be kept simple and non-over-fitted since the relationship between age and volume can be assumed to be linear, although hippocampal volumes were reported to be systemically overestimated to a less extent compared with young subjects when FreeSurfer measured (Wenger et al., 2014). The over-measurement is a function of ICV in elderly subjects. Since we included primary, secondary, and tertiary terms of ICV as predictors in our model, the z-scoring system can reduce the systematical errors caused by the over-measurement. Even if the inclusion of the terms of ICV could not work, the relative relationship between the two races will not change. Additionally, we focused on old age rather than whole life since comparing old and old will be more error-free than comparison between young and old.

We found that the temporal cortex, hippocampus, and amygdala were important for the AD diagnosis and highly influenced by the ethnic factor. Previous studies have shown that the temporal gyrus among cortical structures could be affected by some ethnic or genetic factors resulted in morphological differences such as brain shape or size (Zilles et al., 2001; Chee et al., 2011; Tang et al., 2018), possibly because the Asian brain is relatively wider than the Caucasian brain (Liang et al., 2015) and the temporal cortex is located on both sides of the brain. Our findings align with previous research reporting the significant effects of race or ethnicity on the hippocampus and amygdala volumes even in black and white children (Assari, 2020a,b). In contrast, ventricles and left pallidus did not significantly differ from the ethnicity in our result. Some studies reported the ethnicity effects on the ventricular and pallidal volumes

in diverse racial comparisons such as Hispanic, African vs. white Americans (Minagar et al., 2000; Brickman et al., 2008), and Indigenous Australian vs. Caucasian women except men (Klekamp et al., 1989). The discrepancy with our results might be due to the different racial composition of the subjects in each study and the different aging slopes of the brain structures in each ethnic group that changed the order of the volumes dynamically across races according to age, i.e., Caucasians at relatively early ages showed larger volume than Asians but showed smaller volume at relatively late ages as shown in **Figure 5** (Choi et al., 2020).

Review/Comparison of Previous Studies

Ethnicity, as well as age, was found to affect brain volume significantly. All cortical structures were significantly greater in Koreans compared with Caucasians. Whole-brain size and ICV often has been used interchangeably. Even in old age, the whole brain volume is highly correlated to intracranial capacity (Pearson's $r = 0.75$, $p < 0.001$ for our whole sample). The larger the brain structures, the more proportional it tended to be to intracranial capacity. This tendency is reflected in the results that East Asian's largeness was noticeable, particularly in cortical or lobar volumes rather than in subcortical structures (**Figures 3–5**). Given that Caucasians had a little greater ICV (cf. **Supplementary Table 1**), the East Asian's largeness was rather surprising even after adjusted for ICV. One of the most probable explanations is that Koreans may have a high proportion of GM in the brain, judging from the finding that women show greater cortical GM thickness than men when adjusted for whole-brain size (Luders et al., 2006). Also, it might be due to brain morphometric differences between the ethnic groups, but the exact cause is unknown, and further research is needed.

There are, of course, research papers that take different stances from our data but not converging into one conclusion. Japanese hemispheres were reported to be wider but shorter than European hemispheres (Zilles et al., 2001). Compared with Caucasians, young Chinese men were observed to show larger volumes in temporal and cingulate cortices except for frontal and parietal lobes (Tang et al., 2018). Chinese Singaporeans and non-Asian Americans were not observed to be different for old groups, whereas the young Chinese group was found to have a lower cortical thickness in frontal, parietal, temporal lobes (Chee et al., 2011). All the previous studies involved just fewer than 70 persons as East Asians who are mostly young. The studies are inconsistent with each other. The superior size of our samples may have made the small ethnic difference more reliable.

Limitations

Multi-study MRI analyses combining single- and multi-site datasets have limitations due to different scanner hardware and software versions and MRI protocols between studies. Even a multi-site study like ADNI uses dozens of protocols that contain many types of parameters such as TR, TE, flip angle, voxel size, and FoV. Furthermore, the process by which the complex interplay between the multiple factors affects images has not been clarified. The present study controlled two scanner-related variables: manufacturer and MFS, but not other scan parameters. We expected that the uncontrolled factors would play somewhat more the role of noise that increases variance than of bias that increases ethnic differences since the protocols and scanners used in ADNI were too diverse to produce a bias in a specific direction. As shown in **Supplementary Figures 1**, **2**, the CIs, or variances, of the regression lines for ADNI were wider than those for GARD and OASIS that used only Siemens scanner, and the distances between the lines for ADNI and GARD were narrower than those for OASIS and GARD in most regions. These results made it less plausible that the ethnic differences we found were only due to different MRI protocols. According to Potvin et al. (2016), a combination of data from diverse sources is likely to provide more robust normative values than values generated using data from a single source, although there is a possibility to increase the noise or variance. Nevertheless, it is still necessary to collect brain images from manufacturers other than Siemens to enhance the diversity in the Korean sample.

All studies on humans have limitations in sampling, and our study is no exception. The Korean sample was based upon a population-based cohort in a city, whereas the Caucasian sample was based upon convenience cohorts collected by academic research groups. The GARD dataset can represent the Korean elderly because it is from a city where the prevalence of dementia and the per capita income are moderate in Korea. However, the ADNI and OASIS datasets can hardly represent the Caucasian elderly because of their cohort character. Although some datasets may not be strongly argued to represent the elderly population of their ethnic group, they are one of the largest samples in such studies comparing ethnic groups. Moreover, a study comparing a convenience sample and a population-based sample (Whitwell et al., 2012) reported that the differences in hippocampal volume between the two samples disappeared after matching for demographic information. Indeed, as shown in **Figure 6**, our validation procedure using the matched samples of healthy individuals showed that the z-score distributions overlapped between the two ethnic groups.

Although our study provides an insight into the normal aging of the brain, it has limitations due to its cross-sectional character. The limitations of cross-sectional and longitudinal studies were already discussed in our previous paper (Choi et al., 2020). However, the longitudinal studies have consistently supported the findings of the cross-sectional studies (Fjell et al., 2009), and brain atrophy is found to be greater in the longitudinal data than in cross-sectional data (e.g., Raz et al., 2005; Du et al., 2006; Taki et al., 2011; Fjell et al., 2014). Thus, the effects identified in the cross-sectional study would become more apparent in the longitudinal study, and a large sample-based cross-sectional study could explain a general trend of normal aging at a population level (Schuster et al., 2015).

Ethnicity or race is a very complex construct in which genetic and environmental factors are mixed. So, we do not argue that the observed differences in brain volumes were only caused by genetic background. Alternative explanations involving environmental as well as genetic sub-factors of ethnicity should be considered. For example, since obesity, a

cardiovascular risk factor that may cause brain structure atrophy (Hamer and Batty, 2019; Opel et al., 2020), ethnic differences in obesity measures like body mass index could explain the ethnic differences in brain volumes. The obesity of an ethnic group is related to their dietary culture, which can be considered as an environmental component of ethnicity. However, in the present study, such sub-factors of ethnicity were not rigorously controlled because they could be broadly viewed as constituent elements in the concept of ethnicity. Strictly speaking, our study is not about identifying brain regions affected only by genetic components of ethnicity but rather revealing ethnic norms in brain volume and inventing methods to reduce the discrepancies between the norms at the current time. Further research is needed to dissect which factors cause the ethnic differences in norms. In future studies, the interplay between genetic and environmental factors in ethnicity that affects aging deserves more attention.

CONCLUSION

This normative data for the aging brain considering ethnic backgrounds can render researchers and clinicians with the age-related reference ranges needed to facilitate research and precise diagnosis of degenerative brain diseases in diverse ethnic societies.

DATA AVAILABILITY STATEMENT

The datasets presented in this study can be found in online repositories. The names of the repository/repositories and accession number(s) can be found below: ADNI dataset (https://adni.loni.usc.edu) and the OASIS-3 dataset (https://www.oasis-brains.org/). The GARD data that support the findings of this study are not openly available yet. Until we are ready to share the data publicly, the data could be available from the corresponding author (BCK or KHL), upon reasonable request.

ETHICS STATEMENT

The studies involving human participants were reviewed and approved by the Institutional Review Board of Chosun University Hospital, Gwangju, Republic of Korea. The patients/participants provided their written informed consent to participate in this study.

AUTHOR CONTRIBUTIONS

YYC performed the imaging analysis. YYC and U-SC wrote the preliminary draft. YYC, JJL, and KYC conducted the statistical analysis. EHS, IHC, M-KS, and YC interpreted the neuropsychological results. HK, S-MC, SHC, and BCK interviewed and examined the patients/participants and read the brain MRIs. BCK and KHL designed the study, wrote the manuscript, and provided the overall supervision for the project. All authors contributed to the article and approved the submitted version.

FUNDING

This work was supported by the Original Technology Research Program for Brain Science of the National Research Foundation (NRF) funded by the Korean government, MSIT (NRF-2014M3C7A1046041 and NRF-2016M3C7A1905469 to KHL; NRF-2016M3C7A1905472 and NRF-2019R1A4A1029769 to BCK), and supported by KBRI basic research program through Korea Brain Research Institute funded by Ministry of Science and ICT (21-BR-03-05 to KHL, YC, and BCK). Caucasian data were provided by OASIS (OASIS-3: Principal Investigators: T. Benzinger, D. Marcus, J. Morris; NIH P50 AG00561, P30 NS09857781, P01 AG026276, P01 AG003991, R01 AG043434, UL1 TR000448, R01 EB009352. AV-45 doses were provided by Avid Radiopharmaceuticals, a wholly owned subsidiary of Eli Lilly) and ADNI (NIH Grant U01 AG024904, DOD ADNI W81XWH-12-2-0012). The funding details of ADNI can be found at http://adni.loni.usc.edu/about/funding/.

ACKNOWLEDGMENTS

We are grateful to the volunteers and their families in the GARD, ADNI, and OASIS studies. Some data used in the preparation of this article were obtained from the ADNI dataset (https://adni.loni.usc.edu) and the OASIS-3 dataset (https://www.oasis-brains.org/). Therefore, the investigators within ADNI and OASIS contributed to the design and implementation of their studies and/or provided data but did not participate in the analysis or writing of this report. A complete listing of ADNI investigators can be found at: http://adni.loni.usc.edu/wp-content/uploads/how_to_apply/ADNI_Acknowledgement_List.pdf. The information about OASIS-3 can be found at doi: 10.1101/2019.12.13.19014902.

SUPPLEMENTARY MATERIAL

The Supplementary Material for this article can be found online at: https://www.frontiersin.org/articles/10.3389/fnagi.2021.675016/full#supplementary-material

Supplementary Figure 1 | Lobar volume changes in Caucasian (ADNI and OASIS datasets) and Mongolian elderly peoples (GARD dataset). This figure illustrates ethnic contrast in age effect in each model predicting lobar volumes in a massive sample of cognitively normal people aged 59–89 years. Each line denotes mean volume with 95% confidence intervals in the colored shade.

Supplementary Figure 2 | Subcortical volume changes in Caucasian (ADNI and OASIS datasets) and Mongolian elderly peoples (GARD dataset). This figure illustrates ethnic contrast in age effect in each model predicting subcortical volumes in a massive sample of cognitively normal people aged 59–89 years. Each line denotes mean volume with 95% confidence intervals in the colored shade. Ventricular volumes are $\log_{10}$ transformed.

Supplementary Table 1 | Intracranial volume (ICV) for normal Koreans and Caucasians.

Supplementary Table 2 | Standardized coefficients of the prediction model including the three-way interaction term: MFS x ICV x manufacturer.

Supplementary Table 3 | Standardized coefficients of the prediction model using the image data of Siemens 3T scanners only.

REFERENCES

Assari, S. (2020a). Race, ethnicity, family socioeconomic status, and children's hippocampus volume. *Res. Health Sci.* 5, 25–45. doi: 10.22158/rhs.v5n4p25

Assari, S. (2020b). Socioeconomic status inequalities partially mediate racial and ethnic differences in children's amygdala volume. *Stud. Soc. Sci. Res.* 1, 62–79. doi: 10.22158/sssr.v1n2p62

Ball, R., Shu, C., Xi, P., Rioux, M., Luximon, Y., and Molenbroek, J. (2010). A comparison between Chinese and Caucasian head shapes. *Appl. Ergon.* 41, 832–839. doi: 10.1016/j.apergo.2010.02.002

Beals, K. L., Smith, C. L., and Dodd, S. M. (1984). Brain size, cranial morphology, climate, and time machines. *Curr. Anthropol.* 25, 301–330. doi: 10.1086/203138

Brickman, A. M., Schupf, N., Manly, J. J., Luchsinger, J. A., Andrews, H., Tang, M. X., et al. (2008). Brain morphology in older African Americans, Caribbean Hispanics, and whites from northern Manhattan. *Arch. Neurol.* 65, 1053–1061. doi: 10.1001/archneur.65.8.1053

Carpenter, J., and Bithell, J. (2000). Bootstrap confidence intervals: when, which, what? A practical guide for medical statisticians. *Stat. Med.* 19, 1141–1164. doi: 10.1002/(SICI)1097-0258(20000515)19:9<1141::AID-SIM479>3.0.CO;2-F

Chee, M. W., Zheng, H., Goh, J. O., Park, D., and Sutton, B. P. (2011). Brain structure in young and old East Asians and Westerners: comparisons of structural volume and cortical thickness. *J. Cogn. Neurosci.* 23, 1065–1079. doi: 10.1162/jocn.2010.21513

Choi, Y. Y., Lee, J. J., Choi, K. Y., Seo, E. H., Choo, I. H., Kim, H., et al. (2020). The aging slopes of brain structures vary by ethnicity and sex: evidence from a large magnetic resonance imaging dataset from a single scanner of cognitively healthy elderly people in Korea. *Front. Aging Neurosci.* 12:233. doi: 10.3389/fnagi.2020.00233

Crawford, J. R., Garthwaite, P. H., Denham, A. K., and Chelune, G. J. (2012). Using regression equations built from summary data in the psychological assessment of the individual case: extension to multiple regression. *Psychol. Assess.* 24, 801–814. doi: 10.1037/a0027699

Dale, A. M., Fischl, B., and Sereno, M. I. (1999). Cortical surface-based analysis. I. Segmentation and surface reconstruction. *Neuroimage* 9, 179–194. doi: 10.1006/nimg.1998.0395

Desikan, R. S., Segonne, F., Fischl, B., Quinn, B. T., Dickerson, B. C., Blacker, D., et al. (2006). An automated labeling system for subdividing the human cerebral cortex on MRI scans into gyral based regions of interest. *Neuroimage* 31, 968–980. doi: 10.1016/j.neuroimage.2006.01.021

Du, A. T., Schuff, N., Chao, L. L., Kornak, J., Jagust, W. J., Kramer, J. H., et al. (2006). Age effects on atrophy rates of entorhinal cortex and hippocampus. *Neurobiol Aging* 27, 733–740. doi: 10.1016/j.neurobiolaging.2005.03.021

Fischl, B., and Dale, A. M. (2000). Measuring the thickness of the human cerebral cortex from magnetic resonance images. *Proc. Natl. Acad. Sci. U.S.A.* 97, 11050–11055. doi: 10.1073/pnas.200033797

Fischl, B., Liu, A., and Dale, A. M. (2001). Automated manifold surgery: constructing geometrically accurate and topologically correct models of the human cerebral cortex. *IEEE Med. Imaging* 20, 70–80. doi: 10.1109/42.906426

Fischl, B., Sereno, M. I., and Dale, A. (1999a). Cortical surface-based analysis: ii: inflation, flattening, and a surface-based coordinate system. *NeuroImage* 9, 195–207. doi: 10.1006/nimg.1998.0396

Fischl, B., Sereno, M. I., Tootell, R. B. H., and Dale, A. M. (1999b). High-resolution intersubject averaging and a coordinate system for the cortical surface. *Hum. Brain Map.* 8, 272–284. doi: 10.1002/(SICI)1097-0193(1999)8:4<272::AID-HBM10>3.0.CO;2-4

Fischl, B., Van Der Kouwe, A., Destrieux, C., Halgren, E., Ségonne, F., Salat, D. H., et al. (2004). Automatically parcellating the human cerebral cortex. *Cerebr. Cortex* 14, 11–22. doi: 10.1093/cercor/bhg087

Fjell, A. M., Mcevoy, L., Holland, D., Dale, A. M., Walhovd, K. B., and Alzheimer's Disease Neuroimaging, I. (2014). What is normal in normal aging? Effects of aging, amyloid and Alzheimer's disease on the cerebral cortex and the hippocampus. *Prog. Neurobiol.* 117, 20–40. doi: 10.1016/j.pneurobio.2014.02.004

Fjell, A. M., Westlye, L. T., Amlien, I., Espeseth, T., Reinvang, I., Raz, N., et al. (2009). High consistency of regional cortical thinning in aging across multiple samples. *Cereb. Cortex* 19, 2001–2012. doi: 10.1093/cercor/bhn232

Folstein, M. F., Folstein, S. E., and Mchugh, P. R. (1975). "Mini-mental state." A practical method for grading the cognitive state of patients for the clinician. *J. Psychiatr. Res.* 12, 189–198. doi: 10.1016/0022-3956(75)90026-6

Fox, N. C., and Schott, J. M. (2004). Imaging cerebral atrophy: normal ageing to Alzheimer's disease. *Lancet* 363, 392–394. doi: 10.1016/S0140-6736(04)15441-X

Hamer, M., and Batty, G. D. (2019). Association of body mass index and waist-to-hip ratio with brain structure: UK Biobank study. *Neurology* 92, e594–e600. doi: 10.1212/WNL.0000000000006879

Howells, W. W. (1990). "Skull shapes and the map. craniometric analyses in the dispersion of modern homo," in *Papers of the Peabody Museum of Archaeology and Ethnology, Harvard University* (Cambridge: Harvard University Press).

Kang, Y., Jang, S., and Na, D. L. (2012). *Seoul Neuropsychological Screening Battery (SNSB)*. Seoul: Human Brain Research & Consulting Co.

Klein, A., and Tourville, J. (2012). 101 labeled brain images and a consistent human cortical labeling protocol. *Front. Neurosci.* 6:171. doi: 10.3389/fnins.2012.00171

Klekamp, J., Riedel, A., Harper, C., and Kretschmann, H. J. (1989). Morphometric study on the postnatal growth of non-cortical brain regions in Australian aborigines and Caucasians. *Brain Res.* 485, 79–88. doi: 10.1016/0006-8993(89)90668-9

Kruggel, F. (2006). MRI-based volumetry of head compartments: normative values of healthy adults. *Neuroimage* 30, 1–11. doi: 10.1016/j.neuroimage.2005.09.063

Ledig, C., Schuh, A., Guerrero, R., Heckemann, R. A., and Rueckert, D. (2018). Structural brain imaging in Alzheimer's disease and mild cognitive impairment: biomarker analysis and shared morphometry database. *Sci. Rep.* 8:11258. doi: 10.1038/s41598-018-29295-9

Liang, P., Shi, L., Chen, N., Luo, Y., Wang, X., Liu, K., et al. (2015). Construction of brain atlases based on a multi-center MRI dataset of 2020 Chinese adults. *Sci. Rep.* 5:18216. doi: 10.1038/srep18216

Luders, E., Narr, K. L., Thompson, P. M., Rex, D. E., Woods, R. P., Deluca, H., et al. (2006). Gender effects on cortical thickness and the influence of scaling. *Hum, Brain Mapp,* 27, 314–324. doi: 10.1002/hbm.20187

Minagar, A., Sevush, S., and Bertran, A. (2000). Cerebral ventricles are smaller in Hispanic than non-Hispanic patients with Alzheimer's disease. *Neurology* 55, 446–448. doi: 10.1212/WNL.55.3.446

Morris, J. C. (1993). The Clinical Dementia Rating (CDR): current version and scoring rules. *Neurology* 43, 2412–2414. doi: 10.1212/WNL.43.11.2412-a

Opel, N., Thalamuthu, A., Milaneschi, Y., Grotegerd, D., Flint, C., Leenings, R., et al. (2020). Brain structural abnormalities in obesity: relation to age, genetic risk, and common psychiatric disorders: Evidence through univariate and multivariate mega-analysis including 6420 participants from the ENIGMA MDD working group. *Mol. Psychiatry.* doi: 10.1038/s41380-020-0774-9. [Epub ahead of print].

Potvin, O., Dieumegarde, L., Duchesne, S., and Alzheimer's Disease Neuroimaging, I. (2017). Normative morphometric data for cerebral cortical areas over the lifetime of the adult human brain. *Neuroimage* 156, 315–339. doi: 10.1016/j.neuroimage.2017.05.019

Potvin, O., Mouiha, A., Dieumegarde, L., Duchesne, S., and Alzheimer's Disease Neuroimaging, I. (2016). Normative data for subcortical regional volumes over the lifetime of the adult human brain. *Neuroimage* 137, 9–20. doi: 10.1016/j.neuroimage.2016.05.016

Raz, N., Lindenberger, U., Rodrigue, K. M., Kennedy, K. M., Head, D., Williamson, A., et al. (2005). Regional brain changes in aging healthy adults: general trends, individual differences and modifiers. *Cereb. Cortex* 15, 1676–1689. doi: 10.1093/cercor/bhi044

Resnick, S. M., Pham, D. L., Kraut, M. A., Zonderman, A. B., and Davatzikos, C. (2003). Longitudinal magnetic resonance imaging studies of older adults: a shrinking brain. *J. Neurosci.* 23, 3295–3301. doi: 10.1523/JNEUROSCI.23-08-03295.2003

Rushton, J. P. (2000). *Race, Evolution, and Behavior: A Life History Perspective.* Port Huron, MI: Charles Darwin Research Institute.

Salthouse, T. A. (2011). Neuroanatomical substrates of age-related cognitive decline. *Psychol. Bull.* 137, 753–784. doi: 10.1037/a0023262

Scahill, R. I., Frost, C., Jenkins, R., Whitwell, J. L., Rossor, M. N., and Fox, N. C. (2003). A longitudinal study of brain volume changes in normal aging using serial registered magnetic resonance imaging. *Arch. Neurol.* 60, 989–994. doi: 10.1001/archneur.60.7.989

Schuster, C., Elamin, M., Hardiman, O., and Bede, P. (2015). Presymptomatic and longitudinal neuroimaging in neurodegeneration–from snapshots to motion picture: a systematic review. *J. Neurol. Neurosurg. Psychiatry* 86, 1089–1096. doi: 10.1136/jnnp-2014-309888

Sled, J. G., Zijdenbos, A. P., and Evans, A. C. (1998). A nonparametric method for automatic correction of intensity nonuniformity in MRI data. *IEEE Trans. Med. Imaging* 17, 87–97. doi: 10.1109/42.668698

Sowell, E. R., Peterson, B. S., Thompson, P. M., Welcome, S. E., Henkenius, A. L., and Toga, A. W. (2003). Mapping cortical change across the human life span. *Nat. Neurosci.* 6, 309–315. doi: 10.1038/nn1008

Taki, Y., Kinomura, S., Sato, K., Goto, R., Kawashima, R., and Fukuda, H. (2011). A longitudinal study of gray matter volume decline with age and modifying factors. *Neurobiol. Aging* 32, 907–915. doi: 10.1016/j.neurobiolaging.2009.05.003

Tang, Y., Hojatkashani, C., Dinov, I. D., Sun, B., Fan, L., Lin, X., et al. (2010). The construction of a Chinese MRI brain atlas: a morphometric comparison study between Chinese and Caucasian cohorts. *Neuroimage* 51, 33–41. doi: 10.1016/j.neuroimage.2010.01.111

Tang, Y., Zhao, L., Lou, Y., Shi, Y., Fang, R., Lin, X., et al. (2018). Brain structure differences between Chinese and Caucasian cohorts: a comprehensive morphometry study. *Hum. Brain Mapp.* 39, 2147–2155. doi: 10.1002/hbm.23994

United States Census Bureau (2020). *An Aging World: 2020.* Available online at: https://mtgis-portal.geo.census.gov/arcgis/apps/MapSeries/index.html?appid=3d832796999042daae7982ff36835e2e (accessed March 1, 2021).

Walhovd, K. B., Westlye, L. T., Amlien, I., Espeseth, T., Reinvang, I., Raz, N., et al. (2011). Consistent neuroanatomical age-related volume differences across multiple samples. *Neurobiol. Aging* 32, 916–932. doi: 10.1016/j.neurobiolaging.2009.05.013

Wenger, E., Martensson, J., Noack, H., Bodammer, N. C., Kuhn, S., Schaefer, S., et al. (2014). Comparing manual and automatic segmentation of hippocampal volumes: reliability and validity issues in younger and older brains. *Hum. Brain Mapp.* 35, 4236–4248. doi: 10.1002/hbm.22473

Whitwell, J. L., Wiste, H. J., Weigand, S. D., Rocca, W. A., Knopman, D. S., Roberts, R. O., et al. (2012). Comparison of imaging biomarkers in the Alzheimer Disease Neuroimaging Initiative and the Mayo Clinic Study of Aging. *Arch. Neurol.* 69, 614–622. doi: 10.1001/archneurol.2011.3029

Zilles, K., Kawashima, R., Dabringhaus, A., Fukuda, H., and Schormann, T. (2001). Hemispheric shape of European and Japanese brains: 3-D MRI analysis of intersubject variability, ethnical, and gender differences. *Neuroimage* 13, 262–271. doi: 10.1006/nimg.2000.0688

Conflict of Interest: KHL was employed by the company Neurozen Inc.

The remaining authors declare that the research was conducted in the absence of any commercial or financial relationships that could be construed as a potential conflict of interest.

Publisher's Note: All claims expressed in this article are solely those of the authors and do not necessarily represent those of their affiliated organizations, or those of the publisher, the editors and the reviewers. Any product that may be evaluated in this article, or claim that may be made by its manufacturer, is not guaranteed or endorsed by the publisher.

frontiers in Aging Neuroscience

SYSTEMATIC REVIEW
published: 31 August 2021
doi: 10.3389/fnagi.2021.711023

Altered Patterns of Amplitude of Low-Frequency Fluctuations and Fractional Amplitude of Low-Frequency Fluctuations Between Amnestic and Vascular Mild Cognitive Impairment: An ALE-Based Comparative Meta-Analysis

Xulian Zhang[1†], Chen Xue[1†], Xuan Cao[2], Qianqian Yuan[1], Wenzhang Qi[1], Wenwen Xu[3], Shaojun Zhang[4] and Qingling Huang[1]*

[1] Department of Radiology, The Affiliated Brain Hospital of Nanjing Medical University, Nanjing, China, [2] Division of Statistics and Data Science, Department of Mathematical Sciences, University of Cincinnati, Cincinnati, OH, United States, [3] Department of Neurology, The Affiliated Brain Hospital of Nanjing Medical University, Nanjing, China, [4] Department of Statistics, University of Florida, Gainesville, FL, United States

OPEN ACCESS

Edited by:
Rong Chen,
University of Maryland, Baltimore, United States

Reviewed by:
Yuan Zhong,
Nanjing Normal University, China
Rongfeng Qi,
Nanjing University, China

***Correspondence:**
Qingling Huang
hql_nju@163.com

[†]These authors have contributed equally to this work and share the first authorship

Received: 17 May 2021
Accepted: 26 July 2021
Published: 31 August 2021

Citation:
Zhang X, Xue C, Cao X, Yuan Q, Qi W, Xu W, Zhang S and Huang Q (2021) Altered Patterns of Amplitude of Low-Frequency Fluctuations and Fractional Amplitude of Low-Frequency Fluctuations Between Amnestic and Vascular Mild Cognitive Impairment: An ALE-Based Comparative Meta-Analysis. Front. Aging Neurosci. 13:711023. doi: 10.3389/fnagi.2021.711023

Background: Changes in the amplitude of low-frequency fluctuations (ALFF) and the fractional amplitude of low-frequency fluctuations (fALFF) have provided stronger evidence for the pathophysiology of cognitive impairment. Whether the altered patterns of ALFF and fALFF differ in amnestic cognitive impairment (aMCI) and vascular mild cognitive impairment (vMCI) is largely unknown. The purpose of this study was to explore the ALFF/fALFF changes in the two diseases and to further explore whether they contribute to the diagnosis and differentiation of these diseases.

Methods: We searched PubMed, Ovid, and Web of Science databases for articles on studies using the ALFF/fALFF method in patients with aMCI and vMCI. Based on the activation likelihood estimation (ALE) method, connectivity modeling based on coordinate meta-analysis and functional meta-analysis was carried out.

Results: Compared with healthy controls (HCs), patients with aMCI showed increased ALFF/fALFF in the bilateral parahippocampal gyrus/hippocampus (PHG/HG), right amygdala, right cerebellum anterior lobe (CAL), left middle temporal gyrus (MTG), left cerebrum temporal lobe sub-gyral, left inferior temporal gyrus (ITG), and left cerebrum limbic lobe uncus. Meanwhile, decreased ALFF/fALFF values were also revealed in the bilateral precuneus (PCUN), bilateral cuneus (CUN), and bilateral posterior cingulate (PC) in patients with aMCI. Compared with HCs, patients with vMCI predominantly showed decreased ALFF/fALFF in the bilateral CUN, left PCUN, left PC, and right cingulate gyrus (CG).

Conclusions: The present findings suggest that ALFF and fALFF displayed remarkable altered patterns between aMCI and vMCI when compared with HCs. Thus, the findings of this study may serve as a reliable tool for distinguishing aMCI from vMCI, which may help understand the pathophysiological mechanisms of these diseases.

Keywords: amnestic mild cognitive impairment, vascular mild cognitive impairment, amplitude of low-frequency fluctuations, fractional amplitude of low-frequency fluctuations, resting state

INTRODUCTION

Mild cognitive impairment is a nosological entity referred to as a cognitive decline that is beyond normal peers. The condition is considered to be the transitional state between normal aging and dementia, where activities of daily living are unaffected (Sanford, 2017; Petersen et al., 2018). Amnestic mild cognitive impairment (aMCI) and vascular mild cognitive impairment (vMCI) are the two most common forms of the pre-dementia subtypes (Wentzel et al., 2001; Sun et al., 2016). The aMCI is characterized by isolated episodic memory impairment associated with higher risk; it is also considered as the prodromal state for the development of Alzheimer's disease (AD) (Yan et al., 2019). The vMCI, on the other hand, is described as an abnormal condition caused by vascular diseases, where the cognitive impairment of the patient is not serious and does not meet the criteria of dementia (Consoli et al., 2012). Interests in diagnosing and distinguishing between aMCI and vMCI have attracted a lot of attention and have brought out a great deal of research in both clinical and research settings. From this, researchers proposed that early diagnosis and active intervention could effectively delay the progression from MCI to dementia (Sanford, 2017). Currently, the clinical and research diagnostic criteria for aMCI and vMCI mainly depend on clinical history, neuropsychological assessment, and neuroimaging examination (Sudo et al., 2015; Anderson, 2019), but it is still difficult to distinguish between these two forms of cognitive impairment at an early stage. Therefore, a study on the similarities and specificities between aMCI and vMCI in MRI may provide a new prospect for the diagnosis and differentiation of these two diseases.

Resting-state functional MRI (rs-fMRI) has also been widely used to study the internal brain function of patients with many neuropsychiatric diseases, including MCI (Ni et al., 2016; Yang et al., 2018; Xu et al., 2020). The amplitude of low-frequency fluctuations (ALFF) of the rs-fMRI is a method to measure low-frequency oscillations of the blood-oxygen-level-dependent (BOLD) signal and local spontaneous activity during the resting state (Zang et al., 2007; Zou et al., 2008; Xi et al., 2013). Several studies have shown that ALFF can be used as an indicator of the disease state of the brain (Han et al., 2011; Chen et al., 2015), but it may be affected by a number of non-neurophysiological fluctuations. The fractional amplitude of low-frequency fluctuations (fALFF), on the other hand, represents the ratio of the amplitude in the low-frequency range to the sum of the amplitude in the whole frequency range (Wang et al., 2016). It has high sensitivity and specificity in the detection of spontaneous brain activity, but it is not as reliable as ALFF (Zou et al., 2008). These two indicators reflect the amplitude of low-frequency oscillations from different aspects and are sensitive indicators of related neurodegenerative changes (Wang et al., 2016). Both ALFF and fALFF have been more and more applied in numerous basic and clinical neuroscience studies with high reliability and reproducibility (Liu et al., 2017; Zhao et al., 2018; Luo et al., 2020). Moreover, ALFF and fALFF have been found to be abnormal in a number of neuropsychiatric disorders, such as AD, depression, and schizophrenia, and have also been found to be altered in aMCI and vMCI.

Previous ALFF/fALFF studies revealed abnormal intrinsic brain activity in aMCI. Xi et al. suggested that patients with aMCI, compared with healthy controls (HCs), showed decreased ALFFs in the left lateral temporal cortex, right hippocampus (Hip), parahippocampal gyrus (PHG), and right ventral medial prefrontal cortex (vMPFC), while increased ALFFs were displayed in the left temporal-parietal junction (TPJ) and inferior parietal lobule (IPL) (Xi et al., 2013). Meanwhile, a machine learning method demonstrated the gradual disturbances of the ALFF/fALFF in the AD spectrum as disease advanced. These studies showed several brain regions with decreased ALFF/fALFF within different bands among the bilateral cingulum, bilateral inferior cerebellum lobe, and bilateral precuneus (PCUN). However, increased ALFF/fALFF were also detected in the hip, frontal lobe, and paracentral lobe and involved in default-mode regions, such as the hip, PHG, posterior cingulate gyrus (PCG), and middle frontal gyrus (MFG). These abnormities were significantly correlated with the neuropsychological assessments as diseases progressed (Long et al., 2016; Yang et al., 2018). More recently, vascular risk factors have been found to modulate the spontaneous brain activity in patients with MCI, thus providing preliminary evidence that MCI patients with high vascular risk demonstrated decreased ALFF in the left Hip as compared with HCs with high vascular risk. This may serve as a potential neuroimaging biomarker for an underlying vascular contribution to AD (Zhuang et al., 2020). Previous studies have shown that ALFF/fALFF changes are closely related to cognitive function in patients with AD, MCI, white matter osteoporosis, and cerebral autosomal dominant arteriopathy with subcortical infarcts and leukoencephalopathy (CADASIL), suggesting that ALFF/fALFF may be an imaging biomarker for these diseases (Li et al., 2017; Yang et al., 2018; Su et al., 2019; Wang J. et al., 2019; Wang P. et al., 2019). Thus, the study of ALFF/fALFF changes in aMCI and vMCI can help us find their imaging diagnostic markers and understand their pathophysiological mechanisms.

Considering the above-mentioned ALFF and fALFF findings, in this study, we used the activation likelihood estimation (ALE) method to study ALFF/fALFF changes in aMCI and vMCI to explore their ALFF change pattern compared to HCs and diagnose and differentiate aMCI from vMCI at an early stage. Since there have been many reports of decreased ALFF/fALFF in the PCUN and posterior cingulate cortex (PCC) in aMCI and vMCI (Jing et al., 2012; Ding et al., 2015; Ni et al., 2016; Yang et al., 2018), we hypothesized that aMCI and vMCI also follow this pattern and are expected to find changes in ALFF/fALFF in some other brain regions, which may serve as a reliable neuroimaging biomarker for the two subtypes of MCI.

METHODS

Literature Search and Selection Criteria

This study followed the list of the Preferred Reporting Items for Systematic Reviews and Meta-analyses (PRISMA) statement and the phase flowchart for meta-analysis (Liberati et al., 2009; Moher et al., 2009).

Search Strategy

Studies were comprehensively searched in the PubMed, Web of Science, and Ovid databases. Search keywords were as follows: ("vascular cognitive impairment" OR "vascular cognitive impairment-no dementia" OR "vascular mild cognitive impairment" OR "amnestic mild cognitive impairment" OR "mild cognitive impairment") AND ("amplitude of low-frequency fluctuations" OR "fractional amplitude of low-frequency fluctuations"). Considering that different articles may use different terms to describe vMCI, in order to ensure the comprehensiveness of the search, a supplementary search was made for vMCI. The search keywords are as follows: ("small vessel disease" OR "vascular cognitive impairment not dementia" OR "subcortical ischemic vascular disease" OR "moyamoya disease" OR "Leukoaraiosis" OR "leukodystrophy" OR "CADASIL" OR "vascular deficit" OR "vascular disorder" OR "cerebrovascular disorder" OR "cerebrovascular deficit" OR "vascular" OR "cerebrovascular") AND ("amplitude of low-frequency fluctuations" OR "fractional amplitude of low-frequency fluctuations"). All articles published up to and including March 2021 were examined; thus, a total of 515 articles were studied.

Inclusion and Exclusion Criteria

Criteria for inclusion were as follows: (1) The patients met the diagnostic criteria for aMCI or vMCI; (2) the patients were compared with HCs for ALFF/fALFF; (3) information on three-dimensional Talairach or Montreal Neurological Institute (MNI) coordinates was reported; (4) the study was based on rs-fMRI; and (5) the research was written in English and published in a peer-reviewed journal.

Criteria for exclusion were as follows: (1) The study was based on other diseases, such as schizophrenia and epilepsy; (2) the study was categorized as a case report or secondary literature (e.g., systematic review and meta-analysis).

Data Extraction and Quality Assessment

The research results were screened independently by two authors (Xulian Zhang and Chen Xue) according to the inclusion and exclusion criteria. In case of disagreement, the reviewers (Xuan Cao and Qinlging Huang) evaluated and made the final decision. Firstly, we conducted a preliminary screening of the titles and abstracts of the studies to evaluate whether they conformed to the research content being explored. Secondly, for articles that conformed to the research content or with content that could not be determined according to the title and abstract, the full text was reviewed for a more extensive assessment. Thirdly, the articles obtained after preliminary screening were examined again to assess whether they met the inclusion criteria. Finally, we cross-checked the references of all the retrieval results to find the missing studies.

Data Analysis Procedures

The results of that compared aMCI with HCs and vMCI with HCs were divided into three groups according to decreased or increased ALFF/fALFF values: aMCI increased ALFF/fALFF ($n = 377$; 43 foci); aMCI decreased ALFF/fALFF ($n = 351$; 61 foci); and vMCI decreased ALFF/fALFF ($n = 136$; 20 foci).

JAVA GingerALE Version 2.3.6 (http://www.brainmap.org/ale) was used for meta-analysis free of charge and for calculating the ALFF changes in amnestic and vMCI compared to HCs based on the method of ALE. First, the foci data recorded in the text file were imported into the reading software (Eickhoff et al., 2012), and coordinates in the Talairach space were converted into the MNI 152 standard space using the GingerALE converter foci tool. Then, the threshold for using the error discovery rate in the ALE map was set to $p < 0.05$ (Eickhoff et al., 2012). Finally, the ALE map was overlaid into the MNI 152 template and viewed using the DPABI software (http://rfmri.org/DPABI).

RESULTS

Search Results

After the preliminary screening of the retrieval results, 62 studies were obtained, of which 21 were excluded because they focused on other diseases or meta-analysis, 14 were excluded because they did not have an HC group or group comparison coordinates, and 5 were excluded because they were not published in English. Finally, 22 studies were included in the present meta-analysis (**Figure 1**; **Table 1**).

Meta-Analysis Results

Abnormal ALFF/fALFF in aMCI

Compared with HCs, patients with aMCI showed increased ALFF/fALFF in the bilateral PHG/Hip, right amygdala (AMYG), right cerebellum anterior lobe (CAL), left middle temporal gyrus (MTG), left cerebrum temporal lobe sub-gyral, left inferior temporal gyrus (ITG), and left cerebrum limbic lobe uncus (**Table 2**; **Figure 2A**). Patients with aMCI also showed decreased ALFF/fALFF in the bilateral PCUN, bilateral cuneus (CUN), and bilateral PCC (**Table 2**; **Figure 2B**).

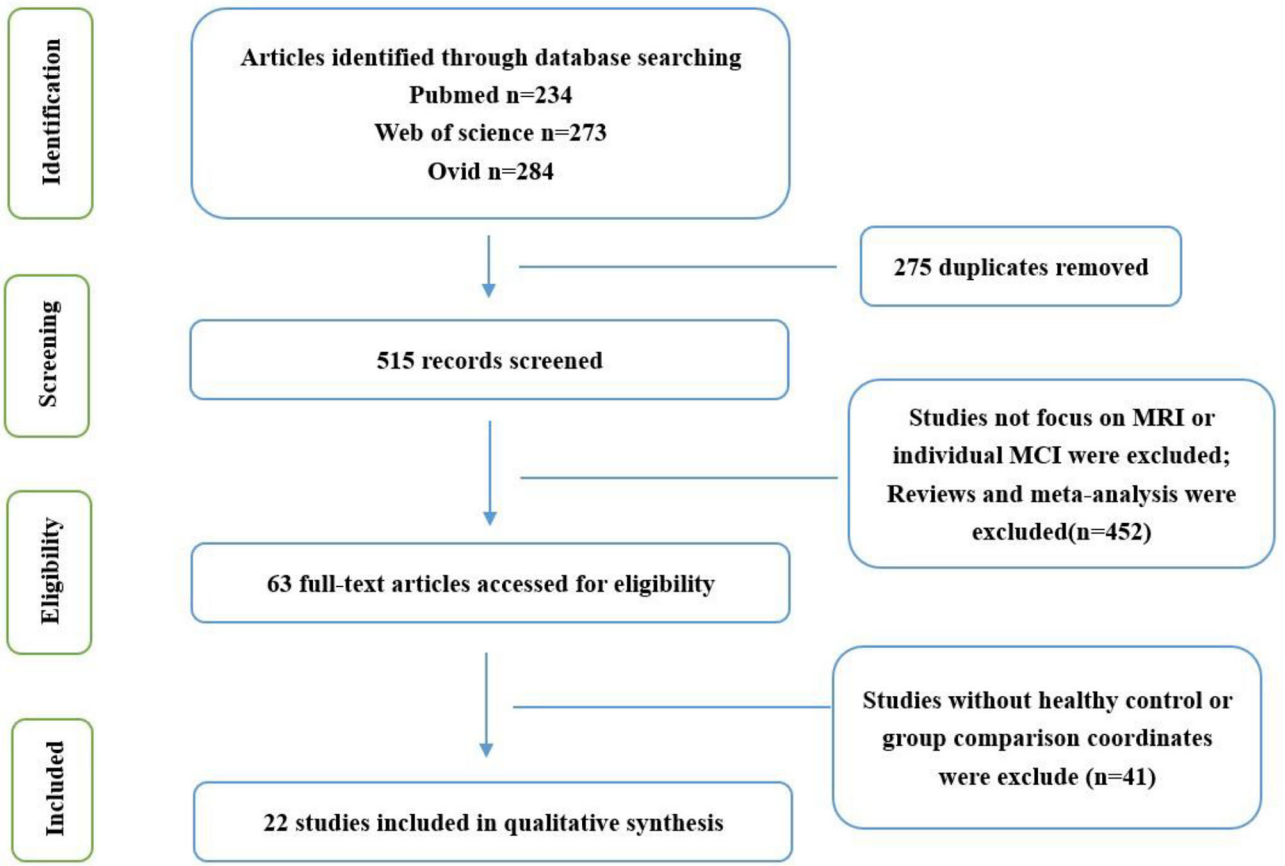

FIGURE 1 | Flowchart to identify the studies that are eligible for systematic review.

Abnormal ALFF/fALFF in vMCI

Compared with HC, patients with vMCI showed decreased ALFF/fALFF in the bilateral CUN, left PCUN, left PCC, and right cingulate gyrus (CG) (**Table 2**; **Figure 3**).

DISCUSSION

This study is the first meta-analysis to investigate the changes of ALFF/fFALFF in aMCI and vMCI and further explore whether these changes contribute to the diagnosis and differentiation of the two diseases. Compared with HCs, we found that the ALFF/fALFF values of both aMCI and vMCI were altered, which was consistent with the findings of the previous studies (Xi et al., 2013; Yin et al., 2014). In patients with aMCI, ALFF/fALFF increased mainly in the bilateral PHG/Hip, right AMYG, right CAL, left MTG, left cerebrum temporal lobe sub-gyral, left ITG, and left cerebrum limbic lobe uncus, while these values decreased mainly in the bilateral PCUN, bilateral CUN, and bilateral cingulate cortex. However, we only found that the ALFF/fALFF decreased in the left side of the bilateral CUN, the left PCC of the PCUN, and the right CG in patients with vMCI, but no brain regions with increased ALFF/fALFF values were found.

In this study, we found that, in aMCI compared to HCs, the brain regions with increased ALFF/fALFF were mainly concentrated in the limbic lobe, MTG, ITG, and anterior cerebellar lobe, while the brain regions with decreased ALFF/fALFF were mainly concentrated in the parietal lobe, occipital lobe, and limbic lobe. A quantitative meta-analysis found that patients with aMCI showed increased ALFF/fALFF in the right CAL, right PCUN, right IPL, and left ITG, while decreased ALFF/fALFF was found in the right PCUN and PCC. These results are mostly consistent with our findings (Xu et al., 2020). Meanwhile, increased ALFF/fALFF also occurred in the right AMYG and right CAL within our meta-data. A voxel-based morphometry meta-analysis found that the aMCI group showed significant GM atrophy in the left AMYG and right Hip, and these findings were highly consistent with the Alzheimer's Disease Neuroimaging Initiative (ADNI) dataset. These abnormalities further confirmed that GM atrophy is accompanied by local ALFF/fALFF abnormalities in patients with aMCI (Zhang J. et al., 2021). However, different results have been reported previously. Studies have revealed that aMCI groups showed increased ALFF in the calcarine, right cuneus, and bilateral PC/PCUN, and decreased ALFFs in the left inferior frontal gyrus, superior temporal gyrus, and insula

TABLE 1 | Demographic characteristics of the included studies.

Study	Imaging modality	N	Age (SD)	Gender (male/female)	MMSE (SD)	Group contrasts	Foci
ALFF/fALFF IN THE aMCI PATIENTS							
ALFF							
Xi et al. (2013)	rs-fMRI	aMCI 18	67.39 (7.67)	8/10	25.16 (3.43)	MCI > HC	2
		HC 20	65.42 (5.75)	9/11	28.14 (1.84)	MCI < HC	3
Cai et al. (2017)	rs-fMRI	aMCI 39	72.4 (5.01)	19/20	25.52 (2.88)	MCI > HC	5
		HC 38	73.92 (3.90)	19/19	29.28 (0.88)	MCI < HC	7
Yin et al. (2014)	rs-fMRI	aMCI 11	66.6 (8.7)	2/9	24.6 (3.2)	MCI > HC	2
		HC 22	62.1 (8.1)	12/10	29.2 (1.1)	MCI < HC	4
Li et al. (2014)	rs-fMRI	aMCI 17	67.0 (7.9)	9/8	25.6 (1.27)	MCI > HC	5
		HC 22	62.6 (5.8)	11/11	28.5 (1.1)	MCI < HC	2
Ni et al. (2016)	rs-fMRI	aMCI 26	71 (9)	12/14	25 (1.48)	MCI > HC	2
		HC 28	70 (9)	17/11	29 (1.09)	MCI < HC	5
Wang et al. (2011)	rs-fMRI	aMCI 16	69.38 (7.00)	7/9	26.50 (1.03)	MCI > HC	0
		HC 22	66.55 (7.67)	7/15	28.59 (0.59)	MCI < HC	2
Zhuang et al. (2020)	rs-fMRI	aMCI 43	64.5 (5.64)	18/25	26.77 (1.66)	MCI > HC	2
		HC 29	66.79 (3.68)	7/22	28.71 (0.91)	MCI < HC	0
Liang et al. (2014)	rs-fMRI	aMCI 53	73.2 (7.3)	22/31	27.1 (2.3)	MCI > HC	1
		HC 35	74.3 (5.9)	17/18	28.9 (1.6)	MCI < HC	8
fALFF							
Yang et al. (2020)	rs-fMRI	aMCI 52	68.06 (9.32)	26/26	24.52 (4.27)	MCI > HC	2
		HC 55	63.41 (7.97)	22/23	28.07 (2.14)	MCI < HC	7
Liu et al. (2020)	rs-fMRI	aMCI 20	68.8 (11.2)	12/8	27.4 (1.66)	MCI > HC	4
		HC 22	72.7 (8.05)	9/13	28.3 (1.42)	MCI < HC	4
Zhou et al. (2020)	rs-fMRI	aMCI 24	69.8 (6.2)	10/14	23.9 (3.6)	MCI > HC	4
		HC 32	67.9 (6.4)	14/18	28.0 (1.9)	MCI < HC	0
Zhao et al. (2015)	rs-fMRI	aMCI 34	68.0 (7.6)	14/20	25.5 (1.6)	MCI > HC	0
		HC 34	66.9 (6.7)	18/16	29.2 (0.9)	MCI < HC	2
Jing et al. (2012)	rs-fMRI	aMCI 10	78.42 (9.65)	5/5	–	MCI > HC	2
		HC 8	75.35 (6.45)	3/5	–	MCI < HC	0
Li et al. (2017)	rs-fMRI	aMCI 27	67.44 (8.49)	13/14	23.52 (3.31)	MCI > HC	0
		HC 32	64.88 (7.54)	16/16	27.69 (1.67)	MCI < HC	9
Yang et al. (2018)	rs-fMRI	aMCI 55	67.51 (9.62)	27/28	24.66 (4.20)	MCI > HC	4
		HC 57	63.77 (8.09)	22/35	28.14 (2.13)	MCI < HC	8
ALFF IN THE vMCI PATIENTS							
Ni et al. (2016)	rs-fMRI	vMCI 22	79 (6)	16/6	25 (1.48)	MCI > HC	2
		HC 28	70 (9)	17/11	29 (1.09)	MCI < HC	2
Ding et al. (2015)	rs-fMRI	vMCI 11	63.09 (4.99)	6/5	–	MCI > HC	4
		HC 12	63.64 (5.35)	6/6	–	MCI < HC	4
Li et al. (2015)	rs-fMRI	vMCI 28	67.9 (6.1)	16/12	27.89 (1.57)	MCI > HC	3
		HC 30	66.6 (4.6)	14/16	28.10 (1.73)	MCI < HC	2
Wang J. et al. (2019)	rs-fMRI	vMCI 28	59.28 (6.12)	14/14	24.96 (1.48)	MCI > HC	1
		HC 28	58.35 (6.82)	13/15	29.46 (1.07)	MCI < HC	1
Su et al. (2019)	rs-fMRI	vMCI 22	49.0 (14.2)	13/9	23.3 (6.3)	MCI > HC	3
		HC 44	48.5 (13.7)	26/18	28.6 (1.1)	MCI < HC	1
Lei et al. (2014)	rs-fMRI	vMCI 11	40.2 (11.2)	4/7	19.6 (4.3)	MCI > HC	15
		HC 22	40.2 (7.2)	10/12	29.0 (1.2)	MCI < HC	3
Ding et al. (2018)	rs-fMRI	vMCI 14	67.9 (8.7)	8/6	26.87 (0.32)	MCI > HC	2
		HC 15	65.8 (7.9)	7/8	28.51 (0.28)	MCI < HC	7

TABLE 2 | All clusters from the activation likelihood estimation (ALE) analysis.

Cluster	Volume (mm^3)	MNI			Anatomical regions	Maximum ALE value	Side	BA
		X	Y	Z				
ALFF/fALFF IN THE aMCI PATIENTS								
MCI > HC								
1	12120	36	−36	−16	Parahippocampal Gyrus	0.009105647	Right	36
1	12120	30	−6	−26	Amygdala	0.008697757	Right	–
1	12120	34	−12	−22	Parahippocampal Gyrus/Hippocampus	0.008655652	Right	–
1	12120	42	−24	−24	Parahippocampal Gyrus	0.008040754	Right	36
1	12120	38	−20	−24	Parahippocampal Gyrus/Hippocampus	0.007865525	Right	–
1	12120	36	−50	−18	Cerebellum Anterior Lobe	0.007794415	Right	–
2	11160	−36	−10	−22	Parahippocampal Gyrus/Hippocampus	0.009343305	Left	–
2	11160	−60	0	−24	Middle Temporal Gyrus	0.009123246	Left	21
2	11160	−50	−18	−16	Sub-Gyral	0.008646758	Left	21
2	11160	−62	−18	−24	Inferior Temporal Gyrus	0.008411912	Left	20
2	11160	−38	−14	−32	Uncus	0.007911957	Left	20
MCI < HC								
1	23032	−10	−60	10	Cuneus	0.014755126	Left	30
1	23032	12	−66	28	Precuneus	0.011124825	Right	31
1	23032	−10	−74	48	Precuneus	0.010285008	Left	7
1	23032	18	−68	42	Precuneus	0.010156754	Right	7
1	23032	10	−72	22	Cuneus	0.00971911	Right	18
1	23032	18	−54	24	Posterior Cingulate	0.009503377	Right	31
1	23032	−14	−72	42	Precuneus	0.009484317	Left	7
1	23032	4	−58	24	Posterior Cingulate	0.009442661	Right	23
1	23032	−4	−52	14	Posterior Cingulate	0.009429278	Left	29
1	23032	10	−66	42	Precuneus	0.008669218	Right	7
1	23032	−6	−60	44	Precuneus	0.006714426	Left	7
1	23032	14	−52	44	Precuneus	0.00636507	Right	7
ALFF/fALFF IN THE vMCI PATIENTS								
MCI < HC								
1	17944	6	−81	30	Cuneus	0.008325707	Right	18
1	17944	−8	−80	42	Cuneus	0.008055744	Left	19
1	17944	0	−66	54	Precuneus	0.006901417	Left	7
1	17944	−2	−52	66	Precuneus	0.006225559	Left	7
2	16000	−4	−46	24	Posterior Cingulate	0.01040697	Left	30
2	16000	−4	−54	20	Posterior Cingulate	0.007187156	Left	30
2	16000	8	−50	32	Cingulate Gyrus	0.006430536	Right	31

(Liu et al., 2014; Zhuang et al., 2019). This may be due to the frequency bands chosen (Slow-4 and Slow-5). An rs-fMRI study showed abnormal ALFF/fALFF in the Slow-5 band of PCC/PCU and PHG, and that several occipital regions were greater than the Slow-4 band in patients with aMCI compared with age- and sex-matched HCs. These abnormalities reflect the functional differences between groups that rely on these frequency bands (Han et al., 2011). In addition, some studies have found that the PICALM rs541458 and TOMM40 gene polymorphisms can regulate ALFF in elderly patients with aMCI (Liu et al., 2014; Zhuang et al., 2019). From the above, we can see that changes in ALFF/fALFF are the result of the combined action of many factors. Although our results are broadly consistent with those of most previous studies (Xi et al., 2013; Yin et al., 2014), there are still some differences, which may be related to the influence of multiple factors on ALFF/fALFF changes.

The limbic lobe mainly includes the hip, parahippocampal gyrus, CG, and AMYG and is mainly involved in emotion and motivation functions (Heimer and Van Hoesen, 2006). Studies have shown that the hip and its parahippocampal gyrus play an important role in memory function, which is mainly related to information storage and episodic memory retrieval (Xi et al., 2013). Heimer et al. found that the hip and CG played a role in regulating emotional state and the AMYG was mainly involved in the recognition of emotional meaning and the generation of emotional state (Heimer and Van Hoesen, 2006). A meta-analysis by Davey et al. found that the MTG is an important junction between the default mode network

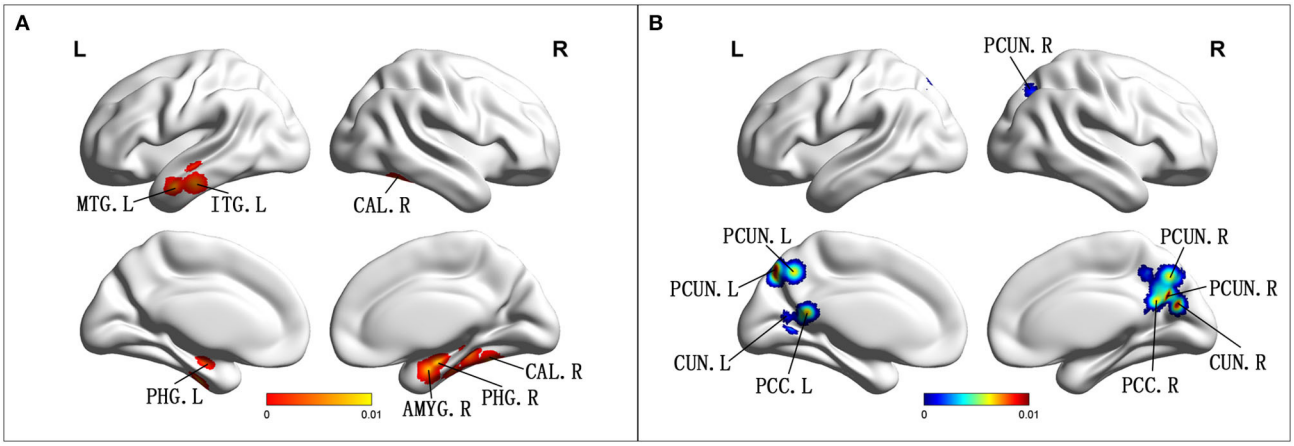

FIGURE 2 | (A) Brain regions showing increased ALFF/fALFF in patients with aMCI compared with HCs. **(B)** Brain regions showing decreased ALFF/fALFF in patients with aMCI compared with HCs. aMCI, amnestic mild cognitive impairment; HCs, healthy controls; ALFF/fALFF, the amplitude of low-frequency fluctuation/fractional amplitude of low-frequency fluctuation; MTG, middle temporal gyrus; ITG, inferior temporal gyrus; CAL, cerebellum anterior lobe; PHG, parahippocampal gyrus; AMYG amygdala; PCUN, precuneus; CUN, cuneus; PCC, posterior cingulate; R, right; L, left.

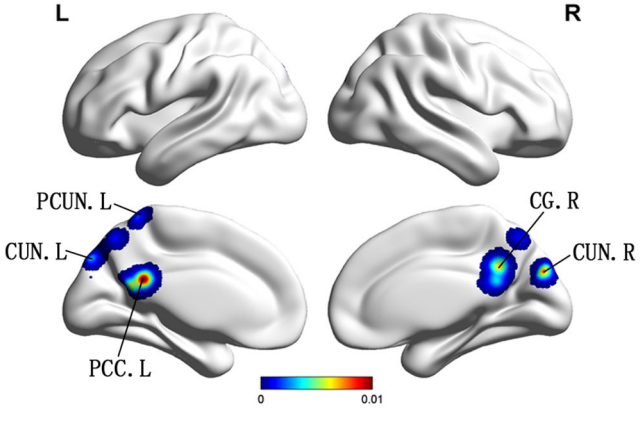

FIGURE 3 | Brain regions showing decreased ALFF in patients with vMCI compared with HCs. PCUN, precuneus; CUN, cuneus; PCC, posterior cingulate; CG, cingulate gyrus R, right; L, left.

(DMN) and the multi-need network and is mainly involved in semantic control, while the ITG is mainly involved in higher cognitive functions such as language and vision (Davey et al., 2016; Lin et al., 2020). The anterior cerebellum is known to be involved in sensorimotor activity, but studies have also suggested that it plays an important role in cognition and emotion (Schmahmann, 2019). In addition, previous studies have found that the PCUN/CUN is structurally and functionally connected to the DMN, which may play a central role in the neural network related to consciousness (Cavanna, 2007; Cunningham et al., 2017; Su et al., 2019). Although the conclusions of studies on ALFF have exhibited some inconsistency, a meta-analysis of rs-fMRI studies using the seed-based mapping software package revealed widespread aberrant regional spontaneous brain activity in aMCI and a regression analysis found that the severity of cognitive impairment in aMCI was negatively correlated with increased ALFFs in the CUN/PCUN cortices. These results were consistent with our meta-analysis results (Pan et al., 2017). We also found a meta-analysis based on brain 18F-fluorodeoxyglucose positron emission tomography (FDG-PET), which found that the left PCC/PCUN was the most robust and reliable metabolic altered brain region for metabolic alterations in aMCI converted to AD. The hypometabolism in the left PCC/PCNU and altered fMRI may serve as a potential biomarker for AD and other forms of cognitive impairment (Ma et al., 2018; Zhang Q. et al., 2021). These findings support our meta-analysis results that found that these aberrant regions may be regarded as early neuroimaging biomarkers for aMCI (Lau et al., 2016).

Our study found that, compared with HCs, vMCI showed no significant difference in ALFF/fALFF increased brain regions, while the decreased brain regions were the bilateral CUN, left PCUN, left PCC, and right CG. These brain areas are essentially the same as those that were decreased in patients with aMCI. Previous researchers have also found consistent results based on rs-fMRI in vMCI. A study on leukoaraiosis (LA) divided LA patients into two groups of LA-vMCI and LA with vascular dementia (LA-VaD). The ANOVA statistical analysis showed the predominant and widespread differences of ALFF in the PCC/PCUN and the right ITG for LA patients compared with the HCs. In particular, ALFF was found to be significantly decreased in the PCC/PCUN and increased in the temporal regions for LA-VaD patients, while the LA-vMCI group showed significantly increased ALFFs in the ITG compared to the HCs and the LA-VaD group. Furthermore, the results revealed that decreased executive functions were correlated with altered ALFF in the left PCUN (Wang J. et al., 2019). In addition, studies have shown that CG is related to cognitive processes and behaviors, which may be the reason why vMCI is mainly shown as decreased processing speed and executive ability (Vasquez and Zakzanis, 2015; Apps et al., 2016). In view of our meta-analysis results between aMCI

and vMCI groups, we found that decreased ALFF/fALFF in the PCC/PCUN and CG both occurred in the two groups. Our results are consistent with the aforementioned meta-analysis, which may indicate that there may be some similarity in cognitive impairment caused by different brain etiologies.

However, decreased ALFF/fALFF in the PCUN/CUN and CG may present a decompensated stage of cognitive impairment in aMCI and vMCI, and this may contribute to the understanding of the pathophysiology and interconnectivity of disparate cognitive processes. Patients with aMCI not only displayed decreased ALFF/fALFFs in several different brain regions but also demonstrated increased ALFF/fALFFs in other brain regions. Meanwhile, we could not achieve satisfactory results regarding the increased ALFF/fALFF in vMCI even after we increased the statistical threshold. Through careful observation, we found that all the included studies on vMCI had brain regions with increased ALFF/fALFF, but there were different opinions on the specific brain regions with increased ALFF/fALFF. We speculated that the inclusion criteria of vMCI and the frequency bands selected in the studies might be related. This may explain the absence of elevated brain regions found in patients with vMCI. Although ALFF/fALFF abnormalities may depend on different frequency bands, these increased ALFF/fALFF in patients with aMCI may still indicate a compensatory mechanism in the early stage of cognitive impairment.

LIMITATIONS

The limitations of this meta-analysis mainly include the following points. Firstly, different studies in the included literature used different criteria to distinguish vMCI from HCs; thus, there is no strict unified standard yet. This may be because the concept of vMCI was only proposed in recent years, and previous studies had inconsistent statements on the disease. Secondly, our meta-analysis was based on a whole-brain analysis, without specific analysis of the various networks in the brain. Finally, although some brain regions of aMCI and vMCI were found to be different from those of HCs, we did not have enough evidence to indicate which brain regions that ALFF/fALFF changes are the early neuroimaging biomarkers of aMCI and vMCI. But finding them is going to be an important part of our future work.

CONCLUSIONS

This study showed that aMCI and vMCI had different ALFF/fALFF changes compared with HCs. Taken together, our findings provide novel insights into the pathophysiological mechanisms of aMCI and vMCI and may be helpful to distinguish aMCI from vMCI for early clinical interventions.

DATA AVAILABILITY STATEMENT

The raw data supporting the conclusions of this article will be made available by the authors, without undue reservation.

AUTHOR CONTRIBUTIONS

XZ, CX, and QH: designed the study. XZ, CX, QH, XC, QY, WQ, WX, and SZ: collected the data. XZ and CX: analyzed the data and prepared the manuscript.

REFERENCES

Anderson, N. D. (2019). State of the science on mild cognitive impairment (MCI). *CNS Spectr*. 24, 78–87. doi: 10.1017/S1092852918001347

Apps, M. A., Rushworth, M. F., and Chang, S. W. (2016). The Anterior cingulate gyrus and social cognition: tracking the motivation of others. *Neuron* 90, 692–707. doi: 10.1016/j.neuron.2016.04.018

Cai, S., Chong, T., Peng, Y., Shen, W., Li, J., von Deneen, K. M., et al. (2017). Altered functional brain networks in amnestic mild cognitive impairment: a resting-state fMRI study. *Brain Imaging Behav*. 11, 619–631. doi: 10.1007/s11682-016-9539-0

Cavanna, A. E. (2007). The precuneus and consciousness. *CNS Spectr*. 12, 545–552. doi: 10.1017/S1092852900021295

Chen, Y. C., Xia, W., Luo, B., Muthaiah, V. P., Xiong, Z., Zhang, J., et al. (2015). Frequency-specific alternations in the amplitude of low-frequency fluctuations in chronic tinnitus. *Front. Neural. Circui.* 9:67. doi: 10.3389/fncir.2015.00067

Consoli, A., Pasi, M., and Pantoni, L. (2012). Vascular mild cognitive impairment: concept, definition, and directions for future studies. *Aging Clin. Exp. Res.* 24, 113–116. doi: 10.1007/BF03325158

Cunningham, S. I., Tomasi, D., and Volkow, N. D. (2017). Structural and functional connectivity of the precuneus and thalamus to the default mode network. *Hum. Brain. Mapp.* 38, 938–956. doi: 10.1002/hbm.23429

Davey, J., Thompson, H. E., Hallam, G., Karapanagiotidis, T., Murphy, C., De Caso, I., et al. (2016). Exploring the role of the posterior middle temporal gyrus in semantic cognition: integration of anterior temporal lobe with executive processes. *Neuroimage* 137: 165–177. doi: 10.1016/j.neuroimage.2016.05.051

Ding, H., Xu, Y., Li, X., Li, D., Li, G., and Han, Y. (2018). Aberrant default mode network in patients with vascular cognitive impairment, no dementia. *Int. J. Clin. Exp. Med.* 11, 1984–1993.

Ding, X., Wu, J., Zhou, Z., and Zheng, J. (2015). Specific locations within the white matter and cortex are involved in the cognitive impairments associated with periventricular white matter lesions (PWMLs). *Behav. Brain. Res.* 289, 9–18. doi: 10.1016/j.bbr.2015.04.021

Eickhoff, S. B., Bzdok, D., Laird, A. R., Kurth, F., and Fox, P. T. (2012). Activation likelihood estimation meta-analysis revisited. *Neuroimage* 59, 2349–2361. doi: 10.1016/j.neuroimage.2011.09.017

Han, Y., Wang, J., Zhao, Z., Min, B., Lu, J., Li, K., et al. (2011). Frequency-dependent changes in the amplitude of low-frequency fluctuations in amnestic mild cognitive impairment: a resting-state fMRI study. *Neuroimage* 55, 287–295. doi: 10.1016/j.neuroimage.2010.11.059

Heimer, L., and Van Hoesen, G. W. (2006). The limbic lobe and its output channels: implications for emotional functions and adaptive behavior. *Neurosci. Biobehav. Rev.* 30, 126–147. doi: 10.1016/j.neubiorev.2005.06.006

Jing, L. L., Li-Yu, H., Deng-Feng, H., Jie, N., and Zheng, Z. (2012). Amplitude of low frequency fluctuation at different frequency bands in early amnestic mild cognitive impairment: results from adnI. *J. Innov. Optic. Health Sci.* 5:39. doi: 10.1142/S1793545811500039

Lau, W. K., Leung, M. K., Lee, T. M., and Law, A. C. (2016). Resting-state abnormalities in amnestic mild cognitive impairment: a meta-analysis. *Transl. Psychiatry* 6:e790. doi: 10.1038/tp.2016.55

Lei, Y., Li, Y., Ni, W., Jiang, H., Yang, Z., Guo, Q., et al. (2014). Spontaneous brain activity in adult patients with moyamoya disease: a

resting-state fMRI study. *Brain Res*. 1546, 27–33. doi: 10.1016/j.brainres.2013.12.022

Li, C., Yang, J., Yin, X., Liu, C., Zhang, L., Zhang, X., et al. (2015). Abnormal intrinsic brain activity patterns in leukoaraiosis with and without cognitive impairment. *Behav. Brain Res*. 292, 409–413. doi: 10.1016/j.bbr.2015.06.033

Li, Q., Zhao, L. Q., and Hu, F. Y. (2017). Characteristics of cognitive impairment and the resting state functional MRI in patients with leukoaraiosis. *Zhonghua Yi Xue Za Zhi* 97, 3529–3533. doi: 10.3760/cma.j.issn.0376-2491.2017.45.003

Li, X., Cao, M., Zhang, J., Chen, K., Chen, Y., Ma, C., et al. (2014). Structural and functional brain changes in the default mode network in subtypes of amnestic mild cognitive impairment. *J Geriatr Psychiatry Neurol*. 27, 188–198. doi: 10.1177/0891988714524629

Liang, P., Xiang, J., Liang, H., Qi, Z., Li, K., and Alzheimer's Disease NeuroImaging, I. (2014). Altered amplitude of low-frequency fluctuations in early and late mild cognitive impairment and Alzheimer's disease. *Curr. Alzheimer Res.* 11, 389–398. doi: 10.2174/1567205011666140331225335

Liberati, A., Altman, D. G., Tetzlaff, J., Mulrow, C., Gøtzsche, P. C., Ioannidis, J. P., et al. (2009). The PRISMA statement for reporting systematic reviews and meta-analyses of studies that evaluate health care interventions: explanation and elaboration. *PLoS Med*. 6:*E*1000100. doi: 10.1371/journal.pmed.1000100

Lin, Y. H., Young, I. M., Conner, A. K., Glenn, C. A., Chakraborty, A. R., Nix, C. E., et al. (2020). Anatomy and White Matter Connections of the Inferior Temporal Gyrus. *World Neurosurg* 143, *E*656–e66. doi: 10.1016/j.wneu.2020.08.058

Liu, P., Jia, X.-Z., Chen, Y., Yu, Y., Zhang, K., Lin, Y.-J., et al. (2020). Gut microbiota interacts with intrinsic brain activity of patients with amnestic mild cognitive impairment. *CNS Neurosci Ther*. 27, 163–173. doi: 10.1111/cns.13451

Liu, X., Bai, F., Yue, C., Shi, Y., Yu, H., Luo, B., et al. (2014). The association between TOMM40 gene polymorphism and spontaneous brain activity in amnestic mild cognitive impairment. *J. Neurol.* 261, 1499–1507. doi: 10.1007/s00415-014-7368-x

Liu, Z. Z., Qu, H. J., Tian, Z. L., Han, M. J., Fan, Y., Ge, L. Z., et al. (2017). Reproducibility of frequency-dependent low frequency fluctuations in reaction time over time and across tasks. *PLoS ONE* 12:e0184476. doi: 10.1371/journal.pone.0184476

Long, Z., Jing, B., Yan, H., Dong, J., Liu, H., Mo, X., et al. (2016). A support vector machine-based method to identify mild cognitive impairment with multi-level characteristics of magnetic resonance imaging. *Neuroscience* 331, 169–176. doi: 10.1016/j.neuroscience.2016.06.025

Luo, F. F., Wang, J. B., Yuan, L. X., Zhou, Z. W., Xu, H., Ma, S. H., et al. (2020). Higher sensitivity and reproducibility of wavelet-based amplitude of resting-state fMRI. *Front. Neurosci.* 14:224. doi: 10.3389/fnins.2020.00224

Ma, H. R., Sheng, L. Q., Pan, P. L., Wang, G. D., Luo, R., Shi, H. C., et al. (2018). Cerebral glucose metabolic prediction from amnestic mild cognitive impairment to Alzheimer's dementia: a meta-analysis. *Transl. Neurodegener.* 7:9. doi: 10.1186/s40035-018-0114-z

Moher, D., Liberati, A., Tetzlaff, J., and Altman, D. G. (2009). Preferred reporting items for systematic reviews and meta-analyses: the PRISMA statement. *PLoS Med*. 6:e1000097. doi: 10.1371/journal.pmed.1000097

Ni, L., Liu, R., Yin, Z., Zhao, H., Nedelska, Z., Hort, J., et al. (2016). Aberrant spontaneous brain activity in patients with mild cognitive impairment and concomitant lacunar infarction: a resting-state functional mri study. *J. Alzheimers Dis.* 50, 1243–1254. doi: 10.3233/JAD-150622

Pan, P., Zhu, L., Yu, T., Shi, H., Zhang, B., Qin, R., et al. (2017). Aberrant spontaneous low-frequency brain activity in amnestic mild cognitive impairment: A meta-analysis of resting-state fMRI studies. *Ageing Res. Rev.* 35, 12–21. doi: 10.1016/j.arr.2016.12.001

Petersen, R. C., Lopez, O., Armstrong, M. J., Getchius, T. S. D., Ganguli, M., Gloss, D., et al. (2018). Practice guideline update summary: mild cognitive impairment: report of the guideline development, dissemination, and implementation subcommittee of the american academy of neurology. *Neurology* 90, 126–135. doi: 10.1212/WNL.0000000000004826

Sanford, A. M. (2017). Mild Cognitive Impairment. *Clin. Geriatr. Med.* 33, 325–337. doi: 10.1016/j.cger.2017.02.005

Schmahmann, J. D. (2019). The cerebellum and cognition. *Neurosci. Lett.* 688, 62–75. doi: 10.1016/j.neulet.2018.07.005

Su, J., Wang, M., Ban, S., Wang, L., Cheng, X., Hua, F., et al. (2019). Relationship between changes in resting-state spontaneous brain activity and cognitive impairment in patients with CADASIL. *J. Headache Pain.* 20:36. doi: 10.1186/s10194-019-0982-3

Sudo, F. K., Alves, G. S., Tiel, C., Ericeira-Valente, L., Moreira, D. M., Laks, J., et al. (2015). Neuroimaging criteria and cognitive performance in vascular mild cognitive impairment: a systematic review. *Dement Neuropsychol.* 9, 394–404. doi: 10.1590/1980-57642015DN94000394

Sun, Q., Luo, L., Ren, H., Wei, C., Xing, M., Cheng, Y., et al. (2016). Semantic clustering and sleep in patients with amnestic mild cognitive impairment or with vascular cognitive impairment-no dementia. *Int. Psychogeriatr.* 28, 1493–1502. doi: 10.1017/S1041610216000739

Vasquez, B. P., and Zakzanis, K. K. (2015). The neuropsychological profile of vascular cognitive impairment not demented: a meta-analysis. *J. Neuropsychol.* 9, 109–136. doi: 10.1111/jnp.12039

Wang, J., Chen, H., Liang, H., Wang, W., Liang, Y., Liang, Y., et al. (2019). Low-frequency fluctuations amplitude signals exhibit abnormalities of intrinsic brain activities and reflect cognitive impairment in leukoaraiosis patients. *Med. Sci. Monit.* 25, 5219–5228. doi: 10.12659/MSM.915528

Wang, J. J., Chen, X., Sah, S. K., Zeng, C., Li, Y. M., Li, N., et al. (2016). Amplitude of low-frequency fluctuation (ALFF) and fractional ALFF in migraine patients: a resting-state functional MRI study. *Clin. Radiol.* 71, 558–564. doi: 10.1016/j.crad.2016.03.004

Wang, P., Yang, J., Yin, Z., Duan, J., Zhang, R., Sun, J., et al. (2019). Amplitude of low-frequency fluctuation (ALFF) may be associated with cognitive impairment in schizophrenia: a correlation study. *BMC Psychiatry* 19:30. doi: 10.1186/s12888-018-1992-4

Wang, Z., Yan, C., Zhao, C., Qi, Z., Zhou, W., Lu, J., et al. (2011). Spatial patterns of intrinsic brain activity in mild cognitive impairment and Alzheimer's disease: a resting-state functional MRI study. *Hum. Brain Mapp*. 32, 1720–1740. doi: 10.1002/hbm.21140

Wentzel, C., Rockwood, K., MacKnight, C., Hachinski, V., Hogan, D. B., Feldman, H., et al. (2001). Progression of impairment in patients with vascular cognitive impairment without dementia. *Neurology* 57, 714–716. doi: 10.1212/WNL.57.4.714

Xi, Q., Zhao, X. H., Wang, P. J., Guo, Q. H., and He, Y. (2013). Abnormal intrinsic brain activity in amnestic mild cognitive impairment revealed by amplitude of low-frequency fluctuation: a resting-state functional magnetic resonance imaging study. *Chin. Med. J. (Engl)* 126, 2912–2917.

Xu, W., Shanshan, C., Chen, X., Guanjie, H., Wenying, M., Wenzhang, Q., et al. (2020). Functional MRI-specific alterations in executive control network in mild cognitive impairment: an ALE meta-analysis. *Front. Aging Neurosci.* 12:578863. doi: 10.3389/fnagi.2020.578863

Yan, T., Wang, Y., Weng, Z., Du, W., Liu, T., Chen, D., et al. (2019). Early-stage identification and pathological development of alzheimer's disease using multimodal MRI. *J. Alzheimers Dis.* 68, 1013–1027. doi: 10.3233/JAD-181049

Yang, L., Yan, Y., Li, Y., Hu, X., Lu, J., Chan, P., et al. (2020). Frequency-dependent changes in fractional amplitude of low-frequency oscillations in Alzheimer's disease: a resting-state fMRI study. *Brain Imaging Behav.* 14, 2187–2201. doi: 10.1007/s11682-019-00169-6

Yang, L., Yan, Y., Wang, Y., Hu, X., Lu, J., Chan, P., et al. (2018). Gradual disturbances of the amplitude of low-frequency fluctuations (ALFF) and fractional ALFF in Alzheimer Spectrum. *Front. Neurosci.* 12:975. doi: 10.3389/fnins.2018.00975

Yin, C., Liye, Y., Longfei, J., Jinhui, W., Pengfei, L., Yanqin, G., et al. (2014). Early morphological brain abnormalities in patients with amnestic mild cognitive impairment. *Transl. Neurosci.* 5, 253–259. doi: 10.2478/s13380-014-0234-6

Zang, Y. F., He, Y., Zhu, C. Z., Cao, Q. J., Sui, M. Q., Liang, M., et al. (2007). Altered baseline brain activity in children with ADHD revealed by resting-state functional MRI. *Brain Dev.* 29, 83–91. doi: 10.1016/j.braindev.2006.07.002

Zhang, J., Liu, Y., Lan, K., Huang, X., He, Y., Yang, F., et al. (2021). Gray Matter Atrophy in Amnestic Mild Cognitive Impairment: A Voxel-Based Meta-Analysis. *Front Aging Neurosci* 13: 627919. doi: 10.3389/fnagi.2021.627919

Zhang, Q., Wang, Q., He, C., Fan, D., Zhu, Y., Zang, F., et al. (2021). Altered regional cerebral blood flow and brain function across the Alzheimer's disease spectrum: a potential biomarker. *Front. Aging Neurosci.* 13:630382. doi: 10.3389/fnagi.2021.630382

Zhao, N., Yuan, L. X., Jia, X. Z., Zhou, X. F., Deng, X. P., He, H. J., et al. (2018). Intra- and inter-scanner reliability of voxel-wise whole-brain analytic metrics for resting state fMRI. *Front. Neuroinform.* 12:54. doi: 10.3389/fninf.2018.00054

Zhao, Z.-L., Fan, F.-M., Lu, J., Li, H.-J., Jia, L.-F., Han, Y., et al. (2015). Changes of gray matter volume and amplitude of low-frequency oscillations in amnestic MCI: An integrative multi-modal MRI study. *Acta Radiol.* 56, 614–621. doi: 10.1177/0284185114533329

Zhou, Q.-H., Wang, K., Zhang, X.-M., Wang, L., and Liu, J.-H. (2020). Differential regional brain spontaneous activity in subgroups of mild cognitive impairment. *Front. Hum. Neurosci.* 14. doi: 10.3389/fnhum.2020.00002

Zhuang, L., Liu, X., Shi, Y., Liu, X., and Luo, B. (2019). Genetic Variants of PICALM rs541458 modulate brain spontaneous activity in older adults with amnestic mild cognitive impairment. *Front. Neurol.* 10:494. doi: 10.3389/fneur.2019.00494

Zhuang, L., Ni, H., Wang, J., Liu, X., Lin, Y., Su, Y., et al. (2020). Aggregation of vascular risk factors modulates the amplitude of low-frequency fluctuation in mild cognitive impairment patients. *Front Aging Neurosci.* 12:604246. doi: 10.3389/fnagi.2020.604246

Zou, Q. H., Zhu, C. Z., Yang, Y., Zuo, X. N., Long, X. Y., Cao, Q. J., et al. (2008). An improved approach to detection of amplitude of low-frequency fluctuation (ALFF) for resting-state fMRI: fractional ALFF. *J. Neurosci. Methods* 172, 137–141. doi: 10.1016/j.jneumeth.2008.04.012

Conflict of Interest: The authors declare that the research was conducted in the absence of any commercial or financial relationships that could be construed as a potential conflict of interest.

Publisher's Note: All claims expressed in this article are solely those of the authors and do not necessarily represent those of their affiliated organizations, or those of the publisher, the editors and the reviewers. Any product that may be evaluated in this article, or claim that may be made by its manufacturer, is not guaranteed or endorsed by the publisher.

frontiers in Aging Neuroscience

METHODS
published: 07 October 2021
doi: 10.3389/fnagi.2021.669490

Connectomics in Brain Aging and Dementia – The Background and Design of a Study of a Connectome Related to Human Disease

Ann D. Cohen[1], Ricardo Bruña[2], Yue-Fang Chang[3], Yu Cheng[4,5], Jack Doman[1], Ted Huppert[6], Tae Kim[7], Fernando Maestu[2], Rebecca E. Roush[8], Beth E. Snitz [8] and James T. Becker[1,8,9] On behalf of the Connectomics in Brain Aging and Dementia Research Team*

[1] Department of Psychiatry, The University of Pittsburgh, Pittsburgh, PA, United States, [2] Department of Experimental Psychology, Universidad Complutense de Madrid, Pozuelo de Alarcón, Madrid, Spain, [3] Department of Neurosurgery, The University of Pittsburgh, Pittsburgh, PA, United States, [4] Department of Statistics, The University of Pittsburgh, Pittsburgh, PA, United States, [5] Department of Biostatistics, The University of Pittsburgh, Pittsburgh, PA, United States, [6] Department of Electrical Engineering, The University of Pittsburgh, Pittsburgh, PA, United States, [7] Department of Radiology, The University of Pittsburgh, Pittsburgh, PA, United States, [8] Department of Neurology, The University of Pittsburgh, Pittsburgh, PA, United States, [9] Department of Psychology, The University of Pittsburgh, Pittsburgh, PA, United States

OPEN ACCESS

Edited by:
Yong Liu,
Beijing University of Posts and Telecommunications (BUPT), China

Reviewed by:
Kun Xiong,
Central South University, China
Miao Cao,
Fudan University, China

***Correspondence:**
Ann D. Cohen
cohenad@upmc.edu

Received: *18 February 2021*
Accepted: *06 September 2021*
Published: *07 October 2021*

Citation:
Cohen AD, Bruña R, Chang Y-F, Cheng Y, Doman J, Huppert T, Kim T, Maestu F, Roush RE, Snitz BE and Becker JT (2021) Connectomics in Brain Aging and Dementia – The Background and Design of a Study of a Connectome Related to Human Disease. Front. Aging Neurosci. 13:669490. doi: 10.3389/fnagi.2021.669490

The natural history of Alzheimer's Disease (AD) includes significant alterations in the human connectome, and this disconnection results in the dementia of AD. The organizing principle of our research project is the idea that the expression of cognitive dysfunction in the elderly is the result of two independent processes — the neuropathology associated with AD, and second the neuropathological changes of cerebrovascular disease. Synaptic loss, senile plaques, and neurofibrillary tangles are the functional and diagnostic hallmarks of AD, but it is the structural changes as a consequence of vascular disease that reduce brain reserve and compensation, resulting in an earlier expression of the clinical dementia syndrome. This work is being completed under the auspices of the Human Connectome Project (HCP). We have achieved an equal representation of Black individuals (vs. White individuals) and enrolled 60% Women. Each of the participants contributes demographic, behavioral and laboratory data. We acquire data relative to vascular risk, and the participants also undergo *in vivo* amyloid imaging, and magnetoencephalography (MEG). All of the data are publicly available under the HCP guidelines using the Connectome Coordinating Facility and the NIMH Data Archive. Locally, we use these data to address specific questions related to structure, function, AD, aging and vascular disease in multi-modality studies leveraging the differential advantages of magnetic resonance imaging (MRI), functional magnetic resonance imaging (fMRI), MEG, and *in vivo* beta amyloid imaging.

Keywords: aging, MRI, amyloid PET imaging, magnetoencepalography, Connectome Related to Human Disease, neuropsychology

INTRODUCTION

The natural history of Alzheimer's Disease (AD) includes significant alterations in the human connectome, and this disconnection results in the dementia of the Alzheimer's type (DAT). Data from structural and functional magnetic resonance imaging (MRI) (Dai and He, 2014; Prescott et al., 2014), as well as magnetoencephalopathy (MEG) (Lopez-Sanz et al., 2019) and electroencephalography (Maestu et al., 2019; Babiloni et al., 2020) all demonstrate significant changes in neural networks even prior to the onset of clinical dementia. While such changes are not explicit in the popular A/T/N (amyloid/tau/neurodegeneration) model of AD (Jack et al., 2016), they appear to be an early consequence of the accumulation of beta amyloid (Busche and Konnerth, 2016; Nakamura et al., 2017), and thus may be an early warning sign of impending neurodegeneration. Indeed, models of the natural history of AD that propose that the loss of synapses is one of the first pathological stages of AD (Selkoe, 2002), imply changes in the connectome.

In 2016 the University of Pittsburgh was awarded funds by the National Institute on Aging under the Connectomes Related to Human Disease[1] of the Human Connectome Project.[2] Our project is organized around the idea that the natural history of AD is affected by multiple independent factors (Ewers et al., 2011), and that the expression of cognitive dysfunction is the result of independent processes including AD and vascular-related neuropathology. Here we describe the general organization of the *Connectomics in Brain Aging and Dementia* project, the sampling frame, a brain imaging protocols, and the behavioral/cognitive data that were acquired as part of the study. All of the study data are currently being uploaded to the *Connectome Coordination Facility*[3] and the NIMH National Data Archive.[4]

To accomplish the study goals, we acquired neuropsychological data, as well as brain structural and functional (functional MRI, MEG) imaging, and positron emission tomography (PET) imaging of *in vivo* of brain amyloid with Pittsburgh Compound B (PET-PiB). We used different measures of brain function because fMRI and MEG rely on fundamentally different biological processes to generate "signal" (Tsvetanov et al., 2015), and this has the potential to provide critical information about the uncoupling of the neural and vascular components in AD (and possibly in normal aging) (Zlokovic, 2011). Because the MEG signal is derived from post-synaptic currents, and fMRI signal also includes a vascular response, they may expose different sources of the disconnection (i.e., degeneration vs. vascular). We also acquire a direct measure of cerebrovascular function – an MRI-based measure of cerebral blood flow, as well as a direct measure of AD pathology using *in vivo* amyloid imaging. These data provide the opportunity to examine the relationship between amyloid deposition and local and distant connectivity (Zhou et al., 2015) among individuals with and without cognitive impairment.

[1]https://grants.nih.gov/grants/guide/pa-files/par-14-281.html

[2]https://en.wikipedia.org/wiki/Human_Connectome_Project

[3]https://www.humanconnectome.org/

[4]https://nda.nih.gov/

METHODS

Study Design

This is a longitudinal, community-based study of brain structural and functional connectivity among cognitively normal and cognitively impaired individuals aged 50–89 years.

Recruitment Sources

There are currently two primary portals of entry into the study: the University of Pittsburgh Alzheimer's Disease Research Center[5] and the Pitt + Me web portal (primarily to recruit Black individuals and Whites without college education).[6] Additional individuals were identified through active links with the Heart SCORE Study (Bambs et al., 2011), the Long Life Family Study (Newman et al., 2011), and by word of mouth.

Study Protocol

All study participants are tested/scanned over three days. On Day One, all study enrollees complete the informed consent process and the intake forms. They are then escorted to the MR Research Center (MRRC) and where they complete the two fMRI tasks (motor, working memory), and the structural imaging. Following a break, the individuals complete the behavioral tests that are *not* components of the NIH Toolbox. On Day Two, the participants undergo a brief exam and fasting blood tests. They are then taken back to the MRRC where they undergo diffusion imaging, task free fMRI and the language/math task fMRI; they then complete all the NIH Toolbox tests. On Day Three the participants undergo MEG and PET-PiB scanning; this is scheduled approximately 1 week after the last MRI scanning session (to avoid any interference of the MRI on the MEG data). The participants are escorted to the Center for Advanced Brain Magnetic Source Imaging[7] where they are prepared for the MEG scan, and complete task training. Once in the magnetically shielded room, the individuals complete task free MEG, and one task MEG (working memory). Individuals will then take for a short break and for the placement of the electrodes for the motor stimulation; then they will complete the Language/Math and Motor MEG task scans. Following a break for either a snack or lunch, the participants are escorted to the UPMC PET Facility for their PiB scan.

Diagnostic Evaluation

Each participant undergoes a brief neuropsychological test battery for group classification purposes. The test battery is based on that of the ADRC and includes the Montreal Cognitive Assessment (MoCA) (Nasreddine et al., 2005), verbal fluency, a 30-item visual naming test (Saxton et al., 2000), Trailmaking (Reitan, 1958; Reitan and Wolfson, 1994), verbal free recall (Welsh et al., 1991, 1994), and the Rey-Osterreith Complex Figure (Rey, 1941). Classification decisions were made independently by JTB, and BES and any differences were resolved

[5]https://www.adrc.pitt.edu/

[6]https://pittplusme.org/studyarms/publicdetails?guid=abdb4de3-0e00-49e6-b0a0-a3ca2d6e7c2a

[7]http://www.neurology.upmc.edu/cabmsi/

in a group discussion. We use the ADRC classification scheme (Lopez et al., 2000) for AD, MCI (both amnestic and non-amnestic), and Subjective Cognitive Complaints (SCC).

Neuropsychological Tests and Questionnaires

The individual tests and questionnaires that serve as outcome variables include items from the *NIH Toolbox*,[8] the *Promis* battery,[9] and additional paper-and-pencil tests (see **Supplementary Tables 1–3**). The questionnaires cover symptomatology, personality, diet, and exercise.

Brain Imaging

Magnetic Resonance Imaging Scanning

We use Siemens Prisma 3-Tesla 64-channel systems equipped with Connectome level gradients operating at 80mT/m. They are equipped with fMRI presentation systems including E-Prime, a MR compatible video projector, and Celeritas response gloves.

The MRI scanning is completed in two 90-min sessions over two days. The scan sequences include: T1-weighted MP-RAGE, T2-weighted SPACE image, FLAIR, susceptibility weighted imaging, diffusion tensor imaging, task-free functional MRI, task-based fMRI, and arterial spin labeling (see **Supplementary Table 4**).

The tasks used were those described for the HCP and, with one exception, used the stimuli provided by the HCP; the exception was the N-back task. For that task all of the original photographs of faces were of White individuals; we substituted photos of Black individuals so that half of all of the N-back trials used White faces, and half Black faces. The same race was used for all of the stimuli within a trial (i.e., race could not be used to select responses).

All the MRI data are processed locally through the HCP pipeline, as modified to work in the local environment. The raw data are stored on an XNAT server[10] and pushed to a receiving server at Washington University in St. Louis for processing by the Connectome Coordination Facility and eventual upload to the on-line, public HCP database.

Magnetoencephalopathy Recording

Magnetoencephalography (MEG) studies are completed on an Elekta-Neuromag Vectorview 306 MEG system. The whole-scalp neuromagnetic measurement system uses 102 triple sensors – 102 magnetometers and 204 planar gradiometers – in a helmet-shaped array. The locations of three cardinal anatomical landmarks (nasion, and two preauricular points) and of four head localization coils are digitized prior to each MEG study using a 3D-digitizer (ISOTRAK; Polhemus, Inc., Colchester VT) to define the subject-specific Cartesian head coordinate system. 30–50 anatomical points are digitized on the head surface to provide for more accurate co-registration of the MEG data with the reconstructed volumetric MR image. Eye movements are measured and recorded simultaneously with the MEG. The MEG sensor unit, the floor-mounted gantry, the subject chair and bed, together with the patient audio-visual monitoring and stimulus delivery systems are contained in a magnetically shielded room.

Once a subject is comfortably positioned in the MEG machine, a short electrical signal is sent to the head coils enabling their localization with respect to the MEG sensor array. The MEG data are acquired at a sampling rate of 1 kHz, with on-line filtering of 0.10–330 Hz. The acquisition includes two memory tasks, as well as 10 min of "resting state" data – 5 min with eyes open followed by 5 min with eyes closed. At the end of the scan, we collect 2 min of "empty room" data to assess the validity of any signal in the test conditions.

Recordings were filtered offline using a tempo-spatial filtering algorithm (tSSS, correlation window 0.9, time window 10 s) (Taulu and Simola, 2006) to eliminate magnetic noise originating outside the head and to compensate for head movements.

The raw data are stored on an XNAT server and are pushed to the NDA for eventual inclusion in the study database (C3159).

Positron Emission Tomography Amyloid Imaging

The PET amyloid tracer, Pittsburgh Compound B (PiB) is synthesized by a simplified radiosynthetic method based on the captive solvent method (Wilson et al., 2000; Price et al., 2005). High specific activity ($>$ 0.50 Ci/μmol at time of injection) PiB (15 mCi) is injected over 20 s and the participant then relaxes quietly in a chair for $\sim$25 min, after which they are positioned in the scanner. A windowed transmission scan (10 min) is acquired for attenuation correction, followed by a 30 min PiB PET study (6×300 s frames).

The Siemens/CTI ECAT HR + scanner gantry is equipped with a Neuro-insert (CTI PET Systems) to reduce the contribution of scattered photon events (Weinhard, 1998). Positron emission tomography data are reconstructed using filtered back-projection (Fourier rebinning and 2D backprojection with Hann filter: kernel FWHM = 3 mm). Data are corrected for photon attenuation, scatter (Watson et al., 1997), and radioactive decay. The final reconstructed PET image resolution is $\sim$ 6 mm (transverse and axial) based on in-house point source measurements.

The raw data are stored on an XNAT server and are pushed to the NDA for inclusion in the study database (C3159). The data include the dynamic images as well as a single SUV image.

Imaging Data Processing (Local)

All the MRI data are pushed to the HCP CCF XNAT server where they are processed using standard quality control measures, and analysis via the HCP Pipeline. The processed data are made available by the CCF. The MEG and PET data are saved to the NIMH Data Archive as.FIF files (MEG) and DICOM images (PET SUV images). What follows below is the description of the local processing of these data.

Magnetic Resonance Imaging Structural Image Processing

We briefly describe here the HCP Minimal Processing Pipelines that are implemented at the CCF prior to the release of the data [See Glasser, et alia (Glasser et al., 2013) for details]. There are three main components to the structural data processing. In the first steps, the goal is to produce a "native" structural space for each subject, align the T1 and T2 images, perform a bias field correction, and co-register the structural volumes into MNI space. The second component which uses FreeSurfer extensively,

[8]http://www.healthmeasures.net/explore-measurement-systems/nih-toolbox

[9]http://www.healthmeasures.net/explore-measurement-systems/promis

[10]https://www.xnat.org/

segments these volumes into predefined subcortical and cortical regions. It also reconstructs cortical surfaces and performs the standard surface registration to the FreeSurfer atlas. Finally, in the third step all the NIFTI and GIFTI surface files are created that can then be used in the Connectome Workbench.

In addition, we also process all the MP-RAGE data through Computational Anatomy Toolbox (CAT12) for SPM.[11] This process provides the basis for a range of morphological analysis methods, including voxel-based morphometry, surface-based morphometry, deformation-based morphometry, and region- or label-based morphometry.

Positron Emission Tomography Processing

The PET data are processed using PMOD[12] and Freesurfer software packages. Correction for subject motion during the multi-frame PET scan is performed using frame-to-frame registration procedure. The PET data are averaged to generate images that correspond to the 50–70 min post-injection uptake. The anatomical T1-weighted MR image is reoriented along the anterior-posterior commissure and the averaged PET images are co-registered to the reoriented MR image. Freesurfer software is used for MR bias field correction, automated ROI parcellation and tissue segmentation. The Freesurfer ROI parcellations are converted into an ROI template and ROI sampling of the PET images is performed to include anterior cingulate, frontal cortex, parietal, precuneus, lateral temporal cortex, primary visual cortex, hippocampus, anterior ventral striatum, thalamus, pons, and cerebellum.

Regional standardized uptake value (SUV) measures are computed for PiB by normalizing tissue uptake to the injected radioligand dose and body mass. Each regional SUV is normalized to a reference ROI in the cerebellum to generate the SUV ratio (SUVR). Cortical SUVRs were measured in anterior cingulate cortex, the superior frontal cortex, orbital frontal cortex, lateral temporal cortex, parietal lobe, precuneus, and the anterior ventral striatum regions and averaged across hemispheres. The volume-weighted average of these seven SUVR values constituted the Global SUVR. The SUVR in each area is compared to a region-specific cut-off determined by sparse k-means clustering; those scores above the cut-off are considered "positive". If *any* of the regions was considered "PiB Positive," then the Global rating was set to positive (Cohen et al., 2013).

Magnetoencephalography Signal Processing

Ocular, muscular and jump artifacts are identified using an automatic procedure from the Fieldtrip package (Oostenveld et al., 2011). The remaining data are segmented into 4 s epochs of artifact-free activity using only the magnetometer data (Garces et al., 2017). An ICA-based procedure is used to remove the electrocardiographic component.

Source Reconstruction. Artifact-free epochs are filtered between 2 and 40 Hz, to remove both low frequency noise and network line artifact. The epochs are padded with 2 s of real signal from both sides prior to the filtering to prevent edge effects inside the data. The source model consists of 2459 sources placed in a homogeneous grid of 1 cm in MNI template, then linearly transformed to subject space by warping the subject T1-weighted MRI into the MNI template. The lead field is calculated using a single shell (the brain-skull interface) generated from the T1 MRI using Fieldtrip[13] and a modified spherical solution (Nolte, 2003). A Linearly Constrained Minimum Variance beamformer (Van Veen et al., 1997) is used to obtain the source time series by using the computed lead field and building the beamforming filter with the epoch-averaged covariance matrix and a regularization factor of 5% of the average channel power.

Spectral Analysis. The estimated spatial filters are used to reconstruct the source-space time series for each epoch and source location. MEG power spectra are calculated between 2 and 40 Hz for every clean epoch using a Hann taper, with 0.25 Hz steps. The resulting spectra for each trial are averaged to build the final spectrum for each source. The obtained power is normalized with the overall power in Rey (1941), Reitan (1958), Welsh et al. (1991, 1994), Reitan and Wolfson (1994), Van Veen et al. (1997), Watson et al. (1997), Weinhard (1998), Lopez et al. (2000), Saxton et al. (2000), Wilson et al. (2000), Selkoe (2002), Nolte (2003), Nasreddine et al. (2005), Price et al. (2005), Rosano et al. (2005), Schinka et al. (2005), Taulu and Simola (2006), Erickson et al. (2010, 2013), Bambs et al. (2011), Ewers et al. (2011), Newman et al. (2011), Oostenveld et al. (2011), Zlokovic (2011), Cohen et al. (2013), Glasser et al. (2013), Lambert et al. (2013), Prescott et al. (2014), Hughes et al. (2015), Tsvetanov et al. (2015), Zhou et al. (2015), Busche and Konnerth (2016), Jack et al. (2016), Garces et al. (2017), Nakamura et al. (2017), Lopez-Sanz et al. (2019), Maestu et al. (2019), and Babiloni et al. (2020) Hz. The normalized spectra of all the sources in each brain lobe were averaged, obtaining one value per frequency step, brain lobe and subject. Last, we calculated the relative power per lobe in each of the standard frequency bands: Delta (2–4 HZ), Theta (4–8 Hz), Alpha (8–12 Hz), Beta (12–30 Hz), and Gamma (30–40 Hz).

Genotyping

We are genotyping each study participant for 21 previously identified susceptibility genes (Lambert et al., 2013) including APOE*4 (see **Supplementary Table 5**). The genetic information is also uploaded to the NDA but requires special permissions for access.

Measures Related to Risk/Protection From Cognitive Impairment

Each of the study subjects provides additional data related to risk for and protection from cognitive impairment based on studies from our prior research. With regard to exercise and motor function, each subject wears an activity monitor (Erickson et al., 2010, 2013) for five days, and we query them about the amount of walking per week, estimate the number of kilocalories burned per week, and measure gait speed (Rosano et al., 2005) (in addition to the motor tasks used by the NIH Toolbox). Each participant completes the Florida Cognitive Activities scale to obtain a measure of activities that might affect cognitive and brain health (Schinka et al., 2005; Hughes et al., 2015).

[11] http://www.neuro.uni-jena.de/cat/

[12] http://www.pmod.com

[13] http://surfer.nmr.mgh.harvard.edu

On Day Two, we measure blood pressure, height, weight, and waist-hip ratio (Mukamal et al., 2003). Laboratory measures include a fasting lipid profile (Wong et al., 2010), cystatin-c, homocysteine (Longstreth et al., 2004), and inflammatory markers (Tracy et al., 1997; Fornage et al., 2008; Braskie et al., 2014).

Quality Control/Assurance Procedures

Quality Control

Magnetic Resonance Imaging Scanner. The MRRC has QC/QA procedures and American College of Radiology certification in place for all scanners. These include daily signal stability scans for echo planar imaging (1% maximum RMS over a continuous 30-min acquisition with a 64 × 64 matrix size) and daily signal-to-noise measurements with the standard RF head coil. In addition to the daily QC testing of the MRI scanner, each imaging protocol is examined visually prior to submitting it to the local data archive. The scans are checked immediately by a member of the Imaging Team and repeated if necessary.

Positron Emission Tomography Scanner. QC/QA procedures are run according to the University of Pittsburgh PET Facility Standard Operating Procedures HR + Quality Assurance Task Schedule. The "Daily QC" protocol runs a scan that is compared to the last standard that was written into the database. That is, the standard that was written by the *Norm 2D and ECF (Customer)* protocol. The resulting deviation between scans must be less than 2.5. The protocol uses the internal rod sources of the gantry, so no phantoms are used.

Magnetoencephalography Scanner. The operating status of the *Elekta NeuroMag* system is tested daily. This includes determining that there is a sufficient level of liquid helium, calibrating and tuning the sensors, determining the proper functioning of the magnetic shielding producing a sufficiently low ambient magnetic interference level.

Neuropsychological Testing. Clinical Team Leader Dr. Snitz trains the staff who are responsible for administering and/or scoring questionnaires or paper-and-pencil tests as she does within the ADRC.

Quality Assurance

Magnetic Resonance Imaging Scanner. We use the ADNI phantom as a reference tool for our structural and functional images.

Positron Emission Tomography Scanner. The ^{68}Ge phantom is run at on a weekly basis to check for changes in the scanner calibration or changes in uniformity. Four times each year the following procedures are performed in order: Full ASIC Bucket Setup; System Normalization; Daily QC; and, Scanner/Well Counter Cross Calibration.

Magnetoencephalography Scanner. Prior to and after every scan we record 2 min of empty room data to measure ambient magnetic noise. We complete a simple spectral analysis and then save the raw data and spectra. This allows for monitoring the noise level and system status over time to help identify changes in the background environment.

Neuropsychological Testing. Dr. Snitz reviews the scoring of all questionnaires and paper-and-pencil tests. Every six months a sample of ten protocols will be "double scored" to ensure inter-rater reliability. Five of these protocols will be repeated annually to check for scoring drift.

PRELIMINARY RESULTS

The data acquired through this protocol are and will continue to be uploaded to the CCF and NDA. However, the team has completed some initial analyses to help to better explicate the participants who had enrolled in the study by March 31, 2020. The data provides critical information about the relationship between the breakdown in functional and structural connectivity and the expression of cognitive impairment along the AD-pathology continuum. Because of our unique sampling frame, we have data from participants who are less likely to enroll in biomedical research studies, and this has revealed several aspects of the normal/pathological aging spectrum that were previously under-appreciated.

The study was reviewed and approved by the University of Pittsburgh Human Research Protection Office. All participants signed written statements of Informed Consent prior to initiation of any research procedures.

Subjects

A total of 472 individuals inquired about the study and of these, 208 either chose not to enroll or failed the initial screening questions related to MR compatibility (e.g., metal implants) or medical history (e.g., clinical stroke). Twenty-seven individuals were excluded after having signed an informed consent form; as of 31 March 2020, 227 individuals had enrolled in the study.

Of these participants, 13 had been diagnosed with DAT; these individuals are not described in this report. Sixty-seven study participants (31%) entered via the ADRC; 97 (45%) came through Pitt + Me, and 27 (13%) were volunteers from the community. Twenty-one participants (10%) entered through HeartScore or the LLFS.

We compared the characteristics of the participants initially classified as having normal cognition to those with some degree of impairment. There were two subgroups among the Cognitively Normal participants: those who reported no limitations in their cognition and those who reported significant concerns [Subjective Cognitive Complaints (SCC)]. There were also two subgroups among the cognitively impaired participants: those who reported no concerns or loss of abilities [Impaired Without Complaints (IWOC)], and those who reported loss of abilities (i.e., MCI) (see **Tables 1–3**).

The proportion of Black individuals was greater within the cognitively impaired group, as was the proportion reporting being left-handed. As would be expected, the Crystallized and Fluid Intelligence measures from the NIH Toolbox were significantly lower among the impaired participants.

The two subgroups of individuals who were cognitively normal did not differ in terms of age, years of education, distribution of men and women, race, or handedness (see

TABLE 1 | Characteristics of study participants as a function of initial classification.

	Study groups		Effect size[1]
	Normal cognition	Impaired cognition	
Number	121	93	
Age	65.6 (8.0)	62.8 (9.7)	0.03*
Education	16.0 (3.1)	13.9 (2.8)	0.13*
Sex [Percent (N) Male]	30.6 (37)	30.4 (32)	0.04
Race [Percent (N) Caucasian]	59.5 (72)	34.4 (32)	0.29*
Handedness [Percent (N) Right]	95.7 (112)	90.0 (81)	0.11*
APOE*4 Present [Percent(N)]	26.1 (29)	34.9 (30)	0.10
Montreal Cognitive Assessment	26.5 (2.3)	23.4 (2.7)	0.44*
Wide Range Achievement Test – 4	63.8 (5.1)	59.1 (7.8)	0.18*
Walk Endurance – *2min distance*	544.4 (177.2)	502.1 (87.0)	0.02
Gait Speed – *4meter walk – time*	3.4 (0.5)	3.4 (0.7)	0.001
Oral reading	6.9 (3.6)	4.6 (2.8_	0.12*
DCCS	29.3 (1.0)	28.2 (2.0)	0.13*
Flanker Inhibitory Control	19.9 (0.8)	19.9 (0.6)	0.00
Pattern Comparison	41.7 (6.3)	38.5 (7.6)	0.05*
Picture Sequence Memory	11.7 (6.8)	7.3 (4.7)	0.14*
Crystalized Cognition	113.5 (9.3)	105.0 (9.1)	0.21
Fluid Cognition	97.5 (9.1)	88.4 (9.2)	0.25*
Total Cognition	105.8 (8.8)	95.4 (7.4)	0.40*
Promis Abilities	30.8 (7.2)	28.1 (8.0)	0.03*
Promis Concerns	16.1 (7.3)	17.0 (7.5)	0.004
Life Satisfaction	19.9 (7.4)	20.1 (10.7)	0.000
Meaning	29.2 (15.3)	30.1 (14.7)	0.001
Positive Affect	18.8 (13.1)	21.2 (15.6)	0.01
Sadness	8.9 (2.4)	9.2 (2.2)	0.004
Self-Efficacy	19.6 (9.4)	18.5 (9.7)	0.003

[1]*Cramer's V for categorical data; Cohen's f^2 for continuous data. *$p < 0.05$.*

Table 2). The MoCA scores were equivalent, but the individuals in the SCC group performed more poorly on the Wide Range Achievement Test. The SCC group reported more cognitive concerns, and lower scores on the measure of Meaning and Purpose. The latter indicates more hopelessness, less goal-directedness, less optimism, and weaker feelings that their life is "worthy".[14]

Between the two subgroups of individuals with Impaired Cognition those in the IWOC group were younger, less well educated, and more likely to self-identify as Black; they had decreased physical endurance (see **Table 3**). The IWOC group reported significantly *better* cognitive abilities (higher scores) and *fewer* cognitive concerns (lower scores) than the people in the MCI group. They reported higher scores on the Meaning and Purpose questions from the Promis battery.

The participants with MCI had significantly lower scores on the Promis Cognitive Abilities questionnaire relative to the healthy controls [$t(132) = -4.39$, $d = 0.76$], and reported significantly more concerns about their cognition [$t(132) = 3.77$, $d = 0.66$]. By contrast, the individuals in the IWOC group did not differ significantly on the Cognitive Abilities scale [$t(125) = 1.20$, $d = 0.21$], and reported *fewer* concerns about their cognition than did the healthy controls [$t(125) = -2.54$, $d = 0.45$]. Finally, when we compared the MCI and IWOC groups, we found that those with MCI had lower scores on the Cognitive Abilities questionnaire [$t(75) = -5.00$, $d = 1.15$], and reported significantly more concerns [$t(75) = 6.12$, $d = 1.41$] about their cognition than the IWOC group.

[14]http://www.healthmeasures.net/index.php?option=com_instruments&view=measure&id=847&Itemid=992

Structural Magnetic Resonance Imaging Data

We calculated an index of the cortical thickness of critical temporal lobe areas including the fusiform gyrus, entorhinal cortex, and the inferior and middle temporal gyri (Jack et al., 2017) using values taken from the standard output of the HCP pipeline. We then classified each case as "normal" or "atrophic" based on the standard cut-off of $\pm$2.70 mm (see **Table 4**).

The mean cortical thickness differed as a function of group (One-Way Analysis of Variance) [$F(3,182) = 3.18$, $f^2 = 0.05$, $p < 0.05$]. Furthermore, the rate of abnormal thickness differed significantly between groups ($X^2 = 7.87$, $df = 3$, $V = 0.21$,

TABLE 2 | Characteristics of cognitively normal participants by subgroup.

	Study groups		Effect size[1]
	Healthy controls	Subjective complaints/ No impairments	
Number	104	17	
Age	65.3 (8.2)	68.6 (6.9)	0.02
Education	16.2 (2.9)	16.4 (4.7)	0.001
Sex [Percent (N) Male]	26.9 (28)	52.9 (9)	0.20*
Race [Percent (N) Caucasian]	56.7 (59)	76.5 (13)	0.15
Handedness [Percent(N) Right]	96.1 (99)	92.9 (13)	0.05
APOE*4 Present [Percent(N)]	27.2 (25)	30.8 (4)	0.01
Montreal Cognitive Assessment	26.4 (2.4)	26.9 (1.4)	0.008
Wide Range Achievement Test – 4	64.1 (5.0)	57.5 (2.1)	0.095
Walk Endurance – *2min distance*	523.0 (82.7)	677.5 (419.0)	0.10*
Gait Speed – *4meter walk – time*	3.4 (0.5)	3.3 (0.4)	0.003
Oral Reading Recognition	6.9 (3.8)	6.7 (2.4)	0.000
Dimensional Change Card Sort Test	29.4 (0.8)	28.7 (1.4)	0.07*
Flanker Inhibitory Control	19.9 (0.8)	20.0 (0.0)	0.002
Pattern Comparison	41.7 (6.1)	41.4 (7.6)	0.000
Picture Sequence Memory	11.8 (6.8)	11.2 (6.9)	0.001
Crystalized Cognition	113.3 (9.6)	114.4 (7.8)	0.002
Fluid Cognition	97.6 (8.9)	97.0 (9.9)	0.001
Total Cognition	105.8 (8.8)	106.0 (9.0)	0.000
Promis Abilities	31.5 (7.0)	27.3 (7.5)	0.04*
Promis Concerns	15.4 (7.0)	20.4 (8.1)	0.06*
General Life Satisfaction	20.0 (7.8)	19.1 (4.5)	0.002
Meaning and Purpose	30.4 (15.9)	21.9 (8.5)	0.04*
Positive Affect	19.3 (13.3)	15.8 (11.7)	0.009
Sadness	8.8 (2.4)	9.0 (2.5)	0.001
Self-Efficacy	20.0 (9.5)	17.2 (8.6)	0.011

[1]*Cramer's V or Cohen's f^2 *$p < 0.05$.*

TABLE 3 | Characteristics of cognitively impaired participants by subgroup.

	Study groups		Effect size[1]
	Mild cognitive impairment	Impaired/No complaints	
Number	52	41	
Age	64.9 (10.4)	60.5 (8.0)	0.06*
Education	14.5 (2.7)	13.1 (2.7)	0.07*
Sex [Percent (N) Male]	28.9 (15)	41.5 (17)	0.13
Race [Percent (N) Caucasian]	48.1 (25)	17.1 (7)	0.32*
Handedness [Percent(N) Right]	92.0 (46)	87.5 (35)	0.08
APOE*4 Present [Percent(N)]	31.3 (15)	39.5 (15)	0.09
Montreal Cognitive Assessment	23.3 (2.6)	23.5 (3.0)	0.001
Wide Range Achievement Test – 4	60.9 (6.8)	56.1 (8.5)	0.10
Walk Endurance – *2min distance*	481.9 (86.3)	528.2 (82.1)	0.08*
Gait Speed – *4meter walk – time*	3.6 (0.7)	3.3 (0.6)	0.04
Oral Reading Recognition	4.9 (2.6)	4.1 (2.9)	0.02
Dimensional Change Card Sort Test	28.2 (2.0)	28.1 (2.1)	0.002
Flanker Inhibitory Control	19.9 (0.8)	20.0 (0.2)	0.01
Pattern Comparison	36.6 (8.3)	40.6 (6.3)	0.08
Picture Sequence Memory	7.1 (4.4)	7.6 (5.0)	0.003
Crystalized Cognition	106.6 (9.0)	103.2 (9.1)	0.04
Fluid Cognition	86.5 (9.2)	90.3 (8.9)	0.05
Total Cognition	95.5 (7.8)	95.3 (7.0)	0.000
Promis Abilities	24.7 (7.9)	32.6 (5.7)	0.32*
Promis Concerns	20.3 (7.5)	12.7 (4.6)	0.35*
General Life Satisfaction	19.6 (8.7)	20.7 (12.6)	0.003
Meaning and Purpose	26.5 (13.2)	34.1 (15.1)	0.07*
Positive Affect	18.1 (12.3)	24.7 (18.1)	0.05
Sadness	8.8 (2.1)	9.5 (2.4)	0.03
Self-Efficacy	17.0 (8.0)	20.2 (11.2)	0.03

[1]*Cramer's V or Cohen's f*^{2}*. *$p < 0.05$.*

$p < 0.05$) with the controls and the IWOC having the lowest rates, and the SCC and MCI groups having the highest.

Positron Emission Tomography Pittsburgh Compound B Data

Positron emission tomography (PET) data were available from 176 of the individuals enrolled in the study. **Table 4** shows the data including the mean SUVR for each of the brain regions used for determining amyloid deposition, as well as the global rate of PiB positivity. There is a significant Main Effect of group (One-Way ANOVA) for each of the seven regions of interest (summed across each hemisphere). In addition, the rate of PiB positivity was significantly different across all groups (chi-square test). However, these effects were due to the lower-than-normal SUVRs in each of the six brain regions for the 35 individuals in the IWOC group compared to the healthy controls (all *d*s > 0.61) and their low rate of PiB positivity (Odds Ratio = 14.0, 95% CI = 1.8−110, Exact Test $p = 0.002$) compared to the controls. Among the normal controls the rate of positivity was greater among the White (51.4%) relative to the Black participants (4.5%; OR = 32.2, 95% CI = 2.7−184; Exact Test $p = 0.0003$).

Amyloid/Neurodegeneration Classification

We compared the rates of PiB retention and temporal lobe atrophy as a function of the clinical classification (see **Table 5**). There was a significant difference in the rates of biomarker abnormality across groups ($\chi^2 = 21.5$, $df = 9$, $V = 0.21$, $p < 0.05$). Fifty-eight percent of the normal controls were biomarker negative, which is similar to the rates for the SCC (53%) and MCI (49%) groups. By contrast, the IWOC group was 74% biomarker negative. Among the participants with MCI, 29% had *only* temporal lobe atrophy, while 9.8% had *only* PiB + imaging.

Magnetoencephalopathy Summary Data

One hundred and eighty-six individuals contributed MEG data that met all quality control standards. We examined the relative power across all five MEG frequency bands in regions of interest (ROI) extracted using the AAL templates (Tzourio-Mazoyer et al., 2002). The repeated measures (band) Analysis of Covariance (age) of temporal lobe power by subject group revealed that the SCC group had elevated theta power compared to the other study groups (see **Figure 1A**), and decreased beta power. There was no significant association (chi-square tests) between elevated theta power (> 75%tile of normal controls) and race, sex, and APOE*4 status. However, an ANCOVA of temporal lobe theta power revealed a significant interaction between group (NC vs. SCC) and PiB status (positive vs. negative) [$F(1,64) = 9.11$, $\xi^2 = 0.13$]. As can be seen in **Figure 1B**, theta power in the temporal lobe (adjusted for age) is similar in the normal controls (PiB ±) and the PiB- SCC group; power is elevated only in the PiB + SCC participants.

DISCUSSION

The purpose of this report is to describe the creation of the Connectomics of Brain Aging and Dementia study.[15] The MRI brain images are being uploaded to the CCF and the behavioral and cognitive data, PET PiB scan regional SUVRs (and raw SUV images), and the raw data from the MEG are being uploaded to the NDA (ID C3159).

Study Advantages, Limitations, Possible Pitfalls, and How to Counteract Them

When this project was initially proposed to the NIH, we specified that the sample would consist of 50% women and 50% black participants. We further proposed that the 50:50 splits be maintained in each subject group. While we were able to achieve this goal in our sample of healthy controls, some subgroups of participants did not conform to these expectations which in fact reveals much about the characteristics of those phenotypes. We believe that the single biggest advantage of using data derived from this study, and which will continue to be acquired and deposited for public consumption, is the composition of the study

[15]https://www.humanconnectome.org/study/connectomics-brain-aging-and-dementia

TABLE 4 | Summary neuroimaging findings among four subject groups.

	Groups				Effect size [1]
	Healthy controls	**Subjective complaints**	**Impaired without complaints**	**Mild cognitive impairment**	
Number	96	17	39	46	
Temporal Lobe Cortical Thickness [2]	2.80 (0.24)	2.72 (0.37)	2.72 (0.27)	2.68 (0.28)	0.04
Grey Matter Atrophy [Percent (N)] [3]	21.9 (21)	29.5 (5)	25.6 (10)	37.0 (17)	0.14
PiB SUVR [4,5,6]					
Ant. Cing.	1.29 (0.33)	1.45 (0.11)	1.12 (0.44)	1.29(0.36)	0.07*
Sup. Front.	1.22 (0.30)	1.36 (0.08)	1.08 (0.36)	1.22 (0.35)	0.07*
Orb. Front.	1.27 (0.30)	1.40 (0.09)	1.11 (0.43)	1.26 (0.36)	0.07*
Lat Temp.	1.18 (0.24)	1.31 (0.07)	1.06 (0.29)	1.18 (0.26)	0.08*
Parietal	1.24 (0.25)	1.35 (0.08)	1.09 (0.33)	1.22 (0.28)	0.08*
Precuneus	1.32 (0.34)	1.46 (0.09)	1.13 (0.42)	1.30 (0.37)	0.08*
Ant. Vent. Striatum	1.29 (0.20)	1.43 (0.12)	1.14 (0.33)	1.28 (0.31)	0.11*
PiB Positive [Percent (N)]	32.5 (26)	40.0 (6)	5.7 (2)	22.2 (10)	0.25*

[1] *Cohen's f^2 for continuous variables; Cramer's V for categorical data.*
[2] *Average of the cortical thickness values from the fusiform gyrus, entorhinal cortex, and the middle and inferior temporal lobe.*
[3] *Abnormal thickness < 2.70 mm (Jack et al., 2017).*
[4] *ANC – Anterior Cingulate Cortex; FRC – Frontal Cortex; LTC – Lateral Temporal Cortex; PAR – Parietal Cortex; PRC – Precuneus; AVS – Anterior Ventral Striatum.*
[5] *PiB SUVR Cut-off scores: Anterior Cingulate = 1.469; Anterior Ventral Striatum = 1.372; Superior Frontal = 1.333; Orbitofrontal = 1.387; Insula = 1.296; Lateral Temporal = 1.278; Parietal = 1.344; Posterior Cingulate = 1.495; Precuneus = 1.508; Global = 1.346.*
[6] *Participants with PiB data: HC = 80, SCC = 15, IWOC = 35, MCI = 45.*
*$p < 0.05$.

TABLE 5 | Summary amyloid and atrophy findings among four subject [Percent(N) Within Group].

	Groups			
	Healthy controls	**Subjective complaints**	**Impaired without complaints**	**Mild cognitive impairment**
Number	74	15	34	41
No Abnormality	58.1 (43)	53.3 (8)	73.5 (25)	48.8 (20)
Amyloid Only	21.6 (16)	13.3 (2)	2.9 (1)	9.8 (4)
Atrophy Only	9.5 (7)	6.7 (1)	20.6 (7)	29.3 (12)
Amyloid and Atrophy	10.8 (8)	26.7 (4)	2.9 (1)	12.2 (5)

Cramer's $V = 0.21$, $p < 0.05$.

sample. We found that by carefully tailoring our public face on Pitt + Me we were able to recruit individuals across a wide range of socioeconomic strata as well as a high rate of Black volunteers. While many studies successfully enroll Black participants at a rate consistent with the population distribution, we specifically chose to oversample Blacks. The individuals that we ended up enrolling, both White and Black, were frequently new to research, and often had relatively low health-related knowledge. In our view, these are the people who need to be enrolled in studies such as COBRA in order to see the process of aging and neurodegeneration as it exists in the broader community.

However, we learned several things about the execution of the protocol that had not been self-evident prior to the study. First, and perhaps most important, the research participants require a great deal of "hands-on" care than the typical research participant. In the end, each participant is assigned to a Research Associate who is, in effect, a concierge. They escort the participant around the medical center for the various procedures. They may be an examiner or interviewer who sits with the participant during neuropsychological testing or completion of healthcare questionnaires. They may take the participant to the cafeteria for lunch, or if time is short, purchase the lunch from the hospital cafeteria. These are also the individuals who make interval telephone calls to maintain the necessary contact with the participants during follow-up. This means that we had underestimated our need for support staff by as much as 50%.

We also learned that because many of these individuals were new to research, many of the procedures that we use must be explained to them in ways that differ from the more research-experienced individuals we are more accustomed to working with. For example, the PET procedures are explained in more detail as the notion of *injecting* radioactive compounds (or any other solution) is not universally accepted without good explanation. To facilitate this process, we talk in terms of the important changes that can occur in the brain with dementia, and that we can take a picture of those changes using that injected solution.

After our participants have completed their baseline examinations, we send them a signed certificate of participation accompanied by a color image of the surface of the brain using

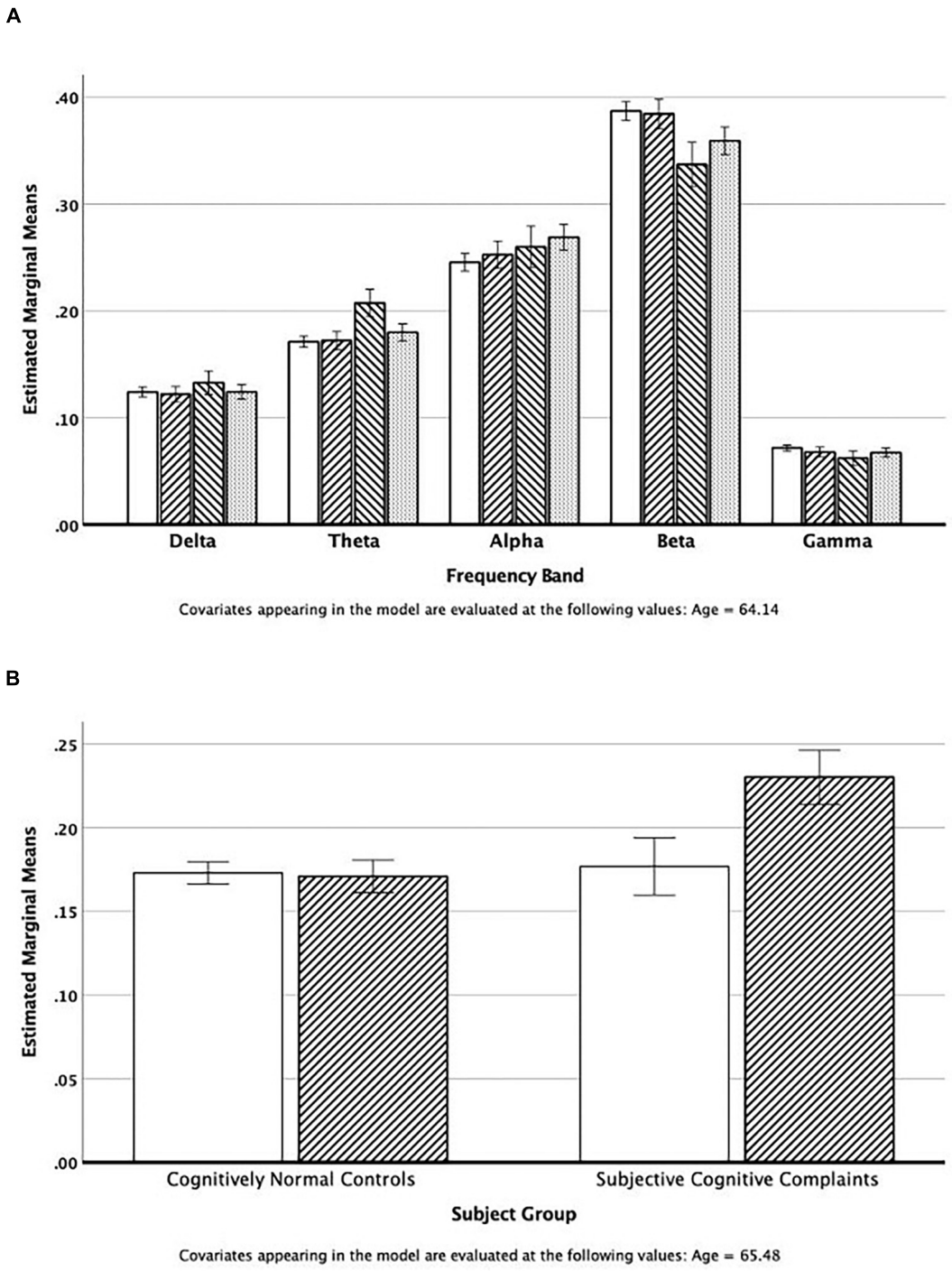

FIGURE 1 | (A) Estimated mean power in the five cortical regions adjusted for mean age of the group. The bars represent values for the Normal Controls, IWOC, SCC, and MCI groups, respectively. **(B)** Estimated theta band power in the temporal lobes adjusted for mean age. The open bars are those individuals classified as PiB−, and the cross-hatched bars are for those individuals who are PiB+.

the Freesurfer parcellations. Frequently, this results in our getting telephone calls being asked to explain "what it means." One of the Investigators always returns these calls; it is critically important to "give back" to the communities. We also attend monthly gatherings at local Community Engagement Centers – just being present increases our familiarity to the community.

We also found that it was important to pay close attention to transportation needs. Many of our participants live in

neighborhoods where public transportation is less than ideal (e.g., two or more transfers needed for a 60-min one-way trip). Consequently, we had to develop relationships with ridesharing services to obtain the quality of service that we wanted for our participants. Everyone is met at the door to the hospital by their "concierge," and from there escorted to all of the tasks that they will do during the day. At the end of the day the ride is scheduled, and the "concierge" takes the volunteer back to the lobby and awaits the arrival of the car.

Finally, while all imaging researchers are familiar with the problem of incidental findings, the quality of those findings in a study such as this is different than that which we have encountered in the past. Many of the individuals in the study had limited healthcare resources which might have identified potential problems; many participants do not have a regular annual physical. However, we have also had instances of more severe brain injury that was a consequence of the participants living environment. One individual, for example, had suffered a severe closed head injury, and the sequalae were evident on the scan. However, there was no mention of this event despite multiple opportunities during screening and interview. The individual seemed surprised that spending more than three days in the hospital, much of the time in coma, would result in brain damage. This view is likely due in part due to lack of awareness of health-related issues.

Comments on Preliminary Data

A significant proportion of the participants in this study have never been involved in biomedical research. Thus, our sample likely includes individuals who are typically under-represented in academic research studies and may be more representative of the population at-risk for cognitive impairment. This has resulted in the identification of a group of study participants who were cognitively impaired but had no complaints or concerns about their cognitive abilities. Further, we found that the rate of amyloid deposition among those individuals with cognitive impairment (i.e., MCI and IWOC) was lower than expected based on prior analyses (Wolk et al., 2009). Among the MCI participants 4/10 individuals (40%) recruited from the ADRC were amyloid positive, whereas only 1/16 among the individuals (6%) recruited via Pitt + Me were amyloid positive (Odds Ratio = 10.0, 95% Confidence Interval = 0.92 – 108, $p = 0.055$) [cf., (Wolk et al., 2009)].

We had assumed when the project began that participants recruited from the community would be, on average, cognitively normal; the cognitively impaired participants (and those with subjective complaints) would enroll through the ADRC. However, experience revealed a more nuanced picture. The group of individuals with impaired cognition, but who did not complain of changes in their behavior or cognition deserve special mention. The participants in this group were predominantly Black (85%) which contrasts sharply with the NC (41.7%) and SCC (14.3%) groups. Their performance on the tests used for classification was equivalent to that of the MCI participants, but without the complaints necessary for that classification. Indeed, on average the IWOC participants reported *better* cognitive abilities, and *fewer* cognitive concerns than did the cognitively normal controls. The near absence of PiB retention means that these individuals were not as yet, on the AD pathology spectrum; although with a mean age of 60 years, the amyloid cascade may not be well developed, or perhaps other non-amyloid factors may be in play [e.g., (Selkoe, 2002)].

Given the age range of the IWOC group there is also a high likelihood that these individuals (as well as other Black participants in the study) are the children or grandchildren of the people who migrated from the rural South to cities like Pittsburgh. Growing up Black in a northern city in the 1950s and 1960s was likely associated with poorer educational quality, poor access to medical care and health maintenance, as well as a range of psychosocial consequences of explicit and implicit discrimination. It may be that any racial inequities in the development of cognitive impairments are driven by pervasive institutionalized inequities that shape risk and disadvantage individuals at multiple levels, including biological, environmental, behavioral, sociocultural (Hill et al., 2015). Although these factors have often been referred to as "modifiable individual risk factors," this term fails to recognize that individual risk is influenced by racism and social determinants *that are outside of an individual's control.* At a population level, Black communities experience racism and more adverse social determinants of health, including negative work, living and educational conditions, that can lead to long-term negative biological consequences (Shonkoff et al., 2009; Braveman P. et al., 2011; Braveman P.A. et al., 2011). Indeed, neighborhood-level disadvantage was associated with an increased likelihood of AD neuropathology at autopsy (Powell et al., 2020). While there are established diagnostic hallmarks of AD, little attention has been paid to the possibility that factors such as neighborhood context may directly and indirectly impact brain changes that alter the connectome, thus resulting in earlier expression of the dementia. To date, little attention has been paid to the possibility that early social structural and social determinants may affect brain structure and function, alter the connectome, and reduce brain reserve and compensation resulting in the earlier expression of DAT and an apparent increased incidence of dementia among Blacks [see also Wilkins et al., 2020]. Indeed, there needs to be a paradigm shift in the field to focus on collecting the contextual and environmental data that may help disentangle apparent differences due to race; "analyzing findings by race/ethnicity without appropriate contextual data could lead to inaccurate, misleading, or stigmatizing conclusions that may detract from the overall goals of diversity in research: to enhance the accuracy, utility, and generalizability of scientific evidence" (Wilkins et al., 2020). This view is supported by the decades of research that argue that racial and socioeconomic inequities are not the result of individual behavior or biological factors but rather are due to the structures, institutional practices, and policies which contribute to adverse outcomes and susceptibilities (Fuller-Thomson et al., 2009; Nuru-Jeter et al., 2009; Mendez et al., 2014a,b; Bailey et al., 2017; Hardeman et al., 2018).

The data included in this project provides investigators around the world with the opportunity to investigate

the spectrum of aging and AD effects on the brain and cognition using true-multimodal imaging, and detailed cognitive/behavioral evaluations. Genetic analyses will be completed starting at the end of 2020, and those restricted data will be available directly from the study investigators. Longitudinal follow-up of the individuals in the study is underway, and there are plans to enrich the sample of pre-DAT participants and continue follow-up. These data, combined with the main HCP dataset, the HCP Lifespan and Aging datasets, and the other CRHD project related to AD provide richest and most comprehensive resource for the neurobiological study of AD and related dementias.

CONCLUSION

The study has two unique characteristics. First, the data are acquired using standard and standardized procedures that are shared by other CRHD studies, including the HCP Lifespan Study (Bookheimer et al., 2019). This provides an international, accessible database for all investigators. Second, and more important, are the characteristics of the study sample. We used multiple portals of entry, including customized web sites that allowed to achieve our goal of ∼50% Black participants, and reaching people who were participating in their first research study. This, we believe, at least partly explains why our measured rates of AD pathology are lower than those in more typical research samples [e.g., (Wolk et al., 2009)]. In addition, we identified a group of participants whose test performance was as poor as that of the MCI participants, but who reports few concerns about their cognition [c.f., (Antinori et al., 2007)]; this group is predominately Black.

This leads us to what we believe is the most important implication of our data, and which is a weakness of the study as currently described. Specifically, we, like many others, make the mistake of "analyzing [our] findings by race/ethnicity without appropriate contextual data [which] could lead to inaccurate, misleading, or stigmatizing conclusions that may detract from the overall goals of diversity in research: to enhance the accuracy, utility, and generalizability of scientific evidence" (Wilkins et al., 2020). Race is a socially determined construct that is not biologically or genetically based (Cooper and David, 1986). In addition to strong data suggesting there are no biologically determined differences between races (Serre and Paabo, 2004), defining race as a social construct has the advantage of capturing the concept of racism more precisely (Jones, 2000). Racism is thus better defined as a system that structures opportunity based on race, providing unfair advantages and disadvantages based on race.

There is still considerable disagreement on the factors contributing to disparities in many AD- related outcomes, e.g., dementia onset and course. Much of this is likely due to the focus on individual behavior or "lifestyle factors" without consideration for the social, physical, and policy environments that are inextricably linked to the individual and are key to understanding health disparities (Cooper et al., 2015). Perhaps a better way to place the factors related to AD and dementia into the NIA Health Disparities Framework is to study the interplay between social determinants of health, racism, and AD and dementia (Hill et al., 2015). Aside from the more direct effects racism on risk factors, we also believe that racism may have the moderating effect of *reducing* the impact of the positive social determinants of health (SDOH) (e.g., education, access to health care) and *increasing* the impact of negative SDOH (e.g., poverty, social isolation). Significant advances in AD and dementia prevention and management will be made as we accumulate more information SDOH and how racism affects their relationship with resilience, diagnosis, prognosis, and response to treatment.

THE CoBRA STUDY TEAM

The CoBRA Study team includes: Ann D. Cohen, Beth E. Snitz, Ted Huppert, Tae Kim, Yue-Fang Chang, Yu Cheng, Jack Doman, Ricardo Bruña, Fernando Maestu, Avniel Ghuman, Anto Bagic, Ilyas Kamboh, Anne Newman, Steven Reis, Rebecca Roush, Lara Fatukasi, Leslie Kovach, Katey Potopenko, Howard J. Aizenstein, Lewis H. Kuller, William E. Klunk, Caterina Rosano, Oscar L. Lopez, and James T. Becker.

With the exceptions of AC and JB, the order of the authors is alphabetical.

DATA AVAILABILITY STATEMENT

The datasets presented in this study can be found in online repositories. The names of the repository/repositories and accession number(s) can be found below: HCP Connectome Central Facility https://www.humanconnectome.org/study/connectomics-brain-aging-and-dementia; NIMH Data Archive https://nda.nih.gov/edit_collection.html?id=3159.

ETHICS STATEMENT

The studies involving human participants were reviewed and approved by Human Research Protection Office; University of Pittsburgh. The patients/participants provided their written informed consent to participate in this study.

AUTHOR CONTRIBUTIONS

AC and JB made the initial draft of the work while the remaining authors revised it for important intellectual content. All authors made substantial contributions to the conception and design of the work, as well as the acquisition, analysis, interpretation of data for the work, and had final approval of the version to be published.

FUNDING

This research and the preparation of this manuscript was supported by funds from the National Institute on Aging (UF1-AG051197), as well as the Neuroimaging Core of the

Alzheimer's Disease Research Center (P50-AG005133 and P30-AG066468).

ACKNOWLEDGMENTS

We are grateful for the support from the Heart Strategies Concentrating on Risk Evaluation (Heart SCORE) study (R01-HL089292) and the Long Life Family Study (U01-AG23744), and the Clinical and Translational Science Institute at the University of Pittsburgh (UL1-TR001857) for managing Pitt + Me.

SUPPLEMENTARY MATERIAL

The Supplementary Material for this article can be found online at: https://www.frontiersin.org/articles/10.3389/fnagi.2021.669490/full#supplementary-material

REFERENCES

Antinori, A., Arendt, G., Becker, J. T., Brew, B. J., Byrd, D. A., Cherner, M., et al. (2007). Updated research nosology for HIV-associated neurocognitive disorders. *Neurology* 69, 1789–1799. doi: 10.1212/01.WNL.0000287431.88658.8b

Babiloni, C., Blinowska, K., Bonanni, L., Cichocki, A., De Haan, W., Del Percio, C., et al. (2020). What electrophysiology tells us about Alzheimer's disease: a window into the synchronization and connectivity of brain neurons. *Neurobiol. Aging* 85, 58–73. doi: 10.1016/j.neurobiolaging.2019.09.008

Bailey, Z. D., Krieger, N., Agenor, M., Graves, J., Linos, N., and Bassett, M. T. (2017). Structural racism and health inequities in the USA: evidence and interventions. *Lancet* 389, 1453–1463. doi: 10.1016/S0140-6736(17)30569-X

Bambs, C., Kip, K. E., Dinga, A., Mulukutla, S. R., Aiyer, A. N., and Reis, S. E. (2011). Low prevalence of "ideal cardiovascular health" in a community-based population: the heart strategies concentrating on risk evaluation (Heart SCORE) study. *Circulation* 123, 850–857. doi: 10.1161/CIRCULATIONAHA.110.980151

Bookheimer, S. Y., Salat, D. H., Terpstra, M., Ances, B. M., Barch, D. M., Buckner, R. L., et al. (2019). The lifespan human connectome project in aging: an overview. *Neuroimage* 185, 335–348. doi: 10.1016/j.neuroimage.2018.10.009

Braskie, M. N., Boyle, C. P., Rajagopalan, P., Gutman, B. A., Toga, A. W., Raji, C. A., et al. (2014). Physical activity, inflammation, and volume of the aging brain. *Neuroscience* 273, 199–209. doi: 10.1016/j.neuroscience.2014.05.005

Braveman, P., Egerter, S., and Williams, D. R. (2011). The social determinants of health: coming of age. *Annu. Rev. Public Health* 32, 381–398. doi: 10.1146/annurev-publhealth-031210-101218

Braveman, P. A., Egerter, S. A., and Mockenhaupt, R. E. (2011). Broadening the focus: the need to address the social determinants of health. *Am. J. Prev. Med.* 40, S4–S18. doi: 10.1016/j.amepre.2010.10.002

Busche, M. A., and Konnerth, A. (2016). Impairments of neural circuit function in Alzheimer's disease. *Philos. Trans. R. Soc. Lond. B Biol. Sci.* 371:20150429. doi: 10.1098/rstb.2015.0429

Cohen, A. D., Mowrey, W., Weissfeld, L. A., Aizenstein, H. J., McDade, E., Mountz, J. M., et al. (2013). Classification of amyloid-positivity in controls: comparison of visual read and quantitative approaches. *Neuroimage* 71, 207–215. doi: 10.1016/j.neuroimage.2013.01.015

Cooper, L. A., Ortega, A. N., Ammerman, A. S., Buchwald, D., Paskett, E. D., Powell, L. H., et al. (2015). Calling for a bold new vision of health disparities intervention research. *Am. J. Public Health* 105(Suppl. 3), S374–S376. doi: 10.2105/AJPH.2014.302386

Cooper, R., and David, R. (1986). The biological concept of race and its application to public health and epidemiology. *J. Health Polit. Policy Law* 11, 97–116. doi: 10.1215/03616878-11-1-97

Dai, Z., and He, Y. (2014). Disrupted structural and functional brain connectomes in mild cognitive impairment and Alzheimer's disease. *Neurosci. Bull.* 30, 217–232. doi: 10.1007/s12264-013-1421-0

Erickson, K. I., Barr, L. L., Weinstein, A. M., Banducci, S. E., Akl, S. L., Santo, N. M., et al. (2013). Measuring physical activity using accelerometry in a community sample with dementia. *J. Am. Geriatr. Soc.* 61, 158–159. doi: 10.1111/jgs.12050

Erickson, K. I., Raji, C. A., Lopez, O. L., Becker, J. T., Rosano, C., Newman, A. B., et al. (2010). Physical activity predicts gray matter volume in late adulthood: the Cardiovascular Health Study. *Neurology* 75, 1415–1422. doi: 10.1212/WNL.0b013e3181f88359

Ewers, M., Frisoni, G. B., Teipel, S. J., Grinberg, L. T., Amaro, E. Jr., Heinsen, H., et al. (2011). Staging Alzheimer's disease progression with multimodality neuroimaging. *Prog. Neurobiol.* 95, 535–546. doi: 10.1016/j.pneurobio.2011.06.004

Fornage, M., Chiang, Y. A., O'Meara, E. S., Psaty, B. M., Reiner, A. P., Siscovick, D. S., et al. (2008). Biomarkers of inflammation and MRI-defined small vessel disease of the brain: the Cardiovascular Health Study. *Stroke* 39, 1952–1959. doi: 10.1161/STROKEAHA.107.508135

Fuller-Thomson, E., Nuru-Jeter, A., Minkler, M., and Guralnik, J. M. (2009). Black-White disparities in disability among older Americans: further untangling the role of race and socioeconomic status. *J. Aging Health* 21, 677–698. doi: 10.1177/0898264309338296

Garces, P., Lopez-Sanz, D., Maestu, F., and Pereda, E. (2017). Choice of magnetometers and gradiometers after signal space separation. *Sensors* 17:2926. doi: 10.3390/s17122926

Glasser, M. F., Sotiropoulos, S. N., Wilson, J. A., Coalson, T. S., Fischl, B., Andersson, J. L., et al. (2013). The minimal preprocessing pipelines for the Human Connectome Project. *Neuroimage* 80, 105–124. doi: 10.1016/j.neuroimage.2013.04.127

Hardeman, R. R., Murphy, K. A., Karbeah, J., and Kozhimannil, K. B. (2018). Naming institutionalized racism in the public health literature: a systematic literature review. *Public Health Rep.* 133, 240–249. doi: 10.1177/0033354918760574

Hill, C. V., Perez-Stable, E. J., Anderson, N. A., and Bernard, M. A. (2015). The National Institute on aging health disparities research framework. *Ethn. Dis.* 25, 245–254. doi: 10.18865/ed.25.3.245

Hughes, T. F., Becker, J. T., Lee, C. W., Chang, C. C., and Ganguli, M. (2015). Independent and combined effects of cognitive and physical activity on incident MCI. *Alzheimers Dement.* 11, 1377–1384. doi: 10.1016/j.jalz.2014.11.007

Jack, C. R. Jr., Bennett, D. A., Blennow, K., Carrillo, M. C., Feldman, H. H., Frisoni, G. B., et al. (2016). A/T/N: An unbiased descriptive classification scheme for Alzheimer disease biomarkers. *Neurology* 87, 539–547. doi: 10.1212/WNL.0000000000002923

Jack, C. R. Jr., Wiste, H. J., Weigand, S. D., Therneau, T. M., Lowe, V. J., Knopman, D. S., et al. (2017). Defining imaging biomarker cut points for brain aging and Alzheimer's disease. *Alzheimers Dement.* 13, 205–216. doi: 10.1016/j.jalz.2016.08.005

Jones, C. P. (2000). Levels of racism: a theoretic framework and a gardener's tale. *Am. J. Public Health* 90, 1212–1215. doi: 10.2105/AJPH.90.8.1212

Lambert, J. C., Ibrahim-Verbaas, C. A., Harold, D., Naj, A. C., Sims, R., Bellenguez, C., et al. (2013). Meta-analysis of 74,046 individuals identifies 11 new susceptibility loci for Alzheimer's disease. *Nat. Genet.* 45, 1452–1458. doi: 10.1038/ng.2802

Longstreth, W. T. Jr., Katz, R., Olson, J., Bernick, C., Carr, J. J., Malinow, M. R., et al. (2004). Plasma total homocysteine levels and cranial magnetic resonance imaging findings in elderly persons: the Cardiovascular Health Study. *Arch. Neurol.* 61, 67–72. doi: 10.1001/archneur.61.1.67

Lopez, O. L., Becker, J. T., Klunk, W., Saxton, J., Hamilton, R. L., Kaufer, D. I., et al. (2000). Research evaluation and diagnosis of possible Alzheimer's disease over the last two decades: II. *Neurology* 55, 1863–1869. doi: 10.1212/WNL.55.12.1863

Lopez-Sanz, D., Bruna, R., de Frutos-Lucas, J., and Maestu, F. (2019). Magnetoencephalography applied to the study of Alzheimer's disease. *Prog. Mol. Biol. Transl. Sci.* 165, 25–61. doi: 10.1016/bs.pmbts.2019.04.007

Maestu, F., Cuesta, P., Hasan, O., Fernandez, A., Funke, M., and Schulz, P. E. (2019). The importance of the validation of M/EEG with current biomarkers in Alzheimer's Disease. *Front Hum Neurosci* 13:17. doi: 10.3389/fnhum.2019.00017

Mendez, D. D., Doebler, D. A., Kim, K. H., Amutah, N. N., Fabio, A., and Bodnar, L. M. (2014a). Neighborhood socioeconomic disadvantage and gestational weight gain and loss. *Matern. Child Health J.* 18, 1095–1103. doi: 10.1007/s10995-013-1339-1

Mendez, D. D., Hogan, V. K., and Culhane, J. F. (2014b). Institutional racism, neighborhood factors, stress, and preterm birth. *Ethn. Health* 19, 479–499. doi: 10.1080/13557858.2013.846300

Mukamal, K. J., Kuller, L. H., Fitzpatrick, A. L., Longstreth, W. T. Jr., Mittleman, M. A., and Siscovick, D. S. (2003). Prospective study of alcohol consumption and risk of dementia in older adults. *JAMA* 289, 1405–1413. doi: 10.1001/jama.289.11.1405

Nakamura, A., Cuesta, P., Kato, T., Arahata, Y., Iwata, K., Yamagishi, M., et al. (2017). Early functional network alterations in asymptomatic elders at risk for Alzheimer's disease. *Sci. Rep.* 7:6517. doi: 10.1038/s41598-017-06876-8

Nasreddine, Z. S., Phillips, N. A., Bedirian, V., Charbonneau, S., Whitehead, V., Collin, I., et al. (2005). The Montreal Cognitive Assessment, MoCA: a brief screening tool for mild cognitive impairment. *J. Am. Geriatr. Soc.* 53, 695–699. doi: 10.1111/j.1532-5415.2005.53221.x

Newman, A. B., Glynn, N. W., Taylor, C. A., Sebastiani, P., Perls, T. T., Mayeux, R., et al. (2011). Health and function of participants in the Long Life Family Study: A comparison with other cohorts. *Aging* 3, 63–76. doi: 10.18632/aging.100242

Nolte, G. (2003). The magnetic lead field theorem in the quasi-static approximation and its use for magnetoencephalography forward calculation in realistic volume conductors. *Phys. Med. Biol.* 48, 3637–3652. doi: 10.1088/0031-9155/48/22/002

Nuru-Jeter, A., Dominguez, T. P., Hammond, W. P., Leu, J., Skaff, M., Egerter, S., et al. (2009). "It's the skin you're in": African-American women talk about their experiences of racism. an exploratory study to develop measures of racism for birth outcome studies. *Matern. Child Health J.* 13, 29–39. doi: 10.1007/s10995-008-0357-x

Oostenveld, R., Fries, P., Maris, E., and Schoffelen, J. M. (2011). FieldTrip: open source software for advanced analysis of MEG, EEG, and invasive electrophysiological data. *Comput. Intell. Neurosci.* 2011:156869. doi: 10.1155/2011/156869

Powell, W. R., Buckingham, W. R., Larson, J. L., Vilen, L., Yu, M., Salamat, M. S., et al. (2020). Association of neighborhood-level disadvantage with alzheimer disease neuropathology. *JAMA Netw. Open* 3:e207559. doi: 10.1001/jamanetworkopen.2020.7559

Prescott, J. W., Guidon, A., Doraiswamy, P. M., Roy Choudhury, K., Liu, C., Petrella, J. R., et al. (2014). The Alzheimer structural connectome: changes in cortical network topology with increased amyloid plaque burden. *Radiology* 273, 175–184. doi: 10.1148/radiol.14132593

Price, J. C., Klunk, W. E., Lopresti, B. J., Lu, X., Hoge, J. A., Ziolko, S. K., et al. (2005). Kinetic modeling of amyloid binding in humans using PET imaging and Pittsburgh compound-B. *J. Cereb. Blood Flow Metab.* 25, 1528–1547. doi: 10.1038/sj.jcbfm.9600146

Reitan, R. M. (1958). Validity of the Trail Making test as an indicator of organic brain damage. *Percep. Mot. Skills* 8, 271–276. doi: 10.2466/pms.1958.8.3.271

Reitan, R. M., and Wolfson, D. (1994). A selective and critical review of neuropsychological deficits and the frontal lobe. *Neuropsychol. Rev.* 4, 161–198. doi: 10.1007/BF01874891

Rey, A. (1941). L'examinen psychologie dans les cas d'encephalopathie traumatique. *Arch. Psychol.* 30, 286–340.

Rosano, C., Kuller, L. H., Chung, H., Arnold, A. M., Longstreth, W. T. Jr., and Newman, A. B. (2005). Subclinical brain magnetic resonance imaging abnormalities predict physical functional decline in high-functioning older adults. *J. Am. Geriatr. Soc.* 53, 649–654.

Saxton, J., Ratcliff, G., Munro, C. A., Coffey, E. C., Becker, J. T., Fried, L., et al. (2000). Normative data on the Boston Naming Test and two equivalent 30-item short forms. *Clin. Neuropsychol.* 14, 526–534.

Schinka, J. A., McBride, A., Vanderploeg, R. D., Tennyson, K., Borenstein, A. R., and Mortimer, J. A. (2005). Florida Cognitive Activities Scale: initial development and validation. *J. Int. Neuropsychol. Soc. JINS* 11, 108–116.

Selkoe, D. J. (2002). Alzheimer's disease is a synaptic failure. *Science* 298, 789–791.

Serre, D., and Paabo, S. (2004). Evidence for gradients of human genetic diversity within and among continents. *Genome Res.* 14, 1679–1685.

Shonkoff, J. P., Boyce, W. T., and McEwen, B. S. (2009). Neuroscience, molecular biology, and the childhood roots of health disparities: building a new framework for health promotion and disease prevention. *JAMA* 301, 2252–2259.

Taulu, S., and Simola, J. (2006). Spatiotemporal signal space separation method for rejecting nearby interference in MEG measurements. *Phys. Med. Biol.* 51, 1759–1768.

Tracy, R. P., Lemaitre, R. N., Psaty, B. M., Ives, D. G., and Evans, R. W. (1997). Relationship of c-reactive protein to risk of cardiovascular disease in the elderly. Results from the Cardiovascular Health Study and the Rural Health Promotion Project. *Arterioscler. Thromb. Vasc. Biol.* 17, 1121–1127.

Tsvetanov, K. A., Henson, R. N., Tyler, L. K., Davis, S. W., Shafto, M. A., Taylor, J. R., et al. (2015). The effect of ageing on fMRI: Correction for the confounding effects of vascular reactivity evaluated by joint fMRI and MEG in 335 adults. *Hum. Brain Mapp.* 36, 2248–2269.

Tzourio-Mazoyer, N., Papathanassiou, D., Crivello, F., Etard, O., Delcroix, N., Mazoyer, B., et al. (2002). Automated anatomical labeling of activations in SPM using a macroscopic anatomical parcellation of the MNI MRI single-subject brain. *NeuroImage* 15, 273–289.

Van Veen, B. D., van Drongelen, W., Yuchtman, M., and Suzuki, A. (1997). Localization of brain electrical activity via linearly constrained minimum variance spatial filtering. *IEEE Trans. Biomed. Eng.* 44, 867–880.

Watson, C. C., Newport, D. F., Casey, M. E., DeKemp, R. A., Beanlands, R. S., and Schmand, M. (1997). Evaluation of simulation-based scatter correction for 3D PET cardiac imaging. *IEEE Trans. Nucl. Sci.* 44, 90–97.

Weinhard, K. (1998). "Applications of 3D PET," in *The Theory and Practice of 3D PET*, ed. B. Bendriem (Boston: Kluwer Academic Publishers), 133–167.

Welsh, K., Butters, N., Hughes, J., Mohs, R., and Heyman, A. (1991). Detection of abnormal memory decline in mild cases of Alzheimer's disease using CERAD neuropsychological measures. *Arch. Neurol.* 48, 278–281.

Welsh, K. A., Butters, N., Mohs, R. C., Beekly, D., Edland, S., Fillenbaum, G., et al. (1994). The consortium to establish a registry for Alzheimer's disease (CERAD). Part V. A normative study of the neuropsychological battery. *Neurology* 44, 609–614.

Wilkins, C. H., Schindler, S. E., and Morris, J. C. (2020). Addressing health disparities among minority populations: why clinical trial recruitment is not enough. *JAMA Neurol.* 77, 1063–1064.

Wilson, A. A., Garcia, A., Jin, L., and Houle, S. (2000). Radiotracer synthesis from [(11)C]-iodomethane: a remarkably simple captive solvent method. *Nucl. Med. Biol.* 27, 529–532.

Wolk, D. A., Price, J. C., Saxton, J., Snitz, B., James, J. A., Lopez, O. L., et al. (2009). Amyloid imaging in mild cognitive impairment subtypes. *Ann. Neurol.* 65, 557–568.

Wong, N. D., Lopez, V. A., Roberts, C. S., Solomon, H. A., Burke, G. L., Kuller, L., et al. (2010). Combined association of lipids and blood pressure in relation to incident cardiovascular disease in the elderly: the cardiovascular health study. *Am. J. Hypertens.* 23, 161–167.

Zhou, Y., Yu, F., Duong, T. Q., and The Alzheimer's Disease Neuroimaging Initiative (2015). White matter lesion load is associated with resting state functional MRI activity and amyloid PET but not FDG in mild cognitive impairment and early Alzheimer's disease patients. *J. Magn. Reson. Imaging* 41, 102–109.

Zlokovic, B. V. (2011). Neurovascular pathways to neurodegeneration in Alzheimer's disease and other disorders. *Nat. Rev. Neurosci.* 12, 723–738.

Conflict of Interest: The authors declare that the research was conducted in the absence of any commercial or financial relationships that could be construed as a potential conflict of interest.

Publisher's Note: All claims expressed in this article are solely those of the authors and do not necessarily represent those of their affiliated organizations, or those of the publisher, the editors and the reviewers. Any product that may be evaluated in this article, or claim that may be made by its manufacturer, is not guaranteed or endorsed by the publisher.

frontiers in Aging Neuroscience

CLINICAL TRIAL
published: 07 October 2021
doi: 10.3389/fnagi.2021.703691

Mechanistic Effects of Aerobic Exercise in Alzheimer's Disease: Imaging Findings From the Pilot FIT-AD Trial

Fang Yu[1,2]*, *Michelle A. Mathiason*[2], *SeungYong Han*[1], *Jeffrey L. Gunter*[3], *David Jones*[3], *Hugo Botha*[3] and *Clifford Jack Jr.*[3]

[1] Arizona State University Edson College of Nursing and Health Innovation, Phoenix, AZ, United States, [2] University of Minnesota School of Nursing, Minneapolis, MN, United States, [3] Mayo Clinic Department of Radiology, Rochester, MN, United States

Despite strong evidence from animal models of Alzheimer's disease (AD) supporting aerobic exercise as a disease-modifying treatment for AD, human mechanistic studies are limited with mixed findings. The objective of this pilot randomized controlled trial was to examine the effects of 6-month aerobic exercise on hippocampal volume, temporal meta-regions of interest (ROI) cortical thickness, white matter hyperintensity (WMH) volume, and network failure quotient (NFQ), measured with MRI, in community-dwelling older adults with AD dementia. Additionally, the relationships between 6- and 12-month changes in MRI biomarkers and the AD Assessment Scale-Cognition (ADAS-Cog) were examined. Sixty participants were randomized, but one was excluded because baseline MRI failed quality control: 38 randomized to cycling and 21 to stretching. The intervention was moderate-intensity cycling for 20–50 mins, three times a week for 6 months. Control was low-intensity stretching. The study outcomes include hippocampal volume, temporal meta-ROI cortical thickness, WMH volume, and NFQ. Outcomes were measured at baseline, 6 months, and 12 months. The sample averaged 77.3 ± 6.3 years old with 15.6 ± 2.9 years of education and 53% men. Both groups experienced significant declines over 6 months in hippocampal volume (2.64% in cycling vs. 2.89% in stretching) and temporal meta-ROI cortical thickness (0.94 vs. 1.54%), and over 12 months in hippocampal volume (4.47 vs. 3.84%) and temporal meta-ROI cortical thickness (2.27 vs. 1.79%). These declines did not differ between groups. WMH volume increased significantly with the cycling group increasing less (10.9%) than stretching (24.5%) over 6 months ($f = 4.47$, $p = 0.04$) and over 12 months (12.1 vs. 27.6%, $f = 5.88$, $p = 0.02$). NFQ did not change significantly over time. Pairwise correlational analyses showed a significant negative correlation between 6-month changes in hippocampal volume and ADAS-Cog ($r = -0.34$, $p < 0.05$). To conclude, aerobic exercise may reduce the decline in hippocampal volume and temporal meta-ROI cortical thickness during the

OPEN ACCESS

Edited by:
Jiu Chen,
Nanjing Medical University, China

Reviewed by:
Avijit Banik,
Emory University, United States
Patrizia Giannoni,
University of Nîmes, France

***Correspondence:**
Fang Yu
Fang.Yu.2@asu.edu

Received: *30 April 2021*
Accepted: *19 July 2021*
Published: *07 October 2021*

Citation:
Yu F, Mathiason MA, Han S, Gunter JL, Jones D, Botha H and Jack C Jr (2021) Mechanistic Effects of Aerobic Exercise in Alzheimer's Disease: Imaging Findings From the Pilot FIT-AD Trial. Front. Aging Neurosci. 13:703691. doi: 10.3389/fnagi.2021.703691

intervention period, but the effect sizes are likely to be very small and dose-dependent and reverse once the intervention stops. Aerobic exercise is effective on slowing down WMH progression but has no effect on NFQ. Hippocampal atrophy was associated with cognitive decline during the intervention period.

Clinical Trial Registration: www.ClinicalTrials.gov, identifier: NCT01954550.

Keywords: exercise, Alzheimer's disease, dementia, imaging, MRI, hippocampal volume, white matter hyperintensity

INTRODUCTION

Dementia affects 47 million people worldwide and is projected to afflict 150 million by 2050 (International, 2016). Alzheimer's disease (AD) is the most common cause of dementia, accounting for 60–80% of all dementia cases (Alzheimer's Association, 2021). No drugs can yet prevent, slow down, or cure AD, and the current Food and Drug Administration (FDA)-approved treatments don't affect AD pathology (Matsunaga et al., 2019). Even when targeting AD neuropathology of abnormal amyloid-beta (Aβ) and tau [hyperphosphorylated tau (p-tau)], recent promising drug trials continued to fail (Tolar et al., 2020). Reasons for these failures are myriad and likely attributable to the facts that these treatments did not address the multifactorial nature of AD neuropathogenesis; the dominant amyloid hypothesis has limited the investigations of other causative factors of AD; and reliance on AD animal models for treatment discovery overly simplifies the complex nature of human cognition, behaviors, emotions, and disease chronicity (Banik et al., 2015). Hence, mechanistic studies on and beyond Aβ and tau biomarkers in humans are critical for developing disease-modifying treatments in AD.

Over the past two decades, aerobic exercise has emerged as a potential disease-modifying treatment for AD. In AD-transgenic animal models, aerobic exercise has been shown to favorably modify the accumulation, degradation, and removal of Aβ and p-tau as well as other abnormal processes occurring in AD such as neuroinflammation (McGurran et al., 2019; da Costa Daniele et al., 2020). On the molecular level, aerobic exercise was found to stimulate the production and function of brain-derived neurotrophic factors (BDNF). BDNF contributes to neurogenesis (particularly in hippocampi), neuronal survival, and synaptic plasticity and mediates memory improvement (Cotman and Berchtold, 2007). Mechanistic studies of aerobic exercise in humans are limited with mixed findings. Observational studies showed that physical activity or exercise was positively (Frederiksen et al., 2019a; Raichlen et al., 2019), not (Best et al., 2015), or negatively (Wagner et al., 2015) associated with hippocampal volume in cognitively normal adults. Self-reported high-intensity physical activity was associated with lower tau in the cerebrospinal fluid (CSF) among cognitively normal older adults (Baker et al., 2012). Engagement in moderate, but not light or vigorous, physical activity was associated with higher CSF Aβ42 and lower CSF total tau and p-tau in asymptomatic late-middle-aged adults at risk for AD (Law et al., 2018). High level of self-reported physical activity was also associated with lower levels of plasma Aβ (Brown et al., 2013), Positron Emission Tomography-qualified Aβ (Liang et al., 2010; Head et al., 2012; Okonkwo et al., 2014), and PET-quantified tau (Brown et al., 2018) in cognitively intact older adults. In contrast, other studies found no associations between physical activity and PET-quantified in this population (de Souto Barreto et al., 2015) or CSF Aβ (Brown et al., 2017). However, self-reported measures of physical activity were prone to recall errors and biases due to varied interpretations of physical activity levels.

Randomized controlled trials (RCTs) to establish the disease-modifying effects of aerobic exercise are even more limited than observational studies. Using MRI in cognitively normal older adults, some studies reported that aerobic exercise increased prefrontal lobe volume (Tamura et al., 2015), gray and white matter volumes in the anterior cingulate (Colcombe et al., 2006), and hippocampal volume (Erickson et al., 2011; Niemann et al., 2014), but other studies showed no (Best et al., 2015) or detrimental effects on brain and hippocampal volume (Wagner et al., 2015). The latter study, however, was conducted with young men only, had large between-participant variations in hippocampal volume changes, and was a short intervention of 6 weeks (Wagner et al., 2015). In older women with mild cognitive impairment (MCI), 6-month aerobic exercise was found to significantly increase hippocampal volume (ten Brinke et al., 2015). In older adults with MCI or mild AD dementia, 26-week aerobic exercise reduced hippocampal atrophy (hippocampal volume in the intervention group decreased 0.8% vs. 1.6% in the control group) (Morris et al., 2017). In older adults with mild-to-moderate AD dementia, 16-week aerobic exercise had no effects on hippocampal volume (Frederiksen et al., 2018), CSF Aβ (Jensen et al., 2016), PET-quantified Aβ (Frederiksen et al., 2019b), and CSF tau (Jensen et al., 2017). Furthermore, emerging findings suggest that aerobic exercise may improve cortical thickness (Bae et al., 2020), functional connectivity (Boa Sorte Silva et al., 2020), and white matter hyperintensity (WMH) (Graff-Radford et al., 2019). Together, these findings suggest the need to examine whether and how aerobic exercise may modify limbic neurodegeneration in humans.

The objective of this pilot RCT, the FIT-AD Trial, was to examine the effects of 6-month aerobic exercise on hippocampal volume, temporal meta-regions of interest (ROI) cortical thickness, WMH volume, and network failure quotient (NFQ) in community-dwelling older adults with mild-to-moderate AD dementia. FIT-AD stands for Functional Impact of aerobic exercise Training in Alzheimer's Disease. We hypothesized that intervention participants will have a smaller decrease in hippocampal volume, cortical thickness, and NFQ and a smaller

increase in WMH volume over 6 and 12 months in comparison to stretching controls. Further, we examined the correlations of the longitudinal changes of these MRI biomarkers and cognition over 6 and 12 months.

MATERIALS AND METHODS

Design

The FIT-AD Trial was a pilot RCT that followed the CONSORT guideline with its CONSORT checklist (Eldridge et al., 2016) provided in the **Supplementary Table**. It first qualified participants based on their eligibility for participating in the exercise interventions. Those who met the eligibility criteria were then approached for their interest in volunteering for the MRI component of the trial, and, if interested, assessed for MRI eligibility. Randomization was performed at the main study level (not the MRI eligibility level) to allocate participants to 6-month intervention (moderate-intensity cycling) or control (low-intensity stretching exercise) for 20–50 mins per session, three times a week on a 2:1 ratio with three age strata (66–75, 76–85, and 85+ years of age). Allocation was generated and concealed to all data collectors and investigators except for the biostatistician. MRI was completed at baseline before randomization and at 6 and 12 months. The biostatistician generated the randomization sequence that was sequentially concealed in an opaque envelop. Once a participant was enrolled, the study interventionist opened the envelop to reveal the group assignment of a participant. This trial was approved by the University of Minnesota's Institutional Review Board (IRB: #1306M35661). The detailed study protocol was published previously (Yu et al., 2014).

Setting

MRI was conducted using 3 Tesla (3T) Siemens Trio system (Siemens, Erlangen, Germany) at the university Center for Magnetic Research and Resources. The MRI protocol was set up and qualified on site by our MRI team located at the Mayo Clinic Aging and Dementia Imaging Research (ADIR) Lab. All scans were securely transmitted to the ADIR lab for evaluation of protocol compliance, scan quality, medical abnormality, and study eligibility. All MRI personnel were blinded to participant group assignment. Any issues were communicated and resolved accordingly. Exercises were delivered in a Young Men's Christian Association gym or the lounge of a senior community.

Participants

Participants were first qualified for the FIT-AD Trial. Community-dwelling older adults, who had a clinical diagnosis of AD dementia, were 66 years old and older, and spoke English were potentially eligible if they scored 15–26 on the Mini-Mental State Examination (MMSE) and 0.5–2 on Clinical Dementia Rating (CDR), had medical clearance for exercise and MRI, and were stable on AD drugs >1 month if prescribed. Potential participants were excluded if their resting heart rate was $\leq$50 or $\geq$100 beats per minute, had neurologic, psychiatric disorders, alcohol/chemical dependency that explained their dementia, exercise contraindications, new symptoms or diseases that had not been evaluated by their providers, and abnormal findings from the symptom-limited cycler-ergometer test. This study was powered on the primary cognitive outcome, not the MRI outcomes (Yu et al., 2014).

The inclusion criteria for the MRI component included consent to volunteer for the MRI and passed MRI safety screening. Participants were excluded from both the MRI component and the main study if MRI showed abnormality (normal pressure hydrocephalus, brain tumor, subdural hematoma, significant posttraumatic encephalomalacia, or one or more large hemispheric infarctions).

A variety of strategies were used for recruitment such as Alzheimer's Association's events, referrals, and flyer/brochure distributions. Recruitment started in March 2014 and ended in March 2019, and the last follow-up was completed in October 2019. Participants were screened through (1) phone screen; (2) in-person interview (consent, MMSE, CDR); (3) medical clearance (exercise/MRI safety); and (4) symptom-limited peak cycle-ergometer test (unknown heart conditions) and MRI if qualified. After completing baseline data collection, participants were enrolled and started their assigned exercise within a week (Yu et al., 2014).

Intervention

The target intervention was supervised, individualized, moderate-intensity cycling on recumbent stationary cycles for 50 mins a session, three times a week, after an adjustment period.

Moderate intensity was prescribed as 65–75% of heart rate reserve (HRR) and 12–14 on the 6–20 Borg Ratings of Perceived Exertion (RPE) scale. The adjustment period was essential to safely progress participants to the target intensity and session duration over time. Hence, the intervention sessions started at a lower than the target dose (50–55% of HRR or RPE 9–11 for 20 mins) in the first week. The session intensity and duration were alternately increased by 5% of HRR (1-point on RPE) or 5-min duration as tolerated over sessions to eventually reach the target dose of 65–75% of HRR or RPE 12–14 for 50 mins a session. The adjustment period lasted for an average of 6–8 weeks. Each session also included a 5-min cardiac warm-up and a 5-min cardiac cool-down before and after the prescribed cycling dose for the session. The control exercise was seated low-intensity stretching at <20% of HRR and RPE 9 with its frequency and session duration matched to those of cycling. The total duration of the exercise programs, including the adjustment period, was 6 months (72 total sessions). A Master's-prepared interventionist supervised every session at no more than 1:3 interventionist-to-participants ratio and monitored heart rate and RPE every 5 mins, blood pressure every 10–15 mins, and overexertion signs and symptoms (Yu et al., 2014).

Outcomes

The outcomes included hippocampal volume, temporal meta-ROI cortical thickness, WMH volume from structural MRI, and NFQ from the resting state functional MRI (rs-fMRI). The protocol for the anatomic sequences and the study data extracted from each sequence were as follows: magnetization prepared rapid gradient echo imaging (MPRAGE) for measuring ROI-wise brain volumes and cortical thickness, axial T2 star

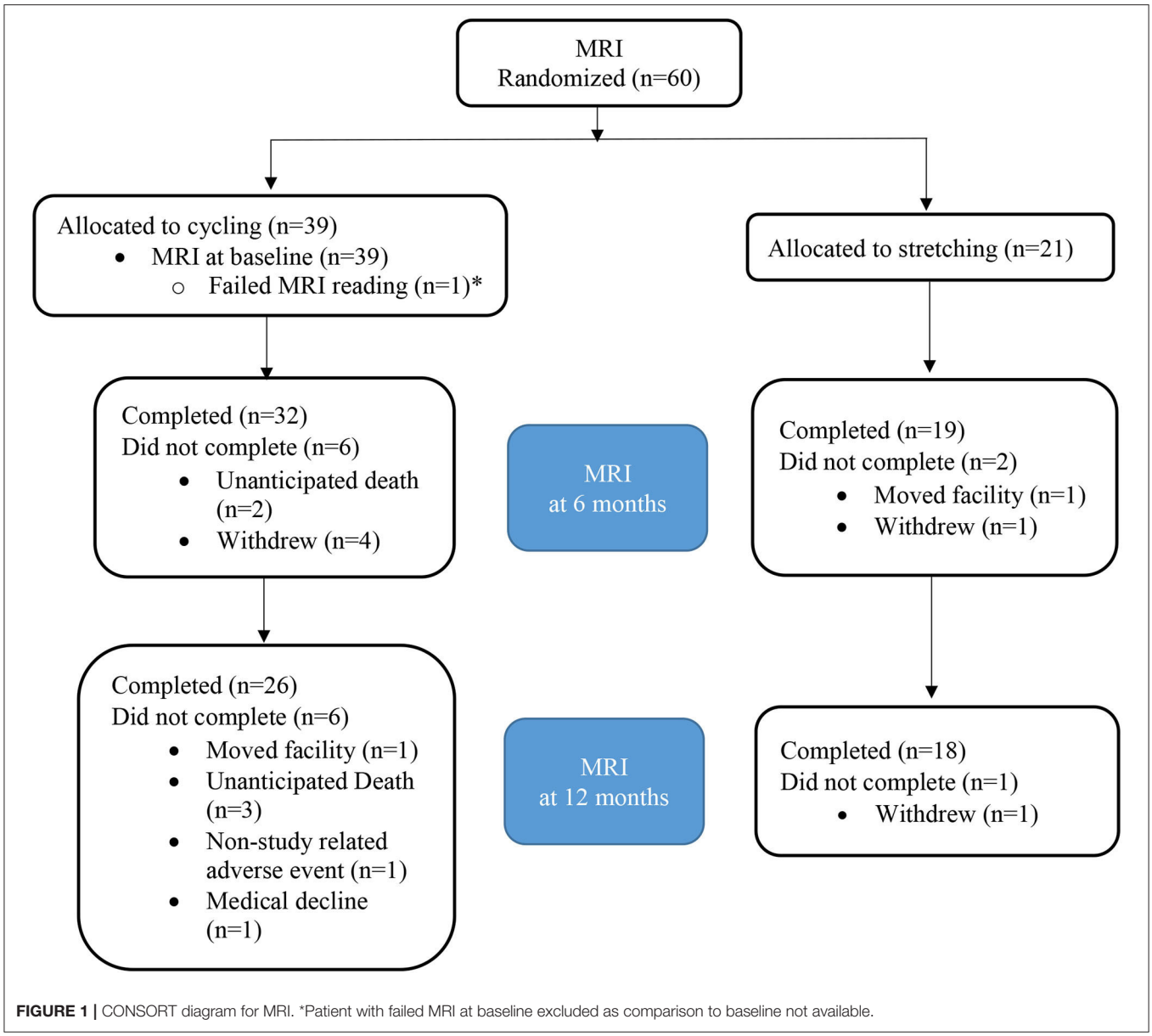

FIGURE 1 | CONSORT diagram for MRI. *Patient with failed MRI at baseline excluded as comparison to baseline not available.

for assessing cerebral micro hemorrhages, T2 fluid-attenuated inversion recovery (FLAIR) for assessing cerebrovascular disease, axial diffusion-weighted imaging (DWI) for assessing acute hemorrhage, and axial multiband fMRI for assessing regional brain perfusion.

Hippocampal volume and cortical thickness of temporal meta-ROI (entorhinal cortex, fusiform, inferior temporal, and middle temporal gyri) (Jack et al., 2017) as shown in **Figure 1** were determined using FreeSurfer (v5.3) (Fischl and Dale, 2000; Fischl et al., 2002). Volume/thickness values were generated for 122 ROIs for each scan. ROI values for hippocampal volume from right and left hemispheres were combined. Global cerebral WMH volume was measured from FLAIR images using a semiautomated segmentation algorithm developed at ADIR (Graff-Radford et al., 2019).

NFQ was calculated from rs-fMRI, following the method described in Wiepert et al. (2017). rs-fMRI data were preprocessed by applying slice timing correction, de-spiking, intra-series motion correction, and simultaneous band pass filtering and nuisance regression. Prior to band pass and nuisance regression steps, a mean-over-time fMRI (3D) volume is created and co-registered with a T1-weighted (T1w) MRI for the same subject. Each T1w image has been processed to create tissue probability maps *via* SPM12 unified segmentation. Additionally, atlases included in the Mayo Clinic Adult Lifespan Template are warped into the space of each T1w image using ANTs registration. Using the EPI-to-T1 registration parameters, atlas parcellations and tissue probability estimates were propagated into space of the fMRI series. Nuisance covariates included intra-series motion

parameters and first derivatives thereof as well as time series of mean signal in white matter, CSF, and a global signal region. Estimates of local co-activation within functional atlas regions and correlation between regions are combined to calculate the NFQ.

Cognition was measured with the AD Assessment Scale-Cognition (ADAS-Cog). The ADAS-Cog is the most widely used measure of global cognition in AD drug RCTs and assesses orientation, memory, recall, language, and praxis. Its total score is 0–70 with higher scores indicating worse cognitive function. The interrater reliability of ADAS-Cog was 0.65–0.99 and test-retest reliability was 0.51–1.0 (Rosen et al., 1984).

Covariates included demographics (age, sex, and education) collected from interviews. Dementia stage was determined as mild stage if MMSE was $\geq$18 and moderate stage if MMSE <18. Exercise adherence was calculated as the percent of attended sessions and the percent of attended sessions that met session intensity and duration goals. Per-protocol adherence was defined as attending >70% sessions and >70% attended sessions met session intensity and duration prescription.

Statistical Analyses

Baseline demographics and characteristics were summarized using standard descriptive statistics. Continuous variables were tested between groups using *t*-tests and categorical variables were tested using χ^2 unless expected cell counts were small, in which case Fischer exact tests were used. Changes at 6 months and at 12 months from baseline were tested using one-way ANCOVA within each group and between groups, following intention-to-treat. In addition, pairwise correlation analyses were conducted to examine the associations of the longitudinal changes in the MRI biomarkers and cognition over 6 and 12 months. Statistical analysis was completed using SAS version 9.4 and $p < 0.05$ was considered statistically significant.

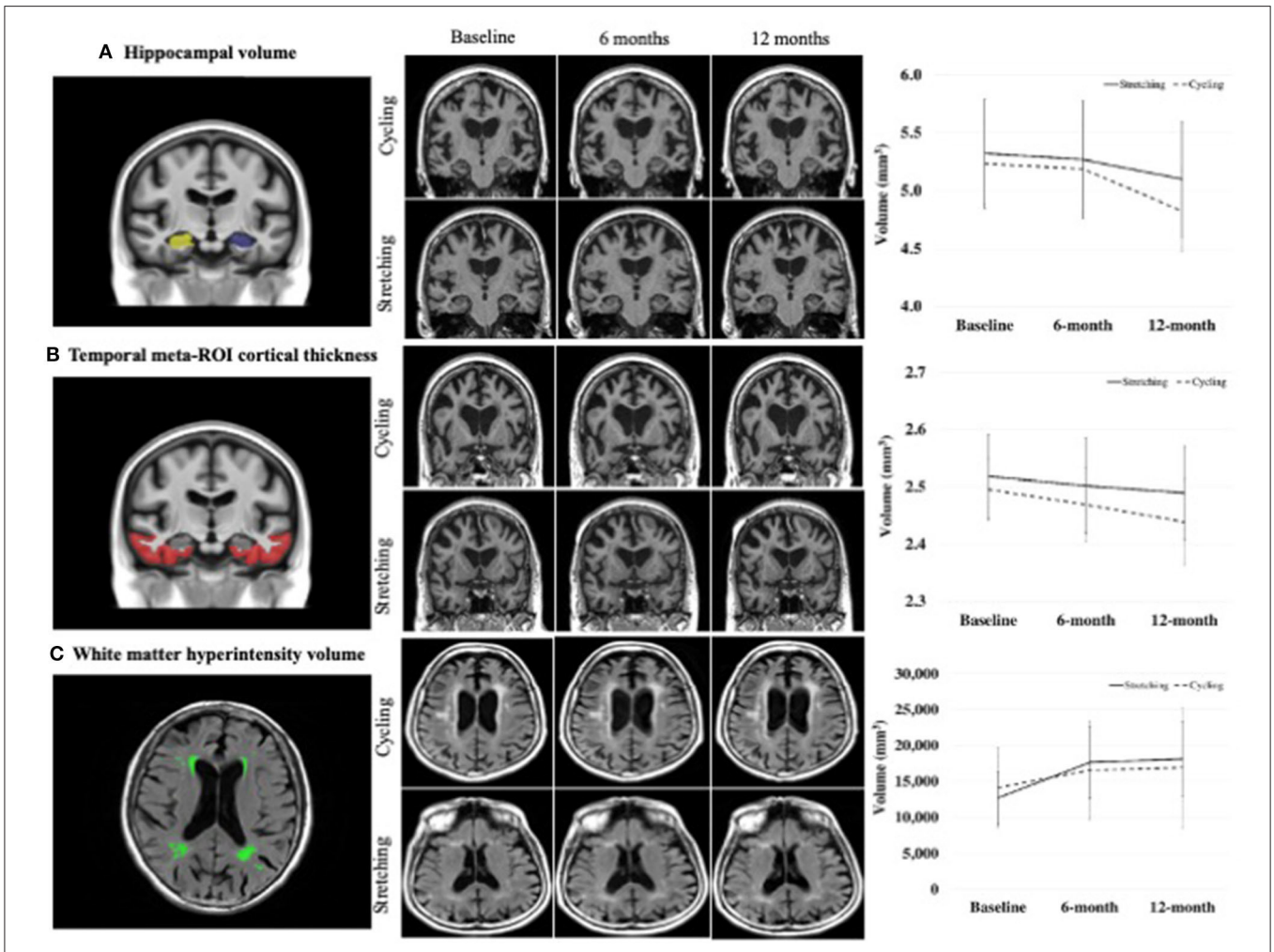

FIGURE 2 | Comparison of changes in MRI biomarkers between groups.

RESULTS

Sixty participants were qualified for the MRI component. One MRI scan at baseline did not meet quality control and was excluded. Among the 59 enrolled participants, 38 were randomized to the intervention group and 21 to the control group (**Figure 2**). The attrition rate was 13.5% at 6 months (15.8 vs. 9.5% for the intervention vs. control group) and 23.7% at 12

TABLE 1 | Characteristics of the study MRI sample at baseline ($n = 59$).

	Overall ($n = 59$) Mean (SD) or n (%)	Cycling ($n = 38$) Mean (SD) or n (%)	Stretching ($n = 21$) Mean (SD) or n (%)	t or χ^{2*}	p
Demographics					
Age, years	77.3 (6.3)	77.2 (6.3)	77.4 (6.5)	0.16	0.876
Sex				1.22	0.268
Male	31 (53%)	22 (58%)	9 (43%)		
Female	28 (47%)	16 (42%)	12 (57%)		
Race/Ethnicity				FET	0.041
Non-Hispanic White	56 (95%)	38 (100%)	18 (86%)		
Hispanic White	2 (3%)	0	2 (10%)		
Black or African American	1 (2%)	0	1 (5%)		
Education, years completed	15.6 (2.6)	15.5 (2.4)	15.8 (3)	0.42	0.673
Marital status				FET	0.685
Married	41 (69%)	27 (71%)	14 (67%)		
Divorced	6 (10%)	4 (11%)	2 (10%)		
Widowed	11 (19%)	7 (18%)	4 (19%)		
Live as married	1 (2%)	0 (0%)	1 (5%)		
Never married	0 (0%)	0 (0%)	0 (0%)		
Living arrangement				FET	0.740
Alone	12 (20%)	8 (21%)	4 (19%)		
With spouse/partner only	35 (59%)	23 (61%)	12 (57%)		
With spouse/partner and other	5 (8%)	2 (5%)	3 (14%)		
With family	7 (12%)	5 (13%)	2 (10%)		
Other	0 (0%)	0 (0%)	0 (0%)		
Clinical indicators					
Dementia severity (MMSE)	21.7 (3.2)	21.5 (3.5)	22.2 (2.7)	0.87	0.390
Body Mass Index (BMI)	27.4 (4.7)	27.2 (4.4)	27.7 (5.3)	0.34	0.736
AD medication				0.44	0.508
Any AD medication	36 (61%)	22 (58%)	14 (67%)		
Not used	23 (39%)	16 (42%)	7 (33%)		
# comorbidities	6 (1.9)	6.3 (1.7)	5.5 (2)	−1.63	0.110
NPI-Q symptom presence	3.4 (2.1)	3.8 (2.0)	2.8 (2.2)	−1.67	0.100
NPI-Q severity	5.1 (3.8)	5.7 (3.7)	4.0 (3.7)	−1.66	0.102
NPI-Q caregiver distress	7.1 (5.7)	7.7 (5.0)	6.0 (6.9)	−1.10	0.274
ADL (DAD percent score)	76.9 (16.3)	76.7 (13.0)	77.3 (21.2)	0.12	0.906
Premorbid intellect (WTAR)	35.2 (10.7)	35.9 (9.4)	33.9 (12.8)	−0.72	0.476
Attrition					
6-month attrition	8 (13.5%)	6 (15.8%)	2 (9.5%)	FET	0.257
12-month attrition	14 (23.7%)	11 (28.9%)	3 (14.3%)	FET	0.338
Exercise adherence					
Sessions attended	55.8 (20.3)	55.5 (19.4)	56.2 (22.4)	0.12	0.906
Attended session meeting prescription	75 (23)	70 (23)	88 (19)	3.06	0.003
Per protocol	32 (54%)	18 (47%)	14 (67%)	2.03	0.154
MRI measures					
Hippocampal volume	5.266 (1.090)	5.236 (1.099)	5.320 (1.099)	0.08	0.780
AD-signature cortical thickness	2.504 (0.170)	2.495 (0.170)	2.518 (0.172)	0.24	0.629
WMH volume	13,608 (14,710)	14,122 (17,321)	12,679 (8,432)	0.13	0.722
NFQ	0.525 (0.221)	0.550 (0.204)	0.480 (0.247)	1.36	0.249

**FET, Fisher Exact Test, if expected cell counts ≤ 5; AD, Alzheimer's disease; DAD, disability in Alzheimer's Disease; MMSE, mini-mental state examination; NPI-Q, neuropsychiatric inventory-caregiver; WTAR, Wechsler Test of Adult Reading.*

TABLE 2 | Adjusted 6- and 12-month Changes in Imaging Biomarkers.

Measure	Cycling		Stretching		Between-group difference
	Mean (SD)	*p* (from baseline)	Mean (SD)	*p* (from baseline)	*p*
6-month changes					
Hippocampal volume	−0.139 (0.198)	0.001*	−0.155 (0.142)	0.001*	0.759
Temporal meta–ROI cortical thickness	−0.024 (0.040)	0.002*	−0.039 (0.047)	0.001*	0.156
WMH volume	1534 (2270)	0.001*	3381 (3612)	0.001*	0.030*
NFQ	0.029 (0.258)	0.531	0.038 (0.247)	0.517	0.687
12-month changes					
Hippocampal volume	−0.227 (0.185)	0.001*	−0.201 (0.142)	0.001*	0.886
Temporal meta-ROI cortical thickness	−0.057 (0.057)	0.001*	−0.045 (0.053)	0.002*	0.936
WMH volume	1829 (2185)	0.001*	3764 (3348)	0.001*	0.015*
NFQ	−0.057 (0.266)	0.285	0.079 (0.357)	0.377	0.174

*$p < 0.05$.

months (28.9 vs. 14.3% for the intervention vs. control group; **Table 1**), respectively.

Overall, the participants were 77.3±6.3 years old and had 15.6±2.9 years of education with 53% male and 95% non-Hispanic white. The two groups did not differ except that the intervention groups were all white (**Table 1**).

The 6- and 12-month within-group changes in hippocampal volume, temporal meta-ROI cortical thickness, and WMH volume were statistically significant for both the cycling and stretching groups, but not in NFQ (**Table 2**). From baseline to 6 months, hippocampal volumes decreased 2.64% in the cycling group vs. 2.89% in the stretching group, temporal meta-ROI cortical thickness decreased 0.94% in cycling and 1.54% in stretching, and WMH volume increased 10.94% in cycling and 24.54% in stretching. From baseline to 12 months, hippocampal volumes decreased 4.47% in the cycling group vs. 3.84% in the stretching group, temporal meta-ROI cortical thickness decreased 2.27% in cycling and 1.79% in stretching, and WMH volume increased 12.08% in cycling and 27.59% in stretching.

The 6-month and 12-month between-group changes in hippocampal volume, temporal meta-ROI cortical thickness, and NFQ were not statistically significant. The 6- and 12-month changes in WMH volume were statistically significant, favoring the cycling group (**Table 2**).

The results of pairwise correlation analyses showed a significant negative correlation between 6-month changes in hippocampal volume and ADAS-Cog ($r = -0.35$, $p < 0.05$). The 12-month changes in hippocampal volume and ADAS-Cog were not significant (**Table 3**). The 6- and 12-month changes in hippocampal volume and temporal meta-ROI cortical thickness were significant ($r = 0.38$ and 0.45 respectively, $p < 0.01$) and 6-month changes in cortical thickness and WMH volume ($r = -0.37$, $p < 0.01$). However, the 6- and 12-month changes in temporal meta-ROI, WMH volume, and NFQ were not significantly associated with the 6- and 12-month changes in ADAS-Cog (**Table 3**).

TABLE 3 | Pairwise correlation coefficients between changes in MRI biomarkers and changes in cognition over 6 and 12 months.

	(1)	(2)	(3)	(4)	(5)
6-month changes in:					
(1) ADAS-Cog	1.00				
(2) Hippocampal volume	−0.34*	1.00			
(3) Cortical thickness	−0.15	0.38**	1.00		
(4) WMH volume	−0.22	−0.09	−0.37**	1.00	
(5) Network failure quotient	0.09	0.06	0.03	−0.11	1.00
12-month changes in:					
(1) ADAS-Cog	1.00				
(2) Hippocampal volume	−0.21	1.00			
(3) Cortical thickness	−0.21	0.45**	1.00		
(4) WMH volume	−0.07	−0.03	−0.19	1.00	
(5) Network failure quotient	0.19	0.04	−0.13	0.14	1.00

*$p < 0.05$; **$p < 0.01$; two tailed; ADAS-Cog, Alzheimer's disease assessment scale-cognition.

DISCUSSIONS

The disease-modifying potential of aerobic exercise for AD has been well-supported in animal research, showing that exercise increases BDNF and reduces AD amyloid plaques and neurofibrillary tangles (McGurran et al., 2019; da Costa Daniele et al., 2020). However, mechanistic studies of effects of aerobic exercise in humans are limited, particularly in older adults with AD dementia, using MRI. An important feature of this study was that the diagnosis of AD dementia was based on clinical criteria and was not verified by biomarkers. Therefore, it is possible that AD played minimal to no role in the cognitive presentation of some participants. Our findings show that hippocampal volume and temporal meta-ROI cortical thickness decreased over 6 and 12 months. The decreases were smaller in the cycling group

than the stretching group over 6 months (2.64 vs. 2.89% for hippocampal volume; 0.94 vs. 1.54% for temporal meta-ROI cortical thickness), but greater over 12 months (4.47 vs. 3.84% for hippocampal volume; 2.27 vs. 1.79% for temporal meta-ROI cortical thickness). The between-group differences did not reach statistical significance. We further found that NFQ did not differ within- or between-groups over 6 and 12 months. In contrast, there are significant within- and between-group differences in WMH volume with the cycling group experiencing substantial less WMH volume increases over both 6 and 12 months. There was a significant negative correlation between 6-month changes in hippocampal volume and ADAS-Cog.

Our findings on hippocampal volume and temporal meta-ROI cortical thickness are consistent with the literature. An important reason for our findings and similar findings that failed to show significant effects of aerobic exercise on these variables is the small detectable changes (Villemagne et al., 2013). For example, the mean annualized rate of hippocampal atrophy was 3.5–3.98% or 1.75–1.99% over 6 months in older adults with AD dementia (Jack et al., 2000). Our participants showed greater 6-month decreases in hippocampal volume (2.64% in the cycling group and 2.89% in the stretching group) than expected (Jack et al., 2000; Morris et al., 2017). In a recent study, aerobic exercise was reported to likely attenuate hippocampal volume decline (0.8% in the intervention group vs. 1.6% in the control group) (Morris et al., 2017). While our cycling group also showed a smaller decline, the between-group difference is smaller (0.23%) than that (0.8%) reported in the other trial (Morris et al., 2017). Similar small detectable changes in PET-quantified brain Aβ have also been reported (Villemagne et al., 2013). In addition, we found a significant negative correlation between 6-month changes in hippocampal volume and ADAS-Cog, suggesting that hippocampal atrophy was significantly associated with cognitive decline during the intervention period. This finding further supports hippocampal atrophy as a potential biological mechanism mediating intervention effects. Together, these results explain the inconsistent and negative results from RCTs because these RCTs including ours are usually not powered to detect such small changes in biomarkers. Future RCTs with large sample sizes and powered on biomarkers such as hippocampal volume are needed to truly establish the disease-modifying abilities of aerobic exercise in AD dementia.

Our participants showed that their temporal meta-ROI cortical thickness decreased 0.94% in cycling and 1.54% for the stretching group over the 6-month intervention period, but the between-group differences were not significant. Two recent trials reported that aerobic exercise alone or in combination with cognitive training increased temporal meta-ROI cortical thickness in older adults with preclinical AD (Bae et al., 2020; Um et al., 2020). Our findings further show that over 12 months, temporal meta-ROI cortical thickness decreased 2.27% in the cycling group and 1.79% in the stretching group. These findings indicate that the effects of aerobic exercise on hippocampal volumes and temporal meta-ROI cortical thickness are most likely intervention dependent. Once the intervention stops, the benefits disappear, and the rate of atrophy appears to accelerate in the intervention group. They may also support the hypotheses that the rates of decline in hippocampal volumes and temporal meta-ROI cortical thickness are likely not linear and are heterogeneous as those who declined faster clinically experienced greater decline in hippocampal atrophy (Jack et al., 2000).

Previously, we have reported that our intervention participants had a smaller increase in global cognition as measured by the ADAS-Cog at 6 months (1.0 ± 4.6) than its natural course (3.2 ± 6.3-point increase; $p = 0.001$) (Yu et al., 2021). In this study, we found a significant negative correlation between the 6-month declines in hippocampal volume and the 6-month increases in ADAS-Cog, meaning that hippocampal atrophy was significantly associated with cognitive decline during the intervention period. The 6- and 12-month changes in temporal meta-ROI cortical thickness were significantly associated with the 6- and 12-month changes in hippocampal volume, and 6-month changes in temporal meta-ROI cortical thickness and WMH volume were associated; however, temporal meta-ROI cortical thickness and WMH volume were not associated with ADAS-Cog changes. Together, these findings suggest hippocampal atrophy as a potential biological mechanism mediating intervention effects and aerobic exercise may affect MRI biomarkers differently. Those hypotheses need to be tested in future studies.

Another potential mechanism may play a bigger role in the effect of aerobic exercise: WMH. WMH results from chronic ischemia and is slowly progressive in nature. Aerobic exercise has been postulated as a potential intervention for mitigating WMH progression. Our findings support this postulation and indicate that there are significant within- and between-group differences over both 6 and 12 months with the cycling group experiencing substantial less increases (∼50%) of WMH volume than the stretching group. However, a recent trial in vascular dementia did not find significant between-group differences in WMH volume; instead, a sex effect was identified, showing women in the control group experienced more WMH progression than women in the aerobic exercise group (Dao et al., 2019). Future studies are needed to examine the effects of aerobic exercise on WMH and the moderating/mediating factors.

We did not find any significant within- or between-group differences in NFQ over 6 and 12 months, although NFQ is a sensitive measure for functional connectivity (Wiepert et al., 2017). Previously, functional connectivity has been associated with cognition and multimodal exercise intervention was shown to improve functional connectivity in older adults (Li et al., 2014). Functional connectivity may also mediate the association between aerobic fitness and cognition (Voss et al., 2010). A recent study showed that multimodal exercise improved task-based functional connectivity (Boa Sorte Silva et al., 2020). Collectively, these findings suggest the need for large-scale studies and the use of not only rs-fMRI but also task-based MRI for measuring functional connectivity.

The striking differences in mechanistic findings between animal and human studies and the inconsistent findings in human research can be explained by many methodological factors, but the aerobic exercise dose likely plays a major role. Animal studies commonly employed high "duration of exercise to lifespan," which means high and desired doses were used

and achieved (Brown et al., 2019), while human studies are often limited in doses. Inter-individual differences in humans further affect the severity and progression of degenerative pathology and exercise dose delivery and may have hidden a wide variety of biomarker responses to aerobic exercise when the conventional "between-group difference" analysis was performed (Williamson et al., 2017). Heterogenous aerobic fitness responses to aerobic exercise that have long been recognized in young adults (Lortie et al., 1984; Bouchard and Rankinen, 2001; Hautala et al., 2003; Rose and Parfitt, 2007; Karavirta et al., 2011; Robinson et al., 2017; Hecksteden et al., 2018; Ross et al., 2019) were shown to be more prominent in older adults (Sisson et al., 2009) and demonstrated by our FIT-AD Trial for the first time in older adults with AD dementia (Yu et al., 2020). Moreover, effects of exercise might be obscured by the high nonresponse rates. Compared to the 17–19% aerobic fitness nonresponse rates to aerobic exercise in young adults (Higgins et al., 2015; Gurd et al., 2016), the nonresponse rates were 19.3–44.9% in older adults when nonresponse was defined as no improvement (Sisson et al., 2009) and rose to 63.4% when nonresponse was defined as <5% improvement (Pandey et al., 2015).

The strengths of our study include a rigorous design and implementation following trial guidelines, the objective measurement of delivered exercise doses, high adherence, the match of exercise frequency and duration between groups, and the use of validated outcome measures.

Weaknesses that inform future trial design include the lack of power to detect between-group differences, the inclusion of both mild and moderate stages of AD dementia, and the unequal representation of mild and moderate stages of AD dementia. In addition, environments might have influenced intervention delivery and adherence. Both the YMCA gym and the lounge of the senior community had open floor plan. Although we delivered exercises during the down time at the YMCA gym, the gym was more crowded and nosier than the lounge of the senior community. Last, our study could have been strengthened with a usual care control group to observe the natural course of changes since both exercises appeared to affect the outcomes. The decision of not including usual care was not made lightly and was influenced by multiple factors (e.g., considerations of the effects of attention and social interaction, the feasibility of recruitment, and retention).

To conclude, aerobic exercise may reduce the decline in hippocampal volume and temporal meta-ROI cortical thickness, but the effect sizes are likely to be small and dose-dependent and reverse once intervention stops. Aerobic exercise appears to slow down WMH progression. Hippocampal atrophy was associated with cognitive decline during the intervention period.

DATA AVAILABILITY STATEMENT

The raw data supporting the conclusions of this article will be made available by the authors, without undue reservation.

ETHICS STATEMENT

The studies involving human participants were reviewed and approved by the University of Minnesota's Institutional Review Board. The patients/participants and their surrogates provided their written informed consent to participate in this study.

AUTHOR CONTRIBUTIONS

FY designed and supervised all aspects of the study implementation and drafted the manuscript. CJ designed all aspects of the study related to the MRI, supervised MRI data collections, and contributed to the draft of the manuscript. MM and SH conducted data analyses, developed figures and tables, and contributed to the draft of the manuscript. JG, DJ, and HB analyzed MRI data and contributed to the draft of the manuscript. All authors read and approved the final manuscript.

FUNDING

The research study reported in this publication was supported by the National Institute on Aging of the National Institutes of Health (1R01AG043392-01A1). The CTSI and Center for Magnetic Resonance Resources were supported by the National Institutes of Health National Center for Advancing Translational Sciences of the National Institutes of Health Award Number UL1TR000114 and the National Institute of Biomedical Imaging and Bioengineering Award Number P41 EB1058941, respectively.

ACKNOWLEDGMENTS

We thank the participants and their families for participating in the study and our community partners who helped with recruitment and study implementation. We are indebted to our dedicated staff who implemented the study with the highest quality as possible.

SUPPLEMENTARY MATERIAL

The Supplementary Material for this article can be found online at: https://www.frontiersin.org/articles/10.3389/fnagi.2021.703691/full#supplementary-material

REFERENCES

Alzheimer's Association. (2021). *2021 Alzheimer's Disease Facts and Figures.* Available online at: https://www.alz.org/media/Documents/alzheimers-facts-and-figures-infographic.pdf (accessed April 21, 2021).

Bae, S., Harada, K., Lee, S., Harada, K., Makino, K., Chiba, I., et al. (2020). The effect of a multicomponent dual-task exercise on cortical thickness in older adults

with cognitive decline: a randomized controlled trial. *J. Clin. Med.* 9:1312. doi: 10.3390/jcm9051312

Baker, L. D., Bayer-Carter, J. L., Skinner, J., Montine, T. J., Cholerton, B. A., Callaghan, M., et al. (2012). High-intensity physical activity modulates diet effects on cerebrospinal amyloid-beta levels in normal aging and mild cognitive impairment. *J. Alzheimers Dis.* 28, 137–146. doi: 10.3233/JAD-2011-111076

Banik, A., Brown, R. E., Bamburg, J., Lahiri, D. K., Khurana, D., Friedland, R. P., et al. (2015). Translation of pre-clinical studies into successful clinical trials for alzheimer's disease: what are the roadblocks and how can they be overcome? *J. Alzheimers. Dis.* 47, 815–843. doi: 10.3233/JAD-150136

Best, J. R., Chiu, B. K., Liang Hsu, C., Nagamatsu, L. S., and Liu-Ambrose, T. (2015). Long-term effects of resistance exercise training on cognition and brain volume in older women: results from a randomized controlled trial. *J. Int. Neuropsychol. Soc.* 21, 745–756. doi: 10.1017/S1355617715000673

Boa Sorte Silva, N. C., Nagamatsu, L. S., Gill, D. P., Owen, A. M., and Petrella, R. J. (2020). Memory function and brain functional connectivity adaptations following multiple-modality exercise and mind-motor training in older adults at risk of dementia: an exploratory sub-study. *Front. Aging Neurosci.* 12:22. doi: 10.3389/fnagi.2020.00022

Bouchard, C., and Rankinen, T. (2001). Individual differences in response to regular physical activity. *Med. Sci. Sports Exerc.* 33 (6 Suppl), S446–S451; discussion S452-3. doi: 10.1097/00005768-200106001-00013

Brown, B. M., Peiffer, J., and Rainey-Smith, S. R. (2019). Exploring the relationship between physical activity, beta-amyloid and tau: a narrative review. *Ageing Res. Rev.* 50: 9–18. doi: 10.1016/j.arr.2019.01.003

Brown, B. M., Peiffer, J. J., Taddei, K., Lui, J. K., Laws, S. M., Gupta, V. B., et al. (2013). Physical activity and amyloid-beta plasma and brain levels: results from the Australian Imaging, Biomarkers and Lifestyle Study of Ageing. *Mol. Psychiatry* 18, 875–881. doi: 10.1038/mp.2012.107

Brown, B. M., Rainey-Smith, S. R., Dore, V., Peiffer, J. J., Burnham, S. C., Laws, S. M., et al. (2018). Self-reported physical activity is associated with tau burden measured by positron emission tomography. *J. Alzheimers. Dis.* 63, 1299–1305. doi: 10.3233/JAD-170998

Brown, B. M., Sohrabi, H. R., Taddei, K., Gardener, S. L., Rainey-Smith, S. R., Peiffer, J. J., et al. (2017). Habitual exercise levels are associated with cerebral amyloid load in presymptomatic autosomal dominant Alzheimer's disease. *Alzheimers. Dement.* 13, 1197–1206. doi: 10.1016/j.jalz.2017.03.008

Colcombe, S. J., Erickson, K. I., Scalf, P. E., Kim, J. S., Prakash, R., McAuley, E., et al. (2006). Aerobic exercise training increases brain volume in aging humans. *J. Gerontol. A Biol. Sci. Med. Sci.* 61, 1166–1170. doi: 10.1093/gerona/61.11.1166

Cotman, C. W., and Berchtold, N. C. (2007). Physical activity and the maintenance of cognition: learning from animal models. *Alzheimer's Dement.* 3, S30–S37. doi: 10.1016/j.jalz.2007.01.013

da Costa Daniele, T. M., de Bruin, C P. F., de Matos, R. S., de Bruin, G. S., Junior Maia Chaves, C., and de Bruin, S. V. M. (2020). Exercise effects on brain and behavior in healthy mice, Alzheimer's disease and Parkinson's disease model—a systematic review and meta-analysis. *Behav. Brain Res.* 383:112488. doi: 10.1016/j.bbr.2020.112488

Dao, E., Barha, C. K., Best, J. R., Hsiung, G. Y., Tam, R., and Liu-Ambrose, T. (2019). The effect of aerobic exercise on white matter hyperintensity progression may vary by sex. *Can. J. Aging* 38, 236–244. doi: 10.1017/S0714980818000582

de Souto Barreto, P., Andrieu, S., Payoux, P., Demougeot, L., Rolland, Y., Vellas, B., et al. (2015). Physical activity and amyloid-beta brain levels in elderly adults with intact cognition and mild cognitive impairment. *J. Am. Geriatr. Soc.* 63, 1634–1639. doi: 10.1111/jgs.13530

Eldridge, S. M., Chan, C. L., Campbell, M. J., Bond, C. M., Hopewell, S., Thabane, L., et al. (2016). CONSORT 2010 statement: extension to randomised pilot and feasibility trials. *BMJ* 355:i5239. doi: 10.1136/bmj.i5239

Erickson, K. I., Voss, M. W., Prakash, R. S., Basak, C., Szabo, A., Chaddock, L., et al. (2011). Exercise training increases size of hippocampus and improves memory. *Proc. Natl. Acad. Sci. USA.* 108, 3017–3022. doi: 10.1073/pnas.1015950108

Fischl, B., and Dale, A. M. (2000). Measuring the thickness of the human cerebral cortex from magnetic resonance images. *Proc. Natl. Acad. Sci. USA.* 97, 11050–11055. doi: 10.1073/pnas.200033797

Fischl, B., Salat, D. H., Busa, E., Albert, M., Dieterich, M., Haselgrove, C., et al. (2002). Whole brain segmentation: automated labeling of neuroanatomical structures in the human brain. *Neuron* 33, 341–355. doi: 10.1016/S0896-6273(02)00569-X

Frederiksen, K. S., Gjerum, L., Waldemar, G., and Hasselbalch, S. G. (2019a). Physical activity as a moderator of alzheimer pathology: a systematic review of observational studies. *Curr. Alzheimer Res.* 16, 362–378. doi: 10.2174/1567205016666190315095151

Frederiksen, K. S., Larsen, C. T., Hasselbalch, S. G., Christensen, A. N., Hogh, P., Wermuth, L., et al. (2018). A 16-week aerobic exercise intervention does not affect hippocampal volume and cortical thickness in mild to moderate alzheimer's disease. *Front. Aging Neurosci.* 10:293. doi: 10.3389/fnagi.2018.00293

Frederiksen, K. S., Madsen, K., Andersen, B. B., Beyer, N., Garde, E., Hogh, P., et al. (2019b). Moderate- to high-intensity exercise does not modify cortical beta-amyloid in Alzheimer's disease. *Alzheimers Dement.* 5, 208–215. doi: 10.1016/j.trci.2019.04.006

Graff-Radford, J., Arenaza-Urquijo, E. M., Knopman, D. S., Schwarz, C. G., Brown, R. D., Rabinstein, A. A., et al. (2019). White matter hyperintensities: relationship to amyloid and tau burden. *Brain* 142, 2483–2491. doi: 10.1093/brain/awz162

Gurd, B. J., Giles, M. D., Bonafiglia, J. T., Raleigh, J. P., Boyd, J. C., Ma, J. K., et al. (2016). Incidence of nonresponse and individual patterns of response following sprint interval training. *Appl. Physiol. Nutr. Metab.* 41, 229–234. doi: 10.1139/apnm-2015-0449

Hautala, A. J., Makikallio, T. H., Kiviniemi, A., Laukkanen, R. T., Nissila, S., Huikuri, H. V., et al. (2003). Cardiovascular autonomic function correlates with the response to aerobic training in healthy sedentary subjects. *Am. J. Physiol. Heart Circ. Physiol.* 285, H1747–H152. doi: 10.1152/ajpheart.00202.2003

Head, D., Bugg, J. M., Goate, A. M., Fagan, A. M., Mintun, M. A., Benzinger, T., et al. (2012). Exercise engagement as a moderator of the effects of APOE genotype on amyloid deposition. *Arch. Neurol.* 69, 636–643. doi: 10.1001/archneurol.2011.845

Hecksteden, A., Pitsch, W., Rosenberger, F., and Meyer, T. (2018). Repeated testing for the assessment of individual response to exercise training. *J. Appl. Physiol.* 124, 1567–1579. doi: 10.1152/japplphysiol.00896.2017

Higgins, T. P., Baker, M. D., Evans, S. A., Adams, R. A., and Cobbold, C. (2015). Heterogeneous responses of personalised high intensity interval training on type 2 diabetes mellitus and cardiovascular disease risk in young healthy adults. *Clin. Hemorheol. Microcirc.* 59, 365–377. doi: 10.3233/CH-141857365-77

International, Alzheimer's Disease. (2016). *World Alzheimer Report*. Available online at: https://www.alz.co.uk/research/world-report-2016 (accessed June 1, 2016).

Jack, C. R. Jr., Petersen, R. C., Xu, Y., O'Brien, P. C., Smith, G. E., Ivnik, R. J., et al. (2000). Rates of hippocampal atrophy correlate with change in clinical status in aging and AD. *Neurology* 55, 484–489. doi: 10.1212/WNL.55.4.484

Jack, C. R. Jr., Wiste, H. J., Weigand, S. D., Therneau, T. M., Lowe, V. J., Knopman, D. S., et al. (2017). Defining imaging biomarker cut points for brain aging and Alzheimer's disease. *Alzheimers. Dement.* 13, 205–216. doi: 10.1016/j.jalz.2016.08.005

Jensen, C. S., Portelius, E., Hogh, P., Wermuth, L., Blennow, K., Zetterberg, H., et al. (2017). Effect of physical exercise on markers of neuronal dysfunction in cerebrospinal fluid in patients with Alzheimer's disease. *Alzheimers Dement.* 3, 284–290. doi: 10.1016/j.trci.2017.03.007

Jensen, C. S., Portelius, E., Siersma, V., Høgh, P., Wermuth, L., Blennow, K., et al. (2016). Cerebrospinal fluid amyloid beta and tau concentrations are not modulated by 16 weeks of moderate- to high-intensity physical exercise in patients with Alzheimer disease. *Dement. Geriatr. Cogn. Disord.* 42, 146–158. doi: 10.1159/000449408

Karavirta, L., Hakkinen, K., Kauhanen, A., Arija-Blazquez, A., Sillanpaa, E., Rinkinen, N., et al. (2011). Individual responses to combined endurance and strength training in older adults. *Med. Sci. Sports Exerc.* 43, 484–490. doi: 10.1249/MSS.0b013e3181f1bf0d

Law, L. L., Rol, R. N., Schultz, S. A., Dougherty, R. J., Edwards, D. F., Koscik, R. L., et al. (2018). Moderate intensity physical activity associates with CSF biomarkers in a cohort at risk for Alzheimer's disease. *Alzheimers Dement.* 10, 188–195. doi: 10.1016/j.dadm.2018.01.001

Li, R., Zhu, X., Yin, S., Niu, Y., Zheng, Z., Huang, X., et al. (2014). Multimodal intervention in older adults improves resting-state functional connectivity

between the medial prefrontal cortex and medial temporal lobe. *Front. Aging Neurosci.* 6:39. doi: 10.3389/fnagi.2014.00039

Liang, K. Y., Mintun, M. A., Fagan, A. M., Goate, A. M., Bugg, J. M., Holtzman, D. M., et al. (2010). Exercise and Alzheimer's disease biomarkers in cognitively normal older adults. *Ann. Neurol.* 68, 311–318. doi: 10.1002/ana.22096

Lortie, G., Simoneau, J. A., Hamel, P., Boulay, M. R., Landry, F., and Bouchard, C. (1984). Responses of maximal aerobic power and capacity to aerobic training. *Int. J. Sports Med.* 5, 232–236. doi: 10.1055/s-2008-1025911

Matsunaga, S., Fujishiro, H., and Takechi, H. (2019). Efficacy and safety of cholinesterase inhibitors for mild cognitive impairment:a systematic review and meta-analysis. *J. Alzheimers. Dis.* 71, 513–523. doi: 10.3233/JAD-190546

McGurran, H., Glenn, J. M., Madero, E. N., and Bott, N. T. (2019). Prevention and treatment of alzheimer's disease: biological mechanisms of exercise. *J. Alzheimers Dis.* 69, 311–338. doi: 10.3233/JAD-180958

Morris, J. K., Vidoni, E. D., Johnson, D. K., Van Sciver, A., Mahnken, J. D., Honea, R. A., et al. (2017). Aerobic exercise for Alzheimer's disease: a randomized controlled pilot trial. *PLoS ONE* 12:e0170547. doi: 10.1371/journal.pone.0170547

Niemann, C., Godde, B., and Voelcker-Rehage, C. (2014). Not only cardiovascular, but also coordinative exercise increases hippocampal volume in older adults. *Front. Aging Neurosci.* 6:170. doi: 10.3389/fnagi.2014.00170

Okonkwo, O. C., Schultz, S. A., Oh, J. M., Larson, J., Edwards, D., Cook, D., et al. (2014). Physical activity attenuates age-related biomarker alterations in preclinical AD. *Neurology* 83, 1753–1760. doi: 10.1212/WNL.0000000000000964

Pandey, A., Ayers, C., Blair, S. N., Swift, D. L., Earnest, C. P., Kitzman, D. W., et al. (2015). Cardiac determinants of heterogeneity in fitness change in response to moderate intensity aerobic exercise training: the DREW study. *J. Am. Coll. Cardiol.* 65, 1057–1058. doi: 10.1016/j.jacc.2014.11.062

Raichlen, D. A., Klimentidis, Y. C., Bharadwaj, P. K., and Alexander, G. E. (2019). Differential associations of engagement in physical activity and estimated cardiorespiratory fitness with brain volume in middle-aged to older adults. *Brain Imaging Behav.* 14, 1994–2003. doi: 10.1007/s11682-019-00148-x

Robinson, M. M., Dasari, S., Konopka, A. R., Johnson, M. L., Manjunatha, S., Esponda, R. R., et al. (2017). Enhanced protein translation underlies improved metabolic and physical adaptations to different exercise training modes in young and old humans. *Cell Metab.* 25, 581–592. doi: 10.1016/j.cmet.2017.02.009

Rose, E. A., and Parfitt, G. (2007). A quantitative analysis and qualitative explanation of the individual differences in affective responses to prescribed and self-selected exercise intensities. *J. Sport Exerc. Psychol.* 29, 281–309. doi: 10.1123/jsep.29.3.281

Rosen, W. G., Mohs, R. C., and Davis, K. L. (1984). A new rating scale for Alzheimer's disease. *Am. J. Psychiatry* 141, 1356–1364. doi: 10.1176/ajp.141.11.1356

Ross, R., Goodpaster, B. H., Koch, L. G., Sarzynski, M. A., Kohrt, W. M., Johannsen, N. M., et al. (2019). Precision exercise medicine: understanding exercise response variability. *Br. J. Sports Med.* 53, 1141–1153. doi: 10.1136/bjsports-2018-100328

Sisson, S. B., Katzmarzyk, P. T., Earnest, C. P., Bouchard, C., Blair, S. N., and Church, T. S. (2009). Volume of exercise and fitness nonresponse in sedentary, postmenopausal women. *Med. Sci. Sports Exerc.* 41, 539–545. doi: 10.1249/MSS.0b013e3181896c4e

Tamura, M., Nemoto, K., Kawaguchi, A., Kato, M., Arai, T., Kakuma, T., et al. (2015). Long-term mild-intensity exercise regimen preserves prefrontal cortical volume against aging. *Int. J. Geriatr. Psychiatry* 30, 686–694. doi: 10.1002/gps.4205

ten Brinke, L. F., Bolandzadeh, N., Nagamatsu, L. S., Hsu, C. L., Davis, J. C., Miran-Khan, K., et al. (2015). Aerobic exercise increases hippocampal volume in older women with probable mild cognitive impairment: a 6-month randomised controlled trial. *Br. J. Sports Med.* 49, 248–254. doi: 10.1136/bjsports-2013-093184

Tolar, M., Abushakra, S., and Sabbagh, M. (2020). The path forward in Alzheimer's disease therapeutics: reevaluating the amyloid cascade hypothesis. *Alzheimers. Dement.* 16, 1553–1560. doi: 10.1016/j.jalz.2019.09.075

Um, Y. H., Wang, S. M., Kim, N. Y., Kang, D. W., Na, H. R., Lee, C. U., et al. (2020). Effects of moderate intensity exercise on the cortical thickness and subcortical volumes of preclinical Alzheimer's disease patients: a pilot study. *Psychiatry Investig.* 17, 613–619. doi: 10.30773/pi.2020.0214

Villemagne, V. L., Burnham, S., Bourgeat, P., Brown, B., Ellis, K. A., Salvado, O., Szoeke, C., et al. (2013). Amyloid beta deposition, neurodegeneration, and cognitive decline in sporadic Alzheimer's disease: a prospective cohort study. *Lancet Neurol.* 12, 357–367. doi: 10.1016/S1474-4422(13)70044-9

Voss, M. W., Erickson, K. I., Prakash, R. S., Chaddock, L., Malkowski, E., Alves, H., et al. (2010). Functional connectivity: a source of variance in the association between cardiorespiratory fitness and cognition? *Neuropsychologia* 48, 1394–1406. doi: 10.1016/j.neuropsychologia.2010.01.005

Wagner, G., Herbsleb, M., de la Cruz, F., Schumann, A., Brunner, F., Schachtzabel, C., et al. (2015). Hippocampal structure, metabolism, and inflammatory response after a 6-week intense aerobic exercise in healthy young adults: a controlled trial. *J. Cereb. Blood Flow Metab.* 35, 1570–1578. doi: 10.1038/jcbfm.2015.125

Wiepert, D. A., Lowe, V. J., Knopman, D. S., Boeve, B. F., Graff-Radford, J., Petersen, R. C., et al. (2017). A robust biomarker of large-scale network failure in Alzheimer's disease. *Alzheimers Dement.* 6, 152–161. doi: 10.1016/j.dadm.2017.01.004

Williamson, P. J., Atkinson, G., and Batterham, A. M. (2017). Inter-individual responses of maximal oxygen uptake to exercise training: a critical review. *Sports Med.* 47, 1501–1513. doi: 10.1007/s40279-017-0680-8

Yu, F., Bronas, U. G., Konety, S., Nelson, N. W., Dysken, M., Jack, C. Jr., et al. (2014). Effects of aerobic exercise on cognition and hippocampal volume in Alzheimer's disease: study protocol of a randomized controlled trial (The FIT-AD trial). *Trials* 15:394. doi: 10.1186/1745-6215-15-394

Yu, F., Salisbury, D., and Mathiason, M.A. (2020). Inter-individual differences in the responses to aerobic exercise in Alzheimer's disease: findings from the FIT-AD trial. *J. Sport Health Sci.* 10, 65–72. doi: 10.1016/j.jshs.2020.05.007

Yu, F., Vock, D. M., Zhang, L., Salisbury, D., Nelson, N. W., Chow, L. S., et al. (2021). Cognitive effects of aerobic exercise in Alzheimer's disease: a pilot randomized controlled trial. *J. Alzheimer's Dis.* 80, 233–244. doi: 10.3233/JAD-201100

Author Disclaimer: The content is solely the responsibility of the authors and does not necessarily represent the official views of the National Institutes of Health.

Conflict of Interest: The authors declare that the research was conducted in the absence of any commercial or financial relationships that could be construed as a potential conflict of interest.

Publisher's Note: All claims expressed in this article are solely those of the authors and do not necessarily represent those of their affiliated organizations, or those of the publisher, the editors and the reviewers. Any product that may be evaluated in this article, or claim that may be made by its manufacturer, is not guaranteed or endorsed by the publisher.

frontiers in Aging Neuroscience

ORIGINAL RESEARCH
published: 15 October 2021
doi: 10.3389/fnagi.2021.750154

Medial Temporal Lobe Subregional Atrophy in Aging and Alzheimer's Disease: A Longitudinal Study

*Léa Chauveau[1], Elizabeth Kuhn[1], Cassandre Palix[1], Francesca Felisatti[1], Valentin Ourry[1,2], Vincent de La Sayette[2], Gaël Chételat[1] and Robin de Flores[1]**

[1] U1237 PhIND, Inserm, Caen-Normandie University, GIP Cyceron, Caen, France, [2] U1077 NIMH, Inserm, Caen-Normandie University, École Pratique des Hautes Études, Caen, France

Medial temporal lobe (MTL) atrophy is a key feature of Alzheimer's disease (AD), however, it also occurs in typical aging. To enhance the clinical utility of this biomarker, we need to better understand the differential effects of age and AD by encompassing the full AD-continuum from cognitively unimpaired (CU) to dementia, including all MTL subregions with up-to-date approaches and using longitudinal designs to assess atrophy more sensitively. Age-related trajectories were estimated using the best-fitted polynomials in 209 CU adults (aged 19–85). Changes related to AD were investigated among amyloid-negative (Aβ−) ($n = 46$) and amyloid-positive (Aβ+) ($n = 14$) CU, Aβ+ patients with mild cognitive impairment (MCI) ($n = 33$) and AD ($n = 31$). Nineteen MCI-to-AD converters were also compared with 34 non-converters. Relationships with cognitive functioning were evaluated in 63 Aβ+ MCI and AD patients. All participants were followed up to 47 months. MTL subregions, namely, the anterior and posterior hippocampus (aHPC/pHPC), entorhinal cortex (ERC), Brodmann areas (BA) 35 and 36 [as perirhinal cortex (PRC) substructures], and parahippocampal cortex (PHC), were segmented from a T1-weighted MRI using a new longitudinal pipeline (LASHiS). Statistical analyses were performed using mixed models. Adult lifespan models highlighted both linear (PRC, BA35, BA36, PHC) and nonlinear (HPC, aHPC, pHPC, ERC) trajectories. Group comparisons showed reduced baseline volumes and steeper volume declines over time for most of the MTL subregions in Aβ+ MCI and AD patients compared to Aβ− CU, but no differences between Aβ− and Aβ+ CU or between Aβ+ MCI and AD patients (except in ERC). Over time, MCI-to-AD converters exhibited a greater volume decline than non-converters in HPC, aHPC, and pHPC. Most of the MTL subregions were related to episodic memory performances but not to executive functioning or speed processing. Overall, these results emphasize the benefits of studying MTL subregions to distinguish age-related changes from AD. Interestingly, MTL subregions are unequally vulnerable to aging, and those displaying non-linear age-trajectories, while not damaged in preclinical AD (Aβ+ CU), were particularly affected from the prodromal stage (Aβ+ MCI). This volume decline in hippocampal substructures

OPEN ACCESS

Edited by:
Yong Liu,
Beijing University of Posts and Telecommunications (BUPT), China

Reviewed by:
Jean-Vianney Haure-Mirande, Icahn School of Medicine at Mount Sinai, United States
Jianxiong Zeng, Kunming Institute of Zoology, China

***Correspondence:**
Robin de Flores
deflores@cyceron.fr

Received: *30 July 2021*
Accepted: *13 September 2021*
Published: *15 October 2021*

Citation:
Chauveau L, Kuhn E, Palix C, Felisatti F, Ourry V, de La Sayette V, Chételat G and de Flores R (2021) Medial Temporal Lobe Subregional Atrophy in Aging and Alzheimer's Disease: A Longitudinal Study. Front. Aging Neurosci. 13:750154. doi: 10.3389/fnagi.2021.750154

might also provide information regarding the conversion from MCI to AD-dementia. All together, these findings provide new insights into MTL alterations, which are crucial for AD-biomarkers definition.

Keywords: medial temporal lobe (MTL), Alzheimer's disease, aging, episodic memory, structural magnetic resonance imaging, mild cognitive impairment, hippocampus

INTRODUCTION

The hippocampus (HPC), entorhinal cortex (ERC), perirhinal cortex (PRC), and parahippocampal cortex (PHC) are subregions of the medial temporal lobe (MTL) that are critical for several cognitive functions such as declarative memory and spatial navigation (Wixted and Squire, 2011; Raslau et al., 2015; Moscovitch et al., 2016; Baumann and Mattingley, 2021). Importantly, these subregions are altered early and severely in Alzheimer's disease (AD), as they are the primary target of neurofibrillary tangles (Braak and Braak, 1991, 1995; Schöll et al., 2016). In this context, hippocampal atrophy, assessed by structural magnetic resonance imaging (MRI), has been extensively studied in Alzheimer's research and is widely used as a biomarker to monitor *in-vivo* AD-related neurodegeneration (Frisoni et al., 2010; Pini et al., 2016). For example, a study focusing on the HPC reported an annual volume reduction of 1.9 ± 0.9% in patients with AD-dementia, and 1.3 ± 0.9% in patients with mild cognitive impairment (MCI) (Henneman et al., 2009). In addition, hippocampal volumetry might be a relevant tool to predict the conversion to AD-dementia in patients with MCI (Pennanen et al., 2004; Apostolova et al., 2006; Devanand et al., 2007; Henneman et al., 2009; Brueggen et al., 2015). As neuropathological changes are known to start several years before symptom onset, more and more studies have focused on the preclinical stage of AD—defined as amyloid-positive (Aβ+) cognitively unimpaired (CU) individuals (Jack et al., 2018)—(Miller et al., 2013; Fortea et al., 2014; Pegueroles et al., 2017; Pettigrew et al., 2017); findings are sparse with only a few studies showing medial temporal lobe subregional atrophy in Aβ+ compared to amyloid-negative (Aβ−) CU (Wolk et al., 2017; Xie et al., 2020), while others have found no difference (Xie et al., 2019).

Interestingly, MTL subregions are also affected in typical aging, and dissociating normal from early pathological changes is sometimes challenging (Fjell et al., 2014). For example, studies report a decline in HPC and ERC volumes with age (Schuff et al., 1999; Jernigan et al., 2001; Du et al., 2006), and trajectories appear to differ across MTL subregions with linear vs. non-linear atrophy over the whole lifespan (Ziegler et al., 2012; Fjell et al., 2013; de Flores et al., 2015; Daugherty et al., 2016; Hasan et al., 2016; Bussy et al., 2021). Thus, a better understanding of the effects of age on the MTL subregions is essential to define the best candidate to be used as an AD biomarker.

Abbreviations: AD, Alzheimer's disease; BA, Brodmann area; CU, cognitively unimpaired; ERC, entorhinal cortex; HPC, hippocampus (a, anterior; p, posterior); LMM, linear mixed model; MCI, mild cognitive impairment; MRI, magnetic resonance imaging; PHC, parahippocampal cortex; PRC, perirhinal cortex; TIV, total intracranial volume.

To date, most of the investigations on MTL structural alterations were performed using cross-sectional designs and were mainly limited to the HPC and ERC (Juottonen et al., 1998; Du et al., 2001, 2003; Pennanen et al., 2004; Barnes et al., 2009; Wisse et al., 2014; Pini et al., 2016). Given that MTL subregions are affected heterogeneously in AD (Braak and Braak, 1995; Krumm et al., 2016; Xie et al., 2020), longitudinal designs accounting for inter-individual variability and including usually neglected MTL subregions such as the PRC and PHC might enhance the clinical utility of these neurodegeneration biomarkers. In addition, automatic procedures recently emerged to segment MTL subregions from standard T1-weighted MRI scans (Pipitone et al., 2014; Iglesias et al., 2015; Xie et al., 2019), and appear promising in characterizing AD-related changes in clinical routines as MRI images are more accessible compared with other neuroimaging techniques which are more expensive and invasive.

In this context, this study aims to better characterize the structural alterations of MTL subregions in typical aging and across the whole Alzheimer's continuum. For this purpose, we took advantage of the longitudinal T1-weighted MRI data acquired from 209 CU participants covering the adult lifespan and 84 patients with MCI and AD. More precisely, we used a tailored methodology to (i) explore the age-related volume trajectories of MTL subregions over the adult lifespan, (ii) examine the differences in MTL subregional atrophy across the Alzheimer's continuum (encompassing Aβ− CU older adults [i.e., controls], Aβ+ CU older adults, Aβ+ MCI patients, and Aβ+ AD patients), (iii) compare MTL subregional atrophy between MCI-to-AD converters and non-converters patients, and finally, (iv) investigate the associations between the volume of MTL subregions and cognitive performances.

MATERIALS AND METHODS

Participants

All participants in this study were enrolled in the *multi-modal neuroimaging in AD* study (IMAP+) (Caen, France) between the years 2008 and 2016, and some of them were included in previous publications from our lab (La Joie et al., 2013; de Flores et al., 2015; Perrotin et al., 2017). All were right-handed, had at least 7 years of education, and had no history of alcoholism, drug abuse, head trauma, or neurological/psychiatric disorder. The IMAP+ study was approved by a regional ethics committee (Comité de Protection des Personnes Nord-Ouest III) and was registered with ClinicalTrials.gov (number NCT01638949). All participants gave written informed consent to the study before the investigation.

Two hundred and nine CU adults from the ages 19–85 were recruited from the community using flyers and advertisements in local newspapers, and had normal cognitive performances according to age and education level, without memory complaints. Patients were recruited from a local memory clinic and then stratified by a senior neurologist and neuropsychologists according to standard clinical criteria. Thirty-one patients with AD fulfilled the standard National Institute of Neurological and Communicative Disorders and Stroke and the Alzheimer's Disease and Related Disorders Association (NINCDS-ADRDA) clinical criteria for mild to moderate probable AD (McKhann et al., 1984), and 53 patients with MCI satisfied Petersen's criteria (Petersen and Morris, 2005) at baseline. Among the 53 patients with MCI, 19 converted to AD-dementia (updated on October 23, 2020, post-study clinical follow-up = 20.7 ± 22.9 months).

Participants were followed up to 47 months with one to three neuroimaging/cognitive assessments (±18 months apart). Florbetapir-PET scans were available for each individual and Aβ−positivity was defined using a global neocortical standardized uptake value ratio (SUVr) measure. The positivity threshold was calculated as the 99.9th percentile of the distribution among 45 healthy individuals younger than 40, corresponding to a SUVr of 0.99. SUVr images were corrected for partial volume effect using the three-compartment method (Müller-Gärtner et al., 1992). Among the CU aged over 60, 46 were Aβ− and 14 were Aβ+, while 33 MCI and 31 AD patients were Aβ+. Of note, Aβ status was determined using scans acquired at baseline for the vast majority of our population. However, when the SUVr value was not available at baseline but values at following times were below the threshold, we considered the individual as Aβ− ($n = 21$). In addition, apolipoprotein E (*APOE*) genotype was available for 203 of the 209 CU, resulting in 53 ε4 allele carriers and 150 non-carriers.

The demographics of our samples are presented in **Table 1**.

MRI Data Acquisition

Participants were repeatedly scanned with a Philips Achieva 3T camera at the Cyceron Center (Caen, France). Longitudinal T1-weighted anatomical images were acquired using a three-dimensional (3D) fast-field echo sequence (3D-T1-FFE sagittal; SENSE factor =2; repetition time = 20 ms; echo time = 4.6 ms; flip angle = 10°; 180 slices with no gap; slice thickness = 1 mm; field of view = 256 × 256 mm²; in-plane resolution = 1 × 1 mm²).

Automatic Segmentation of Medial Temporal Lobe Subregions

MTL subregions, including the anterior and the posterior hippocampus (aHPC and pHPC, respectively), the ERC, Brodmann areas (BA) 35 and 36—as PRC components –, and the PHC were automatically segmented using the *Automatic Segmentation of Hippocampal Subfields* (ASHS) software (Yushkevich et al., 2015; atlas: ashsT1_atlas_upennpmc_07202018; **Supplementary Figure 1**). This multi-atlas segmentation algorithm has the advantage of accounting for the dura mater confounds and MTL cortex anatomic variability (Xie et al., 2019). Participants with a single neuroimaging assessment (usually baseline) were directly segmented using the standard ASHS-T1 pipeline, while the *Longitudinal Automatic Segmentation of Hippocampal Subfields* (LASHiS) pipeline (Shaw et al., 2020) was used to segment images from participants with longitudinal follow-ups (two or three assessments). This method is directly based on the ASHS algorithm but additionally takes account of the longitudinal aspect of the data by building a single subject template, thus, reducing random errors in the labeling procedure. Rigorous quality control was performed by visually evaluating the segmentation of each subregion for all participants. Failed segmentations were manually edited when feasible (∼30%, for aHPC or pHPC only) or were discarded. Note that for the same individual, some subregions were of adequate quality to be included in analyses while others were not, so the number of subjects for a given MTL subregion was not the same (**Supplementary Tables 2–9**).

The aHPC and pHPC volumes were summed to obtain the volume of the whole HPC, as well as the BA 35 and 36 volumes to estimate the PRC volume. Left and right volumes were averaged to limit the number of analyses. Raw bilateral volumes were then normalized by the total intracranial volume (TIV-calculated as the sum of the volumes of gray matter, white matter, and cerebrospinal fluid using SPM12) to account for inter individual variability in head size (normalized volume raw = volume 100/TIV), and then z-transformed to improve comparability between the subregions. For this transformation, we used (i) data from baseline CU adults under 40 for analyses performed in the context of typical aging and (ii) data from baseline Aβ− CU older adults for analyses performed in the context of pathological aging.

Cognitive Functioning

Participants repeatedly underwent the same neuropsychological exams as described in detail previously (Chételat et al., 2005; Mevel et al., 2013). To obtain robust proxies of cognitive abilities and to minimize the issue of multiple statistical testing, we calculated composite scores reflecting executive functions, processing speed, and episodic memory. Composite scores were derived from individual scores z-transformed using baseline Aβ− CU older adults as the reference since cognition was only investigated in patients. We obtained the processing speed score from the duration of the Trail Making Test (TMT) (Reitan, 1958) part A and the Stroop (1935) color naming. The executive functions score was computed from a flexibility score calculated with the TMT ((part B – part A)/part A) and an inhibition score calculated with the Stroop [(interference – color naming)/color naming]. The episodic memory score averaged the free recalls of the Encoding, Storage, Retrieval (ESR) paradigm (Eustache et al., 1998), the adapted *Batterie d'efficience mentale* (BEM)-144 (Signoret, 1991), and the BEM figure. For all composite scores, higher values indicate better performances. Since some patients failed to complete all the tests, the sample size for a given cognitive domain varies (**Supplementary Table 9**).

TABLE 1 | Demographics of the study sample.

	Adult Lifespan		Alzheimer's continuum			MCI-to-AD	
	CU	CU Aβ−	CU Aβ+	MCI Aβ+	AD Aβ+	Non-converters	Converters
Sex: n_{female}/n_{male}	111/98	26/20	8/6	13/20	13/18	15/19	6/13
Age (years)	46.9 ± 18.6 [19.5, 84.6]	69.3 ± 5.9 [60, 81.4]	73.8 ± 7.2* [61.5, 84.6]	73.9 ± 7.2** [59.9, 86.6]	67.3 ± 9.9 [51.7, 84.1]	73.7 ± 7.1 [58.8, 85.1]	72.5 ± 7.1 [60.7, 85.0]
Education (years)	13.4 ± 3.3 [7, 20]	12.3 ± 3.9 [7, 20]	11.3 ± 3.3 [7, 17]	11.6 ± 4 [6, 20]	10.9 ± 3.2 [6, 20]	10.6 ± 2.9 [6, 17]	12 ± 4.7 [7, 20]
APOE4[a]: $n_{carrier}/n_{non-carrier}$	53/150	–	–	–	–	–	–
Follow-up (months)	18.8 ± 11.2 [0, 47.2]	26.9 ± 11.9 [0, 41.2]	20.7 ± 12.5 [0, 39.8]	18.6 ± 13.1 [0, 40.7]	12.8 ± 9.1 [0, 22.6]	21.4 ± 15.5 [0, 43.9]	22.5 ± 12.9 [0, 37.1]
MMSE[b]	29.2 ± 0.9 [26, 30]	28.7 ± 1.2 [26, 30]	29.3 ± 0.7 [28, 30]	26.8 ± 1.9*** [22, 30]	20 ± 4.9*** [12, 29]	26.9 ± 1.9 [22, 30]	26.3 ± 1.8 [22, 30]
Post-study clinical follow-up (months)	–	–	–	–	–	16.3 ± 21.2 [0, 89.7]	28.3 ± 24.5 [0, 78]

Continuous variables are indicated as follows: mean ± SD [minimum, maximum].

Age, education, MMSE from baseline.

*CU Aβ+, MCI Aβ+, and AD Aβ+ were compared with CU Aβ−; converters were compared with non-converters. Independent two-sample t-test (age), Wilcoxon rank-sum test (education and MMSE), and chi-squared test (sex) were used for statistical comparisons. ***p < 0.001; **p < 0.01; *p < 0.05.*

[a]Missing data for six participants. [b]Missing data for two participants.

AD, patients who met McKhann criteria for probable Alzheimer's disease dementia; APOE, apolipoprotein E; CU, cognitively unimpaired participants; MCI, mild cognitive impairment; MMSE, mini-mental state examination.

Statistical Analyses

All statistical analyses were performed using R (version 4.0.3; R Core Team, 2020). Longitudinal data were analyzed using linear mixed models (LMMs). These models are advantageous in handling within-subject observations, as well as missing data and unbalanced designs (e.g., irregular follow-ups as in the current study). LMMs were fitted to the data with restricted maximum likelihood, using the *lme4* package (Bates et al., 2015). Type III F-tests with Satterthwaite's method for degrees of freedom approximation was used to assess the significance of fixed effects. Effect size estimates of the LMMs were assessed using pseudo-R-squared (Nakagawa et al., 2017). Results were considered significant after Holm's family-wise error rate controlling procedure to account for multiple tests ($p < 0.05$) (Holm, 1979). Model quality was assessed using the *performances* package (Lüdecke et al., 2021), and visual inspection of the residual plots did not reveal any obvious deviations from homoscedasticity or normality.

Age-Related Volume Trajectories Over the Adult Lifespan

Relationships between age and MTL subregional volumes were estimated over the adult lifespan in CU participants aged from 19 to 85 years old. LMMs with polynomials of different orders for the age term were considered to best describe the age-related volume trajectories of MTL subregions. Models were tested from the simplest to the most complex. A model was kept as a candidate when the likelihood ratio test (i.e., testing *n* vs. *n-1* order-polynomial) was simultaneously significant ($p < 0.05$) and when all the coefficients were significant using *t*-statistic ($p < 0.05$). Candidate models were compared using the corrected Akaike Information Criterion (AICc) and the Bayesian Information Criterion (BIC) according to criteria (Burnham and Anderson, 2004). As an exception, LMMs were fitted with maximum likelihood for model comparison (Zuur et al., 2009). More details on the model selection are provided in the **Supplementary Method**. For the nonlinear relationships, the inflections in the smoothed curves were estimated from the place where a change in model estimates switches signs. Separate LMMs with each MTL subregion as dependent variable were computed. Fixed effect terms included *age* as an independent variable and *sex* and *education* as covariates. Intercepts for participants were entered as random effects. Differences related to sex, education level, or *APOE* ε4 gene in age trajectories were also investigated by adding the variable of interest (i.e., *sex*, *education,* or *apoe*) and its interaction with the *age* term as fixed effects.

Structural Alterations Across the Alzheimer's Continuum

Structural alterations of MTL subregions across the Alzheimer's continuum were investigated in 124 participants, pooling CU participants over 60 years of age [both Aβ− ($n = 46$) and Aβ+ ($n = 14$)], as well as Aβ+ MCI ($n = 33$) and AD ($n = 31$) patients. Baseline volume differences were assessed using analyses of covariance (ANCOVAs) with group (ie, Aβ− CU, Aβ+ CU, Aβ+ MCI, and Aβ+ AD) as predictors. To estimate the volume changes over time, LMMs with random intercept and slope per participant were then computed with *group*, *time*, and their interaction as fixed effects. In both ANCOVAs and LMMs, each MTL subregion was entered as a dependent variable in separate models. All models were controlled for *age*, *sex,* and *education*. To compare atrophy across groups, independent *t*-tests adjusted for multiple comparisons using Tukey honestly

significant difference test were used as *post-hoc* comparing estimated marginal means with the *emmeans* package (Lenth et al., 2021).

Volume Comparisons Between Converters and Non-converters

MTL subregional atrophy was compared between 19 MCI-to-AD converters and 34 non-converters. Differences in baseline volumes were investigated using ANCOVAs, and differences in volume decreases using LMMs with by-participant random intercepts. Each MTL subregion was entered as a dependent variable in both types of models. The *group* (i.e., converters or non-converters) was included as predictor in ANCOVAs, and *group*, *time,* and their interaction were included as fixed effects in LMMs. In all models, *post-study clinical follow-up*, *age*, *sex,* and *education* were added as covariates.

Relationships Between Cognitive Functioning and Volume

Associations between the cognitive scores and MTL subregions volume were only investigated in Aβ+ MCI and AD patients to avoid ceiling effects and to get enough variance in the scores. Separate LMMs were conducted for each cognitive score (reflecting speed processing, executive functions, and episodic memory) as a dependent variable and for each MTL subregion as a predictor (i.e., 24 tests). Random effects included subject intercepts. All models were adjusted according to the *group*, *time*, *age*, *sex,* and *education*.

RESULTS

Aging Differently Impairs MTL Subregions Over the Adult Lifespan

Structural trajectories over the adult lifespan of all the considered MTL subregions are displayed in **Figure 1**. All MTL subregions volume were significantly related to age using the best-fitted models [HPC: $F_{(317.89)} = 14.58$, $p < 0.001$; aHPC: $F_{(344.43)} = 8.05$, $p < 0.001$; pHCP: $F_{(316.73)} = 17.49$, $p < 0.001$; ERC: $F_{(309.85)} = 16.37$, $p < 0.001$; PRC: $F_{(318.03)} = 37.23$, $p < 0.001$; BA35: $F_{(290.60)} = 14.11$, $p < 0.001$; BA36: $F_{(339.54)} = 35.04$, $p < 0.001$; PHC: $F_{(370.18)} = 48.41$, $p < 0.001$). Both linear and non-linear age-related trajectories were found. More precisely, the BA 35 and 36, PRC, and PHC volumes were linearly associated with age, a quadratic term better described this relationship between volume and age for the aHCP and ERC, and a cubic term better described this relationship for the HPC and pHPC (**Supplementary Table 1**). The estimation of inflection points suggested that the aHPC volume declined from the age of 47 and the ERC volume from the age of 41. The HPC volume approximately increased at the age of 22 and then decreased at 49. The pHPC volume exhibited stability from the ages 37–44 and then started to decline.

When investigating the sex-related differences, a significant main effect of *sex* was observed for pHPC [$F_{(202.88)} = 7.94$, $p = 0.04$] and PHC [$F_{(204.66)} = 23.38$, $p < 0.001$], suggesting that women have greater volumes than men (**Supplementary Figure 2**, **Supplementary Table 2**). No significant *age* × *sex* interaction was found, suggesting that age trajectories were comparable among men and women (**Supplementary Table 2**). With regard to differences related to *APOE4* or education level, results revealed neither an interaction effect with *age* nor a simple effect of the variable of interest (i.e., *apoe* or *education*) for none of all considered MTL subregions (**Supplementary Tables 3**, **4**).

AD Affects MTL Subregions More Severely in the Advanced Stages of the Continuum

Cross-sectional analyses revealed significant effects of *group* on baseline volume for all MTL subregions [HPC: $F_{(3)} = 19.32$, $p < 0.001$; aHPC: $F_{(3)} = 14.25$, $p < 0.001$; pHPC: $F_{(3)} = 14.04$, $p < 0.001$; ERC: $F_{(3)} = 17.36$, $p < 0.001$; PRC: $F_{(3)} = 7.09$, $p < 0.001$; BA35: $F_{(3)} = 9.16$, $p < 0.001$; BA36: $F_{(3)} = 4.56$, $p = 0.005$; PHC: $F_{(3)} = 3.96$, $p = 0.01$]. As illustrated in **Figure 2**, no significant difference between Aβ− and Aβ+ CU was observed. Aβ+ MCI patients showed significantly smaller HPC, aHPC, pHPC, and ERC volumes compared to Aβ− CU, and to Aβ+ CU. Aβ+ AD patients showed significantly smaller volumes in all MTL subregions compared to Aβ− CU, and to Aβ+ CU. Lastly, Abβ+ AD showed significantly smaller ERC volumes compared to Abβ+ MCI patients. The corresponding statistics are depicted in **Supplementary Table 5**.

For longitudinal analyses, the interaction *group* × *time* was significant for all the LMMs, suggesting that volume decline differs along the Alzheimer's continuum [HPC: $F_{(69.55)} = 11.23$, $p < 0.001$; aHPC: $F_{(85.82)} = 4.46$, $p < 0.01$; pHPC: $F_{(126.55)} = 18.37$, $p < 0.001$; ERC: $F_{(87.62)} = 9.67$, $p < 0.001$; PRC: $F_{(77.39)} = 6.21$, $p < 0.001$; BA35: $F_{(93.93)} = 7.28$, $p < 0.001$; BA36: $F_{(82.10)} = 4.71$, $p < 0.01$; PHC: $F_{(85.39)} = 14.26$, $p < 0.001$]. As illustrated in **Figure 3**, Aβ+ MCI patients showed significantly smaller HPC, aHPC, pHPC, ERC, BA35 and PHC volumes compared to Aβ− CU, and significantly smaller HPC, aHPC and pHPC volumes compared to Aβ+ CU. Aβ+ AD patients showed significantly smaller HPC, pHPC, ERC, PRC, BA35, BA36 and PHC volumes compared to Aβ− CU, and significantly smaller HPC, pHPC, PRC, BA35 and PHC volumes compared to Aβ+ CU. No significant differences between Aβ− and Aβ+ CU or between Aβ+ MCI and AD patients were observed (**Supplementary Table 6**).

Volume Decline in Hippocampal Substructures Differs Between MCI-To-AD Converters and Non-converters

Baseline volumes were not significantly different between MCI-to-AD converters and non-converters for any MTL subregion (**Supplementary Table 7**). However, converters showed significantly steeper volume decrease over time in hippocampal substructures compared to non-converters [HPC: $F_{(56.14)} = 15.09$, $p < 0.001$; aHPC: $F_{(58.21)} = 12.44$, $p < 0.001$ and pHPC: $F_{(56.13)} = 9.28$, $p = 0.003$) (**Figure 4**, **Supplementary Table 8**).

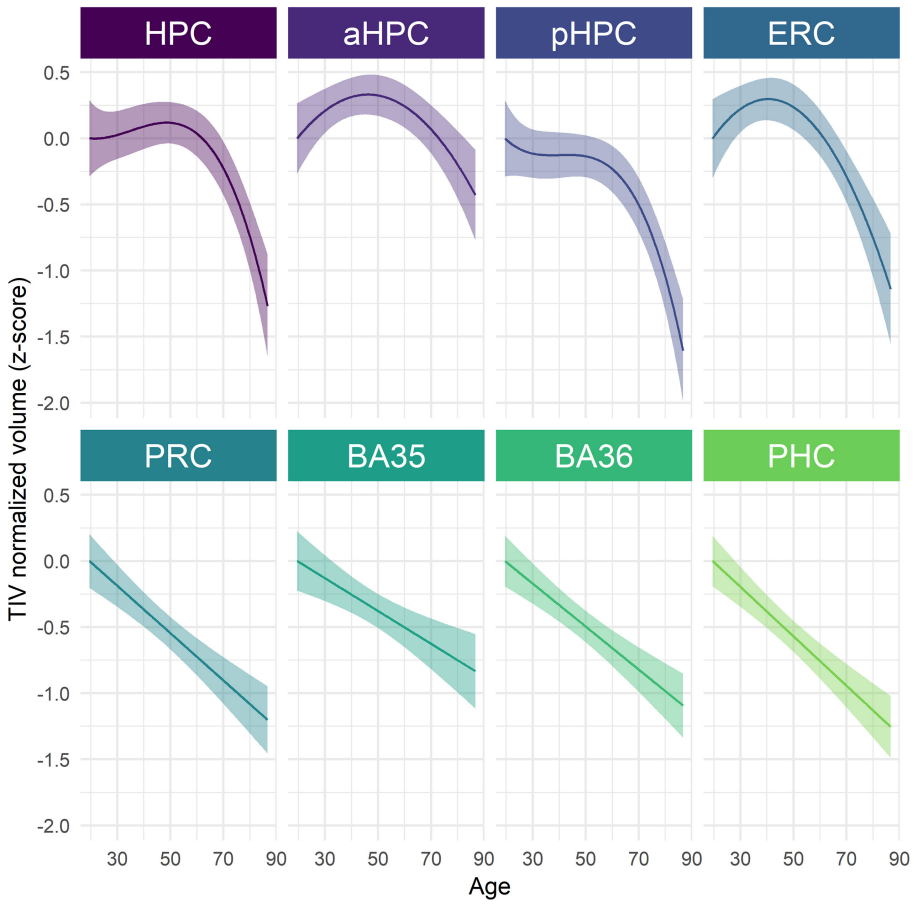

FIGURE 1 | Age-related volume trajectories of MTL subregions over the adult lifespan. All subregions were significantly related to age, $p < 0.001$. Continuous line indicates model-derived estimates. The shaded area represents a 95% confidence interval. BA, Brodmann area; ERC, entorhinal cortex; HPC, hippocampus (a, anterior; p, posterior); PHC, parahippocampal cortex; PRC, perirhinal cortex.

MTL Subregions Are Specifically Associated With Episodic Memory Performances

Volumes in most MTL subregions were positively associated with episodic memory scores (HPC: $\beta = 0.17$, SE $= 0.06$, $p = 0.006$; pHPC: $\beta = 0.21$, SE $= 0.08$, $p = 0.009$; ERC: $\beta = 0.22$, SE $= 0.07$, $p = 0.003$; PRC: $\beta = 0.20$, SE $= 0.07$, $p = 0.007$; and BA35: $\beta = 0.18$, SE $= 0.06$, $p = 0.008$) but not with executive function or speed processing (**Supplementary Table 9**).

DISCUSSION

The present study aims to explore how physiological aging and AD affect the volume of MTL subregions. Our current contribution represents one of the most comprehensive studies on MTL volumetric data using a tailored methodology based on longitudinal data and a dedicated segmentation algorithm. The findings highlight differential effects of age over the adult lifespan and support that AD-related neurodegeneration is more severe in the late stages of the Alzheimer's continuum, reflecting cognitive impairment. Consistently, episodic memory deficit, a key feature of AD, is related to greater atrophy in most MTL subregions. Interestingly, subregions that undergo specific aging mechanisms, as evidence by non-linear age-related volume trajectories, although not different between Aβ− and Aβ+ CU older adults, are particularly affected from the prodromal stage of AD (i.e., Aβ+ MCI). This volume decline in the hippocampal substructures might also give information regarding the conversion to AD-dementia in patients with MCI.

Differential Vulnerabilities of MTL Subregions in Aging

Our results emphasized that MTL subregions differ in their relationships with age over the adult lifespan, with both linear and non-linear age-related trajectories. Linear trajectories were observed for the first time for the PRC (as well as for BA 35 and 36) and PHC volumes, filling a knowledge gap regarding usually neglected MTL subregions. In addition, non-linear trajectories were observed for the HPC (and its anterior and posterior parts) and ERC volumes, strengthening the importance of not

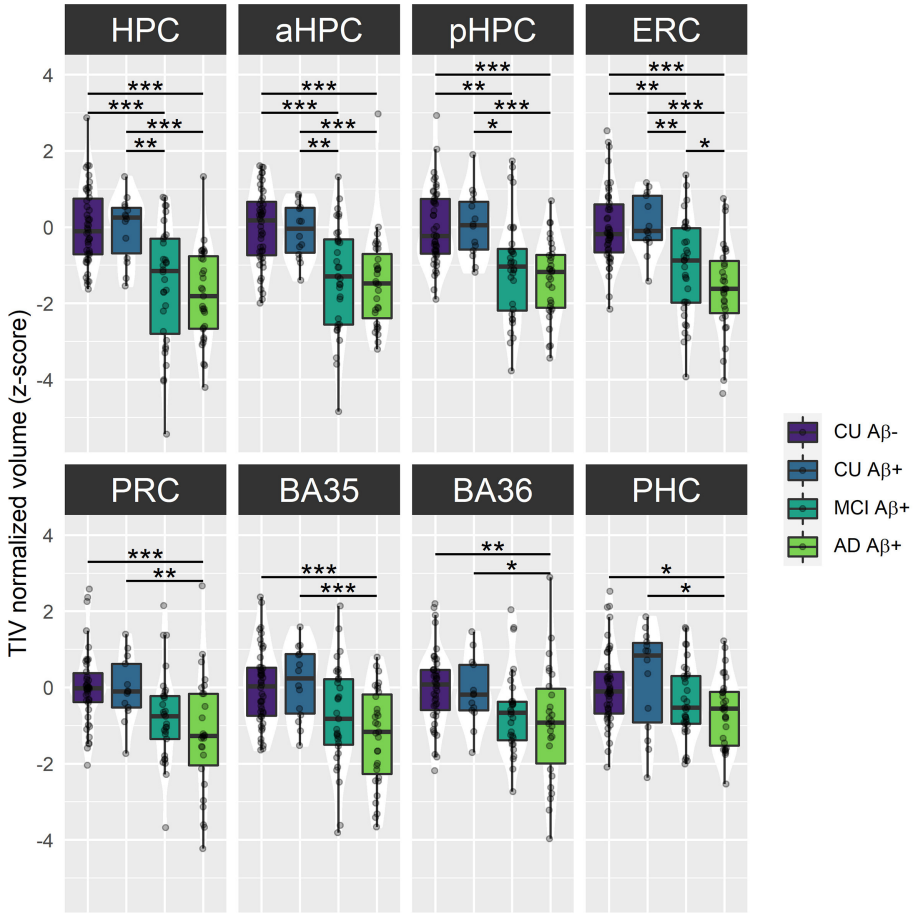

FIGURE 2 | Group comparisons of MTL subregions baseline volume across the Alzheimer's continuum. Boxplots display the median values and distribution of z-transformed TIV normalized volumes at baseline in each group. ***$p < 0.001$; **$p < 0.01$; *$p < 0.05$, as results of Tukey adjusted *post-hoc t*-tests. AD, Alzheimer's dementia; BA, Brodmann area; CU, cognitively unimpaired; ERC, entorhinal cortex; HPC, hippocampus (a, anterior; p, posterior); MCI, mild cognitive impairment; PHC, parahippocampal cortex; PRC, perirhinal cortex. The corresponding statistics are depicted in **Supplementary Table 5**.

restricting analyses to linear models when investigating the effects of age (Chen et al., 2016). In line with previous findings, visual inspection of the trajectories indicates that the HPC and ERC volumes remained stable or expanded until middle age and then declined substantially (Ziegler et al., 2012; Fjell et al., 2013; Coupé et al., 2017; Amlien et al., 2018; Li et al., 2018; Nobis et al., 2019; Langnes et al., 2020; Nyberg et al., 2021). As entorhinal cortical-hippocampal circuits are important in episodic memory processing, this pattern might partly explain the similar trajectory of age-related episodic memory deficit (Rönnlund et al., 2005; Nyberg et al., 2012). Interestingly, the HPC and ERC are strongly involved in neuroplasticity-related mechanisms such as neurogenesis or spinal plasticity (Teter and Ashford, 2002; Neves et al., 2008; Fjell et al., 2014; Yun et al., 2018; Ronaghi et al., 2019). Because these processes are partly dependent on environmental factors, non-linear trajectories in the HPC and ERC volumes might reflect age-related changes in cellular morphology influenced by exogenous events experienced during a lifetime. When compared visually, the HPC and ERC volumes seem to decrease faster from midlife than those of the PRC and PHC, suggesting that they are more vulnerable to late aging; and this vulnerability might be the result of greater plasticity, in line with the proposal of McEwen (1994). Based on the approximation of the decline onset age, the ERC volume was found to decrease earlier than the HPC volume. One speculation behind this observation might be that ERC alterations trigger damage to the HPC, as these structures are strongly connected (Whitwell et al., 2007).

Interestingly, vulnerability to age also seems to vary along the HPC longitudinal axis. Indeed, the pHPC volume declined more severely than the aHPC, suggesting that aging preferentially affects the posterior part of the HPC. This anteroposterior specificity might explain why semantic memory is relatively spared in aging while episodic memory and spatial learning are more damaged (Brickman and Stern, 2009), as semantic memory is particularly associated with the aHPC while episodic memory and spatial navigation are preferentially associated with the pHPC (Ranganath and Ritchey, 2012). Our observations

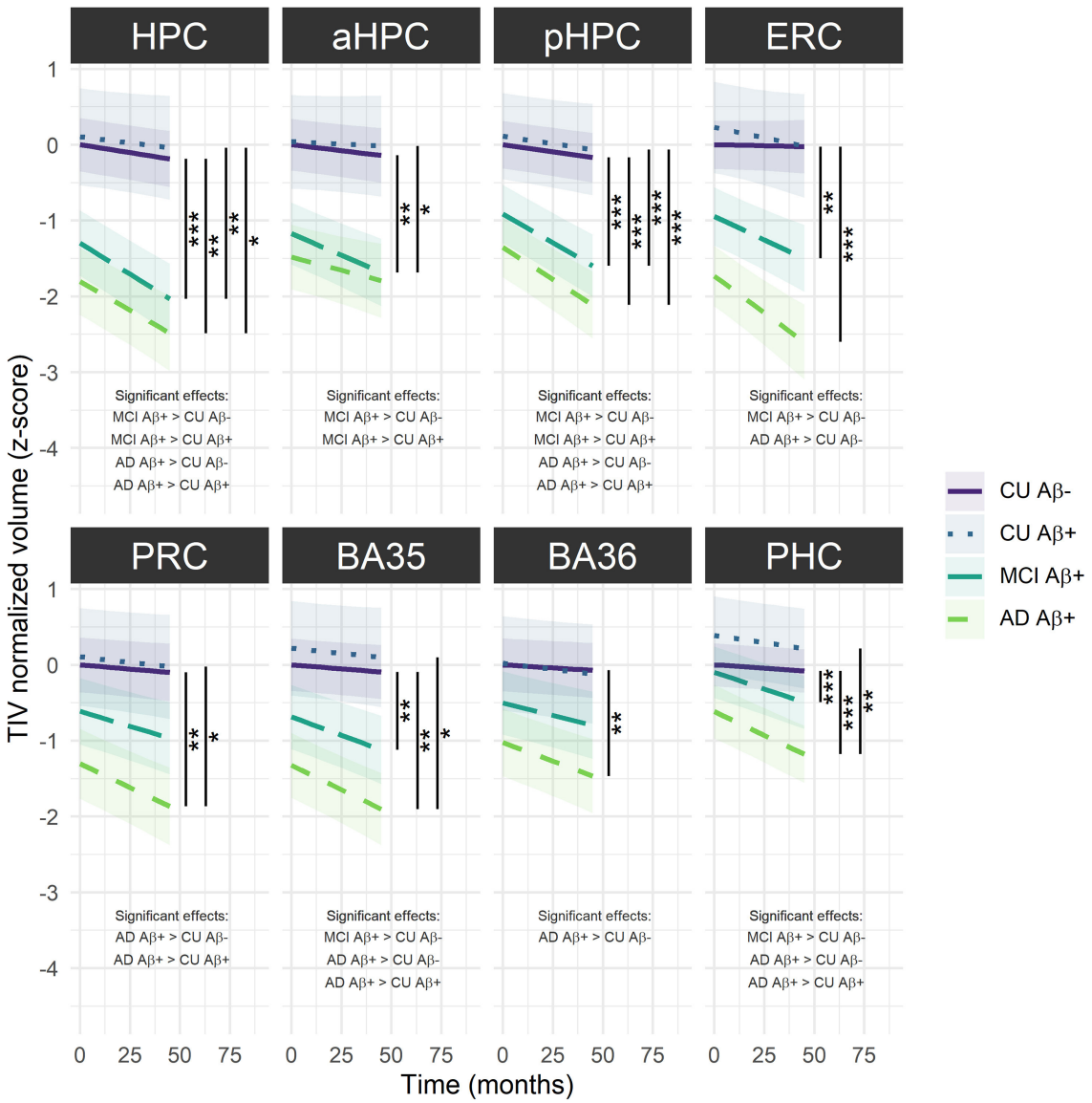

FIGURE 3 | Group comparisons of MTL subregions volume decline over time across the Alzheimer's continuum. The regression line indicates model-derived estimates. The shaded area represents a 95% confidence interval. ***$p < 0.001$; **$p < 0.01$; *$p < 0.05$, as results of Tukey adjusted *post-hoc t*-tests. AD, Alzheimer's dementia; BA, Brodmann area; CU, cognitively unimpaired; ERC, entorhinal cortex; HPC, hippocampus (a, anterior; p, posterior); MCI, mild cognitive impairment; PRC, parahippocampal cortex; PRC, perirhinal cortex. The corresponding statistics are depicted in **Supplementary Table 6**.

support previous results emphasizing less volume alteration in the aHPC compared with pHPC in typical aging (Kalpouzos et al., 2009), but is in contrast with the results showing comparable volume declines (Li et al., 2018) or greater aHPC vulnerability (Chen et al., 2010; Ta et al., 2012). Several methodological differences might explain these discrepancies. For example, the use of longitudinal vs. cross-sectional data might enhance the results reliability, especially since HPC volume varies greatly among individuals (Lupien et al., 2007). Age range, segmentation procedure, and curvilinear pattern might as well account for differences. However, such an anteroposterior gradient of vulnerability was not systematically found in studies comparable to ours (Langnes et al., 2020). Thus, differences between samples might also contribute to the discrepant results because age-related anatomical findings highly depend on inter-individual variance (Ta et al., 2012). From this perspective, CU participants over 60 years old included in our sample were highly educated (12.14 ± 2.85) compared with their peers born in the same period (∼1,940), of whom only 20% had a high school diploma (Clerc et al., 2011), and probably belong to high socioeconomic backgrounds. Following the hypothesis of Baum et al. (1999) stating that stress might be the pathway linking socioeconomic status and health, it is possible that high socioeconomic status is associated with less exposure to stressful life events and might

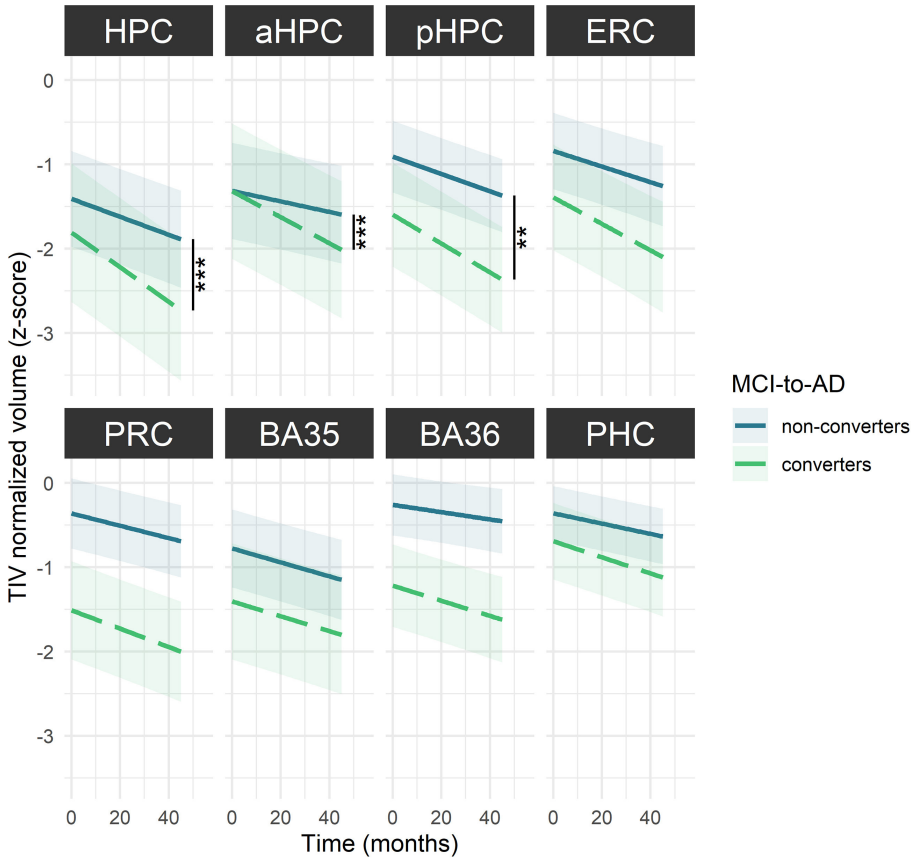

FIGURE 4 | MTL subregions volume decline over time among MCI-to-AD converters and non-converters. The regression line indicates model-derived estimates. The shaded area represents a 95% confidence interval. ***$p < 0.001$; **$p < 0.01$, as results of F-tests after the Holm correction. BA, Brodmann area; ERC, entorhinal cortex; HPC, hippocampus (a, anterior; p, posterior); MCI, mild cognitive impairment; PHC, parahippocampal cortex; PRC, perirhinal cortex. The corresponding statistics are depicted in **Supplementary Table 8**.

prevent individuals from a drastic aHPC volume decline, as the aHPC is particularly sensitive to stress (Vythilingam et al., 2005; Szeszko et al., 2006; Hawley and Leasure, 2012; Hawley et al., 2012; Decker et al., 2020). Further investigations of aHPC and pHPC volume trajectories across the lifespan are needed to draw strong conclusions, and the inclusion of a measure of stressful life events might help explore this possibility. Structural differentiation along the long axis of the HPC was also found in the first decades of the adult lifespan, as the aHPC volume still increased in early adulthood compared with the pHPC volume. This observation is in line with the mean diffusion results indicating that the pHPC microstructural development is completed during childhood whereas the aHPC still develops afterward (Langnes et al., 2020).

Overall, the differential vulnerabilities to age in MTL subregions do not seem to be influenced by sex, *APOE4*, or educational level. While investigating sex differences is not the main focus of this paper, we pointed out that two MTL subregions—pHPC and PHC—exhibited a larger adjusted volume in women than in men. This observation corroborates previous findings, highlighting a larger pHPC in women when adjusted for TIV (Persson et al., 2014; van Eijk et al., 2020). This anteroposterior specificity in sex differences might explain previous inconsistent findings regarding the HPC volume sex differences due to the hippocampus being considered as a whole.

AD Particularly Damages MTL Subregions From the MCI Stage

In line with previous findings, MTL subregional atrophy differed along the Alzheimer's continuum, with later clinical stages being more affected (Wolk et al., 2017; Xie et al., 2019, 2020). Specifically, baseline volumes were significantly greater in CU older adults (either Aβ− or Aβ+) vs. Aβ+ AD patients for all MTL subregions, and vs. Aβ+ MCI patients only for HPC, aHPC, pHPC and ERC. Interestingly, adult lifespan findings describe these subregions as being affected late by the detrimental effects of aging, suggesting that the MTL subregions displaying a late age-related decline were impaired earlier in AD. In addition to significantly smaller baseline volumes, Aβ+ MCI and AD patients exhibited more severe volume decline over time for

most of the MTL subregions compared to Aβ− CU older adults, illustrating the sensitivity of longitudinal analyses in tracking the progression of the disease. Given these findings, MTL subregional atrophy appears as a valid biomarker of the symptomatic stages of the Alzheimer's continuum and seems more widespread at the dementia stage, corroborating studies that have already proven the considerable alteration of the MTL in patients with MCI and AD (Juottonen et al., 1998; Du et al., 2001; Pennanen et al., 2004; Dickerson et al., 2009; Stoub et al., 2010; La Joie et al., 2012). The ERC and HPC (especially the pHPC) were identified as the most damaged subregions from the MCI stage, suggesting that AD preferentially targets long-development MTL subregions, as volume of these subregions keeps increasing until middle age. These subregions might be more vulnerable to the detrimental effects of late aging because of their high plasticity, and this age vulnerability might make them more susceptible to additional pathological AD-related changes, following the hypothesis described in Fjell et al. (2014). Thus, environmental factors that influence volume loss in aging could likely predispose to AD-related alterations. Interestingly, the MTL subregions most prone to atrophy in AD were also the most affected by tau pathology regarding tangles topography (Braak et al., 2006). These observations corroborate the relationship between atrophy and neurofibrillary tangles outlined in previous studies (Whitwell et al., 2008; Harrison et al., 2019; de Flores et al., 2020).

Although our results advocate the benefits of studying MTL subregions to differentiate patients of the Alzheimer's continuum from CU, none of these measures detect early pathological changes defined by the presence of Aβ deposition. Previous cross-sectional findings are inconsistent regarding the potential ability of MTL subregional volumes to differentiate between Aβ− and Aβ+ CU older adults. Some studies report no differences (Xie et al., 2019) while others found smaller BA 35 in Aβ+ CU (Wolk et al., 2017; Xie et al., 2020). Because these results were derived from cortical thickness measurements rather than volumetric measurements, we suppose that cortical thickness may be more sensitive in tracking early signs of AD, especially since extra-hippocampal volume measures are biased by the depth of the collateral sulcus which varies among individuals (Feczko et al., 2009; Schwarz et al., 2016; Berron et al., 2017). Still, the differences were small and did not survive the multiple testing correction. Interestingly, the longitudinal evaluation of MTL subregional atrophy seemed to enhance the clinical utility of these biomarkers. Xie et al. (2020) revealed more robust significant differences between Aβ− and Aβ+ CU older adults using longitudinal data, and these differences were extended to most MTL subregions, yet, we failed to replicate their findings in our analyses. As Xie et al. divided Aβ+ CU participants into tau+ and tau- subgroups and found that only the Aβ+ tau+ subgroup was significantly different from Aβ− CU older adults, we can speculate that most of the participants in our sample did not have significant tau pathology, so no MTL subregional atrophy could be detected. Unfortunately, no tau data was available in our study, so further studies including such measures will be needed to validate this assumption.

Neither the baseline nor longitudinal measures of MTL subregional atrophy dissociated Aβ+ MCI and AD patients, except for the ERC at baseline. This observation corroborates previous findings that found significantly reduced ERC volume in MCI compared with AD patients (Zhou et al., 2016 for review), but do not replicate other previous findings highlighting HPC volume difference between MCI and AD (Lu et al., 2019; Zhao et al., 2019).

Overall, MTL subregional atrophy appears to reflect AD-related cognitive impairments, as it distinguishes patients from CU older adults, but may not be an ideal biomarker of early AD-related pathological changes defined by the presence of Aβ deposits.

Hippocampal Substructures Are Sensitive to Alzheimer's Dementia Conversion in MCI Patients

From a prognostic perspective, the HPC, aHPC, and pHPC volume declines were steeper in MCI-to-AD converters than in non-converters, suggesting that hippocampal substructures atrophy may provide information on the clinical outcomes of MCI patients. These observations corroborate previous findings also highlighting greater hippocampal atrophy in MCI patients who developed AD-dementia compared with those who did not (Pennanen et al., 2004; Apostolova et al., 2006; Devanand et al., 2007; Henneman et al., 2009; Maruszak and Thuret, 2014 for review; Brueggen et al., 2015). The sensitivity of hippocampal substructures in dissociating converters from non-converters was thought to reflect the important alteration of the HPC in AD. Because group differences were found only by comparing the volume declines over time and not the baseline volumes, a longitudinal assessment of atrophy appears to be more sensitive for tracking AD progression than single-time assessment, especially as cross-sectional measures may suffer from cohort effects. In addition, a standardized hippocampal atrophy score based on automatic segmentation procedures, with norms as for neuropsychological testing, might provide a more objective measurement than the subjective appreciation of MTL atrophy used in previous studies (Scheltens et al., 1995, 1997; Korf et al., 2004; Lehmann et al., 2013). In contrast to some studies that have illustrated the ability of ERC volume to predict conversion to AD-dementia in MCI patients, no significant dissociation between converters and non-converters was found for this subregion in our analyses (de Toledo-Morrell et al., 2004; Zhou et al., 2016 for reviews). Still, the ERC was the subregion displaying the greatest groups difference among non-significant models. To the best of our knowledge, the PRC (and its subcomponents BA 35 and 36) and PHC volume differences were investigated for the first time between MCI-to-AD converters and non-converters, and results suggest that none of these subregions discriminate converters from non-converters.

These results might sound promising as they consider a potential prognostic biomarker for AD conversion, but it must be remembered that this is a group comparison and therefore does not directly evaluate the predictive value of these measures.

Further studies entirely dedicated to the predictive ability of MTL subregions volumetry to anticipate AD-dementia conversion in MCI patients might help establish a better clinical routine.

The Volume of Most MTL Subregions Reflects Episodic Memory Performances

According to our hypotheses, we outlined robust relationships between most of MTL subregions volumes and episodic memory performances in Aβ+ MCI and AD patients, suggesting that pronounced MTL subregional atrophy worsens episodic memory. Relative to the cognitive functions investigated, the association between episodic memory and MTL subregions volume was domain-specific, but very few cognitive areas were assessed, which limits our interpretation. Further studies including a more comprehensive assessment of cognitive functioning might complement our results and provide more substantiated information. In particular, indexes of semantic and spatial memory may be relevant, as some MTL subregions are specifically involved in these processes.

Our results suggested that the pHPC, ERC, and PRC volumes were the most strongly associated with episodic memory performances. These MTL subregions were also the most damaged in the late clinical stages of the Alzheimer's continuum, and so substantiate the view of episodic memory deficit as a core feature of AD. Thus, the strong involvement of HPC and ERC in episodic memory function might explain why episodic memory may be enriched by our environment as we suggested that environmental factors could impact their development. Rather, the aHPC, BA36, and PHC volumes were not significantly associated with episodic memory function. The lack of association between PHC volumes and episodic memory performances was quite expected as PHC is more involved in visuospatial processing (Ranganath and Ritchey, 2012; Aminoff et al., 2013; Bohbot et al., 2015; Baumann and Mattingley, 2021). However, the role played by the PHC in episodic memory should not be negated as it is known that PHC supports the representations of the situational context associated with items (Ranganath and Ritchey, 2012; Aminoff et al., 2013). Indeed, our scores might not be sensitive enough to capture the associative processing aspect of episodic memory since tests often fail to capture all reality subtleties, such as contextual details. Thus, new tests assessing episodic memory more realistically have been designed and might be explored to better reflect the complexity of episodic memory (Curot, 2018; Smith, 2019). Interestingly, the aHPC volume was less related to episodic memory performances compared with the pHPC volume. This disparity within hippocampal substructures may reflect the differential role of the two MTL networks, as aHPC belongs to an anterior-temporal network which is known to be more involved in semantic memory compared with pHPC which is included in a posterior-medial network that is preferentially involved in episodic memory (Ranganath and Ritchey, 2012).

Limitations

The present study has some limitations. First, it should be mentioned that the age of our lifespan sample, ranging from 19 and 85, limits the interpretability of age-related changes in the early lifespan. Specifically, the first inflection in the HPC volume trajectory should be considered with caution, and additional analyses including children and adolescents are needed to refine our observations. Also, our sample size can appear relatively small and might prevent us from showing subtle effects, especially early structural changes in preclinical AD, as only the data from 14 Aβ+ CU older adults were available. However, all data used in this article were acquired using the same MRI scanner and this sample size allowed us to rigorously check the scans quality and manually edit the segmentations, thus, greatly improving the accuracy of our data. In addition, we manually corrected about 30% of the segmentations, which may suggest difficulties for MTL volumetry clinical use. However, it is important to note that most of these errors were found in CU young adults, certainly reflecting the inclusion lack of such an age group in the atlas used. Thus, modifying the atlas to better match a specific targeted clinical population would likely optimize the software segmentations.

CONCLUSION

Through this longitudinal study, we gained a better understanding of aging and AD-related mechanisms regarding the volume of MTL subregions. We emphasized the benefits of studying these biomarkers to distinguish age-related changes from AD. Interestingly, the MTL subregions were differently vulnerable to the detrimental effects of aging, and the subregions displaying a late-onset decline, while not affected by the presence of Aβ deposits, were particularly damaged in AD from the MCI stage, as well as closely related to episodic memory performances. In particular, the volume decline in the hippocampal substructures might predict the conversion from MCI to AD-dementia. Overall, we hope that these findings will provide new insights into MTL alterations, which are crucial for the definition of AD-specific biomarkers.

DATA AVAILABILITY STATEMENT

The raw data supporting the conclusions of this article will be made available by the authors, without undue reservation.

ETHICS STATEMENT

The studies involving human participants were reviewed and approved by Comité de Protection des Personnes Nord-Ouest III. The patients/participants provided their written informed consent to participate in this study.

AUTHOR CONTRIBUTIONS

GC and VdLS were the principal investigators of the IMAP+ research protocol. CP, FF, and VO contributed to the data acquisition. RdF and LC conceived the study. LC executed

the study and was responsible for data analysis and data interpretation. RdF and EK contributed to the data analysis and data interpretation. LC drafted the manuscript in close collaboration with RdF. GC, EK, VdLS, CP, FF, and VO provided feedback on the manuscript. All authors have read and approved the manuscript, and so contributed substantially to it.

FUNDING

This work was supported by the Programme Hospitalier de Recherche Clinique (PHRCN 2011-A01493-38 and PHRCN 2012 12-006-0347), the Agence Nationale de la Recherche (ANR LONGVIE 2007), Fondation Plan Alzheimer (Alzheimer Plan 2008–2012), Association France Alzheimer et maladies apparentées AAP 2013, the Région Basse Normandie, and the Institut National de la Santé et de la Recherche Médicale (INSERM).

ACKNOWLEDGMENTS

The authors are grateful to the patients and healthy volunteers who participated in this study. The authors also thank A. Abbas, T. Anquetil, E. Arenaza-Urquijo, L. Barre, JC. Baron, A. Chocat, A. Cognet, J. Dayan, M. Delarue, B Desgranges, S. Egret, F. Eustache, M. Fouquet, M. Gaubert, J. Gonneaud, D. Guilloteau, R. La Joie, B. Landeau, M. Leblond, A. Manrique, F. Mezenge, K. Mevel, J. Mutlu, L. Paly, G. Poisnel, A. Pélerin, A. Quillard, G. Rauchs, C. Schupp, F. Viader, N. Villain for their help with recruitment, cognitive testing and imaging examinations, and the Cyceron MRI-PET staff members for their help with imaging acquisition.

SUPPLEMENTARY MATERIAL

The Supplementary Material for this article can be found online at: https://www.frontiersin.org/articles/10.3389/fnagi.2021.750154/full#supplementary-material

REFERENCES

Aminoff, E. M., Kveraga, K., and Bar, M. (2013). The role of the parahippocampal cortex in cognition. *Trends Cogn. Sci.* 17, 379–390. doi: 10.1016/j.tics.2013.06.009

Amlien, I. K., Sneve, M. H., Vidal-Piñeiro, D., Walhovd, K. B., and Fjell, A. M. (2018). The lifespan trajectory of the encoding-retrieval flip: a multimodal examination of medial parietal cortex contributions to episodic memory. *J. Neurosci.* 38, 8666–8679. doi: 10.1523/JNEUROSCI.1702–17.2018

Apostolova, L. G., Dutton, R. A., Dinov, I. D., Hayashi, K. M., Toga, A. W., Cummings, J. L., et al. (2006). Conversion of mild cognitive impairment to Alzheimer disease predicted by hippocampal atrophy maps. *Arch. Neurol.* 63, 693–699. doi: 10.1001/archneur.63.5.693

Barnes, J., Bartlett, J. W., van de Pol, L. A., Loy, C. T., Scahill, R. I., Frost, C., et al. (2009). A meta-analysis of hippocampal atrophy rates in Alzheimer's disease. *Neurobiol. Aging* 30, 1711–1723. doi: 10.1016/j.neurobiolaging.2008.01.010

Bates, D., Mächler, M., Bolker, B., and Walker, S. (2015). Fitting linear mixed-effects models using lme4. *J. Stat. Softw.* 67, 1–48. doi: 10.18637/jss.v067.i01

Baum, A., Garofalo, J. P., and Yali, A. M. (1999). Socioeconomic Status and chronic stress: does stress account for SES effects on health? *Ann. N. Y. Acad. Sci.* 896, 131–144. doi: 10.1111/j.1749–6632.1999.tb08111.x

Baumann, O., and Mattingley, J. B. (2021). Extrahippocampal contributions to spatial navigation in humans: a review of the neuroimaging evidence. *Hippocampus* 31, 640–657. doi: 10.1002/hipo.23313

Berron, D., Vieweg, P., Hochkeppler, A., Pluta, J., Ding, S.-L., Maass, A., et al. (2017). A protocol for manual segmentation of medial temporal lobe subregions in 7 Tesla MRI. *NeuroImage Clin.* 15, 466–482. doi: 10.1016/j.nicl.2017.05.022

Bohbot, V. D., Allen, J. J. B., Dagher, A., Dumoulin, S. O., Evans, A. C., Petrides, M., et al. (2015). Role of the parahippocampal cortex in memory for the configuration but not the identity of objects: converging evidence from patients with selective thermal lesions and fMRI. *Front. Hum. Neurosci.* 9:431. doi: 10.3389/fnhum.2015.00431

Braak, H., Alafuzoff, I., Arzberger, T., Kretzschmar, H., and Del Tredici, K. (2006). Staging of Alzheimer disease-associated neurofibrillary pathology using paraffin sections and immunocytochemistry. *Acta Neuropathol.* 112, 389–404. doi: 10.1007/s00401–006-0127-z

Braak, H., and Braak, E. (1991). Neuropathological stageing of Alzheimer-related changes. *Acta Neuropathol.* 82, 239–259. doi: 10.1007/BF00308809

Braak, H., and Braak, E. (1995). Staging of Alzheimer's disease-related neurofibrillary changes. *Neurobiol. Aging* 16, 271–278; discussion 278–284. doi: 10.1016/0197–4580(95)00021–6

Brickman, A. M., and Stern, Y. (2009). "Aging and memory in humans," in *Handbook of the Neuroscience of Aging*, eds P. R. Hof and C. V. Mobbs (New York, NY: Elsevier Academic Press), 243–248. doi: 10.1016/B978–008045046-9.00745–2

Brueggen, K., Dyrba, M., Barkhof, F., Hausner, L., Filippi, M., Nestor, P. J., et al. (2015). Basal forebrain and hippocampus as predictors of conversion to Alzheimer's disease in patients with mild cognitive impairment—a multicenter DTI and volumetry study. *J. Alzheimer's Dis.* 48, 197–204. doi: 10.3233/JAD-150063

Burnham, K. P., and Anderson, D. R. (2004). Multimodel inference: understanding AIC and BIC in model selection. *Sociol. Methods Res.* 33, 261–304. doi: 10.1177/0049124104268644

Bussy, A., Patel, R., Plitman, E., Tullo, S., Salaciak, A., Bedford, S. A., et al. (2021). Hippocampus shape across the healthy lifespan and its relationship with cognition. *Neurobiol. Aging.* 106, 153–168. doi: 10.1016/j.neurobiolaging.2021.03.018

Chen, H., Zhao, B., Cao, G., Proges, E. C., O'Shea, A., Woods, A. J., et al. (2016). Statistical approaches for the study of cognitive and brain aging. *Front. Aging Neurosci.* 8:176. doi: 10.3389/fnagi.2016.00176

Chen, K. H. M., Chuah, L. Y. M., Sim, S. K. Y., and Chee, M. W. L. (2010). Hippocampal region-specific contributions to memory performance in normal elderly. *Brain Cogn.* 72, 400–407. doi: 10.1016/j.bandc.2009.11.007

Chételat, G., Eustache, F., Viader, F., De La Sayette, V., Pélerin, A., Mézenge, F., et al. (2005). FDG-PET measurement is more accurate than neuropsychological assessments to predict global cognitive deterioration in patients with mild cognitive impairment. *Neurocase* 11, 14–25. doi: 10.1080/13554790490896938

Clerc, M.-É., Monso, O., and Pouliquen, E. (2011). *Les inégalités entre générations depuis le baby-boom – L'économie française—Comptes et dossiers | Insee*. Available online at: https://www.insee.fr/fr/statistiques/1373852?sommaire=1373855 (accessed June, 2021).

Coupé, P., Catheline, G., Lanuza, E., and Manjón, J. V. (2017). Towards a unified analysis of brain maturation and aging across the entire lifespan: a MRI analysis. *Hum. Brain Mapp.* 38, 5501–5518. doi: 10.1002/hbm.23743

Curot, J. (2018). *Une Exploration Multidimensionnelle des Phénomènes Expérientiels Mnésiques: De la Sémiologie à L'activité Neuronale Unitaire* (Toulouse), 427.

Daugherty, A. M., Bender, A. R., Raz, N., and Ofen, N. (2016). Age differences in hippocampal subfield volumes from childhood to late adulthood. *Hippocampus* 26, 220–228. doi: 10.1002/hipo.22517

de Flores, R., La Joie, R., Landeau, B., Perrotin, A., Mézenge, F., de La Sayette, V., et al. (2015). Effects of age and Alzheimer's disease on hippocampal subfields:

Comparison between manual and FreeSurfer volumetry. *Hum. Brain Mapp.* 36, 463–474. doi: 10.1002/hbm.22640

de Flores, R., Wisse, L. E. M., Das, S. R., Xie, L., McMillan, C. T., Trojanowski, J. Q., et al. (2020). Contribution of mixed pathology to medial temporal lobe atrophy in Alzheimer's disease. *Alzheimer's Dementia* 16, 843–852. doi: 10.1002/alz.12079

de Toledo-Morrell, L., Stoub, T. R., Bulgakova, M., Wilson, R. S., Bennett, D. A., Leurgans, S., et al. (2004). MRI-derived entorhinal volume is a good predictor of conversion from MCI to AD. *Neurobiol. Aging* 25, 1197–1203. doi: 10.1016/j.neurobiolaging.2003.12.007

Decker, A. L., Duncan, K., Finn, A. S., and Mabbott, D. J. (2020). Children's family income is associated with cognitive function and volume of anterior not posterior hippocampus. *Nat. Commun.* 11 :4040. doi: 10.1038/s41467–020-17854–6

Devanand, D. P., Pradhaban, G., Liu, X., Khandji, A., De Santi, S., Segal, S., et al. (2007). Hippocampal and entorhinal atrophy in mild cognitive impairment: prediction of Alzheimer disease. *Neurology* 68, 828–836. doi: 10.1212/01.wnl.0000256697.20968.d7

Dickerson, B. C., Feczko, E., Augustinack, J. C., Pacheco, J., Morris, J. C., Fischl, B., et al. (2009). Differential effects of aging and Alzheimer's disease on medial temporal lobe cortical thickness and surface area. *Neurobiol. Aging* 30, 432–440. doi: 10.1016/j.neurobiolaging.2007.07.022

Du, A., T., Schuff, N., Amend, D., Laakso, M., Hsu, Y., et al. (2001). Magnetic resonance imaging of the entorhinal cortex and hippocampus in mild cognitive impairment and Alzheimer's disease. *J. Neurol. Neurosurg. Psychiatr.* 71, 441–447. doi: 10.1136/jnnp.71.4.441

Du, A.-T., Schuff, N., Chao, L. L., Kornak, J., Jagust, W. J., Kramer, J. H., et al. (2006). Age effects on atrophy rates of entorhinal cortex and hippocampus. *Neurobiol. Aging* 27, 733–740. doi: 10.1016/j.neurobiolaging.2005.03.021

Du, A. T., Schuff, N., Zhu, X. P., Jagust, W. J., Miller, B. L., Reed, B. R., et al. (2003). Atrophy rates of entorhinal cortex in AD and normal aging. *Neurology* 60, 481–486. doi: 10.1212/01.WNL.0000044400.11317.EC

Eustache, F., Desgranges, B., and Lalevée, C. (1998). L'évaluation clinique de la mémoire. [Clinical assessment of memory.]. *Revue Neurol.* 154(Suppl. 2), 2S18–2S32.

Feczko, E., Augustinack, J. C., Fischl, B., and Dickerson, B. C. (2009). An MRI-based method for measuring volume, thickness and surface area of entorhinal, perirhinal, and posterior parahippocampal cortex. *Neurobiol. Aging* 30, 420–431. doi: 10.1016/j.neurobiolaging.2007.07.023

Fjell, A. M., McEvoy, L., Holland, D., Dale, A. M., Walhovd, K. B., and Alzheimer's Disease Neuroimaging Initiative (2014). What is normal in normal aging? Effects of aging, amyloid and Alzheimer's disease on the cerebral cortex and the hippocampus. *Prog. Neurobiol.* 117, 20–40. doi: 10.1016/j.pneurobio.2014.02.004

Fjell, A. M., Westlye, L. T., Grydeland, H., Amlien, I., Espeseth, T., Reinvang, I., et al. (2013). Critical ages in the life course of the adult brain: nonlinear subcortical aging. *Neurobiol. Aging* 34, 2239–2247. doi: 10.1016/j.neurobiolaging.2013.04.006

Fortea, J., Vilaplana, E., Alcolea, D., Carmona-Iragui, M., Sánchez-Saudinos, M.-B., Sala, I., et al. (2014). Cerebrospinal fluid β−amyloid and phospho-tau biomarker interactions affecting brain structure in preclinical Alzheimer disease. *Ann. Neurol.* 76, 223–230. doi: 10.1002/ana.24186

Frisoni, G. B., Fox, N. C., Jack, C. R., Scheltens, P., and Thompson, P. M. (2010). The clinical use of structural MRI in Alzheimer disease. *Nat. Rev. Neurol.* 6, 67–77. doi: 10.1038/nrneurol.2009.215

Harrison, T. M., La Joie, R., Maass, A., Baker, S. L., Swinnerton, K., Fenton, L., et al. (2019). Longitudinal tau accumulation and atrophy in aging and alzheimer disease. *Ann. Neurol.* 85, 229–240. doi: 10.1002/ana.25406

Hasan, K. M., Mwangi, B., Cao, B., Keser, Z., Tustison, N. J., Kochunov, P., et al. (2016). Entorhinal cortex thickness across the human lifespan. *J. Neuroimaging* 26, 278–282. doi: 10.1111/jon.12297

Hawley, D. F., and Leasure, J. L. (2012). Region-specific response of the hippocampus to chronic unpredictable stress. *Hippocampus* 22, 1338–1349. doi: 10.1002/hipo.20970

Hawley, D. F., Morch, K., Christie, B. R., and Leasure, J. L. (2012). Differential response of hippocampal subregions to stress and learning. *PLoS ONE* 7:e53126. doi: 10.1371/journal.pone.0053126

Henneman, W. J. P., Sluimer, J. D., Barnes, J., van der Flier, W. M., Sluimer, I. C., Fox, N. C., et al. (2009). Hippocampal atrophy rates in Alzheimer disease. *Neurology* 72, 999–1007. doi: 10.1212/01.wnl.0000344568.09360.31

Holm, S. (1979). A simple sequentially rejective multiple test procedure. *Scand. J. Statist.* 6, 65–70.

Iglesias, J. E., Augustinack, J. C., Nguyen, K., Player, C. M., Player, A., Wright, M., et al. (2015). A computational atlas of the hippocampal formation using *ex vivo*, ultra-high resolution MRI: application to adaptive segmentation of *in vivo* MRI. *Neuroimage* 115, 117–137. doi: 10.1016/j.neuroimage.2015.04.042

Jack, C. R., Bennett, D. A., Blennow, K., Carrillo, M. C., Dunn, B., Haeberlein, S. B., et al. (2018). NIA-AA Research Framework: toward a biological definition of Alzheimer's disease. *Alzheimer's Dementia* 14, 535–562. doi: 10.1016/j.jalz.2018.02.018

Jernigan, T. L., Archibald, S. L., Fennema-Notestine, C., Gamst, A. C., Stout, J. C., Bonner, J., et al. (2001). Effects of age on tissues and regions of the cerebrum and cerebellum. *Neurobiol. Aging* 22, 581–594. doi: 10.1016/S0197–4580(01)00217–2

Juottonen, K., Laakso, M. P., Insausti, R., Lehtovirta, M., Pitkänen, A., Partanen, K., et al. (1998). Volumes of the entorhinal and perirhinal cortices in Alzheimer's disease. *Neurobiol. Aging* 19, 15–22. doi: 10.1016/S0197–4580(98)00007–4

Kalpouzos, G., Chételat, G., Baron, J.-C., Landeau, B., Mevel, K., Godeau, C., et al. (2009). Voxel-based mapping of brain gray matter volume and glucose metabolism profiles in normal aging. *Neurobiol. Aging* 30, 112–124. doi: 10.1016/j.neurobiolaging.2007.05.019

Korf, E. S. C., Wahlund, L.-O., Visser, P. J., and Scheltens, P. (2004). Medial temporal lobe atrophy on MRI predicts dementia in patients with mild cognitive impairment. *Neurology* 63, 94–100. doi: 10.1212/01.WNL.0000133114.92694.93

Krumm, S., Kivisaari, S. L., Probst, A., Monsch, A. U., Reinhardt, J., Ulmer, S., et al. (2016). Cortical thinning of parahippocampal subregions in very early Alzheimer's disease. *Neurobiol. Aging* 38, 188–196. doi: 10.1016/j.neurobiolaging.2015.11.001

La Joie, R., Perrotin, A., Barr,é, L., Hommet, C., Mézenge, F., Ibazizene, M., et al. (2012). Region-specific hierarchy between atrophy, hypometabolism, and β−amyloid (Aβ) load in Alzheimer's disease dementia. *J. Neurosci.* 32, 16265–16273. doi: 10.1523/JNEUROSCI.2170–12.2012

La Joie, R., Perrotin, A., de La Sayette, V., Egret, S., Doeuvre, L., Belliard, S., et al. (2013). Hippocampal subfield volumetry in mild cognitive impairment, Alzheimer's disease and semantic dementia. *NeuroImage Clin.* 3, 155–162. doi: 10.1016/j.nicl.2013.08.007

Langnes, E., Sneve, M. H., Sederevicius, D., Amlien, I. K., Walhovd, K. B., and Fjell, A. M. (2020). Anterior and posterior hippocampus macro- and microstructure across the lifespan in relation to memory—a longitudinal study. *Hippocampus* 30, 678–692. doi: 10.1002/hipo.23189

Lehmann, M., Koedam, E. L., Barnes, J., Bartlett, J. W., Barkhof, F., Wattjes, M. P., et al. (2013). Visual ratings of atrophy in MCI: prediction of conversion and relationship with CSF biomarkers. *Neurobiol. Aging* 34, 73–82. doi: 10.1016/j.neurobiolaging.2012.03.010

Lenth, R. V., Buerkner, P., Herve, M., Love, J., Riebl, H., and Singmann, H. (2021). *emmeans: Estimated Marginal Means, aka Least-Squares Means* (1.5.4) [Computer software]. Available online at: https://CRAN.R-project.org/package=emmeans (accessed June, 2021).

Li, X., Li, Q., Wang, X., Li, D., and Li, S. (2018). Differential age-related changes in structural covariance networks of human anterior and posterior hippocampus. *Front. Physiol.* 9:518. doi: 10.3389/fphys.2018.00518

Lu, T.esta, Jordan, E.lyan, R., Kanekar, S., Wang, M., Eslinger, P., Yang, Zhang, and Karunanayaka, P. (2019). Functional connectivity between the resting-state olfactory network and the hippocampus in Alzheimer's disease. *Brain Sci.* 9:338. doi: 10.3390/brainsci9120338

Lüdecke, D., Makowski, D., Ben-Shachar, M. S., Patil, I., Waggoner, P., Wiernik, B. M., et al. (2021). *Performance: Assessment of Regression Models Performance (0.7.2) [Computer software]*. Available online at: https://CRAN.R-project.org/package=performance (accessed June, 2021).

Lupien, S. J., Evans, A., Lord, C., Miles, J., Pruessner, M., Pike, B., et al. (2007). Hippocampal volume is as variable in young as in older adults: Implications for the notion of hippocampal atrophy in humans. *Neuroimage* 34, 479–485. doi: 10.1016/j.neuroimage.2006.09.041

Maruszak, A., and Thuret, S. P. (2014). Why looking at the whole hippocampus is not enough—a critical role for anteroposterior axis, subfield and activation analyses to enhance predictive value of hippocampal changes for Alzheimer's disease diagnosis. *Front. Cell. Neurosci.* 8:95. doi: 10.3389/fncel.2014.00095

McEwen, B. S. (1994). The plasticity of the hippocampus is the reason for its vulnerability. *Semin. Neurosci.* 6, 239–246. doi: 10.1006/smns.1994.1031

McKhann, G., Drachman, D., Folstein, M., Katzman, R., Price, D., and Stadlan, E. M. (1984). Clinical diagnosis of Alzheimer's disease: report of the NINCDS-ADRDA Work Group under the auspices of Department of Health and Human Services Task Force on Alzheimer's disease. *Neurology* 34, 939–944. doi: 10.1212/WNL.34.7.939

Mevel, K., Landeau, B., Fouquet, M., La Joie, R., Villain, N., Mézenge, F., et al. (2013). Age effect on the default mode network, inner thoughts, and cognitive abilities. *Neurobiol. Aging* 34, 1292–1301. doi: 10.1016/j.neurobiolaging.2012.08.018

Miller, M. I., Younes, L., Ratnanather, J. T., Brown, T., Trinh, H., Postell, E., et al. (2013). The diffeomorphometry of temporal lobe structures in preclinical Alzheimer's disease. *NeuroImage Clin.* 3, 352–360. doi: 10.1016/j.nicl.2013.09.001

Moscovitch, M., Cabeza, R., Winocur, G., and Nadel, L. (2016). Episodic Memory and beyond: the hippocampus and neocortex in transformation. *Annu. Rev. Psychol.* 67, 105–134. doi: 10.1146/annurev-psych-113011–143733

Müller-Gärtner, H. W., Links, J. M., Prince, J. L., Bryan, R. N., McVeigh, E., Leal, J. P., et al. (1992). Measurement of Radiotracer concentration in brain gray matter using positron emission tomography: MRI-based correction for partial volume effects. *J. Cerebral Blood Flow Metab.* 12, 571–583. doi: 10.1038/jcbfm.1992.81

Nakagawa, S., Johnson, P. C. D., and Schielzeth, H. (2017). The coefficient of determination R2 and intra-class correlation coefficient from generalized linear mixed-effects models revisited and expanded. *J. R. Soc. Interface* 14:20170213. doi: 10.1098/rsif.2017.0213

Neves, G., Cooke, S. F., and Bliss, T. V. P. (2008). Synaptic plasticity, memory and the hippocampus: a neural network approach to causality. *Nat. Rev. Neurosci.* 9, 65–75. doi: 10.1038/nrn2303

Nobis, L., Manohar, S. G., Smith, S. M., Alfaro-Almagro, F., Jenkinson, M., Mackay, C. E., et al. (2019). Hippocampal volume across age: nomograms derived from over 19,700 people in UK Biobank. *NeuroImage Clin.* 23:101904. doi: 10.1016/j.nicl.2019.101904

Nyberg, L., Lövdén, M., Riklund, K., Lindenberger, U., and Bäckman, L. (2012). Memory aging and brain maintenance. *Trends Cogn. Sci.* 16, 292–305. doi: 10.1016/j.tics.2012.04.005

Nyberg, L., Magnussen, F., Lundquist, A., Baaré, W., Bartrés-Faz, D., Bertram, L., et al. (2021). Educational attainment does not influence brain aging. *Proc. Nat. Acad. Sci. U.S.A.* 118:e2101644118. doi: 10.1073/pnas.2101644118

Pegueroles, J., Vilaplana, E., Montal, V., Sampedro, F., Alcolea, D., Carmona-Iragui, M., et al. (2017). Longitudinal brain structural changes in preclinical Alzheimer's disease. *Alzheimer's Dementia* 13, 499–509. doi: 10.1016/j.jalz.2016.08.010

Pennanen, C., Kivipelto, M., Tuomainen, S., Hartikainen, P., Hänninen, T., Laakso, M. P., et al. (2004). Hippocampus and entorhinal cortex in mild cognitive impairment and early AD. *Neurobiol. Aging* 25, 303–310. doi: 10.1016/S0197–4580(03)00084–8

Perrotin, A., La Joie, R., de La Sayette, V., Barr,é, L., Mézenge, F., Mutlu, J., et al. (2017). Subjective cognitive decline in cognitively normal elders from the community or from a memory clinic: differential affective and imaging correlates. *Alzheimer's Dementia* 13, 550–560. doi: 10.1016/j.jalz.2016.08.011

Persson, J., Spreng, R. N., Turner, G., Herlitz, A., Morell, A., Stening, E., et al. (2014). Sex differences in volume and structural covariance of the anterior and posterior hippocampus. *Neuroimage* 99, 215–225. doi: 10.1016/j.neuroimage.2014.05.038

Petersen, R. C., and Morris, J. C. (2005). Mild cognitive impairment as a clinical entity and treatment target. *Arch. Neurol.* 62, 1160–1163. doi: 10.1001/archneur.62.7.1160

Pettigrew, C., Soldan, A., Sloane, K., Cai, Q., Wang, J., Wang, M.-C., et al. (2017). Progressive medial temporal lobe atrophy during preclinical Alzheimer's disease. *NeuroImage Clin.* 16, 439–446. doi: 10.1016/j.nicl.2017.08.022

Pini, L., Pievani, M., Bocchetta, M., Altomare, D., Bosco, P., Cavedo, E., et al. (2016). Brain atrophy in Alzheimer's disease and aging. *Ageing Res. Rev.* 30, 25–48. doi: 10.1016/j.arr.2016.01.002

Pipitone, J., Park, M. T. M., Winterburn, J., Lett, T. A., Lerch, J. P., Pruessner, J. C., et al. (2014). Multi-atlas segmentation of the whole hippocampus and subfields using multiple automatically generated templates. *Neuroimage* 101, 494–512. doi: 10.1016/j.neuroimage.2014.04.054

R Core Team (2020). *R: A Language and Environment for Statistical Computing*. Available online at: https://www.R-project.org/ (accessed June, 2021).

Ranganath, C., and Ritchey, M. (2012). Two cortical systems for memory-guided behaviour. *Nat. Rev. Neurosci.* 13, 713–726. doi: 10.1038/nrn3338

Raslau, F. D., Mark, I. T., Klein, A. P., Ulmer, J. L., Mathews, V., and Mark, L. P. (2015). Memory part 2: the role of the medial temporal lobe. *AJNR Am. J. Neuroradiol.* 36, 846–849. doi: 10.3174/ajnr.A4169

Reitan, R. M. (1958). Validity of the trail making test as an indicator of organic brain damage. *Percept. Mot. Skills* 8, 271–276. doi: 10.2466/pms.1958.8.3.271

Ronaghi, A., Zibaii, M. I., Pandamooz, S., Nourzei, N., Motamedi, F., Ahmadiani, A., et al. (2019). Entorhinal cortex stimulation induces dentate gyrus neurogenesis through insulin receptor signaling. *Brain Res. Bull.* 144, 75–84. doi: 10.1016/j.brainresbull.2018.11.011

Rönnlund, M., Nyberg, L., Bäckman, L., and Nilsson, L.-G. (2005). Stability, growth, and decline in adult life span development of declarative memory: cross-sectional and longitudinal data from a population-based study. *Psychol. Aging* 20, 3–18. doi: 10.1037/0882–7974.20.1.3

Scheltens, P., Launer, L. J., Barkhof, F., Weinstein, H. C., and van Gool, W. A. (1995). Visual assessment of medial temporal lobe atrophy on magnetic resonance imaging: interobserver reliability. *J. Neurol.* 242, 557–560. doi: 10.1007/BF00868807

Scheltens, P., Pasquier, F., Weerts, J. G., Barkhof, F., and Leys, D. (1997). Qualitative assessment of cerebral atrophy on MRI: Inter- and intra-observer reproducibility in dementia and normal aging. *Eur. Neurol.* 37, 95–99. doi: 10.1159/000117417

Schöll, M., Lockhart, S. N., Schonhaut, D. R., O'Neil, J. P., Janabi, M., Ossenkoppele, R., et al. (2016). PET imaging of tau deposition in the aging human brain. *Neuron* 89, 971–982. doi: 10.1016/j.neuron.2016.01.028

Schuff, N., Amend, D. L., Knowlton, R., Norman, D., Fein, G., and Weiner, M. W. (1999). Age-related metabolite changes and volume loss in the hippocampus by magnetic resonance spectroscopy and imaging. *Neurobiol. Aging* 20, 279–285. doi: 10.1016/S0197–4580(99)00022–6

Schwarz, C. G., Gunter, J. L., Wiste, H. J., Przybelski, S. A., Weigand, S. D., Ward, C. P., et al. (2016). A large-scale comparison of cortical thickness and volume methods for measuring Alzheimer's disease severity. *NeuroImage: Clinical* 11, 802–812. doi: 10.1016/j.nicl.2016.05.017

Shaw, T., York, A., Ziaei, M., Barth, M., Bollmann, S., and Alzheimer's Disease Neuroimaging Initiative (2020). Longitudinal Automatic Segmentation of Hippocampal Subfields (LASHiS) using multi-contrast MRI. *Neuroimage* 218 :116798. doi: 10.1016/j.neuroimage.2020.116798

Signoret, J.-L. (1991). *Batterie d'efficience mnésique, BEM 144*. Paris: Elsevier.

Smith, S. A. (2019). Virtual reality in episodic memory research: a review. *Psychon. Bull. Rev.* 26, 1213–1237. doi: 10.3758/s13423–019-01605-w

Stoub, T. R., Rogalski, E. J., Leurgans, S., Bennett, D. A., and deToledo-Morrell, L. (2010). Rate of entorhinal and hippocampal atrophy in incipient and mild AD: relation to memory function. *Neurobiol. Aging* 31, 1089–1098. doi: 10.1016/j.neurobiolaging.2008.08.003

Stroop, J. R. (1935). Studies of interference in serial verbal reactions. *J. Exp. Psychol.* 18, 643–662. doi: 10.1037/h0054651

Szeszko, P. R., Betensky, J. D., Mentschel, C., Gunduz-Bruce, H., Lencz, T., Ashtari, M., et al. (2006). Increased stress and smaller anterior hippocampal volume. *Neuroreport* 17, 1825–1828. doi: 10.1097/01.wnr.0000246322.58814.b8

Ta, A. T., Huang, S.-E., Chiu, M.-J., Hua, M.-S., Tseng, W.-Y. I., Chen, S.-H. A., et al. (2012). Age-related vulnerabilities along the hippocampal longitudinal axis. *Hum. Brain Mapp.* 33, 2415–2427. doi: 10.1002/hbm.21364

Teter, B., and Ashford, J. W. (2002). Neuroplasticity in Alzheimer's disease. *J. Neurosci. Res.* 70, 402–437. doi: 10.1002/jnr.10441

van Eijk, L., Hansell, N. K., Strike, L. T., Couvy-Duchesne, B., de Zubicaray, G. I., Thompson, P. M., et al. (2020). Region-specific sex differences in the hippocampus. *Neuroimage* 215:116781. doi: 10.1016/j.neuroimage.2020.116781

Vythilingam, M., Luckenbaugh, D. A., Lam, T., Morgan, C. A., Lipschitz, D., Charney, D. S., et al. (2005). Smaller head of the hippocampus in

Gulf War-related posttraumatic stress disorder. *Psychiatry Res.* 139, 89–99. doi: 10.1016/j.pscychresns.2005.04.003

Whitwell, J. L., Josephs, K. A., Murray, M. E., Kantarci, K., Przybelski, S. A., Weigand, S. D., et al. (2008). MRI correlates of neurofibrillary tangle pathology at autopsy: a voxel-based morphometry study. *Neurology* 71, 743–749. doi: 10.1212/01.wnl.0000324924.91351.7d

Whitwell, J. L., Przybelski, S., Weigand, S. D., Knopman, D. S., Boeve, B. F., Petersen, R. C., et al. (2007). 3D maps from multiple MRI illustrate changing atrophy patterns as subjects progress from MCI to AD. *Brain* 130, 1777–1786. doi: 10.1093/brain/awm112

Wisse, L. E. M., Biessels, G. J., Heringa, S. M., Kuijf, H. J., Koek, D. H. L., Luijten, P. R., et al. (2014). Hippocampal subfield volumes at 7T in early Alzheimer's disease and normal aging. *Neurobiol. Aging* 35, 2039–2045. doi: 10.1016/j.neurobiolaging.2014.02.021

Wixted, J. T., and Squire, L. R. (2011). The medial temporal lobe and the attributes of memory. *Trends Cogn. Sci.* 15, 210–217. doi: 10.1016/j.tics.2011.03.005

Wolk, D. A., Das, S. R., Mueller, S. G., Weiner, M. W., and Yushkevich, P. A. (2017). Medial temporal lobe subregional morphometry using high resolution MRI in Alzheimer's disease. *Neurobiol. Aging* 49, 204–213. doi: 10.1016/j.neurobiolaging.2016.09.011

Xie, L., Wisse, L. E. M., Das, S. R., Vergnet, N., Dong, M., Ittyerah, R., et al. (2020). Longitudinal atrophy in early Braak regions in preclinical Alzheimer's disease. *Hum. Brain Mapp.* 41, 4704–4717. doi: 10.1002/hbm.25151

Xie, L., Wisse, L. E. M., Pluta, J., de Flores, R., Piskin, V., Manjón, J. V., et al. (2019). Automated segmentation of medial temporal lobe subregions on *in vivo* T1-weighted MRI in early stages of Alzheimer's disease. *Hum. Brain Mapp.* 40, 3431–3451. doi: 10.1002/hbm.24607

Yun, S., Reynolds, R. P., Petrof, I., White, A., Rivera, P. D., Segev, A., et al. (2018). Stimulation of entorhinal cortex–dentate gyrus circuitry is antidepressive. *Nat. Med.* 24, 658–666. doi: 10.1038/s41591–018-0002–1

Yushkevich, P. A., Pluta, J. B., Wang, H., Xie, L., Ding, S.-L., Gertje, E. C., et al. (2015). Automated volumetry and regional thickness analysis of hippocampal subfields and medial temporal cortical structures in mild cognitive impairment. *Hum. Brain Mapp.* 36, 258–287. doi: 10.1002/hbm.22627

Zhao, W., Xuetong, W., Yin, C., He, M., Li, S., and Han, Y. (2019). Trajectories of the hippocampal subfields atrophy in the Alzheimer's disease: a structural imaging study. *Front. Neuroinform.* 13:13. doi: 10.3389/fninf.2019.00013

Zhou, M., Zhang, F., Zhao, L., Qian, J., and Dong, C. (2016). Entorhinal cortex: a good biomarker of mild cognitive impairment and mild Alzheimer's disease. *Rev. Neurosci.* 27, 185–195. doi: 10.1515/revneuro-2015–0019

Ziegler, G., Dahnke, R., Jäncke, L., Yotter, R. A., May, A., and Gaser, C. (2012). Brain structural trajectories over the adult lifespan. *Hum. Brain Mapp.* 33, 2377–2389. doi: 10.1002/hbm.21374

Zuur, A., Ieno, E. N., Walker, N., Saveliev, A. A., and Smith, G. M. (2009). *Mixed Effects Models and Extensions in Ecology with R*. New York, NY: Springer-Verlag. doi: 10.1007/978–0-387–87458-6

Conflict of Interest: The authors declare that the research was conducted in the absence of any commercial or financial relationships that could be construed as a potential conflict of interest.

Publisher's Note: All claims expressed in this article are solely those of the authors and do not necessarily represent those of their affiliated organizations, or those of the publisher, the editors and the reviewers. Any product that may be evaluated in this article, or claim that may be made by its manufacturer, is not guaranteed or endorsed by the publisher.

frontiers in Aging Neuroscience

ORIGINAL RESEARCH
published: 03 November 2021
doi: 10.3389/fnagi.2021.729635

Longitudinal Analysis of Brain-Predicted Age in Amnestic and Non-amnestic Sporadic Early-Onset Alzheimer's Disease

*Morgan Gautherot[1], Grégory Kuchcinski[1,2,3], Cécile Bordier[2], Adeline Rollin Sillaire[4,5], Xavier Delbeuck[4], Mélanie Leroy[2,4], Xavier Leclerc[1,2,3], Jean-Pierre Pruvo[1,2,3], Florence Pasquier[2,4,5] and Renaud Lopes[1,2]**

[1] UMS 2014–US 41–PLBS–Plateformes Lilloises en Biologie & Santé, University of Lille, Lille, France, [2] Inserm, U1172–LilNCog–Lille Neuroscience & Cognition, University of Lille, Lille, France, [3] Neuroradiology Department, Lille University Medical Centre, Lille, France, [4] Memory Center, DISTALZ, Lille, France, [5] Neurology Department, Lille University Medical Centre, Lille, France

Objective: Predicted age difference (PAD) is a score computed by subtracting chronological age from "brain" age, which is estimated using neuroimaging data. The goal of this study was to evaluate the PAD as a marker of phenotypic heterogeneity and severity among early-onset Alzheimer's disease (EOAD) patients.

Methods: We first used 3D T1-weighted (3D-T1) magnetic resonance images (MRI) of 3,227 healthy subjects aged between 18 and 85 years to train, optimize, and evaluate the brain age model. A total of 123 participants who met the criteria for early-onset (<65 years) sporadic form of probable Alzheimer's disease (AD) and presented with two distinctive clinical presentations [an amnestic form ($n = 74$) and a non-amnestic form ($n = 49$)] were included at baseline and followed-up for a maximum period of 4 years. All the participants underwent a work-up at baseline and every year during the follow-up period, which included clinical examination, neuropsychological testing and genotyping, and structural MRI. In addition, cerebrospinal fluid biomarker assay was recorded at baseline. PAD score was calculated by applying brain age model to 3D-T1 images of the EOAD patients and healthy controls, who were matched based on age and sex. At baseline, between-group differences for neuropsychological and PAD scores were assessed using linear models. Regarding longitudinal analysis of neuropsychological and PAD scores, differences between amnestic and non-amnestic participants were analyzed using linear mixed-effects modeling.

Results: PAD score was significantly higher for non-amnestic patients (2.35 ± 0.91) when compared to amnestic patients (2.09 ± 0.74) and controls (0.00 ± 1). Moreover, PAD score was linearly correlated with the Mini-Mental State Examination (MMSE) and the Clinical Dementia Rating Sum of Boxes (CDR-SB), for both amnestic and non-amnestic sporadic forms. Longitudinal analyses showed that the gradual development of the disease in patients was accompanied by a significant increase in PAD score over time, for both amnestic and non-amnestic patients.

OPEN ACCESS

Edited by:
Yong Liu,
Beijing University of Posts and Telecommunications (BUPT), China

Reviewed by:
Henning U. Voss,
Cornell University, United States
Michael Malek-Ahmadi,
Banner Alzheimer's Institute, United States
Fabricio Ferreira de Oliveira,
Elysian Clinic, Brazil

****Correspondence:***
Renaud Lopes
renaud.lopes@univ-lille.fr

Received: *23 June 2021*
Accepted: *27 September 2021*
Published: *03 November 2021*

Citation:
Gautherot M, Kuchcinski G, Bordier C, Sillaire AR, Delbeuck X, Leroy M, Leclerc X, Pruvo J-P, Pasquier F and Lopes R (2021) Longitudinal Analysis of Brain-Predicted Age in Amnestic and Non-amnestic Sporadic Early-Onset Alzheimer's Disease. Front. Aging Neurosci. 13:729635. doi: 10.3389/fnagi.2021.729635

Conclusion: PAD score was able to separate amnestic and non-amnestic sporadic forms. Regardless of the clinical presentation, as PAD score was a way of quantifying an early brain age acceleration, it was an appropriate method to detect the development of AD and follow the evolution of the disease as a marker of severity as MMSE and CDR-SB.

Keywords: brain age, deep learning, structural MRI, longitudinal analysis, early-onset Alzheimer's disease, phenotypic variants

INTRODUCTION

Throughout life, the brain develops and changes (Teissier et al., 2020). The changes do not occur to the same extent in all brain regions (Trollor and Valenzuela, 2001) and are not uniform over the ages (Scahill et al., 2003). Brain aging does not only impact the function of our brain, it also impacts the structures with a decrease in white matter (WM) and gray matter (GM), and an increase in cerebrospinal fluid (CSF) brain volumes in adulthood (Guttmann et al., 1998). In contrast to WM, the volume decrease in GM is less uniform, with the frontoparietal cortex being more affected than the temporo-occipital cortex (Resnick et al., 2003). However, the shrinkage does not necessarily result from a decrease in the number of neurons but mainly from a reduction in their volume (Dickstein et al., 2007). Therefore, normal cellular brain aging is characterized more by subtle changes than a large-scale loss of cells (Teissier et al., 2020). As a result, it is more difficult to characterize the pace of these changes, the biological age of the brain, and all the processes involved in brain aging (Peters, 2006).

It is now widely assumed that Alzheimer's disease (AD) reflects a form of accelerated aging (Cao et al., 2010; Jones et al., 2011; Saetre et al., 2011). For this reason, a growing number of studies investigated both normal and AD age-related changes (Raji et al., 2009; Beheshti et al., 2020). Brain region volumetry may be of interest in the diagnosis of AD with a relatively preserved prefrontal cortex region and an atrophy of hippocampus compared to healthy people (Head et al., 2005; Jack and Holtzman, 2013). However, significant phenotypic heterogeneity of AD is widely recognized, as several atypical variants are described other than the typical limbic-predominant subtype, which is characterized by an amnestic presentation and a pattern of brain atrophy preferentially localized to the limbic areas (Ferreira et al., 2020). Atypical variants are characterized by a hippocampal-sparing pattern of brain atrophy that relatively spares the limbic structures but more severely affects neocortical areas (Whitwell et al., 2012; Cho et al., 2013; Risacher et al., 2017). Moreover, there is significant heterogeneity in the locations of atrophy across individual patients (Tetreault et al., 2020).

Magnetic resonance imaging (MRI) is a powerful non-invasive tool to investigate brain structural changes throughout ages *in vivo* (Guttmann et al., 1998; Sowell et al., 2003). These images can show changes in GM and WM during the maturation of the brain (Giedd et al., 1999; Paus, 1999; Sowell et al., 1999, 2001; Courchesne et al., 2000; Thompson et al., 2000) and during aging (Bartzokis et al., 2001; Jernigan et al., 2001). Many markers, such as cortical thickness and volumetric measures, are associated with brain aging in healthy controls and neurodegenerative diseases (Raji et al., 2009). Although the brain undergoes characteristic changes due to aging over the course of a lifetime, the impact may be slightly different for each individual. Not only are structural characteristics involved in brain change but also education and occupation may be proxies for brain functional reserve, reducing the severity and delaying the clinical expression of AD pathology.

Deep learning techniques, such as convolutional neural networks (CNN), have the benefits to identify MRI markers, and they can model complex non-linear relationships without the need for predefined traditional MRI markers (Cole et al., 2017b; Beheshti et al., 2018). However, these models need large and diverse samples for training the complex deep network, making it possible only by several data sharing initiatives. A growing field of research combining MRI markers and CNN algorithms are focusing on brain age estimation in the healthy population (Sajedi and Pardakhti, 2019), with a mean absolute error (MAE) of 3–5 years in age ranging from 18- to 90-year-olds using T1-weighted (T1w) structural MRI (Cole et al., 2017a; Franke and Gaser, 2019; Couvy-Duchesne et al., 2020). Predicted age difference (PAD), defined as the difference between chronological age and predicted age, is associated with disease status, including AD and mild cognitive impairment (Franke et al., 2010; Franke and Gaser, 2012; Löwe et al., 2016).

Early-onset AD (EOAD), which is defined by an age of onset $\leq$65 years, is of interest in the study of the phenotypic heterogeneity due to the higher frequency of non-amnestic variants than in late-onset AD (LOAD) (Palasí et al., 2015). Atypical presentations affect language abilities, visuospatial abilities, or executive functions (Marshall et al., 2007; Garre-Olmo et al., 2010; Koedam et al., 2010; Balasa et al., 2011; Sá et al., 2012). Patients with EOAD appear to exhibit faster cognitive decline than patients with LOAD (Haxby et al., 1992; Pettigrew et al., 2017). However, studies on LOAD tend to show that the later onset of dementia was the only prominent variable accelerating all cognitive and functional outcomes (de Oliveira et al., 2018). Moreover, studies on cognitive reserve tend to show the same result. The concept of cognitive reserve arose from the idea that life experiences associated with cognitive stimulation could increase brain resilience to neuropathologic lesion and delay the onset of symptoms of functional decline (Haxby et al., 1992; Soldan et al., 2020). However, cognitive reserve did not have a linear effect on the development of brain injuries, and even experienced a paradox. Previous studies suggest that while the cognitive reserve is associated with a delayed symptom onset

(Qiu et al., 2001; Reed et al., 2010; Roe, 2011; Soldan et al., 2013; Pettigrew et al., 2017; Robitaille et al., 2018; van Loenhoud et al., 2019), it could be related to more severe brain atrophy and accelerated cognitive decline in advanced AD stages (Wilson et al., 2000; Scarmeas, 2005; Andel et al., 2006; Bracco et al., 2007; Hall et al., 2007; Yoon et al., 2015; Myung et al., 2016; Soldan et al., 2017). These contradictory results may be explained by a higher proportion of non-amnestic variants and higher education level (which seems to be a proxy for cognitive reserve) in EOAD patients.

Despite the growing interest to better understand the mechanisms underlying phenotypic heterogeneity in EOAD using MRI (Mendez, 2012; Falgàs et al., 2020a; Vanhoutte et al., 2020), there is a potential bridge between these group-level studies and the clinical care of individual AD patients. The aim of this study was to investigate the PAD as a marker of phenotypic heterogeneity in EOAD for diagnostic and follow-up purposes. We hypothesized that (i) PAD marker would distinguish between clinical variants of EOAD, and (ii) progression of PAD marker would follow the functional and cognitive severity of disease for both phenotypes.

MATERIALS AND METHODS

EOAD Population

Participants with EOAD were all recruited at the University Hospital's Memory Resources and Research Center in Lille, France. The participants were part of the COhorte Malade Alzheimer's Jeunes (Early-onset Alzheimer's cohort in French, COMAJ), which was initiated in 2009.

The COMAJ study was approved by the local institutional investigational review board [Ethic committee (CPP Nord-Ouest I); reference: 110-05]. Written informed consent was obtained from all participants and/or their relatives. Inclusion criteria were as follows: (a) participants should meet National Institute on Aging - Alzheimer's Association (NIA-AA) criteria for "probable AD dementia with intermediate evidence of AD pathophysiological process" (McKhann et al., 2011) and International Working Group (IWG) 2 criteria (Dubois et al., 2014); (b) participants must be $\leq$60 years of age at the time of first symptoms; (c) evidence of abnormal CSF biomarkers with $A\beta_{42}$ below 700 pg/mL and total tau and phosphorylated tau above 400 and 60 pg/mL, respectively (Lehmann et al., 2014). The final diagnosis of sporadic EOAD was based upon extensive reviewing of clinical history, CSF biomarkers, and neuropsychological and imaging data by a multidisciplinary board. Criteria for pathological mutations were onset of symptoms $<$ 51 years old or family history of EOAD in the first degree. Individuals with early-onset dementia in first-degree relatives or those with a confirmed mutation in the PSEN1, PSEN2, or APP genes were excluded. Out of 123 participants, 16 participants were searched for APP, PSEN1, and PSEN2.

A total of 217 sporadic EOAD participants were included and classified as amnestic presentation ("typical") or non-amnestic presentation ("atypical") with prominent cognitive impairments in language, visuospatial, or executive functions, based on neuropsychological tests of 4 cognitive domains listed below:

1. Episodic memory: free and cued selective recall, the "doors" part of the Doors and People test, and the Visual Association Test (Lindeboom, 2002; Schoonenboom et al., 2005).
2. Language: the DO80 confrontation naming test with 80 images (Deloche and Hannequin, 1997).
3. Visuospatial function: evaluation of upper limb praxis, evaluation of visuoconstructive abilities using the Rey-Osterrieth complex figure test and the Beery-Buktenica developmental test of visual-motor integration (Beery VMI test) (Lim et al., 2015), evaluation of visual gnosis using subtests from the Visual Object and Space Perception Battery (the screening test, incomplete letters, and number location).
4. Executive functions: evaluation of working memory using the forward and backward digit span task from the Wechsler memory scale (third edition), the Frontal Assessment Battery at bedside, category verbal fluency (animals), and lexical verbal fluency (the letter P) (Godefroy, 2008).

Three-dimensional T1-weighted (3D-T1) images were acquired on a 3T MRI scanner (Achieva, Philips, Best, the Netherlands), using an 8-channel phased-array head coil and whole-body coil transmission (field of view = 256 × 256 × 160 mm^3, isotropic voxel size 1 × 1 × 1 mm^3, TR = 9.9 ms, TE = 4.6 ms, and flip angle = 8°) for initial evaluation and follow-up. In addition to MRI, each patient was evaluated annually for a maximum of 4 years by the Mini-Mental State Examination (MMSE) (Folstein et al., 1985) and the Clinical Dementia Rating Sum of Boxes (CDR-SB) (Hughes et al., 1982). Predicted brain age was obtained from participants who completed a structural MRI scan at least for one time point during follow-up. Based on the availability and quality of MR images of the 217 EOAD participants, 74 amnestic and 49 non-amnestic participants were finally retained (**Figure 1**). Out of the total number, 70, 28, 21, 17, 8 amnestic and 46, 49, 38, 28, 13 non-amnestic patients were finally retained at baseline, year 1, year 2, year 3, and year 4, respectively (**Supplementary Table S1**).

Healthy Population

A total of 3,227 MRI scans from 2,065 healthy participants (48% men, mean age = 33.6 ± 12.3 years, age range from 18 to 85 years) were included in the study. Data were compiled from publicly available sources made available *via* various data sharing initiatives (**Supplementary Table S2**). According to the local study protocols, all participants were free from neurological or psychiatric disease. We retained only images acquired at 3T MRI using 3D-T1 sequence. The subject consent was obtained at each local study site and each contribution was ethically approved.

These images were divided into three datasets—a control dataset to compare with the patients from the COMAJ cohort, the training dataset to train and optimize our model, and the testing dataset to test its performance.

For our control dataset, we used images of 116 age- and sex-matched healthy subjects from the Parkinson's Progression Markers Initiative (PPMI) (www.ppmi-info.org/data) and the Alzheimer's Disease Neuroimaging Initiative (ADNI)

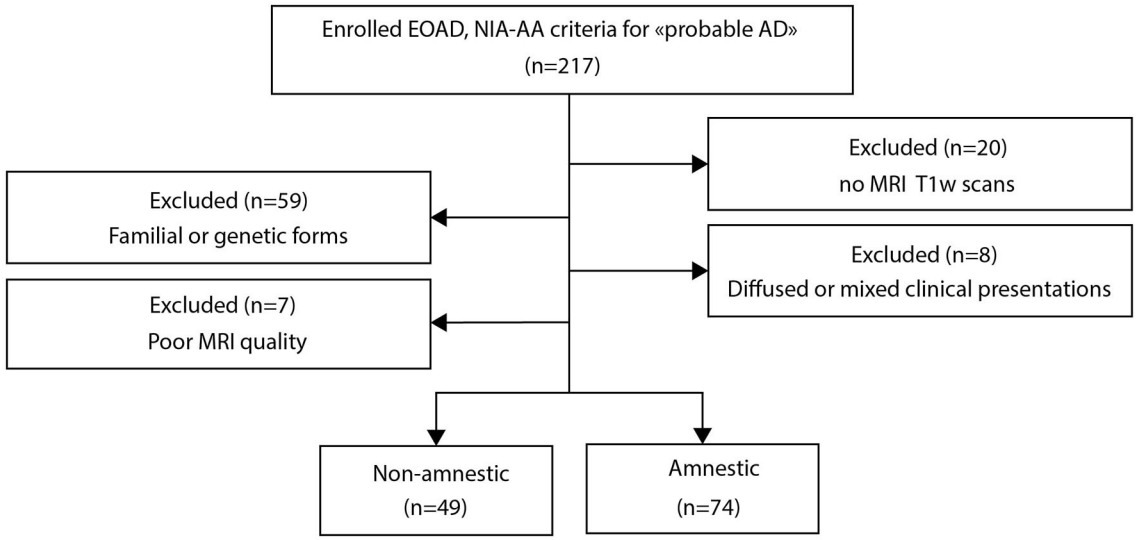

FIGURE 1 | Flowchart of the study population.

(adni.loni.usc.edu). The ADNI was launched in 2003 as a public–private partnership, led by Principal Investigator, Michael W. Weiner, MD. The primary goal of ADNI has been to test whether serial MRI, positron emission tomography and other biological markers, and clinical and neuropsychological assessment can be combined to measure the progression of mild cognitive impairment and early AD. These images were acquired by scanners from the three major MRI manufacturers (General Electric, Philips, and Siemens). These data were never used in the training, the hyperparametrization, or the testing of our brain age model.

The training and testing sets were composed of 3,083 MR acquisitions from 1,955 subjects and 144 MR acquisitions from 110 subjects obtained from 6 data sharing initiatives, which include Information eXtraction from Images (IXI), Human Connectome Project (HCP) (Van Essen et al., 2012), Center Of Biomedical Research Excellence (COBRE), Mind Clinical Imaging Consortium (MCIC), Neuromorphometry by Computer Algorithm Chicago (NMorphCH), and enhanced Nathan Kline Institute-Rockland Sample (NKI-RS) (more details in **Supplementary Table S2**).

Data Preprocessing

Minimal preprocessing steps were performed on 3D-T1 images (Lombardi et al., 2020). First, images were corrected for magnetic field inhomogeneity effects and skull-stripped using VolBrain software (volbrain.upv.es) (Manjón and Coupé, 2016). Brain extractions were systematically checked for possible errors (brain regions missing), and manual corrections were performed by a neuroradiologist (GK), when deemed necessary (Fischl, 2012). Then, preprocessed 3D-T1 images were linearly registered into MNI space and resampled to 1 mm^3 using SPM software (fil.ion.ucl.ac.uk/spm/software/spm12). Finally, intensity normalization was performed using min–max normalization.

Furthermore, for correlation purposes, GM, WM, and CSF brain volumes were estimated using VolBrain software (Manjón and Coupé, 2016).

Brain Age Prediction Model

For the prediction of chronological age using MRI from healthy control subjects, also called "brain age," our model was based on 3D convolutional neural network (CNN) architecture. This architecture, which was inspired by Cole et al. (2017a), is both simple and efficient for the prediction of brain age using 3D-T1 images (**Figure 2**).

The proposed architecture took preprocessed 3D-T1 images with dimensions of $182 \times 218 \times 182$ voxels. The weights of the model were determined by minimizing the cost function, here the mean absolute error (MAE). To optimize the weights, we used stochastic gradient descent optimization algorithm (Sutskever et al., 2013) with a learning rate of 0.001, a momentum of 0.1, and a learning rate decay of 5e-05. We used a batch size of 8 during 150 iterations. We performed an early stopping at the epoch 113 because it gave us the best MAE on the validation set.

During the training phase, we performed a data augmentation strategy on-the-fly consisting of performing translation and rotation of the MR images. This technique generated additional artificial training images to prevent the model from overfitting and was empirically found to yield better performance (Shorten and Khoshgoftaar, 2019).

We used a 5-fold cross-validation procedure on our training set for optimizing hyperparameters and for assessing how our results would generalize to another dataset of the same distribution. The distribution of patient ages was not uniform in the training set, so in the cross-validation, the distribution of the validation set was not uniform either (**Figure 3A**).

To test the performance of our model across the ages, we needed a more balanced testing set. The testing set had 144

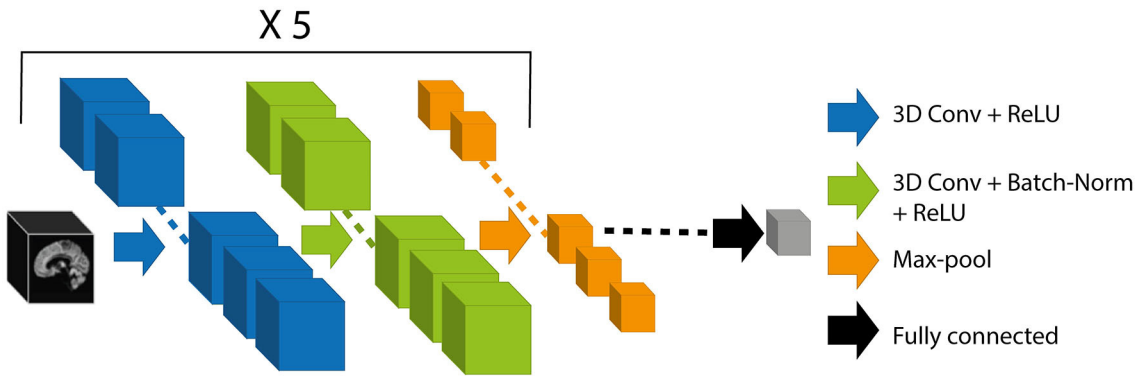

FIGURE 2 | Schematic representation of the CNN architecture. The black box represents the 3D-T1 images as inputs of our model. Each block consisted of 3D convolution of kernel size (3 × 3 × 3), ReLU activation, 3D convolution of kernel size (3 × 3 × 3), batch normalization, rectified linear unit activation, and max-pooling layer of pooling size (2 × 2 × 2). The block was repeated 5 times. The output of the network (gray box) corresponds to the brain-predicted age. CNN, convolutional neural network; ReLU, Rectified Linear Unit.

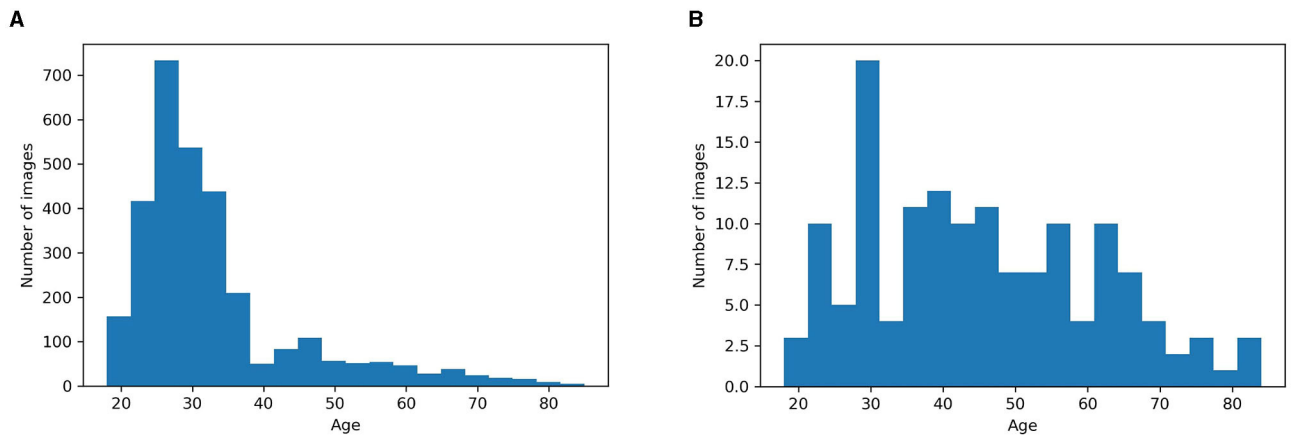

FIGURE 3 | (A) Age distribution of subjects in the training set. **(B)** Age distribution of subjects in our testing set. We randomly selected 10 images every 5 years to obtain a uniform distribution of images throughout the age.

images from 110 subjects, with 10 randomly selected images for each 5 years period from 18 to 70 years, and 10 randomly selected images from 70 years and above. With this pseudo-random selection, we obtained a more uniform distribution than the training age distribution (**Figure 3B**).

Bias Correction in Brain Age Prediction

Like all regression methods, the brain age model is subject to the fundamental phenomenon of "regression toward the mean" (Galton, 1886). This bias overestimates age among younger participants and underestimates it in older participants. Although studies had mainly attributed the bias to inconsistency in the distribution of noise over the life course (Cole et al., 2017a), the reasons are still largely unknown. The bias seems rather universal, regardless of the data, age range, sample size, and even the particular methods used (linear machine learning or deep learning methods) (Liang et al., 2019). To correct the regression toward the mean phenomenon, we used the following equation (Liang et al., 2019):

$$\textit{regressed age predicted} = \textit{intercept} + \alpha^{*}\textit{chronological age} + \textit{error} \quad (1)$$

α is a regression coefficient associated with the chronological age, and in our study $\alpha = 0.13$.

Patient Prediction

Weights from the training model were used for the prediction of brain age of healthy controls and EOAD patients. This age was regressed out using Equation 1. PAD score was calculated as the difference between predicted brain age and chronological age at the acquisition time. We calculated the PAD z-score for the three groups taking the control group as standard.

TABLE 1 | Demographic and clinical characteristics at baseline according to clinical forms of EOAD and controls.

Indicators	Amnestic	Non-amnestic	Control	Effect/*p*-value
N	70	46	116	
CDR-SB	6.71 ± 4.25	7.21 ± 3.81		0.327[a]
MMSE	17.14 ± 6.71	16.13 ± 6.96		0.192[a]
Disease duration, years	5.45 ± 2.91	4.55 ± 2.14		0.157[a]
Education level, years	9.64 ± 2.82	10.41 ± 2.82		0.0357[ac]
Age, years	59.30 ± 4.28	58.61 ± 3.68	59.05 ± 4.05	0.611[b]
Female, n (%)	36 (51%)	26 (56%)	63 (54%)	0.73[a]

Quantitative variables were quoted as the mean ± SD (interquartile range).
[a] χ^2 and Wilcoxon tests were applied to categorical and continuous variables, respectively.
[b] Kruskal–Wallis test was applied to continuous variables for more than two populations.
[c] $p < 0.05$.
CDR-SB, Clinical Dementia Rating Sum of Boxes; MMSE, Mini-Mental State Examination.

TABLE 2 | Model performance on cross-validation datasets.

Folds	1	2	3	4	5	Mean ± SD
MAE validation (year)	3.85	2.74	3.06	2.77	3.48	3.18 ± 0.43

MAE, mean absolute error; SD, standard deviation.

Model Visualization With Gradient Class Activation Maps

Gradient Class Activation Maps (Grad-CAM) approach uses the final convolutional layer gradients to produce a map highlighting the brain regions used for brain age prediction (Selvaraju et al., 2017). Grad-CAM approach was used to create an average map called an attention map for each group of participants (controls, non-amnestic EOAD, and amnestic EOAD participants).

Statistical Analysis

All the analyses were conducted in Python (3.8.5) using scipy (1.6.1) and statsmodels (0.12.1). At baseline, intergroup differences between controls, amnestic, and non-amnestic EOAD participants in demographic, clinical, and neuropsychological features were assessed using Wilcoxon or Kruskal–Wallis tests for continuous variables and chi-squared tests for categorical variables. To quantify the magnitude of effect sizes between groups, we used Cliff's delta (Cliff, 1993). Between-group differences for neuropsychological and PAD scores were assessed using linear models. Regarding the longitudinal analysis of neuropsychological and PAD scores, differences between amnestic and non-amnestic participants were analyzed using univariate linear mixed-effects (LME) models. LME models provide an approach for analyzing longitudinal data while handling variable missing rates and non-uniform timing. These models also make use of participants with a single time point to characterize population-level regionally specific differences. Equality of regression coefficients was assessed by the Chow test (Toyoda, 1974).

The threshold for statistical significance was set to $p < 0.05$. Bonferroni *post-hoc* test was used to correct for multiple comparisons.

Code Availability

Code is available on github at https://github.com/MorganGautherot/Brain_age_model.

RESULTS

Demographic and Clinical Data at Baseline

Baseline demographic and clinical data between amnestic and non-amnestic EOAD forms are shown in **Table 1**. The non-amnestic and amnestic EOAD groups did not differ significantly with regard to age at inclusion, disease duration from the first symptoms, and cognition (CDR-SB and MMSE). The only difference was the education level, which was higher for the non-amnestic patients (10.41 ± 3.68) when compared with the amnestic patients (9.64 ± 2.82). Overall, the EOAD participants had a moderately severe disease (MMSE score was 17.17 ± 6.71 for amnestic, and 16.13 ± 6.96 for non-amnestic patients). Thus, education level was used as a covariate in the comparison of EOAD groups.

Convolutional Neural Networks Accurately Predict Age Using Neuroimaging Data

Analysis showed that our CNN model accurately predicted the chronological age of healthy subjects, using 3D-T1 images. We obtained an MAE of 3.18 ± 0.43 years on training data, after the cross-validation approach (**Table 2**), and 4.34 years on the testing set (**Figure 4A**).

Significant correlation was found between age and prediction error before bias correction ($r = -0.33$, $p < 0.001$), but not after bias correction ($r = 0.00$, $p = 0.99$) (**Figures 4B,C**).

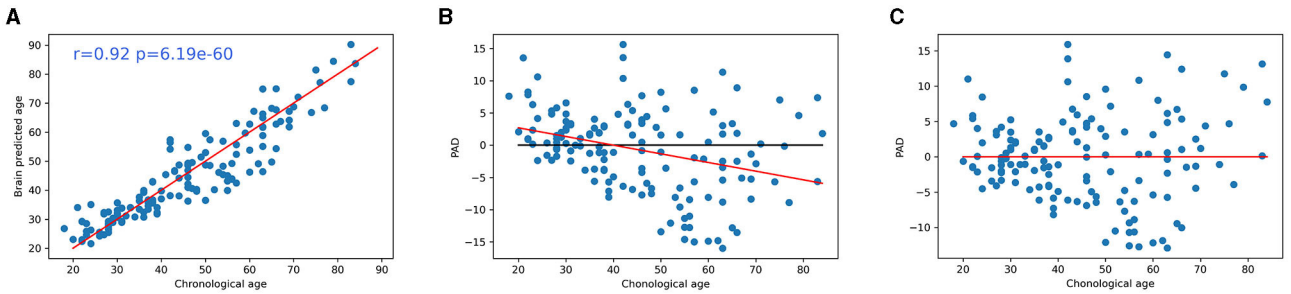

FIGURE 4 | (A) Accuracy of CNN for brain age prediction using testing set. Scatter plots depict chronological age (x-axis) and brain-predicted age (y-axis) on the testing set subjects. The r value was the Pearson's correlation coefficient of brain-predicted age with chronological age and p was the associated *p*-value. Plot of the chronological age in function to PAD z-score **(B)** before and **(C)** after regression. CNN, convolutional neural network; PAD, predicted age difference.

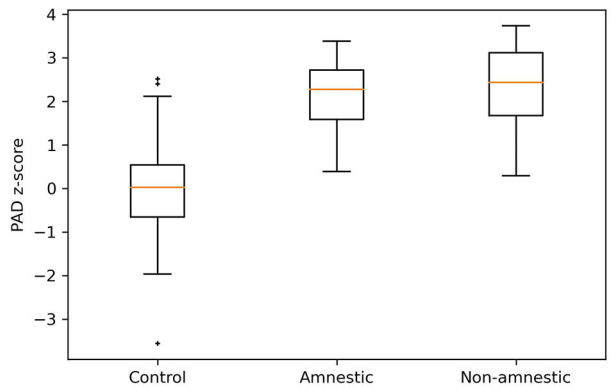

FIGURE 5 | PAD z-scores distribution for controls, amnestic, and non-amnestic EOAD patients. A Kruskal–Wallis test was applied to these groups with a $p < 0.001$. Using Cliff's delta, we showed that there was an effect size between controls and non-amnestic population ($d = 0.91$), controls and amnestic population ($d = 0.90$), and non-amnestic and amnestic population ($d = 0.22$). PAD, predicted age difference. †, ‡; represent the outliers of the distribution.

Comparison of Predicted Brain Age Between Participants of EOAD Subtypes and Controls

Predicted age difference z-scores were different for the three groups ($p < 0.01$), with higher PAD z-scores for non-amnestic patients (2.35 ± 0.91) when compared to amnestic patients (2.09 ± 0.74, $p = 0.022$) and controls (0.00 ± 1, $p < 0.001$) (**Figure 5**). PAD z-scores were higher for amnestic patients when compared to controls ($p < 0.001$) (**Figure 5**). There was a small effect size between amnestic patients and non-amnestic patients (Cliff's delta = 0.22). For controls, there was a large effect size with amnestic (Cliff's delta = 0.90) and non-amnestic (Cliff's delta = 0.91) population.

Predicted age difference z-scores were predictive of a low MMSE (non-amnestic patients: $\alpha = -3.5$, intercept = 22, $p < 0.001$; amnestic patients: $\alpha = -2.5$, intercept = 21, $p =$ 1.7e-02) and a high CDR-SB score (non-amnestic patients: $\alpha = 1.7$, intercept = 3.1, $p < 0.001$; amnestic patients: $\alpha = 2.3$, intercept = 1.8, $p < 0.001$) for EOAD participants (**Figure 6**).

The percentage of CSF brain volume was positively correlated to PAD z-score for non-amnestic EOAD ($r = 0.35$, $p = 0.0025$), amnestic EOAD ($r = 0.35$, $p = 0.0025$), and control participants ($r = 0.30$, $p < 0.001$) (**Figure 7A**). Amnestic ($p < 0.001$) and non-amnestic EOAD patients ($p < 0.001$) had a more rapid evolution of PAD z-scores in relation to the percentage of CSF brain volume when compared to control participants (**Figure 7A**). Amnestic and non-amnestic EOAD patients had no statistical difference between PAD z-scores and percentage of CSF brain volumes ($p = 0.1$).

The percentages of GM volume were strongly negatively correlated to PAD z-scores for non-amnestic EOAD ($r = -0.72$, $p < 0.001$), amnestic EOAD ($r = -0.55$, $p < 0.001$), and control participants ($r = -0.50$, $p < 0.001$) (**Figure 7B**). Amnestic ($p < 0.001$) and non-amnestic EOAD patients ($p < 0.001$) had a more rapid evolution of PAD in relation to the percentage of GM volume when compared to control participants (**Figure 7B**). Amnestic and non-amnestic patients had no statistical difference between PAD z-scores and percentage of GM volumes ($p = 0.092$).

The percentages of WM volume were not correlated to PAD z-scores for non-amnestic ($r = 0.01$, $p = 0.94$), amnestic EOAD ($r = -0.01$, $p = 0.89$), and control participants ($r = 0.11$, $p =$ 0.22) (**Figure 7C**).

Attention Map

For all groups, attention maps showed that mostly subcortical white matter temporo-occipital junction and extension to subcortical white matter middle frontal gyrus were used for brain age prediction (**Figures 8A–C**). In these structures, we noticed a more important involvement of the right hemisphere. For amnestic and non-amnestic EOAD subtypes, attention maps were similar but statistically took into account more information than the controls ($p < 0.05$ FWE-corrected). EOAD subtypes had the involvement of the left superior temporal gyrus and right middle and inferior gyrus and anterior insula (**Figures 9A,B**).

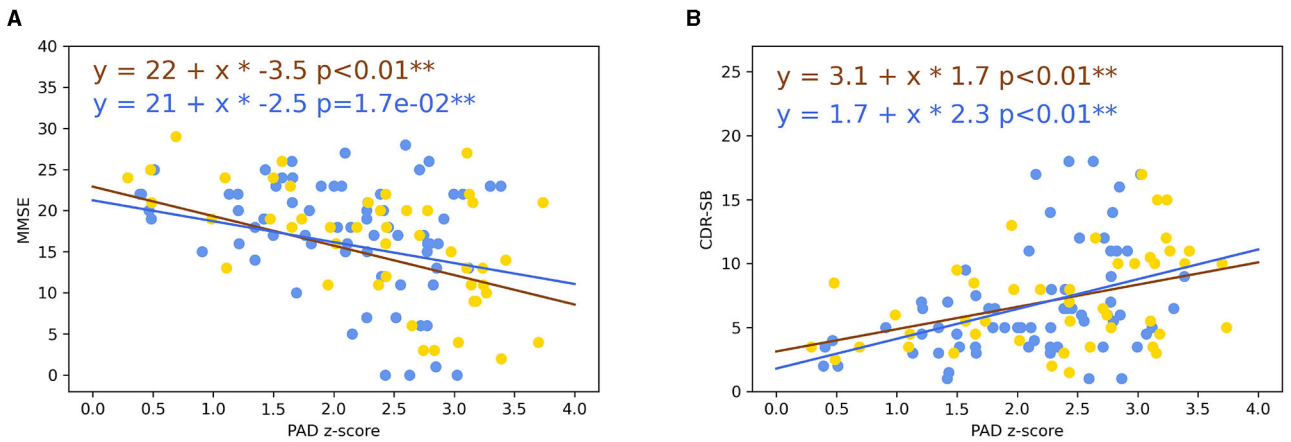

FIGURE 6 | (A) Plot of the MMSE in function of PAD in the EOAD population. **(B)** Plot of the CDR-SB in function of PAD in the EOAD population. Lines represented linear trajectories using linear regression model (blue line: amnestic EOAD and yellow line: non-amnestic EOAD). $^{**}p < 0.05$. MMSE, Mini-Mental State Examination; PAD, predicted age difference; CDR-SB, Clinical Dementia Rating Sum of Boxes; EOAD, early-onset Alzheimer's disease.

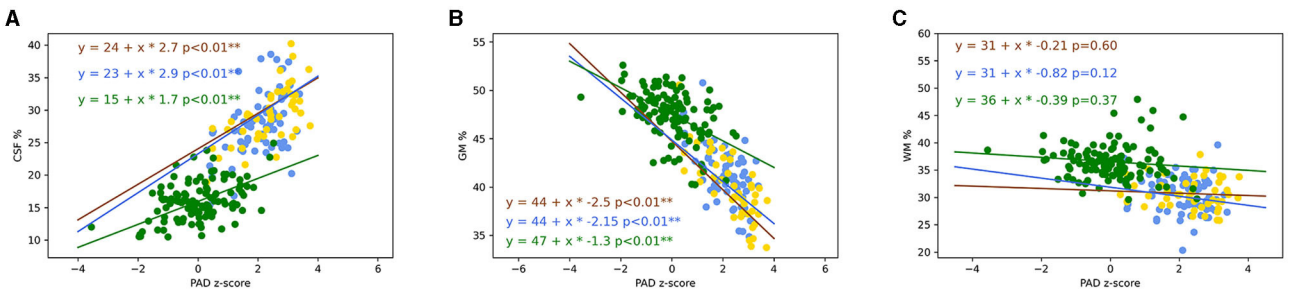

FIGURE 7 | Plot of the percentage of brain CSF **(A)**, GM **(B)**, and WM **(C)** volumes in function of PAD. Lines represented trajectories using linear regression model (blue line: amnestic EOAD; yellow line: non-amnestic EOAD; and green line: control). Pearson correlation was computed between PAD and MMSE on non-amnestic and amnestic EOAD populations. The two coefficients of the regression were not statistically different between non-amnestic and amnestic compared to GM and CSF volumes (Chow test). The two coefficients of the regression for PAD in function of GM and CSF volumes were statistically different between controls and EOAD subtypes (Chow test). $^{**}p < 0.05$. CSF, cerebrospinal fluid; PAD, predicted age difference; GM, gray matter; WM, white matter; EOAD, early-onset Alzheimer's disease; MMSE, Mini-Mental State Examination.

Longitudinal Analysis of Predicted Age Between EOAD Subtypes

The gradual development of disease in patients was accompanied by a significant increase in PAD z-scores over time ($p < 0.01$) (**Figure 10**). Using the Chow test, there was no statistical difference ($p = 0.096$) observed in the PAD z-scores evolution between amnestic and non-amnestic EOAD patients.

DISCUSSION

In this study, we predicted the brain age of EOAD patients based on 3D-T1 images using a 3D CNN algorithm trained on a cohort of 1,955 healthy controls. We compared PAD z-scores in amnestic and non-amnestic EOAD patients and healthy controls. Although the groups of participants were matched with their chronological age, PAD z-scores were higher for EOAD patients when compared to controls. The brain regions used for brain age prediction were also different between groups with the involvement of left superior temporal gyrus and right middle and inferior gyrus and anterior insula in EOAD patients. Moreover, we showed that non-amnestic EOAD patients had a higher PAD z-score than amnestic EOAD patients. Finally, we compared PAD z-scores longitudinally over a period of 4 years and found that the PAD z-score increased with the severity of the disease.

The atrophied regions detected in AD patients largely overlapped with the regions showing a normal age-related decline in healthy control subjects (Raji et al., 2009). As PAD score was a way of quantifying an early brain age acceleration, it was an appropriate method to detect the development of neurodegenerative diseases such as AD. This characteristic of PAD score had already shown its potential to provide clinically relevant information (Franke et al., 2010). Studies showed that PAD score longitudinally increased with the severity of the

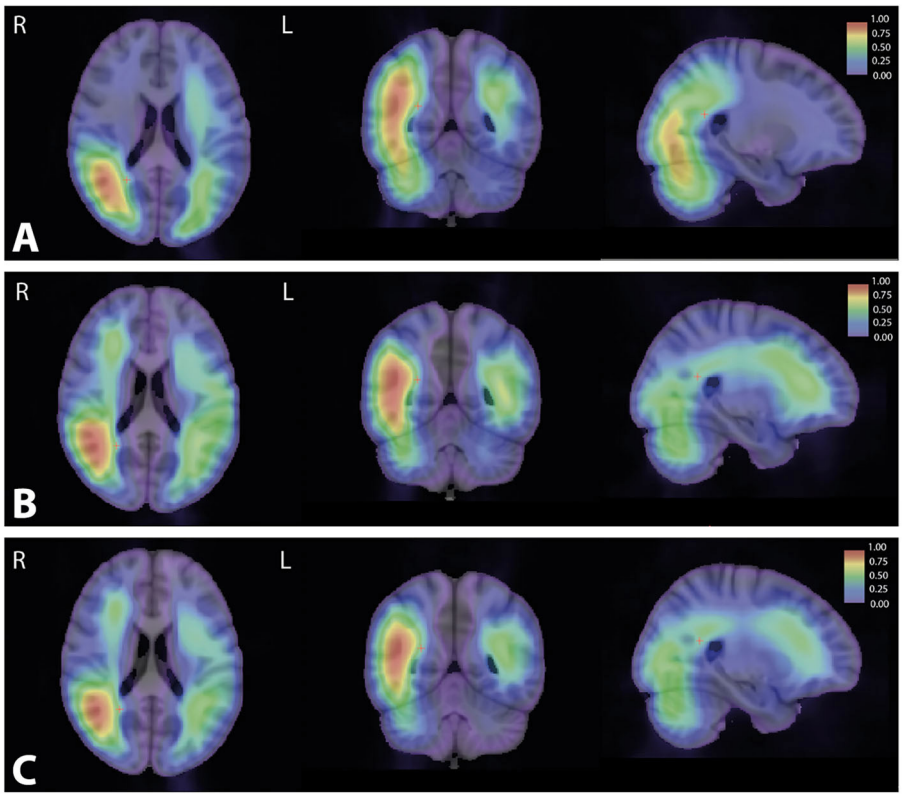

FIGURE 8 | Attention maps computed by Grad-CAM for control, non-amnestic, and amnestic EOAD participants. The resulting averages for each population were overlaid on MNI template space. MNI coordinate of the red cross (25.28, −82.36, 33.42). **(A)** Average of the attention map on the control population. **(B)** Average of the attention map on the non-amnestic EOAD population. **(C)** Average of the attention map on the amnestic EOAD population. R, right hemisphere; L, left hemisphere; Grad-CAM, Gradient-weighted Class Activation Mapping; EOAD, early-onset Alzheimer's disease; MNI, Montreal Neurological Institute.

impairment and allowed the detection of conversions from mild cognitive impairment to AD (Franke and Gaser, 2012; Gaser et al., 2013). However, these studies were based on the comparisons of AD and healthy controls, while several AD subtypes exist. In this study, we studied the EOAD which was defined by an age of onset $\leq$ 65 years. Due to its early onset and the clinical overlap between different diseases, there was a significant delay in the diagnosis of EOAD (van Vliet et al., 2013). One specificity of EOAD is the higher frequency of non-amnestic variants when compared to LOAD (Palasí et al., 2015). Amnestic and non-amnestic forms have different origins and evolution on the cerebral degeneration (Ossenkoppele et al., 2015; Xia et al., 2017; Phillips et al., 2018; Riedel et al., 2018; Vanhoutte et al., 2020). We investigated PAD score as a marker of phenotypic heterogeneity in EOAD for diagnosis.

At baseline, PAD z-scores were positively correlated with MMSE and negatively correlated with CDR-SB. A previous study showed similar results in AD (Beheshti et al., 2018). The correlations of PAD with CDR-SB and MMSE mean that PAD was correlated with the cognitive state of the patients. They confirmed that a more impaired patient tended to have a higher PAD. It was interesting to see that PAD was not only useful in separating healthy population from patients with neurodegenerative diseases, but that it was able to differentiate amnestic and non-amnestic EOAD patients ($p = 0.022$). Non-amnestic patients developed a more marked neocortical and basal nuclei atrophy. However, they had an identical severity on the MMSE, which could be due to a greater cognitive reserve because of a significantly higher level of education or due to the fact that the MMSE is less adapted to quantify the disorders in patients with executive type disorders. One of the strengths of our study is the fact that we analyzed the evolution of PAD z-scores between EOAD phenotypes over a period of 4 years. PAD z-scores increased over time similarly between amnestic and non-amnestic EOAD forms. This result corroborated the positive correlation between the severity of EOAD disease and the increase in PAD z-scores. The evolution of PAD z-scores over time was interesting because it could give a marker of evolution that was independent of the clinical form and of any other element such as cognitive scales that have their limits or clinical scales such as MMSE and CDR-SB (collected subjectively from the caregiver). This would make it possible to get rid of this heterogeneity and show the evolution in an objective way.

One originality of our study was the search for the interpretation of the PAD score in order to know about the brain information on which it was based. We computed the

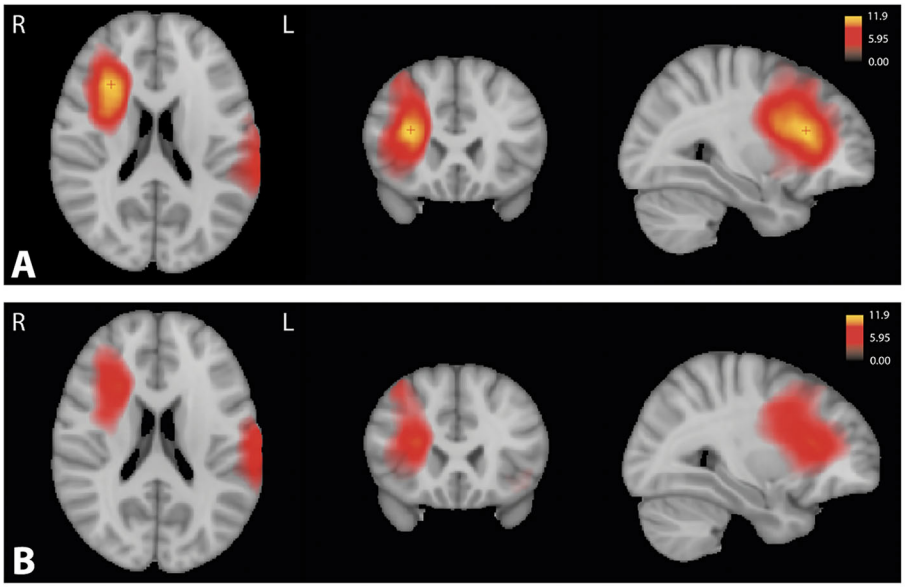

FIGURE 9 | Significant *T*-value map ($p < 0.05$) computed using ANOVA corrected by the family-wise error method between the attention maps of the control group and **(A)** the amnestic and **(B)** the non-amnestic groups. Coordinate of the slice (25.11, 18.40, 25.92). R, right hemisphere; L, left hemisphere; ANOVA, Analysis of variance.

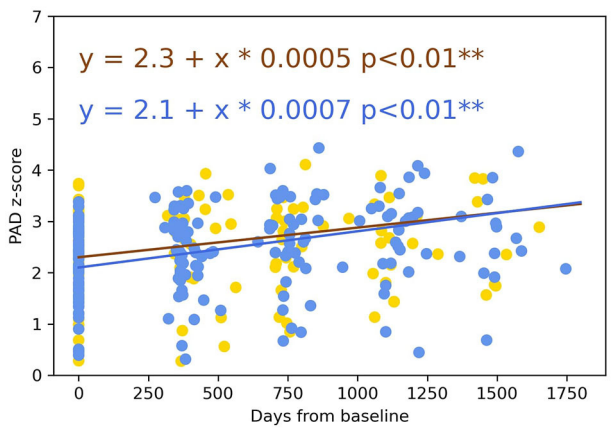

FIGURE 10 | Longitudinal evolution of the PAD over 4 years between amnestic and non-amnestic patients. Lines represented trajectories using linear-mixed-effects models (yellow line: non-amnestic EOAD and blue line: amnestic EOAD). The two coefficients of the regression were not statistically different (Chow test, $p = 0.096$). PAD, predicted age difference; EOAD, early-onset Alzheimer's disease. $^{**}p < 0.05$.

attention maps to show the most involved regions for the brain age prediction. For the three populations, the brain age model took into account common area of the brain with the involvement of the subcortical white matter temporo-parieto-occipital junction and the extension to subcortical white matter middle frontal gyrus. We noticed that the model took more information on the right hemisphere than on the left hemisphere. For the EOAD subtypes, the model statistically accounted for additional structures such as the left superior temporal gyrus and the right middle and inferior frontal gyrus and anterior insula. We also looked for elements of interpretation in the interactions of the PAD with the different tissues of CSF, WM, and GM, which changed throughout life. As GM tissues decreased with age (Narvacan et al., 2017), it was not surprising that PAD score was negatively correlated with the GM volume for each group. The GM volume did not decrease in the same way in all groups. EOAD had lower GM volume, which was consistent with the fact that AD experienced a faster decrease in GM volume when compared to aging subjects (Frings et al., 2014). Even if WM volume changed during the course of life (Guttmann et al., 1998; Courchesne et al., 2000), our brain age model did not use this information to compute PAD score. In aging, due to ventricular dilatation and the decrease of GM and WM volumes, the CSF volume increased with age (Courchesne et al., 2000). We observed a positive correlation between CSF brain volume and PAD score for each group. Nevertheless, EOAD patients had higher CSF brain volume than controls, which was in agreement with the previous studies on EOAD and LOAD patients (Anoop et al., 2010; Teng et al., 2014; Chiaravalloti et al., 2016; Falgàs et al., 2020b). The correlations were also consistent with the attention maps showing the involvement of the junction between the GM and the CSF in the brain age prediction.

To predict PAD score, we used a 3D CNN architecture which allowed us to work directly with raw data with few preprocessing steps. Using raw data allowed the algorithm to search itself for the available information regarding who was the most interesting to solve the brain age problem. There was therefore less bias induced by the preprocessing steps, which were usually more present during feature extraction for a classical machine learning

algorithm. We applied field inhomogeneity correction, skull-stripped extraction, linear registration to common space, and min–max normalization as preprocessing steps. We obtained a cross-validation MAE of 3.18 ± 0.43 and a test MAE of 4.34, which are common results in brain age prediction (Franke and Gaser, 2019; Sajedi and Pardakhti, 2019). The requirement of few preprocessing steps and the fast calculation (around 0.36 s) make the PAD score a marker of sporadic EOAD subtypes classification that can be used in clinical routine.

Our study had some limitations. Even if 3,227 MR images are considered to be a great number in medical studies, CNN models used to be trained on a greater number of images. More complex brain aging models exist, but we made the choice to use a simpler and more flexible architecture to avoid overfitting. In addition, this brain age model had already proven its performance in a previous study (Cole et al., 2017a). Despite the correction of the regression toward mean, the problem was still present and was more pronounced when the model was used on different data from the training set. However, to the best of our knowledge, no alternative has been found to this problem apart from the regression of the error. Our population suffered from an attrition bias, as not all included patients completed the 4 years follow-up. The controls used for comparison to EOAD patients were not acquired with the same MR scanner. We selected healthy subjects not used during the implementation and validation of the brain age prediction model. Moreover, we randomly paired our control with our two EOAD subtypes based on age and sex, to remove the maximum of variability. Lastly, further independent validation will be necessary to assess the PAD score as a marker of global cognitive performance and clinical status.

CONCLUSIONS

In this study, we showed that PAD score could be a valuable marker of disease severity which can be used to distinguish between clinical variants of EOAD. Further studies could determine the robustness of the PAD score in prospective cohorts and can be used in longitudinal studies for developments in pharmacological studies to show the arrest of this progression with treatment.

DATA AVAILABILITY STATEMENT

Publicly available datasets were analyzed in this study. This data can be found at: Information eXtraction from Images (https://brain-development.org/), Human Connectome Project (https://www.humanconnectome.org/), Center of Biomedical Research Excellence (https://www.mrn.org/common/cobre-phase-3), Mind Clinical Imaging Consortium (https://www.nitrc.org/projects/mcic/), Neuromorphometry by Computer Algorithm Chicago (http://schizconnect.org/), Enhanced Nathan Kline Institute-Rockland Sample (http://fcon_1000.projects.nitrc.org/indi/enhanced/), Parkinson's Progression Markers Initiative (www.ppmi-info.org/data), and Alzheimer's Disease Neuroimaging Initiative (adni.loni.usc.edu). Please find the accession numbers of the subjects used for training of the model in the file model_accession_numbers.csv and for the control population in the file control_accession_numbers.csv. (**Supplementary Data Sheets 1, 2**).

ETHICS STATEMENT

The studies involving human participants were reviewed and approved by CPP Nord-Ouest I. The patients/participants provided their written informed consent to participate in this study.

AUTHOR CONTRIBUTIONS

MG: study design, MRI processing, statistical analyses, data interpretation, and writing of the manuscript. GK: study design, MRI processing, data interpretation, and critical revision of the manuscript. CB: acquisition and analysis of MRI data and critical revision of the manuscript. AS: acquisition of neuropsychological and clinical data. XD and ML: acquisition of neuropsychological data and critical revision of the manuscript. XL: critical revision of the manuscript. J-PP: study supervision and critical revision of the manuscript. FP: study supervision, acquisition of clinical data, and critical revision of the manuscript. RL: study concept, design and supervision, data interpretation, and critical revision of the manuscript. All authors contributed to the article and approved the submitted version.

FUNDING

This research was funded by General Electric Healthcare as part of a scientific partnership with Lille University Hospital and the French government's LABEX DISTALZ program (development of innovative strategies for a transdisciplinary approach to Alzheimer's disease). Data collection and sharing for this project was funded by the Alzheimer's Disease Neuroimaging Initiative (ADNI) (National Institutes of Health Grant U01 AG024904) and DOD ADNI (Department of Defense Award Number W81XWH-12-2-0012). ADNI was funded by the National Institute on Aging, the National Institute of Biomedical Imaging and Bioengineering, and through generous contributions from the following: AbbVie, Alzheimer's Association; Alzheimer's Drug Discovery Foundation; Araclon Biotech; BioClinica, Inc.; Biogen; Bristol-Myers Squibb Company; CereSpir, Inc.; Cogstate; Eisai Inc.; Elan Pharmaceuticals, Inc.; Eli Lilly and Company; EuroImmun; F. Hoffmann-La Roche Ltd. and its affiliated company Genentech, Inc.; Fujirebio; GE Healthcare; IXICO Ltd.; Janssen Alzheimer's Immunotherapy Research & Development, LLC.; Johnson & Johnson Pharmaceutical Research & Development, LLC.; Lumosity; Lundbeck; Merck & Co., Inc.; Meso Scale Diagnostics, LLC.; NeuroRx Research; Neurotrack Technologies; Novartis Pharmaceuticals Corporation; Pfizer Inc.; Piramal Imaging; Servier; Takeda Pharmaceutical Company; and Transition Therapeutics. The Canadian Institutes of Health Research was providing funds

to support ADNI clinical sites in Canada. Private sector contributions are facilitated by the Foundation for the National Institutes of Health (www.fnih.org). The grantee organization was the Northern California Institute for Research and Education, and the study was coordinated by the Alzheimer's Therapeutic Research Institute at the University of Southern California. ADNI data were disseminated by the Laboratory for Neuro Imaging at the University of Southern California. PPMI—a public–private partnership—was funded by the Michael J. Fox Foundation for Parkinson's Research and funding partners (the list of all of the PPMI funding partners can be found at: www.ppmi-info.org/fundingpartners). Data were provided by the Human Connectome Project, WU-Minn Consortium (Principal Investigators: David Van Essen and Kamil Ugurbil; 1U54MH091657) funded by the 16 NIH Institutes and Centers that support the NIH Blueprint for Neuroscience Research; and by the McDonnell Center for Systems Neuroscience at Washington University.

ACKNOWLEDGMENTS

The authors thank the patients and their families for their kind participation in the present study. The authors would also like to thank all the members of the Lille Young Onset Dementia study group for their respective contributions to the prospective COMAJ study.

SUPPLEMENTARY MATERIAL

The Supplementary Material for this article can be found online at: https://www.frontiersin.org/articles/10.3389/fnagi.2021.729635/full#supplementary-material

REFERENCES

Andel, R., Vigen, C., Mack, W. J., Clark, L. J., and Gatz, M. (2006). The effect of education and occupational complexity on rate of cognitive decline in Alzheimer's patients. *J. Int. Neuropsychol. Soc.* 12, 147–152. doi: 10.1017/S1355617706060206

Anoop, A., Singh, P. K., Jacob, R. S., and Maji, S. K. (2010). CSF biomarkers for alzheimer's disease diagnosis. *Int. J. Alzheimers. Dis.* 2010, 1–12. doi: 10.4061/2010/606802

Balasa, M., Gelpi, E., Antonell, A., Rey, M. J., Sanchez-Valle, R., Molinuevo, J. L., et al. (2011). Clinical features and APOE genotype of pathologically proven early-onset Alzheimer disease. *Neurology* 76, 1720–1725. doi: 10.1212/WNL.0b013e31821a44dd

Bartzokis, G., Beckson, M., Lu, P. H., Nuechterlein, K. H., Edwards, N., and Mintz, J. (2001). Age-related changes in frontal and temporal lobe volumes in men: a magnetic resonance imaging study. *Arch. Gen. Psychiatry*. 58:461. doi: 10.1001/archpsyc.58.5.461

Beheshti, I., Maikusa, N., and Matsuda, H. (2018). The association between "Brain-Age Score" (BAS) and traditional neuropsychological screening tools in Alzheimer's disease. *Brain Behav*. 8:e01020. doi: 10.1002/brb3.1020

Beheshti, I., Mishra, S., Sone, D., Khanna, P., and Matsuda, H. (2020). T1-weighted MRI-driven brain age estimation in Alzheimer's disease and Parkinson's disease. *Aging Dis*. 11:618. doi: 10.14336/AD.2019.0617

Bracco, L., Piccini, C., Baccini, M., Bessi, V., Biancucci, F., Nacmias, B., et al. (2007). Pattern and progression of cognitive decline in Alzheimer's disease: role of premorbid intelligence and ApoE genotype. *Dement. Geriatr. Cogn. Disord.* 24, 483–491. doi: 10.1159/000111081

Cao, K., Chen-Plotkin, A. S., Plotkin, J. B., and Wang, L.-S. (2010). Age-correlated gene expression in normal and neurodegenerative human brain tissues. *PLoS ONE* 5:e13098. doi: 10.1371/journal.pone.0013098

Chiaravalloti, A., Koch, G., Toniolo, S., Belli, L., Di Lorenzo, F., Gaudenzi, S., et al. (2016). Comparison between early-onset and late-onset Alzheimer's disease patients with amnestic presentation: CSF and 18F-FDG PET study. *Dement. Geriatr. Cogn. Disord. Extra* 6, 108–119. doi: 10.1159/000441776

Cho, H., Hashimoto, T., Wong, E., Hori, Y., Wood, L. B., Zhao, L., et al. (2013). Microfluidic chemotaxis platform for differentiating the roles of soluble and bound amyloid-β on microglial accumulation. *Sci. Rep.* 3:1823. doi: 10.1038/srep01823

Cliff, N. (1993). Dominance statistics: Ordinal analyses to answer ordinal questions. *Psychol. Bull.* 114, 494–509. doi: 10.1037/0033-2909.114.3.494

Cole, J. H., Poudel, P. K. R., Tsagkrasoulis, D., Caan, M. W. A., Steves, C., Spector, T. D., et al. (2017a). Predicting brain age with deep learning from raw imaging data results in a reliable and heritable biomarker. *Neuroimage* 163, 115–124. doi: 10.1016/j.neuroimage.2017.07.059

Cole, J. H., Ritchie, S. J., Bastin, M. E., Valdés Hernández, M. C., Muñoz Maniega, S., Royle, N., et al. (2017b). Brain age predicts mortality. *Mol Psychiatry*. 23, 1385–1392. doi: 10.1038/mp.2017.62

Courchesne, E., Chisum, H. J., Townsend, J., Cowles, A., Covington, J., Egaas, B., et al. (2000). Normal brain development and aging: quantitative analysis at *in vivo* MR imaging in healthy volunteers. *Radiology* 216, 672–682. doi: 10.1148/radiology.216.3.r00au37672

Couvy-Duchesne, B., Faouzi, J., Martin, B., Thibeau-Sutre, E., Wild, A., Ansart, M., et al. (2020). Ensemble learning of convolutional neural network, support vector machine, and best linear unbiased predictor for brain age prediction: ARAMIS contribution to the predictive analytics competition 2019 challenge. *Front. Psychiatry* 11:593336. doi: 10.3389/fpsyt.2020.593336

de Oliveira, F. F., de Almeida, S. S., Chen, E. S., Smith, M. C., Naffah-Mazzacoratti, M. G., and Bertolucci, P. H. F. (2018). Lifetime risk factors for functional and cognitive outcomes in patients with Alzheimer's disease. *J. Alzheimers Dis.* 65, 1283–1299. doi: 10.3233/JAD-180303

Deloche, G., and Hannequin, D. (1997). *DO 80: Epreuve de Dénomination Orale d'images*. Editions du Centre de Psychologie Appliquée.

Dickstein, D. L., Kabaso, D., Rocher, A. B., Luebke, J. I., Wearne, S. L., and Hof, P. R. (2007). Changes in the structural complexity of the aged brain. *Aging Cell*. 6:275–284. doi: 10.1111/j.1474-9726.2007.00289.x

Dubois, B., Feldman, H. H., Jacova, C., Hampel, H., Molinuevo, J. L., Blennow, K., et al. (2014). Advancing research diagnostic criteria for Alzheimer's disease: the IWG-2 criteria. *Lancet Neurol.* 13, 614–629. doi: 10.1016/S1474-4422(14)70090-0

Falgàs, N., Balasa, M., Bargalló, N., Borrego-Écija, S., Ramos-Campoy, O., Fernández-Villullas, G., et al. (2020a). Diagnostic accuracy of MRI visual rating scales in the diagnosis of early onset cognitive impairment. *J. Alzheimers Dis.* 73, 1575–1583. doi: 10.3233/JAD-191167

Falgàs, N., Ruiz-Peris, M., Pérez-Millan, A., Sala-Llonch, R., Antonell, A., Balasa, M., et al. (2020b). Contribution of CSF biomarkers to early-onset Alzheimer's disease and frontotemporal dementia neuroimaging signatures. *Hum. Brain Mapp.* 41, 2004–2013. doi: 10.1002/hbm.24925

Ferreira, D., Nordberg, A., and Westman, E. (2020). Biological subtypes of Alzheimer disease. *Neurology* 94:436. doi: 10.1212/WNL.0000000000009058

Fischl, B. (2012). FreeSurfer. *Neuroimage* 62, 774–781. doi: 10.1016/j.neuroimage.2012.01.021

Folstein, M., Anthony, J. C., Parhad, I., Duffy, B., and Gruenberg, E. M. (1985). The meaning of cognitive impairment in the elderly. *J. Am. Geriatr. Soc.* 33, 228–235. doi: 10.1111/j.1532-5415.1985.tb07109.x

Franke, K., and Gaser, C. (2012). Longitudinal changes in individual BrainAGE in healthy aging, mild cognitive impairment, and Alzheimer's disease. *GeroPsych* 25, 235–245. doi: 10.1024/1662-9647/a000074

Franke, K., and Gaser, C. (2019). Ten years of BrainAGE as a neuroimaging biomarker of brain aging: what insights have we gained? *Front. Neurol.* 10:789. doi: 10.3389/fneur.2019.00789

Franke, K., Ziegler, G., Klöppel, S., and Gaser, C. (2010). Estimating the age of healthy subjects from T1-weighted MRI scans using kernel methods: Exploring the influence of various parameters. *NeuroImage* 50, 883–892. doi: 10.1016/j.neuroimage.2010.01.005

Frings, L., Yew, B., Flanagan, E., Lam, B. Y. K., Hüll, M., Huppertz, H.-J., et al. (2014). Longitudinal grey and white matter changes in frontotemporal dementia and Alzheimer's disease. *PLoS ONE* 9:e90814. doi: 10.1371/journal.pone.0090814

Galton, F. (1886). Regression towards mediocrity in hereditary stature. *J. Anthropol. Inst. G B Irel.* 15:246. doi: 10.2307/2841583

Garre-Olmo, J., Genis Batlle, D., del Mar Fernandez, M., Marquez Daniel, F., de Eugenio Huelamo, R., Casadevall, T., et al. (2010). Incidence and subtypes of early-onset dementia in a geographically defined general population. *Neurology* 75, 1249–1255. doi: 10.1212/WNL.0b013e3181f5d4c4

Gaser, C., Franke, K., Kloppel, S., Koutsouleris, N., and Sauer, H. (2013). BrainAGE in mild cognitive impaired patients: predicting the conversion to Alzheimer's disease. *PLoS ONE* 8:e67346. doi: 10.1371/journal.pone.0067346

Giedd, J. N., Blumenthal, J., Jeffries, N. O., Castellanos, F. X., Liu, H., Zijdenbos, A., et al. (1999). Brain development during childhood and adolescence: a longitudinal MRI study. *Nat. Neurosci.* 2, 861–863. doi: 10.1038/13158

Godefroy, O. (2008). *Fonctions Exécutives et Pathologies Neurologiques et Psychiatriques: Évaluation en Pratique Clinique*. Groupe de Boeck

Guttmann, C. R. G., Jolesz, F. A., Kikinis, R., Killiany, R. J., Moss, M. B., Sandor, T., et al. (1998). White matter changes with normal aging. *Neurology* 50, 972–978. doi: 10.1212/WNL.50.4.972

Hall, C. B., Derby, C., LeValley, A., Katz, M. J., Verghese, J., and Lipton, R. B. (2007). Education delays accelerated decline on a memory test in persons who develop dementia. *Neurology* 69, 1657–1664. doi: 10.1212/01.wnl.0000278163.82636.30

Haxby, J. V., Raffaele, K., Gillette, J., Schapiro, M. B., and Rapoport, S. I. (1992). Individual trajectories of cognitive decline in patients with dementia of the Alzheimer type. *J. Clin. Exp. Neuropsychol.* 14, 575–592. doi: 10.1080/01688639208402846

Head, D., Snyder, A. Z., Girton, L. E., Morris, J. C., and Buckner, R. L. (2005). Frontal-hippocampal double dissociation between normal aging and Alzheimer's disease. *Cereb. Cortex.* 15, 732–739. doi: 10.1093/cercor/bhh174

Hughes, C. P., Berg, L., Danziger, W., Coben, L. A., and Martin, R. L. (1982). A new clinical scale for the staging of dementia. *Br. J. Psychiatry* 140, 566–572. doi: 10.1192/bjp.140.6.566

Jack, C. R., and Holtzman, D. M. (2013). Biomarker modeling of Alzheimer's disease. *Neuron* 80, 1347–1358. doi: 10.1016/j.neuron.2013.12.003

Jernigan, T. L., Archibald, S. L., Fennema-Notestine, C., Gamst, A. C., Stout, J. C., Bonner, J., et al. (2001). Effects of age on tissues and regions of the cerebrum and cerebellum. *Neurobiol. Aging.* 22, 581–594. doi: 10.1016/S0197-4580(01)00217-2

Jones, D. T., Machulda, M. M., Vemuri, P., McDade, E. M., Zeng, G., Senjem, M. L., et al. (2011). Age-related changes in the default mode network are more advanced in Alzheimer disease. *Neurology* 77, 1524–1531. doi: 10.1212/WNL.0b013e318233b33d

Koedam, E. L. G. E., Lauffer, V., van der Vlies, A. E., van der Flier, W. M., Scheltens, P., and Pijnenburg, Y. A. L. (2010). Early-versus late-onset alzheimer's disease: more than age alone. *J. Alzheimers. Dis.* 19, 1401–1408. doi: 10.3233/JAD-2010-1337

Lehmann, S., Dumurgier, J., Schraen, S., Wallon, D., Blanc, F., Magnin, E., et al. (2014). A diagnostic scale for Alzheimer's disease based on cerebrospinal fluid biomarker profiles. *Alzheimers Res. Ther.* 6:38. doi: 10.1186/alzrt267

Liang, H., Zhang, F., and Niu, X. (2019). Investigating systematic bias in brain age estimation with application to post-traumatic stress disorders. *Hum. Brain Mapp.* 40, 3143–3152. doi: 10.1002/hbm.24588

Lim, C. Y., Tan, P. C., Koh, C., Koh, E., Guo, H., Yusoff, N. D., et al. (2015). Beery-buktenica developmental test of visual-motor integration (Beery-VMI): lessons from exploration of cultural variations in visual-motor integration performance of preschoolers: Cultural variation in VMI performance of preschoolers. *Child Care Health Dev.* 41, 213–221. doi: 10.1111/cch.12190

Lindeboom, J. (2002). Visual association test to detect early dementia of the Alzheimer type. *J. Neurol. Neurosurg. Psychiatry* 73, 126–133. doi: 10.1136/jnnp.73.2.126

Lombardi, A., Amoroso, N., Diacono, D., Monaco, A., Tangaro, S., and Bellotti, R. (2020). Extensive evaluation of morphological statistical harmonization for brain age prediction. *Brain Sci.* 10:364. doi: 10.3390/brainsci10060364

Löwe, L. C., Gaser, C., and Franke, K. (2016). The effect of the APOE genotype on individual BrainAGE in normal aging, mild cognitive impairment, and Alzheimer's disease. *PLoS ONE* 11:e0157514. doi: 10.1371/journal.pone.0157514

Manjón, J. V., and Coupé, P. (2016). volBrain: an online MRI brain volumetry system. *Front. Neuroinform.* 10:30. doi: 10.3389/fninf.2016.00030

Marshall, G. A., Fairbanks, L. A., Tekin, S., Vinters, H. V., and Cummings, J. L. (2007). Early-onset Alzheimer's disease is associated with greater pathologic burden. *J. Geriatr. Psychiatry Neurol.* 20, 29–33. doi: 10.1177/0891988706297086

McKhann, G. M., Knopman, D. S., Chertkow, H., Hyman, B. T., Jack, C. R., Kawas, C. H., et al. (2011). The diagnosis of dementia due to Alzheimer's disease: Recommendations from the National Institute on Aging-Alzheimer's Association workgroups on diagnostic guidelines for Alzheimer's disease. *Alzheimers Dement.* 7, 263–269. doi: 10.1016/j.jalz.2011.03.005

Mendez, M. F. (2012). Early-onset Alzheimer's disease: nonamnestic subtypes and type 2 AD. *Arch. Med. Res.* 43, 677–685. doi: 10.1016/j.arcmed.2012.11.009

Myung, W., Lee, C., Park, J. H., Woo, S., Kim, S., Kim, S., et al. (2016). Occupational attainment as risk factor for progression from mild cognitive impairment to Alzheimer's disease: A CREDOS study. *J. Alzheimers Dis.* 55, 283–292. doi: 10.3233/JAD-160257

Narvacan, K., Treit, S., Camicioli, R., Martin, W., and Beaulieu, C. (2017). Evolution of deep gray matter volume across the human lifespan: deep gray matter volume across the lifespan. *Hum. Brain Mapp.* 38, 3771–3790. doi: 10.1002/hbm.23604

Ossenkoppele, R., Cohn-Sheehy, B. I., La Joie, R., Vogel, J. W., Möller, C., Lehmann, M., et al. (2015). Atrophy patterns in early clinical stages across distinct phenotypes of Alzheimer's disease: Origin and Spread of Atrophy in AD Variants. *Hum. Brain Mapp.* 36, 4421–4437. doi: 10.1002/hbm.22927

Palasí, A., Gutiérrez-Iglesias, B., Alegret, M., Pujadas, F., Olabarrieta, M., Liébana, D., et al. (2015). Differentiated clinical presentation of early and late-onset Alzheimer's disease: is 65 years of age providing a reliable threshold? *J. Neurol.* 262, 1238–1246. doi: 10.1007/s00415-015-7698-3

Paus, T. S. A. A. (1999). Structural maturation of neural pathways in children and adolescents: *in vivo* study. *Science* 283, 1908–1911. doi: 10.1126/science.283.5409.1908

Peters, R. (2006). Ageing and the brain. *Postgrad. Med. J.* 82:84–88. doi: 10.1136/pgmj.2005.036665

Pettigrew, C., Soldan, A., Zhu, Y., Wang, M.-C., Brown, T., Miller, M., et al. (2017). Cognitive reserve and cortical thickness in preclinical Alzheimer's disease. *Brain Imaging Behav.* 11, 357–367. doi: 10.1007/s11682-016-9581-y

Phillips, J. S., Re, F. D., Dratch, L., Xie, S. X., Irwin, D. J., McMillan, C. T., et al. (2018). Neocortical origin and progression of gray matter atrophy in nonamnestic Alzheimer's disease. *Neurobiol. Aging* 63, 75–87. doi: 10.1016/j.neurobiolaging.2017.11.008

Qiu, C., Bäckman, L., Winblad, B., Agüero-Torres, H., and Fratiglioni, L. (2001). The influence of education on clinically diagnosed dementia incidence and mortality data from the kungsholmen project. *Arch. Neurol.* 58:2034. doi: 10.1001/archneur.58.12.2034

Raji, C. A., Lopez, O. L., Kuller, L. H., Carmichael, O. T., and Becker, J. T. (2009). Age, Alzheimer disease, and brain structure. *Neurology* 73, 1899–1905. doi: 10.1212/WNL.0b013e3181c3f293

Reed, B. R., Mungas, D., Farias, S. T., Harvey, D., Beckett, L., Widaman, K., et al. (2010). Measuring cognitive reserve based on the decomposition of episodic memory variance. *Brain* 133, 2196–2209. doi: 10.1093/brain/awq154

Resnick, S. M., Pham, D. L., Kraut, M. A., Zonderman, A. B., and Davatzikos, C. (2003). Longitudinal magnetic resonance imaging studies of older adults: a shrinking brain. *J. Neurosci. Off. J. Soc. Neurosci.* 23, 3295–3301. doi: 10.1523/JNEUROSCI.23-08-03295.2003

Riedel, B., Mendez, M., Daianu, M., Desarzant, R., Melrose, R., Jimenez, E., et al. (2018). White matter connectivity differences between typical amnestic and

variant nonamnestic individuals with early-onset Alzheimer's disease (EOAD) (P3.190). *Neurology* 90:15.

Risacher, S. L., Anderson, W. H., Charil, A., Castelluccio, P. F., Shcherbinin, S., Saykin, A. J., et al. (2017). Alzheimer disease brain atrophy subtypes are associated with cognition and rate of decline. *Neurology* 89, 2176–2186. doi: 10.1212/WNL.0000000000004670

Robitaille, A., van den Hout, A., Machado, R. J. M., Bennett, D. A., and Cukić, I., Deary, I. J., et al. (2018). Transitions across cognitive states and death among older adults in relation to education: A multistate survival model using data from six longitudinal studies. *Alzheimers Dement*. 14, 462–472. doi: 10.1016/j.jalz.2017.10.003

Roe, C. M. (2011). Cerebrospinal fluid biomarkers, education, brain volume, and future cognition. *Arch. Neurol.* 68:1145. doi: 10.1001/archneurol.2011.192

Sá, F., Pinto P, Cunha, C., Lemos, R., Letra, L., Simões, M., et al. (2012). Differences between early and late-onset Alzheimer's disease in neuropsychological tests. *Front. Neurol.* 3:81. doi: 10.3389/fneur.2012.00081

Saetre, P., Jazin, E., and Emilsson, L. (2011). Age-related changes in gene expression are accelerated in Alzheimer's disease. *Synapse* 65, 971–974. doi: 10.1002/syn.20933

Sajedi, H., and Pardakhti, N. (2019). Age prediction based on brain MRI image: a survey. *J. Med. Syst.* 43:279. doi: 10.1007/s10916-019-1401-7

Scahill, R. I., Frost, C., Jenkins, R., Whitwell, J. L., Rossor, M. N., and Fox, N. C. (2003). A longitudinal study of brain volume changes in normal aging using serial registered magnetic resonance imaging. *Arch. Neurol.* 60:989. doi: 10.1001/archneur.60.7.989

Scarmeas, N. (2005). Education and rates of cognitive decline in incident Alzheimer's disease. *J. Neurol. Neurosurg. Psychiatry* 77, 308–316. doi: 10.1136/jnnp.2005.072306

Schoonenboom, S. N. M., Visser, P. J., Mulder, C., Lindeboom, J., Van Elk, E. J., Van Kamp, G. J., et al. (2005). Biomarker profiles and their relation to clinical variables in mild cognitive impairment. *Neurocase* 11, 8–13. doi: 10.1080/13554790490896785

Selvaraju, R. R., Cogswell, M., Das, A., Vedantam, R., Parikh, D., and Batra, D. (2017). "Grad-CAM: visual explanations from deep networks via gradient-based localization," in: *2017 IEEE International Conference on Computer Vision (ICCV)* (Venice: IEEE).

Shorten, C., and Khoshgoftaar, T. M. (2019). A survey on image data augmentation for deep learning. *J. Big Data* 6:60. doi: 10.1186/s40537-019-0197-0

Soldan, A., Pettigrew, C., and Albert, M. (2020). Cognitive Reserve from the Perspective of Preclinical Alzheimer Disease. *Clin. Geriatr. Med.* 36, 247–263. doi: 10.1016/j.cger.2019.11.006

Soldan, A., Pettigrew, C., Cai, Q., Wang, J., Wang, M.-C., Moghekar, A., et al. (2017). Cognitive reserve and long-term change in cognition in aging and preclinical Alzheimer's disease. *Neurobiol. Aging* 60, 164–172. doi: 10.1016/j.neurobiolaging.2017.09.002

Soldan, A., Pettigrew, C., Li, S., Wang, M.-C., Moghekar, A., Selnes, O. A., et al. (2013). Relationship of cognitive reserve and cerebrospinal fluid biomarkers to the emergence of clinical symptoms in preclinical Alzheimer's disease. *Neurobiol. Aging* 34, 2827–2834. doi: 10.1016/j.neurobiolaging.2013.06.017

Sowell, E. R., Peterson, B. S., Thompson, P. M., Welcome, S. E., Henkenius, A. L., and Toga, A. W. (2003). Mapping cortical change across the human life span. *Nat. Neurosci.* 6, 309–315. doi: 10.1038/nn1008

Sowell, E. R., Thompson, P. M., Holmes, C. J., Jernigan, T. L., and Toga, A. W. (1999). In vivo evidence for post-adolescent brain maturation in frontal and striatal regions. *Nat. Neurosci.* 2, 859–861. doi: 10.1038/13154

Sowell, E. R., Thompson, P. M., Tessner, K. D., and Toga, A. W. (2001). Mapping continued brain growth and gray matter density reduction in dorsal frontal cortex: inverse relationships during postadolescent brain maturation. *J. Neurosci.* 21, 8819–8829. doi: 10.1523/JNEUROSCI.21-22-08819.2001

Sutskever, I., Martens, J., Dahl, G., and Hinton, G. (2013). "On the importance of initialization and momentum in deep learning," in *Proceedings of the 30th International Conference on Machine Learning ICML'13*.

Teissier, T., Boulanger, E., and Deramecourt, V. (2020). Normal ageing of the brain: histological and biological aspects. *Rev. Neurol.* 176, 649–660. doi: 10.1016/j.neurol.2020.03.017

Teng, E., Yamasaki, T. R., Tran, M., Hsiao, J. J., Sultzer, D. L., and Mendez, M. F. (2014). Cerebrospinal fluid biomarkers in clinical subtypes of early-onset Alzheimer's disease. *Dement. Geriatr. Cogn. Disord.* 37, 307–314. doi: 10.1159/000355555

Tetreault, A. M., Phan, T., Orlando, D., Lyu, I., Kang, H., Landman, B., et al. (2020). Network localization of clinical, cognitive, and neuropsychiatric symptoms in Alzheimer's disease. *Brain* 143, 1249–1260. doi: 10.1093/brain/awaa058

Thompson, P. M., Giedd, J. N., Woods, R. P., MacDonald, D., Evans, A. C., and Toga, A. W. (2000). Growth patterns in the developing brain detected by using continuum mechanical tensor maps. *Nature* 404, 190–193. doi: 10.1038/35004593

Toyoda, T. (1974). Use of the chow test under heteroscedasticity. *Econometrica* 42:601. doi: 10.2307/1911796

Trollor, J. N., and Valenzuela, M. J. (2001). Brain ageing in the new millennium. *Aust. N. Z. J. Psychiatry* 35, 788–805. doi: 10.1046/j.1440-1614.2001.00969.x

Van Essen, D. C., Ugurbil, K., Auerbach, E., Barch, D., Behrens, T. E. J., Bucholz, R., et al. (2012). The Human Connectome Project: A data acquisition perspective. *Neuroimage* 62, 2222–2231. doi: 10.1016/j.neuroimage.2012.02.018

van Loenhoud, A. C., van der Flier, W. M., Wink, A. M., Dicks, E., Groot, C., Twisk, J., et al. (2019). Cognitive reserve and clinical progression in Alzheimer disease: A paradoxical relationship. *Neurology* 93, e334–46. doi: 10.1212/WNL.0000000000007821

van Vliet, D., de Vugt, M. E., Bakker, C., Pijnenburg, Y. A. L., Vernooij-Dassen, M. J. F. J., Koopmans, R. T. C. M., et al. (2013). Time to diagnosis in young-onset dementia as compared with late-onset dementia. *Psychol. Med.* 43, 423–432. doi: 10.1017/S0033291712001122

Vanhoutte, M., Semah, F., Leclerc, X., Sillaire, A. R., Jaillard, A., Kuchcinski, G., et al. (2020). Three-year changes of cortical 18F-FDG in amnestic vs. non-amnestic sporadic early-onset Alzheimer's disease. *Eur. J. Nucl. Med. Mol. Imaging* 47, 304–318. doi: 10.1007/s00259-019-04519-w

Whitwell, J. L., Dickson, D. W., Murray, M. E., Weigand, S. D., Tosakulwong, N., Senjem, M. L., et al. (2012). Neuroimaging correlates of pathologically defined subtypes of Alzheimer's disease: a case-control study. *Lancet Neurol.* 11, 868–877. doi: 10.1016/S1474-4422(12)70200-4

Wilson, R. S., Bennett, D. A., Gilley, D. W., Beckett, L. A., Barnes, L. L., and Evans, D. A. (2000). Premorbid reading activity and patterns of cognitive decline in Alzheimer disease. *Arch. Neurol.* 57:1718. doi: 10.1001/archneur.57.12.1718

Xia, C., Makaretz, S. J., Caso, C., McGinnis, S., Gomperts, S. N., Sepulcre, J., et al. (2017). Association of *in vivo* [18 F]AV-1451 Tau PET imaging results with cortical atrophy and symptoms in typical and atypical Alzheimer disease. *JAMA Neurol.* 74:427. doi: 10.1001/jamaneurol.2016.5755

Yoon, B., Shim, Y. S., Park, H.-K., Park, S. A., Choi, S. H., and Yang, D. W. (2015). Predictive factors for disease progression in patients with early-onset Alzheimer's disease. *J. Alzheimers. Dis.* 49, 85–91. doi: 10.3233/JAD-150462

Conflict of Interest: The authors declare that the research was conducted in the absence of any commercial or financial relationships that could be construed as a potential conflict of interest.

frontiers in Aging Neuroscience

ORIGINAL RESEARCH
published: 22 November 2021
doi: 10.3389/fnagi.2021.735508

Neuroimaging Biomarkers Predicting the Efficacy of Multimodal Rehabilitative Intervention in the Alzheimer's Dementia Continuum Pathology

Sonia Di Tella[1,2†], Monia Cabinio[1†], Sara Isernia[1], Valeria Blasi[1], Federica Rossetto[1], Francesca Lea Saibene[1], Margherita Alberoni[1], Maria Caterina Silveri[2,3], Sandro Sorbi[1,4], Mario Clerici[1,5] and Francesca Baglio[1]*

[1] IRCCS Fondazione Don Carlo Gnocchi ONLUS, Milan, Italy, [2] Department of Psychology, Università Cattolica del Sacro Cuore, Milan, Italy, [3] Fondazione Policlinico Universitario "Agostino Gemelli" IRCCS, Rome, Italy, [4] Università degli Studi di Firenze, NEUROFARBA, Firenze, Italy, [5] Department of Physiopathology and Transplants, Università degli Studi di Milano, Milan, Italy

OPEN ACCESS

Edited by:
Jiu Chen, Nanjing Medical University, China

Reviewed by:
Sindhuja T. Govindarajan, University of Pennsylvania, United States
Ernest Marek Tyburski, Pomeranian Medical University in Szczecin, Poland
Geon Ha Kim, Ewha Womans University, South Korea
Maria L. Bringas, University of Electronic Science and Technology of China, China
Rafael González-Redondo, Neuromedical Center, Spain

***Correspondence:**
Sara Isernia
sisernia@dongnocchi.it

† These authors have contributed equally to the work

Received: *02 July 2021*
Accepted: *30 September 2021*
Published: *22 November 2021*

Citation:
Di Tella S, Cabinio M, Isernia S, Blasi V, Rossetto F, Saibene FL, Alberoni M, Silveri MC, Sorbi S, Clerici M and Baglio F (2021) Neuroimaging Biomarkers Predicting the Efficacy of Multimodal Rehabilitative Intervention in the Alzheimer's Dementia Continuum Pathology. Front. Aging Neurosci. 13:735508. doi: 10.3389/fnagi.2021.735508

In this work we aimed to identify neural predictors of the efficacy of multimodal rehabilitative interventions in AD-continuum patients in the attempt to identify ideal candidates to improve the treatment outcome. Subjects in the AD continuum who participated in a multimodal rehabilitative treatment were included in the analysis [$n = 82$, 38 Males, mean age = 76 ± 5.30, mean education years = 9.09 ± 3.81, Mini Mental State Examination (MMSE) mean score = 23.31 ± 3.81]. All subjects underwent an MRI acquisition (1.5T) at baseline (T0) and a neuropsychological evaluation before (T0) and after intervention (T1). All subjects underwent an intensive multimodal cognitive rehabilitation (8–10 weeks). The MMSE and Neuropsychiatric Inventory (NPI) scores were considered as the main cognitive and behavioral outcome measures, and Delta change scores (T1–T0) were categorized in Improved (ΔMMSE $>$ 0; ΔNPI $<$ 0) and Not Improved (ΔMMSE $\leq$ 0; ΔNPI $\geq$ 0). Logistic Regression (LR) and Random Forest classification models were performed including neural markers (Medial Temporal Brain; Posterior Brain (PB); Frontal Brain (FB), Subcortical Brain indexes), neuropsychological (MMSE, NPI, verbal fluencies), and demographical variables (sex, age, education) at baseline. More than 50% of patients showed a positive effect of the treatment (ΔMMSE $>$ 0: 51%, ΔNPI $<$ 0: 52%). LR model on ΔMMSE (Improved vs. Not Improved) indicate a predictive role for MMSE score ($p = 0.003$) and PB index ($p = 0.005$), especially the right PB ($p = 0.002$) at baseline. The Random Forest analysis correctly classified 77% of cognitively improved and not improved AD patients. Concerning the NPI, LR model on ΔNPI (Improved vs. Not Improved) showed a predictive role of sex ($p = 0.002$), NPI ($p = 0.005$), PB index ($p = 0.006$), and FB index ($p = 0.039$) at baseline. The Random Forest reported a classification accuracy of 86%. Our data indicate that cognitive and behavioral status

alone are not sufficient to identify best responders to a multidomain rehabilitation treatment. Increased neural reserve, especially in the parietal areas, is also relevant for the compensatory mechanisms activated by rehabilitative treatment. These data are relevant to support clinical decision by identifying target patients with high probability of success after rehabilitative programs on cognitive and behavioral functioning.

Keywords: neurodegenerative diseases, dementia, rehabilitation, biomarker, MRI, brain reserve, cognitive reserve

INTRODUCTION

Cognitive disability affects 10.8% of adults living with a chronic condition, and is characterized by a complex impairment in attention, memory and/or decision making. With the aging of the general population (World Health Organization, 2012) cognitive disabilities in the adult are often observed as clinical signs of neurodegenerative diseases as in Alzheimer's continuum conditions, ranging from Mild Cognitive Impairment (MCI) to Alzheimer's Dementia (AD) (Aisen et al., 2017; Jack et al., 2018).

MCI is a mild neurocognitive disorder (American Psychiatric Association, 2013; Stokin et al., 2015), affecting 6–25% of people aged over 60, characterized by isolated impairment in one or more cognitive processes, often involving memory (amnestic MCI), with a complete autonomy in functional activities of daily living (Langa and Levine, 2014; Petersen et al., 2018). Each year, 5–25% of amnestic MCI individuals develop AD (Hänninen et al., 2002; Grundman et al., 2004), thus experiencing a worsening of cognitive abilities, gradual loss of functional autonomies and different degrees of behavioral and psychological symptoms (Lyketsos et al., 2000, 2002) such as depression, agitation, apathy and delusions (Cummings, 2004; Steinberg et al., 2008). Especially, behavioral symptoms associated to AD impact seriously on patient's management in daily living, as well as caregiver distress (Steinberg et al., 2008). Unfortunately, behavioral changes represent a mark of the disease and is strictly linked with the need of hospitalization (Spector et al., 2013; Maki et al., 2018).

Clinical, neuropsychological and behavioral aspects of AD continuum are, in its typical form, paralleled by the pathophysiological counterpart of the disease: a progressive accumulation and spreading of amyloid plaques and neurofibrillary T-tau protein tangles starting even years before the clinical onset of symptoms (Aisen et al., 2017; Ekman et al., 2018). The pathology starts in the medial temporal lobe and limbic areas (enthorinal cortex, hippocampus, parahippocampal regions) and reaches associative cortices (Braak and Braak, 1991). Different patterns of cortical atrophy are associated with the diffusion of tangles in the brain, such as the earlier involvement of posterior-parietal regions (Lehmann et al., 2013; Ekman et al., 2018) or the presence of frontal lobe atrophy in "executive AD" presentation (Ferreira et al., 2016). Given this progression, specific brain changes such as hippocampal atrophy rates and local atrophy indices are established neuroimaging biomarkers of AD-associated downstream neuronal degeneration (McKhann et al., 2011; Ekman et al., 2018). To date, AD is the most diffuse form of dementia, affecting globally 4.7 million individuals aged 65 + and a projected rise to 130 million individuals worldwide by 2,050 (Lopez and Kuller, 2019).

Despite the great efforts spent in clinical and translational research, the possible effect of symptomatic drugs on patients suffering from AD continuum remains controversial (Birks, 2006; Birks and Grimley Evans, 2015) with a single molecule, Aducanumab, recently obtaining the FDA approval (Fillit and Green, 2021) and new disease-modifying pharmacological treatments still in clinical developing stages (Sabbagh et al., 2020).

The most-adopted intervention is thus rehabilitation, tested in manifold settings: from single-cognitive-domain approaches to the most recent holistic multi-modal interventions (Fabbri et al., 2018; Maki et al., 2018), amply documented to be effective in neurodegenerative conditions (Baglio et al., 2015; Chew et al., 2015; Realdon et al., 2016; Isernia et al., 2019). In fact, considering the difficulties faced by individuals in the AD continuum, often impacting cognitive and behavioral functionality, multidisciplinary models of care are taken in consideration to manage such a great variety of symptoms. Multidisciplinary approaches have the advantage to mutually complement and optimize benefits on different target of rehabilitation (Maki et al., 2018). Importantly, the main effects of multimodal approaches are demonstrated in several domains, including daily living skills, global physical functions and cognition (McDermott et al., 2019). These effects are the results of multi-domain cognitive stimulation, motor enhancement and occupational activities which are implemented in the framework of a multidisciplinary clinical team. This complex setting drives a parallel action on both enhancement and maintenance of cognitive residual abilities, attaining and aligning with the values of the International Classification of Functioning, Disability and Health and supporting the quality of life of people regardless their level of functioning (Gitlin et al., 2013; World Health Organization, 2017; Maki et al., 2018).

To our knowledge, to date no clear evidences have been proposed to forecast which patients can mostly benefit from these rehabilitation treatments. This can be partially explained by the observation that, despite the known neuropathological progression of the disease, a disjunction between brain damage and clinical outcome is often observed, accounting for individual differences in coping with the pathology (Williams et al., 2018). In particular, genetic, epigenetic and environmental factors can mitigate the effects of neural decline caused by aging and age-related diseases (Cabeza et al., 2018). Identifying which neuro-clinical features are prognostic of

treatment success is urgent with potentially vast implications for the personalization of interventions and maximizing the effectiveness of rehabilitation programs. This would allow to *a priori* differentiate between people who potentially benefit from the treatment and those who not.

Concepts such as cognitive and brain reserves (Stern, 2009) can catch the individual differences both in how people process cognitive tasks and in how their brains can morphologically differ each other, aspects well known to be mediated by life experiences (Maguire et al., 2006; Stern, 2009). Cognitive reserve has been defined as the processing resources gained over time as a result of engaging in mentally stimulating activities, i.e., education, professional attainment, and leisure activities (Stern, 2009). Although the relevance to measure cognitive reserve, a plethora of "convenience proxies" to operationalized this construct, as socio-behavioral indices, such as education, has been reported (Stern, 2009). In this framework, brain reserve is hypothesized to be the result of the accumulation of neural resources before the brain is affected by age-related processes, over a period of years (Cabeza et al., 2018). Brains with higher reserve can sustain more insult before clinical deficit emerges, and thus individual differences in brain reserve can led to differences in the clinical expression of a particular degree of damage to the brain (Stern, 2009). Brain reserve has been operatively quantified in terms of functional or morphometric measures (gross whole-brain measures reflective of peak or premorbid brain volume, including Total Intracranial Volume or head circumference) (Katzman et al., 1988; Stern, 2009). Ongoing research has begun to incorporate more finegrained measures such as specific patterns of gray matter volume, cortical surface area, and cortical thickness. Changes after treatment have been reported, such as changes in medial temporal lobe structures in subjects that performed intensive mnestic training (Maguire et al., 2006), but the detection of specific neural structures as critical hub of neural reserve has not yet been demonstrated.

Despite the association between a good brain reserve and the increased probability to positively cope with neural injuries, to date no clear indications can forecast the effects of a given brain reserve on the results of a rehabilitative intervention, and the prognostic characteristics of treatment success still remain a matter of debate. A better knowledge of the prognostic neural profile of rehabilitation candidates, in terms of level of probability of treatment effectiveness, could be beneficial both for individual patients, who would receive a more efficacious intervention, and for the healthcare system.

In this work we aim to identify the best candidates for effective rehabilitative interventions in AD-continuum disease patients. We included neuroimaging biomarkers as aspects of brain reserve and, in line with our previous work (Di Tella et al., 2020), we used classification approaches including Random Forest and logistic regression to define which neural (brain reserve), demographical and clinical aspects of the disease might predict the best outcome for multimodal rehabilitation. Given the literature supporting the role of brain reserve on clinical expression of diseases and deficits (Stern, 2009), we hypothesize to find a significant predictor of neurorehabilitation success in critical hub of neural reserve, such as specific morphometric volumes.

MATERIALS AND METHODS

All the patients with a diagnosis in the AD-continuum, consecutively admitted to the Memory Clinic of IRCCS Fondazione Don Carlo Gnocchi ONLUS, Centro Santa Maria Nascente (Milan) from 2011 to 2019 and fulfilling the admission criteria (see below) had the possibility to participate in a multimodal rehabilitation treatment. This IRCCS Don Carlo Gnocchi is a scientific institute for rehabilitation and research with a specific focus on neurodegenerative diseases. For this reason, all subjects at admission are asked to provide an informed consent (by signing the informed consent module approved by Don Gnocchi Foundation Ethics Committee) allowing the use of clinical data collected during evaluation and rehabilitation for research purposes. No procedures different from standard were performed for the present study.

Admission criteria were: (1) a diagnosis of an AD-continuum condition, from MCI to mild-to- moderate AD according to National Institute on Aging-Alzheimer's Association guidelines (Albert et al., 2011; McKhann et al., 2011) reported in the clinical documentation; (2) age $\geq$ 65 years old; (3) minimum education level being alphabetization (2 years); (4) right-hand dominance (Oldfield, 1971); (5) attendance of a multimodal intensive rehabilitation intervention tailored for mild-to-moderate stages of AD continuum followed at IRCCS Santa Maria Nascente for at least 80% of program's sessions (see below); (6) presence of a MRI examination not earlier than 2 months before the beginning of rehabilitation treatment; (7) presence of a neuropsychological evaluation pre- and post- intervention; (8) a stable pharmacological treatment (acetylcholine esterase inhibitors and neuropsychiatric drugs, if any) at least for 3 months before starting the rehabilitation. Exclusion criteria were indeed considered: (1) presence of a prodromic condition or a diagnosis of other types of dementia different from AD-continuum; (2) presence of major psychiatric disorders; (3) absence of a written informed consent.

All patients fulfilling the criteria were admitted in an intensive rehabilitation program (8–10 weeks, 3–5 times a week) based on a holistic approach (Baglio et al., 2015; Fabbri et al., 2018). Rehabilitation was conceived to train cognition by enhancing several domains (cognition, physical, and social) *via* neuropsychological activities (both paper-and-pencil and computerized tasks addressing different cognitive domains, such as memory, executive functions, language, attention, abstraction, praxis), psychomotor exercises (stretching, postural changes, gait exercises, balance, and postural control), and recreational/occupational activities (functional and goal-based exercises in order to readapting the use of daily tools and performing everyday tasks to recover personal autonomy and to improve targeted domains of quality of life) were proposed. By training different domains of functioning, the treatments aimed to act in an integrated manner on residual cognitive functions of AD-continuum people, triggering neuroplasticity

mechanisms (e.g., Venna et al., 2014). The principal setting of the intervention was in a small group (2–4 person) with a therapist who helped the rehabilitation program for patients, and the dose of the treatment was intense: about 3–5 times a week, about 60-min per session. The programs were based on multi-stimulation therapy (Baglio et al., 2015) and a multidisciplinary rehabilitation team (physiotherapist, neuropsychologist, and occupational therapist) cooperated in the rehabilitation plan implementation and monitoring.

Retrospectively, demographic and clinical data have been extracted from clinical charts by a single researcher (FR) and inserted in an anonymized database, subsequently used for the statistical analyses of the present research. The database included, for each recruited subject:

- Age, gender, education diagnosis and anamnesis (disease history and mood evaluation Hamilton, 1960);
- *Mini-Mental State Examination* (MMSE; Folstein et al., 1983) as index of the global cognitive level of patients. The total score, ranged 0–30, suggests the absence of cognitive impairment (MMSE score: 27–30), the presence of borderline impairment (MMSE score: 24–26), mild cognitive impairment (MMSE score: 18–23), moderate cognitive impairment (MMSE score: 14–17), or severe cognitive impairment (MMSE score: 0–13).
- *Verbal Fluencies* (Novelli et al., 1986; Carlesimo et al., 1996) assessing language and executive functions. In details, both letter (FAS) and categorical (CAT) fluencies were extracted from charts and included in the analysis. The raw total score of the test performance was adjusted for age and education following the instructions' procedure of Novelli et al. (1986) and Carlesimo et al. (1996).
- *Neuropsychiatric Inventory* (NPI; Cummings et al., 1994; Cummings, 1997) as a measure of the frequency and severity of behavioral symptoms related to the clinical condition, including delusions, hallucinations, dysphoria, anxiety, euphoria, aggression, apathy, irritability, disinhibition, troublesome behavior. Both the scores of frequencies and severity of symptoms (NPI_{f*s}) and distress of caregiver ($NPI_{distress}$) were reported.

Moreover, from the MRI examinations (1.5T Siemens Magnetom Avanto scanner, Erlangen, Germany) acquired before the rehabilitation treatment, we retrieved anonymized conventional sequences to exclude gross brain abnormalities and a high-resolution T1-3D MPR (TR/TE = 1,900/3.37 ms; FoV = 192 × 256 mm, isometric in-plane resolution 1 mm, 176 axial slices) to assess brain morphometry.

Statistics

MRI Data Analysis and Computation of Neuroimaging Biomarkers

To extract morphometrical data, MPR acquisitions have been analyzed using the recon-all pipeline of Freesurfer software (v.5.3).[1] Quality check have been performed for each subject according to ENIGMA guidelines[2] and manual corrections performed to improve automatic segmentation when necessary. Brain parcellation were performed according to Fischl et al. (2002) and Desikan et al. (2006) atlases. As neuroimaging biomarkers, volumetric measurements were computed considering brain areas strongly related to AD-continuum conditions, according to Ekman et al. (2018). In particular, we computed (a) Medial Temporal Brain (MTB) index (sum of volumes in: hippocampal and parahippocampal volumes); (b) Posterior Brain (PB) index (sum of volumes in: posterior cingulate, precuneus, superior parietal, inferior parietal, supramarginal gyrus); (c) Frontal Brain (FB) index (sum of volumes in: caudal middle frontal, rostral middle frontal, pars opercularis, pars triangularis, pars orbitalis, frontal pole, superior frontal, rostral anterior cingulate, caudal anterior cingulate, precentral, lateral orbito-frontal, medial orbitofrontal). In addition, we also computed a (d) Subcortical Brain (SBCB) index (sum of volumes in: thalamus, amygdala, nucleus accumbens, caudate nucleus) (Roh et al., 2011). In each subject, the brain neuroimaging biomarkers have been computed separately for left and right hemispheres, as well as globally (MTB_{rh}, MTB_{lh}, MTB_{global}, PB_{rh}, PB_{lh}, PB_{global}, FB_{rh}, FB_{lh}, FB_{global}, $SBCB_{rh}$, $SBCB_{lh}$, $SBCB_{global}$). All indices have been normalized to the estimated Total Intracranial Volume, and converted in *z*-values considering MRI mean and SD data from an age- gender- and education-matched sample of healthy controls (n = 32, 13 M, mean age 74.16 ± 4.33, internal laboratory dataset). These *Z*-values have been included in subsequent statistical analyses ($Z\text{-}MTB_{rh}$, $Z\text{-}MTB_{lh}$, $Z\text{-}MTB_{global}$, $Z\text{-}PB_{rh}$, $Z\text{-}PB_{lh}$, $Z\text{-}PB_{global}$, $Z\text{-}FB_{rh}$, $Z\text{-}FB_{lh}$, $Z\text{-}FB_{global}$, $Z\text{-}SBCB_{rh}$, $Z\text{-}SBCB_{lh}$, $Z\text{-}SBCB_{global}$).

Demographic, Clinical, and Behavioral Measures

Statistical analyses were performed with IBM SPSS Statistics software (version 24) and JASP (JASP Team 2020, JASP version 0.14.1). Means, frequencies, and standard deviations were computed to describe sample characteristics. χ^2-test was used to verify if sex distribution and education were balanced in the whole sample.

The MMSE score was considered the primary clinical outcome measure for the cognitive status. Delta change score (T1–T0) of MMSE was categorized in Improved ($\Delta MMSE > 0$) and Not Improved ($\Delta MMSE \leq 0$). The NPI_{f*s} was considered the primary clinical outcome measure for the behavioral status. Delta scores (T1–T0) of NPI was categorized in Improved ($\Delta NPI_{f*s} < 0$) and Not Improved ($\Delta NPI_{f*s} \geq 0$).

Logistic Regression classification models including demographical characteristics (age, sex, years of education), neural markers ($Z\text{-}MTB_{global}$, $Z\text{-}PB_{global}$, $Z\text{-}FB_{global}$, $Z\text{-}SBCB_{global}$) and neuropsychological variables (MMSE T0, NPI_{f*s} T0, FAS T0, CAT T0) at baseline were performed to identify the subjects that significantly benefited from treatment ($\Delta MMSE > 0$ and $\Delta NPI_{f*s} < 0$) as in Di Tella et al. (2020). Wald forward option was used as a stepwise selection method (entry criterion $p < 0.05$, removal criterion $p > 0.10$). Only for cognitive outcome neural markers were split in left and right side.

[1] http://surfer.nmr.mgh.harvard.edu/

[2] http://enigma.ini.usc.edu/protocols/imaging-protocols

For confirmatory purposes, Random Forest classification models were run including only predictors retained in the last step of the logistic regressions. We built Random Forest with the default parameter values in JASP (version 0.14.1), specifically with respect to data split we partitioned the data set into a training (60%), validation (20%), and test set (20%). In relation to the number of trees, we selected an optimal number of trees [Ntrees (maximum) = 100], optimized with respect to the out-of-bag accuracy. Performance of the classification model was evaluated by calculating the classification accuracy that represents the proportion of the instances that were classified correctly, summing up true positive and true negative cases.

RESULTS

Demographical Characteristics of the Sample

In total, 82 people (38 males) with a diagnosis of AD-continuum condition (n_{MCI} = 54, n_{AD} = 28) were included in the study. **Table 1** shows data referred to neuropsychological assessment and morphometrical z-scores of the computed brain neuroimaging biomarkers.

TABLE 1 | Neuropsychological assessment and morphometrical z-scores of the sample.

	25th percentile	75th percentile	Mean	*SD*
Age (years)	72.25	79.00	76.00	5.30
Education (years)	6.00	13.00	9.09	3.81
Hamilton T0*	3.75	8.00	6.62	4.55
MMSE T0 (0–30)	21.00	26.00	23.32	4.08
FAS T0	16.25	30.50	23.10	10.55
CAT T0	18.00	30.75	24.33	9.96
NPI_{f*s} T0 (0–144)	4.75	19.50	12.75	9.47
$NPI_{distress}$ T0 (0–60)	3.00	10.00	6.67	4.83
$Z\text{-}MTB_{global}$	−2.70	−1.18	−1.86	1.43
$Z\text{-}MTB_{lh}$	−2.72	−1.13	−1.88	1.39
$Z\text{-}MTB_{rh}$	−2.73	−0.82	−1.75	1.54
$Z\text{-}PB_{global}$	−2.54	−0.71	−1.54	1.38
$Z\text{-}PB_{lh}$	−2.28	−0.49	−1.35	1.29
$Z\text{-}PB_{rh}$	−2.54	−0.61	−1.58	1.43
$Z\text{-}FB_{global}$	−2.82	−0.45	−1.56	1.80
$Z\text{-}FB_{lh}$	−3.08	−0.50	−1.69	1.87
$Z\text{-}FB_{rh}$	−2.52	−0.29	−1.40	1.72
$Z\text{-}SBCB_{global}$	−1.21	−0.13	−0.65	0.84
$Z\text{-}SBCB_{lh}$	−1.23	−0.15	−0.70	0.87
$Z\text{-}SBCB_{rh}$	−1.16	−0.08	−0.58	0.87

Hamilton T0, Hamilton Depression Scale; MMSE T0, Mini-Mental State Examination at baseline; FAS T0, Phonological Fluency at baseline; CAT T0, Categorial Fluency at baseline; NPI_{f*s} T0, Neuropsychiatric Inventory frequencies and severity of symptoms at baseline; $NPI_{distress}$ T0, Neuropsychiatric Inventory caregiver distress; $Z\text{-}MTB_{global}$, Z-values of Medial Temporal Brain index; $Z\text{-}MTB_{lh}$, Z-values of left Medial Temporal Brain index; $Z\text{-}MTB_{rh}$, Z-values of right Medial Temporal Brain index; $Z\text{-}PB_{global}$, Z-values of Posterior Brain index; $Z\text{-}PB_{lh}$, Z-values of left Posterior Brain index; $Z\text{-}PB_{rh}$, Z-values of right Posterior Brain index; $Z\text{-}FB_{global}$, Z-values of Frontal Brain index; $Z\text{-}FB_{lh}$, Z-values of left Frontal Brain index; $Z\text{-}FB_{rh}$, Z-values of right Frontal Brain index; $Z\text{-}SBCB_{global}$, Z-values of Subcortical Brain index; $Z\text{-}SBCB_{lh}$, Z-values of left Subcortical Brain index; $Z\text{-}SBCB_{rh}$, Z-values of right Subcortical Brain index.

**This data was available only for 64 participants.*

TABLE 2 | Percentages of responders and not responders to the treatment in cognitive and behavioral outcomes.

	Not responders at NPI_{f*s} (%)	Responders at NPI_{f*s} (%)
Not responders at MMSE (%)	22.0%	26.8%
Responders at MMSE (%)	25.6%	25.6%

MMSE, Mini-Mental State Examination; NPI_{f*s}, Neuropsychiatric Inventory frequencies and severity of symptoms at baseline.

Response to the Treatment

The percentage of not responders to the treatment in both cognitive and behavioral outcome was 22% (see **Table 2**). Fifty-one percent of patients showed an improvement on global cognitive functioning after the treatment (ΔMMSE > 0: 51%; AD: 38%; MCI: 13%) showing a mean ΔMMSE = 2.24 ($\Delta MMSE_{AD}$ = 2.13; $\Delta MMSE_{MCI}$ = 2.55), Cohen's d = 2.15. A reduction of behavioral symptoms after the treatment was observed in a large number of cases ($\Delta NPI_{f*s} < 0$= 52%, AD: 32%; MCI: 20%), showing a mean $\Delta NPI_{f*s} = -5.60$ ($\Delta NPI_{f*sAD} = -6.67$; $\Delta NPI_{f*sMCI} = -3.81$), Cohen's d = 2.18 (**Table 2**). Baseline characteristics comparison between responders and not responders to rehabilitation program are reported in **Supplementary Tables 1,2**.

Improvement in the Cognitive Status

Significant logistic regression model (Wald method, Nagelkerke R^2 = 0.229) on ΔMMSE (Improved vs. Not Improved) showed in the final second step a predicted role of MMSE score at baseline (p = 0.003) and $Z\text{-}PB_{global}$ index (p = 0.005) (**Table 3**). Age, sex, educational years, FAS at baseline, CAT at baseline, NPI_{f*s} at baseline, $Z\text{-}MTB_{global}$ index, $Z\text{-}FB_{global}$ index, $Z\text{-}SBCB_{global}$ index were excluded from the equation ($p > 0.05$).

When considering the left and right hemisphere separately, only MMSE score at baseline (p = 0.002) and $Z\text{-}PB_{rh}$ index (p = 0.002) remained in the final second regression model (Nagelkerke R^2 = 0.259) (**Table 4**). Age, sex, educational years, FAS at baseline, CAT at baseline, NPI_{f*s} at baseline, Z-values of $Z\text{-}MTB_{lh}$ and $Z\text{-}MTB_{rh}$ index, $Z\text{-}PB_{lh}$ index; $Z\text{-}FB_{lh}$ and $Z\text{-}FB_{rh}$ index, $Z\text{-}SBCB_{lh}$ and $Z\text{-}SBCB_{rh}$ index were excluded from the equation ($p > 0.05$).

When considering predicted probability of success, ideal candidate for the multimodal treatment was a person with lower MMSE at baseline and higher brain volume in PB-index, especially in the right PB-index (see **Figure 1**).

The Random Forest analysis, run to confirm the classification model, gave an accuracy score of approximately 77% including only variables retained at the last step of the regression model for the identification of participants who significantly benefited from the treatment and those which did not (**Table 5**).

Improvement in Behavioral Symptoms

Significant logistic regression model (Wald method, Nagelkerke R^2 = 0.352) on ΔNPI_{f*s} (Improved vs. Not Improved) showed in the final fourth step a predicted role of sex (p = 0.002), ΔNPI_{f*s} at

TABLE 3 | Binary logistic regression model to test best predictors of the MMSE change after rehabilitation.

		β	S.E.	Wald	*p*-value	Exp(β)	95% C.I. for Exp(β)	
							Lower	Upper
Step 1	MMSE baseline	−0.142	0.061	5.474	**0.019**	0.868	0.770	0.977
	Constant	3.358	1.439	5.444	0.020	28.727		
Step 2	MMSE baseline	−0.214	0.072	8.947	**0.003**	0.807	0.702	0.929
	Z-PB_{global} index	0.594	0.211	7.929	**0.005**	1.811	1.198	2.739
	Constant	6.006	1.870	10.310	0.001	405.674		

MMSE T0, Mini-Mental State Examination at baseline; Z-PB_{global}, Z-values of Posterior Brain index; S.E., standard error; C.I., confidence intervals. Relevant statistically significant results are reported in bold.

TABLE 4 | Binary logistic regression model to test best predictors of the MMSE change after rehabilitation.

		β	S.E.	Wald	*p-value*	Exp(β)	95% C.I. for Exp(β)	
							Lower	Upper
Step 1	MMSE baseline	−0.142	0.061	5.474	**0.019**	0.868	0.770	0.977
	Constant	3.358	1.439	5.444	0.020	28.727		
Step 2	MMSE baseline	−0.229	0.074	9.633	**0.002**	0.795	0.688	0.919
	Z-PB_{rh} index	0.657	0.214	9.409	**0.002**	1.929	1.268	2.935
	Constant	6.478	1.940	11.151	0.001	650.428		

MMSE, Mini-Mental State Examination; Z-PB_{rh}, Z-values of right Posterior Brain index; S.E., standard error; C.I., confidence intervals. Relevant statistically significant results are reported in bold.

baseline ($p = 0.005$), Z-PB_{global} index ($p = 0.006$), and Z-FB_{global} ($p = 0.039$) (**Table 6**). Age, educational years, FAS at baseline, CAT at baseline, MMSE at baseline, Z-MTB_{global} index, Z-$SBCB_{global}$ index were excluded from the equation ($p > 0.05$).

When exploring predicted probability of success, ideal candidate for the multimodal treatment was a person with higher severity of NPI_{f^*s} at baseline, lower brain volume in FB-index and higher brain volume in PB-index (see **Figure 2**).

Finally, for confirmatory purposes we ran Random Forest analysis. This analysis reported an accuracy of prediction approximately of 86% including demographical, neurostructural, and neuropsychological variables at baseline retained in the last step of the regression model for the identification of participants who significantly benefited from the treatment and those which did not (**Table 7**).

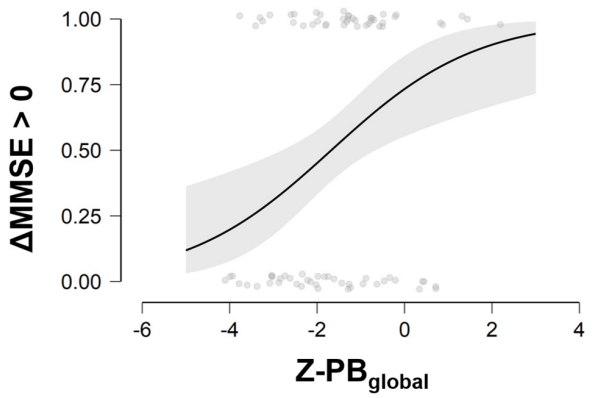

FIGURE 1 | Probability to improve in the cognitive status at different scores of MMSE at baseline and Z-PB_{global}. MMSE, Mini-Mental State Examination; ΔMMSE > 0, Delta change score (T1–T0) of Mini-Mental State Examination; Z-PB_{global}, *Z*-values of Posterior Brain index. Three ranks of PB index values can be considered for interpretation purposes: Low PB: Z-score ranges −4.10 to −2.22; Intermediate PB: Z-score ranges −2.15 to −0.95; High PB: Z-score ranges −0.88 to 2.19.

DISCUSSION

We investigated the best predictors able to forecast the efficacy of rehabilitative intervention according to multimodal approach on cognitive and behavioral aspects in AD-continuum conditions. While recent evidence supports the effectiveness of these interventions (Baglio et al., 2015; Realdon et al., 2016; McDermott et al., 2019; Di Tella et al., 2020; Cafferata et al., 2021), little is known about the associated neural reserve mechanisms underlying cognitive and behavioral functions recovery. We identified brain reserve neuroimaging biomarkers and clinical features associated with the best rehabilitative outcomes, thus giving the opportunity to

TABLE 5 | Random Forest results.

			Predicted	
	ΔMMSE		Not responders	Responders
Actual	Not responder	Count	28	12
		%	70.0%	30.0%
	Responder	Count	7	35
		%	16.7%	83.3%

Confusion matrix summarizing the performance of the RF classification algorithm on the cognitive outcome. The column targets (Predicted Not responders/Responders) are predicted values by the RF and the row targets (Actual Not responders/Responders) are the actual values. Classification accuracy represents the proportion of the instances that were classified correctly (Actual Not responders and Predicted Not responders + Actual Responders and Predicted Responders/Total sample). MMSE, Mini-Mental State Examination.

TABLE 6 | Binary logistic regression model to test best predictors of the NPI f*s change after rehabilitation.

							95% C.I. for Exp(β)	
		β	S.0E.	Wald	*p*-value	Exp(β)	Lower	Upper
Step 1	Sex	−1.333	0.475	7.888	**0.005**	0.264	0.104	0.669
	Constant	0.762	0.324	5.545	0.019	2.143		
Step 2	Sex	−1.314	0.497	6.984	**0.008**	0.269	0.101	0.712
	NPI_{f*s} T0	0.070	0.029	5.879	**0.015**	1.073	1.014	1.136
	Constant	−0.117	0.470	0.062	0.803	0.889		
Step 3	Sex	−1.424	0.519	7.521	**0.006**	0.241	0.087	0.666
	NPI_{f*s} T0	0.079	0.030	7.051	**0.008**	1.082	1.021	1.147
	$Z\text{-}PB_{global}$ index	0.428	0.204	4.388	**0.036**	1.534	1.028	2.288
	Constant	0.555	0.576	0.929	0.335	1.742		
Step 4	Sex	−1.758	0.580	9.175	**0.002**	0.172	0.055	0.538
	NPI_{f*s} T0	0.086	0.031	7.711	**0.005**	1.090	1.026	1.157
	$Z\text{-}PB_{global}$ index	1.123	0.408	7.588	**0.006**	3.073	1.382	6.830
	$Z\text{-}FB_{global}$ index	−0.605	0.294	4.243	**0.039**	0.546	0.307	0.971
	Constant	0.754	0.613	1.511	0.219	2.125		

NPI_{f*s}, Neuropsychiatric Inventory frequencies and severity of symptoms at baseline; $Z\text{-}PB_{global}$, Z- values of Posterior Brain index; $Z\text{-}FB_{global}$, Z-values of Frontal Brain index; S.E., standard error; C.I., confidence intervals. Relevant statistically significant results are reported in bold.

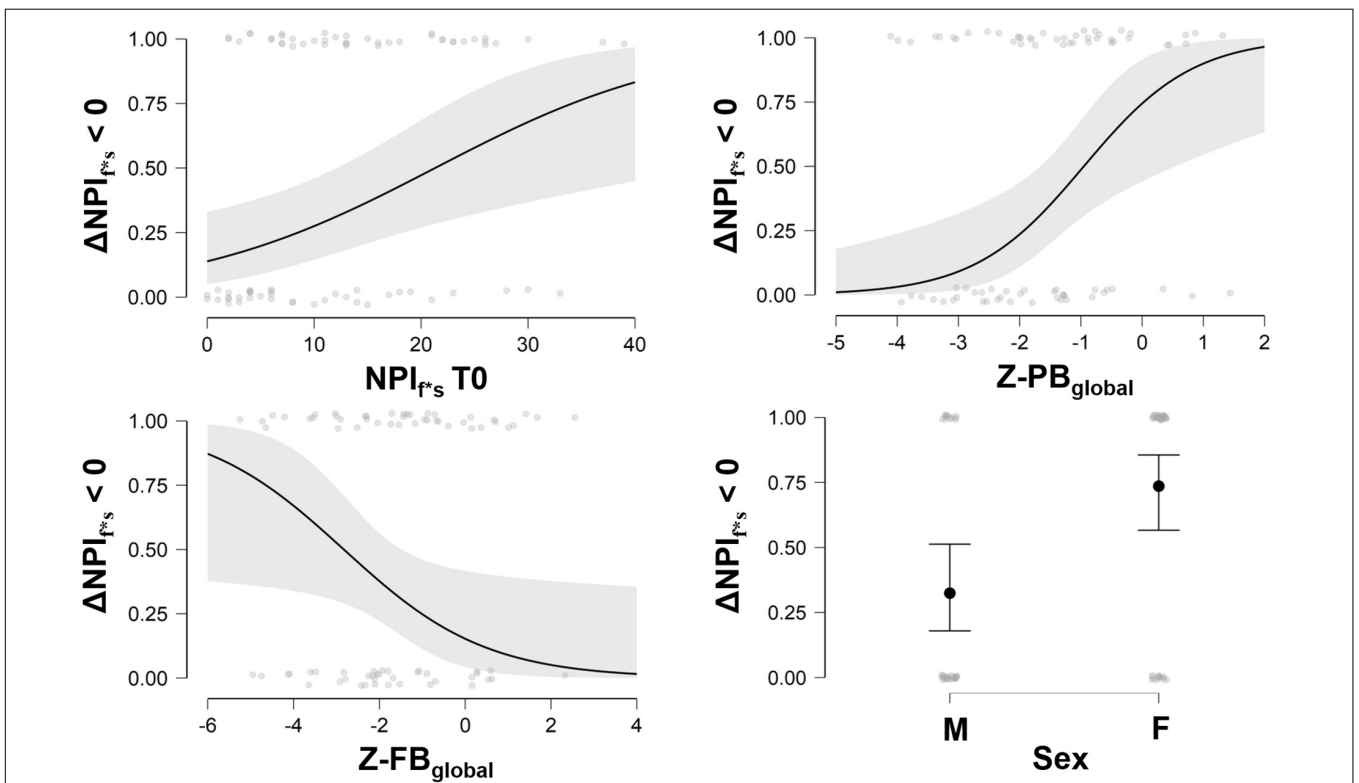

FIGURE 2 | Probability to reduce behavioral symptoms at different scores of NPI_{f*s} at baseline, and $Z\text{-}PB_{global}$, $Z\text{-}FB_{global}$, and sex. NPI, Neuropsychiatric Inventory; $\Delta NPI_{f*s} > 0$, Delta change score (T1–T0) of Neuropsychiatric Inventory frequencies and severity of symptoms; $Z\text{-}PB_{global}$, *Z*-values of Posterior Brain index; $Z\text{-}FB_{global}$, *Z*-values of Frontal Brain index; M, males, F, females. Three ranks values can be considered for interpretation purposes for PB index (Low PB: Z-score ranges −4.10 to −2.22; Intermediate PB: Z-score ranges −2.15 to −0.95; High PB: Z-score ranges −0.88 to 2.19) and FB index (Low FB: Z-score ranges −5.25 to −2.32; Intermediate FB: Z-score ranges −2.30 to −0.87; High FB: Z-score ranges −0.81 to 2.56).

both clinicians and the healthcare system to exploit the available resources at best, by selecting the best tailored rehabilitative interventions for each patient. Despite the large consensus regarding the impact of cognitive and brain reserve in coping with age-related diseases (Valenzuela and Sachdev, 2006; Cabeza et al., 2018), a paucity of studies is available on the prognostic significance of structural brain measures in neurorehabilitation. To our knowledge,

TABLE 7 | Random Forest results.

			Predicted	
	ΔNPI_{f*s}		Not responders	Responders
Actual	Not responders	Count	35	2
		%	94.6%	5.4%
	Responders	Count	9	34
		%	20.9%	79.1%

Confusion matrix summarizing the performance of the RF classification algorithm on the behavioral outcome. The column targets (Predicted Not responders/Responders) are predicted values by the RF and the row targets (Actual Not responders/Responders) are the actual values. Classification accuracy represents the proportion of the instances that were classified correctly (Actual Not responders and Predicted Not responder + Actual Responder and Predicted Responder/Total sample). NPI_{f*s}, Neuropsychiatric Inventory frequencies and severity of symptoms.

this is the first study focusing on the effects of brain reserves on the efficacy of rehabilitation interventions in AD-continuum conditions.

Considering the cognitive outcome of rehabilitation, our findings show that patients with low cognitive residual capabilities (MMSE level) at the time of admission and a high PB reserve in the parietal hemispheres (i.e., the normalized volume of AD-related parietal areas according to Ekman et al., 2018) are the best candidates to benefit from the rehabilitative treatment by achieving a significant improvement in global cognitive level. Neither FB nor MTL areas play a crucial role in the prediction of the cognitive outcome of intervention in our cohort of individuals.

The PB index (sum of volumes in: posterior cingulate, precuneus, superior parietal, inferior parietal, supramarginal gyrus) is not yet importantly compromised by the pathology progression as MTL index (Ekman et al., 2018) and can sustain the rehabilitation process in the mild to moderate stage of AD by integrating cognition, physical, and social activities (e.g., Venna et al., 2014). Such regions are importantly involved in the focusing of attention in internally directed cognition processes through the "tuning" of brain network activity and in the retrieval of autobiographical memories and in the planning of future acts (Zhang and Li, 2010; Leech and Sharp, 2014), somatosensory processing and visuo-spatial perception (Studer et al., 2014), socio-cognitive abilities (Rossetto et al., 2020; Tholen et al., 2020; Lion et al., 2021), and high-order processes (Culham and Kanwisher, 2001; Coull, 2004; Jubault et al., 2007; Desmurget and Sirigu, 2012). These aspects are well represented in the considered multimodal rehabilitation treatment, consisting in multifaced tasks touching cognitive, motor and social aspects of the patient's wellbeing.

Interestingly, when exploring the contribution of lateralization, we observed that the right, but not left, PB areas alone are strongly associated with cognitive improvement after the multimodal rehabilitation. This confirms previous findings (Thompson et al., 2003; Karas et al., 2008; Derflinger et al., 2011; Cabinio et al., 2018; Yang et al., 2019) that report an asymmetrical degeneration of gray matter in AD, in terms of a greater atrophy of left than right hemispheres: the so called "left hemisphere susceptibility" (Shi et al., 2009; Donix et al., 2013). This is particularly true considering cortical thickness and surface areas in both amnestic mild cognitive impairment and mild AD. fMRI studies highlighted the role of bilateral activation as an effective way to counteract the effects of aging and neurodegeneration by reorganizing its function. In our previous work using fMRI we looked for a hypoactivation pattern in AD, and after a period of intensive multimodal rehabilitation, we found increased fMRI activation in some PB areas for restoring neural functioning (Baglio et al., 2015). We can assume that although there is some neural asymmetric deterioration occurring with the disease, the brain can increase bilateral neural activity to improve cognitive function recruiting residual areas from brain reserve.

Results herein also show that the best predictors to achieve a significant improvement in behavioral domain include the level of behavioral symptomatology at baseline, the volume of FB and PB areas, as well as sex. In details, lower brain volume in FB-index is associated with a greater probability to improve in the behavioral outcome. In fact, participants showing a high volume in FB-index are plausibly people without significant behavioral symptoms and are likely to remain stable over time. The behavioral symptoms associated with dementia are particularly disabling aspects of the disease, with a relevant impact on both patients and caregivers (Bessey and Walaszek, 2019). These symptoms include apathy, depression, anxiety, irritability, agitation, delusions, hallucinations, aberrant motor behavior, and appetite disorder. A recent study demonstrated that FB areas constitute the best predictor of behavioral impairment of dementia (Boublay et al., 2020), considering the strictly link between the frontal-limbic pathways in the etiopathogenesis of the main behavioral symptoms of the disease. In fact, changes in behavior represent a mark of the disease linked with impairment in executive functions and subserved by frontal lobe degenerative damage. Our findings indicate that the parietal reserve may also trigger a mechanism of improvement during rehabilitation even when a frontal degeneration is evident in behavioral aspects of AD-continuum. Accordingly, a paradigm shift is currently leading to new approaches in neurorehabilitation for older adults, favoring a functional-led multimodal method to enhance a wide range of cognitive functions, such as art-based tools. This approach is based on evidence supporting the potential benefit of the modulation of neural activity in brain areas that are better preserved in the aging process, such as parietal areas (Prakash et al., 2014). In particular, art-based stimulation resulted in a high effectiveness on different domains of functioning in AD, by acting on emotional channels and brain areas in which overactivation is observed in older adult age (Bucks and Radford, 2004; Klein-Koerkamp et al., 2012; Savazzi et al., 2020). Finally, a predictive role of sex on the

behavioral outcome was found as females were more likely to benefit from rehabilitation. To the best of our knowledge no consistent data are available on sex and the prognostic rehabilitation effect in AD. Only pilot evidence suggests that sex may influence the cognitive effectiveness of motor treatment: older females show greater cognitive benefits from exercise than males (Barha and Liu-Ambrose, 2018). However, the mechanisms underlying this finding are still unknown.

This study is not without limitation: only one MRI examination per patient has been carried out at baseline. Subsequent studies may investigate neural plasticity induced by rehabilitation programs. Another limitation consists in the restricted neuropsychological battery considered for the outcome measures, not including measures with high ecological validity, which could have prevented the study from additional significant findings. Finally, our results should be interpreted with caution also considering that the effects of rehabilitation programs are variable depending on different factors, related to the contents of the program, the ability of therapists, the compliance of the participants. However, the relatively large sample size of the study renders the work relevant in the neurorehabilitation field. Future works will refine the predictive models by considering additional variables, such as the symptom duration and biomarkers (TAU protein and genotypes). Also, more sophisticated models including other proxy measures of cognitive reserve (employment/socio-behavioral indices) should investigate the possible mediating and/or moderating role of these variables explaining the association between treatment response and brain reserve.

These results indicate that cognitive behavioral improvement fostered by non-pharmacological treatments (Crescentini et al., 2014; Stinear et al., 2014), strictly depends on the actual brain reserve and functions of patients. This evidence supported the concept that structural characteristics of the brain have a protective role in AD. Cognitive and behavioral status alone are not sufficient to identify best responders to a multidomain rehabilitation treatment. Increased neural reserve, especially in the parietal areas, is relevant for the compensatory mechanisms activated by rehabilitative treatment. These data support clinical decision by identifying target patients with high probability of success after rehabilitative programs on cognitive and behavioral functioning.

CONCLUSION

Our findings suggest that increased neural reserve, especially in the posterior brain structures, is a relevant predictor of the response to a rehabilitative treatment based on a holistic approach. Finally, baseline assessment of neural reserve indexes is fundamental to support clinical decision by identifying those patients that might most benefit from of multidomain rehabilitation.

DATA AVAILABILITY STATEMENT

The raw data supporting the conclusions of this article will be made available by the authors, without undue reservation.

ETHICS STATEMENT

The studies involving human participants were reviewed and approved by the Don Gnocchi Ethics Committee. The patients/participants provided their written informed consent to participate in this study.

AUTHOR CONTRIBUTIONS

FB, MCl, MS, and SS conceived the work. FS, FR, and MA collected the data. MCa, SI, and SD performed the analyses. FB, SD, SI, MCa, and VB interpreted the results. FB, SD, SI, and MCa wrote the draft of the manuscript. All authors read and reviewed the final version of the manuscript.

FUNDING

This work was supported by the Italian Ministry of Health—Ricerca Corrente (Ricerca Corrente and Rete IRCCS delle Neuroscienze e della Neuroriabilitazione – Teleneuroriabilitazione).

ACKNOWLEDGMENTS

We thank all patients who voluntarily participated in the research.

SUPPLEMENTARY MATERIAL

The Supplementary Material for this article can be found online at: https://www.frontiersin.org/articles/10.3389/fnagi.2021.735508/full#supplementary-material

REFERENCES

Aisen, P. S., Cummings, J., Jack, C. R., Morris, J. C., Sperling, R., Frolich, L., et al. (2017). On the path to 2025: understanding the Alzheimer's disease continuum. *Alzheimers Res. Ther.* 9:60. doi: 10.1186/s13195-017-0283-5

Albert, M. S., DeKosky, S. T., Dickson, D., Dubois, B., Feldman, H. H., Fox, N. C., et al. (2011). The diagnosis of mild cognitive impairment due to Alzheimer's disease: recommendations from the National Institute on Aging-Alzheimer's Association workgroups on diagnostic guidelines for Alzheimer's disease. *Alzheimers Dement.* 7, 270–279. doi: 10.1016/j.jalz.2011.03.008

American Psychiatric Association (2013). *The Diagnostic and Statistical Manual of Mental Disorders: DSM 5*. Virginia: American Psychiatric Association. doi: 10.1176/appi.books.9780890425596

Baglio, F., Griffanti, L., Saibene, F. L., Ricci, C., Alberoni, M., Critelli, R., et al. (2015). Multistimulation group therapy in Alzheimer's disease promotes changes in brain functioning. *Neurorehabil. Neural. Repair* 29, 13–24. doi: 10.1177/1545968314532833

Barha, C. K., and Liu-Ambrose, T. (2018). Exercise and the Aging Brain: Considerations for Sex Differences. *Brain Plast.* 4, 53–63. doi: 10.3233/bpl-180067

Bessey, L. J., and Walaszek, A. (2019). Management of behavioral and psychological symptoms of dementia. *Curr. Psychiatry Rep.* 21:66. doi: 10.1007/s11920-019-1049-5

Birks, J. (2006). Cholinesterase inhibitors for Alzheimer's disease. *Cochrane. Database Syst. Rev.* 2006:Cd005593. doi: 10.1002/14651858.CD005593

Birks, J. S., and Grimley Evans, J. (2015). Rivastigmine for Alzheimer's disease. *Cochrane. Database Syst. Rev.* 2015:Cd001191. doi: 10.1002/14651858.CD001191.pub3

Boublay, N., Bouet, R., Dorey, J. M., Padovan, C., Makaroff, Z., Gallice, I., et al. (2020). Brain volume predicts behavioral and psychological symptoms in Alzheimer's Disease. *J. Alzheimers Dis.* 73, 1343–1353. doi: 10.3233/jad-190612

Braak, H., and Braak, E. (1991). Neuropathological stageing of Alzheimer-related changes. *Acta Neuropatho.l* 82, 239–259. doi: 10.1007/bf00308809

Bucks, R. S., and Radford, S. A. (2004). Emotion processing in Alzheimer's disease. *Aging Ment. Health* 8, 222–232. doi: 10.1080/13607860410001669750

Cabeza, R., Albert, M., Belleville, S., Craik, F. I. M., Duarte, A., Grady, C. L., et al. (2018). Maintenance, reserve and compensation: the cognitive neuroscience of healthy ageing. *Nat. Rev. Neurosci.* 19, 701–710. doi: 10.1038/s41583-018-0068-2

Cabinio, M., Saresella, M., Piancone, F., LaRosa, F., Marventano, I., Guerini, F. R., et al. (2018). association between hippocampal shape, neuroinflammation, and cognitive decline in Alzheimer's Disease. *J. Alzheimers Dis.* 66, 1131–1144. doi: 10.3233/jad-180250

Cafferata, R. M. T., Hicks, B., and von Bastian, C. C. (2021). Effectiveness of cognitive stimulation for dementia: A systematic review and meta-analysis. *Psychol. Bullet.* 147:325. doi: 10.1037/bul0000325

Carlesimo, G. A., Caltagirone, C., and Gainotti, G. (1996). The Mental Deterioration Battery: normative data, diagnostic reliability and qualitative analyses of cognitive impairment. The Group for the standardization of the mental deterioration battery. *Eur. Neurol.* 36, 378–384. doi: 10.1159/000117297

Chew, J., Chong, M. S., Fong, Y. L., and Tay, L. (2015). Outcomes of a multimodal cognitive and physical rehabilitation program for persons with mild dementia and their caregivers: a goal-oriented approach. *Clin. Interv. Aging* 10, 1687–1694. doi: 10.2147/cia.s93914

Coull, J. T. (2004). fMRI studies of temporal attention: allocating attention within, or towards, time. *Brain Res. Cogn. Brain Res.* 21, 216–226. doi: 10.1016/j.cogbrainres.2004.02.011

Crescentini, C., Urgesi, C., Fabbro, F., and Eleopra, R. (2014). Cognitive and brain reserve for mind-body therapeutic approaches in multiple sclerosis: a review. *Restor. Neurol. Neurosci.* 32, 575–595. doi: 10.3233/rnn-130364

Culham, J. C., and Kanwisher, N. G. (2001). Neuroimaging of cognitive functions in human parietal cortex. *Curr. Opin. Neurobiol.* 11, 157–163. doi: 10.1016/s0959-4388(00)00191-4

Cummings, J. L. (1997). The Neuropsychiatric Inventory: assessing psychopathology in dementia patients. *Neurology* 48, S10–S16. doi: 10.1212/WNL.48.5_Suppl_6.10S

Cummings, J. L. (2004). Alzheimer's disease. *N Engl. J. Med.* 351, 56–67. doi: 10.1056/NEJMra040223

Cummings, J. L., Mega, M., Gray, K., Rosenberg-Thompson, S., Carusi, D. A., and Gornbein, J. (1994). The Neuropsychiatric Inventory: comprehensive assessment of psychopathology in dementia. *Neurology* 44, 2308–2314. doi: 10.1212/wnl.44.12.2308

Derflinger, S., Sorg, C., Gaser, C., Myers, N., Arsic, M., Kurz, A., et al. (2011). Grey-matter atrophy in Alzheimer's disease is asymmetric but not lateralized. *J. Alzheimers Dis.* 25, 347–357. doi: 10.3233/jad-2011-110041

Desikan, R. S., Segonne, F., Fischl, B., Quinn, B. T., Dickerson, B. C., Blacker, D., et al. (2006). An automated labeling system for subdividing the human cerebral cortex on MRI scans into gyral based regions of interest. *Neuroimage* 31, 968–980. doi: 10.1016/j.neuroimage.2006.01.021

Desmurget, M., and Sirigu, A. (2012). Conscious motor intention emerges in the inferior parietal lobule. *Curr. Opin. Neurobiol.* 22, 1004–1011. doi: 10.1016/j.conb.2012.06.006

Di Tella, S., Isernia, S., Pagliari, C., Jonsdottir, J., Castiglioni, C., Gindri, P., et al. (2020). A Multidimensional virtual reality neurorehabilitation approach to improve functional memory: who is the ideal candidate? *Front. Neurol.* 11:618330. doi: 10.3389/fneur.2020.618330

Donix, M., Burggren, A. C., Scharf, M., Marschner, K., Suthana, N. A., Siddarth, P., et al. (2013). APOE associated hemispheric asymmetry of entorhinal cortical thickness in aging and Alzheimer's disease. *Psychiatry Res.* 214, 212–220. doi: 10.1016/j.pscychresns.2013.09.006

Ekman, U., Ferreira, D., and Westman, E. (2018). The A/T/N biomarker scheme and patterns of brain atrophy assessed in mild cognitive impairment. *Sci. Rep.* 8:8431. doi: 10.1038/s41598-018-26151-8

Fabbri, L., Mosca, I. E., Gerli, F., Martini, L., Pancani, S., Lucidi, G., et al. (2018). The Games for Older Adults Active Life (GOAL) project for people with mild cognitive impairment and vascular cognitive impairment: a study protocol for a randomized controlled trial. *Front. Neurol.* 9:1040. doi: 10.3389/fneur.2018.01040

Ferreira, D., Cavallin, L., Granberg, T., Lindberg, O., Aguilar, C., Mecocci, P., et al. (2016). Quantitative validation of a visual rating scale for frontal atrophy: associations with clinical status. APOE e4, CSF biomarkers and cognition. *Eur. Radiol.* 26, 2597–2610. doi: 10.1007/s00330-015-4101-9

Fillit, H., and Green, A. (2021). Aducanumab and the FDA - where are we now? *Nat. Rev. Neurol.* 17, 129–130. doi: 10.1038/s41582-020-00454-9

Fischl, B., Salat, D. H., Busa, E., Albert, M., Dieterich, M., Haselgrove, C., et al. (2002). Whole brain segmentation: automated labeling of neuroanatomical structures in the human brain. *Neuron* 33, 341–355. doi: 10.1016/S0896-6273(02)00569-X

Folstein, M. F., Robins, L. N., and Helzer, J. E. (1983). The Mini-mental state examination. *Arch. Gen. Psychiatry* 40:812. doi: 10.1001/archpsyc.1983.01790060110016

Gitlin, L. N., Mann, W. C., Vogel, W. B., and Arthur, P. B. (2013). A non-pharmacologic approach to address challenging behaviors of Veterans with dementia: description of the tailored activity program-VA randomized trial. *BMC Geriatr.* 13:96. doi: 10.1186/1471-2318-13-96

Grundman, M., Petersen, R. C., Ferris, S. H., Thomas, R. G., Aisen, P. S., Bennett, D. A., et al. (2004). Mild cognitive impairment can be distinguished from Alzheimer′s disease and normal aging for clinical trials. *Arch. Neurol.* 61, 59–66. doi: 10.1001/archneur.61.1.59

Hamilton, M. (1960). A rating scale for depression. *J. Neurol. Neurosurg. Psychiatry* 23, 56–62. doi: 10.1136/jnnp.23.1.56

Hänninen, T., Hallikainen, M., Tuomainen, S., Vanhanen, M., and Soininen, H. (2002). Prevalence of mild cognitive impairment: a population-based study in elderly subjects. *Acta Neurol. Scand.* 106, 148–154. doi: 10.1034/j.1600-0404.2002.01225.x

Isernia, S., Pagliari, C., Jonsdottir, J., Castiglioni, C., Gindri, P., Gramigna, C., et al. (2019). Efficiency and patient-reported outcome measures from clinic to home: the human empowerment aging and disability program for digital-health rehabilitation. *Front. Neurol.* 10:1206. doi: 10.3389/fneur.2019.01206

Jack, C. R. Jr., Bennett, D. A., Blennow, K., Carrillo, M. C., Dunn, B., Haeberlein, S. B., et al. (2018). NIA-AA Research Framework: Toward a biological definition of Alzheimer's disease. *Alzheimers Dement.* 14, 535–562. doi: 10.1016/j.jalz.2018.02.018

Jubault, T., Ody, C., and Koechlin, E. (2007). Serial organization of human behavior in the inferior parietal cortex. *J. Neurosci.* 27, 11028–11036. doi: 10.1523/jneurosci.1986-07.2007

Karas, G., Sluimer, J., Goekoop, R., van der Flier, W., Rombouts, S. A., Vrenken, H., et al. (2008). Amnestic mild cognitive impairment: structural MR imaging findings predictive of conversion to Alzheimer′s disease. *AJNR Am. J. Neuroradiol.* 29, 944–949. doi: 10.3174/ajnr.a0949

Katzman, R., Terry, R., DeTeresa, R., Brown, T., Davies, P., Fuld, P., et al. (1988). Clinical, pathological, and neurochemical changes in dementia: a subgroup with preserved mental status and numerous neocortical plaques. *Ann. Neurol.* 23, 138–144. doi: 10.1002/ana.410230206

Klein-Koerkamp, Y., Beaudoin, M., Baciu, M., and Hot, P. (2012). Emotional decoding abilities in Alzheimer's disease: a meta-analysis. *J. Alzheimers Dis.* 32, 109–125. doi: 10.3233/jad-2012-120553

Langa, K. M., and Levine, D. A. (2014). The diagnosis and management of mild cognitive impairment: a clinical review. *Jama* 312, 2551–2561. doi: 10.1001/jama.2014.13806

Leech, R., and Sharp, D. J. (2014). The role of the posterior cingulate cortex in cognition and disease. *Brain* 137, 12–32. doi: 10.1093/brain/awt162

Lehmann, M., Koedam, E. L., Barnes, J., Bartlett, J. W., Barkhof, F., Wattjes, M. P., et al. (2013). Visual ratings of atrophy in MCI: prediction of conversion and relationship with CSF biomarkers. *Neurobiol. Aging* 34, 73–82. doi: 10.1016/j.neurobiolaging.2012.03.010

Lion, K. M., Szczesniak, D., Bulinska, K., Mazurek, J., Evans, S. B., Evans, S. C., et al. (2021). Does the Meeting Centre Support Programme decrease the experience of stigmatisation among people with cognitive deficits? *Aging Ment. Health* 25, 160–169. doi: 10.1080/13607863.2019.1683815

Lopez, O. L., and Kuller, L. H. (2019). Epidemiology of aging and associated cognitive disorders: Prevalence and incidence of Alzheimer's disease and other dementias. *Handb. Clin. Neurol.* 167, 139–148. doi: 10.1016/B978-0-12-804766-8.00009-1

Lyketsos, C. G., Lopez, O., Jones, B., Fitzpatrick, A. L., Breitner, J., and DeKosky, S. (2002). Prevalence of neuropsychiatric symptoms in dementia and mild cognitive impairment: results from the cardiovascular health study. *Jama* 288, 1475–1483. doi: 10.1001/jama.288.12.1475

Lyketsos, C. G., Steinberg, M., Tschanz, J. T., Norton, M. C., Steffens, D. C., and Breitner, J. C. (2000). Mental and behavioral disturbances in dementia: findings from the Cache County Study on Memory in Aging. *Am. J. Psychiatry* 157, 708–714. doi: 10.1176/appi.ajp.157.5.708

Maguire, E. A., Woollett, K., and Spiers, H. J. (2006). London taxi drivers and bus drivers: a structural MRI and neuropsychological analysis. *Hippocampus* 16, 1091–1101. doi: 10.1002/hipo.20233

Maki, Y., Sakurai, T., Okochi, J., Yamaguchi, H., and Toba, K. (2018). Rehabilitation to live better with dementia. *Geriatr. Gerontol. Int.* 18, 1529–1536. doi: 10.1111/ggi.13517

McDermott, O., Charlesworth, G., Hogervorst, E., Stoner, C., Moniz-Cook, E., Spector, A., et al. (2019). Psychosocial interventions for people with dementia: a synthesis of systematic reviews. *Aging Ment. Health* 23, 393–403. doi: 10.1080/13607863.2017.1423031

McKhann, G. M., Knopman, D. S., Chertkow, H., Hyman, B. T., Jack, C. R. Jr., Kawas, C. H., et al. (2011). The diagnosis of dementia due to Alzheimer's disease: recommendations from the National Institute on Aging-Alzheimer's Association workgroups on diagnostic guidelines for Alzheimer's disease. *Alzheimers Dement.* 7, 263–269. doi: 10.1016/j.jalz.2011.03.005

Novelli, G., Papagno, C., Capitani, E., and Laiacona, M. (1986). Tre test clinici di ricerca e produzione lessicale. Taratura su sogetti normali. [Three clinical tests to research and rate the lexical performance of normal subjects.]. *Archivio di Psicologia, Neurologia e Psichiatria* 47, 477–506.

Oldfield, R. C. (1971). The assessment and analysis of handedness: the Edinburgh inventory. *Neuropsychologia* 9, 97–113. doi: 10.1016/0028-3932(71)90067-4

Petersen, R. C., Lopez, O., Armstrong, M. J., Getchius, T. S. D., Ganguli, M., Gloss, D., et al. (2018). Practice guideline update summary: mild cognitive impairment: report of the guideline development, dissemination, and implementation subcommittee of the american academy of neurology. *Neurology* 90, 126–135. doi: 10.1212/WNL.0000000000004826

Prakash, R. S., De Leon, A. A., Patterson, B., Schirda, B. L., and Janssen, A. L. (2014). Mindfulness and the aging brain: a proposed paradigm shift. *Front. Aging Neurosci.* 6:120. doi: 10.3389/fnagi.2014.00120

Realdon, O., Rossetto, F., Nalin, M., Baroni, I., Cabinio, M., Fioravanti, R., et al. (2016). Technology-enhanced multi-domain at home continuum of care program with respect to usual care for people with cognitive impairment: the Ability-TelerehABILITation study protocol for a randomized controlled trial. *BMC Psychiatry* 16:425. doi: 10.1186/s12888-016-1132-y

Roh, J. H., Qiu, A., Seo, S. W., Soon, H. W., Kim, J. H., Kim, G. H., et al. (2011). Volume reduction in subcortical regions according to severity of Alzheimer's disease. *J. Neurol.* 258, 1013–1020. doi: 10.1007/s00415-010-5872-1

Rossetto, F., Baglio, F., Massaro, D., Alberoni, M., Nemni, R., Marchetti, A., et al. (2020). Social cognition in rehabilitation context: different evolution of affective and cognitive theory of mind in mild cognitive impairment. *Behav. Neurol.* 2020:5204927. doi: 10.1155/2020/5204927

Sabbagh, M. N., Boada, M., Borson, S., Chilukuri, M., Doraiswamy, P. M., Dubois, B., et al. (2020). Rationale for Early Diagnosis of Mild Cognitive Impairment (MCI) Supported by Emerging Digital Technologies. *J. Prev. Alzheimers Dis.* 7, 158–164. doi: 10.14283/jpad.2020.19

Savazzi, F., Isernia, S., Farina, E., Fioravanti, R., D'Amico, A., Saibene, F. L., et al. (2020). Art, Colors, and Emotions" Treatment (ACE-t): a pilot study on the efficacy of an art-based intervention for people with alzheimer's disease. *Front. Psychol.* 11:1467. doi: 10.3389/fpsyg.2020.01467

Shi, F., Liu, B., Zhou, Y., Yu, C., and Jiang, T. (2009). Hippocampal volume and asymmetry in mild cognitive impairment and Alzheimer's disease: Meta-analyses of MRI studies. *Hippocampus* 19, 1055–1064. doi: 10.1002/hipo.20573

Spector, A., Orrell, M., and Goyder, J. (2013). A systematic review of staff training interventions to reduce the behavioural and psychological symptoms of dementia. *Ageing Res. Rev.* 12, 354–364. doi: 10.1016/j.arr.2012.06.005

Steinberg, M., Shao, H., Zandi, P., Lyketsos, C. G., Welsh-Bohmer, K. A., Norton, M. C., et al. (2008). Point and 5-year period prevalence of neuropsychiatric symptoms in dementia: the Cache County Study. *Int. J. Geriatr. Psychiatry* 23, 170–177. doi: 10.1002/gps.1858

Stern, Y. (2009). Cognitive reserve. *Neuropsychologia* 47, 2015–2028. doi: 10.1016/j.neuropsychologia.2009.03.004

Stinear, C. M., Byblow, W. D., and Ward, S. H. (2014). An update on predicting motor recovery after stroke. *Ann. Phys. Rehabil. Med.* 57, 489–498. doi: 10.1016/j.rehab.2014.08.006

Stokin, G. B., Krell-Roesch, J., Petersen, R. C., and Geda, Y. E. (2015). Mild Neurocognitive disorder: an old wine in a new bottle. *Harv. Rev. Psychiatry* 23, 368–376. doi: 10.1097/HRP.0000000000000084

Studer, B., Cen, D., and Walsh, V. (2014). The angular gyrus and visuospatial attention in decision-making under risk. *Neuroimage* 103, 75–80. doi: 10.1016/j.neuroimage.2014.09.003

Tholen, M. G., Trautwein, F. M., Böckler, A., Singer, T., and Kanske, P. (2020). Functional magnetic resonance imaging (fMRI) item analysis of empathy and theory of mind. *Hum. Brain Mapp.* 41, 2611–2628. doi: 10.1002/hbm.24966

Thompson, P. M., Hayashi, K. M., de Zubicaray, G., Janke, A. L., Rose, S. E., Semple, J., et al. (2003). Dynamics of gray matter loss in Alzheimer's disease. *J. Neurosci.* 23, 994–1005. doi: 10.1523/JNEUROSCI.23-03-00994.2003

Valenzuela, M. J., and Sachdev, P. (2006). Brain reserve and dementia: a systematic review. *Psychol. Med.* 36, 441–454. doi: 10.1017/S0033291705006264

Venna, V. R., Xu, Y., Doran, S. J., Patrizz, A., and McCullough, L. D. (2014). Social interaction plays a critical role in neurogenesis and recovery after stroke. *Transl. Psychiatry* 4:e351. doi: 10.1038/tp.2013.128

Williams, B., Jalilianhasanpour, R., Matin, N., Fricchione, G. L., Sepulcre, J., Keshavan, M. S., et al. (2018). Individual differences in corticolimbic structural profiles linked to insecure attachment and coping styles in motor functional neurological disorders. *J. Psychiatr Res.* 102, 230–237. doi: 10.1016/j.jpsychires.2018.04.006

World Health Organization (2012). *Dementia: a public health priority*. Geneva: World Health Organization.

World Health Organization (2017). *International Classification of Functioning, Disability and Health*. Geneva: World Health Organization.

Yang, H., Xu, H., Li, Q., Jin, Y., Jiang, W., Wang, J., et al. (2019). Study of brain morphology change in Alzheimer's disease and amnestic mild cognitive impairment compared with normal controls. *Gen. Psychiatr.* 32:e100005. doi: 10.1136/gpsych-2018-100005

Zhang, S., and Li, C. S. (2010). A neural measure of behavioral engagement: task-residual low-frequency blood oxygenation level-dependent activity in the precuneus. *Neuroimage* 49, 1911–1918. doi: 10.1016/j.neuroimage.2009.09.004

Conflict of Interest: The authors declare that the research was conducted in the absence of any commercial or financial relationships that could be construed as a potential conflict of interest.

frontiers in Aging Neuroscience

ORIGINAL RESEARCH
published: 26 November 2021
doi: 10.3389/fnagi.2021.710172

Functional Integrity of Executive Control Network Contributed to Retained Executive Abilities in Mild Cognitive Impairment

Wan Liu[1†], Li Liu[1†], Xinxin Cheng[1], Honglin Ge[2,3], Guanjie Hu[2,4], Chen Xue[2,4], Wenzhang Qi[2,4], Wenwen Xu[5], Shanshan Chen[5], Run Gao[1], Jiang Rao[1] and Jiu Chen[2,3]**

[1] Department of Rehabilitation, The Affiliated Brain Hospital of Nanjing Medical University, Nanjing, China, [2] Institute of Brain Functional Imaging, Nanjing Medical University, Nanjing, China, [3] Institute of Neuropsychiatry, The Affiliated Brain Hospital of Nanjing Medical University, Nanjing, China, [4] Department of Radiology, The Affiliated Brain Hospital of Nanjing Medical University, Nanjing, China, [5] Department of Neurology, The Affiliated Brain Hospital of Nanjing Medical University, Nanjing, China

OPEN ACCESS

Edited by:
Thomas Wisniewski,
NYU Grossman School of Medicine,
United States

Reviewed by:
Jiaojian Wang,
University of Electronic Science and Technology of China, China
Liang Gong,
Chengdu Second People's Hospital, China

***Correspondence:**
Jiang Rao
46190782@qq.com
Jiu Chen
ericcst@aliyun.com

[†] These authors have contributed equally to this work and share first authorship

Received: 15 May 2021
Accepted: 19 October 2021
Published: 26 November 2021

Citation:
Liu W, Liu L, Cheng X, Ge H, Hu G, Xue C, Qi W, Xu W, Chen S, Gao R, Rao J and Chen J (2021) Functional Integrity of Executive Control Network Contributed to Retained Executive Abilities in Mild Cognitive Impairment. Front. Aging Neurosci. 13:710172. doi: 10.3389/fnagi.2021.710172

Background: Mild cognitive impairment (MCI) is considered to be a transitional state between normal aging and Alzheimer's dementia (AD). Recent studies have indicated that executive function (EF) declines during MCI. However, only a limited number of studies have investigated the neural basis of EF deficits in MCI. Herein, we investigate the changes of regional brain spontaneous activity and functional connectivity (FC) of the executive control network (ECN) between high EF and low EF groups.

Methods: According to EF composite score (ADNI-EF) from the Alzheimer's Disease Neuroimaging Initiative (ADNI), we divided MCI into two groups, including the MCI-highEF group and MCI-lowEF group. Resting-state functional MRI was utilized to investigate the fractional amplitude of low-frequency fluctuation (fALFF) and ECN functional connectivity across 23 healthy controls (HC), 11 MCI-highEF, and 14 MCI-lowEF participants. Moreover, a partial correlation analysis was carried out to examine the relationship between altered fALFF or connectivity of the ECN and the ADNI-EF.

Results: Compared to HC, the MCI-highEF participants demonstrated increased fALFF in the left superior temporal gyrus (STG), as well as decreased fALFF in the right precentral gyrus, right postcentral gyrus, and left middle frontal gyrus (MFG). The MCI-lowEF participants demonstrated increased fALFF in the cerebellar vermis and decreased fALFF in the left MFG. Additionally, compared to HC, the MCI-highEF participants indicated no significant difference in connectivity of the ECN. Furthermore, the MCI-lowEF participants showed increased ECN FC in the left cuneus and left MFG, as well as decreased ECN functional connectivity in the right parahippocampal gyrus (PHG). Notably, the altered fALFF in the left MFG was positively correlated to ADNI-EF, while the altered fALFF in cerebellar vermis is negatively correlated with ADNI-EF across the two MCI groups and the HC group. Altered ECN functional connectivity in the right PHG is negatively correlated to ADNI-EF, while altered ECN functional connectivity in the left cuneus is negatively correlated to ADNI-EF across the three groups.

Conclusions: Our current study demonstrates the presence of different patterns of regional brain spontaneous activity and ECN FC in the MCI-highEF group and MCI-lowEF group. Furthermore, the ECN FC of the MCI-highEF group was not disrupted, which may contribute to retained EF in MCI.

Keywords: mild cognitive impairment, executive function, executive control network, functional connectivity, fractional amplitude of low-frequency fluctuation

1. INTRODUCTION

Mild cognitive impairment (MCI) is a transitional state between normal aging and Alzheimer's dementia (AD) (Bohlken et al., 2019; Thomas et al., 2019). Among patients with MCI, it has been well-established that patients with memory impairment (amnestic MCI, aMCI) are at a high risk of developing AD (Park et al., 2017; Thomas et al., 2017). Although memory deficits during disease progression have been widely studied and represent a benchmark of a probable AD diagnosis (Scheltens et al., 2018), more recent research has investigated executive function (EF) decline during MCI, which is also referred to as the preclinical stage of AD (Chang et al., 2009; Ewers et al., 2014; Kirova et al., 2015). EF has the ability required to plan, organize, operate on working memory, as well as switch between tasks (Bettcher et al., 2016). A recent study has developed a composite measure of EF, ADNI-EF, utilizing neuropsychological data from the Alzheimer's Disease Neuroimaging Initiative (ADNI), and has reported that ADNI-EF is a major predictor of transition from MCI to AD (Gibbons et al., 2012a). It has been concluded that poor EF in patients with MCI is characterized by very early cognitive decline in the initial course of AD, and indicates a transition from MCI to AD. Thus, it is greatly significant to clarify neuropathological mechanism of EF impairment and identify features that can predict their progression to AD.

While a large number of studies have examined the neuropathological factors related to MCI memory impairment (Perrotin et al., 2015; Terry et al., 2015; Vijayakumari et al., 2020), only a limited number of studies have examined the neural basis of EF deficits in MCI. Therefore, these limited studies have explored neural mechanisms of EF decline in patients with MCI from different aspects of brain morphology, metabolism, and network function. A study from the perspective of brain morphology has demonstrated that among patients with aMCI, the atrophic brain areas associated with decreasing of EF are located in the frontal and temporal cortex and that the atrophy of the right inferior frontal gyrus is more closely related to decreasing EF (Zheng et al., 2014). However, results from the metabolic point of view are not consistent with this, and the results indicated that EF impairment in aMCI is related to cerebral glucose metabolic abnormalities in the anterior cingulate cortex (ACC) and posterior cingulate cortex (PCC) (Yoon et al., 2020). Damage to the EF in MCI is not only related to the abnormality of local brain structure and brain metabolism but also to the brain network. A functional MRI (fMRI) study validated that the presence of increased connectivity of the ACC and dorsal lateral prefrontal cortex (DLPFC) in the ECN is positively correlated to EF in aMCI (Wu et al., 2014). Similarly, a diffusion tensor imaging (DTI) study demonstrated that MCI with high EF has a larger network size, density, and clustering coefficient (Farrar et al., 2018). However, results from fewer previous studies were not entirely consistent, and little was known about the changes in both spontaneous brain activity and brain functional networks.

In recent years, resting-state fMRI (rs-fMRI), attracted significant research interest in studying neural mechanisms of cognitive dysfunction (d'Ambrosio et al., 2020; Lee et al., 2020; Li et al., 2020). Among them, the fractional amplitude of low-frequency fluctuation (fALFF) was utilized to reliably measure the intensity of brain activity (Shu et al., 2020; Li et al., 2021). As it is a whole-brain data-driven method with high test-retest reliability, the fALFF has been chosen to carry out many studies among patients with MCI (Qiu et al., 2019; Yu et al., 2019; Zeng et al., 2019). In addition, it is well-known that EF requires several distinct brain regions that work together to perform complex tasks effectively (Farrar et al., 2018). Therefore, EF is suitable for network analysis. Moreover, the ECN comprising the main brain regions in the medial frontal cortex, ACC, DLPFC, is involved in top-down, attention-dependent EF such as cognitive control and response inhibition (Chen et al., 2008; Brown et al., 2019).

Therefore, according to ADNI-EF, patients with MCI were divided into two groups, including the high EF group and the low EF group. The objective of this current study is to investigate changes in regional brain spontaneous activity and FC of ECN between the two groups, as well as to further investigate the relationship between changes in the brain activity or FC of the ECN and EF. We hypothesized that there are different altered brain spontaneous activity and FC of ECN between the two groups, and changes of the low EF group may be more significant and similar to the pathological patterns of AD.

2. MATERIALS AND METHODS

In total, 109 subjects participated in the current study, which included 84 patients with MCI and 25 healthy controls (HC). All participants were chosen from the in-house database, the Nanjing Brain Hospital-Alzheimer's Disease Spectrum Neuroimaging Project (NBH-ADsnp) (Nanjing, China), which is continuously updated. The details of the NBH-ADsnp-related information are provided in **Supplementary Material**. The diagnostic and exclusion criteria of MCI and HC were in accordance with our previous studies (Xue et al., 2019; Wang et al., 2021b). This study was granted approval by the responsible Human Participants

Ethics Committee of the Affiliated Brain Hospital of Nanjing Medical University (Nos. 2018-KY010-01 and 2020-KY010-02), located in Nanjing, China. All participants were granted written informed consent prior to participation.

2.1. Neuropsychological Assessments

All participants underwent a comprehensive and standard assessment of neurocognitive function, including general cognitive function, information processing speed, episodic memory, visuo-spatial function, and EF. Details regarding each of these assessments were consistent with previous studies (Xue et al., 2019; Wang et al., 2021a).

2.2. Grouping

First, the EF composite score (ADNI-EF) of 84 patients with MCI was calculated according to the model provided by the ADNI website (http://adni.loni.usc.edu/). This model contains a WAIS-R Digit Symbol Substitution, Digit Span Backwards, Trails A and B, Category Verbal Fluency Test (CVFT), and Clock Drawing (Gibbons et al., 2012b). In our study, the average score was −0.91, with a SD of 0.46. Individuals with MCI with high executive abilities (MCI-highEF participants) were classified as being one SD above the group mean EF score, which led to 13 participants having a score above −0.45. Individuals with cognitive impairment that have low executive abilities (MCI-lowEF participants) were categorized as being one standard deviation below the group mean, leading to 15 participants with a score below −1.37. Similarly, 25 HCs were matched with 28 MCI participants (13 MCI-highEF participants and 15 MCI-lowEF participants). However, two MCI-highEF participants, one MCI-lowEF participant, and two HCs were excluded due to excessive head movement ($> 3mm$ *or* $> 3^{\circ}$). Finally, 25 patients with MCI were enrolled, which included 11 MCI-highEF participants, 14 MCI-lowEF participants, and 23 HCs.

2.3. MRI Data Acquisition

The detailed parameters of MRI acquisition of NBH-ADsnp were summarized in **Supplementary Material**.

2.4. Image Preprocessing

Data processing was conducted utilizing Data Processing Assistant for Resting-State fMRI (DPARSF 4.4, http://www.restfmri.net) based on the Matlab2013b platform. The first 10 volumes of functional images were removed for each subject. Then, the remaining images were corrected using slice-timing and realignment, accounting for head motion, normalized to standard space using DARTEL, resampled to a $3\times3\times3mm^3$ voxel size, regress nuisance variable, and spatially smoothed with 4 mm full width at half maximum (FWHM). The nuisance variables include 24 motion parameters (six head motion parameters, six head motion parameters one time point before, and the 12 corresponding squared items), a global signal, a white matter signal, and a cerebrospinal fluid signal. Finally, we carried out filtering band-pass (0.01-0.08 Hz) (Chen et al., 2016) prior to calculating seed-based functional connectivity (FC), and after calculating fALFF. In addition, participants with excessive head motion (cumulative translation or rotation >3.0 mm or 3.0) were excluded(Chen et al., 2020; Wang et al., 2021a).

2.5. fALFF Analysis

After data preprocessing, we carried out fALFF for each scan. The fast Fourier transform helped transform the time series of each voxel to the frequency domain in order to obtain the power spectrum. Then, the square root of the power spectrum was calculated. The fALFF was attained using the ratio of the power spectrum in a given frequency band (0.01–0.08 Hz) to total power in the entire detectable frequency range (Zou et al., 2008). Finally, the fALFF value of each voxel was divided using the global mean value in order to decrease global effects across participants.

2.6. FC Analysis

A seed-based FC analysis was carried out to examine the alteration of ECN. Seed region of interest (ROI) by drawing the 6-mm spheres located in the right DLPFC (MNI space: 48, 12, 34) was determined by converging data from previous studies (Smith et al., 2009; Wang et al., 2016). The DLPFC was consistently considered to be a key region within the ECN. Individual mean time series were extracted based on the coregistered seed region as the reference time series. The correlation analyses were conducted on the seed region and whole brain in a voxel-wise manner. The correlation coefficients of each voxel were normalized to Z-scores using Fisher's r-to-z transformation. Therefore, an entire brain Z-score map was developed for each subject for subsequent statistical analyses.

2.7. Statistical Analyses

The ANOVA was conducted to compare the demographics, neuropsychological assessment, and head rotation parameters among the three groups, except for gender (chi-square test). The two-sample *t*-test was used for *post-hoc* comparisons. The *p*-value was set as <0.05 for significant differences. A one-way analysis of covariance (ANCOVA) was utilized for comparison of the differences of FC in ECN and fALFF among HC, MCI-highEF, and MCI-lowEF participants. We used demographic data (age, gender, and education level), and gray matter volume as covariables. As suggested in the previous study, a non-parametric permutation test was able to precisely control the false positive rate in cluster-level inference (Qi et al., 2010). Therefore, we set the permutation times at 1,000. The corrected p <0.01 (fALFF results) or p <0.05 (FC results) was used for statistical significance and cluster size >50 voxels (1,350 mm^3) was applied for multiple comparisons at the voxel level. Then, the two-sample *t*-test was used for *post-hoc* comparisons, and the mask resulted from ANCOVA analyses after controlling the effects of demographic data (age, gender, and education level), and gray matter volume. We also set significance with the threshold free cluster enhancement and family-wise error (TFCE-FWE) corrected cluster $p < 0.05$ and the cluster size $>$ 10 voxels (270 mm^3). Finally, FCs or fALFF of significantly altered regions were extracted and later utilized for correlation analyses. The partial correlation analyses were carried out to reveal relationships between the altered fALFF or FCs and ADNI-EF after adjusting for the effects of age, gender, and education

TABLE 1 | Demographics and clinical measures of patients with mild cognitive impairment (MCI) and healthy controls (HC).

	HCs (n = 23)	MCI-highEF (n = 11)	MCI-lowEF (n = 14)	F(χ^2)	P
Age (years)	60.96 ± 9.45	60.00 ± 6.68	70.00 ± 7.47^{b,c}	6.27	0.004*
Gender (M/F), n	8/15	2/9	4/10	1.00	0.608
Education (years)	12.70 ± 2.24	12.18 ± 2.32	10.68 ± 3.16	2.75	0.075
MMSE	28.430 ± 1.56	27.73 ± 1.01	26.36 ± 1.45^{b,c}	9.30	<0.001*
MoCA	26.65 ± 1.70	23.91 ± 1.70	22.21 ± 2.46^{a,b,c}	9.30	<0.001*
ADNI-EF	-0.11 ± 0.36	−0.33 ± 0.18	−1.60 ± 0.20^{a,b,c}	121.81	<0.001*

*Data is represented by mean ± SD unless otherwise indicated. M, male; F, female; MMSE, Mini-Mental State Examination; MoCA, Montreal Cognitive Assessment. *Significant differences were found among HC, MCI-highEF, and MCI-lowEF subjects. Most p-values were obtained using ANOVA, except for gender (chi-square test). Comparisons of each paired group were conducted to further reveal the source of ANOVA difference (a: MCI-highEF vs. HCs; b: MCI-lowEF vs. HCs; c: MCI-lowEF vs. MCI-highEF).*

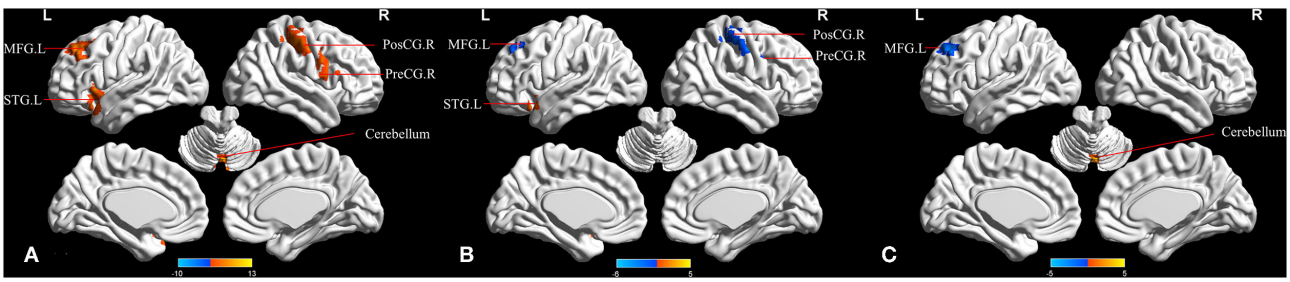

FIGURE 1 | Regions that demonstrate between-group differences in the fractional amplitude of low-frequency fluctuation (fALFF). **(A)** Regions with significant differences across the three groups in fALFF (one-way analysis of covariance (ANCOVA), cluster p <0.01, cluster size >50 voxels). **(B)** Regions with significant differences of MCI-highEF group vs. HC in fALFF [two-sample t-test; cluster p <0.05; cluster size >10 voxels; TFCE-FWE (family-wise error) corrected]. **(C)** Regions with significant differences of the MCI-lowEF group vs. HC in fALFF (two-sample t-test; cluster p <0.05; cluster size >10 voxels; TFCE-FWE corrected). MFG.L, left middle frontal gyrus; PosCG.R, right postcentral gyrus; PreCG.R, right precentral gyrus; STG.L, left superior temporal gyrus.

level. Because of the relatively small sample size, we did not correct the correlation analysis results for multiple comparisons in order to better present the results. The statistical significance was determined by an uncorrected p <0.05.

3. RESULTS

3.1. Demographic and Neuropsychological Characteristics

In parallel, EF of the MCI-lowEF group was lower compared to the MCI-high group (p <0.05) (**Table 1**). We found no significant differences in gender, head motion parameters (**Supplementary Table 1**) or education level were observed between the MCI-highEF group, MCI-lowEF group, and the HC group (all p >0.05). The MCI-lowEF group was older, compared to the HC subjects (70 ± 7.47 vs. 60.96 ± 9.45, p <0.05) and MCI-highEF group (70 ± 7.47 vs. 60 ± 7.47, p <0.05). In comparison to HCs, MCI-highEF patients only showed significantly decreased MoCA and ADNI-EF scores, while MCI-lowEF patients exhibited significantly reduced MMSE, MoCA, and ADNI-EF (all p <0.05). In addition, compared to the MCI-highEF group, the MCI-lowEF group demonstrated a significant decline in MMSE, MoCA, and ADNI-EF (all p <0.05) (**Table 1**).

3.2. Comparison of fALFF Between the Patients With MCI and the HC

When comparing the three groups, the ANCOVA analysis demonstrated significantly altered fALFF across the five brain regions among the groups, including in the cerebellar vermis, left superior temporal gyrus (STG), right precentral gyrus, left middle frontal gyrus (MFG), and right postcentral gyrus (**Figure 1A** and **Table 2**). Compared to HC, the MCI-highEF participants had significantly higher fALFF in the left STG, and decreased fALFF in the right precentral gyrus, right postcentral gyrus, and left MFG (**Figure 1B** and **Table 2**). The MCI-lowEF participants also showed significantly increased fALFF in the cerebellar vermis and decreased fALFF in the left MFG (**Figure 1C** and **Table 2**). Compared to the MCI-highEF participants, the MCI-lowEF participants demonstrated no significant differences in fALFF in these brain regions.

3.3. Comparison of FC Between the Patients With MCI and the HC

In the ECN, upon the comparison of the three groups, the ANCOVA analysis demonstrated the seven significantly altered FCs between the right DLPFC and brain regions among the groups, including the left cerebelum_crus, right parahippocampal gyrus (PHG), left cerebelum_4_5, left calcarine, left MFG, and left middle cingulum (**Figure 2A** and **Table 3**). Compared to the HC, the MCI-highEF participants demonstrated no significant difference in the connectivity of the ECN. In addition, the MCI-lowEF participants indicated significantly increased FC in the left cuneus, left MFG, and decreased FC in the right PHG (**Figure 2B** and **Table 3**). Compared to the MCI-highEF participants, the MCI-lowEF

TABLE 2 | The differences in the fractional amplitude of low-frequency fluctuation (fALFF) among the three groups.

Region (aal)	Peak MNI coordinate			F/t	Cluster number
	x	y	z		
ANCOVA					
Cerebellar vermis	6	−72	−24	12.697	57
Left superior temporal gyrus	−39	21	−18	9.852	89
Right precentral gyrus	57	9	39	11.033	77
Left middle frontal gyrus	−24	36	42	11.557	100
Right postcentral gyrus	54	−30	48	10.570	124
MCI-highEF>HC					
Left superior temporal gyrus	−39	18	−18	4.782	35
MCI-highEF<HC					
Right precentral gyrus	54	6	39	−5.359	16
Right postcentral gyrus1	60	−12	42	−4.354	12
Right postcentral gyrus2	36	−33	60	−5.025	59
Left middle frontal gyrus	−30	30	48	−4.323	27
MCI-lowEF>HC					
Cerebellar vermis	3	−72	−15	4.656	24
MCI-lowEF<HC					
Left middle frontal gyrus	−24	36	42	−4.782	48

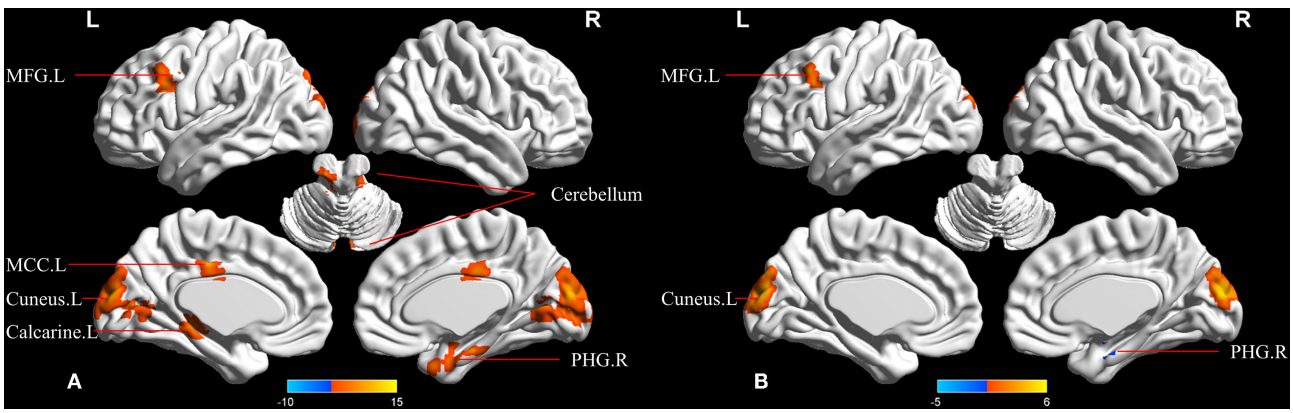

FIGURE 2 | Regions showing between-group differences in functional connectivity (FC) of the executive control network (ECN). **(A)** Regions with significant differences among the three groups in FC of ECN. (one-way ANCOVA; cluster p <0.05; cluster size >50 voxels). **(B)** Regions with significant differences of MCI-lowEF group vs. HC in FC of ECN (two-sample t-test; cluster p <0.05; cluster size >10 voxels; TFCE-FWE corrected). MCC.L, left middle cingulum cortex; MFG.L, left middle frontal gyrus; PHG.R, right parahippocampal gyrus.

participants demonstrated no significant difference in FC of the ECN.

3.4. Association Between Changes in fALFF or FC and ADNI-EF

Among the groups that consist of HC and MCI, the analysis demonstrated that altered fALFF in the left MFG is positively correlated to ADNI-EF ($r = 0.41$, $p = 0.005$, **Figure 3A**), while altered fALFF in cerebellar vermis is negatively correlated to ADNI-EF ($r = -0.32$, $p = 0.033$, **Figure 3B**). Altered FC between the right DLPFC and the right PHG is negatively correlated to ADNI-EF ($r = 0.31$, $p = 0.038$, **Figure 3C**), while altered FC between the right DLPFC and left cuneus is negatively correlated to ADNI-EF ($r = -0.31$, $p = 0.039$, **Figure 3D**). Age, gender, and education level are all used as covariates for these results (If Bonferroni-corrected used, the result is that only the fALLF value of the left MFG is significantly positively correlated with ADNI-EF).

4. DISCUSSION

Using the fALFF and FC, we evaluated the differences in resting regional brain activity and FC of ECN among patients with MCI-highEF and MCI-lowEF subtypes. We also explored the relationship between these changes and EF. The results demonstrated that only the regional brain activity was impaired

TABLE 3 | The differences in functional connectivity (FC) of executive control network (ECN) among the three groups.

Region (aal)	Peak MNI coordinate			F/t	Cluster number
	x	y	z		
ANCOVA					
Left cerebelum_crus	−3	−78	−33	7.962	52
Right parahippocampal	24	−6	−24	9.787	74
Left cerebelum_4_5	−9	−36	−9	11.632	93
Left cuneus	0	−90	18	14.376	409
Left calcarine	−12	−78	9	6.252	54
Left middle frontal gyrus	−42	18	33	10.072	71
Left middle cingulum	−3	−21	39	9.708	52
MCI-lowEF>HC					
Left cuneus	0	−93	15	5.515	189
Left middle frontal gyrus	−42	21	36	4.634	22
MCI-lowEF<HC					
Right parahippocampal	24	−9	−24	−4.698	10

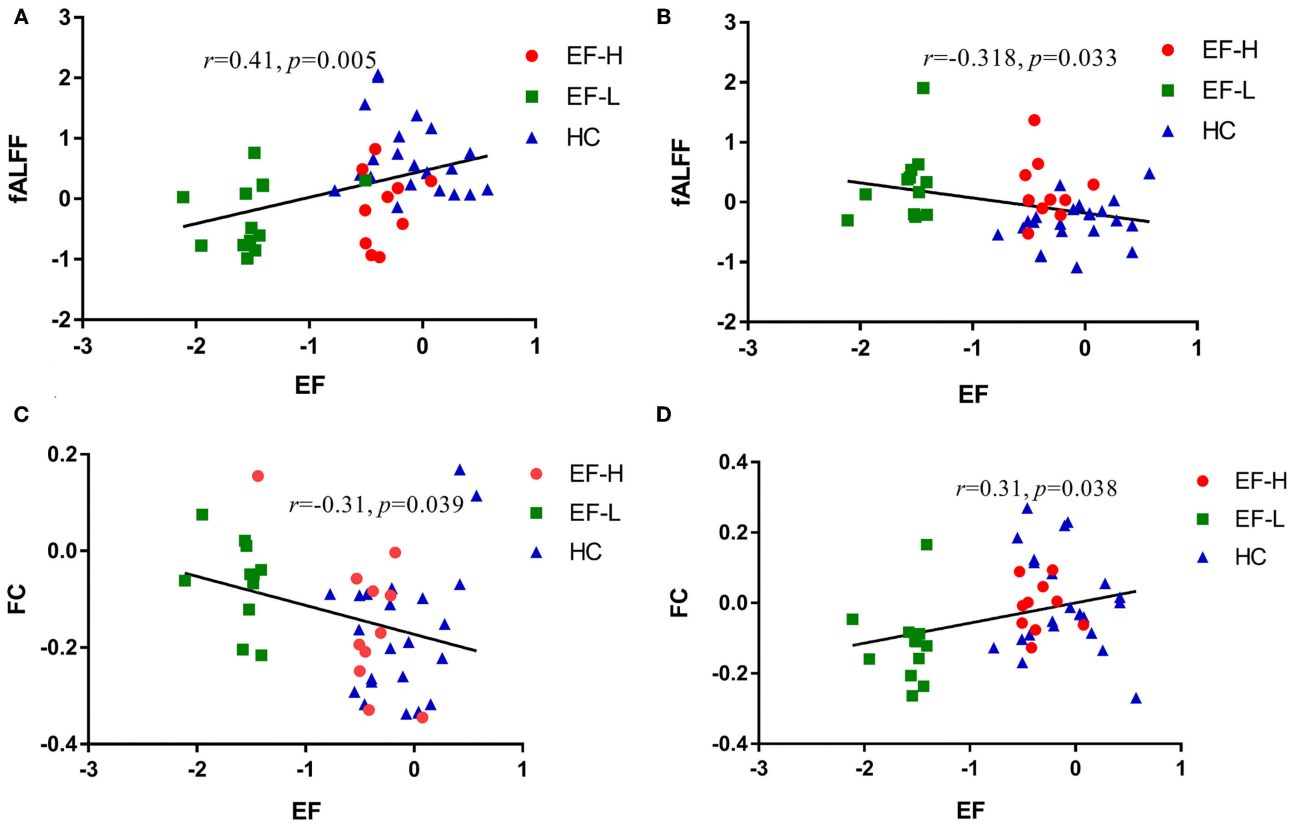

FIGURE 3 | (A) Significant relationships between the altered fALFF in the left MFG and ADNI-EF. **(B)** Significant relationships between altered fALFF in the cerebellar vermis and ADNI-EF. **(C)** Significant relationships between altered FC in the right parahippocampal gyrus and ADNI-EF. **(D)** Significant relationships between altered FC in the left cuneus and ADNI-EF. EF-H, MCI-highEF group; EF-L, MCI-lowEF group; HC, healthy controls; EF, ADNI-EF.

in MCI-highEF, while the FC of ECN did not change. On the other hand, not only was the regional brain activity of MCI-lowEF impaired, but the FC patterns of ECN changed. Additionally, correlation analysis indicated that altered fALFF and FC were related to impaired EF. These results suggest that the two subtypes of MCI can have different patterns of spontaneous brain activity and FC of the ECN, and the functional integrity of ECN may contribute to retained executive abilities in MCI.

Our first important finding was that the fALFF in the right precentral gyrus, right postcentral gyrus, and left MFG in the MCI-highEF group is lower than that in the HC group, while the fALFF in the left STG is higher than in the HC group. Contrastingly, the fALFF in the left MFG in the MCI-lowEF group is lower compared to HC, while fALFF of the cerebellar vermis is higher than HC. The majority of regions have been reported in prior MCI or AD studies (Cai et al., 2018; Long et al., 2018; Shi and Liu, 2020; Wang et al., 2021c). Compared to HC, the two groups all demonstrated significant fALFF differences in the left MFG. On the other hand, the frontal lobe itself was found to be an important component of ECN. A large number of previous studies have shown that the frontal lobe is closely related to cognitive function (Zhao et al., 2018; Catani, 2019; Jung et al., 2020) and EF (Cristofori et al., 2019; Zanto and Gazzaley, 2019). Herein, a study aimed to investigate the differences in atrophy patterns in the frontal-subcortical circuits between MCI and AD subjects, results of which indicated that both MCI and AD subjects had a thinner cortex in the left MFG compared to HC individuals (Zhao et al., 2015). Another structural MRI study also determined that frontal lobe atrophy was related to decreased EF in patients with aMCI (Zheng et al., 2014). Moreover, the study examined the relation between reward processing and performance on a working memory task. Results revealed that left MFG was activated by both working memory demands and increasing levels of reward (Pochon et al., 2002). Another task fMRI study showed that bilateral MFG were activated while participants performed a color-word Stroop task (Spielberg et al., 2011). Previous studies have validated that the structural and neurophysiological basis of abnormal frontal lobe spontaneous brain activity in patients with MCI, and have further verified the results of this current study. Furthermore, correlation analysis demonstrates that the fALFF of the left MFG is positively correlated to the ADNI-EF (The left MFG remained significantly positively correlated with ADNI-EF if Bonferroni-corrected was used). In other words, the lower the fALFF of the left MFG, the more severe the impairment of EF. Therefore, we hypothesize that the two groups have different patterns of spontaneous brain activity, but that the left MFG is not only a common site of injury but also closely related to EF.

In addition, our study also found that fALFF in cerebellar vermis is negatively correlated to ADNI-EF. Traditionally, the cerebellum plays an important role in the movement, maintaining body balance, regulating muscle tension, and forming voluntary movements. Thus, it was not considered to influence human cognitive function. Such an approach changed in the 1980s when research demonstrated that patients with cerebellar damage exhibited cognitive deficits (Schmahmann, 1991). Recently, much evidence has shown that the cerebellum affects not only visuospatial and verbal function, and declarative memory but also more complex behavior regulation processes, namely EF (Mak et al., 2016; Myers et al., 2017; Beuriat et al., 2020). A study found that patients with cerebellar infarction exhibited impaired cognitive function and had reduced fALFF values in the cerebellum compared to HC (Fan et al., 2019). Similarly, patients with bipolar disorder executive dysfunction showed significant hypoactivation in the cerebellum during the performance of EF tasks (Tian et al., 2020). Numerous studies have confirmed the important role of the cerebellum in EF, which is consistent with our study.

At the same time, our study indicated that the ECN connectivity pattern altered in the MCI-lowEF group, as we observed a decrease in the connection to the right PHG and an increase in the connection to the left MFG and left cuneus. However, there were no significant FC changes in the MCI-highEF group, which suggests that the functional integrity of the ECN may have contributed to retained executive abilities in MCI. More importantly, there is a positive correlation between FC and EF in the right PHG, but a negative correlation between the FC and EF in the left cuneus. Therefore, we speculate a decrease of the connection between the right PHG may be the diseased brain area related to damaging EF, while an increase in the connection of the left cuneus may be a compensatory mechanism. The PHG is known to be an important node of the hippocampal network (Zhu et al., 2020), which is vulnerable in AD for convergence of amyloid deposition, brain atrophy, functional disconnection, and hypometabolism (Sanchez et al., 2011; Trachtenberg et al., 2012). Prior studies have also shown a role of PHG in the progression of AD (Qiu et al., 2016; Wang et al., 2017). For example, some studies have demonstrated that the thickness of the PHG cortex is significantly thinner among patients with MCI (Devanand et al., 2012; Spulber et al., 2012; Machulda et al., 2020). Additionally, a longitudinal study showed that, compared to the normal control group, the converted patients with MCI showed insufficient perfusion in the right precuneus and PHG, while the MCI patients with MCI demonstrated low perfusion in the left PHG. The results of this study suggest that hypoperfusion in PHG is the earliest sign of progression from MCI to AD (Park et al., 2012). In addition, results from a meta-analysis showed the presence of significant regional resting-state differences between the aMCI and control group, which includes the posterior cingulate gyrus, right angular gyrus, right PHG, left fusiform gyrus, left supramarginal gyrus and bilateral middle temporal gyrus. The regions can be utilized as neuroimaging markers of aMCI. Thus, it can be seen that the right PHG is not only a neuroimaging marker of MCI but also a sign of progression from MCI to AD (Lau et al., 2016). This is consistent with our results and also validates that patients with MCI having low EF are more likely to progress to AD. Additionally, we identified an increase in FC in the left MFG and left cuneus. This is consistent with the majority of our previous research results, and is considered to be a compensatory mechanism.

Combining the results of fALFF and FC, both groups demonstrated the abnormal intensity of spontaneous brain activity. However, only the FC of the ECN in the MCI-lowEF group changed. This indicates that it was not just local brain regions involved, but also ECN changes with the aggravation of EF damage among patients with MCI. Executive abilities are known to require many distinct brain regions working together in order to efficiently perform complex tasks (Reineberg et al., 2018). As EF depends on global brain function, as the damage increases, the brain network needs to change. Our results further validate this point. Another important finding is that the left MFG is a commonly damaged brain area. The fALFF in the

MCI-highEF group and MCI-lowEF group is lower compared to the HC group, while FC between the right DLPFC and left MFG in the MCI-lowEF group is higher compared to the HC group. Similarly, correlation analysis demonstrated that there was a positive relationship between ADNI-EF and fALFF in the left MFG (If Bonferroni-corrected was used, the left MFG remained significantly positively correlated with ADNI-EF). These results suggest that with a decrease of EF in MCI, the spontaneous brain activity of left MFG decreases, while FC of the left MFG and ECN increases, in order to compensate part of the function. At the same time, it has also been validated that the retained executive abilities in MCI are related to the functional integrity of ECN. Hence, our study provides an important and novel idea that the left MFG can be used as a target of neuroregulatory techniques for early intervention.

In addition, our current study utilized ADNI-EF to assess the EF of patients with MCI. Studies have verified that ADNI-EF is a useful comprehensive measurement of EF in MCI, as good or better as any composite part. Importantly, ADNI-EF performed the same or better than all other EF indicators in detecting changes over time, as well as in predicting dementia (Gibbons et al., 2012a). Therefore, it is more reasonable to separate patients with MCI into either the low EF group or the high EF group, according to ADNI-EF.

5. LIMITATIONS

Despite these results, there are still several limitations to our study. First, to ensure the authenticity of the data, we did not censor the data for matching demographics between groups, which led to significant differences in age among the three groups and, thus, may cause confusion to our results. However, in order to avoid the effect of these confounding factors, we carried out all statistical analyses with age, gender, and education level as covariates. Meanwhile, MCI - highEF group only includes two men, which will also affect our results. Therefore, we are still working on enrolling participants, and we will further validate the results after demographics matching. Second, our cross-sectional design can limit the assessment of the role of regional brain activity and changes in FC in the left MFG in the subsequent development of AD. Changes of fALFF and FC in the left MFG after the conversion of two MCI groups into AD need to be further prospectively studied. Meanwhile, differences in fALFF and FC in the left MFG between patients with MCI who will be converted into AD and those who were not converted to AD also need to be further prospectively researched. Third, the sample size in our study is small, so the results are corrected by strict multiple comparisons to ensure reliability. However, recent studies have shown that even if the results are corrected by multiple comparisons, the results of a small sample size are inconsistent. Small *P*-values may not yield robust findings (Jia et al., 2021). Therefore, we are still working on enrolling participants, and we will further validate the results when the sample size is expanded in the future.

6. CONCLUSION

Our current study demonstrates that there are different patterns of spontaneous brain activity and FC of the ECN in the MCI-highEF group and MCI-lowEF group. Furthermore, the two groups demonstrated the abnormal intensity of spontaneous brain activity, but only FC of the ECN in MCI-lowEF group changed. This suggests that not only are the local brain regions involved but also that ECN changes with the aggravation of EF damage in patients with MCI. Additionally, the functional integrity of the ECN may contribute to retained executive abilities in MCI. Furthermore, the left MFG showed synchronous abnormalities in regional brain activity and FC with peripheral brain regions, and this was positively correlated with EF. Therefore, it has been suggested that the left MFG can be utilized as a target of neuroregulatory techniques for early intervention in MCI.

DATA AVAILABILITY STATEMENT

The raw data supporting the conclusions of this article will be made available by the authors, without undue reservation.

ETHICS STATEMENT

The studies involving human participants were reviewed and approved by Human Participants Ethics Committee of the Affiliated Brain Hospital of Nanjing Medical University (Nos. 2018-KY010-01 and 2020-KY010-02), located in Nanjing, China. The patients/participants provided their written informed consent to participate in this study.

AUTHOR CONTRIBUTIONS

JR, JC, and RG designed the study. XC, HG, GH, CX, WQ, WX, and SC collected the data. WL and LL analyzed the data and prepared the manuscript. All authors contributed to the article and approved the submitted version.

FUNDING

This study was supported by the National Natural Science Foundation of China (No. 81701675); the key project supported by Medical Science and Technology Development Foundation, Nanjing Department of Health (No. JQX18005); the Key Research and Development Plan (Social Development) Project of Jiangsu Province (No. BE2018608).

SUPPLEMENTARY MATERIAL

The Supplementary Material for this article can be found online at: https://www.frontiersin.org/articles/10.3389/fnagi.2021.710172/full#supplementary-material

REFERENCES

Bettcher, B. M., Mungas, D., Patel, N., Elofson, J., Dutt, S., Wynn, M., et al. (2016). Neuroanatomical substrates of executive functions: beyond prefrontal structures. *Neuropsychologia* 85, 100–109. doi: 10.1016/j.neuropsychologia.2016.03.001

Beuriat, P.-A., Cohen-Zimerman, S., Smith, G. N., Krueger, F., Gordon, B., and Grafman, J. (2020). A new insight on the role of the cerebellum for executive functions and emotion processing in adults. *Front. Neurol*. 11:1668. doi: 10.3389/fneur.2020.593490

Bohlken, J., Jacob, L., and Kostev, K. (2019). Progression of mild cognitive impairment to dementia in german specialist practices. *Dementia* 18, 380–390. doi: 10.1177/1471301216673919

Brown, C. A., Schmitt, F. A., Smith, C. D., and Gold, B. T. (2019). Distinct patterns of default mode and executive control network circuitry contribute to present and future executive function in older adults. *Neuroimage* 195, 320–332. doi: 10.1016/j.neuroimage.2019.03.073

Cai, S., Wang, Y., Kang, Y., Wang, H., Kim, H., von Deneen, K. M., et al. (2018). Differentiated regional homogeneity in progressive mild cognitive impairment: a study with *post hoc* label. *Am. J. Alzheimers Dis. Other Dement*. 33, 373–384. doi: 10.1177/1533317518778513

Catani, M. (2019). "Chapter 6: the anatomy of the human frontal lobe," in *The Frontal Lobes, volume 163 of Handbook of Clinical Neurology*, eds M. D'Esposito and J. Grafman (Amsterdam: Elsevier), 95–122. doi: 10.1016/B978-0-12-804281-6.00006-9

Chang, Y.-L., Jacobson, M. W., Fennema-Notestine, C., Hagler, D. J. Jr., Jennings, R. G., Dale. A. M. et al. (2009). Level of executive function influences verbal memory in amnestic mild cognitive impairment and predicts prefrontal and posterior cingulate thickness. *Cereb. Cortex* 20, 1305–1313. doi: 10.1093/cercor/bhp192

Chen, J., Ma, N., Hu, G., Nousayhah, A., Xue, C., Qi, W., et al. (2020). RTMs modulates precuneus-hippocampal subregion circuit in patients with subjective cognitive decline. *Aging* 13, 1314–1331. doi: 10.18632/aging.202313

Chen, J., Shu, H., Wang, Z., Zhan, Y., Liu, D., Liao, W., et al. (2016). Convergent and divergent intranetwork and internetwork connectivity patterns in patients with remitted late-life depression and amnestic mild cognitive impairment. *Cortex* 83, 194–211. doi: 10.1016/j.cortex.2016.08.001

Chen, S., Ross, T. J., Zhan, W., Myers, C. S., Chuang, K.-S., Heishman, S. J., et al. (2008). Group independent component analysis reveals consistent resting-state networks across multiple sessions. *Brain Res*. 1239, 141–151. doi: 10.1016/j.brainres.2008.08.028

Cristofori, I., Cohen-Zimerman, S., and Grafman, J. (2019). "Chapter 11: executive functions," in *The Frontal Lobes, volume 163 of Handbook of Clinical Neurology*, eds M. D'Esposito and J. Grafman (Amsterdam: Elsevier), 197–219. doi: 10.1016/B978-0-12-804281-6.00011-2

d'Ambrosio, A., Valsasina, P., Gallo, A., Stefano, N. D., Pareto, D., Barkhof, F., et al. (2020). Reduced dynamics of functional connectivity and cognitive impairment in multiple sclerosis. *Multiple Sclerosis J*. 26, 476–488. doi: 10.1177/1352458519837707

Devanand, D., Bansal, R., Liu, J., Hao, X., Pradhaban, G., and Peterson, B. S. (2012). MRI hippocampal and entorhinal cortex mapping in predicting conversion to Alzheimer's disease. *Neuroimage* 60, 1622–1629. doi: 10.1016/j.neuroimage.2012.01.075

Ewers, M., Brendel, M., Rizk-Jackson, A., Rominger, A., Bartenstein, P., Schuff, N., et al. (2014). Reduced FDG-pet brain metabolism and executive function predict clinical progression in elderly healthy subjects. *Neuroimage Clin*. 4, 45–52. doi: 10.1016/j.nicl.2013.10.018

Fan, L., Hu, J., Ma, W., Wang, D., Yao, Q., and Shi, J. (2019). Altered baseline activity and connectivity associated with cognitive impairment following acute cerebellar infarction: a resting-state fmri study. *Neurosci. Lett*. 692, 199–203. doi: 10.1016/j.neulet.2018.11.007

Farrar, D. C., Mian, A. Z., Budson, A. E., Moss, M. B., Koo, B. B., and Ronald, J. (2018). Alzheimer's disease neuroimaging initiative. retained executive abilities in mild cognitive impairment are associated with increased white matter network connectivity. *Eur. Radiol.* 28, 340–347. doi: 10.1007/s00330-017-4951-4

Gibbons, L., Carle, A., Mackin, R., Harvey, D., Mukherjee, S., Insel, P., et al. (2012a). A composite score for executive functioning, validated in Alzheimer's disease neuroimaging initiative (ADNI) participants with baseline mild cognitive impairment. *Brain Imaging Behav*. 6, 517–527. doi: 10.1007/s11682-012-9176-1

Gibbons, L. E., Carle, A. C., Mackin, R. S., Mukherjee, S., Insel, P., Curtis, S., et al. (2012b). Composite measures of executive function and memory: Adni_ef and adni_mem. *Alzheimers Dis. Neuroimaging Initiat*.

Jia, X.-Z., Zhao, N., Dong, H.-M., Sun, J.-W., Barton, M., Burciu, R., et al. (2021). Small p values may not yield robust findings: an example using rest-meta-PD. *Sci. Bull*. 66, 2148–2152. doi: 10.1016/j.scib.2021.06.007

Jung, Y. H., Park, S., Jang, H., Cho, S. H., Kim, S. J., Kim, J. P., et al. (2020). Frontal-executive dysfunction affects dementia conversion in patients with amnestic mild cognitive impairment. *Sci. Rep*. 10:772. doi: 10.1038/s41598-020-57525-6

Kirova, A.-M., Bays, R. B., and Lagalwar, S. (2015). Working memory and executive function decline across normal aging, mild cognitive impairment, and alzheimer's disease. *Biomed. Res. Int*. 2015:748212. doi: 10.1155/2015/748212

Lau, W. K. W., Leung, M.-K., Lee, T. M. C, and Law, A. C. K. (2016). Resting-state abnormalities in amnestic mild cognitive impairment: a meta-analysis. *Transl. Psychiatry* 26:e790. doi: 10.1038/tp.2016.55

Lee, Y. H., Bak, Y., Park, C., Chung, S. J., Yoo, H. S., Baik, K., et al. (2020). Patterns of olfactory functional networks in Parkinson's disease dementia and Alzheimer's dementia. *Neurobiol. Aging* 89, 63–70. doi: 10.1016/j.neurobiolaging.2019.12.021

Li, F., Lu, L., Shang, S., Hu, L., Chen, H., Wang, P., et al. (2020). Disrupted functional network connectivity predicts cognitive impairment after acute mild traumatic brain injury. *CNS Neurosci. Therapeut*. 26, 1083–1091. doi: 10.1111/cns.13430

Li, H.-L., Chou, X.-M., Liang, Y., Pan, T., Zhou, Q., Pei, C.-G., et al. (2021). Use of rsfMRI-fALFF for the detection of changes in brain activity in patients with normal-tension glaucoma. *Acta Radiol*. 62, 414–422. doi: 10.1177/0284185120926901

Long, Z., Jing, B., Guo, R., Li, B., Cui, F., Wang, T., et al. (2018). A brainnetome atlas based mild cognitive impairment identification using hurst exponent. *Front. Aging Neurosci*. 10:103. doi: 10.3389/fnagi.2018.00103

Machulda, M. M., Lundt, E. S., Albertson, S. M., Spychalla, A. J., Schwarz, C. G., Mielke, M. M., et al. (2020). Cortical atrophy patterns of incident mci subtypes in the Mayo clinic study of aging. *Alzheimers Dement*. 16, 1013–1022. doi: 10.1002/alz.12108

Mak, M., Tyburski, E., Madany, Ł., Sokoł owski, A., and Samochowiec, A. (2016). Executive function deficits in patients after cerebellar neurosurgery. *J. Int. Neuropsychol. Soc*. 22, 47–57. doi: 10.1017/S1355617715001174

Myers, P. S., McNeely, M. E., Koller, J. M., Earhart, G. M., and Campbell, M. C. (2017). Cerebellar volume and executive function in parkinson disease with and without freezing of gait. *J. Parkinsons Dis*. 7, 149–157. doi: 10.3233/JPD-161029

Park, J.-H., Park, H., Sohn, S. W., Kim, S., and Park, K. W. (2017). Memory performance on the story recall test and prediction of cognitive dysfunction progression in mild cognitive impairment and Alzheimer's dementia. *Geriatr. Gerontol. Int*. 17, 1603–1609. doi: 10.1111/ggi.12940

Park, K. W., Yoon, H. J., Kang, D.-Y., Kim, B. C., Kim, S., and Kim, J. W. (2012). Regional cerebral blood flow differences in patients with mild cognitive impairment between those who did and did not develop Alzheimer's disease. *Psychiatry Res. Neuroimaging* 203, 201–206. doi: 10.1016/j.pscychresns.2011.12.007

Perrotin, A., Desgranges, B., Landeau, B., Mézenge, F., La Joie, R., Egret, S., et al. (2015). Anosognosia in Alzheimer disease: Disconnection between memory and self-related brain networks. *Ann. Neurol.* 78, 477–486. doi: 10.1002/ana.24462

Pochon, J. B., Levy, R., Fossati, P., Lehericy, S., Poline, J. B., Pillon, B., et al. (2002). The neural system that bridges reward and cognition in humans: an fMRI study. *Proc. Natl. Acad. Sci. U.S.A*. 99, 5669–5674. doi: 10.1073/pnas.082111099

Qi, Z., Wu, X., Wang, Z., Zhang, N., Dong, H., Yao, L., et al. (2010). Impairment and compensation coexist in amnestic mci default mode network. *Neuroimage* 50, 48–55. doi: 10.1016/j.neuroimage.2009.12.025

Qiu, H., Li, X., Luo, Q., Li, Y., Zhou, X., Cao, H., et al. (2019). Alterations in patients with major depressive disorder before and after electroconvulsive therapy measured by fractional amplitude of low-frequency fluctuations (fALFF). *J. Affect. Disord*. 244, 92–99. doi: 10.1016/j.jad.2018.10.099

Qiu, T., Luo, X., Shen, Z., Huang, P., Xu, X., and Zhou, J. (2016). Disrupted brain network in progressive mild cognitive impairment measured by eigenvector

centrality mapping is linked to cognition and cerebrospinal fluid biomarkers. *J. Alzheimers Dis*. 54, 1483–1493. doi: 10.3233/JAD-160403

Reineberg, A. E., Gustavson, D. E., Benca, C., Banich, M. T., and Friedman, N. P. (2018). The relationship between resting state network connectivity and individual differences in executive functions. *Front. Psychol*. 9:1600. doi: 10.3389/fpsyg.2018.01600

Sanchez, M. M., Moghadam, S., Naik, P., Martin, K. J., and Salehi, A. (2011). Hippocampal network alterations in alzheimer's disease and down syndrome: from structure to therapy. *J. Alzheimers Dis*. 26(Suppl 3):29–47. doi: 10.3233/JAD-2011-0050

Scheltens, N., Tijms, B., Heymans, M., Rabinovici, G., Cohn-Sheehy, B., Miller, B., et al. (2018). Prominent non-memory deficits in alzheimer's disease are associated with faster disease progression. *J. Alzheimers Dis*. 65, 1029–1039. doi: 10.3233/JAD-171088

Schmahmann, J. D. (1991). An emerging concept: the cerebellar contribution to higher function. *Arch. Neurol*. 48, 1178–1187. doi: 10.1001/archneur.1991.00530230086029

Shi, J., and Liu, B. (2020). Stage detection of mild cognitive impairment via fMRI using hilbert huang transform based classification framework. *Med. Phys*. 47, 2902–2915. doi: 10.1002/mp.14183

Shu, Y., Kuang, L., Huang, Q., and He, L. (2020). Fractional amplitude of low-frequency fluctuation (falff) alterations in young depressed patients with suicide attempts after cognitive behavioral therapy and antidepressant medication cotherapy: a resting-state fMRI study. *J. Affect. Disord*. 276, 822–828. doi: 10.1016/j.jad.2020.07.038

Smith, S. M., Fox, P. T., Miller, K. L., Glahn, D. C., Fox, P. M., and Mackay, C. E. (2009). Correspondence of the brain's functional architecture during activation and rest. *Proc. Natl. Acad. Sci. U.S.A*. 106, 13040–13045. doi: 10.1073/pnas.0905267106

Spielberg, J. M., Miller, G. A., Engels, A. S., Herrington, J. D., Sutton, B. P., Banich, M. T., et al. (2011). Trait approach and avoidance motivation: lateralized neural activity associated with executive function. *Neuroimage* 54, 661–670. doi: 10.1016/j.neuroimage.2010.08.037

Spulber, G., Niskanen, E., MacDonald, S., Kivipelto, M., Padilla, D. F., and Julkunen, V. (2012). Evolution of global and local grey matter atrophy on serial MRI scans during the progression from MCI to AD. *Curr. Alzheimer Res*. 9, 516–524. doi: 10.2174/156720512800492486

Terry, D. P., Sabatinelli, D., Puente, A. N., Lazar, N. A., and Miller, L. S. (2015). A meta-analysis of fMRI activation differences during episodic memory in Alzheimer's disease and mild cognitive impairment. *J. Neuroimaging* 25, 849–860. doi: 10.1111/jon.12266

Thomas, B., Sheelakumari, R., Kannath, S., Sarma, S., and Menon, R. (2019). Regional cerebral blood flow in the posterior cingulate and precuneus and the entorhinal cortical atrophy score differentiate mild cognitive impairment and dementia due to Alzheimer disease. *Am. J. Neuroradiol*. 40, 1658–1664. doi: 10.3174/ajnr.A6219

Thomas, B. P., Sheng, M., Tseng, B. Y., Tarumi, T., Martin-Cook, K., Womack, K. B., et al. (2017). Reduced global brain metabolism but maintained vascular function in amnestic mild cognitive impairment. *J. Cereb. Blood Flow Metab*. 37, 1508–1516. doi: 10.1177/0271678X16658662

Tian, F., Diao, W., Yang, X., Wang, X., Roberts, N., Feng, C., et al. (2020). Failure of activation of striatum during the performance of executive function tasks in adult patients with bipolar disorder. *Psychol. Med*. 50, 653–665. doi: 10.1017/S0033291719000473

Trachtenberg, A. J., Filippini, N., Ebmeier, K. P., Smith, S. M., Karpe, F., and Mackay, C. E. (2012). The effects of apoe on the functional architecture of the resting brain. *Neuroimage* 59, 565–572. doi: 10.1016/j.neuroimage.2011.07.059

Vijayakumari, A. A., Menon, R. N., Thomas, B., Arun, T. M., Nandini, M., and Kesavadas, C., (2020). Glutamatergic response to a low load working memory paradigm in the left dorsolateral prefrontal cortex in patients with mild cognitive impairment: a functional magnetic resonance spectroscopy study. *Brain Imaging Behav*. 14, 451–459. doi: 10.1007/s11682-019-00122-7

Wang, S., Rao, J., Yue, Y., Xue, C., Hu, G., Qi, W., et al. (2021a). Altered frequency-dependent brain activation and white matter integrity associated with cognition in characterizing preclinical Alzheimer's disease stages. *Front. Hum. Neurosci*. 15:11. doi: 10.3389/fnhum.2021.625232

Wang, S., Sun, H., Hu, G., Xue, C., Qi, W., Rao, J., et al. (2021b). Altered insular subregional connectivity associated with cognitions for distinguishing the spectrum of pre-clinical Alzheimer's disease. *Front. Aging Neurosci*. 13:25. doi: 10.3389/fnagi.2021.597455

Wang, X., Cui, X., Ding, C., Li, D., Cheng, C., Wang, B., et al. (2021c). Deficit of cross-frequency integration in mild cognitive impairment and Alzheimer's disease: a multilayer network approach. *J. Magnet. Reson. Imaging* 53, 1387–1398. doi: 10.1002/jmri.27453

Wang, Y., Yang, S., Sun, W., Shi, Y., and Duan, H. (2016). Altered functional interaction hub between affective network and cognitive control network in patients with major depressive disorder. *Behav. Brain Res*. 298, 301–309. doi: 10.1016/j.bbr.2015.10.040

Wang, Z., Dai, Z., Shu, H., Liu, D., Guo, Q., He, Y. (2017). Cortical thickness and microstructural white matter changes detect amnestic mild cognitive impairment. *J. Alzheimers Dis*. 56, 415–428. doi: 10.3233/JAD-160724

Wu, L., Soder, R. B., Schoemaker, D., Carbonnell, F., Sziklas, V., Rowley, J. (2014). Resting state executive control network adaptations in amnestic mild cognitive impairment. *J. Alzheimers Dis*. 40, 993–1004. doi: 10.3233/JAD-131574

Xue, C., Yuan, B., Yue, Y., Xu, J., Wang, S., Wu, M., et al. (2019). Distinct disruptive patterns of default mode subnetwork connectivity across the spectrum of preclinical Alzheimer's disease. *Front. Aging Neurosci*. 11:307. doi: 10.3389/fnagi.2019.00307

Yoon, H.-J., Kim, S.-G., Kim, S.H., Choo, I. H., Park, S.H., Seo, E. H. (2020). Distinct neural correlates of executive function by amyloid positivity and associations with clinical progression in mild cognitive impairment. *Yonsei Med. J*. 60, 935–943. doi: 10.3349/ymj.2019.60.10.935

Yu, Y., Li, Z., Lin, Y., Yu, J., Peng, G., Zhang, K., et al. (2019). Depression affects intrinsic brain activity in patients with mild cognitive impairment. *Front. Neurosci*. 13:1333. doi: 10.3389/fnins.2019.01333

Zanto, T. P., and Gazzaley, A. (2019). "Chapter 20: aging of the frontal lobe, in *The Frontal Lobes, volume 163 of Handbook of Clinical Neurology*, eds M. D'Esposito and J. Grafman (Amsterdam: Elsevier), 369–389. doi: 10.1016/B978-0-12-804281-6.00020-3

Zeng, Q., Luo, X., Li, K., Wang, S., Zhang, R., Hong, H., et al. (2019). Distinct spontaneous brain activity patterns in different biologically-defined Alzheimer's disease cognitive stage: a preliminary study. *Front. Aging Neurosci*. 11:350. doi: 10.3389/fnagi.2019.00350

Zhao, H., Li, X., Wu, W., Li, Z., Qian, L., Li, S. (2015). Atrophic patterns of the frontal-subcortical circuits in patients with mild cognitive impairment and Alzheimer's disease. *PLoS ONE* 10:e0130017. doi: 10.1371/journal.pone.0130017

Zhao, Q., Lu, H., Metmer, H., Li, W. X., and Lu, J. (2018). Evaluating functional connectivity of executive control network and frontoparietal network in Alzheimer's disease. *Brain Res*. 1678, 262–272. doi: 10.1016/j.brainres.2017.10.025

Zheng, D., Sun, H., Dong, X., Liu, B., Xu, Y., Chen, S., et al. (2014). Executive dysfunction and gray matter atrophy in amnestic mild cognitive impairment. *Neurobiol. Aging* 35, 548–555. doi: 10.1016/j.neurobiolaging.2013.09.007

Zhu, Y., Zang, F., Liu, X., Fan, D., qian Zhang, Q., Ren, Q.-G., et al. (2020). Endocytosis-pathway polygenic scores affects the hippocampal network connectivity and individualized identification across the high-risk of Alzheimer's disease. *Brain Imaging Behav*. 15, 1155–1169. doi: 10.1007/s11682-020-00316-4

Zou, Q.-H., Zhu, C.-Z., Yang, Y., Zuo, X.-N., Long, X.-Y., Cao, Q.-J., et al. (2008). An improved approach to detection of amplitude of low-frequency fluctuation (ALFF) for resting-state fMRI: fractional ALFF. *J. Neurosci. Methods* 172, 137–141. doi: 10.1016/j.jneumeth.2008.04.012

Conflict of Interest: The authors declare that the research was conducted in the absence of any commercial or financial relationships that could be construed as a potential conflict of interest.

Publisher's Note: All claims expressed in this article are solely those of the authors and do not necessarily represent those of their affiliated organizations, or those of the publisher, the editors and the reviewers. Any product that may be evaluated in this article, or claim that may be made by its manufacturer, is not guaranteed or endorsed by the publisher.

Advantages of publishing in Frontiers

OPEN ACCESS
Articles are free to read for greatest visibility and readership

FAST PUBLICATION
Around 90 days from submission to decision

HIGH QUALITY PEER-REVIEW
Rigorous, collaborative, and constructive peer-review

TRANSPARENT PEER-REVIEW
Editors and reviewers acknowledged by name on published articles

Frontiers
Avenue du Tribunal-Fédéral 34
1005 Lausanne | Switzerland

Visit us: www.frontiersin.org
Contact us: frontiersin.org/about/contact

REPRODUCIBILITY OF RESEARCH
Support open data and methods to enhance research reproducibility

DIGITAL PUBLISHING
Articles designed for optimal readership across devices

FOLLOW US
@frontiersin

IMPACT METRICS
Advanced article metrics track visibility across digital media

EXTENSIVE PROMOTION
Marketing and promotion of impactful research

LOOP RESEARCH NETWORK
Our network increases your article's readership